

**Isolation and Characterization of Antioxidative and
Anti-inflammatory Small Molecular Bioactives from Bivalve Clams
Villorita cyprinoides (Gray) and *Paphia malabarica* (Chemnitz)**

Thesis submitted in partial fulfillment of the requirement for the degree of

DOCTOR OF PHILOSOPHY

in

CHEMISTRY

Submitted to

MANGALORE UNIVERSITY

By

Ms. MINJU JOY

(Ref. No. MU/EXB/Ph.D/CR.137/Chem./2014-15/E.13, dated 20.02.2015)

Under the Faculty of Science and Technology



MANGALORE UNIVERSITY

MANGALAGANGOTHRI - 574 199

Dakshina Kannada Dist., Karnataka, India

Guided By

Dr. KAJAL CHAKRABORTY

Senior Scientist (Organic Chemistry)

Marine Biotechnology Division, Central Marine Fisheries Research Institute (CMFRI)



Central Marine Fisheries Research Institute

Post Box No. 1603, Ernakulam North P.O.

Kochi - 682 018, Kerala, India



November 2017



भारतीय कृषि अनुसंधान परिषद
Indian Council of Agricultural Research
केन्द्रीय समुद्री मात्स्यिकी अनुसंधान संस्थान
Central Marine Fisheries Research Institute

(कृषि अनुसंधान एवं शिक्षा विभाग, केन्द्र कृषि एवं किसान कल्याण मंत्रालय, भारत सरकार)
(Department of Agricultural Research and Education, Ministry of Agriculture and Farmers' Welfare, Govt. of India)

पोस्ट बॉक्स नं. 1603, एरणाकुलम नॉर्थ पी.ओ., कोच्ची - 682 018, केरल, भारत
Post Box No. 1603, Ernakulam North P.O., Kochi - 682 018, Kerala, India

Phone: 91 484 2394867/2391407, Fax: 91 484 2394909/2396685, Email: director@cmfri.org.in, Web: www.cmfri.org.in



CMFRI Platinum Jubilee - Celebrating 70 years of Excellence in Research

Dr. Kajal Chakraborty

Senior Scientist (Organic Chemistry)

Certificate

This is to certify that this thesis entitled "Isolation and Characterization of Antioxidative and Anti-inflammatory Small Molecular Bioactives from Bivalve Clams Villorita cyprinoides (Gray) and Paphia malabarica (Chemnitz)" submitted by Ms. MINJU JOY, Research Fellow of Marine Biotechnology Division of Central Marine Fisheries Research Institute, for the award of the degree of Doctor of Philosophy in Chemistry is the result of bonafide research work carried out by her in the Marine Biotechnology Division of Central Marine Fisheries Research Institute in Chemistry, Kochi-682018, under my guidance and direct supervision. I further certify that this thesis or part thereof has not previously formed the basis for the award of any degree, diploma and associateship of any other University or Institution.

Kajal Chakraborty

Place: Kochi

Date: 21/11/2017

Declaration

*I do hereby declare that the thesis entitled “Isolation and Characterization of Antioxidative and Anti-inflammatory Small Molecular Bioactives from Bivalve Clams *Villorita cyprinoides* (Gray) and *Paphia malabarica* (Chemnitz)” is an authentic record of research work carried out by me under the guidance and supervision of Dr. Kajal Chakraborty, Senior Scientist (Organic Chemistry), Marine Biotechnology Division, Central Marine Fisheries Research Institute, Kochi-682018 and the same has not previously formed the basis for the award of any degree or diploma. Whenever the work described is based on the findings of other researchers, due acknowledgement is made in keeping with the general practice of reporting scientific observations. However, errors and unintentional oversights, if any are regretted.*

MINJU JOY

Place: Kochi

Date: 21/11/2017

Acknowledgements

First and foremost, praises and thanks to Jesus Christ, the Almighty, for His showers of blessings throughout my research work to complete my research work successfully. You have given me the power to believe in myself and pursue my dreams. You have given me the strength and confidence to face all my difficult situations and hardships throughout my journey. I express my sincere gratitude and thanks to God for giving me strength, wisdom, health and luck to accomplish this endeavor. I could never have done this without the faith I have in you, the Almighty.

I would like to thank all those people who made my thesis possible and a memorable experience. The successful completion of any task would be imperfect without mentioning the people who helped in every stage. At the end of my thesis, it is very pleasant task and my privilege to express a few words of gratitude, respect and special thanks to one and all those who contributed in many ways to the achievement of my thesis work.

I express my sincere gratitude and thanks to my supervising guide Dr. Kajal Chakraborty, Senior Scientist (Organic Chemistry), Central Marine Fisheries Research Institute Kochi, for his inspiring guidance, support, valuable suggestions, encouragement, scholarly inputs and intellectual support throughout the research work. I am deeply grateful to him for providing all the facilities and freedom in doing the experiments. I record my deep sense of gratitude to him for all his efforts and the moral support for the successful completion of my thesis. Thank you so much, Sir.

I feel extremely thankful to Dr. A. Gopalakrishnan, Director, Central Marine Fisheries Research Institute, for all the necessary facilities and support required to carry out my research work. I record my heartfelt respect and gratitude to Dr. A. Gopalakrishnan, for providing me absolute freedom for the successful completion of this thesis.

I feel extremely express my sincere respect and gratitude to Dr. Vijayagopal Pananghat, Head of the Department, Marine Biotechnology Division, Central Marine

Fisheries Research Institute, for facilitating my research activities and support during the doctoral work. I feel privileged to place on record my sincere gratitude for Dr. Bobby Ignatius, Principal Scientist and Head of HRD Cell of CMFRI, for kindly facilitating my research activities during the doctoral work. I extremely express my sincere respect and gratitude to the scientists of Marine Biotechnology Division, Dr. N. K. Sanil, Dr. Sandhya Sukumaran and Dr. M. A. Pradeep. I would like to express my sincere thanks to Dr. Rekhadevi Chakraborty, Senior Scientist, Crustacean Fisheries Division, CMFRI.

I wish to express my heartfelt thanks to Dr. M. P. Paulton (Senior Technical Officer), Mr. Nandakumar Rao, Mrs. G. Shylaja (Technical Officer, CMFRI) and Mrs. P. Vineetha, SIC librarian, library support staff, staff members of the HRD Cell, the canteen, security personnel and all the employees of CMFRI, Kochi, for their sincere help and cooperation extended during the tenure.

I express my deep sense of gratitude for the support extended by my lab mates and colleagues Prima Francis, Vamshi Krishna Raola, Deepu Joseph, Bini Thilakan, Selsa J. Chakkalakkal, Anusree Venugopal, Fasina Makkar, Dexy Joseph, Shubhajit Dhara, Tima Antony, Soumya Krishnan, Vinaya K. K., Soumya Salas, Rajesh T. K., Purushothaman P., Aswathy Elizabeth Mani, and all other research scholars of Marine Biotechnology Division.

I acknowledge the staffs of Sophisticated Analytical Instrument Facility (SAIF), Indian Institute of Technology (IIT), Chennai, Tamil Nadu especially, Dr. S. S. Bhattacharya, Head of SAIF, Dr. C. Baby (Technical officer), Dr. Murugesan, Mr. Bhaskar, Mr. V. Srinivasan, Mr. R. Sathiyamoorthi and Mr. Shankar for their help and support extended towards the NMR, FTIR and Mass spectroscopic analyses. I also acknowledge the staffs of Sophisticated Test and Instrumentation Centre (STIC), Cochin University of Science and Technology (CUSAT) for their help in analytical experiments.

I take this opportunity to thank Indian Council of Agricultural Research, New Delhi for providing Research Fellowships under different schemes and Ministry of Earth Science (MoES), New Delhi, India for funding under the project “Drugs from the sea” for providing the necessary facilities.

I would like to thank my parents for allowing me to realize my own potential. All the support and time they have provided me over these years was the greatest gift anyone has ever given me. I am thankful to my Chachan, Joy K. J. and Mummy, Molly Joy with tearful gratitude for their selfless sacrifice, painful efforts, prayers, blessings and their trust on me. I don't have words to express my sincere gratitude to my father for allowing me to complete my thesis work and for his patience and sacrifice to fulfil my wishes, without him, I may never have gotten to where I am today. Thank you so much, Chachan and Mummy. I remember my grandmother, Rosy Joseph and my heavenly grandparents Joseph Kaitharan, Antony Koikkara, Kochuthresia Antony for their prayers, blessings and I never achieve this in my life without their prayers. My special gratitude and thanks to my younger brother, Manu Joy for his loving support and selfless care throughout my studies. I extend my deep sense of gratitude to all my dearest 'Koikkara' and 'Kaithran' family members for their prayers and good wishes. I am forever indebted to all my cousin sisters and brothers, uncles and aunties for their understanding, endless patience and encouragement when it was most required.

I express my sincere thanks and gratitude to my beloved husband, Regith R., for his constant support, prayers and selfless helps which made my task much easier and comfortable throughout my research work. He has loved me, cared for me and trusted me in all my difficult situations and encouraged me to achieve my goals. Words fail me to convey the sort of heavenly benediction he has been to me.

I express my gratitude and thanks from my bottom of heart to my dear friend, Sr. Helga Pereira, for her inspiring words, boundless prayers and supports throughout my life.

Finally, I thank all those who have helped me directly or indirectly in the successful completion of my thesis.

MINJU JOY

Place: Kochi

Date: 21/11/2017

Dedicated to my Beloved

Chachan-Mummy

ABSTRACT

The bivalve clams are traditional seafoods occupying a leading share to the edible bivalve mollusks in the estuarine and marine ecosystems of India. Corbiculid clam *Villorita cyprinoides* (black clam) and venerid clam *Paphia malabarica* (yellow-foot clam) are recognized to be the common bivalve clam resources in the coastal areas of the southwest coast of India. The bivalve clams, though regarded as low-value by-catch, believed to possess valuable nutritional qualities and pharmacological properties.

The bivalve clams, *V. cyprinoides* and *P. malabarica* collected from the estuarine system of the southwest coastal waters of India, and evaluated for their nutritional composition. A balanced essential to non-essential amino acid ratio (> 1.0) with a greater quantity of sulfur containing amino acids in these species demonstrated that they could provide well-balanced protein depositions. *P. malabarica* displayed lesser atherogenicity (0.7) and thrombogenicity (0.3) indices and greater hypocholesterolemic to hypercholesterolemic ratio (1.7) when compared with those in *V. cyprinoides*, thereby indicating the nutritional superiority of former. A greater content of vitamin D₃ (> 150 IU), along with significant quantities of calcium and phosphorus (> 500 mg/100 g) in clams signified their importance in preventing osteoporosis.

The ethyl acetate:methanol (EtOAc:MeOH) solvent extract of *V. cyprinoides* and *P. malabarica* assessed for their bioactive potentials, namely antioxidant, anti-diabetic, anti-inflammatory and anti-hypertension using various *in vitro* analyses. No significant difference was apparent for antioxidant potentials evaluated by 1,1-diphenyl-2-picryl-hydrazil (IC₅₀ DPPH 0.76 mg/mL) among *P. malabarica* and *V. cyprinoides* ($p > 0.05$). However, EtOAc:MeOH extract of *P. malabarica* demonstrated greater 2,2'-azino-bis-3-ethylbenzothiozoline-6-sulfonic acid (IC₅₀ ABTS⁺ 1.27 mg/mL) radical scavenging activities along with lipid peroxidation inhibitory potentials (2.39 mM MDAEQ/kg) than those recorded with *V. cyprinoides* ($p < 0.05$). Likewise, anti-inflammatory effects of EtOAc:MeOH solvent extract of *P. malabarica* against pro-inflammatory cyclooxygenase-2 (IC₅₀ COX-2 0.92 mg/mL) and 5-lipoxygenase (IC₅₀ 5-LOX 1.51 mg/mL) enzymes registered significant potencies than *V. cyprinoides* (IC₅₀ 1.03 and 1.64 mg/mL, respectively). A greater anti-hypertensive property against angiotensin converting enzyme-1 (IC₅₀ ACE-1 1.11 mg/mL) and anti-diabetic potentials against dipeptidyl peptidase-4 (IC₅₀ DPP-4 1.00 mg/mL) were recorded for EtOAc:MeOH extract of *P. malabarica* than those recorded with *V. cyprinoides*. A significant co-linearity has observed among various bioactivities and deshielded electronegative functionalities present in proton NMR spectra of EtOAc:MeOH extracts of the studied bivalve clams.

The bioassay guided chemical investigations of EtOAc:MeOH extract of *V. cyprinoides* led to the isolation of bioactive metabolites classified under various classes of chemistries, like spirocyclic ether derivatives (**1-2**), meroterpenoids (**3-5**), hexahydro isochromenyl analogues (**6-7**) and cholesterol derivatives (**8-10**). The chemical investigations of EtOAc:MeOH extract of *P. malabarica* led to the isolation of different metabolites classified under aryl polyketide derivatives (**1-3**), tetrahydro chromenyl analogues (**4-5**), isopimarane norditerpenoid (**6**), meroterpeno 2H-pyranoids (**7-8**) and cholesterol derivatives (**9-10**). The structures of isolated compounds were unambiguously assigned by 1D (¹H, ¹³C, ¹³⁵DEPT), 2D (¹H-¹H COY, HSQC, HMBC, NOESY) nuclear magnetic resonances (NMR) spectroscopy, Fourier transform infrared (FTIR) and mass spectrometric experiments. The spirocyclic ether derivatives, **1** and **2** isolated from *V. cyprinoides* were displayed significantly greater ($p < 0.05$) antioxidant activities against DPPH radical (IC₅₀ < 0.60 mg/mL) as equated with other compounds and standard, α -tocopherol (IC₅₀ > 0.60 mg/mL). Likewise, the compounds **1** and **2** (IC₅₀ 0.62-0.67 mg/mL), which along with furano meroterpenoid derivative, **5** (IC₅₀ 0.64 mg/mL) displayed significantly greater ABTS⁺ scavenging effects ($p < 0.05$) as compared to those exhibited by other compounds and commercial antioxidative agent, α -tocopherol (IC₅₀ $>$

0.70 mg/mL). The spirocyclic ether derivative, **2** recorded significantly greater inhibitory activity against COX-1 and COX-2 (IC_{50} 0.86 and 0.65 mg/mL, respectively) as related to other compounds with higher IC_{50} values of > 0.90 and > 0.70 mg/mL, respectively ($p < 0.05$). In addition, the compounds from *V. cyprinoides* (**1-10**) displayed potential bioactivities against pro-inflammatory inducible enzyme, COX-2 than the constitutive isoform COX-1, and consequently recorded greater selectivity indices (SI, IC_{50} anti-COX-1/ IC_{50} anti-COX-2 > 1.00) than the anti-inflammatory drug, ibuprofen (SI 0.63). Similarly, spirocyclic ether derivatives, **1-2** (IC_{50} 0.75-0.77 mg/mL), hexahydrobenzo furanone, **3** (IC_{50} 0.76 mg/mL) and furano meroterpenoid derivative, **5** (IC_{50} 0.80 mg/mL) exhibited significantly greater inhibitory potentials against pro-inflammatory 5-LOX when compared to other compounds and ibuprofen ($IC_{50} > 0.90$ mg/mL; $p < 0.05$).

The hydroxy oxo-pyran enclosed benzoate derivative, **3** (IC_{50} 0.59 mg/mL) and furanyl-2H-tetrahydro-chromenyl, **4** (IC_{50} 0.56 mg/mL) isolated from *P. malabarica* were found to exhibit significantly greater DPPH inhibitory activity related to other compounds in the series and α -tocopherol ($IC_{50} \geq 0.65$ mg/mL; $p < 0.05$). Likewise, the compounds, **3** (IC_{50} 0.69 mg/mL) and **4** (IC_{50} 0.67 mg/mL) did not display noteworthy difference in ABTS⁺ scavenging ($p > 0.05$) potentials. These compounds were found to display significantly greater ($p < 0.05$) ABTS⁺ scavenging effects when equated to other compounds and α -tocopherol ($IC_{50} \geq 0.74$ mg/mL). The hydroxy benzoate derivative, **3** (IC_{50} 0.68 mg/mL) registered greater inhibitory properties against COX-2 followed by that of hydroxy benzoate, **1** (IC_{50} 0.74 mg/mL) and furanyl-2H-tetrahydro-chromenyl, **4** (IC_{50} 0.72 mg/mL), in descending order. The compounds, **1-10** isolated from *P. malabarica* registered greater selectivity indices (SI > 1.05) than that recorded with ibuprofen (SI 0.63), which appropriately demonstrated the greater anti-inflammatory activity of former against pro-inflammatory COX-2 than COX-1. Moreover, these compounds (**3**, **6** and **4**) exhibited significantly greater 5-LOX inhibitory properties when compared to other compounds and ibuprofen ($IC_{50} > 0.77$ mg/mL; $p < 0.05$).

The target bioactivities of the studied compounds from *V. cyprinoides* and *P. malabarica* correlated with their structural parameters using different physicochemical descriptor variables, wherein the bioactivities of the studied compounds were directly proportional to their electronic parameters. An optimum hydrophobic-hydrophilic balance along with lesser steric bulk of the studied compounds manifested towards their greater bioactivities. Putative antioxidative mechanisms proposed for the studied bioactive secondary metabolites from *V. cyprinoides* and *P. malabarica* in the DPPH radical scavenging model. The modes of inhibition of COX-2 and 5-LOX pro-inflammatory enzymes by the candidate compounds from these bivalve clams determined by *in silico* molecular docking simulations. The present study envisaged the significance of nutritional and bio-potential functionalities of commonly available seafoods, *V. cyprinoides* and *P. malabarica*.

Among various mollusks, bivalve clams, particularly *V. cyprinoides* and *P. malabarica* have considered as traditional health food and natural dietary source, even though, the scientific investigations to acknowledge the health benefits of these species were relatively confined. Considering the underutilization of these species, exploring bioactive compounds has dual benefits as health products and their commercial farming in coastal habitats of southwest coast of India. The current findings of bioassay guided isolation and characterization of secondary metabolites from *V. cyprinoides* and *P. malabarica* appropriately recommended their utilities as potential bioactive leads in the functional food formulations and templates for therapeutic applications.

ABBREVIATIONS

1D NMR	-	One Dimensional Nuclear Magnetic Resonance
¹ H NMR	-	Proton Nuclear Magnetic Resonance
2D NMR	-	Two Dimensional Nuclear Magnetic Resonance
5-LOX	-	5-Lipoxygenase
AA	-	Arachidonic Acid
ABTS ⁺	-	2,2-Azino-Bis-3ethylbenzothiozoline-6-Sulfonic Acid
AI	-	Atherogenicity Index
ANOVA	-	Analysis of Variance
BHA	-	Butylated Hydroxy Anisole
BSA	-	Bovine Serum Albumin
CC	-	Column Chromatography
COSY	-	Correlation Spectroscopy
COX	-	Cyclooxygenase
DCM	-	Dichloromethane
DDW	-	Double Distilled Water
DEPT	-	Distortionless Enhancement by Polarization Transfer
DHA	-	Docosahexaenoic acid
DMSO	-	Dimethyl Sulfoxide
DPPH	-	1,1-Diphenyl-2-Picrylhydrazyl
EDTA	-	Ethylenediaminetetra Acetic Acid
EI-MS	-	Electron Ionization Mass Spectra
EPA	-	Eicosapentaenoic acid
EtOAc	-	Ethyl Acetate
FAs	-	Fatty Acids
FAME	-	Fatty Acid Methyl Esters
FC	-	Flash Chromatography
FFA	-	Free Fatty Acid
FTIR	-	Fourier Transform Infra Red
GAE	-	Gallic Acid Equivalence
GC-MS	-	Gas Chromatography-Mass Spectrometry
GLC	-	Gas Liquid chromatography
GSD	-	Global Spectral Deconvolution
H ₂ O ₂	-	Hydrogen Peroxide
HH	-	Hypocholesterolaemic/hypercholesterolaemic
HMBC	-	Heteronuclear Multiple Bond Correlation
HPLC	-	High-Performance Liquid Chromatography
HRESIMS	-	High Resolution Electro Spray Mass Spectrometry
HSQC	-	Heteronuclear Single Quantum Coherence
IC ₅₀	-	Inhibition Concentration at 50%
LMWC	-	Low Molecular Weight Compounds
<i>m/z</i>	-	Mass-to-Charge ratio
MDA	-	Malondialdehyde/Malonaldehyde

MDAEQ	-	Malondialdehyde Equivalent
MeOH	-	Methanol
MNP	-	Marine Natural Products
MUFA	-	Mono Unsaturated Fatty Acid
NMR	-	Nuclear Magnetic Resonance
NOESY	-	Nuclear Overhauser Effect Spectroscopy
PCA	-	Principal Component Analysis
PDA	-	Photodiode Array
PGE ₂	-	Prostaglandin E ₂
PGF ₂	-	Prostaglandin F ₂
PGG ₂	-	Prostaglandin G ₂
ppm	-	Parts Per Million
PTLC	-	Preparative Thin Layer Chromatography
PUFA	-	Poly Unsaturated Fatty Acid
R _f	-	Retardation Factor
RMSD	-	Root Mean Square Deviation
RNS	-	Reactive Nitrogen Species
ROS	-	Reactive Oxygen Species
RP-HPLC	-	Reverse Phase High-Performance Liquid Chromatography
R _t	-	Retention Time
SD	-	Standard Deviation
SFA	-	Saturated Fatty Acid
SPSS	-	Statistical Program for Social Sciences
TAA	-	Total Amino Acids
TArAA	-	Total aromatic amino acids
TBA	-	Thiobarbituric Acid
TBARS	-	Thiobarbituric Acid Reactive Species
Tbhq	-	Tertbutylhydroquinone
TCA	-	Trichloroacetic Acid
TEAA	-	Total essential amino acid
TEAA	-	Total essential amino acids
TI	-	Thrombogenicity Index
TLC	-	Thin Layer Chromatography
TNEAA	-	Total non-essential amino acids
TNF- α	-	Tumor Necrosis Factor- α
TPC	-	Total Phenolic Content
TSAA	-	Total Sulphur containing Amino Acid
UV-VIS	-	Ultra Violet-Visible

CONTENTS

CHAPTER 1: INTRODUCTION	1
1.1. Background	1
1.2. Biological potentials of secondary metabolites from marine and estuarine habitats	4
1.2.1. Importance of small molecular weight secondary metabolites	5
1.3. Pharmacological significance of antioxidant and anti-inflammatory properties	6
1.3.1. Free radicals and its relation to various life threatening disorders	6
1.3.2. The biological defense against free radicals	9
1.3.3. The importance of natural alternatives	11
1.4. Importance of mollusks and bivalves as potential resources of bioactive compounds	12
1.5. Bioactive potentials of bivalve mollusks and with reference to marine and estuarine clams	14
1.6. Objectives	16
1.7. Thesis outline	19
 CHAPTER 2: REVIEW OF LITERATURE	 20
2.1. Background	20
2.2. Oxidative stress and related health problems	21
2.3. Marine habitat as a productive resource of bioactive metabolites	25
2.4. Mollusks	28
2.5. Cephalopods	30
2.5.1. Nutritional importance of cephalopods	31
2.5.2. Bioactive potentials of cephalopods	32
2.5.3. Secondary metabolites from cephalopods	33

2.6.	Gastropods	34
2.6.1.	Nutritional importance of gastropods	35
2.6.2.	Bioactive potentials of gastropods	36
2.6.3.	Secondary metabolites from gastropods	37
2.7.	Bivalves	48
2.7.1.	Nutritional importance of bivalves	50
2.7.2.	Bioactive potentials of bivalves	51
2.7.3.	Secondary metabolites from bivalves	54
2.7.3.1.	Secondary metabolites from bivalve clams	54
2.7.3.2.	Secondary metabolites from bivalve mussels	57
2.7.3.3.	Secondary metabolites from bivalve oysters	61
2.7.3.4.	Secondary metabolites from bivalve scallops	63
2.8.	Conclusions	64

CHAPTER 3: NUTRITIONAL PROFILING OF *VILLORITA CYPRINOIDES* AND *PAPHIA MALABARICA*

		66
3.1.	Background	66
3.2.	Materials and methods	68
3.2.1.	Chemicals, reagents and instrumentations	68
3.2.2.	Study area and samples	69
3.2.3.	Determination of biometric parameters, condition indices and meat yield	71
3.2.4.	Proximate composition	71
3.2.5.	Estimation of protein and amino acid	71
3.2.5.1.	Estimation of protein	71
3.2.5.2.	Estimation of amino acid	72
3.2.6.	Estimation of lipid and fatty acid	74
3.2.6.1.	Estimation of lipid	74

3.2.6.2.	Estimation of fatty acid	74
3.2.7.	Estimation of minerals	75
3.2.8.	Estimation of cholesterol and vitamins	76
3.2.8.1.	Estimation of cholesterol	76
3.2.8.2.	Estimation of vitamins	77
3.2.9.	Statistical analyses	78
3.3.	Results and discussion	78
3.3.1.	Morphometric characteristics	78
3.3.2.	Proximate composition	79
3.3.3.	Lipid content and fatty acid composition	81
3.3.4.	Protein content and amino acid composition	85
3.3.5.	Mineral composition	88
3.3.6.	Cholesterol content and vitamin composition	90
3.3.7.	Principal component analyses	92
3.4.	Conclusions	94

CHAPTER 4: BIOACTIVE POTENTIALS OF *VILLORITA*

***CYPRINOIDES AND PAPHIA MALABARICA* 96**

4.1.	Background	96
4.2.	Materials and methods	97
4.2.1.	Chemicals, reagents and instrumentations	97
4.2.2.	Sample collection and pretreatment	99
4.2.3.	Preparation of the crude extracts of bivalve clams	99
4.2.4.	Determination of bioactive potentials of extracts of bivalve clams	100
4.2.4.1.	<i>In vitro</i> antioxidant assays	100
4.2.4.1.1.	Determination of total phenolic content	100
4.2.4.1.2.	Free radical scavenging assays	101
4.2.4.1.2.A.	1,1-Diphenyl-2-picryl-hydrazil (DPPH) radical scavenging assay	101
4.2.4.1.2.B.	2,2'-Azino-bis-3-ethylbenzothiozoline -6 sulfonic acid diammonium salt	

	(ABTS ⁺) radical scavenging assay	101
4.2.4.1.2.C.	Hydrogen peroxide (H ₂ O ₂) radical scavenging assay	102
4.2.4.1.2.D.	Ferrous ion (Fe ²⁺ ion) chelating assay	102
4.2.4.1.2.E.	Lipid peroxidation inhibitory assay	103
4.2.4.2.	<i>In vitro</i> anti-inflammatory assays	104
4.2.4.2.1.	Cyclooxygenases (COX) inhibition assay	104
4.2.4.2.2.	5-Lipoxygenase (5-LOX) inhibition assay	104
4.2.4.3.	<i>In vitro</i> anti-diabetic assays	105
4.2.4.3.1.	α -Amylase inhibition assay	105
4.2.4.3.2.	α -Glucosidase inhibition assay	105
4.2.4.3.3.	Dipeptidyl Peptidase-4 (DPP-4) inhibition assay	106
4.2.4.4.	<i>In vitro</i> anti-hypertensive assay	106
4.2.4.4.1.	Angiotensin converting enzyme-1 (ACE-1) inhibitory assay	106
4.2.5.	Spectroscopic analyses	107
4.2.5.1.	Fourier transform infrared (FTIR) spectroscopy	107
4.2.5.2.	Proton (¹ H) and carbon (¹³ C) nuclear magnetic resonance (NMR) spectroscopy	107
4.2.6.	Statistical analyses	108
4.3.	Results and discussion	108
4.3.1.	Yield of EtOAc:MeOH extracts of <i>V. cyprinoides</i> and <i>P. malabarica</i>	108
4.3.2.	Total phenolic content and antioxidant activities	108
4.3.3.	Anti-inflammatory activities	110
4.3.4.	Anti-diabetic and anti-hypertensive activities	112

4.3.5.	Spectroscopic labeling of the functional groups in the EtOAc:MeOH extracts of bivalve clams	113
4.3.5.1.	NMR based proton and carbon labeling	113
4.3.5.2.	FTIR analyses	117
4.3.6.	Correlation analyses	120
4.4.	Conclusions	122

CHAPTER 5: ISOLATION AND CHARACTERIZATION OF SECONDARY METABOLITES FROM *VILLORITA CYPRINOIDES*

5.1.	Background	123
5.2.	Materials and methods	125
5.2.1.	Chemicals, reagents and instrumentations	125
5.2.2.	Chromatographic analyses	126
5.2.2.A.	Column chromatography (CC)	126
5.2.2.B.	Flash chromatography (FC)	127
5.2.2.C.	Thin layer chromatography (TLC)	127
5.2.2.D.	High pressure liquid chromatography (HPLC)	127
5.2.3.	Spectrophotometric analyses	128
5.2.4.	Spectroscopic analyses	128
5.2.4.A.	Fourier transform infrared (FTIR) spectroscopy	128
5.2.4.B.	Mass spectrometry	129
5.2.4.C.	Nuclear magnetic resonance (NMR) spectroscopy	129
5.2.5.	Animal material and extraction	130
5.2.6.	Chromatographic purification of pure compounds from <i>V. cyprinoides</i>	132
5.2.7.	Physicochemical data of bioactive secondary metabolites from EtOAc:MeOH extract of <i>V. cyprinoides</i>	135
5.2.7.1.	Physicochemical data of compound 1	

	(VC ₃₋₆₋₁₋₁)	135
5.2.7.2.	Physicochemical data of compound 2	
	(VC ₃₋₆₋₂₋₁)	136
5.2.7.3.	Physicochemical data of compound 3	
	(VC ₂₋₆₋₂₋₁₋₂)	136
5.2.7.4.	Physicochemical data of compound 4	
	(VC ₂₋₆₋₄₋₁)	137
5.2.7.5.	Physicochemical data of compound 5	
	(VC ₂₋₆₋₆₋₂₋₂)	137
5.2.7.6.	Physicochemical data of compound 6	
	(VC ₃₋₄₋₃₋₁)	138
5.2.7.7.	Physicochemical data of compound 7	
	(VC ₃₋₄₋₃₋₂)	138
5.2.7.8.	Physicochemical data of compound 8	
	(VC ₂₋₆₋₅₋₂)	139
5.2.7.9.	Physicochemical data of compound 9	
	(VC ₂₋₅₋₁)	139
5.2.7.10.	Physicochemical data of compound 10	
	(VC ₂₋₄₋₁)	140
5.2.8.	Determination of bioactive potentials	140
5.2.8.1.	<i>In vitro</i> antioxidant assays	140
5.2.8.1.A.	1,1-diphenyl-2-picryl-hydrazil (DPPH) radical scavenging assay	140
5.2.8.1.B.	2,2'-Azino-bis-3-ethylbenzothiozoline -6-sulfonic acid diammonium salt (ABTS ⁺) radical scavenging assay	140
5.2.8.2.	<i>In vitro</i> anti-inflammatory assays	141
5.2.8.2.A.	Cyclooxygenases (COX) inhibition assay	141
5.2.8.2.B.	5-Lipoxygenase (5-LOX) inhibition assay	141
5.2.9.	The structure-activity relationship analyses of	

secondary metabolites isolated from EtOAc:MeOH extract of <i>V. cyprinoides</i>	141
5.2.10. <i>In silico</i> molecular modeling	141
5.2.10.1. Molecular structures of protein and energy minimization	142
5.2.10.2. Preparation of ligands	142
5.2.10.3. Molecular docking	142
5.2.11. Statistical analyses	143
5.3. Results and discussion	143
5.3.1. Chromatographic fractionation, bioactive potentials and spectroscopic analyses of intermediate fractions from EtOAc:MeOH extract of <i>V. cyprinoides</i>	143
5.3.1.1. Chromatographic fractionation and bioactive potentials of intermediate fractions from EtOAc:MeOH extract of <i>V. cyprinoides</i>	143
5.3.1.2. Spectroscopic analyses of intermediate fractions from EtOAc:MeOH extract of <i>V. cyprinoides</i>	144
5.3.1.3. Isolation of bioactive secondary metabolites from EtOAc:MeOH extract of <i>V. cyprinoides</i>	147
5.3.2. Spectroscopic analyses of bioactive secondary metabolites isolated from EtOAc:MeOH extract of <i>V. cyprinoides</i>	155
5.3.2.1. Structural characterization of spirocyclic ether derivatives (1-2)	155
5.3.2.1.A. Structural characterization of compound 1 (VC ₃₋₆₋₁₋₁)	156
5.3.2.1.B. Structural characterization of compound 2 (VC ₃₋₆₋₂₋₁)	166
5.3.2.2. Structural characterization of irregular	

	meroterpenoid derivatives (3-5)	176
5.3.2.2.A.	Structural characterization of compound 3 (VC ₂₋₆₋₂₋₁₋₂)	177
5.3.2.2.B.	Structural characterization of compound 4 (VC ₂₋₆₋₄₋₁)	186
5.3.2.2.C.	Structural characterization of compound 5 (VC ₂₋₆₋₆₋₂₋₂)	195
5.3.2.3.	Structural characterization of hexahydro isochromenyl meroterpenoid derivatives (6-7)	205
5.3.2.3.A.	Structural characterization of compound 6 (VC ₃₋₄₋₃₋₁)	205
5.3.2.3.B.	Structural characterization of compound 7 (VC ₃₋₄₋₃₋₂)	214
5.3.2.4.	Structural characterization of cholestenol derivatives (8-10)	223
5.3.2.4.A.	Structural characterization of compound 8 (VC ₂₋₆₋₅₋₂)	224
5.3.2.4.B.	Structural characterization of compound 9 (VC ₂₋₅₋₁)	234
5.3.2.4.C.	Structural characterization of compound 10 (VC ₂₋₄₋₁)	243
5.3.3.	Bioactive (antioxidant and anti-inflammatory) potentials of secondary metabolites isolated from EtOAc:MeOH extract of <i>V. cyprinoides</i>	254
5.3.3.1.	Antioxidative potentials of secondary metabolites isolated from EtOAc:MeOH extract of <i>V. cyprinoides</i>	254
5.3.3.2.	Anti-inflammatory potentials of secondary metabolites isolated from EtOAc:MeOH extract of <i>V. cyprinoides</i>	256

5.3.4.	Structure-activity relationship analyses of secondary metabolites isolated from EtOAc:MeOH extract of <i>V. cyprinoides</i>	259
5.3.4.1.	Structure-activity relationship analyses of secondary metabolites from EtOAc:MeOH extract of <i>V. cyprinoides</i> using various molecular parameters	259
5.3.4.2.	Suggested antioxidative mechanism of secondary metabolites isolated from EtOAc:MeOH extract of <i>V. cyprinoides</i> in the DPPH radical model system	264
5.3.5.	<i>In silico</i> molecular docking studies of selected compounds (1-5) from <i>V. cyprinoides</i>	268
5.4.	Conclusions	274

CHAPTER 6: ISOLATION AND CHARACTERIZATION OF SECONDARY METABOLITES FROM <i>PAPHIA MALABARICA</i>	276
6.1. Background	276
6.2. Materials and methods	277
6.2.1. Chemicals, reagents and instrumentations	277
6.2.2. Chromatographic analyses	277
6.2.2.A. Column chromatography (CC)	277
6.2.2.B. Flash chromatography (FC)	277
6.2.2.C. Thin layer chromatography (TLC)	277
6.2.2.D. High pressure liquid chromatography (HPLC)	277
6.2.3. Spectrophotometric analyses	277
6.2.4. Spectroscopic analyses	278
6.2.4.A. Fourier transform infrared (FTIR) spectroscopy	278
6.2.4.B. Mass spectrometry	278
6.2.4.C. Nuclear magnetic resonance (NMR)	

	spectroscopy	278
6.2.5.	Animal material and extraction	278
6.2.6.	Chromatographic purification of pure compounds from <i>P. malabarica</i>	280
6.2.7.	Physicochemical data of bioactive secondary metabolites from EtOAc:MeOH extract of <i>P. malabarica</i>	284
6.2.7.1.	Physicochemical data of compound 1 (PM ₄₋₅₋₃₋₁)	284
6.2.7.2.	Physicochemical data of compound 2 (PM ₆₋₃₋₁₋₁)	285
6.2.7.3.	Physicochemical data of compound 3 (PM ₃₋₁₋₁₋₁)	285
6.2.7.4.	Physicochemical data of compound 4 (PM ₄₋₂₋₁)	286
6.2.7.5.	Physicochemical data of compound 5 (PM ₃₋₁₋₂₋₂)	286
6.2.7.6.	Physicochemical data of compound 6 (PM ₄₋₄₋₁)	287
6.2.7.7.	Physicochemical data of compound 7 (PM ₄₋₃₋₁)	287
6.2.7.8.	Physicochemical data of compound 8 (PM ₄₋₁₋₁)	288
6.2.7.9.	Physicochemical data of compound 9 (PM ₃₋₃₋₂₋₁)	288
6.2.7.10.	Physicochemical data of compound 10 (PM ₃₋₃₋₁₋₁)	289
6.2.8.	Determination of bioactive potentials	289
6.2.8.1.	<i>In vitro</i> antioxidant assays	289
6.2.8.1.A.	1,1-diphenyl-2-picryl-hydrazil (DPPH) radical scavenging assay	289
6.2.8.1.B.	2,2'-Azino-bis-3-ethylbenzothiozoline-6-	

	sulfonic acid diammonium salt (ABTS ⁺)	
	radical scavenging assay	290
6.2.8.2.	<i>In vitro</i> anti-inflammatory assays	290
6.2.8.2.A.	Cyclooxygenases (COX) inhibition assay	290
6.2.8.2.B.	5-Lipoxygenase (5-LOX) inhibition assay	290
6.2.9.	The structure-activity relationship analyses of secondary Metabolites isolated from EtOAc:MeOH extract of <i>P. malabarica</i>	290
6.2.10.	<i>In silico</i> molecular modeling	290
6.2.11.	Statistical analyses	290
6.3.	Results and discussion	291
6.3.1.	Chromatographic fractionation, bioactive potentials and spectroscopic analyses of intermediate fractions from EtOAc:MeOH extract of <i>P. malabarica</i>	291
6.3.1.1.	Chromatographic fractionation and bioactive potentials of intermediate fractions from EtOAc:MeOH extract of <i>P. malabarica</i>	291
6.3.1.2.	Spectroscopic analyses of intermediate fractions from EtOAc:MeOH extract of <i>P. malabarica</i>	292
6.3.1.3.	Isolation of bioactive secondary metabolites from EtOAc:MeOH extract of <i>P. malabarica</i>	294
6.3.2.	Spectroscopic analyses of bioactive secondary metabolites isolated from EtOAc:MeOH extract of <i>P. malabarica</i>	302
6.3.2.1.	Structural characterization of aryl polyketide derivatives (1-3)	302
6.3.2.1.A.	Structural characterization of compound 1 (PM ₄₋₅₋₃₋₁)	304
6.3.2.1.1.	Biogenic origin of the polyketide	

	synthase (PKS) catalyzed aryl polyketide derivative (1)	314
6.3.2.1.B.	Structural characterization of compound 2 (PM ₆₋₃₋₁₋₁)	314
6.3.2.1.2.	Biogenic origin of the polyketide synthase (PKS) catalyzed aryl polyketide derivative (2)	324
6.3.2.1.C.	Structural characterization of compound 3 (PM ₃₋₁₋₁₋₁)	325
6.3.2.1.3.	Biogenic origin of the polyketide synthase (PKS) catalyzed aryl polyketide derivative (3)	335
6.3.2.2.	Structural characterization of tetrahydro chromenyl derivatives (4-5)	337
6.3.2.2.A.	Structural characterization of compound 4 (PM ₄₋₂₋₁)	338
6.3.2.2.B.	Structural characterization of compound 5 (PM ₃₋₁₋₂₋₂)	349
6.3.2.3.	Structural characterization of isopimarane norditerpenoid derivative (6)	360
6.3.2.3.A.	Structural characterization of compound 6 (PM ₄₋₄₋₁)	360
6.3.2.4.	Structural characterization of meroterpeno pyranoids (7-8)	371
6.3.2.4.A.	Structural characterization of compound 7 (PM ₄₋₃₋₁)	371
6.3.2.4.B.	Structural characterization of compound 8 (PM ₄₋₁₋₁)	381
6.3.2.5.	Structural characterization of cholestenol derivatives (9-10)	392
6.3.2.5.A.	Structural characterization of compound 9 (PM ₃₋₃₋₂₋₁)	392

6.3.2.5.B.	Structural characterization of compound 10 (PM ₃₋₃₋₁₋₁)	403
6.3.3.	Bioactive (antioxidant and anti-inflammatory) potentials of secondary metabolites isolated from EtOAc:MeOH extract of <i>P. malabarica</i>	414
6.3.3.1.	Antioxidative potentials of secondary metabolites isolated from EtOAc:MeOH extract of <i>P. malabarica</i>	414
6.3.3.2.	Anti-inflammatory potentials of secondary metabolites isolated from EtOAc:MeOH extract of <i>P. malabarica</i>	416
6.3.4.	Structure-activity relationship analyses of secondary metabolites isolated from EtOAc:MeOH extract of <i>P. malabarica</i>	420
6.3.4.1.	Structure-activity relationship analyses of secondary metabolites from EtOAc:MeOH extract of <i>P. malabarica</i> using various molecular parameters	420
6.3.4.2.	Suggested antioxidative mechanism of secondary metabolites isolated from EtOAc:MeOH extract of <i>P. malabarica</i> in the DPPH radical model system	424
6.3.5.	<i>In silico</i> molecular docking studies of selected compounds (1-4, 6) from <i>P. malabarica</i>	429
6.4.	Conclusions	435
CHAPTER 7: SUMMARY		438
REFERENCES		451
PUBLICATIONS		488

LIST OF TABLES

<i>Table No.</i>	<i>Title</i>	<i>Page No.</i>
Table 3.1.:	Meat yield (%) and biometric measurement (length, width, thickness) of <i>P. malabarica</i> and <i>V. cyprinoides</i>	78
Table 3.2.:	Condition indices of <i>P. malabarica</i> and <i>V. cyprinoides</i> ...	79
Table 3.3.:	Proximate compositions (g/100 g wet weight) of <i>P. malabarica</i> and <i>V. cyprinoides</i>	80
Table 3.4.:	Lipid content (g/100 g wet weight) and fatty acid composition (% total fatty acids wet weight) in <i>P. malabarica</i> and <i>V. cyprinoides</i>	81
Table 3.5.:	Protein and amino acid composition (mg/100 g wet weight) in <i>P. malabarica</i> and <i>V. cyprinoides</i>	86
Table 3.6.:	Mineral composition (mg/100 g wet weight) in <i>P. malabarica</i> and <i>V. cyprinoides</i>	89
Table 3.7.:	Cholesterol and vitamin composition in <i>P. malabarica</i> and <i>V. cyprinoides</i>	91
Table 4.1.:	Phenolic content and antioxidant activities (IC ₅₀) of EtOAc:MeOH extracts of <i>P. malabarica</i> and <i>V. cyprinoides</i>	109
Table 4.2.:	Anti-inflammatory activities (IC ₅₀) of EtOAc:MeOH extracts of <i>P. malabarica</i> and <i>V. cyprinoides</i>	111
Table 4.3.:	Anti-diabetic and anti-hypertensive activities (IC ₅₀) of EtOAc:MeOH extracts of <i>P. malabarica</i> and <i>V. cyprinoides</i>	112
Table 5.1.:	Yield and bioactive (antioxidant and anti-inflammatory) potentials of sub-fractions from EtOAc:MeOH extract of <i>V. cyprinoides</i>	144
Table 5. 2.:	Type and integral values of protons obtained from the ¹ H NMR spectra of sub-fractions from EtOAc:MeOH extract of <i>V. cyprinoides</i>	145
Table 5.3.:	The yield (in mg and in %), retention factor (R _f), bioactivities (antioxidant/anti-inflammatory) of column/flash/PTLC/PHPLC fractions obtained from the sub-fraction, VC ₂ of EtOAc:MeOH extract of <i>V. cyprinoides</i>	149
Table 5.4.:	The yield (in mg and in %), retention factor (R _f), bioactivities (antioxidant/anti-inflammatory) of column/flash/PTLC/PHPLC fractions obtained from the sub-fraction, VC ₃ of EtOAc:MeOH extract of <i>V.</i>	

	<i>cyprinoides</i>	153
Table 5.5.:	NMR spectroscopic data of 16-hydroxyhexyl-(2-ethyl-2,6-dimethyl-1-oxaspiro[4.5]dec-3,8-dien)-10-propanoate (1) in CDCl ₃	159
Table 5.6.:	NMR spectroscopic data of (<i>E</i>)-18-ethyl-17,19-dihydroxyhept-14-enyl-(2-ethyl-2,6-dimethyl-1-oxaspiro[4.5]dec-3,8-dien)-10-acetate (2) in CDCl ₃	169
Table 5.7.:	NMR spectroscopic data of 8-(1,3,3a,4,5,7a-hexahydro-1-(hydroxymethyl)-3-oxoisobenzofuran-4-yl)-ethyl pentanoate (3) in CDCl ₃	179
Table 5.8.:	NMR spectroscopic data of tetrahydro-3-methoxy-5-((<i>E</i>)-8,12-dimethyloct-8-enyl)-pyran-2-one (4) in CDCl ₃ ^a	189
Table 5.9.:	NMR spectroscopic data of dihydro-5-(8-(9,12-dihydro-8-methyl-11-propyl-2 <i>H</i> -pyran-8-yl)-ethyl)-furan-2-(3 <i>H</i>)-one (5) in CDCl ₃ ^a	198
Table 5.10.:	NMR spectroscopic data of (10 <i>E</i>)-butyl-9-(6-ethyl-3,4,6,7,8,8a-hexahydro-1 <i>H</i> -isochromen-3-yl)-pent-10-enoate (6) in CDCl ₃	208
Table 5.11.:	NMR spectroscopic data of (12 <i>E</i>)-(3,4,6,7,8,8a-hexahydro-1 <i>H</i> -isochromen-3-yl)-methylhept-12-enoate (7) in CDCl ₃	217
Table 5.12.:	NMR spectroscopic data of 19 (10→5) abeo-20-methylpregn-1-en-3-yl-3β-methoxy-hex-25-enoate (8) in CDCl ₃ .	227
Table 5.13.:	NMR spectroscopic data of (22 <i>E</i>)-24 ¹ -homocholesta-5,22-dien-(3β,24 ¹ β)-diol (9) in CDCl ₃	236
Table 5.14.:	NMR spectroscopic data of (22 <i>E</i>),(24 ¹ <i>E</i>)-24 ¹ ,24 ² -dihomocholesta-5,22,24 ¹ -trien-3β-ol (10) in CDCl ₃	247
Table 5.15.:	<i>In vitro</i> antioxidant {2,2-diphenyl-1-picrylhydrazyl (DPPH) and 2,2'-azino-bis(3-ethylbenzothiazoline-6-sulphonic acid) (ABTS ⁺) radical scavenging assays} activities of secondary metabolites (1-10) isolated from EtOAc:MeOH extract of <i>V. cyprinoides</i> against commercially available standard, α-tocopherol	255
Table 5.16.:	<i>In vitro</i> anti-inflammatory {cyclooxygenase-1/2 (COX-1/2) and 5-lipoxygenase (5-LOX)} radical scavenging assays) activities of secondary metabolites (1-10) isolated from EtOAc:MeOH extract of <i>V. cyprinoides</i> against commercially available standard, ibuprofen	257
Table 5.17.:	The molecular descriptors of secondary metabolites from EtOAc:MeOH extract of <i>V. cyprinoides</i> (1-10) and commercially available products	261
Table 5.18.:	Number of hydrogen bonds, hydrogen bonded (H-	

	bonded) amino acid residue, binding energy, docking score, inhibition constant, intermolecular energy and torsional free energy between the ligands (compounds 1-5) and the active sites of COX-2	272
Table 5.19.:	Number of hydrogen bonds, hydrogen bonded (H-bonded) amino acid residue, binding energy, docking score, inhibition constant, intermolecular energy and torsional free energy between the ligands (compounds 1-5) and the active sites of 5-LOX	273
Table 6.1.:	Yield and bioactive (antioxidant and anti-inflammatory) potentials of sub-fractions from EtOAc:MeOH extract of <i>P. malabarica</i>	292
Table 6. 2.:	Type and integral values of protons obtained from the ¹ H NMR spectra of sub-fractions from EtOAc:MeOH extract of <i>P. malabarica</i>	294
Table 6.3.:	The yield (in mg and in %), retention factor (R _f), bioactivities (antioxidant/anti-inflammatory) of column/flash/PTLC fractions obtained from the sub-fraction, PM ₃ of EtOAc:MeOH extract of <i>P. malabarica</i> .	296
Table 6.4.:	The yield (in mg and in %), retention factor (R _f), bioactivities (antioxidant/anti-inflammatory) of column/flash/PTLC fractions obtained from the sub-fraction, PM ₄ of EtOAc:MeOH extract of <i>P. malabarica</i> .	299
Table 6.5.:	The yield (in mg and in %), retention factor (R _f), bioactivities (antioxidant/anti-inflammatory) of column/flash/PTLC fractions obtained from the sub-fraction, PM ₆ of EtOAc:MeOH extract of <i>P. malabarica</i> .	301
Table 6.6.:	NMR spectroscopic data of 13-(methoxycarbonyl)-11-((<i>E</i>)-18-ethylhexa-16,19-dienyl)-12-propylcyclohex-10-enyl)-methyl-4-hydroxy benzoate (1) in CDCl ₃	306
Table 6.7.:	NMR spectroscopic data of isobutyl-13-(6-(benzoyloxy)-10-methylpentyl)-tetrahydro-13-methyl-2 <i>H</i> -pyran-17-carboxylate (2) in CDCl ₃	317
Table 6.8.:	NMR spectroscopic data of (<i>E</i>)-12-(17-ethyl-tetrahydro-16-hydroxy-15-(methylpentanoate)-14-oxo-2 <i>H</i> -pyran-13-yl)-9-methylbut-11-enyl benzoate (3) in CDCl ₃	328
Table 6.9:	NMR spectroscopic data of 6 ¹ -(3-((<i>E</i>)-3 ^{1b} -(furan-2'-yl)-prop-3 ^{1b} -en-3 ¹ -yl)-4a,5,6,8a-tetrahydro-8-methyl-2 <i>H</i> -chromen-6-yl)-ethyl-5''-methyl-hexanoate (4) in CDCl ₃ ..	342
Table 6.10.:	NMR spectroscopic data of 7-(2'-ethyl-1'-hydroxynonan-2'-yl)-6,7,8,8a-tetrahydro-3 <i>H</i> -isochromen-1-(5 <i>H</i>)-one (5) in CDCl ₃	353

Table 6.11.:	NMR spectroscopic data of 18 (4→14),19 (4→8) bis-abeo-nor-isopimarane-1,5-diene-3-yl-3 β -methoxy-propyl pentanoate (6) in CDCl ₃	363
Table 6.12.:	NMR spectroscopic data of 1'-((10 <i>E</i>)-10-(10-(pentan-4-yl)-cyclohex-4-enyl)-allyloxy)-tetrahydro-2',2'-dimethyl-2 <i>H</i> -pyran (7) in CDCl ₃	374
Table 6.13.:	NMR spectroscopic data of 2-((<i>E</i>)-deca-1,8-dien-10-yl)-11,12-dihydro-13-propyl-2 <i>H</i> -pyran (8) in CDCl ₃	385
Table 6.14.:	NMR spectroscopic data of (22 <i>E</i>)-24 ¹ ,24 ² -methylidihomocholesta-5,22-dien-3 β -ol (9) in CDCl ₃	395
Table 6.15.:	NMR spectroscopic data of 23- <i>gem</i> -dimethylcholesta-5-en-3 β -ol (10) in CDCl ₃	407
Table 6.16.:	<i>In vitro</i> antioxidant {2,2-diphenyl-1-picrylhydrazyl (DPPH) and 2,2'-azino-bis(3-ethylbenzothiazoline-6-sulphonic acid) (ABTS ⁺) radical scavenging assays} activities of secondary metabolites (1-10) isolated from EtOAc:MeOH extract of <i>P. malabarica</i> against commercially available standard, α -tocopherol	415
Table 6.17.:	<i>In vitro</i> anti-inflammatory {cyclooxygenase-1/2 (COX-1/2) and 5-lipoxygenase (5-LOX)) radical scavenging assays} activities of secondary metabolites (1-10) isolated from EtOAc:MeOH extract of <i>P. malabarica</i> against commercially available standard, ibuprofen	418
Table 6.18.:	The molecular descriptors of secondary metabolites from EtOAc:MeOH extract of <i>P. malabarica</i> (1-10) and commercially available products	422
Table 6.19.:	Number of hydrogen bonds, hydrogen bonded (H-bonded) amino acid residue, binding energy, docking score, inhibition constant, intermolecular energy and torsional free energy between the ligands (compounds 1-4, 6) and the active sites of COX-2	433
Table 6.20.:	Number of hydrogen bonds, hydrogen bonded (H-bonded) amino acid residue, binding energy, docking score, inhibition constant, intermolecular energy and torsional free energy between the ligands (compounds 1-4, 6) and the active sites of 5-LOX	434

LIST OF FIGURES

<i>Figure No.</i>	<i>Title</i>	<i>Page No.</i>
Figure 1.1.:	The coastal and estuarine waters of India gifted with bivalve mollusks	3
Figure 1.2.:	The percentage share of marine and coastal mollusks among various classes of marine organisms	4
Figure 1.3.:	Formation of reactive oxygen species and their reaction mechanisms. O ₂ -molecular oxygen, H ₂ O ₂ -hydrogen peroxide, NO-nitric oxide, H ₂ O-water, .NO ₂ -nitrogen dioxide, ONOO ⁻ -peroxynitrite, .O ₂ ⁻ -superoxide anion, HOCl-hypochlorous acid, ONOOH-peroxynitrous acid, .OH-hydroxyl radical, SCN ⁻ -thiocyanate, HOSCN-hypothiocyanous acid, NOX- NADPH oxidase, SOD-superoxide dismutase	7
Figure 1.4.:	The mechanisms of oxidative cellular damage. The formation of hydroxy free radicals from hydroperoxide induces oxidative cellular damage, impairment of DNA, protein carboxylation, peroxidation of lipids and damages in mitochondria. These mechanisms lead to oxidative injury and finally to cell death	8
Figure 1.5.:	The free radical associated diseases in human	8
Figure 1.6.:	Mechanism of neutralization of free radicals by antioxidant agents	10
Figure 1.7.:	Antioxidant mechanisms against free radical induced damages. The antioxidants inhibit the oxidative stress and constrain the nuclear factor kappa-enhancer of activated B cell (NF-kB), redox reactions, inflammations and interferes metal chelation. The antioxidants activate superoxide dismutase (SOD), thioredoxin reductase (TR) and catalase (CAT). ROS-reactive oxygen species, H ₂ O ₂ -hydrogen peroxide, O ₂ ⁻ -superoxide anion, .HO-hydroxyl radical	10
Figure 1.8.:	The coastline of Kerala is bestowed with large assemblage of bivalve mollusks	15
Figure 1.9.:	A collection site of bivalve mollusk, <i>V. cyprinoides</i>	16
Figure 1.10.:	A collection site of bivalve mollusk, <i>P. malabarica</i>	16
Figure 1.11.:	Sample collection sites of the bivalve clams from the southwest coast of India bordering the Arabian Sea in Kerala State (A); <i>P. malabarica</i> from Ashtamudi Lake at 8°59' N and 76°36' E (B) and <i>V. cyprinoides</i> from Vembanad Lake (9°35' N and 76°25' E) (C) along with	

	shell-on samples of <i>V. cyprinoides</i> and <i>P. malabarica</i> ...	17
Figure 2.1.:	A schematic representation of mitochondrial ROS production. The ROS produced by mitochondria can leads to oxidative damages in the protein, lipid and DNA. The damaged mitochondrial cells increase the release of inter-membrane proteins like cytochrome c (cyt c) by mitochondrial outer membrane permeabilization and likewise, the cell death. Also, the mitochondrial ROS leads to initiation of mitochondrial permeability transition pore (PTP), which results in the tissue injury (Murphy 2009)	22
Figure 2.2.:	Inflammatory mediators and mechanism of ROS mediated inflammatory responses. COX-cyclooxygenase, LOX-lipoxygenase, H ₂ O ₂ -hydrogen peroxide, HO.-hydroxyl radical	23
Figure 2.3.:	Relationship among reactive oxygen species induced inflammatory responses and the role of antioxidants to inhibit the production of inflammatory enzymes. ROS-reactive oxygen species, NOX-NADPH oxidase, TNF- α -tumour necrosis factor alpha, NF- κ B-nuclear factor kappa B	24
Figure 2.4.:	Number of marine natural products over the period 1965 to 2005 (Blunt <i>et al.</i> , 2006)	26
Figure 2.5.:	Distribution of marine natural products by phylum (Blunt <i>et al.</i> , 2003)	27
Figure 2.6.:	Distribution of marine organisms among phylum collected for natural product isolations over the period from 1971 to 2015 (Blunt <i>et al.</i> , 2016)	27
Figure 2.7.:	Schematic representation of the distribution of molluskan phylum	29
Figure 2.8.:	Photographic description of cephalopods	31
Figure 2.9.:	Photographic description of gastropods	35
Figure 2.10.:	The percentage share of bivalves, particularly clams among bivalve mollusks (FAO 2014)	49
Figure 2.11.:	Photographic illustration of bivalves	49
Figure 3.1.:	Sample collection site of edible clam, <i>V. cyprinoides</i> along the southwest coast of India bordering the Arabian Sea. (A) Vembanad Lake at 9°35' N and 76°25' E; (B) the shell on <i>V. cyprinoides</i> ; (C) the inside view of <i>V. cyprinoides</i> with edible part	70
Figure 3.2.:	Sample collection sites of edible clam, <i>P. malabarica</i> from the southwest coast of India bordering the Arabian	

	Sea. (A) Ashtamudi Lake at 8°59' N and 76°36' E; (B) the shell on <i>P. malabarica</i> ; (C) the inside view of <i>P. malabarica</i> with edible part	70
Figure 3.3.:	Comparison of <i>n</i> -3/ <i>n</i> -6, <i>n</i> -6/ <i>n</i> -3, DHA/EPA and Σ PUFA/ Σ SFA between <i>P. malabarica</i> and <i>V. cyprinoides</i>	84
Figure 3.4.:	Comparison of essential amino acid scores between <i>P. malabarica</i> and <i>V. cyprinoides</i>	88
Figure 3.5.:	Loading plot diagrams (PCA) showing the correlation of vitamins, lipid, cholesterol, SFA, MUFA, PUFA, DHA, EPA, <i>n</i> -3 and <i>n</i> -6 of <i>V. cyprinoides</i> (VC) and <i>P. malabarica</i> (PM)	93
Figure 3.6.:	Loading plot diagrams showing the correlation of protein content, AA, EA, NEAA, ArAA, SA of <i>V. cyprinoides</i> (VC) and <i>P. malabarica</i> (PM)	93
Figure 4.1.:	The stacked plot representing the ¹ H NMR spectra of EtOAc:MeOH extracts of <i>P. malabarica</i> and <i>V. cyprinoides</i> . (A) deconvoluted ¹ H NMR and (B) acquired ¹ H NMR spectra of EtOAc:MeOH extract of <i>P. malabarica</i> . (C) Deconvoluted ¹ H NMR and (D) acquired ¹ H NMR spectra of EtOAc:MeOH extract of <i>V. cyprinoides</i> . The protons at the defined regions of the ¹ H NMR spectra were integrated to get the number of protons in specific regions. The functional groups representing the distinct regions of the ¹ H NMR spectra were illustrated as insets	114
Figure 4.2.:	The stacked plot representing the (A) deconvoluted and (B) acquired ¹³ C NMR spectra of EtOAc:MeOH extract of <i>P. malabarica</i> . (C) deconvoluted and (D) acquired ¹³ C NMR spectra of EtOAc:MeOH extract of <i>V. cyprinoids</i> . Chemical shift (δ) values are expressed in parts per million (ppm) and were referenced to the residual solvent signals of CDCl ₃	115
Figure 4.3.:	Type and integral values of protons obtained from the ¹ H NMR spectra of EtOAc:MeOH extracts of <i>P. malabarica</i> and <i>V. cyprinoides</i>	116
Figure 4.4.:	FTIR spectra of EtOAc:MeOH extracts of (A) <i>P. malabarica</i> and (B) <i>V. cyprinoides</i> . The functional groups representing the distinct regions of the IR spectra were illustrated	118
Figure 4.5.:	Loading plot diagram (PC-1 and PC-2 in rotated space) of antioxidant potentials compared with anti-	

	inflammatory, anti-diabetic and anti-hypertensive potentials of solvent extracts from <i>P. malabarica</i> (PM) and <i>V. cyprinoides</i> (VC)	121
Figure 5.1.:	The fresh shelled <i>V. cyprinoides</i> samples collected from the southwestern coast of the Indian Penninsula (9°35' N and 76°25' E), bordering the Arabian Sea	131
Figure 5.2.:	Schematic diagram of purification of EtOAc:MeOH extract of <i>V. cyprinoides</i> . CC-column chromatography; FC-flash chromatography; PTLC-preparative thin layer chromatography; TLC-thin layer chromatography; RP C18 PHPLC-reverse phase C18 preparatory high pressure liquid chromatography; E-ethyl acetate; H- <i>n</i> -hexane; M-methanol. The coloured boxes represented the pure compounds and were characterized by detailed spectroscopic experiments	134
Figure 5.3.:	¹ H NMR spectra of intermediate sub-fractions, (A) VC ₁ , (B) VC ₂ , (C) VC ₃ and (D) VC ₄ from the EtOAc:MeOH extract of <i>V. cyprinoides</i> with integration values	146
Figure 5.4.:	UV spectrum of 16-hydroxyhexyl-(2-ethyl-2,6-dimethyl-1-oxaspiro[4.5]dec-3,8-dien)-10-propanoate (1)	156
Figure 5.5.:	HPLC chromatogram of 16-hydroxyhexyl-(2-ethyl-2,6-dimethyl-1-oxaspiro[4.5]dec-3,8-dien)-10-propanoate (1)	157
Figure 5.6.:	¹ H- ¹ H COSY (A) and HMBC (B) correlations of 16-hydroxyhexyl-(2-ethyl-2,6-dimethyl-1-oxaspiro[4.5]dec-3,8-dien)-10-propanoate (1). The key ¹ H- ¹ H COSY couplings have been represented by bold face bonds. The HMBC couplings were indicated by double barbed arrow	160
Figure 5.7.:	NOESY correlations of 16-hydroxyhexyl-(2-ethyl-2,6-dimethyl-1-oxaspiro[4.5]dec-3,8-dien)-10-propanoate (1). The NOESY relations were represented by double barbed arrow	160
Figure 5.8.:	¹ H NMR spectrum of 16-hydroxyhexyl-(2-ethyl-2,6-dimethyl-1-oxaspiro[4.5]dec-3,8-dien)-10-propanoate (1)	161
Figure 5.9.:	¹³ C NMR spectrum of 16-hydroxyhexyl-(2-ethyl-2,6-dimethyl-1-oxaspiro[4.5]dec-3,8-dien)-10-propanoate (1)	161

Figure 5.10.:	$^{135}\text{DEPT}$ NMR spectrum of 16-hydroxyhexyl-(2-ethyl-2,6-dimethyl-1-oxaspiro[4.5]dec-3,8-dien)-10-propanoate (1)	162
Figure 5.11.:	^1H - ^1H COSY NMR spectrum of 16-hydroxyhexyl-(2-ethyl-2,6-dimethyl-1-oxaspiro[4.5]dec-3,8-dien)-10-propanoate (1)	162
Figure 5.12.:	HSQC NMR spectrum of 16-hydroxyhexyl-(2-ethyl-2,6-dimethyl-1-oxaspiro[4.5]dec-3,8-dien)-10-propanoate (1)	163
Figure 5.13.:	HMBC NMR spectrum of 16-hydroxyhexyl-(2-ethyl-2,6-dimethyl-1-oxaspiro[4.5]dec-3,8-dien)-10-propanoate (1)	163
Figure 5.14.:	NOESY NMR spectrum of 16-hydroxyhexyl-(2-ethyl-2,6-dimethyl-1-oxaspiro[4.5]dec-3,8-dien)-10-propanoate (1)	164
Figure 5.15.:	FTIR spectrum of 16-hydroxyhexyl-(2-ethyl-2,6-dimethyl-1-oxaspiro[4.5]dec-3,8-dien)-10-propanoate (1) .	164
Figure 5.16.:	EIMS spectrum of 16-hydroxyhexyl-(2-ethyl-2,6-dimethyl-1-oxaspiro[4.5]dec-3,8-dien)-10-propanoate (1) .	165
Figure 5.17.:	Mass fragmentation pattern of 16-hydroxyhexyl-(2-ethyl-2,6-dimethyl-1-oxaspiro[4.5]dec-3,8-dien)-10-propanoate (1)	166
Figure 5.18.:	UV spectrum of (<i>E</i>)-18-ethyl-17,19-dihydroxyhept-14-enyl-(2-ethyl-2,6-dimethyl-1-oxaspiro[4.5]dec-3,8-dien)-10-acetate (2)	167
Figure 5.19.:	HPLC chromatogram of (<i>E</i>)-18-ethyl-17,19-dihydroxyhept-14-enyl-(2-ethyl-2,6-dimethyl-1-oxaspiro[4.5]dec-3,8-dien)-10-acetate (2)	167
Figure 5.20.:	^1H - ^1H COSY (A) and HMBC (B) correlations of (<i>E</i>)-18-ethyl-17,19-dihydroxyhept-14-enyl-(2-ethyl-2,6-dimethyl-1-oxaspiro[4.5]dec-3,8-dien)-10-acetate (2). The key ^1H - ^1H COSY couplings have been represented by the bold face bonds. The HMBC couplings were indicated by double barbed arrow	170
Figure 5.21.:	NOESY correlations of (<i>E</i>)-18-ethyl-17,19-dihydroxyhept-14-enyl-(2-ethyl-2,6-dimethyl-1-oxaspiro [4.5]dec-3,8-dien)-10-acetate (2). The NOESY relations were represented by double barbed arrow	170
Figure 5.22.:	^1H NMR spectrum of (<i>E</i>)-18-ethyl-17,19-dihydroxyhept-14-enyl-(2-ethyl-2,6-dimethyl-1-oxaspiro[4.5]dec-3,8-dien)-10-acetate (2)	171
Figure 5.23.:	^{13}C NMR spectrum of (<i>E</i>)-18-ethyl-17,19-	

	dihydroxyhept-14-enyl-(2-ethyl-2,6-dimethyl-1-oxaspiro [4.5]dec-3,8-dien)-10-acetate (2)	171
Figure 5.24.:	¹³⁵ DEPT NMR spectrum of (<i>E</i>)-18-ethyl-17,19-dihydroxyhept-14-enyl-(2-ethyl-2,6-dimethyl-1-oxaspiro [4.5]dec-3,8-dien)-10-acetate (2)	172
Figure 5.25.:	¹ H- ¹ H COSY NMR spectrum of (<i>E</i>)-18-ethyl-17,19-dihydroxyhept-14-enyl-(2-ethyl-2,6-dimethyl-1-oxaspiro [4.5]dec-3,8-dien)-10-acetate (2)	172
Figure 5.26.:	HSQC NMR spectrum of (<i>E</i>)-18-ethyl-17,19-dihydroxy hept-14-enyl-(2-ethyl-2,6-dimethyl-1-oxaspiro[4.5]dec-3,8-dien)-10-acetate (2)	173
Figure 5.27.:	HMBC NMR spectrum of (<i>E</i>)-18-ethyl-17,19-dihydroxy hept-14-enyl-(2-ethyl-2,6-dimethyl-1-oxaspiro [4.5]dec-3,8-dien)-10-acetate (2)	173
Figure 5.28.:	NOESY NMR spectrum of (<i>E</i>)-18-ethyl-17,19-dihydroxyhept-14-enyl-(2-ethyl-2,6-dimethyl-1-oxaspiro [4.5]dec-3,8-dien)-10-acetate (2)	174
Figure 5.29.:	FTIR spectrum of (<i>E</i>)-18-ethyl-17,19-dihydroxyhept-14-enyl-(2-ethyl-2,6-dimethyl-1-oxaspiro[4.5]dec-3,8-dien)-10-acetate (2)	174
Figure 5.30.:	EIMS spectrum of (<i>E</i>)-18-ethyl-17,19-dihydroxyhept-14-enyl-(2-ethyl-2,6-dimethyl-1-oxaspiro[4.5]dec-3,8-dien)-10-acetate (2)	175
Figure 5.31.:	Mass fragmentation pattern of (<i>E</i>)-18-ethyl-17,19-dihydroxyhept-14-enyl-(2-ethyl-2,6-dimethyl-1-oxaspiro [4.5]dec-3,8-dien)-10-acetate (2)	175
Figure 5.32.:	UV spectrum of 8-(1,3,3a,4,5,7a-hexahydro-1-(hydroxy methyl)-3-oxoisobenzofuran-4-yl)-ethyl pentanoate (3) ..	177
Figure 5.33.:	HPLC chromatogram of 8-(1,3,3a,4,5,7a-hexahydro-1-(hydroxymethyl)-3-oxoisobenzofuran-4-yl)-ethyl pentanoate (3)	178
Figure 5.34.:	¹ H- ¹ H COSY (A), HMBC (B) and NOESY (C) correlations of 8-(1,3,3a,4,5,7a-hexahydro-1-(hydroxy methyl)-3-oxoisobenzofuran-4-yl)-ethyl pentanoate (3). The key ¹ H- ¹ H COSY couplings have been represented by the bold face bonds. The HMBC couplings were indicated by double barbed arrow. The NOESY relations were represented by double barbed arrow	180
Figure 5.35.:	¹ H NMR spectrum of 8-(1,3,3a,4,5,7a-hexahydro-1-(hydroxymethyl)-3-oxoisobenzofuran-4-yl)-ethyl pentanoate (3)	181
Figure 5.36.:	¹³ C NMR spectrum of 8-(1,3,3a,4,5,7a-hexahydro-1-	

	(hydroxymethyl)-3-oxoiso-benzofuran-4-yl)-ethyl pentanoate (3)	181
Figure 5.37.:	¹³⁵ DEPT NMR spectrum of 8-(1,3,3a,4,5,7a-hexahydro- 1-(hydroxymethyl)-3-oxoisobenzofuran-4-yl)-ethyl pentanoate (3)	182
Figure 5.38.:	¹ H- ¹ H COSY NMR spectrum of 8-(1,3,3a,4,5,7a- hexahydro-1-(hydroxymethyl)-3-oxoisobenzofuran-4- yl)-ethyl pentanoate (3)	182
Figure 5.39.:	HSQC NMR spectrum of 8-(1,3,3a,4,5,7a-hexahydro-1- (hydroxymethyl)-3-oxoisobenzofuran-4-yl)-ethyl pentanoate (3)	183
Figure 5.40.:	HMBC NMR spectrum of 8-(1,3,3a,4,5,7a-hexahydro-1- (hydroxymethyl)-3-oxoisobenzofuran-4-yl)-ethyl pentanoate (3)	183
Figure 5.41.:	NOESY NMR spectrum of 8-(1,3,3a,4,5,7a-hexahydro- 1-(hydroxymethyl)-3-oxoisobenzofuran-4-yl)-ethyl pentanoate (3)	184
Figure 5.42.:	FTIR spectrum of 8-(1,3,3a,4,5,7a-hexahydro-1- (hydroxymethyl)-3-oxoisobenzofuran-4-yl)-ethyl pentanoate (3)	184
Figure 5.43.:	EIMS spectrum of 8-(1,3,3a,4,5,7a-hexahydro-1- (hydroxymethyl)-3-oxoisobenzofuran-4-yl)-ethyl pentanoate (3)	185
Figure 5.44.:	Mass fragmentation pattern of 8-(1,3,3a,4,5,7a-hexa hydro-1-(hydroxymethyl)-3-oxoisobenzofuran-4-yl)- ethyl pentanoate (3)	185
Figure 5.45.:	UV spectrum of tetrahydro-3-methoxy-5-((<i>E</i>)-8,12- dimethyloct-8-enyl)-pyran-2-one (4)	186
Figure 5.46.:	HPLC chromatogram of tetrahydro-3-methoxy-5-((<i>E</i>)- 8,12-dimethyloct-8-enyl)-pyran-2-one (4)	187
Figure 5.47.:	¹ H- ¹ H COSY (A) and HMBC (B) correlations of tetrahydro-3-methoxy-5-((<i>E</i>)-8,12-dimethyloct-8-enyl)- pyran-2-one (4). The key ¹ H- ¹ H COSY couplings have been represented by bold face bonds. The HMBC couplings were indicated by double barbed arrow	190
Figure 5.48.:	NOESY correlations of tetrahydro-3-methoxy-5-((<i>E</i>)- 8,12-dimethyloct-8-enyl)-pyran-2-one (4). The NOESY relations were represented by double barbed arrow	190
Figure 5.49.:	¹ H NMR spectrum of tetrahydro-3-methoxy-5-((<i>E</i>)-8,12- dimethyloct-8-enyl)-pyran-2-one (4)	190
Figure 5.50.:	¹³ C NMR spectrum of tetrahydro-3-methoxy-5-((<i>E</i>)- 8,12-dimethyloct-8-enyl)-pyran-2-one (4)	191

Figure 5.51.:	¹³⁵ DEPT NMR spectrum of tetrahydro-3-methoxy-5-((<i>E</i>)-8,12-dimethyloct-8-enyl)-pyran-2-one (4)	191
Figure 5.52.:	¹ H- ¹ H COSY NMR spectrum of tetrahydro-3-methoxy-5-((<i>E</i>)-8,12-dimethyloct-8-enyl)-pyran-2-one (4)	192
Figure 5.53.:	HSQC NMR spectrum of tetrahydro-3-methoxy-5-((<i>E</i>)-8,12-dimethyloct-8-enyl)-pyran-2-one (4)	192
Figure 5.54.:	HMBC NMR spectrum of tetrahydro-3-methoxy-5-((<i>E</i>)-8,12-dimethyloct-8-enyl)-pyran-2-one (4)	193
Figure 5.55.:	NOESY NMR spectrum of tetrahydro-3-methoxy-5-((<i>E</i>)-8,12-dimethyloct-8-enyl)-pyran-2-one (4)	193
Figure 5.56.:	FTIR spectrum of tetrahydro-3-methoxy-5-((<i>E</i>)-8,12-dimethyloct-8-enyl)-pyran-2-one (4)	194
Figure 5.57.:	EIMS spectrum of tetrahydro-3-methoxy-5-((<i>E</i>)-8,12-dimethyloct-8-enyl)-pyran-2-one (4)	195
Figure 5.58.:	Mass fragmentation of tetrahydro-3-methoxy-5-((<i>E</i>)-8,12-dimethyloct-8-enyl)-pyran-2-one (4)	195
Figure 5.59.:	UV spectrum of dihydro-5-(8-(9,12-dihydro-8-methyl-11-propyl-2 <i>H</i> -pyran-8-yl)-ethyl)-furan-2-(3 <i>H</i>)-one (5) ...	196
Figure 5.60.:	HPLC chromatogram of dihydro-5-(8-(9,12-dihydro-8-methyl-11-propyl-2 <i>H</i> -pyran-8-yl)-ethyl)-furan-2-(3 <i>H</i>)-one (5)	196
Figure 5.61.:	¹ H- ¹ H COSY (A) and HMBC (B) correlations of dihydro-5-(8-(9,12-dihydro-8-methyl-11-propyl-2 <i>H</i> -pyran-8-yl)-ethyl)-furan-2-(3 <i>H</i>)-one (5). The key ¹ H- ¹ H COSY couplings have been represented by the bold face bonds. The HMBC couplings were indicated by double barbed arrow	199
Figure 5.62.:	NOESY correlations of dihydro-5-(8-(9,12-dihydro-8-methyl-11-propyl-2 <i>H</i> -pyran-8-yl)-ethyl)-furan-2-(3 <i>H</i>)-one (5). The NOESY relations were represented by double barbed arrow	199
Figure 5.63.:	¹ H NMR spectrum of dihydro-5-(8-(9,12-dihydro-8-methyl-11-propyl-2 <i>H</i> -pyran-8-yl)-ethyl)-furan-2-(3 <i>H</i>)-one (5)	199
Figure 5.64.:	¹³ C NMR spectrum of dihydro-5-(8-(9,12-dihydro-8-methyl-11-propyl-2 <i>H</i> -pyran-8-yl)-ethyl)-furan-2-(3 <i>H</i>)-one (5)	200
Figure 5.65.:	¹³⁵ DEPT NMR spectrum of dihydro-5-(8-(9,12-dihydro-8-methyl-11-propyl-2 <i>H</i> -pyran-8-yl)-ethyl)-furan-2-(3 <i>H</i>)-one (5)	200
Figure 5.66.:	¹ H- ¹ H COSY NMR spectrum of dihydro-5-(8-(9,12-dihydro-8-methyl-11-propyl-2 <i>H</i> -pyran-8-yl)-ethyl)-	

	furan-2-(3 <i>H</i>)-one (5)	201
Figure 5.67.:	HSQC NMR spectrum of dihydro-5-(8-(9,12-dihydro-8-methyl-11-propyl-2 <i>H</i> -pyran-8-yl)-ethyl)-furan-2-(3 <i>H</i>)-one (5)	201
Figure 5.68.:	HMBC NMR spectrum of dihydro-5-(8-(9,12-dihydro-8-methyl-11-propyl-2 <i>H</i> -pyran-8-yl)-ethyl)-furan-2-(3 <i>H</i>)-one (5)	202
Figure 5.69.:	NOESY NMR spectrum of dihydro-5-(8-(9,12-dihydro-8-methyl-11-propyl-2 <i>H</i> -pyran-8-yl)-ethyl)-furan-2-(3 <i>H</i>)-one (5)	202
Figure 5.70.:	FTIR spectrum of dihydro-5-(8-(9,12-dihydro-8-methyl-11-propyl-2 <i>H</i> -pyran-8-yl)-ethyl)-furan-2-(3 <i>H</i>)-one (5) ...	203
Figure 5.71.:	EIMS spectrum of dihydro-5-(8-(9,12-dihydro-8-methyl-11-propyl-2 <i>H</i> -pyran-8-yl)-ethyl)-furan-2-(3 <i>H</i>)-one (5) ...	203
Figure 5.72.:	Mass fragmentation pattern of dihydro-5-(8-(9,12-dihydro-8-methyl-11-propyl-2 <i>H</i> -pyran-8-yl)-ethyl)-furan-2-(3 <i>H</i>)-one (5)	204
Figure 5.73.:	UV spectrum of (10 <i>E</i>)-butyl-9-(6-ethyl-3,4,6,7,8,8a-hexahydro-1 <i>H</i> -isochromen-3-yl)-pent-10-enoate (6)	206
Figure 5.74.:	HPLC chromatogram of (10 <i>E</i>)-butyl-9-(6-ethyl-3,4,6,7,8,8a-hexahydro-1 <i>H</i> -isochromen-3-yl)-pent-10-enoate (6)	206
Figure 5.75.:	¹ H- ¹ H COSY (A) and HMBC (B) correlations of (10 <i>E</i>)-butyl-9-(6-ethyl-3,4,6,7,8,8a-hexahydro-1 <i>H</i> -isochromen-3-yl)-pent-10-enoate (6). The key ¹ H- ¹ H COSY couplings have been represented by the bold face bonds. The HMBC couplings were indicated by double barbed arrow	209
Figure 5.76.:	NOESY correlations of (10 <i>E</i>)-butyl-9-(6-ethyl-3,4,6,7,8,8a-hexahydro-1 <i>H</i> -isochromen-3-yl)-pent-10-enoate (6). The NOESY relations were represented by double barbed arrow	209
Figure 5.77.:	¹ H NMR spectrum of (10 <i>E</i>)-butyl-9-(6-ethyl-3,4,6,7,8,8a-hexahydro-1 <i>H</i> -isochromen-3-yl)-pent-10-enoate (6) ..	209
Figure 5.78.:	¹³ C NMR spectrum of (10 <i>E</i>)-butyl-9-(6-ethyl-3,4,6,7,8,8a-hexahydro-1 <i>H</i> -isochromen-3-yl)-pent-10-enoate (6) ..	210
Figure 5.79.:	¹³⁵ DEPT NMR spectrum of (10 <i>E</i>)-butyl-9-(6-ethyl-3,4,6,7,8,8a-hexahydro-1 <i>H</i> -isochromen-3-yl)-pent-10-enoate (6)	210
Figure 5.80.:	¹ H- ¹ H COSY NMR spectrum of (10 <i>E</i>)-butyl-9-(6-ethyl-3,4,6,7,8,8a-hexahydro-1 <i>H</i> -isochromen-3-yl)-pent-10-enoate (6)	211

Figure 5.81.:	HSQC NMR spectrum of (10 <i>E</i>)-butyl-9-(6-ethyl-3,4,6,7,8,8a-hexahydro-1 <i>H</i> -isochromen-3-yl)-pent-10-enoate (6)	211
Figure 5.82.:	HMBC NMR spectrum of (10 <i>E</i>)-butyl-9-(6-ethyl-3,4,6,7,8,8a-hexahydro-1 <i>H</i> -isochromen-3-yl)-pent-10-enoate (6)	212
Figure 5.83.:	NOESY NMR spectrum of (10 <i>E</i>)-butyl-9-(6-ethyl-3,4,6,7,8,8a-hexahydro-1 <i>H</i> -isochromen-3-yl)-pent-10-enoate (6)	212
Figure 5.84.:	FTIR spectrum of (10 <i>E</i>)-butyl-9-(6-ethyl-3,4,6,7,8,8a-hexahydro-1 <i>H</i> -isochromen-3-yl)-pent-10-enoate (6)	213
Figure 5.85.:	EIMS spectrum of (10 <i>E</i>)-butyl-9-(6-ethyl-3,4,6,7,8,8a-hexahydro-1 <i>H</i> -isochromen-3-yl)-pent-10-enoate (6)	214
Figure 5.86.:	Mass fragmentation pattern of (10 <i>E</i>)-butyl-9-(6-ethyl-3,4,6,7,8,8a-hexahydro-1 <i>H</i> -isochromen-3-yl)-pent-10-enoate (6)	214
Figure 5.87.:	UV spectrum of (12 <i>E</i>)-(3,4,6,7,8,8a-hexahydro-1 <i>H</i> -isochromen-3-yl)-methylhept-12-enoate (7)	215
Figure 5.88.:	HPLC chromatogram of (12 <i>E</i>)-(3,4,6,7,8,8a-hexahydro-1 <i>H</i> -isochromen-3-yl)-methylhept-12-enoate (7)	215
Figure 5.89.:	¹ H- ¹ H COSY (A) and HMBC (B) correlations of (12 <i>E</i>)-(3,4,6,7,8,8a-hexahydro-1 <i>H</i> -isochromen-3-yl)-methylhept-12-enoate (7). The key ¹ H- ¹ H COSY couplings have been represented by the bold face bonds. The HMBC couplings were indicated by double barbed arrow	218
Figure 5.90.:	NOESY correlations of (12 <i>E</i>)-(3,4,6,7,8,8a-hexahydro-1 <i>H</i> -isochromen-3-yl)-methylhept-12-enoate (7). The NOESY relations were represented by double barbed arrow	218
Figure 5.91.:	¹ H NMR spectrum of (12 <i>E</i>)-(3,4,6,7,8,8a-hexahydro-1 <i>H</i> -isochromen-3-yl)-methylhept-12-enoate (7)	218
Figure 5.92.:	¹³ C NMR spectrum of (12 <i>E</i>)-(3,4,6,7,8,8a-hexahydro-1 <i>H</i> -isochromen-3-yl)-methylhept-12-enoate (7)	219
Figure 5.93.:	¹³⁵ DEPT NMR spectrum of (12 <i>E</i>)-(3,4,6,7,8,8a-hexahydro-1 <i>H</i> -isochromen-3-yl)-methylhept-12-enoate (7) ...	219
Figure 5.94.:	¹ H- ¹ H COSY NMR spectrum of (12 <i>E</i>)-(3,4,6,7,8,8a-hexahydro-1 <i>H</i> -isochromen-3-yl)-methylhept-12-enoate (7)	220
Figure 5.95.:	HSQC NMR spectrum of (12 <i>E</i>)-(3,4,6,7,8,8a-hexahydro-1 <i>H</i> -isochromen-3-yl)-methylhept-12-enoate (7) ...	220
Figure 5.96.:	HMBC NMR spectrum of (12 <i>E</i>)-(3,4,6,7,8,8a-hexa	

	hydro-1 <i>H</i> -isochromen-3-yl)-methylhept-12-enoate (7) ...	221
Figure 5.97.:	NOESY NMR spectrum of (12 <i>E</i>)-(3,4,6,7,8,8a-hexahydro-1 <i>H</i> -isochromen-3-yl)-methylhept-12-enoate (7) ...	221
Figure 5.98.:	FTIR spectrum of (12 <i>E</i>)-(3,4,6,7,8,8a-hexahydro-1 <i>H</i> -isochromen-3-yl)-methylhept-12-enoate (7)	222
Figure 5.99.:	EIMS spectrum of (12 <i>E</i>)-(3,4,6,7,8,8a-hexahydro-1 <i>H</i> -isochromen-3-yl)-methylhept-12-enoate (7)	222
Figure 5.100.:	Mass fragmentation pattern of (12 <i>E</i>)-(3,4,6,7,8,8a-hexahydro-1 <i>H</i> -isochromen-3-yl)-methylhept-12-enoate (7) ...	223
Figure 5.101.:	Sterol analogues from <i>V. cyprinoides</i> with bioactive potentials	224
Figure 5.102.:	UV spectrum of 19 (10→5) abeo-20-methyl-pregn-1-en-3-yl-3β-methoxy-hex-25-enoate (8)	225
Figure 5.103.:	HPLC chromatogram of 19 (10→5) abeo-20-methyl-pregn-1-en-3-yl-3β-methoxy-hex-25-enoate (8)	225
Figure 5.104.:	¹ H- ¹ H COSY (A) and HMBC (B) correlations of 19 (10→5) abeo-20-methyl-pregn-1-en-3-yl-3β-methoxy-hex-25-enoate (8). The key ¹ H- ¹ H COSY couplings have been represented by the bold face bonds. The HMBC couplings were indicated by double barbed arrow	228
Figure 5.105.:	NOESY correlations of 19 (10→5) abeo-20-methyl-pregn-1-en-3-yl-3β-methoxy-hex-25-enoate (8). The NOESY relations were represented by double barbed arrow	228
Figure 5.106.:	¹ H NMR spectrum of 19 (10→5) abeo-20-methyl-pregn-1-en-3-yl-3β-methoxy-hex-25-enoate (8)	229
Figure 5.107.:	¹³ C NMR spectrum of 19 (10→5) abeo-20-methyl-pregn-1-en-3-yl-3β-methoxy-hex-25-enoate (8)	229
Figure 5.108.:	¹³⁵ DEPT NMR spectrum of 19 (10→5) abeo-20-methyl-pregn-1-en-3-yl-3β-methoxy-hex-25-enoate (8)	230
Figure 5.109.:	¹ H- ¹ H COSY NMR spectrum of 19 (10→5) abeo-20-methyl-pregn-1-en-3-yl-3β-methoxy-hex-25-enoate (8) ..	230
Figure 5.110.:	HSQC NMR spectrum of 19 (10→5) abeo-20-methyl-pregn-1-en-3-yl-3β-methoxy-hex-25-enoate (8)	231
Figure 5.111.:	HMBC NMR spectrum of 19 (10→5) abeo-20-methyl-pregn-1-en-3-yl-3β-methoxy-hex-25-enoate (8)	231
Figure 5.112.:	NOESY NMR spectrum of 19 (10→5) abeo-20-methyl-pregn-1-en-3-yl-3β-methoxy-hex-25-enoate (8)	232
Figure 5.113.:	FTIR spectrum of 19 (10→5) abeo-20-methyl-pregn-1-en-3-yl-3β-methoxy-hex-25-enoate (8)	232
Figure 5.114.:	EIMS spectrum of 19 (10→5) abeo-20-methyl-pregn-1-en-3-yl-3β-methoxy-hex-25-enoate (8)	233

Figure 5.115.:	Mass fragmentation pattern of 19 (10→5) abeo-20-methyl-pregn-1-en-3-yl-3β-methoxy-hex-25-enoate (8) ..	233
Figure 5.116.:	UV spectrum of (22 <i>E</i>)-24 ¹ -homocholesta-5,22-dien-(3β,24 ¹ β)-diol (9)	234
Figure 5.117.:	HPLC chromatogram of (22 <i>E</i>)-24 ¹ -homocholesta-5,22-dien-(3β,24 ¹ β)-diol (9)	235
Figure 5.118.:	¹ H- ¹ H COSY (A) and HMBC (B) correlations of (22 <i>E</i>)-24 ¹ -homocholesta-5,22-dien-(3β,24 ¹ β)-diol (9). The key ¹ H- ¹ H COSY couplings have been represented by the bold face bonds. The HMBC couplings were indicated by double barbed arrow	238
Figure 5.119.:	NOESY correlations of (22 <i>E</i>)-24 ¹ -homocholesta-5,22-dien-(3β,24 ¹ β)-diol (9). The NOESY relations were represented by double barbed arrow	238
Figure 5.120.:	¹ H NMR spectrum of (22 <i>E</i>)-24 ¹ -homocholesta-5,22-dien-(3β,24 ¹ β)-diol (9)	238
Figure 5.121.:	¹³ C NMR spectrum of (22 <i>E</i>)-24 ¹ -homocholesta-5,22-dien-(3β,24 ¹ β)-diol (9)	239
Figure 5.122.:	¹³⁵ DEPT NMR spectrum of (22 <i>E</i>)-24 ¹ -homocholesta-5,22-dien-(3β,24 ¹ β)-diol (9)	239
Figure 5.123.:	¹ H- ¹ H COSY NMR spectrum of (22 <i>E</i>)-24 ¹ -homocholesta-5,22-dien-(3β,24 ¹ β)-diol (9)	240
Figure 5.124.:	HSQC NMR spectrum of (22 <i>E</i>)-24 ¹ -homocholesta-5,22-dien-(3β,24 ¹ β)-diol (9)	240
Figure 5.125.:	HMBC NMR spectrum of (22 <i>E</i>)-24 ¹ -homocholesta-5,22-dien-(3β,24 ¹ β)-diol (9)	241
Figure 5.126.:	NOESY NMR spectrum of (22 <i>E</i>)-24 ¹ -homocholesta-5,22-dien-(3β,24 ¹ β)-diol (9)	241
Figure 5.127.:	FTIR spectrum of (22 <i>E</i>)-24 ¹ -homocholesta-5,22-dien-(3β,24 ¹ β)-diol (9)	242
Figure 5.128.:	EIMS spectrum of (22 <i>E</i>)-24 ¹ -homocholesta-5,22-dien-(3β,24 ¹ β)-diol (9)	243
Figure 5.129.:	Mass fragmentation pattern of (22 <i>E</i>)-24 ¹ -homocholesta-5,22-dien-(3β,24 ¹ β)-diol (9)	243
Figure 5.130.:	UV spectrum of (22 <i>E</i>),(24 ¹ <i>E</i>)-24 ¹ ,24 ² -dihomocholesta-5,22,24 ¹ -trien-3β-ol (10)	244
Figure 5.131.:	HPLC chromatogram of (22 <i>E</i>),(24 ¹ <i>E</i>)-24 ¹ ,24 ² -dihomocholesta-5,22,24 ¹ -trien-3β-ol (10)	244
Figure 5.132.:	¹ H- ¹ H COSY (A) and HMBC (B) correlations of (22 <i>E</i>),(24 ¹ <i>E</i>)-24 ¹ ,24 ² -dihomocholesta-5,22,24 ¹ -trien-3β-ol (10). The key ¹ H- ¹ H COSY couplings have been represented by the bold face bonds. The HMBC	

	couplings were indicated by double barbed arrow	248
Figure 5.133.:	NOESY correlations of (22 <i>E</i>),(24 ¹ <i>E</i>)-24 ¹ ,24 ² -dihomocholesta-5,22,24 ¹ -trien-3β-ol (10). The NOESY relations were represented by double barbed arrow.....	248
Figure 5.134.:	¹ H NMR spectrum of (22 <i>E</i>),(24 ¹ <i>E</i>)-24 ¹ ,24 ² -dihomocholesta-5,22,24 ¹ -trien-3β-ol (10)	249
Figure 5.135.:	¹³ C NMR spectrum of (22 <i>E</i>),(24 ¹ <i>E</i>)-24 ¹ ,24 ² -dihomocholesta-5,22,24 ¹ -trien-3β-ol (10)	249
Figure 5.136.:	¹³⁵ DEPT NMR spectrum of (22 <i>E</i>),(24 ¹ <i>E</i>)-24 ¹ ,24 ² -dihomocholesta-5,22,24 ¹ -trien-3β-ol (10)	250
Figure 5.137.:	¹ H- ¹ H COSY NMR spectrum of (22 <i>E</i>),(24 ¹ <i>E</i>)-24 ¹ ,24 ² -dihomocholesta-5,22,24 ¹ -trien-3β-ol (10)	250
Figure 5.138.:	HSQC NMR spectrum of (22 <i>E</i>),(24 ¹ <i>E</i>)-24 ¹ ,24 ² -dihomocholesta-5,22,24 ¹ -trien-3β-ol (10)	251
Figure 5.139.:	HMBC NMR spectrum of (22 <i>E</i>),(24 ¹ <i>E</i>)-24 ¹ ,24 ² -dihomocholesta-5,22,24 ¹ -trien-3β-ol (10)	251
Figure 5.140.:	NOESY NMR spectrum of (22 <i>E</i>),(24 ¹ <i>E</i>)-24 ¹ ,24 ² -dihomocholesta-5,22,24 ¹ -trien-3β-ol (10)	252
Figure 5.141.:	FTIR spectrum of (22 <i>E</i>),(24 ¹ <i>E</i>)-24 ¹ ,24 ² -dihomocholesta-5,22,24 ¹ -trien-3β-ol (10)	252
Figure 5.142.:	EIMS spectrum of (22 <i>E</i>),(24 ¹ <i>E</i>)-24 ¹ ,24 ² -dihomocholesta-5,22,24 ¹ -trien-3β-ol (10)	253
Figure 5.143.:	Mass fragmentation pattern of (22 <i>E</i>),(24 ¹ <i>E</i>)-24 ¹ ,24 ² -dihomocholesta-5,22,24 ¹ -trien-3β-ol (10)	254
Figure 5.144.:	A comparison of selectivity indices (IC ₅₀ of anti-COX-1/IC ₅₀ of anti-COX-2) calculated for the secondary metabolites (1-10) isolated from EtOAc:MeOH extract of <i>V. cyprinoides</i> along with commercially available standard, ibuprofen	258
Figure 5.145.:	Suggested antioxidative mechanism of spirocyclic ether derivatives (1-2) in DPPH radical model system	265
Figure 5.146.:	Suggested antioxidative mechanism of irregular meroterpenoid derivatives (3-5) in DPPH radical model system	266
Figure 5.147.:	Suggested antioxidative mechanism of hexahydro isochromenyl derivatives (6-7) in DPPH radical model system	267
Figure 5.148.:	Suggested antioxidative mechanism of cholesterol derivatives (8-10) in DPPH radical model system	268
Figure 5.149.:	The molecular binding interactions of compounds (A) 1 , (B) 2 , (C) 3 , (D) 4 and (E) 5 in the active site of cyclooxygenase (COX-2) were comprehended from the	

	docking studies. The orange and blue coloured bonds were indicated the H-bonding correlations with COX-2 ..	270
Figure 5.150.:	The molecular binding interactions of compounds (A) 1 , (B) 2 , (C) 3 , (D) 4 and (E) 5 in the active site of lipoxigenase (5-LOX) were comprehended from the docking studies. The orange and blue coloured bonds were indicated the H-bonding correlations with 5-LOX ..	271
Figure 6.1.:	The fresh shelled <i>P. malabarica</i> samples collected from the estuarine waters of Ashtamudi Lake (8°59' N and 76°36' E) located along the southwest coast of Arabian Sea, India	280
Figure 6.2.:	Schematic diagram of purification of EtOAc:MeOH extract of <i>P. malabarica</i> . CC-column chromatography; FC-flash chromatography; PTLC-preparative thin layer chromatography; TLC-thin layer chromatography; E-ethyl acetate; H- <i>n</i> -hexane; M-methanol. The coloured boxes represented the pure compounds and were characterized by detailed spectroscopic experiments	283
Figure 6.3.:	¹ H NMR spectra of intermediate sub-fractions of (A) PM ₁ , (B) PM ₂ , (C) PM ₃ , (D) PM ₄ , (E) PM ₅ and (F) PM ₆ from EtOAc:MeOH extract of <i>P. malabarica</i> with integration values	293
Figure 6.4.:	UV spectrum of (13-(methoxycarbonyl)-11-((<i>E</i>)-18-ethylhexa-16,19-dienyl)-12-propylcyclohex-10-enyl)-methyl-4-hydroxy benzoate (1)	304
Figure 6.5.:	HPLC chromatogram of (13-(methoxycarbonyl)-11-((<i>E</i>)-18-ethylhexa-16,19-dienyl)-12-propylcyclohex-10-enyl)-methyl-4-hydroxy benzoate (1)	305
Figure 6.6.:	¹ H- ¹ H COSY (A) and HMBC (B) correlations of (13-(methoxy carbonyl)-11-((<i>E</i>)-18-ethylhexa-16,19-dienyl)-12-propylcyclohex-10-enyl)-methyl-4-hydroxy benzoate (1). The key ¹ H- ¹ H COSY couplings have been represented by bold face bonds. The HMBC couplings were indicated by double barbed arrow	307
Figure 6.7.:	NOESY correlations of (13-(methoxycarbonyl)-11-((<i>E</i>)-18-ethylhexa-16,19-dienyl)-12-propylcyclohex-10-enyl)-methyl-4-hydroxy benzoate (1). The NOESY relations were represented by double barbed arrow	308
Figure 6.8.:	¹ H NMR spectrum of (13-(methoxycarbonyl)-11-((<i>E</i>)-18-ethylhexa-16,19-dienyl)-12-propylcyclohex-10-enyl)-methyl-4-hydroxy benzoate (1)	308
Figure 6.9.:	¹³ C NMR spectrum of (13-(methoxycarbonyl)-11-((<i>E</i>)-	

	18-ethylhexa-16,19-dienyl)-12-propylcyclohex-10-enyl)-methyl-4-hydroxy benzoate (1)	309
Figure 6.10.:	¹³⁵ DEPT NMR spectrum of (13-(methoxycarbonyl)-11-((<i>E</i>)-18-ethylhexa-16,19-dienyl)-12-propylcyclohex-10-enyl)-methyl-4-hydroxy benzoate (1)	309
Figure 6.11.:	¹ H- ¹ H COSY NMR spectrum of (13-(methoxycarbonyl)-11-((<i>E</i>)-18-ethylhexa-16,19-dienyl)-12-propylcyclohex-10-enyl)-methyl-4-hydroxy benzoate (1)	310
Figure 6.12.:	HSQC NMR spectrum of (13-(methoxycarbonyl)-11-((<i>E</i>)-18-ethylhexa-16,19-dienyl)-12-propylcyclohex-10-enyl)-methyl-4-hydroxy benzoate (1)	310
Figure 6.13.:	HMBC NMR spectrum of (13-(methoxycarbonyl)-11-((<i>E</i>)-18-ethylhexa-16,19-dienyl)-12-propylcyclohex-10-enyl)-methyl-4-hydroxy benzoate (1)	311
Figure 6.14.:	NOESY NMR spectrum of (13-(methoxycarbonyl)-11-((<i>E</i>)-18-ethylhexa-16,19-dienyl)-12-propylcyclohex-10-enyl)-methyl-4-hydroxy benzoate (1)	311
Figure 6.15.:	FTIR spectrum of (13-(methoxycarbonyl)-11-((<i>E</i>)-18-ethylhexa-16,19-dienyl)-12-propylcyclohex-10-enyl)-methyl-4-hydroxy benzoate (1)	312
Figure 6.16.:	EIMS spectrum of (13-(methoxycarbonyl)-11-((<i>E</i>)-18-ethylhexa-16,19-dienyl)-12-propylcyclohex-10-enyl)-methyl-4-hydroxy benzoate (1)	313
Figure 6.17.:	Mass fragmentation pattern of (13-(methoxycarbonyl)-11-((<i>E</i>)-18-ethylhexa-16,19-dienyl)-12-propylcyclohex-10-enyl)-methyl-4-hydroxy benzoate (1)	313
Figure 6.18.:	Schematic representation of biosynthetic pathway of (13-(methoxycarbonyl)-11-((<i>E</i>)-18-ethylhexa-16,19-dienyl)-12-propylcyclohex-10-enyl)-methyl-4-hydroxy benzoate (1)	314
Figure 6.19.:	UV spectrum of isobutyl-13-(6-(benzoyloxy)-10-methylpentyl)-tetrahydro-13-methyl-2 <i>H</i> -pyran-17-carboxylate (2)	315
Figure 6.20.:	HPLC chromatogram of isobutyl-13-(6-(benzoyloxy)-10-methylpentyl)-tetrahydro-13-methyl-2 <i>H</i> -pyran-17-carboxylate (2)	316
Figure 6.21.:	¹ H- ¹ H COSY (A) and HMBC (B) correlations of isobutyl-13-(6-(benzoyloxy)-10-methylpentyl)-tetrahydro-13-methyl-2 <i>H</i> -pyran-17-carboxylate (2). The key ¹ H- ¹ H COSY couplings have been represented by the bold face bonds. The HMBC couplings were indicated by double barbed arrow	318

Figure 6.22.:	NOESY correlations of isobutyl-13-(6-(benzoyloxy)-10-methylpentyl)-tetrahydro-13-methyl-2 <i>H</i> -pyran-17-carboxylate (2). The NOESY relations were represented by double barbed arrow	319
Figure 6.23.:	¹ H NMR spectrum of isobutyl-13-(6-(benzoyloxy)-10-methylpentyl)-tetrahydro-13-methyl-2 <i>H</i> -pyran-17-carboxylate (2)	319
Figure 6.24.:	¹³ C NMR spectrum of isobutyl-13-(6-(benzoyloxy)-10-methylpentyl)-tetrahydro-13-methyl-2 <i>H</i> -pyran-17-carboxylate (2)	320
Figure 6.25.:	¹³⁵ DEPT NMR spectrum of isobutyl-13-(6-(benzoyloxy)-10-methylpentyl)-tetrahydro-13-methyl-2 <i>H</i> -pyran-17-carboxylate (2)	320
Figure 6.26.:	¹ H- ¹ H COSY NMR spectrum of isobutyl-13-(6-(benzoyloxy)-10-methylpentyl)-tetrahydro-13-methyl-2 <i>H</i> -pyran-17-carboxylate (2)	321
Figure 6.27.:	HSQC NMR spectrum of isobutyl-13-(6-(benzoyloxy)-10-methylpentyl)-tetrahydro-13-methyl-2 <i>H</i> -pyran-17-carboxylate (2)	321
Figure 6.28.:	HMBC NMR spectrum of isobutyl-13-(6-(benzoyloxy)-10-methyl pentyl)-tetrahydro-13-methyl-2 <i>H</i> -pyran-17-carboxylate (2)	322
Figure 6.29.:	NOESY NMR spectrum of isobutyl-13-(6-(benzoyloxy)-10-methylpentyl)-tetrahydro-13-methyl-2 <i>H</i> -pyran-17-carboxylate (2)	322
Figure 6.30.:	FTIR spectrum of isobutyl-13-(6-(benzoyloxy)-10-methylpentyl)-tetrahydro-13-methyl-2 <i>H</i> -pyran-17-carboxylate (2)	323
Figure 6.31.:	EIMS spectrum of isobutyl-13-(6-(benzoyloxy)-10-methylpentyl)-tetrahydro-13-methyl-2 <i>H</i> -pyran-17-carboxylate (2)	324
Figure 6.32.:	Mass fragmentation pattern of isobutyl-13-(6-(benzoyloxy)-10-methylpentyl)-tetrahydro-13-methyl-2 <i>H</i> -pyran-17-carboxylate (2)	324
Figure 6.33.:	Schematic representation of biosynthetic pathway of isobutyl-13-(6-(benzoyloxy)-10-methylpentyl)-tetrahydro-13-methyl-2 <i>H</i> -pyran-17-carboxylate (2)	325
Figure 6.34.:	UV spectrum of (<i>E</i>)-12-(17-ethyl-tetrahydro-16-hydroxy-15-(methylpentanoate)-14-oxo-2 <i>H</i> -pyran-13-yl)-9-methylbut-11-enyl benzoate (3)	326
Figure 6.35.:	HPLC chromatogram of (<i>E</i>)-12-(17-ethyl-tetrahydro-16-hydroxy-15-(methylpentanoate)-14-oxo-2 <i>H</i> -pyran-13-	

	yl)-9-methylbut-11-enyl benzoate (3)	326
Figure 6.36.:	¹ H- ¹ H COSY (A) and HMBC (B) correlations of (<i>E</i>)-12-(17-ethyl-tetrahydro-16-hydroxy-15-(methylpentanoate)-14-oxo-2H-pyran-13-yl)-9-methylbut-11-enyl benzoate (3). The key ¹ H- ¹ H COSY couplings have been represented by the bold face bonds. The HMBC couplings were indicated by double barbed arrow	329
Figure 6.37.:	NOESY correlations of (<i>E</i>)-12-(17-ethyl-tetrahydro-16-hydroxy-15-(methylpentanoate)-14-oxo-2H-pyran-13-yl)-9-methylbut-11-enyl benzoate (3). The NOESY relations were represented by double barbed arrow	329
Figure 6.38.:	¹ H NMR spectrum of (<i>E</i>)-12-(17-ethyl-tetrahydro-16-hydroxy-15-(methylpentanoate)-14-oxo-2H-pyran-13-yl)-9-methylbut-11-enyl benzoate (3)	330
Figure 6.39.:	¹³ C NMR spectrum of (<i>E</i>)-12-(17-ethyl-tetrahydro-16-hydroxy-15-(methylpentanoate)-14-oxo-2H-pyran-13-yl)-9-methylbut-11-enyl benzoate (3)	330
Figure 6.40.:	¹³⁵ DEPT NMR spectrum of (<i>E</i>)-12-(17-ethyl-tetrahydro-16-hydroxy-15-(methylpentanoate)-14-oxo-2H-pyran-13-yl)-9-methylbut-11-enyl benzoate (3)	331
Figure 6.41.:	¹ H- ¹ H COSY NMR spectrum of (<i>E</i>)-12-(17-ethyl-tetrahydro-16-hydroxy-15-(methylpentanoate)-14-oxo-2H-pyran-13-yl)-9-methylbut-11-enyl benzoate (3)	331
Figure 6.42.:	HSQC NMR spectrum of (<i>E</i>)-12-(17-ethyl-tetrahydro-16-hydroxy-15-(methylpentanoate)-14-oxo-2H-pyran-13-yl)-9-methylbut-11-enyl benzoate (3)	332
Figure 6.43.:	NMR HMBC spectrum of (<i>E</i>)-12-(17-ethyl-tetrahydro-16-hydroxy-15-(methylpentanoate)-14-oxo-2H-pyran-13-yl)-9-methylbut-11-enyl benzoate (3)	332
Figure 6.44.:	NOESY NMR spectrum of (<i>E</i>)-12-(17-ethyl-tetrahydro-16-hydroxy-15-(methylpentanoate)-14-oxo-2H-pyran-13-yl)-9-methylbut-11-enyl benzoate (3)	333
Figure 6.45.:	FTIR spectrum of (<i>E</i>)-12-(17-ethyl-tetrahydro-16-hydroxy-15-(methylpentanoate)-14-oxo-2H-pyran-13-yl)-9-methylbut-11-enyl benzoate (3)	333
Figure 6.46.:	EIMS spectrum of (<i>E</i>)-12-(17-ethyl-tetrahydro-16-hydroxy-15-(methylpentanoate)-14-oxo-2H-pyran-13-yl)-9-methylbut-11-enyl benzoate (3)	334
Figure 6.47.:	Mass fragmentation pattern of (<i>E</i>)-12-(17-ethyl-tetrahydro-16-hydroxy-15-(methylpentanoate)-14-oxo-2H-pyran-13-yl)-9-methylbut-11-enyl benzoate (3)	335
Figure 6.48.:	Schematic representation of biosynthetic pathway of (<i>E</i>)-	

	12-(17-ethyl-tetrahydro-16-hydroxy-15-(methylpentanoate)-14-oxo-2 <i>H</i> -pyran-13-yl)-9-methylbut-11-enyl benzoate (3)	336
Figure 6.49.:	Tetrahydro chromenyl derivatives from <i>P. malabarica</i> with bioactive potentials	337
Figure 6.50.:	UV spectrum of 6 ¹ -(3-((<i>E</i>)-3 ^{1b} -(furan-2'-yl)-prop-3 ^{1b} -en-3 ¹ -yl)-4a,5,6,8a-tetrahydro-8-methyl-2 <i>H</i> -chromen-6-yl)-ethyl-5''-methyl-hexanoate (4)	339
Figure 6.51.:	HPLC chromatogram of 6 ¹ -(3-((<i>E</i>)-3 ^{1b} -(furan-2'-yl)-prop-3 ^{1b} -en-3 ¹ -yl)-4a,5,6,8a-tetrahydro-8-methyl-2 <i>H</i> -chromen-6-yl)-ethyl-5''-methyl-hexanoate (4)	339
Figure 6.52.:	¹ H- ¹ H COSY (A) and HMBC (B) correlations of 6 ¹ -(3-((<i>E</i>)-3 ^{1b} -(furan-2'-yl)-prop-3 ^{1b} -en-3 ¹ -yl)-4a,5,6,8a-tetrahydro-8-methyl-2 <i>H</i> -chromen-6-yl)-ethyl-5''-methyl-hexanoate (4). The key ¹ H- ¹ H COSY couplings have been represented by bold face bonds. The HMBC couplings were indicated by double barbed arrow	343
Figure 6.53.:	NOESY correlations of 6 ¹ -(3-((<i>E</i>)-3 ^{1b} -(furan-2'-yl)-prop-3 ^{1b} -en-3 ¹ -yl)-4a,5,6,8a-tetrahydro-8-methyl-2 <i>H</i> -chromen-6-yl)-ethyl-5''-methyl-hexanoate (4). The NOESY relations were represented by double barbed arrow	343
Figure 6.54.:	¹ H NMR spectrum of 6 ¹ -(3-((<i>E</i>)-3 ^{1b} -(furan-2'-yl)-prop-3 ^{1b} -en-3 ¹ -yl)-4a,5,6,8a-tetrahydro-8-methyl-2 <i>H</i> -chromen-6-yl)-ethyl-5''-methyl-hexanoate (4)	344
Figure 6.55.:	¹³ C NMR spectrum of 6 ¹ -(3-((<i>E</i>)-3 ^{1b} -(furan-2'-yl)-prop-3 ^{1b} -en-3 ¹ -yl)-4a,5,6,8a-tetrahydro-8-methyl-2 <i>H</i> -chromen-6-yl)-ethyl-5''-methyl-hexanoate (4)	344
Figure 6.56.:	¹³⁵ DEPT NMR spectrum of 6 ¹ -(3-((<i>E</i>)-3 ^{1b} -(furan-2'-yl)-prop-3 ^{1b} -en-3 ¹ -yl)-4a,5,6,8a-tetrahydro-8-methyl-2 <i>H</i> -chromen-6-yl)-ethyl-5''-methyl-hexanoate (4)	345
Figure 6.57.:	¹ H- ¹ H COSY NMR spectrum of 6 ¹ -(3-((<i>E</i>)-3 ^{1b} -(furan-2'-yl)-prop-3 ^{1b} -en-3 ¹ -yl)-4a,5,6,8a-tetrahydro-8-methyl-2 <i>H</i> -chromen-6-yl)-ethyl-5''-methyl-hexanoate (4)	345
Figure 6.58.:	HSQC NMR spectrum of 6 ¹ -(3-((<i>E</i>)-3 ^{1b} -(furan-2'-yl)-prop-3 ^{1b} -en-3 ¹ -yl)-4a,5,6,8a-tetrahydro-8-methyl-2 <i>H</i> -chromen-6-yl)-ethyl-5''-methyl-hexanoate (4)	346
Figure 6.59.:	HMBC NMR spectrum of 6 ¹ -(3-((<i>E</i>)-3 ^{1b} -(furan-2'-yl)-prop-3 ^{1b} -en-3 ¹ -yl)-4a,5,6,8a-tetrahydro-8-methyl-2 <i>H</i> -chromen-6-yl)-ethyl-5''-methyl-hexanoate (4)	346
Figure 6.60.:	NOESY NMR spectrum of 6 ¹ -(3-((<i>E</i>)-3 ^{1b} -(furan-2'-yl)-prop-3 ^{1b} -en-3 ¹ -yl)-4a,5,6,8a-tetrahydro-8-methyl-2 <i>H</i> -	

	chromen-6-yl)-ethyl-5''-methyl-hexanoate (4)	347
Figure 6.61.:	FTIR spectrum of 6 ¹ -(3-((<i>E</i>)-3 ^{1b} -(furan-2'-yl)-prop-3 ^{1b} -en-3 ¹ -yl)-4a,5,6,8a-tetrahydro-8-methyl-2 <i>H</i> -chromen-6-yl)-ethyl-5''-methyl-hexanoate (4)	347
Figure 6.62.:	EIMS spectrum of 6 ¹ -(3-((<i>E</i>)-3 ^{1b} -(furan-2'-yl)-prop-3 ^{1b} -en-3 ¹ -yl)-4a,5,6,8a-tetrahydro-8-methyl-2 <i>H</i> -chromen-6-yl)-ethyl-5''-methyl-hexanoate (4)	348
Figure 6.63.:	Mass fragmentation of 6 ¹ -(3-((<i>E</i>)-3 ^{1b} -(furan-2'-yl)-prop-3 ^{1b} -en-3 ¹ -yl)-4a,5,6,8a-tetrahydro-8-methyl-2 <i>H</i> -chromen-6-yl)-ethyl-5''-methyl-hexanoate (4)	348
Figure 6.64.:	UV spectrum of 7-(2'-ethyl-1'-hydroxynonan-2'-yl)-6,7,8,8a-tetrahydro-3 <i>H</i> -isochromen-1-(5 <i>H</i>)-one (5)	350
Figure 6.65.:	HPLC chromatogram of 7-(2'-ethyl-1'-hydroxynonan-2'-yl)-6,7,8,8a-tetrahydro-3 <i>H</i> -isochromen-1-(5 <i>H</i>)-one (5) .	350
Figure 6.66.:	¹ H- ¹ H COSY (A) and HMBC (B) correlations of 7-(2'-ethyl-1'-hydroxynonan-2'-yl)-6,7,8,8a-tetrahydro-3 <i>H</i> -isochromen-1-(5 <i>H</i>)-one (5). The key ¹ H- ¹ H COSY couplings have been represented by the bold face bonds. The HMBC couplings were indicated by double barbed arrow	353
Figure 6.67.:	NOESY correlations of 7-(2'-ethyl-1'-hydroxynonan-2'-yl)-6,7,8,8a-tetrahydro-3 <i>H</i> -isochromen-1-(5 <i>H</i>)-one (5). The NOESY relations were represented by double barbed arrow	354
Figure 6.68.:	¹ H NMR spectrum of 7-(2'-ethyl-1'-hydroxynonan-2'-yl)-6,7,8,8a-tetrahydro-3 <i>H</i> -isochromen-1-(5 <i>H</i>)-one (5) ...	354
Figure 6.69.:	¹³ C NMR spectrum of 7-(2'-ethyl-1'-hydroxynonan-2'-yl)-6,7,8,8a-tetrahydro-3 <i>H</i> -isochromen-1-(5 <i>H</i>)-one (5) ...	355
Figure 6.70.:	¹³⁵ DEPT NMR spectrum of 7-(2'-ethyl-1'-hydroxynonan-2'-yl)-6,7,8,8a-tetrahydro-3 <i>H</i> -isochromen-1-(5 <i>H</i>)-one (5)	355
Figure 6.71.:	¹ H- ¹ H COSY NMR spectrum of 7-(2'-ethyl-1'-hydroxynonan-2'-yl)-6,7,8,8a-tetrahydro-3 <i>H</i> -isochromen-1-(5 <i>H</i>)-one (5)	356
Figure 6.72.:	HSQC NMR spectrum of 7-(2'-ethyl-1'-hydroxynonan-2'-yl)-6,7,8,8a-tetrahydro-3 <i>H</i> -isochromen-1-(5 <i>H</i>)-one (5)	356
Figure 6.73.:	HMBC NMR spectrum of 7-(2'-ethyl-1'-hydroxynonan-2'-yl)-6,7,8,8a-tetrahydro-3 <i>H</i> -isochromen-1-(5 <i>H</i>)-one (5)	357
Figure 6.74.:	NOESY NMR spectrum of 7-(2'-ethyl-1'-hydroxynonan-2'-yl)-6,7,8,8a-tetrahydro-3 <i>H</i> -isochromen	

	-1-(5 <i>H</i>)-one (5)	357
Figure 6.75.:	FTIR spectrum of 7-(2'-ethyl-1'-hydroxynonan-2'-yl)-6,7,8,8a-tetrahydro-3 <i>H</i> -isochromen-1-(5 <i>H</i>)-one (5)	358
Figure 6.76.:	EIMS spectrum of 7-(2'-ethyl-1'-hydroxynonan-2'-yl)-6,7,8,8a-tetrahydro-3 <i>H</i> -isochromen-1-(5 <i>H</i>)-one (5)	359
Figure 6.77.:	Mass fragmentation pattern of 7-(2'-ethyl-1'-hydroxynonan-2'-yl)-6,7,8,8a-tetrahydro-3 <i>H</i> -isochromen-1-(5 <i>H</i>)-one (5)	359
Figure 6.78.:	UV spectrum of 18 (4→14),19 (4→8) bis-abeo-nor-isopimarane-1,5-dien-3-yl-3β-methoxy propyl pentanoate (6)	361
Figure 6.79.:	HPLC chromatogram of 18 (4→14),19 (4→8) bis-abeo-nor-isopimarane-1,5-dien-3-yl-3β-methoxy propyl pentanoate (6)	361
Figure 6.80.:	¹ H- ¹ H COSY (A) and HMBC (B) correlations of 18 (4→14),19 (4→8) bis-abeo-nor-isopimarane-1,5-dien-3-yl-3β-methoxy propyl pentanoate (6). The key ¹ H- ¹ H COSY couplings have been represented by the bold face bonds. The HMBC couplings were indicated by double barbed arrow	364
Figure 6.81.:	NOESY correlations of 18 (4→14),19 (4→8) bis-abeo-nor-isopimarane-1,5-dien-3-yl-3β-methoxy propyl pentanoate (6). The NOESY relations were represented by double barbed arrow	364
Figure 6.82.:	¹ H NMR spectrum of 18 (4→14),19 (4→8) bis-abeo-nor-isopimarane-1,5-dien-3-yl-3β-methoxy propyl pentanoate (6)	365
Figure 6.83.:	¹³ C NMR spectrum of 18 (4→14),19 (4→8) bis-abeo-nor-isopimarane-1,5-dien-3-yl-3β-methoxy propyl pentanoate (6)	365
Figure 6.84.:	¹³⁵ DEPT NMR spectrum of 18 (4→14),19 (4→8) bis-abeo-nor-isopimarane-1,5-dien-3-yl-3β-methoxy propyl pentanoate (6)	366
Figure 6.85.:	¹ H- ¹ H COSY NMR spectrum of 18 (4→14),19 (4→8) bis-abeo-nor-isopimarane-1,5-dien-3-yl-3β-methoxy propyl pentanoate (6)	366
Figure 6.86.:	HSQC NMR spectrum of 18 (4→14),19 (4→8) bis-abeo-nor-isopimarane-1,5-dien-3-yl-3β-methoxy propyl pentanoate (6)	367
Figure 6.87.:	HMBC NMR spectrum of 18 (4→14),19 (4→8) bis-abeo-nor-isopimarane-1,5-dien-3-yl-3β-methoxy propyl pentanoate (6)	367
Figure 6.88.:	NOESY NMR spectrum of 18 (4→14),19 (4→8) bis-	

	abeo-nor-isopimarane-1,5-dien-3-yl-3 β -methoxy propyl pentanoate (6)	368
Figure 6.89.:	FTIR spectrum of 18 (4 \rightarrow 14),19 (4 \rightarrow 8) bis-abeo-nor-iso pimarane-1,5-dien-3-yl-3 β -methoxy propyl pentanoate (6)	368
Figure 6.90:	EIMS spectrum of 18 (4 \rightarrow 14),19 (4 \rightarrow 8) bis-abeo-nor-iso pimarane-1,5-dien-3-yl-3 β -methoxy propyl pentanoate (6)	369
Figure 6.91.:	Mass fragmentation pattern of 18 (4 \rightarrow 14),19 (4 \rightarrow 8) bis-abeo-nor-isopimarane-1,5-dien-3-yl-3 β -methoxy propyl pentanoate (6)	370
Figure 6.92.:	UV spectrum of 1'-((10 <i>E</i>)-10-(10-(pentan-4-yl)-cyclohex-4-enyl)-allyloxy)-tetrahydro-2',2'-dimethyl-2 <i>H</i> -pyran (7)	372
Figure 6.93.:	HPLC chromatogram of 1'-((10 <i>E</i>)-10-(10-(pentan-4-yl)-cyclohex-4-enyl)-allyloxy)-tetrahydro-2',2'-dimethyl-2 <i>H</i> -pyran (7)	372
Figure 6.94.:	¹ H- ¹ H COSY (A) and HMBC (B) correlations of 1'-((10 <i>E</i>)-10-(10-(pentan-4-yl)-cyclohex-4-enyl)-allyloxy)-tetrahydro-2',2'-dimethyl-2 <i>H</i> -pyran (7). The key ¹ H- ¹ H COSY couplings have been represented by the bold face bonds. The HMBC couplings were indicated by double barbed arrow	375
Figure 6.95.:	NOESY correlations of 1'-((10 <i>E</i>)-10-(10-(pentan-4-yl)-cyclohex-4-enyl)-allyloxy)-tetrahydro-2',2'-dimethyl-2 <i>H</i> -pyran (7). The NOESY relations were represented by double barbed arrow	375
Figure 6.96.:	¹ H spectrum NMR of 1'-((10 <i>E</i>)-10-(10-(pentan-4-yl)-cyclohex-4-enyl)-allyloxy)-tetrahydro-2',2'-dimethyl-2 <i>H</i> -pyran (7)	376
Figure 6.97.:	¹³ C NMR spectrum of 1'-((10 <i>E</i>)-10-(10-(pentan-4-yl)-cyclohex-4-enyl)-allyloxy)-tetrahydro-2',2'-dimethyl-2 <i>H</i> -pyran (7)	376
Figure 6.98.:	¹³⁵ DEPT NMR spectrum of 1'-((10 <i>E</i>)-10-(10-(pentan-4-yl)-cyclohex-4-enyl)-allyloxy)-tetrahydro-2',2'-dimethyl-2 <i>H</i> -pyran (7)	377
Figure 6.99.:	¹ H- ¹ H COSY NMR spectrum of 1'-((10 <i>E</i>)-10-(10-(pentan-4-yl)-cyclohex-4-enyl)-allyloxy)-tetrahydro-2',2'-dimethyl-2 <i>H</i> -pyran (7)	377
Figure 6.100.:	HSQC NMR spectrum of 1'-((10 <i>E</i>)-10-(10-(pentan-4-yl)-cyclohex-4-enyl)-allyloxy)-tetrahydro-2',2'-dimethyl-2 <i>H</i> -pyran (7)	378
Figure 6.101.:	HMBC NMR spectrum of 1'-((10 <i>E</i>)-10-(10-(pentan-4-yl)-cyclohex-4-enyl)-allyloxy)-tetrahydro-2',2'-dimethyl-	

	2 <i>H</i> -pyran (7)	378
Figure 6.102.:	NOESY NMR spectrum of 1'-((10 <i>E</i>)-10-(10-(pentan-4-yl)-cyclohex-4-enyl)-allyloxy)-tetrahydro-2',2'-dimethyl-2 <i>H</i> -pyran (7)	379
Figure 6.103.:	FTIR spectrum of 1'-((10 <i>E</i>)-10-(10-(pentan-4-yl)-cyclohex-4-enyl)-allyloxy)-tetrahydro-2',2'-dimethyl-2 <i>H</i> -pyran (7)	379
Figure 6.104.:	EIMS spectrum of 1'-((10 <i>E</i>)-10-(10-(pentan-4-yl)-cyclohex-4-enyl)-allyloxy)-tetrahydro-2',2'-dimethyl-2 <i>H</i> -pyran (7)	380
Figure 6.105.:	Mass fragmentation pattern of 1'-((10 <i>E</i>)-10-(10-(pentan-4-yl)-cyclohex-4-enyl)-allyloxy)-tetrahydro-2',2'-dimethyl-2 <i>H</i> -pyran (7)	381
Figure 6.106.:	UV spectrum of 2-((<i>E</i>)-deca-1,8-dien-10-yl)-11,12-dihydro-13-propyl-2 <i>H</i> -pyran (8)	382
Figure 6.107.:	HPLC chromatogram of 2-((<i>E</i>)-deca-1,8-dien-10-yl)-11,12-dihydro-13-propyl-2 <i>H</i> -pyran (8)	382
Figure 6.108.:	¹ H- ¹ H COSY (A) and HMBC (B) correlations of 2-((<i>E</i>)-deca-1,8-dien-10-yl)-11,12-dihydro-13-propyl-2 <i>H</i> -pyran (8). The key ¹ H- ¹ H COSY couplings have been represented by the bold face bonds. The HMBC couplings were indicated by double barbed arrow	385
Figure 6.109.:	NOESY correlations of 2-((<i>E</i>)-deca-1,8-dien-10-yl)-11,12-dihydro-13-propyl-2 <i>H</i> -pyran (8). The NOESY relations were represented by double barbed arrow	386
Figure 6.110.:	¹ H NMR spectrum of 2-((<i>E</i>)-deca-1,8-dien-10-yl)-11,12-dihydro-13-propyl-2 <i>H</i> -pyran (8)	386
Figure 6.111.:	¹³ C NMR spectrum of 2-((<i>E</i>)-deca-1,8-dien-10-yl)-11,12-dihydro-13-propyl-2 <i>H</i> -pyran (8)	387
Figure 6.112.:	¹³⁵ DEPT NMR spectrum of 2-((<i>E</i>)-deca-1,8-dien-10-yl)-11,12-dihydro-13-propyl-2 <i>H</i> -pyran (8)	387
Figure 6.113.:	¹ H- ¹ H COSY NMR spectrum of 2-((<i>E</i>)-deca-1,8-dien-10-yl)-11,12-dihydro-13-propyl-2 <i>H</i> -pyran (8)	388
Figure 6.114.:	HSQC NMR spectrum of 2-((<i>E</i>)-deca-1,8-dien-10-yl)-11,12-dihydro-13-propyl-2 <i>H</i> -pyran (8)	388
Figure 6.115.:	HMBC NMR spectrum of 2-((<i>E</i>)-deca-1,8-dien-10-yl)-11,12-dihydro-13-propyl-2 <i>H</i> -pyran (8)	389
Figure 6.116.:	NOESY NMR spectrum of 2-((<i>E</i>)-deca-1,8-dien-10-yl)-11,12-dihydro-13-propyl-2 <i>H</i> -pyran (8)	389
Figure 6.117.:	FTIR spectrum of 2-((<i>E</i>)-deca-1,8-dien-10-yl)-11,12-dihydro-13-propyl-2 <i>H</i> -pyran (8)	390
Figure 6.118.:	EIMS spectrum of 2-((<i>E</i>)-deca-1,8-dien-10-yl)-11,12-	

	dihydro-13-propyl-2 <i>H</i> -pyran (8)	390
Figure 6.119.:	Mass fragmentation pattern of 2-((<i>E</i>)-deca-1,8-dien-10-yl)-11,12-dihydro-13-propyl-2 <i>H</i> -pyran (8)	391
Figure 6.120.:	UV spectrum of (22 <i>E</i>)-24 ¹ ,24 ² -methyldihomocholesta-5,22-dien-3β-ol (9)	393
Figure 6.121.:	HPLC chromatogram of (22 <i>E</i>)-24 ¹ ,24 ² -methyldihomocholesta-5,22-dien-3β-ol (9)	393
Figure 6.122.:	¹ H- ¹ H COSY (A) and HMBC (B) correlations of (22 <i>E</i>)-24 ¹ ,24 ² -methyldihomocholesta-5,22-dien-3β-ol (9). The key ¹ H- ¹ H COSY couplings have been represented by the bold face bonds. The HMBC couplings were indicated by double barbed arrow	397
Figure 6.123.:	NOESY correlations of (22 <i>E</i>)-24 ¹ ,24 ² -methyl dihomocholesta-5,22-dien-3β-ol (9). The NOESY relations were represented by double barbed arrow	397
Figure 6.124.:	¹ H NMR spectrum of (22 <i>E</i>)-24 ¹ ,24 ² -methyldihomocholesta-5,22-dien-3β-ol (9)	397
Figure 6.125.:	¹³ C NMR spectrum of (22 <i>E</i>)-24 ¹ ,24 ² -methyldihomocholesta-5,22-dien-3β-ol (9)	398
Figure 6.126.:	¹³⁵ DEPT NMR spectrum of (22 <i>E</i>)-24 ¹ ,24 ² -methyldihomocholesta-5,22-dien-3β-ol (9)	398
Figure 6.127.:	¹ H- ¹ H COSY NMR spectrum of (22 <i>E</i>)-24 ¹ ,24 ² -methyldihomocholesta-5,22-dien-3β-ol (9)	399
Figure 6.128.:	HSQC NMR spectrum of (22 <i>E</i>)-24 ¹ ,24 ² -methyldihomocholesta-5,22-dien-3β-ol (9)	399
Figure 6.129.:	HMBC NMR spectrum of (22 <i>E</i>)-24 ¹ ,24 ² -methyldihomocholesta-5,22-dien-3β-ol (9)	400
Figure 6.130.:	NOESY NMR spectrum of (22 <i>E</i>)-24 ¹ ,24 ² -methyldihomocholesta-5,22-dien-3β-ol (9)	400
Figure 6.131.:	FTIR spectrum of (22 <i>E</i>)-24 ¹ ,24 ² -methyldihomocholesta-5,22-dien-3β-ol (9)	401
Figure 6.132.:	EIMS spectrum of (22 <i>E</i>)-24 ¹ ,24 ² -methyldihomocholesta-5,22-dien-3β-ol (9)	402
Figure 6.133.:	Mass fragmentation pattern of (22 <i>E</i>)-24 ¹ ,24 ² -methyldihomocholesta-5,22-dien-3β-ol (9)	402
Figure 6.134.:	UV spectrum of 23- <i>gem</i> -dimethylcholesta-5-en-3β-ol (10)	403
Figure 6.135.:	HPLC chromatogram of 23- <i>gem</i> -dimethylcholesta-5-en-3β-ol (10)	404
Figure 6.136.:	¹ H- ¹ H COSY (A) and HMBC (B) correlations of 23- <i>gem</i> -dimethylcholesta-5-en-3β-ol (10). The key ¹ H- ¹ H COSY couplings have been represented by the bold face	

	bonds. The HMBC couplings were indicated by double barbed arrow	408
Figure 6.137.:	NOESY correlations of 23- <i>gem</i> -dimethylcholesta-5-en- 3 β -ol (10). The NOESY relations were represented by double barbed arrow	408
Figure 6.138.:	¹ H NMR spectrum of 23- <i>gem</i> -dimethylcholesta-5-en-3 β - ol (10)	408
Figure 6.139.:	¹³ C NMR spectrum of 23- <i>gem</i> -dimethylcholesta-5-en- 3 β -ol (10)	409
Figure 6.140.:	¹³⁵ DEPT NMR spectrum of 23- <i>gem</i> -dimethylcholesta-5- en-3 β -ol (10)	409
Figure 6.141.:	¹ H- ¹ H COSY NMR spectrum of 23- <i>gem</i> - dimethylcholesta-5-en-3 β -ol (10)	410
Figure 6.142.:	HSQC NMR spectrum of 23- <i>gem</i> -dimethylcholesta-5-en- 3 β -ol (10)	410
Figure 6.143.:	HMBC NMR spectrum of 23- <i>gem</i> -dimethylcholesta-5- en-3 β -ol (10)	411
Figure 6.144.:	NOESY NMR spectrum of 23- <i>gem</i> -dimethylcholesta-5- en-3 β -ol (10)	411
Figure 6.145.:	FTIR spectrum of 23- <i>gem</i> -dimethylcholesta-5-en-3 β -ol (10)	412
Figure 6.146.:	EIMS spectrum of 23- <i>gem</i> -dimethylcholesta-5-en-3 β -ol (10)	412
Figure 6.147.:	Mass fragmentation pattern of 23- <i>gem</i> -dimethylcholesta- 5-en-3 β -ol (10)	413
Figure 6.148.:	A comparison of selectivity indices (IC ₅₀ of anti-COX- 1/IC ₅₀ of anti-COX-2) of were calculated for the secondary metabolites (1-10) isolated from EtOAc:MeOH extract of <i>P. malabarica</i> along with commercially available standard, ibuprofen	419
Figure 6.149.:	Suggested antioxidative mechanism of aryl polyketides (1-3) in DPPH radical model system	425
Figure 6.150.	Suggested antioxidative mechanism of chromenyl derivatives (4-5) in DPPH radical model system	427
Figure 6.151.	Suggested antioxidative mechanism of isopimarane derivative (6) in DPPH radical model system	427
Figure 6.152.	Suggested antioxidative mechanism of meroterpeno pyranoids (7-8) in DPPH radical model system	428
Figure 6.153.	Suggested antioxidative mechanism of cholestenol derivatives (9-10) in DPPH radical model system	428
Figure 6.154.	The molecular binding interactions of compounds (A) 1 , (B) 2 , (C) 3 , (D) 4 and (E) 6 in the active site of	

cyclooxygenase (COX-2) were comprehended from the docking studies. The orange and blue coloured bonds were indicated the H-bonding correlations with COX-2 .

431

Figure 6.155. The molecular binding interactions of compounds (A) **1**, (B) **2**, (C) **3**, (D) **4** and (E) **6** in the active site of lipoxxygenase (5-LOX) were comprehended from the docking studies. The orange and blue coloured bonds were indicated the H-bonding correlations with 5-LOX ..

432

INTRODUCTION

Contents

- 1.1. *Background*
- 1.2. *Biological potentials of secondary metabolites from marine and estuarine habitats*
- 1.3. *Pharmacological significance of antioxidant and anti-inflammatory properties*
- 1.4. *Importance of mollusks and bivalves as potential resources of bioactive compounds*
- 1.5. *Bioactive potentials of bivalve mollusks and with reference to marine and estuarine clams*
- 1.6. *Objectives*
- 1.7. *Thesis outline*

1.1. Background

During the previous decades, the marine organisms have significantly contributed towards the development of bioactive metabolites as potential therapeutic agents in functional foods and pharmaceuticals. An increase in the number of patents filed and granted in the subject area of marine bio-prospecting and pharmacophores from the organisms dwelling in the marine and coastal habitats is a ready testimony to this statement. Among various marine organisms, those belonging to the class *Mollusca* are of particular interest, and have been extensively distributed in the marine and estuarine habitats. Estuarine and coastal mollusks, especially bivalves contribute significantly towards the total fish catch in the coastal and estuarine waters of India (Figure 1.1.). The bivalve mollusk fishery is constituted predominantly by clams, mussels and oysters. Over the past decades, the importance of the bivalve clams has been increased as unconventional resources to conventional finfish fishery in different regions of the world. Due to their potential market values and nutritional qualities, clam aquaculture recorded an increasing trend in the recent years. The greater interest in this field could be corroborated by the increased number of research publications with regard to the isolation and characterization of hitherto undescribed chemistries from mollusks and bivalve clams (Blunt *et al.*, 2012; Blunt *et al.*, 2014), which appropriately

signified the wider scope of the bivalves in medicinal chemistry research and applications. The recently published reports on bivalve mollusks of marine and estuarine origin, as natural bioactive products and their applications as health foods, nutraceuticals, cosmetics and medications (Watanabe *et al.*, 2012) additionally explained the increased interest to explore these groups of invertebrates to develop functional food supplements and high value compounds for human health.

Mollusks are the predominant marine phylum that appeared 545 million years back comprising around 1,20,000 described and 2,00,000 undescribed species (Chapman 2009; FAO 2012). These species are abundantly available in the coastal, estuarine and brackish water environments. These groups of organisms are sessile (*L. mollis*, soft) preferably with a hard shell for the purpose of defense. The percentage distribution of prominent group of marine organisms *vis-à-vis* marine and estuarine mollusks were presented in the Figure 1.2. The largest class among the mollusks is Gastropoda, followed by Bivalvia. The later broadly includes clams, oysters and mussels. Among the mollusks, clams formed 27.2%, cockles 21.9%, scallops 15.7% and the remaining 4.2% has been constituted by other mollusks (Chapman 2009). The estimated annual landings of mussels, oysters and clams in India during 2015 were 92513 tonnes (CMFRI Annual Report 2015-2016), and are therefore, found as a valuable fishery resources in various parts of coastal regions of the southwest India. The southwest coastal waters of Arabian Sea are the main productive marine fishery sectors in India, signifying around 90% of the collective bivalve clam production (Gosling 2002).

Bivalve mollusks are important seafood resources in estuarine and coastal regions of the world constituting a predominant share in the international trade markets (Xie *et al.*, 2012). Among various classes of molluskan bivalves, clams occupied a major share of edible mollusks in the world (Murray and Burt 2001). In general, these species are repeatedly undervalued and regarded as by-catch or discard fishery resources (Gosling 2002), and have been widely exploited for their meat and shell for industrial purposes. However, they were not comprehensively investigated for their nutritional, biochemical and pharmacological properties. The importance of low value bivalve clams as potential health food has been recognized very recently and the medicinal properties of these species began to receive considerable attention. Due to

their ecological significance, nutritional and market values over different parts of the world, bivalve clams have acknowledged for substantial interest in recent years.



Figure 1.1.: The coastal and estuarine waters of India gifted with bivalve mollusks

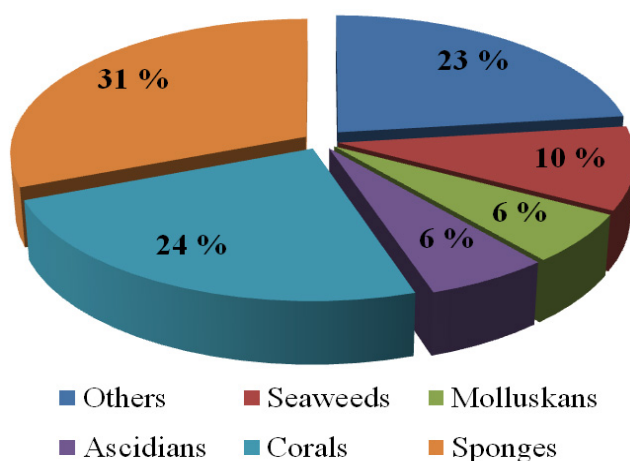


Figure 1.2.: The percentage share of marine and coastal mollusks among various classes of marine organisms

1.2. Biological potentials of secondary metabolites from marine and estuarine habitats

Over the previous decades, the investigations on the natural products from coastal, marine and estuarine environments have showed an increasing trend in the medicinal, nutritional and organic chemistry fields. The marine or estuarine creatures are inexhaustible producers of chemically or structurally distinctive and diverse bio-potent secondary metabolites, which have been originated through the varied biosynthetic mechanisms (Costa-Lotufo *et al.*, 2009). Benthic species (bivalves, gastropods, bryozoans, tunicates etc.) were capable of biosynthesizing specialized metabolites that were found to aid these organisms to survive in the adverse saline habitats. Marine and estuarine environments are an extremely complex ecosystem with broad pressure limits (1-1000 atm), thermal range (from less than freezing point in Antarctic areas to 350°C in deep hydrothermal vents), nutrient limits (oligotrophic to eutrophic) along with their broad photic and non-photoc regions. These extensive eco-chemical variations in the marine habitats have facilitated speciation at all phylogenetic ranks with various collections of life forms. In the view of enormous taxonomic varieties of the marine organisms, explorations related to the investigations of newer bioactive complexes from marine or estuarine habitats can be seen as an unlimited field. Of note is that the chemical compounds with pluralities of bioactive properties are present in the marine organisms as an adaptive mechanism to survive against the

extreme stress factors in the oceanic ecosystems, which cannot be found in terrestrial organisms. “*Poison kills the poison*”, a popular proverb is the base of researchers in the discovery of biomedical components or metabolites from aquatic organisms. Therefore, the marine living organisms were found to be an important source to develop high value compounds and pharmaceutically active leads (McClintock and Baker 2001). The rich variety of mollusk species belonging to marine and estuarine origin represents unexploited resources of bioactive compounds with valuable biomedical and pharmaceutical potencies, and there is a substantial exploitation of these compounds as pharmaceuticals and functional food supplements (Lordan *et al.*, 2011).

1.2.1. Importance of small molecular weight secondary metabolites

The low molecular weight metabolites (LMWM) are organic compounds from biological sources with molecular weight below 900 Dalton (Macielag 2011). Different terminologies are used to represent LMWMs. The pharmaceutical researchers categorized them as natural products (eg. antibiotics) and the biologists denoted them as primary and secondary metabolites. The primary metabolites are crucial for the growth and development of an organism and the secondary metabolites are required to survive in their unfavourable habitats. The LMWMs constitute a major share of bioactives in marine organisms, and were found to possess potential health benefits (Blunt *et al.*, 2015; Hadacek and Bachmann 2015).

The molecular size of LMWMs depended on the presence and absence of polar functional groups and it can be either volatile or non-volatile. These have been characterized by diverse combinations of functional groups, such as unsaturated bonds, oxygenated and/or other heteroatoms that define their chemical, structural and potential peculiarities (Hadacek and Bachmann 2015). The various classes of compounds, such as lipids, flavonoids, polyketides, terpenoids, steroids, tetrapyrroles and pyranoids are some common examples of small molecular weight secondary metabolites. Predominantly, these LMWMs were prominent in the sessile organisms, such as sponges, mollusks, corals, plants and in all types of microorganisms. The antioxidant LMWMs can scavenge free radicals, and depending on their chemical environment, it can act as pro-oxidant agents by reducing molecular oxygen. These molecules can also permeate through the lipid trans-membrane barrier with relative ease. The natural

components with small molecular weights can perform with more effectiveness and specificity in the protein receptor sites and have excellent platforms for natural product-based drug design and development (Clardy and Walsh 2004). Moreover, due to their greater diversity and specificity, the investigations of newer small molecular bioactive components from marine and estuarine organisms were found to be an unlimited field of research.

1.3. Pharmacological significance of antioxidant and anti-inflammatory properties

1.3.1. Free radicals and its relation to various life threatening disorders

The knowledge of reactive oxygen species (ROS) or free radicals are an important area of pharmaceutical research (Aruoma 2003). Notably, the free radicals are formed due to the normal metabolic processes in the body or due to external exposures, such as ozone rays, UV radiations, X-rays, pollutants, chemicals/metals from industrial wastes and by enzymatic/non-enzymatic reactions (Aruoma 1994). The incidence of unpaired electrons makes the free radicals extremely unstable and potentially reactive reductants or oxidants, which can donate or accept electron(s) from other molecules (Cheeseman and Slater 1993). The major oxygen bearing free radicals were hydrogen peroxide (H_2O_2), hypochlorite (ClO^-), hydroxyl ($\cdot\text{OH}$), superoxide anion (O_2^-) and singlet oxygen. These extremely reactive species were potentially capable to destruct the biologically significant molecules like lipids, DNA, proteins and carbohydrates in the nucleus along with cell membranes which leads to cell damage and cellular disorders (Young and Woodside 2001). The ROS reaction mechanisms and oxidative cellular damages were depicted in the Figure 1.3.-1.4.

Non-radical products ($\text{H}_2\text{O}_2/\text{HOCl}$) were also found to be powerful oxidizing agents in free radical induced reactions. The radical and non-radical species were generally accounted as “reactive oxygen species” (ROS) and the term “oxidative stress” was used to account for the damages in cellular membranes by mitochondrial respiratory chains (Poyton *et al.*, 2009). The redox active components in the intracellular environment (reducing medium) were present in reduced state (RH_2) by the autoxidation mechanisms that forwarding to the development of superoxide (O_2^-) radicals. The thiol-bound amino acid (cysteine), nucleotides, reducing sugars,

catecholamines etc. were easily subjected to autoxidation reactions (Carrell *et al.*, 1975) catalyzed by different metal ions along with enzymes (especially lipoxygenase, cyclooxygenase and myeloperoxidase) and these autoxidized products were the potential sources of free radicals (ROS) in the tissues (Bartosz 2003). The formation of hydrogen peroxide/peroxide radicals were catalyzed by superoxide dismutases (SOD) leading to the propagation of hypochlorite radicals by the oxidation reactions of Cl^- with hydrogen peroxide catalyzed by myeloperoxidases (MPO) (Halliwell and Gutteridge 2006; Kanofsky 1986). The hydroxyl radicals are formed in the biological systems by Fenton reaction between iron/copper ions ($\text{Cu}^+/\text{Fe}^{2+}$ and H_2O_2) (Kanofsky 1989). Overall, the formation of primary ROS, such as superoxides resulted in the propagation of other reactive oxygen species.

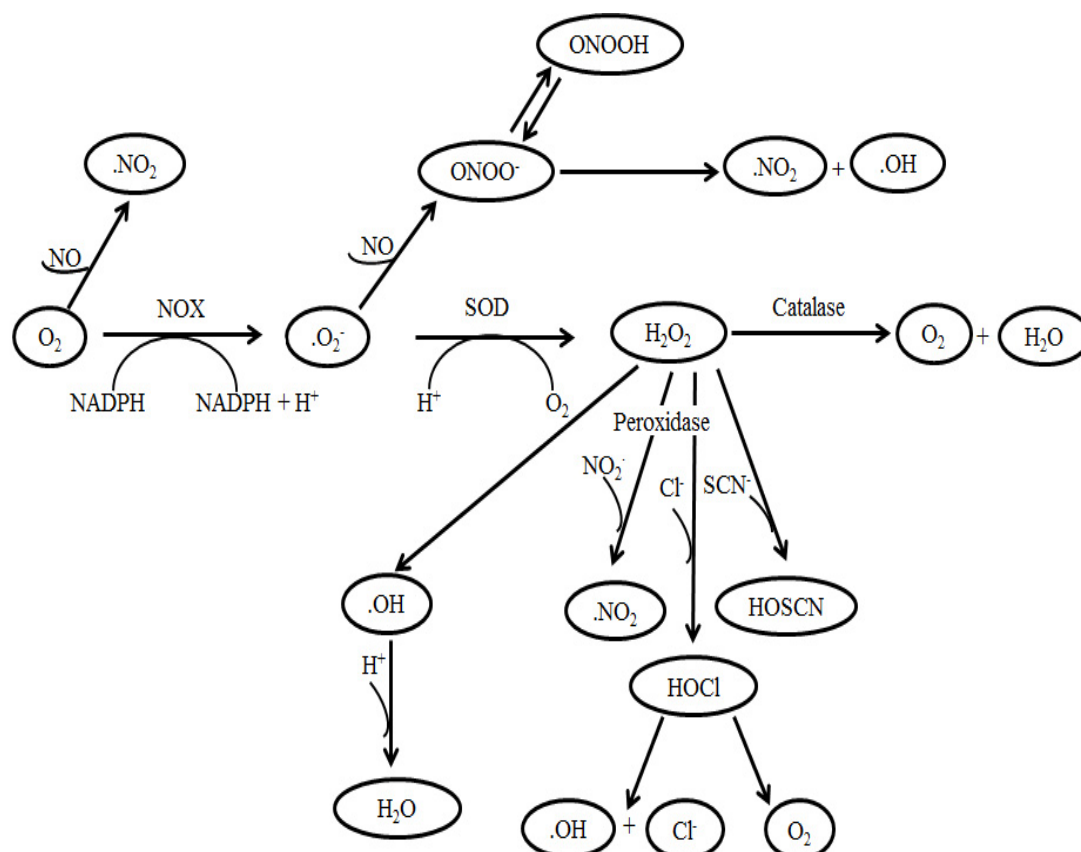


Figure 1.3.: Formation of reactive oxygen species and their reaction mechanisms. O_2 -molecular oxygen, H_2O_2 -hydrogen peroxide, NO -nitric oxide, H_2O -water, $\cdot\text{NO}_2$ -nitrogen dioxide, ONOO^- -peroxynitrite, $\cdot\text{O}_2^-$ -superoxide anion, HOCl -hypochlorous acid, ONOOH -peroxynitrous acid, $\cdot\text{OH}$ -hydroxyl radical, SCN^- -thiocyanate, HOSCN -hypothiocyanous acid, NOX - NADPH oxidase, SOD -superoxide dismutase

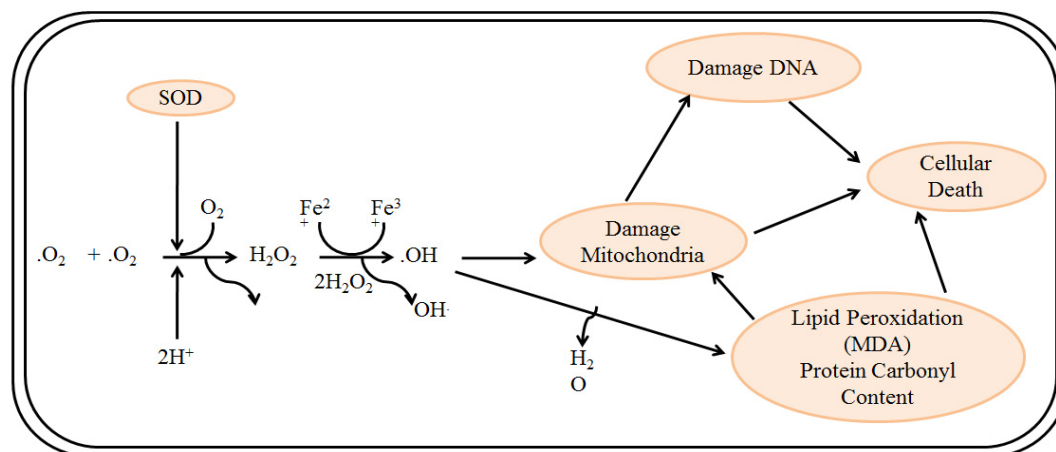


Figure 1.4.: The mechanisms of oxidative cellular damage. The formation of hydroxyl free radicals from hydrogen peroxide induces oxidative cellular damage, impairment of DNA, protein carboxylation, peroxidation of lipids and damages in mitochondria. These mechanisms lead to oxidative injury and finally to cell death

The unrestrained free radical generation is closely related to peroxidation of lipids and proteins. An imbalance in the production of free radicals and the antioxidant resistance mechanisms appeared to cause oxidative stress in the cell organelles. The ROS are also demonstrated as the mediators of inflammation, atherosclerosis, cancer, diabetes, gastric ulcers, hypertension and other age related problems (Stefanis *et al.*, 1997). The free radical associated diseases in humans were described (Figure 1.5.).

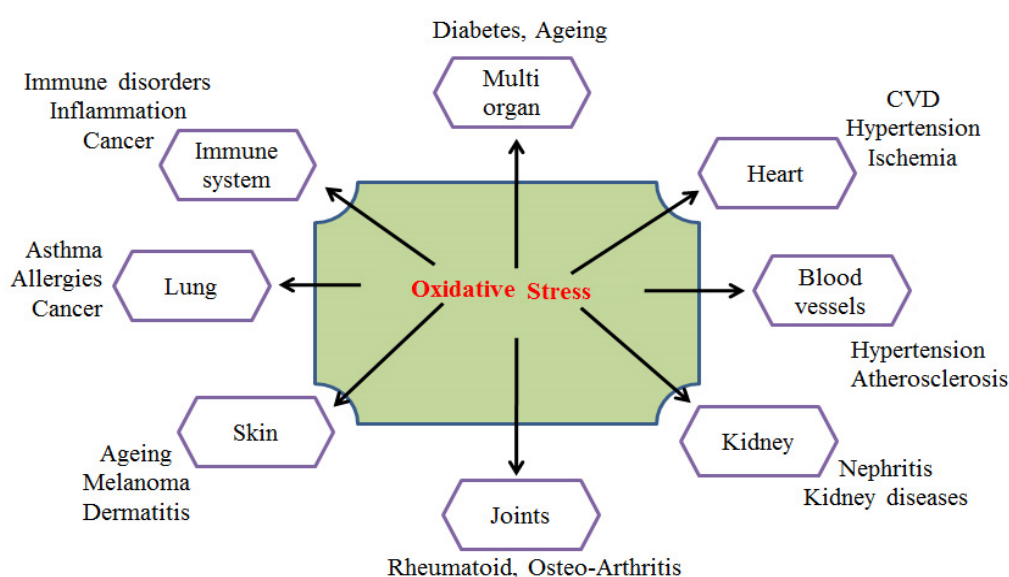


Figure 1.5.: The free radical associated diseases in human

The development and propagation of inflammations were manifested by the neutrophils, which is the major causes of free radicals at the pro-inflammation site (Mathy-Hartert *et al.*, 2002). The generation of ROS led to the signaling cascades that activate the formation of pro-inflammatory mediators, such as tumour necrosis factor, cyclooxygenases (COX-1 and COX-2 isoforms), lipoxygenases (5-LOX isoforms), cytokines, interleukins, inducible nitric oxide synthases (iNOS) and chemokines. These, in turn, found to produce more ROS and inflammatory prostaglandins in the damaged sites leading to oxidative stress induced inflammations (Ryan *et al.*, 2004). The sustained inflammatory responses can potentially lead to cell damages and ROS overproduction in the inflammatory cells. The chronic inflammation cause damages to DNA leading to cellular malignancy and cancer. The oxidative stress was too found to have major role in the development of diabetes, predominantly, type-2 diabetes. The diabetic complications were due to the variations in the catalases, SOD and glutathione peroxidase, which disposed the cells to oxidative stress (Lipinski 2001). The glucose or insulin levels along with dyslipidemia in diabetic patients form macroangiopathies were reported to cause oxidative stress and atherosclerosis (Giugliano *et al.*, 1995). Increase in the levels of ROS linked to non-enzymatic glycation of proteins, lipid peroxidation and glucose oxidation were contributed to diabetes and related complications. The ROS generated within the vascular wall, vascular/endothelial smooth muscles and in the fibroblasts, also appeared to have significant role in causing vascular inflammation. In normal circumstances, the controlled or low level ROS productions can act as a signaling agent for vascular contractions and relaxations. The ROS production from NADPH oxidase was reported to activate angiotensin-2 (Ang-2) in vascular tissues which resulted in hypertension. Ang-2 exerted harmful functional or structural damages through the NADPH oxidase which resulted in the ROS generation (Virdis *et al.*, 2011).

1.3.2. The biological defense against free radicals

The uncontrolled generation and propagation of radicals led to oxidative strain in the tissues. The antioxidant molecules are termed as “free radical scavengers” that can neutralize the free radical(s) by the transfer of electron(s) (Antolovic *et al.*, 2002) (Figure 1.6.). The word antioxidant has been defined as “any matter that removes or prevents oxidative damages in the targeted molecules” by Halliwell (2007), whereas

Khlebnikov *et al.*, (2007) defined as “any matter that directly prevents ROS or indirectly plays to up-regulate the antioxidant defenses or hinder ROS productions”.

The human body neutralizes the free radicals by using antioxidants, which were either supplied by external foods/supplements (exogenous) or naturally produced in the tissue organelles (endogenous). The antioxidant molecules also quench oxidative reactions related to ROS, thus counterbalancing the adverse effects of free radicals and free radical induced ailments (Sevanian and Ursini 2000). The antioxidant mechanisms against free radical induced damages were illustrated (Figure 1.7.).

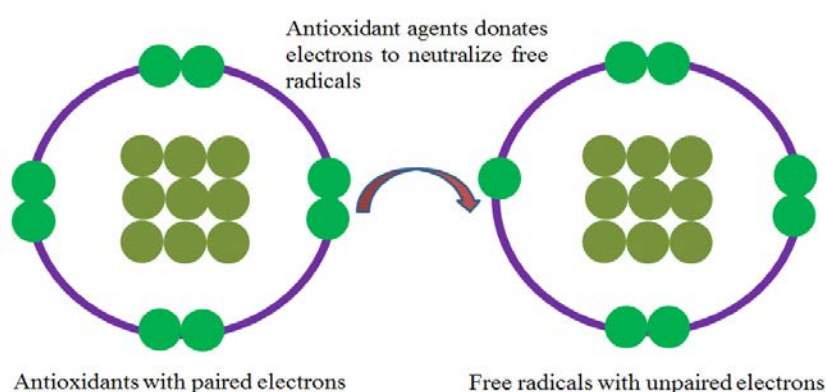


Figure 1.6.: Mechanism of neutralization of free radicals by antioxidant agents

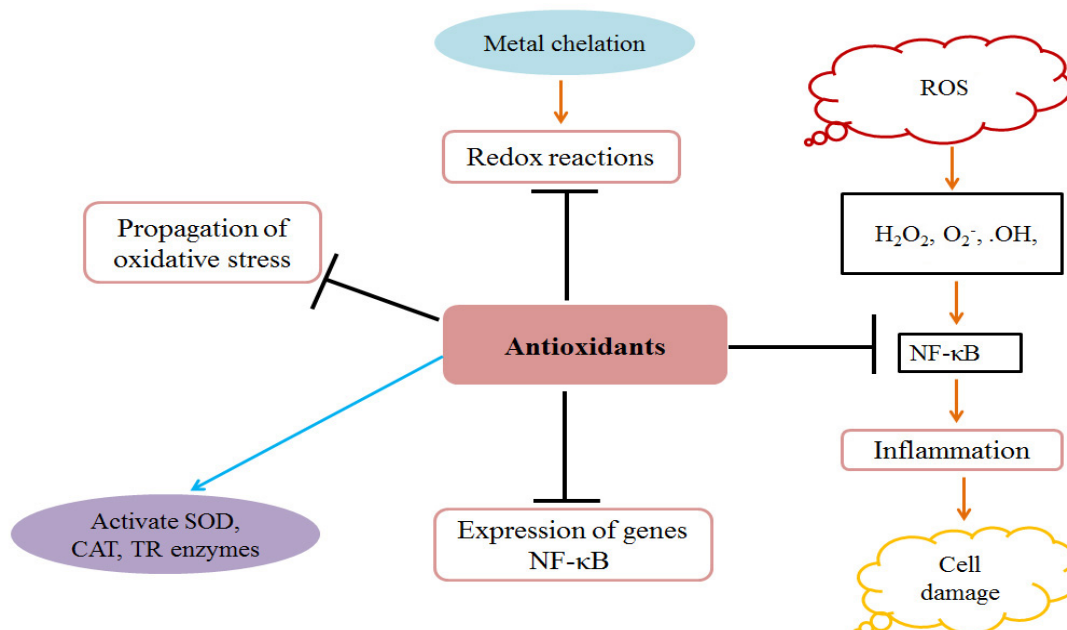


Figure 1.7.: Antioxidant mechanisms against free radical induced damages. The antioxidants inhibit the oxidative stress and constrain the nuclear factor kappa-enhancer

of activated B cell (NF- κ B), redox reactions, inflammations and interferes metal chelation. The antioxidants activate superoxide dismutase (SOD), thioredoxin reductase (TR) and catalase (CAT). ROS-reactive oxygen species, H_2O_2 -hydrogen peroxide, O_2^- -superoxide anion, $\cdot\text{HO}$ -hydroxyl radical

Antioxidant molecules mechanized in different ways, such as (i) preventing and maintaining the generation of ROS to least level, (ii) quenching of ROS by catalytic or non-catalytic molecules and (iii) repairing the impaired targets (Zhivotovsky and Orrenius 2011). The two categories of antioxidant systems were found to be enzymatic and non-enzymatic, which can synergistically alleviate or deactivate the free radicals before attacking the target cells. The most effective enzymatic antioxidants are superoxide dismutase, glutathione peroxidase, catalase etc. (Mates *et al.*, 1999), whereas non-enzymatic classes include ascorbic acid, tocopherol, thiols, carotenoids and flavonoids (McCall and Frei 1999). Endogenous antioxidants were potential free radical quenchers, even though, in certain circumstances, such as extreme oxidative stress, these endogenous molecules may not exhibit their efficacies. Therefore, the exogenous dietary antioxidant supplements (vitamins, minerals etc.) required for normal metabolic functions. Some antioxidants regenerate each other and develop an antioxidant network, which can effectively inhibit the production of ROS, thus the oxidative stress related diseases can be controlled (Kohen and Nyska 2002).

1.3.3. The importance of natural alternatives

Efficient antioxidant defense systems are necessary to scavenge, minimize or cease the formation and propagation of ROS. The free radicals are mostly connected with lipid peroxidation in foods resulting in the decreased nutritional qualities. Therefore, antioxidants were used in food/food ingredients to minimize their oxidative damages. Synthetic antioxidants, such as butylated hydroxyanisole (BHA), tert-butylhydro-quinone (TBHQ) and butylated hydroxytoluene (BHT) were used to prevent lipid peroxidation in foodstuffs and pharmaceutical principles to increase their shelf-life. However, these synthetic antioxidants were reported to be carcinogenic and their continuous uptake can potentially lead to organ damages (Schnitzer *et al.*, 1999). Therefore, the natural antioxidants have acknowledged for substantial consideration in

the recent days to overcome the adverse effects of synthetic agents. The commonly used natural antioxidants were ascorbic acid, vitamin K, tocopherol etc. Flavonoids are another group of antioxidants, which include flavanols, flavonols, isoflavonoids, anthocyanins, flavanones etc., and have been typically found in the fruits and plants (Rice-Evans *et al.*, 1996). Antioxidant phenolics, such as phenolic acids (rosmarinic, caffeic, gallic, protocatechuic), flavonoids (catechin, quercetin) and volatile oils (thymol, carvacrol, eugenol) have reported in literatures (Shan *et al.*, 2007). The natural pigments and carotenoids were comparatively unreactive, but it can form non-radical compounds that can terminate radical induced damages by forming non-radical adducts with toxic radical intermediates (Paiva and Russell 1999). The selenium composites (or sulfur containing seleno-amino acids particularly in marine organisms) do not directly act on free radicals, but reported to exhibit their activities by inhibiting antioxidant enzymes (glutathione peroxidase, metalloenzymes, etc.) (Tabassum *et al.*, 2010).

The inflammatory ailments were mostly cured by NSAIDs (non-steroidal anti-inflammatory drugs). These were linked with various side effects, such as gastrointestinal disorders leading to mild to severe damages of gastric and intestinal mucosa (Weil *et al.*, 1995). The NSAIDs deter inflammatory responses by interfering with cyclooxygenase (COX) pathways. In particular, the nonselective NSAIDs exert their effects through the quenching of constitutive COX-1 isoforms, and therefore, cause various side effects (Parente and Perretti 2003).

Synthetic agents were associated with adverse effects on various clinical parameters, and the researchers have been interested in finding natural anti-inflammatory agents and antioxidative formulations as substitutes of synthetics. Therefore, the target specified inhibitory agents from natural resources have gained importance in these years. Recently, antioxidant components from marine or estuarine organisms become a broad and widespread subject due to the safety concerns and increasing demand for nutraceuticals and functional food components.

1.4. Importance of mollusks and bivalves as potential resources of bioactive compounds

Antioxidant defense mechanism is an extremely well-maintained biochemical process that guards the organisms from destructive effects of ROS. The organisms have

been endowed with complex defensive mechanisms for biosynthesizing specialized bioactive metabolites to challenge the unfavourable oxidative stress conditions (Chainy *et al.*, 2016). The marine-derived nutrients and other bioactive components were found to possess potential functional foods and high value compounds with health benefits. Previous studies established that the bioactive components from mollusks have vital role in the development of functional health foods and pharmaceutical leads (Datta *et al.*, 2015; Hamed *et al.*, 2015).

The mollusks are important class of organisms representing about 23% of the total marine flora and fauna. Mollusks (phylum: Molluska) have been stratified into various classes, named as Scaphopoda, Monoplacophora, Aplacophora, Bivalvia, Polyplacophora, Cephalopoda and Gastropoda. Previous research findings characterized various groups of specialized metabolites in mollusks with antioxidant, anti-inflammatory, anti-diabetic, anti-hypertensive, anti-cholesterol, anti-microbial, anti-cancer and anti-HIV properties (Benkendorff 2010; Chakraborty and Joy 2017; Chellaram and Edward 2009; Nagash *et al.*, 2010; Schwartzmann *et al.*, 2001; Wei *et al.*, 2007). Small (low) molecular weight compounds (LMWC), such as alkaloids, carotenoids, steroids, phenolics and terpenoides were found to be the predominant groups of bioactive compounds in mollusks (Andersen *et al.*, 1985; Baunbaek *et al.*, 2008; Chattopadhyay and Pattenden 2000; Pettit *et al.*, 2005). The gastropod mollusk, *Dolabella auricularia* (Sea hare) (Yamada *et al.*, 2000) was reported for dolastatin analogues and *Elysia rufescens* was reported for anti-cancer agent, Kahalalide F (Lopez-Macia *et al.*, 2001).

Bivalves in the coastal or estuarine areas were reported as potential sources of *n*-3 PUFAs comprising docosahexaenoic acid and eicosapentaenoic acid. Moreover, the utilization of bivalve mollusks afforded as an inexpensive resources of vitamins, minerals and protein (Astorga-Espana *et al.*, 2007; Taylor and Savage 2006). Previous literatures have been established the antioxidative and anti-inflammatory functionalities of bivalve mussel (Chakraborty *et al.*, 2014a; Chakraborty *et al.*, 2016a). Recently, an anti-inflammatory nutraceutical, CadalminTM Green Mussel Extract (CadalminTM GMe) from *Perna viridis* (mussel) was developed to combat arthritis (Chakraborty *et al.*, 2014a; Chakraborty *et al.*, 2014b). Whitehouse *et al.*, (1997) have formulated the anti-inflammatory potency of the oil fractionated from Green Lipped Mussel (LyprinolTM)

against polyarthritis. The anti-tumour and immune-stimulating effects of *Crassostrea gigas* (Oyster) hydrolysates were studied previously (Wang *et al.*, 2010c).

1.5. Bioactive potentials of bivalve mollusks and with reference to marine and estuarine clams

Bivalve clams occupy a major share of the total edible mollusks in the world, yet they were not been explored for their biomedical and pharmaceutical properties (Murray and Burt 2001). The soft tissue bivalves have been adapted to adverse environments and believed that the cells of these sessile organisms were prolific producers of diverse classes of bioactive compounds and functional foods with biomedical significance. The antagonistic living habitats, ecological strain and filter feeding practices of bivalve clams were attributed towards their capacities to biosynthesize high value compounds (Goldberg 1975) with potential activities against various diseases (Lushchak 2011). The bivalve clams were exposed to extreme salinity, temperature and free radicals inducing noxious chemicals, even if, it's cellular damage was not reported and therefore, regarded as potential natural antioxidant candidates (Gonzalez *et al.*, 2015). The soft shell clam, *Mya arenaria* was reported to deter the oxidative stress conditions in response to adverse environmental circumstances (Abele *et al.*, 2002), although they were not extensively explored in greater details for their pharmaceutical, nutraceutical and biomedical applications (Mohite *et al.*, 2009). Earlier reports on bivalve clams were recognized their nutritional values as well as bioactive potentials (Pawar *et al.*, 2013; Tsai *et al.*, 2008; Wei *et al.*, 2007). Higher α -tocopherol (antioxidant) and α -carotene contents were reported in the digestive gland of Antarctic bivalve clam, *Laternula elliptica* and *M. arenaria* (Estevez *et al.*, 2002). Another carotenoid, fucoxanthin and its fatty acid ester derivatives were found in *Macrura chinensis* (Maoka *et al.*, 2007).

An anti-proliferative compound, Spisulosine ES-285 from *Spisula polynyma* (surf clam) and antioxidant chitosan from *Donax scortum* (clam) were characterized by extensive spectroscopic experiments (Hamann *et al.*, 1993; Sanmugam *et al.*, 2012). *Meretrix lusoria* (hard clam, Taiwan) was used as a remedy for hepatitis and liver ailments, and its metabolites were recognized to combat apoptosis in the HL-60 cell lines (Gauvin *et al.*, 2000; Pan *et al.*, 2007). An anticoagulant heparin-like compound

was isolated and characterized from the Italian clam, *Callista chione* (Luppi *et al.*, 2005) and from marine clam, *Anomalocardia brasiliana* (Cesaretti *et al.*, 2004). The iron chelating Ferritin-H unit from Manila clam, *Ruditapes philippinarum* was found to display potential anti-bacterial properties (Kim *et al.*, 2012). A novel antioxidant peptide was isolated and characterized from *R. philippinarum* with potential hydroxyl radical scavenging ability (Kim *et al.*, 2013). The peptides from hard clam, *M. lusoria* were recorded ACE-inhibitory activity (Tsai *et al.*, 2008) and polysaccharide from *Meretrix petechialis* was recorded anti-HIV activity (Amornrut *et al.*, 1999). These results explained that, the bivalve clams were potential natural sources of small molecular weight secondary metabolites with bioactive potentials, and therefore, it is imperative to discover potential bioactive molecules from the bivalve clams. The coastline of Kerala is bestowed with large assemblage of different bivalve mollusks which illustrated in the Figure 1.8.



Figure 1.8.: The coastline of Kerala bestowed with large assemblage of bivalve mollusks

1.6. Objectives

The rich diversity of edible bivalve clams in the coastal and marine waters of India represents an untapped reservoir of bioactive compounds with valuable pharmaceutical and biomedical use. Among various bivalve clams, the Corbiculid black clam, *Villorita cyprinoides* (family, Corbiculidae) and yellow-foot Venerid clam, *Paphia malabarica* (family, Veneridae) are the common seafood resources in the coastal waters of India (Suja and Mohamed 2010) (Figure 1.9.-1.10.). These low-valued bivalve clams are traditional health food items among the coastal populace of India and various regions of the World. However, there were limited research findings to characterize the bioactive principles in these organisms, and the significant attention to develop potential pharmaceutical/nutraceutical leads and health-foods received considerable attentions in the recent years.



Figure 1.9.: A collection site of bivalve mollusk, *V. cyprinoides*



Figure 1.10.: A collection site of bivalve mollusk, *P. malabarica*

The samples of *V. cyprinoides* and *P. malabarica* were collected from the estuarine waters of Vembanad Lake (9°35' N and 76°25' E) and Ashtamudi Lake (8°59' N and 76°36' E), respectively, situated on the southwest coast of India, bordering the Arabian Sea (Figure 1.11.).

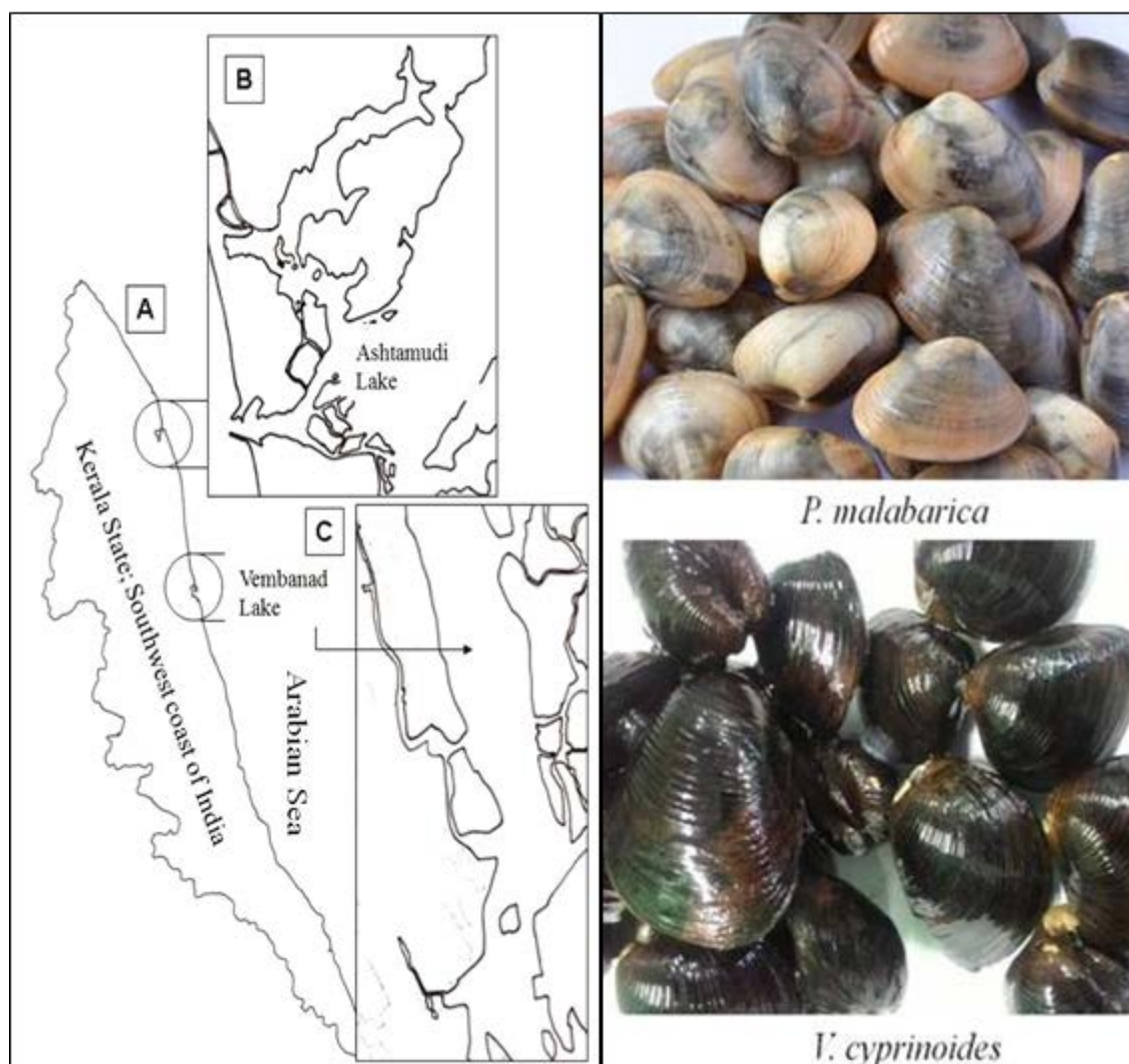


Figure 1.11.: Sample collection sites of the bivalve clams from the southwest coast of India bordering the Arabian Sea in Kerala State (A); *P. malabarica* from Ashtamudi Lake at 8°59' N and 76°36' E (B) and *V. cyprinoides* from Vembanad Lake (9°35' N and 76°25' E) (C) along with shell-on samples of *V. cyprinoides* and *P. malabarica*

The aim of current research points to the evaluation of nutritional qualities and bioactive potentials of bivalve clams *V. cyprinoides* and *P. malabarica*. The ethyl acetate-methanol (EtOAc:MeOH) solvent extract of these species were subjected for

repeated chromatographic fractionation and bioactive analyses. Furthermore, we aimed at the isolation of bioactive lead molecules with special reference to small molecular weight compounds from these bivalve clam species and their structural characterization using extensive spectroscopic analyses including mass, Fourier transform infrared (FTIR) and one/two dimensional nuclear magnetic resonance spectroscopic experiments (1D and 2D NMR). The bioactive potentials of newly described compounds from the candidate species were carried out by various *in vitro* analyses. The work also aimed to utilize different molecular descriptor variables to corroborate the structure-activity correlations of the titled compounds. Molecular docking simulations were carried out with special reference to inflammation (COX-2 and 5-LOX isoforms) and the binding energies obtained for the compounds were determined to understand their potential enzyme-ligand interactions. The hitherto undescribed bioactive compounds were reported in this study can be used as therapeutic leads and pharmacophore templates.

Based on this background, the objectives of the thesis are as follows:

- ❖ To develop an optimized procedure at laboratory for the extraction of anti-inflammatory and antioxidant metabolites from *Villorita cyprinoides* (Family, Corbiculidae) and *Paphia malabarica* (family, Veneridae) available in southwestern coast of India.
- ❖ To document the *in vitro* anti-inflammatory and antioxidant potentials of the crude extracts from these marine invertebrates.
- ❖ To purify the active principles with special reference to small molecular weight bioactives by bioassay-guided chromatography, and to elucidate the structures of purified molecules by spectroscopic techniques like infrared (IR), mass and extensive NMR techniques, in conjunction with 2D NMR experiments.
- ❖ To identify the molecular parameters of the lead molecules responsible for the bioactivities by quantitative structure-activity relationship analyses (QSAR).

1.7. Thesis outline

Based upon the above mentioned objectives, the present Thesis has been summarized into seven chapters. The importance of this study on the nutritional and bioactive potentials of mollusks and bivalves, with objectives were discussed in the introductory chapter (Chapter 1). The detailed review of the studies based on the significance of mollusks and bivalves as antioxidative and anti-inflammatory bioactive agents along with the characterized bioactive secondary metabolites were envisaged in the Chapter 2. Chapter 3 described the nutritional parameters and biochemical compositions of bivalve clams *V. cyprinoides* and *P. malabarica* to understand their nutritional qualities. Chapter 4 explained the bioactive potentials, specifically antioxidant and anti-inflammatory effects of the titled organisms and additionally reported their anti-diabetic and anti-hypertensive properties using different *in vitro* models. The isolation and characterization of small molecular weight secondary metabolites responsible for antioxidant and anti-inflammatory activities from *V. cyprinoides* and *P. malabarica* were described in the Chapter 5 and Chapter 6, respectively. Chapter 7 summarized the important research findings of the present study.

REVIEW OF LITERATURE

Contents

- 2.1. *Background*
- 2.2. *Oxidative stress and related health problems*
- 2.3. *Marine habitat as a productive resource of bioactive metabolites*
- 2.4. *Mollusks*
- 2.5. *Cephalopods*
- 2.6. *Gastropods*
- 2.7. *Bivalves*
- 2.8. *Conclusions*

2.1. Background

Bio-prospecting of previously undescribed natural products mainly from the marine or estuarine environment has been improved considerably over the previous few decades, resulting into an investigation of newer secondary metabolites (Blunt *et al.*, 2015; Blunt *et al.*, 2016; Faulkner 2000a; Faulkner 2000b). It has been stated that the marine/estuarine invertebrates particularly mollusks were the most prominent sources of natural products, and therefore, have been favourite choices of natural product chemists (Blunt *et al.*, 2013; Blunt *et al.*, 2014; Faulkner 1999). Newer natural compounds of marine origin have delivered promising bioactive compounds with previously undescribed structures/skeletons, and these could be used as promising nutraceuticals and therapeutic agents against various ailments (Lordan *et al.*, 2011). Large numbers of newer natural compounds have been reported for their bioactivities, and as candidate molecules for potential drugs, even though, only a few of them qualified as drug candidates. Nonetheless, the worldwide and widespread bio-prospecting attempts have not been stopped, and continuous search for chemically and structurally different secondary metabolites were increased. Several novel compounds of marine origin were added to the natural products library, and among which, mollusks have significantly contributed towards the discovery of compounds with potential pharmacological properties (Blunt *et al.*, 2015; Blunt *et al.*, 2016). During the past few years, various

bio-potential components have been isolated, identified and characterized from different marine or estuarine organisms, such as mollusks, bryozoans, sponges, tunicates, corals etc. The key objective of this review is to emphasize the bioactive components from marine/estuarine mollusks, particularly from bivalves.

2.2. Oxidative stress and related health problems

The normal metabolic processes in the body or external exposures leads to the formation of free radicals and the studies on free radicals were found to be useful in the proper management of disease and health (Aruoma 2003). Free radicals were highly reactive species and reported to damage cellular components leading to cellular disorders (Young and Woodside 2001) (Figure 2.1.). The uncontrolled free radical generation followed by lipid and protein peroxidations resulted in various health disorders. The imbalance between the free radical production and the mechanism of antioxidant defenses pointed out to oxidative stresses. The reactive oxygen species (ROS) were the mediators of various ailments, such as inflammation, atherosclerosis, cancer, diabetes, hypertension etc. (Stefanis *et al.*, 1997).

The free radical accumulation in the body was found to be the primary cause for inflammatory responses as described in various literatures (Lushchak 2011; Wilcox 2002). Therefore, it is anticipated that the antioxidant components can control the formation and propagation of free radicals. The lipid peroxidation caused by the free radicals transmutes fatty acids, lipoproteins and lipids to their corresponding hydroperoxides resulting in inflammatory responses (Camacho-Ruiz and Mendex 2010). The cell membrane phospholipid generates arachidonic acid (AA), a substrate for prostaglandin H_2 (PGH₂), by the action of phospholipase enzymes. The cyclooxygenases and lipoxygenases catalyzes the synthesis of prostaglandins (PGs) to thromboxane A₂ (TXA₂), prostaglandin F_{2 α} (PGF_{2 α}), prostaglandin E₂ (PGE₂), 5-hydroperoxyicosatetraenoic acid, 5-hydroxyeicosatetraenoic acid and leukotriene B₄ (Figure 2.2.). These were reported as mediators to develop inflammatory pathogenesis, and play a critical role to cause inflammatory disorders, such as arthritis (Morteau 2000). The antioxidants were reported to effectually hinder the pro-inflammatory enzymes, such as cyclooxygenases and lipoxygenases (Fernandes *et al.*, 2004) (Figure 2.3.). Therefore, it has been anticipated that free radical inhibiting agents are better anti-

inflammatory candidate molecules. The human metabolic system neutralizes oxidative stress by using antioxidants, which were either supplied by external foods/supplements (exogenous) or naturally produced in the tissue organelles (endogenous). The natural antioxidants like vitamin K, vitamin C (ascorbic acid), vitamin E (tocopherol) etc. were found to be effective radical scavengers. Flavonoids were found to be another group of antioxidants composed of flavanols, isoflavonoids, anthocyanins, flavanones etc. found in fruits and plants (Rice-Evans *et al.*, 1996).

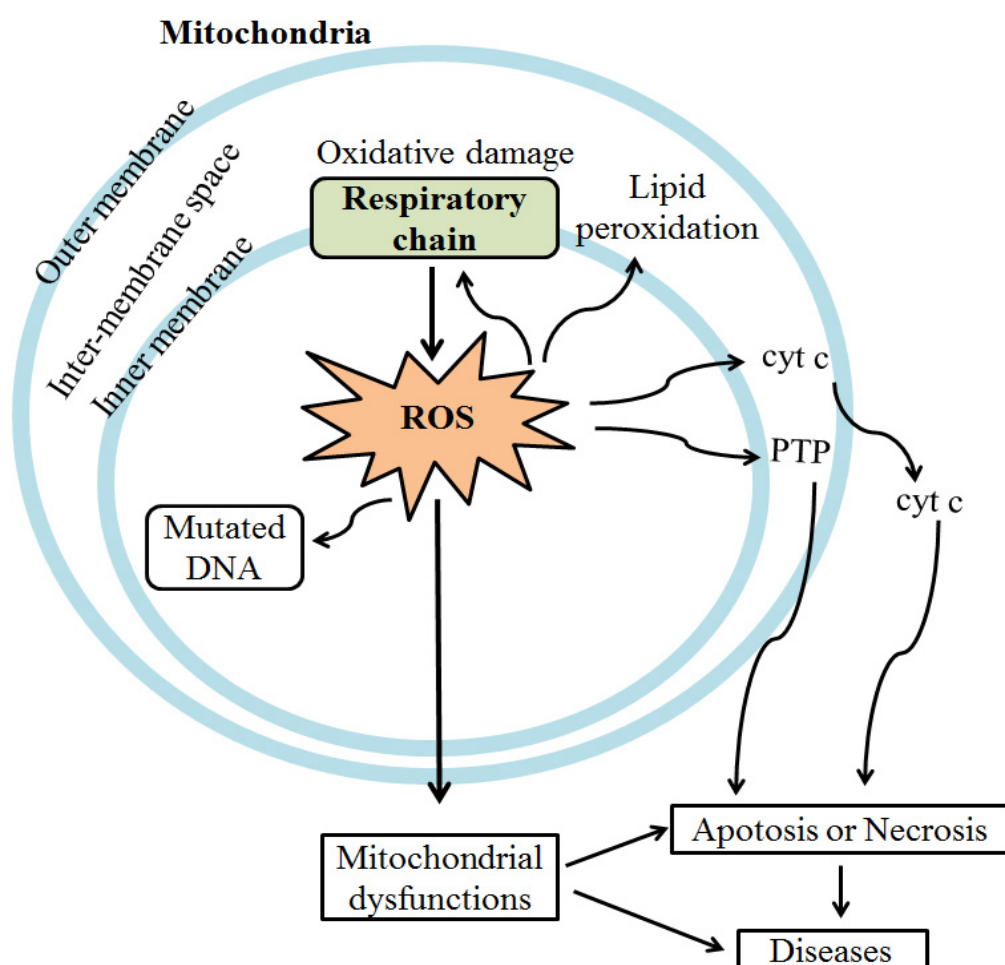


Figure 2.1.: A schematic representation of mitochondrial ROS production. The ROS produced by mitochondria can lead to oxidative damages in the protein, lipid and DNA. The damaged mitochondrial cells increase the release of inter-membrane proteins like cytochrome c (cyt c) by mitochondrial outer membrane permeabilization and likewise, cell death. Also, mitochondrial ROS leads to the initiation of mitochondrial permeability transition pore (PTP) resulting in tissue injury (Murphy 2009)

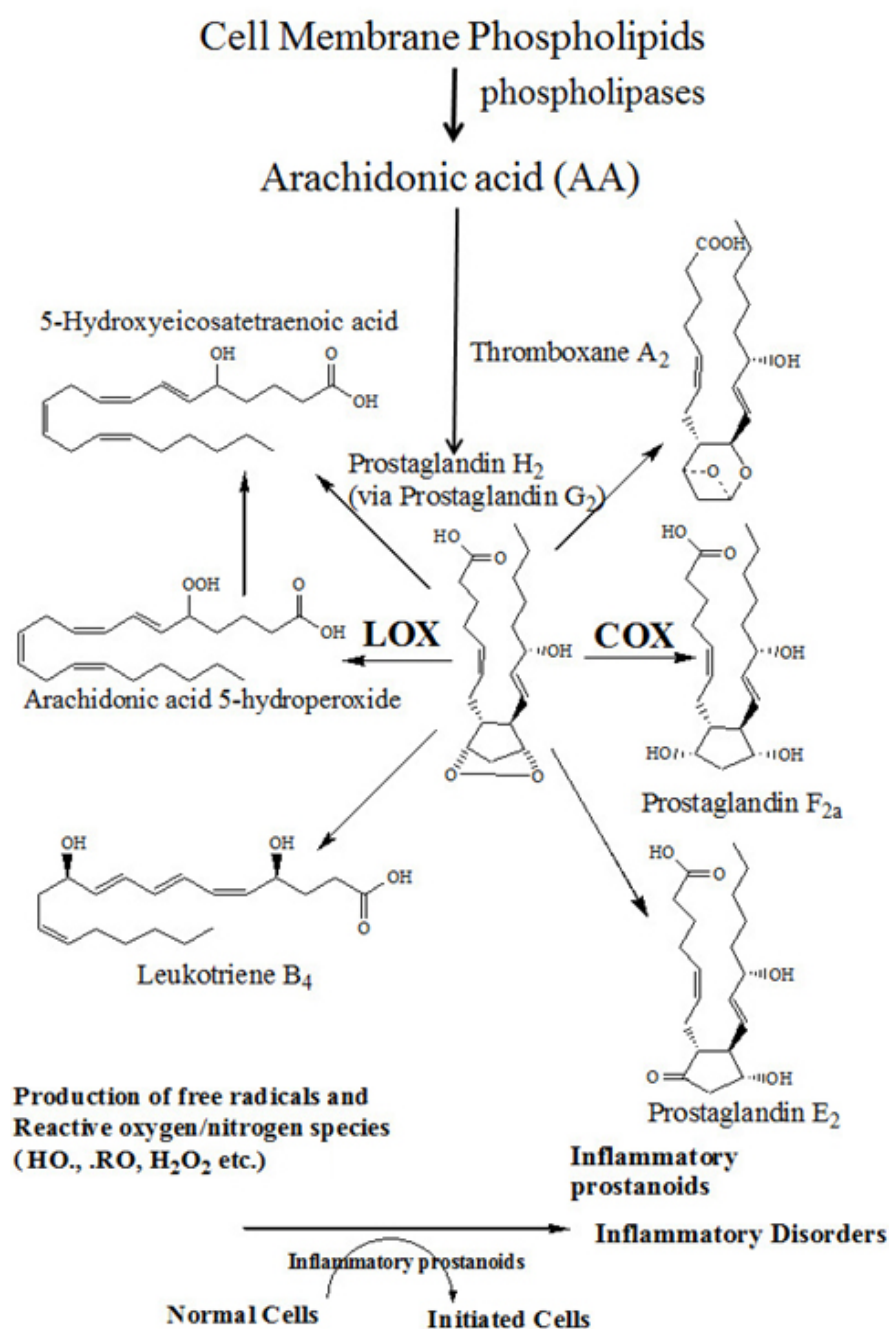


Figure 2.2.: Inflammatory mediators and mechanism of ROS mediated inflammatory responses. COX-cyclooxygenase, LOX-lipoxygenase, H₂O₂-hydrogen peroxide, HO.-hydroxyl radical

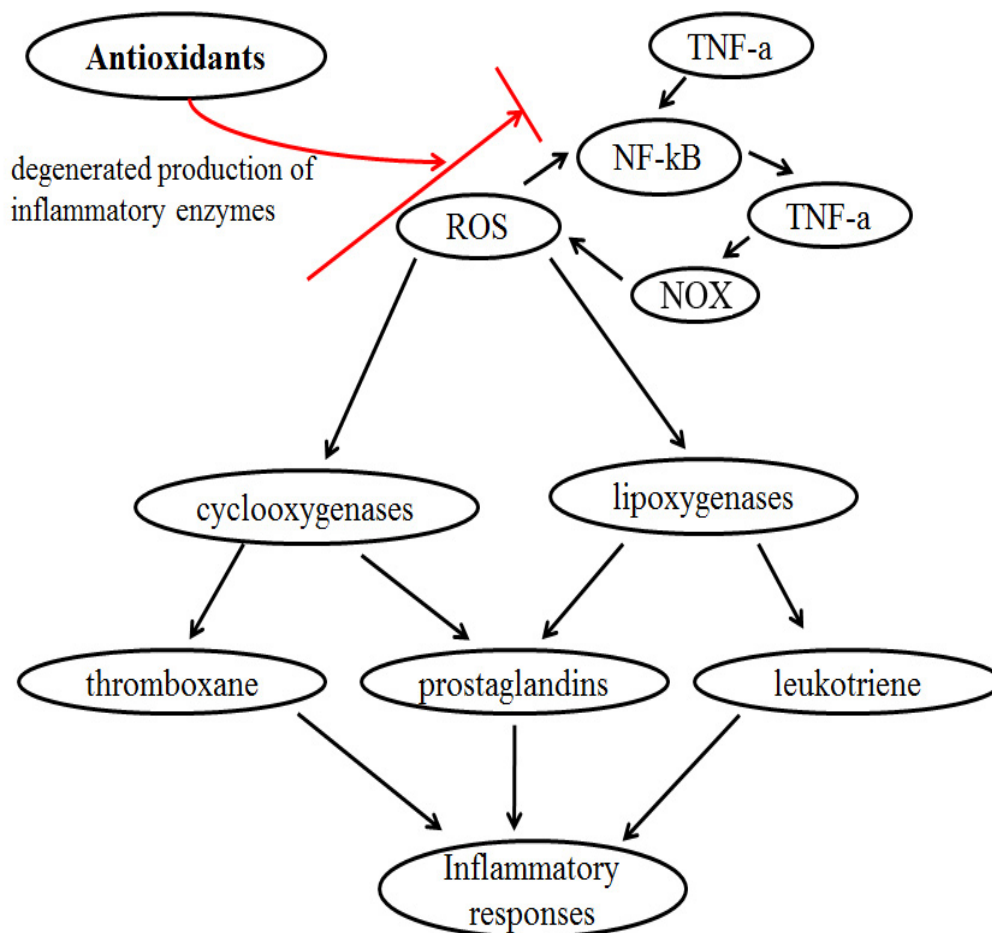


Figure 2.3.: Relationship among reactive oxygen species induced inflammatory responses and the role of antioxidants to inhibit the production of inflammatory enzymes. ROS-reactive oxygen species, NOX-NADPH oxidase, TNF-a-tumour necrosis factor alpha, NF-kB-nuclear factor kappa B

Synthetic antioxidants to oils/foods utilized to prevent lipid oxidations, although their adverse effects has been motivated the scientists to assess the natural compounds with bio-potential functionalities. Several synthetic antioxidants were reported to deter various intermediates of free radicals by reacting as oxygen scavengers and reduce free radical associated diseases. However, these synthetics were reported for serious side effects on multiple clinical parameters (Schnitzer *et al.*, 1999). The non-steroidal anti-inflammatory (NSAIDs) medications are common suppositories against inflammations. However, usage of these drugs was not safe due to the increased risk of gastrointestinal (GI) and cardiovascular (CVD) complications. The NSAIDs has reported to injure the mucosal layers of gut by reducing COX-1 derived prostaglandins

causing ulcers (Sostres *et al.*, 2010). Therefore, there is an increasing trend to search for natural alternatives to overcome the side effects of synthetic agents and to develop bioactive lead molecules with greater selectivity profiles. Safety of natural agent is not assured, even though, there is some ease to know that these were extracted or purified from natural resources. Recently, bioactive agents from nature become a widespread and broad subject of research due to the increasing demand for functional food and nutraceuticals as natural therapeutic agents against various life threatening diseases.

2.3. Marine habitat as a productive resource of bioactive metabolites

Marine natural product chemistry (MNP) research was started during the 1970's and rapidly developed during the 1980's before being full-fledged in the recent decade from 2000-2015 (Blunt *et al.*, 2016; Faulkner 2000b). There were several publications available and it is very difficult to select individual papers that significantly impacted to the MNP field. The MNP chemistry has considerably influenced other fields, such as pharmaceuticals, nutraceuticals, cosmetics, functional foods, drug developments etc. (Faulkner 2000b). The combinations of marine biomedical, marine chemical ecology and marine toxins have cumulatively substantiated the marine natural products with unique identity (Faulkner 2000a). The increase in the number of identified or published compounds from the year 1965 to 2005 were compared in the Figure 2.4., which envisaged the increased interest in the field of MNPs (Blunt *et al.*, 2006). However, the investigations have not led to prominent pharmaceutical or medicinal candidates, although there is a probability that many marine compounds could be recognized in the drug level.

Marine habitats harbour more than 2,00,000 identified invertebrates and algae species, although, a greater number of species were yet to be identified (Gosling 2002; Gosling 2015). It is significant that the marine ecosystem is an untapped reservoir of novel components with therapeutic potentials, and therefore, has been a key attraction of natural product chemists due to its comparatively unexplored biodiversity than the terrestrial systems. The main resources of bioactive metabolites with pharmaceutical potentials were algae, mollusks, bryozoans etc. Reviews on various marine organisms, including bio-prospecting of mollusks, sponges, bryozoans, algae etc. were common and the classification of marine natural products among various phyla (Figure 2.5.).

Most of the marine organisms are sessile or soft bodied, and therefore, they have to protect themselves from the unfavourable marine ecosystems, such as salinity, temperature and attack of predators and pathogens in their habitats. Evolutionally, the response to this unfavourable condition is the development of in-built defense mechanisms leading to the generation and accumulation of biologically active metabolites. The distribution of various marine organisms evaluated for chemical investigations and natural product isolations over the period from 1971 to 2015 among different phyla was plotted in the Figure 2.6. (Blunt *et al.*, 2016). The diverse chemical compounds, which were biosynthesized by the organisms for defense purpose other than basic metabolic requirements, defined as secondary metabolites. The compounds include alkaloids, peptides, terpenoids or steroids which provide natural immunities to the organisms. Likewise, the marine ecosystem encompasses a wide array of organisms with unique bio-potentials and bioactive metabolites. Moreover, it is one of the greatest underutilized biological resources and the search for newer bioactive compounds from marine/estuarine ecosystem is found to be an unlimited field of investigation and delight for natural product chemists. It is appropriate to state that MNPs have had an important impact on chemistry, pharmaceutical and drug development areas over past few years, and found to be valuable sources for newer bioactive templates in upcoming years.

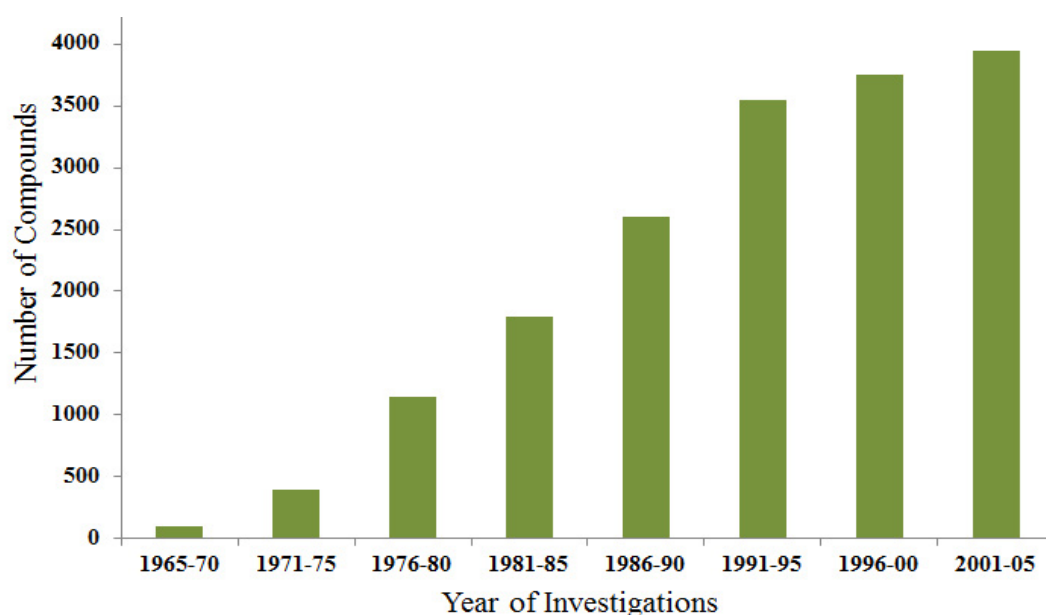


Figure 2.4.: Number of marine natural products over the period 1965 to 2005 (Blunt *et al.*, 2006)

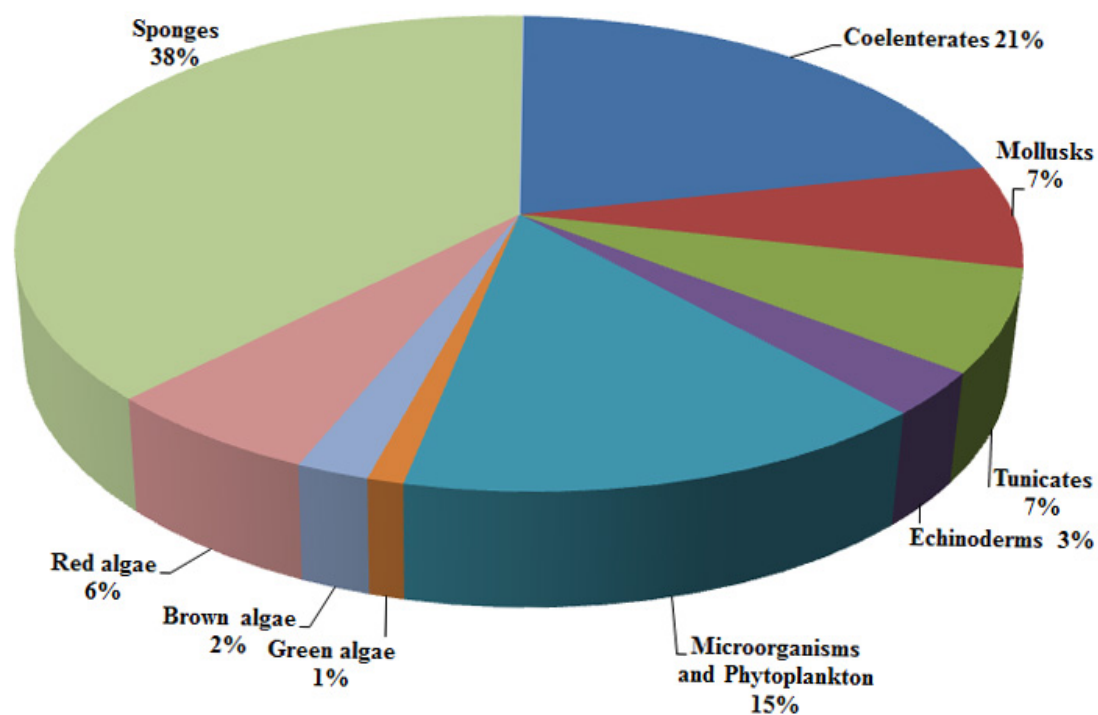


Figure 2.5.: Distribution of marine natural products by phylum (Blunt *et al.*, 2003)

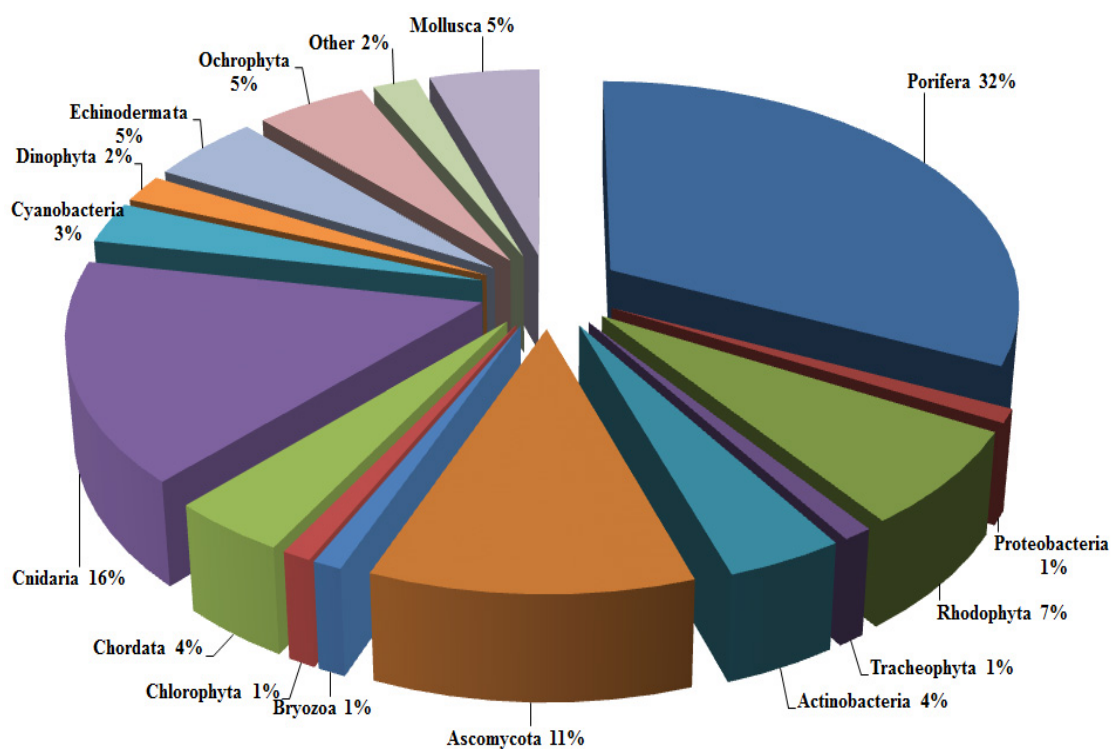


Figure 2.6.: Distribution of marine organisms among phylum collected for natural product isolations over the period from 1971 to 2015 (Blunt *et al.*, 2016)

2.4. Mollusks

The phylum Molluska represents as one of the main and diverse classes of marine animals, and which contributed significantly greater to the total available marine fish catches in the world. These are soft bodied organisms as described by the Latin word “*Molluscus*” which means “soft”. These soft, sessile and heterogenous classes of animals were protected with shells to escape from pathogens and predators. The mollusks were found to be the valuable sources of food, shells, medicines, dyes etc. from time immemorial. The compounds from mollusk species were reported a significant role in the production of functional foods and nutraceuticals, which considered as a combination of nutritional and pharmaceutical elements (Herbert *et al.*, 2003; Lordan *et al.*, 2011). However, the scientific investigations were comparatively lesser to understand the health benefits of mollusks. It is significant to record that the coastal populace of different parts of the world trusted on these animals as their livelihood since ancient times, whereas the molluskan shells were used by them to make various tools, decoratives and symbols (Benkendorff 2010; Brusca and Brusca 1990).

The unfavourable climate and habitats were developed a definite adaptation mechanisms in the coastal and marine mollusks to defend themselves from the adverse conditions, and thus, many bioactive metabolites were evolutionally developed in these soft bodied organisms. Various pathogenic organisms living in the marine environment tend to attack the molluskan species distributed in the Sea surface, although these species were appeared to be resistant towards the microbial invasion. It is also to be noted that mollusks do not have acquired immunological systems, and therefore, it might have developed a substitute defense pathways to defend themselves in the coastal or marine ecosystems (Hooper *et al.*, 2007). Under the extreme pressure of competitions, a wide variety of metabolites have been evolved by the mollusks, and these secondary metabolites have used as a part of their communication systems, predation and defense (Cimino and Gavagnin 2006). These species was found to synthesize various primary metabolites, such as sugars, lipids, amino acids etc., and secondary metabolites, such as alkaloids, terpenoids, steroids, polypropionates etc. with bioactive potentials (Blunt *et al.*, 2015; Blunt *et al.*, 2016). Mollusks were regarded as one of the key resources to develop valuable bioactive compounds with specific anti-tumour, anti-hypertensive, anti-microbial, anti-HIV, anti-inflammatory, anti-diabetic

and antioxidant potencies (Anbuselvi *et al.*, 2009; Benkendorff *et al.*, 2011; Chellaram and Edward 2009). The compounds identified from these species exhibited bioactivities within the nanomolar range, and therefore, can be developed as potential drug candidates or lead compounds (Cimino and Gavagnin 2006). Previous studies established that the chemical defense mechanisms/systems were differently evolved and modified in different types of marine organisms. This apparently resulted in the formation and production of different and distinct chemical structures with bio-potentials within the various classes of mollusks under the extreme environmental conditions (Cimino and Ghiselin 2001). The objective of the review is to investigate and understand the existing studies/literatures on the nutritional, bio-potential and the characterized bioactive secondary metabolites from molluskan species and to enhance our knowledge of chemistry of mollusks. This assessment will help to improve the upcoming natural product investigations.

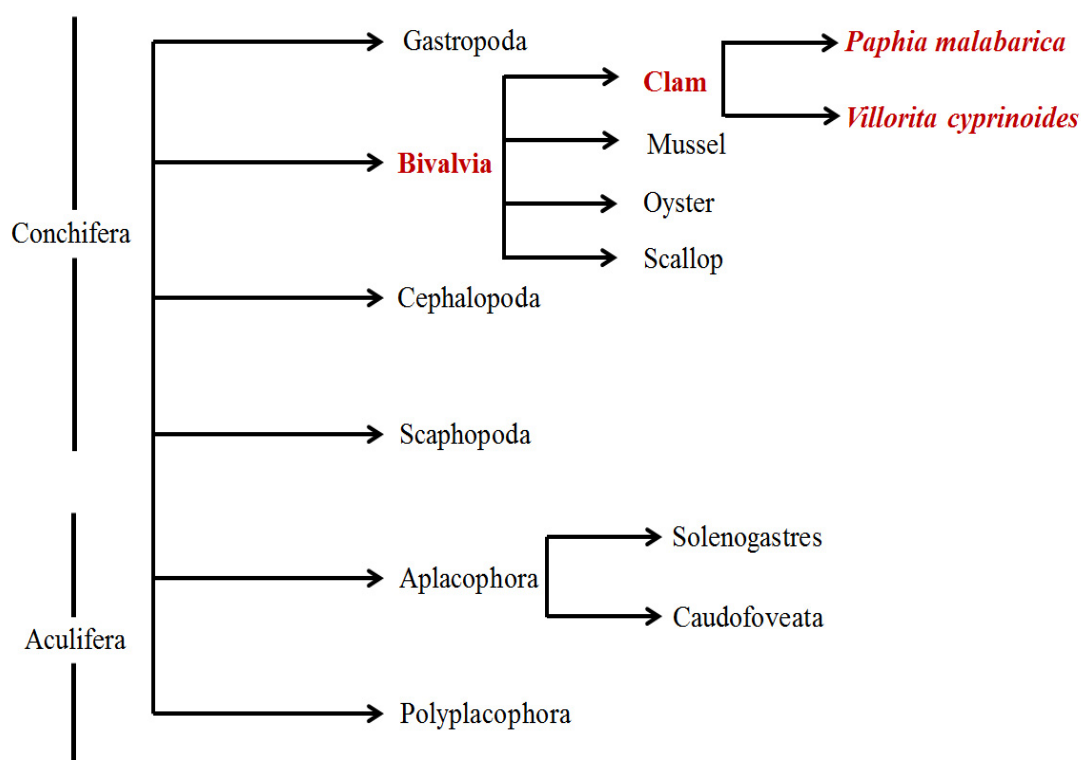


Figure 2.7.: Schematic representation of the distribution of molluscan phylum

Mollusks are one of the largest and utmost varied classes of marine and estuarine organisms. Indian coasts have broad ecosystems such as lagoons, mangroves,

rocky regions and coral reefs in which rocky and corals regions were flourished with molluskan fauna. The largest phylum Molluska enclosed 50,000 described mollusk species, and as numerous as 200,000 living species, most of which were of marine origin. They feed on various food items, whereas their size ranged from big squids and clams to small snails with millimetre long. Mollusks are classified into seven classes, which belonged to Aplacophora including two classes, such as Solenogastres (~250 species) and Caudofoveata (~150 species), Polyplacophora (~100 species), Monoplacophora (~30 species), Scaphopoda (~600 species), Gastropoda (> 100,000 species), Bivalvia (~9200 species) (Huber 2010) and Cephalopoda (~1000 species) (Gosling 2015). Among these, gastropods are the largest and diverse class of organisms whereas, bivalves are the second largest and cephalopods are the most organized and specialized groups (Gosling 2002). Herein, we have discussed these three major classes of organisms, particularly the importance of bivalve class (Figure 2.7.).

2.5. Cephalopods

The class Cephalopoda symbolizes the greatly evolved, organized and edible class of phylum Molluska, which distributed throughout the world. These were purely coastal and marine organisms, whereas most of them were reported as free swimming shallow water predators. These species lacks calcium carbonate shell as protection with a compartmentalized structure (Gosling 2002). Cephalopods include squids, octopods, cuttlefishes etc., and these were reported to be single-time spawners with short life span, and therefore, adapted a rapid growth (Boyle and Rodhouse 2005). These species plays an important role in the exploited fisheries sectors all over the world, and began to receive more interest due to the cumulative export demands (Kreuzer 1984). This might be attributed due to the enhanced alertness about their dietary potentials (Okuzumi and Fujii 2000). Deteriorating catches of groundfishes have tempted to practice the potential non-traditional cephalopod species. During the last forty years, cephalopod stockings increased from 1 million metric tonnes (1970) to 4 million metric tonnes (2010), whereas the share of squids, cuttlefishes and octopuses in world's fish market increased to 4% (2010) with greater market price. The countries like Spain, Japan, Korea, Italy and Hawaii have been the major consumers of cephalopods (FAO 2012). As a result of their nutritional and market values along with the bioactive potentials, cephalopod

fishery demonstrated a cumulative interest in the recent years (Lee 1995). The photographic representation of commonly available cephalopods in the southwestern coastal regions of Arabian Sea, bordering India illustrated in the Figure 2.8.



Figure 2.8.: Photographic description of cephalopods

2.5.1. Nutritional importance of cephalopods

Cephalopods were found to be rich in protein content, and 80% of their total fleshy material was considered to be the edible portion for human consumption (Chakraborty *et al.*, 2016c; Lee 1995). The edible portions of these species were accounted for *n*-3 polyunsaturated fatty acids, minerals, vitamins along with essential amino acids including antioxidative selenium (Zlatanov *et al.*, 2006). Several reports were available on the biological description, occurrence, proximate composition and nutritional qualities of the cephalopod species (Okuzumi and Fujii, 2000; Pierce *et al.*, 2008). The compositions of fatty acid profiles and its relation to seasonal or annual variations studied for cephalopods (Ozyurt *et al.*, 2006). As compared to marine finfishes, cephalopods found to be lesser in lipid content (Njinkou *et al.*, 2002). The previous study of *Sepia pharaonis*, *Amphioctopus neglectus* and other species of

cuttlefish, octopus and squids exhibited prominent lipid contents (> 2 mg/100 g), which were lesser than those recorded in the edible portion of the marine fishes (Chakraborty *et al.*, 2014c; Chakraborty *et al.*, 2016c; Zlatanov *et al.*, 2006). The edible portions of cephalopod species, *Uroteuthis duvauceli*, *Sepiella inermis*, *S. pharaonis*, *Cistopus indicus*, and *A. neglectus* found to possess considerable amounts of PUFAs (Chakraborty *et al.*, 2016c; Ozyurt *et al.*, 2006). The long-chain C_{20} - C_{22} PUFAs were found to be key biochemical markers of cephalopods, whereas C_{20} - C_{22} FAs like docosahexaenoic acid and eicosapentaenoic acid were described to be vital for various human metabolic and physiological functions, and were predominant in cephalopods. Long chain n -3 PUFAs were essential to prevent the occurrences of numerous health concerns, such as cardiovascular illnesses, type-2 diabetes, hypertension, inflammation, asthma and cancer (Simopoulos 2009). As stated by Boucaud-Camou (1990), cuttlefish was composed of water (81%), protein (16.1%), lower lipids (1%), and with no carbohydrates. Previous studies described that the cephalopods were rich source of protein, EPA, DHA, micro and macro minerals, vitamins, amino acids, and therefore, this species can be regarded as effective health foods (Chakraborty *et al.*, 2016c).

2.5.2. Bioactive potentials of cephalopods

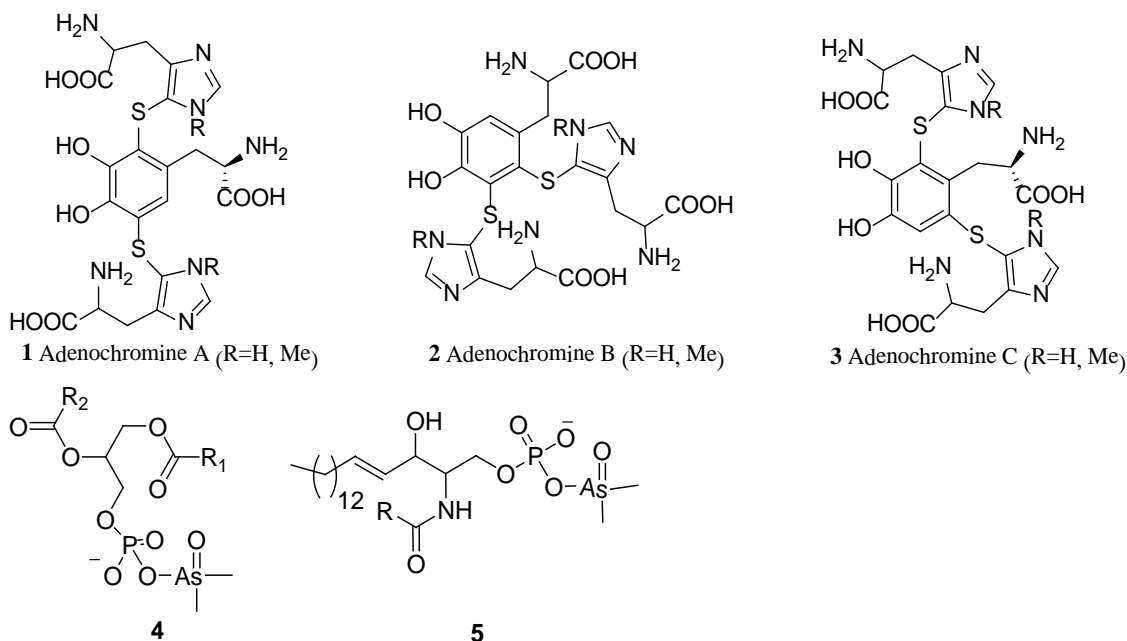
The cephalopods were considered as significant resources of bioactive metabolites representing various bioactive potentials (Chakraborty *et al.*, 2017a; Chakraborty and Joy 2017). However, these species were not explored in significant details with respect to their bioactivities. The knowledge of bioactive compounds from these organisms will develop newer perspectives to harvest potential pharmacological benefits. Cephalopods believed to possess unique biological compounds or secondary metabolites at higher concentrations. Most of these species lacks outer protective shell and found to produce venom and liquid ink materials to defend themselves from the predators (Cooke *et al.*, 2015). Cephalopods comprised of structurally and chemically diverse and distinct anti-stress metabolites, therefore, can be considered as important health food items and also, can be used for formulating various nutraceuticals to combat diabetes and inflammatory diseases (Chakraborty and Joy 2017). The C_{20} - C_{22} n -3 fatty acids present in these species were found to be accountable for their anti-inflammatory activities (Russo and Tringali 1983). Cephalopods including squid and octopus have

broad physiological actions, such as immune and anti-inflammatory responses along with neural function and reproduction (Miliou *et al.*, 2006). The antioxidant/anti-hypertensive potencies of *S. pharaonis*, *U. duvaucelii*, *C. indicus*, *S. inermis* and *A. marginatus* based upon spectroscopic evolution were previously reported (Chakraborty *et al.*, 2017a). The ink extract of *Sepia officinalis* displayed anti-inflammatory and antioxidant potentials (Soliman *et al.*, 2015). The cephalopod species *Paraoctopus limaculatus* (octopus) studied for their anti-mutagenic and anti-proliferative effects (Moreno-Felix *et al.*, 2013). A number of investigations on antioxidant potentials of tissues and ink extracts of cephalopods were published (Choi *et al.*, 2015). The anti-hypertensive (angiotensin converting enzyme-1 (ACE-1) inhibitors) components were reported from squids, cuttlefish and octopus (Balti *et al.*, 2015; Chakraborty *et al.*, 2017a; Lin *et al.*, 2012). Various anti-tumour metabolites were isolated from squid (Chen *et al.*, 2010), octopus (Karthigayan *et al.*, 2006) and cuttlefish (Senan *et al.*, 2013).

Remarkably, advanced efforts have been aimed at the small molecular bioactive compounds and their ability to inhibit different target sites. This will lead towards the identification of specific regions/moieties in the compounds, which were responsible for particular therapeutic potentials. Likewise, the preparations or formulations from the cephalopods will occupy a key place in the wider range of pharmaceutical industry (Besednova *et al.*, 2017).

2.5.3. Secondary metabolites from cephalopods

There are limited research works and fewer publications on the biologically active molecules from the cephalopods. Most of the works were carried out on their physiology, bioluminescence, mimicry and ink productions (Kornprobst 2010). The pigments, adeno chromines **1-3** were discovered from *Octopus vulgaris* (Ito *et al.*, 1976; Prota *et al.*, 1977). Arsenolipids **4-5** were reported from squid, *Todarodes pacificus* (Ninh *et al.*, 2007).



Cephalopods used in wide range of traditional medications, even though chemical investigations were relatively lesser (Benkendorff 2010). Sepia ink used as a remedy for depression in China (Cazalet 2007). The cephalopod, *Spirula spirula* is an expensive marine mollusk as traditional medication in the Durban market (Herbert *et al.*, 2003). Cyclophosphamine extracted from squid ink was a well-known chemotherapeutic drug (Zhong 2009). Cytotoxic tyrosinase (Russo *et al.*, 2003) and peptides (from ovarian jelly) were isolated from *Sepia officinalis* (Bernay *et al.*, 2006). The novel cardioactive peptides were purified from brain of *Octopus vulgaris* (Kanda and Minakata 2006) and Japanese octopus, *Octopus minor* (Iwakoshi *et al.*, 2000). Astaxanthin and its ester derivatives were the major carotenoids in octopus and cuttlefish species (Maoka *et al.*, 1989).

2.6. Gastropods

Gastropoda is the largest class with regard to the number and diversity of species. Among all other classes of mollusks, gastropods have been mostly investigated and reported for their bioactive secondary metabolites (Kornprobst 2010). The photographic representation of commonly available gastropods was illustrated in the Figure 2.9.



Figure 2.9.: Photographic description of Gastropods

Gastropods were classified into three sub-classes, such as Prosobranchia (strongly wound within the shell), Opisthobranchia (weakly wound within the shell or shell-less) and Pulmonata (they can breathe air through the lungs), which includes Sea slugs, Sea snails, abalones, Sea hares, etc. Edible gastropods collected throughout the world for their flesh, which was found to be the essential sources of economic value to world's fishery sectors. Majority of molluskan fishery promoted by cephalopods and bivalves whereas, gastropods shared lower than 2% of whole yield (FAO 2015). Even though, some of the gastropods have reported comparatively higher economic and commercial values (Leiva and Castilla 2002).

2.6.1. Nutritional importance of gastropods

The gastropods are gaining more significance among mollusks during the recent years due to their commercial potential. Subsequently, there is an increasing requirement for the supply of underutilized species. Previous studies were established that the predator gastropod whelks possessed higher protein content than the herbivore

gastropods. The predatory carnivore gastropods, such as *Chicoreus ramosus* (Ramesh and Ayyakkannu 1992), *Hexaplex trunculus* (Zarai *et al.*, 2011), *Thais haemastoma* (Belisle and Stickle 1978), *Rapana venosa* (Celik *et al.*, 2014) were reported for their higher protein contents. The herbivorous snails were also good candidate source of protein. The nutritional profiles of gastropods varied according to the type of organisms, body parts, seasonal changes, collection sites, spatial changes, temporal variations and reproductive cycles (Smoothey 2013). Lipid content was found to be lesser in the predatory gastropods than those in herbivorous (Belisle and Stickle 1978; Lah *et al.*, 2017; Ramesh and Ayyakkannu 1992). Visceral lipid content was greater when compared to foot tissue and it has been recommended that visceral tissues were the lipid storing part of gastropods. Usually visceral tissue in larger gastropods not recommended for consumption and foot tissues were typically consumed by the people (Saito and Aono 2014). Therefore, previous studies concluded that foot tissues were suitable for human diet due to higher protein and lower lipid contents (Lah *et al.*, 2017). The fatty acid composition especially, PUFA contents along with DHA and EPA was previously reported in various gastropods particularly, in snails (Brazao *et al.*, 2003; Lah *et al.*, 2017; Morais *et al.*, 2003). Gastropods were found to possess various minerals, such as potassium, sodium, selenium, zinc, iron and sulphur (Lah *et al.*, 2017). Also, the essential amino acid components reported to be considerably higher in gastropods such as *Chicoreus virginineus*, *Phalium glaucum*, *Rapana rapiformis* and *Tonna dolium* (Babu *et al.*, 2011). These studies described the nutritional qualities of gastropods and suggested that these could contribute towards the people's diets as nutritional health food, particularly in the developing countries.

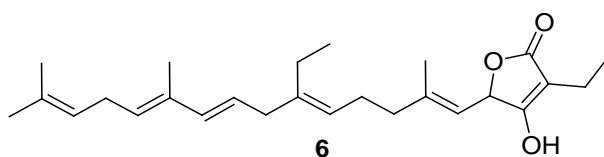
2.6.2. Bioactive potentials of gastropods

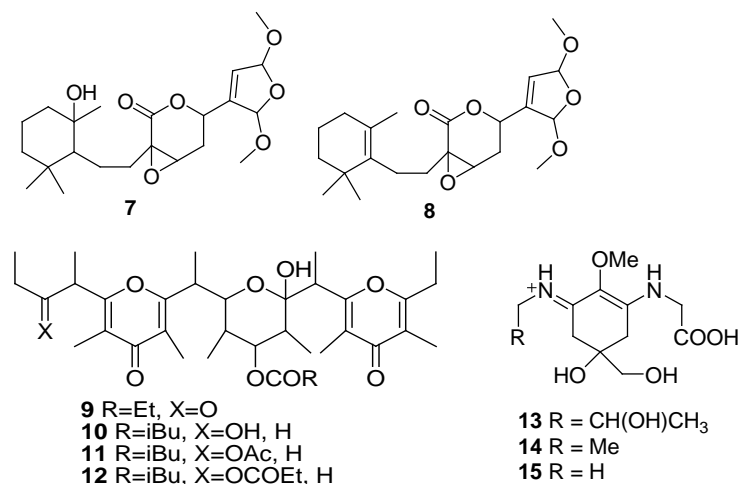
Gastropods reported for various bioactive potentials and believed to be rich sources of bioactive metabolites. These bioactive molecules generated from the immune response tissues of gastropods as a result of host defense mechanisms (Rajaganapathi *et al.*, 2002). The gastropod snail, Abalone is an important marine mollusk with potential therapeutic properties, and has been recommended for physically weak patients. Abalone extracts exhibited anti-cancer (Lee *et al.*, 2010), antioxidant, anti-hypertensive and anti-coagulant (Kim *et al.*, 2006) properties. Conopeptides from the cone snails

reported for various biomedical pluralities, such as anti-noceptive, analgesic, neuroprotectives and anti-cancer (Han *et al.*, 2008; Twede *et al.*, 2009). Sea hares, *Dolabella*, *Bursatella* and *Aplysia* were found to be potential sources of anti-bacterial and anti-HIV metabolites (Rajaganapathi *et al.*, 2002; Yamazaki 1993). The tissues and eggs of gastropods were reported to possess bioactive metabolites with anti-microbial properties to protect the embryos in the capsule (Kaviarasan *et al.*, 2011). The anti-bacterial and anti-fungal potentials of *Babylonia spirata*, *P. glaucum*, *T. dolium*, *Hemifusus pugilinus*, *C. ramosus* and *Babylonia zeylanica* collected from the southeast coast of India were investigated previously (Govindarajalu *et al.*, 2016). The extract of Australian muricid gastropod, *Dicathais orbita* was found to exhibit anti-inflammatory properties along with nutraceutical functionalities (Ahmad *et al.*, 2017). The methanol and ethyl acetate tissue extracts of *Littorina littorea* exhibited antioxidant and anti-microbial properties (Borquaye *et al.*, 2016). However, there were only few investigations were conducted to understand the commercial importance and utilities of gastropods.

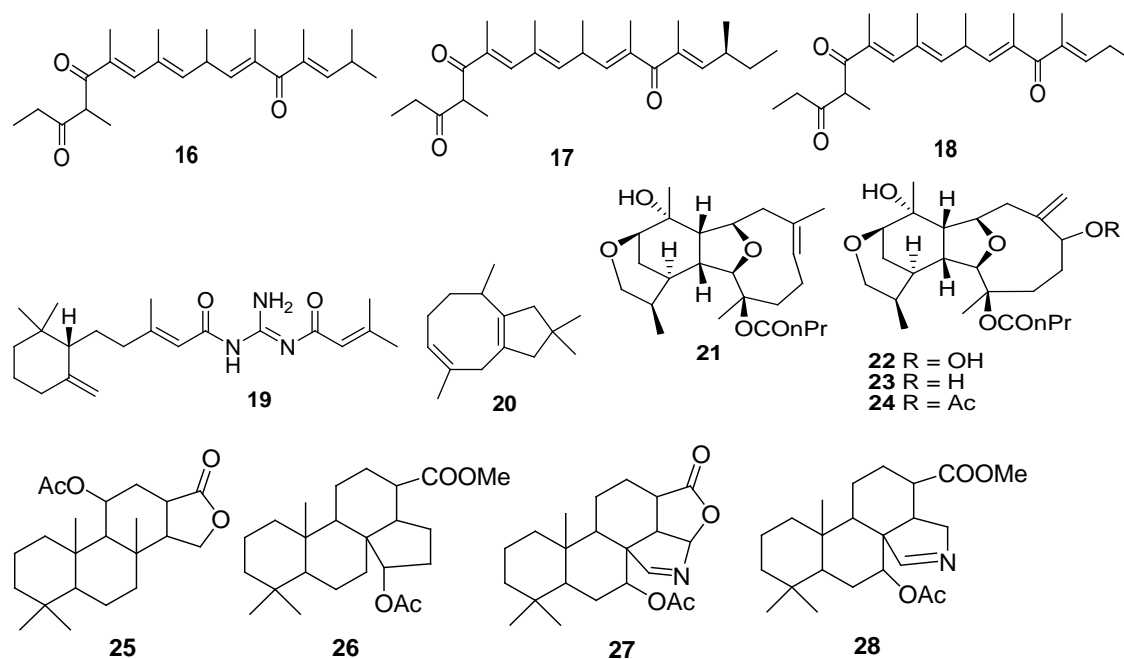
2.6.3. Secondary metabolites from gastropods

Numerous bio-potent secondary metabolites were identified and characterized from gastropod mollusks. A linear homosesterterpene, granulocide (**6**) was isolated from gastropod *Charcotia granulosa* (Cutignano *et al.*, 2015) and diterpene metabolites thuridillins **7-8** were isolated from *Thuridilla splendens* (Somerville *et al.*, 2012). Rare Δ^8 unsaturated 4,4-dimethyl and 4-methyl sterols were isolated from Japanese gastropod, *Cellana grata* and *C. toreuma* (Kawashima *et al.*, 2013) and pyranone ester derivatives or analogues **9-12** were identified from *Onchidium* sp. (Carbone *et al.*, 2013). An anti-leishmaniasis compound, 5 α ,8 α -epidioxycholest-6-en-3 β -ol was characterized from *Dolabrifera dolabrifera* (Clark *et al.*, 2013). Mycosporine-type amino acids **13-15** isolated from the protective ink of *Aplysia californica* (Sea hare) (Kamio *et al.*, 2011).

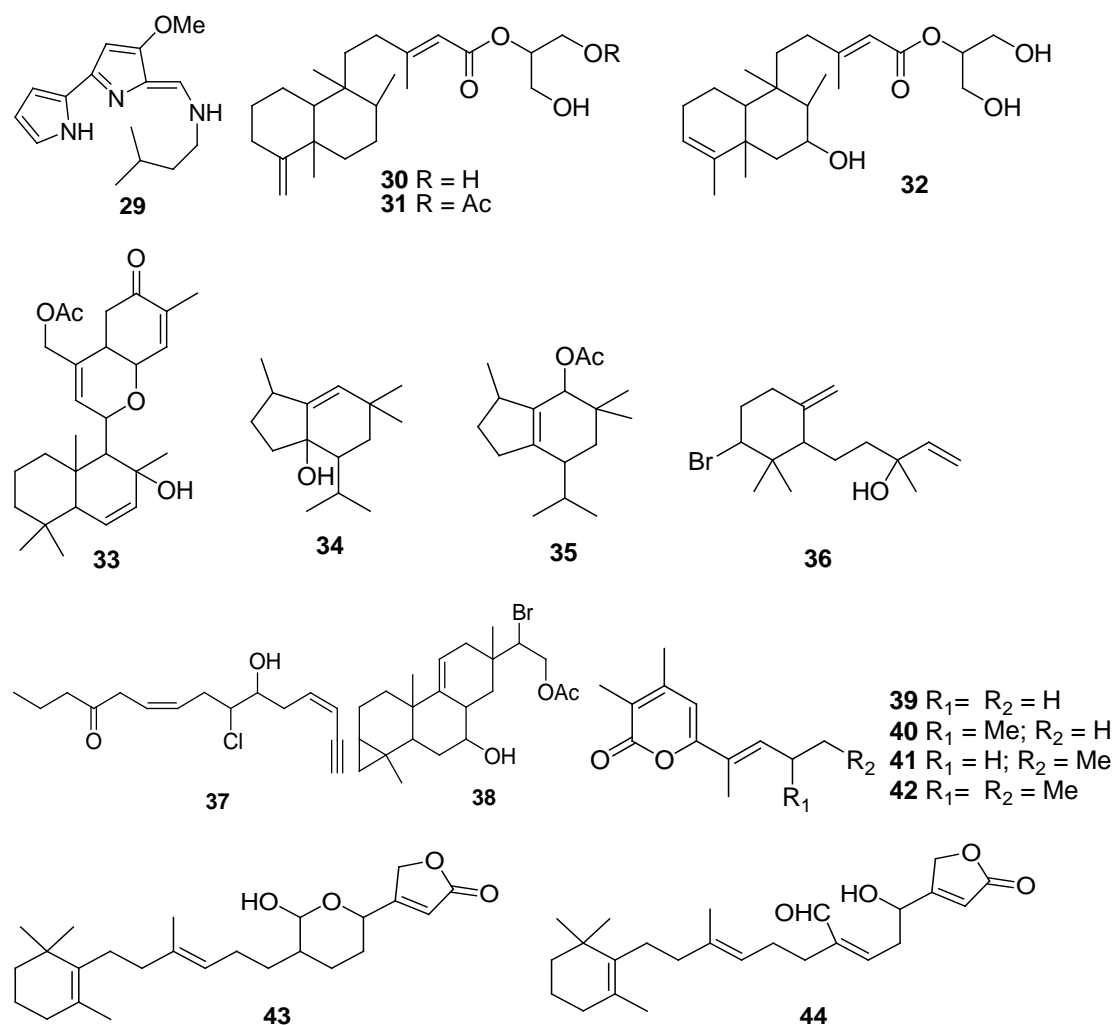




The polypropionate derivatives, niuhinone A-C **16-18** identified from carnivorous mollusk, *Philineopsis speciosa* and herbivore mollusk, *Bulla occidentalis*. These suggested that the origin of these metabolites in *P. speciosa* was due to the consumption of *Bulla* sp. (Coval *et al.*, 1985; Cutignano *et al.*, 2011). A guanidine-bound terpene derivative **19** identified from *Doto pinnatida* (Putz *et al.*, 2011), an asteriscane sesquiterpenoid **20** afforded from *Phyllodesmium magnum* (Mao *et al.*, 2011) and rare pyran-enclosed cladiellane diterpene derivatives, tritoniopsin A-D **21-24** isolated from *Tritoniopsis elegans* and its feed *Cladiella krempfi* (coral) (Ciavatta *et al.*, 2011). Novel diterpenoids **25-26** and chromoculatimine A-B **27-28** were identified and the tissue localisation studies revealed that these diterpenes have been obtained from their mantle and internal organs (Suciati *et al.*, 2011).

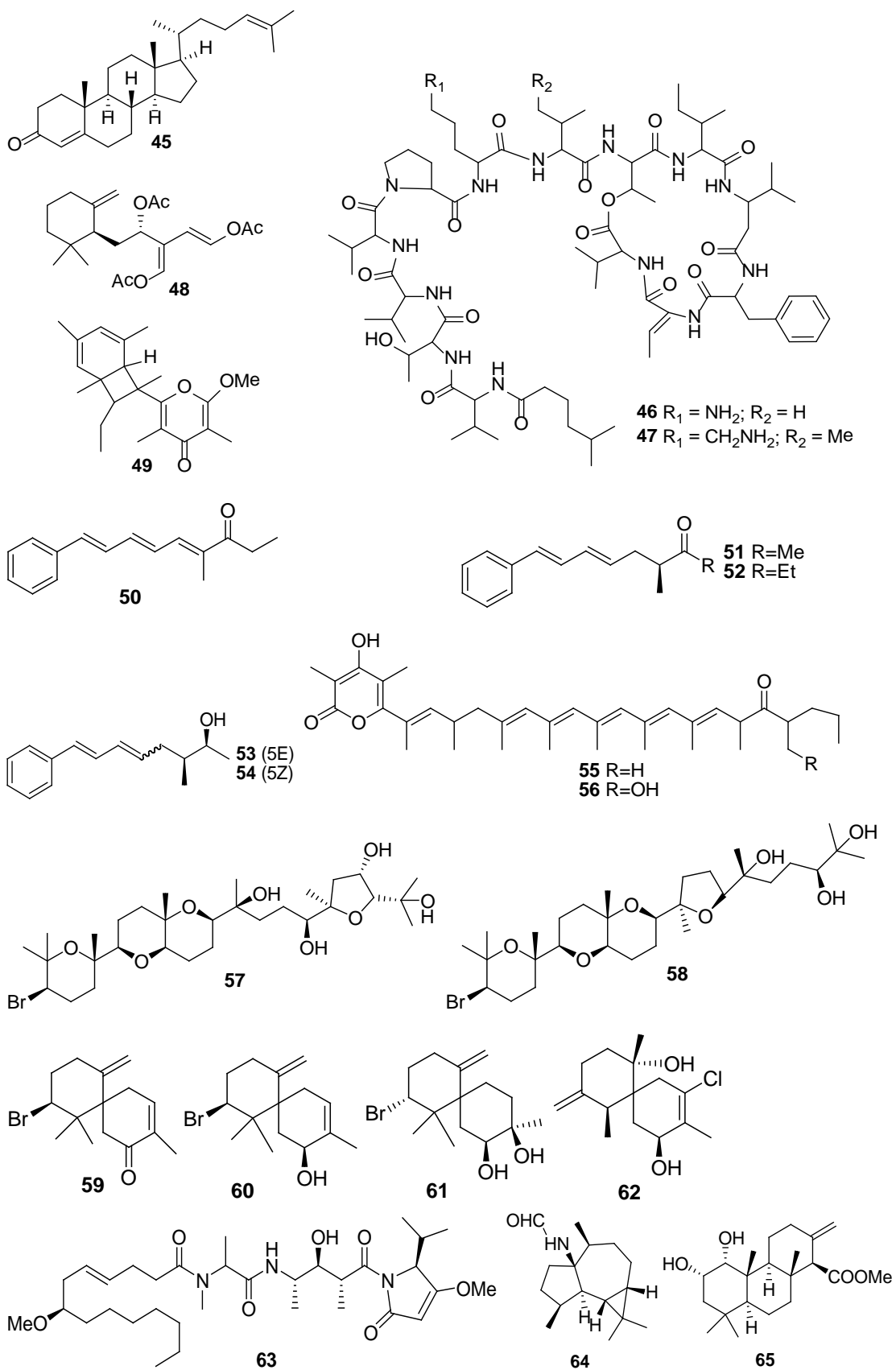


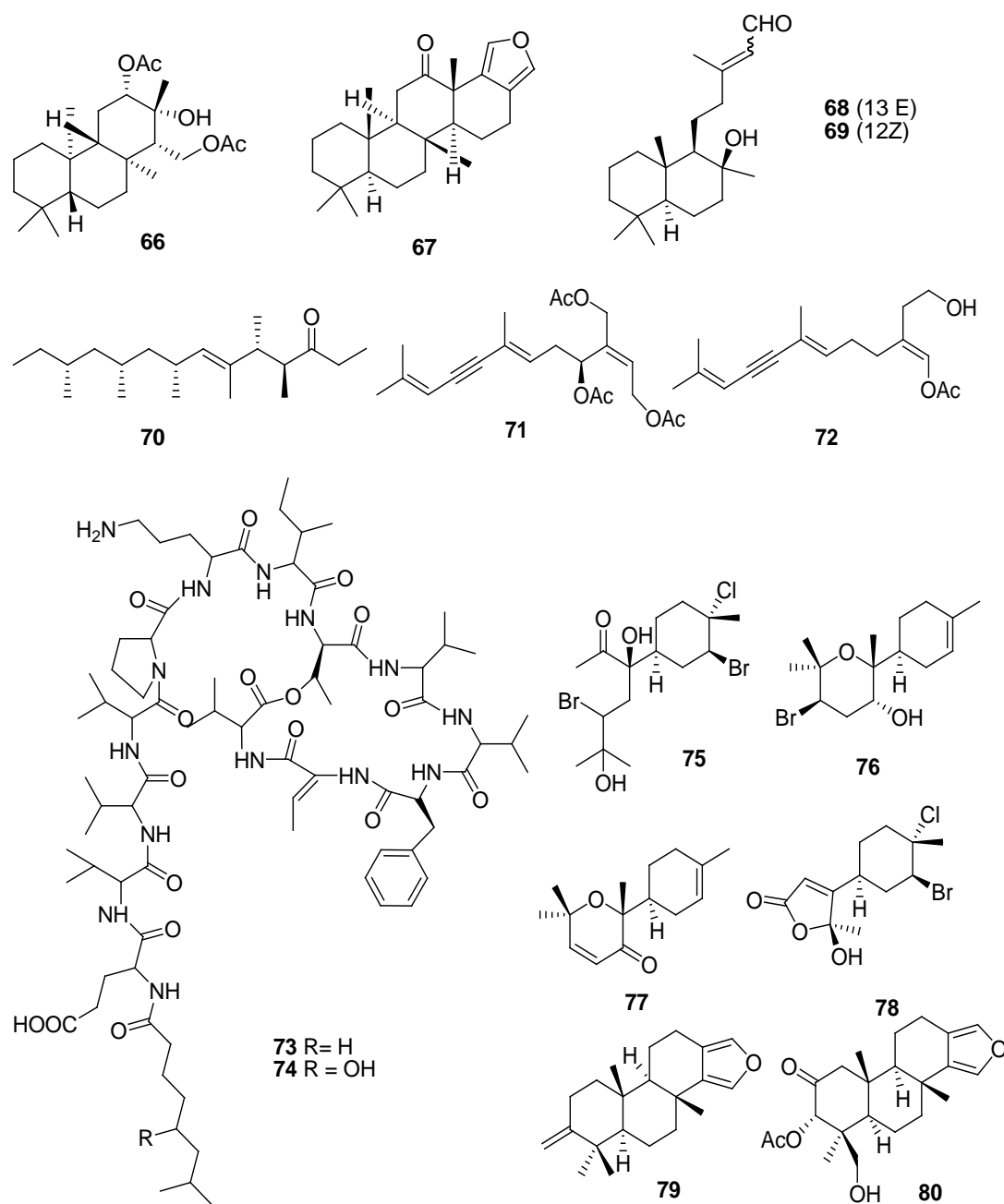
The isopentyl-containing alkaloids, tambjamine K **29** was identified from *Tambja ceutae* (Carbone *et al.*, 2010). The clerodane diterpenes palmadorin A-C **30-32** were isolated from nudibranch, *Austrodoris kerguelenensis* (Diyabalanage *et al.*, 2010) and sesterterpenoid, ansellone A **33** was isolated from *Cadlina luteromarginata* (Daoust *et al.*, 2010). The extraction of digestive and hermaphroditic glands of *Aplysia fasciata* (Sea hare) yielded sesquiterpenoids **34-36**, acetogenin **37**, and diterpenoid **38** (Ioannou *et al.*, 2009). The α -pyrone polyketides, aplysiopsene A-D **39-42** has isolated from herbivorous *Aplysiopsis formosa* (slug) (Ciavatta *et al.*, 2009). Chemical investigation of *Chromodoris willani* reported for its deoxy analogues of manoalide **43** and secomanoalide **44** with anti-microbial activity (Uddin *et al.*, 2009). The anti-fungal compound Kabiramide B was reported from Pacific nudibranch *Hexabranchus sanguineus* (Matsunaga *et al.*, 1989).



The prosobranch mollusk, *Onchidiopsis variegata* reported for number of ketosteroid derivatives **45** (Santalova *et al.*, 2007) and sacoglossan mollusk, *Elysia grandifolia* reported for two new members of cyclic depsipeptides **46-47** in kahalalide family (Tilvi and Naik 2007). The absolute conformation of crispatenine (sesquiterpenoid) **48** formerly identified from *Tridachia crispata* (Gavagnin *et al.*, 1997), and further recognized by its enantioselective synthesis (Bourdron *et al.*, 2007). New pyrone compound reported from *Placobranchus ocellatus* **49** (Manzo *et al.*, 2005a) and an aromatic benzene enclosed compounds, named lignarenones reported from *Scaphander lignarius* **50-54** (Sala *et al.*, 2007). The polypropionate analogues, fusaripyrones A and B **55-56** were reported from Mediterranean *Haminoea fusari* (Cutignano *et al.*, 2007). The polyether triterpenes named as aplysiols A and B **57-58** were identified from *Aplysia dactylomela* (Sea hare) collected from South China Sea (Manzo *et al.*, 2007a) and the chemical investigation of this same species from Madagascar afforded halogenated chamigrane sesquiterpenoids **59-62** (Shubina *et al.*, 2007). Another Sea hare, *Bursatella leachii* was reported to produce 7R-configured malynamide **63** (Suntornchashwej *et al.*, 2007). A sesquiterpenoid **64** and a diterpenoid **65** were isolated from *Hexabranhus sanguineus* (Spanish dancer mollusk) (Zhang *et al.*, 2007). Isocopalane diester **66** was isolated from unrevealed gastropod of Marion Island (van Wyk *et al.*, 2007). A 12-keto scalarane type of compound, **67** reported from *Glossodoris averni* (Queensland, Australia) and *G. pallida* (Hainan, China) (Manzo *et al.*, 2007b). The labdane class of diterpenoids **68-69** reported from *Pleurobranchus meckelii* (Ciavatta *et al.*, 1995).

The pulmonate, *Siphonaria lessoni* was the major source of **70**, a nor-homologue of well known metabolite, siphonarienolone (Roviroso and San-Martin 2006). The cytotoxic alkaloid lamellarin N reported from *Lamellaria* sp. and further structure activity analyses on lamellarin D have been carried out (Pla *et al.*, 2006). The sacoglossan mollusk, *Elysia cf. expansa* collected from Mandapam, India was afforded caulerpenyne typed metabolites, dihydrocaulerpenyne **71** and expansinol **72** (Ciavatta *et al.*, 2006).

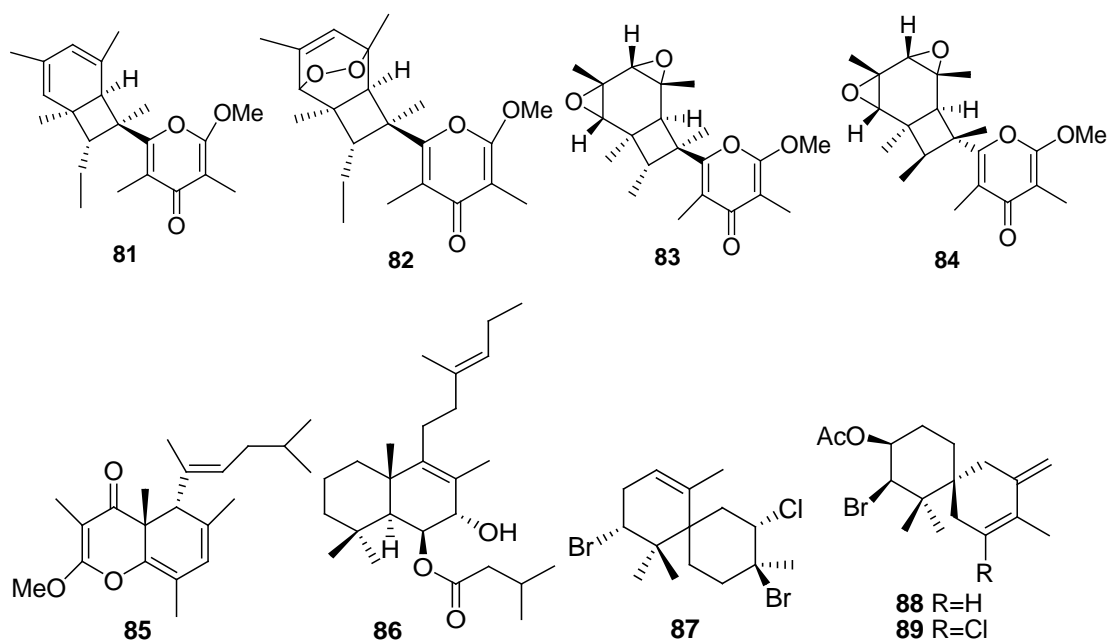


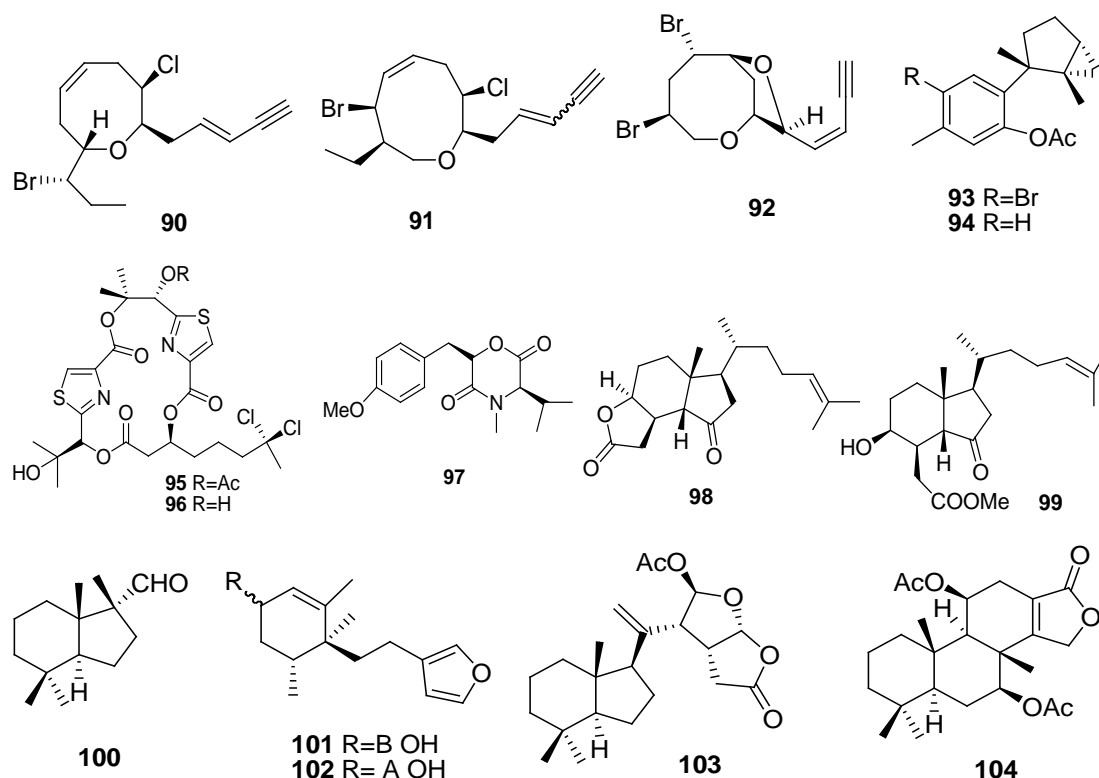


The cyclic depsipeptides, kahalalide R-S, **73-74** were reported from *E. grandifolia* (Ashour *et al.*, 2006). Bisabolene typed sesquiterpenes **75-78** identified from the crude extracts of *A. dactylomela* (Brito *et al.*, 2006) and anti-tumour compound, aplyronine A isolated from *A. kurodai* (Yamada *et al.*, 1993). The chemical investigation of Australian mollusk, *Glossodoris atromarginata* led to the identification of **79** and **80** for the first time (Andersen *et al.*, 2006).

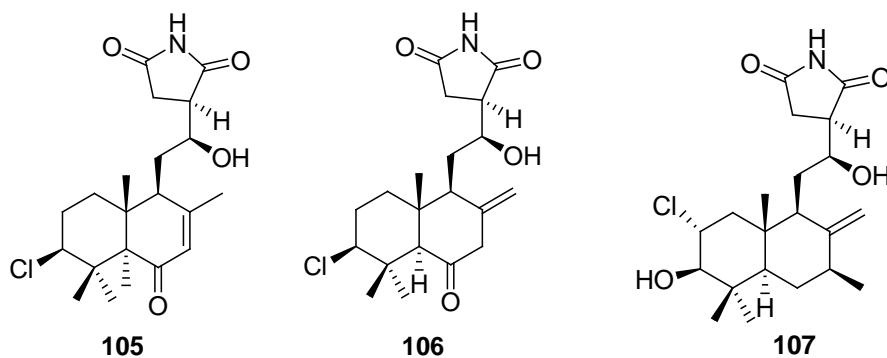
The pyrone **81** and its possible peroxy analogue **82** from *Placobranchus ocellatus* were reported previously (Manzo *et al.*, 2005a). Cueto *et al.*, (2005) reported

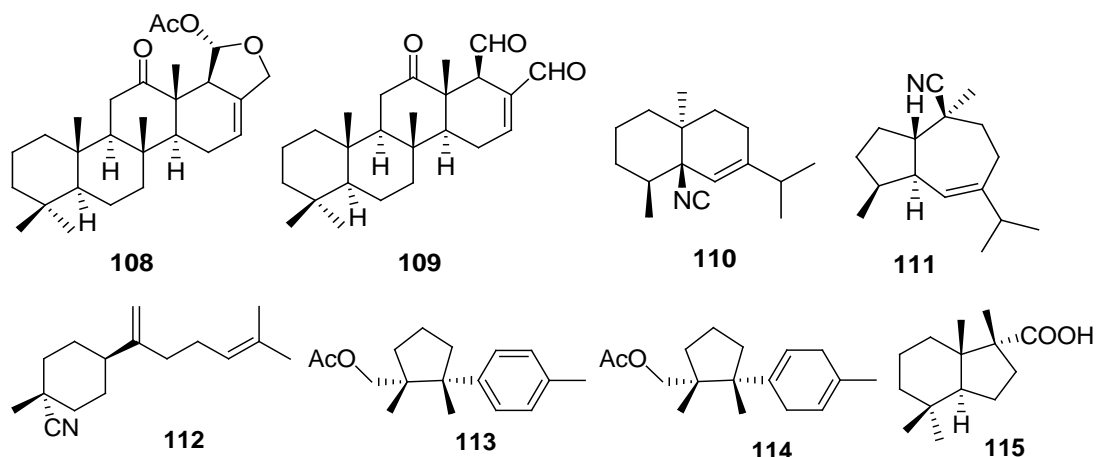
elysiapyrone metabolites A-B **83-84** from *Elysia diomedea*. Tridachiahdropyrone **85** isolated from *Tridachia crispata* and *trans*-decalin compound, **86** were isolated from *T. reticulatus* (Gavagnin *et al.*, 1996; Manker and Faulkner 1987). The sesquiterpene derivatives **87-89** were isolated from *A. dactylomela* (Dias *et al.*, 2005) with *in vitro* anti-tumour activity. The C15-halogenated derivatives **90-91** were identified from *A. dactylomela* (Manzo *et al.*, 2005b). The metabolite (3*Z*)-bromofucin **92** isolated from *A. parvula* extracts (McPhail and Davies-Coleman 2005) and bioactive laurinterol **93** and debromolaurinterol **94** were reported from *A. kurodai* (Tsukamoto *et al.*, 2005). *Bursatella leachii* was the predominant source of cytotoxic metabolites such as hectochlorin **95**, deacetyl derivatives **96-97** (Suntornchashwej *et al.*, 2005). Degraded sterols, such as aplykurodinone 1-2 (**98** and **99**) were purified from the skin extract of mollusk, *Syphonota geographica* (Gavagnin *et al.*, 2005). Derivatives of dolastatin 11 from *D. auricularia* (Pettit *et al.*, 1989) and nor-sesquiterpenoid, (+)-austrodoral **100** from *Austrodoris kerguelensis* (Antarctic mollusk) were reported (Gavagnin *et al.*, 2003b). Furanosesquiterpene alcohol derivatives, pelseneeriols-1 **101** and 2 **102** were reported from *Doriopsilla pelseneeri* (Gaspar *et al.*, 2005). The hydroquinone and dodecadienonyl-benzoquinone derivatives were purified from *Leminda millecra* (African gastropod) (McPhail *et al.*, 2001). The norrisolide **103** was isolated from *Chromodoris norrisi* (Hochlowski *et al.*, 1983) and dorisenone C **104** was identified from *C. obsolete* (Miyamoto *et al.*, 1996).



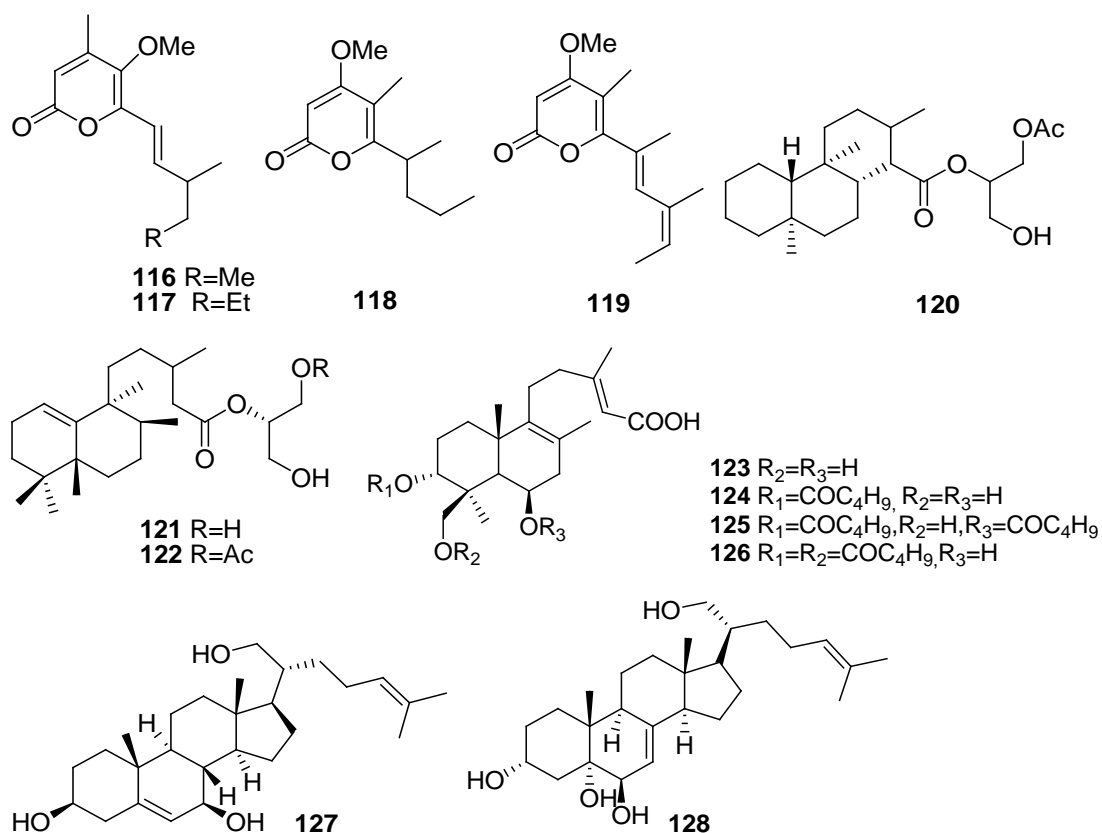


The cytotoxic components, haterumaimides L **105** and M **106** along with 3β -hydroxychlorolissoclimide **107** were obtained from *Pleurobranchus albiguttatus* and *P. forskalii* (Fu *et al.*, 2004). The isolation of scalarane-framework metabolites **108** and **109** from *G. rufomarginata* was reported previously (Gavagnin *et al.*, 2004). The sesquiterpenes **110-112** were fractionated from *Phyllidiella pustulosa* found at South China (Manzo *et al.*, 2004). The sesquiterpenes (-)-tochuinyl acetate **113** and (-)-dihydrotochuinyl acetate **114** were identified from *Tochuina tetraquetra* (Williams and Andersen 1987). The pyrone polypropionate, cyercene was reported by Vardaro *et al.*, (1991) from Mediterranean *Cyerce cristallina* and austrodoric acid **115** from Antarctic *A. kerguelensis* was previously reported by Gavagnin *et al.*, (2003b).

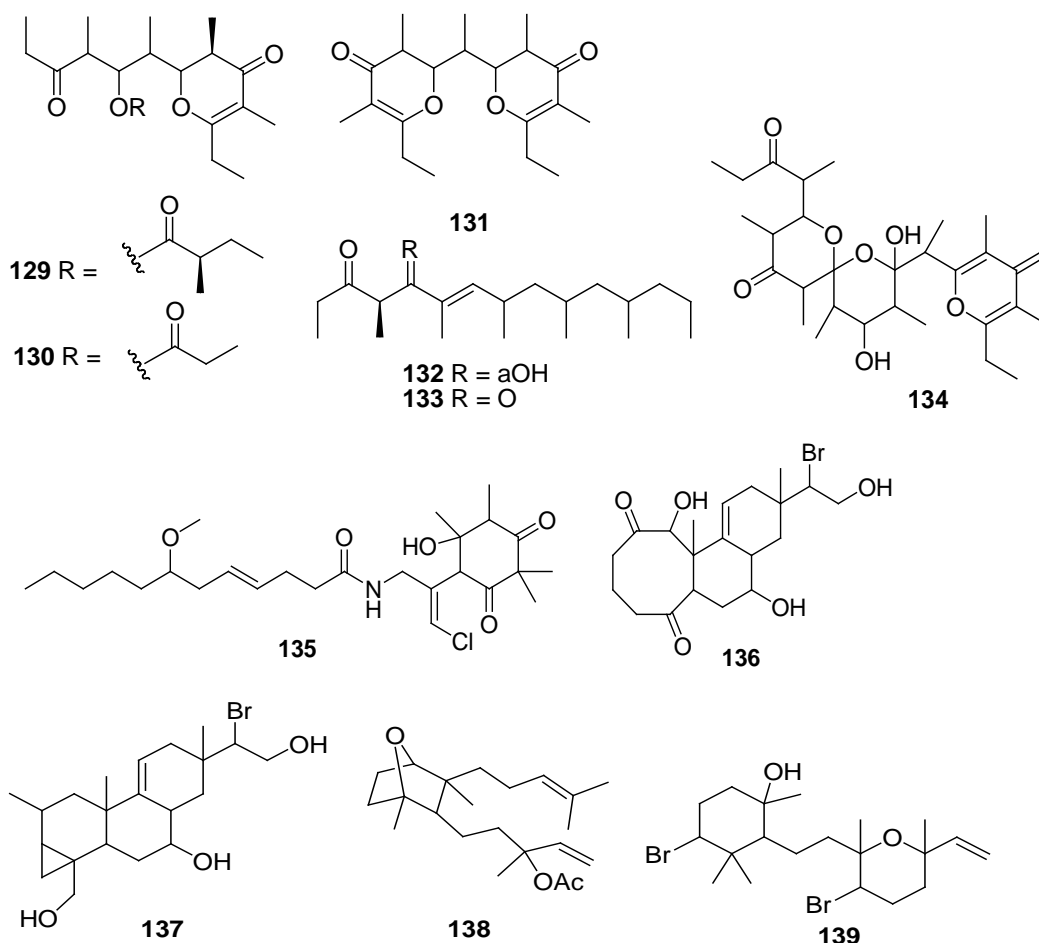


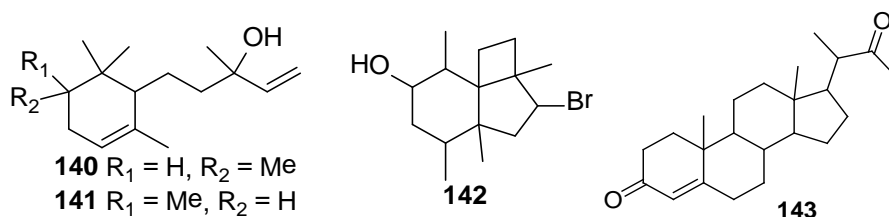


Asymmetrical polypropionate derivatives, placidenes C-F **116-119** characterized by Cutignano *et al.*, (2003) from *Placida dendritica*. Chemical investigation of diterpenoid acylglycerol fraction from the Antarctic gastropod, *A. kerguelensis* yielded acylglycerols **120-122** (Gavagnin *et al.*, 2003a). The labdane diterpenes **123-126** were identified from *T. peruvianus* (pulmonate) along with cytotoxic polyhydroxylated steroids **127-128** (Diaz-Marrero *et al.*, 2003a; Diaz-Marrero *et al.*, 2003b).

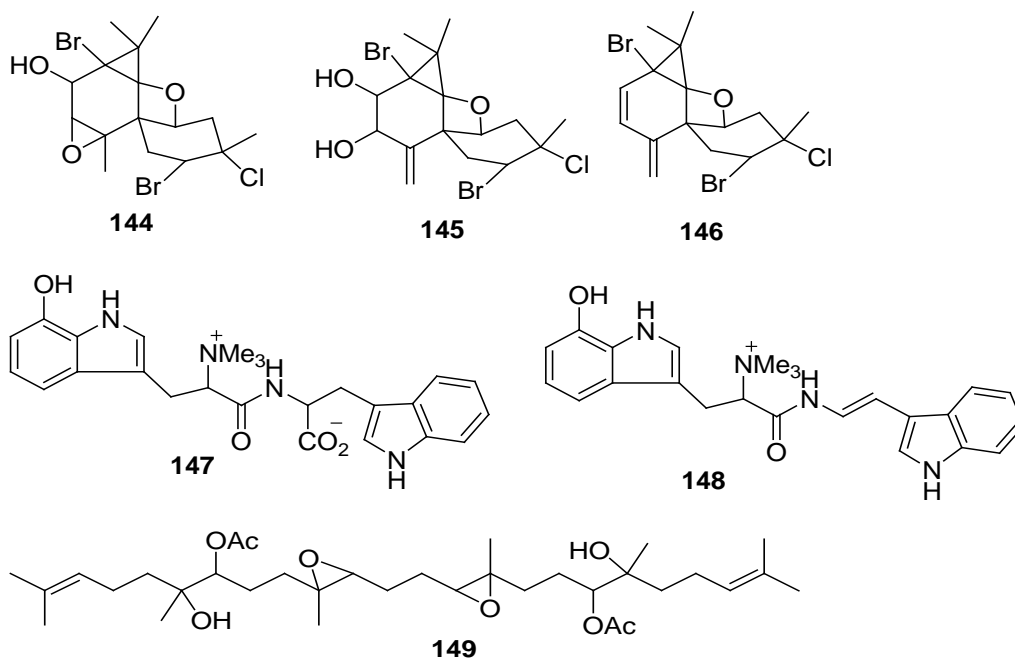


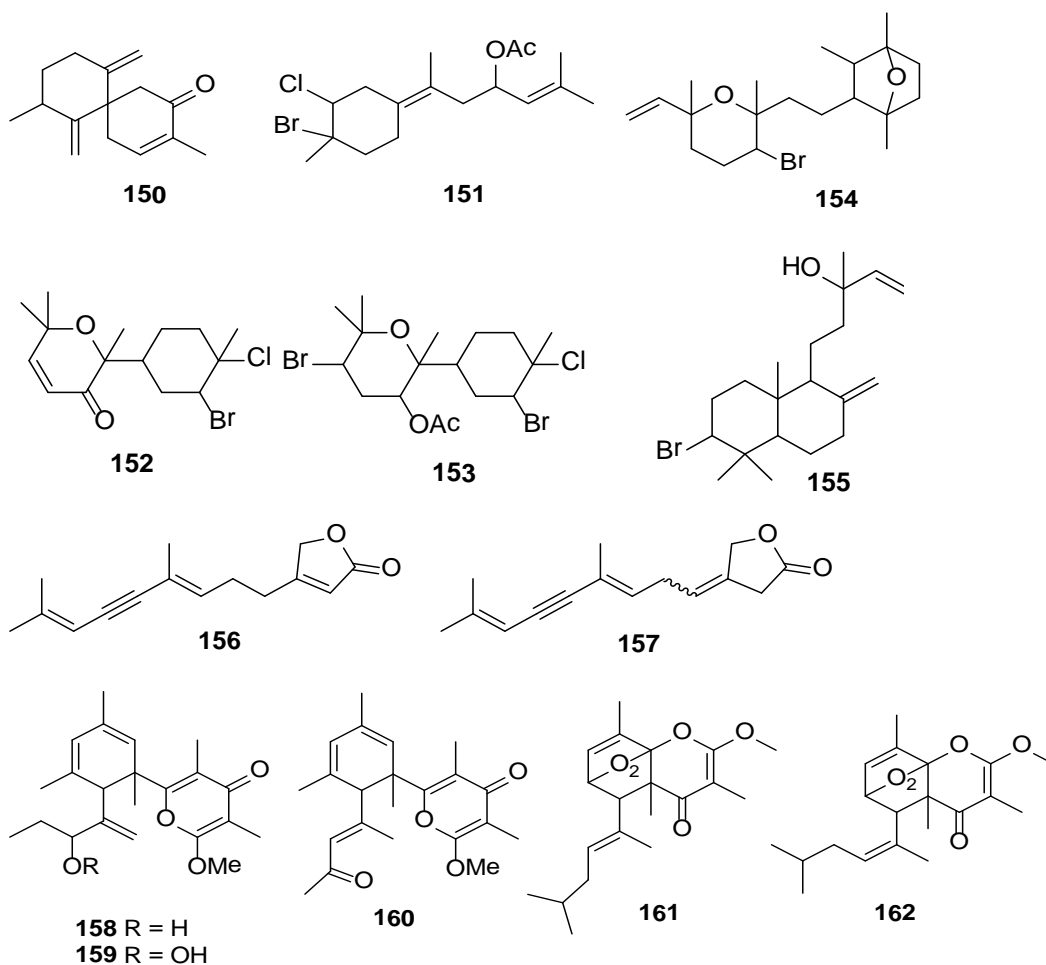
The membrenones A-C **129-131** and γ -dihydropyrone enclosed polypropionates were extracted from *Pleurobranchus membranaceus* by Ciavatta *et al.*, (1993). The chemical investigation of *Siphonaria grisea* was reported the characterization of siphonarienolone **132** and siphonarienedione **133** (Calter and Liao 2002) polypropionates and their relative and absolute stereochemistries were established (Norte *et al.*, 1990). The compound, siphonarin B **134** was reported from *Siphonaria zelandica* and *S. atra* (Hochlowski *et al.*, 1984). A novel malyngamide S derivative **135** was reported from mollusk *Bursatella leachii* and the compound was found to exhibit potential anti-inflammatory activities (Appleton *et al.*, 2002). A wide range of diterpene metabolites **136-139** and new sesquiterpenes **140-142** were reported by Findlay and Li (2002) from Sardinian Sea hare *Aplysia punctata*. A progesterone analogue **143** was isolated by Gavagnin *et al.*, (2002) from nudibranch *Aldisa smaragdina* (Spain).





The extensive NMR assignments of the *A. dactylomela* metabolites, such as johnstonol **144**, pacifenediol **145** and pacifidiene **146** (Kaiser *et al.*, 2001) along with tryptophan based dipeptides **147** and **148** (Appleton *et al.*, 2001) have been previously reported. Another Sea hare from Japanese collection *Dolabella auricularia* contained a novel cytotoxic squalene metabolite named as auriculol **149** (Kigoshi *et al.*, 2001). A non-halogenated sesquiterpene **150** that was possibly a rearranged product of a known chamigrane found from *Aplysia* sp. collected from Madagascar coast (Federov *et al.*, 2000). *A. dactylomela* contained new sesquiterpenes puertitol-B acetate **151**, caespitenone **152** and 8-acetyl-caespitol **153** along with diterpenoids, such as dactylopyranoid **154** and isopinnatol B **155** with bioactivity profiles (Wessels *et al.*, 2000). Also, the sesquiterpenes ascobullins A **156** and B **157** metabolites were reported from *Ascobulla ulla* (Gavagnin *et al.*, 2000). The polypropionate pyrones such as tridachiapyrones G **158** - J **160** and tridachiahydro pyrones B **161** - C **162** were reported from mollusk, *P. ocellatus* (Fu *et al.*, 2000).





2.7. Bivalves

In the bivalve molluscan aquaculture, the major bivalve species includes clams (along with cockles, arkshells etc.), mussels, oysters, scallops and other various bivalves of minor importance. It was found that clams, oysters, mussels and scallops were the four foremost groups, based upon the production census of 2012 (FAO 2012). The percentage of aquaculture production among various bivalves illustrated in the Figure 2.10., and in which bivalve clams were found to possess major share to the total bivalves (FAO 2014). The photographic representation of commonly available bivalves in the coastal regions of Arabian Sea, bordering India illustrated in the Figure 2.11.

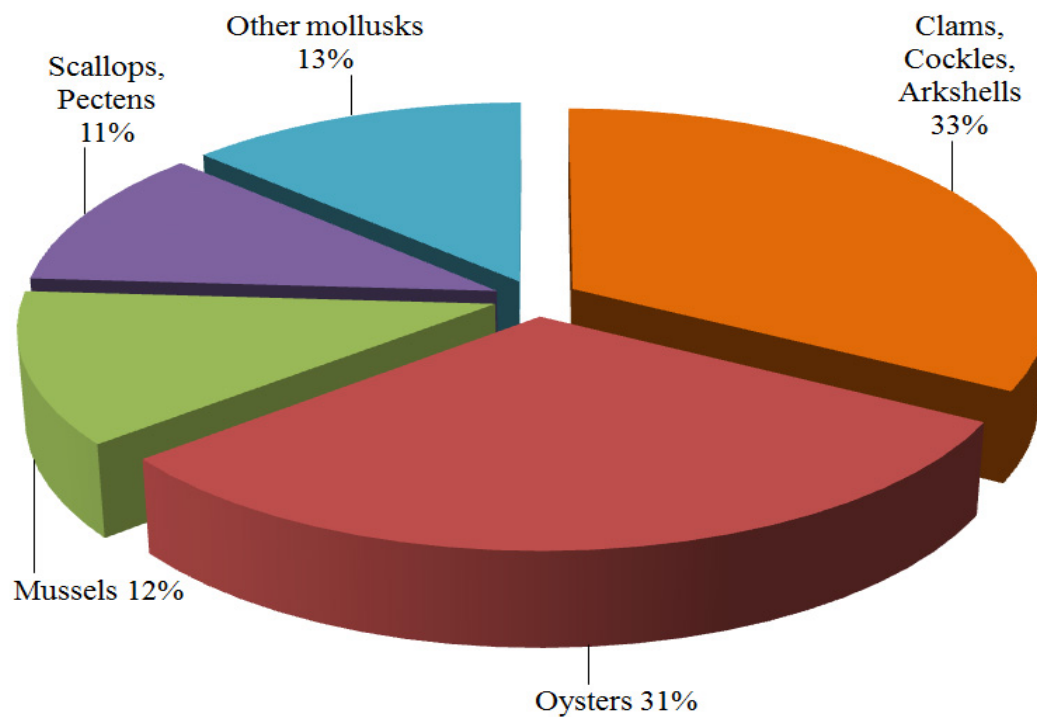


Figure 2.10.: The percentage share of bivalves, particularly clams among bivalve mollusks (FAO 2014)



Figure 2.11.: Photographic illustration of bivalves

2.7.1. Nutritional importance of bivalves

The bivalve mollusks are prominent seafoods at coastline regions and found to be a dominant share to the global trade markets (Chakraborty *et al.*, 2014b; Xie *et al.*, 2012). However, these were not comprehensively investigated for their dietary and nutritional potentials. Bivalves are potential resources of *n*-3 polyunsaturated fatty acids comprising EPA and DHA. The bivalve mollusks were found to be the originators of anti-inflammatory agents (E and D sequences), which described to combat the biosynthesis of inflammatory prostanoids (Chakraborty *et al.*, 2014a). In general, these species reported to provide an inexpensive source of proteins, minerals, amino acids and vitamins (Astorga-Espana *et al.*, 2007). The bivalves, *Ruditapes decussatus* and *Mytilus galloprovincialis* collected from the Mediterranean Sea exhibited greater contents of lipid and protein (Saba 2011). The Asian hard clam, *Meretrix lusoria* and *M. meretrix* displayed good nutritional qualities (Supatra *et al.*, 2013; Xie *et al.*, 2012), and were considered as low-value health food items. Bivalves were regarded next to finfish and prawns in the view of nutritional qualities, and also reported for the presence of bioactive lipids, for example diacylglycerols, sphingolipids, and phytosterols that can effect human health and alleviate inflammatory conditions (Li and Sinclair 2002). The nutritional qualities of green mussels (*Perna viridis*) and oysters (*Crassostrea madrasensis*) were reported previously, therefore, suggested as a substitute to equilibrate the greater consumption of inflammatory *n*-6 FAs (Chakraborty *et al.*, 2016a; Chakraborty *et al.*, 2016b). The nutritional quality parameters, such as mineral composition, fatty acids, glycogen, cholesterol, vitamins, carotenes and the commercial quality indicators of meat of striped venus clam, *Chamelea gallina* were studied previously (Orban *et al.*, 2006). The proteins, minerals, lipids, glycogen along with minor components of lipophilic and hydrophilic nature were found to contribute towards the nutritive importance along with organoleptic features of clams (Orban *et al.*, 2006). The clam, *M. meretrix* was historical seafood and valued resources of ancient Chinese therapeutics (Xie *et al.*, 2012). These previous studies established the nutritional importance of marine and coastal bivalve mollusks for use as nutritional health foods, particularly in the coastal regions of the world.

2.7.2. Bioactive potentials of bivalves

The unfavourable living environments, such as salinity and oxidative stress, predators along with the filter-feeding nature of marine or estuarine bivalves were found to be accountable for their utilities as potent resources. Bivalves were equipped with bioactive metabolites having various functionalities specifically against free radical induced oxidations and related disorders (Goldberg 1975). In general, the bivalve clams exposed to higher salinity and radical inducing noxious agents, although these were not subjected to cellular damages, and therefore, appeared as potential candidates to harness antioxidant molecules (Gonzalez *et al.*, 2015). Bivalves occupied a highest share in the hierarchy of total eatable mollusks, although they were not extensively recognized for their pharmaceutical and biomedical properties (Mohite *et al.*, 2009). Earlier reports demonstrated that the bivalves possessed numerous bioactive effects, like antioxidant, anti-inflammatory and anti-tumour characteristics (Benkendorff 2010; Chakraborty *et al.*, 2014a; Nagash *et al.*, 2010). The lipid fraction of *Perna canaliculus* was marketed as Lyprinol® which demonstrated potential activity against cyclooxygenase-2 (COX-2) and 5-lipoxygenase (5-LOX) inflammatory enzymes (Whitehouse *et al.*, 1997). The clam, *M. meretrix* has displayed to harbour anti-hypertensive, hypolipidemic and antioxidant pluralities (Wei *et al.*, 2007). The mollusk muscle protein hydrolysates reported for anti-hypertensive potentials against angiotensin-1 converting enzyme (Tsai *et al.*, 2008). There were reports for the occurrence of antioxidants in mollusks which can constrain the cell damages from the oxidative reactions (Nagash *et al.*, 2010). The methanolic or ethyl acetate extracts of bivalve mussel, *Perna viridis* was described for its scavenging properties against DPPH radical (Jena *et al.*, 2010; Sreejamole and Radhakrishnan 2013). The ACE inhibitor (anti-hypertensive) peptides from mussel, *Mytilus coruscus* reported in a previous literature (Wu *et al.*, 2013). The commercial freeze-dried extract of New Zealand green lipped mussel *P. canaliculus* was found to down-regulate the inflammatory responses (Tiffany and Bui 2002). The green mussel extract (CadaminTM GMe) prepared from bivalve mollusk, *P. viridis* displayed potential anti-inflammatory effects against pro-inflammatory prostanoids (Chakraborty *et al.*, 2014a).

It was stated that the extracts of some oysters and clams showed anti-microbial and anti-viral potentials (Lin-rui *et al.*, 2012). The extract of edible clam,

Mercenaria mercenaria was found to prevent the development of tumours in Swiss mice (Schmeer and Huala 1965). The polysaccharides from *Mactra chinensis* (Chinese surf clam) were reported to possess scavenging activities against hydroxyl and superoxide anion free radicals (Lin-rui *et al.*, 2012), whereas the aqueous and alcoholic extracts of *M. veneriformis* showed *in vitro* antioxidant potentials (Luan *et al.*, 2011). It was stated that the presence of hydrophilic/lipophilic antioxidant components like polyunsaturated fatty acids, amino acids and carotenoids were found to be accountable for therapeutic potentials of clam species (Luan *et al.*, 2011). The aqueous and ethanolic extracts of New Zealand surf clams, *Crassula aequilatera*, *Mactra murchisoni* and *Paphies donacina* were found to possess potential antioxidant properties (Odeleye *et al.*, 2016). Anti-microbial activity of the gill extract from the bivalve *P. viridis* was reported (Chandran *et al.*, 2009). A natural thrombolytic agent, C-type hemolytic lectin with activity against myocardial infarction, was purified from *Villorita cyprinoides* (Sudhakar and Vincent 2014). Earlier study revealed that the extract of *V. cyprinoides* has potential anti-ulcer activity (Ajithkumar *et al.*, 2012). Anti-bacterial activity of crude solvent fractions of marine clam, *Anadara granosa* (Linn.) and *M. casta* (Chemnitz) against pathogenic bacteria were reported (Ramasamy and Balasubramanian 2012; Ramasamy and Balasubramanian 2014). The extracts from bivalves, *P. viridis*, *C. madrasensis*, *C. gryphoides*, *M. casta*, *V. cyprinoides* and *Polymesoda erosa* were found to possess antiviral activities against influenza virus type-A and type-B (Chatterji *et al.*, 2002).

The dose-dependent antioxidant responses of methanolic extracts of *P. malabarica* and its lipid peroxidation inhibition potentials against reactive oxygen species were reported in earlier works (Pawar *et al.*, 2013). The anti-inflammatory, anti-tumour and antioxidant activities of mussel, *Coelatura aegyptiaca* were evaluated by Fahmy and Soliman (2013). A new polysaccharide bearing galactan sulfate isolated from clam, *Meretrix petechialis* exhibited anti-HIV activity (Amornrut *et al.*, 1999). The Asiatic hard clam, *M. meretrix* (Veneridae) was reported to exhibit several pharmacological activities, such as anti-tumour, antioxidant, immuno-modulatory, anti-hyperglycemia, and anti-hyperlipemia along with detoxification effects (Xie *et al.*, 2012). The earliest Chinese pharmacopeia Compendium of material (Li Shizhen, 16th century) stated that the clam, *M. meretrix* could diminish the inflammation, and has used in the

treatment of typhoid fever and to relieve pain. Another Chinese medicinal book, Treatise on Fevers (Zhang Zhongjing, 2nd century), suggested its potentials to eliminate cyst and detoxification. Several bioactive components, such as peptides, proteins, and enzyme inhibitors identified from *M. meretrix* with anti-hypertensive, anti-neoplastic, hypolipidemic and antioxidant effects (Huang *et al.*, 2005; Wei *et al.*, 2007; Xu *et al.*, 1999; Zhao 1992). Recent studies showed that greatly polyunsaturated cardiolipids (particularly EPA and DHA) were the characteristic of the marine and coastal bivalves (Kraffe *et al.*, 2005). An interesting correlation was observed among the cardiolipin fatty acid profile and bivalve's phylogeny (Kraffe *et al.*, 2005).

The methanol, ethanol and aqueous extracts acquired from *P. viridis* exhibited anti-inflammatory properties in different *in vivo* models (Sreejamole *et al.*, 2011). In addition, *P. viridis* has been reported for anti-microbial, radioprotective, anti-angiogenic and anti-HIV potencies (Annamalai *et al.*, 2007; Mirshahi *et al.*, 2009; Mitra and Chatterji 2004; Sreekumar 2007), and also, attributed for various bioactive components (Bichurina *et al.*, 1994; Blunt *et al.*, 2015; Chatterji *et al.*, 2002). Earlier studies of *P. viridis* highlighted the potential antioxidant activities related to free radical inhibition and lipid peroxidation, thus suggested its utility as health food and valuable antioxidant source (Chakraborty *et al.*, 2016a). A nutraceutical supplement was formulated from *P. viridis* (CadaminTM Green Mussel extract) which exhibited potent *in vitro* and *in vivo* anti-inflammatory effects (Chakraborty *et al.*, 2012; Chakraborty *et al.*, 2014a; Chakraborty *et al.*, 2014b). The nutritional supplement, Seatone[®] developed from *P. canaliculus* has been used as an anti-inflammatory supplement (Cobb and Ernst 2006). *P. canaliculus* and *M. galloprovincialis* were reported for anti-inflammatory potentials. The *P. canaliculus* was used against osteoarthritis and rheumatoid arthritis (McPhee *et al.*, 1995). Okinawan mollusk, *Pinna muricata* reported for Ca²⁺ channel activation and possesses anti-inflammatory properties (Murphy *et al.*, 2002). There were various reports on the nutraceutical formulations and bioactive potentials of bivalve mollusks, even though, these were not extensively investigated for their bioactive components, structural characterizations and their effectiveness as functional food supplements.

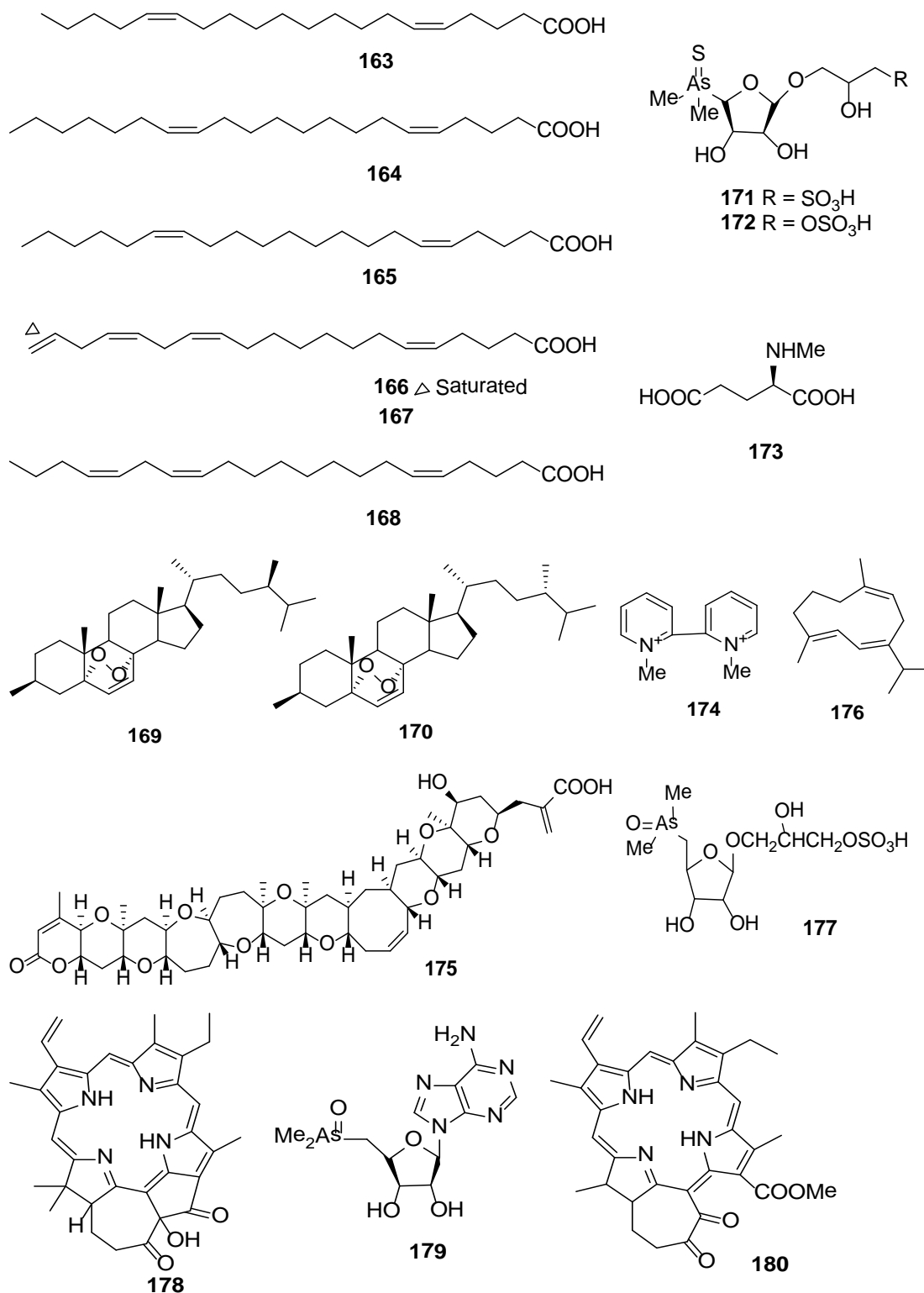
2.7.3. Secondary metabolites from bivalves

Recently, the research efforts on marine natural products were focused towards the bivalves and, there have been a sharp logarithmic increase in the number of reported components from these organisms. In this section, the reported secondary metabolites were classified under the various classes of bivalves, such as clams, oysters, mussels and cockles.

2.7.3.1. Secondary metabolites from bivalve clams

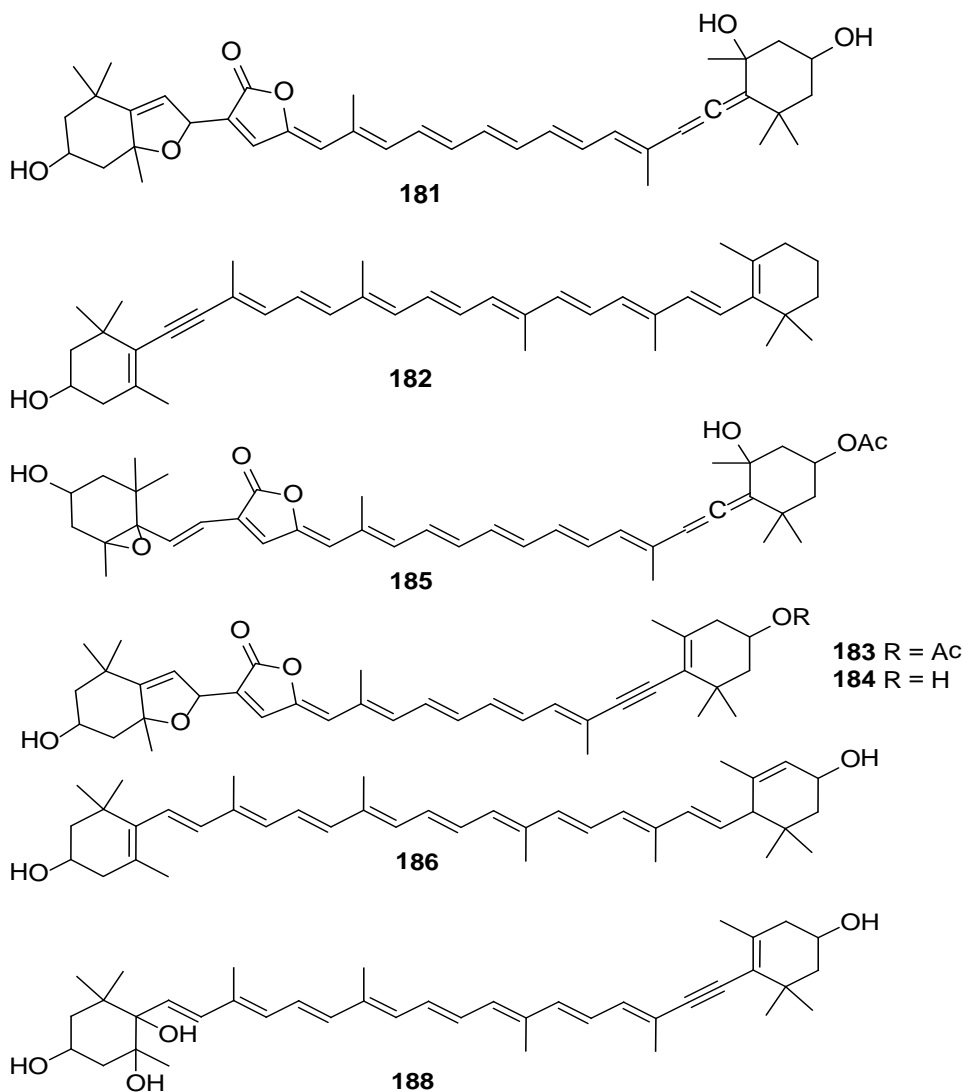
A novel sequence of *n*-4 PUFAs **163-168** were identified from *Calyptogena phaseoliformis* (deep Sea clam) collected from the Japan Trench (Saito 2007). The hard clam, *M. lusoria* (Taiwan) which was the primary resources of the Chinese antidote for hepatitis and liver illness, contained two previously reported epidioxysterols **169-170** with anti-cancer properties (Pan *et al.*, 2007). Two new thioarsenosugars, **171** and **172** were identified from the extracts of brackishwater clam, *Venus verrucosa* (Nischwitz *et al.*, 2006). The isolation and characterization of N-methyl-D-glutamic acid **173** from Japanese blood clam or Ark clam, *Scapharca broughtonii* was the first report of this kind of amino acid derivative as natural compound (Tarui *et al.*, 2003). The smooth clam, *Callista chione* contained 1,1'-dimethyl-[2,2']-bipyridyldium salt **174** which was acknowledged for the first time from a natural resource (Vagias *et al.*, 2000). A brevetoxin B5 **175** was reported from *Austrovenus stutchburyi* (New Zealand cockle) (Ishida *et al.*, 2004).

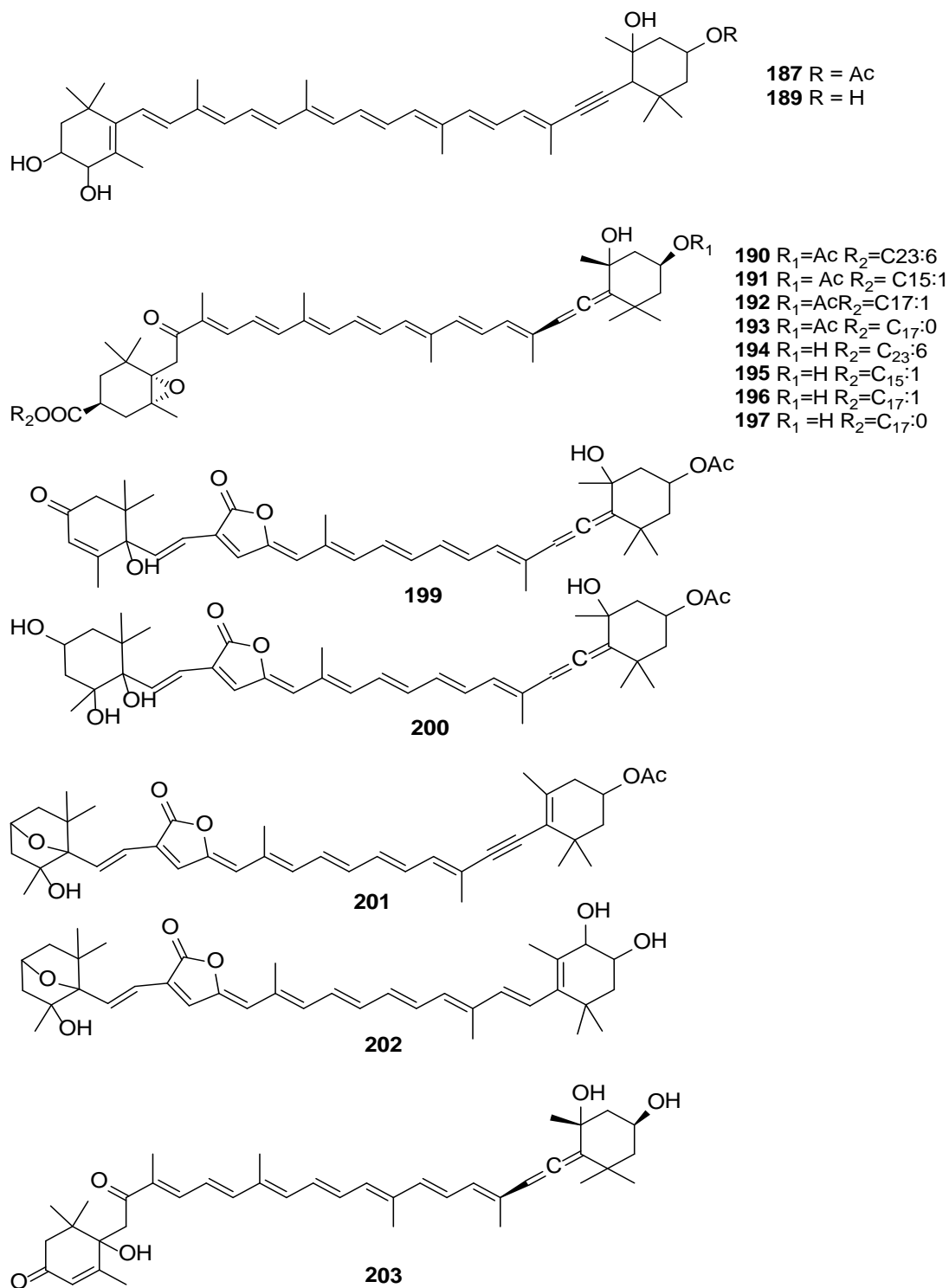
The terpenoid constituent from *Tridacna maxima* (giant clam) was found to be germacrene-C **176** (Bowden *et al.*, 1980). The *T. maxima* was afforded an arsenic-enclosed sugar sulphate **177** (Edmonds *et al.*, 1982) by X-ray crystallography. A new antioxidative pigment, Chlorophyllone A **178** was isolated from short-necked clam, *R. philippinarum* (Sakata *et al.*, 1990). An arsenic containing nucleoside, 5'-deoxy-5'-dimethylarsinyl- adenosine **179** was isolated from *T. maxima* (Francesconi *et al.*, 1991). The antioxidant, chlorophyllonic acid A methyl ester **180** was identified from *R. philippinarum* by single crystal experiments (Yamamoto *et al.*, 1992).



Bivalve clams contained different carotenoids with structural modifications and these were obtained from their micro-algal diets. Most of the carotenoids were derivatives of fucoxanthin, diadinoxanthin, diatoxanthin etc. Many carotenoids were isolated from freshwater and brackishwater corbicula clams such as *Corbicula japonica*,

C. Sandai etc. The peridininol-5,8-furanoxide (**181**), 7,8-didehydro- β -cryptoxanthin (**182**) pyrrhoxanthinol-5,8-furanoxide (**183**) and pyrrhoxanthin 5,8-furanoxide (**184**) were newly reported from the mollusks. The peridinin (**185**) and its analogues were the main carotenoids in *C. japonica* and lutein (**186**) was the main carotenoid in *C. sandai*. The corbiculaxanthin 3'-acetate (**187**), 6-epiheteroxanthin (**188**) and corbiculaxanthin (**189**) isolated from these species were not reported previously from other shellfishes (Maoka *et al.*, 2005a). A series of fucoxanthin **190-195** and fucoxanthinol **196-198** fatty acid esters were identified from edible *M. chinensis* (Chinese surf clam) (Maoka *et al.*, 2007), *R. philippinarum* and *M. petechialis* (Maoka *et al.*, 2010). The amarouciaxanthin A (**199**) and its ester derivatives were identified from *Paphia amabilis* and *P. amabilis* along with C37-skeletal carotenoids (**200-203**) (Maoka *et al.*, 2008).

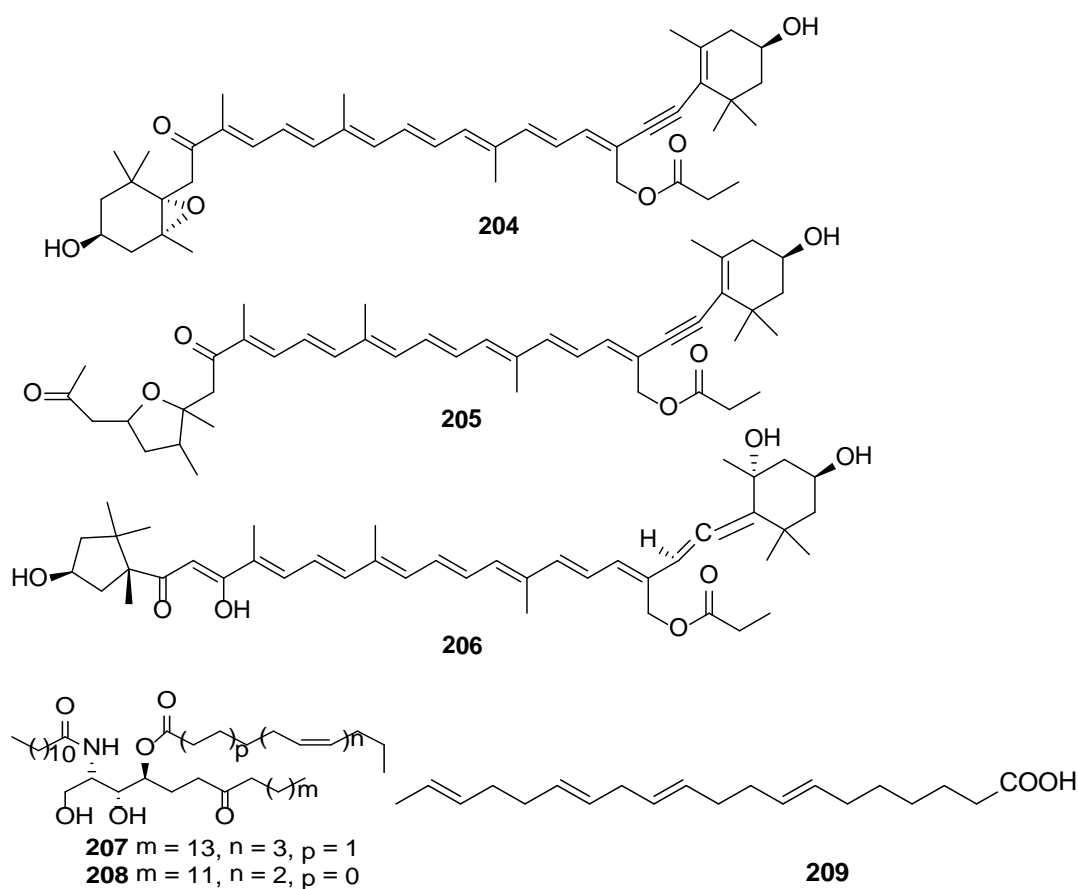


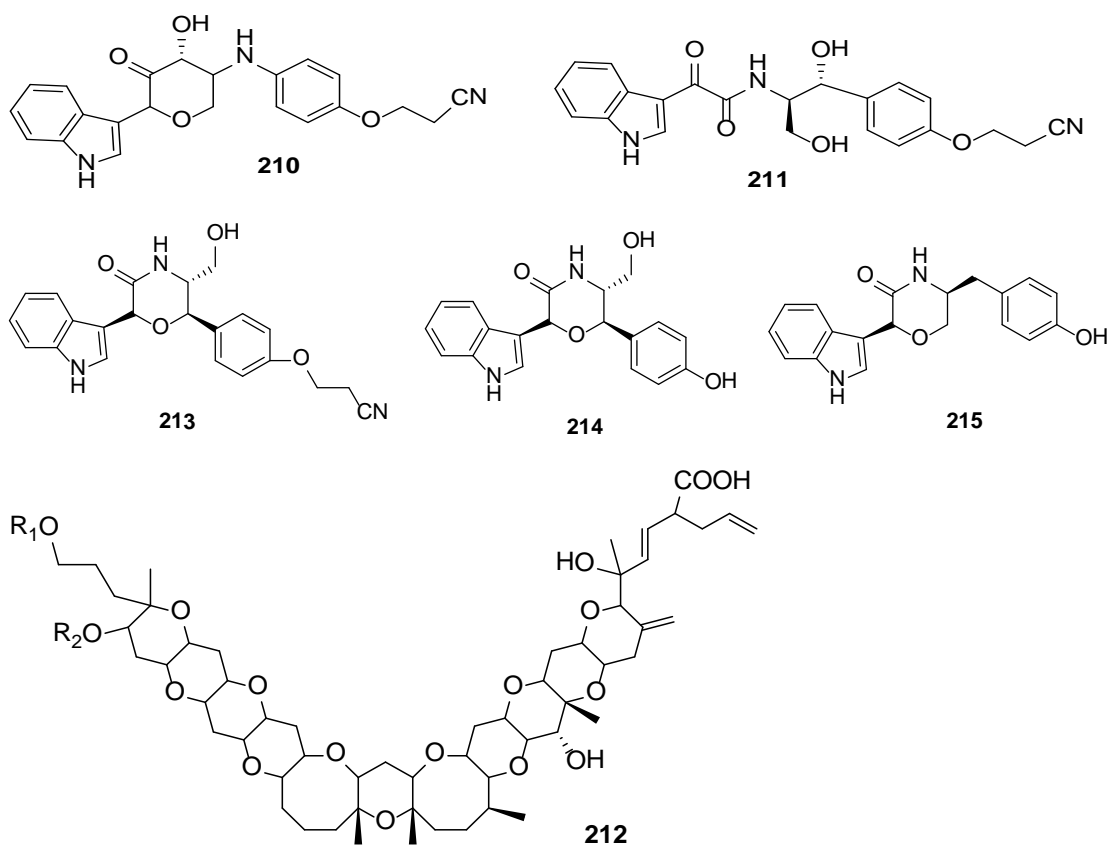


2.7.3.2. Secondary metabolites from bivalve mussels

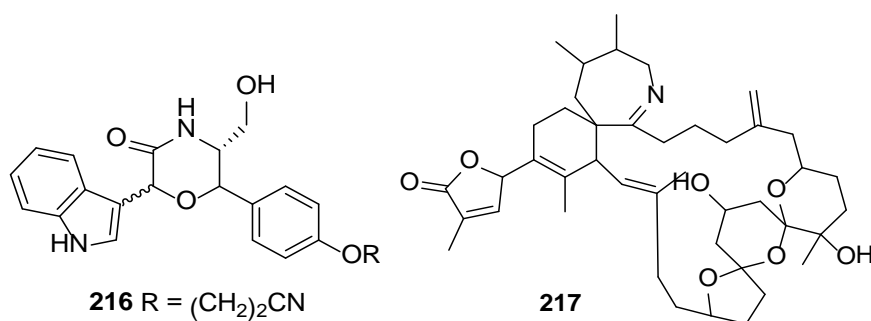
The azaspiracids were isolated from the extracts of *Mytilus edulis* (mussel) and their chemical structures characterised by NMR or mass spectroscopy (Kilcoyne *et al.*, 2015). Several carotenoids **204-206** were isolated from *M. galloprovincialis*

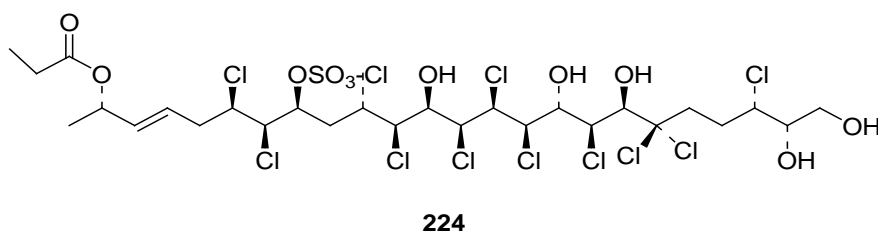
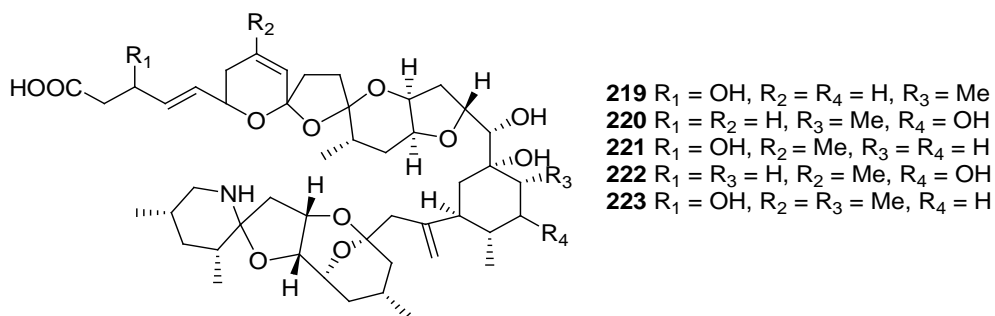
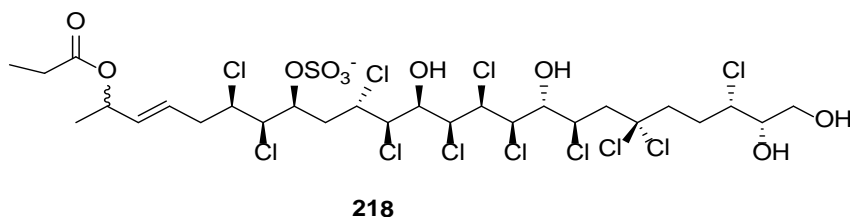
collected from Black Sea of Ukraine (Maoka *et al.*, 2011). Bathymodiolamides A **207** and B **208** with anti-tumour potentials were isolated from deep Sea mussel, *Bathymodiolus thermophilus* (Andrianasolo *et al.*, 2011). Anti-microbial peptide, Mytilin-A was purified from bivalve *M. edulis* (Charlet *et al.*, 1996), and the peptide analogue was exhibited activity towards marine *Vibrio*, yeasts and fungi. An homologous series of *n*-3 PUFAs along with 7,11,14,17-eicosatetraenoic acid **209** were identified as anti-inflammatory components in New Zealand green-lipped mussel *P. canaliculus* (Treschow *et al.*, 2007). The chemical investigation of *M. galloprovincialis* yielded oxazinin-5 **210** and a linear precursor preoxazinin-7 **211** (Ciminiello *et al.*, 2007b) along with desulfoyessotoxin **212** from the same mussel species (Ciminiello *et al.*, 2007a). The pinnatoxins and its fatty acid ester metabolites were identified from mussels (*M. edulis*) (McCarron *et al.*, 2012), whereas oxazinin compounds **213**, **214** and **215** and their analogues were identified from digestive glands of *M. galloprovincialis* (Ciminiello *et al.*, 2001).



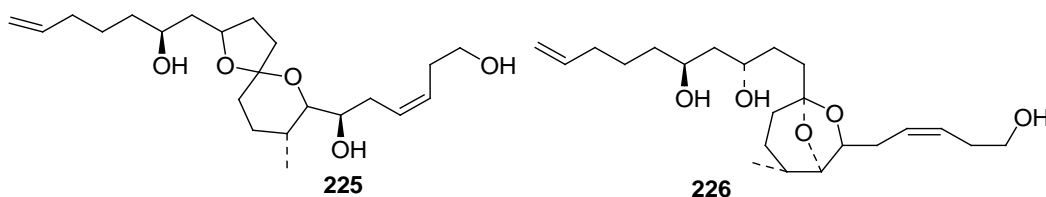


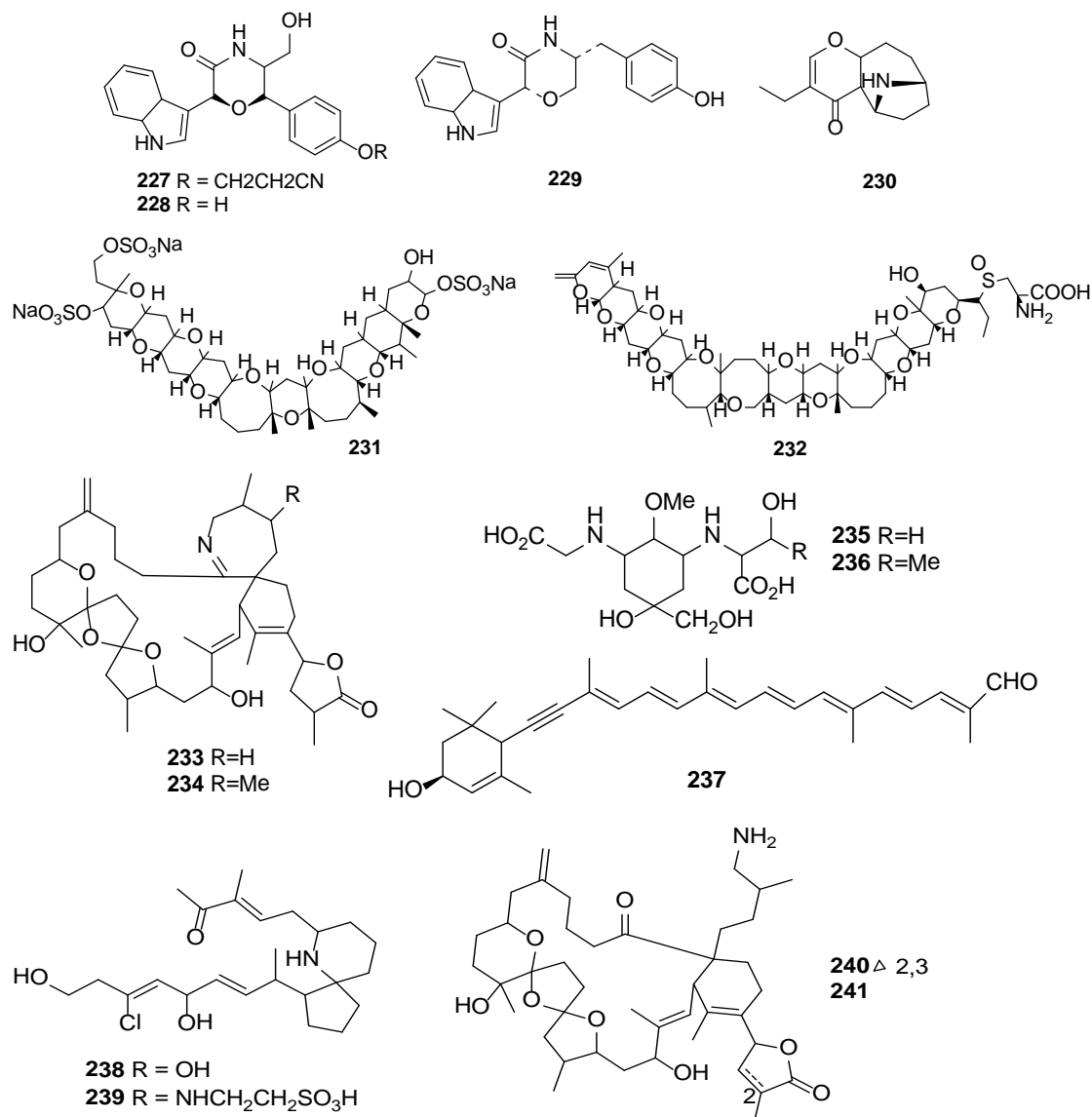
The oxazinin alkaloid, oxazinin-4 **216** was reported from mussel, *M. galloprovincialis* extract (Ciminiello *et al.*, 2006). The compound, 20-methyl spirolide G **217** was identified from *M. edulis* (Aasen *et al.*, 2005). The chromatographic fractionation of *M. galloprovincialis* extracts were found to yield cytotoxic chlorosulfolipid **218** (Ciminiello *et al.*, 2004) and brevetoxin analogue, brevetoxin B5 **175** identified from *P. canaliculus* (Ishida *et al.*, 2004). Five undescribed azaspiracid analogues **219-223** were characterized by tandem mass spectrometric methods from *M. edulis* (Ireland) (James *et al.*, 2003). The structure of polychlorinated sulfolipid **224** was reported from *M. galloprovincialis* (Ciminiello *et al.*, 2002).





The cytotoxic spiro-acetals, attenols A **225** and B **226** isolated from *Pinna attenuate* (Takada *et al.*, 1999). New bioactive alkaloids, oxazinins 1-3 **227-229** identified from *M. galloprovincialis* (Ciminiello *et al.*, 2001). An alkaloidal toxin, pinnamine **230** was identified from *P. muricata* (Takada *et al.*, 2000). The yessotoxin analogue, adriatoxin **231** isolated from *M. galloprovincialis* (Ciminiello *et al.*, 1998) and brevetoxin analogue, brevetoxin B2 **232** isolated from *P. canaliculus* (Murata *et al.*, 1998). The macrolides, spirolides B-C **233-234** were isolated from *M. edulis* (Hu *et al.*, 1995). The mycosporine derivatives such as mytilin A (**235**) and B (**236**) were acquired from *M. galloprovincialis* (Chioccaro *et al.*, 1979). The apocarotenoid, apoalloxanthinal **237** isolated from the Japanese mussel, *M. coruscus* (Maoka 1997). The cytosolic phospholipase A2 inhibitors, pinnaic acid **238** and taupinnaic acid **239** isolated from *P. muricata* (Chou *et al.*, 1996). The spirolides E **240** and F **241** metabolites from *M. edulis* helped to define pharmacophores of spirolides (Hu *et al.*, 1996).

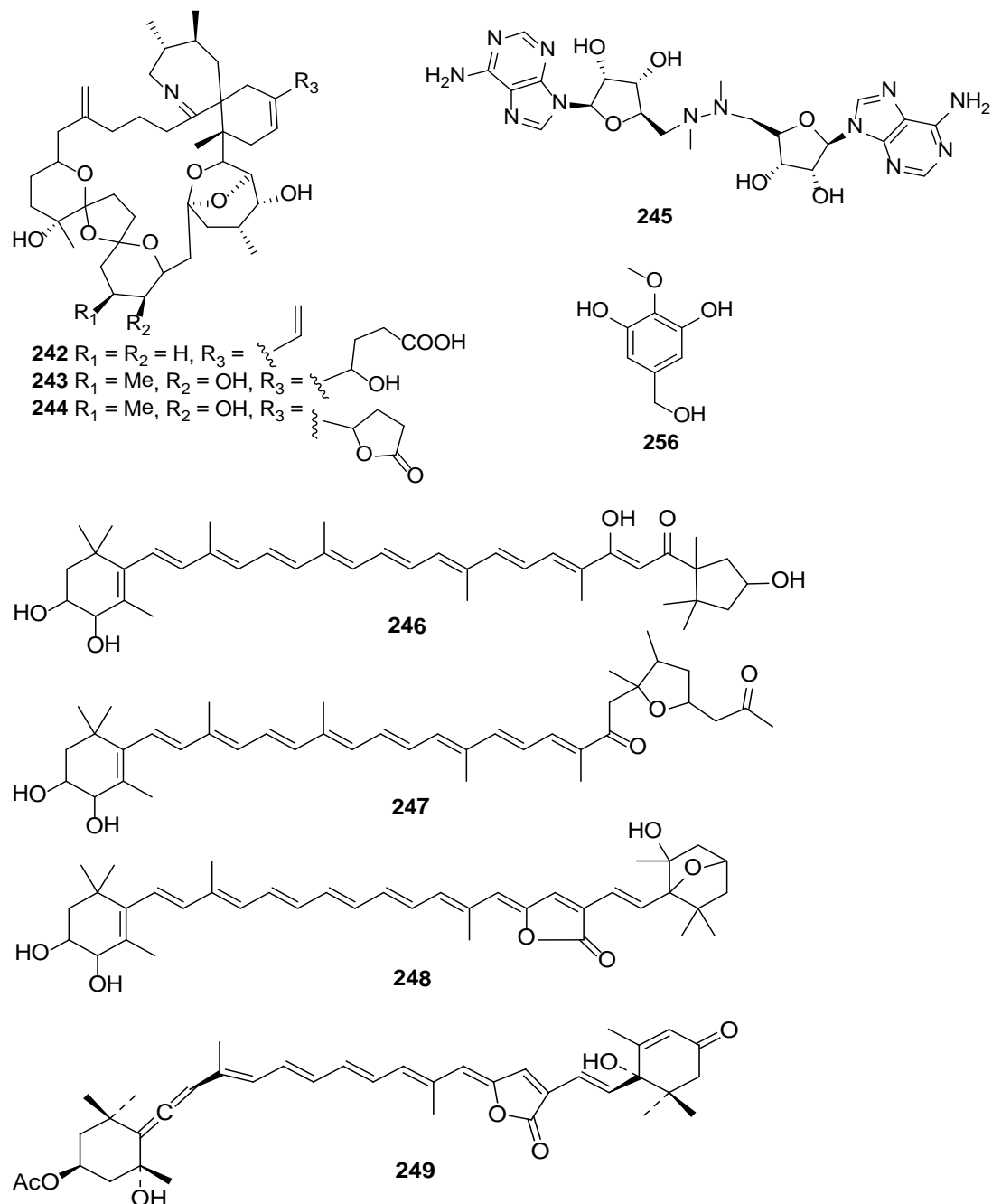


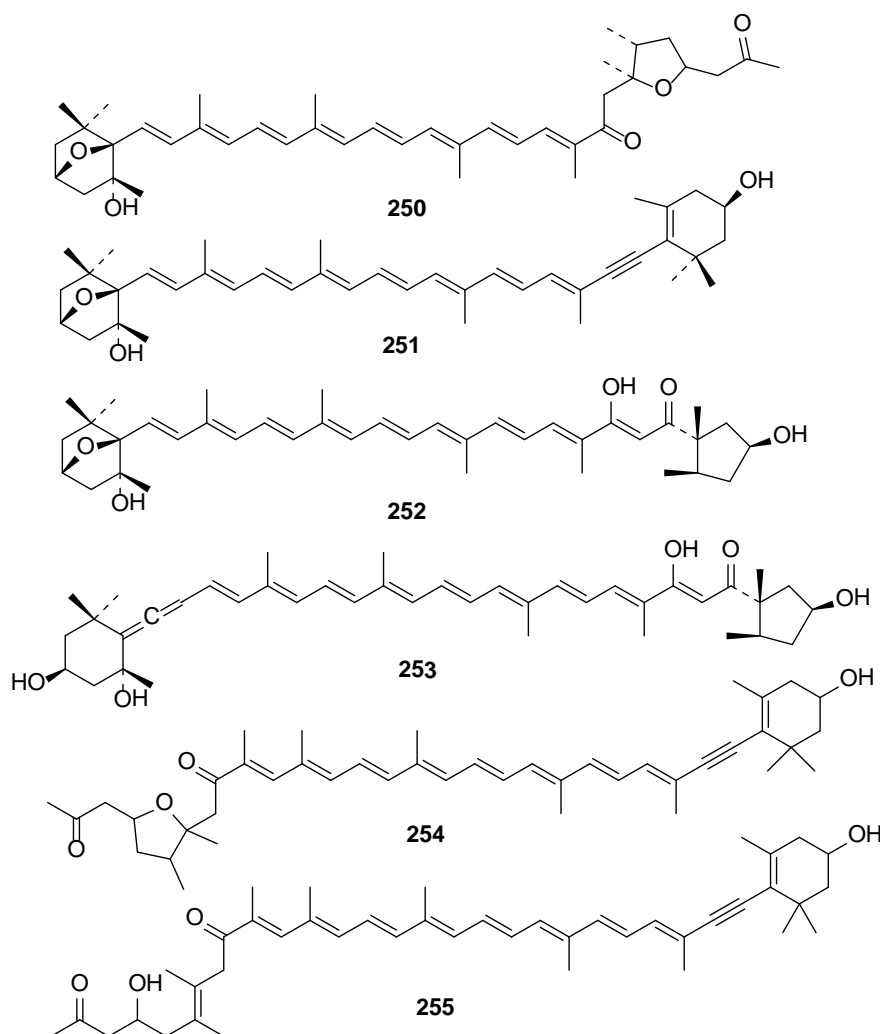


2.7.3.3. Secondary metabolites from bivalve oysters

The known spiroimine toxins pinnatoxin A and D, pinnatoxin E-G **242-244** were isolated from digestive glands of Pacific oyster *Crassostrea gigas* (Selwood *et al.*, 2010). Ostrerine A **245** acknowledged from the extracts of *Ostrea rivularis*, which has been used as foodstuff and conventional Chinese medication (Ouyang 2006). The carotenoids **246-248** were reported from *C. gigas* (Japan) (Maoka *et al.*, 2005b), whereas an anti-microbial peptide, defensin (molecular weight of 4265 Da) was isolated from the oyster, *C. virginica* (Seo *et al.*, 2005). *C. gigas* was used to isolate and characterize brevetoxin B5 **175** (Ishida *et al.*, 2004). The carotenoids **249-253** were reported from *C. gigas* (Maoka *et al.*, 2001). The metabolites of fucoxanthin,

crassostreaxanthin A (**254**) and crassostreaxanthin B (**255**) (Fujiwara *et al.*, 1992) along with C37-skeletal carotenoids (**200-203**) were identified from mollusk *C. gigas* (Maoka *et al.*, 2005b). The polyphenolic compound, 3,5-dihydroxy-4-methoxybenzyl **256** alcohol was identified from the Pacific edible oyster (*C. gigas*) and its potential antioxidant activity was determined (Watanabe *et al.*, 2012).

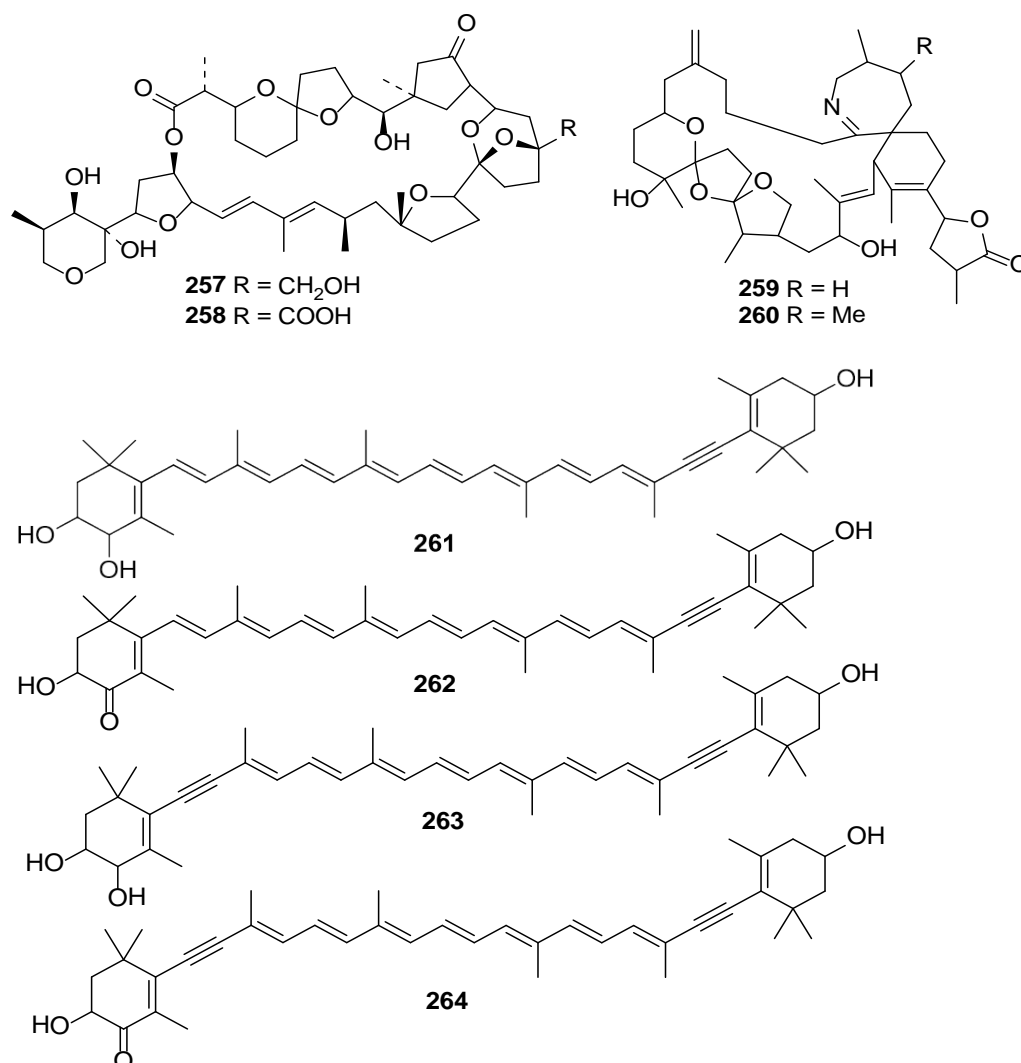




2.7.3.4. Secondary metabolites from bivalve scallops

The biosynthesis of elongated PUFA found in scallop *Chlamys nobilis* has revealed the occurrence of a novel elongase that can extend 20:5 n -3 and 20:4 n -6 FAs to C22 and C24 acids along with Δ^8 -desaturase (Liu *et al.*, 2014). This PUFA biosynthesising enzyme exhibited an advanced adaptation to its marine environment. Pectenotoxin 4 (**257**) and Pectenotoxin 7 (**258**) were purified from Japanese scallop, *Patinopecten yessoensis* (Sasaki *et al.*, 1998). Comparable macrolides, spirolides B **259** and D **260** were reported from scallop, *Placopecten magellanicus* (Hu *et al.*, 1995). The spirolides E and F metabolites were isolated from the scallop *P. magellanicus* (Hu *et al.*, 1996). The yessotoxin analogues, 45-hydroxyyessotoxin and 45,46,47-trinoryessotoxin from the Japanese scallop *P. yessoensis* were identified (Satake *et al.*, 1996; Takahashi *et al.*, 1996). The metabolites of alloxanthin and diatoxanthin, such as pectenol (**261**),

pectenolone (**262**), 4-hydroxyalloxanthin (**263**) and 4-ketoalloxanthin (**264**) were reported from scallops (Matsuno 2001).



2.8. Conclusions

The marine natural product research focused at the purification, isolation and characterization of previously undescribed specialized secondary metabolites with bioactive pluralities. These investigations were initially biased towards the soft bodied shelled or shell-less mollusks due to their vulnerability, adverse living conditions and lack of physical protections, even though, these were not reported for cellular damages. The newer approaches envisaged to identify an extremely diverse range of compounds including various pharmacophore templates, which aimed towards the drug discovery. The natural products derived from mollusks, particularly of shelled origin, have been used as traditional medicines and functional foods. The preliminary data on nutritional

assessments, bioactive potentials and bioactive components from bivalves, gastropods and cephalopods appropriately suggested their potential pharmacological utilities. Among various mollusks, bivalve clams were considered as traditional health food and natural dietary source, even though, the scientific investigations to acknowledge the health benefits of these species were confined. There are scanty and scattered information on bioactive lead molecules from these low value species, whereas the investigations on the structural characterizations of bioactive molecules were limited or yet to be studied. There is an increasing demand for more target oriented investigations related to bioactive components from mollusk, specifically from the bivalve clams. The bioactives from bivalve clams can be used as potential pharmacophore leads to develop drug templates, nutraceuticals and functional food supplements for human health and wellness.

NUTRITIONAL PROFILING OF *VILLORITA CYPRINOIDES* AND *PAPHIA MALABARICA*

Contents

- 3.1. *Background*
- 3.2. *Materials and methods*
- 3.3. *Results and discussion*
- 3.4. *Conclusion*

3.1. Background

Bivalve mollusks are one of the most important seafoods in the coastal areas of the world contributing a predominant share among the marine and estuarine organisms (Xie *et al.*, 2012). Among the molluscan bivalves, the clams occupy a predominant share to the total edible bivalve mollusks in the world (Murray and Burt 2001) although these are frequently underestimated and regarded as by-catch fishery resources (Gosling 2002). The black clam *Villorita cyprinoides* (family, Corbiculidae) and short-neck yellow-foot clam, *Paphia malabarica* (family, Veneridae), are the most important and common seafood resources in the coastal regions of India. These low valued clam species will be recognized as preferred food items among the coastal populace of the underdeveloped and developing countries of Africa and Asia, provided if their nutritional qualities be studied extensively (Saba 2011). The mollusks were accounted for possessing the essential nutritional elements, which are not present in sufficient quantities in our staple food items, such as cereals and pulses (Chakraborty *et al.*, 2016a; Chakraborty *et al.*, 2016b; Murray and Burt 2001). For example, the essential nutritional elements such as lysine and sulfur containing amino acids are reported to be absent in cereals, and were present in adequate quantities in the bivalve mollusks, this showed that these species can viably supplement the limiting amino acids in our daily diets (Chakraborty *et al.*, 2016a; Chakraborty *et al.*, 2016b). It is additionally significant to note that the consumption of staple food items in the daily diets, such as cereals and pulses can't fulfil the obliged nutritional necessities. The quest

for balanced nutritional components from the low value food items are of greater importance particularly due to the fact that lack of proper nutrition continues to be a major risk factor causing death in developing and underdeveloped countries (Schofield and Ashworth 2002). Most of the populace in these nations can't stand to have the relatively expensive food items with balanced nutritional elements.

Marine fishes are rich in minerals and vitamins (Chakraborty and Joseph 2015; Chakraborty *et al.*, 2016c). The clam species have a place with the group of bivalve mollusks, and therefore, constitute potential low valued food items of the coastal populace in this area. The clam fisheries in Ashtamudi Lake of Kerala have acquired India's first MSC certification (Marine Stewardship Council certification), which will facilitate in promoting the clam fishery in this region. The development of clam fishery in Ashtamudi was determined by the requirements in Thailand, Japan and Vietnam in 1980s to 1990s. Clam fisheries have continuous landings of approximately 10,000 tonnes per year for as long as decade in this fishing area of India (Mohamed *et al.*, 2013).

The fat content in pulse based food items and edible oils were accounted for to have elevated contents of saturated fat and *n*-6 fatty acids. Prior reports have expressed those large amounts of *n*-6 PUFA in the human diet realizes numerous health disorders due to their biotransformation to the inflammatory prostaglandin leading to various oxidative stresses induced inflammatory diseases (Cleland *et al.*, 2006). It was reported that the *n*-3 PUFAs accounted for to change the unfavourable effects of *n*-6 PUFAs (Calder 2004). Notably, long-chain C₂₀-C₂₂ *n*-3 PUFAs are vital for healthy diet, which has a significant part in different structural and metabolic capacities, for example, inflammation, immunity and allergic responses (Calder 2012). The *n*-3 polyunsaturated fatty acid content is predominant than saturated fatty acids in bivalve mollusks as demonstrated in earlier studies (Chakraborty *et al.*, 2016a; Orban *et al.*, 2002).

Bivalves are good sources of C₂₀-C₂₂ *n*-3 PUFAs, such as EPA and DHA, which are the precursors of anti-inflammatory resolvins (E- and D-series), and reported to be anti-inflammatory agents (Chakraborty *et al.*, 2014a). In this way, shellfish were considered as low saturated fat and high protein food, which can be included in the low fat and affordable healthy diets (Food and Nutrition Board 2007). The low valued clam species may constitute the significant raw materials for the functional food supplements

and may substitute the relatively expensive nutraceuticals available in the market. Over the previous decades, the importance of bivalve clam has significantly expanded as alternative resources to the traditional finfish fishery in the distinctive parts of the world. Because of their nutritional and market value, clam aquaculture has additionally demonstrated an increment amid the recent years.

As of late, after the significance of low valued bivalve clams as a potential health food had been acknowledged, the studies on its biochemical composition began to receive considerable attention. The coastal waters of the southwest coast of Arabian Sea was found to be the most productive fishery zone in India, representing around 90% of the aggregate bivalve clam production. Albeit, a few studies have been directed to the biological description and distribution of these species (Gosling 2002; Heslinga 1989), there has no published studies were available on its nutritional composition. Hence, the present study envisaged to carry out on the essential nutritional qualities with respect to proximate composition, meat yield, condition indices, amino acids, cholesterol, proteins, lipids, fatty acids, vitamins and mineral contents of the two common clam species, *V. cyprinoides* (Gary) and *P. malabarica* (Chemnitz), available in abundance at the coastal waters of the southwest coast of India.

3.2. Materials and methods

3.2.1. Chemicals, reagents and instrumentations

The solvents utilized in the study were of analytical or HPLC category (E-Merck, Frankfurter, Darmstadt, Germany; Sigma-Aldrich, Missouri, USA) and carried out for redistillation. MiiliQ or double distilled (DDW) or HPLC grade water was used during the experimentations. The reagents were of spectroscopic or analytical category (E-Merck, Frankfurter, Darmstadt, Germany; Sigma-Aldrich, Missouri, USA). Potassium hydroxide, sodium hydroxide, sodium phosphate buffer, acetic acid, metaphosphoric acid, tertbutylhydroquinone (TBHQ), sodium sulfate (Na_2SO_4), boron trifluoride in methanol (BF_3 in MeOH), bovine serum albumin, sodium carbonate (Na_2CO_3), copper sulfate (CuSO_4), potassium-sodium tartarate, Folin-Ciocalte reagent (F.C. reagent), trichloro acetic acid (TCA), cholesterol (standard), *O*-phtalaldehyde, glacial acetic acid, fatty acid methyl ester (FAME) standards (Catalog No. 47885-U, SupelcoTM 37 Component FAME Mix), vitamin (A, D₃, E, K, C) standards were

procured from E-Merck (Frankfurter, Darmstadt, Germany) or Sigma-Aldrich (Missouri, USA). The amino acid standards procured from Thermo Scientific (PIERS amino acid standard H) and the standards for mineral analyses were purchased from Perkin Elmer (Shelton, USA). All glasswares procured from Borosil (India) or Magnum glassworks (Cochin, Kerala, India).

Gas liquid chromatography (GLC) data recorded on a Perkin-Elmer AutoSystem XL gas chromatograph (HP 5890 Series II, Perkin Elmer, Shelton, CT, USA). The spectrophotometric data acquired on ultraviolet-visible spectrophotometer (Varian Cary 50, Walnut Creek, California, USA). The amino acid analyses performed on a reversed phase binary gradient high performance liquid chromatography (HPLC, Waters Corp., Milford, MA, USA). The analyses of fat soluble vitamins such as A, D₃, E, K performed using HPLC instrument (Shimadzu LC 20AD, Shimadzu Corp., Nakagyo-ku, Japan). Mineral profiles analyzed using atomic absorption spectrometer (AAAnalyst™ 200, Perkin Elmer, Shelton, CT, USA). The solvents were evaporated by rotary evaporator (Heidolph Instruments GmbH and Company, Schwabach, Germany). The refrigerated centrifuge (Thermo Scientific, Thermo Electron LED GmbH, Langenselbold, Germany) used for centrifugation. Samples were dried using laboratory oven (Labline, India).

3.2.2. Study area and samples

The two bivalve clams selected for this study were,

- *Villorita cyprinoides* Family - Corbiculidae
- *Paphia malabarica* Family – Veneridae

The samples of *V. cyprinoides* and *P. malabarica* (5 kg each) were collected during the month of September (post-monsoon season) from the estuarine waters of Vembanad Lake (9°35' N and 76°25' E) and Ashtamudi Lake (8°59' N and 76°36' E), respectively situated at the southwest coast of India, which is predominantly influenced by oceanic waters from the Arabian Sea. The photographs of sample collection sites, the shell on samples and the inside view of edible part of *V. cyprinoides* and *P. malabarica* were illustrated (Figure 3.1.-3.2.).

After cleaning the fouling matters and externalities, *V. cyprinoides* and *P. malabarica* were transported to the laboratory in an ice box. They were thoroughly washed to remove mucus, debris, fecal matters, and other particles. The surface water on the clam samples blotted with filter paper, and the edible meat (1 kg each) separated from the shells before being analyzed for the biometric and nutritional parameters.

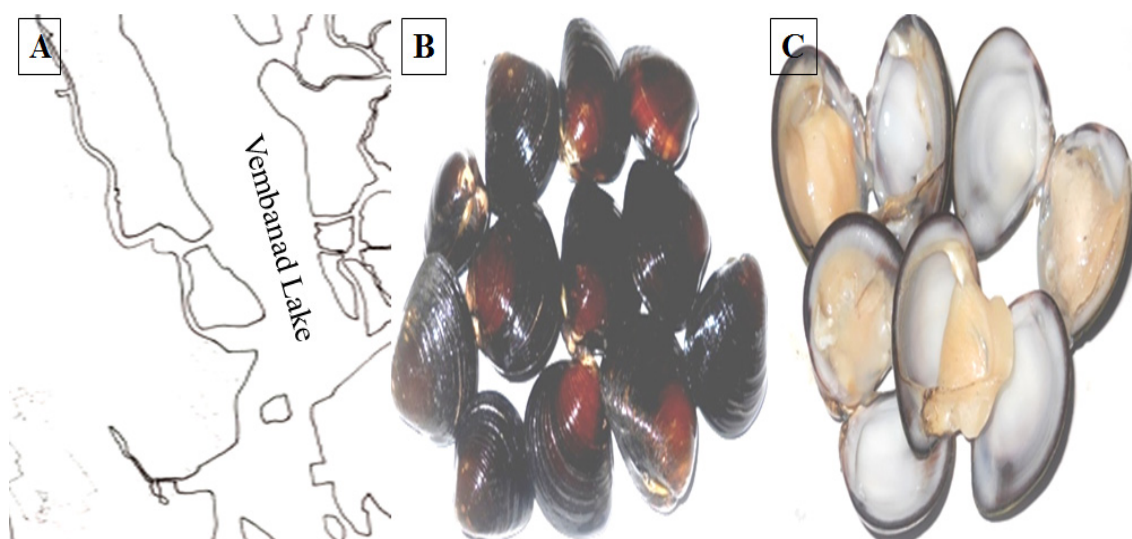


Figure 3.1.: Sample collection site of edible clam, *V. cyprinoides* along the southwest coast of India bordering the Arabian Sea. (A) Vembanad Lake at 9°35' N and 76°25' E; (B) the shell on *V. cyprinoides*; (C) the inside view of *V. cyprinoides* with edible part

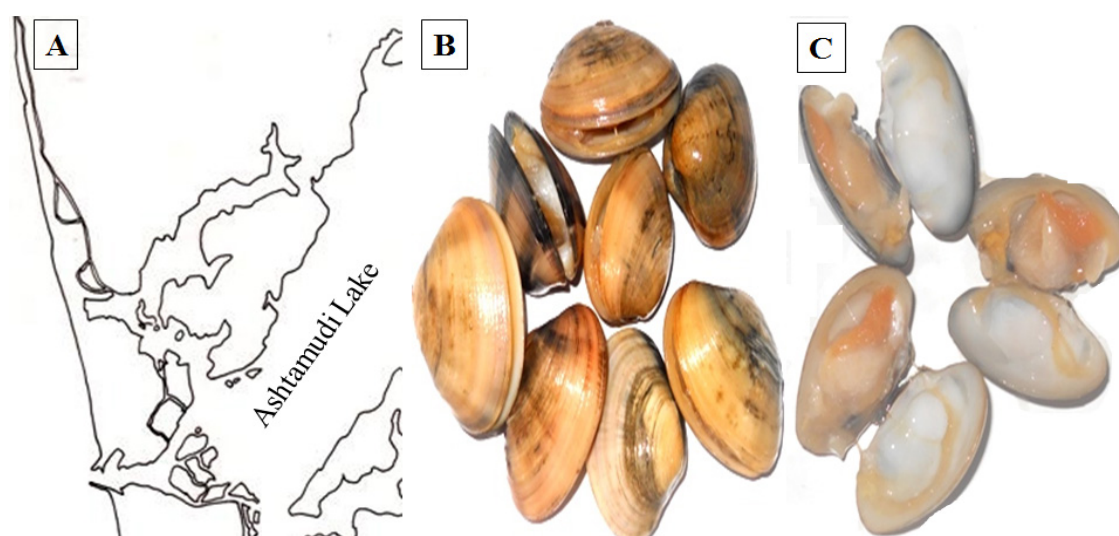


Figure 3.2.: Sample collection sites of edible clam, *P. malabarica* from the southwest coast of India bordering the Arabian Sea. (A) Ashtamudi Lake at 8°59' N and 76°36' E; (B) the shell on *P. malabarica*; (C) the inside view of *P. malabarica* with edible part

3.2.3. Determination of biometric parameters, condition indices and meat yield

The samples of *V. cyprinoides* and *P. malabarica* measured for their biometrical parameters, namely length, width and thickness. The length (maximum anterior-posterior axis), width (maximum lateral axis), and thickness (height of maximum longitudinal axis) of fifty randomly selected samples measured using a Vernier calipers. The samples were weighed, opened by cutting the adductor muscle and the wet meat and shell weight were noted. The tissues were oven dried for 48 h at 60°C, and the dry weight was determined. Condition indices (CI) used to characterize the apparent health and quality of the biological entity. Three condition indices (CI) were taken into account in this study were as follows: (1) economic CI calculated using the formula: $\text{thickness} / [0.5 * (\text{length} + \text{width})]$ (Imai and Sakai 1961); (2) Booth CI calculated as wet flesh weight/total weight (Booth 1983) and (3) ecophysiological CI expressed as dry flesh weight/dry shell weight (Walne 1976). The dry weights of shells were calculated by oven drying (80°C).

3.2.4. Proximate composition

Moisture content in the samples were analyzed by drying the known weights of samples at 60°C in a hot air oven until acquiring a constant weight, followed by drying in a hot air oven for 2 h at 100°C (AOAC 1990). The crude protein (total nitrogen content) was determined by micro Kjeldhal method and the results were multiplied by 6.25 to attain the crude protein percentage. The crude fat was calculated by Soxhlet apparatus method using petroleum ether (b.p. 60-80°C). Crude fibre was estimated by the fraction remained after the reflux with standard, H₂SO₄ (1.25% w/v) and NaOH (1.25% w/v) solution for 30 min, under controlled condition. The carbohydrate content was determined by following AOAC (2005) method.

3.2.5. Estimation of protein and amino acid

3.2.5.1. Estimation of protein

The protein contents in the flesh of clams were determined by recognized procedure of Lowry *et al.*, (1951). The standard, bovine serum albumin stock was prepared and from this solution, different concentrations (0-800 µg/mL) of working standard were prepared by serial dilutions. Each of the above working standard solution

(5 mL) was added with 5 mL of freshly prepared alkaline reagent (96% of Na_2CO_3 2% in 0.1 N NaOH + 2% of CuSO_4 0.5% in DDW + 2% of potassium-sodium tartarate 1% in DDW). This solution was mixed well and kept for 10 min incubation, along with addition of 0.5 mL of freshly prepared Folin-Ciocalte (1:2, v/v, F.C. reagent:DDW). This mixture was homogenized properly and kept for 30 min in dark (a blue colour was formed). The absorbance of aliquot of protein was recorded at 660 nm against the reagent blank by UV-Visible spectrophotometer. A linear curve of standard was plotted between the concentration (X-axis) and the absorbance (Y-axis). The edible tissues of respective clam samples (0.1-0.2 g) were mixed with DDW (1 mL) and 1 mL of 5% trichloro acetic acid followed by centrifugation (4°C , 20 min, 10,000 rpm). To the supernatant solution of samples (1 mL) were added with 5 mL of freshly prepared alkaline reagent (96% of Na_2CO_3 2% in 0.1 N NaOH + 2% of CuSO_4 0.5% in DDW + 2% of potassium-sodium tartarate 1% in DDW). This solution was mixed well and kept for incubation (10 min), followed by addition of 0.5 mL of freshly prepared F.C. reagent (1:2, v/v, F.C. reagent:DDW). This mixture was homogenized properly and kept in dark for 30 min (a blue colour was formed) before being measured the absorbance at 660 nm. The protein content was calculated from standard curve of bovine serum albumin, and expressed as mg/g of wet weight using the equation given below.

Protein in mg/g sample = (concentration in $\mu\text{g/mL}$ (x) * 2 mL)/(weight of sample in g * 1000)

Concentration in $\mu\text{g/mL}$ (x) was obtained from the linear graph of standard using the equation

$y = mx + c$ (where “y = absorbance of sample”)

(1000 = g converted to mg; 2 = sample dissolved in 1 mL TCA and 1 mL DDW)

3.2.5.2. Estimation of amino acid

The percentages of amino acids were calculated by earlier methods (Chakraborty and Joseph, 2015). The samples (0.2 g) were hydrolyzed at 110°C using HCl (10 mL, 6 N) in a closed glass tube on multi-place heating mantle for 24 h. After cooling the glass tubes, the seal was broken and filtered the samples through Whatman filter paper (No. 41) to a flask followed by evaporation to dryness in vacuum rotary

evaporator (75-85°C) to afford a residue. This residue was washed using DDW and vacuum concentrated at 75-85°C. This procedure was repeated for 3-4 times to remove the presence of acid and finally, the concentrate or aliquot was reconstituted in 5 mL 0.05 N HCl. The hydrolyzed amino acids in the aliquot treated with the redrying agent (2:2:1, v/v/v, methanol 95%:water:triethylamine) and subsequently pre-column derivatization of hydrolyzable amino acids were treated with phenyl isothiocyanate (PITC or Edman's reagent) to yield phenylthiocarbamyl amino acids (PTC). The reagent was freshly processed and composition of derivatizing agent consisted of methanol 95%:triethylamine:phenylisothiocyanate (20 µL, 7:1:1, v/v/v; 70 µL methanol + 10 µL DDW + 10 µL triethylamine + 10 µL phenyl isothiocyanate). The 20 µL of PTC derivative (derivatized sample) was diluted with 20 µL of diluent (5:95, v/v, acetonitrile:5 mM sodium phosphate buffer, pH 7.4) before injecting into reversed phase HPLC equipped with column, retained at 38°C in a column oven and identified by UV absorbance at λ_{\max} 254 nm (Waters Corporation, Milford, MA 01757, USA). Mobile phase has been consisted of sodium acetate trihydrate (pH 6.4, 0.14 M, 940 mL; A) including 0.05% triethylamine was homogenized with 60 mL acetonitrile and 60:40 (v/v) acetonitrile:water (B). The gradient elution method with increasing eluent B employed for this use. The quantification of amino acids was carried out by comparing the peak area of sample with the peak area of standard and the amino acid content was expressed as mg/100 g protein. The total essential amino acids (\sum EAA), total non-essential amino acids (\sum NEAA), total amino acids (\sum AA), total aromatic amino acids (\sum ArAA), total sulfur containing amino acids (\sum SAA), ratio of total essential amino acid to total amino acid (\sum EAA/ \sum AA), ratio of total non-essential amino acid to total amino acid (\sum NEAA/ \sum AA) and ratio of total essential amino acid to total non-essential amino acid (\sum EAA/ \sum NEAA) were determined.

The amino acid score for essential amino acids determined by utilizing FAO/WHO (FAO, WHO 1990) method:

amino acid score = amount of amino acid per protein in sample (mg/g)/amount of amino acid per protein in standard protein (mg/g) with regard to standard amino acid requirements for adults (FAO, WHO, UNU 2007).

3.2.6. Estimation of lipid and fatty acid

3.2.6.1. Estimation of lipid

The extractions of lipids in tissues of bivalve clams were performed by Folch extraction (Folch *et al.*, 1957) method by 2:1 chloroform:methanol (v/v, 200 mL). Edible portion of each species (10-30 g) were mixed with 1:1 of chloroform:methanol (v/v) and distilled water (200 mL). This mixture was homogenized with 0.002% TBHQ and kept for overnight in the dark at 4°C in the nitrogen atmosphere to extract lipids. The solutions were filtered through separating funnel using Whatman filter paper and chloroform layer (bottom layer) containing lipids was collected through Na₂SO₄ to a pre-weighed flask (w2). The filtrate was evaporated at 40-45°C and final weight of the flask was calculated. The percentage (%) of lipid content was calculated using the equation,

$$\text{Lipid (\%)} = [(W1-W2)/W3] * 100$$

(W1 - weight of flask + lipid; W2 - weight of flask; W3 - weight of sample)

3.2.6.2. Estimation of fatty acid

The fatty acid compositions of total lipids from *V. cyprinoides* and *P. malabarica* were estimated as mentioned earlier (Metcalf *et al.*, 1966). The methanolic KOH was added to the above obtained lipid and refluxed for 30 min at 80°C under nitrogen atmosphere. A solution of BF₃ in methanol (5 mL) was added to the above mixture and again refluxed under nitrogen atmosphere (5 min). This solution was allowed to cool and added with petroleum ether (twice the volume of solution) to a separating funnel to separate the layers using distilled water. The organic layer (upper) was washed with distilled water for 3-4 times and collected the petroleum ether layer (organic) through Na₂SO₄ and concentrated in rotary evaporator (40°C). The concentrates were reconstituted in minimum amount of petroleum ether and injected in gas liquid chromatography (GLC). GLC data recorded on a Perkin-Elmer AutoSystem XL gas chromatograph (HP 5890 Series II, Perkin Elmer, Bridgeport Ave, Shelton, CT, USA) connected with a SP 2560 (crossbond 5% diphenyl-95% dimethyl polysiloxane) capillary column (100 m X 0.25 mm i.d., 0.50 µm film thickness, Supelco, Bellfonte, PA) utilizing a flame ionization detector (FID) equipped with a split/splitless injector,

which was used in the split (1:15) mode. The GLC analyses were carried out using oven temperature ramp program: 140°C for 1 min, rising at 30°C/min to 250°C, where it was held for 1.0 min, followed by an increase of 25°C/min to 285°C, where it was held for 2.0 min, until all peaks were appeared. The injector and detector were held at 285°C and 290°C, respectively. Nitrogen (ultra high purity > 99.99%) was used as carrier gas at 25 cm/s flow rate. Hydrogen was used as the carrier gas at a head pressure of 20 psi. The injection volume was 0.02 µL. The evaluation of retention times with standards (Supelco™ 37 Component FAME Mix) was identified as FAMES and results were calculated as total fatty acids percentage (% TFA). Total Σ PUFA (polyunsaturated fatty acids), Σ MUFA (total monounsaturated fatty acids) and Σ SFA (total saturated fatty acids) were calculated. The different ratios of fatty acid indicating nutritional values of the edible clams namely, n -3/ n -6, n -6/ n -3, DHA/EPA and Σ PUFA/ Σ SFA were calculated.

The indices of atherogenicity (AI) and thrombogenicity (TI) (Ulbricht and Southgate 1991) have been calculated as:

$$AI = (4 * 14:0 + 18:0 + 16:0) / (\text{MUFA} + \Sigma n\text{-3PUFA} + \Sigma n\text{-6PUFA})$$

$$TI = (14:0 + 18:0 + 16:0) / [(0.5 * \text{MUFA}) + (0.5 * n\text{-3PUFA}) + (3 * n\text{-3PUFA}) + (n\text{-3PUFA}/n\text{-6PUFA})]$$

The hypocholesterolaemic/hypercholesterolaemic (HH) ratio determined by (Santos-Silva *et al.*, 2002).

$$HH = (18:1n\text{-9} + 18:2n\text{-6} + 20:4n\text{-6} + 18:3n\text{-3} + 20:5n\text{-3} + 22:5n\text{-3} + 22:6n\text{-3}) / (14:0 + 16:0)$$

3.2.7. Estimation of minerals

The mineral contents were estimated by atomic absorption spectrometer (AAnalyst™ 200 spectrometer, Perkin Elmer, USA). The samples were kept for ashing, followed by acid (HCl) digestion and aspiration. The dry samples of clam (2 g) were kept at 525°C in muffle furnace and the ashed samples were digested in 50 mL of 6N HCl, and filtered through Whatman No.1 filter paper before being diluted with milliQ water. The sample solution was aspirated in an atomic absorption spectrometer for the

determination of minerals. The analyses of calcium (Ca), sodium (Na), potassium (K), magnesium (Mg), copper (Cu), iron (Fe), and zinc (Zn) were performed by flame atomic absorption spectrometer equipped with a hollow cathode lamp containing D₂ lamp background correction system. The continuous flow hydride generator fixed with atomic absorption spectrometer was utilized for selenium (Se) contents (Chakraborty *et al.*, 2016b). The analyses of phosphorus was carried out by alkalimetric ammonium molybdophosphate experiment as established in AOAC (AOAC 2005) official procedure 964.06. Macro (Mg, Na, Ca, K and P) and micro minerals (Fe, Cu, Mn and Zn) were represented as mg/100 g wet weight except for Se which was represented in µg/100 g wet weight.

3.2.8. Estimation of cholesterol and vitamins

3.2.8.1. Estimation of cholesterol

The total cholesterol content in bivalve clams were resolved spectrophotometrically (Varian Cary, USA) with appropriate alterations using *O*-phthalaldehyde (50 mg/dL in glacial acetic acid) (Wanasundara and Shahidi 1999). The stock standard solution of cholesterol in ethanol (10 mg in 10 mL, 1000 ppm) and its working stock solutions were prepared (0-1000 µg/mL by serial dilution). About 0.1 mL of stock solution from each of the different concentration was mixed with *O*-phthalaldehyde (2 mL) and Con. H₂SO₄ (1 mL). The absorbance of solution was recorded after 10 min at 550 nm. Then, a linear curve of standard was plotted by the concentration against (X-axis) absorbance (Y-axis). The edible tissue of respective clam samples (0.1 g) mixed with 33% KOH (0.3 mL) and ethanol (3 mL) followed by heating for 15 min in water bath (60°C). This solution was allowed to cool and mixed with hexane (10 mL) and DDW (3 mL). The hexane supernatant was pipetted out and evaporated, followed by slow addition of Con. H₂SO₄ (1 mL). The mixture was homogenized thoroughly and absorbance was recorded after 10 min at 550 nm. The collective cholesterol content determined from standard curve of cholesterol. The values were reported as mg/100 g on wet weight basis using the equation given below,

$$\text{Cholesterol in mg/100 g} = (\text{concentration in } \mu\text{g/mL (x)} * 100) / (\text{sample weight in g} * 1000)$$

Concentration in $\mu\text{g/mL}$ (x) obtained from the linear graph of standard using the equation

$y = mx + c$ (where “y = absorbance of sample”)

(1000 = conversion of μg to mg, 100 = 100 g sample)

3.2.8.2. Estimation of vitamins

The vitamins, A, D₃, E and K were estimated by Salo-Vaananen *et al.*, (2000) method. The vitamin standard (Sigma-Aldrich Chemical Co. Inc, St. Louis, MO) solutions (1/10/ 25/50/100 ppm) were maintained at -20°C except vitamin D₃ (stored at 4°C). Lipids were yielded by the method described as in 3.2.6.1. before hydrolyzation (KOH/MeOH, 0.5 N, 2 mL) (Chakraborty *et al.*, 2014b). The hydrolyzed mixture (2 mL) was extracted with petroleum ether (fraction of 40-60°C, 15 mL) before being washed with deionized water (2 X 10 mL) to remove alkali content. The non-saponifiable portion was concentrated under vacuum using a rotary evaporator (Heidolph Instruments GmbH and Co., Schwabach, Germany) at 50°C before being reconstituted in MeOH. The latter was filtered through a syringe filter (0.2 mm) before being injected (20 mL) in the HPLC (Shimadzu LC 20AD, Shimadzu Corporation, Nakagyo-ku, Japan). The HPLC system was equipped with a reverse phase column (phenomenex, C18 250 mm length, 4.6 mm i.d., 5 μm) that was housed in a column oven (32°C) and connected to a photodiode array detector. The gradient programme was as follows: 20% MeOH (HPLC grade) up to 3 min, which was increased to 100% in the next 5 min and held for 37 min with a complete run time of 45 min. The flow rate was 1 mL/min. The vitamin C was determined based upon the quantitative discolouration of 2,6-dichlorophenol indophenol titrimetric method (AOAC 2005). In brief, ascorbic acid was extracted from the clam samples (M, 15-20 g) using an acetic acid and metaphosphoric acid solution (HPO₃-CH₃COOH, 10 mL X 2). The extracts were transferred with distilled water into a known volume (B, mL) and filtered rapidly. The known volume (C, mL) of the above solution was pipetted out and titrated with the redox dye, 2,6-dichlorophenol indophenol solution until the faint pink colour persisted for 15 s. The vitamins A, D₃, E and C were reported in IU (International Unit) whereas, vitamin K in $\mu\text{g}/100$ g wet weight.

Ascorbic acid content was calculated as: $\{(A - A_0) * D * B * 10\} / (M * C)$,

Where A = average volume of test solution for titration in mL, A_0 = average volume for blank titration in mL and D = mg ascorbic acid equal to 1 mL of standard indophenol solution.

3.2.9. Statistical analyses

One way analyses of variance (ANOVA) was carried out with the Statistical Program for Social Sciences 13.0 (SPSS, USA, ver. 13.0) to assess significant differences between the means. The significant differences were represented as $p < 0.05$. The values were given as mean of triplicates \pm standard deviation. The mean variance in the data set was detected using principal component analyses (PCA). The various nutritional parameters were selected as the variables for PCA.

3.3. Results and discussion

3.3.1. Morphometric characteristics

The biometric estimations of clams were determined by measuring their length, width and thickness. The meat yield of the edible clams from their habitat showed that this morphometric index was not significantly distinctive between *V. cyprinoides* and *P. malabarica* (20-21%, $p > 0.05$) (Table 3.1.). The present study exhibited no significant difference in condition indices between the edible clams by the methods of Imai and Sakai, Walne and Booth ($p > 0.05$).

Table 3.1.: Meat yield (%) and biometric measurement (length, width, thickness) of *P. malabarica* and *V. cyprinoides*

	<i>P. malabarica</i>	<i>V. cyprinoides</i>
Meat yield (%)	20.33 ± 1.15^a	21.67 ± 1.53^a
Length (cm)	3.67 ± 0.15^a	3.37 ± 0.15^a
Width (cm)	2.67 ± 0.15^a	2.70 ± 0.10^a
Thickness (cm)	1.40 ± 0.10^a	1.33 ± 0.15^a

Data were reported as mean \pm standard deviation of three replicates. No significant differences were observed between the variants ($p > 0.05$)

Table 3.2.: Condition indices of *P. malabarica* and *V. cyprinoides*

	<i>P. malabarica</i>	<i>V. cyprinoides</i>
Imai and Sakai	0.44 ± 0.05^a	0.44 ± 0.04^a
Booth	0.20 ± 0.01^a	0.22 ± 0.02^a
Walne	0.05 ± 0.01^a	0.07 ± 0.01^a

Data were reported as mean \pm standard deviation of three replicates. No significant differences were observed between the variants ($p > 0.05$)

Percentage edibility or the condition indices (CI) have been utilized to comprehend the biological value of these shellfishes used in the present study. The commercial quality and physiological condition of mollusks were depicted by condition indices. CI is closely identified with the nutrient storage and meat quality. The good CIs which were dictated by different methods suggested that these shellfish species can be used as potential sources for human consumption.

3.3.2. Proximate composition

The proximate compositions of clams were recorded in Table 3.3. No significant differences in the contents of crude fibre and crude ash were apparent among the clam species ($p > 0.05$). The crude protein content varied from 13-15 g/100 g wet weight; the maximum of 15 g/100 g wet weight recorded for *P. malabarica*. The crude fat content ranged from 2.01-3.75 g/100 g wet weight, which was found to be significantly greater for *V. cyprinoides* ($p < 0.05$). The moisture content was ranged from 74-76 g/100 g wet weight, and found to be significantly greater for *P. malabarica* as compared to that in *V. cyprinoides* ($p < 0.05$). A direct relationship between moisture and protein content was apparent. *V. cyprinoides* was demonstrated significantly greater ($p < 0.05$) carbohydrate content (8.57 g/100 g wet weight) than that observed in *P. malabarica* (4.65 g/100 g on wet weight basis).

Proximate compositions were depicted by the accumulation and depletion of food reserves and accessibility of food. The results were showed the inverse relationship between crude fat and moisture. The changes in crude protein in these two species were only due to the variation in moisture content and these variations were found to be within the normal range. The principle constituent of the edible part of the clam is

water, an index of freshness, which was around 76% and 74% for *V. cyprinoides* and *P. malabarica*, respectively. These results were upheld by previous works of Murray and Burt (2001). The water content was found to be more than 70% that demonstrated the freshness of the edible bivalve mollusks. *V. cyprinoides* and *P. malabarica* possessed greater crude protein (13-15% wet weight) and fat (2.01-3.75% wet weight) contents when contrasted with other bivalve mollusks, *Mytilus galloprovincialis* and *Ruditapes decussatus* (12-13%) from Porto Pozzo Lagoon of central-western Mediterranean Sea. The crude fat content of *M. galloprovincialis* and *R. decussatus* 1.3-2.0%, which were lesser than those reported in the present study (Saba 2011). The term crude fibre is a measure of the amount of indigestible lignin, cellulose, and other components of this type in the food items. A lesser content of crude fibre is directly proportional to the digestibility of the food sample and therefore, a good quality food should contain lesser content of crude fibre. The crude fibre contents of *V. cyprinoides* and *P. malabarica* considered in the present study were 0.04-0.05 g/100 g wet weight, which indicated the greater digestibility of their edible parts. No significant differences in proximate composition of *V. cyprinoides* and *P. malabarica* with that of Asian hard clam, *M. lusoria* was noted (Supatra *et al.*, 2013). Notwithstanding, *M. meretrix* from China reported 10-15% and 1-6% fat (Xie *et al.*, 2012), which were equivalent with *V. cyprinoides* and *P. malabarica*.

Table 3.3.: Proximate compositions (g/100 g wet weight) of *P. malabarica* and *V. cyprinoides*

	<i>P. malabarica</i>	<i>V. cyprinoides</i>
Dry matter	23.40 ± 0.02 ^a	26.83 ± 0.02 ^b
Moisture	76.62 ± 0.03 ^a	74.17 ± 0.02 ^b
Crude protein	15.47 ± 0.01 ^a	13.42 ± 0.02 ^b
Crude fat	2.01 ± 0.02 ^a	3.75 ± 0.02 ^b
Crude fibre	0.05 ± 0.02 ^a	0.04 ± 0.02 ^a
Crude ash	1.22 ± 0.01 ^a	0.93 ± 0.02 ^a
Carbohydrate	4.65 ± 0.04 ^a	8.57 ± 0.02 ^b

Data were reported as mean ± standard deviation (n = 3). Different superscripts (a-b) within the same row denoted the significant differences ($p < 0.05$)

3.3.3. Lipid content and fatty acid composition

The lipid contents of the experimental samples were denoted in Table 3.4. Significant difference in lipid content was noted in the edible parts of clam species ($p < 0.05$), wherein *V. cyprinoides* recorded greater lipid content (2.27 g/100 g wet weight) than *P. malabarica* (1.77 g/100 g wet weight).

The fatty acid compositions of bivalve mollusk samples were given in Table 3.4. *V. cyprinoides* was demonstrated significantly greater contents of ($p < 0.05$) total SFAs (48% TFA wet weight) than that in *P. malabarica* (34% TFA wet weight). The palmitic (16:0) and stearic acids (18:0) were found to be the predominant SFAs in *V. cyprinoides* and *P. malabarica*. The content of 16:0 was greater in *V. cyprinoides* and contributed about 64% of the total SFA content, whereas *P. malabarica* contributed about 53% wet weight of the aggregate SFAs. The odd chain saturated fatty acid pentadecanoic acid (15:0) was found to be present in significantly greater quantity (1.55% TFA wet weight) in *P. malabarica* than that in *V. cyprinoides* (0.42% TFA wet weight), whilst the concentration of docosanoic acid (22:0) was significantly greater in *V. cyprinoides* (0.77% TFA wet weight) than that in *P. malabarica* (0.19% TFA wet weight) ($p < 0.05$). No significant differences in the 18:0 fatty acid contents among both the clam species ($p > 0.05$) were apparent. The aggregate MUFA content in *V. cyprinoides* and *P. malabarica* were differed from 23-26% wet weight. The palmitoleic (16:1*n*-7), erucic acid (22:1*n*-9) and oleic acid (18:1*n*-9) were found to be the predominant MUFAs. The content of 16:1*n*-7 fatty acid was significantly greater in *V. cyprinoides* ($p < 0.05$), whereas *P. malabarica* exhibited significantly greater 18:1*n*-9 cis and 22:1*n*-9 contents when contrasted with those in *V. cyprinoides* ($p < 0.05$). The fatty acid 16:1*n*-7 in *V. cyprinoides* and *P. malabarica* contributed 41% and 25% of the total fatty acids, respectively on wet weight basis.

Table 3.4.: Lipid content (g/100 g wet weight) and fatty acid composition (% total fatty acids wet weight) in *P. malabarica* and *V. cyprinoides*

Fatty acids	<i>P. malabarica</i>	<i>V. cyprinoides</i>
Lipid	1.77 ± 0.01 ^a	2.27 ± 0.02 ^b
Saturated fatty acids		
12:0	0.05 ± 0.01 ^a	0.03 ± 0.01 ^a

14:0	2.62 ± 0.01^a	4.35 ± 0.02^b
15:0	1.55 ± 0.01^a	0.42 ± 0.02^b
16:0	17.92 ± 0.03^a	30.57 ± 0.02^b
17:0	2.43 ± 0.02^a	2.66 ± 0.02^a
18:0	8.73 ± 0.02^a	8.33 ± 0.02^a
20:0	0.31 ± 0.01^a	0.71 ± 0.01^b
22:0	0.19 ± 0.01^a	0.77 ± 0.02^b
24:0	0.04 ± 0.00^a	0.03 ± 0.00^a
Σ SFA*	33.84 ± 0.01^a	47.77 ± 0.15^b
Monounsaturated fatty acids		
14:1 <i>n</i> -7	0.20 ± 0.01^a	0.42 ± 0.01^b
15:1 <i>n</i> -7	1.19 ± 0.01^a	0.84 ± 0.01^b
16:1 <i>n</i> -7 cis	5.76 ± 0.02^a	10.39 ± 0.02^b
18:1 <i>n</i> -7	0.12 ± 0.01^a	0.31 ± 0.02^b
18:1 <i>n</i> -9 cis	8.87 ± 0.01^a	6.77 ± 0.02^b
20:1 <i>n</i> -9	2.10 ± 0.1^a	4.37 ± 0.01^b
22:1 <i>n</i> -9	4.33 ± 0.01^a	2.32 ± 0.01^b
24:1 <i>n</i> -9	0.71 ± 0.01^a	0.11 ± 0.01^b
Σ MUFA**	23.15 ± 0.01^a	25.57 ± 0.01^a
Polyunsaturated fatty acids		
18:2 <i>n</i> -6 cis	1.34 ± 0.01^a	2.68 ± 0.02^b
18:3 <i>n</i> -6	2.72 ± 0.01^a	5.05 ± 0.01^b
18:3 <i>n</i> -3	0.22 ± 0.01^a	0.36 ± 0.01^a
20:2 <i>n</i> -6	2.92 ± 0.01^a	1.68 ± 0.01^b
20:3 <i>n</i> -6	2.63 ± 0.01^a	0.39 ± 0.01^b
20:4 <i>n</i> -6	0.76 ± 0.01^a	0.60 ± 0.01^a
20:5 <i>n</i> -3 EPA	7.68 ± 0.02^a	3.57 ± 0.01^b
22:5 <i>n</i> -3	1.62 ± 0.02^a	0.92 ± 0.01^b
22:6 <i>n</i> -3 DHA	14.35 ± 0.01^a	3.22 ± 0.01^b
Σ PUFA***	34.33 ± 0.15^a	18.46 ± 0.01^b
Σ <i>n</i> -3	23.84 ± 0.01^a	8.07 ± 0.02^b
Σ <i>n</i> -6	10.37 ± 0.02^a	10.39 ± 0.01^a

$\Sigma n-3/\Sigma n-6$	2.31±0.01 ^a	0.77±0.01 ^b
DHA/EPA	1.88±0.01 ^a	0.91±0.01 ^b
Σ PUFA/ Σ SFA	1.02±0.01 ^a	0.39±0.01 ^b
Atherogenicity index (AI)	0.66±0.01 ^a	1.25±0.03 ^b
Thrombogenicity index (TI)	0.31±0.01 ^a	1.04±0.03 ^b
HH ratio	1.71±0.01 ^a	0.52±0.03 ^b

*Total saturated fatty acids, ** total monounsaturated fatty acids, *** total polyunsaturated fatty acids. Data were presented as mean values of three samples (mean ± standard deviation). Different superscripts (a-b) within the same row indicate the significant difference ($p < 0.05$). HH ratio-hypocholesterolaemic/hypercholesterolaemic ratio

P. malabarica has recorded significantly greater content of PUFAs (34% TFA wet weight) ($p < 0.05$) as compared to that recorded in *V. cyprinoides* (18% TFA wet weight). The total content of *n*-3 PUFAs was found to be significantly greater ($p < 0.05$) in *P. malabarica* (23.84% TFA wet weight) as compared to that in *V. cyprinoides* (8.07% TFA wet weight). The EPA and DHA contents of the edible parts of *P. malabarica* (7% and 14% TFA, respectively on wet weight basis) were found to be greater than those in *V. cyprinoides* (3.5% and 3.2% TFA, respectively on wet weight basis). Accordingly, the *n*-3/*n*-6 fatty acid ratio recorded to be greater (2.3) in *P. malabarica* than that in *V. cyprinoides* (< 1.0). *P. malabarica* was displayed significantly greater ($p < 0.05$) DHA/EPA (1.88) and Σ PUFA/ Σ SFA (1.02) than edible parts of *V. cyprinoides* [DHA/EPA (0.91) and Σ PUFA/ Σ SFA (0.39)].

The AI and TI indices were evaluated in *V. cyprinoides* (1.25 and 1.04, respectively) and *P. malabarica* (0.66 and 0.31, respectively). The HH ratio was found to be significantly greater in *P. malabarica* as compared to that of the edible part of *V. cyprinoides* ($p < 0.05$). Figure 3.3. represented the comparison of *n*-3/*n*-6, *n*-6/*n*-3, DHA/EPA and Σ PUFA/ Σ SFA between *P. malabarica* and *V. cyprinoides*.

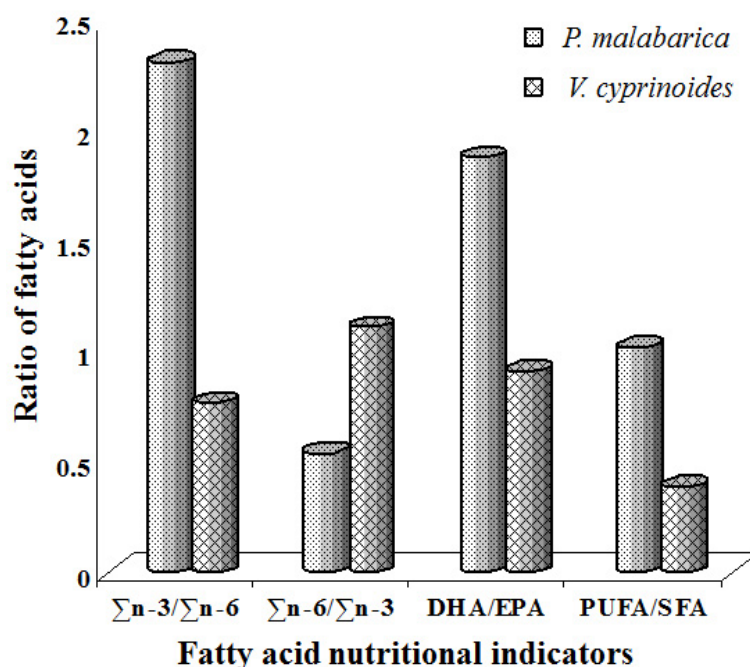


Figure 3.3.: Comparison of $n-3/n-6$, $n-6/n-3$, DHA/EPA and Σ PUFA/ Σ SFA between *P. malabarica* and *V. cyprinoides*

Among different saturated fatty acids, palmitic acid was found to be predominant in *V. cyprinoides* (31% TFA on wet weight basis) when contrasted with that in related bivalves, for example, *Donax incarnates* (28%) (Periyasamy *et al.*, 2014) and *M. casta* (15-16% TFA) (Srilatha *et al.*, 2013). Palmitic acid has been accounted for as the major SFA in mussels (Alkanani *et al.*, 2007). SFAs with their more prominent caloric substance are basically used as a storage form of energy. Diets that are more prominent in PUFAs are connected with decreased danger of cardiovascular illness and atherogenesis (Andrade *et al.*, 2012). The health Department of UK has been prescribed a perfect percentage of $n-6/n-3$ as 4.0 and the qualities greater than 4.0 are viewed as harmful to human wellbeing, and may prompt cardiovascular maladies (HMSO 2001). The $n-6/n-3$ degree in the present study was lesser than 2 and, in this manner, the bivalves can be considered as a healthy diet.

The aggregate $n-3$ PUFA content in *P. malabarica* was found to be fundamentally more prominent ($p < 0.05$). PUFAs are essential biochemical markers of bivalves contributing to their nutritional qualities. The EPA and DHA contents in *P. malabarica* were found to be 7% and 14%, respectively, on wet weight basis which were more noteworthy when contrasted with the normally devoured finfish *Epinephelus*

diacanthus (4.7% and 11%, respectively) (Chakraborty *et al.*, 2014c). The long-chain (C₂₀-C₂₂) *n*-3 PUFAs were known to have variety of health benefits against cardiovascular ailments including anti-inflammatory, antihypertensive, antioxidant, and anti-arthritis effects (Siriwardhana *et al.*, 2012).

AI is a marker of risk for cardiovascular maladies, whilst TI is an indicator of potential for blood platelets conglomeration. Lesser estimations of AI and TI in edible part of *P. malabarica* and *V. cyprinoides* were practically identical with the prior studies identified with the bivalves, *R. decussates* and *M. galloprovincialis* (Saba 2011).

3.3.4. Protein content and amino acid composition

No significant differences in protein contents in *V. cyprinoides* and *P. malabarica* were apparent (11-12 mg/g wet weight, $p < 0.05$) (Table 3.5.).

A total of seventeen amino acids were identified and quantified in *V. cyprinoides* and *P. malabarica* (Table 3.5.). *V. cyprinoides* was exhibited significantly greater ($p < 0.05$) content of total essential amino acid (300 mg/100 g wet weight) as compared to *P. malabarica* (285 mg/100 g wet weight). No significant differences in the total non-essential amino acids (Σ NEAA) contents were recorded in these species ($p > 0.05$). The most abundant essential amino acid was found to be arginine in *V. cyprinoides* (54 mg/100 g wet edible weight), followed by leucine (48 mg/100 g) and lysine (42 mg/100 g). Arginine was found to be abundant in *P. malabarica* (53 mg/100 g), followed by lysine and leucine. Among the non-essential amino acids, glutamine was constituted the major share followed by aspartic acid (Table 3.5.). However, the content of aspartic acid was found to be significantly greater in *P. malabarica* as compared to that in *V. cyprinoides* ($p < 0.05$). No significant difference was noted for glutamine content in these samples ($p > 0.05$). The total sulfated and aromatic amino acid contents were found to be significantly greater in *V. cyprinoides* as compared to those in *P. malabarica* ($p < 0.05$). The arginine-lysine proportion was found to be varied from 1.22-1.29. *V. cyprinoides* recorded significantly higher leucine/isoleucine ratio as compared to that in *P. malabarica* ($p < 0.05$, Table 3.5.).

Table 3.5.: Protein and amino acid composition (mg/100 g wet weight) in *P. malabarica* and *V. cyprinoides*

	<i>P. malabarica</i>	<i>V. cyprinoides</i>
Protein	12.64 ± 0.08 ^a	11.15 ± 0.07 ^a
Essential amino acids		
Histidine*	14.64 ± 0.01 ^a	13.54 ± 0.07 ^a
Methionine*	16.67 ± 0.08 ^a	18.32 ± 0.02 ^b
Valine*	29.47 ± 0.15 ^a	30.57 ± 0.03 ^a
Threonine*	27.23 ± 0.03 ^a	29.95 ± 0.03 ^b
Isoleucine*	29.62 ± 0.03 ^a	31.12 ± 0.03 ^a
Leucine*	42.95 ± 0.04 ^a	48.35 ± 0.05 ^b
Lysine*	43.57 ± 0.04 ^a	41.67 ± 0.04 ^b
Phenylalanine *	28.20 ± 0.03 ^a	33.11 ± 0.17 ^b
Arginine *	52.94 ± 0.05 ^a	53.57 ± 0.05 ^a
Non-essential amino acids		
Alanine **	28.24 ± 0.14 ^a	27.23 ± 0.03 ^a
Aspartic acid **	57.73 ± 0.06 ^a	55.20 ± 0.06 ^b
Glutamic acid **	78.39 ± 0.08 ^a	77.23 ± 0.08 ^a
Serine **	26.53 ± 0.03 ^a	26.83 ± 0.03 ^a
Glycine **	32.75 ± 0.03 ^a	30.95 ± 0.03 ^b
Proline **	22.66 ± 0.11 ^a	25.72 ± 0.03 ^b
Tyrosine **	13.34 ± 0.07 ^a	13.90 ± 0.07 ^a
Cysteine **	6.85 ± 0.03 ^a	8.86 ± 0.04 ^b
ΣAA	551.78 ± 1.01 ^a	566.12 ± 0.57 ^b
ΣEA	285.29 ± 0.41 ^a	300.20 ± 0.25 ^b
ΣNEA	266.49 ± 0.59 ^a	265.92 ± 0.32 ^a
ΣEA/ΣAA	0.52 ± 0.00 ^a	0.53 ± 0.00 ^a
ΣNEA/ΣAA	0.48 ± 0.00 ^a	0.47 ± 0.02 ^a
ΣEA/ΣNEA	1.07 ± 0.01 ^a	1.13 ± 0.00 ^a
ΣArAA	41.54 ± 0.15 ^a	47.01 ± 0.03 ^b
ΣSAA	23.52 ± 0.12 ^a	27.18 ± 0.00 ^b
Arg:Lys	1.22 ± 0.00 ^a	1.29 ± 0.01 ^a

Leu:Ile	1.45 ± 0.03 ^a	1.55 ± 0.00 ^b
Cys:ΣSAA	0.29 ± 0.02 ^a	0.33 ± 0.00 ^a

*Essential amino acids; **non-essential amino acids; ΣEAA-total essential amino acids; ΣNEAA-total non-essential amino acids; ΣAA-total amino acids; ΣArAA-total aromatic amino acids; TSAA-total sulfur containing amino acids; Data were expressed as mean ± standard deviation; Tryptophan was not determined; Different superscripts (a, b) within the same row indicates the significant difference ($p < 0.05$)

The amino acid scores with respect to histidine, threonine, valine, methionine plus lysine, aromatic amino acids (phenylalanine and tyrosine), and lysine of the bivalve mollusks were plotted in Figure 3.4., and these scores were found to be significantly greater in *V. cyprinoides* as compared to those in *P. malabarica* ($p < 0.05$). The isoleucine score was found to be greatest in the edible parts of *V. cyprinoides* and *P. malabarica* (99% and 84%, respectively). *V. cyprinoides* and *P. malabarica* were found to be rich in protein content that are fundamental for human proper growth and survival. The proteins, lipids and minerals are considered as the significant contributors to the nutritional value and organoleptic properties of mollusks (Orban *et al.*, 2006).

The amino acids alanine, glycine and arginine were available at a generally greater level in marine bivalve mollusks. In the present study, *V. cyprinoides* and *P. malabarica* were indicated arginine, leucine and lysine as leading fundamental amino acids, which were similar with the prior study of mollusk, *P. viridis* (Chakraborty *et al.*, 2016a). Any proportion of ΣEAA/NEAA greater than 1.0 is considered to be useful for wellbeing. The ΣEA/ΣNEA proportion in the edible parts of *V. cyprinoides* and *P. malabarica* were ranged from 1.07-1.13 which is above the threshold limit of 1.0. It is demonstrated that these bivalve clams are good sources of decently adjusted and high-quality protein source. The ΣEA/ΣNEA ratio for razor clam, *Ensis siliqua* was found to be lesser (0.80) (Baptista *et al.*, 2014) as looked at to those in the present study. The measures of aggregate aromatic amino acids (ΣArAA) were found to be more prominent for these bivalve shellfishes accordingly implying their part in keeping up thyroxine metabolism. The protein contents in *V. cyprinoides* and *P. malabarica* were found to be rich in lysine, which is the limiting amino acid in cereal-based eating regimens utilized as essential foods in the developing nations (Kim and Lall 2000).

Glutamine, a donor of nitrogen for the synthesis of purines and pyrimidines that are fundamental for the proliferation of cells, was found to be present in *V. cyprinoides* and *P. malabarica* (77-78 mg/100 g) in considerable amounts. The shellfishes displayed the leucine-isoleucine proportion as prescribed by FAO/WHO (FAO, WHO, UNU 2007). Arginine-lysine proportion (1.22-1.29) in the present study was additionally found to be tantamount with those in vegetables and meat (Unusan 2007). *V. cyprinoides* and *P. malabarica* were demonstrated good amino acid scores, an index of good quality of protein.

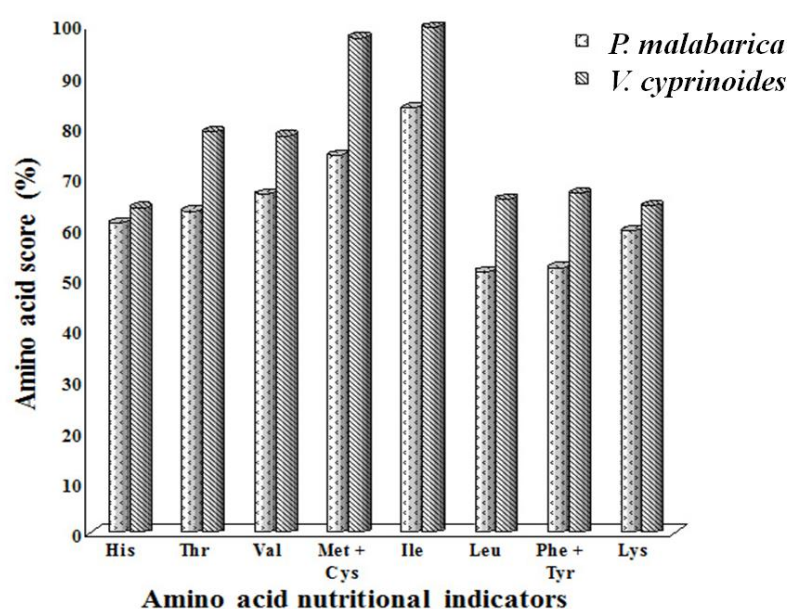


Figure 3.4.: Comparison of essential amino acid scores between *P. malabarica* and *V. cyprinoides*

3.3.5. Mineral composition

The edible part of shellfishes used in this study was found to be rich in macro (K, Ca, Mg and P) and micro (Mn, Fe, Cu, Zn and Se) minerals and their concentrations were delineated in Table 3.6. The concentrations of macro minerals were significantly greater for *P. malabarica* when compared with *V. cyprinoides* ($p < 0.05$). The concentration of K and P concentration were found in appreciable quantities in *P. malabarica* (94 and 584 mg/100 g wet weight, respectively). The Na/K ratio in the clams was ranged from 1.3-1.5 mg/100 g wet weight. The Ca+P content were essentially greater for *P. malabarica* (> 600 mg/100 g) than *V. cyprinoides* ($p < 0.05$).

No significant variations were observed in micro mineral compositions with the exception of Fe between *P. malabarica* and *V. cyprinoides*. *P. malabarica* showed significantly greater content of Fe (7.64 mg/100 g wet weight) than recorded in *V. cyprinoides* (5.65 mg/100 g wet weight; $p < 0.05$). The aggregate micronutrient content was found to be varied from 11-13 mg/100 g wet weight in the edible part of the clam samples. The Se concentration was significantly greater ($p < 0.05$) for *P. malabarica* (30 µg/100 g wet weight) compared with *V. cyprinoides* (27 µg/100 g wet weight).

Table 3.6.: Mineral composition (mg/100 g wet weight) in *P. malabarica* and *V. cyprinoides*

	<i>P. malabarica</i>	<i>V. cyprinoides</i>
Macronutrients		
Na	118.50 ± 0.57 ^a	92.00 ± 0.90 ^b
K	94.23 ± 0.87 ^a	60.21 ± 0.12 ^b
Na/K	1.25 ± 0.01 ^a	1.51 ± 0.02 ^a
Ca	34.25 ± 0.61 ^a	28.52 ± 0.69 ^b
P	583.62 ± 0.99 ^a	534.23 ± 0.75 ^b
Ca/P	0.06 ± 0.00 ^a	0.06 ± 0.00 ^a
Ca+P	617.87 ± 1.24 ^a	562.75 ± 1.43 ^b
Mg	36.75 ± 0.38 ^a	25.86 ± 0.45 ^b
Micronutrients		
Mn	2.03 ± 0.05 ^a	1.75 ± 0.09 ^a
Cu	0.46 ± 0.06 ^a	0.30 ± 0.02 ^a
Zn	3.01 ± 0.13 ^a	3.26 ± 0.07 ^a
Fe	7.64 ± 0.14 ^a	5.65 ± 0.04 ^b
Se (µg/100 g wet weight)	30.15 ± 0.09 ^a	27.27 ± 0.04 ^b

Data were expressed as mean ± standard deviation (n = 3). Different superscripts (a, b) within the same row indicate significant difference ($p < 0.05$)

Shellfish meat is rich in key minerals needed for vital enzymes and for different metabolic pools. The bivalves were demonstrated more prominent content of P (534-583 mg/100 g wet weight) evidently due to more noteworthy extent of

phospholipid and phosphoprotein contents in the bivalves. The K contents of *V. cyprinoides* and *P. malabarica* were found to be at 94 and 60 mg/100 g, respectively on wet weight basis, which is basic to keep up legitimate osmotic equalization of body liquid and pH of the body (Ensminger *et al.*, 1995). It was accounted for that the mean K and P contents of molluskan fauna (*P. globosa*, *B. bengalensis*, *M. tuberculata*, *L. marginalis*, *A. convexiusculus* and *Helix sp*) were around 48 and 103 mg/100 g sample, respectively (Baby *et al.*, 2010), which were lesser when contrasted with the present study. The Ca, Fe and Cu contents in the edible bivalves were notably lesser as compared to those in the edible part of the hard clam, *M. meretrix*, reaped from the shoreline of China (Xie *et al.*, 2012). It is to note that the bivalves in current investigation appeared to possess higher than 20 mg/100 g of Mg as well as Ca on wet weight basis. Ca is responsible for bone development and maintenances, whereas, Mg is crucial cofactor to complete different biochemical responses in the body. The Zn content in *V. cyprinoides* and *P. malabarica* was found to be around 3 mg/100 g edible part. Zn is vital for recuperating wounds and bone advancement. *D. incarnates*, a wedge clam demonstrated Fe and Zn contents of around 1.4 and 0.3 mg/g dry weight, respectively, which were tantamount with those reported in the present study (Periyasamy *et al.*, 2014). Selenium has been connected with security of body tissues against oxidative stress, upkeep of protections against contamination and balance of development and improvement. A more prominent bit of the selenoproteins has enzyme activities and selenocysteine as a key segment of the catalytic cycle (Liu *et al.*, 2012). This element was found to change between 27-30 µg/100 g on wet weight basis in *V. cyprinoides* and *P. malabarica*, and was fundamentally more noteworthy than in grains, fruits, vegetables (Levander and Burk 1994), and various marine finfishes (10-20 µg/100 g) (Chakraborty *et al.*, 2014c). It is subsequently, important to consume these clam species in our day by day eating regimens to meet the base prerequisite of selenium.

3.3.6. Cholesterol content and vitamin composition

The cholesterol contents of the edible part of these species were found to be lesser than 60 mg/100 g wet weight, and were within the threshold limits (Table 3.7.). The cholesterol content of *P. malabarica* was found to be significantly greater (59

mg/100 g wet weight) than that recorded in *V. cyprinoides* (56 mg/100 g wet weight) ($p < 0.05$).

Vitamin contents of *V. cyprinoides* and *P. malabarica* were shown in Table 3.7. No significant differences in vitamin A, E, K and C contents were discernable between these species ($p > 0.05$). The vitamin D₃ content was significantly greater ($p < 0.05$) in *V. cyprinoides* (183 IU wet weight) as compared to that in *P. malabarica* (161 IU wet weight). Vitamin A contents varied from 39-41 IU wet weight. The vitamins with antioxidative properties such as E and C contents in *P. malabarica* and *V. cyprinoides* were found to vary from 0.32-0.39 IU and 10-11 IU, respectively on wet weight basis.

Table 3.7.: Cholesterol and vitamin composition in *P. malabarica* and *V. cyprinoides*

	<i>P. malabarica</i>	<i>V. cyprinoides</i>
Cholesterol (mg/100 g)	59.02 ± 0.72 ^a	56.27 ± 0.38 ^b
Vitamins		
Retinol A (IU)	39.46 ± 0.38 ^a	41.11 ± 0.86 ^a
Cholecalciferol D ₃ (IU)	161.29 ± 1.05 ^a	183.28 ± 1.13 ^b
α-tocopherol E (IU)	0.39 ± 0.01 ^a	0.32 ± 0.01 ^a
Phylloquinone K ₁ (μg/100 g)	0.75 ± 0.04 ^a	0.65 ± 0.03 ^a
Ascorbic acid C (IU)	10.2 ± 0.11 ^a	11.36 ± 0.16 ^a

Data were expressed as mean ± standard deviation (n = 3). Different superscripts (a, b) within the same row indicate significant difference ($p < 0.05$)

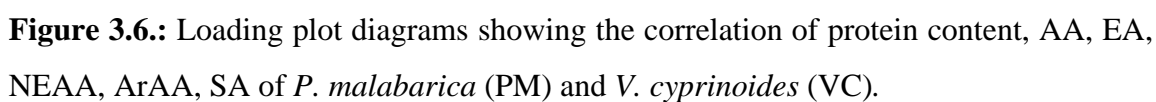
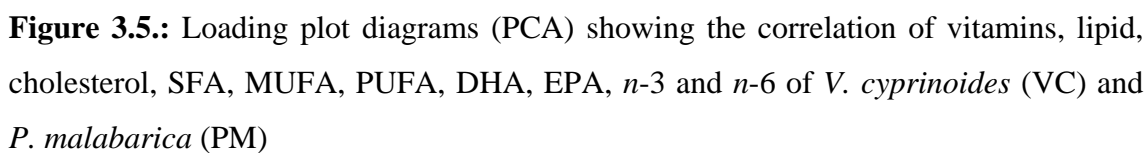
V. cyprinoides and *P. malabarica* were demonstrated cholesterol level within the threshold levels. Cholesterol was accounted as the significant sterol in *M. edulis* and *P. canaliculus* (Murphy *et al.*, 2002). The present study has been exhibited that the mollusks are good sources of vitamins. The content of vitamin D₃ of the shellfishes was found to be greater than 160 IU, which is fundamental for the support of ordinary blood levels of Ca and phosphate (Trivedi *et al.*, 2003). The vitamin A and D₃ contents were more prominent in *V. cyprinoides* and *P. malabarica* than those reported in *M. casta* (Srilatha *et al.*, 2013). The vitamin C content reported in *V. cyprinoides* and *P. malabarica* were found to vary from 10-11 IU wet weight, and was greater than that in

M. meretrix (5.83 $\mu\text{g}/\text{mg}$) (Gopalakrishnan and Vijayavel 2008). This water soluble vitamin is a crucial antioxidative supplement for people, yet an extra outer dietary source is obliged in light of the fact that it is not biosynthesized by human digestion system (Jeevitha *et al.*, 2013). It furthermore helps the body assimilate to iron and calcium, backs in wound recovering, and helps cerebrum capacity (Iqbal *et al.*, 2004).

3.3.7. Principal component analyses

The similarities and contrasts among the nutritional parameters of *V. cyprinoides* and *P. malabarica* were statistically assessed by utilizing the principle component analyses (PCA). The distinctive parameters, which were considered to PCA, were vitamins, lipid, cholesterol, ΣSFA , ΣMUFA , ΣPUFA , DHA, EPA, $\Sigma n-3$ and $\Sigma n-6$ fatty acids (Figure 3.5.). The stacking of the first and second order principal components (PC1 and PC2) represented 55.28% and 44.72% of the variance, respectively. PC1 was fundamentally impacted by vitamins of *P. malabarica*, vitamin C, D and E of *V. cyprinoides*. PC2 was principally affected by lipid, SFA, DHA of *P. malabarica* and SFA of *V. cyprinoides*. The more prominent positive loadings were for the variables, vitamin D and EPA of *P. malabarica* and negative loadings for the variables, lipid and PUFA of *V. cyprinoides* on PC1.

The PCA was performed to focus the similarities between protein, ΣEA , ΣNEA , ΣAA , ΣArAA , and ΣSAA of *V. cyprinoides* and *P. malabarica*, and were demonstrated in Figure 3.6. The PC1 clarified 66.17% variances, which accounted for the similarities between the total sulfur containing aromatic acid (TSAAVC), total amino acid (TAAVC) and total non-essential amino acid (TNEAVC) of *V. cyprinoides*. The PC2 axis explained 33.83% variances with greater similarities of total essential amino acid (TEAPM), total non-essential amino acid (TNEAPM) and total amino acid (TAAPM) of *P. malabarica*. The more noteworthy positive loadings were for the variables, total aromatic amino acid content of *V. cyprinoides* (TArAAVC) on PC1 axis and total essential amino acid of *V. cyprinoides* (TEAVC) on PC2 axis.



The principal component analyses plot (Figure 3.5.) delineated that there was no clear relationship between lipid content (lipidPM) and vitamins, except vitamin A (VitAPM). Nonetheless, the lipid content (lipidPM) was displayed similarity with SFA (SFAPM), DHA (DHAPM) and *n*-3 fatty acids (n3PM). The lipid content of *V. cyprinoides* demonstrated similitude with Σ PUFA (PUFAVC), Σ MUFA (MUFAVC), DHA (DHAVC) and *n*-3 fatty acids (n3VC) which indicated the more noteworthy comparability with the PUFA contents. It may be because of the way that the lipid content of *V. cyprinoides* was contained greater share of PUFAs. The Figure 3.6. demonstrated that the protein content of *V. cyprinoides* was at negative correlation with the protein content of *P. malabarica*. The aggregate non-essential amino acid (TNEAAPM) and total essential amino acid (TEAPM) contents of *P. malabarica* was showed closer similarities, while aggregate sulfur containing amino acids (TSAVC) and total aromatic amino acids (TAAVC) of *V. cyprinoides* exhibited greater correlation than other parameters.

3.4. Conclusions

The present study has been provided comprehensive biochemical profile of the bivalve clams, *V. cyprinoides* and *P. malabarica* collected from the estuarine waters of southwest shoreline of India. Clam is a source of high valued nutrients and is abundantly available, principally to the individuals living in the coastal areas. It is a rich source of minerals, vitamin, long-chain *n*-3 polyunsaturated fatty acid contents, and which can conceivably supplant the artificial food supplements available in the market. The present study likewise provided useful information in regards to the importance of these candidate species for fisheries and aquaculture.

The present study has been presented a better understanding into nutritional composition of two bivalve clams, *V. cyprinoides* and *P. malabarica* harvested from the estuarine waters situated at the southwest coast of Arabian Sea. Greater levels of long-chain C₂₀-C₂₂ *n*-3 polyunsaturated fatty acids, especially, eicosapentaenoic acid, docosahexaenoic acid and higher *n*-3/*n*-6 fatty acid proportions were characterized for these species. The more prominent contents of essential/non-essential amino acid ratio, vitamin D₃, calcium and phosphorus were showed that these bivalves are good sources of well-balanced diet. The present study demonstrated that *V. cyprinoides* and *P.*

malabarica can be utilized as nutritionally rich sources of sea food. The ideal atherogenic index, thrombogenicity index, hypocholesterolemic/hypercholesterolemic ratio along with fatty acid and amino acid based health markers were qualified these low-esteemed mollusk species as potential health food. These low-value bivalve clam species can be considered as an ideal raw material for further bio-potential analyses as explained in the upcoming chapters.

BIOACTIVE POTENTIALS OF *VILLORITA CYPRINOIDES* AND *PAPHIA MALABARICA*

Contents

- 4.1. *Background*
- 4.2. *Materials and methods*
- 4.3. *Results and discussion*
- 4.4. *Conclusion*

4.1. Background

The adverse living conditions, such as environmental stress and filter feeding habits of bivalves are responsible for their utilities as potential sources to harness bioactive metabolites with different functional properties, particularly, the prevention of free radical induced metabolic disorders (Goldberg 1975). The reactive oxygen species (ROS) formed during the regular metabolic activities and their overproduction plays a vital role in the progression of oxidative stress induced diseases, such as inflammation, type-2 diabetes, hypertension, atherosclerosis, cancer, ageing and cell death (Lushchak 2011). It is, therefore, anticipated that the antioxidants assume greater importance in controlling the initiation and development of these life threatening diseases. The origin of hypertension together with various pathophysiological manifestations including type-2 diabetes were reported to be due to excessive production of ROS leading to oxidative stress and inflammatory responses (Wilcox 2002). Several synthetic drugs were capable of deterring free radical intermediates by acting as oxygen scavengers and decrease the free radical induced diseases, but they were reported to cause severe side effects (Schnitzer *et al.*, 1999).

The bivalve clams have been exposed to high salinity and free radical inducing toxic chemicals, even though, they were not reported for cellular damage, and therefore, are considered as potential candidates as natural antioxidants (Gonzalez *et al.*, 2015). These species occupy a major share of the total edible clams in the world, and have high percentage edibility, yet they were not been explored for their biomedical and

pharmaceutical properties (Mohite *et al.*, 2009). The mollusk, *P. canaliculus* was demonstrated to be active against inflammatory cyclooxygenase-2 (COX-2) and 5-lipoxygenase enzymes (5-LOX) (Whitehouse *et al.*, 1997). Bioactive components and enzyme inhibitors were identified from *M. meretrix* with anti-hypertensive, hypolipidemic and antioxidant properties (Wei *et al.*, 2007).

With innumerable edible clams from the coastal ecosystem representing a large community of marine fauna, the Indian coasts are acknowledged for their particular richness. Among different clams, the black clam *Villorita cyprinoides* (family, Corbiculidae) and yellow-foot clam, *Paphia malabarica* (family, Veneridae) are the common seafood resources abundantly available in the coastal regions of India, and their cultivation methodologies were developed and standardized. Considering the promising perspective for the utilization of these groups of bivalve clams, and limited research reports on their utilization as potential health food, as a result their pharmaceutical potentials began to receive considerable attention. Therefore, the current study aims to evaluate the free radical scavenging guided evaluation of the anti-inflammatory, anti-diabetic and anti-hypertensive properties of ethyl acetate:methanol extract (EtOAc:MeOH, 1:1, v/v) of *V. cyprinoides* and *P. malabarica* by various *in vitro* assays. Nuclear magnetic resonance spectroscopy based proton and carbon fingerprinting of the solvent extracts derived from these species were used to understand the various functional groups, which might be a useful tool for the preliminary prediction of biological activities associated with these extracts.

4.2. Materials and methods

4.2.1. Chemicals, reagents and instrumentations

All chemicals and reagents used in this study were of analytical/spectroscopic grade and were obtained from E-Merck (E-Merck, Frankfurter, Darmstadt, Germany) and Sigma Aldrich (Missouri, USA). Double distilled or milliQ or HPLC grade water was used throughout the work. Sodium carbonate (Na_2CO_3), malondialdehyde standard, thiobarbituric acid (TBA), acetic acid, 1,1-diphenyl-2-picryl-hydrazil (DPPH), potassium persulfate ($\text{K}_2\text{S}_2\text{O}_8$), 2,2'-azino-bis-3-ethylbenzothiazoline-6-sulfonic acid diammonium salt (ABTS⁺), gallic acid, Folin-Ciocalteu (F.C.) reagent, hydrogen peroxide (H_2O_2), potassium phosphate buffer, ferrozine, ferrous sulfate (FeSO_4), leuco-

2,7-dichlorofluoresce in diacetate, sodium hydroxide (NaOH), tris-buffer, hematin, phenol, arachidonic acid, linoleic acid, sodium phosphate buffer, 3,5-dinitrosalicylic acid reagent were acquired from E-Merck/Sigma-Aldrich/HiMedia (HiMedia Laboratories LLC, Pennsylvania, USA). The dipeptidyl peptidase-4 (DPP-4, from porcine kidney), angiotensin converting enzyme-1 (ACE-1, from rabbit lung), N-(3-[2-furyl]acryloyl)-Phe-Gly-Gly (FAPGG), Gly-Pro-p-nitroanilide, cyclooxygenase-1 (COX-1, from sheep), cyclooxygenase-2 (COX-2, human recombinant) were procured from Sigma-Aldrich and 5-lipoxygenase (5-LOX, from soybean) extra pure, α -amylase (obtained from porcine pancreas) and lyophilized powder of α -glucosidase (acquired from yeast) were purchased from Sisco Research Laboratories (SRL, Mumbai, India). All glasswares were procured from Borosil (India) or Magnum glassworks (Kochi, Kerala, India).

The solvents evaporated using rotary vacuum evaporators (Heidolph instruments GmbH and Co., Schwabach, Germany; Ika rotary evaporator, IKA[®] Works, North Chase Pkwy SE, Wilmington, USA) and rotational vacuum concentrators (RVC, Martin Christ, GmbH, Osterode, Germany). The refrigerated centrifuge (Thermo Scientific, Thermo Electron LED GmbH, Robert-Bosch-Str-1, Langenselbold, Germany) was used to perform centrifugation. UV-VIS absorbances were acquired on an ultraviolet-visible (UV-VIS) spectrophotometer (Varian Cary 50, Walnut Creek, California, USA) and microplate spectrophotometer (Thermo Scientific[™] Multiskan[™] GO, Waltham, MA USA). The glass cuvettes (1 cm X 1 cm X 4.5 cm) were utilized in the UV-VIS spectrophotometer and 96-well microplates (Nunclon[™] Plates with Delta Surface, Thermo Fisher Scientific, Suzhou, Jiangsu, China) used in the microplate spectrophotometer for the absorbance measurements. A laboratory scale lyophilizers (Alpha 1-4 LD plus, Martin Christ, Osterode, Germany; Scanvac, Coolsafe[™], LaboGene, DK-3540 Lyngby, Denmark) used for freeze drying. The samples were kept in the -80°C deep freezer (ultra-low temperature freezer, Eppendorf, Hamburg, Germany). The solvent extractions of samples were carried out using rotary shaker (Orbital shaker, Labline, India) and ultrasound sonicator (water bath sonicator, Elma, Hohentwiel, Germany). Perkin-Elmer Series 2000 Fourier transform infrared (FTIR) spectrometer recorded FTIR spectra between the scan range of 4000 and 400 cm⁻¹ on KBr pellets (Perkin-Elmer FTIR, Winter Street, Waltham, Massachusetts, USA). The

samples (15 mg) were homogenized with KBr (150 mg) and applied a pressure of around 5×10^6 Pa to afford clear transparent disc (1 mm thickness X 13 mm diameter). The IR absorption readings were represented as percentage transmittance (%T). The proton (^1H) and carbon (^{13}C) (one-dimensional) nuclear magnetic resonance (NMR) spectra were documented on Bruker Avance DPX 500 (500 MHz) spectrometer utilizing deuteriated chloroform (CDCl_3) with internal standard tetramethylsilane (δ 0 ppm), (TMS, Cortec, Paris, France) (Bruker, Karlsruhe, Germany) and connected with 5 mm probes. The ^1H and ^{13}C NMR spectroscopic interpretations were carried out using the software MestReNova version 7.1.1-9649© 2012 (Mestrelab Research, S.L. Feliciano Barrera, Santiago de Compostela, Spain).

4.2.2. Sample collection and pretreatment

The bivalve clams, *V. cyprinoides* and *P. malabarica* (10 kg each) used for this study were freshly collected from their natural habitat at the estuarine waters of Vembanad Lake ($9^\circ 35'$ N and $76^\circ 25'$ E) and Ashtamudi Lake ($8^\circ 59'$ N and $76^\circ 36'$ E), respectively situated along the southwest coast of the Arabian Sea, bordering India. After cleaning the externalities, *V. cyprinoides* and *P. malabarica* were transported to the laboratory in an ice box. The shell-on samples were systematically cleaned in running distilled water and edible meat (6 kg each) was separated from the shells by manually without heating. The edible flesh samples were subsequently homogenized by grinding machine and kept back for overnight in the deep freezer (ultra-low temperature freezer, Eppendorf, Hamburg, Germany) at -80°C for freezing. It was then lyophilized by utilizing freeze drier (Scanvac, CoolsafeTM Denmark; Martin Christ, Alpha 1-4 LD plus, Germany) to yield the freeze dried clam samples (1500 g each; yield 25 g/100 g). This was powdered and preserved in vacuum packed polythene biohazard autoclavable bags (Fisherbrand TM, Fischer Scientific) in the deep freezer at -80°C until further processing. The freeze lyophilized powder of clam samples used for solvent extraction.

4.2.3. Preparation of the crude extracts of bivalve clams

The lyophilized powder (1500 g; yield 25 g/100 g on wet basis) of bivalve clam material extracted with 1:1 (v/v) ethyl acetate:methanol (EtOAc:MeOH) by sonication (Elma, Hohentwiel, Germany) and shaking (Orbital shaker, Labline, India)

for 4 h under an inert atmosphere of nitrogen. This extraction procedure repeated for three times to recover maximum bioactive components in the crude extract. The extract contents then filtered through filter paper (Whatman No. 1) to yield the clarified filtrates and again filtered through Na₂SO₄ (30 g). The solvent filtrates concentrated (40°C) by rotary vacuum evaporator (Ika, USA; Heidolph, Germany) to afford concentrated extracts of *V. cyprinoides* and *P. malabarica*. The extracts dried in the rotational vacuum concentrators (RVC, Martin Christ, Germany) to yield corresponding solvent extracts of *V. cyprinoides* (50 g; yield 3.33 g/100 g on dry weight basis) and *P. malabarica* (55 g; yield 3.67 g/100 g on dry weight basis). This EtOAc:MeOH crude extracts of clam samples used for the evaluation of bioactive potentials against various targets.

4.2.4. Determination of bioactive potentials of extracts of bivalve clams

4.2.4.1. *In vitro* antioxidant assays

4.2.4.1.1. Determination of total phenolic content

Total phenolic content in EtOAc:MeOH extracts of *V. cyprinoides* and *P. malabarica* assessed according to established method (Chew *et al.*, 2008). Briefly, the known quantities of the extracts (10 mg) were added into a vial containing MeOH (1 mL). It was mixed with 5 mL of Folin-Ciocalteu (F.C.) solution and 4 mL of 0.7 M sodium carbonate followed by incubation at 25°C for 120 min. The absorbances were recorded at 760 nm by UV-VIS spectrophotometer, relative to the blank (MeOH). A standard curve of various concentrations of gallic acid (0.2-0.005 mg/mL) along X-axis and absorbance along Y-axis were plotted. The amounts of total phenolic contents calculated in milligram of gallic acid equivalents (mg GAE)/g of extracts using the following equation:

mg Gallic acid equivalent/g of sample =

(concentration of mg/g gallic acid equivalent (x) * weight of sample in g)/volume of extract

Concentration of mg/mL gallic acid equivalent (x) was obtained from the linear graph of standard using the equation: $y = mx + c$ (where “y = absorbance of sample”)

4.2.4.1.2. Free radical scavenging assays**4.2.4.1.2.A. 1,1-Diphenyl-2-picryl-hydrazil (DPPH) radical scavenging assay**

The free radical scavenging activity of the solvent extracts of *V. cyprinoides* and *P. malabarica* were estimated by utilizing the stable free radical, DPPH based on earlier methods (Chew *et al.*, 2008). In brief, stock solutions of extracts in methanol were prepared followed by the preparation of the serial dilutions from the corresponding stock solutions to afford various concentrations (0.25 to 2.0 mg/mL) of the extracts. The various concentrations of extracts were added to equal volumes of 0.1 mM DPPH in methanol (2.0 mL). The solutions were mixed properly and kept for 30 min at room temperature in dark. The absorbance of various concentrations of extracts and control solutions (2.0 mL DPPH solution + 2.0 mL methanol) were recorded against a reagent blank (MeOH) after 20 min at 517 nm using UV-VIS spectrophotometer. The triplicate experiments were carried out. An equal volume of test samples with different concentrations (0.25-2.00 mg/mL) were analyzed to determine the percentage inhibition and the IC₅₀ values. The percentage inhibition (%) was calculated as follows: $((A_C - A_S)/A_C) * 100$, where A_C and A_S represented the absorbance of control and sample, respectively. 50% Inhibitory Concentration (IC₅₀) can be calculated from the graph plotted with concentrations of sample (X-axis) against percentage inhibition (Y-axis). The results were expressed as IC₅₀, the concentration of samples at which it inhibits/scavenge 50% of enzyme/radical activities and were expressed in mg/mL.

4.2.4.1.2.B. 2,2'-Azino-bis-3-ethylbenzothiozoline-6-sulfonic acid diammonium salt (ABTS⁺) radical scavenging assay

The radical scavenging potentials of EtOAc:MeOH extracts of *V. cyprinoides* and *P. malabarica* were determined by ABTS⁺ decolourization assay (Vijayabaskar and Shiyamala 2012). In brief, ABTS⁺ (7 mM) and potassium persulfate (2.45 mM) were mixed and kept for 16 h in dark at room temperature. The intensely coloured resultant ABTS⁺ stock solution was diluted with MeOH to get ~0.70 absorbance at 734 nm. The diluted ABTS⁺ (5 mL) was mixed with 0.1 mL of extracts (0.25 to 2.0 mg/mL; in MeOH) and their corresponding absorbance were recorded at 734 nm against blank solution (MeOH) using UV-VIS spectrophotometer. The triplicate analyses were performed. An equal volume of test samples with different concentrations (0.25-2.00

mg/mL) were analyzed to determine the percentage inhibition and the IC₅₀ values. The percentage inhibition (%) was calculated as follows: $((A_C - A_S)/A_C) * 100$, where A_C and A_S represented the absorbance of control and sample, respectively. 50% Inhibitory Concentration (IC₅₀) can be calculated from the graph plotted with concentrations of sample (X-axis) against percentage inhibition (Y-axis). The results were expressed as IC₅₀, the concentration of samples at which it inhibits/scavenge 50% of enzyme/radical activities and were expressed in mg/mL.

4.2.4.1.2.C. Hydrogen peroxide (H₂O₂) radical scavenging assay

The ability of EtOAc:MeOH extracts to inhibit H₂O₂ was measured by the established method (Gulcin 2007). The 40 mM H₂O₂ in phosphate (pH 7.4) buffer was prepared. The different concentrations of extracts, ranging from 0.25-2.0 mg/mL in methanol were prepared by serial dilutions using a stock solution of extracts (2 mg/mL). Equal volumes of extracts (3.0 mL) and H₂O₂ solution (3.0 mL) were mixed and kept for 10 min incubation. The absorbance of various concentrations of extracts and control (H₂O₂ solution + MeOH) recorded at 230 nm against phosphate buffer without H₂O₂ (blank) using UV-VIS spectrophotometer after 10 min. This assay performed in triplicates. An equal volume of test samples with different concentrations (0.25-2.00 mg/mL) analyzed to determine the percentage inhibition and the IC₅₀ values. The percentage inhibition (%) was calculated as follows: $((A_C - A_S)/A_C) * 100$, where A_C and A_S represented the absorbance of control and sample, respectively. 50% Inhibitory Concentration (IC₅₀) can be calculated from the graph plotted with concentrations of sample (X-axis) against percentage inhibition (Y-axis). The results were expressed as IC₅₀, the concentration of samples at which it inhibits/scavenge 50% of enzyme/radical activities and expressed in mg/mL.

4.2.4.1.2.D. Ferrous ion (Fe²⁺ ion) chelating assay

The ferrous ion (Fe²⁺ ion) chelating ability of EtOAc:MeOH extracts evaluated according to the established method (Gulcin 2007). The crude extracts (1 mL) with various concentrations (0.25 to 2.0 mg/mL) mixed to ferrozine (1.0 mL, 0.3125 mM) and FeSO₄ (1 mL, 0.125 mM). This was homogenized and equilibrated for 10 min. The absorbance of extracts and control (consisting of FeSO₄ and ferrozine

solution) recorded at 562 nm against blank (MeOH) using UV-VIS spectrophotometer after 10 min. The investigations carried out in triplicates. An equal volume of test samples with different concentrations (0.25-2.00 mg/mL) were analyzed to determine the percentage inhibition and the IC₅₀ values (mg/mL). The percentage inhibition (%) was calculated as follows: $((A_C - A_S)/A_C) * 100$, where A_C and A_S represented the absorbance of control and sample, respectively. 50% Inhibitory Concentration (IC₅₀) can be calculated from the graph plotted with concentrations of sample (X-axis) against percentage inhibition (Y-axis). The results were expressed as IC₅₀, the concentration of samples at which it inhibits/scavenge 50% of enzyme/radical activities and were expressed in mg/mL.

4.2.4.1.2.E. Lipid peroxidation inhibitory assay

The ability of clam extracts to arrest lipid peroxidation assessed by thiobarbituric acid reactive species (TBARS) assay (Kulisic *et al.*, 2004). The extracts of *V. cyprinoides* and *P. malabarica* (10 mg) added to 20% ice cold acetic acid (2 mL) and 2 mL of thiobarbituric acid (0.78% in acetic acid). This was incubated for 45 min in water bath at 95°C and cooled followed by centrifugation (8000 rpm/10 min). The corresponding absorbances were recorded at 532 nm. The mixture of 2 mL acetic acid (20%) and 2 mL TBA was used for the blank reading. The different concentrations of malondialdehyde (0.1mL; 0.1, 0.05, 0.025, 0.0125 and 0.00625 µg/mL) was mixed with 20% ice cold acetic acid (2 mL) and 2 mL of thiobarbituric acid (0.78% in acetic acid) followed by water bath incubation (95°C/45 min). The absorbance was reported at 532 nm and a standard curve of mM MDA was plotted [concentration (µg/mL) at X-axis and absorbance at Y-axis]. The lipid peroxidation inhibitory potency was expressed as mM of malondialdehyde equivalent compounds per kg sample (MDAEQ/kg sample) using the following equation:

$$\text{mM MDA/kg sample} = (\text{mM MDA equivalent (x)} * 1000000)/(4 * W1)$$

where, (4 = total sample volume; W1 = sample weight in mg; 1000000 = conversion of mg to kg)

The mM MDA equivalent (x) was obtained from the standard curve using the equation:

$$y = mx + c \text{ (where "y = absorbance of sample")}$$

4.2.4.2. *In vitro* anti-inflammatory assays

4.2.4.2.1. Cyclooxygenases (COX) inhibition assay

The cyclooxygenase (COX-1 and COX-2) inhibition assays were performed by 2,7-dichlorofluorescein method (Larsen *et al.*, 2009). In brief, 5 mg of leuco-2,7-dichlorofluorescein diacetate hydrolyzed in 1 M NaOH (50 μ L) at room temperature (10 min) followed by adding of 30 μ L HCl (1 M) to counteract additional NaOH before resultant leuco-dichlorofluorescein was dissolved in tris-buffer (0.1 M; pH 8). The cyclooxygenase enzymes, COX-1 and COX-2 were dissolved in 0.1 M tris-buffer. The various concentrations of samples (0.25 to 2.0 mg/mL) were pre-incubated with enzymes in hematin (5 min). The phenol, arachidonic acid and 1-DCF were mixed with enzymes to get a final mixture of 1 μ M hematin, 500 μ M phenol, 50 μ M arachidonic acid and 20 μ M 1-DCF in 1 mL of tris-buffer. The absorbances were assessed at 502 nm. Also, a blank (without enzyme) solution was evaluated in the same wavelength. The investigations were performed in triplicate. An equal volume of test samples with different concentrations (0.25-2.00 mg/mL) were analyzed to determine the percentage inhibition and the IC₅₀ values. The percentage inhibition (%) was calculated as follows: $((A_C - A_S)/A_C) * 100$, where A_C and A_S represented the absorbance of control and sample, respectively. 50% Inhibitory Concentration (IC₅₀) can be calculated from the graph plotted with concentrations of sample (X-axis) against percentage inhibition (Y-axis). The results were expressed as IC₅₀, the concentration of samples at which it inhibits/scavenge 50% of enzyme/radical activities and were expressed in mg/mL.

4.2.4.2.2. 5-Lipoxygenase (5-LOX) inhibition assay

The 5-lipoxygenase inhibitory analyses were carried out using earlier method (Baylac and Racine 2003). An aliquot of the various concentrations (0.25 to 2.0 mg/mL) of extracts (29:1, w/w, 50 μ L, in DMSO and Tween 20 mixture) were prepared and mixed with 2.95 mL of pre-heated potassium phosphate buffer (0.1 M, pH 6.3) and 48 μ L of linoleic acid. Then, ice-cold potassium phosphate buffers (12 μ L) were added to 5-LOX (100 U). The absorbances were obtained spectrophotometrically at 234 nm. The control was prepared with DMSO:Tween 20 mixture without enzyme. The triplicate evaluations were carried out. An equal volume of test samples with different concentrations (0.25-2.00 mg/mL) analyzed to determine the percentage inhibition and

the IC₅₀ values. The percentage inhibition (%) was calculated as follows: $((A_C - A_S)/A_C) * 100$, where A_C and A_S represented the absorbance of control and sample, respectively. 50% Inhibitory Concentration (IC₅₀) can be calculated from the graph plotted with concentrations of sample (X-axis) against percentage inhibition (Y-axis). The results were expressed as IC₅₀, the concentration of samples at which it inhibits/scavenge 50% of enzyme/radical activities and were expressed in mg/mL.

4.2.4.3. *In vitro* anti-diabetic assays

4.2.4.3.1. α -Amylase inhibition assay

The *in vitro* anti-diabetic investigations against α -amylase were measured by previously described assay (Hamdan and Afifi 2004). Equal volumes of the test samples (0.25-2.00 mg/mL) and α -amylase (0.5 mg/mL) enzyme in phosphate buffer (0.20 mM/pH 6.9) which were incubated for 10 min at 25°C. Thereafter, it was incubated with 1% solution of starch in phosphate buffer (0.02 M/pH 6.9) for 10 min at 25°C and the reaction was ceased using 3,5 dinitrosalicylic acid followed by keeping in boiling (for 5 min) water bath. The absorbances were reported at 540 nm subsequent to diluting with DDW. The α -amylase inhibitory potency of control was carried out in the same way by replacing the extracts with vehicle. The investigations were repeated. An equal volume of test samples with different concentrations (0.25-2.00 mg/mL) were analyzed to determine the percentage inhibition and the IC₅₀ values. The percentage inhibition (%) was calculated as follows: $((A_C - A_S)/A_C) * 100$, where A_C and A_S represented the absorbance of control and sample, respectively. 50% Inhibitory Concentration (IC₅₀) can be calculated from the graph plotted with concentrations of sample (X-axis) against percentage inhibition (Y-axis). The results were expressed as IC₅₀, the concentration of samples at which it inhibits/scavenge 50% of enzyme/radical activities and expressed in mg/mL.

4.2.4.3.2. α -Glucosidase inhibition assay

The α -glucosidase scavenging effects (Hamdan and Afifi 2004) determined by incubating various concentrations of clam extracts (0.25-2.00 mg/mL) in tris-buffer (pH 8, 0.2 M) with starch substrate (2%) at 37°C (5 min). The experiment started by mixing α -glucosidase (1 U/mL) enzyme followed by incubation (37°C/10 min). The

reaction mixture heated for 2 min, then 3,5-dinitrosalicylic acid was added to stop the reaction followed by incubation and dilution. The amount of glucose liberation was calculated by glucose oxidase peroxidase experiment. An equal volume of test samples with different concentrations (0.25-2.00 mg/mL) were analyzed to determine percentage inhibition and the IC₅₀ values. The percentage inhibition (%) was calculated as follows: $((A_C - A_S)/A_C) * 100$, where A_C and A_S represented the absorbance of control and sample, respectively. 50% Inhibitory Concentration (IC₅₀) can be calculated from the graph plotted with concentrations of sample (X-axis) against percentage inhibition (Y-axis). The results were expressed as IC₅₀, the concentration of samples at which it inhibits/scavenge 50% of enzyme/radical activities and were expressed in mg/mL.

4.2.4.3.3. Dipeptidyl peptidase-4 (DPP-4) inhibition assay

The DPP-4 inhibitory potency (Kojima *et al.*, 1980) was performed by using different concentration of extracts (0.25-2.00 mg/mL; 350 µL) in tris-HCl buffer (50 mM/pH 7.5) pre-incubated with 0.05 U/mL of DPP-4 enzyme (15 µL) in 100 mM tris-HCl buffer (pH 8). This was incubated at 37°C (30 min), followed by mixing of 50 µL of 1.4 mM Gly-Pro-p-nitroanilide (0.2 M in tris-HCl buffer). This mixture was kept at 37°C (30 min) and the absorbances were measured at 405 nm. DPP-4 inhibitory activity of control was carried out in the same way by replacing extracts with vehicle. The investigations were repeated. An equal volume of test samples with different concentrations (0.25-2.00 mg/mL) were analyzed to determine the percentage inhibition and the IC₅₀ values. The percentage inhibition (%) was calculated as follows: $((A_C - A_S)/A_C) * 100$, where A_C and A_S represented the absorbance of control and sample, respectively. 50% Inhibitory Concentration (IC₅₀) can be calculated from the graph plotted with concentrations of sample (X-axis) against percentage inhibition (Y-axis). The results were expressed as IC₅₀, the concentration of samples at which it inhibits/scavenge 50% of enzyme/radical activities and were expressed in mg/mL.

4.2.4.4. *In vitro* anti-hypertensive assay

4.2.4.4.1. Angiotensin converting enzyme-1 (ACE-1) inhibitory activity

The ACE-1 scavenging ability was evaluated by earlier technique of Holmquist *et al.*, (1979). Briefly, 20 µL of 20 mU ACE-1 (1 U/mL) was added to

EtOAc:MeOH extracts of *V. cyprinoides* and *P. malabarica* (concentrations of 0.2, 0.3, 0.4 and 0.7 mg). Then, FAPGG (1 mL/0.5 mM) suspended in tris-buffer (50 mM/pH 7.5) comprising sodium chloride (0.3 M) was added. The declined absorbances were recorded at 345 nm. An equal volume of test samples with different concentrations (0.2, 0.3, 0.4 and 0.7 mg) were analyzed to determine the percentage inhibition and the IC₅₀ values. The percentage inhibition (%) was calculated as follows: $((A_C - A_S)/A_C) * 100$, where A_C and A_S represented the absorbance of control and sample, respectively. 50% Inhibitory Concentration (IC₅₀) can be calculated from the graph plotted with concentrations of sample (X-axis) against percentage inhibition (Y-axis). The results were expressed as IC₅₀, the concentration of samples at which it inhibits/scavenge 50% of enzyme/radical activities and were expressed in mg/mL.

4.2.5. Spectroscopic analyses

4.2.5.1. Fourier transform infrared (FTIR) spectroscopy

The Fourier transform infrared (FTIR) spectra of EtOAc:MeOH extracts of *V. cyprinoides* and *P. malabarica* were scanned between 4000 and 400 cm⁻¹ (Perkin-Elmer FTIR, Winter Street, Waltham, Massachusetts, USA).

4.2.5.2. Proton (¹H) and carbon (¹³C) nuclear magnetic resonance spectroscopy

The ¹H and ¹³C spectroscopic analyses of the EtOAc:MeOH extracts of bivalve clams, *V. cyprinoides* and *P. malabarica* were recorded on a Bruker Avance DPX 500 (500 MHz) spectrometer in deuteriated chloroform (CDCl₃) with standard, tetramethylsilane (TMS) (Bruker, Karlsruhe, Germany).

The ¹H spectra were mainly categorized in six different regions, including saturated hydrocarbons (RCH₃, R₂CH₂ and R₃CH) from δ 0.1-2.0, RC(=O)-CH₃ (acetyl) or -CH₂=CH-CH₃ (allylic) from δ 2.0-2.5, RCH₂-X (alkyl halide) or -OCH₃ (methoxy) or RCH₂OH (alkanols) from δ 2.5-3.5, directly attached protons to oxygen of ester linkages or RCH₂C(=O)-OCH₃ (alkyl alkanoates) from δ 3.5-4.5, olefinic (RCH=CHR₁) protons from δ 4.5-6.5 and aromatic protons from δ 6.5-8.5. The protons at characterized zones of the ¹H NMR were solved and integrated to obtain numbers of protons in the corresponding areas. The ¹³C NMR spectra partitioned into characteristic carbons in the specific positions which were found to be carbonyl carbon atoms from δ

180-210, alkanolate ester carbon atoms from δ 160-180, aryls from δ 140-160, olefinic from δ 110-140, carbon atom bonded to hydride moiety of alkyl alkanolates from δ 70-80, alkoxy (RCH_2OR_1) from δ 45-70 and saturated hydrocarbons from δ 10-40. The spectroscopic analyses were carried out to study the nature, characteristics of components present in the extract, and its relation to bioactive potentials.

4.2.6. Statistical analyses

One way analyses of variance (ANOVA) was carried out using Statistical Program for Social Sciences 13.0 (SPSS, USA, ver. 13.0) to assess the significant differences between the means of bioactivities. The significant differences were represented as $p < 0.05$ and the values were given as the means of triplicates \pm standard deviation. The variances in the data were evaluated by utilizing the principal component analyses (PCA) in which specific factors for PCA were anti-diabetic, anti-inflammatory, antioxidant and anti-hypertensive potentials demonstrated by EtOAc:MeOH extracts of *V. cyprinoides* and *P. malabarica*.

4.3. Results and discussion

4.3.1. Yield of EtOAc:MeOH crude extracts of *V. cyprinoides* and *P. malabarica*

The recovery of EtOAc:MeOH crude extracts derived from the bivalve clams, *V. cyprinoides* and *P. malabarica* were found to be 3.33% and 3.67%, respectively based on the dry weight of clam samples.

4.3.2. Total phenolic content and antioxidant activities

The total phenolic content and antioxidant potentials against various targets along with ferrous ion chelating potentials were tabulated in the Table 4.1. The EtOAc:MeOH extracts of *P. malabarica* was showed significantly greater ($p < 0.05$) total phenolic content (88.62 mg GAE/g, 5 mg/mL) than recorded in *V. cyprinoides* (73.87 mg GAE/g, 5 mg/mL).

The EtOAc:MeOH extract derived from *P. malabarica* displayed significantly greater ABTS⁺ scavenging activity (IC_{50} 1.27 mg/mL) than that of *V. cyprinoides* (IC_{50} 1.41 mg/mL), whilst no characteristic differences in H_2O_2 /DPPH quenching and Fe^{2+} ion chelating activities of *V. cyprinoides* and *P. malabarica* were

apparent (Table 4.1.). Both the species exhibited greater DPPH scavenging potentials with lower IC₅₀ value of 0.76 mg/mL. Also, the IC₅₀ values of Fe²⁺ ion chelating activities and H₂O₂ scavenging potentials were found to be ~1.86 and ~1.42 mg/mL, respectively for both the studied clam species. The lipid peroxidation inhibition activity was found to be significantly greater ($p < 0.05$) for *P. malabarica* than those from *V. cyprinoides*. This was apparent from the lower value of TBARS (malondialdehyde, MDA) formation by the EtOAc:MeOH extracts of *P. malabarica* (2.39 mM MDAEQ/kg) when compared to *V. cyprinoides* (3.18 mM MDAEQ/kg).

The EtOAc:MeOH extract of *P. malabarica* showed significantly greater total phenolic contents (~88.6 mg GAE/g) than those in *V. cyprinoides* (~73.9 mg GAE/g). The phenolic compounds reported to possess radical scavenging properties and were assured to shield the delicate bodied mollusks from photooxidation. The present work likewise observed a significant correlation between the phenolic contents and the antioxidant activities which signified the role of phenolics as antioxidants like earlier reports of other marine living organisms (Escrig *et al.*, 2001; Karawita *et al.*, 2004).

Table 4.1.: Phenolic content and antioxidant activities (IC₅₀) of EtOAc:MeOH extracts of *P. malabarica* and *V. cyprinoides*

	<i>P. malabarica</i>	<i>V. cyprinoides</i>
^w Total phenolic content (5 mg/mL)	88.62 ± 0.33 ^a	73.87 ± 0.33 ^b
^x DPPH radical scavenging activity	0.76 ± 0.02 ^a	0.76 ± 0.03 ^a
^x ABTS ⁺ radical scavenging activity	1.27 ± 0.02 ^a	1.41 ± 0.00 ^b
^x Fe ²⁺ ion chelating activity	1.86 ± 0.02 ^a	1.87 ± 0.02 ^a
^x H ₂ O ₂ scavenging activity	1.41 ± 0.03 ^a	1.44 ± 0.04 ^a
^y Lipid peroxidation inhibitory activity	2.39 ± 0.07 ^a	3.18 ± 0.04 ^b

The samples were analyzed in triplicate (n=3) and expressed as mean ± standard deviation. Means followed by the different superscripts (a-b) within the same row indicated significant differences ($p < 0.05$). ^wTotal phenolic contents were presented as mg of gallic acid equivalence (mg GAE)/g. ^xThe IC₅₀ values were expressed as mg/mL. ^yLipid peroxidation inhibitory (TBARS assay) was expressed as mM MDAEQ/kg

It is evident that owing to their greater number of hydroxyl groups, polyphenols display higher redox potential and in this manner are efficient electron donors. By virtue of this, they can act as reducing agents, metal chelating agents or singlet oxygen quenchers. The EtOAc:MeOH extract of *V. cyprinoides* and *P. malabarica* were demonstrated greater Fe^{2+} ion chelating ability ($\text{IC}_{50} \sim 1.86$ mg/mL) therefore, efficient in neutralizing the H_2O_2 ($\text{IC}_{50} \sim 1.42$ mg/mL), ABTS^+ radicals (IC_{50} 1.27-1.41 mg/mL) and DPPH (IC_{50} 0.76 mg/mL). Significant positive correlations between total phenolic contents and various antioxidant activities of the solvent extracts, as acknowledged by correlation analyses, showed the vicinity of phenolic compounds responsible for free radical scavenging ability. Previous studies showed that the extracts containing phenolic or electronegative groups were potential antioxidants (Hodzic *et al.* 2009; Lindsay 1996). In the present study, the EtOAc:MeOH extracts derived from the bivalve clams were demonstrated higher TPC content, which might explain the greater ABTS^+ and DPPH radical scavenging properties. The methanolic and EtOAc extract of bivalve mollusk, *P. viridis* reported to exhibit significant scavenging property against DPPH radical, which support the outcome of the present study (Jena *et al.*, 2010; Sreejamole and Radhakrishnan 2013).

4.3.3. Anti-inflammatory activities

The EtOAc:MeOH extract of *P. malabarica* exhibited significantly greater anti-inflammatory properties as determined by COX-1 and COX-2 enzyme inhibitory activities (IC_{50} 2.36 and 0.92 mg/mL, respectively) ($p < 0.05$) than those extracted from *V. cyprinoides* (IC_{50} 2.54 and 1.03 mg/mL, respectively) (Table 4.2.). *P. malabarica* also exhibited significantly ($p < 0.05$) greater 5-LOX inhibitory activity (IC_{50} 1.51 mg/mL) than the EtOAc:MeOH extract derived from *V. cyprinoides* (IC_{50} 1.64 mg/mL). The selectivity indices (IC_{50} value of anti-cyclooxygenase-1/ IC_{50} value of anti-cyclooxygenase-2) of EtOAc:MeOH extract obtained from *P. malabarica* and *V. cyprinoides* were 2.57 and 2.47, respectively which was found to be greater than the commercially available non-steroidal anti-inflammatory drugs (NSAIDs, SI < 2.0).

Table 4.2.: Anti-inflammatory activities (IC₅₀) of EtOAc:MeOH extracts of *P. malabarica* and *V. cyprinoides*

	<i>P. malabarica</i>	<i>V. cyprinoides</i>
^x COX-1 inhibitory activity	2.36 ± 0.03 ^a	2.54 ± 0.04 ^b
^x COX-2 inhibitory activity	0.92 ± 0.01 ^a	1.03 ± 0.02 ^b
^y Selectivity index	2.57 ± 0.02 ^a	2.47 ± 0.03 ^b
^x 5-LOX inhibitory activity	1.51 ± 0.01 ^a	1.64 ± 0.02 ^b

The samples were analyzed in triplicate (n=3) and expressed as mean ± standard deviation. Means followed by the different superscripts (a-b) within the same row indicated significant differences ($p < 0.05$). ^xThe IC₅₀ values were expressed as mg/mL. ^ySelectivity index is the ratio of IC₅₀ value of anti-COX-1 to IC₅₀ value of anti-COX-2 (IC₅₀ anti-COX-1/IC₅₀ anti-COX-2)

The EtOAc:MeOH extract derived from *P. malabarica* was exhibited significantly greater anti-COX-2/anti-5-LOX properties (IC₅₀ 0.92 and 1.51 mg/mL, respectively) than those extracted from *V. cyprinoides*, which indicated that these antioxidants might have significant role in deterring pro-inflammatory enzymes in the system. The EtOAc:MeOH extracts of bivalve clams registered the ratio of inhibitory concentration for COX-1/COX-2 as greater than 2.0 compared to non-steroidal anti-inflammatory drugs (< 1.0), which confirmed their greater selectivity against inflammatory reactions and greater selectivity profiles. The EtOAc:MeOH extracts derived from the bivalve clams considered in the present study were found to effectively inhibit pro-inflammatory enzymes, which leads to the declined production of inflammatory prostaglandins, such as prostaglandin E₂ (PGE₂) and prostaglandin F_{2a} (PGF_{2a}) (Fernandes *et al.*, 2004). It is of note that the lipid peroxidation transforms lipids, fatty acids and lipoproteins to hydroperoxide lipids by free radicals resulting in inflammation (Camacho-Ruiz *et al.*, 2010). It is therefore apparent that the free radical quenching species were good anti-inflammatory candidates. Earlier studies reported that commercially prepared freeze dried extract of New Zealand green lipped mussel *P. canaliculus* was down regulate the inflammatory sequence (Tiffany and Bui 2002). Green mussel (*P. viridis*) reported to exhibit anti-inflammatory properties against COX-2 (50%) and 5-LOX (47%) enzymes (Chakraborty *et al.*, 2014a).

4.3.4. Anti-diabetic and anti-hypertensive activities

The EtOAc:MeOH extract of *P. malabarica* exhibited greater α -amylase and α -glucosidase inhibitory activities (IC_{50} 1.39 and 1.47 mg/mL, respectively) than *V. cyprinoides* (IC_{50} ~1.54 mg/mL for anti- α -amylase and anti- α -glucosidase) (Table 4.3.). Likewise the DPP-4 inhibition activity of EtOAc:MeOH extract of *P. malabarica* appeared to be appreciably higher (IC_{50} 1.00 mg/mL) than the same derived from *V. cyprinoides* (IC_{50} 1.06 mg/mL).

The EtOAc:MeOH extract derived from *P. malabarica* was displayed significantly greater anti-hypertensive properties as dictated by angiotensin-1 converting enzyme inhibitory activity (IC_{50} 1.11 mg/mL) compared to *V. cyprinoides* (IC_{50} 1.16 mg/mL).

Oxidative stress was found to be an important reason for increased blood sugar level and type-2 diabetes related disorders in human. More recently, inflammatory mediators have become increasingly implicated in the development of type-2 diabetes. The present studies has been demonstrated the potentials of *P. malabarica* to prevent the formation of free radicals due to the presence of greater numbers of electronegative functional groups, to decelerate the digestion of starch and carbohydrate by inhibiting α -amylase along with α -glucosidase enzymes (Brayer *et al.*, 2000).

Table 4.3.: Anti-diabetic and anti-hypertensive activities (IC_{50}) of EtOAc:MeOH extracts of *P. malabarica* and *V. cyprinoides*.

	<i>P. malabarica</i>	<i>V. cyprinoides</i>
Anti-diabetic activities		
^x α -amylase inhibitory activity	1.39 \pm 0.04 ^a	1.54 \pm 0.05 ^b
^x α -glucosidase inhibitory activity	1.47 \pm 0.02 ^a	1.54 \pm 0.04 ^b
^x DPP-4 inhibitory activity	1.00 \pm 0.06 ^a	1.06 \pm 0.06 ^b
Anti-hypertensive activity		
^x ACE-1 inhibitory activity	1.11 \pm 0.05 ^a	1.16 \pm 0.04 ^b

The samples were analyzed in triplicate (n=3) and expressed as mean \pm standard deviation. Means followed by the different superscripts (a-b) within the same row indicated significant differences ($p < 0.05$). ^xThe IC_{50} values were expressed as mg/mL

Earlier studies were demonstrated that the mollusks, *Hemifusus pugilinus* and *Natica didyma* possessed anti-diabetic potential (Ravi *et al.*, 2012). Inhibition of DPP-4 enzyme was considered to be the potential target in the treatment of diabetics. The positive control, diprotein A (Ile-Pro-Ile), a reported DPP-4 inhibitor, was found to covalently bound to Ser⁶³⁰ forming a hemiacetal and trapped as a tetrahedral intermediate of the hydrolysis reaction. The anti-diabetic potentials assessed by DPP-4 scavengers reported to possess electrophilic functionalities that can directly interact with the hydroxyl group of catalytic serine⁶³⁰ in active site of DPP-4 enzyme.

The EtOAc:MeOH extract obtained from *P. malabarica* showed significantly greater anti-hypertensive properties than that from *V. cyprinoides* as displayed by ACE-1 inhibitory activity. This apparently showed that the antioxidants from the solvent extract of *P. malabarica* might have a prominent role in deterring the hypertensive modulators. Likewise significant co-linearity was found to exist between anti-inflammatory and anti-diabetic properties *vis-à-vis* antioxidative activities of solvent extracts from bivalve clams.

Many synthetic drugs developed to combat elevated blood pressure though they cause unfavourable side effects. To overcome the side effects of these drugs, targeted ACE inhibitors were developed particularly from the marine resources, for example, ACE inhibitor peptides from mussel, *Mytilus coruscus* (Wu *et al.*, 2013). Numerous reports have recognized that hypertension is associated with decreased antioxidant capacity (Lacy *et al.*, 2000), greater levels of lipid peroxidation (Manning *et al.*, 2005) and the formation H₂O₂ (Russo *et al.*, 1998), which appropriately suggested the relationship between free radicals and hypertension.

4.3.5. Spectroscopic labeling of the functional groups in the EtOAc:MeOH extracts of bivalve clams

4.3.5.1. NMR based proton and carbon labeling

The labeling of protons and carbons associated with different magnetic environments of the prominent functional groups in the EtOAc:MeOH extracts of bivalve clams were analyzed by ¹H NMR spectroscopy (Figure 4.1.) conjugated with ¹³C NMR approach (Figure 4.2.). A comparison of proton integrals at different regions were plotted for EtOAc:MeOH extracts derived from these species (Figure 4.3.).

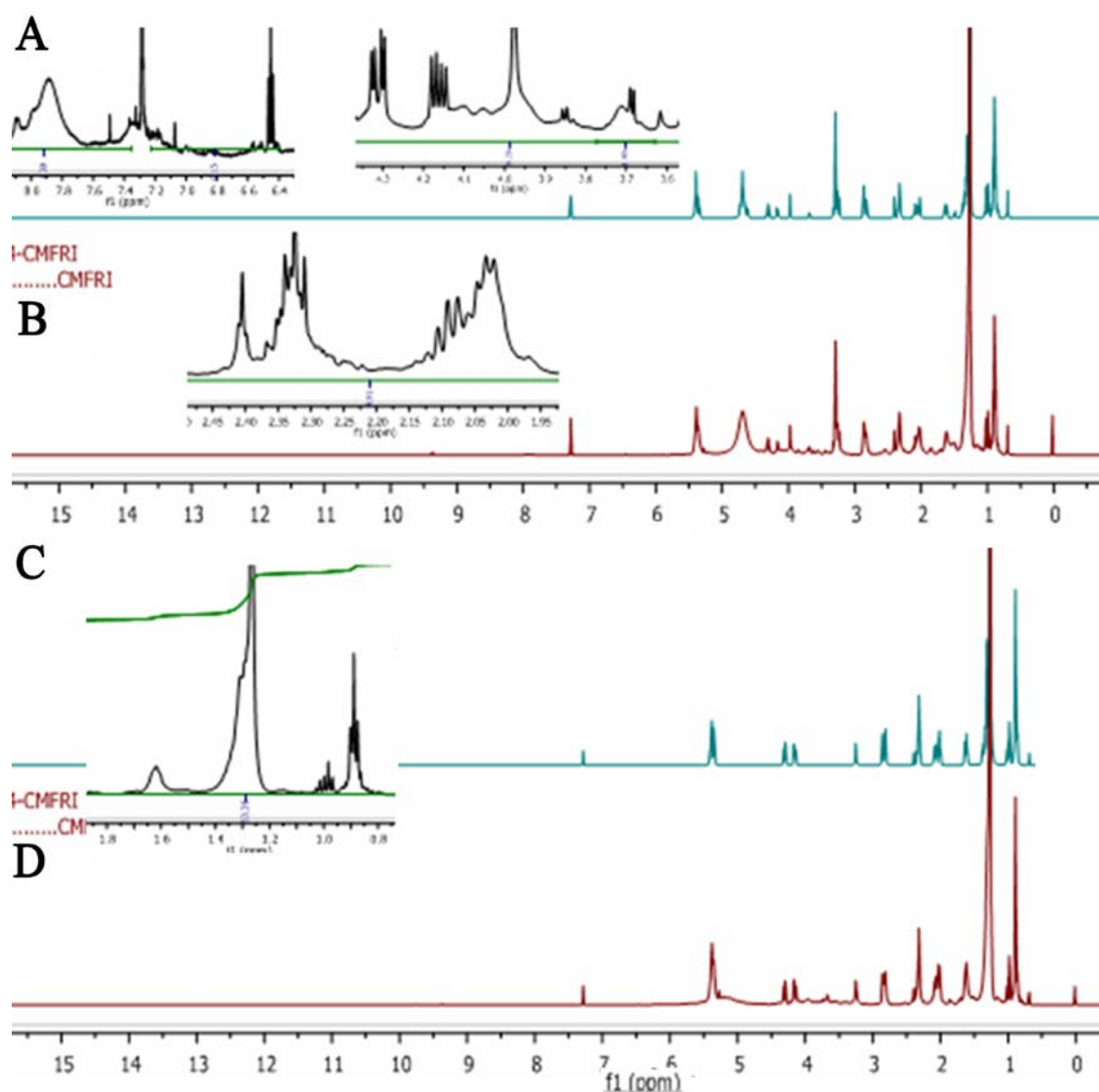


Figure 4.1.: The stacked plot representing the ^1H NMR spectra of EtOAc:MeOH extracts of *P. malabarica* and *V. cyprinoides*. (A) deconvoluted ^1H NMR and (B) acquired ^1H NMR spectra of EtOAc:MeOH extract of *P. malabarica*. (C) Deconvoluted ^1H NMR and (D) acquired ^1H NMR spectra of EtOAc:MeOH extract of *V. cyprinoides*. The protons at the defined regions of the ^1H NMR spectra were integrated to get the number of protons in specific regions. The functional groups representing the distinct regions of the ^1H NMR spectra were illustrated as insets

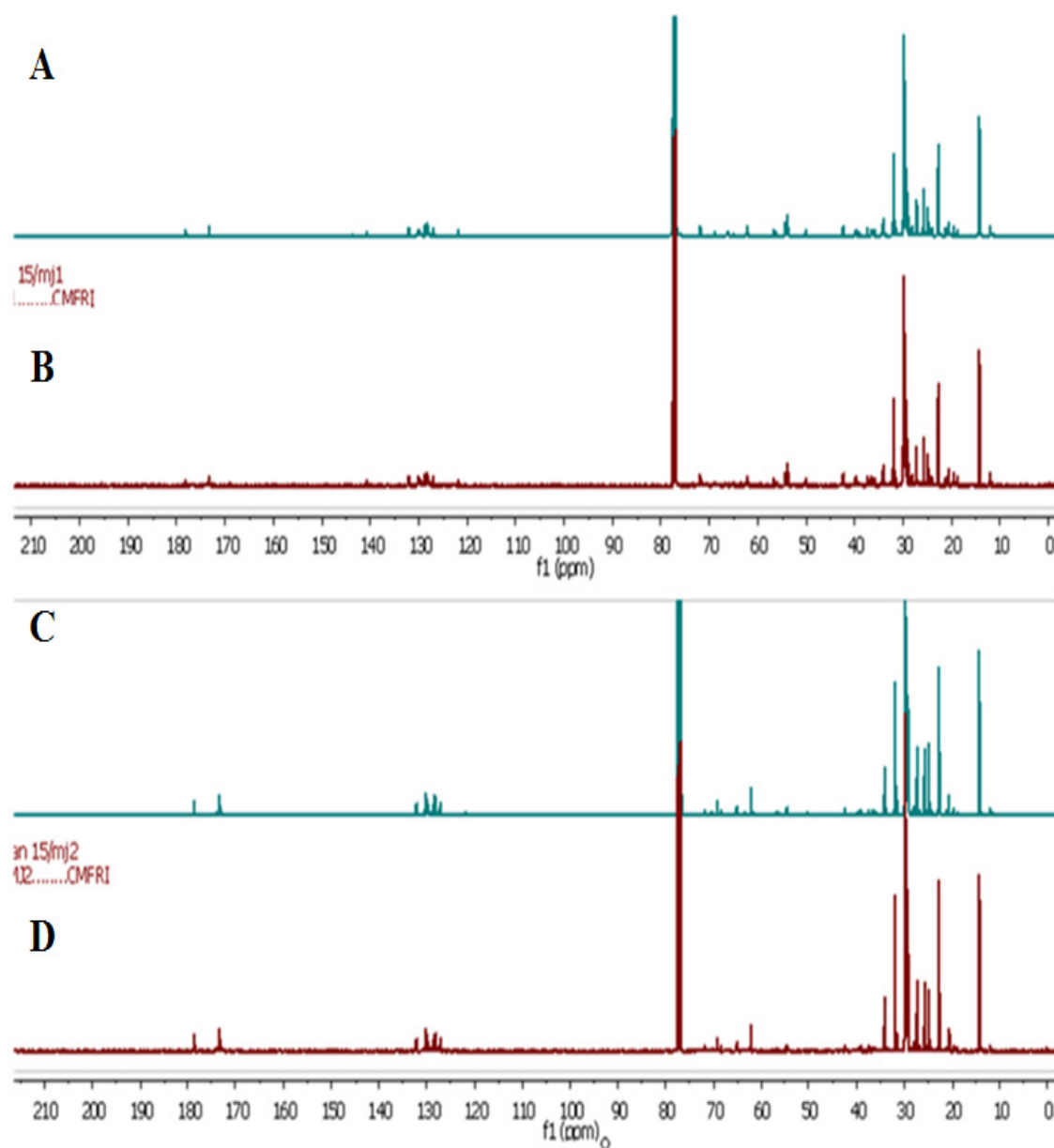


Figure 4.2.: The stacked plot representing the (A) deconvoluted and (B) acquired ^{13}C NMR spectra of EtOAc:MeOH extract of *P. malabarica*. (C) deconvoluted and (D) acquired ^{13}C NMR spectra of EtOAc:MeOH extract of *V. cyprinoides*. Chemical shift (δ) values are expressed in parts per million (ppm) and were referenced to the residual solvent signals of CDCl_3

The ^1H NMR spectra of EtOAc:MeOH extract from *V. cyprinoides* and *P. malabarica* showed that the total proton integral due to saturated hydrocarbon groups were more prominent in *V. cyprinoides* (63.36) than that in *P. malabarica* (57.23). The proton integrals at the olefinic region (δ 4.5-6.5) of the EtOAc:MeOH extract of *P.*

malabarica were more prominent (22.23) than *V. cyprinoides* (13.79). The number of protons at δ 2.5-3.5, presumably of methoxy ($-\text{OCH}_3$)/alkyl halide ($\text{RCH}_2\text{-X}$)/functionalized hydride H of the substituted alkanol (RCH_2OH), were found to be greater in *P. malabarica* (proton integral of 12.24), whilst, exceptionally frail proton signals at this locale for *V. cyprinoides* (total proton integral of 6.68) were obvious. The ^1H integrals at δ 3.5-4.5 corresponded towards the alkyl alkanoates ($\text{RCH}_2\text{C(=O)OCH}_3$) or protons directly attached to oxygen of ester linkages were greater for *P. malabarica* (proton integral of 8.29) when compared to *V. cyprinoides* (7.27).

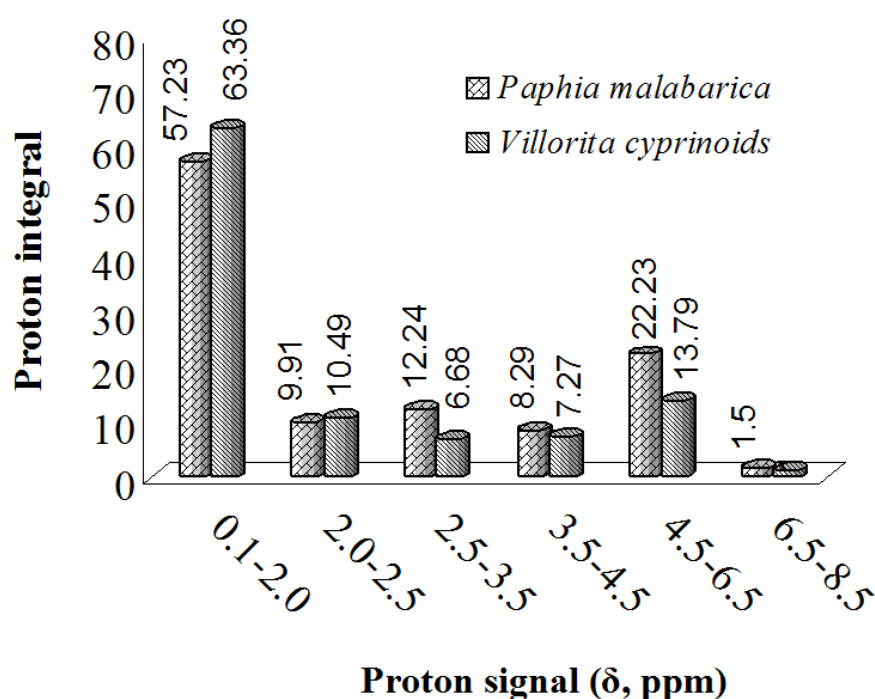


Figure 4.3.: Type and integral values of protons obtained from the ^1H NMR spectra of EtOAc:MeOH extracts of *P. malabarica* and *V. cyprinoides*

The signal intensity and number of carbon atoms with saturated hydrocarbons (δ 10-40) were more noteworthy in the EtOAc:MeOH extracts derived from *P. malabarica* than in *V. cyprinoides*. The number of methine ($-\text{CH}-$) signals at δ 30-40 was found to be greater in the EtOAc:MeOH extracts of *V. cyprinoides* and *P. malabarica*. The characteristic peaks due to alkanoate carbon atom of esters (RC(=O)OR_1) were discernible at δ 160-180 present in these species. The number of sp^2 hybridized olefinic carbon atoms in the region between δ 110-140 were found to be

greater in the EtOAc:MeOH extracts derived from *P. malabarica* than in *V. cyprinoides*. The signals at δ 45-70 due to the alkoxy carbon ($\text{R}\underline{\text{C}}\text{H}_2\text{OR}_1$) were present in greater intensity in EtOAc:MeOH extracts of *P. malabarica*. These signals were found to be absent or present in minor quantity in *V. cyprinoides*.

4.3.5.2. FTIR analyses

The FTIR spectra of the EtOAc:MeOH extracts from the bivalve clams were used to analyze the various functional groups (Figure 4.4.). The dominant differences of the characteristic FTIR signals of the EtOAc:MeOH extracts of *V. cyprinoides* and *P. malabarica* were due to the carbonyl bands in infrared spectra. Two intense absorption bands in $1736\text{-}1636\text{ cm}^{-1}$ region of the FTIR spectra of the EtOAc:MeOH extract derived from *P. malabarica* was demonstrated the presence of esters (at 1736 cm^{-1}) and carbonyl groups (such as esters or ketones, at 1636 cm^{-1}) adjacent to the electron withdrawing functional groups preferably of olefinic nature. Unlike *P. malabarica*, the IR spectrum of *V. cyprinoides* was showed only one intense signal at 1740 cm^{-1} and that the peak at 1646 cm^{-1} in EtOAc:MeOH extract obtained from *V. cyprinoides* was feeble, which evidently suggested the absence of electron withdrawing functional groups adjacent to the carbonyl functionalities. A particularly intense signal was recorded in the EtOAc:MeOH extract derived from *P. malabarica* at $1461\text{-}1405\text{ cm}^{-1}$, which is particular to the C-C stretching frequency of the aryl ring framework. The signals at this region were weak in the EtOAc:MeOH extract derived from *V. cyprinoides*. The broad absorption peaks around $3000\text{-}3500\text{ cm}^{-1}$ in the FTIR spectra of the EtOAc:MeOH extracts of *V. cyprinoides* and *P. malabarica* were because of more prominent intensities of H-bonded -OH stretching vibrations of the characteristic lead molecules present in the solvent extracts, although, it is hard to precisely foresee the molecular interactions due to their broad character. The peaks were likewise recognized at $1200\text{-}1000\text{ cm}^{-1}$ in the EtOAc:MeOH extract obtained from *P. malabarica*, evidently because of the vicinity of C=C stretching vibration due to the olefinic groups. The peaks in this region were feeble in the solvent extract of *V. cyprinoides*.

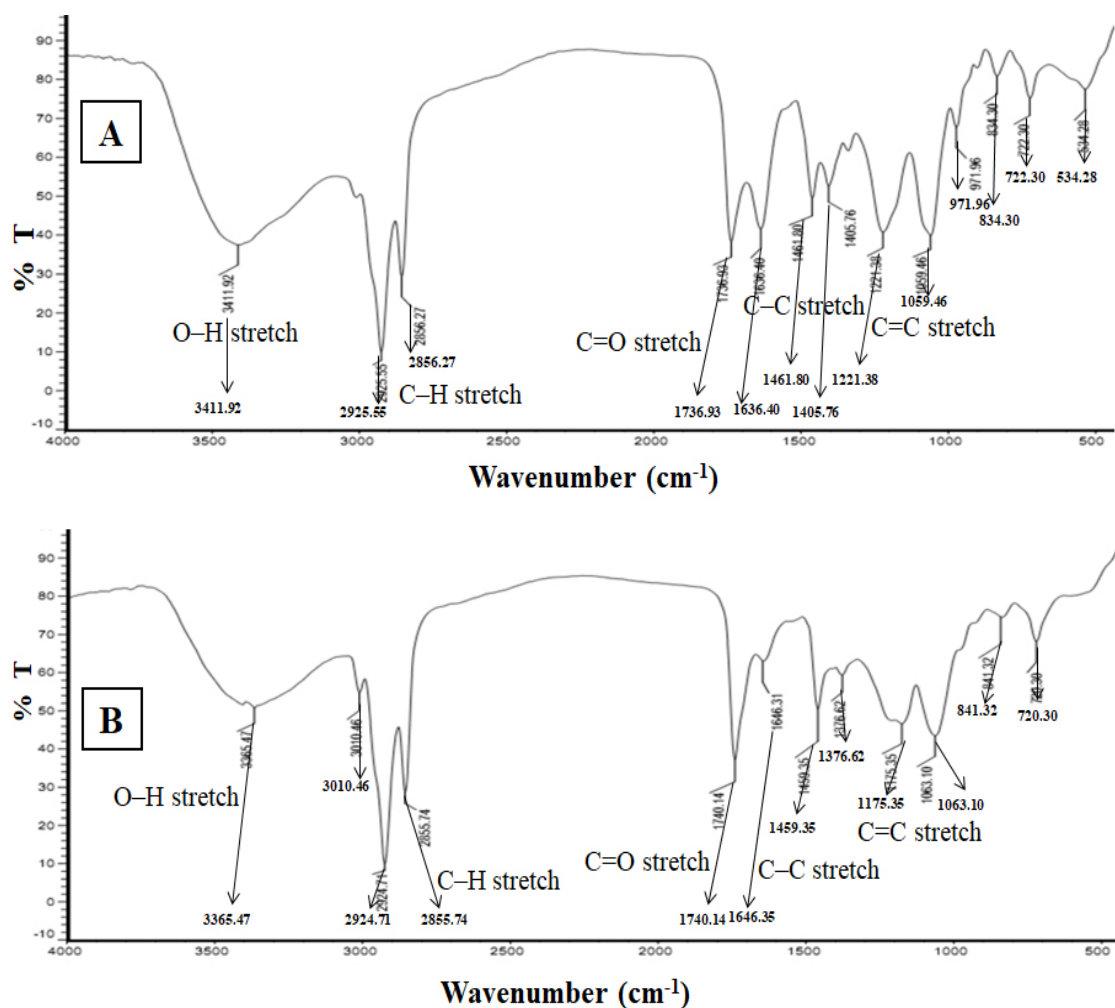


Figure 4.4.: FTIR spectra of EtOAc:MeOH extracts of (A) *P. malabarica* and (B) *V. cyprinoides*. The functional groups representing the distinct regions of the IR spectra were illustrated.

Spectroscopic analyses, for instance, ^1H and ^{13}C NMR of EtOAc:MeOH extracts of the bivalve clam species were provided a clear idea to comprehend and compare the signal pattern and component intensities of the distinctive sorts of protons and carbons. This gave an understanding into the distinctive functional groups connected with the EtOAc:MeOH extracts. Since the spectra is a mixture of different compounds, it is apparently difficult to break down some multiplets because of their complexity to interpret and peak overlaps as a result of regular line width impediment imposed by the T2 (spin-spin relaxation), which forestalls significant data to be identified in the multiplets. The large numbers of transitions in ^1H spectra of compounds were made disentangled by the peak analyses algorithm, Global Spectral

Deconvolution (GSD), which applies a deconvolution of the entire range of the spectrum in this way making us to work out the signature peaks in an effective manner.

The total number of protons at the region depicting the saturated hydrocarbons (δ 0.1-2.0) was fundamentally lesser (an aggregate proton integral of about 57.23) in *P. malabarica* than the EtOAc:MeOH extract derived from *V. cyprinoides* (63.36). It is intriguing to note that the bioactivity of the latter was lesser due to the presence of more prominent saturated hydrocarbons leading to greater hydrophobicity. This might result in lesser electrostatic or dipole-dipole interactions with the enzyme active site. The ^1H NMR spectrum of EtOAc:MeOH extract from *P. malabarica* acquired well resolved, deshielded signals at about δ 4.5-6.5, which presumably showed the vicinity of the olefinic protons or those associated with the parent hydride group of alkyl alkanoates ($\text{RCH}_2\text{C}(=\text{O})\text{OCH}_3$). This explained the greater antioxidant capacity of *P. malabarica* compared to *V. cyprinoides*. These observations have been further validated with the ^{13}C NMR data of the EtOAc:MeOH extract. The strong signals in the ^1H NMR spectrum of the EtOAc:MeOH extract of *P. malabarica* at δ 2.5-3.5 (proton integral of 12.24) could be ascribed to the vicinity of protons because of the presumably of methoxy ($-\text{OCH}_3$)/alkyl halide ($\text{RCH}_2\text{-X}$)/functionalized hydride H of the substituted alkanol (RCH_2OH) groups capable of preventing lipid peroxidation. The greater radical scavenging activity (antioxidant activity) of the EtOAc:MeOH extracts from *P. malabarica* could also be explained with the presence of electron donating methoxy ($-\text{OMe}$) or hydroxyl groups ($-\text{OH}$) (Cai *et al.*, 2006).

The EtOAc:MeOH extracts of the bivalve clams were recorded the occurrence of electronegative groups, such as $\text{RC}(=\text{O})\text{CH}_3$ or $\text{RCH}_2\text{C}(=\text{O})\text{OR}_1$ or $\text{CH}_2=\text{CH}-\text{CH}_3$ at δ 2.0-2.5 in the ^1H NMR spectra that might be responsible for the significant inhibition towards pro-inflammatory 5-LOX, COX-1 and COX-2 along with diabetic (DPP-4) enzymes. The EtOAc:MeOH extracts of *P. malabarica* displayed very intense signals at δ 2.5-3.5, which ascribed to be because of the vicinity of electronegative auxochromes, for example, alkoxy/alkyl halide/functionalized hydride H of the substituted alkanols. In general, the EtOAc:MeOH extract derived from *P. malabarica* was showed greater proton integrals than *V. cyprinoides* when these potentially electronegative regions were taken into consideration. This assumption was

further validated by the presence of bands in the FTIR and ^{13}C NMR spectra. It can therefore be inferred that the functional electronegative groups present in the downfield space of the ^1H and ^{13}C NMR spectra might frame strong electrostatic linkage with the amino acid residues in the enzyme active site leading to greater bioactivity.

4.3.6. Correlation analyses

The similarities and differences of antioxidant, anti-inflammatory, anti-diabetic and anti-hypertension activities of EtOAc:MeOH extracts of bivalve clams *P. malabarica* and *V. cyprinoides* were statistically analyzed using principle component analyses (PCA). The loadings of first and second principal components (PC1 and PC2) accounted for 78.70% and 21.30% of the variance, respectively (Figure 4.5.). The IC_{50} value of DPPH activity (DPPHPM) for *P. malabarica* was displayed similarity with COX-2 (COX2PM), 5-LOX (LOXPM), α -glucosidase (GlucoPM) and α -amylase (AmylPM) activities on PC1. Nonetheless, the IC_{50} value of DPPH activity of *V. cyprinoides* (DPPHVC) demonstrated resemblance with the IC_{50} values of ABTS $^{+}$ (ABTSVC), Fe^{2+} ion chelating (FeCh^{+}VC), H_2O_2 scavenging (HyPeroVC), COX-2 (COX2PM) and DPP-4 inhibition (DPPIVVC) on PC1. Similarly, the IC_{50} value of total phenolic content of *V. cyprinoides* (TPCVVC) displayed positive similarity with its COX-1 (COX1VC) and α -amylase (AmylVC) activities on PC2 component. Nevertheless, the lipid peroxidation inhibitory potency of *V. cyprinoides* (TBARSVC) demonstrated closer resemblance with the IC_{50} values of 5-LOX (LOXVC) and α -glucosidase (GlucoVC) on PC2 axis. The EtOAc:MeOH extract derived from *P. malabarica* and *V. cyprinoides* were exhibited significantly greater anti-inflammatory properties as determined by COX-2 inhibitory activity, which apparently indicated that these antioxidants might have significant role in deterring inflammatory modulators in the system.

A positive correlation as portrayed by PCA analyses was showed the co-linearity between antioxidative properties and anti-ACE activities. A considerable co-linearity was found to exist between the olefinic groups and the ACE-inhibitory activity. A positive correlation might suggest an interaction depending on the polarizability of the bioactive leads present in the extract. It is of note that the proton integral of the olefinic protons (at δ 4.5-6.5) in the EtOAc:MeOH extract derived from *P. malabarica*

was about 22.23 (as compared to 13.79 in *V. cyprinoides*), which possibly interact with the contacting polar space in the enzyme (ACE), thereby inhibiting the enzyme responsible for hypertensive activity. It can therefore be inferred that the electronic descriptors might significantly contribute towards the greater anti-ACE activity of the solvent extracts derived from the experimental clam species.

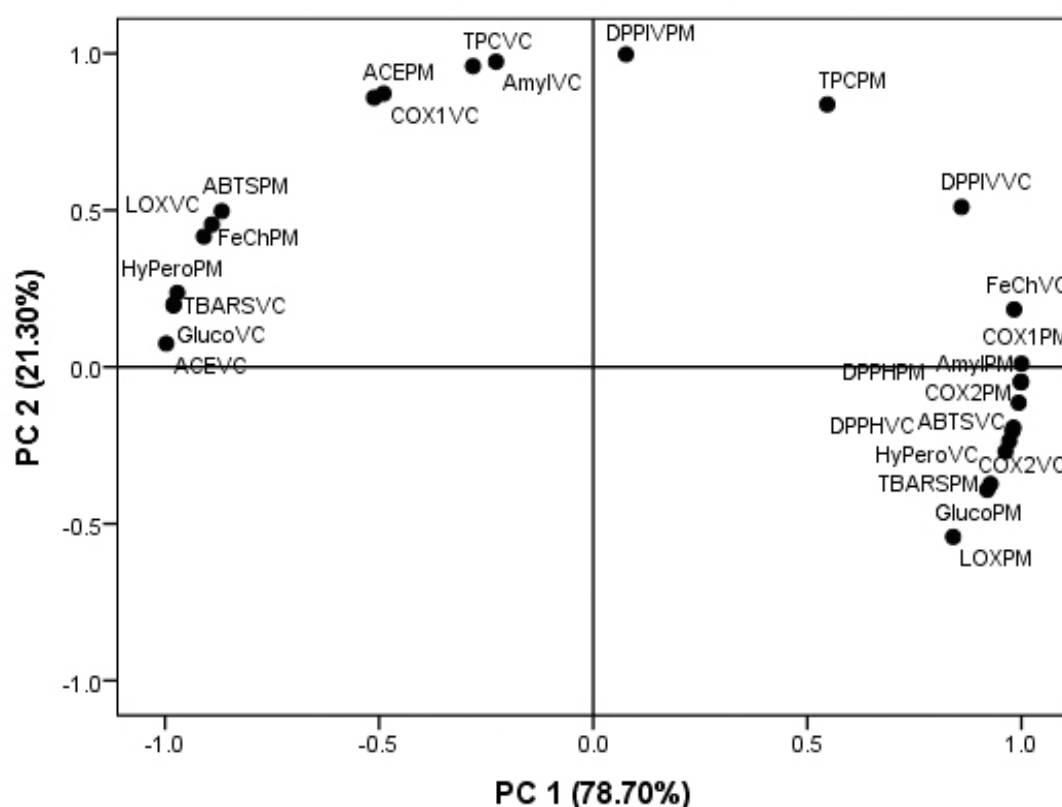


Figure 4.5.: Loading plot diagram (PC-1 and PC-2 in rotated space) of antioxidant potentials compared with anti-inflammatory, anti-diabetic and anti-hypertensive potentials of solvent extracts from *P. malabarica* (PM) and *V. cyprinoides* (VC).

Antioxidant compounds play immense role against various diseases, for example, inflammation, type-2 diabetes, hypertension, atherosclerosis etc (Kohen and Nyska 2002), which explain their potential use in pharmaceutical field and functional food industry. Bivalve mollusks have been described as very important marine fauna, which were reported to be endowed with potential antioxidative and anti-inflammatory properties (Chakraborty *et al.*, 2014a). The rich diversity of bivalve clams were

accessible throughout the southwest coast of Arabian Sea represented an untapped reservoir of antioxidative principles with potential health benefits. There were reports for the presence of antioxidants in mollusks that can prevent cell damage from oxidative responses (Conforti *et al.*, 2005; Nagash *et al.*, 2010; Nawar 1996). The present study has been demonstrated the potentials of EtOAc:MeOH extracts of the bivalve clams *V. cyprinoides* and *P. malabarica* as antioxidative, anti-diabetic, anti-inflammatory, and anti-ACE-1 activities.

4.4. Conclusion

The present study has been revealed that the EtOAc:MeOH extract of bivalve clam *P. malabarica* registered greater antioxidative properties and the activities were showed a significant positive correlation with the anti-hypertensive, anti-inflammatory and anti-diabetic activities. The utilities of spectroscopic tools for analyzing the signature peaks and relative abundance of the vital functional groups present in the solvent extracts and to furnish with essential rules regarding the presence of these functional groups responsible for bioactivities were illustrated. A significant co-linearity was found to exist between the electronegative groups present in the deshielded position of the NMR spectra and the bioactivities of the EtOAc:MeOH extracts derived from the bivalve clam species. The results from the present study will be helpful to develop nutraceutical supplements from these bivalve clam species in combating oxidative stress induced disorders, for example, diabetes, inflammation, and hypertension. The present study demonstrated that the bivalve clams, particularly *P. malabarica* have been well equipped with potential sources of antioxidants and anti-inflammatory principles. Therefore, the following chapters (5 and 6) were focused towards the bioactivity-guided isolation and characterization of compounds with bioactive potentials, particularly with reference to the antioxidative and anti-inflammatory activities.

ISOLATION AND CHARACTERIZATION OF SECONDARY METABOLITES FROM *VILLORITA CYPRINOIDES*

Contents

- 5.1. *Background*
- 5.2. *Materials and methods*
- 5.3. *Results and discussion*
- 5.4. *Conclusions*

5.1. Background

Novel secondary metabolites from the natural resources have been increasingly recognized in the field of natural product chemistry research for use against reactive oxygen species (ROS) and inflammatory mediators. The ROS has been considered as major end products of several metabolic reaction cascades and believed to be the potential initiators or intermediates for the inflammatory reactions through lipid peroxidation and generation of pro-inflammatory cyclooxygenases and lipoxygenases (Vapaatalo 1986). There were reports of synthetic derivatives being used as antioxidants or anti-inflammatory agents, while they were found for acute toxicities and severe carcinogenic origin (Schnitzer *et al.*, 1999). With the increasing requirement for enhanced life expectancy and improved lifestyle, the newer term “nutraceuticals” or “functional foods” with natural bioactive molecules were developed (Fung *et al.*, 2013). In a successive attempt to this area of interest, numerous investigations were focused on natural dietary components, particularly from unharnessed marine or estuarine resources that could prevent the oxidative damages and related ailments (Luan *et al.*, 2011; Odeleye *et al.*, 2016). Research on the extracts of various marine and estuarine bivalve mollusks, such as oysters, mussels, clams etc. were found to display anti-bacterial, antioxidant, anti-inflammatory, anti-cancer and anti-diabetic activities (Chakraborty *et al.*, 2016a; Chakraborty *et al.*, 2016b; Lin-rui *et al.*, 2012). Exhaustive investigations have described the effectiveness of various edible bivalve clams, such as surf clams,

black clams, hard clams etc. for their bioactive and nutritional properties (Odeleye *et al.*, 2016).

Earlier reports on secondary metabolites from mollusks and bivalves were suggested different classes of compounds, such as chromenyls, pyranoids, spiro compounds, polyketides, polypropionates, steroids, heterocyclics with bioactive properties (Blunt *et al.*, 2015; Ciavatta *et al.*, 2011). The oxygen heterocyclic ring systems as the principle antioxidative domain and electronegative ester groups as lipophilic components coupled with lesser steric bulk and lipophilic (recommended $\log P_{ow} < 5$) factors (that implies the absence of an extended side chain moiety) in the bioactive compounds were vital for their greater bioavailability and bioactivity. Extensive study of naturally occurring chromenyl, furanyl, cholestene or pyranyl enclosed compounds with substitutions of different electronegative functionalities, such as hydroxyls, esters, ethers, alkenes etc. can lead to potential high value templates for functional health foods and antioxidative nutraceuticals. The α -pyrone methyl derivatives were reported from mollusks, *H. fusari* and *Siphonaria lesson* (Cutignano *et al.*, 2007; Rovirosa and San-Martin 2006). Spirocyclic ether possessing unrearranged monocyclofarnesane skeleton were reported from mollusk, *Aplysia dactylomela* (Schmitz *et al.*, 1978). Steroidal compounds with unusual structures were predominant in the mollusks along with terpenoids and meroterpenoid analogues (Fontana *et al.*, 1993; Zhao *et al.*, 2013).

Bivalve clam, *Villoritta cyprinoides* (Corbiculidae) are traditional seafoods among the coastal populations of the southwestern coast of the Indian Peninsula. These predominantly available bivalve clams were found to have commercial/export values, and reported for its nutritional properties and bio-potentials, even though, these commercially significant species have not been investigated to its entirety for the presence of specialized bioactive metabolites, and their application as potential pharmacophores. Hence, this chapter directed towards the isolation and characterization of bioactive secondary metabolites from the ethyl acetate:methanol extract of bivalve clam, *V. cyprinoides* by repetitive chromatographic fractionation methods. The characterized bioactive secondary metabolites classified under various classes of chemistries, named as irregular spirocyclic ether derivatives (**1-2**), irregular meroterpenoids (**3-5**), hexahydro isochromenyl analogues (**6-7**) and cholestenol

derivatives (**8-10**). These compounds characterized by various spectroscopic techniques, such as nuclear magnetic resonance (NMR) comprising one/two dimensional (1D/2D NMR), FTIR and mass experiments. The chromatographic fractions and pure metabolites assessed for their anti-inflammatory {anti-cyclooxygenase (anti-COX)/anti-lipoxygenase (anti-5-LOX)} and free radical inhibitory (DPPH/ABTS⁺ scavenging) potentials. The target bioactivities of these compounds correlated with their structural parameters using different physicochemical descriptors, such as hydrophobic parameter (logarithmic octanol-water partition value, log P_{ow}), electronic (polarizability, PI/topological polar surface area, tPSA) and steric {molar refractivity (MR)/molar volume (MV)/parachor (Pr)} factors. This chapter also proposed the antioxidative mechanisms of secondary metabolites (**1-10**) isolated from *V. cyprinoides* in the DPPH radical model system. The modes of COX-2 and 5-LOX enzyme inhibitions by selected compounds were determined by molecular docking models.

5.2. Materials and methods

5.2.1. Chemicals, reagents and instrumentations

All chemicals and reagents used in this study were of analytical/spectroscopic grade and obtained from E-Merck (E-Merck, Frankfurter, Darmstadt, Germany) and Sigma-Aldrich (Missouri, USA). Redistilled or milliQ or HPLC grade water used throughout the work. 1,1-Diphenyl-2-picryl-hydrazil, potassium persulfate, 2,2'-azino-bis-3-ethylbenzothiozoline-6-sulfonic acid diammonium salt, leuco-2,7-dichloro fluorescein diacetate, sodium hydroxide, tris-buffer, hematin, phenol, arachidonic acid, linoleic acid, sodium phosphate buffer, 3,5-dinitrosalicylic acid reagent were purchased (E-Merck, Germany and Sigma-Aldrich, USA). Pro-inflammatory enzymes, such as cyclooxygenase-1 (sheep) and cyclooxygenase-2 (human recombinant) were procured from Sigma-Aldrich, whereas 5-lipoxygenase extra pure (5-LOX from soybean) procured from Sisco Research Laboratories (SRL, Mumbai, India). The natural compound, α -tocopherol (Himedia, Pennsylvania, USA) was used as a standard for antioxidant assays and synthetic compound, ibuprofen (Sigma Aldrich, USA) was used as a standard for anti-inflammatory assays. All glasswares were procured from Borosil (India) or Magnum glassworks (Cochin, India).

The solvents were evaporated using rotary vacuum evaporators (Heidolph instruments GmbH and Co., Schwabach, Germany; Ika rotary evaporator, IKA[®] Works, North Chase Pkwy SE, Wilmington, USA) and rotational vacuum concentrator (RVC, Martin Christ, GmbH, Osterode, Germany). Laboratory scale lyophilizers (Alpha 1-4 LD plus, Martin Christ, Osterode, Germany; Scanvac, Coolsafe[™], LaboGene, DK-3540 Lyngø, Denmark) were used for freeze drying. The samples were kept in the -80°C deep freezer (ultra-low temperature freezer, Eppendorf, Hamburg, Germany). The extractions of samples were carried out using rotary shaker (Orbital shaker, Labline, India) and ultrasound sonicator (water bath sonicator, Elma, Hohentwiel, Germany). The melting points of pure compounds were determined using melting point apparatus (VMP-DS, Veego, Mumbai, India) and the angle of rotation of compounds recorded on a polarimeter (AP-300, ATAGO, Japan). The UV lamp (short/long-wave UV lamp, wavelength 254/365 nm; Cole-Parmer, India) was used to identify the various spots or bands developed in the TLC/PTLC plates.

5.2.2. Chromatographic analyses

5.2.2.A. Column chromatography (CC)

The column chromatographic purifications were carried out using various mesh sized dry silica (230-400, 100-200 and 60-120 mesh size; E-Merck, Darmstadt, Germany) pre-packed in a vertically clamped glass columns (10 mm X 300 mm, 10 mm X 450 mm, 18 mm X 450 mm, 18 mm X 600 mm and 40 mm X 1000 mm; Borosil, India; Magnum glassworks, India). The column was packed and saturated with the desired non-polar solvent as mobile phase (mainly *n*-hexane) prior to sample loading. The extracts were mixed with the same solvent in small volume and silica gel (60-120 mesh, 4.5 g) to make into slurry before being filled into glass column. This slurry was thereafter packed onto the column using modified syringe. The mobile phase was added by step gradient elution with non-polar/medium polar solvent(s) (*n*-hexane/dichloromethane) and polarity was regularly increased using the increasing amounts of polar solvents (EtOAc/MeOH). The successive column fractions were collected separately. The mobile phase was pumped through the column using the air pressure.

5.2.2.B. Flash chromatography (FC)

The extracts or fractions resolved by flash (Biotage AB SP1-B1A, Sweden) chromatography on silica column (230-400 mesh silica; Biotage No. 25 + M KP Si or 12 + M Si). The desired collection/monitor wavelengths and a step gradient elution of non-polar to polar solvents as mobile phase were used for chromatographic fractionation. The extracts were packed onto the column either as slurry (extracts mixed with silica gel) or as liquid (extracts dissolved in solvents) using modified syringe. The various fractions were separately collected based on the chromatograph.

5.2.2.C. Thin layer chromatography (TLC)

Thin layer chromatographic technique was used for the separation of various components from mixtures and for checking the purity of isolated compounds. The pre-coated preparative TLC (PTLC) glass plates with silica gel 60 GF₂₅₄ (thickness 0.2 mm and size 20 X 20 cm; Merck KGaA, Germany) was used for the purification of compounds from various column fractions using various percentages of mobile phases (*n*-hexane, dichloromethane, EtOAc, MeOH). The spots or bands separated on PTLC were detected under the UV lamp (short/long-wave UV lamp, wavelength 254/365 nm; Cole-Parmer, India) at 254 nm (short UV) and 365 nm (long UV).

Thin layer chromatography was carried out on a pre-packed aluminium sheets with silica 60F₂₅₄ of size 20 X 20 cm (Kieselgel-60F₂₅₄; E-Merck, Frankfurter, Darmstadt, Germany) to check the purity of isolated compounds and to screen the various components present in the mixtures by considering their retention factors (R_f : ratio of distance travelled by spot to distance travelled by solvent front). Various percentages of solvents (*n*-hexane, dichloromethane, EtOAc, MeOH) were used as mobile phases. The spots or bands on TLC were detected under the UV lamp (short/long-wave UV lamp, wavelength 254/365 nm; Cole-Parmer, India) at 254 nm (short UV) and 365 nm (long UV). The extracts dissolved in small volume of desired solvents and applied on the PTLC or TLC plates using capillary tubes.

5.2.2.D. High pressure liquid chromatography (HPLC)

The preparatory high pressure liquid chromatograph (PHPLC) system (Shimadzu Corporation, Nakagyo-ku, Japan) connected with a bonded reverse phase

C18 (RP C18) column (Shimadzu; Luna 250 mm X 14.0 mm, 5 μ m) fitted with binary gradient pump (Shimadzu LC-20AP), column oven (CTO-20AC, Shimadzu), photodiode array detector (SPD-M20A, Kyoto, Japan) and a controller (CBM-20A, Shimadzu) were used for the purification of compounds. The injection volume was 2 mL and the column temperature retained at 40°C. The various percentages of MeOH and acetonitrile utilized as mobile phase with 6-8 mL/min flow rate. The absorbances recorded between the ranges of 200-800 nm wavelengths.

An analytical HPLC system (Shimadzu Corporation, Nakagyo-ku, Japan) bonded with reverse phase C18 (RP C18) column (Phenomenex, Torrance, California, USA; Luna 250 mm X 4.6 mm, 5 μ m) fitted to binary gradient pump (Shimadzu LC-20AD), column oven (CTO-20A, Shimadzu), photodiode array detector (SPD-M20A, Kyoto, Japan) and a controller (CBM-20A, Shimadzu) were used to analyze the purity of isolated compounds. The injection volume was 20 μ L and column temperature was maintained to 40°C. The mobile phase comprised of various percentages of MeOH and acetonitrile with 1 mL/min flow rate. The absorbances recorded between 200-800 nm.

The samples were passed through the solid phase extraction (SPE) cartridges (Strata C18-E; 55 Mm, 70 Å; Phenomenex, Torrance, California, USA) and filtered through the syringe filter (0.20 μ m, PTFE, Minisart syringe filter, Sartorius, Goettingen, Germany) before being injected into reversed phase HPLC instruments.

5.2.3. Spectrophotometric analyses

The UV-VIS spectra of chromatographic fractions/isolated pure compounds along with UV-VIS absorbances acquired on ultraviolet-visible (UV-VIS) spectrophotometer (Varian Cary 50, Walnut Creek, California, USA) and microplate spectrophotometer (Thermo Scientific™ Multiskan™ GO, Waltham, MA USA), as appropriate. The glass cuvettes (1 cm X 1 cm X 4.5 cm) were used in the UV-VIS spectrophotometer and 96-well microplates (Nunc™ Plates with Delta Surface, Thermo Fisher Scientific, Jiangsu, China) used in the microplate spectrophotometer.

5.2.4. Spectroscopic analyses

5.2.4.A. Fourier transform infrared (FTIR) spectroscopy

The Perkin-Elmer Series 2000 Fourier transform infrared (FTIR) spectrometer used to record FTIR spectra between the scan range of 4000 and 400 cm^{-1} on KBr (Perkin-Elmer FTIR, Winter Street, Waltham, Massachusetts, USA). The samples (15 mg) prepared in KBr (150 mg) and applied 5×10^6 Pa pressure to afford clear transparent disc (thickness 1 mm X diameter 13 mm). The IR values have been expressed in percentage transmittance (% T). The FTIR spectrometer-Alpha from Bruker Optics (Bruker, Karlsruhe, Germany) also used for the FTIR analysis.

5.2.4.B. Mass spectrometry

The gas-chromatographic mass-spectrometric (GC-MS) experiments carried out by using the EI (electronic impact) ionization method (GC-MS Perkin-Elmer Clarus-680, Winter Street, Waltham, Massachusetts, USA). Helium (He) was used as the carrier gas and the flow rate was 1 mL/min. The injection volume was 1 μL in a split mode and temperature of the injector was 280°C. Electron ionization energy was set at 70 eV. The scan rates were set as 10 spectra/s and ion source temperature maintained at 200°C. The compounds fractionated with non-polar capillary column (Elite-5 bonded phase, 50 m X 0.22 mm i.d. X 0.25 μm film thicknesses). The exact molecular ion weights of pure compounds have been acquired by direct injection in high resolution mass spectrometer {HRESIMS, $[\text{M}+\text{H}]^+$ } and compared with the MarinLit database (Royal Society of Chemistry, London, Burlington House, London W1J 0BA dedicated to marine natural products) and NIST database (NIST standard reference database 1A v17, National Institute of Standards and Technology, Gaithersburg, MD, USA).

5.2.4.C. Nuclear magnetic resonance (NMR) spectroscopy

The one dimensional NMR analyses, such as proton (^1H ; 500 MHz), carbon (^{13}C ; 125 MHz), distortionless enhancement by polarization transfer ($^{135}\text{DEPT}$) and two dimensional NMR analyses, such as ^1H - ^1H correlation spectroscopy (^1H - ^1H COSY), heteronuclear single-quantum coherence spectroscopy (^1H - ^{13}C HSQC), heteronuclear multiple-bond correlation spectroscopy (^1H - ^{13}C HMBC) and nuclear overhauser effect spectroscopy (NOESY) were analyzed on Bruker AVANCE III 500MHz (AV 500) spectrometer (Bruker, Karlsruhe, Germany) in CDCl_3 as aprotic solvent at ambient temperature with internal standard (TMS; δ 0 ppm) fitted to 5 mm probes. The ^1H NMR

signals corresponding to the types of hydrogen nuclei in a molecule and numbers of characteristic protons were obtained from the proton integral values. The ^{13}C NMR signals recognized the various types of carbons in a molecule. The multiplicities of carbons established from $^{135}\text{DEPT}$ spectra, which differentiated the number or possibilities of methylenes ($-\text{CH}_2$; signals appeared in the downward direction), methyls ($-\text{CH}_3$; signals appeared in the upward direction with lower chemical shift values in the range δ 10-40) and methines ($-\text{CH}$; signals appeared in the upward direction with higher chemical shift values in the range δ 45-160). The signal that was apparent in the ^{13}C NMR spectra and absent in the $^{135}\text{DEPT}$ spectra denoted the occurrence of quaternary carbons. The ^1H - ^1H COSY spectra determined the signals, which were correlated with the neighbouring protons by J couplings through-bond and the spectra were obtained by diagonal peaks and cross peaks. The resonances in HSQC spectra represented ^1H - ^{13}C correlations, which determined the unique proton directly attached to unique carbon heteronucleus. The HMBC spectra denoted correlations between protons and carbons, which were separated by two, three and four bond distances. The NOESY spectra were similar to ^1H - ^1H COSY and attained with diagonal peaks and cross peaks. But, the cross peaks represented the resonances from nucleus, and were spatially close to each other than the direct bond couplings. In short, NOESY spectra determined the special arrangements and close proximities of adjacent spin systems.

The NMR spectral interpretations carried out using the software MestReNova ver. 7.1.1-9649 © 2012 (Mestrelab Research, S.L. Feliciano Barrera, Santiago de Compostela, Spain).

5.2.5. Animal material and extraction

The shelled *V. cyprinoides* (10 kg) samples were freshly gathered from their natural locality, Vembanad Lake situated at the southwestern coast of the Indian Peninsula ($9^\circ 35'$ N and $76^\circ 25'$ E), bordering the Arabian Sea (Figure 5.1.). After cleaning the externalities, the samples were transported to the laboratory in an ice box. The shell-on samples thoroughly washed in distilled water and the edible meat (6 kg) was manually separated from the shells without applying heat. The edible flesh samples thereafter homogenized by a grinding machine before being kept overnight in the deep freezer at -80°C (ultra-low temperature freezer, Eppendorf, Hamburg, Germany) for

freezing. It was then lyophilized by freeze drier (Alpha 1-4 LD plus, Martin Christ, Germany; Scanvac, Coolsafe™ Denmark) for 48 h to yield the lyophilized black clam powder (1500 g; yield 25 g/100 g wet weight basis). This was stored in vacuum packed polyethylene biohazard autoclave bags (Fisherbrand™, Fischer Scientific) in the deep freezer at -80°C until further processing. The lyophilized powder was used for the solvent extraction.



Figure 5.1.: The fresh shelled *V. cyprinoides* samples collected from the southwestern coast of the Indian Peninsula (9°35' N and 76°25' E), bordering the Arabian Sea

The lyophilized powder (1500 g) of black clam material was homogenized with ethyl acetate:methanol (1:1, v/v, EtOAc:MeOH) by sonication (Elma, Hohentwiel, Germany) and shaking (Orbital shaker, Labline, India) for 4 h under an inert atmosphere of nitrogen. This extraction procedure repeated for three times to recover maximum bioactive components in the crude extract. The extract contents were then filtered through filter paper (Whatman No. 1) using Na₂SO₄ (30 g) to obtain the clarified filtrates. The solvent filtrates concentrated (40°C) in rotary evaporator (Heidolph,

Germany; Ika, USA) to afford the brown viscous crude solvent extract of *V. cyprinoides*. Then, the extracts were completely dried in the rotational vacuum concentrators (RVC, Martin Christ, Germany) to yield the corresponding solvent extracts of *V. cyprinoides* (50 g; yield on dry weight basis 3.33%). The crude solvent extract was kept under an inert nitrogenous atmosphere and used for the isolation of bioactive compounds by repeated chromatographic fractionations.

5.2.6. Chromatographic purification of pure compounds from *V. cyprinoides*

The crude extract of *V. cyprinoides* (45.0 g) was partitioned by exhaustive column chromatography over silica gel as adsorbent. The schematic diagram showing the purification of EtOAc:MeOH extract of *V. cyprinoides* was illustrated in Figure 5.2. The extract was made into slurry with silica (5 g, 60-120 mesh) before being filled into column (1000 mm X 40 mm) enclosing silica gel as adsorbent (60-120 mesh, 50 g). The column was primarily eluted with *n*-hexane (100%) followed by dichloromethane (DCM, 100%), ethyl acetate (EtOAc, 100%) and finally methanol (MeOH, 100%) to obtain a total of 4 column fractions, such as VC₁, VC₂, VC₃ and VC₄, respectively. The column fractions were assessed for their anti-inflammatory and antioxidant activities. The two fractions, VC₂ and VC₃ were selected for further purifications as it exhibited reasonably better antioxidant and anti-inflammatory activities compared to other fractions.

The fraction, VC₂ (8 g; 17.78%), which obtained by eluting with 100% DCM was fractionated by vacuum liquid chromatography on a glass column (450 mm X 30 mm) packed with silica (230-400 mesh) using *n*-hexane/EtOAc/MeOH to acquire 25 fractions of 25 mL each, which reduced to 9 fractions (VC₂₋₁-VC₂₋₉) after TLC (*n*-hexane:EtOAc, 9:1, v/v) analysis. The VC₂₋₄ fraction (10% EtOAc:*n*-hexane, v/v; 1023 mg; 2.27%), VC₂₋₅ (12% EtOAc:*n*-hexane, v/v; 1136 mg; 2.52%) and VC₂₋₆ (15% EtOAc:*n*-hexane, v/v; 1323 mg; 2.94%) were acquired in greater yields compared to other fractions. Also, the sub-fractions were checked for their potentials in which VC₂₋₄, VC₂₋₅ and VC₂₋₆ registered greater bioactive properties, and therefore, selected for further fractionation. The fraction, VC₂₋₄ eluted at 10% EtOAc:*n*-hexane (v/v) appeared to be mixture and purified to homogeneity by preparative HPLC (reverse phase C18 PHPLC) using 80% MeCN:MeOH (v/v) to yield compound **10** (195 mg; 0.43%). The

another fraction, VC₂₋₅ was found to be mixture, and therefore, sub-fractionated on preparative HPLC (RP C18 PHPLC; 80% MeCN:MeOH, v/v) to yield pure compound **9** (134 mg; 0.30%). The solvents allowed to evaporate from their respective fractions followed by TLC analysis by utilizing 95:5, v/v, *n*-hexane:EtOAc to support its purity.

The VC₂₋₆ fraction (1323 mg; 2.94%) was flash chromatographed (Biotage AB SP1-B1A, 25+M, 230-400 mesh, 12 g; Biotage AB, Uppsala, Sweden) on silica column at collection UV wavelength of 250 nm using *n*-hexane/EtOAc/MeOH to afford total of 52 fractions (8 mL each) and pooled to six fractions (VC₂₋₆₋₁-VC₂₋₆₋₆). The sub-fractions, such as VC₂₋₆₋₂, VC₂₋₆₋₄, VC₂₋₆₋₅ and VC₂₋₆₋₆ were exhibited greater bioactive potentials, therefore, selected for further purifications. The fraction VC₂₋₆₋₂ (205 mg; 0.46%) on repeated column chromatography followed by PTLC (4% EtOAc:*n*-hexane) purifications afforded **3** (79 mg; 0.18%) and its purity was checked with silica gel GF₂₅₄ TLC using *n*-hexane:EtOAc (9:1, v/v). The fraction, VC₂₋₆₋₄ (214 mg; 0.48%), on repeated RP C18 PHPLC (80% MeCN:MeOH X 5) purification techniques yielded **4** (59 mg; 0.13%), and the homogeneity was confirmed by TLC analysis using 15% EtOAc:*n*-hexane (v/v). The fraction, VC₂₋₆₋₅ (510 mg; 1.13%) on repeated PTLC (4% EtOAc:*n*-hexane, v/v) acquired compound **8** (143 mg; 0.32%) and its purity was checked by TLC analyses (10% EtOAc:*n*-hexane, v/v). The VC₂₋₆₋₆ (196 mg; 0.44%) fraction on repeated column chromatography was afforded sub-fractions, VC₂₋₆₋₆₋₁-VC₂₋₆₋₆₋₄ and in which the sub-fraction, VC₂₋₆₋₆₋₂ (134 mg; 0.30%) exhibited greater bioactivities. The sub-fraction, VC₂₋₆₋₆₋₂ on RP C18 PHPLC (80% MeCN:MeOH, v/v) fractionation yielded compound **5** (69 mg; 0.15%) and its purity was checked by TLC analysis (15% EtOAc:*n*-hexane, v/v).

Another active fraction, VC₃ (11 g; 24.44%), which eluted at 100% EtOAc, was further fractionated on flash chromatography (Biotage AB SP1-B1A, 230-400 mesh, 25+M; 12 g; Biotage AB, Uppsala, Sweden) using *n*-hexane/EtOAc/MeOH on silica gel column at a collection UV wavelength of 264 nm. The solvent polarity was initiated from 100% *n*-hexane followed by EtOAc and MeOH to afford 85 (12 mL each) fractions and were reduced to 6 (VC₃₋₁-VC₃₋₆) fractions. The sub-fraction, VC₃₋₄ (1640 mg; 3.64%) and VC₃₋₆ (1540 mg; 3.42%) were acquired in greater yields with greater bioactive potentials, and therefore, considered for further purifications. The sub-fraction, VC₃₋₄ fractionated by flash (Biotage AB SP1-B1A, 230-400 mesh, 12+M;

Figure 5.2.: Schematic diagram of purification of EtOAc:MeOH extract of *V. cyprinoides*. CC-column chromatography; FC-flash chromatography; PTLC-preparative thin layer chromatography; TLC-thin layer chromatography; RP C18 PHPLC-reverse

phase C18 preparatory high pressure liquid chromatography; E-ethyl acetate; H-*n*-hexane; M-methanol. The coloured boxes represented the pure compounds and were characterized by detailed spectroscopic experiments

Another active fraction, VC₃₋₆ fractionated by flash chromatographic purification (Biotage AB SP1-B1A, 230-400 mesh, 12+M; Biotage AB, Uppsala, Sweden) on a silica gel column at a collection UV wavelength of 252 nm with *n*-hexane/EtOAc/MeOH to furnish three sub-fractions, which were designated as VC₃₋₆₋₁-VC₃₋₆₋₃. The fractions, VC₃₋₆₋₁ (546 mg; 1.21%) and VC₃₋₆₋₂ (489 mg; 1.09%) were selected for repeated purifications. The fraction, VC₃₋₆₋₁ on PTLC using 2% EtOAc:*n*-hexane (v/v) solvent system resulted in the isolation of compound **1** (147 mg; 0.33%) and its purity was determined using TLC {*n*-hexane:EtOAc (90:10, v/v)}. The other fraction, VC₃₋₆₋₂ on PTLC (5% EtOAc:*n*-hexane, v/v) fractionation yielded compound **2** (96 mg; 0.21%) and its purity was checked using TLC (90:10, v/v, *n*-hexane:EtOAc) and RP C18 HPLC (8:2, v/v, MeOH/MeCN).

5.2.7. Physicochemical data of bioactive secondary metabolites from EtOAc:MeOH extract of *V. cyprinoides*

5.2.7.1. Physicochemical data of compound **1** (VC₃₋₆₋₁₋₁)

16-Hydroxyhexyl-(2-ethyl-2,6-dimethyl-1-oxaspiro[4.5]dec-3,8-dien)-10-propanoate: Yellow oily; UV (MeOH) λ_{\max} (log ϵ): 231.9 nm (2.55); TLC (Si gel GF₂₅₄ 15 mm; 10:90, v/v, EtOAc/*n*-hexane) R_f : 0.63; R_t (RP C18 HPLC, 8:2, v/v, MeOH:MeCN): 5.33 min; IR (cm⁻¹) (stretching ν , bending δ , rocking ρ): 3411 (br, O-H ν), 2924, 2854 (C-H ν), 1731 (C=O ν), 1460 (C-H δ), 1376 (C-H ρ), 1167 (C-C ν), 1045 (C-O ν), 972 (=C-H δ), 826, 657 (C-H δ); ¹H (CDCl₃, 500 MHz): δ 6.50 (1H α , d, J =8.84 Hz), 6.25 (1H α , d, J =8.84 Hz), 5.36 (1H α , t, J =3.54 Hz), 5.35 (1H α , t, J =3.93 Hz), 4.18 (1H α , t), 4.14 (1H β , t), 3.97 (1H α , m), 2.35 (2H, t), 2.32 (1H β , m), 2.10 (1H α , m), 2.02 (2H, t), 1.92 (2H, m), 1.86 (2H, m), 1.61 (2H, m), 1.52 (2H, m), 1.30 (2H, m), 1.25 (3H α , s), 1.01 (3H β , s), 0.88 (3H, t), 0.82 (3H, t); ¹³C (125 MHz, CDCl₃): δ 173.95, 135.40, 132.30, 130.73, 129.94, 82.17, 79.47, 66.47, 65.04, 39.43, 36.89, 34.69, 34.11, 31.92, 30.06, 29.70, 27.22, 24.88, 22.69, 22.54, 18.17, 14.12; COSY and HMBC data were given in Table 5.5. EIMS (Electron impact ionization mass spectrometry): found

m/z 364.2620 $[M]^+$, cal. for $C_{22}H_{36}O_4$ 364.2614 (Δ 1.6 ppm). HRESI-MS (positive mode) m/z : for $C_{22}H_{37}O_4$ 365.2692 $[M+H]^+$.

5.2.7.2. Physicochemical data of compound 2 (VC₃₋₆₋₂₋₁)

(*E*)-18-Ethyl-17,19-dihydroxyhept-14-enyl-(2-ethyl-2,6-dimethyl-1-

oxaspiro[4.5]dec-3,8-dien)-10-acetate: Yellow oily; UV (MeOH) λ_{\max} (log ϵ): 236 nm (2.17); TLC (Si gel GF₂₅₄ 15 mm; 10:90, v/v, EtOAc/*n*-hexane) R_f : 0.51; R_t (RP C18 HPLC, 8:2, v/v, MeOH:MeCN): 3.28 min; IR (cm^{-1}): 3389 (br, O-H ν), 2923, 2855 (C-H ν), 1728 (C=O ν), 1459 (C-H δ), 1375 (C-H ρ), 1042 (C-O ν), 971 (=C-H δ), 730, 650 (C-H δ); 1H (CDCl₃, 500 MHz): δ 6.50 (1H α , d, J =8.64 Hz), 6.25 (1H α , d, J =8.64 Hz), 5.41 (1H α , t, J =3.74 Hz), 5.38 (1H α , q, J =3.29 Hz), 5.21 (1H β , q, J =10.77 Hz), 5.17 (1H α , q, J =10.14 Hz), 4.18 (1H α , d), 4.15 (1H β , d), 3.97 (1H α , m), 3.69 (1H β , d), 3.60 (1H α , d), 2.81 (1H β , m), 2.35 (2H, d), 2.10 (1H α , m), 2.02 (2H, t), 1.92 (2H, t), 1.63 (2H, q), 1.58 (1H α , m), 1.33 (2H, m), 1.25 (3H α , s), 1.01 (3H β , s), 0.88 (3H, t), 0.80 (3H, t); ^{13}C (125 MHz, CDCl₃): δ 174.36, 135.40, 135.18, 132.30, 130.76, 130.73, 129.94, 82.17, 79.44, 66.46, 65.15, 63.33, 39.43, 36.89, 34.69, 31.92, 29.69, 27.98, 25.54, 23.40, 22.69, 22.53, 18.16, 14.11; COSY and HMBC data were given in Table 5.6. EIMS: found m/z 406.2725 $[M]^+$, cal. for $C_{24}H_{38}O_5$ 406.2719 (Δ 1.5 ppm). HRESI-MS (positive mode) m/z : for $C_{24}H_{39}O_5$ 407.2797 $[M+H]^+$.

5.2.7.3. Physicochemical data of compound 3 (VC₂₋₆₋₂₋₁₋₂)

8-(1,3,3a,4,5,7a-Hexahydro-1-(hydroxymethyl)-3-oxoisobenzofuran-4-yl)-

ethyl pentanoate: Dark brown oily; UV (MeOH) λ_{\max} (log ϵ): 235.3 nm (2.76); TLC (Si gel GF₂₅₄ 15 mm; 1:9, v/v, EtOAc/*n*-hexane) R_f : 0.81; R_t (RP C18 HPLC, 2:3, v/v, MeOH:MeCN): 3.03 min; IR (cm^{-1}): 3089 (br, O-H ν), 2984 (C-H ν), 1737 (C=O ν), 1446 (C-H δ), 1233, 1043 (C-O ν), 847 (=C-H δ), 786, 734 (C-H δ); 1H (CDCl₃, 500 MHz): δ 5.37 (1H α , q, J =3.53 Hz), 5.35 (1H α , t, J =3.64 Hz), 4.17 (1H β , d), 4.15 (1H α , d), 4.08 (1H β , m), 3.73 (3H, d), 2.81 (1H α , m), 2.35 (2H, t), 2.32 (1H α , d), 2.08 (1H β , m), 2.02 (2H, m), 1.63 (2H, m), 1.30 (2H, m), 1.29 (2H, m), 0.88 (3H, t); ^{13}C (125 MHz, CDCl₃): δ 178.41, 173.95, 129.99, 129.70, 68.26, 65.00, 61.42, 50.10, 34.10, 31.92, 29.69, 27.21, 25.62, 24.88, 22.68, 14.11; COSY and HMBC data were given in Table 5.7.

EIMS: found m/z 296.1630 $[M]^+$, cal. for $C_{16}H_{24}O_5$ 296.1624 (Δ 2.0 ppm). HRESI-MS (positive mode) m/z : for $C_{16}H_{25}O_5$ 297.1702 $[M+H]^+$.

5.2.7.4. Physicochemical data of compound 4 (VC₂₋₆₋₄₋₁)

Tetrahydro-3-methoxy-5-((*E*)-8,12-dimethyloct-8-enyl)-pyran-2-one: Pale yellow oily; UV (MeOH) λ_{\max} (log ϵ): 218.6 nm; (3.76); TLC (Si gel GF₂₅₄ 15 mm; 15:85, v/v, EtOAc/*n*-hexane) R_f : 0.67; R_t (RP C18 HPLC, 1:4, v/v, MeOH:MeCN): 3.41 min; IR (cm⁻¹): 2922, 2852 (C-H_v), 1740 (C=O_v), 1462 (C-H δ), 1376 (C-H ρ), 1116, 1049 (C-O_v), 910 (=C-H δ), 732, 648 (C-H δ); ¹H (CDCl₃, 500 MHz): δ 5.35 (1H, t, $J=3.95$ Hz), 4.17 (1H α , d), 4.14 (1H β , d), 4.08 (1H α , t), 3.67 (3H, s), 2.35 (2H, t), 2.01 (2H, m), 1.86 (3H α , s), 1.82 (2H, d), 1.63 (1H β , m), 1.50 (1H α , m), 1.30 (2H, m), 1.13 (2H, m), 0.99 (3H β , d), 0.87 (3H, t); ¹³C (125 MHz, CDCl₃): δ 173.92, 135.14, 130.02, 68.40, 65.04, 50.68, 34.11, 31.93, 30.97, 28.03, 27.22, 24.90, 23.73, 22.69, 15.26, 14.02; COSY and HMBC data were given in Table 5.8. EIMS: found m/z 268.2044 $[M]^+$, cal. for $C_{16}H_{28}O_3$ 268.2038 (Δ 2.2 ppm). HRESI-MS (positive mode) m/z : for $C_{16}H_{29}O_3$ 269.2117 $[M+H]^+$.

5.2.7.5. Physicochemical data of compound 5 (VC₂₋₆₋₆₋₂₋₂)

Dihydro-5-(8-(9,12-dihydro-8-methyl-11-propyl-2*H*-pyran-8-yl)-ethyl)-furan-2-(3*H*)-one: Pale brown oily; UV (MeOH) λ_{\max} (log ϵ): 234.6 nm (2.52); TLC (Si gel GF₂₅₄ 15 mm; v/v, 15:85, EtOAc/*n*-hexane) R_f : 0.73; R_t (RP C18 HPLC, 1:4, v/v, MeOH:MeCN): 4.38 min; IR (cm⁻¹): 2919, 2851 (C-H_v), 1739, 1710 (C=O_v), 1462 (C-H δ), 1375 (C-H ρ), 1168, 1114 (C-O_v), 971 (=C-H δ), 721 (C-H δ); ¹H (CDCl₃, 500 MHz): δ 5.35 (1H β , t, $J=7.23$ Hz), 4.17 (1H β , d), 4.14 (1H α , d), 4.08 (1H β , m), 2.35 (2H, t), 2.02 (2H, d), 1.86 (2H, t), 1.65 (2H, m), 1.60 (2H, m), 1.30 (2H, t), 1.28 (2H, m), 1.25 (3H α , s), 0.89 (3H, t); ¹³C (125 MHz, CDCl₃): δ 177.63, 135.84, 130.02, 72.12, 68.41, 65.04, 34.11, 33.67, 31.93, 30.73, 29.69, 27.23, 24.72, 22.69, 14.11; COSY and HMBC data were given in Table 5.9. EIMS: found m/z 252.1730 $[M]^+$ cal. for $C_{15}H_{24}O_3$ 252.1725 (Δ 2.0 ppm). HRESI-MS (positive mode) m/z : for $C_{15}H_{25}O_3$ 253.1804 $[M+H]^+$.

5.2.7.6. Physicochemical data of compound 6 (VC₃₋₄₋₃₋₁)

(10E)-Butyl-9-(6-ethyl-3,4,6,7,8,8a-hexahydro-1H-isochromen-3-yl)pent-10-enoate: Light yellow oily; UV (MeOH) λ_{\max} (log ϵ): 231 nm (3.13); TLC (Si gel GF₂₅₄ 15 mm; 2:98, v/v, EtOAc/*n*-hexane) R_f : 0.62; R_t (RP C18 HPLC, 1:4, v/v, MeOH:MeCN): 8.31 min; IR (cm⁻¹): 2974, 2853 (C-H ν), 1711 (C=O ν), 1460 (C-H δ), 1377 (C-H ρ), 1167 (C-C ν), 1094 (C-O ν), 910 (=C-H δ), 731 (C-H δ); ¹H (CDCl₃, 500 MHz): δ 5.43 (1H β , q, J =10.97 Hz), 5.40 (1H α , q, J =10.52 Hz), 5.36 (1H α , d, J =7.72 Hz), 4.20 (1H β , t), 4.17 (1H α , t), 3.94 (1H β , p), 3.70 (1H β , d), 3.63 (1H α , d), 2.86 (2H, d), 2.44 (2H, d), 2.36 (1H, p), 2.07 (2H, t), 2.03 (1H β , m), 1.73 (2H, m), 1.64 (2H, m), 1.62 (2H, m), 1.32 (2H, m), 1.29 (2H, m), 0.99 (3H, t), 0.90 (3H, t); ¹³C (125 MHz, CDCl₃): δ 174.34, 132.04, 129.93, 128.29, 128.07, 70.27, 65.14, 63.36, 34.15, 34.04, 31.91, 31.51, 29.68, 29.65, 27.21, 25.64, 24.90, 22.68, 14.10, 14.05; COSY and HMBC data were given in Table 5.10. EIMS: found m/z 320.2356 [M]⁺, cal. for C₂₀H₃₂O₃ 320.2351 (Δ 1.6 ppm). HRESI-MS (positive mode) m/z : for C₂₀H₃₃O₃ 321.2430 [M+H]⁺.

5.2.7.7. Physicochemical data of compound 7 (VC₃₋₄₋₃₋₂)

(12E)-(3,4,6,7,8,8a-Hexahydro-1H-isochromen-3-yl)-methyl-hept-12-enoate: Light yellow oily; UV (MeOH) λ_{\max} (log ϵ): 229 nm (2.08); TLC (Si gel GF₂₅₄ 15 mm; 2:98, v/v, EtOAc/*n*-hexane) R_f : 0.68; R_t (RP C18 HPLC, 1:4, v/v, MeOH:MeCN): 6.66 min; IR (cm⁻¹): 2923, 2853 (C-H ν), 1711 (C=O ν), 1460, 1412 (C-H δ), 1377 (C-H ρ), 1167 (C-C ν), 1094 (C-O ν), 974, 910 (=C-H δ), 731, 647 (C-H δ); ¹H (CDCl₃, 500 MHz): δ 5.30 (1H β , q, J =10.96 Hz), 5.29 (1H α , q, J =10.53 Hz), 5.27 (1H α , d, J =7.02 Hz), 4.07 (1H β , d), 4.06 (1H α , d), 3.84 (1H, p), 3.59 (1H β , d), 3.52 (1H α , d), 2.73 (2H, d), 2.30 (2H β , d), 2.26 (1H, p), 1.98 (2H, m), 1.94 (2H, m), 1.54 (2H, m), 1.22 (2H, m), 1.20 (2H, m), 0.80 (3H, t); ¹³C (125 MHz, CDCl₃): δ 174.37, 135.46, 129.99, 129.80, 129.68, 70.22, 65.05, 63.35, 34.14, 31.89, 31.75, 29.67, 29.63, 27.20, 24.88, 22.66, 14.08; COSY and HMBC data were given in Table 5.11. EIMS: found m/z 278.1886 [M]⁺, cal. for C₁₇H₂₆O₃ 278.1882 (Δ 1.4 ppm). HRESI-MS (positive mode) m/z : for C₁₇H₂₇O₃ 279.1960 [M+H]⁺.

5.2.7.8. Physicochemical data of compound 8 (VC₂₋₆₋₅₋₂)**19 (10→5) Abeo-20-methyl-pregn-1-en-3-yl-3β-methoxy-hex-25-enoate:**

White solid; melting point (m.p.) 138.2°C; $[\alpha]_D^{26}$ -20.5° (CHCl₃, c0.011); UV (MeOH) λ_{\max} (log ϵ): 222.3 nm (3.61); TLC (Si gel GF₂₅₄ 15 mm; 10:90, v/v, EtOAc/*n*-hexane) R_f: 0.42; R_t (RP C18 HPLC, 3:2, v/v, MeOH:MeCN): 3.19 min; IR (cm⁻¹): 2923, 2855 (C-H_v), 1719 (C=O_v), 1457 (C-H δ), 1375 (C-H ρ), 1167 (C-C_v), 1050 (C-O_v), 973 (=C-H δ), 722, 655 (C-H δ); ¹H (CDCl₃, 500 MHz): δ 5.41 (1H, td, *J*=9.02, 7.03 Hz), 5.40 (1H, td, *J*=9.14, 7.05 Hz), 5.39 (1H α , t, *J*=6.50 Hz), 4.62 (1H α , p), 2.87 (2H, d), 2.32 (1H β , t), 2.29 (1H α , t), 2.08 (1H α , m), 2.05 (2H, m), 1.97 (1H β , m), 1.86 (2H, m), 1.72 (1H β , d), 1.59 (2H, m), 1.57 (1H α , d), 1.52 (2H, m), 1.35 (2H, m), 1.32 (2H, m), 1.15 (2H, t), 1.10 (1H α , m), 1.04 (3H β , s), 1.00 (1H β , m), 0.98 (1H β , m), 0.95 (3H, t), 0.90 (3H, d), 0.88 (3H, d), 0.70 (3H β , s); ¹³C (125 MHz, CDCl₃): δ 173.28, 139.70, 132.01, 128.20, 122.57, 73.66, 56.70, 56.15, 50.04, 42.32, 39.53, 38.17, 37.02, 36.60, 36.20, 35.81, 31.91, 31.88, 29.71, 28.02, 25.64, 24.29, 22.83, 22.57, 21.05, 19.33, 18.73, 11.86; COSY and HMBC data were given in Table 5.12. EIMS: found *m/z* 412.3347 [M+1]⁺, cal. for C₂₈H₄₄O₂ 412.3341 (Δ 1.4 ppm). HRESI-MS (positive mode) *m/z*: for C₂₈H₄₅O₂ 413.3420 [M+H]⁺.

5.2.7.9. Physicochemical data of compound 9 (VC₂₋₅₋₁)**(22E)-24¹-Homocholesta-5,22-dien-(3β,24¹β)-diol:**

White solid; m.p. 139.1°C; $[\alpha]_D^{26}$ -18.3° (CHCl₃, c0.014); UV (MeOH) λ_{\max} (log ϵ): 221.5 nm (3.46); TLC (Si gel GF₂₅₄ 5:95, v/v, 15 mm; EtOAc/*n*-hexane) R_f: 0.54; R_t (RP C18 HPLC, 3:2, v/v, MeOH:MeCN): 6.00 min; IR (cm⁻¹): 3366 (br, O-H_v), 2934, 2865 (C-H_v), 1653 (C=C_v), 1459 (C-H δ), 1327 (C-H ρ), 1242, 1191 (C-C_v), 1107 (C-O_v), 928, 881, 801 (=C-H δ), 737, 625 (C-H δ); ¹H (CDCl₃, 500 MHz): δ 5.34 (1H α , dd, *J*=6.25, 6.31 Hz), 5.18 (1H, m, *J*=9.81 Hz), 5.17 (1H, td, *J*=10.44, 9.61 Hz), 3.64 (1H α , m), 3.52 (1H α , p), 2.28 (1H α , d), 2.23 (1H β , d), 2.03 (2H, t), 2.00 (1H α , t), 1.95 (1H, t), 1.86 (1H, m), 1.85 (1H α , t), 1.83 (1H α , m), 1.69 (2H, m), 1.53 (1H α , m), 1.52 (1H, m), 1.51 (1H β , m), 1.49 (1H β , m), 1.47 (2H, m), 1.14 (1H β , t), 1.10 (1H α , m), 1.08 (1H β , m), 1.03 (1H β , t), 1.01 (3H β , s), 0.95 (1H β , m), 0.92 (1H α , m), 0.90 (3H α , d), 0.86 (3H, d), 0.84 (3H, d), 0.69 (3H β , s); ¹³C (125 MHz, CDCl₃): δ 140.75, 135.83, 131.72, 121.70, 71.80, 70.44, 56.77, 56.02, 50.14, 46.25, 42.81, 42.30, 40.16, 39.79, 37.27, 36.51, 33.10, 31.91, 31.65,

28.54, 28.02, 24.30, 22.69, 21.09, 19.89, 19.40, 17.62, 11.87; COSY and HMBC data were given in Table 5.13. EIMS: found m/z 414.3504 $[M]^+$, cal. for $C_{28}H_{46}O_2$ 414.3498 (Δ 1.4 ppm). HRESI-MS (positive mode) m/z : for $C_{28}H_{47}O_2$ 415.3576 $[M+H]^+$.

5.2.7.10. Physicochemical data of compound 10 (VC₂₋₄₋₁)

(22*E*),(24¹*E*)-24¹,24²-dihomocholesta-5,22,24¹-trien-3 β -ol: White solid; m.p. 140.4°C; $[\alpha]_D^{26}$ -17.3° (CHCl₃, c0.016); UV (MeOH) λ_{max} (log ϵ): 220 nm (3.32); TLC (Si gel GF254 15 mm; 20:80, v/v, EtOAc/*n*-hexane) R_f : 0.58; R_t (RP C18 HPLC, 3:2, v/v, MeOH:MeCN): 8.99 min; IR (cm⁻¹): 3366 (br, O-Hv), 2934, 2894 (C-Hv), 1663 (C=Cv), 1459 (C-H δ), 1329 (C-Hp), 1242, 1133 (C-Cv), 1044 (C-Ov), 963, 836, 801 (=C-H δ), 737 (C-H δ); ¹H (CDCl₃, 500 MHz): δ 5.39 (1H, q, J =10.49 Hz), 5.35 (1H α , dd, J =6.77, 5.03 Hz), 5.20 (1H, t, J =11.02 Hz), 5.16 (1H, td, J =9.55, 9.00 Hz), 5.03 (1H, t, J =9.04 Hz), 3.52 (1H α , p), 2.28 (1H α , d), 2.25 (1H β , d), 2.02 (2H, t), 2.00 (1H α , t), 1.95 (1H, t), 1.85 (1H, m), 1.84 (1H α , t), 1.83 (1H α , m), 1.68 (2H, m), 1.53 (1H α , m), 1.51 (1H, m), 1.50 (1H β , m), 1.49 (1H β , m), 1.47 (2H, m), 1.16 (1H β , t), 1.12 (1H α , m), 1.08 (1H, m), 1.03 (1H β , t), 1.01 (3H β , s), 0.95 (1H β , m), 0.92 (1H α , m), 0.90 (3H α , d), 0.87 (3H, d), 0.86 (3H, d), 0.68 (3H β , s); ¹³C (125 MHz, CDCl₃): δ 140.75, 138.26, 135.83, 131.72, 129.32, 121.70, 71.80, 56.85, 56.02, 50.17, 42.81, 42.30, 42.25, 40.16, 39.69, 37.26, 36.52, 33.10, 31.91, 31.66, 28.24, 28.02, 24.30, 22.82, 21.19, 19.86, 19.40, 17.62, 11.87; COSY and HMBC data were given in Table 5.14. EIMS: found m/z 410.3555 $[M]^+$, cal. for $C_{29}H_{46}O$ 410.3549 (Δ 1.5 ppm). HRESI-MS (positive mode) m/z : for $C_{29}H_{47}O$ 411.3627 $[M+H]^+$.

5.2.8. Determination of bioactive potentials

5.2.8.1. *In vitro* antioxidant assays

5.2.8.1.A. 1, 1-Diphenyl-2-picryl-hydrazil (DPPH) radical scavenging assay

The antioxidant activities of chromatographic fractions and pure compounds isolated from the EtOAc:MeOH extracts of *V. cyprinoides* were measured using the stable free radical, DPPH as explained in the section 4.2.4.1.2.A. under Chapter 4.

5.2.8.1.B. 2,2'-Azino-bis-3-ethylbenzothiozoline-6-sulfonic acid diammonium salt (ABTS⁺) radical scavenging assay

The free radical scavenging activity of chromatographic fractions and pure compounds isolated from the EtOAc:MeOH extracts of *V. cyprinoides* were determined by ABTS⁺ decolourization assay as explained in the sections 4.2.4.1.2.B. under Chapter 4.

5.2.8.2. *In vitro* anti-inflammatory assays

5.2.8.2.A. Cyclooxygenases (COX) inhibition assay

The cyclooxygenase (COX-1 and COX-2) inhibitory analyses of chromatographic fractions and pure compounds isolated from EtOAc:MeOH extracts of *V. cyprinoides* were carried out as explained in the sections 4.2.4.2.1. under Chapter 4.

5.2.8.2.B. 5-Lipoxygenase (5-LOX) inhibition assay

The 5-lipoxygenase (5-LOX) inhibitory analyses of chromatographic fractions and pure compounds isolated from EtOAc:MeOH extracts of *V. cyprinoides* were carried out as explained in the sections 4.2.4.2.2. under Chapter 4.

5.2.9. The structure-activity relationship analyses of bioactive secondary metabolites isolated from EtOAc:MeOH extract of *V. cyprinoides*

All the structures in this chapter were produced with the use of ChemDraw drawing program by presetting in ACS style-sheet format in the ChemDraw (CambridgeSoft Corporation, Cambridge, MA, USA; ver. 8.0 and ver. 12.0).

Structure-activity relationship analyses of the characterized bioactive secondary metabolites isolated from *V. cyprinoides* and the standards (α -tocopherol and ibuprofen) were analyzed by the molecular descriptor variables, named hydrophobic (logarithm of octanol-water partition co-efficient, log P_{ow}), steric bulk {molar refractivity (MR), molar volume (MV), parachor (Pr)} and electronic (topological polar surface area tPSA, polarizability PI) descriptors (Chakraborty *et al.*, 2017b; Lipinski 2000) using ChemDraw Ultra (CambridgeSoft Corporation, Cambridge, MA, USA; ver. 8.0 and vers. 12.0) and ACD ChemSketch (Advanced Chemistry Development, Inc., Canada; ver. 12.0) softwares.

5.2.10. *In silico* molecular modeling

5.2.10.1. Molecular structures of protein and energy minimization

The X-ray crystal structures of cyclooxygenase-2 (COX-2) (PDB ID 3LN1; resolution 2.4 Å) bound with celecoxib (Wang *et al.*, 2010b) and 5-lipoxygenase enzyme (5-LOX) (PDB ID 1N8Q; resolution 2.1 Å) bound with protocatechuic acid (Borbulevych *et al.*, 2004) were recovered from the Protein Data Bank (www.pdb.org) as PDB file (text). The water molecules were removed and the two target enzymes energetically minimized by Swiss-PdbViewer (SPDBV v4.1.0) software tool. The minimized protein was further taken for the docking studies.

5.2.10.2. Preparation of ligands

The titled compounds (**1-10**) were constructed by utilizing ACD/ChemSketch (Freeware) 2016.2.2. (Advanced Chemistry Development, Inc. Toronto, Canada) and saved as MDL Molfiles (V2000). These MDL molfiles were converted to PDB format using the software OpenBabelGUI 2.4.1 (O'Boyle *et al.*, 2011).

5.2.10.3. Molecular docking

The molecular docking of title compounds (**1-10**) were carried out to evaluate their possible binding modes between COX-2 and 5-LOX enzyme active sites other than calculating the binding strength, energy of the complex and binding affinity. The docking studies were performed using AutoDock 4 (AutoDock Tools ver. 1.5.6). In the Autodock software, all ligands, protein bound water and cofactors were eliminated. The macromolecules were assigned for polar hydrogens, atomic solvation parameters and Kollman charges. Thereafter, the ligands were selected and their torsion bonds were defined. To assign the perfect grid for each ligand, grid box was generated by Auto Grid algorithm and grid box values were selected by trial and error and also, based on the previous studies. Grid map set values for the docking of COX-2 was selected as x=47.975, y=-33.687, z=18.295 (54 Å X 56 Å X 106 Å) points and the grid box values for the docking of 5-LOX was found to be x=10.500, y=0.583, z=18.972 (48 Å X 32 Å X 42 Å). Each map was centered so that it can cover the entire protein particularly, all probable binding sites. The molecular docking studies were performed using Genetic Algorithm and Lamarckian genetic algorithm (LGA) docking methods. Cygwin-I terminal was used for running the docking algorithm. After the successful completion of

autodocking, the RMSD (Root-Mean-Square Deviation of atomic positions) results were analyzed. The docked conformations of the title compounds were ranked based on their binding energies and the conformation with the lowest free binding energies were selected for further studies. Among the ten compounds described in this chapter, the best five molecules with lowest binding energies were selected and carried out Cygwin-II terminal for optimization and visualization. The visualization and interpretation of molecular docking analyses of the selected (five) molecules were carried out by using USCF Chimera 1.11.2 software to recognize the hydrogen-bond interactions between the selected molecules and targeted enzymes (COX-2 and 5-LOX).

5.2.11. Statistical analysis

One way analysis of variance (ANOVA) was analyzed using SPSS software (Statistical Program for Social Sciences, USA, ver. 13.0) to study the significant differences among the means of bioactivities. The significant differences were signified as $p < 0.05$ and values were represented as means of triplicates \pm standard deviation.

5.3. Results and discussion

5.3.1. Chromatographic fractionation, bioactive potentials and spectroscopic analysis of intermediate fractions from EtOAc:MeOH extract of *V. cyprinoides*

5.3.1.1. Chromatographic fractionation and bioactive potentials of intermediate fractions from EtOAc:MeOH extract of *V. cyprinoides*

Chromatographic fractionation of EtOAc:MeOH extract of *V. cyprinoides* afforded four pooled sub-fractions, named VC₁ to VC₄ based upon the TLC (8:2, *n*-hexane:EtOAc, v/v) and RP C18 HPLC (3:2, v/v, MeOH/acetonitrile) experiments. The four sub-fractions checked for their target bioactive potentials against free radicals and pro-inflammatory enzymes. The yields and bioactivities of these column fractions presented in Table 5.1.

The percentage yields of sub-fractions, VC₁ (10.0 g), VC₂ (8.0 g), VC₃ (11.0 g) and VC₄ (13.0 g) were found to be 22.22%, 17.78%, 24.44% and 28.89%, respectively on EtOAc:MeOH crude extract weight basis. The sub-fractions, VC₂ and VC₃ exhibited significantly greater ($p < 0.05$) DPPH radical scavenging potentials and

their IC₅₀ values were found to be 0.93 and 1.06 mg/mL, respectively compared to VC₁ (IC₅₀ 1.23 mg/mL) and VC₄ (IC₅₀ 1.16 mg/mL). Similarly, the ABTS⁺ radical inhibitory effects were significantly greater ($p < 0.05$) for VC₂ (IC₅₀ 1.03 mg/mL) and VC₃ (IC₅₀ 1.06 mg/mL) compared to VC₁ (IC₅₀ 1.43 mg/mL) and VC₄ (IC₅₀ 1.34 mg/mL). The anti-inflammatory potentials against inflammatory enzymes COX-2 and 5-LOX were found to be considerably higher for sub-fractions, VC₂ and VC₃ and their IC₅₀ values were ranged from 1.06-1.10 and 0.96-1.01 mg/mL, respectively when compared to VC₁ and VC₄. The sub-fractions, VC₁ and VC₄ registered IC₅₀ of > 1.45 and > 1.25 mg/mL, respectively for anti-COX-2 and anti-5-LOX. Hence, the sub-fractions VC₂ and VC₃ were regarded as appropriate for sequential fractionation to obtain bioactive compounds.

Table 5.1.: Yield and bioactive (antioxidant and anti-inflammatory) potentials of sub-fractions from EtOAc:MeOH extract of *V. cyprinoides*

Sub-fractions	#Yield		Bioactive potentials (IC ₅₀ value)			
			Antioxidant		Anti-inflammatory	
	g	%	*DPPH	*ABTS ⁺	*COX-2	*5-LOX
VC ₁	10	22.22	1.23 ± 0.04 ^a	1.43 ± 0.05 ^a	1.52 ± 0.06 ^a	1.39 ± 0.07 ^a
VC ₂	8	17.78	0.93 ± 0.02 ^b	1.03 ± 0.03 ^b	1.06 ± 0.04 ^b	0.96 ± 0.05 ^b
VC ₃	11	24.44	1.06 ± 0.05 ^b	1.06 ± 0.06 ^b	1.10 ± 0.07 ^b	1.01 ± 0.08 ^b
VC ₄	13	28.89	1.16 ± 0.03 ^c	1.34 ± 0.04 ^c	1.46 ± 0.05 ^a	1.26 ± 0.06 ^c

[#]The percentage of yield was calculated on the basis of crude EtOAc:MeOH extract (45.0 g EtOAc:MeOH crude extract weight). The samples were analyzed in triplicate (n=3) and expressed as mean ± standard deviation. Means followed by the different superscripts (a-c) within the same column indicated the significant differences ($p < 0.05$). *The IC₅₀ values were expressed as mg/mL

5.3.1.2. Spectroscopic analysis of intermediate fractions from EtOAc:MeOH extract of *V. cyprinoides*

The intermediate sub-fractions (VC₁-VC₄) subjected to ¹H NMR analysis (Figure 5.3.) to acquire proton integral values corresponded to characteristic functional group signals (Table 5.2.). The proton integrals for VC₂ in the regions δ 0.1-2.0

(saturated hydrocarbons), 2.0-2.5 (Ar-CH and acetylinic groups), 2.5-3.5 (-CH-C=O and -CH-Ar), 3.5-4.5 (electronegative groups) and 4.5-6.5 (vinylic, conjugated) were found to be 54.00, 4.09, 1.85, 4.44 and 2.73, respectively. Likewise, the proton integrals in the regions δ 0.1-2.0, 2.0-2.5, 2.5-3.5, 3.5-4.5 and 4.5-6.5 were found to be 47.42, 5.85, 4.03, 1.73 and 4.15, respectively for VC₃. The sub-fractions, VC₁ and VC₄ were registered lesser proton integrals in the regions of δ 2.0-2.5 and 3.5-4.5, which were found to be ~2.15 and ~0.92, respectively. In general, VC₂ and VC₃ sub-fractions showed significantly greater proton integrals than the other fractions (VC₁ and VC₄) when the potentially electronegative regions δ 3.5-4.5 and 2.0-2.5 were taken into consideration. The signals at δ 0.1-2.0 respective to saturated hydrocarbons were more prominent in the fraction, VC₃ (47.42) and VC₂ (54.0), which could be attributed towards the methylene or end methyls in alkyl chains.

Table 5.2.: Types and integral values of protons obtained from the ¹H NMR spectra of sub-fractions from EtOAc:MeOH extract of *V. cyprinoides*

Proton signal	Proton integral (ΣH)			
	VC ₁	VC ₂	VC ₃	VC ₄
0.1-2.0	24.14	54.00	47.42	33.13
2.0-2.5	2.13	4.09	5.85	2.19
2.5-3.5	0.03	1.85	4.03	2.96
3.5-4.5	0.87	4.44	1.73	0.96
4.5-6.5	0.21	2.73	4.15	2.81
6.5-8.5	0.00	0.04	0.05	0.20

The greater radical scavenging property of VC₃ and VC₂ might be attributed to more electron donating methoxy/hydroxyl groups (δ 3.5-4.5) whereas, VC₁ and VC₄ recorded comparatively lesser number of olefinic/oxygenated groups, and therefore, exhibited significantly lower activities. The sub-fraction, VC₃ displayed very intense signals and greater number of proton integrals at δ 2.0-2.5, 2.5-3.5 and 4.5-6.5 followed by VC₂, which was ascribed to the alkenic and electronegative auxochromes, such as alkoxy/alkyl halide/functionalized hydride H of substituted alkanols. In general, VC₃ and VC₂ fractions derived from EtOAc:MeOH extract of *V. cyprinoides* showed greater proton integrals than other column fractions when these potentially electronegative regions were taken into consideration. A significant co-linearity was found between

bioactive properties and the deshielded electronegative groups present in intermediate fractions from EtOAc:MeOH extract of *V. cyprinoides*. The proton NMR based bioactivity analyses of intermediate fractions (VC₁-VC₄) suggested that the sub-fractions, VC₃ and VC₂ could be considered as better candidate fractions for further chromatographic purifications to isolate the bioactive compounds.

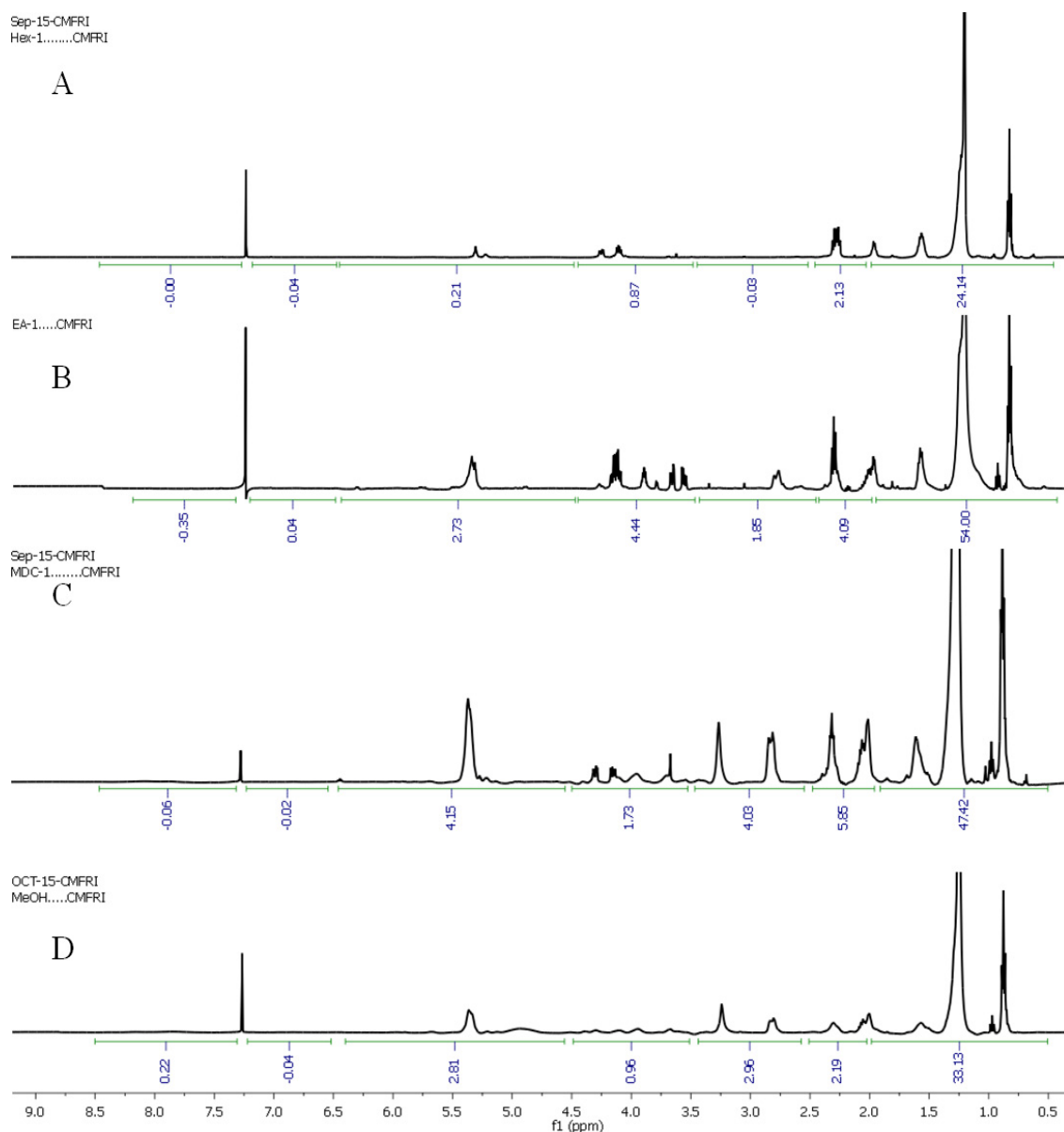


Figure 5.3.: ¹H NMR spectra of intermediate sub-fractions, (A) VC₁, (B) VC₂, (C) VC₃ and (D) VC₄ from the EtOAc:MeOH extract of *V. cyprinoides* with integration values

5.3.1.3. Isolation of bioactive secondary metabolites from EtOAc:MeOH extract of *V. cyprinoides*

The sub-fractions, VC₂ and VC₃ were selected for the isolation of bioactive principles. The yield (in mg and in %), retention factor (R_f), bioactivities (antioxidant/anti-inflammatory) of each column/flash/PTLC/PHPLC sub-fractions obtained from the candidate fractions were recorded in Table 5.3.-5.4.

The fraction, VC₂ (8.0 g; 17.78%) eluted at 100% DCM was subjected to vacuum liquid chromatography using the step-wise elution of *n*-hexane/EtOAc/MeOH to furnish 9 sub-groups (VC₂₋₁-VC₂₋₉). Among these, column fractions such as VC₂₋₄ (1023 mg; 2.27%), VC₂₋₅ (1136 mg; 2.52%) and VC₂₋₆ (1323 mg; 2.94%) exhibited significantly higher antioxidant activities with respect to scavenge DPPH (IC₅₀ 0.69-0.98 mg/mL) and ABTS⁺ (IC₅₀ 0.71-0.99 mg/mL) radicals. The anti-inflammatory effects were also greater for VC₂₋₄ (IC₅₀ anti-COX-2 0.65 mg/mL and IC₅₀ anti-5-LOX 0.73 mg/mL), VC₂₋₅ (IC₅₀ anti-COX-2 1.03 mg/mL and IC₅₀ anti-5-LOX 0.94 mg/mL) and VC₂₋₆ (IC₅₀ anti-COX-2 0.83 mg/mL and IC₅₀ anti-5-LOX 0.84 mg/mL) when compared to other fractions (IC₅₀ > 1.15 mg/mL).

The bioactive fraction, VC₂₋₄ was found to be mixture, and therefore, fractionated by preparative HPLC (80% MeCN:MeOH) to yield compound **10** (195 mg; 0.43%; VC₂₋₄₋₁). Likewise, VC₂₋₅ on preparative HPLC (80% MeCN:MeOH) fractionation yielded compound **9** (134 mg, 0.30%; VC₂₋₅₋₁). The fraction, VC₂₋₆ (1323 mg; 2.94%) was subjected to flash chromatography using *n*-hexane/EtOAc/MeOH to afford six fractions (VC₂₋₆₋₁-VC₂₋₆₋₆). The sub-fractions, such as VC₂₋₆₋₂ (205 mg; 0.46%), VC₂₋₆₋₄ (214 mg; 0.48%), VC₂₋₆₋₅ (510 mg; 1.13%) and VC₂₋₆₋₆ (196 mg; 0.44%) displayed greater bioactive potentials, and therefore, selected for further purifications (Table 5.3.).

The fractions, VC₂₋₆₋₂, VC₂₋₆₋₄, VC₂₋₆₋₅ and VC₂₋₆₋₆ registered greater antioxidant (IC₅₀ 0.72-0.86 mg/mL for DPPH scavenging; IC₅₀ 0.70-0.89 mg/mL for ABTS⁺ scavenging) and anti-inflammatory potentials (IC₅₀ 0.78-0.93 mg/mL for anti-COX-2; IC₅₀ 0.81-0.96 mg/mL for anti-5-LOX). The fraction, VC₂₋₆₋₂ on column chromatography using *n*-hexane/EtOAc/MeOH afforded three sub-fractions, VC₂₋₆₋₂₋₁ (138 mg; 0.31%), VC₂₋₆₋₂₋₂ (26 mg; 0.06%) and VC₂₋₆₋₂₋₃ (34 mg; 0.08%), wherein VC₂₋₆₋₂₋₁ was registered greater antioxidant (IC₅₀ DPPH scavenging 0.79 mg/mL and IC₅₀

ABTS⁺ scavenging 0.78 mg/mL) and anti-inflammatory (IC₅₀ anti-COX-2 0.77 mg/mL and IC₅₀ anti-5-LOX 0.83 mg/mL) potentials. The VC₂₋₆₋₂₋₁ on PTLC purification afforded compound **3** (79 mg; 0.18%; VC₂₋₆₋₂₋₁₋₂). The fraction, VC₂₋₆₋₄ on repeated RP C18 PHPLC purification techniques yielded compound **4** (59 mg; 0.13%; VC₂₋₆₋₄₋₁) with greater antioxidant (IC₅₀ 0.71-0.76 mg/mL) and anti-inflammatory (IC₅₀ 0.89-0.92 mg/mL) potentials, along with a minor fraction, VC₂₋₆₋₄₋₂. The fraction VC₂₋₆₋₅ on repeated PTLC acquired compound **8** (143 mg; 0.32%; VC₂₋₆₋₅₋₂) with anti-inflammatory (IC₅₀ ~1.04 mg/mL) and antioxidant (IC₅₀ ~0.90 mg/mL) potentials, along with a minor fraction, VC₂₋₆₋₅₋₁ (Table 5.3.).

The VC₂₋₆₋₆ on repeated column chromatography afforded four sub-fractions, VC₂₋₆₋₆₋₁ (14 mg; 0.03%), VC₂₋₆₋₆₋₂ (134 mg; 0.30%), VC₂₋₆₋₆₋₃ (16 mg; 0.04%) and VC₂₋₆₋₆₋₄ (24 mg; 0.05%). Among these, VC₂₋₆₋₆₋₂ exhibited greater DPPH (IC₅₀ 0.81 mg/mL) and ABTS⁺ scavenging (IC₅₀ 0.79 mg/mL) along with COX-2 (IC₅₀ 0.85 mg/mL) and 5-LOX (IC₅₀ 0.91 mg/mL) inhibitory potentials. Therefore, the fraction, VC₂₋₆₋₆₋₂ was opted for further fractionation. The sub-fraction, VC₂₋₆₋₆₋₂ on RP C18 PHPLC purification yielded the pure compound **5** (69 mg; 0.15%; VC₂₋₆₋₆₋₂₋₂) along with two minor fractions (VC₂₋₆₋₆₋₂₋₁ and VC₂₋₆₋₆₋₂₋₃) (Table 5.3.).

Table 5.3.: The yield (in mg and in %), retention factor (R_f), bioactivities (antioxidant/anti-inflammatory) of column/flash/PTLC/PHPLC fractions obtained from the sub-fraction, VC₂ of EtOAc:MeOH extract of *V. cyprinoides*

	#Yield		R _f	*Bioactive Potentials (IC ₅₀ value; mg/mL)			
	mg	%		Antioxidant		Anti-inflammatory	
				DPPH	ABTS ⁺	COX-2	5-LOX
VC ₂ CC (<i>n</i> -hexane/EtOAc/MeOH)	8000	17.78		0.93 ± 0.02	1.03 ± 0.03	1.06 ± 0.04	0.96 ± 0.05
VC ₂₋₁ (100% <i>n</i> -hexane)	849	1.89		1.76 ± 0.03	1.68 ± 0.10	1.76 ± 0.02	1.68 ± 0.09
VC ₂₋₂ (2% EtOAc: <i>n</i> -hexane)	231	0.51		2.35 ± 0.05	2.42 ± 0.04	2.16 ± 0.04	2.12 ± 0.00
VC ₂₋₃ (5% EtOAc: <i>n</i> -hexane)	126	0.28		1.26 ± 0.07	1.07 ± 0.01	1.55 ± 0.03	1.23 ± 0.05
VC ₂₋₄ (10% EtOAc: <i>n</i> -hexane)	1023	2.27		0.69 ± 0.02	0.71 ± 0.02	0.65 ± 0.01	0.73 ± 0.02
VC ₂₋₅ (12% EtOAc: <i>n</i> -hexane)	1136	2.52		0.98 ± 0.00	0.99 ± 0.02	1.03 ± 0.02	0.94 ± 0.01
VC ₂₋₆ (15% EtOAc: <i>n</i> -hexane)	1323	2.94		0.88 ± 0.01	0.89 ± 0.03	0.83 ± 0.03	0.84 ± 0.02
VC ₂₋₇ (25% EtOAc: <i>n</i> -hexane)	351	0.78		1.25 ± 0.00	1.84 ± 0.04	1.85 ± 0.04	1.36 ± 0.05
VC ₂₋₈ (100% EtOAc)	960	2.13		1.21 ± 0.02	2.35 ± 0.05	1.42 ± 0.03	1.17 ± 0.08
VC ₂₋₉ (100% MeOH)	1042	2.32	1.92 ± 0.04	2.16 ± 0.04	2.12 ± 0.00	2.42 ± 0.04	
VC ₂₋₄ RP C18 PHPLC (80% MeCN:MeOH)	1023	2.27	0.58	0.91 ± 0.01	1.08 ± 0.01	1.12 ± 0.03	1.19 ± 0.02
VC ₂₋₄₋₁ (Compound 10)	195	0.43					
VC ₂₋₄₋₂	665	1.48					
VC ₂₋₅ RP C18 PHPLC (80% MeCN:MeOH)	1136	2.52	0.54	0.93 ± 0.01	1.05 ± 0.01	1.15 ± 0.03	1.17 ± 0.02
VC ₂₋₅₋₁ (Compound 9)	134	0.30					
VC ₂₋₅₋₂	712	1.58					

VC₂₋₆ FC (<i>n</i>-hexane/EtOAc/MeOH)	1323	2.94					
VC ₂₋₆₋₁ (5% EtOAc: <i>n</i> -hexane)	54	0.12		1.70 ± 0.01	1.72 ± 0.01	1.61 ± 0.03	1.84 ± 0.02
VC₂₋₆₋₂ (10% EtOAc:<i>n</i>-hexane)	205	0.46		0.84 ± 0.04	0.88 ± 0.02	0.92 ± 0.01	0.96 ± 0.01
VC ₂₋₆₋₃ (20% EtOAc: <i>n</i> -hexane)	82	0.18		1.76 ± 0.02	1.78 ± 0.02	1.91 ± 0.04	1.80 ± 0.03
VC ₂₋₆₋₄ (25% EtOAc: <i>n</i> -hexane)	214	0.48		0.86 ± 0.05	0.89 ± 0.03	0.93 ± 0.02	0.94 ± 0.02
VC ₂₋₆₋₅ (100% EtOAc)	510	1.13		0.72 ± 0.03	0.70 ± 0.03	0.78 ± 0.05	0.81 ± 0.04
VC ₂₋₆₋₆ (100% MeOH)	196	0.44		0.84 ± 0.06	0.81 ± 0.04	0.90 ± 0.03	0.94 ± 0.03
VC₂₋₆₋₂ CC (<i>n</i>-hexane/EtOAc/MeOH)	205	0.46					
VC₂₋₆₋₂₋₁ (10% EtOAc:<i>n</i>-hexane)	138	0.31		0.79 ± 0.01	0.78 ± 0.01	0.77 ± 0.03	0.83 ± 0.02
VC ₂₋₆₋₂₋₂ (50% EtOAc: <i>n</i> -hexane//MeOH)	26	0.06		1.85 ± 0.04	1.82 ± 0.02	1.96 ± 0.01	1.89 ± 0.01
VC ₂₋₆₋₂₋₃ (100% MeOH)	34	0.08		2.70 ± 0.02	2.65 ± 0.02	2.41 ± 0.04	2.60 ± 0.03
VC₂₋₆₋₂₋₁ PTLC (4% EtOAc:<i>n</i>-hexane)	138	0.31					
VC ₂₋₆₋₂₋₁₋₁	29	0.06		1.54 ± 0.01	1.49 ± 0.01	1.79 ± 0.03	1.84 ± 0.02
VC₂₋₆₋₂₋₁₋₂ (Compound 3)	79	0.18	0.81	0.63 ± 0.04	0.72 ± 0.02	0.74 ± 0.01	0.76 ± 0.01
VC₂₋₆₋₄ RP C18 PHPLC (80% MeCN:MeOH)	214	0.48					
VC₂₋₆₋₄₋₁ (Compound 4)	59	0.13	0.67	0.71 ± 0.01	0.76 ± 0.01	0.89 ± 0.03	0.92 ± 0.02
VC ₂₋₆₋₄₋₂	121	0.27		1.84 ± 0.04	2.02 ± 0.02	2.11 ± 0.01	2.15 ± 0.01
VC₂₋₆₋₅ PTLC (4% EtOAc:<i>n</i>-hexane)	510	1.13					
VC ₂₋₆₋₅₋₁	342	0.76		1.36 ± 0.01	1.94 ± 0.01	1.49 ± 0.03	1.64 ± 0.02

VC₂₋₆₋₅₋₂ (Compound 8)	143	0.32	0.42	0.86 ± 0.04	0.94 ± 0.02	1.05 ± 0.01	1.03 ± 0.01
VC₂₋₆₋₆ CC (<i>n</i>-hexane/EtOAc/MeOH)	196	0.44					
VC ₂₋₆₋₆₋₁ CC (<i>n</i> -hexane/EtOAc/MeOH)	14	0.03		1.65 ± 0.01	1.67 ± 0.01	1.68 ± 0.03	1.57 ± 0.02
VC₂₋₆₋₆₋₂ CC (<i>n</i>-hexane/EtOAc/MeOH)	134	0.30		0.81 ± 0.04	0.79 ± 0.02	0.85 ± 0.01	0.91 ± 0.01
VC ₂₋₆₋₆₋₃ CC (<i>n</i> -hexane/EtOAc/MeOH)	16	0.04		1.97 ± 0.02	1.87 ± 0.02	1.67 ± 0.04	1.54 ± 0.03
VC ₂₋₆₋₆₋₄ CC (<i>n</i> -hexane/EtOAc/MeOH)	24	0.05		2.01 ± 0.03	2.10 ± 0.03	2.08 ± 0.05	2.09 ± 0.04
VC₂₋₆₋₆₋₂ RP C18 PHPLC (80% MeCN:MeOH)	134	0.30					
VC ₂₋₆₋₆₋₂₋₁	23	0.05		1.70 ± 0.01	1.76 ± 0.01	1.79 ± 0.03	1.76 ± 0.02
VC₂₋₆₋₆₋₂₋₂ (Compound 5)	69	0.15	0.73	0.69 ± 0.04	0.78 ± 0.02	0.76 ± 0.01	0.80 ± 0.01
VC ₂₋₆₋₆₋₂₋₂	32	0.07		1.76 ± 0.01	1.87 ± 0.02	1.54 ± 0.03	1.79 ± 0.03

[#]The percentage of yield was calculated on the basis of crude EtOAc:MeOH extract (45.0 g EtOAc:MeOH crude extract weight). CC-column chromatography; FC-flash chromatography; PTLC-preparative thin layer chromatography; PHPLC-preparatory high pressure liquid chromatography; EtOAc-ethyl acetate; MeOH-methanol. The samples were analyzed in triplicate (n=3) and expressed as mean ± standard deviation. *The IC₅₀ values were expressed as mg/mL

The fraction, VC₃ (11.0 g; 24.44%) eluted at 100% EtOAc was subjected to vacuum liquid chromatography using the step-wise elution of *n*-hexane/EtOAc/MeOH to furnish 6 sub-groups (VC₃₋₁-VC₃₋₆). Among these, the column fractions, such as VC₃₋₄ (1640 mg; 3.64%) and VC₃₋₆ (1540 mg; 3.42%) were displayed significantly higher antioxidant activities with respect to scavenge DPPH (IC₅₀ 0.98 and 0.69 mg/mL, respectively) and ABTS⁺ (IC₅₀ 1.03 and 0.71 mg/mL, respectively) radicals. The anti-inflammatory effects were also greater for VC₃₋₄ (IC₅₀ anti-COX-2 0.93 mg/mL and IC₅₀ anti-5-LOX 1.01 mg/mL) and VC₃₋₆ (IC₅₀ anti-COX-2 0.65 mg/mL and IC₅₀ anti-5-LOX 0.74 mg/mL) when compared to other fractions (IC₅₀ > 1.25 mg/mL) (Table 5.4.).

The sub-fraction, VC₃₋₄ fractionated by flash chromatographic purification using *n*-hexane/EtOAc/MeOH to yield five pooled sub-fractions (VC₃₋₄₋₁-VC₃₋₄₋₅). The fraction, VC₃₋₄₋₃ has registered greater antioxidant (IC₅₀ DPPH quenching 0.84 mg/mL and IC₅₀ ABTS⁺ quenching 0.79 mg/mL) and anti-inflammatory (IC₅₀ anti-COX-2 0.76 mg/mL and IC₅₀ anti-5-LOX 0.68 mg/mL) potentials when compared to other fractions (IC₅₀ > 1.40 mg/mL). The RP C18 PHPLC purification of VC₃₋₄₋₃ afforded two pure bioactive compounds, **6** (169 mg; 0.38%; VC₃₋₄₋₃₋₁) and **7** (156 mg; 0.35%; VC₃₋₄₋₃₋₂) (Table 5.4.).

Another active fraction, VC₃₋₆ fractionated by flash chromatographic purification with *n*-hexane/EtOAc/MeOH to acquire three sub-fractions, VC₃₋₆₋₁ (546 mg; 1.21%), VC₃₋₆₋₂ (489 mg; 1.09%) and VC₃₋₆₋₃ (213 mg; 0.47%). The fractions, VC₃₋₆₋₁ and VC₃₋₆₋₂ were selected for further purifications due to their greater antioxidant (IC₅₀ DPPH scavenging 0.71-0.81 mg/mL and IC₅₀ ABTS⁺ scavenging 0.73-0.86 mg/mL) and anti-inflammatory (IC₅₀ anti-COX-2 0.74-0.81 mg/mL and IC₅₀ anti-5-LOX 0.79-0.84 mg/mL) potentials. The fraction, VC₃₋₆₋₁ on further purification by PTLC (using 2% EtOAc:*n*-hexane) resulted in the isolation of compound **1** (147 mg; 0.33%; VC₃₋₆₋₁₋₁) along with a minor fraction, VC₃₋₆₋₁₋₂. The other fraction, VC₃₋₆₋₂ on PTLC (5% EtOAc:*n*-hexane) fractionation yielded the compound **2** (96 mg; 0.21%; VC₃₋₆₋₂₋₁) along with two minor fractions (VC₃₋₆₋₂₋₂) (Table 5.4.).

Table 5.4.: The yield (in mg and in %), retention factor (R_f), bioactivities (antioxidant/anti-inflammatory) of column/flash/PTLC/PHPLC fractions obtained from the sub-fraction, VC₃ of EtOAc:MeOH extract of *V. cyprinoides*

	#Yield		R _f	*Bioactive potentials (IC ₅₀ value; mg/mL)			
	mg	%		Antioxidant		Anti-inflammatory	
				DPPH	ABTS ⁺	COX-2	5-LOX
VC ₃ FC (<i>n</i> -hexane/EtOAc/MeOH)	11000	24.44		1.06 ± 0.05	1.06 ± 0.06	1.10 ± 0.07	1.01 ± 0.08
VC ₃₋₁	2500	5.56		2.16 ± 0.04	1.25 ± 0.00	1.21 ± 0.02	1.92 ± 0.04
VC ₃₋₂	1113	2.47		2.35 ± 0.05	2.42 ± 0.04	2.16 ± 0.04	2.12 ± 0.00
VC ₃₋₃	1320	2.93		2.05 ± 0.06	2.02 ± 0.05	2.06 ± 0.05	2.02 ± 0.01
VC ₃₋₄	1640	3.64		0.98 ± 0.00	1.03 ± 0.02	0.93 ± 0.03	1.01 ± 0.04
VC ₃₋₅	1227	2.73		2.42 ± 0.04	2.12 ± 0.00	1.42 ± 0.03	1.26 ± 0.07
VC ₃₋₆	1540	3.42		0.69 ± 0.02	0.71 ± 0.02	0.65 ± 0.01	0.74 ± 0.01
VC ₃₋₄ FC (<i>n</i> -hexane/EtOAc/MeOH)	1640	3.64					
VC ₃₋₄₋₁	281	0.62		1.94 ± 0.04	1.66 ± 0.05	1.56 ± 0.03	1.82 ± 0.10
VC ₃₋₄₋₂	240	0.53		1.40 ± 0.03	1.63 ± 0.04	1.67 ± 0.02	1.86 ± 0.09
VC ₃₋₄₋₃	398	0.88		0.84 ± 0.02	0.79 ± 0.03	0.76 ± 0.01	0.68 ± 0.08
VC ₃₋₄₋₄	291	0.65		1.54 ± 0.04	1.30 ± 0.05	1.49 ± 0.03	1.85 ± 0.10
VC ₃₋₄₋₅	289	0.64		1.68 ± 0.09	1.76 ± 0.02	1.84 ± 0.03	1.36 ± 0.04
VC ₃₋₄₋₃ RP C18 PHPLC (80% MeCN:MeOH)	398	0.88					
VC ₃₋₄₋₃₋₁ (Compound 6)	169	0.38	0.62	0.76 ± 0.01	0.85 ± 0.01	0.90 ± 0.03	0.96 ± 0.02
VC ₃₋₄₋₃₋₂ (Compound 7)	156	0.35	0.68	0.79 ± 0.04	0.87 ± 0.02	0.89 ± 0.01	0.98 ± 0.01

VC₃₋₆ FC (<i>n</i>-hexane/EtOAc/MeOH)	1540	3.42					
VC₃₋₆₋₁	546	1.21		0.71 ± 0.01	0.73 ± 0.01	0.74 ± 0.03	0.79 ± 0.02
VC₃₋₆₋₂	489	1.09		0.81 ± 0.04	0.86 ± 0.02	0.81 ± 0.01	0.84 ± 0.01
VC ₃₋₆₋₃	213	0.47		1.85 ± 0.05	1.82 ± 0.03	1.99 ± 0.02	1.89 ± 0.02
VC₃₋₆₋₁ PTLC (2% EtOAc:<i>n</i>-hexane)	546	1.21					
VC₃₋₆₋₁₋₁ (Compound 1)	147	0.33	0.63	0.59 ± 0.01	0.67 ± 0.01	0.70 ± 0.03	0.77 ± 0.02
VC ₃₋₆₋₁₋₂	213	0.47		1.82 ± 0.03	1.99 ± 0.02	1.91 ± 0.01	1.85 ± 0.05
VC₃₋₆₋₂ PTLC (5% EtOAc:<i>n</i>-hexane)	489	1.09					
VC₃₋₆₋₂₋₁ (Compound 2)	96	0.21	0.51	0.54 ± 0.01	0.62 ± 0.01	0.65 ± 0.03	0.75 ± 0.02
VC ₃₋₆₋₂₋₂	195	0.43		1.80 ± 0.04	2.35 ± 0.05	2.42 ± 0.04	1.94 ± 0.01

[#]The percentage of yield was calculated on the basis of crude EtOAc:MeOH extract (45.0 g EtOAc:MeOH crude extract weight). CC-Column chromatography; FC-Flash chromatography; PTLC-Preparative thin layer chromatography; PHPLC-Preparatory high pressure liquid chromatography; EtOAc-Ethyl acetate; MeOH-Methanol. The samples were analyzed in triplicate (n=3) and expressed as mean ± standard deviation. *The IC₅₀ values were expressed as mg/mL

5.3.2. Spectroscopic analysis of bioactive secondary metabolites isolated from EtOAc:MeOH extract of *V. cyprinoides*

Repetitive chromatographic fractionations of EtOAc:MeOH extract of *V. cyprinoides* yielded potent bioactive secondary metabolites. The structures of identified metabolites assigned by extensive one (^1H , ^{13}C and $^{135}\text{DEPT}$ NMR) and two (^1H - ^1H COSY, HSQC, HMBC and NOESY) dimensional spectroscopic experimentations combined with mass and FTIR experiments. The characterized bioactive secondary metabolites from *V. cyprinoides* classified under various classes, such as spirocyclic ether derivatives (**1-2**), irregular meroterpenoids (**3-5**), hexahydro isochromenyls (**6-7**) and cholesterol derivatives (**8-10**).

5.3.2.1. Structural characterization of spirocyclic ether derivatives (**1-2**)

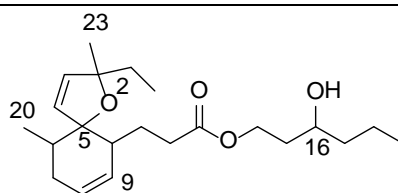
The compounds with *O*-heterocyclic-spiro functionalities were found to be significant bioactive agents among various classes of organic compounds and present in many natural products (Blunt *et al.*, 2015; Perron and Albizati 1989; Wermuth 1996; Zheng *et al.*, 2014). Spiro compounds enclosed two rings (identical or different rings) shared with one atom (the quaternary spiroatom). The conformation of ligands (compounds) has been rigidified by the introduction of ring framework and the cyclic derivatives apparently experience a reduced conformational stress when it binds to a target site (enzymes or proteins). Moreover, the conformational restraint can be executed by the addition of spiro ring skeletons (Wermuth 1996). A search for newer compounds with *O*-heterocyclic-spiro ring systems as principle bioactive domains along with lower lipophilic ($\log P_{\text{ow}} < 5$) factor and greater electronegative functionalities in the pharmacophore templates appeared to be vital for bioactive potentials and bioavailability. Spirocyclic ether compounds enclosed rearranged monocyclofarnesyl framework (Schmitz and McDonald 1974) with a dihydrofuran ring spiro fused to substituted cyclohexene framework coupled with an oxaspiro[4.5]deca-dienyl skeleton. The di-tertiary ether natures of these compounds were detailed in previous literatures of dactyloxene derivatives (Schmitz *et al.*, 1981).

The spirocyclic ether possessing unrearranged monocyclofarnesane skeleton were previously reported from mollusk, *Aplysia dactylomela* (Schmitz *et al.*, 1978). Herein, we have reported the characterization of two spirocyclic ether derivatives,

named as 16-hydroxyhexyl-(2-ethyl-2,6-dimethyl-1-oxaspiro[4.5]dec-3,8-dien)-10-propanoate (**1**) and (*E*)-18-ethyl-17,19-dihydroxyhept-14-enyl-(2-ethyl-2,6-dimethyl-1-oxaspiro[4.5]dec-3,8-dien)-10-acetate (**2**) with the help of comprehensive NMR and mass analyses.

5.3.2.1.A. Structural characterization of compound **1** (VC₃₋₆₋₁₋₁)

16-Hydroxyhexyl-(2-ethyl-2,6-dimethyl-1-oxaspiro[4.5]dec-3,8-dien)-10-propanoate (**1**)



Yield	147 mg; 0.33%
Physical description	Yellow oily
Molecular formula	C ₂₂ H ₃₆ O ₄
Molecular mass	364.2614

The irregularly prenylated spirocyclic ether derivative, 16-hydroxyhexyl-(2-ethyl-2,6-dimethyl-1-oxaspiro[4.5]dec-3,8-dien)-10-propanoate isolated as yellow oily compound. It displayed UV absorbance (in MeOH) at λ_{max} (log ϵ 2.55) 231.9 nm assigned to a chromophore with olefinic and carbonyl systems (Figure 5.4.). The purity of compound supported by RP C18 HPLC {using 8:2 MeOH:MeCN, v/v (R_t 5.33)} experiments (Figure 5.5.).

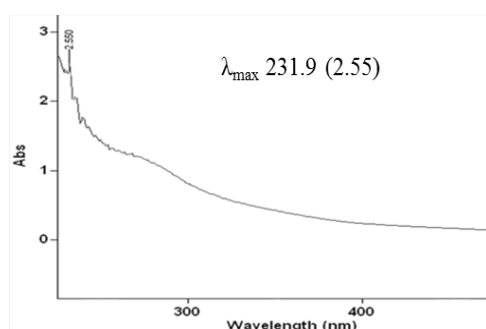


Figure 5.4.: UV spectrum of 16-hydroxyhexyl-(2-ethyl-2,6-dimethyl-1-oxaspiro[4.5]dec-3,8-dien)-10-propanoate (**1**)

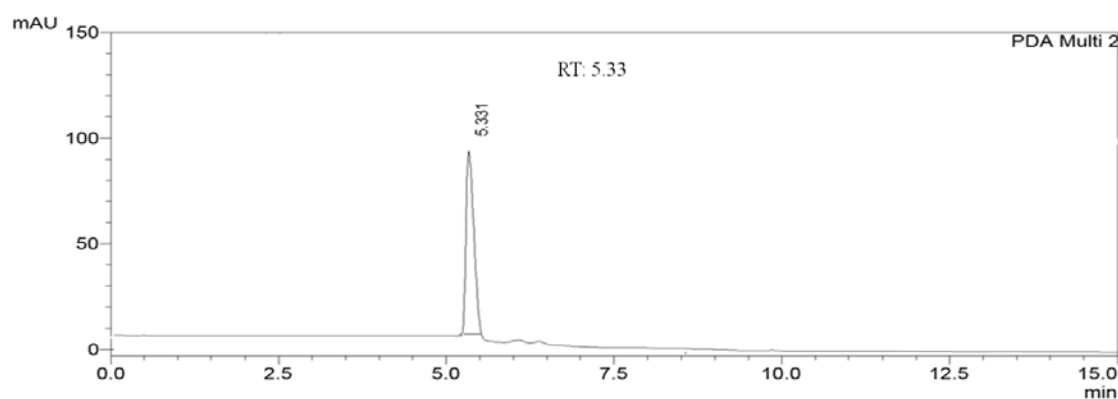


Figure 5.5.: HPLC chromatogram of 16-hydroxyhexyl-(2-ethyl-2,6-dimethyl-1-oxaspiro[4.5]dec-3,8-dien)-10-propanoate (**1**)

The irregularly spirocyclic ether derivative (**1**) with molecular formula $C_{22}H_{36}O_4$, recorded its molecular ion peak at m/z 364 (EIMS found m/z 364.2620 $[M]^+$, cal. for $C_{22}H_{36}O_4$ 364.2614), which exhibited double bond indices of five corresponding to three double bonds and two rings. The compound has a rearranged monocyclofarnesyl framework (Schmitz and McDonald 1974) with a dihydrofuran ring spiro-fused to substituted cyclohexene framework, and found to possess an oxaspiro[4.5]deca-dienyl skeleton. This spirocyclic ether skeleton bonded to hydroxyhexyl fragment through carboxylate $\{-(C=O)-O-\}$ group which was attributed by COSY, HSQC and HMBC experiments (Figure 5.11.-5.13.). The titled compound exhibited chemical shifts for four each of methyls and sp^2 methines, three sp^3 methines, eight sp^3 methylenes and three quaternary (one carboxylate and two oxygenated) carbons, which were assigned by exhaustive 1H along with ^{13}C NMR and DEPT experiments (Figure 5.8.-5.10.; Table 5.5.). The 1H and ^{13}C resonances were exhibited characteristic signals for one each of ester carbonyl (δ_C 173.95), oxygenated methylene (δ_H 4.18, 4.14/ δ_C 65.04), hydroxylated methine (δ_H 3.97/ δ_C 66.47) and carbonyl methylene (δ_H 2.35/ δ_C 34.69), along with two isolated disubstituted alkenes (δ_H 6.50/ δ_C 130.73, δ_H 6.25/ δ_C 135.40 and δ_H 5.35/ δ_C 132.30, δ_H 5.36/ δ_C 129.94). The ^{13}C spectrum enclosed highly deshielded singlet resonances for two carbon atoms directly bonded to oxygen, and were found at δ 82.17 (C-2) and 79.47 (C-5). These attributions demonstrated the di-tertiary ether nature of the title compound, as supported by previous literatures of dactyloxene derivatives (Schmitz *et al.*, 1981). Greatly deshielded sp^2 protons at δ 6.50 (H-3) and 6.25 (H-4) with doublet splitting were

attached to δ 130.73 and 135.40, respectively as derived from the HSQC data. Both protons were directly connected by one bond ^1H - ^1H COSY conjunctions (H-3 to H-4) and exhibited HMBC interactions with the carbons at δ 82.17 (C-2) and 79.47 (C-5). Also, HMBC relations were apparent from H-3 to C-4 and H-4 to C-3, thus, the dihydrofuran ring with two quaternary carbon atoms at C-2 and C-5 were confirmed. The C-2 position was satisfied by one each of singlet methyl (δH 1.25/ δC 22.54) and ethyl groups. The spin system was apparent between the H-21 and H-22 $\{\delta$ 1.86 (H-21)/0.88 (H-22); $-\text{CH}_2-\text{CH}_3\}$ (Figure 5.6.A). The attachment of ethyl and methyl groups to the basic dihydrofuran ring of spirocyclic ether was confirmed by HMBCs from δ 1.86 (H-21) to δ 82.17 (C-2); δ 0.88 (H-22) to δ 22.54 (C-23), 82.17 (C-2) and δ 1.25 (H-23) to δ 82.17 (C-2), 130.73 (C-3) (Figure 5.6.B). The two spin systems, H-6 to H-8 $\{\delta$ 2.10 (H-6)/2.02 (H-7)/5.35 (H-8) $\}$ comprising H-6 to H-20 $\{\delta$ 2.10 (H-6)/1.01 (H-20) $\}$ and H-9 to H-10 $\{\delta$ 5.36 (H-9)/2.32 (H-10) $\}$ together with HMBC correlations from δ 2.02 (H-7) to δ 129.94 (C-9), 34.11 (C-10); δ 1.01 (H-20) to δ 36.89 (C-6), 132.30 (C-8), 34.11 (C-10) attributed for 6-methyl cyclohexene ring system. This 6-methyl cyclohexene directly linked to 2-ethyl-2-methyl dihydrofuran at C-5 quaternary carbon (δ 79.47), hence the bicyclic framework, oxaspiro[4.5]deca-diene was satisfied. The oxaspiro[4.5]deca-dienyl skeleton ascertained by HMBC relations, such as δ 6.25 (H-4) to δ 36.89 (C-6); δ 2.02 (H-7) to δ 79.47 (C-5); δ 2.32 (H-10) to δ 79.47 (C-5) and δ 1.01 (H-20) to δ 135.40 (C-4), 79.47 (C-5). The short bond ^1H - ^1H COSYs from H-10 to H-12 $\{\delta$ 2.32 (H-10)/1.61 (H-11)/2.35 (H-12) $\}$ proved the attachment of propanoate part of 16-hydroxyhexyl-propanoate at C-10. Further, long bond relations, such as δ 2.32 (H-10) to δ 173.95 (C-13); δ 1.61 (H-11) to δ 173.95 (C-13) and δ 2.35 (H-12) to δ 24.88 (C-11) confirmed the side chain assignments. Higher chemical shift signals at δ 4.18, 4.14 (H-14) exhibiting HSQC cross peaks with δC 65.04 was located at the oxygen end of carboxylate $\{-\text{C}(=\text{O})-\text{O}-\text{CH}_2-\}$ and signal at δ 3.94 (H-16, m) displayed HSQC correlation with δC 66.47 was directly bonded to hydroxyl $\{-\text{CH}(\text{OH})-\}$ group of 16-hydroxyhexyl-10-propanoate side chain. The occurrence of side chain affirmed by spin systems from H-14 to H-19 $\{\delta$ 4.18, 4.14 (H-14)/1.92 (H-15)/3.97 (H-16)/1.52 (H-17)/1.30 (H-18)/0.82 (H-19) $\}$ and HMBCs from δ 4.18 (H-14) to δ 66.47 (C-16); δ 3.97 (H-16) to δ 65.04 (C-14) and δ 1.30 (H-18) to δ 14.12 (C-19). The linkage of 16-hydroxyhexyl part to the oxygenated end of 10-propanoate moiety established by

HMBC connections from δ 4.18 (H-14) to δ 173.95 (C-13) and δ 1.92 (H-15) to δ 173.95 (C-13). Remarkably, the two di-substituted olefinic groups at δ 6.50 (H-3), 6.25 (H-4) and δ 5.35 (H-8), 5.36 (H-9) had lower coupling constants (J) of 8.84, 8.84 and 3.93, 3.54 Hz, respectively. Thus, the configuration of these olefinic groups in oxaspiro[4.5]dec-3,8-diene affirmed as *cis* (*Z*) orientation. The relative configurations at chiral centers, mainly at C-6, C-10 and C-16 were deduced by extensive NOESY experiments (Figure 5.14.). The NOE correlations from δ 3.97 (H-16)/2.10 (H-6)/6.25 (H-4)/6.50 (H-3)/5.35 (H-2)/2.02 (H-7)/1.25 (H-23)/4.18 (H-14 α) confirmed the close proximity of these protons with each other and their same plane of alignment, and therefore, were arbitrarily assigned as α -disposed. The alkenic protons exhibited NOE couplings with each other, and this further confirmed its *cis* (*Z*) orientation. The hydroxyl (-OH) group at C-16 position was placed opposite to α -disposed proton at δ 3.97 and it was attributed as β -hydroxylated. The ethyl and singlet methyl at C-2 disposed at β and α disposition, respectively, as deduced from NOESYs and previous reports (Schmitz *et al.*, 1978). Other NOEs recorded among δ 1.01 (H-20)/2.32 (H-10)/4.14 (H β -14), which implied that these were on identical molecular plane, but did not show couplings with α -oriented protons, and therefore, assigned as β -aligned with regard to molecular plane of symmetry. The β -disposed H-10 proton further confirmed the α -disposition of the side chain, 16-hydroxyhexyl-10-propanoate (Figure 5.7.).

Table 5.5.: NMR spectroscopic data of 16-hydroxyhexyl-(2-ethyl-2,6-dimethyl-1-oxaspiro[4.5]dec-3,8-dien)-10-propanoate (**1**) in CDCl₃

C. No.	¹³ C	¹ H (int.,mult., J in Hz) ^a	COSY	HMBC
1	-	-	-	-
2	82.17	-	-	-
3	130.73	6.50 (1H α ,d,8.84)	H-4	C-4,2,5
4	135.40	6.25 (1H α ,d,8.84)	-	C-3,2,5,6
5	79.47	-	-	-
6	36.89	2.10 (1H α ,m)	H-20,7	-
7	27.22	2.02 (2H,t)	H-8	C-8,9,5,10
8	132.30	5.35 (1H α ,t,3.93)	-	C-7
9	129.94	5.36 (1H α ,t,3.54)	H-10	-
10	34.11	2.32 (1H β ,m)	H-11	C-5,13,11
11	24.88	1.61 (2H,m)	H-12	C-10,12,13
12	34.69	2.35 (2H,t)	-	C-11,13
13	173.95	-	-	-

14	65.04	4.18 (1H α ,t) 4.14 (1H β ,t)	H-15	C-13,16
15	39.43	1.92 (2H,m)	H-16	C-14,16,13
16	66.47	3.97 (1H α ,m)	H-17	C-14
17	31.92	1.52 (2H,m)	H-18	C-18
18	29.70	1.30 (2H,m)	H-19	C-19
19	14.12	0.82 (3H,t)	-	C-18,17
20	22.69	1.01 (3H β ,s)	-	C-4,5,6,10,8
21	30.06	1.86 (2H,m)	H-22	C-22,2
22	18.17	0.88 (3H,t)	-	C-23,21,2
23	22.54	1.25 (3H α ,s)	-	C-2,3

^1H NMR spectra recorded using Bruker AVANCE III 500MHz (AV 500) spectrometer (Bruker, Karlsruhe, Germany) in CDCl_3 as aprotic solvent at ambient temperature with TMS as the internal standard (δ 0 ppm). The ^1H NMR spectra were recorded at 500MHz, while the ^{13}C NMR spectra were recorded at 125MHz. ^aValues in ppm, multiplicity and coupling constants ($J=\text{Hz}$) were indicated in parentheses. The assignments were made with the aid of the ^1H - ^1H COSY, HSQC, HMBC and NOESY experiments

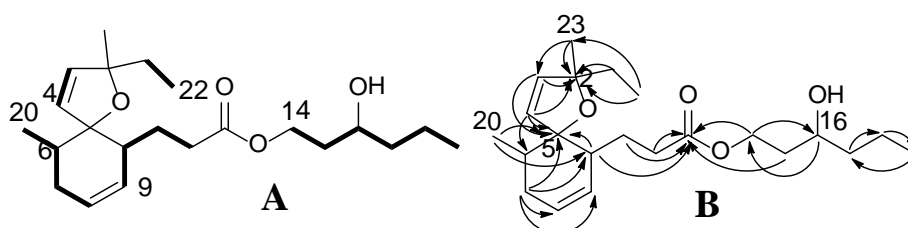


Figure 5.6.: ^1H - ^1H COSY (A) and HMBC (B) correlations of 16-hydroxyhexyl-(2-ethyl-2,6-dimethyl-1-oxaspiro[4.5]dec-3,8-dien)-10-propanoate (**1**). The key ^1H - ^1H COSY couplings have been represented by bold face bonds. The HMBC couplings were indicated by double barbed arrow

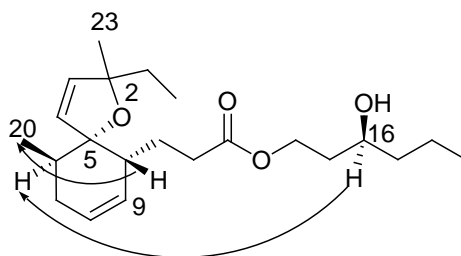


Figure 5.7.: NOESY correlations of 16-hydroxyhexyl-(2-ethyl-2,6-dimethyl-1-oxaspiro[4.5]dec-3,8-dien)-10-propanoate (**1**). The NOESY relations were represented by double barbed arrow

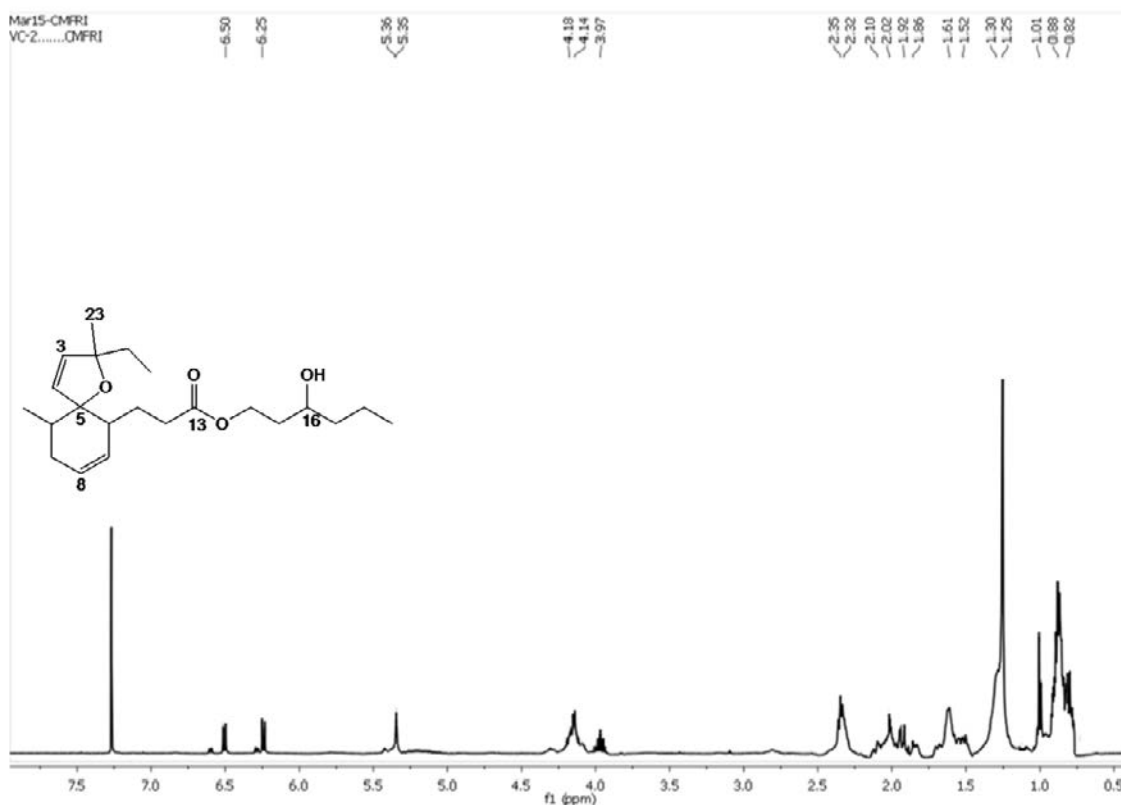


Figure 5.8.: ^1H NMR spectrum of 16-hydroxyhexyl-(2-ethyl-2,6-dimethyl-1-oxaspiro[4.5]dec-3,8-dien)-10-propanoate (**1**)

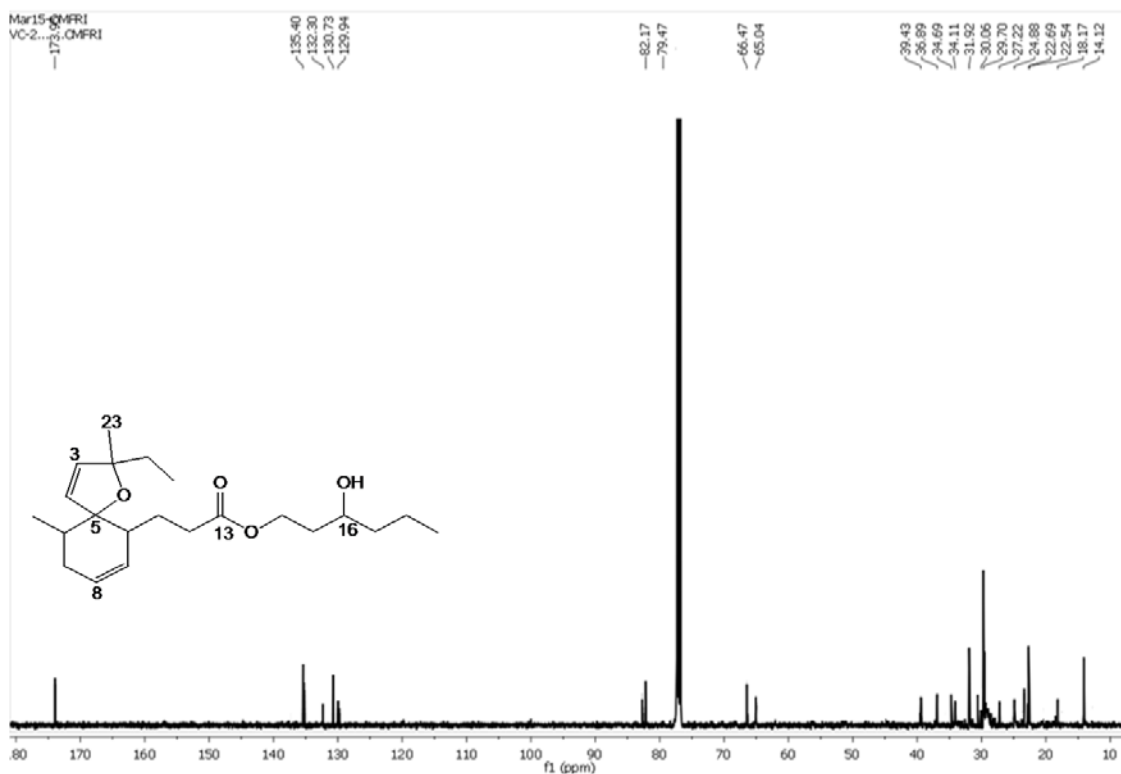


Figure 5.9.: ^{13}C NMR spectrum of 16-hydroxyhexyl-(2-ethyl-2,6-dimethyl-1-oxaspiro[4.5]dec-3,8-dien)-10-propanoate (**1**)

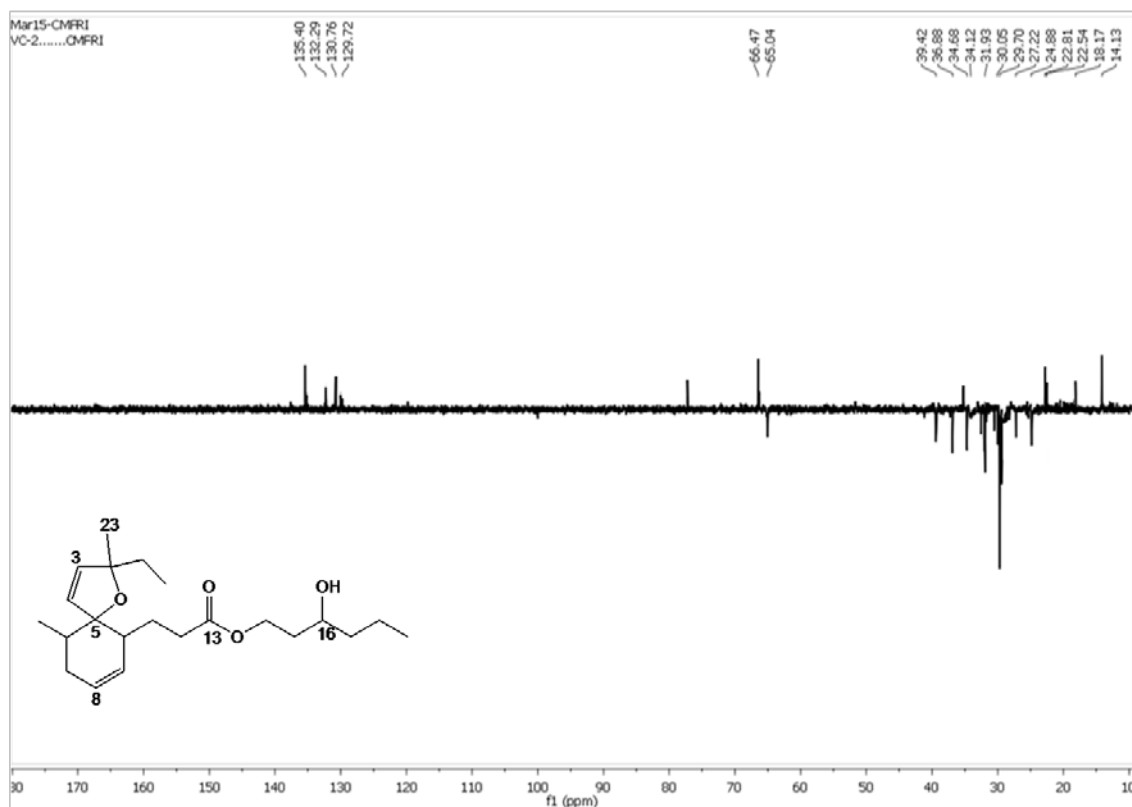


Figure 5.10.: $^{135}\text{DEPT}$ NMR spectrum of 16-hydroxyhexyl-(2-ethyl-2,6-dimethyl-1-oxaspiro[4.5]dec-3,8-dien)-10-propanoate (**1**)

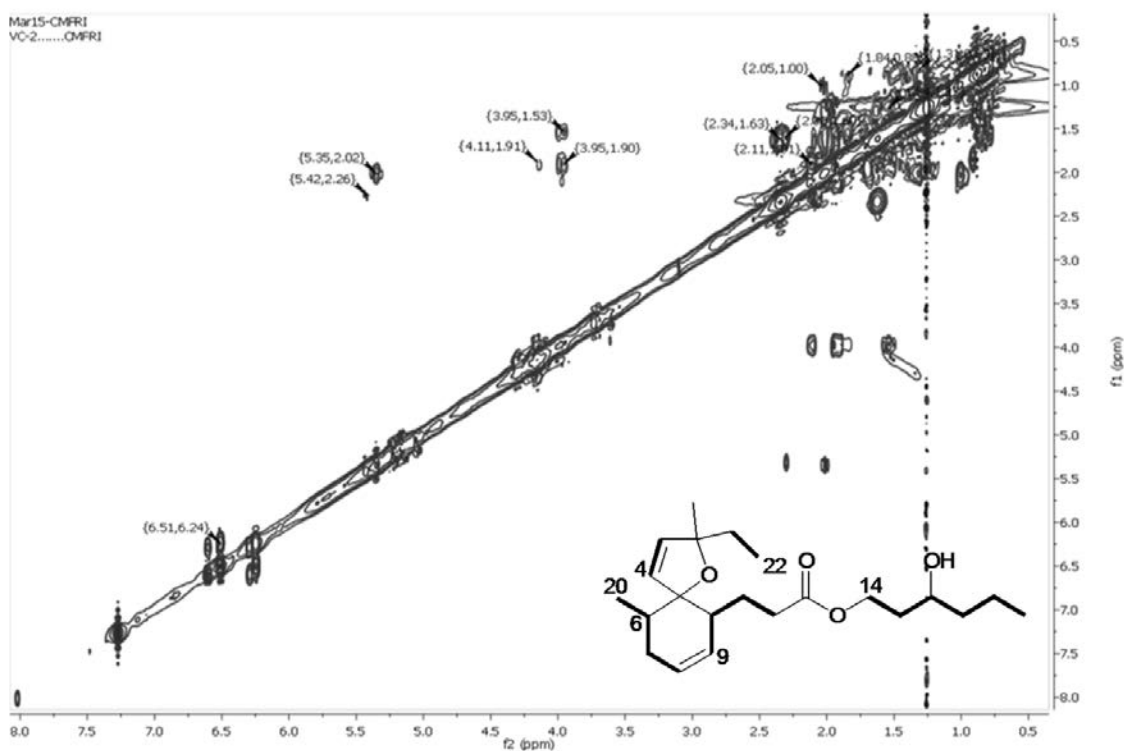


Figure 5.11.: ^1H - ^1H COSY NMR spectrum of 16-hydroxyhexyl-(2-ethyl-2,6-dimethyl-1-oxaspiro[4.5]dec-3,8-dien)-10-propanoate (**1**)

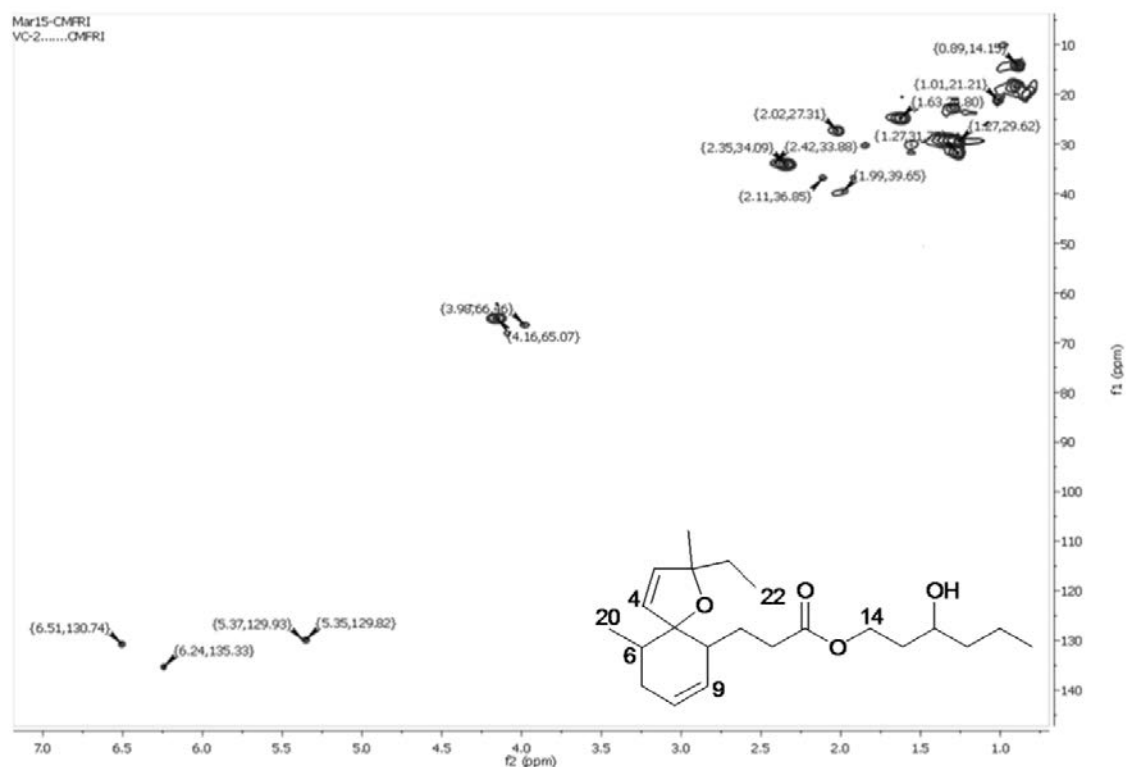


Figure 5.12.: HSQC NMR spectrum of 16-hydroxyhexyl-(2-ethyl-2,6-dimethyl-1-oxaspiro[4.5]dec-3,8-dien)-10-propanoate (**1**)

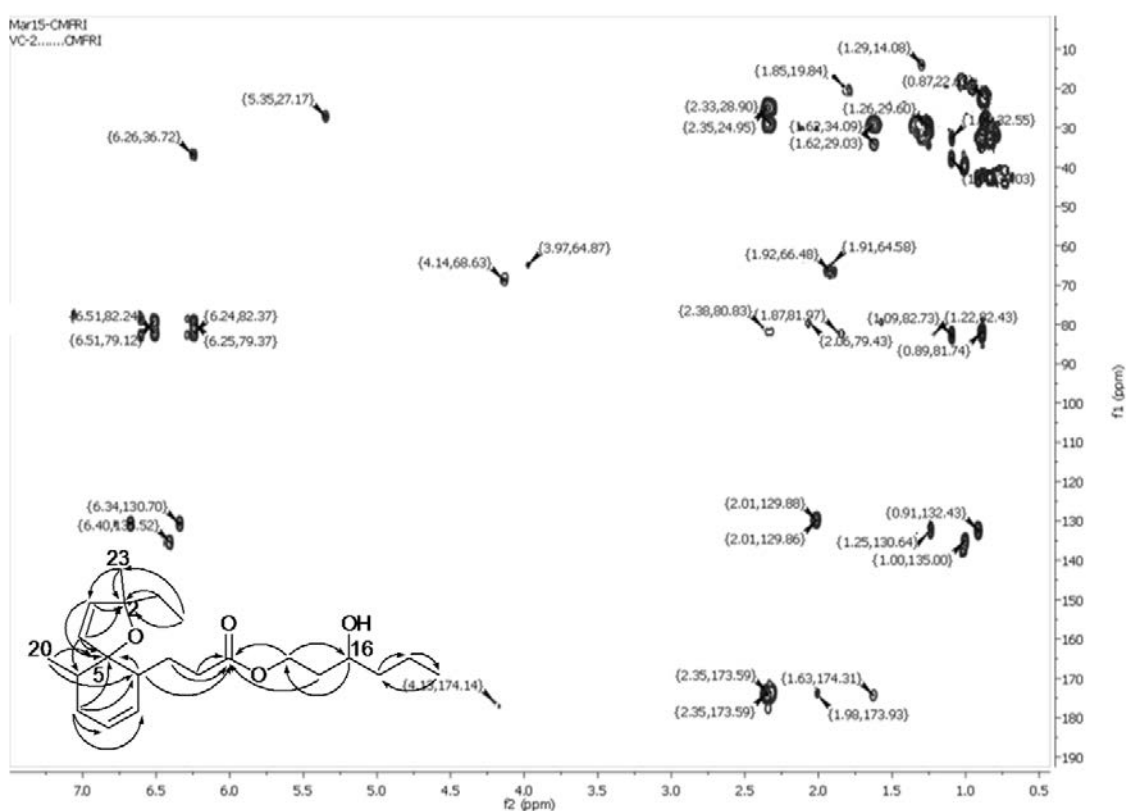


Figure 5.13.: HMBC NMR spectrum of 16-hydroxyhexyl-(2-ethyl-2,6-dimethyl-1-oxaspiro[4.5]dec-3,8-dien)-10-propanoate (**1**)

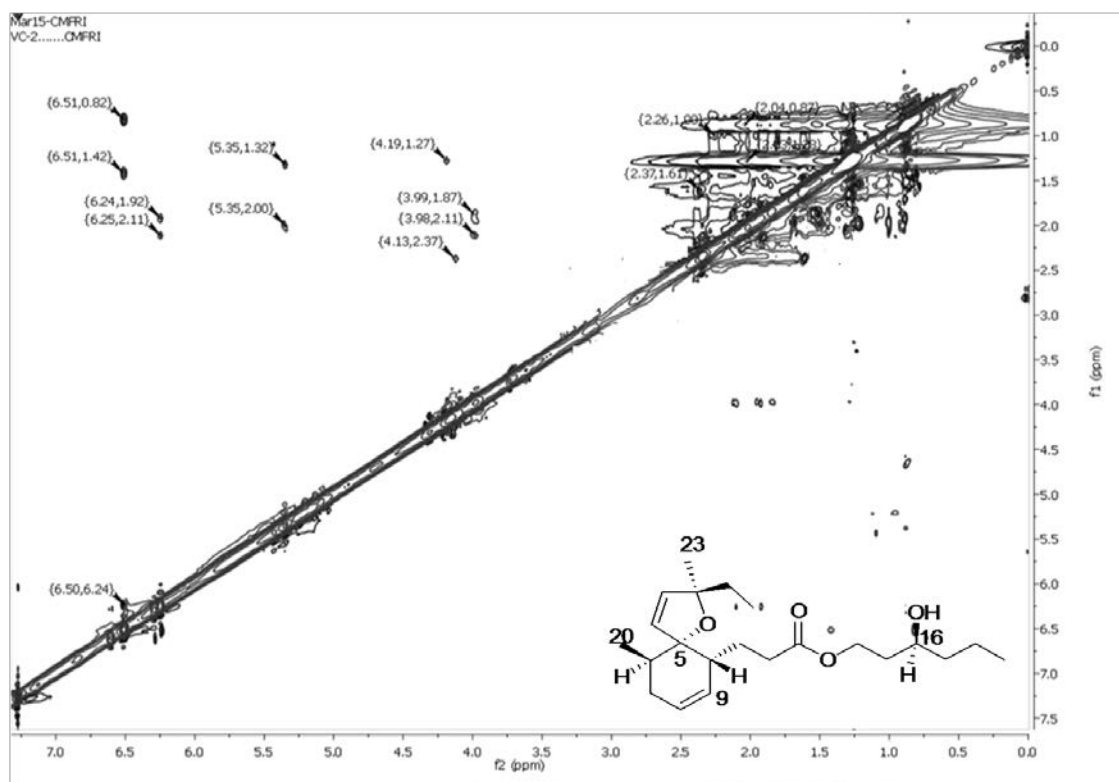


Figure 5.14.: NOESY NMR spectrum of 16-hydroxyhexyl-(2-ethyl-2,6-dimethyl-1-oxaspiro[4.5]dec-3,8-dien)-10-propanoate (**1**)

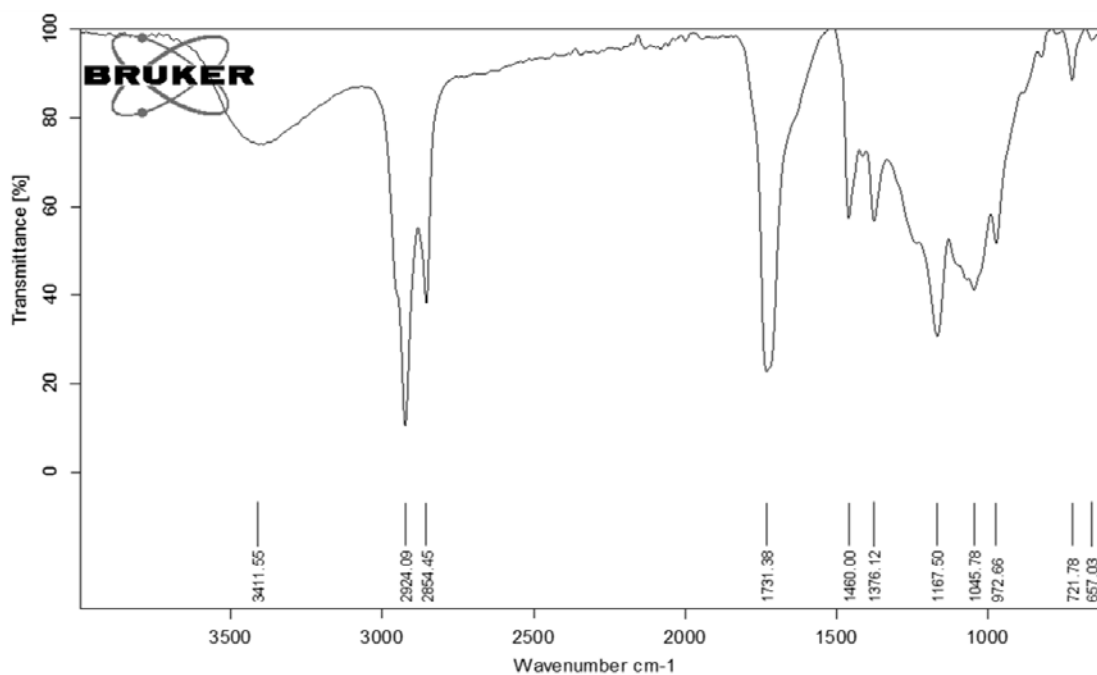


Figure 5.15.: FTIR spectrum of 16-hydroxyhexyl-(2-ethyl-2,6-dimethyl-1-oxaspiro[4.5]dec-3,8-dien)-10-propanoate (**1**)

The compound **1** exhibited infrared absorption stretching vibrations equivalent of hydroxyl at 3411 cm^{-1} , alkoxy (-C-O) at 1045 cm^{-1} and alkanes at 2924 , 2854 cm^{-1} . The absorption band was appeared at 1731 cm^{-1} which recognized the occurrence of an ester carbonyl group (Figure 5.15.).

The mass fragmentation spectrum (Figure 5.16.) indicated that the molecular ion at m/z 364 eliminated a methyl radical to afford an ion at m/z 347 (**a**). The later underwent elimination of methyl and ethyl side chains at C-3 to acquire an ion at m/z 304 (**b**) followed by C_2H_5^+ and two successive $\text{C}_2\text{H}_5\text{O}^+$ radical eliminations registered peaks at m/z 279 (**c**) and 195 (**e**), respectively. The fragment ion at m/z 167 (**f**) was formed from m/z 195 (**e**) by removal of CHO^\bullet radical. The later appeared to undergo ethyl elimination and rearrangements to acquire 3-cyclohexylpropan-1-ol radical (**h**, m/z 140), which fragmented a methoxy and two sequential methyl radicals to yield a base peak of cyclohexane radical (**k**, $\text{C}_6\text{H}_{11}^+$) at m/z 83. Further fragmentations of this cyclohexane radical by two consecutive methyl radical eliminations resulted in the formation of stable butane radical with m/z 57 (**m**) (Figure 5.17.).

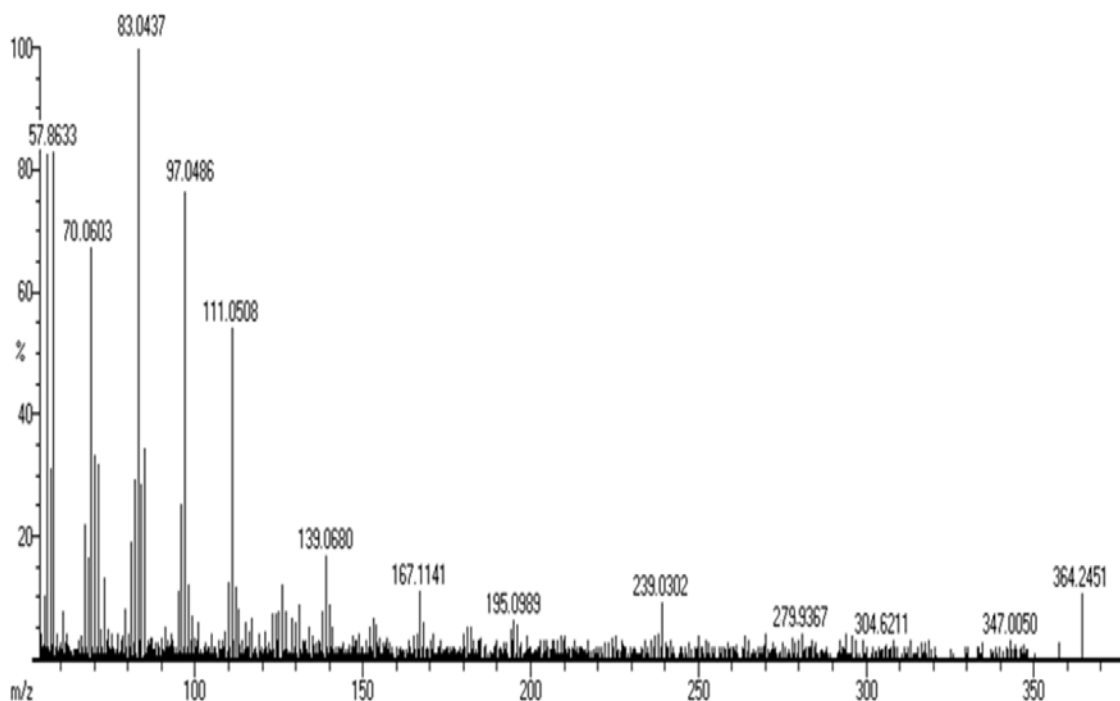


Figure 5.16.: EIMS spectrum of 16-hydroxyhexyl-(2-ethyl-2,6-dimethyl-1-oxaspiro [4.5]dec-3,8-dien)-10-propanoate (**1**)

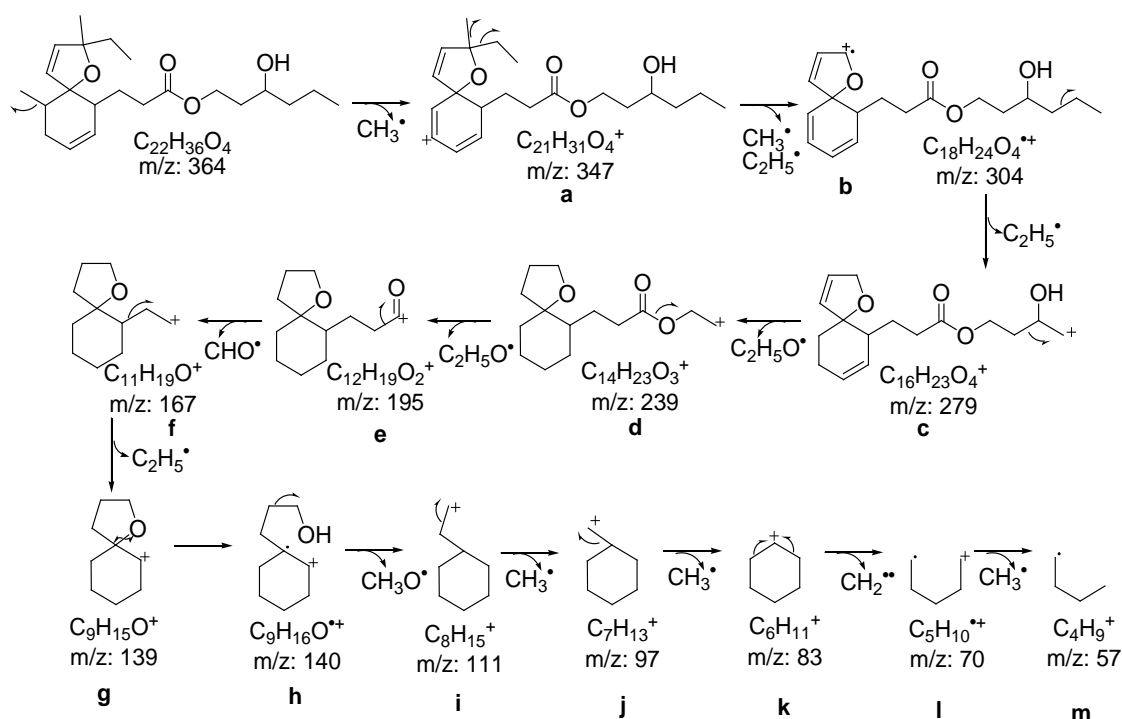
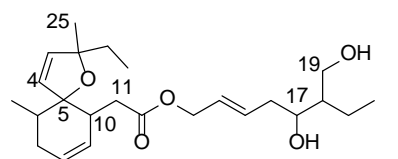


Figure 5.17.: Mass fragmentation pattern of 16-hydroxyhexyl-(2-ethyl-2,6-dimethyl-1-oxaspiro[4.5]dec-3,8-dien)-10-propanoate (**1**)

5.3.2.1.B. Structural characterization of compound 2 (VC₃₋₆₋₂₋₁)

(*E*)-18-Ethyl-17,19-dihydroxyhept-14-enyl-(2-ethyl-2,6-dimethyl-1-oxaspiro[4.5]dec-3,8-dien)-10-acetate (**2**)

	
Yield	96 mg; 0.21%
Physical description	Yellow oily
Molecular formula	$C_{24}H_{38}O_5$
Molecular mass	406.2719

The irregularly prenylated spirocyclic ether derivative, (*E*)-18-ethyl-17,19-dihydroxyhept-14-enyl-(2-ethyl-2,6-dimethyl-1-oxaspiro[4.5]dec-3,8-dien)-10-acetate isolated as yellow oily compound. It displayed UV absorbance (in MeOH) at λ_{max} (log ϵ 2.17) 236 nm and was assigned to a chromophore with olefinic and carbonyl systems

(Figure 5.18.). The purity of the compound was supported by RP C18 HPLC using 8:2 (v/v) MeOH:MeCN (R_t 3.29) experiments (Figure 5.19.).

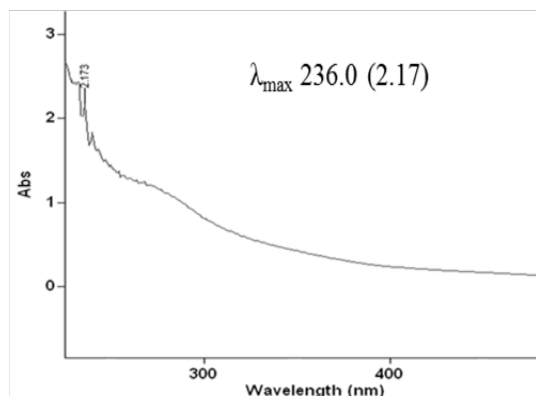


Figure 5.18.: UV spectrum of (*E*)-18-ethyl-17,19-dihydroxyhept-14-enyl-(2-ethyl-2,6-dimethyl-1-oxaspiro[4.5]dec-3,8-dien)-10-acetate (**2**)

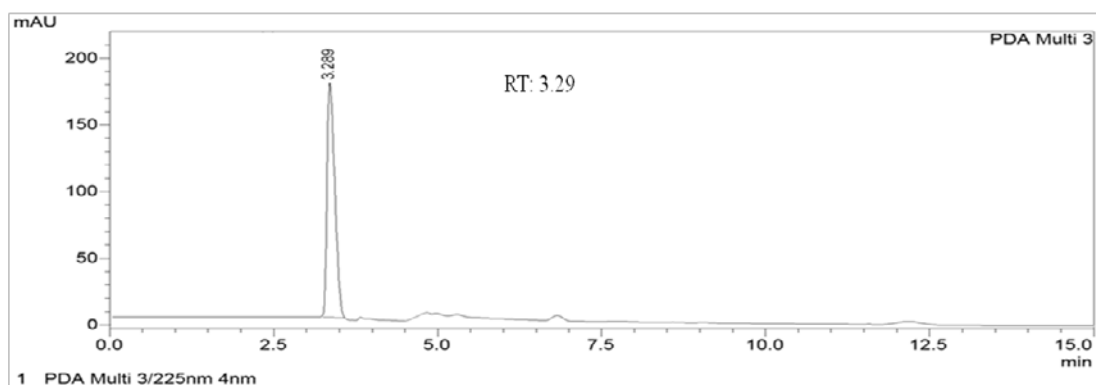


Figure 5.19.: HPLC chromatogram of (*E*)-18-ethyl-17,19-dihydroxyhept-14-enyl-(2-ethyl-2,6-dimethyl-1-oxaspiro[4.5]dec-3,8-dien)-10-acetate (**2**)

The extensive one and two dimensional NMR experimentations (^1H - ^1H COSY, HSQC and HMBC) of irregularly prenylated spirocyclic ether derivative, (**2**) ascertained that the structural attributions of this compound was found to be similar to those of **1** apart from the presence of distinctive 18-ethyl-17,19-dihydroxyhept-14-enyl-10-acetate unit (in **2**) at C-10 (Figure 5.22.-5.27.). Its molecular ion peak was appeared at m/z 406 (EIMS m/z : 406.2725 $[\text{M}]^+$, cal. for $\text{C}_{24}\text{H}_{38}\text{O}_5$, 406.2719) demonstrated the occurrence of six degrees of unsaturations equivalent to four double bonds and two rings. The irregular spirocyclic ether exhibited resonances for four methyls, ten methines, seven sp^3 methylenes and three quaternary (one carboxylate and two oxygenated) carbons (Table 5.6.). The characteristic chemical shift signals

corresponding to ester carbonyl (δ 174.36), three sets of isolated disubstituted alkenes (δ H 6.50/ δ C 130.76, δ H 6.25/ δ C 135.40; δ H 5.38/ δ C 132.30, δ H 5.41/ δ C 129.94 and δ H 5.21/ δ C 130.73, δ H 5.17/ δ C 135.18), one oxygenated methylene (δ H 4.18, 4.15/ δ C 65.15), one hydroxylated methine (δ H 3.97/ δ C 66.46), one hydroxylated methylene (δ H 3.69, 3.60/ δ C 63.33) and one carbonyl methylene (δ H 2.35/ δ C 34.69) characterized from ^1H and ^{13}C resonances. The occurrence of dihydrofuran ring with two oxygenated quaternary carbon shifts at C-2 and C-5 and its attachment to 6-methyl cyclohexene ring moiety at C-5 junction was similar to those as **1**, and these assignments confirmed by extensive ^1H - ^1H COSY and HMBC connections along with earlier reports of dactyloxene compounds (Schmitz *et al.*, 1981). The ^1H - ^1H COSY correlations from H-10 to H-11 { δ 2.81 (H-10)/ δ 2.35 (H-11)} proved the attachment of acetate part of 18-ethyl-17,19-dihydroxyhept-14-enyl-10-acetate side chain at C-10, and this attributions were verified by HMBC from δ 2.35 (H-11) to δ 174.36 (C-12), 65.15 (C-13). The deshielded protons at δ 4.15, 4.18 (H-13) exhibiting HSQC correlation with δ 65.15 was placed at oxygen end of acetate $\{-\text{C}(=\text{O})-\text{O}-\underline{\text{CH}_2}-\}$ unit at C-10. The methine group at C-14 (δ H 3.94 (m)/ δ C 66.47) and methylene group at C-19 (δ H 3.69 (d), 3.60 (d)/ δ C 63.33) directly bonded to hydroxyls (-OH) which were represented by $-\underline{\text{CH}}(-\text{OH})-$ and $-\underline{\text{CH}_2}(-\text{OH})-$ moieties, respectively in heptenyl side chain. Two ^1H - ^1H COSY spin systems from H-13 to H-14 { δ 4.15, 4.18 (H-13)/ δ 5.21 (H-14)} and H-15 to H-19 { δ 5.17 (H-15)/1.92 (H-16)/3.97 (H-17)/1.58 (H-18)/3.69, 3.60 (H-19)} including δ 1.58 (H-18)/1.33 (H-20)/0.80 (H-21) supported 18-ethyl-17,19-dihydroxyhept-14-enyl side chain moiety (Figure 5.20.A). This side chain moiety and its attachment to acetate at C-10 were further clarified by long range conjunctions from δ 4.15 (H-13) to δ 174.36 (C-12); δ 5.17 (H-15) to δ 3.97 (C-17); δ 1.92 (H-16) to δ 29.69 (C-20); δ 3.97 (H-17) to δ 63.33 (C-19) and δ 3.69 (H-19) to δ 23.40 (C-18) (Figure 5.20.B). Noticeably, the geometric alignment of two di-substituted olefinic groups in oxaspiro[4.5]dec-3,8-diene ring was *cis* (*Z*) oriented and this assignment confirmed by its lesser coupling constant values (*J*), such as 8.64 (δ 6.50, H-3), 8.64 (δ 6.25, H-4), 3.29 (δ 5.38, H-8) and 3.74 (δ 5.35, H-9) Hz. However, di-substituted alkene in side chain, 18-ethyl-17,19-dihydroxyhept-14-enyl-10-acetate has higher coupling constant of 10.77 and 10.14 Hz, respectively for H-14 (δ 5.21) and H-15 (δ 5.17) protons, and therefore, the *trans* (*E*) orientation of the respective alkene established. The relative configurations at chiral

positions C-18, C-17, C-6 and C-10 were established by NOESY relations (Figure 5.21.). NOE connections among the protons at δ 3.94 (H-17)/3.60 (H α -19)/2.10 (H-6)/6.25 (H-4)/6.50 (H-3)/5.38 (H-2)/2.02 (H-7)/1.25 (H-25)/4.18 (H-13 α)/5.41 (H-9)/1.58 (H-18)/5.17 (H-15) attributed to their close special proximity and their disposition at identical plane of molecular geometry, and therefore, arbitrarily assigned as α -disposed. The hydroxyl (-OH) group at C-17 position was placed opposite to the α -disposed proton at δ 3.97, likewise the β -position of hydroxyl was correlated. The ethyl and singlet methyl at C-2 oriented towards β and α plane of compound, respectively, as elucidated by NOESY conjunctions and previous reports (Schmitz *et al.*, 1978). Further, NOE relations were recorded between δ 5.21 (H-14)/1.01 (H-20)/2.81 (H-10)/4.15 (H β -13)/3.69 (H β -19) which indicated that these were disposed on identical plane, but no correlations with α -oriented protons, consequently assigned at β -disposition (Figure 5.21.). The β -disposed, H-10 proton further confirmed the α -disposition of bulky side chain, 18-ethyl-17,19-dihydroxyhept-14-enyl-10-acetate.

Table 5.6.: NMR spectroscopic data of (*E*)-18-ethyl-17,19-dihydroxyhept-14-enyl-(2-ethyl-2,6-dimethyl-1-oxaspiro[4.5]dec-3,8-dien)-10-acetate (**2**) in CDCl₃

C. No.	¹³ C	¹ H (int.,mult.,J in Hz) ^a	COSY	HMBC
1	-	-	-	-
2	82.17	-	-	-
3	130.76	6.50 (1H α ,d,8.64)	H-4	C-2,4,5
4	135.40	6.25 (1H α ,d,8.64)	-	C-2,3,5,6
5	79.44	-	-	-
6	36.89	2.10 (1H α ,m)	H-22,7	C-5
7	27.98	2.02 (2H,t)	H-8	C-8
8	132.30	5.38 (1H α ,q,3.29)	-	C-6
9	129.94	5.41 (1H α ,t,3.74)	H-10	C-7
10	25.54	2.81 (1H β ,m)	H-11	C-9
11	34.69	2.35 (2H,d)	-	C-10,12,13
12	174.36	-	-	-
13	65.15	4.15 (1H β ,d) 4.18 (1H α ,d)	H-14 -	C-12 -
14	130.73	5.21 (1H β ,q,10.77)	-	C-13
15	135.18	5.17 (1H α ,q,10.14)	H-16	C-17
16	39.43	1.92 (2H,t)	H-17	C-17,20
17	66.46	3.97 (1H α ,m)	H-18	C-19
18	23.40	1.58 (1H α ,m)	H-20,19	-
19	63.33	3.69 (1H β ,d)	-	C-18

		3.60 (1H α ,d)	-	-
20	29.69	1.33 (2H,m)	H-21	C-21
21	14.11	0.80 (3H,t)	-	C-20
22	22.69	1.01 (3H β ,s)	-	C-8,6
23	31.92	1.63 (2H,q)	H-24	C-5
24	18.16	0.88 (3H,t)	-	C-23,2,25
25	22.53	1.25 (3H α ,s)	-	C-23,2,3

^1H NMR spectra recorded using Bruker AVANCE III 500MHz (AV 500) spectrometer (Bruker, Karlsruhe, Germany) in CDCl_3 as aprotic solvent at ambient temperature with TMS as the internal standard (δ 0 ppm). The ^1H NMR spectra were recorded at 500MHz, while the ^{13}C NMR spectra were recorded at 125MHz. ^aValues in ppm, multiplicity and coupling constants (J =Hz) were indicated in parentheses. The assignments were made with the aid of the ^1H - ^1H COSY, HSQC, HMBC and NOESY experiments

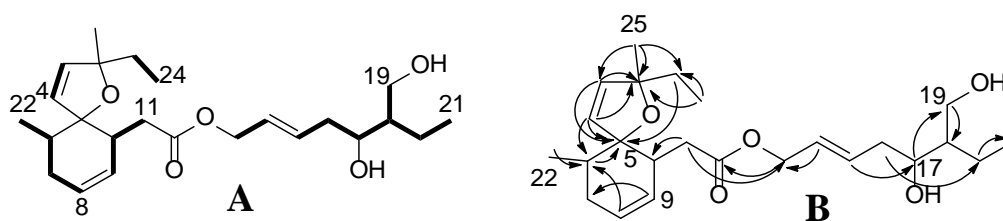


Figure 5.20.: ^1H - ^1H COSY (A) and HMBC (B) correlations of (*E*)-18-ethyl-17,19-dihydroxyhept-14-enyl-(2-ethyl-2,6-dimethyl-1-oxaspiro[4.5]dec-3,8-dien)-10-acetate (**2**). The key ^1H - ^1H COSY couplings have been represented by the bold face bonds. The HMBC couplings were indicated by double barbed arrow

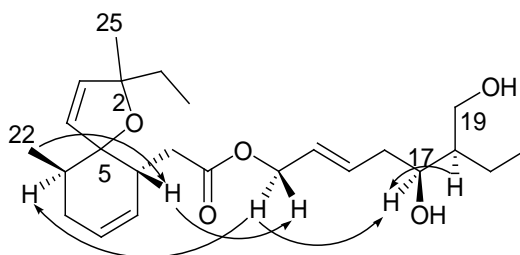


Figure 5.21.: NOESY correlations of (*E*)-18-ethyl-17,19-dihydroxyhept-14-enyl-(2-ethyl-2,6-dimethyl-1-oxaspiro[4.5]dec-3,8-dien)-10-acetate (**2**). The NOESY relations were represented by double barbed arrow

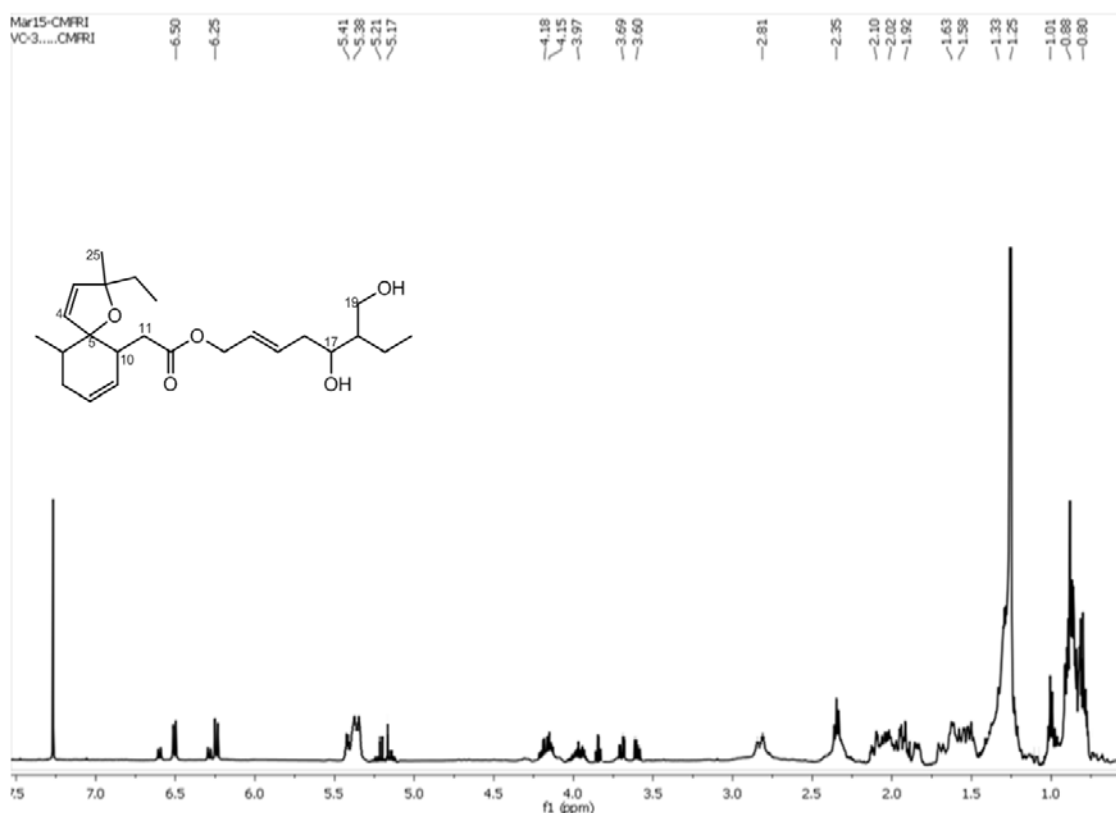


Figure 5.22.: ¹H NMR spectrum of (*E*)-18-ethyl-17,19-dihydroxyhept-14-enyl-(2-ethyl-2,6-dimethyl-1-oxaspiro[4.5]dec-3,8-dien)-10-acetate (**2**)

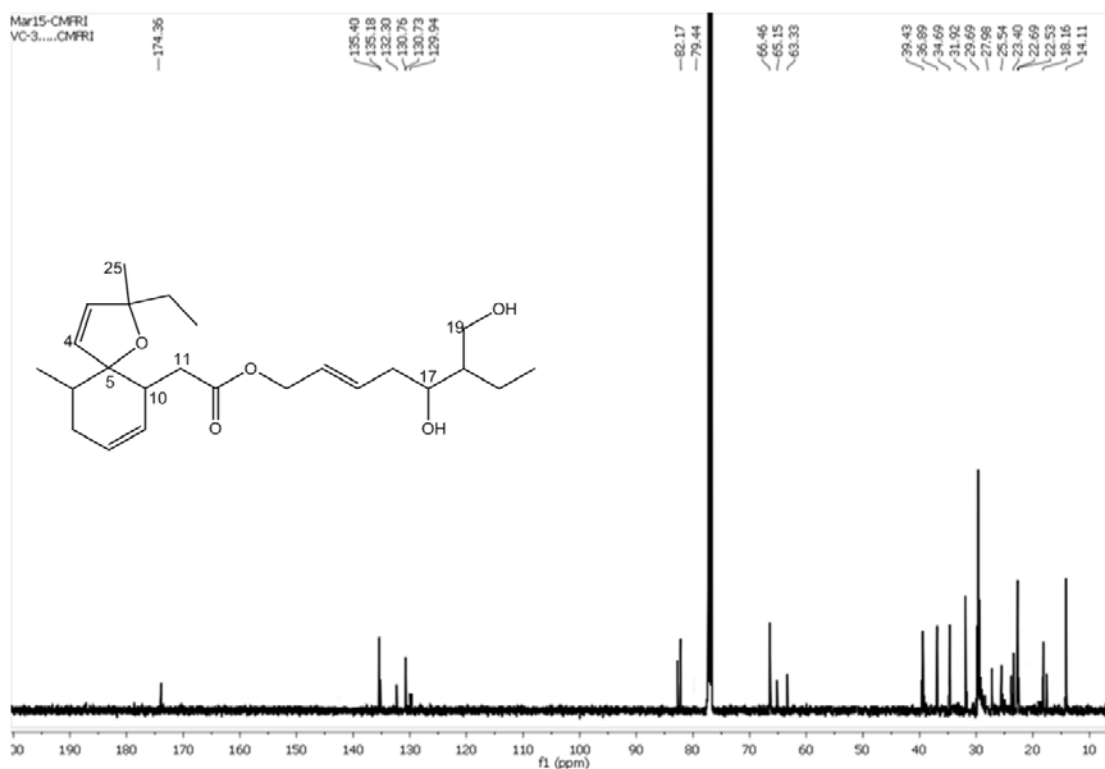


Figure 5.23.: ¹³C NMR spectrum of (*E*)-18-ethyl-17,19-dihydroxyhept-14-enyl-(2-ethyl-2,6-dimethyl-1-oxaspiro[4.5]dec-3,8-dien)-10-acetate (**2**)

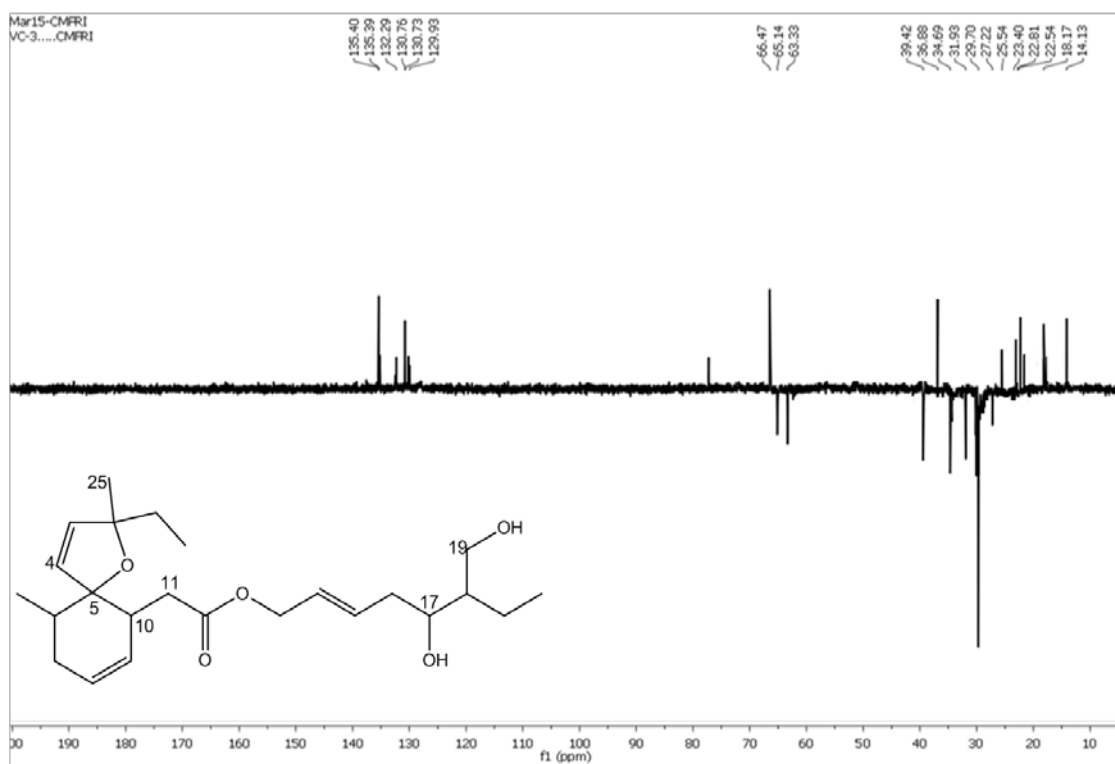


Figure 5.24.: $^{135}\text{DEPT}$ NMR spectrum of (*E*)-18-ethyl-17,19-dihydroxyhept-14-enyl-(2-ethyl-2,6-dimethyl-1-oxaspiro[4.5]dec-3,8-dien)-10-acetate (**2**)

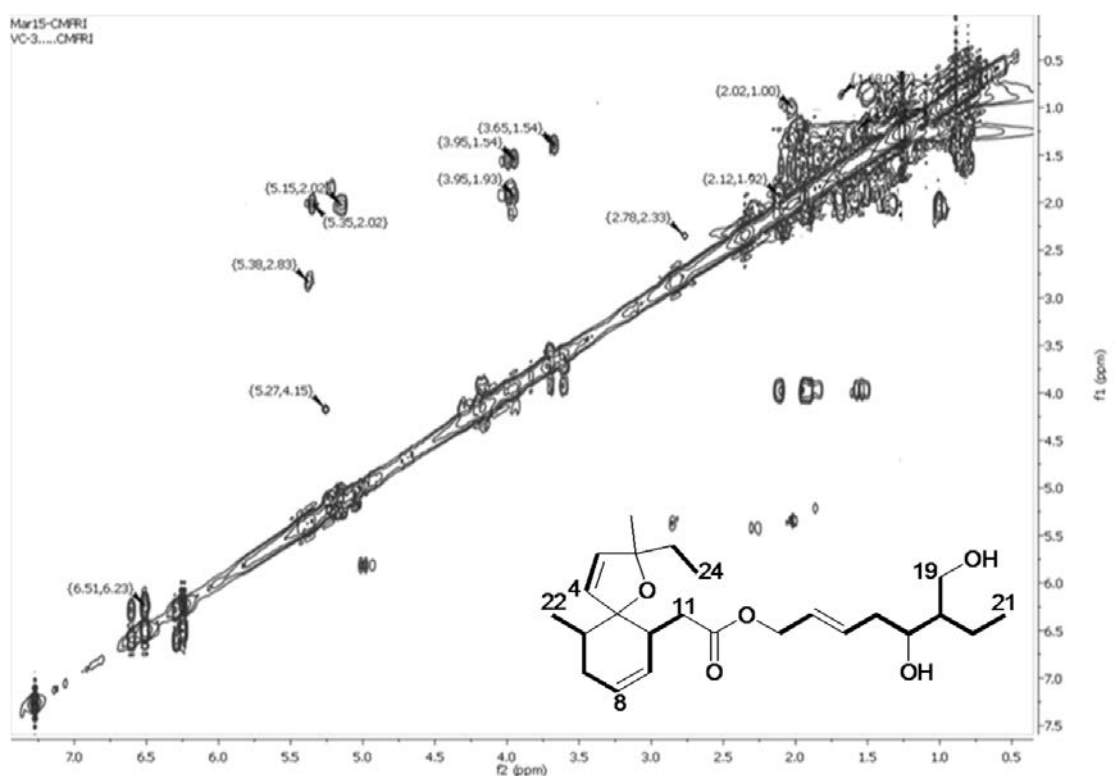


Figure 5.25.: ^1H - ^1H COSY NMR spectrum of (*E*)-18-ethyl-17,19-dihydroxyhept-14-enyl-(2-ethyl-2,6-dimethyl-1-oxaspiro[4.5]dec-3,8-dien)-10-acetate (**2**)

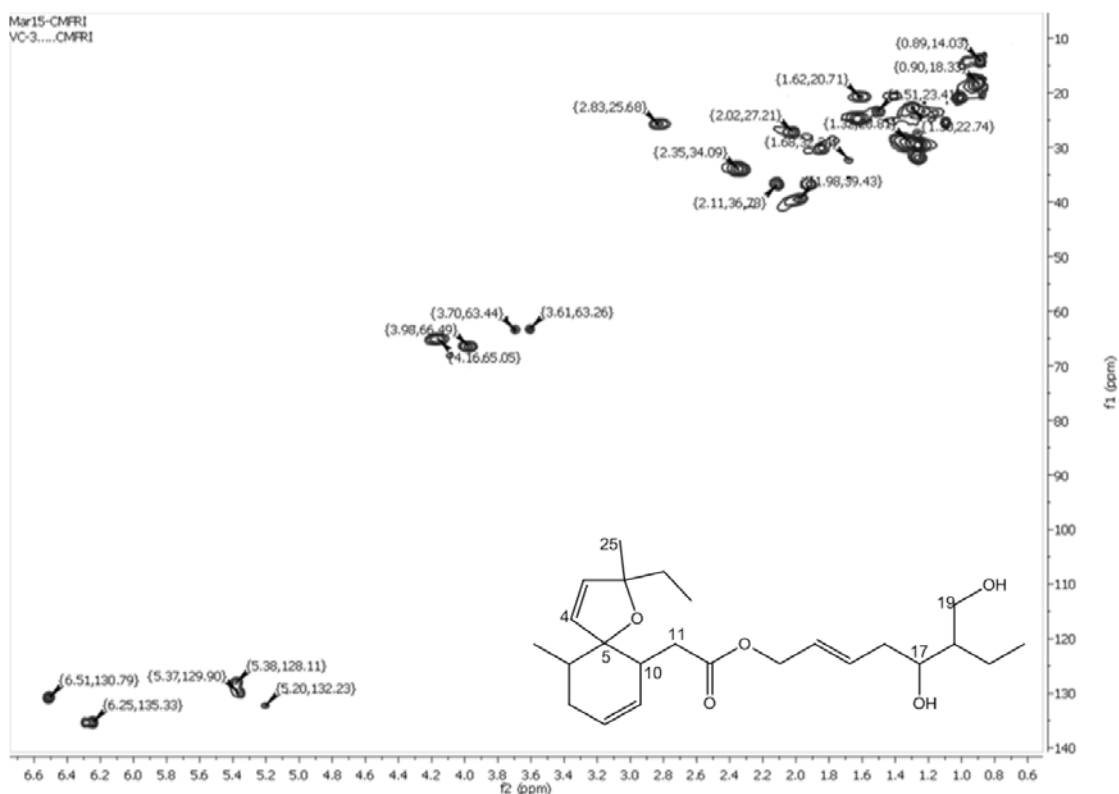


Figure 5.26.: HSQC NMR spectrum of (*E*)-18-ethyl-17,19-dihydroxyhept-14-enyl-(2-ethyl-2,6-dimethyl-1-oxaspiro[4.5]dec-3,8-dien)-10-acetate (**2**)

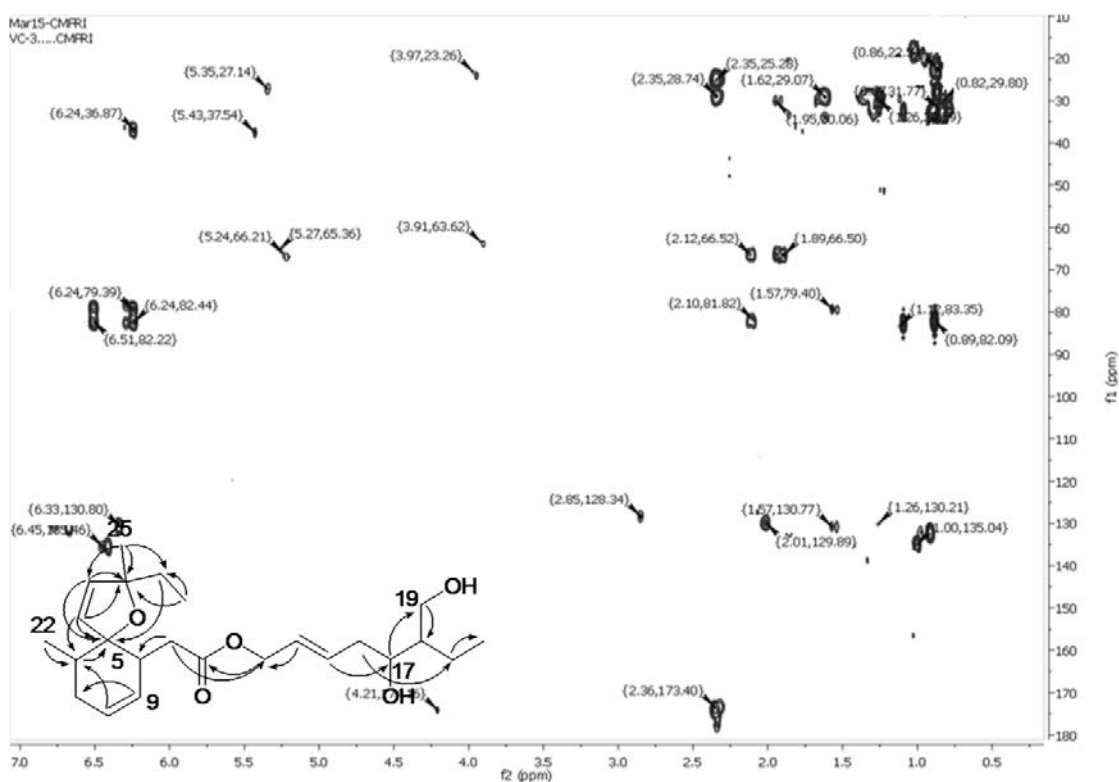


Figure 5.27.: HMBC NMR spectrum of (*E*)-18-ethyl-17,19-dihydroxyhept-14-enyl-(2-ethyl-2,6-dimethyl-1-oxaspiro[4.5]dec-3,8-dien)-10-acetate (**2**)

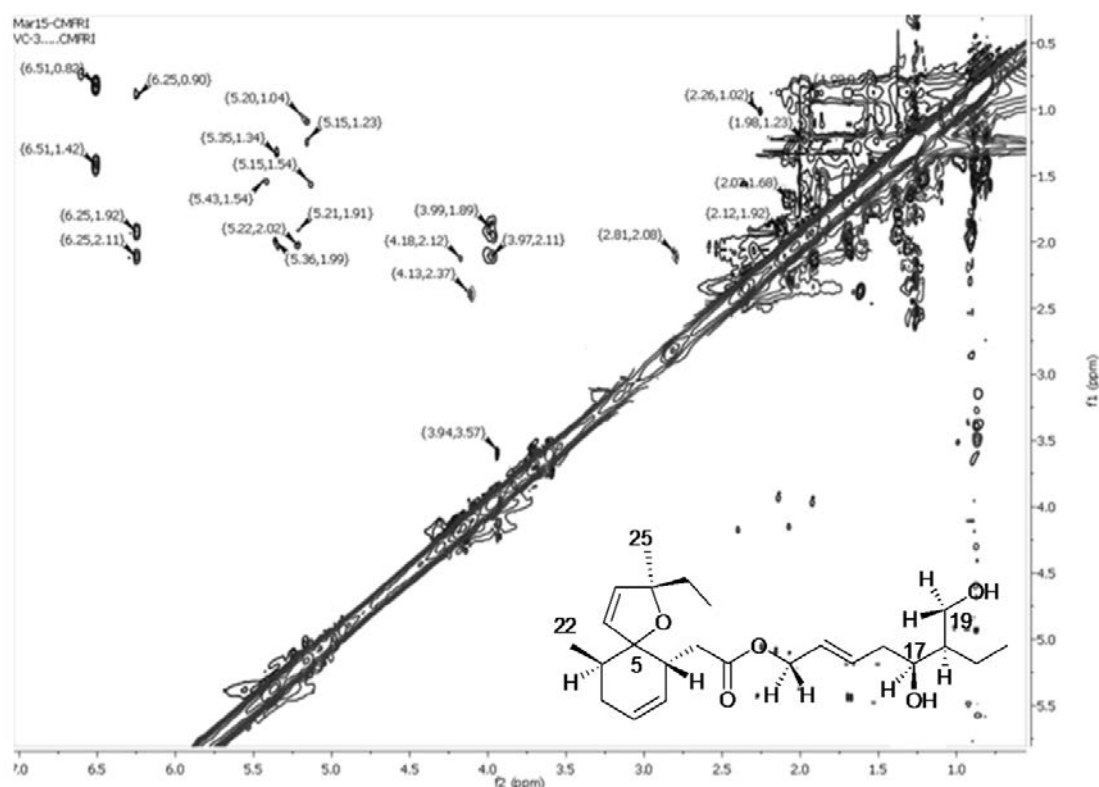


Figure 5.28.: NOESY NMR spectrum of (*E*)-18-ethyl-17,19-dihydroxyhept-14-enyl-(2-ethyl-2,6-dimethyl-1-oxaspiro[4.5]dec-3,8-dien)-10-acetate (**2**)

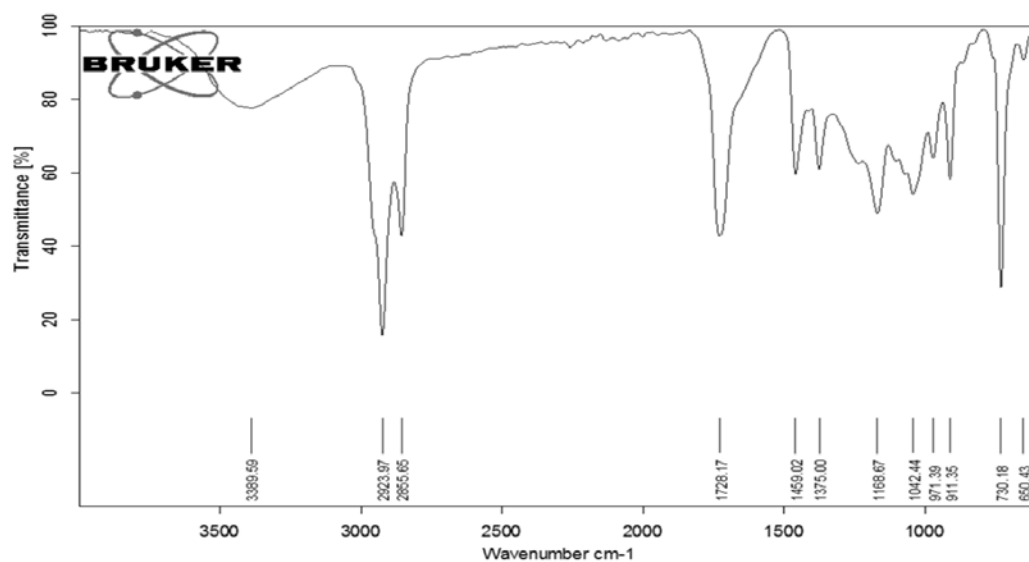


Figure 5.29.: FTIR spectrum of (*E*)-18-ethyl-17,19-dihydroxyhept-14-enyl-(2-ethyl-2,6-dimethyl-1-oxaspiro[4.5]dec-3,8-dien)-10-acetate (**2**)

The present compound exhibited IR stretching absorptions of hydroxyl at 3389 cm⁻¹, alkoxy group (-C-O) at 1042 cm⁻¹ and alkanes at 2923, 2855 cm⁻¹. The ester carbonyl group absorption band was found at 1728 cm⁻¹ (Figure 5.29.).

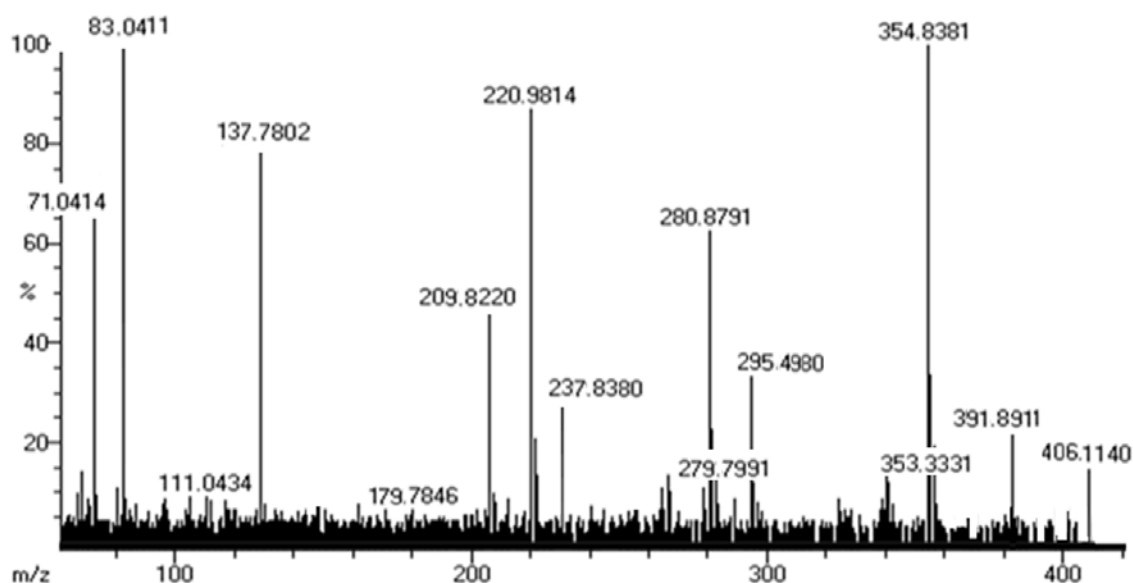


Figure 5.30.: EIMS spectrum of (*E*)-18-ethyl-17,19-dihydroxyhept-14-enyl-(2-ethyl-2,6-dimethyl-1-oxaspiro[4.5]dec-3,8-dien)-10-acetate (**2**)

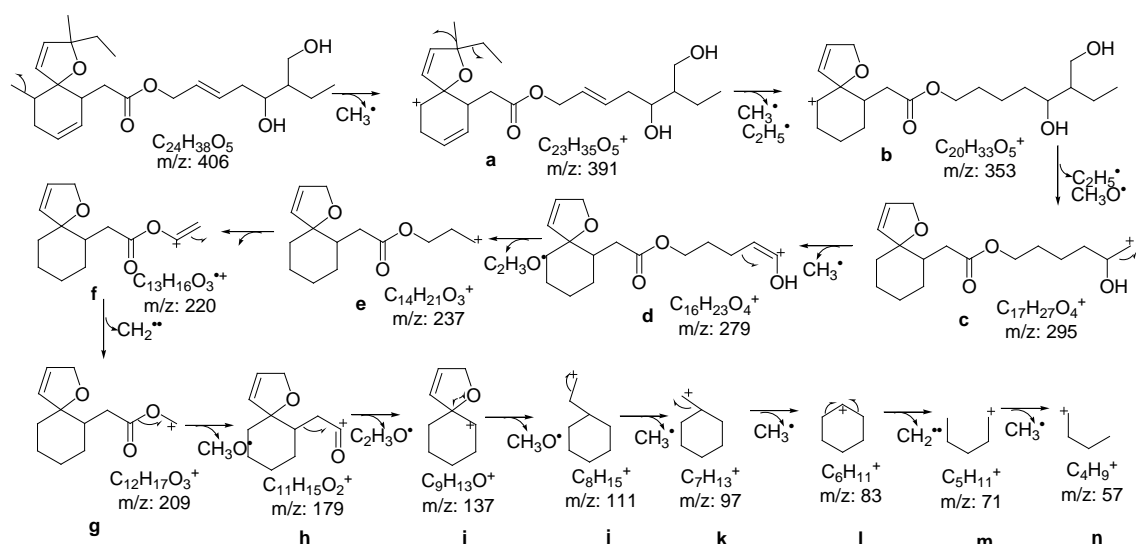


Figure 5.31.: Mass fragmentation pattern of (*E*)-18-ethyl-17,19-dihydroxyhept-14-enyl-(2-ethyl-2,6-dimethyl-1-oxaspiro[4.5]dec-3,8-dien)-10-acetate (**2**)

The mass fragmentation spectrum (Figure 5.30.) indicated that the molecular ion at m/z 406 eliminated a methyl radical to afford an ion at m/z 391 (**a**). The later appeared to undergo elimination of methyl and ethyl side chains at C-3 acquired an ion at m/z 353 (**b**) followed by $C_2H_5^\bullet/CH_3O^\bullet$ and methyl radical eliminations were registered peaks at m/z 295 (**c**) and 279 (**d**), respectively. The ion at m/z 279 (**d**) fragmented to m/z 237 (**e**), 220 (**f**), 209 (**g**), 179 (**h**), 137 (**i**) and followed by rearrangement to 3-cyclohexylpropan-1-ol fragment. The later on removal of methoxy and two methyl

radicals yielded a base peak of cyclohexane radical (**1**, $C_6H_{11}^+$) at m/z 83. Further fragmentations of this cyclohexane radical by two consecutive methyl radical eliminations were resulted in the formation of stable butane radical ($C_4H_9^+$) with m/z 57 (**m**) (Figure 5.31.).

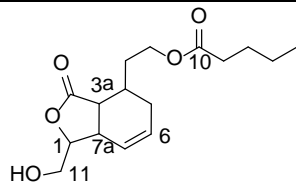
Two bioactive prenylated spirocyclic ether derivatives (**1-2**) were characterized from *V. cyprinoides*. It envisaged the significance and the better efficacy of natural compounds isolated from commonly available seafood, *V. cyprinoides*. The furanyl, hydroxyl and carboxyl enclosed titled natural compounds can develop a constructive and cardinal bioactive pharmacophore templates.

5.3.2.2. Structural characterization of irregular meroterpenoid derivatives (3-5)

The secondary metabolites from marine mollusks grouped into different classes of compounds based on their structural frameworks, particularly, pyranoids, furanoids, polypropionates etc. (Blunt *et al.*, 2015; Ciavatta *et al.*, 2011). Pyran/pyrone and furan/furanone derivatives were important class of heterocyclic organic compounds, which found in marine and estuarine organisms with greater pharmacological potentials (Ciavatta *et al.*, 2011). The bioactive pyran, pyrone, furan and furanone containing compounds reported previously (Cutignano *et al.*, 2007; Fishedick *et al.*, 2013). The α -pyrone methyl derivatives reported from mollusks, *Haminoea fusari* and *S. lesson* (Cutignano *et al.*, 2007; Roviroso and San-Martin 2006). The furanoid monoterpenes, furoplocamioids from *Plocamium cartilagineum* (Darias *et al.*, 2001) and an anti-bacterial compound, 6-pentyl-2*H*-pyran-2-one were previously reported (Parker *et al.*, 1997). Herein, we have detailed the characterization of hexahydro isobenzofuranone derivative (**3**), tetrahydro pyranone derivative (**4**) and dihydrofurano-dihydropyran derivative (**5**) isolated from *V. cyprinoides*.

5.3.2.2.A. Structural characterization of compound 3 (VC₂₋₆₋₂₋₁₋₂)

8-(1,3,3a,4,5,7a-Hexahydro-1-(hydroxymethyl)-3-oxoisobenzofuran-4-yl)-ethyl pentanoate (3)



Yield	79 mg; 0.18%
Physical description	Dark brown oily
Molecular formula	C ₁₆ H ₂₄ O ₅
Molecular mass	296.1624

An irregular C₁₆ hexahydro oxoisobenzofuran-meroterpenoid, 8-(1,3,3a,4,5,7a-hexahydro-1-(hydroxymethyl)-3-oxoisobenzofuran-4-yl)-ethyl pentanoate (**3**) isolated as dark brown oily compound. It displayed UV absorbance (in MeOH) at λ_{\max} (log ϵ 2.76) 235.3 nm was assigned to a chromophore with olefinic and two isolated carbonyl systems (Figure 5.32.). The purity of the compound supported by RP C₁₈ HPLC using 2:3 (v/v) MeOH:MeCN (R_t 3.04) experiments (Figure 5.33.).

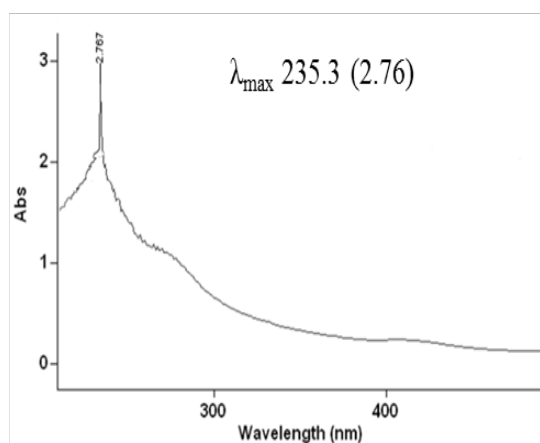


Figure 5.32.: UV spectrum of 8-(1,3,3a,4,5,7a-hexahydro-1-(hydroxymethyl)-3-oxoisobenzofuran-4-yl)-ethyl pentanoate (**3**)

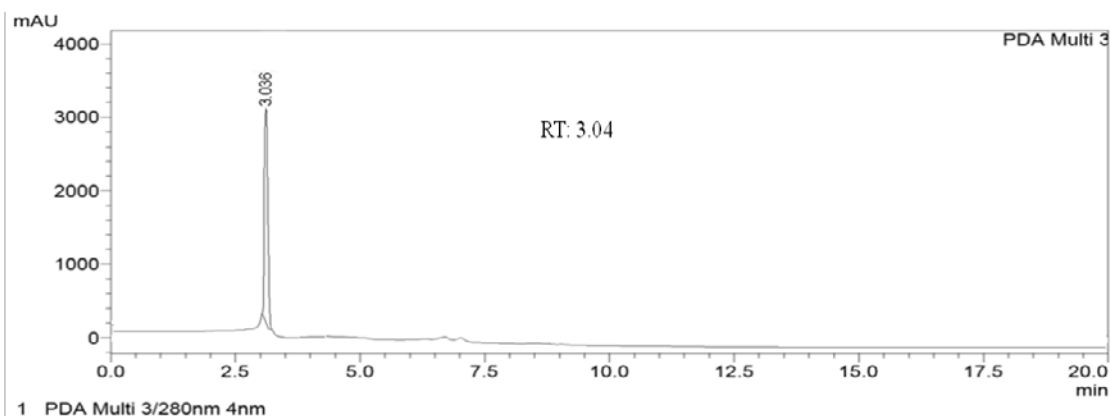


Figure 5.33.: HPLC chromatogram of 8-(1,3,3a,4,5,7a-hexahydro-1-(hydroxymethyl)-3-oxoisobenzofuran-4-yl)-ethyl pentanoate (**3**)

An irregular C16 hexahydrobenzo furanone derivative, (**3**) recorded its molecular ion peak at m/z 296 (EIMS 296.1630 $[M]^+$, cal. 296.1624 for $C_{16}H_{24}O_5$) and its double bond equivalences were calculated as five (three double bonds and two ring moieties). It housed a C11 diterpene based skeleton, which attached with the pentanoate side chain at C-9, and these attributions were based on exhaustive 1H - 1H COSY, HSQC, HMBC NMR experimental data (Figure 5.38-5.40.). The chemical shift resonances of one methyl (doublet), three sp^3 methines, two sp^2 methines, two sp^3 methylenes (one oxygenated and one hydroxylated), five aliphatic methylenes and two quaternary carbons were recorded in the 1H , ^{13}C and DEPT spectra (Table 5.7.; Figure 5.35.-5.37.). The characteristic disubstituted alkene (δH 5.37/ δC 129.99; δH 5.35/ δC 129.70), two ester carbonyls (δC 178.41 and 173.95) (Jin *et al.*, 2016), one oxygenated methine (δH 4.08/ δC 68.26), one carbonyl methine (δH 2.32/ δC 50.01), and one oxygenated methylene (δH 4.17, 4.15/ δC 65.00) groups were identified. The title compound composed of a basic C11 skeleton including the hexahydro oxoisobenzofuran and pentanoate side chain, which linked through the ethyl linkage among C-4 and C-10. The 1H - 1H COSY spectrum of the titled compound revealed that it enclosed two spin systems in the 8-(hexahydro-1-(hydroxymethyl)-3-oxoisobenzofuran-4-yl)-ethyl part and one spin system in the pentanoate side chain. The correlations between the proton shifts at δ 3.73 (H-1¹)/4.08 (H-1)/2.81 (H-7a)/5.35 (H-7); δ 2.81 (H-7a)/2.32 (H-3a)/2.08 (H-4)/1.30 (H-8)/4.17, 4.15 (H-9); δ 2.02 (H-5)/5.37 (H-6) along with δ 2.35 (H-11)/1.63 (H-12)/1.29 (H-13)/0.88 (H-14) were satisfied the above mentioned spin systems (Figure 5.34.A). The hexahydro-3-oxoisobenzofuranyl framework was further

supported by long range conjunctions from δ 4.08 (H-1) to δ 178.41 (C-3), 25.62 (C-7a); δ 2.32 (H-3a) to δ 178.41 (C-3), 27.21 (C-5); δ 2.08 (H-4) to δ 50.10 (C-3a); δ 2.02 (H-5) to 129.70 (C-7); δ 5.37 (H-6) to δ 27.21 (C-5) and δ 2.81 (H-7a) to δ 129.99 (C-6), 129.70 (C-7) (Figure 5.34.B). The position of hydroxymethyl (-CH₂-OH) at C-1 of dihydro furanone was confirmed by the HMBCs from δ 3.73 (C-1¹) to δ 68.26 (C-1), 25.62 (C-7a). The isolated double bonds, δ 5.37 and 5.35 at C-6 and C-7, respectively had lesser *J* (coupling constant) values (3.53 and 3.64 Hz, respectively), and this affirmed its *cis* (*Z*) orientation in hexahydro-oxoisobenzofuranyl ring. The pentanoate side chain validated by long range correlations such as, δ 2.35 (H-11) to δ 173.95 (C-10); δ 1.63 (H-12) to δ 173.95 (C-10) and δ 0.88 (H-14) to δ 34.10 (C-11). The ethyl linkage between hexahydro-3-isobenzofuranone skeleton and pentanoate side chain further supported by HMBCs from δ 1.30 (H-8) to δ 50.10 (C-3a), δ 129.99 (C-6); δ 4.17 (H-9) to δ 173.95 (C-10), 31.92 (C-4) along with δ 2.08 (H-4) and δ 2.02 to δ 29.69 (C-8). Comparison of proton and carbon signals of **3** with 1-acetoxy-6 α -(2-methylbutyryl)-eriolanolide suggested that the former enclosed hexahydro-isobenzofuran-3-one as basic skeleton and tetrahydro-3-methylene benzo furan-2-one in the latter (Jin *et al.*, 2016). The relative stereochemistries of chiral protons at H-1, H-3a, H-7a and H-4 were confirmed by correlations in NOE spectrum (Figure 5.41.). The NOE correlations recorded between δ 2.32 (H-3a)/5.37 (H-6)/2.81 (H-7a)/5.35 (H-7)/4.15 (H α -9) that signified their equiplanar orientation and arbitrarily designated as α -disposed. The α -disposition of ring junction protons at C-3a and C-7a was also confirmed from previous studies (Fischedick *et al.*, 2013). The protons at δ 4.08 (H-1)/4.17 (H β -9)/2.08 (H-4) exhibited intense NOE correlation and found to be opposite to α -protons, which signified that H-1, H β -9, H-4 protons were at their β -disposition (Figure 5.34.C).

Table 5.7.: NMR spectroscopic data of 8-(1,3,3a,4,5,7a-hexahydro-1-(hydroxymethyl)-3-oxoisobenzofuran-4-yl)-ethyl pentanoate (**3**) in CDCl₃

C. No.	¹³ C	¹ H (int.,mult., <i>J</i> in Hz) ^a	COSY	HMBC
1	68.26	4.08 (1H β ,m)	H-1 ¹ ,7a	C-3,7a
1 ¹	61.42	3.73 (3H,d)	-	C-1,7a
2	-	-	-	-
3	178.41	-	-	-
3a	50.10	2.32 (1H α ,d)	H-7a,4	C-3,5

4	31.92	2.08 (1H β ,m)	H-8	C-8,3a
5	27.21	2.02 (2H,m)	H-6	C-6,7,8
6	129.99	5.37 (1H α ,q,3.53)	-	C-5
7	129.70	5.35 (1H α ,t,3.64)	H-7a	C-5
7a	25.62	2.81 (1H α ,m)	-	C-6,7
8	29.69	1.30 (2H,m)	H-9	C-3a,6
9	65.00	4.17 (1H β ,d)	-	C-10,4
		4.15 (1H α ,d)	-	-
10	173.95	-	-	-
11	34.10	2.35 (2H,t)	H-12	C-12,10
12	24.88	1.63 (2H,m)	H-13	C-10,11
13	22.68	1.29 (2H,m)	H-14	-
14	14.11	0.88 (3H,t)	-	C-13,11

^1H NMR spectra recorded using Bruker AVANCE III 500MHz (AV 500) spectrometer (Bruker, Karlsruhe, Germany) in CDCl_3 as aprotic solvent at ambient temperature with TMS as the internal standard (δ 0 ppm). The ^1H NMR spectra were recorded at 500MHz, while the ^{13}C NMR spectra were recorded at 125MHz. ^aValues in ppm, multiplicity and coupling constants (J =Hz) were indicated in parentheses. The assignments were made with the aid of the ^1H - ^1H COSY, HSQC, HMBC and NOESY experiments

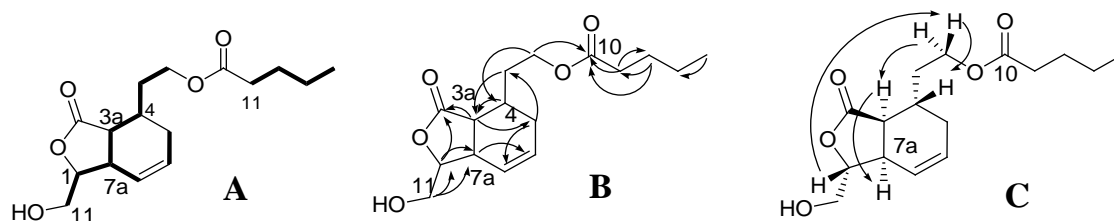


Figure 5.34.: ^1H - ^1H COSY (A), HMBC (B) and NOESY (C) correlations of 8-(1,3,3a,4,5,7a-hexahydro-1-(hydroxymethyl)-3-oxoisobenzofuran-4-yl)-ethyl pentanoate (**3**). The key ^1H - ^1H COSY couplings have been represented by the bold face bonds. The HMBC couplings were indicated by double barbed arrow. The NOESY relations were represented by double barbed arrow

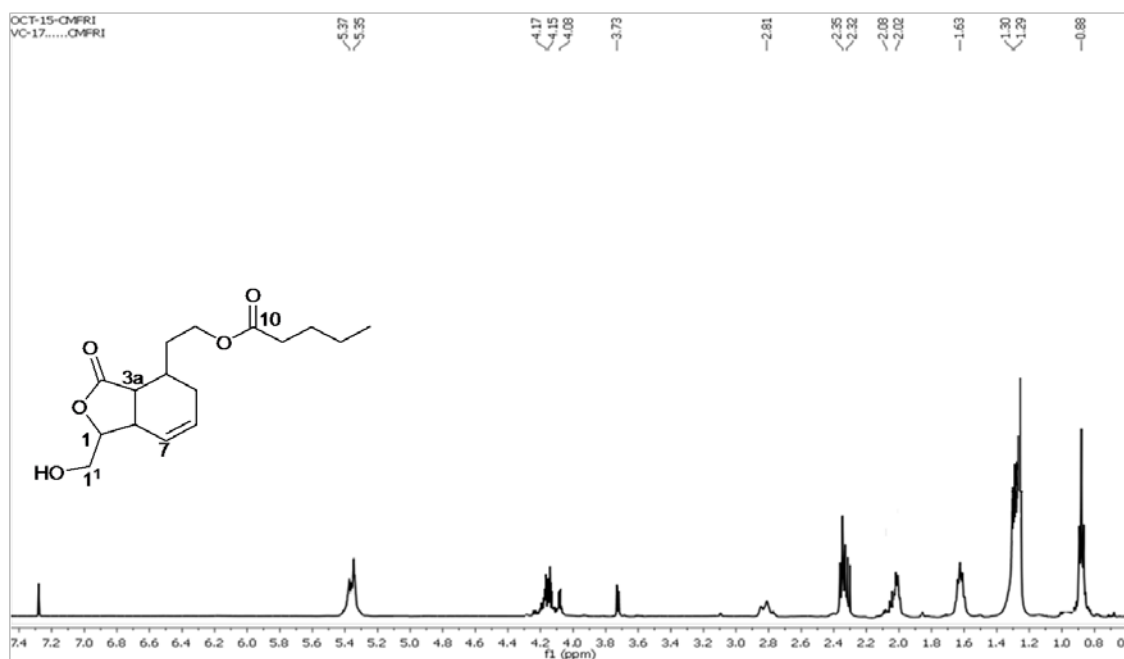


Figure 5.35.: ^1H NMR spectrum of 8-(1,3,3a,4,5,7a-hexahydro-1-(hydroxymethyl)-3-oxoisobenzofuran-4-yl)-ethyl pentanoate (**3**)

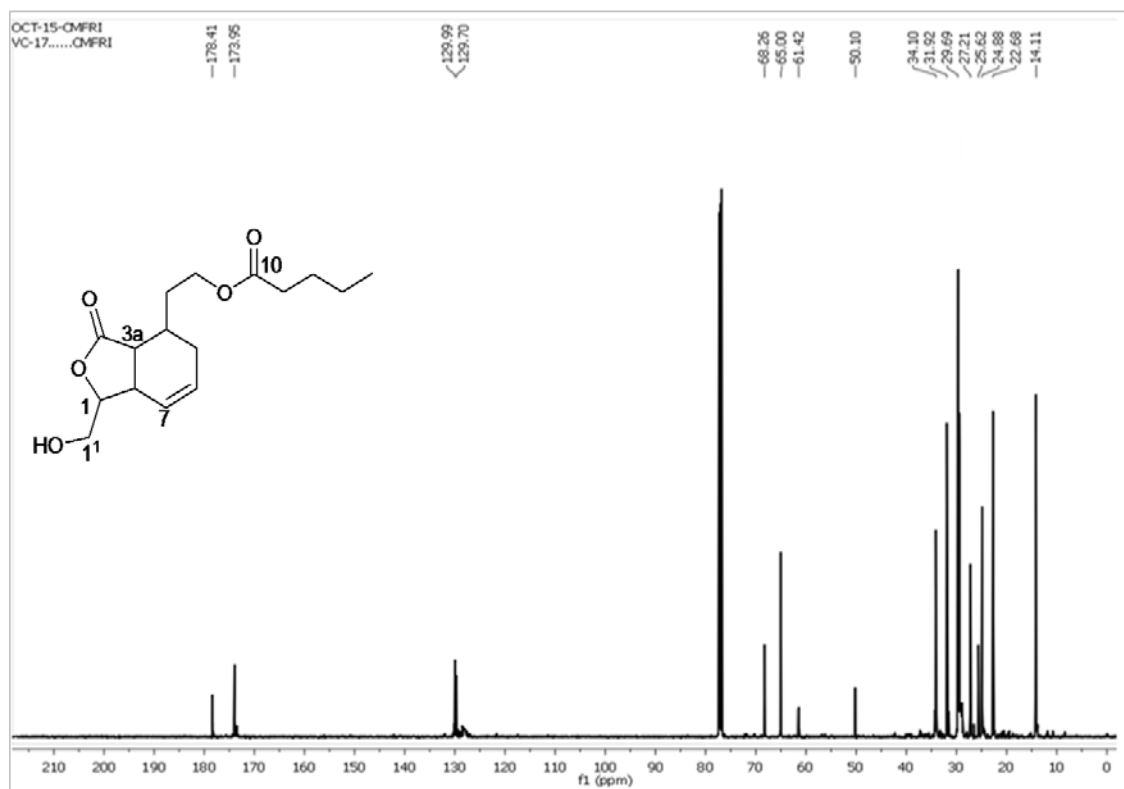


Figure 5.36.: ^{13}C NMR spectrum of 8-(1,3,3a,4,5,7a-hexahydro-1-(hydroxymethyl)-3-oxoisobenzofuran-4-yl)-ethyl pentanoate (**3**)

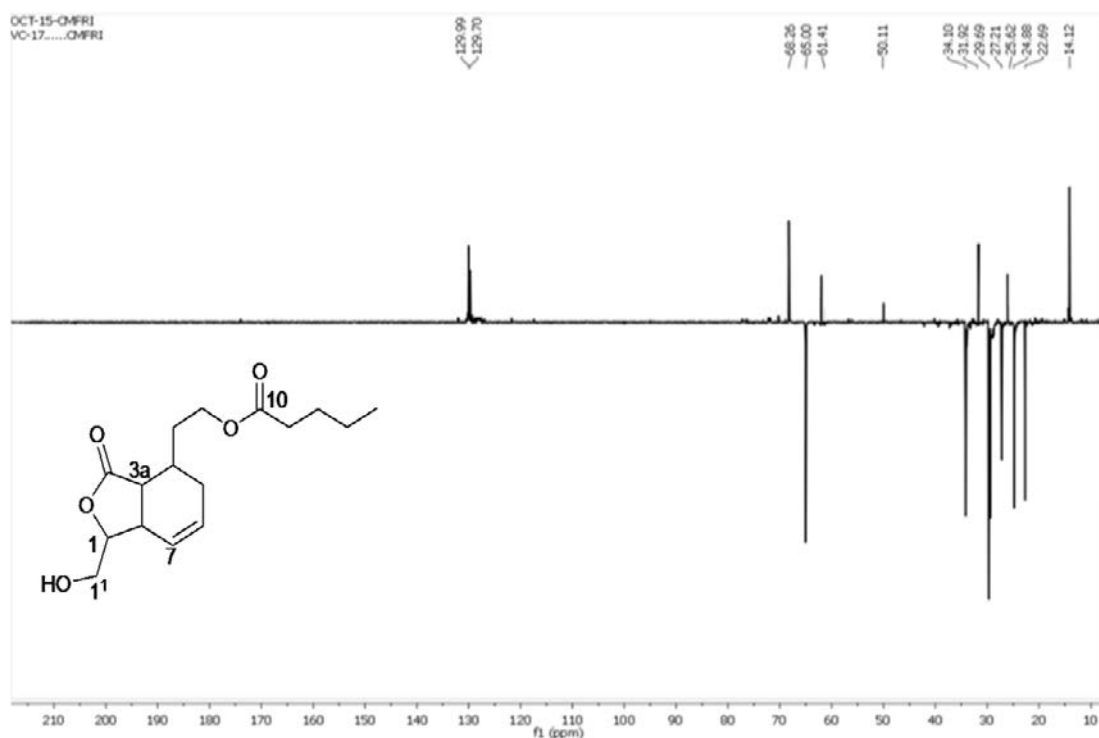


Figure 5.37.: $^{135}\text{DEPT}$ NMR spectrum of 8-(1,3,3a,4,5,7a-hexahydro-1-(hydroxymethyl)-3-oxoisobenzofuran-4-yl)-ethyl pentanoate (**3**)

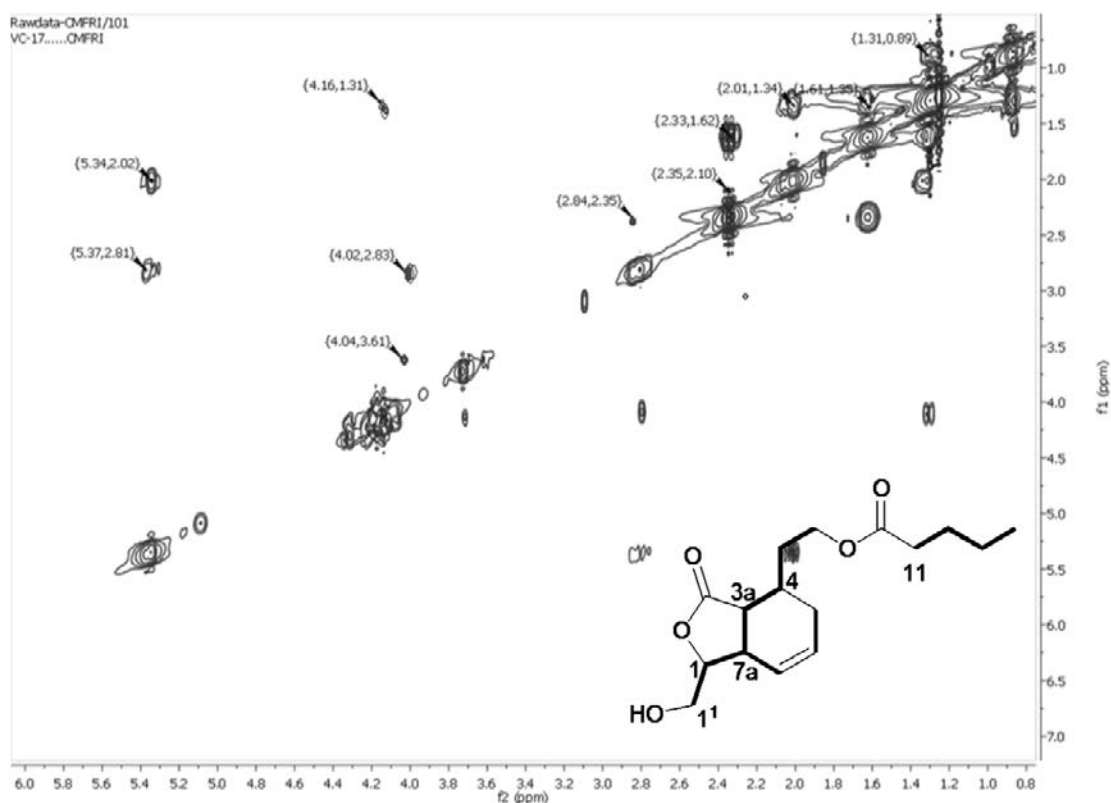


Figure 5.38.: ^1H - ^1H COSY NMR spectrum of 8-(1,3,3a,4,5,7a-hexahydro-1-(hydroxymethyl)-3-oxoisobenzofuran-4-yl)-ethyl pentanoate (**3**)

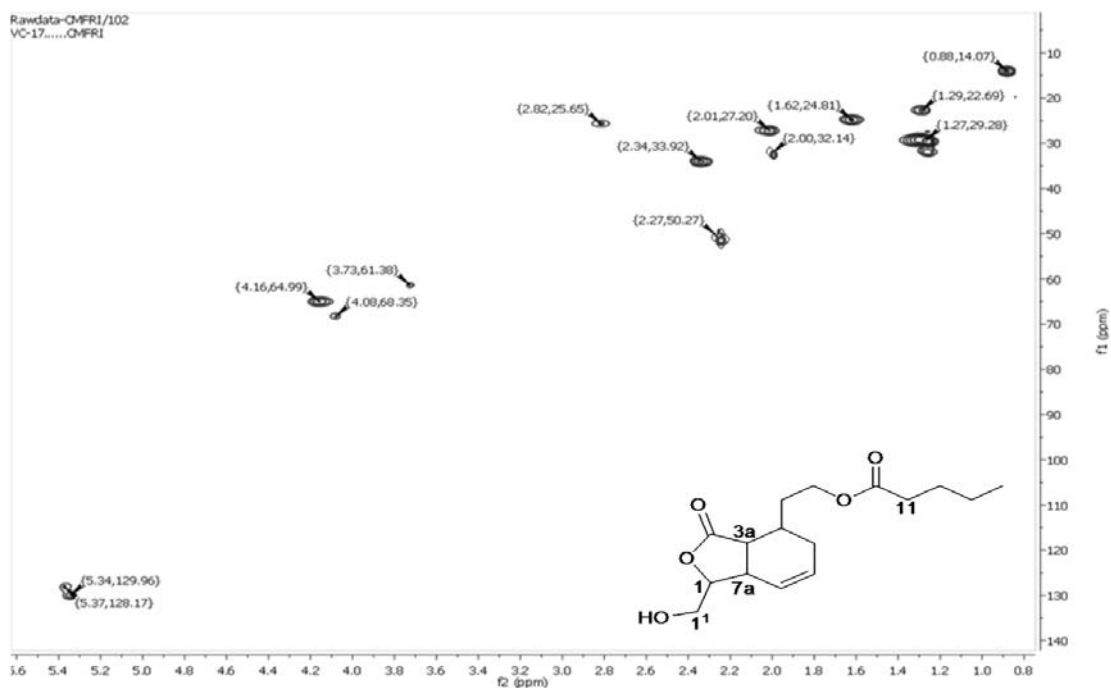


Figure 5.39.: HSQC NMR spectrum of 8-(1,3,3a,4,5,7a-hexahydro-1-(hydroxymethyl)-3-oxoisobenzofuran-4-yl)-ethyl pentanoate (**3**)

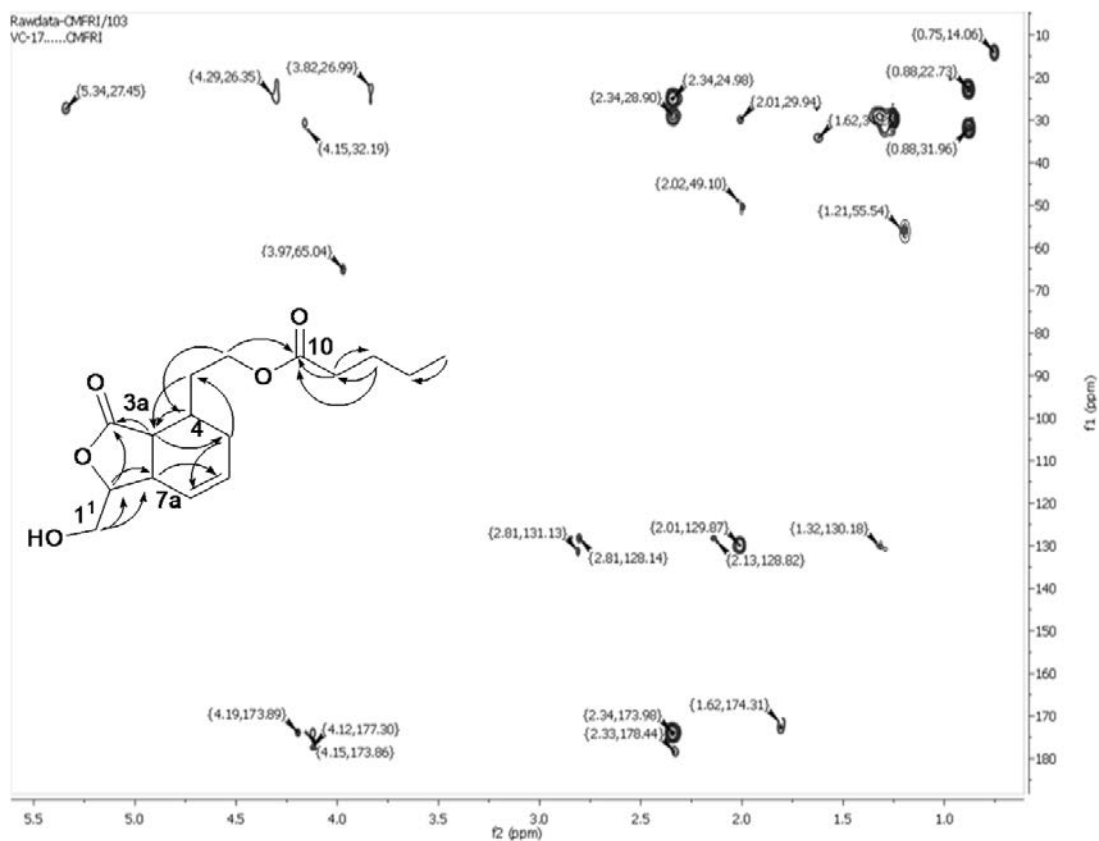


Figure 5.40.: HMBC NMR spectrum of 8-(1,3,3a,4,5,7a-hexahydro-1-(hydroxymethyl)-3-oxoisobenzofuran-4-yl)-ethyl pentanoate (**3**)

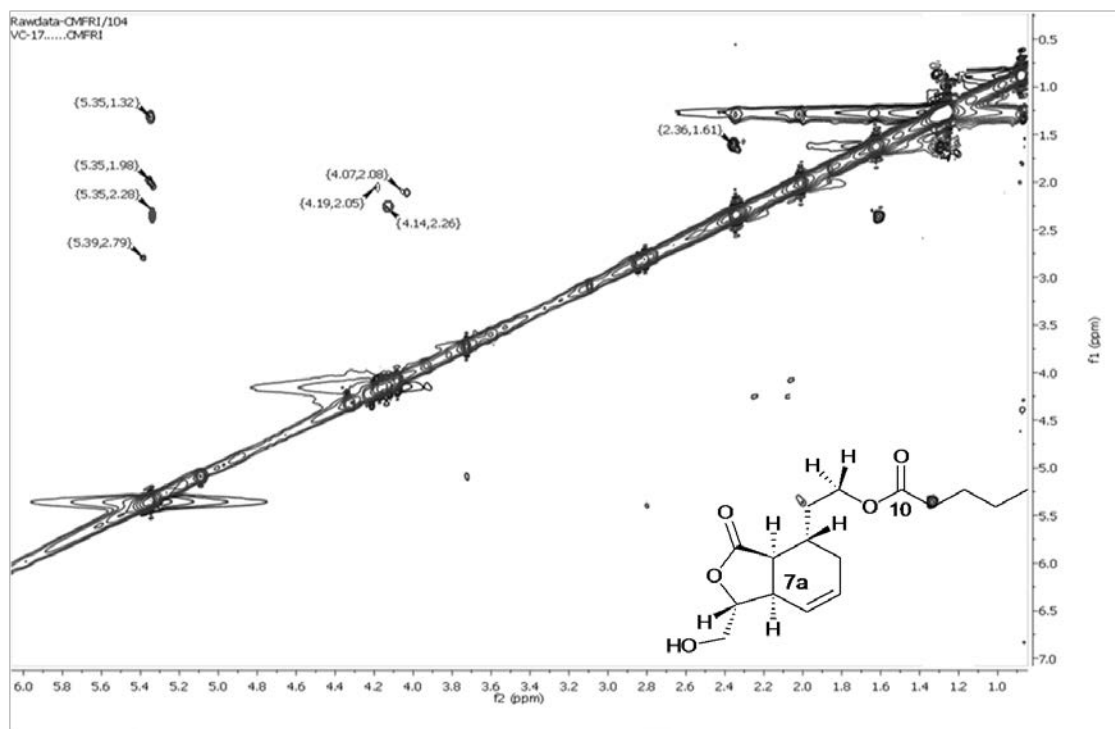


Figure 5.41.: NOESY NMR spectrum of 8-(1,3,3a,4,5,7a-hexahydro-1-(hydroxymethyl)-3-oxoisobenzofuran-4-yl)-ethyl pentanoate (**3**)

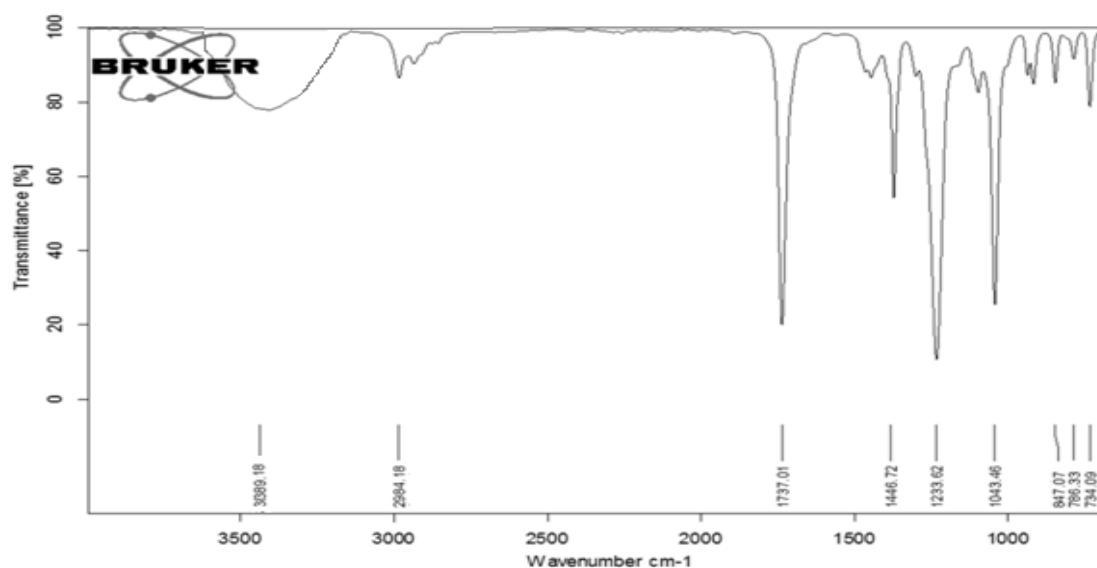


Figure 5.42.: FTIR spectrum of 8-(1,3,3a,4,5,7a-hexahydro-1-(hydroxymethyl)-3-oxoisobenzofuran-4-yl)-ethyl pentanoate (**3**)

The IR spectrum illustrated absorption bands at 1737 cm^{-1} , which was indicative of ester group. The alkane (2984 cm^{-1}), acyl (1233 cm^{-1}), hydroxyl (3089 cm^{-1}) and alkoxy (1043 cm^{-1}) stretching vibrations were also accounted for this compound (Figure 5.42.).

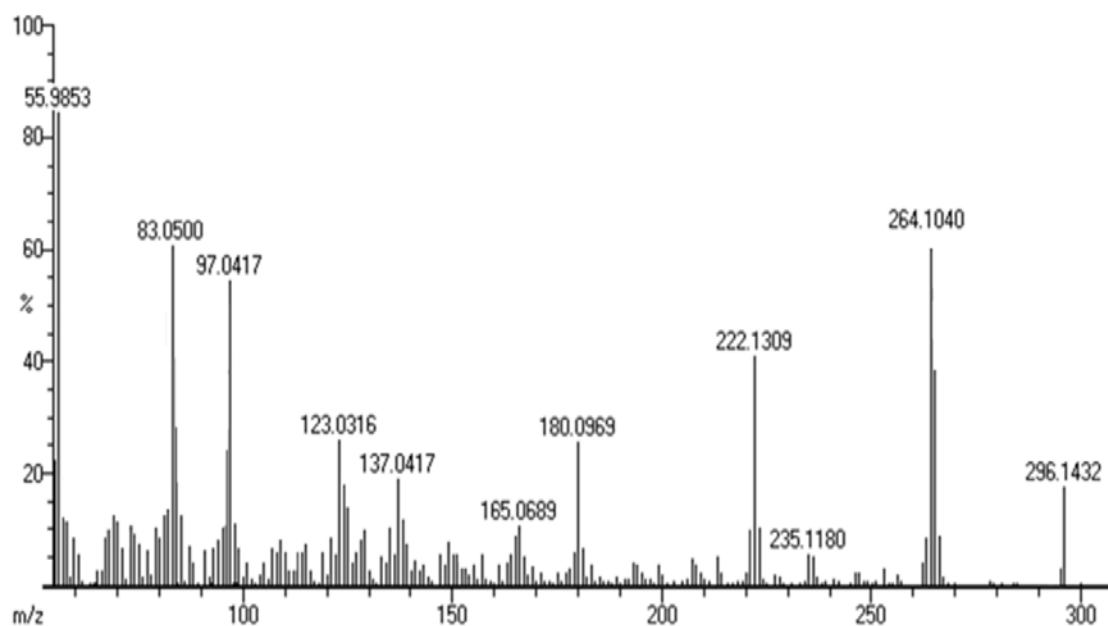


Figure 5.43.: EIMS spectrum of 8-(1,3,3a,4,5,7a-hexahydro-1-(hydroxymethyl)-3-oxoisobenzofuran-4-yl)-ethyl pentanoate (**3**)

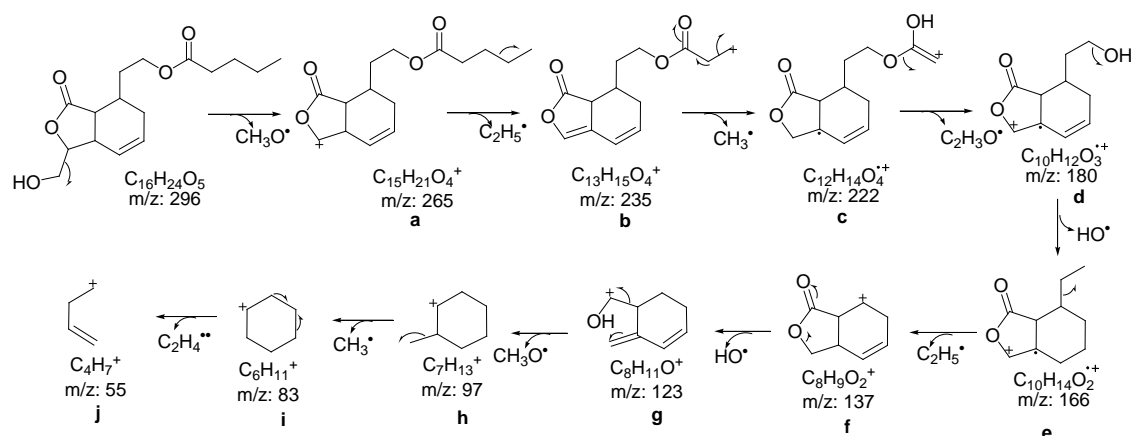


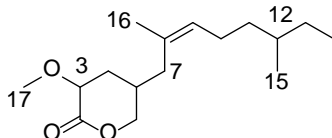
Figure 5.44.: Mass fragmentation pattern of 8-(1,3,3a,4,5,7a-hexahydro-1-(hydroxymethyl)-3-oxoisobenzofuran-4-yl)-ethyl pentanoate (**3**)

The mass spectrum has registered a molecular ion peak for the current compound at m/z 296 (Figure 5.43.). It fragmented a methoxy radical to yield an ion at m/z 265 (**a**, $C_{15}H_{21}O_4^+$). This appeared to undergo sequential elimination of ethyl followed by methyl radical afforded a fragment at m/z 222 (**c**). The later underwent sequential elimination of $C_2H_3O^\bullet$ and $C_2H_5^\bullet$ radicals yielded ion peak of tetrahydro isobenzofuranone at m/z 137 (**f**), which on removal of hydroxy radical yielded a peak at $C_8H_{11}O^\bullet$ (**g**) with m/z 123. This further fragmented to $C_7H_{13}^\bullet$ with m/z 97 (**h**) and $C_6H_{11}^\bullet$ with m/z 83 (**i**) after eliminating methoxy and methyl radicals, respectively. The base

ion peak of butene radical was obtained at m/z 55 (**j**, $C_4H_7^{\bullet}$) by the fragmentation of $C_2H_4^{\bullet\bullet}$ radical from $C_6H_{11}^{\bullet}$ (**i**) (Figure 5.44.).

5.3.2.2.B. Structural characterization of compound 4 (VC₂₋₆₋₄₋₁)

Tetrahydro-3-methoxy-5-((*E*)-8,12-dimethyloct-8-enyl)-pyran-2-one (**4**)



Yield	59 mg; 0.13%
Physical description	Pale yellow oily
Molecular formula	$C_{16}H_{28}O_3$
Molecular mass	268.2038

The compound, tetrahydro-3-methoxy-5-((*E*)-8,12-dimethyloct-8-enyl)-pyran-2-one (**4**) isolated as yellowish oily compound. It displayed UV absorbance (in MeOH) at λ_{max} (log ϵ 3.76) 218.6 nm assigned to chromophore with olefinic and carbonyl systems (Figure 5.45.). The purity of compound was supported by RP C18 HPLC using 1:4 (v/v) MeOH:MeCN (R_t 3.41) experiments (Figure 5.46.).

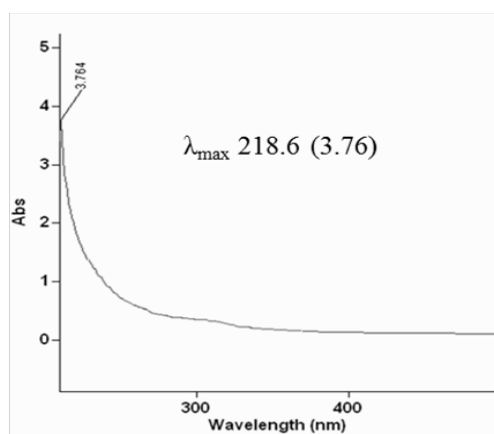


Figure 5.45.: UV spectrum of tetrahydro-3-methoxy-5-((*E*)-8,12-dimethyloct-8-enyl)-pyran-2-one (**4**)

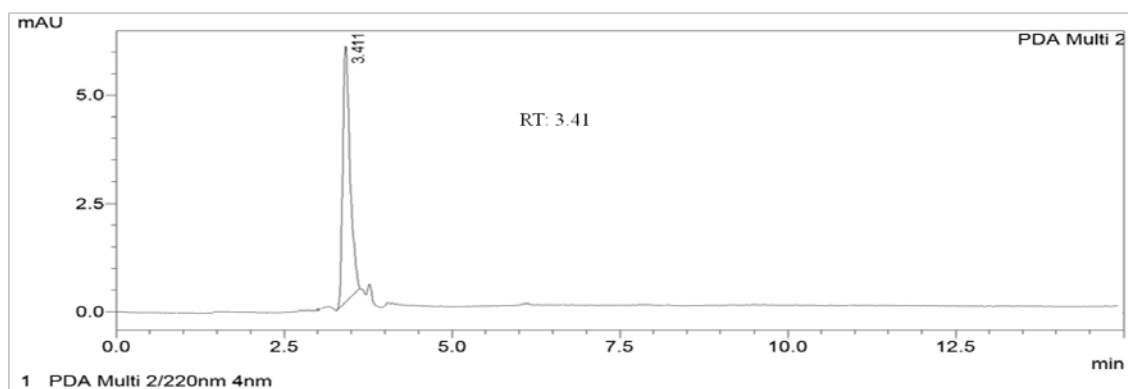


Figure 5.46.: HPLC chromatogram of tetrahydro-3-methoxy-5-((*E*)-8,12-dimethyloct-8-enyl)-pyran-2-one (**4**)

The compound, **4** was found to be α -pyrone enclosed sesquiterpene based C16 prenylated bisabolene type of meroterpenoid. Its molecular formula, $C_{16}H_{28}O_3$ was assigned by molecular ion peak at m/z 268 (EIMS: found m/z 268.2044 $[M]^+$, cal. 268.2038) indicating the occurrence of three indices of hydrogen deficiencies. The ^{13}C NMR in combination with DEPT validated the presence of four methyls (one methoxy), six methylenes, and four methines along with two quaternary (carboxylate and alkene) carbons (Table 5.8.; Figure 5.50-5.51.), which was comparable with basic skeleton of α -pyrone analogues from *Dysidea cinerea* (sponge) and fungus *Nectria* sp (Kiem *et al.*, 2013; Li *et al.*, 2015a). It is interesting to note that the basic skeletons of tetrahydro pyran-2-one and the side chain 5-(*E*)-8,12-dimethyloct-8-enyl were formed as C15 terpenoid by irregular array of three isoprene units yielding a sesquiterpene-type prenylated bisabolene meroterpenoid. Notably, the title compound was found to house the pyrone ring skeleton. Highly deshielded ^{13}C resonances at δ 173.92 (C-2), 135.14 (C-8) and 130.02 (C-9) were accounted for carboxyl $\{-C=O(O)-\}$, 4° alkene ($>C=CH$; C-8) and secondary alkene (C-9), respectively. Investigations of 1H , ^{13}C NMR and HSQC data of **4** revealed the occurrence of olefinic bond (δC 130.02 (C-9)/ δH 5.35), methoxy (17-OMe; δC 50.68 (C-17)/ δH 3.67), methines with higher $\{-(O=C)-CH-O-$; δC 68.40 (C-3)/ δH 4.08} and lower (δC 24.90 (C-5)/ δH 1.63; δC 30.97 (C-12)/ δH 1.50) chemical shifts and four deshielded methylenes $\{(\delta C$ 65.04 (C-6)/ δH 4.17/4.14 for $CH_2-O-(C=O)-$; δC 34.11 (C-4)/ δH 2.35; δC 27.22 (C-10)/ δH 2.01; δC 31.93 (C-7)/ δH 1.82)} (Figure 5.49.-5.50., 5.53.). The shielded methyl protons at δ 0.87 $\{\delta C$ 14.02 (C-14)} and δ 0.99 $\{\delta C$ 15.26 (C-15)} along with deshielded singlet proton at δ 1.86 $\{\delta C$

28.03 (C-16)} were recorded. The α -pyrone ring part was deduced by ^1H - ^1H COSY cross peaks from H-3 to H-6, which were δ 4.08 (H-3)/2.35 (H-4)/1.63 (H-5)/4.17, 4.14 (H-6) (Figure 5.47.A, 5.52.). The pyrone ring further validated with HMBC peaks from δ 4.08 (H-3) to δ 65.04 (C-6); δ 2.35 (H-4) to δ 173.92 (C-2), 24.90 (C-5); δ 1.63 (H-5) to δ 173.92 (C-2); δ 4.17 (H-6) to δ 173.92 (C-2), 68.40 (C-3) (Figure 5.47.B, 5.54.). The distinctive cross peaks from 17-OMe δ 3.67 (H-17) to δ 173.92 (C-2) and 68.40 (C-3) in the HMBC spectrum assigned the methoxyl group at C-4, which was comparable with the chemical shifts values in previous reports (Ding *et al.*, 2012). The title compound exhibited similarity with skeletons of α -pyrone based polypropionate derivatives (Cutignano *et al.*, 2007). The fusaripyrone polypropionates isolated from mollusk *H. fusari* and necpyrone from fungus *Nectria* sp. were found to enclose a methoxy group bonded at the sp^2 alkenic quaternary carbon, C-4 (Cutignano *et al.*, 2007), whereas the methoxy (17-OMe) in title compound was at sp^3 methine carbon located at C-3. The attachment of side chain 8,12-dimethyloct-8-enyl at C-5 was assigned by ^1H - ^1H COSY correlation from δ 1.63 (H-5) to 1.82 (H-7). The acyclic chain assignments were made by ^1H - ^1H COSY connectivities from H-9 to H-15, which were δ 5.35 (H-9)/2.01 (H-10)/1.30 (H-11)/1.50 (H-12)/1.13 (H-13)/0.87 (H-14) including δ 1.50 (H-12)/0.99 (H-15). This was further established from the HMBC correlations, such as δ 1.63 (H-5) to δ 135.14 (C-8), 31.93 (C-7); δ 1.82 (H-7) to δ 135.14 (C-8), 130.02 (C-9); δ 2.01 (H-10) to δ 30.97 (C-12); δ 1.50 (H-12) to δ 130.02 (C-9); δ 0.87 (H-14) to δ 30.97 (C-12), 22.69 (C-11); δ 0.99 (H-15) to δ 30.97 (C-12), 22.69 (C-11). The ^{13}C NMR signal at δ 135.14 was lesser in intensity than alkenic shift at δ 130.02, which was attributed to slow relaxation due to sp^2 quaternary carbon. The relaxation delay has been too small (RD = 1.7 s) for the carbons, which were not attached to any protons, that determined the closeness of protons. The presence of tri-substituted alkene, $>\text{C}(8)\text{-CH}(9)\text{-}$ was assigned by HMBCs from δ 5.35 (H-9) to sp^2 quaternary carbon at δ 135.14 (C-8) in side chain moiety (Roviroso and San-Martin 2006). The low-field singlet methyl (C-16) was bonded to alkenic quaternary carbon at C-8, which was proposed by HMBC relations from δ 1.86 (H-16) to δ 130.02 (C-9), 135.14 (C-8) and based on earlier literatures (Bromley *et al.*, 2012). The *cis* (Z) geometrical configuration of alkenic proton at C-9 (δ 5.35) in dimethyloct-8-ene confirmed from its lesser *J* value (3.95 Hz). The greater chemical resonance of C-16 alkenic methyl (δC 28.03) than

typical alkenic shift values (δ C 13-19) further specified the *cis*-configuration (*Z*) of C-8 alkene (Bromley *et al.*, 2012; Rovirosa and San-Martin 2006). The relative configurations at chiral centre, mainly that of C-3 with methoxy proton and C-5 with (*E*)-8,12-dimethyloct-8-enyl chain deduced from NOESY experiments (Figure 5.55.). NOE cross relations among the protons, δ 4.08 (H-3)/4.17 (H α -6)/5.35 (H-9)/1.86 (H-16)/1.50 (H-12)/0.87 (H-14) affirmed their close proximity and equiplaner alignment, and arbitrarily assigned as α -disposed. Other NOEs recorded between δ 1.63 (H-5)/4.14 (H β -6)/0.99 (H-15) designated that these moieties were on same side of molecular plane, and thus, orientated at β -plane of reference (Figure 5.48.A). The α -disposed H-3 proton confirmed the β -orientation of 17-OMe group, likewise the β -oriented H-5 proton established the α -geometry of (*E*)-8,12-dimethyloct-8-enyl side chain.

Table 5.8.: NMR spectroscopic data of tetrahydro-3-methoxy-5-((*E*)-8,12-dimethyloct-8-enyl)-pyran-2-one (**4**) in CDCl₃

C. No.	¹³ C	¹ H (int.,mult., <i>J</i> in Hz) ^a	COSY	HMBC
1	-	-	-	-
2	173.92	-	-	-
3	68.40	4.08 (1H α ,t)	H-4	C-6
4	34.11	2.35 (2H,t)	H-5	C-2,7,5
5	24.90	1.63 (1H β ,m)	H-6,7	C-4,2,8,7
6	65.04	4.17 (1H α ,d) 4.14 (1H β ,d)	- -	C-2,3 -
7	31.93	1.82 (2H,d)	-	C-8,9
8	135.14	-	-	-
9	130.02	5.35 (1H,t,3.95)	H-10	C-10,8
10	27.22	2.01 (2H,m)	H-11	C-9,12
11	22.69	1.30 (2H,m)	H-12	C-12
12	30.97	1.50 (1H α ,m)	H-13,15	C-9
13	23.73	1.13 (2H,m)	H-14	C-12
14	14.02	0.87 (3H,t)	-	C-12,11
15	15.26	0.99 (3H β ,d)	-	C-12,11
16	28.03	1.86 (3H α ,s)	-	C-8,9
17	50.68	3.67 (3H,s)	-	C-3,2

¹H NMR spectra recorded using Bruker AVANCE III 500MHz (AV 500) spectrometer (Bruker, Karlsruhe, Germany) in CDCl₃ as aprotic solvent at ambient temperature with TMS as the internal standard (δ 0 ppm). The ¹H NMR spectra were recorded at 500MHz, while the ¹³C NMR spectra were recorded at 125MHz. ^aValues in ppm, multiplicity and coupling constants (*J*=Hz) were indicated in parentheses. The

assignments were made with the aid of the ^1H - ^1H COSY, HSQC, HMBC and NOESY experiments

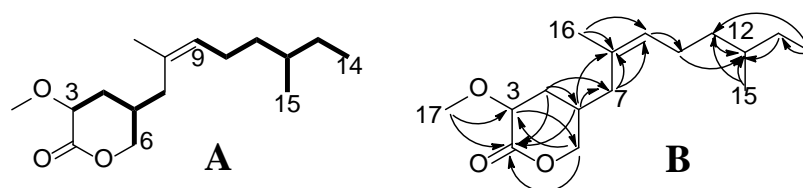


Figure 5.47.: ^1H - ^1H COSY (A) and HMBC (B) correlations of tetrahydro-3-methoxy-5-((E)-8,12-dimethyloct-8-enyl)-pyran-2-one (4). The key ^1H - ^1H COSY couplings have been represented by bold face bonds. The HMBC couplings were indicated by double barbed arrow

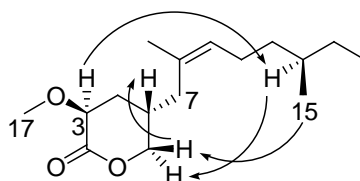


Figure 5.48.: NOESY correlations of tetrahydro-3-methoxy-5-((E)-8,12-dimethyloct-8-enyl)-pyran-2-one (4). The NOESY relations were represented by double barbed arrow

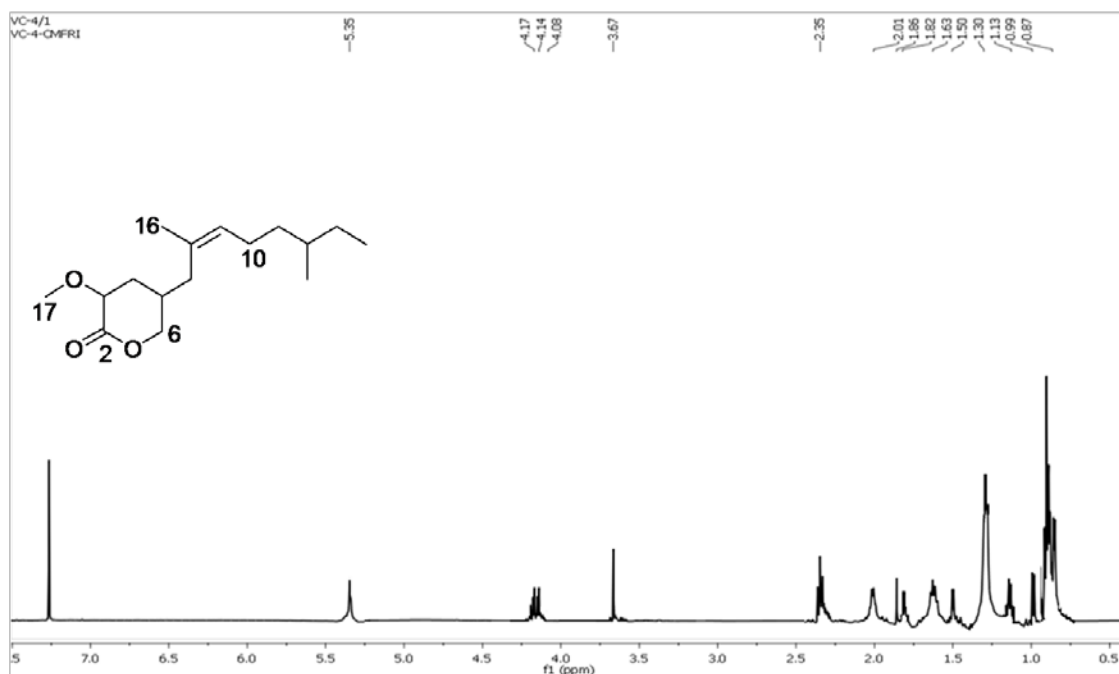


Figure 5.49.: ^1H NMR spectrum of tetrahydro-3-methoxy-5-((E)-8,12-dimethyloct-8-enyl)-pyran-2-one (4)

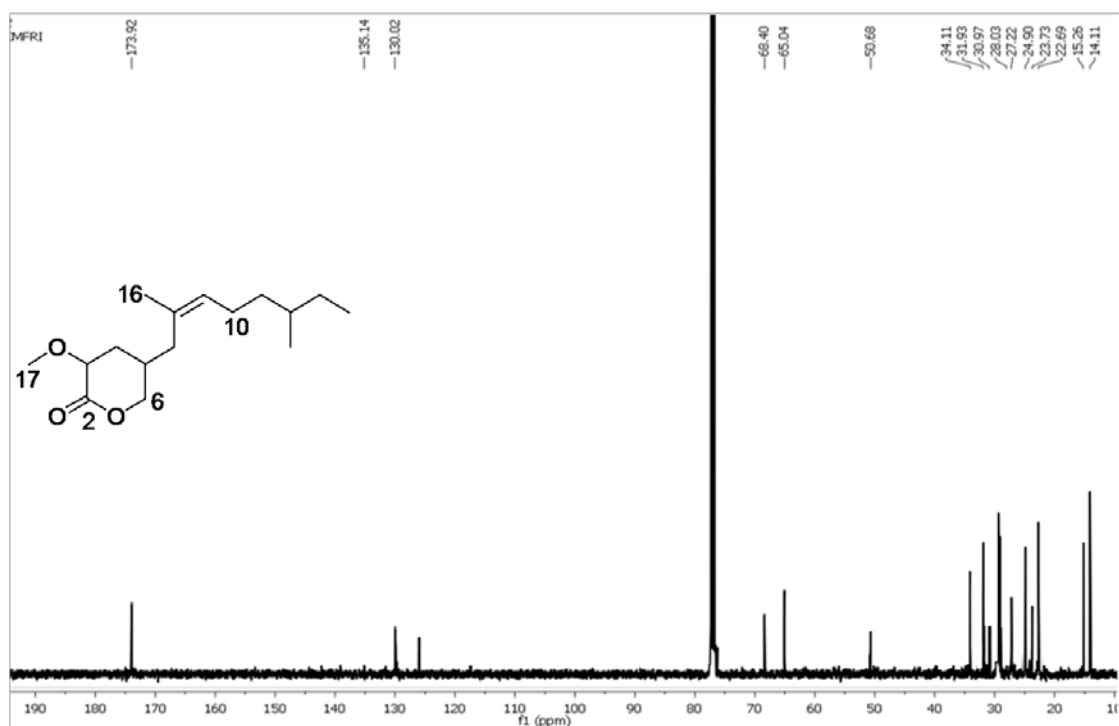


Figure 5.50.: ^{13}C NMR spectrum of tetrahydro-3-methoxy-5-((E)-8,12-dimethyloct-8-enyl)-pyran-2-one (4)

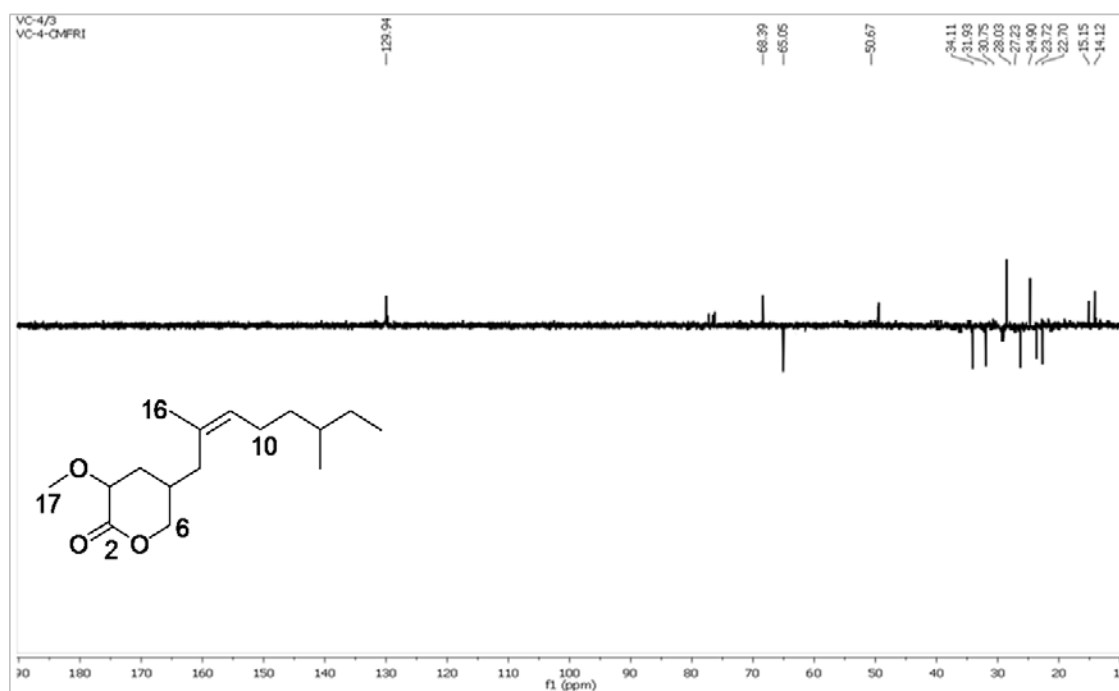


Figure 5.51.: $^{135}\text{DEPT}$ NMR spectrum of tetrahydro-3-methoxy-5-((E)-8,12-dimethyloct-8-enyl)-pyran-2-one (4)

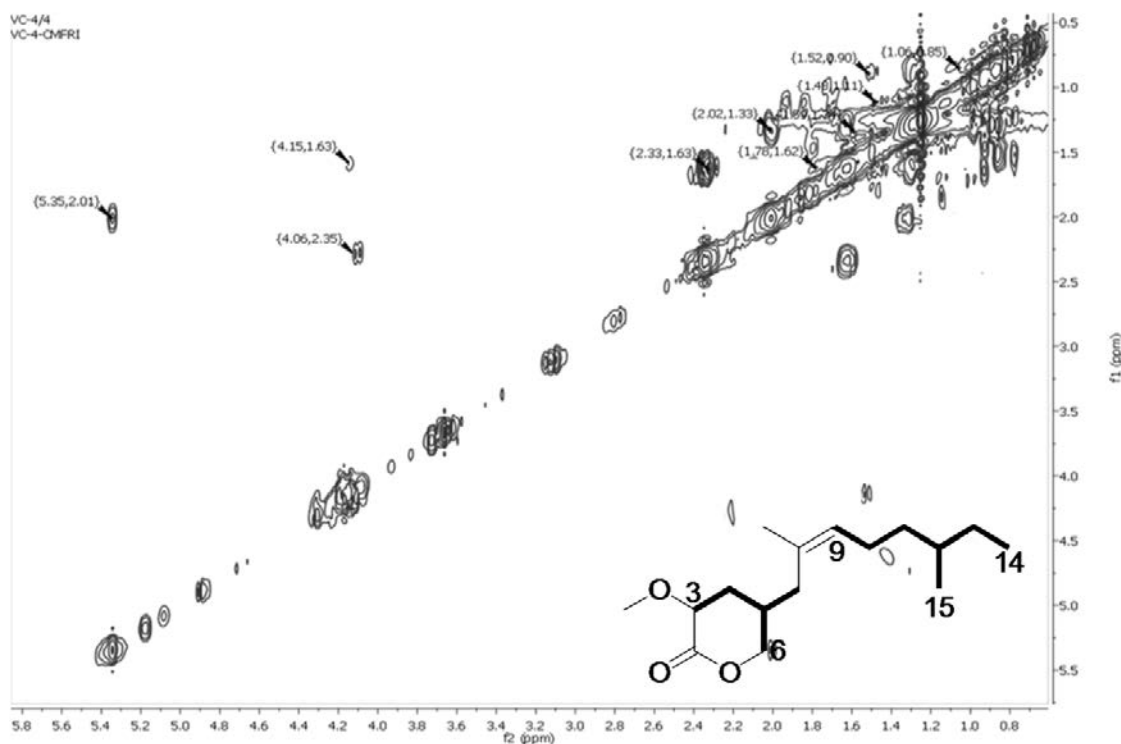


Figure 5.52.: ^1H - ^1H COSY NMR spectrum of tetrahydro-3-methoxy-5-((*E*)-8,12-dimethyl-oct-8-enyl)-pyran-2-one (**4**)

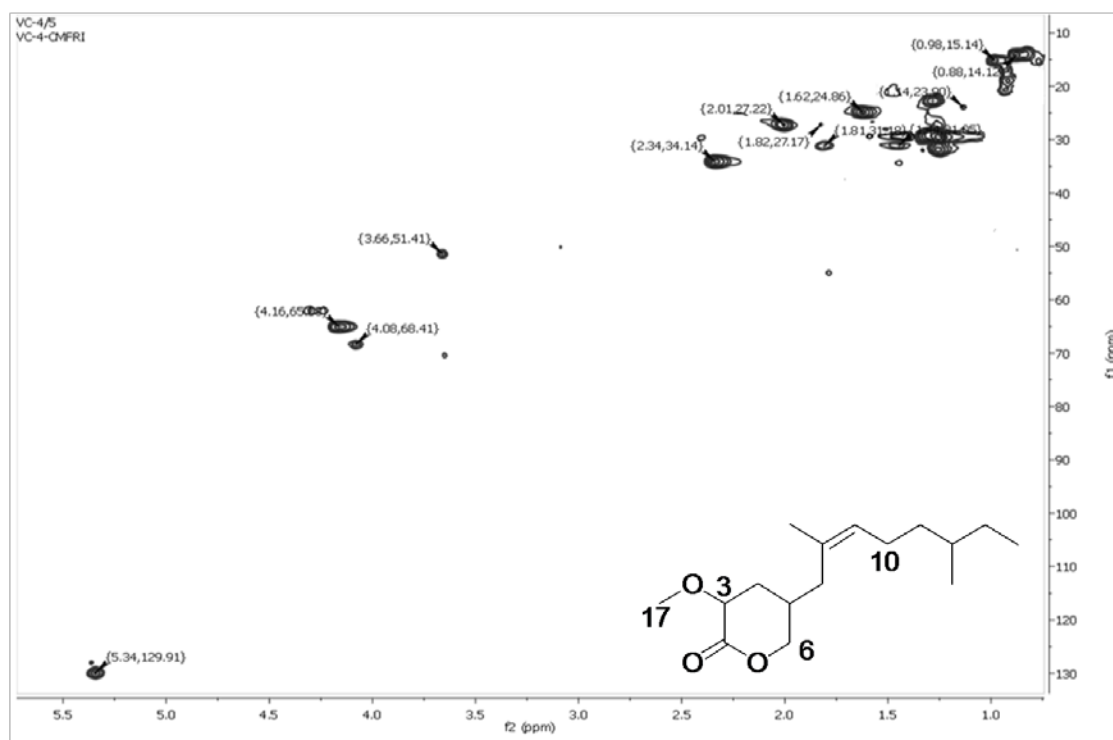


Figure 5.53.: HSQC NMR spectrum of tetrahydro-3-methoxy-5-((*E*)-8,12-dimethyloct-8-enyl)-pyran-2-one (**4**)

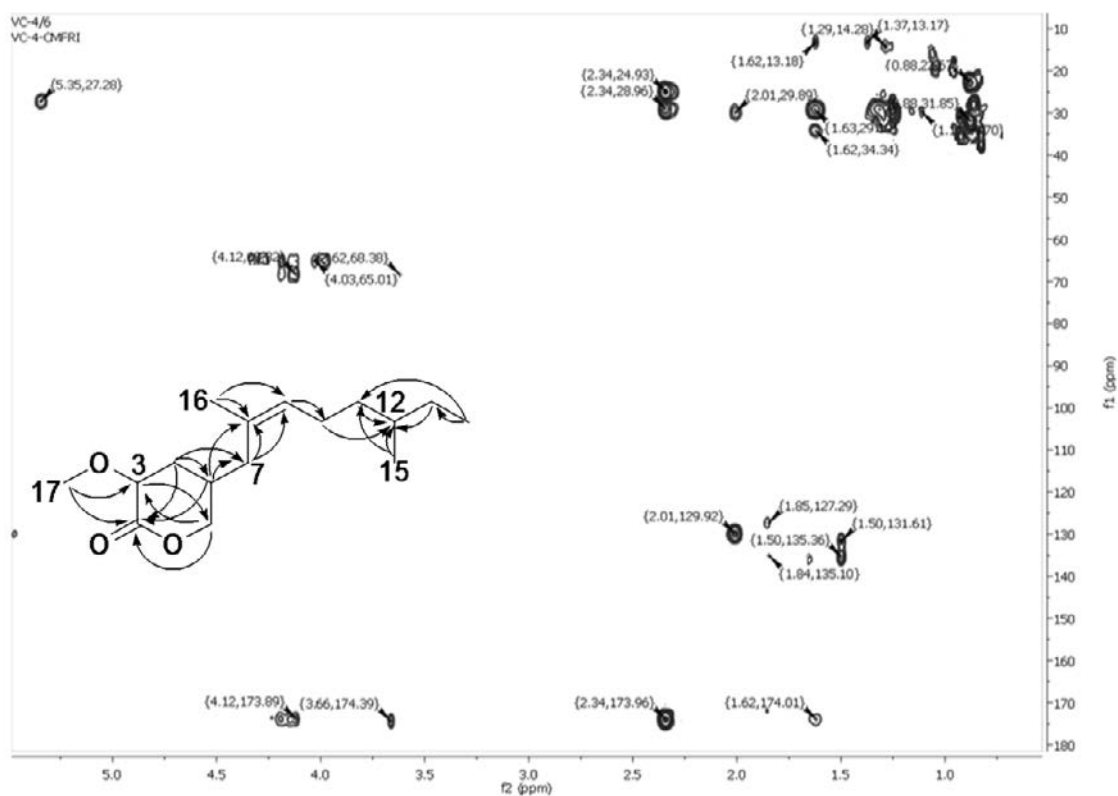


Figure 5.54.: HMBC NMR spectrum of tetrahydro-3-methoxy-5-((*E*)-8,12-dimethyloct-8-enyl)-pyran-2-one (**4**)

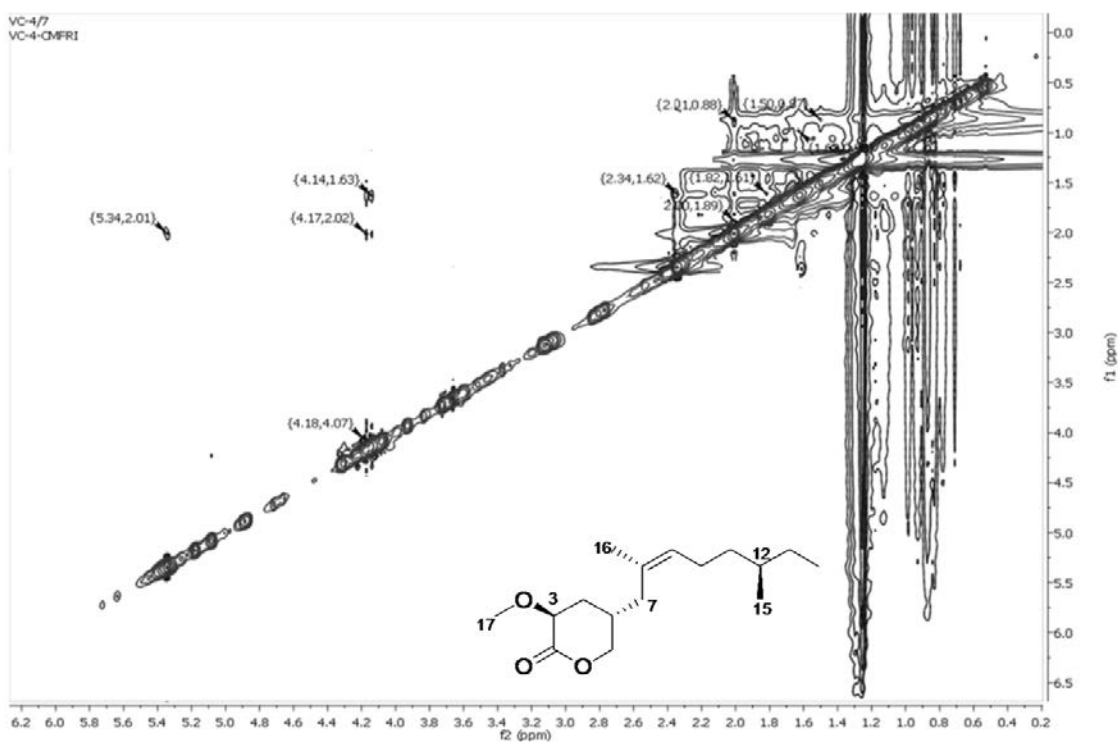


Figure 5.55.: NOESY NMR spectrum of tetrahydro-3-methoxy-5-((*E*)-8,12-dimethyloct-8-enyl)-pyran-2-one (**4**)

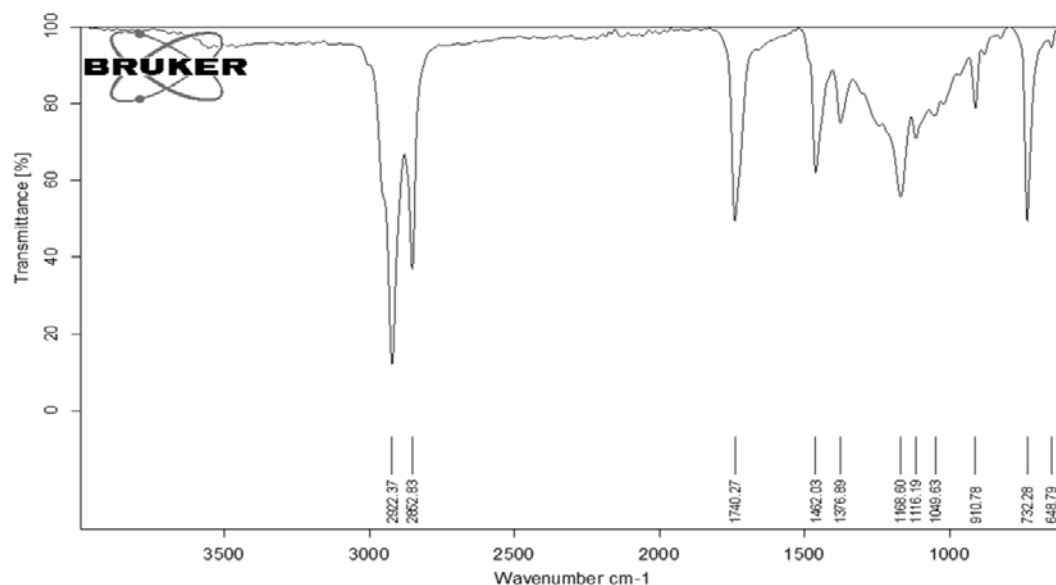


Figure 5.56.: FTIR spectrum of tetrahydro-3-methoxy-5-((*E*)-8,12-dimethyloct-8-enyl)-pyran-2-one (**4**)

The IR spectrum was exhibited absorption bands at 1740 cm^{-1} which indicated the presence of pyrone ring. The presence of alkane and alkoxy stretching vibrations were recorded at 2922 and 1049 cm^{-1} , respectively (Figure 5.56.).

The mass fragmentation spectrum (Figure 5.57.) designated that the molecular ion peak at m/z 268 that eliminated a methoxy radical to afford an ion at m/z 236 (**a**). The later seemed to undergo methyl and ethyl eliminations to acquire an ion at m/z 194 (**b**), followed two ethyl radical eliminations registering peaks at m/z 166 (**c**) and 141 (**d**), respectively. The ion at m/z 141 (**d**) fragmented into m/z 113 (**e**) and 97 (**f**) by the removal of ethyl and methyl radicals, respectively. The fragment ion at m/z 97 (**f**), underwent removal of oxygen radical followed by the intermolecular rearrangements to resulted in the generation of penta-dienol ion at m/z 83 (**f**). The hydroxyl radical was eliminated from later ion followed by $\text{CH}_2^{\bullet\bullet}$ elimination yielded the base peak of butene (**i**, $\text{C}_4\text{H}_8^{\bullet+}$) at m/z 56 (Figure 5.58.).

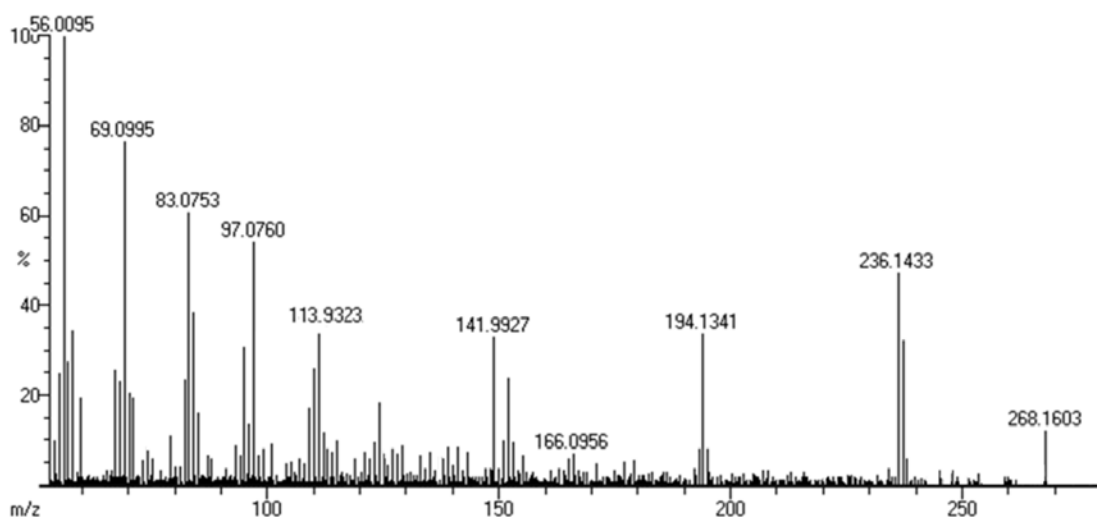


Figure 5.57.: EIMS spectrum of tetrahydro-3-methoxy-5-((*E*)-8,12-dimethyloct-8-enyl)-pyran-2-one (**4**)

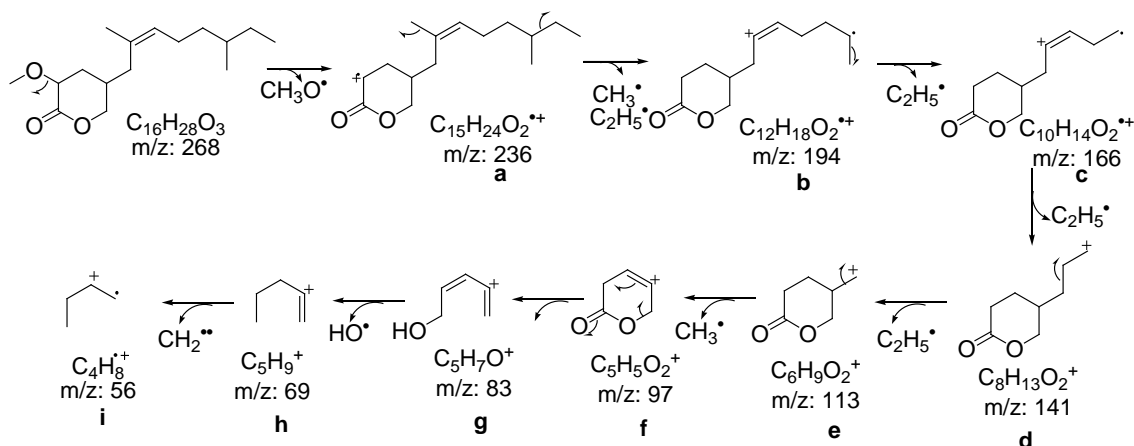
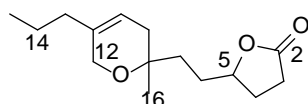


Figure 5.58.: Mass fragmentation of tetrahydro-3-methoxy-5-((*E*)-8,12-dimethyloct-8-enyl)-pyran-2-one (**4**)

5.3.2.2.C. Structural characterization of compound 5 (VC₂₋₆₋₆₋₂₋₂)

Dihydro-5-(8-(9,12-dihydro-8-methyl-11-propyl-2*H*-pyran-8-yl)-ethyl)-furan-2-(3*H*)-one (**5**)



Yield	69 mg; 0.15%
Physical description	Pale brown oily
Molecular formula	C ₁₅ H ₂₄ O ₃
Molecular mass	252.1725

The irregular C15 furano meroterpenoid, dihydro-5-(8-(9,12-dihydro-8-methyl-11-propyl-2*H*-pyran-8-yl)ethyl)-furan-2(3*H*)-one (**5**) yielded as pale brown oily compound. It displayed UV absorbance (in MeOH) at λ_{max} (log ϵ 2.52) 234.2 nm was assigned to carbonyl systems (Figure 5.59.). The purity of the compound supported by RP C18 HPLC using 1:4 (v/v) MeOH:MeCN (R_t 4.38) experiments (Figure 5.60.).

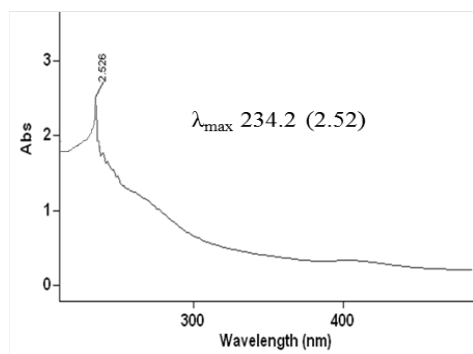


Figure 5.59.: UV spectrum of dihydro-5-(8-(9,12-dihydro-8-methyl-11-propyl-2*H*-pyran-8-yl)-ethyl)-furan-2-(3*H*)-one (**5**)

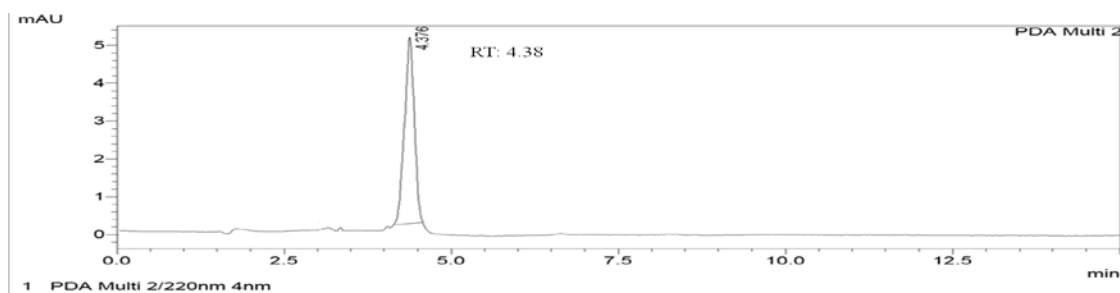


Figure 5.60.: HPLC chromatogram of dihydro-5-(8-(9,12-dihydro-8-methyl-11-propyl-2*H*-pyran-8-yl)-ethyl)-furan-2-(3*H*)-one (**5**)

The irregular C15 furano meroterpenoid, (**5**) with molecular formula $C_{15}H_{24}O_3$ having double bond equivalences of four (two double bonds and two ring moieties). The sesquiterpene based furano meroterpenoid was elucidated on the basis of extensive ^1H - ^1H COSY, HSQC and HMBC analyses (Figure 5.66.-5.68.). Resonances for two methyls, one sp^3 methine, one sp^2 methine, eight sp^3 methylenes and three quaternary (alkenic, carboxylate and oxygenated) groups were accounted in the ^1H NMR in conjugation with ^{13}C NMR and DEPT spectra (Table 5.9.; Figure 5.63.-5.65). The molecular ion peak was recorded at m/z 252 (EIMS: found m/z 252.1730 $[\text{M}]^+$ cal. 252.1725). The characteristic trisubstituted alkene (δH 5.35/ δC 130.02 and δC 135.84),

one each of ester carbonyl (δ C 177.63) (Huang *et al.*, 2008), oxygenated methine (δ H 4.08/ δ C 68.41), and oxygenated methylene (δ H 4.17, 4.14/ δ C 65.04) were recognized by HSQC resonances. The two dimensional NMR of **5** explained that it was composed of two parts, (A) {dihydro-furan-2(3*H*)-one part from C-2 to C-5} and (B) {8-(9,12-dihydro-8-methyl-11-propyl)-2*H*-pyran-8-yl from C-8 to C-12 comprising C-13 to C-16}. The ring structure A was evident by the spin system from H-3 to H-5 { δ 2.35 (assigned to H-3)/1.65 (H-4)/4.08 (H-5)} as deduced from the ^1H - ^1H COSY spectrum (Figure 5.61.A, 5.66.). In addition, HMBC couplings from δ 2.35 (H-3) to δ 177.63 (C-2), 24.72 (C-4); δ 1.65 (H-4) to δ 177.63 (C-2) and δ 4.08 (H-5) to δ 177.63 (C-2), 33.67 (C-3) supported the presence of dihydro-furan-2-one ring system (A) (Figure 5.61.B, 5.68.). The two spin systems from H-9 to H-10 { δ 2.02 (H-9)/5.35 (H-10)} and H-13 to H-15 { δ 1.86 (H-13)/1.28 (H-14)/0.89 (H-15)} validated the partial structure of B. The long range HMBCs from δ 2.02 (H-9) to δ 135.84 (C-11); δ 5.35 (H-10) to δ 135.84 (C-11); δ 1.86 (H-13) to δ 135.84 (C-11) attributed that these two spin systems were linked through a quaternary carbon at C-11. Furthermore, HMBC correlations from δ 2.02 (H-9) to δ 72.12 (C-8); δ 5.35 (H-10) to δ 65.04 (C-12); δ 4.17 (H-12) to δ 72.12 (C-8); δ 1.86 (H-13) to δ 130.02 (C-10), 135.84 (C-11) and δ 1.28 (H-14) to δ 14.11 (C-15) assigned 9,12-dihydro-11-propyl-2*H*-pyran-8-yl framework. The methyl singlet at δ 1.25 (H-16) was verified with its HMBC correlations to δ 72.12 (C-8) and 27.23 (C-9). The partial-units, (A) {dihydro-furan-2(3*H*)-one} and (B) {8-(9,12-dihydro-8-methyl-11-propyl)-2*H*-pyran-8-yl} were deduced to be connected through ethyl linkage C-6 to C-7 by the examination of spin system from H-5 to H-7 { δ 4.08 (H-5)/1.60 (H-6)/1.30 (H-7)} along with ^1H - ^{13}C long range correlations, such as δ 1.65 (H-4) to δ 31.93 (C-6); δ 4.08 (H-5) to δ 31.93 (H-6); δ 1.60 (H-6) to δ 33.67 (C-3); δ 1.30 (H-7) to δ 31.93 (C-6), 72.12 (C-8) and δ 2.02 (H-9) to δ 29.69 (C-7). This can be compared with an ionone derivative enclosing the partial structures, furan-2-one and cyclohexane connected through a vinyl linkage (Huang *et al.*, 2016). Biologically active furanosesquiterpenes composed of furanone and cyclohexane ring network through ethyl linkage from marine invertebrates was reported (Huang *et al.*, 2008). Another furanosesquiterpene from marine sponge enclosing hydroxy furanone and cyclohexane moieties were also found to be connected by ethyl linkage (Venkateswarlu *et al.*, 1994). The structures of previously reported sesquiterpene alcohol, pelseneeriols and furanosesquiterpenoid

isomicrocionins were comprised of furan rings connected to cyclohexane ring through ethyl bond (Gaspar *et al.*, 2005; Gaspar *et al.*, 2008). These compounds were composed of cyclohexane rings, whereas the present compound (**5**) enclosed a pyran ring moiety. There is one chiral center (C-5) around the dihydro-furan-2-one ring and its relative orientations were determined by extensive NOESY correlations (Figure 5.62., 5.69.). The NOE couplings between δ 4.14 (H α -12)/1.25 (H-16) confirmed their equiplaner disposition with each other, and therefore, arbitrarily considered as α -oriented with reference to molecular plane of reference. Furthermore, NOEs between δ 4.08 (H-5)/5.35 (H-10)/4.17 (H β -12) indicated their disposition at identical molecular plane, and were found to be *trans* with α -oriented protons (H α -12, H-16), which determined their β -position. Since, methyl singlet at C-8 was determined as α -disposed, the ethyl moiety at C-8 adopted β -orientation (Huang *et al.*, 2008).

Table 5.9.: NMR spectroscopic data of dihydro-5-(8-(9,12-dihydro-8-methyl-11-propyl-2H-pyran-8-yl)-ethyl)-furan-2-(3H)-one (**5**) in CDCl₃

C. No.	¹³ C	¹ H (int.,mult.,J in Hz) ^a	COSY HMBC	
1	-	-	-	-
2	177.63	-	-	-
3	33.67	2.35 (2H,t)	H-4	C-2,4
4	24.72	1.65 (2H,m)	H-5	C-2,3,6
5	68.41	4.08 (1H β ,m)	H-6	C-2,3,6
6	31.93	1.60 (2H,m)	H-7	C-3,7
7	29.69	1.30 (2H,t)	-	C-6,8,9
8	72.12	-	-	-
9	27.23	2.02 (2H,d)	H-10	C-10,11,8,7
10	130.02	5.35 (1H β , t,7.23)	-	C-11,12,9
11	135.84	-	-	-
12	65.04	4.17 (1H β ,d) 4.14 (1H α ,d)	-	C-11,8 -
13	34.11	1.86 (2H,t)	H-14	C-10,11,9
14	22.69	1.28 (2H,m)	H-15	C-13,15
15	14.11	0.89 (3H,t)	-	C-13,14
16	30.73	1.25 (3H α ,s)	-	C-8,9

¹H NMR spectra recorded using Bruker AVANCE III 500MHz (AV 500) spectrometer (Bruker, Karlsruhe, Germany) in CDCl₃ as aprotic solvent at ambient temperature with TMS as the internal standard (δ 0 ppm). The ¹H NMR spectra were recorded at 500MHz, while the ¹³C NMR spectra were recorded at 125MHz. ^aValues in ppm,

multiplicity and coupling constants (J =Hz) were indicated in parentheses. The assignments were made with the aid of the ^1H - ^1H COSY, HSQC, HMBC and NOESY experiments

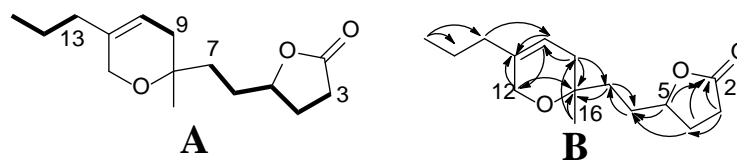


Figure 5.61.: ^1H - ^1H COSY (A) and HMBC (B) correlations of dihydro-5-(8-(9,12-dihydro-8-methyl-11-propyl-2H-pyran-8-yl)-ethyl)-furan-2-(3H)-one (**5**). The key ^1H - ^1H COSY couplings have been represented by the bold face bonds. The HMBC couplings were indicated by double barbed arrow

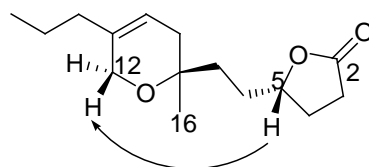


Figure 5.62.: NOESY correlations of dihydro-5-(8-(9,12-dihydro-8-methyl-11-propyl-2H-pyran-8-yl)-ethyl)-furan-2-(3H)-one (**5**). The NOESY relations were represented by double barbed arrow

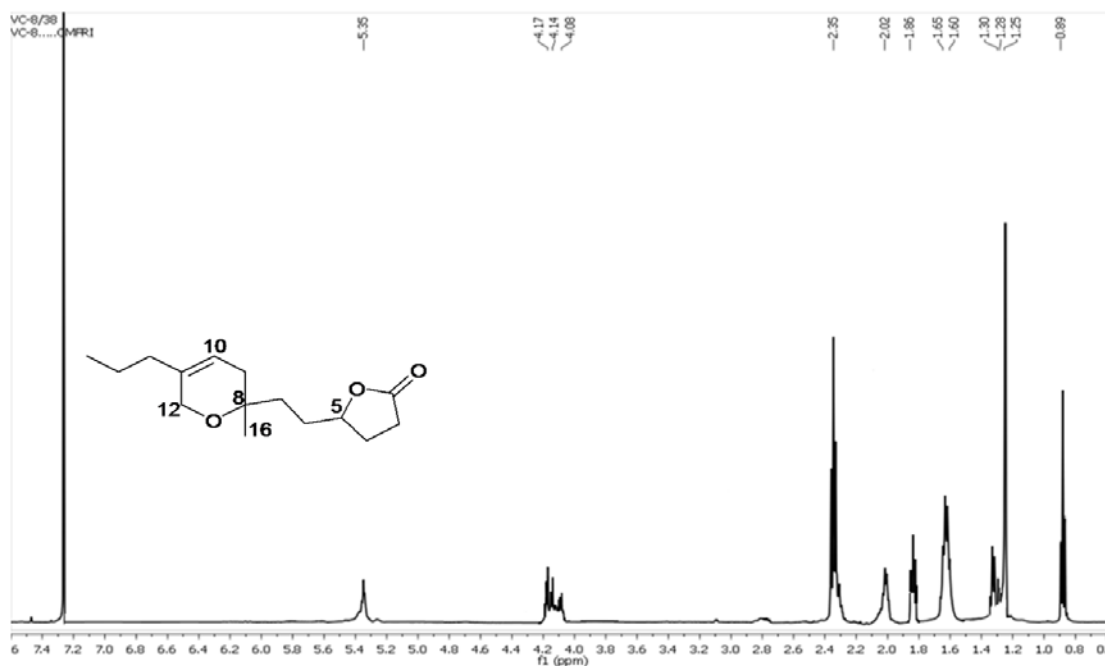


Figure 5.63.: ^1H NMR spectrum of dihydro-5-(8-(9,12-dihydro-8-methyl-11-propyl-2H-pyran-8-yl)-ethyl)-furan-2-(3H)-one (**5**)

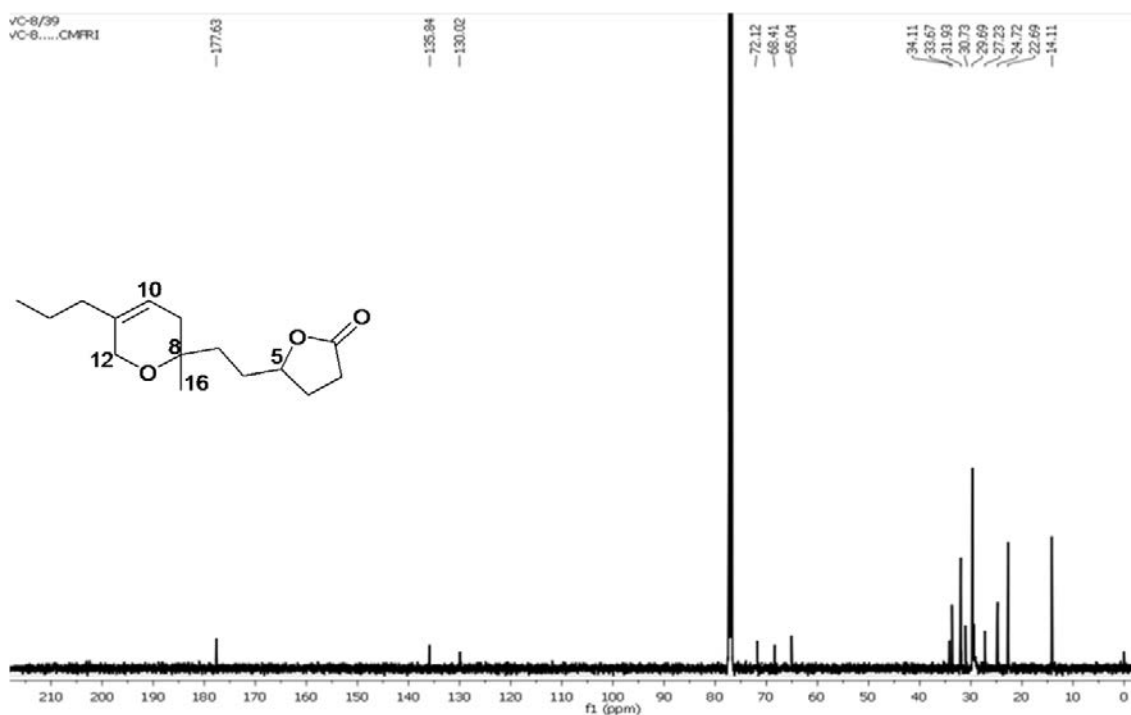


Figure 5.64.: ¹³C NMR spectrum of dihydro-5-(8-(9,12-dihydro-8-methyl-11-propyl-2H-pyran-8-yl)-ethyl)-furan-2-(3H)-one (**5**)

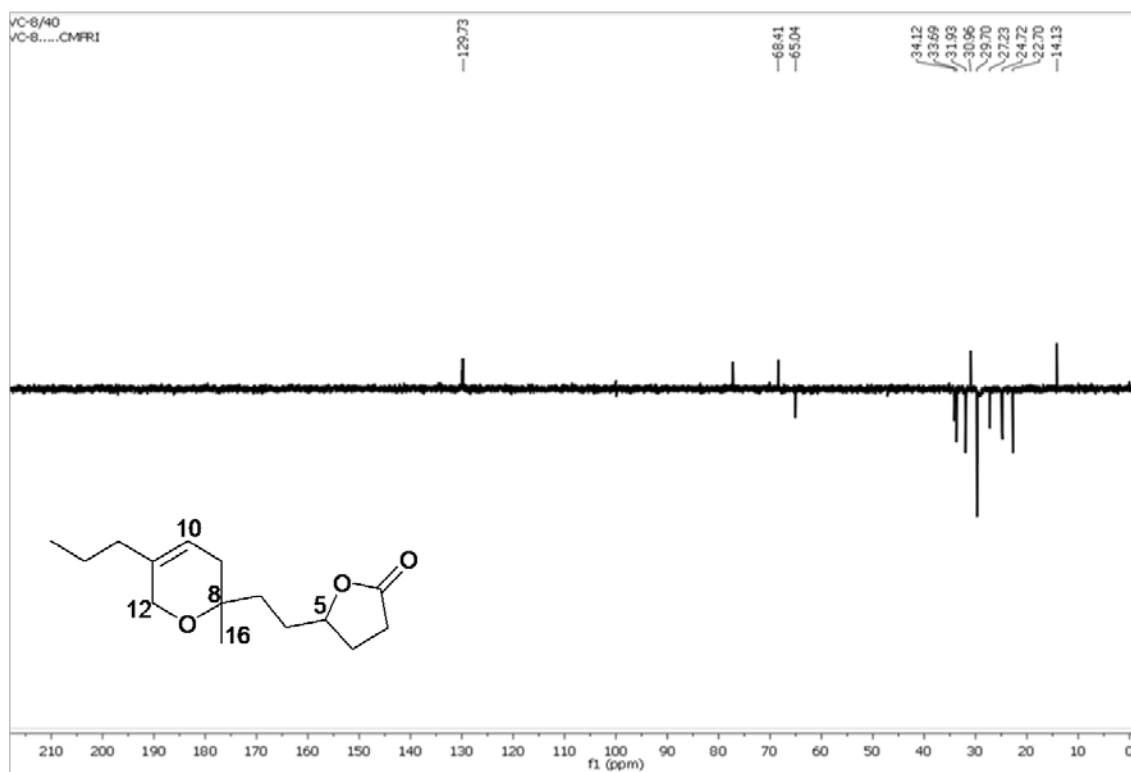


Figure 5.65.: ¹³⁵DEPT NMR spectrum of dihydro-5-(8-(9,12-dihydro-8-methyl-11-propyl-2H-pyran-8-yl)-ethyl)-furan-2-(3H)-one (**5**)

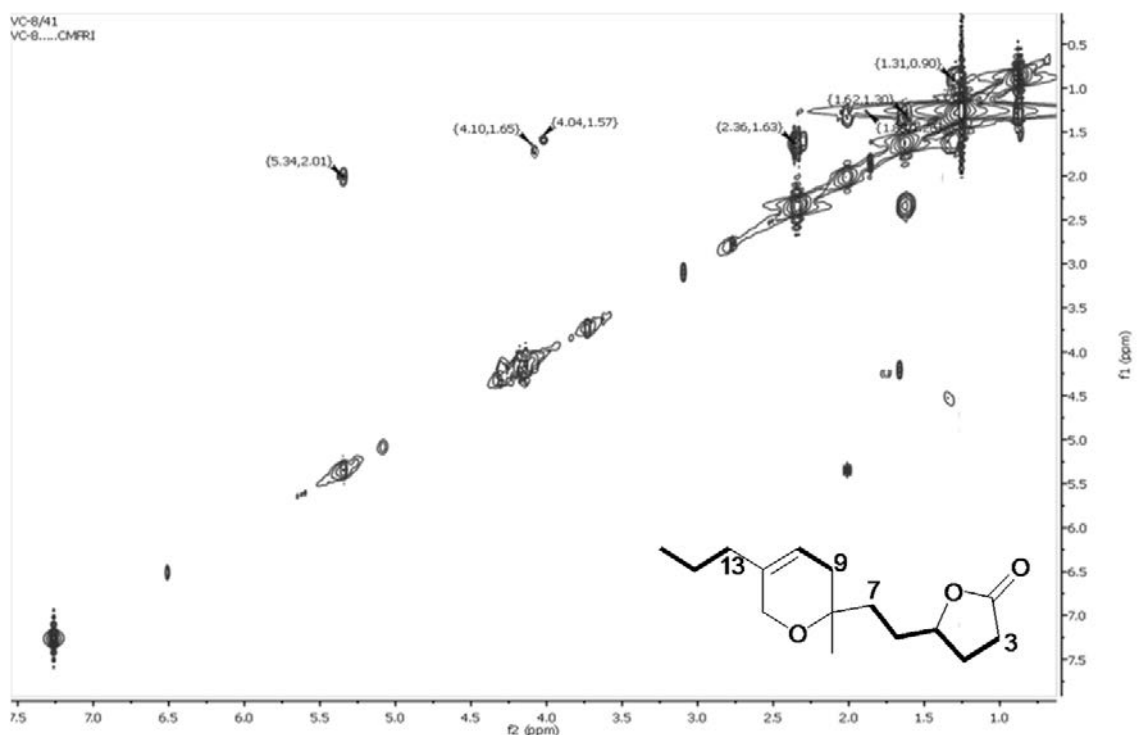


Figure 5.66.: ^1H - ^1H COSY NMR spectrum of dihydro-5-(8-(9,12-dihydro-8-methyl-11-propyl-2H-pyran-8-yl)-ethyl)-furan-2-(3H)-one (**5**)

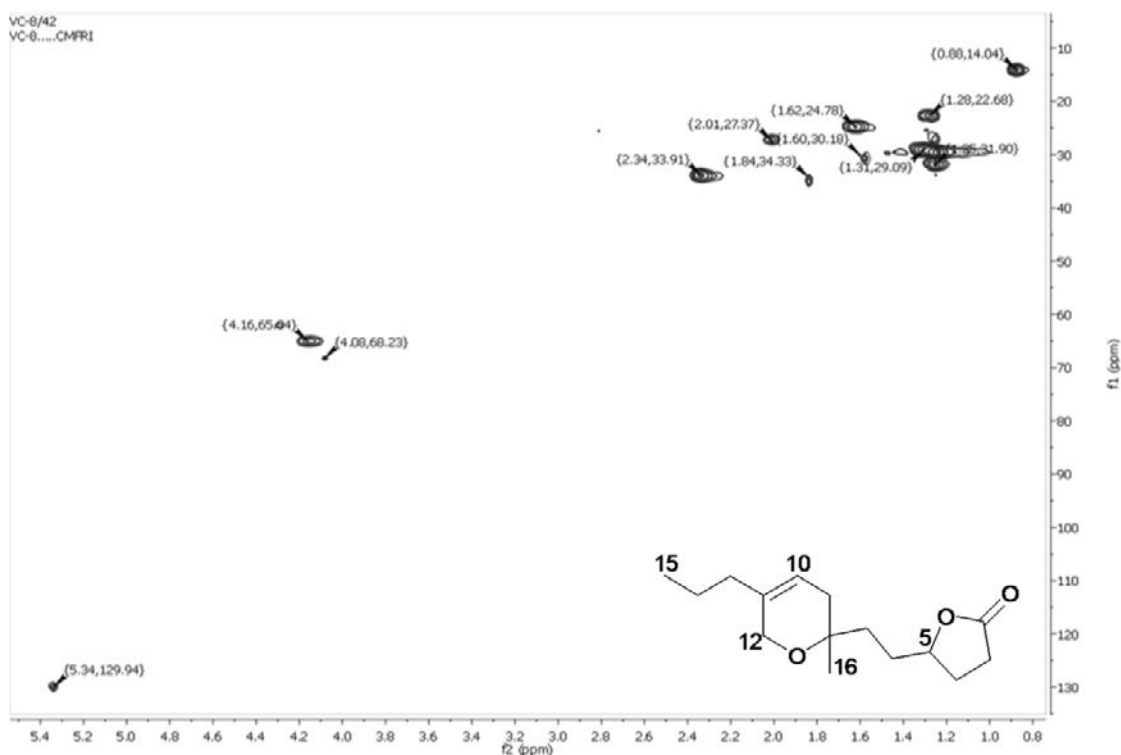


Figure 5.67.: HSQC NMR spectrum of dihydro-5-(8-(9,12-dihydro-8-methyl-11-propyl-2H-pyran-8-yl)-ethyl)-furan-2-(3H)-one (**5**)

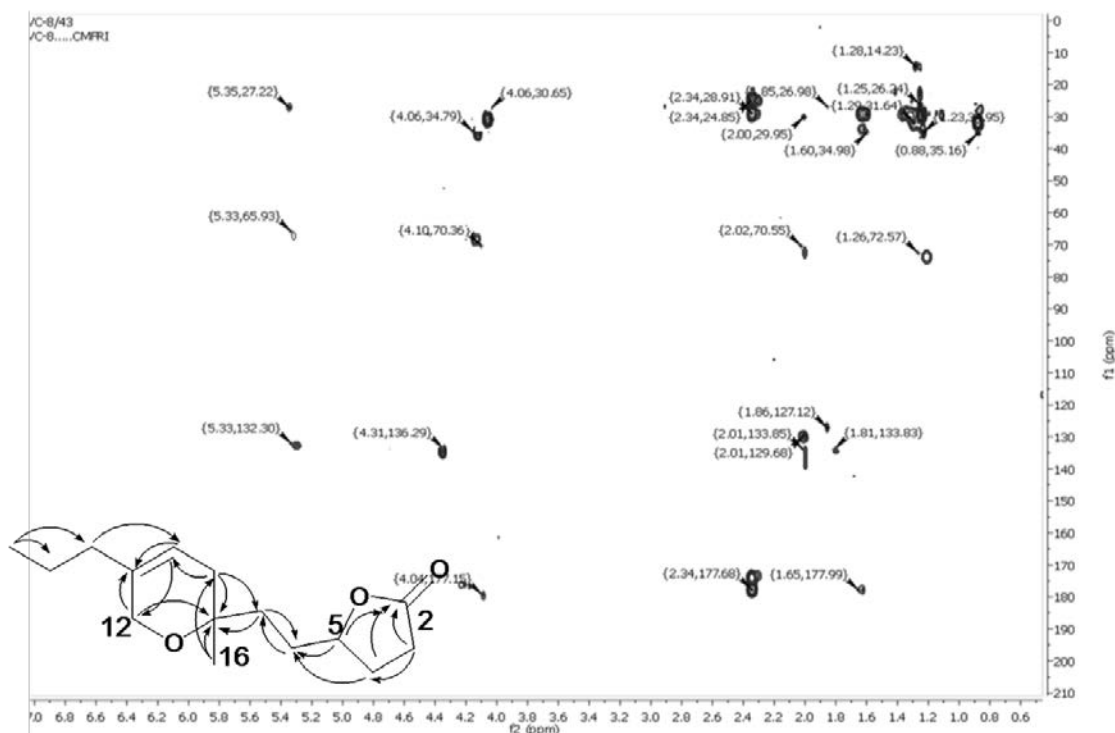


Figure 5.68.: HMBC NMR spectrum of dihydro-5-(8-(9,12-dihydro-8-methyl-11-propyl-2H-pyran-8-yl)-ethyl)-furan-2-(3H)-one (5)

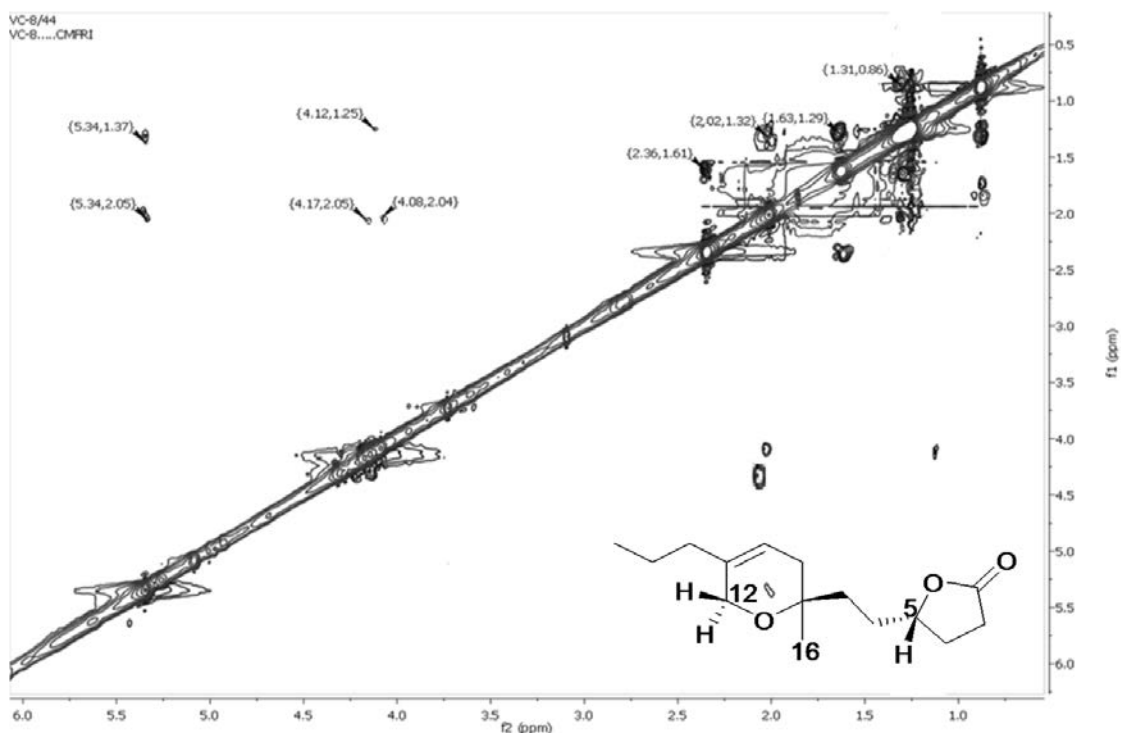


Figure 5.69.: NOESY NMR spectrum of dihydro-5-(8-(9,12-dihydro-8-methyl-11-propyl-2H-pyran-8-yl)-ethyl)-furan-2-(3H)-one (5)

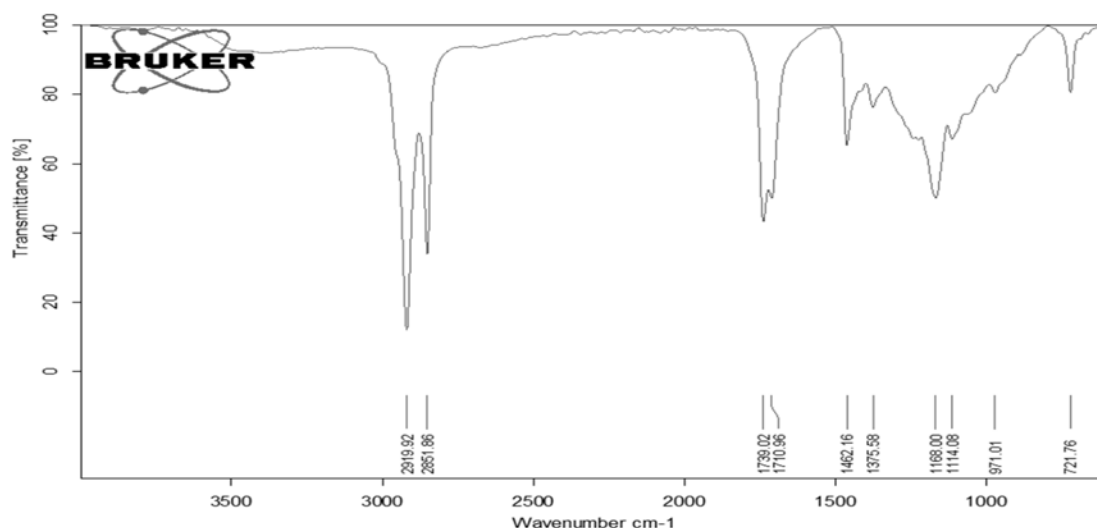


Figure 5.70.: FTIR spectrum of dihydro-5-(8-(9,12-dihydro-8-methyl-11-propyl-2*H*-pyran-8-yl)-ethyl)-furan-2-(3*H*)-one (**5**)

The IR spectrum was exhibited absorption bands at 1739 and 1710 cm^{-1} , which indicated the presence of a lactone group and a furanone ring in it. The alkane (2919 and 2851 cm^{-1}) and alkoxy (1168 and 1114 cm^{-1}) stretching vibrations were also recorded for the compound (Figure 5.70.).

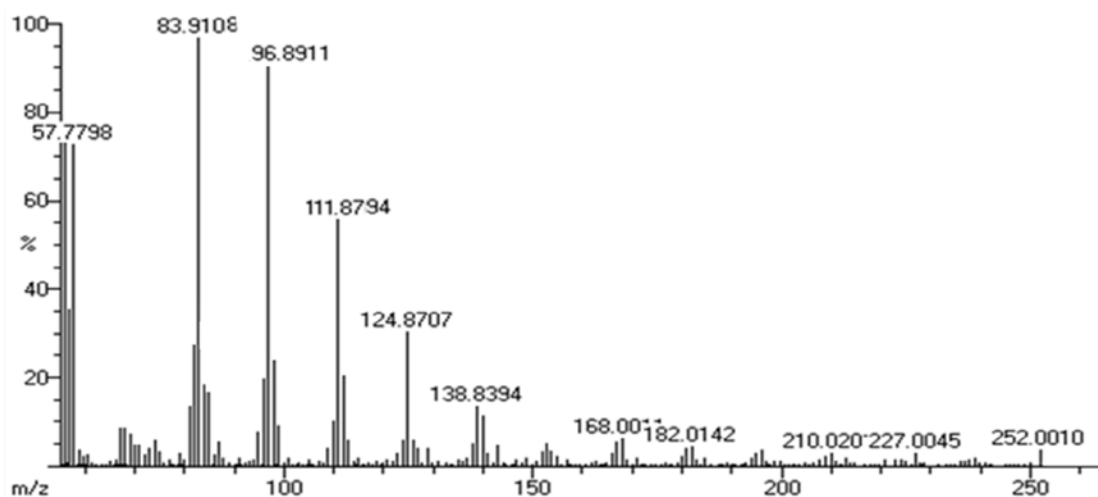


Figure 5.71.: EIMS spectrum of dihydro-5-(8-(9,12-dihydro-8-methyl-11-propyl-2*H*-pyran-8-yl)-ethyl)-furan-2-(3*H*)-one (**5**)

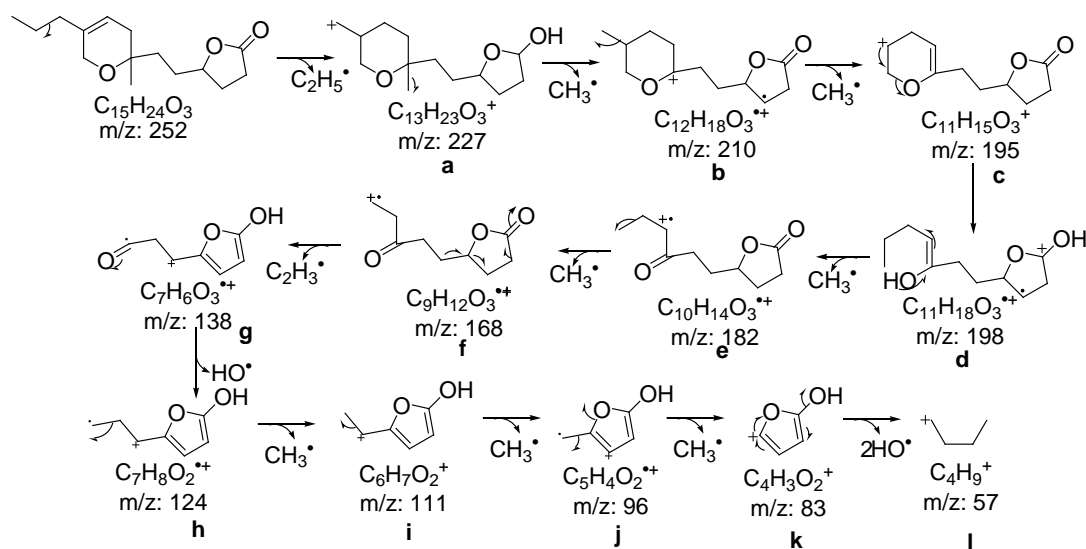


Figure 5.72.: Mass fragmentation pattern of dihydro-5-(8-(9,12-dihydro-8-methyl-11-propyl-2H-pyran-8-yl)-ethyl)-furan-2-(3H)-one (**5**)

The mass spectrum recorded its molecular ion peak at m/z 252, which was found to dissociate an ethyl radical to afford an ion at m/z 227 (**a**) for $C_{13}H_{23}O_3^+$ radical (Figure 5.71). This appeared to undergo sequential elimination of four methyl radicals afforded $C_9H_{12}O_3^{++}$ radical with m/z 168 (**f**). The later underwent elimination of $C_2H_3^{\bullet}$ radical, followed by hydroxy and two methyl radical to yield peaks at m/z 138 (**g**) 124 (**h**) and 96 (**j**). The base peak of furanol radical was obtained at m/z 83 (**k**, $C_4H_3O_2^+$) from the methylfuranol radical at m/z 96 (**j**). The base peak of furanol ion (m/z 83, **k**) underwent fragmentation to yield butane radical ($C_4H_9^+$) with m/z 57 (**l**) (Figure 5.72.).

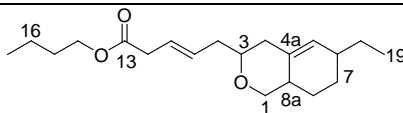
The furan enclosed metabolites were reported from *Hypocrea koningii*, *Doriopsilla pelseneeri* and *P. canaliculus* and these metabolites were found to be potent DPPH radical scavengers and strong anti-inflammatory agents (Ding *et al.*, 2015; Gaspar *et al.*, 2005; Wakimoto *et al.*, 2011). The titled hexahydro isobenzofuranone (**3**), tetrahydro pyranone (**4**) and dihydrofuran-dihydropyran (**5**) derivatives isolated from *V. cyprinoides* constitute a major part in the natural products and changes in the substitutions or rearrangements of functional groups can lead to better antioxidant candidates with greater selectivity in the food supplements and functional foods along with anti-inflammatory effects.

5.3.2.3. Structural characterization of hexahydro isochromenyl meroterpenoid derivatives (6-7)

The isochromenyl derivatives were found to be valuable bioactive pharmacophores with structural and functional peculiarities in the field of natural product research (Milan *et al.*, 2011; Nitin *et al.*, 2012). The 1*H*/3*H*-benzopyrans and hydrogenated 1*H*/3*H*-benzopyrans are the different forms of isochromene or isochromenone based skeletons (Boeckman *et al.*, 1988). The α -tocopherol is a popular example of natural benzopyran with antioxidant properties (Kindleysides *et al.*, 2012). The isochromenone secondary metabolite identified from a fungus, *Camptotheca acuminata* (Lin *et al.*, 2011) with medicinal properties. Herein, we have characterized two new substituted isochromenyl analogues, such as (10*E*)-butyl-9-(6-ethyl-3,4,6,7,8,8a-hexahydro-1*H*-isochromen-3-yl)-pent-10-enoate (**6**) and (12*E*)-(3,4,6,7,8,8a-hexahydro-1*H*-isochromen-3-yl)-methyl hept-12-enoate (**7**) from EtOAc:MeOH extract of *V. cyprinoides*.

5.3.2.3.A. Structural characterization of compound 6 (VC₃₋₄₋₃₋₁)

(10*E*)-Butyl- 9-(6-ethyl-3,4,6,7,8,8a-hexahydro-1*H*-isochromen-3-yl)-pent-10-enoate (**6**)



Yield	169 mg; 0.38%
Physical description	Light yellow oily
Molecular formula	C ₂₀ H ₃₂ O ₃
Molecular mass	320.2351

The irregularly arranged C₂₀ isochromenyl-meroterpenoid, (10*E*)-butyl-9-(6-ethyl-3,4,6,7,8,8a-hexahydro-1*H*-isochromen-3-yl)-pent-10-enoate was found to be in light yellow oily nature. It displayed UV absorbance (in MeOH) at λ_{max} (log ϵ 3.13) 231 nm assigned to a chromophore with olefinic and carbonyl systems (Figure 5.73.). The purity of the compound supported by RP C₁₈ HPLC using 1:4 (v/v) MeOH:MeCN (R_t 8.31) experiments (Figure 5.74.).

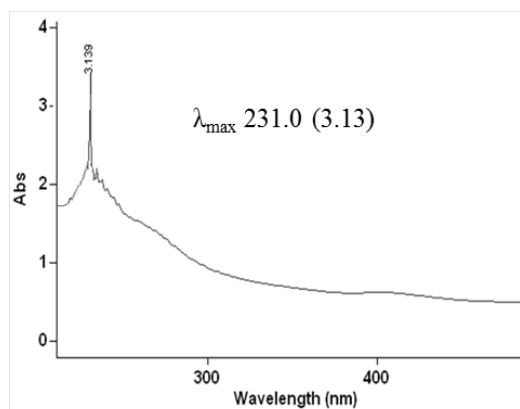


Figure 5.73.: UV spectrum of (10*E*)-butyl-9-(6-ethyl-3,4,6,7,8,8a-hexahydro-1*H*-isochromen-3-yl)-pent-10-enoate (**6**)

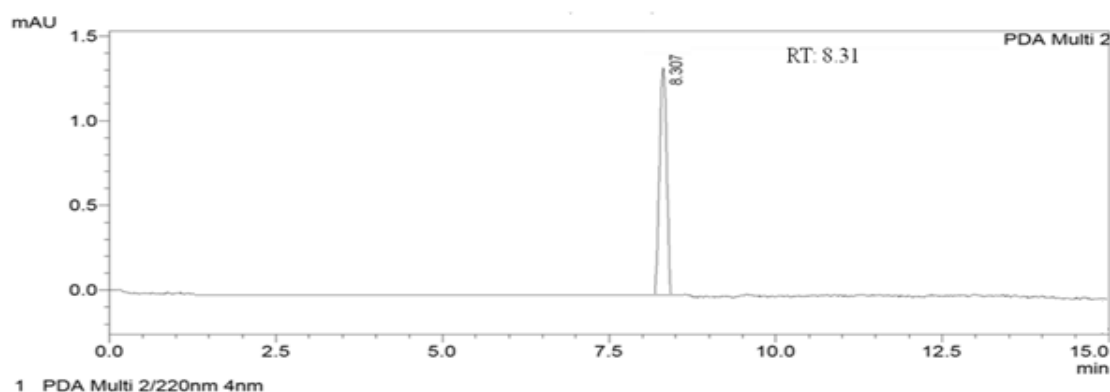


Figure 5.74.: HPLC chromatogram of (10*E*)-butyl-9-(6-ethyl-3,4,6,7,8,8a-hexahydro-1*H*-isochromen-3-yl)-pent-10-enoate (**6**)

The irregularly arranged C₂₀ hexahydro isochromenyl meroterpenoid, (**6**) deduced as C₂₀H₃₂O₃ based on comprehensive NMR and mass spectroscopy. The title compound exhibited five indices of hydrogen deficiency, which was satisfied by three double bonds and two cyclic systems. The molecular ion peak at 320 (EIMS: found m/z 320.2356 [M]⁺, cal. 320.2351) was recorded. The sesquiterpene type of chromenyl meroterpenoid determined on the basis of ¹H-¹H COSY, HSQC and HMBC experiments (Table 5.10.; Figure 5.80.-5.82). Chemical resonances for two quaternary (alkenic and carboxylate), three sp² methine, three sp³ methine, ten sp³ methylenes and two methyls (doublets) were determined by ¹H together with ¹³C NMR and DEPT experiments (Figure 5.77.-5.79.). The significant tri-substituted olefine (δ H 5.36/ δ C 129.93 and δ C 132.04), disubstituted alkene (δ H 5.40/ δ C 128.07 and δ H 5.43/ δ C 128.29), two oxygenated methylenes (δ H 3.70, 3.63/ δ C 63.36; δ H 4.20, 4.17/ δ C 65.14),

along with one each of carbonyl carbon (δC 174.34), oxygenated methine (δH 3.94/ δC 70.27), and carbonyl methylene (δH 2.86/ δC 25.64) were supported with detailed HSQC experiments. The extensive 2D NMR experiments of **6** demonstrated that it enclosed 6-ethyl-hexahydro-isochromenyl ring as basic skeleton and a butyl pentenoate moiety bonded at C-3 position of hexahydro chromenyl ring. Greatly downfielded ^1H NMR peaks at δ 4.17/4.20 HSQC with δC 65.14 (C-14) demonstrated the presence of oxygenated sp^3 hybridized groups, such as ester, whereas the signals at δ 3.63-3.70 and 3.94 HSQC with δC 63.36 (C-1) and 70.27 (C-3), respectively demonstrated the presence of oxygenated sp^3 hybridized methylene and methine, respectively ($^{135}\text{DEPT}$). The two oxygenated carbons at δ 63.36 (C-1) and 70.27 (C-3) implied that the oxygen atom found its place between the C-1 and C-3 positions, and the presence of an ether linkage ($-\text{CH}_2\text{-O-CH}<$), was therefore, attributed. Four spin systems were recorded at δ 3.70, 3.63 (H-1)/2.36 (H-8a)/1.73 (H-8)/1.62 (H-7)/2.03 (H-6)/5.36 (H-5); δ 2.03 (H-6)/1.29 (H-18)/0.90 (H-19) due to ethyl side chain at C-6; δ 2.44 (H-4)/3.94 (H-3)/2.07 (H-9)/5.40 (H-10) along with δ 5.43 (H-11)/2.86 (H-12), which attributed the pentenoate side chain at C-3; and δ 4.20, 4.17 (H-14)/1.64 (H-15)/1.32 (H-16)/0.99 (H-17) accounting for butyl substitution (Figure 5.75.A). The bicyclic hexahydro chromenyl ring affirmed by HMBCs from δ 3.70 (H-1) to δ 70.27 (C-3), 132.04 (C-4a); δ 3.94 (H-3) to δ 132.04 (C-4a); δ 2.44 (H-4) to δ 132.04 (C-4a), 31.91 (C-8), 34.04 (C-6); δ 5.36 (H-5) to δ 132.04 (C-4a) and δ 2.36 (H-8a) to δ 34.15 (C-4), 34.04 (C-6) (Figure 5.75.B). The HMBCs from δ 1.29 (H-18) to δ 34.04 (C-6) and δ 0.90 (H-19) to δ 22.68 (C-18), 29.65 (C-7) established the attachment of ethyl group $\{-\text{CH}_2(18)\text{-CH}_3(19)\}$ to C-6 of hexahydro-chromenyl ring. Other long bond connections were recorded from δ 2.07 (H-9) to δ 70.27 (C-3), 128.07 (C-10); δ 5.40 (H-10) to δ 27.21 (C-9), 25.64 (C-12) and δ 2.86 (H-12) to δ 174.34 (C-13) that suggested the attachment of pentenoate side chain at C-3. The butyl moiety of butyl pentenoate framework was assigned by HMBCs at δ 4.20 (H-14) to δ 174.34 (C-13) and δ 0.99 (H-17) to δ 29.68 (C-16). The geometrical arrangement of isolated alkene in pentenoate side chain calculated from their greater J values, which were δ 5.40 ($J=10.52$ Hz; H-10) and 5.43 ($J=10.97$ Hz; H-11), thus their *trans* (*E*) configuration was established. The relative stereochemistries of chiral centres at H-3, H-6 and H-8a were deduced by NOESY (Figure 5.76., 5.83.). NOESY correlations of δ 3.63 (H-1) with δ 5.36 (H-5) and 5.40

(H-10) and that between δ 5.36 (H-5) and 4.17 (H-14) indicated that these protons were on identical face of hexahydro isochromenyl ring. Thus, these protons could be arbitrarily considered as α -disposed with respect to molecular plane of symmetry. NOESYs between δ 3.70 (H-1)/2.03 (H-6)/3.94 (H-3)/5.43 (H-11)/4.20 (H-14) displayed that these protons were aligned at identical molecular plane, and assigned as β -disposed. Based on these, side chain attachments at C-6 and C-3 positions of ring was located at α -face of the ring, being opposite to β -protons in that position. The protons of olefinic bond, -C(10)=(C11)- in side chain did not exhibit any cross peaks with each other in NOESY, thus their *trans* disposition was ascertained.

Table 5.10.: NMR spectroscopic data of (10*E*)-butyl-9-(6-ethyl-3,4,6,7,8,8a-hexahydro-1*H*-isochromen-3-yl)-pent-10-enoate (**6**) in CDCl₃

C. No.	¹³ C	¹ H (int.,mult.,J in Hz) ^a	COSY	HMBC
1	63.36	3.70 (1H β ,d) 3.63 (1H α ,d)	H-8a -	C-3,4a -
2	-	-	-	-
3	70.27	3.94 (1H β ,p)	H-9,4	C-4a
4	34.15	2.44 (2H,d)	-	C-5,4a,8,6
4a	132.04	-	-	-
5	129.93	5.36 (1H α ,d,7.72)	H-6	C-4a
6	34.04	2.03 (1H β ,m)	H-7,18	C-5,7,8
7	29.65	1.62 (2H,m)	H-8	-
8	31.91	1.73 (2H,m)	H-8a	C-8a
8a	31.51	2.36 (1H,p)	-	C-4,6
9	27.21	2.07 (2H,t)	H-10	C-3,4,10,11
10	128.07	5.40 (1H α ,q,10.52)	-	C-9,12,13
11	128.29	5.43 (1H β ,q,10.97)	H-12	C-12
12	25.64	2.86 (2H,d)	-	C-11,13
13	174.34	-	-	-
14	65.14	4.20 (1H β ,t) 4.17 (1H α , t)	H-15 -	C-13,15 -
15	24.90	1.64 (2H,m)	H-16	C-16
16	29.68	1.32 (2H,m)	H-17	-
17	14.10	0.99 (3H,t)	-	C-16
18	22.68	1.29 (2H,m)	H-19	C-6
19	14.05	0.90 (3H,t)	-	C-18,7

¹H NMR spectra recorded using Bruker AVANCE III 500MHz (AV 500) spectrometer (Bruker, Karlsruhe, Germany) in CDCl₃ as aprotic solvent at ambient temperature with TMS as the internal standard (δ 0 ppm). The ¹H NMR spectra were recorded at

500MHz, while the ^{13}C NMR spectra were recorded at 125MHz. ^aValues in ppm, multiplicity and coupling constants ($J=\text{Hz}$) were indicated in parentheses. The assignments were made with the aid of the ^1H - ^1H COSY, HSQC, HMBC and NOESY experiments

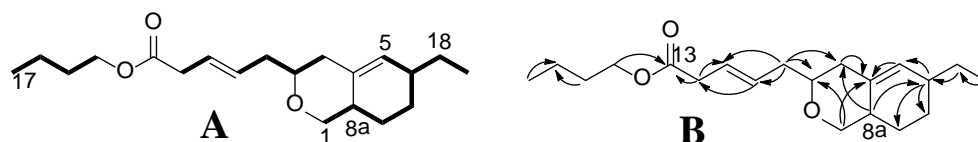


Figure 5.75.: ^1H - ^1H COSY (A) and HMBC (B) correlations of (10*E*)-butyl- 9-(6-ethyl-3,4,6,7,8,8a-hexahydro-1*H*-isochromen-3-yl)-pent-10-enoate (**6**). The key ^1H - ^1H COSY couplings have been represented by the bold face bonds. The HMBC couplings were indicated by double barbed arrow

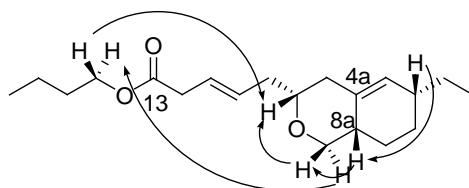


Figure 5.76.: NOESY correlations of (10*E*)-butyl- 9-(6-ethyl-3,4,6,7,8,8a-hexahydro-1*H*-isochromen-3-yl)-pent-10-enoate (**6**). The NOESY relations were represented by double barbed arrow

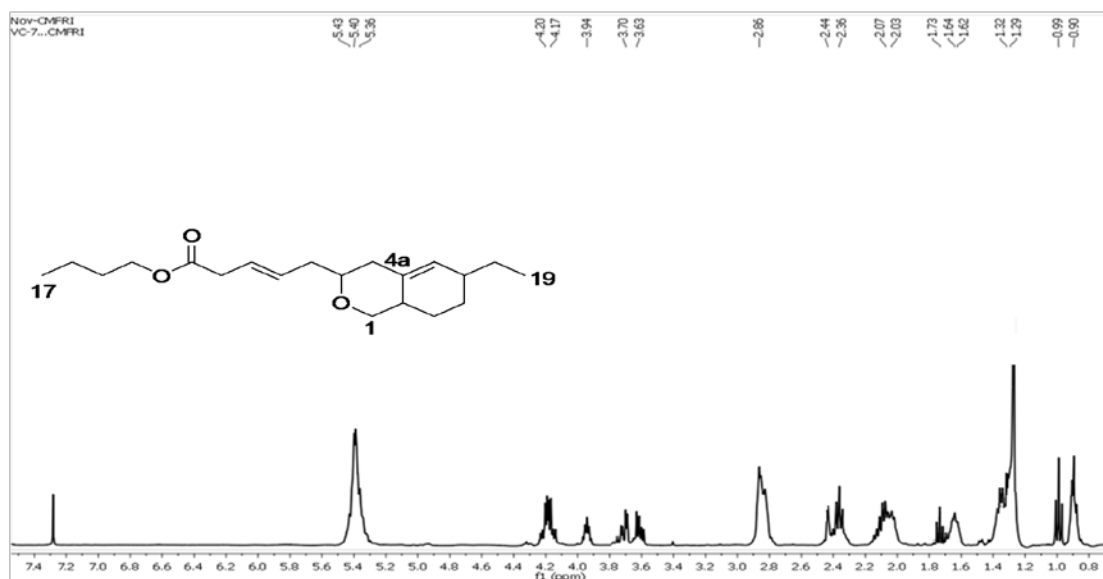


Figure 5.77.: ^1H NMR spectrum of (10*E*)-butyl-9-(6-ethyl-3,4,6,7,8,8a-hexahydro-1*H*-isochromen-3-yl)-pent-10-enoate (**6**)

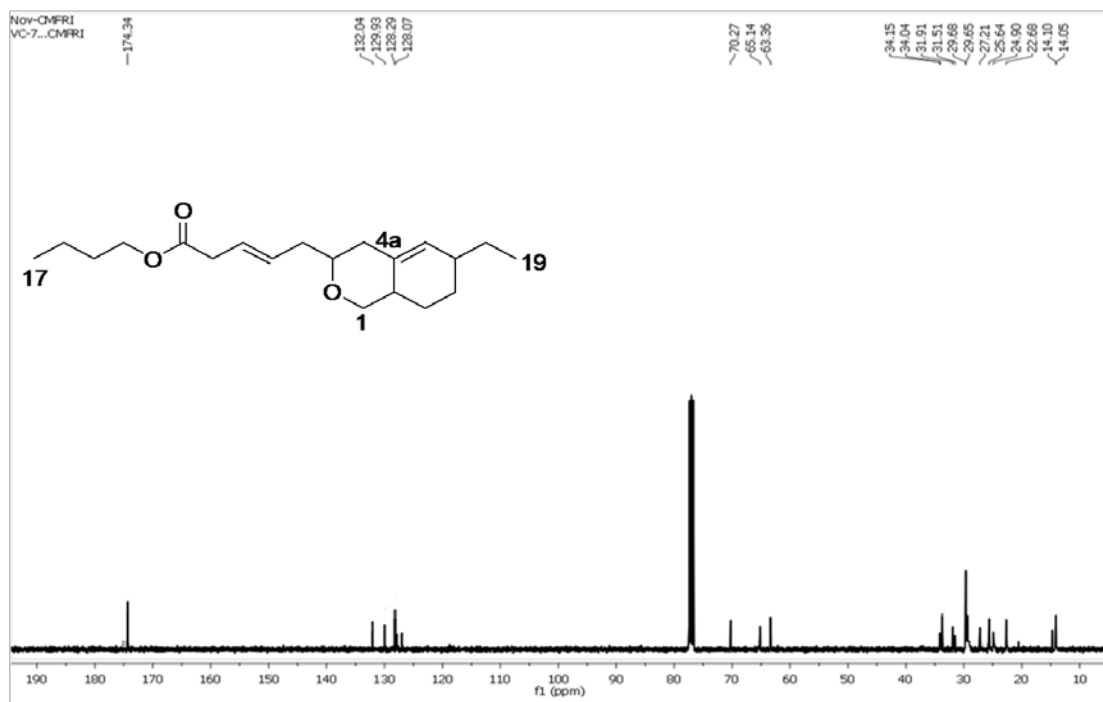


Figure 5.78.: ^{13}C NMR spectrum of (10*E*)-butyl-9-(6-ethyl-3,4,6,7,8,8a-hexahydro-1*H*-isochromen-3-yl)-pent-10-enoate (**6**)

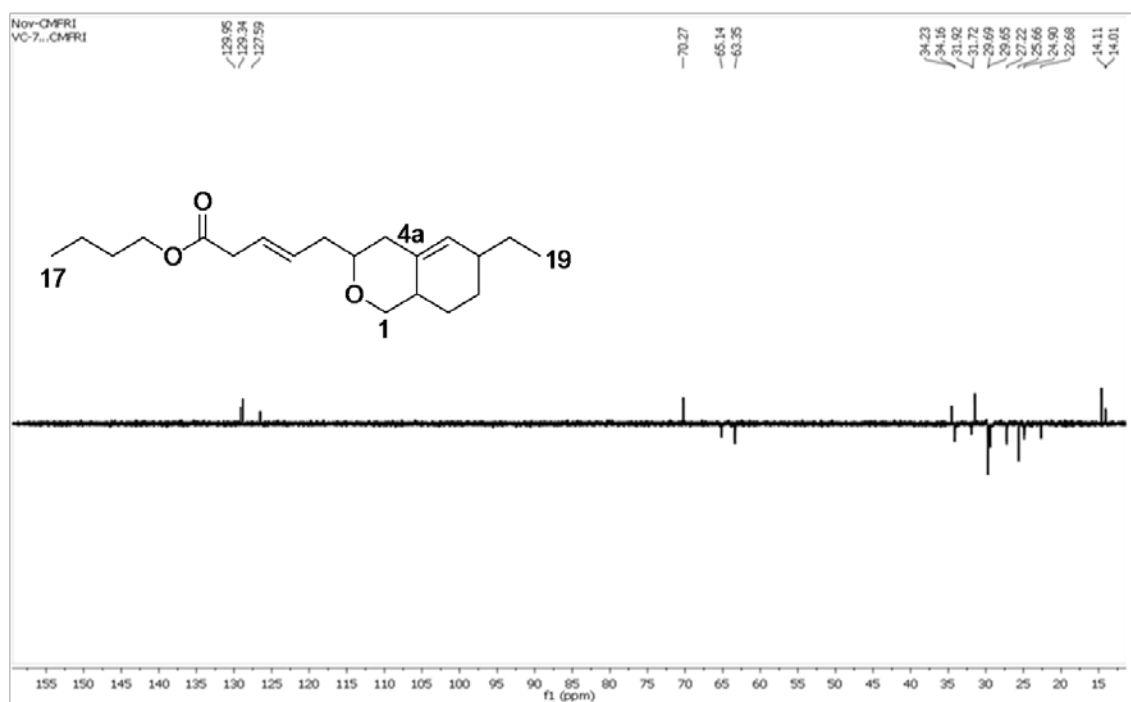


Figure 5.79.: $^{135}\text{DEPT}$ NMR spectrum of (10*E*)-butyl-9-(6-ethyl-3,4,6,7,8,8a-hexahydro-1*H*-isochromen-3-yl)-pent-10-enoate (**6**)

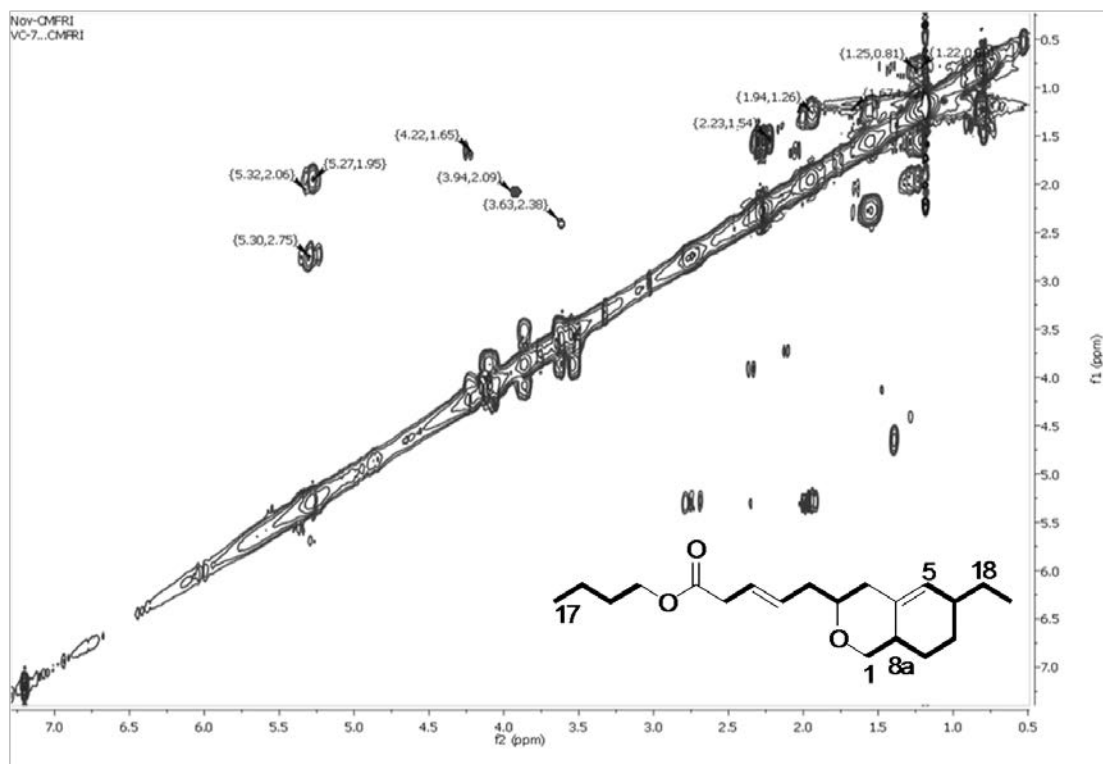


Figure 5.80.: ^1H - ^1H COSY NMR spectrum of (10*E*)-butyl-9-(6-ethyl-3,4,6,7,8,8a-hexahydro-1*H*-isochromen-3-yl)-pent-10-enoate (**6**)

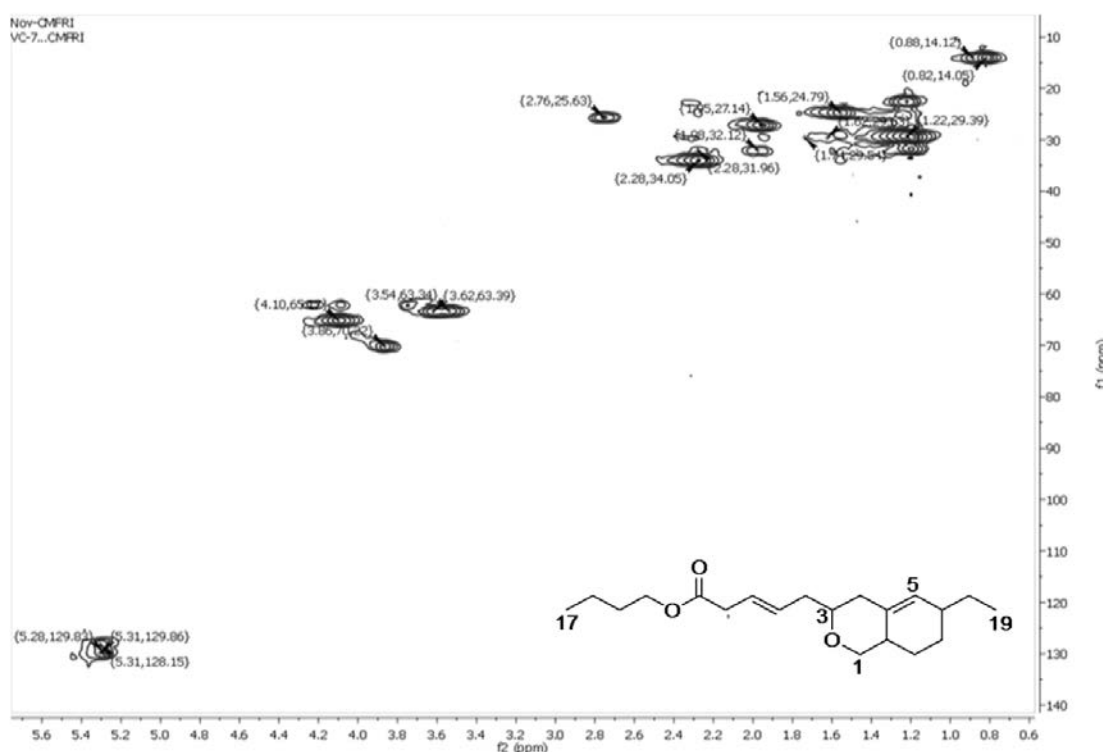


Figure 5.81.: HSQC NMR spectrum of (10*E*)-butyl-9-(6-ethyl-3,4,6,7,8,8a-hexahydro-1*H*-isochromen-3-yl)-pent-10-enoate (**6**)

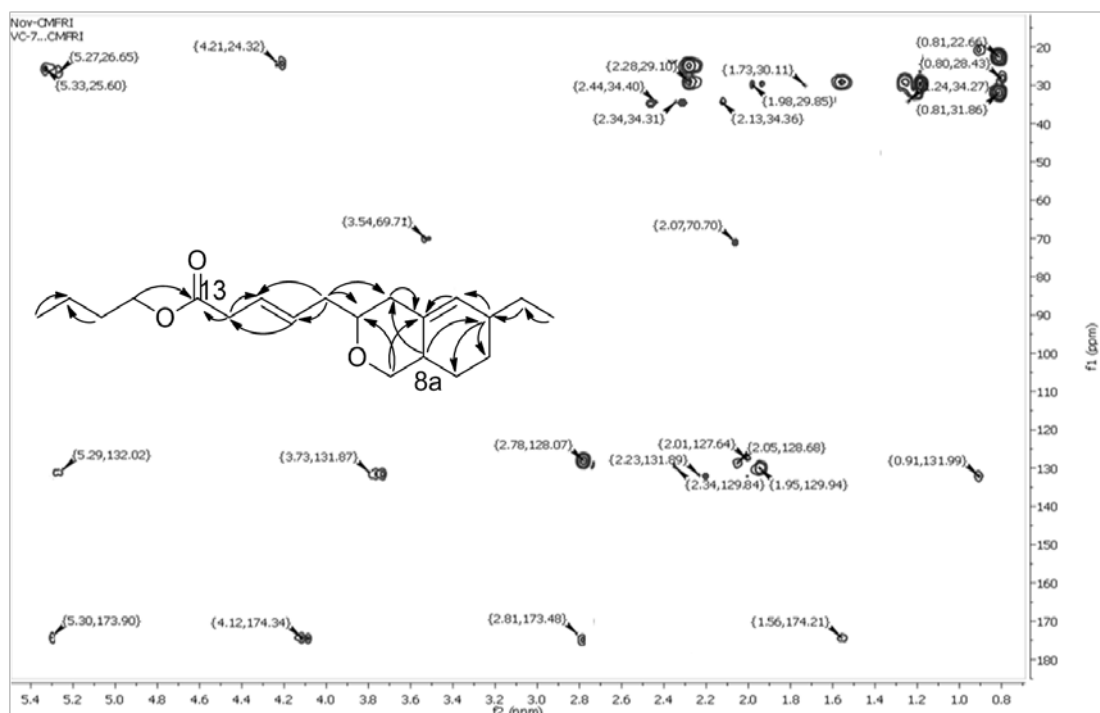


Figure 5.82.: HMBC NMR spectrum of (10*E*)-butyl-9-(6-ethyl-3,4,6,7,8,8a-hexahydro-1*H*-isochromen-3-yl)-pent-10-enoate (**6**)

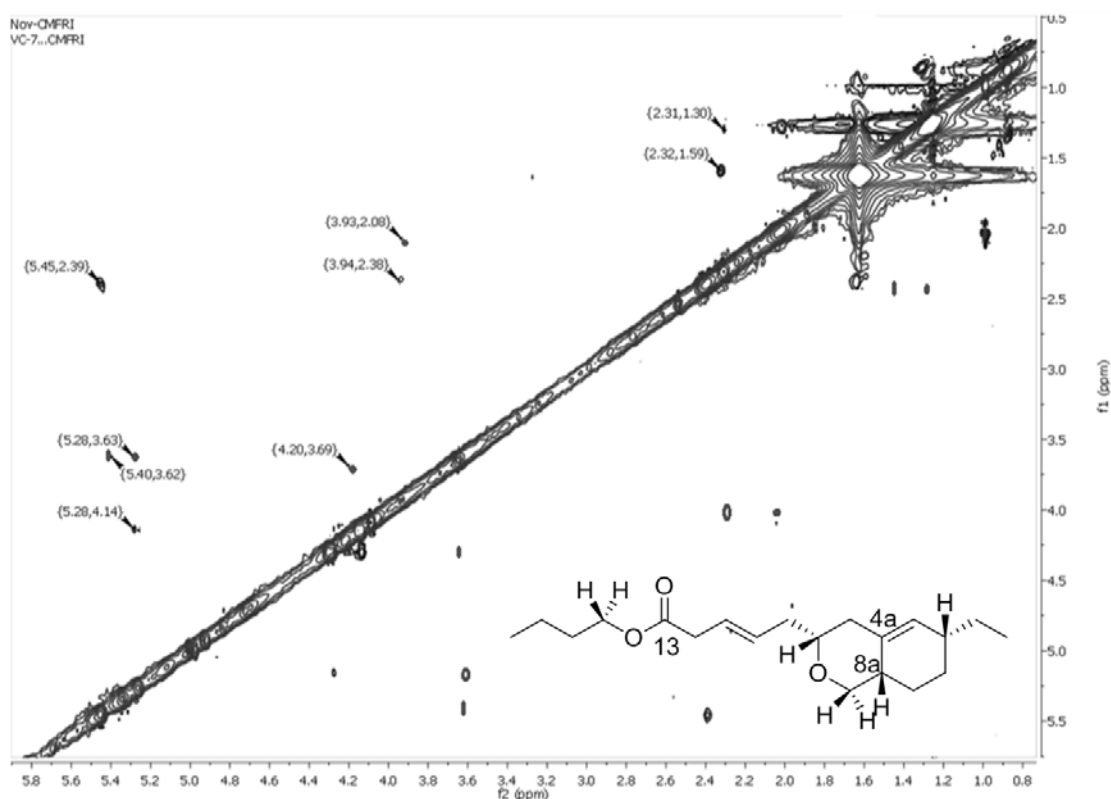


Figure 5.83.: NOESY NMR spectrum of (10*E*)-butyl-9-(6-ethyl-3,4,6,7,8,8a-hexahydro-1*H*-isochromen-3-yl)-pent-10-enoate (**6**)

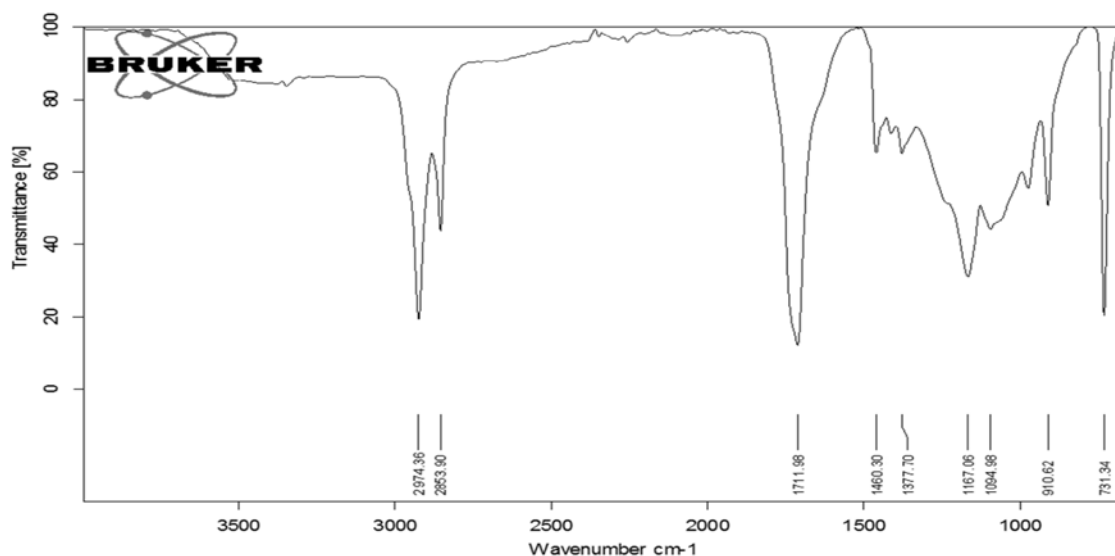


Figure 5.84.: FTIR spectrum of (10*E*)-butyl-9-(6-ethyl-3,4,6,7,8,8*a*-hexahydro-1*H*-isochromen-3-yl)-pent-10-enoate (**6**)

The typical IR absorptions at 2974 and 2853 cm^{-1} were represented alkyl stretching vibrations along with the stretching vibrations for ester carbonyl (1711 cm^{-1}) and alkoxy (1094 cm^{-1}) groups (Figure 5.84.).

The sequential elimination of ethyl, propyl and methyl radicals from the molecular ion peak (m/z 320) of the titled compound resulted in the formation of fragment ions with m/z 291 (**a**, $\text{C}_{18}\text{H}_{27}\text{O}_3^+$), 249 (**b**, $\text{C}_{15}\text{H}_{21}\text{O}_3^+$) and 238 (**c**, $\text{C}_{14}\text{H}_{22}\text{O}_3$), respectively. The later appeared to undergo sequential elimination of hydroxyls, followed by methyl and ethyl radicals to yield $\text{C}_{14}\text{H}_{23}\text{O}^+$ fragment with m/z 207 (**e**), $\text{C}_{13}\text{H}_{21}\text{O}^+$ with 193 (**f**) and $\text{C}_{11}\text{H}_{17}\text{O}^+$ with 165 (**g**). The repeated methyl radical elimination from ethyl-hexahydro-isochromene (**g**) and intramolecular rearrangements afforded the fragment ion peak at m/z 94 corresponding to methylcyclohexene (**l**, $\text{C}_7\text{H}_{10}^+$). Base peak of cyclohexene ($\text{C}_6\text{H}_{10}^+$) recorded at m/z 82 (**m**) by elimination of CH_3^\bullet from methylcyclohexene (**l**). This further eliminated two methyl radicals from the base peak ion (**m**) to acquire m/z 55 (**o**, butene cation) (Figure 5.85.-5.86.).

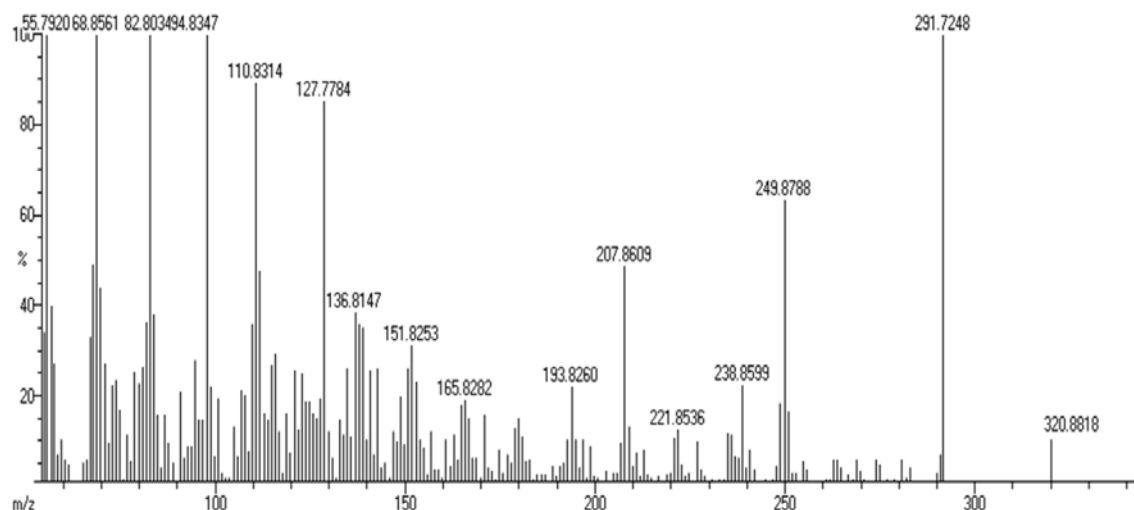


Figure 5.85.: EIMS spectrum of (10*E*)-butyl-9-(6-ethyl-3,4,6,7,8,8a-hexahydro-1*H*-isochromen-3-yl)-pent-10-enoate (**6**)

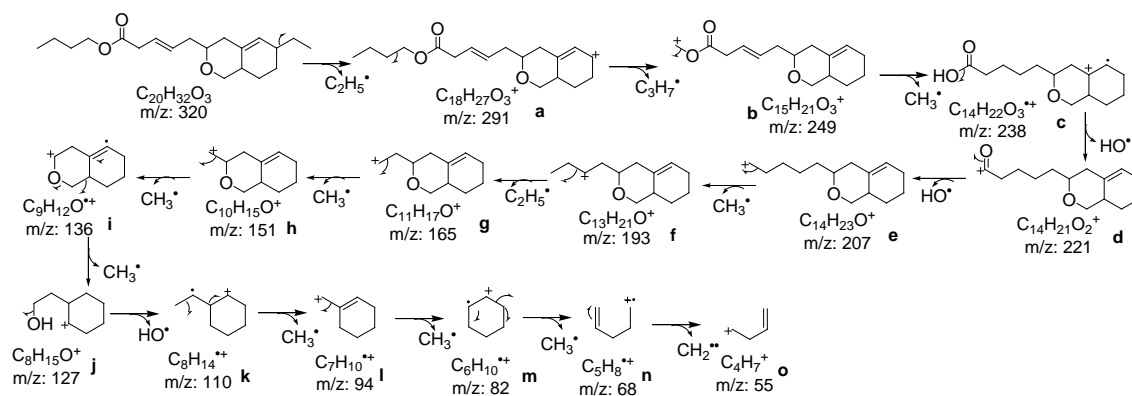
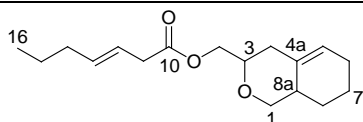


Figure 5.86.: Mass fragmentation pattern of (10*E*)-butyl-9-(6-ethyl-3,4,6,7,8,8a-hexahydro-1*H*-isochromen-3-yl)-pent-10-enoate (**6**)

5.3.2.3.B. Structural characterization of compound **7** (VC₃₋₄₋₃₋₂)

(12*E*)-(3,4,6,7,8,8a-Hexahydro-1*H*-isochromen-3-yl)-methylhept-12-enoate (**7**)



Yield	156 mg; 0.35%
Physical description	Light yellow oily
Molecular formula	C ₁₇ H ₂₆ O ₃
Molecular mass	278.1882

An irregularly arranged C17 isochromenyl meroterpenoid, (12*E*)-(3,4,6,7,8,8a-hexahydro-1*H*-isochromen-3-yl)-methylhept-12-enoate purified as light yellow oily compound. It displayed UV absorbance (in MeOH) at λ_{max} (log ϵ 2.08) 229 nm assigned to olefinic and carbonyl systems (Figure 5.87.). The purity was supported by RP C18 HPLC using 1:4 (v/v) MeOH:MeCN (R_t 6.66) (Figure 5.88.).

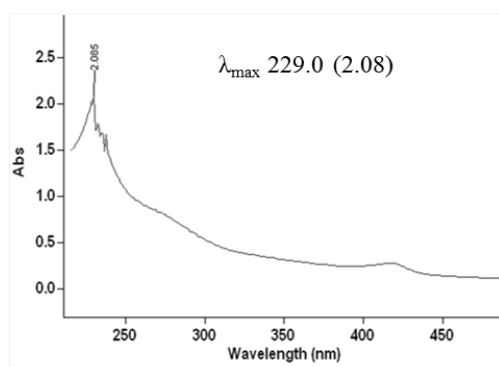


Figure 5.87.: UV spectrum of (12*E*)-(3,4,6,7,8,8a-hexahydro-1*H*-isochromen-3-yl)-methylhept-12-enoate (**7**)

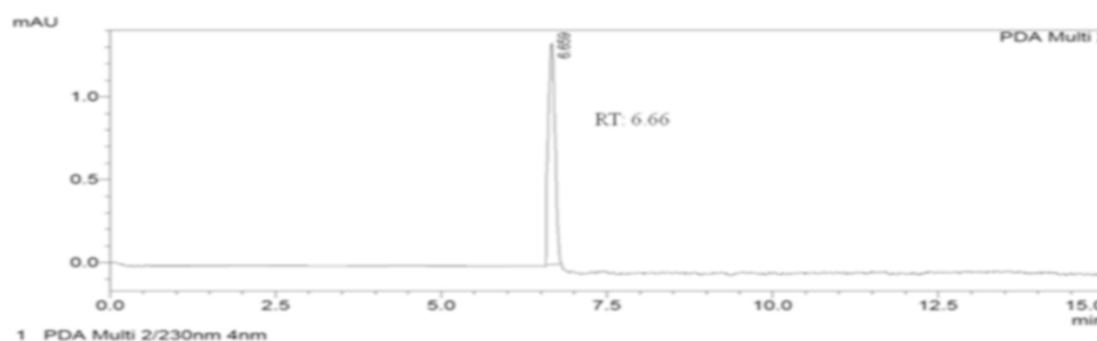


Figure 5.88.: HPLC chromatogram of (12*E*)-(3,4,6,7,8,8a-hexahydro-1*H*-isochromen-3-yl)-methylhept-12-enoate (**7**)

The isochromenyl meroterpenoid, (12*E*)-(3,4,6,7,8,8a-hexahydro-1*H*-isochromen-3-yl)-methylhept-12-enoate (**7**) with molecular formula of $C_{17}H_{26}O_3$ was characterized by extensive spectroscopic experiments (Table 5.11.; Figure 5.91.-5.97.). The five indices of hydrogen deficiencies accounted for the molecular formula, which assigned three double bonds and two cyclic systems. The peak at m/z 278 was recorded as molecular ion peak (EIMS: found m/z 278.1886 $[M]^+$, cal. for $C_{17}H_{26}O_3$ 278.1882). This hexahydro isochromenyl meroterpenoid proposed through extensive 1H - 1H COSY, HSQC and HMBC experiments. The basic hexahydro isochromenyl moiety was

comparable to compound **6**, except the absence of ethyl moiety at C-6 and presence of (12*E*)-methylhept-12-enoate side chain at C-3. The chemical shifts corresponding to two quaternary (ester carbonyl and olefinic), three sp^2 methine, two sp^3 methine, nine sp^3 methylenes and one methyl (doublet) were identified by 1H together with ^{13}C NMR and DEPT spectra. The characteristic peaks with regard to di-substituted alkene (δH 5.30/ δC 129.99 and 5.29/129.80), tri-substituted olefine (δH 5.27/ δC 129.68 and δC 135.46), ester carbon (δC 174.37), two oxygenated methylene (δH 3.59, 3.52/ δC 63.35; δH 4.07, 4.06/ δC 65.05), along with one each of oxygenated methine (δH 3.84/ δC 70.22) and carbonyl methylene (δH 2.86/ δC 25.64) were supported with HSQC. The extensive 2D NMR experiments attributed hexahydro isochromene framework attached to a methyl-heptenoate at C-3 position. Four spin systems were recorded in 1H - 1H COSY, such as δ 3.59, 3.52 (H-1)/2.26 (H-8a)/1.54 (H-8)/1.22 (H-7)/1.98 (H-6)/5.27 (H-5); δ 2.30 (H-4)/3.84 (H-3)/4.07, 4.06 (H-9); δ 2.73 (H-11)/5.30 (H-12) and δ 5.29 (H-13)/1.94 (H-14)/1.20 (H-15)/0.80 (H-16), which established the presence of hexahydro-1*H*-isochromen-3-yl-methylhept-12-enoate moiety (Figure 5.89.A). The 3-methyl-isochromenyl moiety constructed on the basis of 1H - ^{13}C conjunctions from δ 3.59 (H-1) to δ 70.22 (C-3), 65.05 (C-9); δ 3.84 (H-3) to δ 65.05 (C-9); δ 2.30 (H-4) to δ 31.89 (C-8a); δ 1.98 (H-6) to δ 135.46 (C-4a); δ 1.54 (H-8) to δ 31.89 (C-8a), 34.14 (C-4); δ 2.26 (H-8a) to δ 29.67 (C-7) and δ 4.07 (H-9) to δ 63.35 (C-1) (Figure 5.89.B). The linkage between isochromenyl and methyl groups deduced by HMBCs from δ 2.30 (H-4) to δ 174.37 (C-10) and δ 4.07 (H-9) to δ 174.37 (C-10). The heptenoate chain attached at C-9 of 3-methyl-hexahydro isochromenyl through oxygen atom (-O-) was apparent from HMBCs, such as δ 5.30 (H-12) to δ 174.37 (C-10), 27.20 (C-14) and δ 0.80 (H-16) to δ 27.20 (C-14). Notably, olefinic protons at δ 5.30 (H-12) and 5.29 (H-13) displayed higher coupling constants of 10.96 and 10.53 Hz, correspondingly, hence the geometrical arrangement was affirmed as *trans* (*E*) for -CH(12)=CH(13)- olefinic linkage. The stereochemical arrangement of chiral centers at H-3 and H-8a in **7** was deduced by NOESY experiments (Figure 5.90., 5.97.). NOE correlations between δ 5.27 (H-5) and δ 3.52 (H α -1)/4.06 (H α -9) designated that these protons were on same side of hexahydro isochromenyl ring, and therefore, were considered as α -disposed. NOE couplings between the protons at δ 3.59 (H β -1)/3.84 (H-3)/5.30 (H-12)/4.07 (H β -9) showed that they were disposed at the reverse side of ring system, and therefore, were

denoted as β -oriented with reference to the molecular plane of symmetry. Therefore, the side chain attachment at C-3 was on the α -face of ring, being reverse to β -protons in that position.

Table 5.11.: NMR spectroscopic data of (12*E*)-(3,4,6,7,8,8a-hexahydro-1*H*-isochromen-3-yl)-methylhept-12-enoate (**7**) in CDCl₃

C. No.	¹³ C	¹ H (int.,mult., <i>J</i> in Hz) ^a	COSY	HMBC
1	63.35	3.59 (1H β ,d) 3.52 (1H α ,d)	H-8a -	C-3,9 -
2	-	-	-	-
3	70.22	3.84 (1H,p)	H-9,4	C-9
4	34.14	2.30 (2H β ,d)	-	C-8a,10
4a	135.46	-	-	-
5	129.68	5.27 (1H α ,d,7.02)	H-6	C-4
6	31.75	1.98 (2H,m)	H-7	C-5,4a
7	29.67	1.22 (2H,m)	H-8	-
8	29.63	1.54 (2H,m)	H-8a	C-8a,4,7
8a	31.89	2.26 (1H,p)	-	C-4,8,7
9	65.05	4.07 (1H β ,d) 4.06 (1H α ,d)	- -	C-3,10,1 -
10	174.37	-	-	-
11	24.88	2.73 (2H,d)	H-12	C-10
12	129.99	5.30 (1H β ,q,10.96)	-	C-10,14
13	129.80	5.29 (1H α ,q,10.53)	H-14	C-14
14	27.20	1.94 (2H,m)	H-15	C-12,13,11,15
15	22.66	1.20 (2H,m)	H-16	C-16,14
16	14.08	0.80 (3H,t)	-	C-15,14

¹H NMR spectra recorded using Bruker AVANCE III 500MHz (AV 500) spectrometer (Bruker, Karlsruhe, Germany) in CDCl₃ as aprotic solvent at ambient temperature with TMS as the internal standard (δ 0 ppm). The ¹H NMR spectra were recorded at 500MHz, while the ¹³C NMR spectra were recorded at 125MHz. ^aValues in ppm, multiplicity and coupling constants (*J*=Hz) were indicated in parentheses. The assignments were made with the aid of the ¹H-¹H COSY, HSQC, HMBC and NOESY experiments

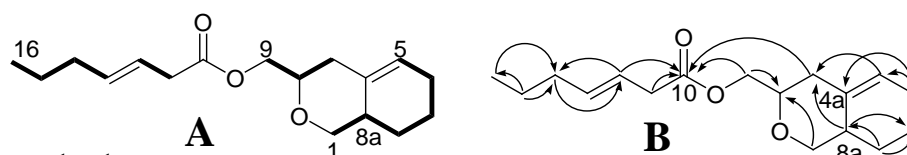


Figure 5.89.: ^1H - ^1H COSY (A) and HMBC (B) correlations of (12*E*)-(3,4,6,7,8,8a-hexahydro-1*H*-isochromen-3-yl)-methylhept-12-enoate (**7**). The key ^1H - ^1H COSY couplings have been represented by the bold face bonds. The HMBC couplings were indicated by double barbed arrow

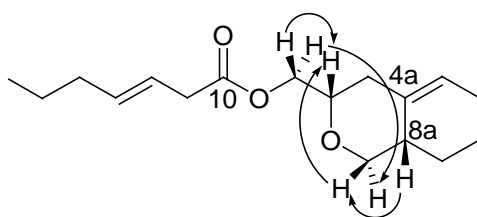


Figure 5.90.: NOESY correlations of (12*E*)-(3,4,6,7,8,8a-hexahydro-1*H*-isochromen-3-yl)-methylhept-12-enoate (**7**). The NOESY relations were represented by double barbed arrow

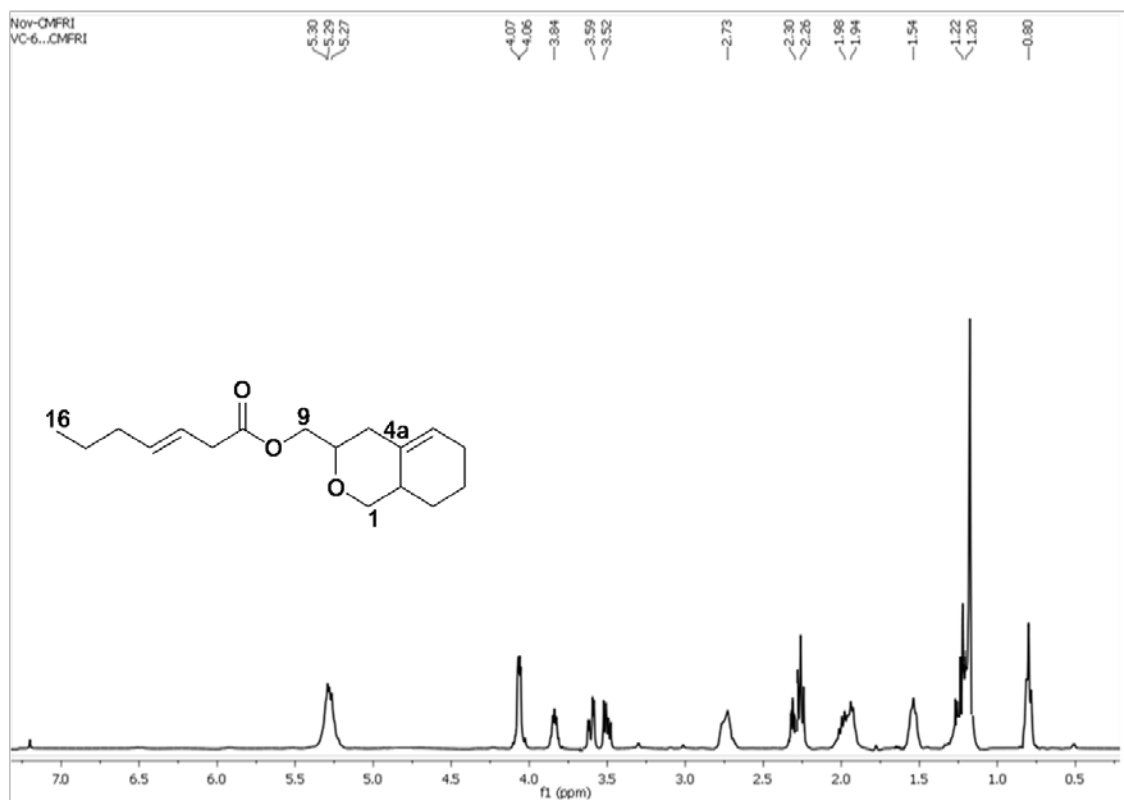


Figure 5.91.: ^1H NMR spectrum of (12*E*)-(3,4,6,7,8,8a-hexahydro-1*H*-isochromen-3-yl)-methylhept-12-enoate (**7**)

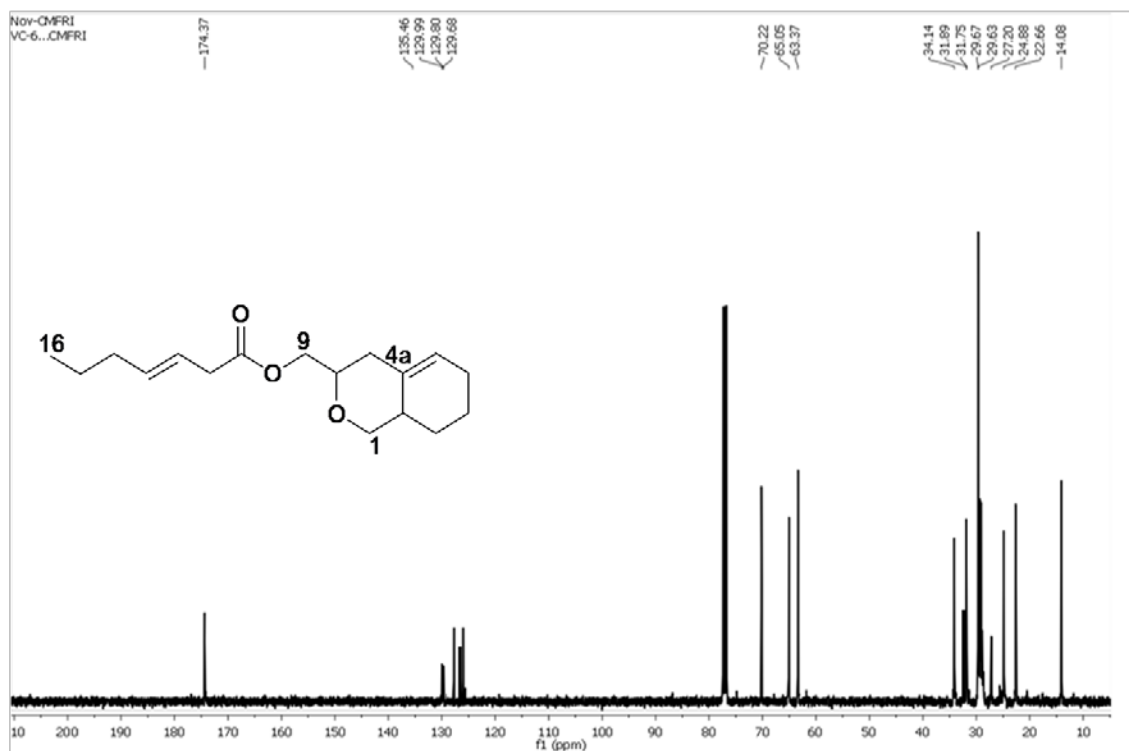


Figure 5.92.: ^{13}C NMR spectrum of (12E)-(3,4,6,7,8,8a-hexahydro-1H-isochromen-3-yl)-methylhept-12-enoate (7)

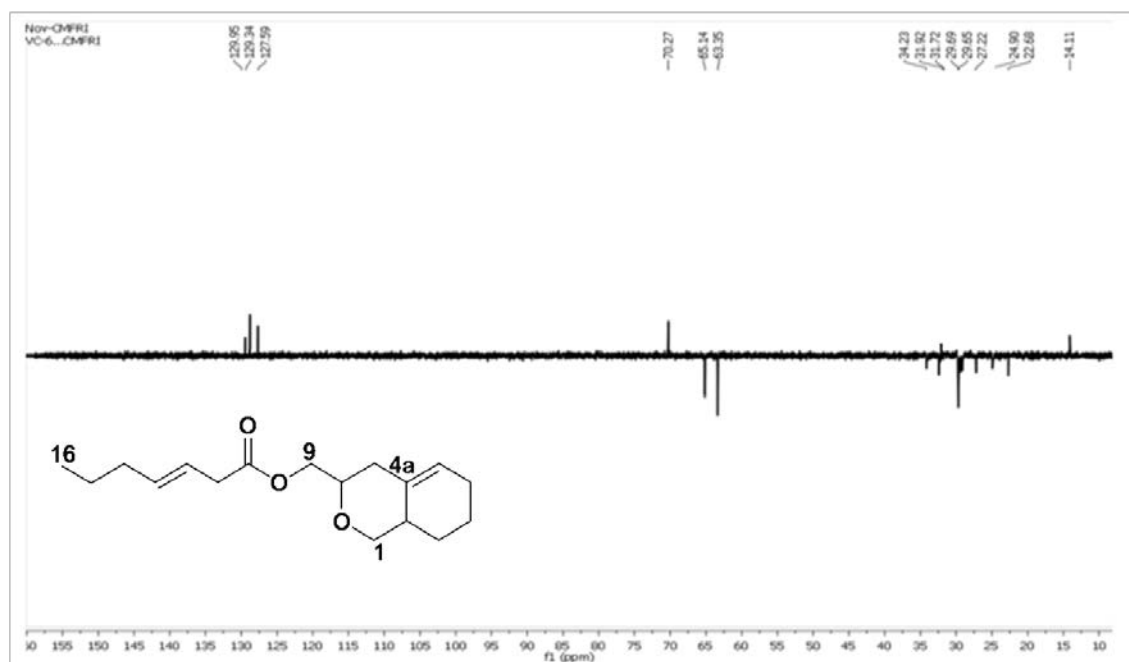


Figure 5.93.: $^{135}\text{DEPT}$ NMR spectrum of (12E)-(3,4,6,7,8,8a-hexahydro-1H-isochromen-3-yl)-methylhept-12-enoate (7)

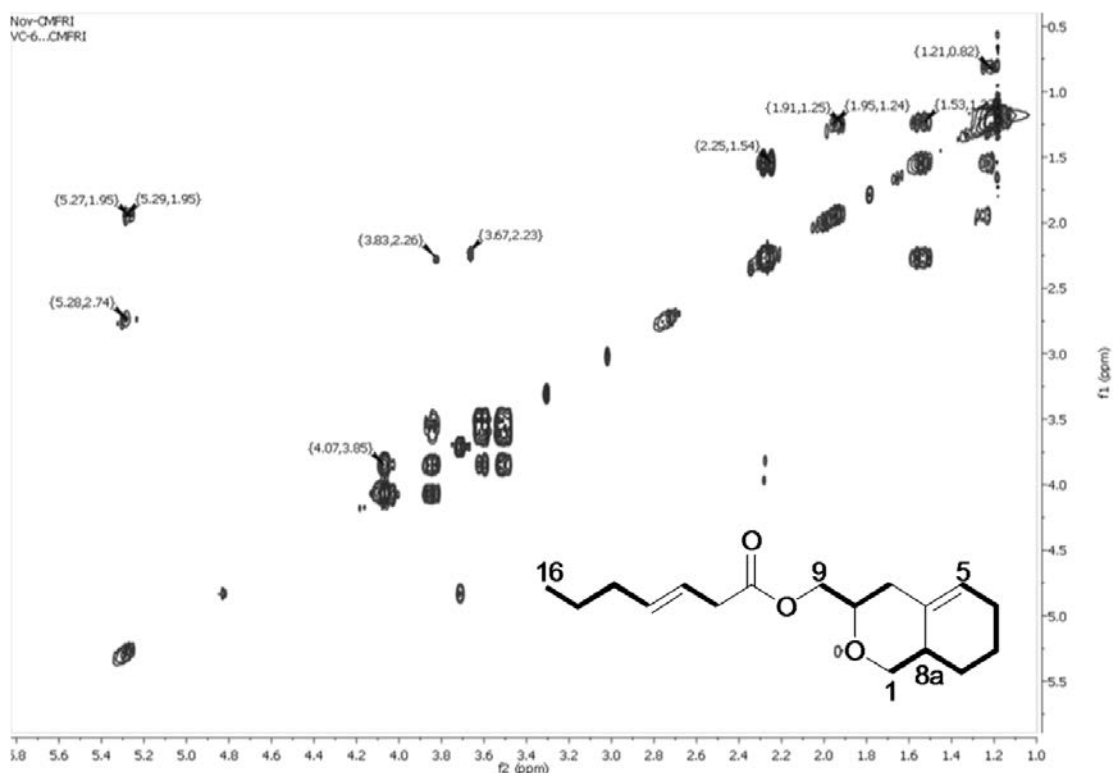


Figure 5.94.: ^1H - ^1H COSY NMR spectrum of (12*E*)-(3,4,6,7,8,8a-hexahydro-1*H*-isochromen-3-yl)-methylhept-12-enoate (**7**)

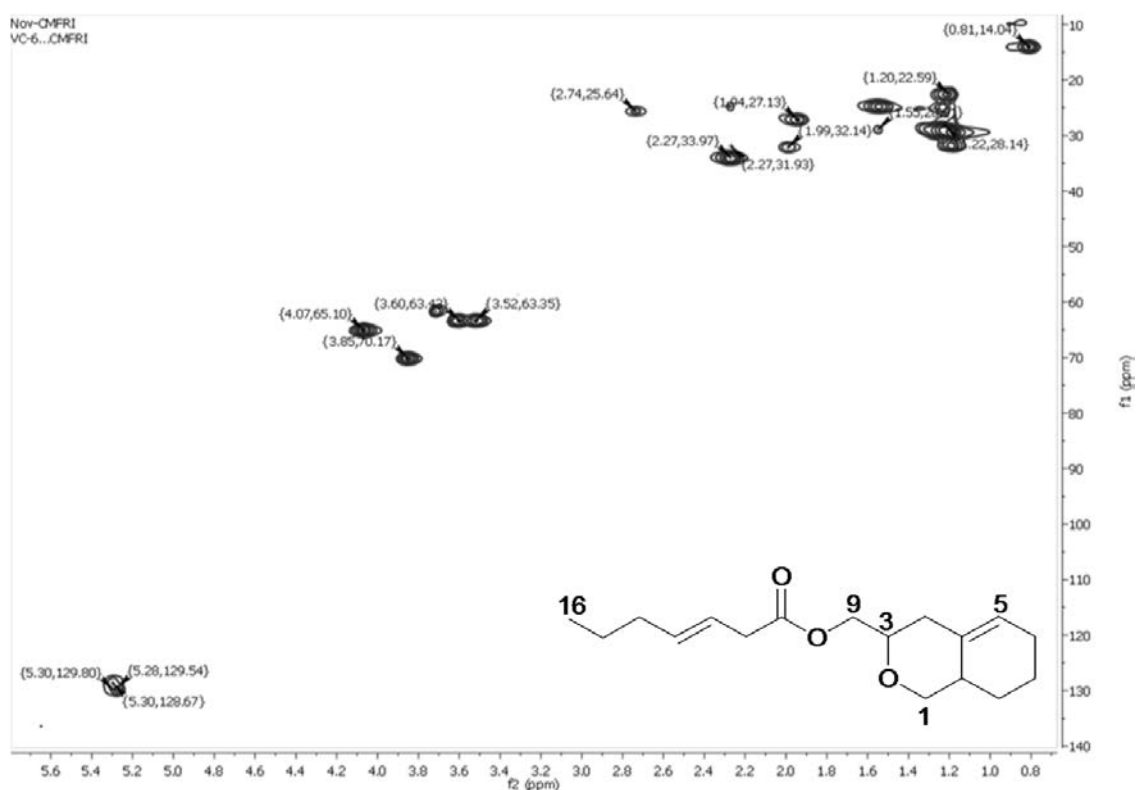


Figure 5.95.: HSQC NMR spectrum of (12*E*)-(3,4,6,7,8,8a-hexahydro-1*H*-isochromen-3-yl)-methylhept-12-enoate (**7**)

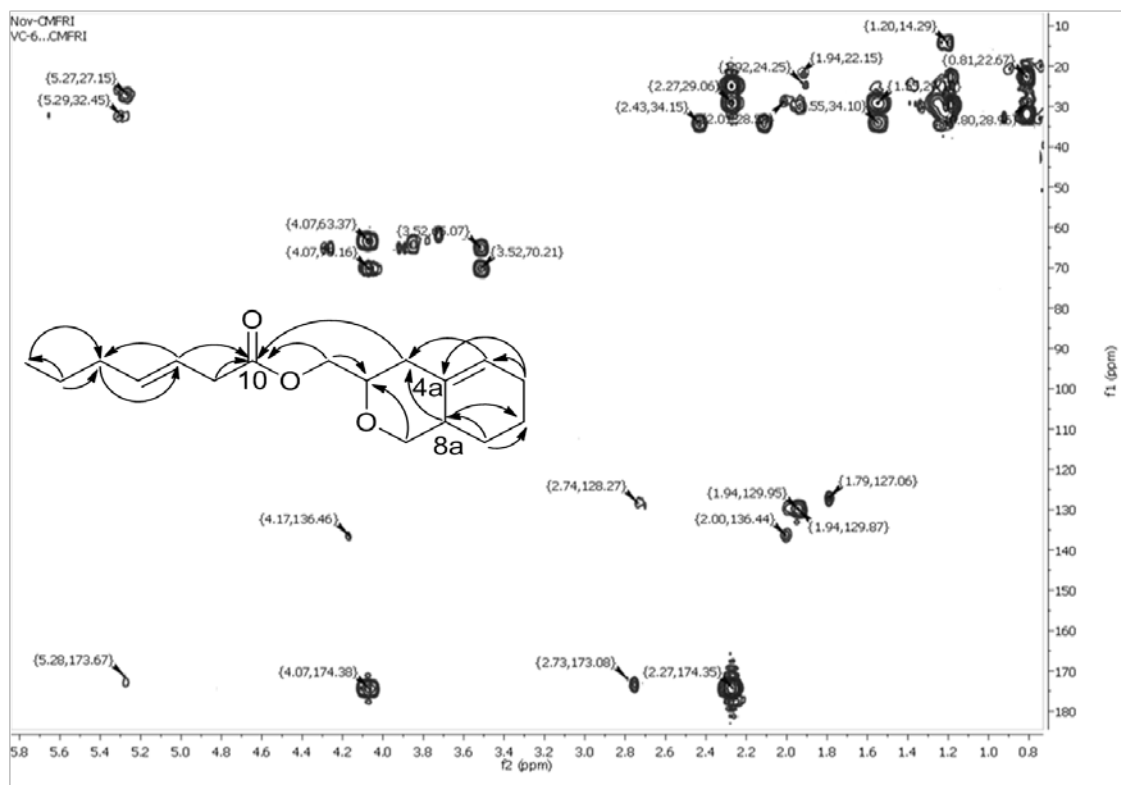


Figure 5.96.: HMBC NMR spectrum of (12*E*)-(3,4,6,7,8,8a-hexahydro-1*H*-iso chromen-3-yl)-methylhept-12-enoate (**7**)

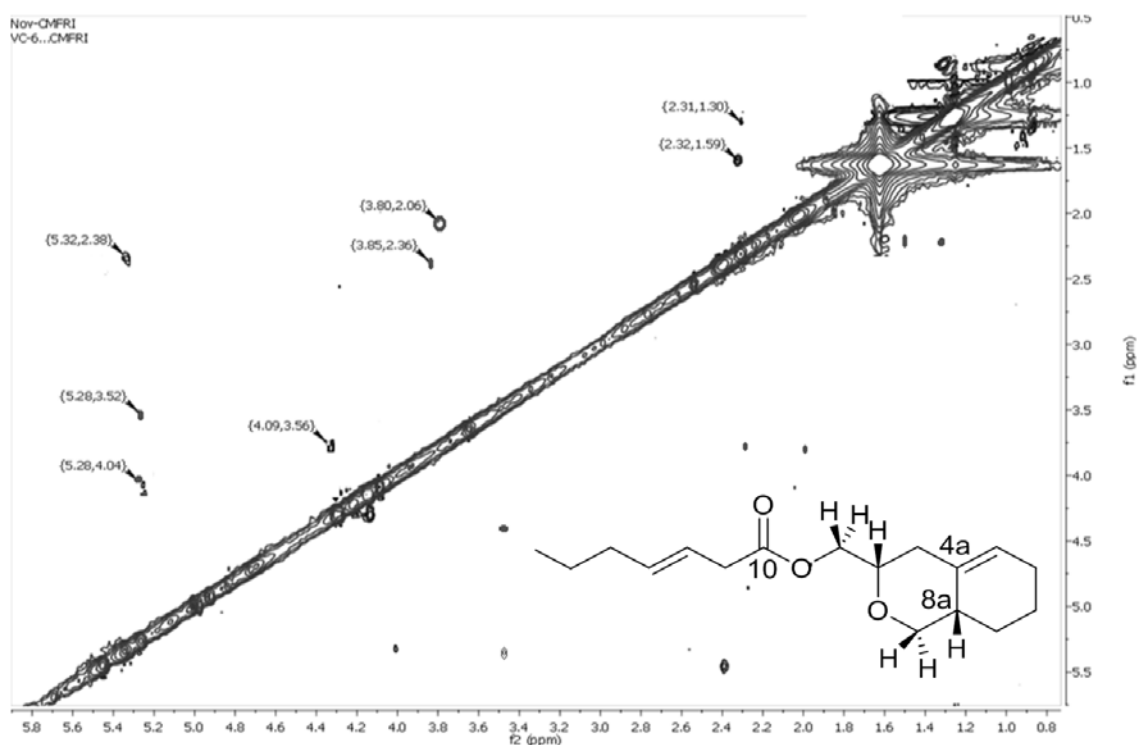


Figure 5.97.: NOESY NMR spectrum of (12*E*)-(3,4,6,7,8,8a-hexahydro-1*H*-iso chromen-3-yl)-methylhept-12-enoate (**7**)

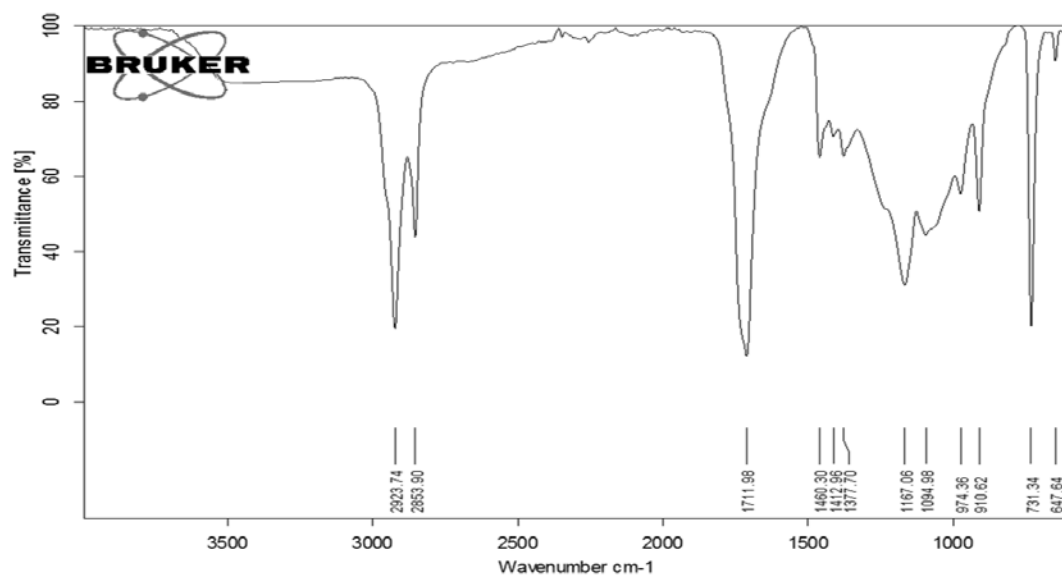


Figure 5.98.: FTIR spectrum of (12*E*)-(3,4,6,7,8,8a-hexahydro-1*H*-isochromen-3-yl)-methylhept-12-enoate (**7**)

The IR stretching vibrations corresponding to the ester carbonyl (C=O) and alkoxy groups were symbolized by 1711 and 1094 cm^{-1} bands, respectively. The characteristic absorptions at 2923 and 2853 cm^{-1} represented alkyl stretching vibrations (Figure 5.98.).

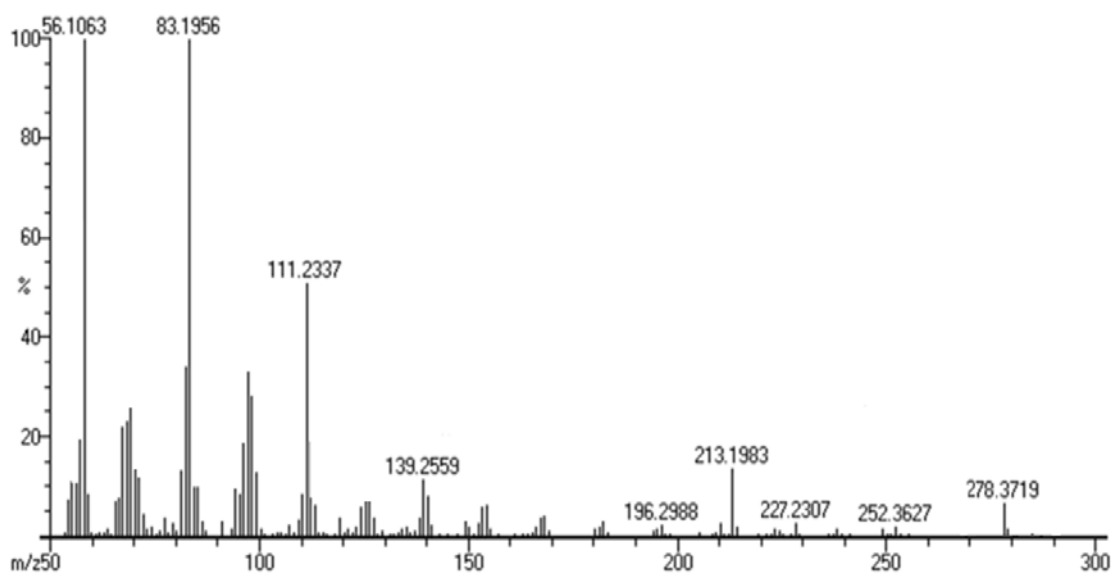


Figure 5.99.: EIMS spectrum of (12*E*)-(3,4,6,7,8,8a-hexahydro-1*H*-isochromen-3-yl)-methylhept-12-enoate (**7**)

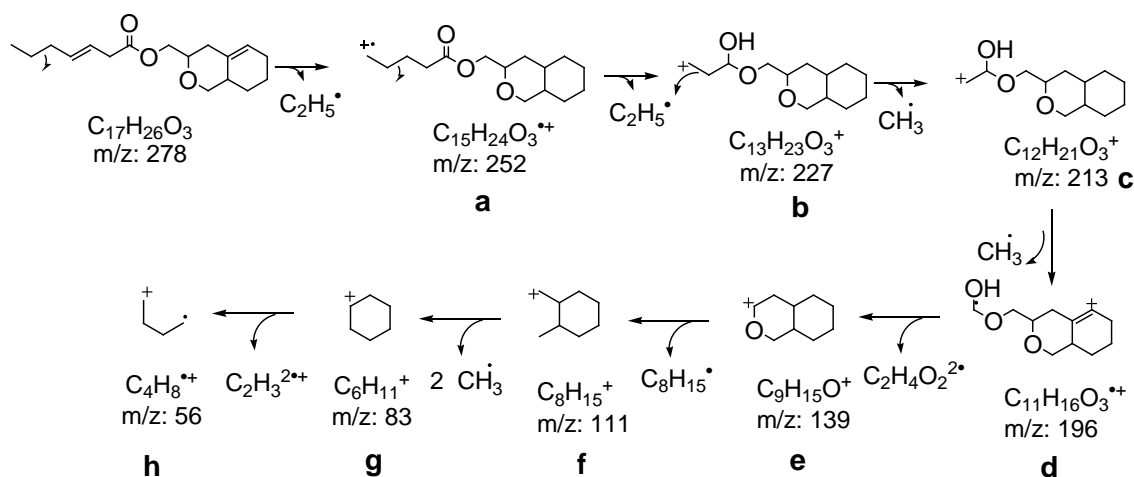


Figure 5.100.: Mass fragmentation pattern of (12E)-(3,4,6,7,8,8a-hexahydro-1H-isochromen-3-yl)-methylhept-12-enoate (7)

The molecular ion peak was observed at m/z 278 (Figure 5.99.). The sequential elimination of two ethyl and two methyl radicals from the side chain moiety of the titled compound resulted into fragments with m/z 227 (b) and 196 (d), respectively. The later was seemed to undergo sequential fragmentations resulted in the fragment peak at m/z 111 (f). The twomethyl radical elimination from the fragment at m/z 111 (f) resulted in the base peak of cyclohexane ($C_6H_{11}^+$) radical at m/z 83 (g). The latter on further mass fragmentation acquired a peak at m/z 56 (h), which was characteristic of butene ($C_4H_8^{++}$) (Figure 5.100.).

The titled chromenyl derivatives constitute a major part in the natural products and changes in the substitution of functional groups might probably led to better antioxidant candidates with greater selectivity in the food supplements and functional foods.

5.3.2.4. Structural characterization of cholestenol derivatives (8-10)

Sterols are the major constituents in marine invertebrates, such as corals, bryozoans and mollusks (Goad and Scheuer 1978). In particular, sponges, corals and mollusks were extensively investigated for different types of steroids (Joosse 1978; Sica 1980). Most of the pregnanes reported to possess significant bioactivities, such as anti-inflammatory (Chao *et al.*, 2008) and anti-bacterial (Diaz-Marrero *et al.*, 2011) activities. We herein described the NMR guided structural elucidation of one pregnane-type steroids, 19 (10→5) abeo-20-methyl-pregn-1-en-3-yl-3β-methoxy-hex-25-enoate

(8) and two new cholestenol derivatives, (22*E*)-24¹-homocholesta-5,22-dien-(3 β ,24¹ β)-diol (9) and (22*E*),(24¹*E*)-24¹,24²-dihomocholesta-5,22,24¹-trien-3 β -ol (10) from *V. cyprinoides* (Figure 5.101.).

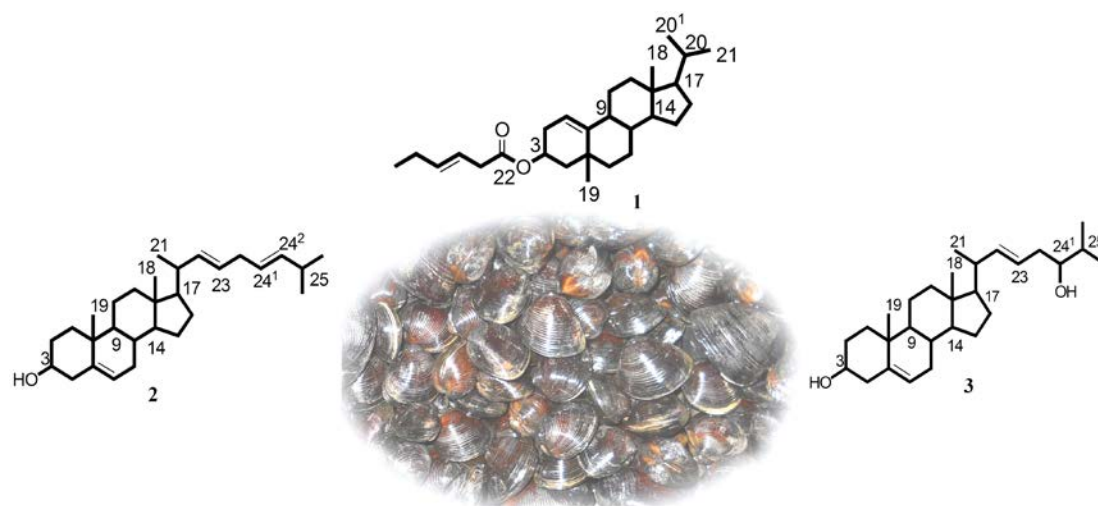
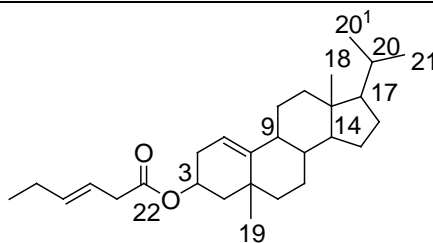


Figure 5.101.: Sterol analogues from *V. cyprinoides* with bioactive potentials

5.3.2.4.A. Structural characterization of compound 8 (VC₂₋₆₋₅₋₂)

19 (10→5) Abeo-20-methyl-pregn-1-en-3-yl-3 β -methoxy-hex-25-enoate (8)



Yield	143 mg; 0.32%
Physical description	White solid
Molecular formula	C ₂₈ H ₄₄ O ₂
Molecular mass	412.3341

The pregnane steroid, 19 (10→5) abeo-20-methyl-pregn-1-en-3-yl-3 β -methoxy hex-25-enoate was isolated as white solid. It exhibited UV absorbance (in MeOH) at λ_{\max} (log ϵ 3.61): 222.3 nm was assigned to a chromophore with carbonyl and olefinic groups (Figure 5.102.). The purity of the compound was supported by RP C18 HPLC using 3:2 (v/v) MeOH:MeCN (R_t 3.19) experiments (Figure 5.103.).

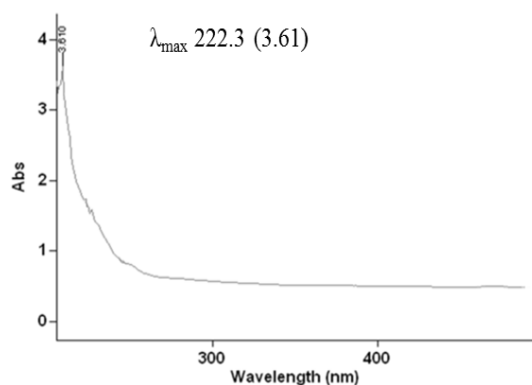


Figure 5.102.: UV spectrum of 19 (10→5) abeo-20-methyl-pregn-1-en-3-yl-3 β -methoxy-hex-25-enoate (**8**)

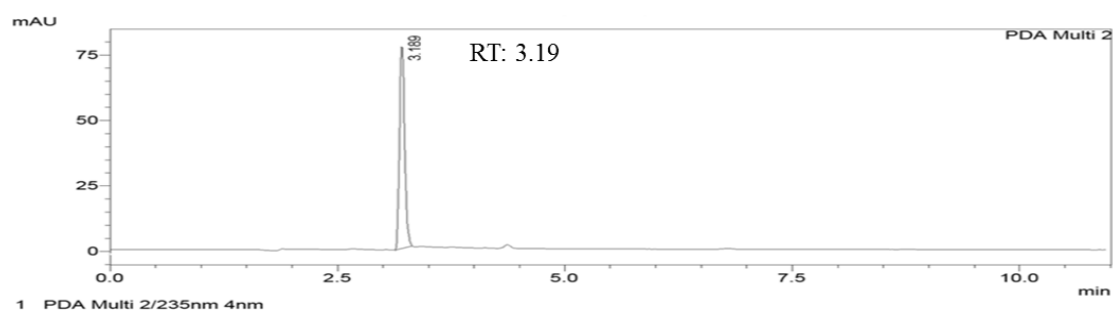


Figure 5.103.: HPLC chromatogram of 19 (10→5) abeo-20-methyl-pregn-1-en-3-yl-3 β -methoxy-hex-25-enoate (**8**)

A pregnane class of steroid, **8** exhibited its molecular formula as $\text{C}_{28}\text{H}_{44}\text{O}_2$ (EIMS: found m/z 412.3347 $[\text{M}+1]^+$, cal. for $\text{C}_{28}\text{H}_{44}\text{O}_2$ 412.3341). The double bond equivalence was calculated as seven, which included three unsaturations and four ring moieties. The absence of ^1H NMR aromatic signals in the δ 6.5-8.5 regions confirmed that these cyclic rings were not related to the aromatic class of chemistry. The proton and carbon shift values were assigned on the basis of earlier reports (Huang *et al.*, 2006; Kuo *et al.*, 2014). The ^{13}C NMR along with DEPT spectroscopic analyses recorded signals for 28 carbons, enclosing five methyls (including two singlets), ten methylenes, nine methines (including an oxymethine) and four quaternary carbon (including carbonyl carbon) (Table 5.12.; Figure 5.107.-5.108.). The proton spectrum displayed the occurrences of two each of terminal (δ 0.90, 0.88, d, 3H each) and tertiary methyls (δ 0.70, 1.04, s, 3H each), one oxymethine (δ 4.62, p, 1H), along with a tri-substituted alkene (δ 5.39, t, 1H) (Figure 5.106.). The side chain was comprised of one terminal

methyl (δ 0.95, t, 3H), a carboxymethylene (δ 2.87, d, 2H) and two di-substituted alkene (δ 5.40, m, 1H; 5.41, m, 1H). The NMR data shared close resemblance to the basic skeleton of pregnane (Huang *et al.*, 2006). Highly deshielded proton at δ 4.62 with δ C 73.66 positioned at C-3, confirmed the presence of highly oxygenated group. The -OH group at C-3 with δ H 3.5/ δ C 71 was the characteristic resonances for sterols (Chen *et al.*, 2014), whereas the present compound exhibited greater chemical shift value at C-3 (δ H ~4.5) than the characteristic hydroxy or methoxy groups. Therefore, it was assumed that C-3 position was directly bonded to strong electronegative groups, such as carboxylates { $\underline{\text{CH}}\text{-O(O)-C-}$ }. The 3β -acetoxy-5,20-pregnadiene isolated from *Scleronephthya flexilis* identified as carboxylate (C-3) derivative and its chemical shifts at C-3 position (δ H 4.60 (1H, m)/ δ C 73.9) was comparable with those of the titled compound in the same vicinity (δ H 4.62 (1H, p)/ δ C 73.66) (Kuo *et al.*, 2014). The ^1H - ^1H COSY correlations attributed for two spin systems in the pregnane skeleton and two spin systems in the hexenoate side chain attached at C-3. The short range couplings, such as δ 5.39 (H-1)/2.32, 2.29 (H-2)/4.62 (H-3)/1.72, 1.57 (H-4) and δ 1.15 (H-6)/1.32 (H-7)/0.98 (H-8)/2.08 (H-9)/1.59 (H-11)/1.35 (H-12); δ 0.98 (H-8)/1.10 (H-14)/1.86 (H-15)/1.52 (H-16)/1.00 (H-17)/1.97 (H-20)/0.90 (H-20¹), 0.88 (H-21) were accounted for the basic tetracyclic framework (Figure 5.104.A, 5.109.). HMBC relations from δ 5.39 (H-1) to δ 35.81 (C-9); δ 2.32 (H-2) to δ 122.57 (C-1), δ 73.66 (C-3), 139.70 (C-10); δ 1.72 (H-4) to δ 73.66 (C-3), 139.70 (C-10); δ 1.57 (H-4) to δ 139.70 (C-10); δ 0.98 (H-8) to δ 139.70 (C-10) confirmed the A/B ring system of **8** (Figure 5.104.B, 5.111.). Other couplings, such as δ 1.10 (H-14) to δ 42.32 (C-13); δ 1.52 (H-16) to δ 31.88 (C-20); δ 1.00 (H-17) to δ 42.32 (C-13), 31.88 (C-20); δ 1.97 (H-20) to δ 56.70 (C-17); δ 0.90 (H-20¹) to δ 56.70 (C-17); δ 0.88 (H-21) to δ 56.70 (C-17) supported the pregnane network. The singlet methyl proton at δ 0.70 (C-18) exhibited HMBC correlations with δ C 42.32 (attributed to C-13), 21.05 (C-12) and 56.70 (C-17), thus the position of -CH₃-18 at C-13 was validated (Fang *et al.*, 2013). The position of methyl at C-5 was confirmed due to the couplings from δ 1.04 (H-19) to δ 36.20 (C-5). The methyl group (-CH₃-19) at C-10 position of the pregnane steroids (Zhao *et al.*, 2013) was shifted to C-5 in the titled compound (**8**), and therefore, it was named as 19 (10→5) abeo pregnane derivative. Highly deshielded ^{13}C resonances at δ 173.28 (C-22) and 128.20 (C-24)/132.01 (C-25) were recorded, in which the former corresponded to ester carbonyl,

whereas the latter was accounted for the sp^2 hybridized alkenic carbons. The protons at δ 5.40 (H-24) and 5.41 (H-25) displayed HSQC correlation with two different ^{13}C shifts at δ 128.20 (C-24) and 132.01 (C-25) with greater coupling constants (J) of 9.14 and 9.02 Hz, respectively, that established the *trans* (*E*) configuration of the alkenic group. The presence of 3-methoxy-hex-25-enoate moiety was evident at C-3 by HMBC coupling from δ 2.32 (H-2) to δ 173.28 (C-22) and δ 1.72 (H-4) to δ 173.28 (C-22). This side chain embedded two spin systems, which were δ 2.87 (H-23)/5.40 (H-24) and δ 5.41 (H-25)/2.05 (H-26)/0.95 (H-27). The presence of carbonyl carbon at δ 173.28 (C-23) and its extended side chain were further corroborated by long range correlations, such as δ 2.87 (H-23) to δ 173.28 (C-22); δ 5.41 (H-25) to δ 25.64 (C-23); δ 2.05 (H-26) to δ 128.20 (C-24); δ 0.95 (H-27) to δ 128.20 (C-24). The relative stereochemistries of **8** were determined by extensive NOE correlations (Figure 5.105., 5.112.). The NOEs among δ 5.39 (H-1)/4.62 (H-3)/1.57 (H α -4)/2.08 (H-9)/1.10 (H-14) suggested that these protons were aligned in same plane, and therefore, arbitrarily assigned as α -oriented. NOEs found among δ 2.32 (H-2a)/1.72 (H β -4)/0.98 (H-8)/1.00 (H-17), which together with methyl signals at δ 1.04 (H-19) and δ 0.70 (H-18) established their β -disposition.

Table 5.12.: NMR spectroscopic data of 19 (10 \rightarrow 5) abeo-20-methyl-pregn-1-en-3-yl-3 β -methoxy-hex-25-enoate (**8**) in CDCl₃

C. No.	^{13}C	1H (int.,mult., J in Hz) ^a	COSY	HMBC
1	122.57	5.39 (1H α ,t,6.50)	H-2	C-2,9
2	38.17	2.32 (1H β ,t) 2.29 (1H α ,t)	H-3 -	C-1,22,3,10,5 -
3	73.66	4.62 (1H α ,p)	H-4	-
4	37.02	1.72 (1H β ,d) 1.57 (1H α ,d)	- -	C-3,22,10,6 C-10,6,22
5	36.2	-	-	-
6	29.71	1.15 (2H,t)	H-7	C-19,7
7	31.91	1.32 (2H,m)	H-8	-
8	50.04	0.98 (1H β ,m)	H-9,14	C-10,5
9	35.81	2.08 (1H α ,m)	H-11	C-11
10	139.70	-	-	-
11	24.29	1.59 (2H,m)	H-12	-
12	21.05	1.35 (2H,m)	-	-
13	42.32	-	-	-
14	56.15	1.10 (1H α ,m)	H-15	C-13
15	39.53	1.86 (2H,m)	H-16	C-16
16	36.60	1.52 (2H,m)	H-17	C-15,20
17	56.70	1.00 (1H β ,m)	H-20	C-13,14,20,18

18	11.86	0.70 (3H β ,s)	-	C-13,12,17
19	19.33	1.04 (3H β ,s)	-	C-5
20	31.88	1.97 (1H β ; m)	H-21,20 ¹	C-17,21,20 ¹
20 ¹	22.57	0.90 (3H,d)	-	C-17,21
21	22.83	0.88 (3H,d)	-	C-17,20 ¹
22	173.28	-	-	-
23	25.64	2.87 (2H,d)	H-24	C-24,22
24	128.20	5.40 (1H, td, 9.14, 7.05)	-	-
25	132.01	5.41 (1H, td, 9.02, 7.03)	H-26	C-23
26	28.02	2.05 (2H,m)	H-27	C-25,24
27	18.73	0.95 (3H,t)		C-26,24,25

¹H NMR spectra recorded using Bruker AVANCE III 500MHz (AV 500) spectrometer (Bruker, Karlsruhe, Germany) in CDCl₃ as aprotic solvent at ambient temperature with TMS as the internal standard (δ 0 ppm). The ¹H NMR spectra were recorded at 500MHz, while the ¹³C NMR spectra were recorded at 125MHz. ^aValues in ppm, multiplicity and coupling constants (J =Hz) were indicated in parentheses. The assignments were made with the aid of the ¹H-¹H COSY, HSQC, HMBC and NOESY experiments

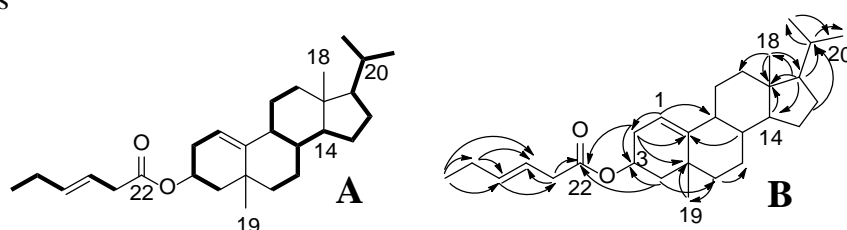


Figure 5.104.: ¹H-¹H COSY (A) and HMBC (B) correlations of 19 (10→5) abeo-20-methyl-pregn-1-en-3-yl-3 β -methoxy-hex-25-enoate (**8**). The key ¹H-¹H COSY couplings have been represented by the bold face bonds. The HMBC couplings were indicated by double barbed arrow

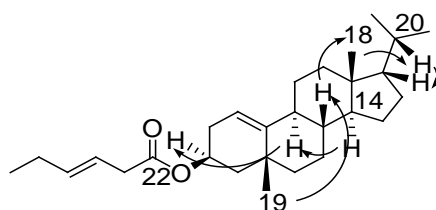


Figure 5.105.: NOESY correlations of 19 (10→5) abeo-20-methyl-pregn-1-en-3-yl-3 β -methoxy-hex-25-enoate (**8**). The NOESY relations were represented by double barbed arrow

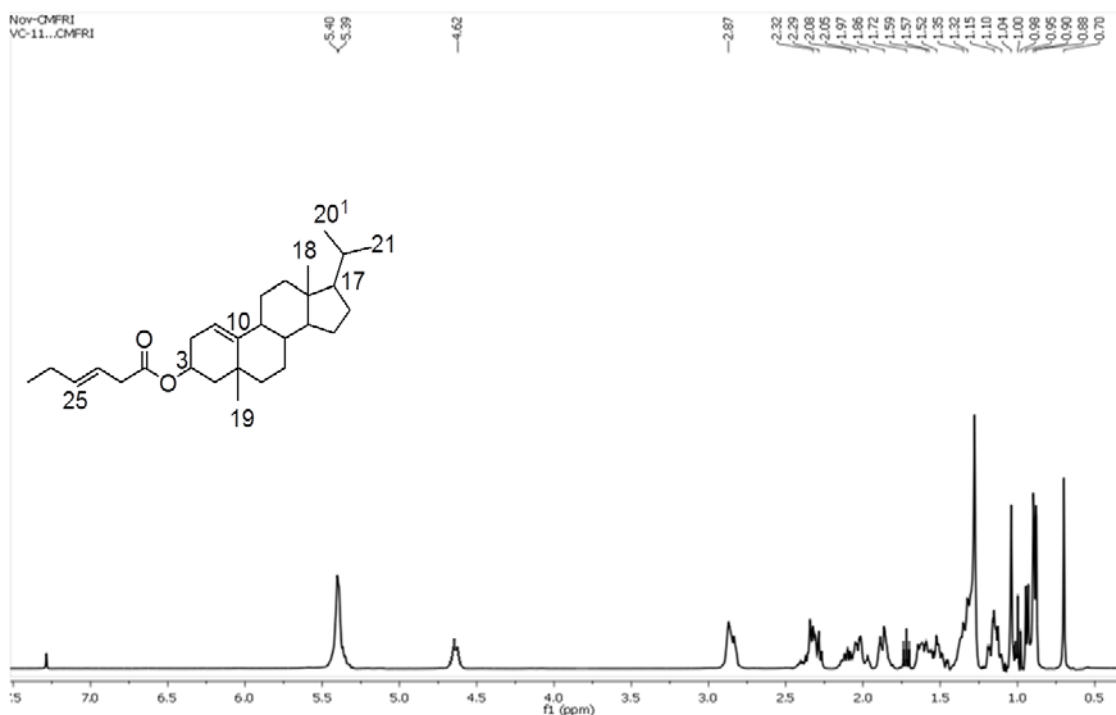


Figure 5.106.: ^1H NMR spectrum of 19 (10 \rightarrow 5) abeo-20-methyl-pregn-1-en-3-yl-3 β -methoxy-hex-25-enoate (**8**)

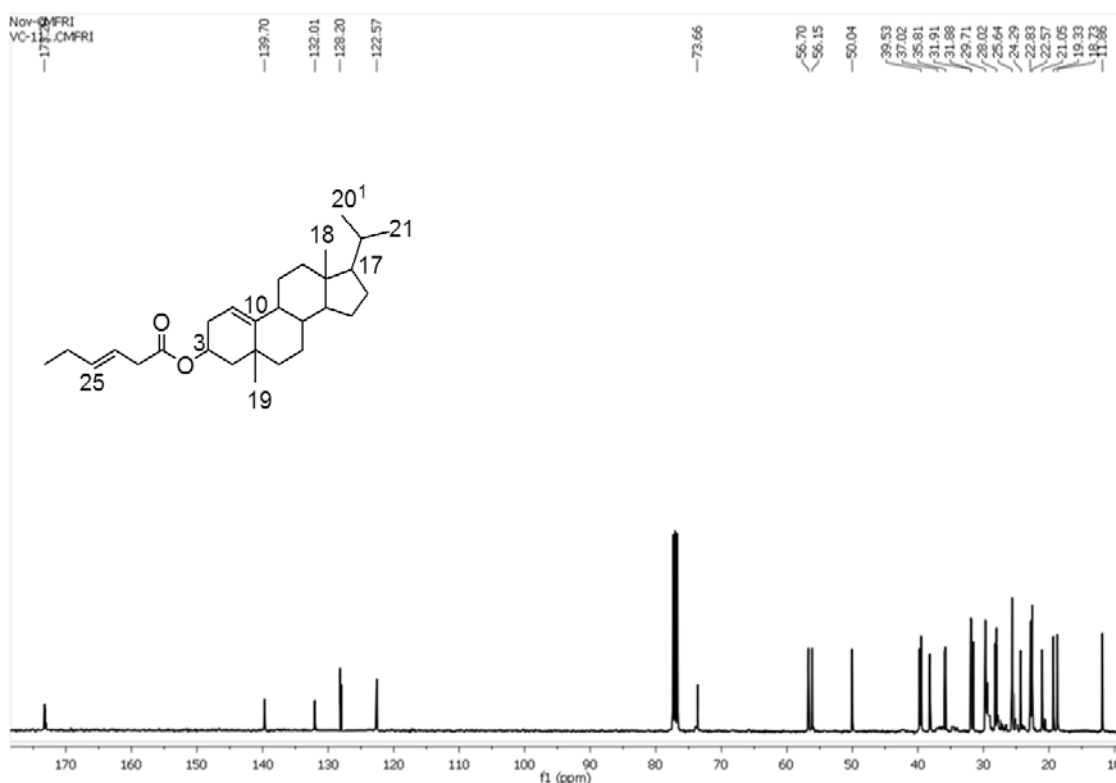


Figure 5.107.: ^{13}C NMR spectrum of 19 (10 \rightarrow 5) abeo-20-methyl-pregn-1-en-3-yl-3 β -methoxy-hex-25-enoate (**8**)

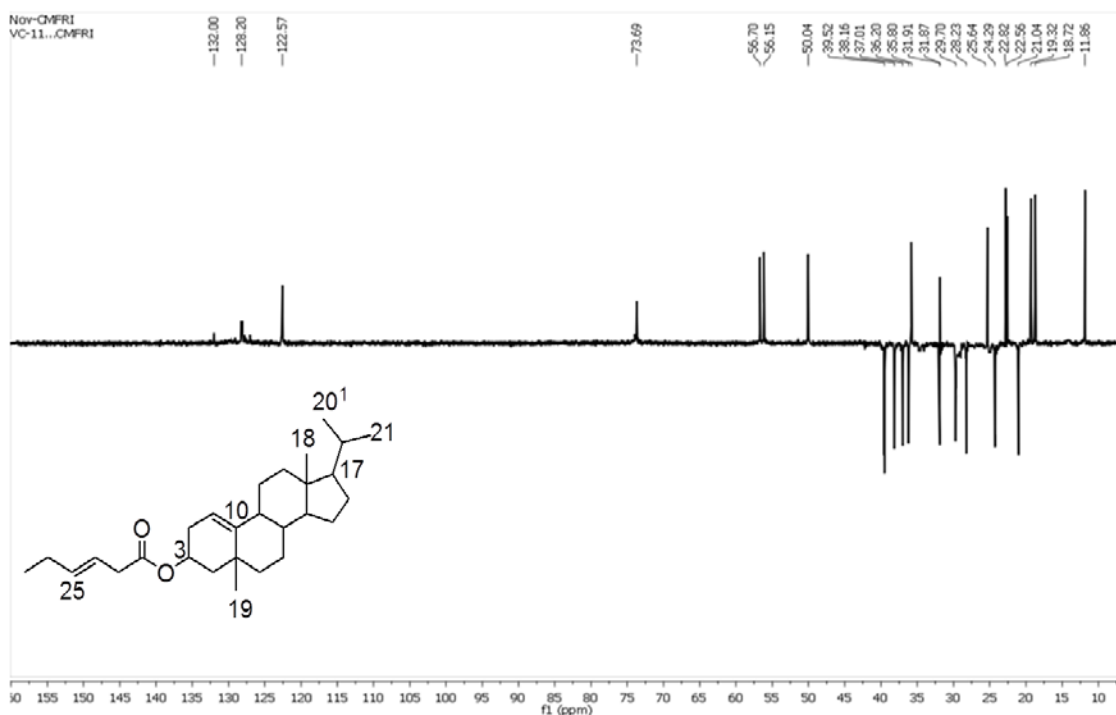


Figure 5.108.: $^{135}\text{DEPT}$ NMR spectrum of 19 (10→5) abeo-20-methyl-pregn-1-en-3-yl-3 β -methoxy-hex-25-enoate (**8**)

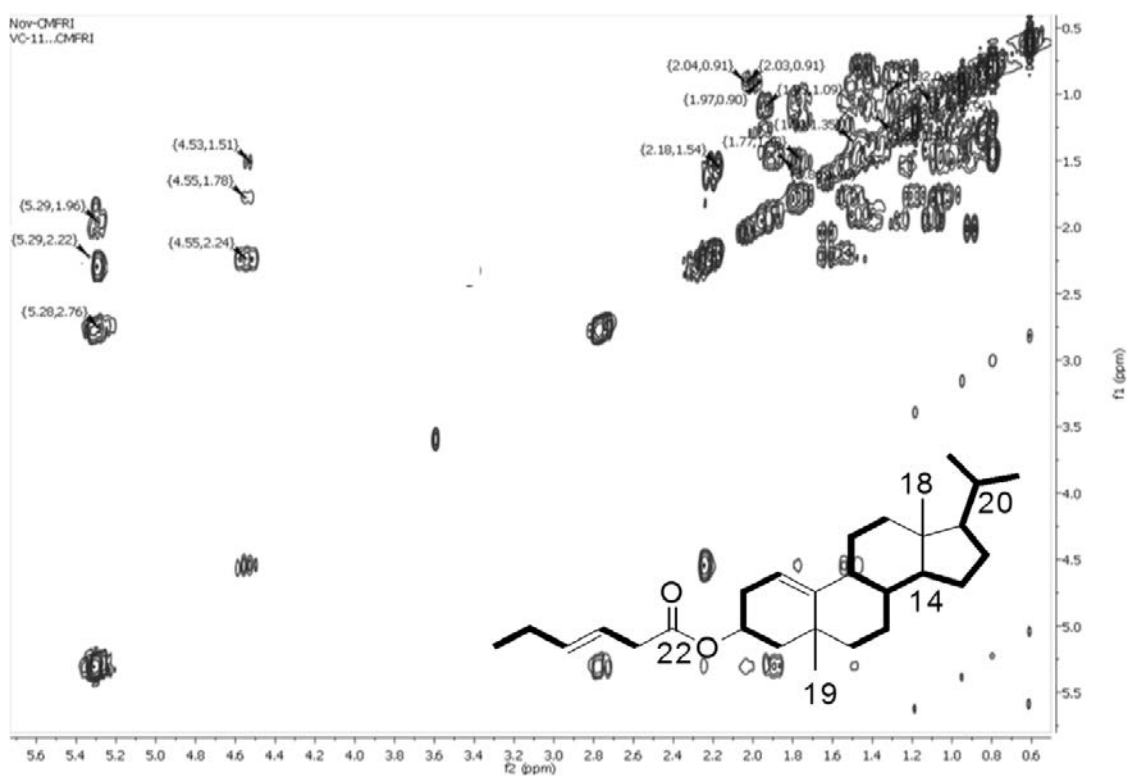


Figure 5.109.: ^1H - ^1H COSY NMR spectrum of 19 (10→5) abeo-20-methyl-pregn-1-en-3-yl-3 β -methoxy-hex-25-enoate (**8**)

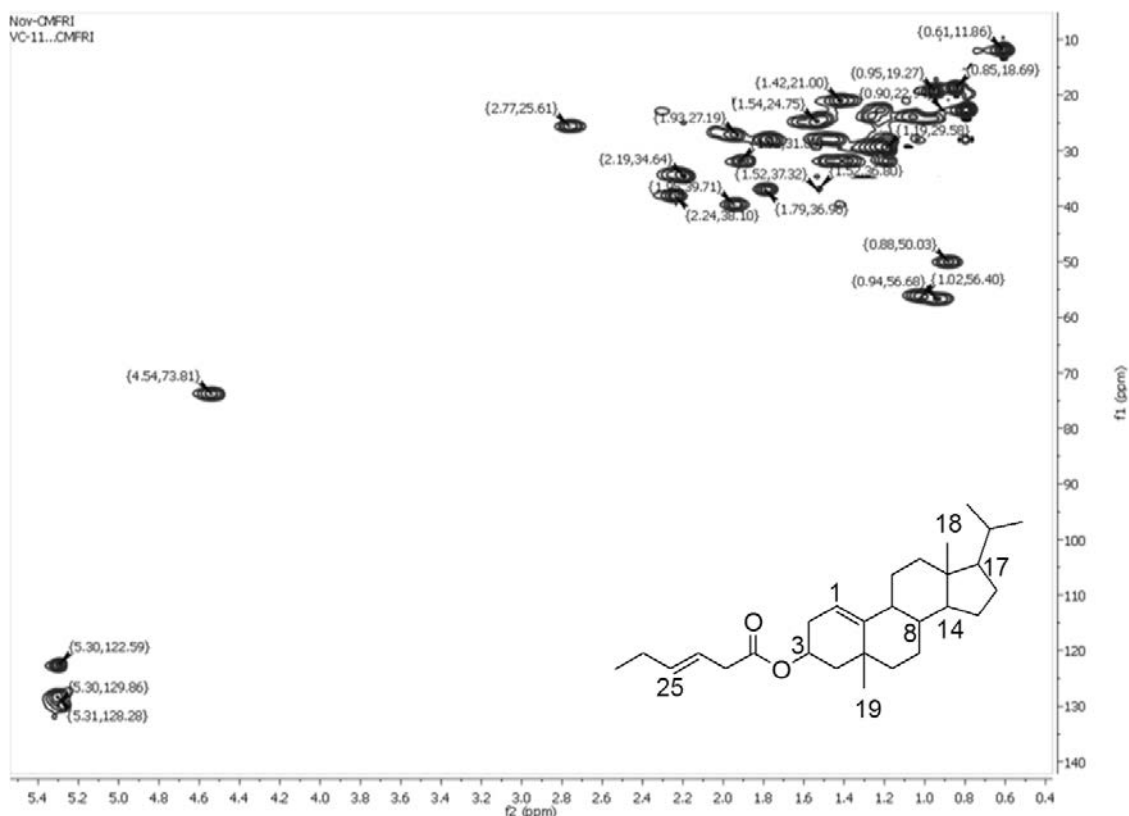


Figure 5.110.: HSQC spectrum of 19 (10→5) abeo-20-methyl-pregn-1-en-3-yl-3 β -methoxy-hex-25-enoate (**8**)

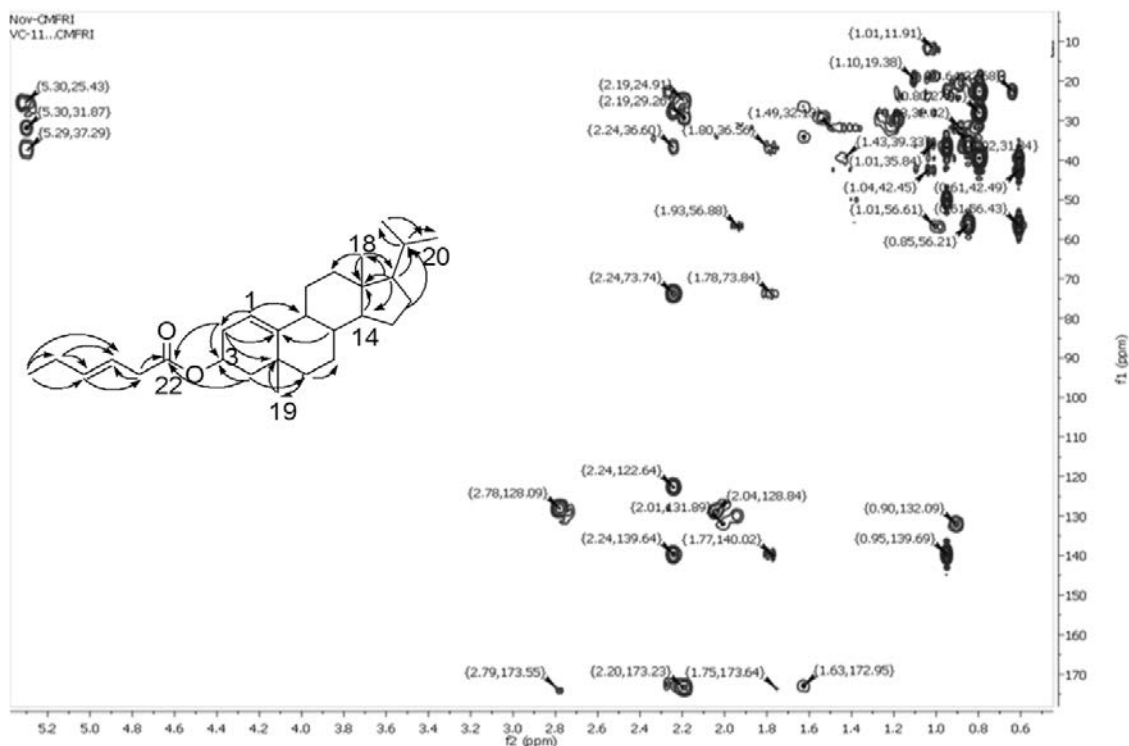


Figure 5.111.: HMBC NMR spectrum of 19 (10→5) abeo-20-methyl-pregn-1-en-3-yl-3 β -methoxy-hex-25-enoate (**8**)

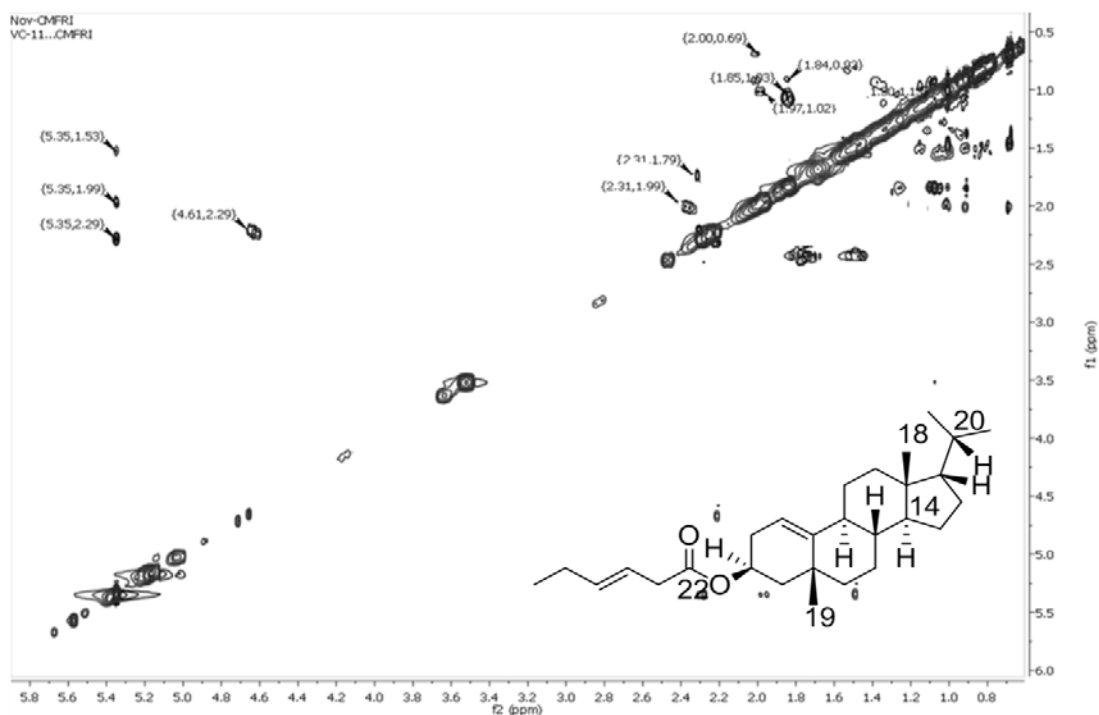


Figure 5.112.: NOESY NMR spectrum of 19 (10→5) abeo-20-methyl-pregn-1-en-3-yl-3β-methoxy-hex-25-enoate (**8**)

The IR stretching vibrations for ester carbonyl (C=O) and alkoxy functionalities were implied by signals at 1719 and 1050 cm^{-1} , respectively. The characteristic absorption bands at 2923 and 2855 cm^{-1} represented alkyl stretching vibrations (Figure 5.113.).

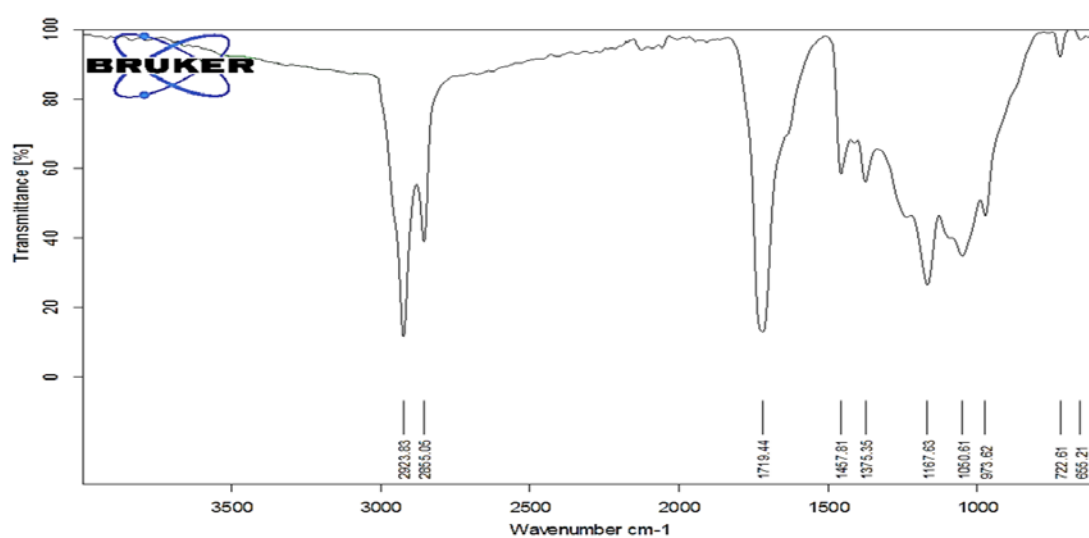


Figure 5.113.: FTIR spectrum of 19 (10→5) abeo-20-methyl-pregn-1-en-3-yl-3β-methoxy-hex-25-enoate (**8**)

The molecular ion peak was recorded at m/z 412 (Figure 5.114.). The sequential elimination of two methyl radicals from the side chain moiety resulted into fragment with m/z 380 (**b**, $C_{26}H_{36}O_2^{+}$). This appeared to undergo sequential elimination of radicals such as $C_2H_3^{\bullet}$, $C_2H_3O_2^{\bullet}$, $C_3H_7^{\bullet}$, two CH_3^{\bullet} , and $C_2H_2^{++}$ resulted into corresponding peaks at m/z 354 (**c**, $C_{24}H_{34}O_2^{+}$), 301 (**d**, $C_{22}H_{37}^{+}$), 254 (**e**, $C_{19}H_{26}^{+}$), 226 (**f**, $C_{17}H_{22}^{+}$) and 201 (**g**, $C_{15}H_{21}^{+}$), respectively. The fragment, dodecahydro-cyclopropa-phenanthrene (**g**) appeared to undergo repeated fragmentations to yield methylenecyclohexene at m/z 94 (**k**, $C_7H_{10}^{+}$), which was on fragmentation of two molecules of methyl radical registered base ion peak at m/z 70 ($C_5H_{10}^{+}$) corresponding to the pentene moiety (Figure 5.115.).

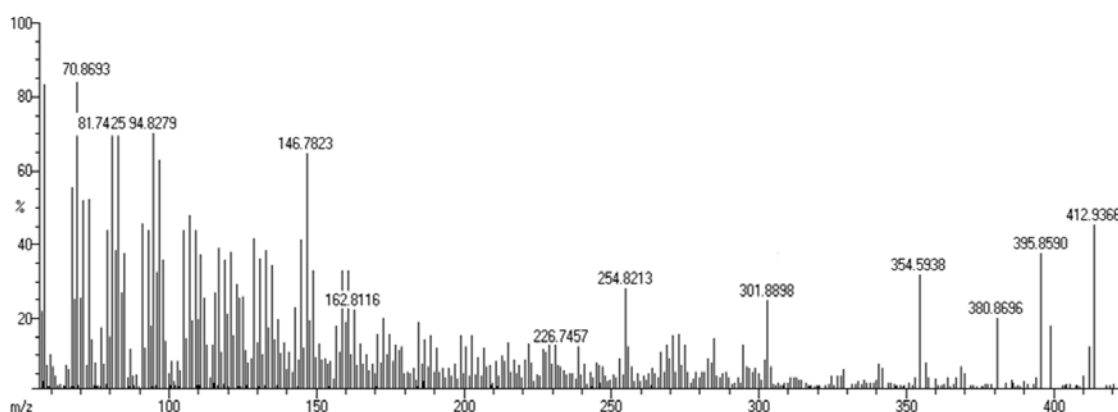


Figure 5.114.: EIMS spectrum of 19 (10→5) abeo-20-methyl-pregn-1-en-3-yl-3 β -methoxy-hex-25-enoate (**8**)

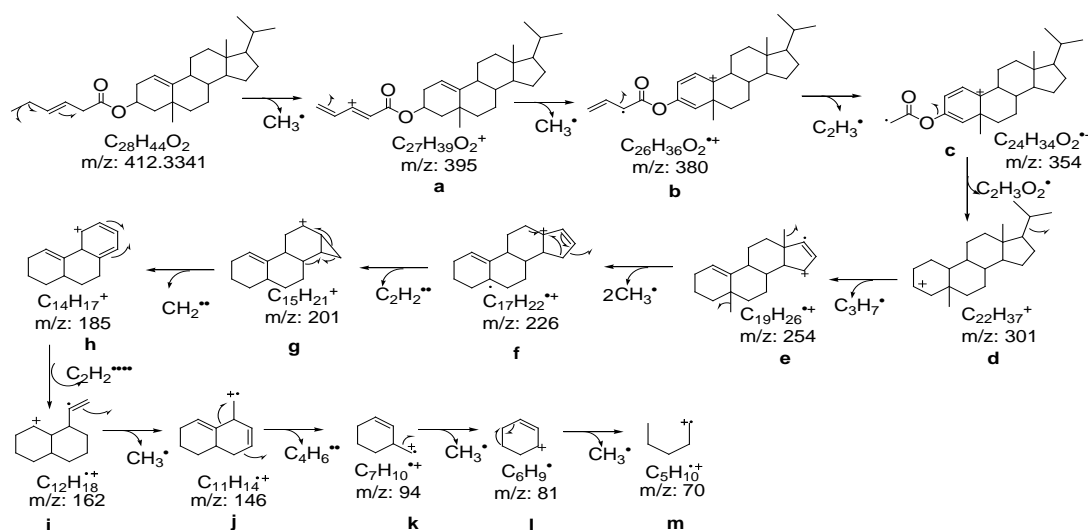
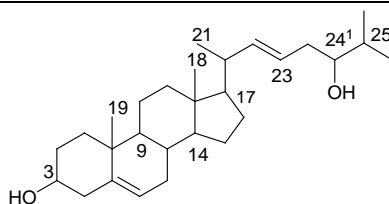


Figure 5.115.: Mass fragmentation pattern of 19 (10→5)-abeo-20-methyl-pregn-1-en-3-yl-3 β -methoxy-hex-25-enoate (**8**)

5.3.2.4.B. Structural characterization of compound 9 (VC₂₋₅₋₁)**(22E)-24¹-Homcholesta-5,22-dien-(3 β ,24¹ β)-diol (9)**

Yield	134 mg; 0.30%
Physical description	White solid
Molecular formula	C ₂₈ H ₄₆ O ₂
Molecular mass	414.3498

The cholestene compound, (22E)-24¹-homcholesta-5,22-dien-(3 β ,24¹ β)-diol (**9**) was isolated as white solid after repeated chromatographic purification techniques. It exhibited UV absorbance (in MeOH) at λ_{max} (log ϵ 3.46) 221.5 nm, which was assigned to a chromophore with olefinic groups and hydroxyl systems (Figure 5.116.). The purity of the compound was supported by RP C18 HPLC using 3:2 MeOH:MeCN (R_t 6.00) experiments (Figure 5.117.).

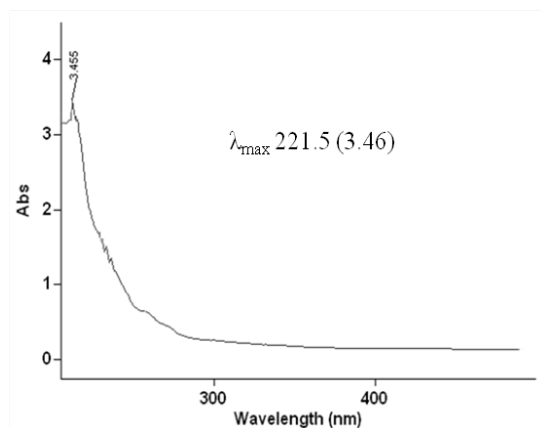


Figure 5.116.: UV spectrum of (22E)-24¹-homcholesta-5,22-dien-(3 β ,24¹ β)-diol (**9**)

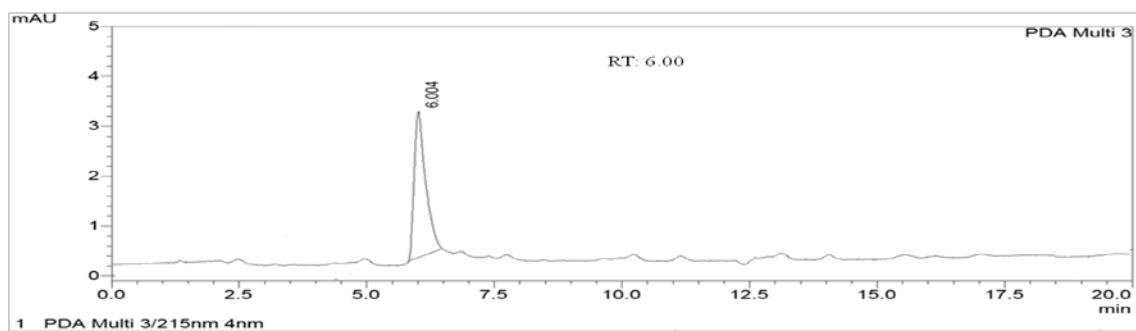


Figure 5.117.: HPLC chromatogram of (22*E*)-24¹-homocholesta-5,22-dien-(3β,24¹β)-diol (**9**)

The cholesterol derivative, characterized as (22*E*)-24¹-homocholesta-5,22-dien-(3β,24¹β)-diol (**9**) was found to enclose an olefinic and hydroxyl groups in side chain framework attached at C-17. The molecular ion peak at m/z 414 (EIMS found m/z 414.3504 $[M]^+$, cal. 414.3498) along with the proton and carbon spectroscopic data represented its molecular formula as $C_{28}H_{46}O_2$. The present compound was corroborated with the spectroscopic data of the sterol derivatives in the previous works (Tian *et al.*, 2011). The cumulative DEPT and ^{13}C NMR analyses confirmed the occurrence of 28 carbons, which was distributed among nine methylenes, five methyls, and eleven methines along with three quaternary carbons (Table 5.13.; Figure 5.122.-5.123.). Highly deshielded protons at δ 5.34, 5.18 and 5.17 displayed HSQC correlations with δC 121.70, 131.72 and 135.83, respectively, which were placed at C-6, C-22 and C-23 positions, respectively. The lesser chemical shifts for $-CH_3$ groups at δH 1.01 (s), 0.69 (s), 0.84 (d), 0.86 (d) and 0.90 (d) exhibited HSQC correlation with the carbons at δC 19.40, 11.87, 19.89, 22.69 and 17.62, respectively arranged at C-19, C-18, C-26, C-27 and C-21, positions, in that order. The HSQC cross peaks with δH 0.92/ δC 50.14, δH 1.10/ δC 56.02 and δH 0.95/ δC 56.77 (Figure 5.124.) assigned the presence of characteristic methines ($-CH-$) at C-9, C-14 and 17, respectively (Reich *et al.*, 1969). The 1H - 1H COSY spectrum specified three spin systems in the title compound. The first spin system was exhibited by proton cross peaks at δ 1.85, 1.03 (H-1)/1.49, 1.83 (H-2)/3.52 (H-3)/2.23, 2.28 (H-4) in ring A. The second spin system was found at δ 5.34 (H-6)/1.95 (H-7)/1.51 (H-8)/0.92 (H-9)/1.47 (H-11)/1.14, 2.00 (H-12); δ 1.51 (H-8)/1.10 (H-14)/1.08, 1.53 (H-15)/1.69 (H-16)/0.95 (H-17) in B/C/D ring along with δ 0.95 (H-17)/1.86 (H-20)/0.90 (H-21), 5.18 (H-22), which confirmed the side chain attachment to parent steroid group at C-17 (Figure 5.118.A, 5.123.). Other spin system

was attributed to δ 5.17 (H-23)/2.03 (H-24)/3.64 (H-24¹)/1.52 (H-25)/0.84 (H-26), 0.86 (H-27), which formed the part of side chain. The HMBCs from δ 1.85 (H-1) to δ 36.51 (C-10); δ 1.49 (H-2) to δ 140.75 (C-5); δ 2.23 (H-4) to δ 36.52 (C-10); δ 5.35 (H-6) to δ 42.30 (C-4), 36.51 (C-10); δ 1.95 (H-7) to δ 50.14 (C-9); δ 1.51 (H-8) to δ 140.75 (C-5); δ 0.92 (H-9) to δ 140.75 (C-5), δ 36.52 (C-10) confirmed the presence of ring A/B. Further HMBC cross peaks from δ 1.47 (H-11) to δ 50.14 (C-9), 19.40 (C-19); δ 1.14 (H-12) to δ 11.87 (C-18); δ 1.10 (H-14) to δ 21.09 (C-11) and δ 0.95 (H-17) to δ 46.25 (C-13), 56.02 (C-14) were attributed to C/D bicyclic ring system (Figure 5.118.B, 5.125.). The long range HMBCs from δ 1.01 (H-19) to δ 36.51 (C-10), 140.75 (C-5) confirmed the attachment of -CH₃-19 to C-10 and those between δ 0.69 (H-18) to δ 42.81 (C-20), 46.25 (C-13) assigned the attachment of -CH₃-18 to C-13. The side chain attachment at C-17 was corroborated with HMBC correlations from δ 1.86 (H-20) to δ 56.77 (C-17) and δ 0.90 (H-21) to δ 56.77 (C-17). Long-range HMBC couplings from δ 1.86 (H-20) to δ 131.72 (C-22); δ 0.90 (H-21) to δ 131.72 (C-22); δ 2.03 (H-24) to δ 42.81 (C-20) and δ 0.86 (H-27) to δ 40.16 (C-24) were attributed to side chain moiety. Highly deshielded methine proton at δ 3.64 displaying HSQC with the δ C 70.44 was accounted for the presence of a hydroxyl group and its position was attributed from the long distance HMBC couplings from δ 2.03 (H-24) to δ 70.44 (C-24¹) and δ 1.52 (H-25) to δ 70.44 (C-24¹). Thus, the side chain with one each of olefinic centre (C-22) and hydroxyl group (C-24¹) were attributed. The greater coupling constants (*J*) of 9.81 and 10.44/9.61 Hz, corresponding to olefinic signals at H-22 and H-23, respectively suggested their *trans* (*E*) orientation. The β -orientation of -OH at C-3 was assumed from NOE relations, such as δ 3.52 (H-3)/2.28 (H α -4)/1.03 (H α -1)/1.83 (H α -2) and δ 5.34 (H-6)/2.28 (H α -4) (Figure 5.119., 5.126.) (Sun *et al.*, 2013). The intense NOE correlations, such as δ 1.01 (H-19)/ δ 2.23 (H β -4)/1.51 (H β -8)/0.68 (H-18) corroborated the β -orientation of singlet methyls at H-19 and H-18 bonded to sp³ hybridized quaternary carbons, C-10 and C-13, respectively (Calderon *et al.*, 2004).

Table 5.13.: NMR spectroscopic data of (22*E*)-24¹-homocholesta-5,22-dien-(3 β ,24¹ β)-diol (**9**) in CDCl₃

C. No.	¹³ C	¹ H (int.,mult., <i>J</i> in Hz) ^a	COSY	HMBC
1	37.27	1.85 (1H α ,t) 1.03 (1H β ,t)	H-2 H-2	C-3,10 -

2	31.65	1.49 (1H β ,m) 1.83 (1H α ,m)	H-3 -	C-3,5 -
3	71.80	3.52 (1H α ,p)	H-4	-
4	42.30	2.23 (1H β ,d) 2.28 (1H α ,d)	- -	C-3,10,5 -
5	140.75	-	-	-
6	121.70	5.34 (1H α ,dd,6.25, 6.31)	H-7	C-4,10
7	31.91	1.95 (1H,t)	H-8	C-6,9,8
8	28.02	1.51 (1H β ,m)	H-9,14	C-5
9	50.14	0.92 (1H α ,m)	H-11	C-10,5,14
10	36.51	-	-	-
11	21.09	1.47 (2H,m)	H-12	C-9,19,12
12	39.79	1.14 (1H β ,t) 2.00 (1H α ,t)	- -	C-11,18 -
13	46.25	-	-	-
14	56.02	1.10 (1H α ,m)	H-15	C-11,15
15	24.30	1.08 (1H β ,m) 1.53 (1H α ,m)	H-16 -	C-16 -
16	28.54	1.69 (2H,m)	H-17	C-15
17	56.77	0.95 (1H β ,m)	H-20	C-13,14,15,16
18	11.87	0.69 (3H β ,s)	-	C-20,17,12,13
19	19.40	1.01 (3H β ,s)	-	C-1,10,5,9
20	42.81	1.86 (1H,m)	H-21,22	C-21,22,23,17
21	17.62	0.90 (3H α ,d)	-	C-17,22
22	131.72	5.18 (1H,t,9.81)	-	-
23	135.83	5.17 (1H,td,10.44, 9.61)	H-24	C-22
24	40.16	2.03 (2H,t)	H-24 ¹	C-20,24 ¹
24 ¹	70.44	3.64 (1H α ,m)	H-25	-
25	33.10	1.52 (1H,m)	H-26,27	C-24 ¹
26	19.89	0.84 (3H,d)	-	C-25,27
27	22.69	0.86 (3H,d)	-	C-25,26,24

¹H NMR spectra recorded using Bruker AVANCE III 500MHz (AV 500) spectrometer (Bruker, Karlsruhe, Germany) in CDCl₃ as aprotic solvent at ambient temperature with TMS as the internal standard (δ 0 ppm). The ¹H NMR spectra were recorded at 500MHz, while the ¹³C NMR spectra were recorded at 125MHz. ^aValues in ppm, multiplicity and coupling constants (J =Hz) were indicated in parentheses. The assignments were made with the aid of the ¹H-¹H COSY, HSQC, HMBC and NOESY experiments

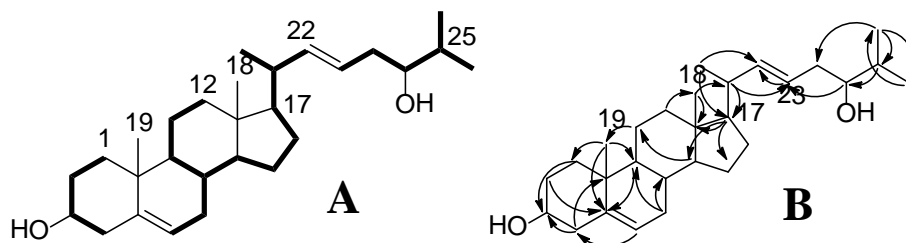


Figure 5.118.: ¹H-¹H COSY (A) and HMBC (B) correlations of (22E)-24¹-homocholesta-5,22-dien-(3 β ,24¹ β)-diol (9). The key ¹H-¹H COSY couplings have been represented by the bold face bonds. The HMBC couplings were indicated by double barbed arrow

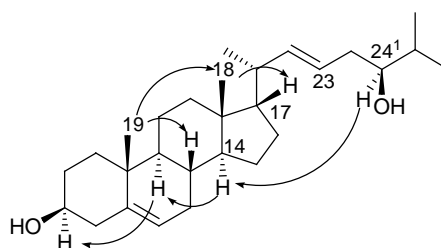


Figure 5.119.: NOESY correlations of (22E)-24¹-homocholesta-5,22-dien-(3 β ,24¹ β)-diol (9). The NOESY relations were represented by double barbed arrow

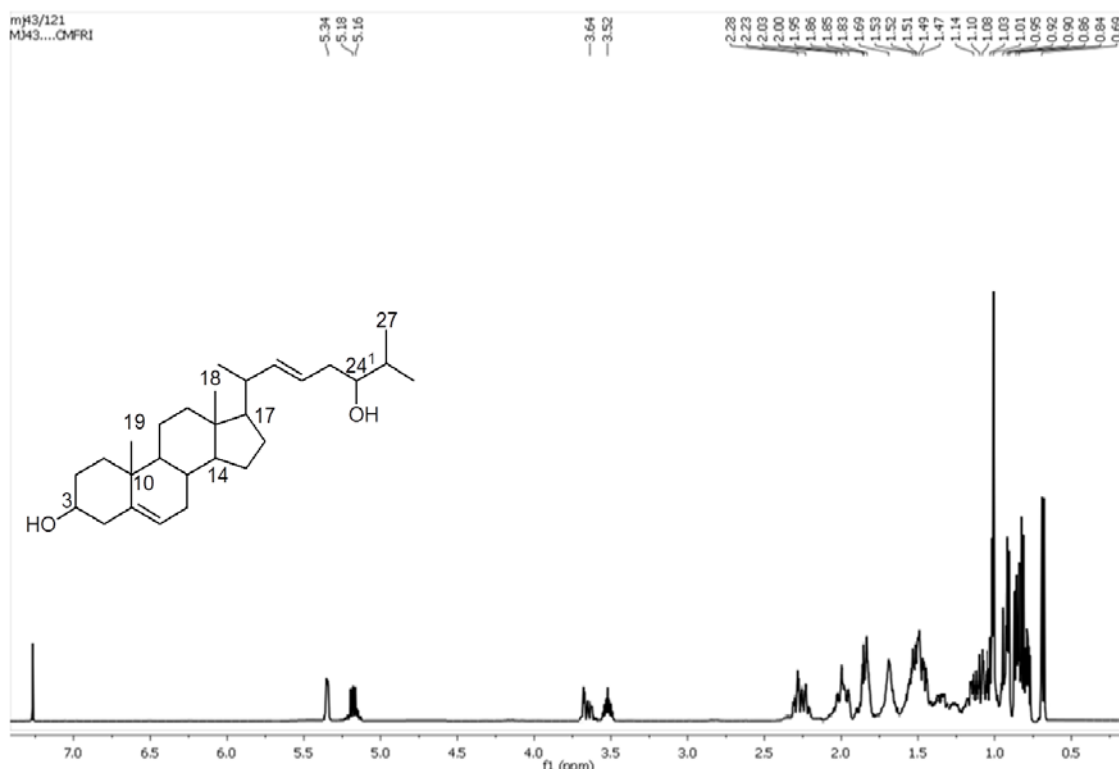


Figure 5.120.: ¹H NMR spectrum of (22E)-24¹-homocholesta-5,22-dien-(3 β ,24¹ β)-diol (9)

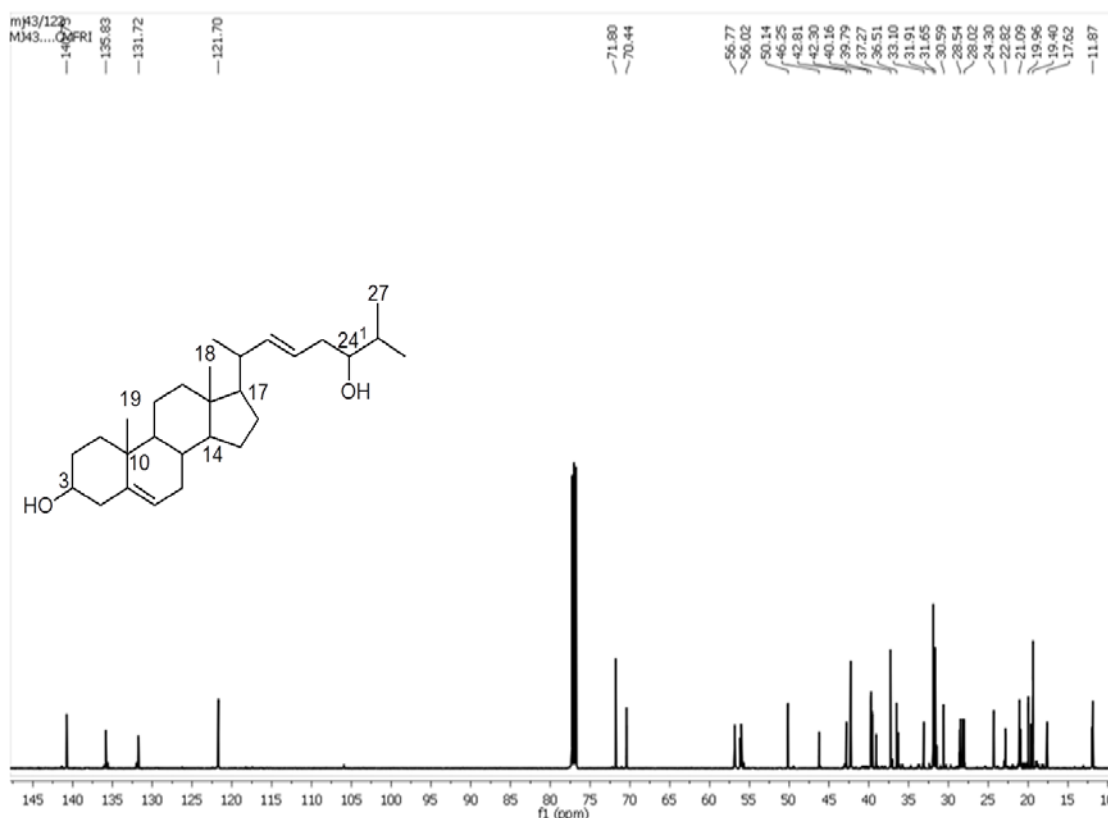


Figure 5.121.: ¹³C NMR spectrum of (22E)-24¹-homocholesta-5,22-dien-(3 β ,24¹ β)-diol (9)

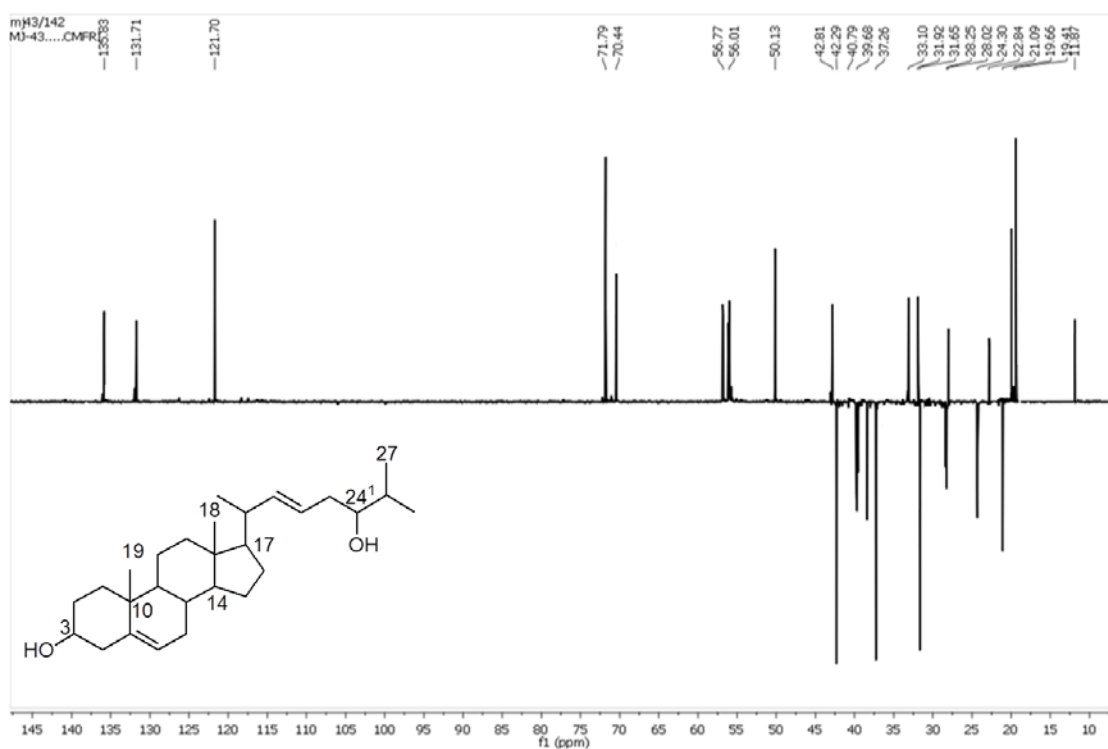


Figure 5.122.: ¹³⁵DEPT NMR spectrum of (22E)-24¹-homocholesta-5,22-dien-(3 β ,24¹ β)-diol (9)

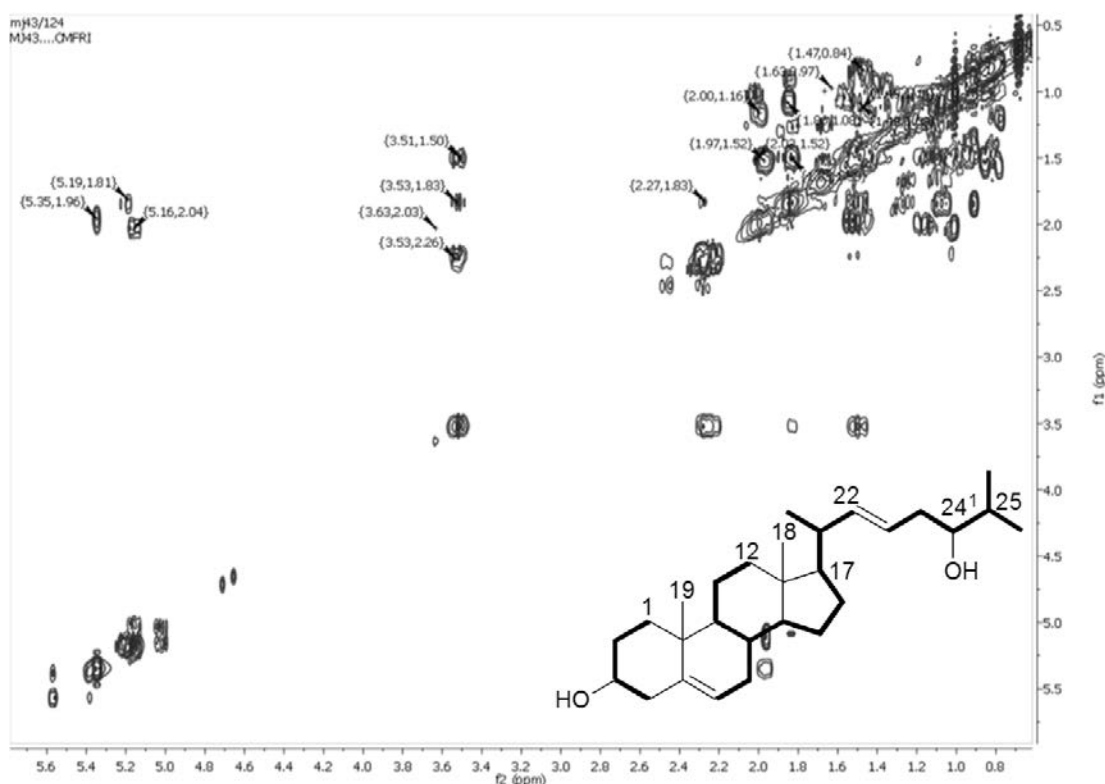


Figure 5.123.: ^1H - ^1H COSY NMR spectrum of (22*E*)-24¹-homocholesta-5,22-dien-(3 β , 24¹ β)-diol (**9**)

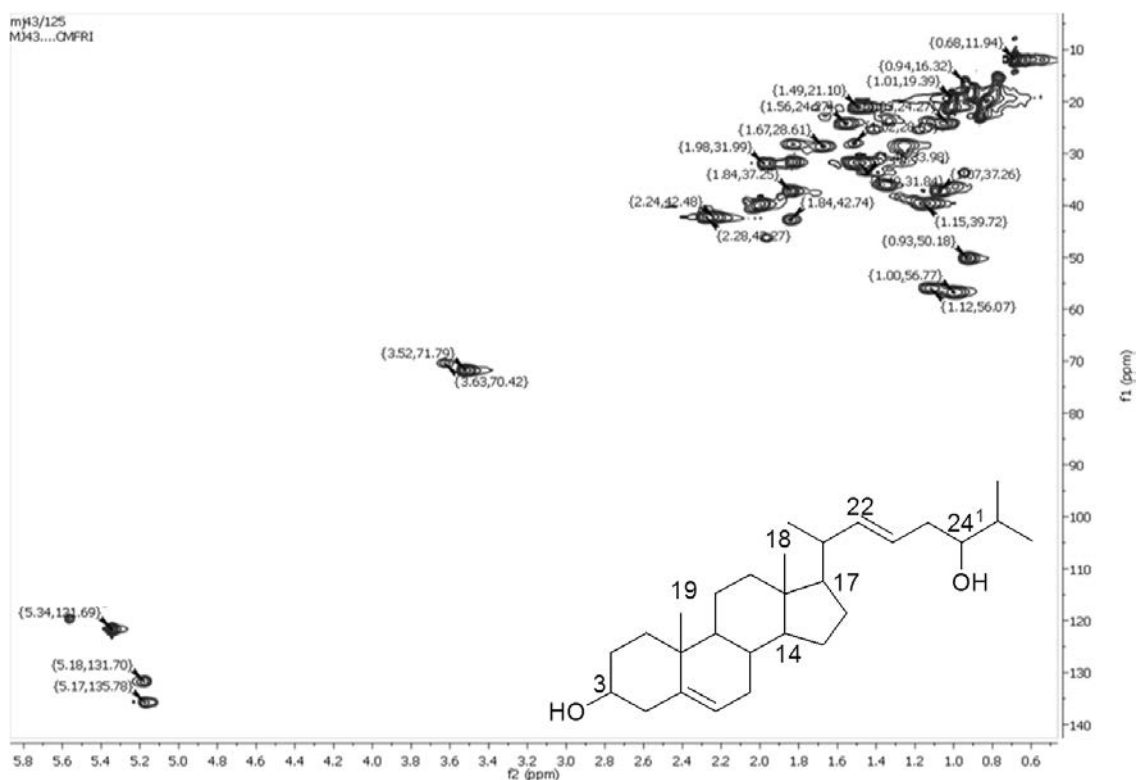


Figure 5.124.: HSQC NMR spectrum of (22*E*)-24¹-homocholesta-5,22-dien-(3 β , 24¹ β)-diol (**9**)

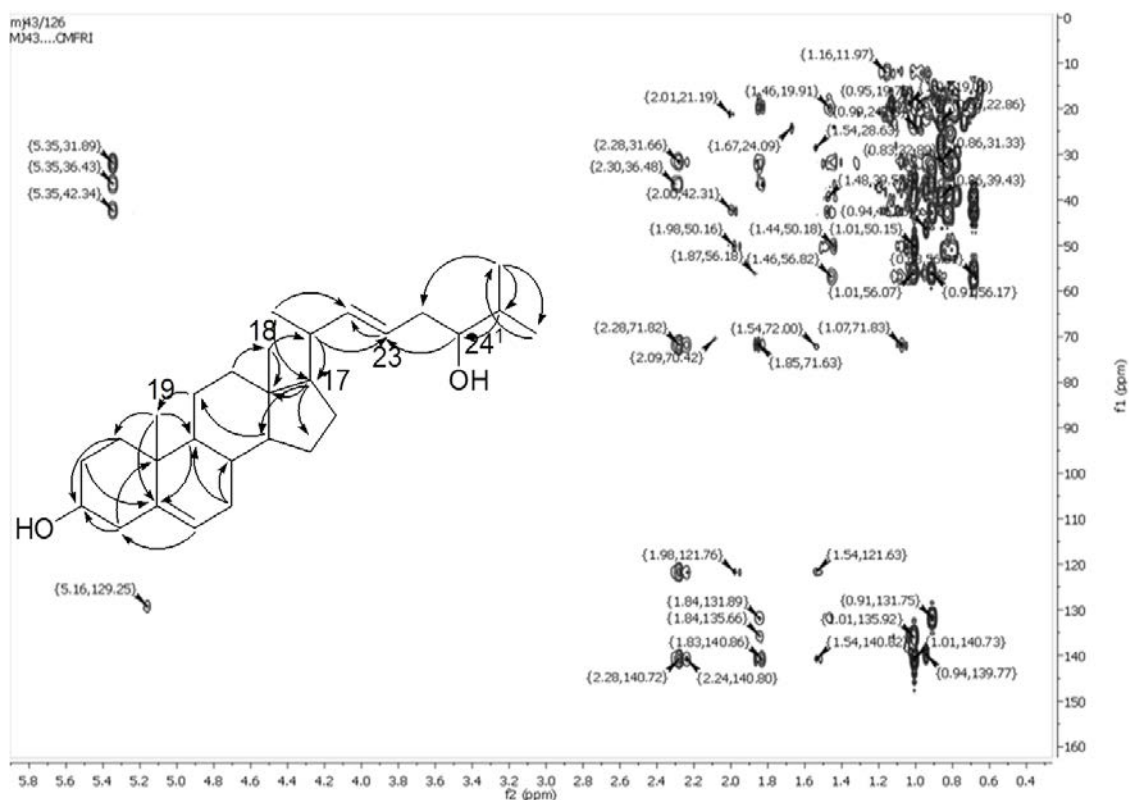


Figure 5.125.: HMBC NMR spectrum of (22E)-24¹-homocholesta-5,22-dien-(3 β ,24¹ β)-diol (**9**)

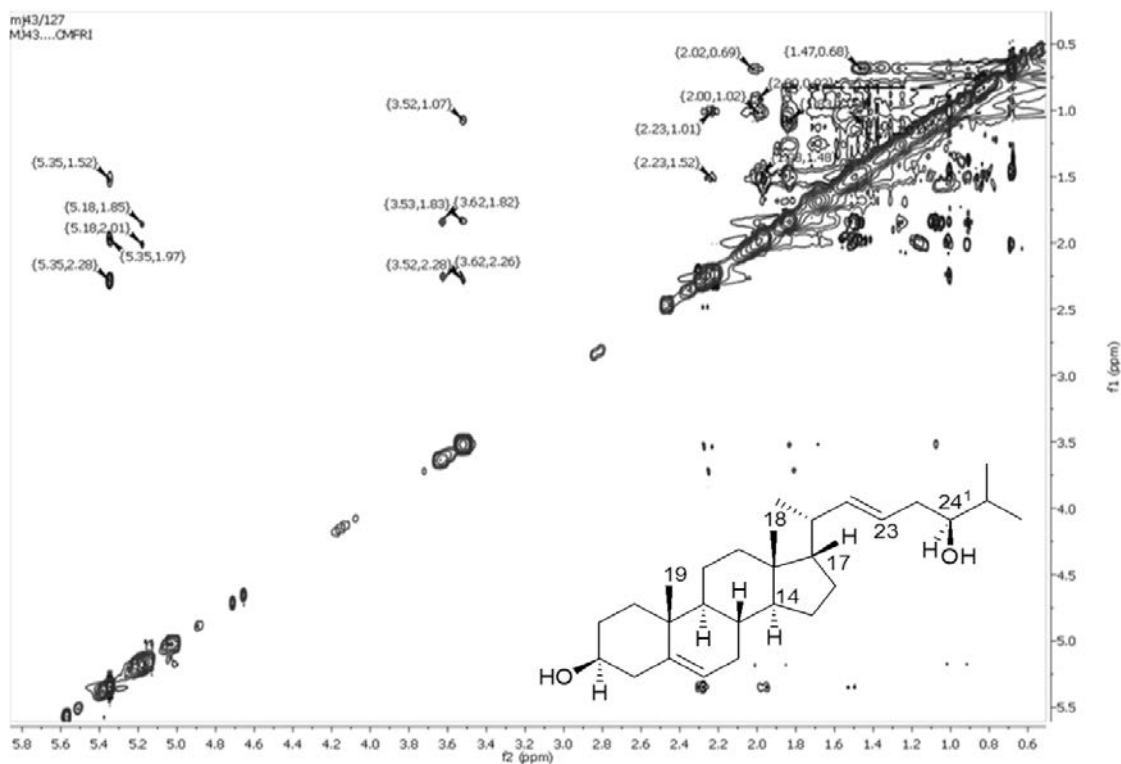


Figure 5.126.: NOESY NMR spectrum of (22E)-24¹-homocholesta-5,22-dien-(3 β ,24¹ β)-diol (**9**)

The IR stretching vibrations for C=C and alkyl moieties were implied through absorptions at 1663 and 2934 cm^{-1} , respectively (Figure 5.127.). The characteristic absorption at 3366 cm^{-1} represented hydroxyl stretching vibration.

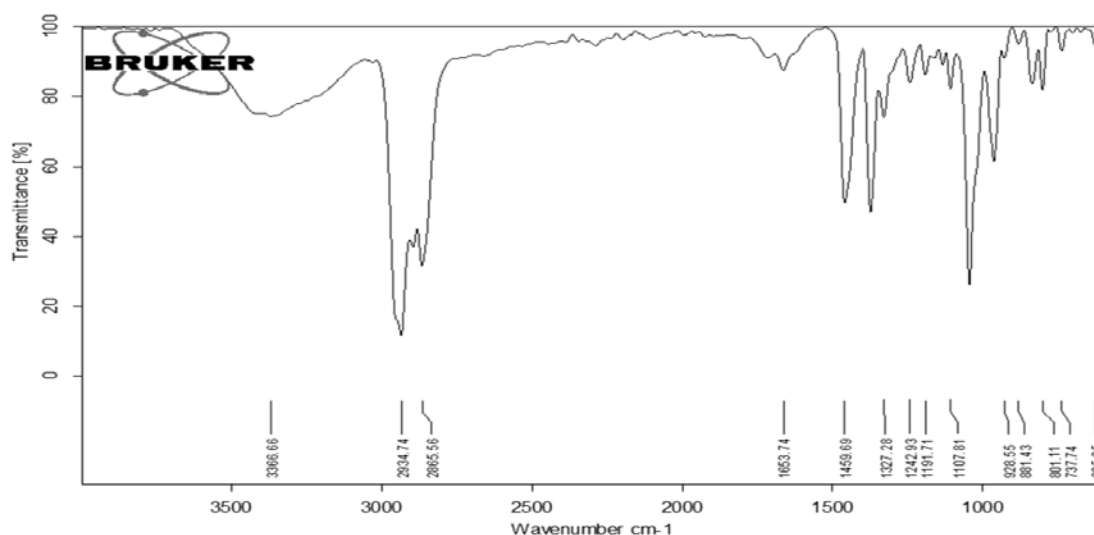


Figure 5.127.: FTIR spectrum of (22*E*)-24¹-homocholesta-5, 22-dien-(3 β , 24¹ β)-diol (**9**)

The molecular ion peak in the mass spectra was recorded at m/z 414 (Figure 5.128.). The elimination of hydroxyl radical at C-24¹ of hydrocarbon chain of sterol reported a fragment peak at m/z 396 (**a**). This appeared to undergo elimination of angular methyl radical at C-18 and C-19 to yield a peak at m/z 369 (**b**, $\text{C}_{26}\text{H}_{41}\text{O}^+$), which appeared to dissociate the methyl/ethyl radicals in the hydrocarbon tail of sterol along with the elimination of hydroxyl radical at C-3 to register a peak at m/z 221 (**h**, $\text{C}_{17}\text{H}_{17}^+$) due to the hexahydro-cyclopenta-phenanthrene moiety. The later appeared to undergo sequential elimination of ions, such as CH_2^\bullet , $\text{C}_2\text{H}_3^\bullet$, CH_2^\bullet , $\text{C}_2\text{H}_3^\bullet$, $\text{C}_2\text{H}_4^\bullet$ and CH_3^\bullet corresponding to the peaks at m/z 207 (**i**, $\text{C}_{16}\text{H}_{15}^+$), 185 (**j**, $\text{C}_{14}\text{H}_{17}^+$), 171 (**k**, $\text{C}_{13}\text{H}_{15}^+$), 147 (**l**, $\text{C}_{11}\text{H}_{15}^+$), 117 (**m**, C_9H_9^+) and 105 (**n**, C_8H_9^+), respectively. The ethylenecyclohexadiene (**n**) radical eliminated methyl radical to obtain a base peak of methylcyclohexadiene at m/z 94 (**o**, $\text{C}_7\text{H}_{10}^+$) which further dissociated two methyl radicals to yield pentadiene cation with m/z 67 (**q**) (Figure 5.129.).

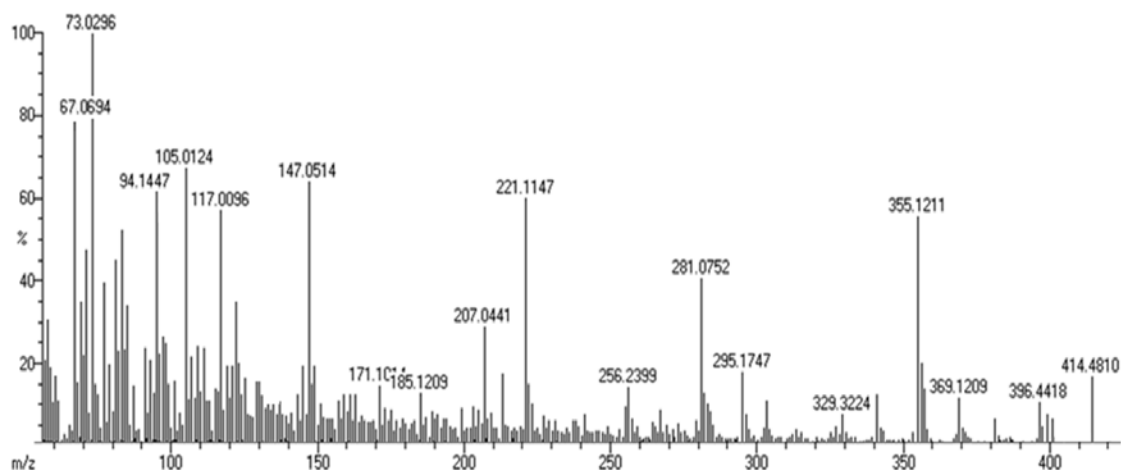


Figure 5.128.: EIMS spectrum of (22*E*)-24¹-homocholesta-5,22-dien-(3β,24¹β)-diol (**9**)

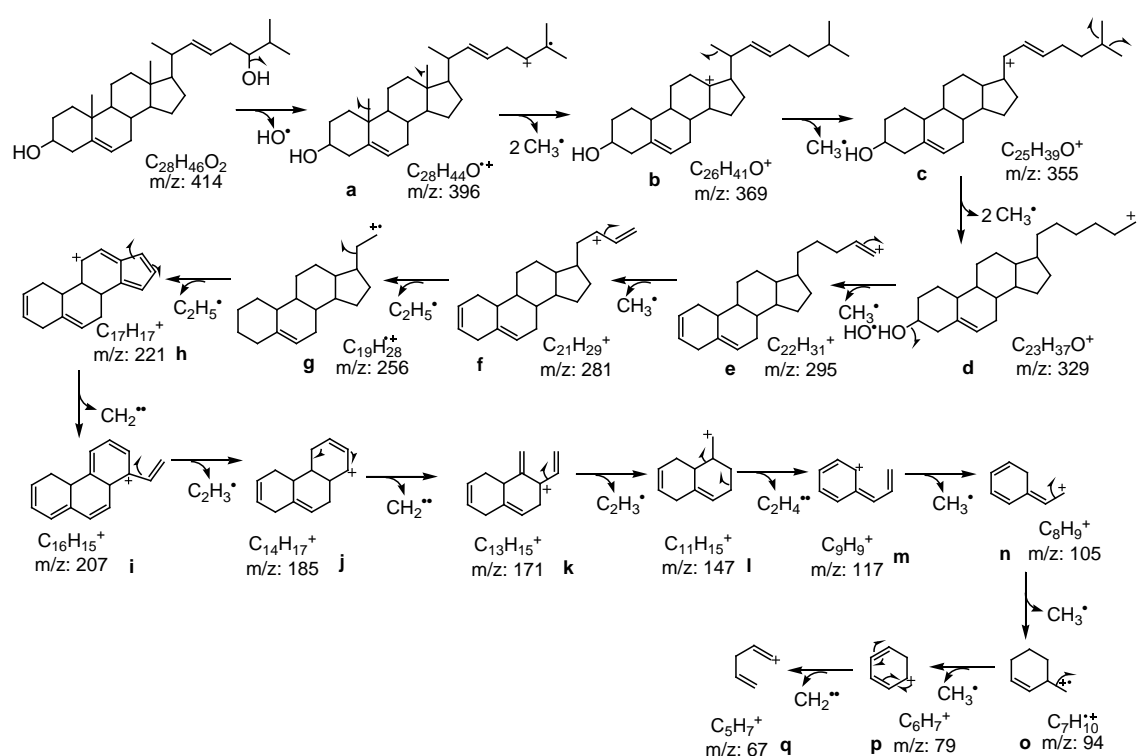
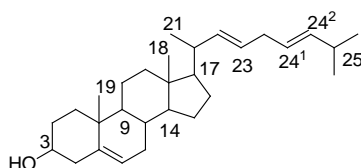


Figure 5.129.: Mass fragmentation pattern of (22*E*)-24¹-homocholesta-5,22-dien-(3β,24¹β)-diol (**9**)

5.3.2.4.C. Structural characterization of compound 10 (VC₂₋₄₋₁)

(22*E*),(24¹*E*)-24¹,24²-Dihomocholesta-5,22,24¹-trien-3β-ol (**10**)



Yield	195 mg; 0.43%
Physical description	White solid
Molecular formula	$C_{29}H_{46}O$
Molecular mass	410.3549

A new cholestene compound, (22*E*),(24¹*E*)-24¹,24²-dihomocholest-5,22,24¹-trien-3 β -ol (**10**) isolated as a white solid. It exhibited UV absorbance (in MeOH) at λ_{\max} (log ϵ 3.32) 220.1 nm related to alkenes (Figure 5.130.). The purity of compound was supported by RP C18 HPLC using 3:2 (v/v) MeOH:MeCN (R_t 8.99) experiments (Figure 5.131.).

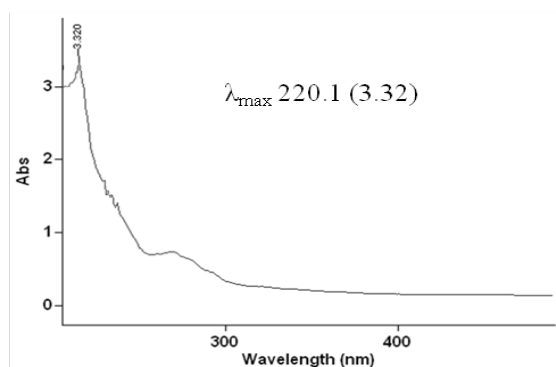


Figure 5.130.: UV spectrum of (22*E*),(24¹*E*)-24¹,24²-dihomocholesta-5,22,24¹-trien-3 β -ol (**10**)

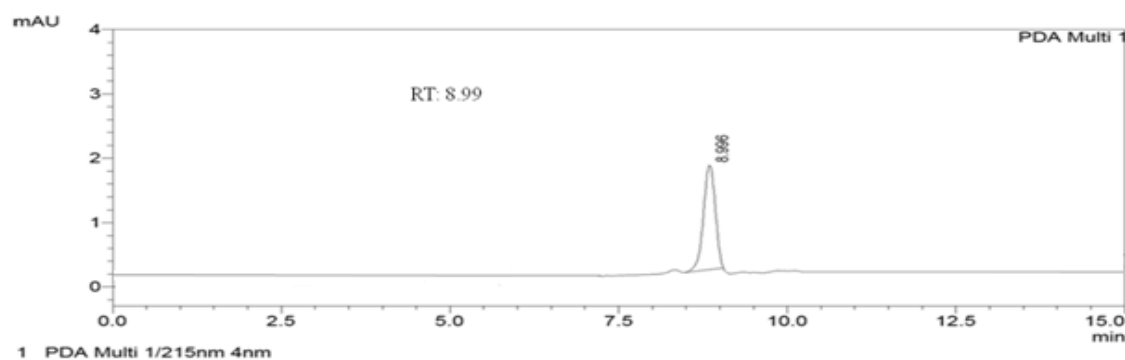


Figure 5.131.: HPLC chromatogram of (22*E*),(24¹*E*)-24¹,24²-dihomocholesta-5,22,24¹-trien-3 β -ol (**10**)

A cholestenol derivative, (22*E*),(24¹*E*)-24¹,24²-dihomocholesta-5,22,24¹-trien-3 β -ol (**10**), with two isolated alkenes at C-22 and C-24¹ positions in side chain (C-17) was identified. The molecular ion peak at m/z 410 (EIMS: found m/z 410.3555 $[M]^+$, cal. for $C_{29}H_{46}O$ 410.3549) along with 1H and ^{13}C data represented its molecular

formula as $C_{29}H_{46}O$ with seven degrees of unsaturation (three double bond and four rings). It exhibited six alkenic carbon signals at δ 140.75, 121.70, 131.72, 135.83, 138.26 and 129.32 in which the signal at δ 140.75 was attributed to the alkenic quaternary carbon as deduced from ^{13}C spectrum supported by DEPT analysis (Table 5.14.; Figure 5.134.-5.5.139.). The highly deshielded protons at H-6 (δ 5.35, dd) and that at H-3 (δ 3.52, p) were attached to the respective carbons at δ 121.70 and 71.80, were attributed to $>C=\underline{CH}$ and $-\underline{C(H)}-OH$ groups, respectively (Reich *et al.*, 1969). The ^{13}C signal at δ 140.75 appeared downfield, and was lesser in intensity than the olefinic peak at δ 121.70 due to the slow relaxation, and therefore, it was deduced to be alkenic quaternary carbon. The carbons that were not attached to protons, relaxed gradually and exhibited lesser intense peak, if relaxation delay is small (RD = 1.7 s), thus the closeness of protons could be determined. The greater chemical shift value of carbinol proton and carbon were due to the higher electron withdrawing effects of hydroxyl moiety at C-3, which was identified from the absence of deuterated -OH proton signal in NMR spectrum by deuteration of hydroxyl proton. The NMR spectral signals of the title cholestene framework were found to be related with previous disclosures (Tian *et al.*, 2011). Five high-field methyls ($-CH_3$) δ 0.68 (s), 1.01 (s), 0.90 (d), 0.86 (d), 0.87 (d) were attributed to the carbons at δ 11.87 (C-18), 19.40 (C-19), 17.62 (C-21), 19.86 (C-26) and 22.82 (C-27), respectively; whereas the methines ($-CH-$) at δ 1.12 (m), 0.92 (m) and 0.95 (m) were assigned to carbons at δ 56.02 (C-14), 50.17 (C-9) and 56.85 (C-17), respectively in that order. The titled compound registered three significant quaternary carbons at δ 36.52 (C-10), 42.25 (C-13) and 140.75 (C-5), which were the characteristic shift signals for sterols (Reich *et al.*, 1969). The combined DEPT and ^{13}C NMR analyses confirmed that the compound enclosed 29 carbon atoms, which were distributed into five $-CH_3$, nine $-CH_2$ and twelve $-CH$ groups. It exhibited four spin systems in COSY data, which include δ 1.84, 1.03 (H-1)/1.49, 1.83 (H-2)/3.52 (H-3)/2.25, 2.28 (H-4) in the ring A, whereas the second spin arrangement enclosed correlations among the protons at δ 5.35 (H-6)/1.95 (H-7)/1.50 (H-8)/0.92 (H-9)/1.47 (H-11)/1.16, 2.00 (H-12); δ 1.50 (H-8)/1.12 (H-14)/1.08, 1.53 (H-15)/1.68 (H-16)/0.95 (H-17) in ring B/C/D along with δ 0.95 (H-17)/1.85 (H-20)/0.90 (H-21), 5.20 (H-22) that confirmed the attachment of side chain fragment to parent steroid moiety at C-17 (Figure 5.132.A, 5.137.). Other two spin systems were found to enclose in the side

chain, which were δ 5.16 (H-23)/2.02 (H-24)/5.39 (H-24¹) and δ 5.03 (H-24²)/1.51 (H-25)/0.86 (H-26), 0.87 (H-27). The HMBC attachments from δ 1.84 (H-1) to δ 140.75 (C-5), 19.40 (C-19); δ 1.49 (H-2) to δ 140.75 (C-5); δ 2.25 (H-4) to δ 121.70 (C-6), 36.52 (C-10); δ 5.35 (H-6) to δ 42.30 (C-4), 36.52 (C-10); δ 1.95 (H-7) to δ 50.17 (C-9), 56.02 (C-14); δ 1.50 (H-8) to δ 121.70 (C-6); δ 0.92 (H-9) to δ 31.91 (C-7), 37.26 (C-1) confirmed the presence of A/B ring moiety. The HMBC relations from δ 1.47 (H-11) to δ 50.17 (C-9), 56.02 (C-14); δ 1.16 (H-12) to δ 11.87 (C-18); δ 1.12 (H-14) to δ 50.17 (C-9) and δ 0.95 (H-17) to δ 24.30 (C-15) attributed the C/D bicyclic moiety (Figure 5.132.B, 5.139.). The characteristic singlet methyls of steroids at C-18 and C-19 positions were furthermore attributed by HMBC correlations from δ 0.68 (H-18) to δ 42.25 (C-13), 56.02 (C-14) and δ 1.01 (H-19) to δ 50.17 (C-9), 140.75 (C-5), 37.26 (C-1), respectively in that order. The attachment of side chain at Δ^{17} was confirmed by HMBCs from δ 1.85 (H-20) to δ 56.85 (C-17) and δ 0.90 (H-21) to δ 56.85 (C-17). Other HMBC couplings, such as δ 0.90 (H-21) to δ 131.72 (C-22), 135.83 (C-23); δ 5.20 (H-22) to δ 40.16 (C-24); δ 5.16 (H-23) to δ 40.16 (C-24); δ 5.39 (H-24¹) to δ 135.83 (C-23); δ 5.03 (H-24²) to δ 135.83 (C-23); δ 1.51 (H-25) to δ 22.82 (C-27), 129.32 (C-24²); δ 0.86 (H-26) to δ 129.32 (C-24²) and δ 0.87 (H-27) to δ 33.10 (C-24) assigned the presence of dihomom side chain with two olefinic centres (C-22 and C-24¹). The side chain attachments (Δ^{20} to Δ^{27}) could be compared readily with compounds discussed in earlier reports (Diaz-Marrero *et al.*, 2003b). The greater coupling constants (J), 11.02 and 9.55/9.00 Hz corresponding to H-22 and H-23 alkenic protons, respectively along with other coupling constants (J), 10.49 and 9.04 Hz for olefinic protons at H-24¹ and H-24², respectively attributed to their *E* (*trans*) configuration, which were further supported by earlier studies (Goad and Akihisa 1997). The relative configurations were assigned by their extensive NOESY correlations (Figure 5.133., 5.140.). The proton signal at δ 3.52 (H-3) displayed NOESY correlation with δ 5.35 (H-6)/2.28 (H-4)/1.84 (H-1)/1.83 (H-2), which were distributed in same plane, and therefore, have been arbitrarily assigned to dispose at α -plane of molecule. This explained the β -orientation of hydroxyl at C-3 (Sun *et al.*, 2013). The singlet methyl groups at δ 0.68 (attributed to H-18) and δ 1.01 (H-19) of sterol derivative were correlated with proton shifts at δ 2.25 (H-4)/1.50 (H-8) that accordingly suggested their β -disposition (Calderon *et al.*, 2004).

Table 5.14.: NMR spectroscopic data of (22*E*),(24¹*E*)-24¹,24²-dihomocholesta-5,22,24¹-trien-3β-ol (**10**) in CDCl₃

C. No.	¹³ C	¹ H (int.,mult., <i>J</i> in Hz) ^a	COSY	HMBC
1	37.26	1.84 (1H α ,t) 1.03 (1H β ,t)	H-2	C-3,5,19 -
2	31.66	1.49 (1H β ,m) 1.83 (1H α ,m)	H-3	C-4,5 -
3	71.80	3.52 (1H α ,p)	H-4	-
4	42.30	2.25 (1H β ,d) 2.28 (1H α ,d)	- -	C-3,5,6,10 -
5	140.75	-	-	-
6	121.70	5.35 (1H α ,dd,6.77,5.03)	H-7	C-4,10,7
7	31.91	1.95 (1H,t)	H-8	C-9,14,8
8	28.02	1.50 (1H β ,m)	H-9,14	C-6,9
9	50.17	0.92 (1H α ,m)	H-11	C-7,1
10	36.52	-	-	-
11	21.19	1.47 (2H,m)	H-12	C-9,14
12	39.69	1.16 (1H β ,t) 2.00 (1H α ,t)	- -	C-11,18 -
13	42.25	-	-	-
14	56.02	1.12 (1H α ,m)	H-15	C-9,15
15	24.30	1.08 (1H β ,m) 1.53 (1H α ,m)	H-16 -	- -
16	28.24	1.68 (2H,m)	H-17	C-15
17	56.85	0.95 (1H β ,m)	H-20	C-16,15
18	11.87	0.68 (3H β ,s)	-	C-13,14,17,12
19	19.40	1.01 (3H β ,s)	-	C-9,5,1
20	42.81	1.85 (1H,m)	H-21,22	C-17,21
21	17.62	0.90 (3H α ,d)	-	C-20,17,22,23
22	131.72	5.20 (H,t,11.02)	-	C-24
23	135.83	5.16 (1H,td,9.55,9.00)	H-24	C-22,24
24	40.16	2.02 (2H,t)	H-25	-
24 ¹	138.26	5.39 (1H,q,10.49)	-	C-23
24 ²	129.32	5.03 (1H,t,9.04)	H-27	C-23
25	33.10	1.51 (1H,m)	H-28,29	C-26,27,24 ²
26	19.86	0.86 (3H,d)	-	C-25,24 ²
27	22.82	0.87 (3H,d)	-	C-25

¹H NMR spectra recorded using Bruker AVANCE III 500MHz (AV 500) spectrometer (Bruker, Karlsruhe, Germany) in CDCl₃ as aprotic solvent at ambient temperature with TMS as the internal standard (δ 0 ppm). The ¹H NMR spectra were recorded at 500MHz, while the ¹³C NMR spectra were recorded at 125MHz. ^aValues in ppm, multiplicity and coupling constants (*J*=Hz) were indicated in parentheses. The

assignments were made with the aid of the ^1H - ^1H COSY, HSQC, HMBC and NOESY experiments

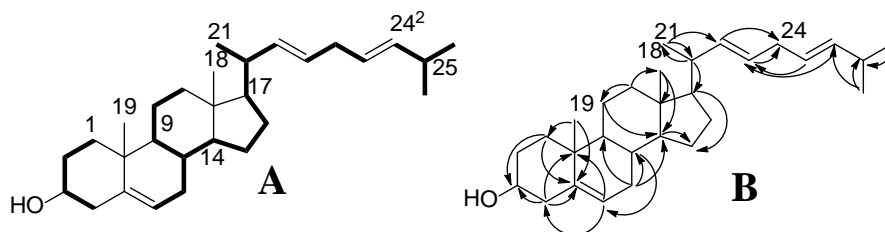


Figure 5.132.: ^1H - ^1H COSY (**A**) and HMBC (**B**) correlations of (22E),(24¹E)-24¹,24²-dihomocholesta-5,22,24¹-trien-3β-ol (**10**). The key ^1H - ^1H COSY couplings have been represented by the bold face bonds. The HMBC couplings were indicated by double barbed arrow

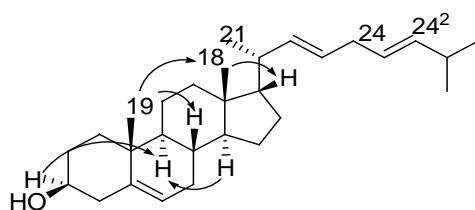


Figure 5.133.: NOESY correlations of (22E),(24¹E)-24¹,24²-dihomocholesta-5,22,24¹-trien-3β-ol (**10**). The NOESY relations were represented by double barbed arrow

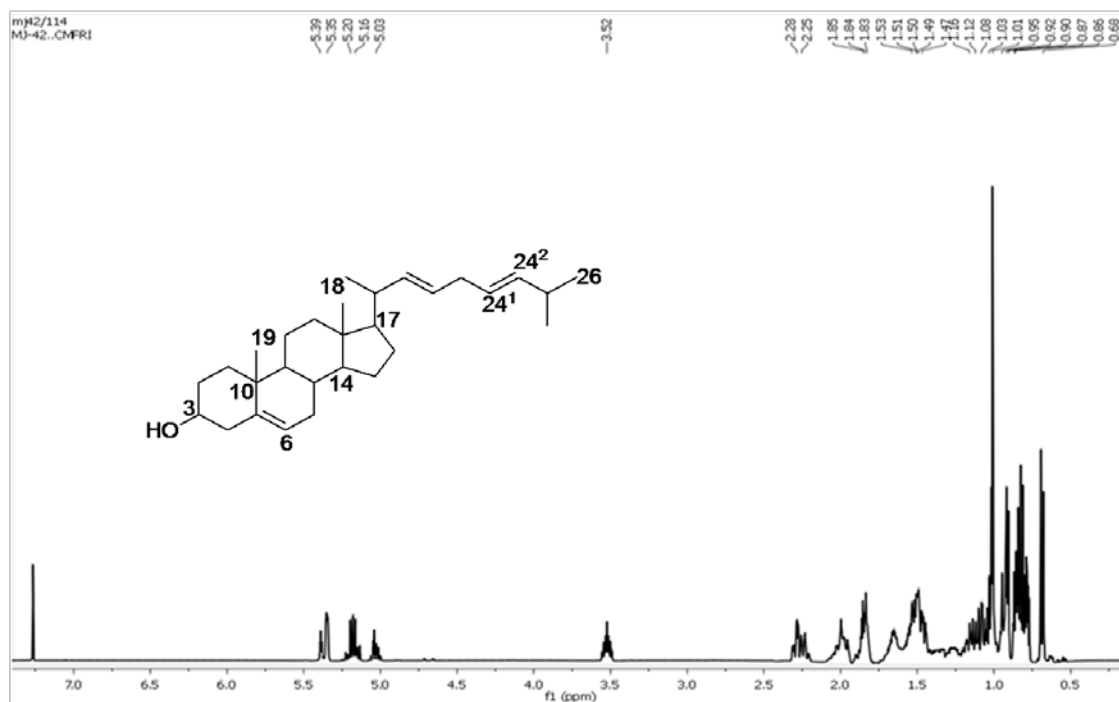


Figure 5.134.: ^1H NMR spectrum of (22*E*),(24¹*E*)-24¹,24²-dihomocholesta-5,22,24¹-trien-3 β -ol (**10**)

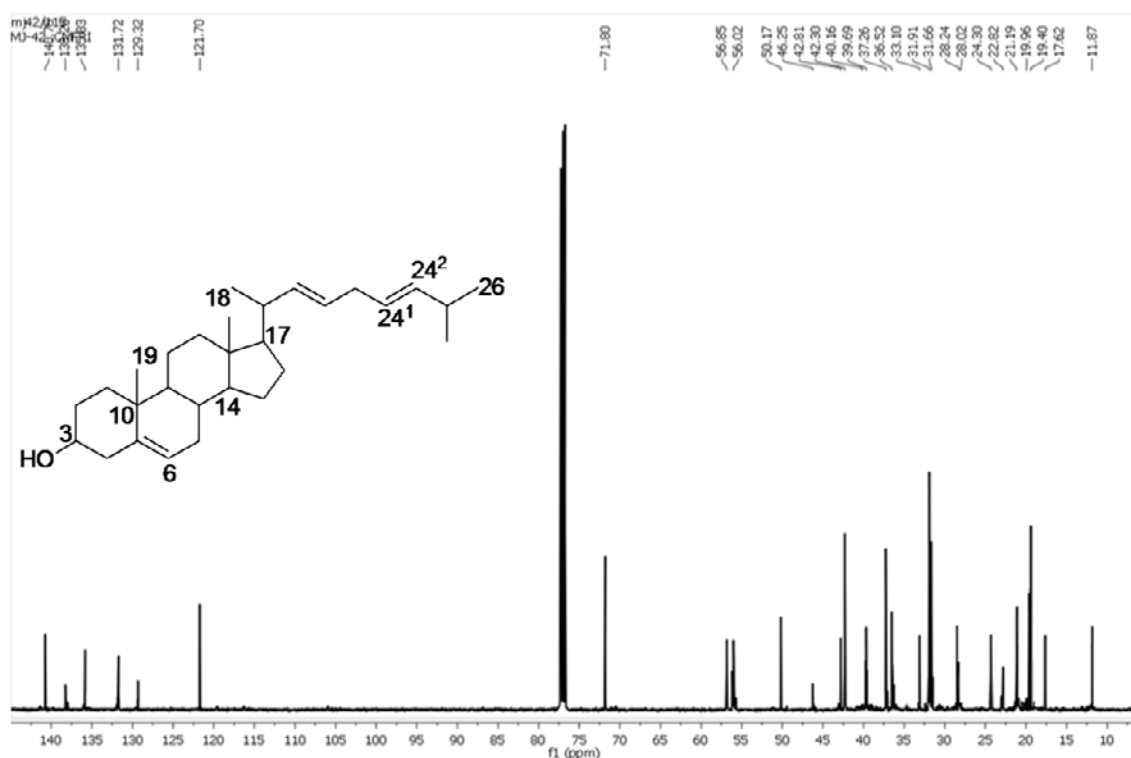


Figure 5.135.: ^{13}C NMR spectrum of (22*E*),(24¹*E*)-24¹,24²-dihomocholesta-5,22,24¹-trien-3 β -ol (**10**)

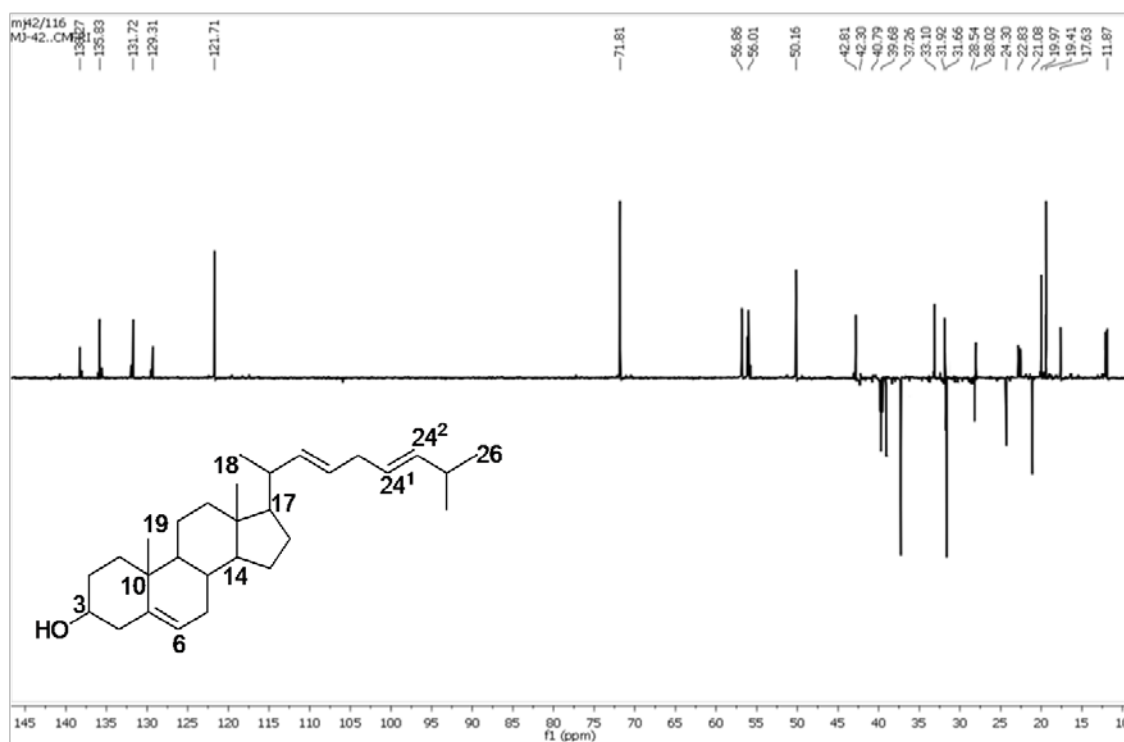


Figure 5.136.: $^{135}\text{DEPT}$ NMR spectrum of (22E),(24¹E)-24¹,24²-dihomocholesta-5,22,24¹-trien-3 β -ol (10)

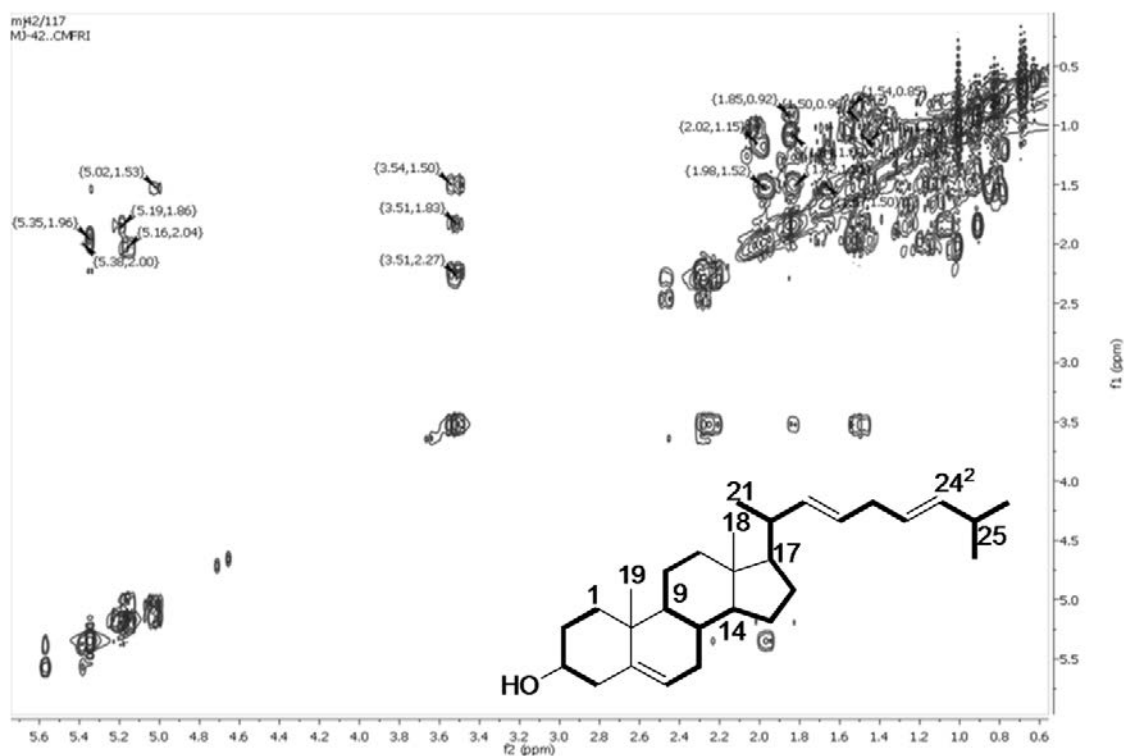


Figure 5.137.: COSY NMR spectrum of (22E),(24¹E)-24¹,24²-dihomocholesta-5,22,24¹-trien-3 β -ol (10)

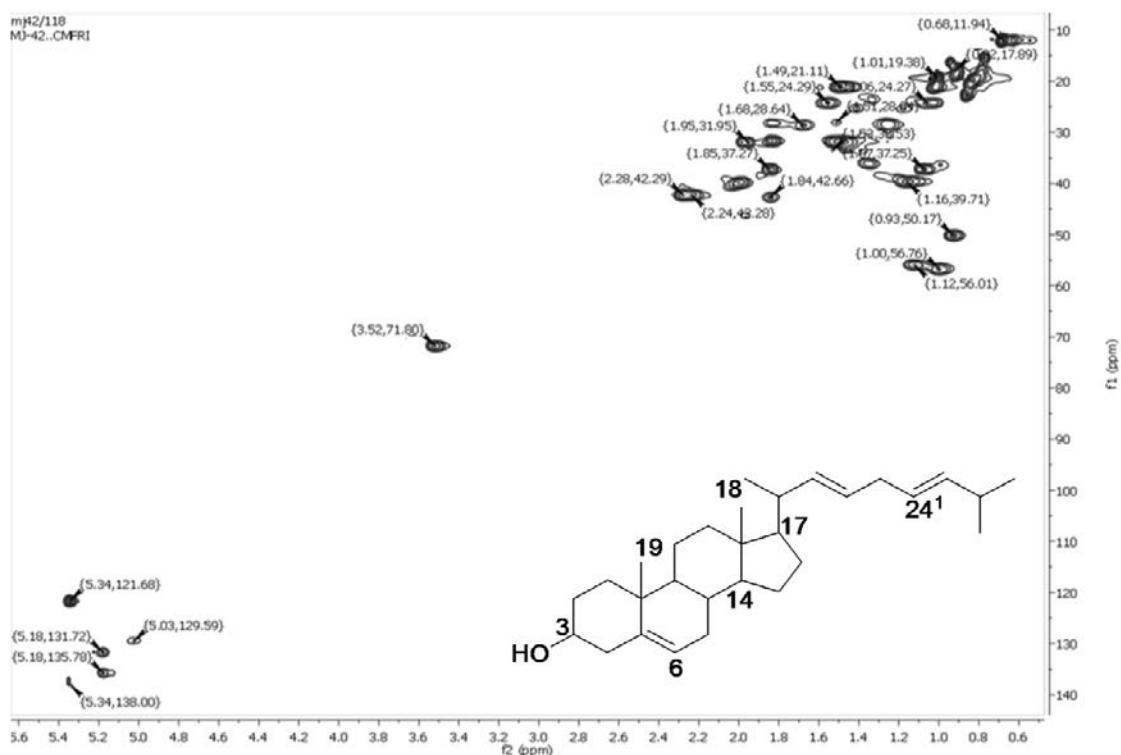


Figure 5.138.: HSQC NMR spectrum of (22*E*),(24¹*E*)-24¹,24²-dihomocholesta-5,22,24¹-trien-3β-ol (**10**)

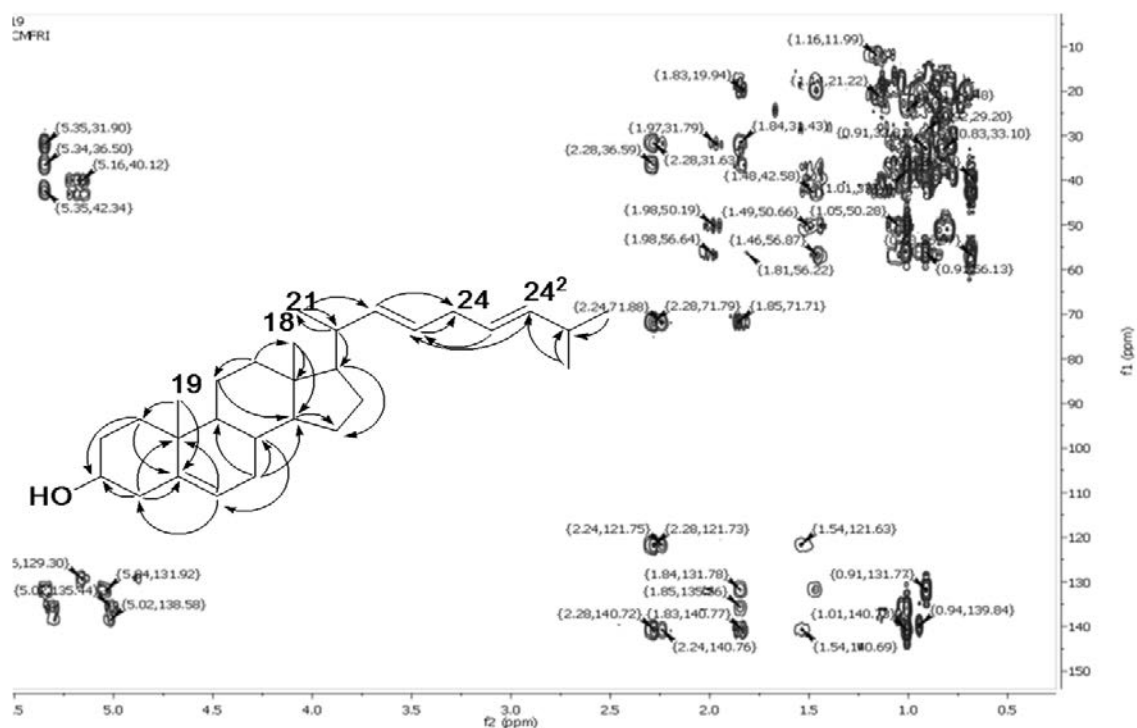


Figure 5.139.: HMBC NMR spectrum of (22*E*),(24¹*E*)-24¹,24²-dihomocholesta-5,22,24¹-trien-3β-ol (**10**)

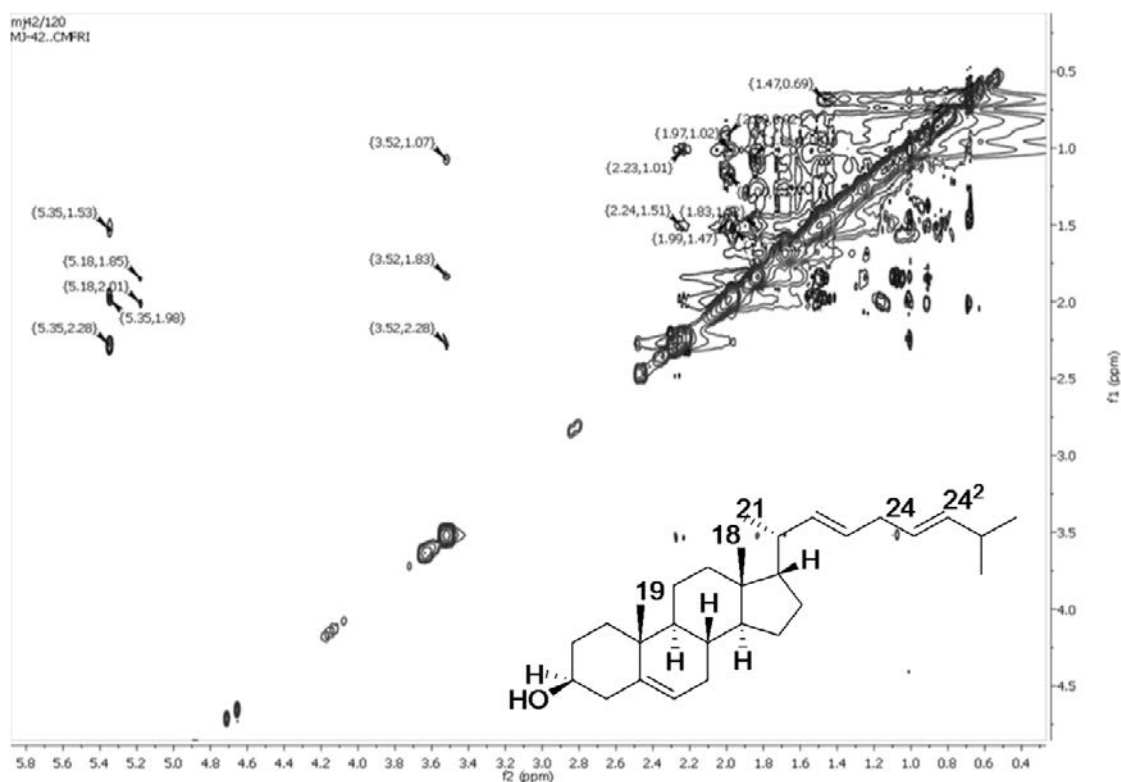


Figure 5.140.: NOESY spectrum of (22*E*), (24¹*E*)-24¹,24²-dihomocholesta-5,22,24¹-trien-3β-ol (**10**)

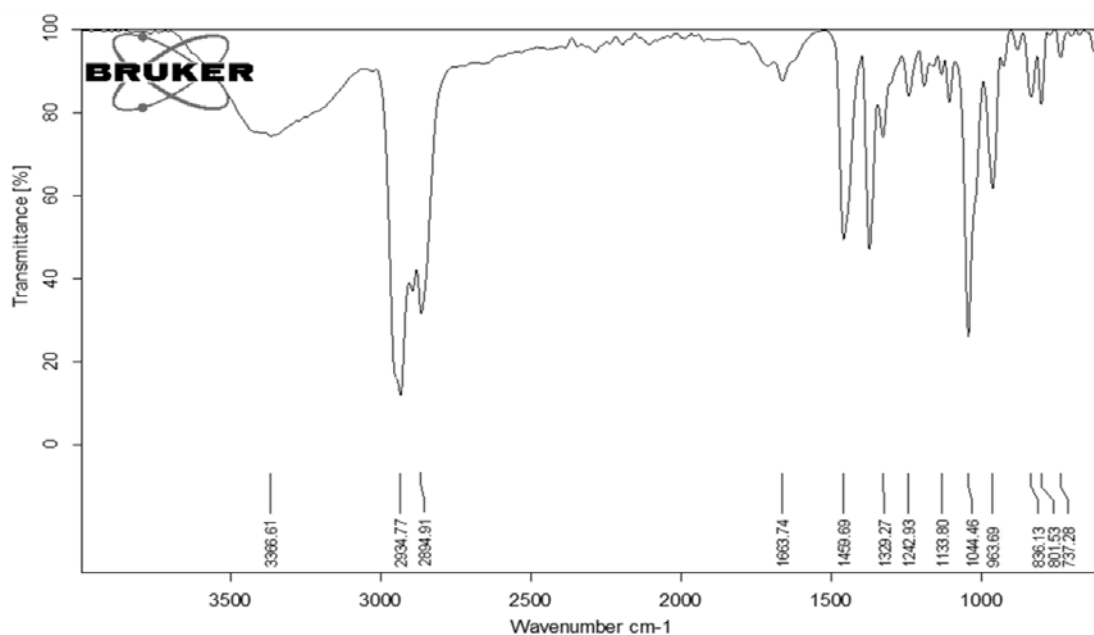


Figure 5.141.: FTIR spectrum of (22*E*),(24¹*E*)-24¹,24²-dihomocholesta-5,22,24¹-trien-3β-ol (**10**)

The IR stretching vibrations for C=C and alkyl functionalities were denoted by absorptions at 1663 and 2934 cm⁻¹, respectively. The characteristic band at 3366 cm⁻¹

¹ was represented the hydroxyl moiety. All these data substantiated the structure of cholestene derivative (Figure 5.141.).

The molecular ion peak was recorded in the mass spectrum at m/z 410 (Figure 5.142.). The sequential elimination of methyl, isopropyl and two methyl radicals from the side chain moiety at C-17 appeared to result in the fragment peaks with m/z 395 (**a**, $C_{28}H_{43}O^+$), 354 (**b**, $C_{25}H_{38}O^+$) and 324 (**d**, $C_{23}H_{32}O^+$), respectively. The later appeared to undergo sequential elimination of ions, such as $C_3H_5^+$, $C_2H_4^+$, $C_2H_2^+$, hydroxyl, ethyl, methyl, $C_2H_3^+$ and finally $C_3H_6^+$ corresponding to peaks at m/z 284 (**e**, $C_{20}H_{28}O^+$), 256 (**f**, $C_{18}H_{24}O^+$), 236 (**g**, $C_{16}H_{20}O^+$), 211 (**h**, $C_{16}H_{19}^+$), 185 (**i**, $C_{14}H_{17}^+$), 171 (**j**, $C_{13}H_{15}^+$), 146 (**k**, $C_{11}H_{14}^+$) and 112 (**l**, $C_8H_{16}^+$), respectively. The ethylcyclohexane (**l**) fragment appeared to dissociate methyl radical to yield a base peak of methylenecyclohexene at m/z 94 (**m**, $C_7H_{10}^+$), which further fragmented to pentadiene cation with m/z 67 (**n**) (Figure 5.143.).

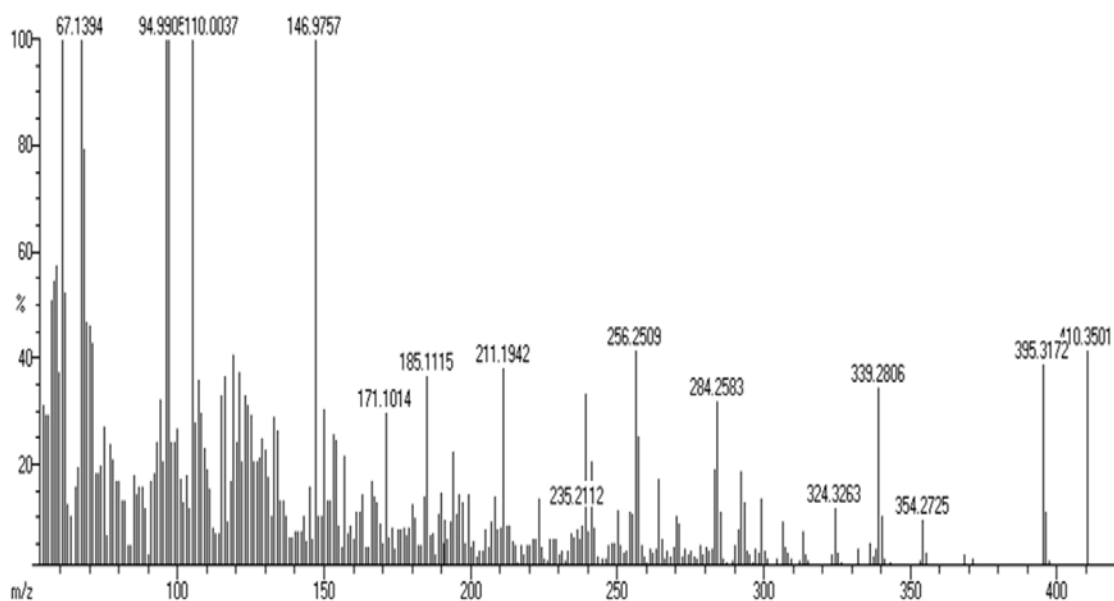


Figure 5.142.: EIMS spectrum of (22*E*),(24¹*E*)-24¹,24²-dihomocholesta-5,22,24¹-trien-3β-ol (**10**)

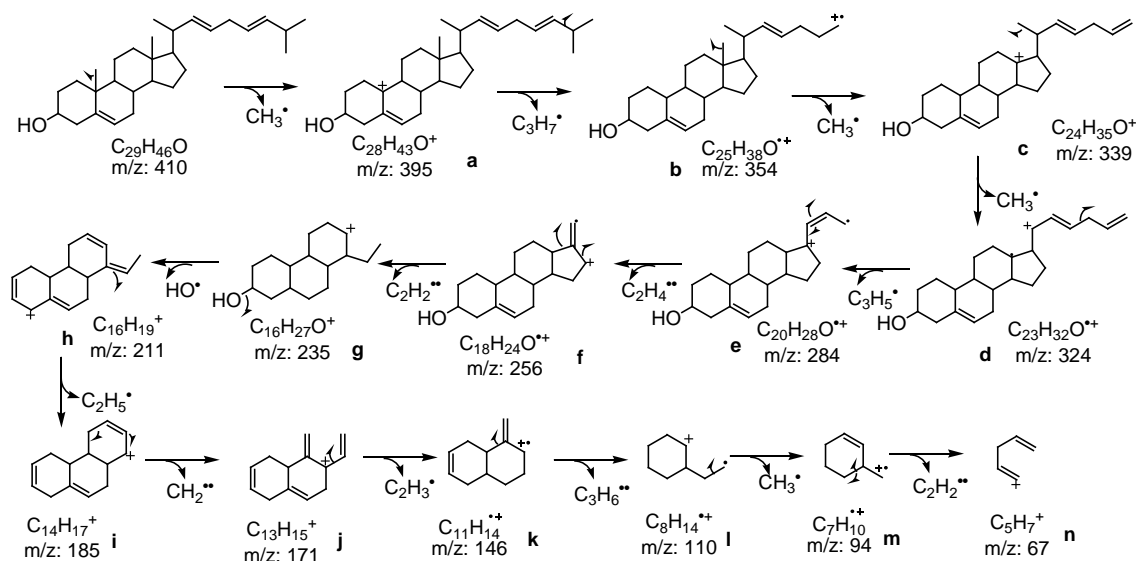


Figure 5.143.: Mass fragmentation pattern of (22*E*),(24¹*E*)-24¹,24²-dihomocholesta-5,22,24¹-trien-3β-ol (**10**)

The steroids with diverse structures were found to exhibit interesting therapeutic properties (Goad and Akihisa 1997; Whitson *et al.*, 2009). Anti-inflammatory properties of di-unsaturated C-27 polyhydroxy sterols isolated from the marine gastropod, *Trimusculus peruvianus* (Chao *et al.* 2008; Diaz-Marrero *et al.* 2003b; Su *et al.*, 2008). The anti-inflammatory pregnane-type steroids from soft coral, *Scleronephthya gracillimum* were reported in prior studies (Fang *et al.*, 2013). The steroids that can act as COX-2/5-LOX specific dual inhibitors will be helpful in the treatment of inflammatory disorders.

5.3.3. Bioactive (antioxidant and anti-inflammatory) potentials of secondary metabolites isolated from EtOAc:MeOH extract of *V. cyprinoides*

5.3.3.1. Antioxidative potentials of secondary metabolites isolated from EtOAc:MeOH extract of *V. cyprinoides*

The free radical inhibiting activities of title compounds (**1** to **10**) isolated from EtOAc:MeOH extract of *V. cyprinoides* were described in Table 5.15. The antioxidant activities of isolated compounds were determined by the *in vitro* DPPH and ABTS⁺ scavenging experiments.

Table 5.15.: *In vitro* antioxidant {2,2-diphenyl-1-picrylhydrazyl (DPPH) and 2,2'-azino-bis(3-ethylbenzothiazoline-6-sulphonic acid) (ABTS⁺) radical scavenging assays} activities of secondary metabolites (**1-10**) isolated from EtOAc:MeOH extract of *V. cyprinoides* against commercially available standard, α -tocopherol

Compounds	Antioxidant activities IC ₅₀ values (mg/mL)	
	*DPPH scavenging activity	*ABTS ⁺ scavenging activity
1	0.59 ± 0.01 ^a	0.67 ± 0.01 ^a
2	0.54 ± 0.01 ^a	0.62 ± 0.01 ^a
3	0.63 ± 0.04 ^b	0.72 ± 0.02 ^b
4	0.71 ± 0.01 ^b	0.76 ± 0.01 ^b
5	0.69 ± 0.04 ^b	0.64 ± 0.02 ^a
6	0.76 ± 0.01 ^c	0.85 ± 0.01 ^c
7	0.79 ± 0.04 ^c	0.87 ± 0.02 ^c
8	0.86 ± 0.04 ^d	0.94 ± 0.02 ^d
9	0.93 ± 0.01 ^e	1.05 ± 0.01 ^e
10	0.91 ± 0.01 ^e	1.08 ± 0.01 ^e
α -tocopherol	0.65 ± 0.04 ^b	0.76 ± 0.05 ^b

The samples were analyzed in triplicate (n = 3) and expressed as mean ± standard deviation. Means followed by different superscripts (a-e) within the same column indicated significant differences ($p < 0.05$). *The bioactivities were expressed as IC₅₀ values (mg/mL)

The prenylated spirocyclic ether derivatives, **1** and **2** displayed significantly greater ($p < 0.05$) antioxidant activities against DPPH radical (IC₅₀ 0.59 and 0.54 mg/mL, respectively) compared to other compounds and standard, α -tocopherol (IC₅₀ 0.65 mg/mL). However, no noteworthy dissimilarity in DPPH quenching potencies were observed among furano meroterpenoid derivative, **5** (IC₅₀ 0.69 mg/mL), α -pyrone, **4** (IC₅₀ 0.71 mg/mL), hexahydrobenzo furanone, **3** (IC₅₀ 0.63 mg/mL) and α -tocopherol (IC₅₀ 0.65 mg/mL) ($p > 0.05$) (Table 5.15.). The compounds, **1-5** registered greater DPPH radical scavenging activity as compared to hexahydro isochromenyls, **6-7** (IC₅₀ ~0.77 mg/mL) followed by steroidal analogues, **8** (IC₅₀ 0.86 mg/mL) and **9-10** (IC₅₀ ~0.92 mg/mL), in descending order ($p < 0.05$).

The prenylated spirocyclic ether derivatives, **1** and **2** (IC₅₀ 0.62-0.67 mg/mL) and furano meroterpenoid, **5** (IC₅₀ 0.64 mg/mL) did not display any significant

difference with each other in ABTS⁺ radical scavenging activity ($p > 0.05$). The compounds **1-2** and **5** exhibited significantly greater ABTS⁺ radical scavenging properties ($p < 0.05$) when compared to other compounds ($IC_{50} > 0.70$ mg/mL) and commercially available α -tocopherol (IC_{50} 0.76 mg/mL). Significantly greater ($p < 0.05$) ABTS⁺ radical potentials were recorded for α -pyrone derivative, **4** (IC_{50} 0.76 mg/mL), hexahydrobenzo furanone derivative, **3** (IC_{50} 0.72 mg/mL) followed by hexahydro isochromenyls, **6-7** (IC_{50} ~0.86 mg/mL) and steroidal analogues, **8-10** (IC_{50} 0.94-1.08 mg/mL), in descending order (Table 5.15.).

5.3.3.2. Anti-inflammatory potentials of secondary metabolites isolated from EtOAc:MeOH extract of *V. cyprinoides*

The anti-inflammatory potentials of title compounds (**1** to **10**) isolated from EtOAc:MeOH extract of *V. cyprinoides* were described in Table 5.16. The anti-inflammatory potentials of these compounds determined by *in vitro* cyclooxygenase-1/2 (COX-1/2) and 5-lipoxygenase (5-LOX) enzyme inhibitory assays. In addition, the selectivity indices were calculated from the ratio of IC_{50} values of anti-COX-1 to IC_{50} values of anti-COX-2 potentials and the values were compared among the isolated bioactive compounds and standard, ibuprofen in Figure 5.144.

The spirocyclic ether derivative, **2** implied significantly greater inhibitory activity ($p < 0.05$) against pro-inflammatory COX-1 and COX-2 (IC_{50} 0.86 and 0.65 mg/mL, correspondingly) as compared to other studied compounds ($IC_{50} > 0.90$ and > 0.70 mg/mL, correspondingly). No significant difference ($p > 0.05$) in COX-1 inhibitory potentials was apparent among the spirocyclic ether derivative, **1** (IC_{50} 0.94 mg/mL), furano meroterpenoid, **5** (IC_{50} 0.91 mg/mL), α -pyrone, **4** (IC_{50} 1.00 mg/mL) and hexahydrobenzo furanone derivative, **3** (IC_{50} 0.96 mg/mL) (Table 5.16.). The anti-COX-1 potencies were significantly higher for the compounds **1-5** ($p > 0.05$) followed by those recorded with hexahydro isochromenyl derivatives, **6-7** (IC_{50} ~1.08 mg/mL) and steroidal analogues, **8-10** (IC_{50} 1.07-1.19 mg/mL). No significant similarity ($p > 0.05$) was observed for anti-COX-2 potentials among spirocyclic ether derivatives, **1** (IC_{50} 0.70 mg/mL), furano meroterpenoid derivative, **5** (IC_{50} 0.76 mg/mL) along with hexahydrobenzo furanone, **3** (IC_{50} 0.74 mg/mL) (Table 5.16.). The anti-COX-2 potentials were notably higher for the compounds, **1-3** and **5** ($p > 0.05$) followed by α -

pyrone, **4** (IC_{50} 0.89 mg/mL), hexahydro isochromenyls, **6-7** (IC_{50} ~0.89 mg/mL) and steroidal analogues, **8-10** (IC_{50} 1.05-1.15 mg/mL). Moreover, these compounds (**1-10**) displayed greater activity against inducible COX-2 than constitutive COX-1, and accordingly recorded greater selectivity indices (SI, IC_{50} anti-COX-1/ IC_{50} anti-COX-2 > 1.00) than anti-inflammatory drug, ibuprofen (0.63; selective towards constitutive pro-inflammatory enzyme COX-1) (Figure 5.144.). The selectivity index was significantly greater for spirocyclic ether derivatives, **1-2** (SI ~1.33) followed by the compounds, **3-7** (SI 1.12-1.22) and **8-10** (SI 1.02-1.04).

Table 5.16.: *In vitro* anti-inflammatory {cyclooxygenase-1/2 (COX-1/2) and 5-lipoxygenase (5-LOX)) radical scavenging assays} activities of secondary metabolites (**1-10**) isolated from EtOAc:MeOH extract of *V. cyprinoides* against commercially available standard, ibuprofen

Compounds	Anti-inflammatory activities		
	IC_{50} values (mg/mL)		
	*COX-1 scavenging activity	*COX-2 scavenging activity	*5-LOX scavenging activity
1	0.94 ± 0.05^a	0.70 ± 0.03^{ab}	0.77 ± 0.02^a
2	0.86 ± 0.06^b	0.65 ± 0.03^b	0.75 ± 0.02^a
3	0.96 ± 0.02^a	0.74 ± 0.01^a	0.76 ± 0.01^a
4	1.00 ± 0.06^{ac}	0.89 ± 0.03^c	0.92 ± 0.02^b
5	0.91 ± 0.06^a	0.76 ± 0.01^a	0.80 ± 0.01^a
6	1.05 ± 0.05^c	0.90 ± 0.03^c	0.96 ± 0.02^b
7	1.09 ± 0.02^c	0.89 ± 0.01^c	0.98 ± 0.01^b
8	1.07 ± 0.05^c	1.05 ± 0.03^d	1.03 ± 0.02^b
9	1.19 ± 0.04^d	1.15 ± 0.03^e	1.17 ± 0.02^c
10	1.16 ± 0.04^d	1.12 ± 0.05^e	1.19 ± 0.03^c
Ibuprofen	0.05 ± 0.02^e	0.08 ± 0.05^f	0.96 ± 0.03^b

The samples were analyzed in triplicate ($n = 3$) and expressed as mean \pm standard deviation. Means followed by different superscripts (a-f) within the same column indicated significant differences ($p < 0.05$). *The bioactivities were expressed as IC_{50} values (mg/mL)

Spirocyclic ether derivatives, **1-2** (IC_{50} 0.75-0.77 mg/mL), hexahydrobenzo furanone, **3** (IC_{50} 0.76 mg/mL) and furano meroterpenoid derivative, **5** (IC_{50} 0.80

mg/mL) did not display any significant difference with each other with regard to anti-5-LOX properties ($p > 0.05$). These compounds showed significantly greater ($p < 0.05$) activity when compared to other compounds and ibuprofen ($IC_{50} > 0.90$ mg/mL). The α -pyrone derivative, **4** (IC_{50} 0.92 mg/mL), hexahydro isochromenyls, **6-7** (IC_{50} ~0.97 mg/mL) and sterol analogues, **8** (IC_{50} 1.03 mg/mL) were showed anti-5-LOX activities greater than or comparable to the standard, ibuprofen (IC_{50} 0.96 mg/mL) (Table 5.16.).

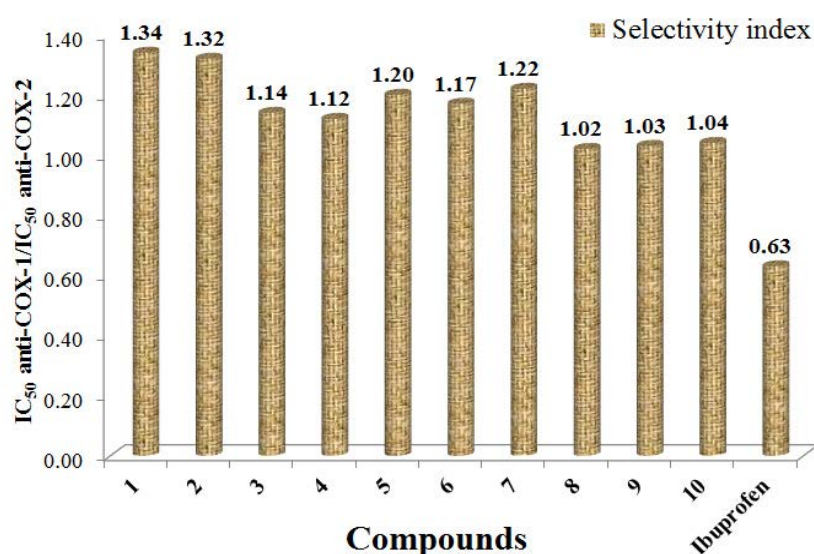


Figure 5.144.: A comparison of selectivity indices (IC_{50} of anti-COX-1/ IC_{50} of anti-COX-2) calculated for the secondary metabolites (**1-10**) isolated from EtOAc:MeOH extract of *V. cyprinoides* along with commercially available standard, ibuprofen

The commercially available NSAIDs, such as ibuprofen, were reported to inhibit both pro-inflammatory COX-1 and COX-2. The lesser selectivity ratio (anti-COX-1/ IC_{50} /anti-COX-2/ IC_{50}) of the NSAIDs also explained the larger selective inhibition of constitutive COX-1 that can cause severe side effects such as gastric related health problems (Laneuville *et al.*, 1994). Therefore, the search for compounds with specificity towards COX-2 inhibition was preferred due to the lesser gastrointestinal difficulties and safer therapeutic profiles. The greater selectivity index of the secondary metabolites (**1-10**) isolated from EtOAc:MeOH extract of *V. cyprinoides* (SI > 1.02) appropriately explained its specific inhibition towards COX-2 activity than COX-1, and therefore, can be suggested as potential anti-inflammatory lead molecules (Figure 5.144.).

5.3.4. Structure-activity relationship analysis of secondary metabolites isolated from EtOAc:MeOH extract of *V. cyprinoides*

5.3.4.1. Structure-activity relationship analysis of secondary metabolites from EtOAc:MeOH extract of *V. cyprinoides* using various molecular parameters

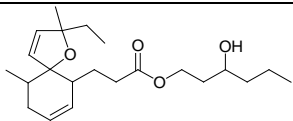
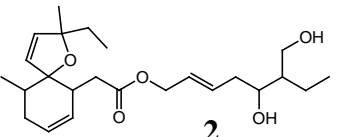
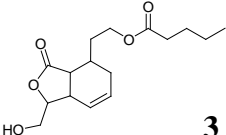
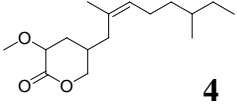
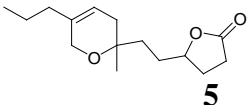
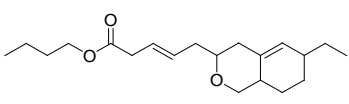
The free radical scavenging and anti-inflammatory properties of the title compounds (**1-10**) were correlated between their structures and corresponding hydrophobic ($\log P_{ow}$) and electronic (tPSA/PI) factors along with the steric bulk (MR/MV/Pr) to explain their bioactivities (Chakraborty *et al.*, 2016d; Lipinski 2000). The molecular descriptor values for bioactive secondary metabolites isolated from *V. cyprinoides* (**1-10**) and commercially available products, α -tocopherol and ibuprofen were tabulated in the Table 5.17.

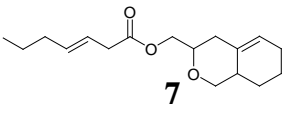
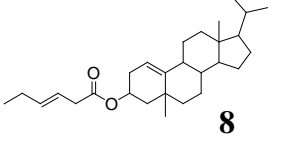
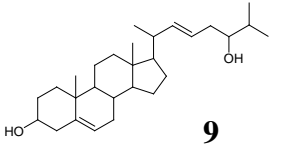
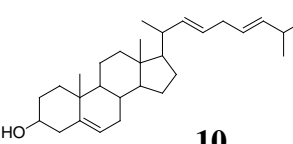
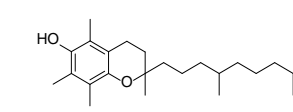
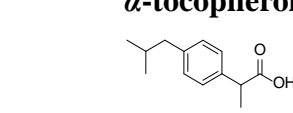
The hydrophobicity factor (logarithmic scale of the octanol-water partition coefficient, $\log P_{ow}$) was considered to be useful in predicting the antioxidant potentials of compounds. A drug with $\log P_{ow}$ value lesser than 5 has been considered to possess a balanced hydrophobic-lipophilic properties leading to an effective intermembrane permeability (Lipinski and Hopkins 2004). The $\log P_{ow}$ values of spirocyclic ether derivatives, **1-2** ($\log P_{ow}$ 3.32-3.79), hexahydrobenzo furanone, **3** ($\log P_{ow}$ 1.81), α -pyrone, **4** ($\log P_{ow}$ 3.59), furano meroterpenoid derivative, **5** ($\log P_{ow}$ 2.25) and hexahydro isochromenyl analogues, **6-7** ($\log P_{ow}$ 3.11-4.00) were found to be within the acceptable limits for optimum hydrophobic-lipophilic properties (Lipinski and Hopkins 2004). The hydrophobicity of title compounds, **1-10** were found to be lesser ($\log P_{ow} < 7.6$) when compared to the reference, α -tocopherol ($\log P_{ow}$ 9.98) (Table 5.17.). The greater antioxidant activity of the compounds, **1-5** and their acceptable lipophilic levels demonstrated their potential utilities as selective pharmacophore molecules. The importance of hydrophobicity to determine the inter-membrane permeability and antioxidative properties was previously illustrated (Ishige *et al.*, 2001). The significantly greater hydrophobicity of α -tocopherol thus, explained its lesser antioxidant properties. Further, the bioactivities of the isolated compounds were correlated with their steric bulk values, such as molar refractivity (MR), molar volume (MV) and parachor (Pr) values. The lower steric parameters of titled secondary metabolites, **1-2** (MR 106-119 cm^3/mol ; MV 348-371 cm^3 ; Pr 876-959 cm^3), irregular meroterpenoids, **3-5** (MR 71-78

cm³/mol; MV 251-278 cm³; Pr 595-665 cm³) and hexahydro isochromenyl derivatives, **6-7** (MR 81-95 cm³/mol; MV 268-317 cm³; Pr 665-783 cm³) appropriately explained their relatively lesser steric hindrance and greater antioxidative activities compared to α -tocopherol with greater steric bulk (MR 135.06 cm³/mol; MV 462.7 cm³; Pr 1123 cm³) values.

The electronic property of a compound could be directly correlated to its greater free radical scavenging and anti-inflammatory activities (Chakraborty *et al.*, 2017c). Notably, α -tocopherol recorded lesser values of total polar surface area, tPSA (29.46) compared to the spirocyclic ether derivatives, **1-2** (tPSA > 55), irregular meroterpenoids, **4-5** (tPSA 35.53) and hexahydro isochromenyl derivatives, **6-7** (tPSA 35.53), which signified their greater electronic interaction resulting in potentially higher free radical scavenging activities.

Table 5.17.: The molecular descriptors of secondary metabolites from EtOAc:MeOH extract of *V. cyprinoides* (**1-10**) and commercially available products

	Electronic		Steric			Hydrophobic
	tPSA	PI ($\times 10^{-24} \text{ cm}^3$)	MR (cm^3/mol)	MV (cm^3)	Pr (cm^3)	Log P _{ow}
 1	55.76	41.51	106.90	348.1	876.8	3.79
 2	75.99	45.75	119.01	371.7	959.6	3.32
 3	72.83	30.43	78.14	263.6	659.4	1.81
 4	35.53	30.64	78.72	278.0	665.0	3.59
 5	35.53	27.89	71.22	251.1	595.8	2.25
 6	35.53	37.14	95.91	317.4	783.4	4.00

 7	35.53	31.64	81.93	268.1	665.2	3.11
 8	26.30	49.49	126.91	405.8	1011.1	7.21
 9	40.46	49.96	128.28	398.7	1015.5	6.33
 10	20.23	51.16	132.76	410.3	1028.2	7.59
 α-tocopherol	29.46	53.54	135.06	462.7	1123.0	9.98
 Ibuprofen	37.30	23.96	60.44	200.1	499.3	3.75

tPSA: Topological Polar Surface Area; PI: polarizability; MR: molar refractivity; MV: molar volume; Pr: parachor; Log P_{ow}: logarithm of octanol-water coefficient. The molecular descriptors were calculated by using ChemDraw[®] Ultra (CambridgeSoft Corporation, Cambridge, MA, USA; ver. 8.0) and ACD ChemSketch (Advanced Chemistry Development, Inc., Canada; vers. 12.0) softwares

Likewise, the studied compounds, **1** (tPSA 55.76), **2** (tPSA 75.99) and **3** (tPSA 72.83) displayed greater tPSA values when compared to reference, ibuprofen (tPSA 37.30) consequently, echoed its significantly higher inhibiting activities towards pro-inflammatory 5-LOX (IC₅₀ anti-5-LOX 0.75-0.77 mg/mL) than ibuprofen (IC₅₀ 0.96 mg/mL). The electronic property determined by polarizability factor, PI was found to be greater for title compounds, **1-10** (PI > 26) as compared to that recorded with ibuprofen (PI 23.96). The polarizability factor registered for spirocyclic ether derivatives (**1-2**), hexahydro isochromenyls (**6-7**), irregular meroterpenoids (**3-5**) and steroidal analogues (**8-10**) were found to be 41-45, 31-37, 27-30 and 49-51, respectively (Table 5.17.). The hydroxy and oxaspiro-dec-diene in **1-2**, hydroxy hexahydro-oxoisobenzofuranyl skeleton of **3**, methoxy pyran ring in **4**, pyran-furanone moiety in **5** and hexahydro isochromenyl in **6-7** appeared to play predominant roles to increase the electron delocalizations and provide free hydrogens to efficiently neutralize the free radicals by hydrogen atom transfer (HAT) mechanism, which in turn, appeared to diminish the inflammatory responses (Chakraborty *et al.*, 2016d). The presence of greater numbers of electron withdrawing groups and centre of unsaturations, such as oxo-pyran, furanones, hydroxyl, carboxylates and furanyl moieties in compounds **1-3** appeared to increase its electronic properties (tPSA**1-3** > 55) than other compounds in the series (tPSA**4-10** 20-35). Greater number of electronegative centers enhances its higher bioactive properties due to effective electron transfer (Cai *et al.*, 2006). Therefore, greater electronic property of **2** appropriately manifested its superior bioactivities compared to other compounds in the series.

Free radical formation and accumulation in body was the focal cause for various oxidative stress induced disorders, for instance, inflammation, and therefore, the antioxidant property of a compound can appropriately describe its anti-inflammatory activity. Recent studies indicated that the selective inhibition of 5-LOX is a preferred mechanism to inhibit inflammatory responses in metabolic systems (Martel-Pelletier *et al.*, 2003). Principally, ibuprofen showed significantly lesser activity against 5-LOX enzyme compared to the compounds isolated from *V. cyprinoides* in this study. Furthermore, the significantly greater selectivity indices of compounds **1** to **10** compared to ibuprofen demonstrated their capacities to selectively inhibit inductive inflammatory response. The primary origin of inflammatory response was found to be

due to the excessive free radical species. A statistically significant similarity between the capacity of the compounds purified in the present study to suppress free radicals and pro-inflammatory COX-2 and 5-LOX further corroborated the closer relation between oxidative stress and inflammatory response. Based on these results, greater antioxidant or anti-inflammatory activities were observed for compounds, **1-5**, especially spirocyclic ether derivatives, **2**. It can therefore, be inferred that the radical scavenging or anti-inflammatory activity of compound **2** is primarily caused by the oxaspiro-dec-diene, hydroxyl and ester moieties present in it. Bioactive potentials of the studied compounds were corroborated with their molecular descriptor values and suggested its greater selectivity as pharmacophore molecules.

5.3.4.2. Suggested antioxidative mechanism of secondary metabolites isolated from *V. cyprinoides* in the DPPH radical model system

The compound **1** comprised of two antioxidant reaction centres and compound **2** enclosed three reaction sites of bioactivity (Figure 5.145.). The two primary reaction centres were similar for both the compounds. The alkenic proton at C-8 in the oxaspiro[4.5]dec-3,8-dienyl group contributed in the extended conjugation, and thus can be easily transferred to the DPPH radical. The proton at C-12 (in the of side chain) assisting in keto-enol resonance with the adjacent $>\text{C}=\text{O}$ group (at C-13) leading to the formation of $\text{CH}=\text{C}(\text{-OH})\text{-}$ moiety by relocating the proton at C-12 to DPPH radical. The second one was related to the proton in the hydroxyl attached at C-16 position in the side chain. In compound **2**, one reaction center was at C-8 in conjugation with the proton at C-11 (in the side chain) assisted in keto-enol resonance with the adjacent $>\text{C}=\text{O}$ group (at C-12) leading to the formation of $\text{CH}=\text{C}(\text{-OH})\text{-}$ moiety (Figure 5.145.). This was found to be the primary active reaction site for transferring the protons to neutralize the DPPH radical. The remaining two reaction sites were related to the protons in the hydroxyl groups located at C-17 and C-19 positions in the side chain. Thus, the greater DPPH scavenging potentials of compound **2** (IC_{50} 0.54 mg/mL) compared to that exhibited by **1** (IC_{50} 0.59 mg/mL) was correlated with the suggested antioxidative mechanism in DPPH radical model.

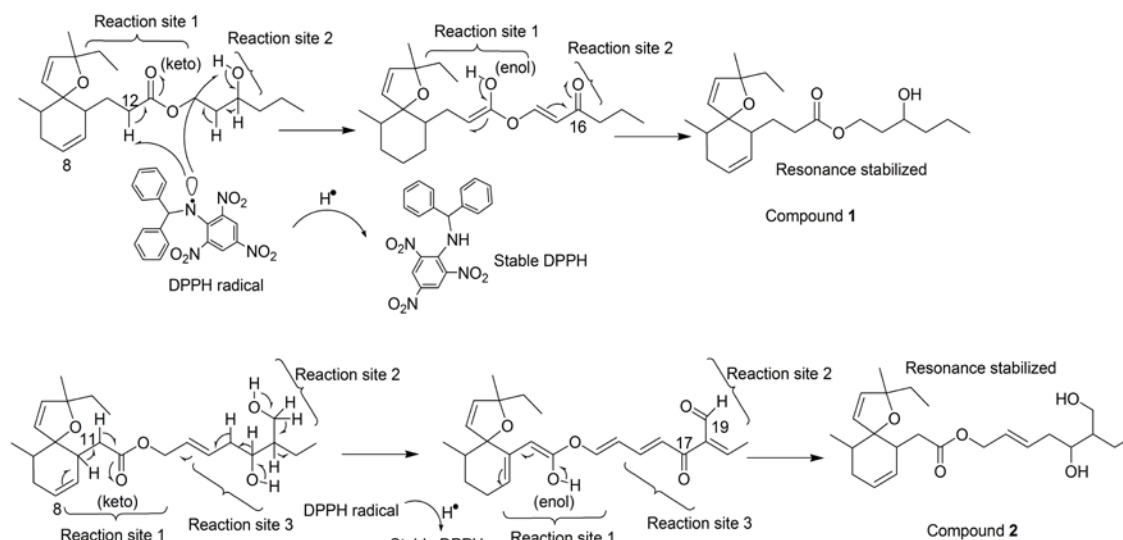


Figure 5.145.: Suggested antioxidative mechanism of spirocyclic ether derivatives (**1-2**) in DPPH radical model system

The compound **3** was found to comprise with three active antioxidant reaction centers (Figure 5.146.). The hydroxy hexahydro oxoisobenzofuranyl ring of **3** enclosed one active center in extended alkenic conjugation along with hydroxyl group and the second one was related to the ester group in the ring. The proton at olefinic group (C-6) appeared to take part in extended conjugation, and intramolecular rearrangement, to enable interacting with the DPPH radical. The proton at C-3a (in the ring junction linked to the furanone group) might probably assist in keto-enol resonance with the adjacent $>\text{C}=\text{O}$ group (at C-3) leading to the formation of $\text{CH}=\text{C}(\text{-OH})\text{-}$ moiety by relocating the proton to DPPH radical. The third active site was found to be in the ethyl pentanoate side chain. The proton at C-11 (in the side chain next to ester linkage) might assist in keto-enol resonance with the adjacent $>\text{C}=\text{O}$ group (at C-10) leading to the formation of $\text{CH}=\text{C}(\text{-OH})\text{-}$ moiety by transferring the proton to neutralize the DPPH radical. These three reaction centres might participate in the resonance stabilization, and therefore, appeared to exhibit primary role stabilizing the DPPH radical.

Compound **4** comprises a tetrahydro-3-methoxy-pyranone conjugated system as the basic skeleton that can potentially transfer proton from C-3 to DPPH radical (HAT mechanism) to form 3-methoxy-dihydro-pyranol (Figure 5.146.). The proton at C-3 could be involved in keto-enol resonance by relocating the proton at C-3 to DPPH radical. Likewise, two bioactive reaction centers at C-2 and C-3 with hydroxyl (keto to

hydroxyl) groups might play predominant role to enhance the radical scavenging ability of compound **4**.

The dihydro-pyran and dihydro-furanone were the two active centers in **5** (Figure 5.146.). The readily available proton at C-3 was transferred to DPPH radical and appeared to undergo resonance stabilization with keto group at C-2 (dihydro-furanone) leading to the formation of hydroxyl group (dihydro-furanol). Similarly, the protons in dihydro-pyran ring of **5** might be relocated and resonance stabilized to form hydroxyl group at C-8 that could potentially scavenge the free radicals.

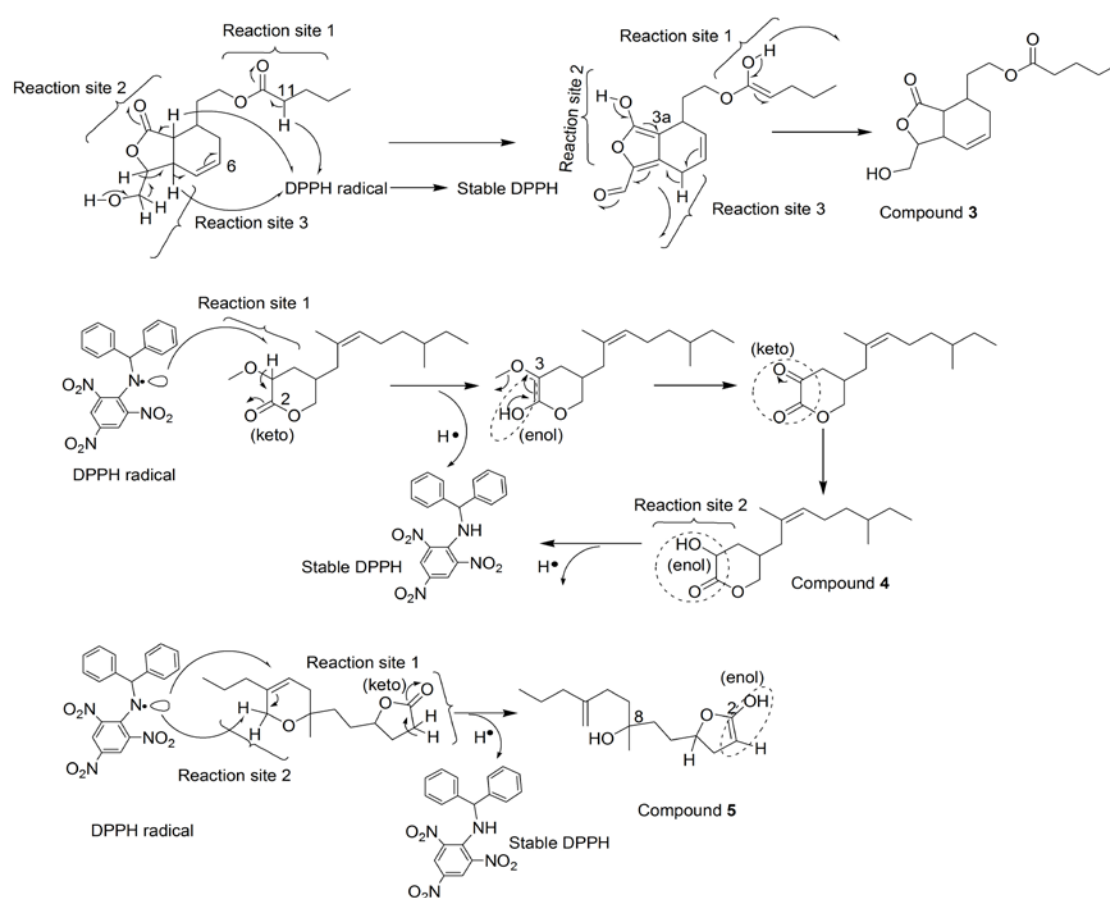


Figure 5.146.: Suggested antioxidative mechanism of irregular meroterpenoid derivatives (**3-5**) in DPPH radical model system

The compounds, **6** and **7** were found to comprise two reaction sites each, whereas one of them were located in the hexahydro isochromenyl ring and the other at the carboxylate group (Figure 5.147.). The protons at C-12 and C-11 of compounds **6** and **7**, respectively appeared to participate in the keto-enol delocalization with the

neighboring $>C=O$ group resulting in the formation of $-CH-(OH)-$ moiety by the replacement of proton to DPPH radical. The presence of hydroxyl containing compounds were effective in neutralizing the free radical species in the biological system (Derochette *et al.*, 2014), and this could be attributed to the antioxidant properties of hexahydro isochromenyl compounds.

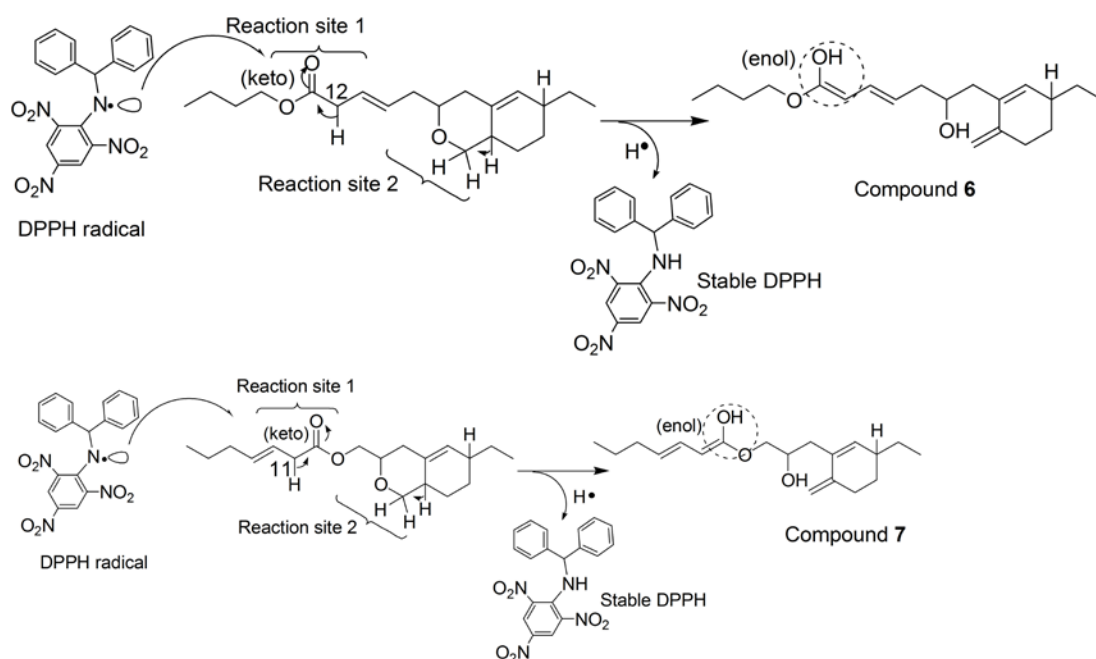


Figure 5.147.: Suggested antioxidative mechanism of hexahydro isochromenyl derivatives (6-7) in DPPH radical model system

The cholesterol derivative, **8** possess two active sites, whereas one of them were located at the ester group in the side chain was found to be primary active site and the second one was related to olefinic proton at C-1 in extended conjugation (Figure 5.148.). The compounds, **9** and **10** enclosed identical antioxidative reaction centers at hydroxyl attached position, C-3 in conjugation with olefinic proton at C-6. The free electron pair of the $-OH$ may not effectively participate in the resonance with the tetracyclic ring (Figure 5.148.). The protons of $-CHOH$ group located at C-3 position of **9** and **10** are weakly acidic in nature, and therefore, might form a weakly stabilized diphenyl picryl-hydrazine (DPPH-H). The compound **9** contained an additional reaction center in the side chain (related to hydroxyl), and that could potentially transfer protons to the DPPH radical through the keto-enol resonance stabilization.

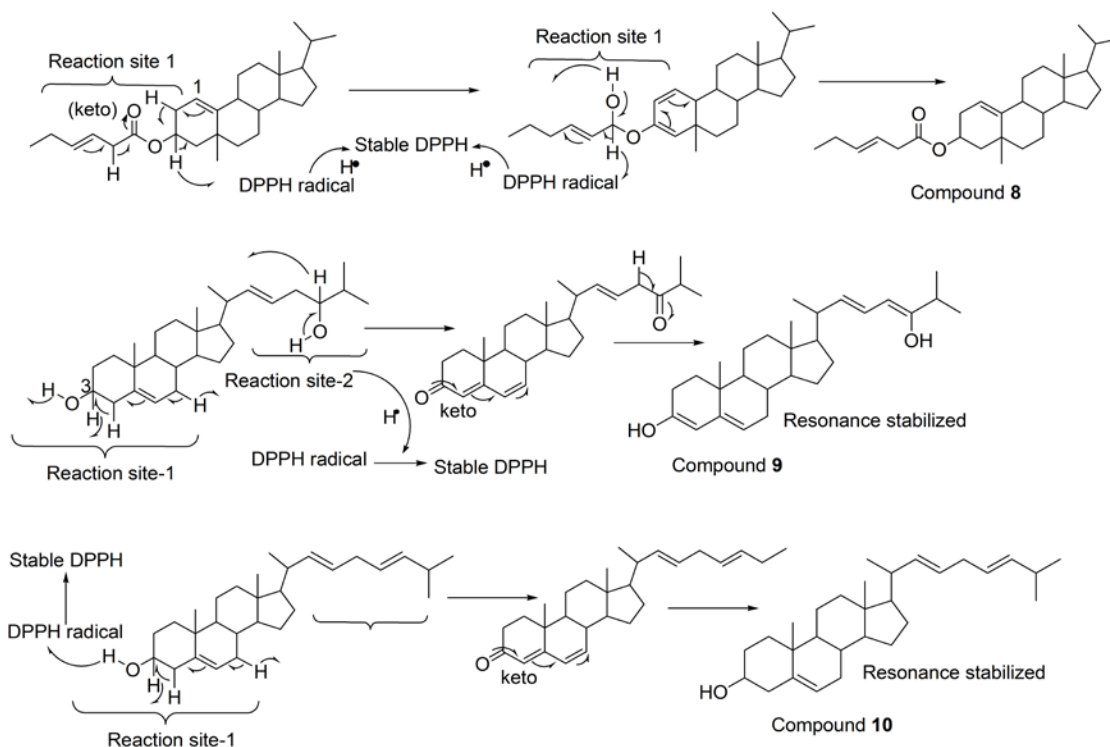


Figure 5.148.: Suggested antioxidative mechanism of cholestenol derivatives (8-10) in DPPH radical model system

The proposed antioxidative mechanism of titled secondary metabolites (1-10) from *V. cyprinoides* in DPPH radical model system corroborated with the *in vitro* DPPH radical scavenging assay. The spirocyclic ether derivative, **2** was found to possess greater number of active antioxidant reaction centers and electronegative groups in extended conjugation. Accordingly, it can potentially transfer H atom to neutralize the DPPH radical to form resonance stabilized structures, consequently demonstrated its greater antioxidant activity. Similarly, the spirocyclic ether derivative, **1** and hexahydrobenzo furanone derivative, **3** were found to comprise primarily active reaction centres along with electronegative groups, which might actively interact with the DPPH radical.

5.3.5. *In silico* molecular docking studies of selected compounds (1-5) from *V. cyprinoides*

The molecular docking studies were revealed the interactions between the selected compounds from *V. cyprinoides* with the active sites of target pro-inflammatory COX-2 and 5-LOX. The molecular docking studies were performed for

the ten compounds against COX-2 and 5-LOX enzymes, respectively and their RMSD results were analyzed. The docked conformations with lowest binding energies (compounds **1-5**) were selected for docking visualization to calculate the number of hydrogen bonds and the molecular binding interactions with the active sites of COX-2 and 5-LOX. The number of hydrogen bonds, hydrogen bonded amino acid residues, binding energy, docking score, inhibition constant, intermolecular energy and torsional free energy between the compounds **1-5** and the active sites of COX-2 and 5-LOX enzymes were recorded in the Table 5.18. and 5.19., respectively.

In silico molecular docking studies of the selected compounds with COX-2 receptor revealed that all the docked ligands might bind with the targets and exhibited lowest binding energies ranging from -7.06 to -8.98 kcal/mol along with lowest docking scores of -7.60 to -10.85 kcal/mol (Table 5.18.). Particularly, irregular spirocyclic ether derivative, **2** registered lowest binding energy and docking score of -8.98 and -10.85 kcal/mol, respectively followed by spirocyclic ether derivative, **1** (-8.72 and -10.26 kcal/mol, respectively) and hexahydrobenzo furanone derivative, **3** (-7.39 and -8.70 kcal/mol, respectively). The enzyme inhibition constants, K_i was found to be lesser for compound **2** (1.01 μ M) followed by **1** (1.31 μ M) and **3** (3.82 μ M) when compared to **4-5** (5.38-6.68 μ M). Also, the intermolecular energy and torsional free energies were found to be lesser for irregular spirocyclic ether derivatives, **1-2** (-10.21 to -10.97 and 1.39 to 1.49 kcal/mol, respectively) followed by hexahydrobenzo furanone, **3** (-8.88 and -1.49 kcal/mol, respectively) (Table 5.18.). These results demonstrated the lowest binding energy and docking score of **2** that in turn, indicated its greater enzyme inhibition activities against COX-2. The compound **2** has showed four H-bond residues such as LEU 224.B, GLU 126.A (two H-bonds), TRP 125.A (Figure 5.149.B) in the active pocket site whereas, the compound **1** exerted two hydrogen bonding interactions with GLU 222.B (Figure 5.149.A). The compounds **3** (ARG 319.B, THR 223.B, LEU 131.A (two H-bonds); Figure 5.149.C) and **4** (GLN 227.B, THR 223.B, GLU 222.B, ARG 319.B; Figure 5.149.D) displayed four hydrogen bonds whereas, compound **5** showed three hydrogen bonded residues (ARG 319.B (two H-bonds), GLY 227.B; Figure 5.149.E). The greater number of hydrogen bonds in the active site of COX-2 and the lower values of docking parameters (binding energy, docking energy and inhibition

recorded by **4-5** (7.34-8.21 μM). The intermolecular energy and torsional free energies were found to be lesser for compounds **1-3** (-6.28 to -9.37 and 1.49 to 1.79 kcal/mol, respectively). These results appropriately substantiated the greater enzyme inhibition activities of compound **2** against 5-LOX.

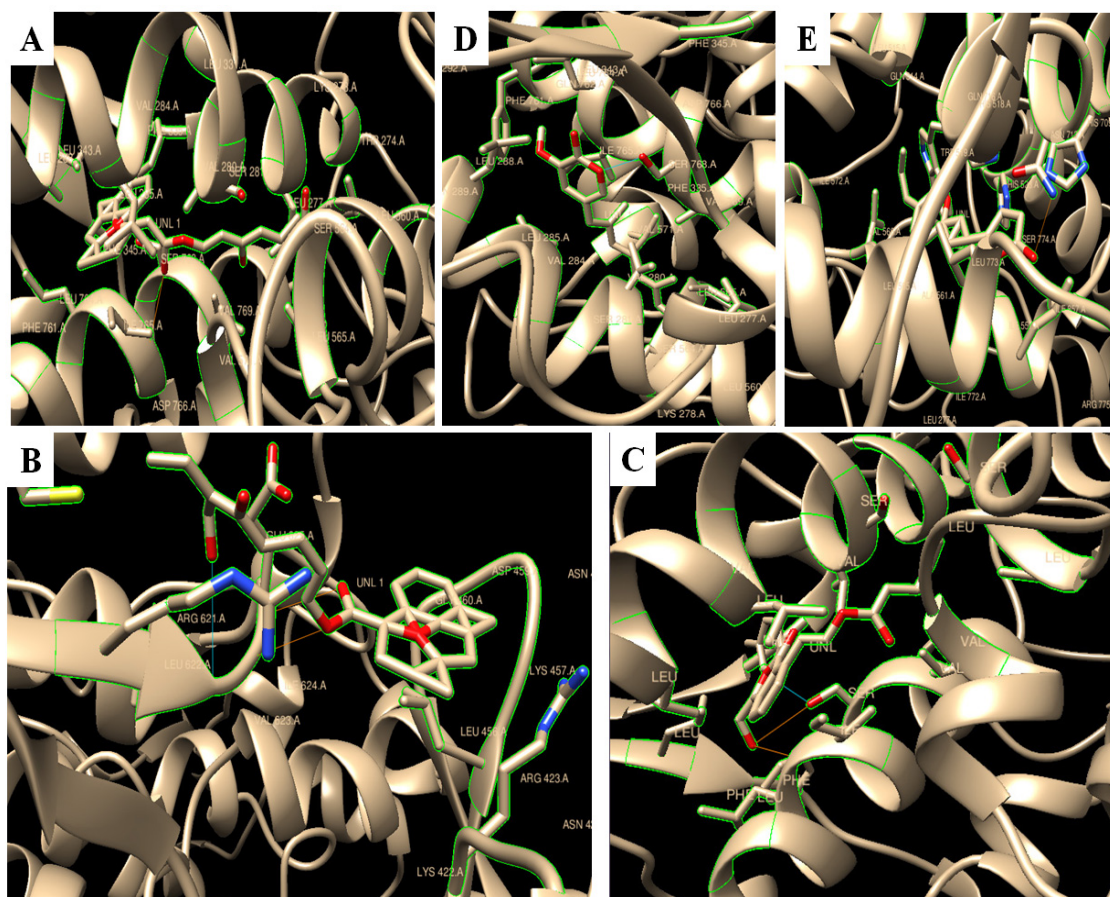


Figure 5.150.: The molecular binding interactions of compounds (A) **1**, (B) **2**, (C) **3**, (D) **4** and (E) **5** in the active site of lipooxygenase (5-LOX) were comprehended from the docking studies. The orange and blue coloured bonds were indicated the H-bonding correlations with 5-LOX

Table 5.18.: Number of hydrogen bonds, hydrogen bonded (H-bonded) amino acid residue, binding energy, docking score, inhibition constant, intermolecular energy and torsional free energy between the ligands (compounds **1-5**) and the active sites of COX-2

Ligands	†No. of H-bonds	#H-bonded amino acid residues	*Binding energy (kcal/mol)	*Docking score (kcal/mol)	*Inhibition constant, Ki (μM)	*Intermolecular energy (kcal/mol)	*Torsional free energy (kcal/mol)
1	2	GLU 222.B GLU 222.B	-8.72	-10.26	1.31	-10.21	1.49
2	4	LEU 224.B GLU 126.A GLU 126.A TRP 125.A	-8.98	-10.85	1.01	-10.97	1.39
3	4	ARG 319.B THR 223.B LEU 131.A LEU 131.A	-7.39	-8.70	3.82	-8.88	1.49
4	4	GLN 227.B THR 223.B GLU 222.B ARG 319.B	-7.06	-8.69	6.68	-8.85	1.79
5	3	ARG 319.B ARG 319.B GLY 227.B	-7.19	-7.60	5.38	-7.79	1.60

†Molecular docking studies were carried out using the software Autodock 4. #Hydrogen bonding interactions between protein and ligand.

*Values were obtained from the energy minimization based calculations

Table 5.19.: Number of hydrogen bonds, hydrogen bonded (H-bonded) amino acid residue, binding energy, docking score, inhibition constant, intermolecular energy and torsional free energy between the ligands (compounds **1-5**) and the active sites of 5-LOX

Ligands	†No. of H-bonds	#H-bonded amino acid residues	*Binding energy (kcal/mol)	*Docking score (kcal/mol)	*Inhibition constant, Ki (μM)	*Intermolecular energy (kcal/mol)	*Torsional free energy (kcal/mol)
1	1	ILE 765.A	-5.06	-8.54	3.32	-8.57	1.49
2	3	LEU 622.A GLU 625.A ILE 624.A	-7.58	-9.20	2.78	-9.37	1.79
3	3	SER 768.A SER 768.A LEU 764.A	-5.49	-6.26	2.90	-6.28	1.79
4	1	SER 768.A	-5.62	-7.07	7.34	-7.12	1.49
5	1	ASN 713.A	-1.75	-2.15	8.21	-2.45	1.69

†Molecular docking studies were carried out using the software Autodock 4. #Hydrogen bonding interactions between protein and ligand.

*Values were obtained from the energy minimization based calculations.

The compounds, **2** and **3** on molecular docking simulation displayed four hydrogen bonded residues, named LEU 622.A, GLU 625.A, ILE 624.A (Figure 5.150.B) and SER 768.A (two H-bonds), LEU 764.A, respectively (Figure 5.150.C) in the active pocket site, whereas **1** (ILE 765.A; Figure 5.150.A), **4** (SER 768.A; Figure 5.150.D) and **5** (ASN 713.A; Figure 5.150.E) displayed one hydrogen bonding each. The greater number of hydrogen bonds in the active site of 5-LOX and lesser values of binding energy/docking energy obtained for **1**, **3** and **4** were found to be linear with the greater *in vitro* anti-5-LOX potentials (IC₅₀ 0.75-0.77 mg/mL).

The docking study of selected compounds (**1-5**) isolated from *V. cyprinoides* on binding sites of 5-LOX and COX-2 showed that these ligands were dual COX-2/5-LOX inhibitors. The good binding interactions of the ligands with the target pro-inflammatory enzymes were explained the significant biological activity of the compounds, **1** through **5** isolated in the present study. Also, it revealed the specificity of these compounds with COX-2 and 5-LOX enzymes that in turn, suggested their greater selectivities towards the target anti-inflammatory properties.

5.4. Conclusions

The ethyl acetate:methanol extract of venerid bivalve clam, *Villorita cyprinoides* was chromatographically fractionated to acquire bioactive secondary metabolites, which were classified under various classes of chemistries, such as irregular spirocyclic ether derivatives (**1-2**), irregular meroterpenoids (**3-5**), isochromenyl analogues (**6-7**) and cholestenol derivatives (**8-10**). The chemical structures of these previously undescribed specialized metabolites were resolved by detailed spectroscopic analysis.

The titled compounds were assessed for antioxidant (DPPH and ABTS⁺ scavenging) and anti-inflammatory (COX-1, COX-2 and 5-LOX inhibition) properties. The compounds, 16-hydroxyhexyl-(2-ethyl-2,6-dimethyl-1-oxaspiro[4.5]dec-3,8-dien)-10-propanoate (**1**), (*E*)18-ethyl-17,19-dihydroxyhept-14-enyl-(2-ethyl-2,6-dimethyl-1-oxaspiro[4.5]dec-3,8-dien)-10-acetate (**2**) and 8-(1,3,3a,4,5,7a-hexahydro-1-(hydroxy methyl)-3-oxoisobenzofuran-4-yl)-ethyl pentanoate (**3**) were exhibited comparatively greater pro-inflammatory 5-lipoxygenase (5-LOX) inhibition potential (IC₅₀ 0.75-0.77 mg/mL) in consonant with significantly greater anti-inflammatory selectivity indices

(SI, anti-cyclooxygenase-1IC₅₀/anti-cyclooxygenase-2IC₅₀ > 1.10) than that displayed by non-steroidal anti-inflammatory drug, ibuprofen (IC₅₀ 0.96 mg/mL, SI < 1). Likewise, the irregular meroterpenoids (**4-5**) and hexahydro isochromenyl derivatives (**6-7**) were exhibited comparable pro-inflammatory 5-lipoxygenase (5-LOX) inhibition potentials (IC₅₀ 0.80-0.98 mg/mL) to that displayed by the reference, ibuprofen (IC₅₀ 0.96 mg/mL) and significantly greater anti-inflammatory selectivity indices (SI > 1.10) than ibuprofen (SI < 1).

The antioxidant activities of the spirocyclic ether derivatives **1-2**, as determined by DPPH and ABTS⁺ inhibitory activities (IC₅₀ 0.54-0.59 and 0.62-0.67 mg/mL, respectively) were appeared to be greater than those recorded with commercially available α -tocopherol (IC₅₀ 0.65 and 0.76 mg/mL, correspondingly). The compounds, **3**, **4** and **5** were displayed comparable antioxidant potentials (IC₅₀ 0.63-0.71 and 0.64-0.76 mg/mL, correspondingly) to α -tocopherol. Structure activity correlation studies displayed that antioxidative and anti-inflammatory pluralities of studied compounds were linearly related to the electronic factors, whereas steric bulk and hydrophobic parameters were inversely correlated. The proposed antioxidative mechanisms of titled secondary metabolites in DPPH radical model system could be corroborated with the *in vitro* DPPH radical scavenging assay. These mechanisms further supported the greater antioxidant potentials of the spirocyclic ether derivative, **2** followed by hexahydrobenzo furanone, **3** and spirocyclic ether derivative, **1**, which can easily dislocate the DPPH radical in the system. The docking studies of selected compounds (**1-5**) from *V. cyprinoides* on the binding sites of 5-LOX and COX-2 demonstrated their COX-2/5-LOX dual inhibitory action, particularly, the inhibitory action of spirocyclic ether derivative, **2**. The binding interactions explained their significant biological activity and revealed the specificity of the titled compounds towards pro-inflammatory COX-2 and 5-LOX enzymes. Utilization of the hitherto undescribed compounds isolated from *V. cyprinoides* predominantly, spirocyclic ether derivatives could effectively substitute the commercially available synthetic antioxidative food additives and can act as potential anti-inflammatory pharmacophore leads.

ISOLATION AND CHARACTERIZATION OF SECONDARY METABOLITES FROM *PAPHIA MALABARICA*

Contents

- 6.1. *Background*
- 6.2. *Materials and methods*
- 6.3. *Results and discussion*
- 6.4. *Conclusions*

6.1. Background

The oxidative stress in the cell organelles stimulate several unfavourable effects in our body leading to various ailments, particularly ageing, hypertension, inflammatory reactions, diabetes, cancer, etc., that were found to depend on the accumulation of reactive oxygen species (Lushchak 2011). Thus, there is an increased interest in pharmacological agents that can control or quench the free radicals from accumulating in the biological systems. The natural products from marine or estuarine organisms, such as bivalves were adapted to the adverse living conditions in their ecosystems. These organisms were reported to biosynthesize bioactive secondary metabolites as an adaptive mechanism and recognized as valuable pharmacophores for use against various oxidative stress and inflammatory disorders (Gonzalez *et al.*, 2015). The recent research efforts on natural bioactives with lesser side effects and improved effectiveness over synthetics are concerted from the marine/estuarine bivalve mollusks with greater radical quenching potentials, to sustain in their unfavourable habitats. Bivalve mollusks are traditional seafoods with wide variety of bioactive secondary metabolites and considered as valuable nutritional and commercial resources (Chakraborty *et al.*, 2014a; Chakraborty *et al.*, 2016a; Chakraborty *et al.*, 2016b; Wakimoto *et al.*, 2011).

The mollusks were reported for the occurrence of several bioactive small molecular weight secondary metabolites belonging to heterocyclics, chromenes, pyranoids, terpenes and sterols with diverse biological functions such as antioxidative, anti-diabetic, anti-inflammatory, etc. (Appleton *et al.*, 2002; Wu *et al.*, 2013). Ciavatta *et al.*, (2011) reported pyranoid cladiellane diterpene derivatives from mollusk, *Tritoniopsis elegans*. The mollusk, *Kelletia kelletii* was reported for anti-bacterial compounds, such as erythrityl-tetrakis-hydroxybenzoate and 2-deoxy-D-ribityl-tetrakis-hydroxybenzoate which enclosed benzoate frameworks in their chemical structure (Tymiak and Rinehart 1983). The steroidal alkaloids, steroid-amino acid conjugates, spiro A/B ring containing steroids were isolated from marine organisms (Amagata *et al.*, 2003; Su *et al.*, 2007).

Paphia malabarica (Veneridae) is a filter feeding organism which mainly scattered in the southwestern coasts of India. The EtOAc:MeOH (1:1, v/v) solvent extract of *P. malabarica* was showed promising anti-inflammatory and antioxidative potencies by different *in vitro* experiments. In this point of view, this chapter was directed towards the isolation and characterization of bioactive secondary metabolites from the EtOAc:MeOH extract of *P. malabarica* by repeated chromatographic fractionation techniques. The characterized secondary metabolites were classified under various classes of compounds, such as aryl polyketide derivatives (**1-3**), tetrahydro chromenyl analogues (**4-5**), isopimarane norditerpenoid (**6**), meroterpeno pyranoids (**7-8**) and cholestenol derivatives (**9-10**). The titled compounds were characterized by various spectroscopic techniques, such as nuclear magnetic resonance (NMR) including one and two dimensional (2D NMR) experiments, FTIR and mass analyses. A putative biosynthetic pathways catalyzed by polyketide synthase leading to the formation of three aryl polyketide compounds were used to corroborate the structural attributions of compounds, **1-3**. The chromatographic fractions and pure compounds were evaluated for their *in vitro* anti-inflammatory and free radical inhibition potentials. The target bioactivities of titled compounds were correlated with their structural parameters using different physicochemical descriptors, such as hydrophobic parameter, electronic descriptor variables and steric factors. This chapter also proposed putative antioxidative mechanisms for the titled bioactive secondary metabolites (**1-10**) in the DPPH radical

model system. The modes of inhibitions of 5-LOX/COX-2 enzymes by candidate compounds were determined by molecular docking simulations.

6.2. Materials and methods

6.2.1. Chemicals, reagents and instrumentations

The chemicals, reagents and instrumentations were utilized as mentioned in the section 5.2.1. under Chapter 5.

6.2.2. Chromatographic analyses

6.2.2.A. Column chromatography (CC)

The column chromatographic experimentations were used as mentioned in the section 5.2.2.A. under Chapter 5.

6.2.2.B. Flash chromatography

The fractions were resolved by flash chromatography as mentioned in the section 5.2.2.B. under Chapter 5.

6.2.2.C. Thin layer chromatography (TLC)

The thin layer chromatographic techniques and preparative thin layer chromatographic methods were performed as mentioned in the section 5.2.2.C. under Chapter 5.

6.2.2.D. High pressure liquid chromatography (HPLC)

The preparatory high pressure liquid chromatography (HPLC) and analytical high pressure liquid chromatography (HPLC) systems were used as explained in the section 5.2.2.D. under Chapter 5.

6.2.3. Spectrophotometric analyses

The UV-VIS spectrophotometric experimentations were carried out as mentioned in the section 5.2.3. under Chapter 5.

6.2.4. Spectroscopic analyses**6.2.4.A. Fourier transform infrared (FTIR) spectroscopy**

The Fourier transform infrared (FTIR) analyses were carried out as explained in the section 5.2.4.A. under Chapter 5.

6.2.4.B. Mass spectrometry

The mass spectrometry experiments were executed by the technique as demonstrated in the section 5.2.4.B. under Chapter 5.

6.2.4.C. Nuclear magnetic resonance (NMR) spectroscopy

The one and two dimensional NMR experimentations were carried out as explained in the section 5.2.4.C. under Chapter 5.

6.2.5. Animal material and extraction

The shell-on samples of *P. malabarica* (10 kg) were freshly acquired from their natural habitat at the Ashtamudi Lake (8°59' N and 76°36' E) located along the southwest coast of Arabian Sea. After cleaning the external matters, *P. malabarica* (Figure 6.1.) were transported to laboratory in ice boxes. The shell-on samples were thoroughly washed in running distilled water and the edible flesh (6 kg) was manually taken from shells without applying heat. The edible flesh samples were thereafter homogenized by grinding before being kept for overnight in the deep freezer (ultra-low temperature freezer, Eppendorf, Hamburg, Germany) for freezing at -80°C. The contents were thereafter lyophilized by freeze drier (Alpha 1-4 LD plus, Martin Christ, Germany; Scanvac, CoolsafeTM Denmark) for 48 h to yield the freeze dried clam samples (1500 g; yield 25 g/100 g on dry weight). This was powdered and stored in vacuum packed polyethylene biohazard autoclave bags (FisherbrandTM, Fischer Scientific) in the deep freezer at -80°C until further processing. The dried clam powder was used for the solvent extraction.

The lyophilized powder (1500 g) of bivalve clam material was homogenized with ethyl acetate:methanol (EtOAc:MeOH, 1:1, v/v) by sonication (Elma, Hohentwiel, Germany) followed by shaking (Orbital shaker, Labline, India) in the presence of nitrogen for 4 h. This procedure was continued for three to four times to afford

maximum bioactive components in crude extract. The extracts were then filtered through filter paper (Whatman No. 1) using Na_2SO_4 (30 g) to obtain the clarified filtrates. The solvent filtrates were concentrated (40°C) in the rotary evaporator (Heidolph, Germany; IKA, Germany) to afford concentrated extracts of *P. malabarica*. The extracts were completely dried in the rotational vacuum concentrators (RVC, Martin Christ, Germany) to yield corresponding solvent extracts of *P. malabarica* (55 g; 3.67 g/100 g yield on dry weight basis). The solvent extract was kept under an inert nitrogen atmosphere and used for the chromatographic purifications to isolate bioactive principles.



Figure 6.1.: The fresh shelled *P. malabarica* samples collected from the estuarine waters of Ashtamudi Lake ($8^\circ 59'$ N and $76^\circ 36'$ E) located along the southwest coast of Arabian Sea, India

6.2.6. Chromatographic purification of pure compounds from *P. malabarica*

The crude extract of *P. malabarica* (50.0 g) was partitioned by repeated column chromatographic experiments over adsorbent silica. The schematic diagram

showing the purification of EtOAc:MeOH extract of *P. malabarica* was shown in Figure 6.2. The extract was made into slurry with silica (60-120 mesh, 6 g) and pre-packed into a column (1000 mm X 40 mm) enclosing silica gel as adsorbent (60-120 mesh). The column was initiated with 100% *n*-hexane followed by EtOAc and methanol to obtain six different fractions (PM₁ to PM₆). The column fractions were assessed for anti-inflammatory and antioxidant activities. The fractions, PM₃, PM₄ and PM₆ were subjected to further chromatographic fractionation due to its relatively greater antioxidant and anti-inflammatory activities compared to other fractions.

The fraction, PM₃ (6.42 g; 12.84%) was carried out to vacuum liquid chromatography on a glass column (450 mm X 30 mm) packed with silica (230-400 mesh). The polarity of eluent was regularly increased by the addition of *n*-hexane/EtOAc/MeOH to endow 21 fractions of 32 mL each and were compiled to 8 groups (PM₃₋₁ to PM₃₋₈) based upon TLC (*n*-hexane:EtOAc, 9:1, v/v) experiments. Fraction, PM₃₋₃ (1.52 g; 3.04%) eluted with 10% *n*-hexane:EtOAc (v/v) was flash chromatographed (Biotage AB SP1-B1A, 230-400 mesh, 12 g; Biotage AB, Uppsala, Sweden) on a silica gel column at a collection UV wavelength of 254 nm. The eluent polarity was initiated from 100% *n*-hexane followed by EtOAc and MeOH to furnish a total of 55 fractions (9 mL each), which were pooled to four fractions (PM₃₋₃₋₁ through PM₃₋₃₋₄) based on analytical TLC (*n*-hexane:EtOAc, 9:1, v/v). The fraction, PM₃₋₃₋₁ was further fractionated over preparatory TLC on silica gel GF₂₅₄ using *n*-hexane:EtOAc (49:1, v/v) afforded compound **10** (82 mg; 0.16%) as major component. The solvents were evaporated and assessed for TLC (silica GF₂₅₄; *n*-hexane:EtOAc, 95:5, v/v) to confirm its purity. The fraction, PM₃₋₃₋₂ was further fractionated over preparatory TLC on silica gel GF₂₅₄ using *n*-hexane:EtOAc (46:4, v/v) afforded compound **9** (148 mg; 0.30%), as major component. The TLC of this fraction over silica gel GF₂₅₄ using 10% *n*-hexane:EtOAc (v/v) supported its purity. The sub-fraction PM₃₋₁ (1.5 g; yield 3.00%) was found to be mixture and exhibited higher bioactivity. It was further resolved by flash chromatography (BiotageAB SP1-B1A, Sweden) on 230-400 mesh silica at 256 nm (collection wavelength) with increasing eluent polarity of *n*-hexane/EtOAc/MeOH to furnish 15 fractions (8 mL each), which were combined into PM₃₋₁₋₁ and PM₃₋₁₋₂ sub-fractions based on analytical TLC (*n*-hexane:EtOAc, 23:2, v/v) and RP C18 HPLC (3:2 MeOH/MeCN). The sub-fraction, PM₃₋₁₋₂ (668 mg; 1.34%) on preparatory TLC (silica

GF₂₅₄) using *n*-hexane:EtOAc (24:1 v/v) yielded pure compound **5** (90 mg; 0.18%), and checked for its purity on TLC (GF₂₅₄) using *n*-hexane:EtOAc (9:1 v/v). The sub-fraction, PM₃₋₁₋₁ was further purified by preparatory TLC (on silica gel GF₂₅₄) using *n*-hexane:EtOAc (24:1, v/v) to purify compound **3** (75 mg; 0.15%), which was homogenous on TLC (1:19, v/v, EtOAc/*n*-hexane) and RP C18 HPLC (MeOH/MeCN, 3:2, v/v).

The fraction, PM₄ (eluted at 70% EtOAc:*n*-hexane, v/v) was selected for further purification to afford pure bioactive metabolites since the percentage yield (3.53 g; 7.06%) and bioactive potentials were significantly higher. This fraction was flash chromatographed (Biotage AB SP1-B1A, Uppsala, Sweden) on a silica gel column (Biotage, 230-400 mesh, 12 g, Biotage No. 25+M) at a collection UV wavelength of 258 nm and a monitor wavelength of 264 nm with a step gradient elution of *n*-hexane/EtOAc/MeOH to afford 29 fractions (10 mL each), which were pooled to seven fractions (PM₄₋₁ to PM₄₋₇) based upon analytical TLC. The purification of sub-fraction, PM₄₋₂ over preparatory TLC (GF₂₅₄) using *n*-hexane:EtOAc (47:3, v/v) yielded compound **4** (110 mg; 0.22%) as major component. The TLC analysis over silica (*n*-hexane:EtOAc; 17:3, v/v) was supported its purity. The sub-fraction, PM₄₋₁ was further fractionated over PTLC on silica gel GF₂₅₄ using *n*-hexane:EtOAc (49:1, v/v) to afford compound **8** (90 mg; 0.18%; 94% purity by RP C18 HPLC, MeOH:MeCN, 3:2 v/v) as major component, which was homogenous by TLC (Si gel GF₂₅₄ 15 mm; 100% *n*-hexane, R_f: 0.75). The fraction, PM₄₋₃ was fractionated over preparatory TLC over silica GF₂₅₄ using *n*-hexane:EtOAc (22:3, v/v) to yield compound **7** (118 mg; 0.24%; 97% purity by C18 HPLC RP, MeOH:MeCN, 3:2, v/v) as the main component. Evaporation of solvents from the fractions followed by TLC (silica GF₂₅₄ using 5% EtOAc:*n*-hexane, v/v) analysis were confirmed its purity. The fraction, PM₄₋₄ was further fractionated by PTLC over silica gel (GF₂₅₄) using *n*-hexane/EtOAc (43:7, v/v) to achieve the title compound **6** (95 mg; 0.19%) and its TLC analysis over silica gel using 15% EtOAc/*n*-hexane (v/v) confirmed its purity. Fraction, PM₄₋₅ (1.15 g) was flash chromatographed (collection wavelength of 254 nm) on silica gel using gradient elution of *n*-hexane/EtOAc to acquire 10 fractions (13 mL each), which were combined to three (PM₄₋₅₋₁-PM₄₋₅₋₃) fractions after TLC (3:17, v/v, EtOAc:*n*-hexane). The bioactive sub-fraction, PM₄₋₅₋₃ was found to be a mixture, and therefore, fractionated by PTLC with EtOAc:*n*-hexane solvent

system (10:90, v/v) to acquire **1** (65 mg; 0.13%). The purity of **1** was supported by TLC using 3% EtOAc/*n*-hexane (v/v) along with RP C18 HPLC (3:2, v/v, MeOH:MeCN) experiments.

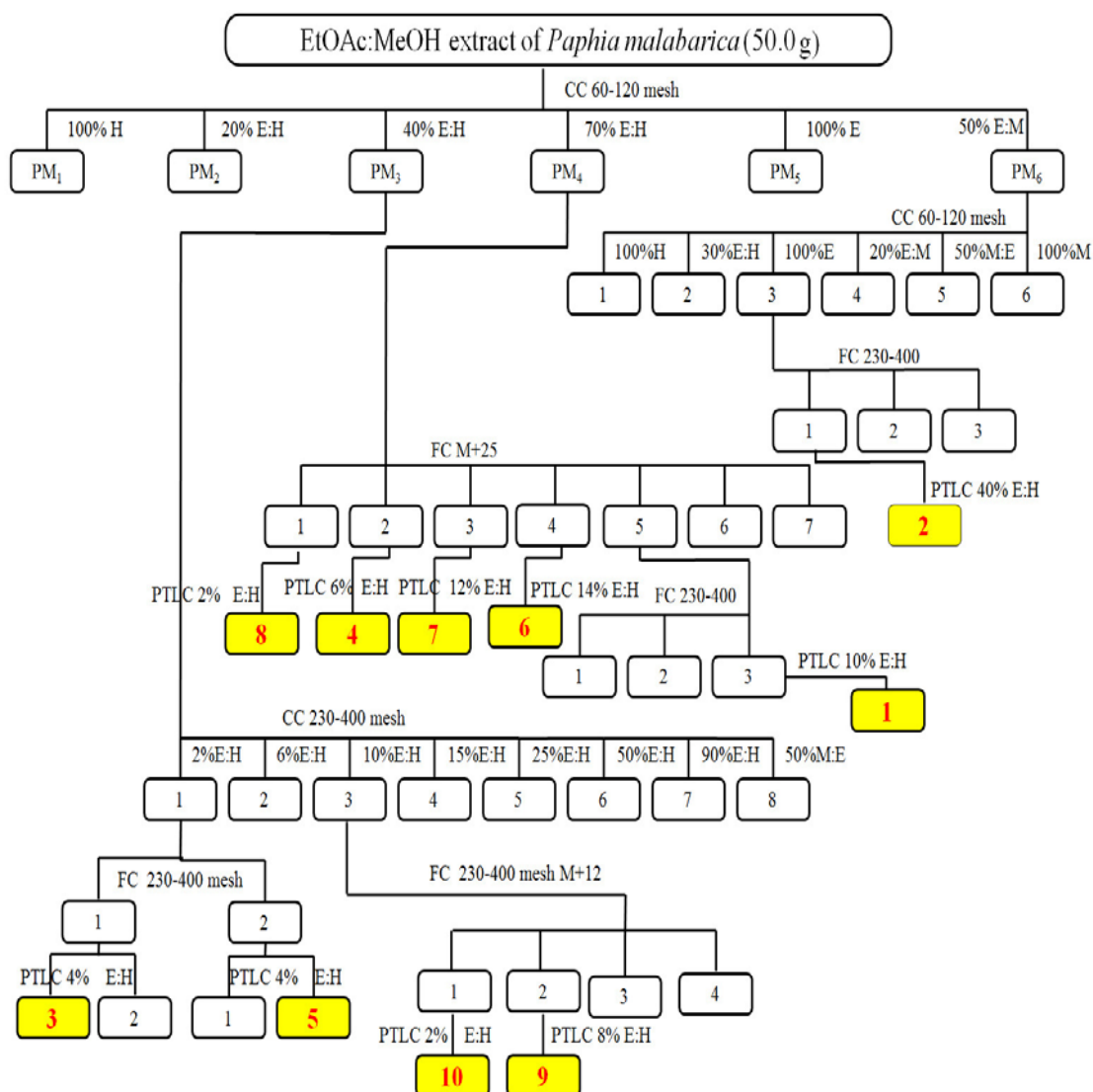


Figure 6.2.: Schematic diagram of purification of EtOAc:MeOH extract of *P. malabarica*. CC-column chromatography; FC-flash chromatography; PTLC-preparative thin layer chromatography; TLC-thin layer chromatography; E-ethyl acetate; H-*n*-hexane; M-methanol. The coloured boxes represented the pure compounds and were characterized by detailed spectroscopic experiments

The fraction, PM₆ (18.0 g; 36.0%) was subjected to chromatographic fractionation on column (45 cm X 3 cm) packed with silica (60-120 mesh, 8 g). A

gradient elution of *n*-hexane/EtOAc/MeOH afforded 65 column fractions (16 mL each), which were compiled to 6 pooled fractions after TLC analysis (PM₆₋₁-PM₆₋₆). The sub-fraction PM₆₋₃ (2136 mg, eluted with 100% EtOAc) was appeared to be a mixture and therefore, chosen for flash chromatography on a silica gel column (Biotage, 230-400 mesh, 12 g, Biotage No. 25+M) connected with UV detector (collection wavelength of 260 nm) using *n*-hexane and EtOAc to yield 7 sub-fractions (11 mL each). These were combined to three sub-fractions (PM₆₋₃₋₁ to PM₆₋₃₋₃) after TLC (20% EtOAc:*n*-hexane, v/v) and RP C18 HPLC (3:2, v/v, MeOH/MeCN). Repeated preparatory thin layer chromatographic fractionation of bioactive sub-fraction, PM₆₋₃₋₁ using EtOAc:*n*-hexane (40:60, v/v) yielded **2** (92 mg; 0.18%) as pure compound, which was homogenous on thin layer chromatography (1:4, v/v, EtOAc/*n*-hexane) and RP C18 HPLC (MeOH/MeCN, 3:2, v/v).

6.2.7. Physicochemical data of bioactive secondary metabolites from EtOAc:MeOH extract of *P. malabarica*

6.2.7.1. Physicochemical data of compound 1 (PM₄₋₅₋₃₋₁)

13-(Methoxycarbonyl)-11-((*E*)-18-ethylhexa-16,19-dienyl)-12-propylcyclohex-10-enyl)-methyl-4-hydroxy benzoate: Brown oily; UV (MeOH) λ_{\max} (log ϵ): 286.0 nm (3.90); TLC (Si gel GF₂₅₄ 15 mm; 3:17, v/v, EtOAc/*n*-hexane) R_f : 0.61; R_t (RP C18 HPLC, 3:2, v/v, MeOH:MeCN): 6.79 min; IR (cm⁻¹) (stretching ν , bending δ , rocking ρ): 3349 (br, O-H ν), 2919, 2851 (C-H ν), 1709 (C=O ν), 1683 (C=C ν), 1575, 1593 (C=C ν), 1483 (C-H δ), 1374 (C-H ρ), 1203 (C-O ν), 1184, 1140 (C-C ν), 971 (=C-H δ), 841, 802, 722 (C-H ρ). ¹H (500 MHz, CDCl₃): δ 8.10 (1H, s), 7.52 (1H, d, J =10.48 Hz), 7.36 (1H, t, J =7.89 Hz), 7.12 (1H, d, J =9.36 Hz), 5.82 (1H, p, J =11.26 Hz), 5.36 (1H, t, J =10.46 Hz), 5.35 (1H β , d, J =8.95 Hz), 5.34 (1H, q, J =10.48 Hz), 4.97 (2H, dd, J =16.45, 12.31 Hz), 4.08 (2H, d), 3.70 (3H, s), 2.85 (2H, dd), 2.62 (1H α , m), 2.31 (1H α , m), 2.03 (1H β , m), 2.02 (1H β , m), 1.33 (2H, t), 1.32 (2H, m), 1.31 (2H, m), 1.28 (2H, m), 0.98 (3H, t), 0.88 (3H, t); ¹³C (125 MHz, CDCl₃): δ 174.89, 167.98, 155.50, 146.92, 139.28, 137.23, 136.47, 133.63, 129.74, 129.73, 129.73, 128.25, 124.45, 114.06, 67.55, 50.55, 33.82, 31.93, 31.44, 30.20, 29.66, 29.36, 27.23, 25.63, 22.69, 19.23, 14.12; COSY and HMBC data were given in Table 6.6. EIMS: found m/z 440.2565 [M]⁺, cal.

for $C_{27}H_{36}O_5$ 440.2563 (Δ 0.91 ppm). HRESI-MS (positive mode) m/z : for $C_{27}H_{37}O_5$ 441.2641 $[M+H]^+$.

6.2.7.2. Physicochemical data of compound 2 (PM₆₋₃₋₁₋₁)

Isobutyl-13-(6-(benzoyloxy)-10-methylpentyl)-tetrahydro-13-methyl-2H-pyran-17-carboxylate: Yellow oily; UV (MeOH) λ_{max} (log ϵ): 261.0 nm (3.50); TLC (Si gel GF₂₅₄ 15 mm; 1:4, v/v, EtOAc/*n*-hexane) R_f : 0.57; R_t (RP C18 HPLC, 3:2, v/v, MeOH:MeCN): 5.32 min; IR (cm⁻¹): 2959, 2930 (C-H ν), 1722 (C=O ν), 1599, 1580 (C=C ν), 1448 (C-H δ), 1380 (C-H ρ), 1276 (C-O ν), 1072, 1039 (C-C ν), 741 (C-H δ), 703, 651 (C-H ρ). ¹H (500 MHz, CDCl₃): δ 7.65 (1H, d, J =7.15 Hz), 7.64 (1H, d, J =9.17 Hz), 7.46 (1H, t, J =8.58 Hz), 7.45 (1H, t, J =9.53 Hz), 7.45 (1H, d, J =10.21 Hz), 5.10 (1H β , dd), 4.23 (2H, t), 4.02 (2H, d), 1.97 (1H, m), 1.64 (2H, m), 1.61 (1H α , m), 1.27 (1H β , m), 1.52 (2H, t), 1.47 (2H, m), 1.37 (1H α , m), 1.34 (2H, m), 1.26 (2H, m), 1.18 (3H β , s), 0.92 (3H, d), 0.91 (3H, d), 0.88 (3H β , d); ¹³C (125 MHz, CDCl₃): δ 167.69, 167.01, 132.32, 130.90, 130.83, 130.74, 128.81, 128.71, 72.38, 71.77, 67.23, 65.51, 38.05, 31.92, 30.57, 29.69, 27.73, 26.20, 22.69, 19.75, 19.16, 19.13, 18.81, 13.77; COSY and HMBC data were given in Table 6.7. EIMS: found m/z 404.2567 $[M]^+$, cal. for $C_{24}H_{36}O_5$ 404.2563 (Δ 0.99 ppm). HRESI-MS (positive mode) m/z : for $C_{24}H_{37}O_5$ 405.2641 $[M+H]^+$.

6.2.7.3. Physicochemical data of compound 3 (PM₃₋₁₋₁₋₁)

(E)-12-(17-Ethyl-tetrahydro-16-hydroxy-15-(methylpentanoate)-14-oxo-2H-pyran-13-yl)-9-methylbut-11-enyl benzoate: Pale yellow oily; UV (MeOH) λ_{max} (log ϵ): 274.0 nm (3.80); TLC (Si gel GF₂₅₄ 15 mm; 1:19, v/v, EtOAc/*n*-hexane) R_f : 0.75; R_t (RP C18 HPLC, 3:2, v/v, MeOH:MeCN): 6.28 min; IR (cm⁻¹): 3308 (br, O-H ν), 2921, 2852 (C-H ν), 1724 (C=O ν), 1607 (C=C ν), 1509 (C=C ν), 1457 (C-H δ), 1374 (C-H ρ), 1280 (C-O ν), 1165, 1125 (C-C ν), 988 (=C-H δ), 826 (C-H δ), 742 (C-H δ). ¹H (500 MHz, CDCl₃): δ 7.72 (1H, d, J =7.48 Hz), 7.71 (1H, d, J =8.57 Hz), 7.54 (1H, dd, J =9.46 Hz), 7.53 (1H, dd, J =8.24 Hz), 7.51 (1H, dd, J =7.59 Hz), 5.37 (1H, t, J =9.86 Hz), 5.35 (1H, t, J =9.54 Hz), 5.27 (1H α , dt), 4.32 (1H α , t), 4.15 (1H α , dd), 4.29 (1H β , dd), 4.09 (2H, d), 2.85 (1H β , t), 2.31 (2H, t), 2.03 (1H β , m), 1.73 (1H β , p), 1.61 (2H, p), 1.45 (2H, m), 1.30 (2H, m), 1.26 (2H, m), 0.98 (3H α , d), 0.96 (3H, t), 0.89 (3H, t); ¹³C (125

MHz, CDCl₃): δ 173.25, 172.83, 167.68, 132.33, 130.88, 130.88, 130.88, 129.92, 129.80, 128.83, 128.70, 71.78, 68.88, 65.54, 62.09, 34.05, 30.58, 29.70, 27.73, 25.63, 24.82, 22.69, 19.19, 19.16, 14.11, 13.72; COSY and HMBC data were given in Table 6.8. EIMS: found m/z 460.2466 [M]⁺, cal. for C₂₆H₃₆O₇ 460.2461 (Δ 1.1 ppm). HRESI-MS (positive mode) m/z : for C₂₆H₃₇O₇ 461.2539 [M+H]⁺.

6.2.7.4. Physicochemical data of compound 4 (PM₄₋₂₋₁)

6¹-(3-((*E*)-3^{1b}-(Furan-2'-yl)-prop-3^{1b}-en-3¹-yl)-4a,5,6,8a-tetrahydro-8-methyl-2*H*-chromen-6-yl)-ethyl-5''-methyl-hexanoate: Brown oily; UV (MeOH) λ_{\max} (log ϵ): 284.0 nm (3.98), 286.0 nm (3.90); TLC (3:17, v/v, EtOAc/*n*-hexane) R_f: 0.38; R_t (RP C18 HPLC, MeOH:MeCN, 3:2, v/v): 12.92 min; IR (cm⁻¹): 2922, 2853 (C-H_v), 1737 (C=O_v), 1481 (C-H δ), 1365, 1257 (C-H ρ), 1161 (C-O_v), 1079 (C-H δ_{furan}), 967, 879, 801 (=C-H δ), 720 (C-H ρ); ¹H (500 MHz, CDCl₃): δ 7.46 (1H, d, J =9.91 Hz), 7.29 (1H, d, J =5.51 Hz), 7.07 (1H, t, J =10.48 Hz), 6.92 (1H β , s), 5.30 (1H, d, J =11.20 Hz), 5.27 (1H, d, J =11.00 Hz), 4.22 (1H, dd), δ 4.08 (1H, dd), 4.00 (2H, t), 2.78 (1H β , t), 2.54 (1H β , dt), 2.24 (2H, m), 1.98 (1H α , m), 1.95 (1H β , m), 1.54 (2H, m), 1.51 (2H, m), 1.38 (2H, t), 1.36 (3H β , s), 1.26 (3H α , s), 1.21 (2H, m), 0.81 (3H, d), 0.81 (3H, d); ¹³C (125 MHz, CDCl₃): δ 173.30, 152.10, 147.00, 135.80, 131.10, 130.80, 128.80, 124.70, 124.40, 123.90, 119.10, 64.60, 62.10, 36.50, 34.30, 31.90, 31.40, 30.23, 30.22, 30.21, 29.30, 27.21, 25.92, 22.70, 14.18, 14.10; COSY and HMBC data were given in Table 6.9. EIMS: found m/z 412.2616 [M]⁺, cal. for C₂₆H₃₆O₄ 412.2613 (Δ 0.72 ppm). HRESI-MS (positive mode) m/z : for C₂₆H₃₇O₄ 413.2692 [M+H]⁺.

6.2.7.5. Physicochemical data of compound 5 (PM₃₋₁₋₂₋₂)

7-(2'-Ethyl-1'-hydroxynonan-2'-yl)-6,7,8,8a-tetrahydro-3*H*-isochromen-1-(5*H*)-one: Yellow oily; UV (MeOH) λ_{\max} (log ϵ): 277.0 nm (3.99); TLC (1/9, v/v, EtOAc/*n*-hexane) R_f: 0.48; R_t (RP C18 HPLC, 3:2, v/v, MeOH:MeCN): 3.80 min; IR (cm⁻¹): 3433 (br, O-H_v), 2922, 2852 (C-H_v), 1736 (C=O_v), 1481, 1414 (C-H δ), 1376 (C-H ρ), 1163, 1096 (C-O_v), 976 (=C-H δ), 721 (C-H ρ); ¹H (500 MHz, CDCl₃): δ 5.34 (1H α , t, J =9.85 Hz), 4.28 (1H α , d), 4.14 (1H β , d), 3.48 (2H, s), 2.31 (2H, t), 2.30 (1H β , t), 2.01 (2H, t), 1.60 (2H, m), 1.33 (1H β , m), 1.29 (2H), 1.28 (2H), 1.28 (2H), 1.28 (2H), 1.27 (2H), 1.25 (2H), 1.25 (2H), 0.88 (3H, t), 0.86 (3H, t); ¹³C (125 MHz, CDCl₃): δ

173.30, 144.40, 130.80, 61.90, 50.60, 42.40, 38.20, 34.00, 34.00, 31.90, 31.70, 29.60, 29.30, 29.20, 29.10, 27.20, 24.80, 22.60, 22.50, 14.10; COSY and HMBC data were given in Table 6.10. EIMS: found m/z 322.2512 $[M]^+$, cal. for $C_{20}H_{34}O_3$ 322.2508 (Δ 1.2 ppm). HRESI-MS (positive mode) m/z : for $C_{20}H_{35}O_3$ 323.2586 $[M+H]^+$.

6.2.7.6. Physicochemical data of compound 6 (PM₄₋₄₋₁)

18 (4→14),19 (4→8) Bis-abeo-nor-isopimarane-1,5-diene-3-yl-3 β -methoxy-propyl pentanoate: White solid; melting point (m.p.) 172°C (decom.); UV (MeOH) λ_{max} (log ϵ): 270.0 nm (3.12); TLC (Si gel GF₂₅₄ 15 mm; 15% EtOAc:*n*-hexane, v/v) R_f : 0.65; R_t (RP C18 HPLC, 3:2, v/v, MeOH:MeCN): 3.85 min; IR (cm⁻¹): 2922, 2853 (C-Hv), 1722 (C=Ov), 1642 (C=Cv), 1375, 1260, 1035 (C-Ov); ¹H (CDCl₃, 500 MHz): δ 5.37 (1H, t, $J=7.24$ Hz), 5.38 (1H, t, $J=8.51$ Hz), 5.34 (1H, t, $J=6.61$ Hz), 4.15 (2H, t), 3.64 (2H, t), 3.53 (1H, td), 2.81 (1H, dd), 2.33 (2H, t), 2.29 (2H, d), 2.01 (2H, d), 1.85 (1H, m), 1.83 (1H, t), 1.63 (2H, m), 1.61 (2H, m), 1.49 (1H, m), 1.44 (2H, m), 1.15 (2H, d), 1.12 (1H, m), 1.08 (1H, t), 1.01 (3H, s), 0.91 (1H, m), 0.89 (3H, t), 0.87 (3H, t), 0.86 (3H, d), 0.68 (3H, s); ¹³C (125 MHz, CDCl₃): δ 178.23, 140.72, 130.01, 129.71, 121.72, 71.83, 68.35, 65.03, 56.77, 50.14, 42.32, 42.24, 39.52, 37.25, 36.50, 33.87, 31.93, 29.70, 28.23, 24.75, 22.82, 22.69, 21.09, 19.39, 18.72, 14.11, 11.86; COSY and HMBC data were given in Table 6.11. EIMS: found m/z 416.3295 $[M]^+$, cal. for $C_{27}H_{44}O_3$, 416.3290 (Δ 1.2 ppm). HRESI-MS (positive mode) m/z : for $C_{27}H_{45}O_3$ 417.3367 $[M+H]^+$.

6.2.7.7. Physicochemical data of compound 7 (PM₄₋₃₋₁)

1'-((10*E*)-10-(10-(Pentan-4-yl)-cyclohex-4-enyl)-allyloxy)-tetrahydro-2',2'-dimethyl-2*H*-pyran: Light green solid; m.p. 148.7°C (decom.); UV (MeOH) λ_{max} (log ϵ): 260.0 nm (3.46); TLC (Si gel GF₂₅₄ 15 mm; 5% EtOAc:*n*-hexane, v/v) R_f : 0.43; R_t (RP C18 HPLC, 3:2, v/v, MeOH:MeCN): 22.18 min; IR (cm⁻¹): 2932, 2860 (C-Hv), 1661 (C=Cv), 1455 (C-H δ), 1372, 1241, 1187, 1108, 1042 (C-Ov), 965 (=C-H δ), 803 (C-H ρ). ¹H (500 MHz, CDCl₃): δ 5.38 (1H, t, $J=8.50$), 5.35 (1H, t, $J=9.21$), 5.34 (1H, t, $J=9.22$), 4.59 (1H, s), 4.14 (1H, d), 4.12 (1H, d), 3.64 (2H, t), 2.35 (1H, t), 2.31 (2H, m), 2.02 (2H, d), 1.99 (2H, t), 1.63 (2H, m), 1.57 (2H, m), 1.55 (2H, m), 1.48 (3H, s), 1.46 (3H, s), 1.43 (2H, m), 1.42 (2H, m), 0.89 (3H, t), 0.87 (3H, t); ¹³C (125 MHz, CDCl₃): δ

143.18, 139.27, 127.67, 124.47, 68.39, 65.05, 63.11, 39.07, 34.37, 32.84, 31.93, 30.25, 30.09, 29.62, 29.37, 27.23, 25.74, 22.69, 22.69, 14.15, 14.15; COSY and HMBC data were given in Table 6.12. EIMS: found m/z 320.2718 $[M]^+$, cal. for $C_{21}H_{36}O_2$ 320.2715 (Δ 0.93 ppm). HRESI-MS (positive mode) m/z : for $C_{21}H_{37}O_2$ 321.2794 $[M+H]^+$.

6.2.7.8. Physicochemical data of compound 8 (PM₄₋₁₋₁)

2-((*E*)-Deca-1,8-dien-10-yl)-11,12-dihydro-13-propyl-2*H*-pyran: Yellow solid; m.p. 169.6°C (decom.); UV (MeOH) λ_{max} (log ϵ): 265.0 nm (3.37); TLC (Si gel GF₂₅₄ 15 mm; 100% *n*-hexane, v/v) R_f : 0.75; R_t (RP C18 HPLC, 3:2, v/v, MeOH:MeCN): 20.52 min; IR (cm⁻¹): 2955, 2921, 2852 (C-H_v), 1641 (C=C_v), 1462 (C-H δ), 1376, 1259, 1200, 1098, 1034 (C-O_v), 992 (=C-H δ), 802, 721, 636 (C-H_p). ¹H (500 MHz, CDCl₃): δ 6.96 (1H, s), 5.81 (1H, p, J =10.24, 6.90 Hz), 5.35 (1H, t, J =10.68, 5.52 Hz), 5.01 (1H, m, J =14.52 Hz), 4.94 (1H, m, J =10.21 Hz), 4.68 (1H, t), 2.06 (2H, t), 2.03 (2H, t), 2.02 (2H, t), 1.97 (2H, t), 1.58 (2H, m), 1.44 (3H, s), 1.37 (2H, m), 1.36 (2H, m), 1.30 (2H, m), 1.26 (2H, m), 0.88 (3H, t); ¹³C (125 MHz, CDCl₃): δ 139.27, 130.38, 129.91, 123.34, 114.06, 112.37, 108.30, 37.11, 33.83, 31.94, 30.41, 29.71, 29.52, 29.37, 28.97, 26.72, 22.70, 14.12; COSY and HMBC data were given in Table 6.13. EIMS: found m/z 262.2300 $[M]^+$, cal. for $C_{18}H_{30}O$ 262.2297 (Δ 1.1 ppm). HRESI-MS (positive mode) m/z : for $C_{18}H_{31}O$ 263.2375 $[M+H]^+$.

6.2.7.9. Physicochemical data of compound 9 (PM₃₋₃₋₂₋₁)

(22*E*)-24¹,24²-Methyldihomocholesta-5,22-dien-3 β -ol: White solid; m.p. 140.7°C; $[\alpha]_D^{26}$ 18.6° (CHCl₃, c0.012); UV (MeOH) λ_{max} (log ϵ): 228.9 (1.74); TLC (Si gel GF₂₅₄ 15 mm; 10:90, v/v, EtOAc:*n*-hexane) R_f : 0.48; R_t (RP C18 HPLC, 6:4, v/v, MeOH:MeCN): 5.33 min; IR (cm⁻¹): 3427 (br, O-H_v), 2945 (C-H_v), 1664 (C=C_v), 1459, 1374, 1332 (C-H_p), 1243, 1188, 1122 (C-C_v), 881 (=C-H δ), 835, 806, 733, 596 (C-H_p); ¹H (500 MHz, CDCl₃): δ 5.35 (1H α , dd, J =5.28, 3.58 Hz), 5.18 (1H α , dd, J =12.41, 6.09 Hz), 5.17 (1H, dt, J =16.10, 7.31 Hz), 3.50 (1H α , p), 2.28 (1H α , d), 2.24 (1H β , d), 2.03 (2H, m), 2.01 (1H β , t), 1.96 (1H α , t), 1.86 (1H α , t), 1.85 (2H, m), 1.83 (1H β , t), 1.82 (1H, m), 1.57 (1H β , m), 1.56 (1H β , m), 1.52 (1H α , m), 1.50 (1H β , m), 1.49 (2H, m), 1.35 (1H β , m), 1.25 (2H, m), 1.15 (1H α , t), 1.10 (1H β , m), 1.08 (1H α , t), 1.06 (1H α , m), 1.01 (3H β , s), 1.00 (1H, m), 0.96 (1H α , m), 0.93 (1H β , m), 0.92 (3H α , d), 0.91 (3H α , d),

0.87 (3H, d), 0.86 (3H, d), 0.68 (3H β , s); ^{13}C (125 MHz, CDCl_3): δ 140.76, 135.83, 131.71, 121.71, 71.81, 56.70, 56.16, 50.14, 46.05, 42.54, 42.33, 42.32, 41.90, 39.72, 37.22, 36.50, 35.72, 31.91, 31.83, 28.42, 28.22, 28.02, 24.26, 22.69, 21.14, 20.53, 19.89, 19.40, 18.39, 11.68; COSY and HMBC data were given in Table 6.14. EIMS: found m/z 426.3868 $[\text{M}]^+$, cal. for $\text{C}_{30}\text{H}_{50}\text{O}$ 426.3862 (Δ 1.4 ppm). HRESI-MS (positive mode) m/z : for $\text{C}_{30}\text{H}_{51}\text{O}$ 427.3910 $[\text{M}+\text{H}]^+$.

6.2.7.10. Physicochemical data of compound 10 (PM_{3.3-1-1})

23-Gem-dimethylcholesta-5-en-3 β -ol: White solid; m.p. 139.4°C; $[\alpha]_D^{26}$ 16.4° (CHCl_3 , c0.015); UV (MeOH) λ_{max} (log ϵ): 226.4 (1.36); TLC (Si gel GF₂₅₄ 15 mm; 5:95, v/v, EtOAc:*n*-hexane) R_f : 0.39; R_t (RP C18 HPLC, 6:4, v/v, MeOH:MeCN): 5.99 min; IR (cm^{-1}): 3427 (br O-H ν), 2945 (C-H ν), 1664 (C=C ν), 1374, 1332 (C-H ρ), 1243, 1188 (C-C ν), 881 (=C-H δ), 835, 733 (C-H ρ); ^1H (500 MHz, CDCl_3): δ 5.35 (1H, dd, $J=5.13, 3.36$ Hz), 3.50 (1H α , p), 2.29 (1H α , d), 2.25 (1H β , d), 2.01 (1H β , t), 1.98 (1H α , t), 1.85 (1H α , m), 1.84 (1H β , t), 1.83 (2H, t), 1.59 (3H, s), 1.56 (1H α , t), 1.52 (1H β , t), 1.50 (1H β , m), 1.49 (1H, m), 1.46 (2H, q), 1.35 (1H β , m), 1.30 (2H, d), 1.25 (3H, s), 1.15 (1H α , t), 1.14 (2H, d), 1.10 (1H α , m), 1.08 (1H α , t), 1.06 (1H β , m), 1.02 (1H β , m), 1.01 (3H β , s), 0.95 (1H α , t), 0.92 (3H α , d), 0.91 (1H β , m), 0.87 (3H, d), 0.86 (3H, d), 0.68 (3H β , s); ^{13}C (125 MHz, CDCl_3): δ 140.76, 121.72, 71.82, 56.72, 56.11, 50.14, 46.06, 42.52, 42.31, 39.79, 39.61, 37.22, 36.52, 36.27, 36.22, 35.71, 31.91, 31.66, 29.72, 28.33, 28.01, 24.21, 23.83, 22.82, 21.09, 19.41, 19.31, 18.72, 11.87; COSY and HMBC HMBC data were given in Table 6.15. EIMS: found m/z 414.3868 $[\text{M}]^+$, cal. for $\text{C}_{29}\text{H}_{50}\text{O}$ 414.3862 (Δ 1.4 ppm). HRESI-MS (positive mode) m/z : for $\text{C}_{29}\text{H}_{51}\text{O}$ 415.3940 $[\text{M}+\text{H}]^+$.

6.2.8. Determination of bioactive potentials

6.2.8.1. *In vitro* antioxidant assays

6.2.8.1.A. 1,1-Diphenyl-2-picryl-hydrazil (DPPH) radical scavenging assay

The antioxidant activities of various chromatographic fractions and pure compounds isolated from the EtOAc:MeOH extracts of *P. malabarica* were measured using stable free radical, DPPH as explained in the sections 4.2.4.1.2.A. under Chapter 4.

6.2.8.1.B. 2,2'-Azino-bis-3-ethylbenzothiozoline-6-sulfonic acid diammonium salt (ABTS⁺) radical scavenging assay

The free radical quenching potentials of chromatographic fractions and pure compounds isolated from EtOAc:MeOH extracts of *P. malabarica* were evaluated by ABTS⁺ decolourization assay as explained in the sections 4.2.4.1.2.B. under Chapter 4.

6.2.8.2. *In vitro* anti-inflammatory assays**6.2.8.2.A. Cyclooxygenases (COX) inhibition assay**

The cyclooxygenase inhibitory experiments of chromatographic fractions along with pure compounds isolated from EtOAc:MeOH extracts of *P. malabarica* were carried out as explained in the sections 4.2.4.2.1. under Chapter 4.

6.2.8.2.B. 5-Lipoxygenase (5-LOX) inhibition assay

The 5-lipoxygenase inhibitory activity of chromatographic fractions and pure compounds isolated from EtOAc:MeOH extracts of *P. malabarica* were carried out as explained in the sections 4.2.4.2.2. under Chapter 4.

6.2.9. The structure-activity relationship analyses of secondary metabolites isolated from EtOAc:MeOH extract of *P. malabarica*

The structure-activity relationship analyses of bioactive secondary metabolites isolated EtOAc:MeOH extract of *P. malabarica* and standards (α -tocopherol and ibuprofen) were analyzed as explained in the section 5.2.9. under Chapter 5.

6.2.10. *In silico* molecular modeling

The *in silico* molecular modeling of secondary metabolites isolated EtOAc:MeOH extract of *P. malabarica* were performed by the method described in the sections 5.2.10.1. to 5.2.10.3. under Chapter 5.

6.2.11. Statistical analysis

Statistical analysis was carried out as detailed in section 5.2.11. under Chapter 5.

6.3. Results and discussion

6.3.1. Chromatographic fractionation, bioactive potentials and spectroscopic analysis of intermediate fractions from EtOAc:MeOH extract of *P. malabarica*

6.3.1.1. Chromatographic fractionation and bioactive potentials of intermediate fractions from EtOAc:MeOH extract of *P. malabarica*

The chromatographic fractionation of EtOAc:MeOH extract of *P. malabarica* afforded six pooled sub-fractions, named PM₁ to PM₆ based upon TLC (9:1, *n*-hexane:EtOAc, v/v) and RP C18 HPLC (MeOH/acetonitrile, 3:2, v/v) experiments. Also, six sub-fractions were checked for their target bioactive potentials against free radicals and pro-inflammatory enzymes. The yield and bioactivities of six column fractions were given in Table 6.1. The percentage yields of sub-fractions, PM₁ (5.80 g), PM₂ (8.66 g), PM₃ (6.42 g), PM₄ (3.53 g), PM₅ (1.70 g) and PM₆ (18.0 g) were found to be 11.60%, 17.32%, 12.84%, 7.06%, 3.40% and 36.00%, respectively. The sub-fractions PM₃, PM₄ and PM₆ were exhibited significantly greater ($p < 0.05$) DPPH radical scavenging potentials and their IC₅₀ values were found to be 0.73, 0.68 and 0.83 mg/mL, respectively when compared to PM₁ (IC₅₀ 1.32 mg/mL), PM₂ (IC₅₀ 1.68 mg/mL) and PM₅ (IC₅₀ 1.55 mg/mL). Similarly, the ABTS⁺ inhibitory effects were significantly greater ($p < 0.05$) for PM₃ (IC₅₀ 0.94 mg/mL), PM₄ (IC₅₀ 0.95 mg/mL) and PM₆ (IC₅₀ 0.84 mg/mL) when compared to PM₁ (IC₅₀ 1.53 mg/mL), PM₂ (IC₅₀ 1.90 mg/mL) and PM₅ (IC₅₀ 2.22 mg/mL). The anti-inflammatory potentials against COX-2 and 5-LOX enzymes were found to be significantly greater ($p < 0.05$) for the sub-fractions, PM₃, PM₄ and PM₆ and their IC₅₀ values were ranged from 0.88-0.92 and 0.84-0.89 mg/mL, respectively when compared to other sub-fractions (PM₁, PM₂ and PM₅). The sub-fractions, PM₁, PM₂ and PM₅ were registered IC₅₀ values of > 1.55 and > 1.70 mg/mL, respectively for COX-2 and 5-LOX inhibitions. Hence, the sub-fractions PM₃, PM₄ and PM₆ were regarded as appropriate for sequential fractionation to obtain potential bioactive compounds.

Table 6.1.: Yield and bioactive (antioxidant and anti-inflammatory) potentials of sub-fractions of EtOAc:MeOH extract of *P. malabarica*

Sub-fractions	#Yield		Bioactive potentials (IC ₅₀ values)			
			Antioxidant		Anti-inflammatory	
	g	%	*DPPH	*ABTS ⁺	*COX-2	*5-LOX
PM₁	5.80	11.60	1.32 ± 0.04 ^a	1.53 ± 0.05 ^a	1.72 ± 0.06 ^a	1.79 ± 0.07 ^a
PM₂	8.66	17.32	1.68 ± 0.04 ^b	1.90 ± 0.10 ^b	1.60 ± 0.17 ^a	1.72 ± 0.11 ^a
PM₃	6.42	12.84	0.73 ± 0.03 ^{cd}	0.94 ± 0.07 ^c	0.89 ± 0.03 ^b	0.87 ± 0.01 ^b
PM₄	3.53	7.06	0.68 ± 0.03 ^d	0.95 ± 0.05 ^c	0.88 ± 0.03 ^b	0.84 ± 0.01 ^b
PM₅	1.70	3.40	1.55 ± 0.05 ^b	2.22 ± 0.02 ^d	1.94 ± 0.01 ^c	1.96 ± 0.10 ^c
PM₆	18.00	36.00	0.83 ± 0.03 ^c	0.84 ± 0.07 ^c	0.92 ± 0.03 ^b	0.89 ± 0.01 ^b

[#]The percentage of yield was calculated on the basis of crude EtOAc:MeOH extract (50.0 g EtOAc:MeOH crude extract weight). *The IC₅₀ values were reported as mg/mL. The samples were analyzed in triplicate (n=3) and expressed as mean ± standard deviation. Means followed by different superscripts (a-d) within same column indicate significant differences ($p < 0.05$)

6.3.1.2. Spectroscopic analysis of intermediate fractions from EtOAc:MeOH extract of *P. malabarica*

The intermediate sub-fractions (PM₁-PM₆) were subjected to ¹H NMR analysis (Figure 6.3.) to acquire proton integral values corresponding to characteristic functional group signals (Table 6.2.). The proton integrals for fraction, PM₃ at δ 0.1-2.0 (saturated hydrocarbons), 2.0-2.5 (Ar-CH and acetylinic groups), 2.5-3.5 (-CH-C=O and -CH-Ar), 3.5-4.5 (electronegative groups) and 4.5-6.5 (vinylic, conjugated) were found to be 106.93, 14.04, 1.78, 1.76 and 3.13, respectively. Likewise, the proton integrals in regions δ 0.1-2.0, 2.0-2.5, 2.5-3.5, 3.5-4.5 and 4.5-6.5 were found to be 76.71, 5.60, 1.66, 3.05 and 2.70, respectively for PM₄ and 42.24, 4.07, 15.56, 3.28 and 18.14, respectively for PM₆. The sub-fractions, PM₁, PM₂ and PM₅ was registered lesser proton integrals in the regions of δ 2.0-2.5, 3.5-4.5 and 4.5-6.5, which were found to be 1.4-3.2, 0.26-1.1 and 0.11-2.5, respectively. In general, PM₃, PM₄ and PM₆ were displayed significantly greater proton integrals than PM₁, PM₂ and PM₅ when the potentially electronegative regions, δ 3.5-4.5 due to auxochromes and at δ 2.0-2.5 due to -CH₂=CH-CH₃ groups were taken into consideration. The signals at δ 0.1-2.0 were found to be

more prominent in fraction PM₃ (106.93), PM₄ (76.71) and PM₆ (42.24) which could be attributed to methylene $[-(\text{CH}_2)_n]$ envelope or end methylys in long alkyl chains.

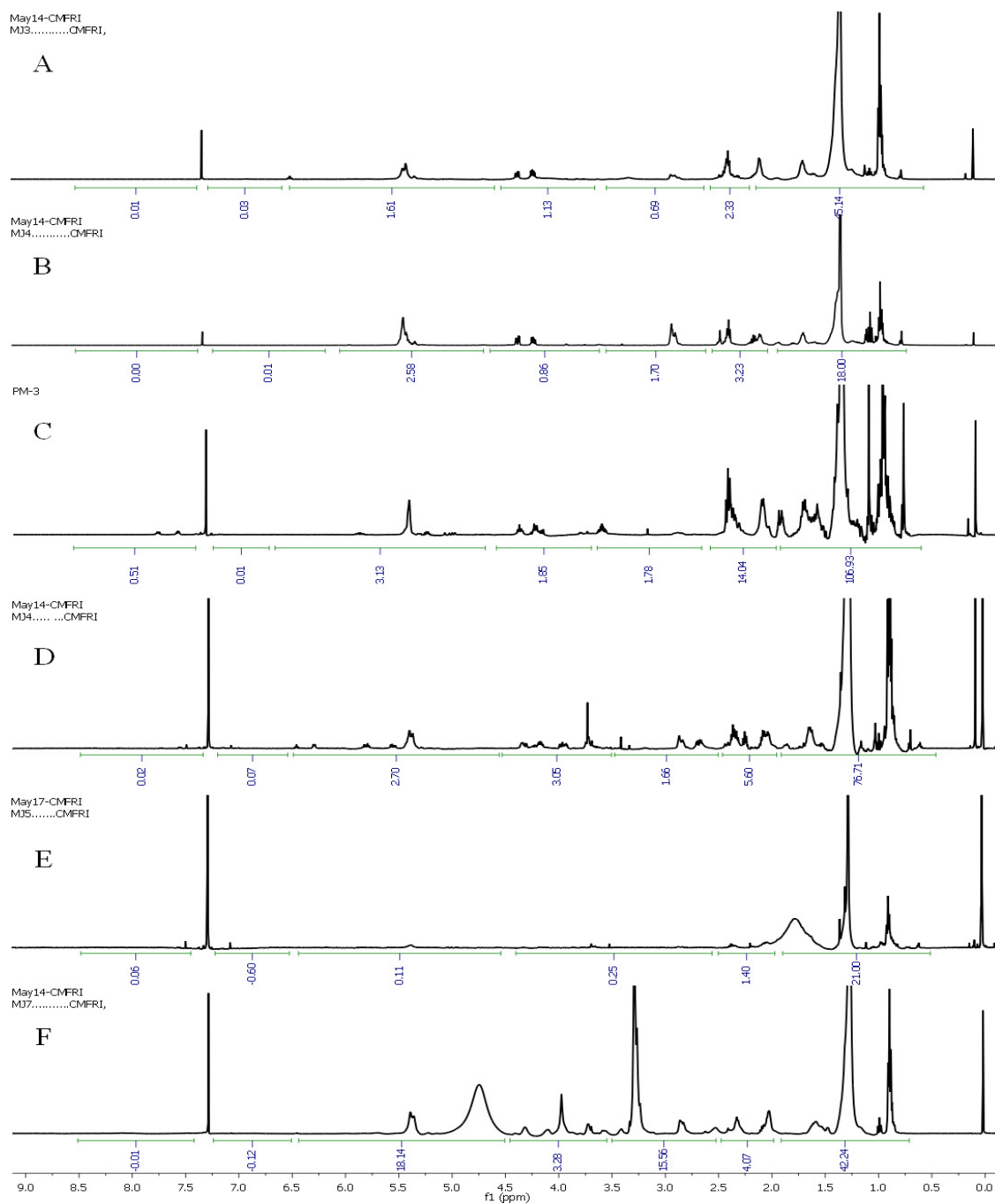


Figure 6.3.: ¹H NMR spectra of intermediate sub-fractions of (A) PM₁, (B) PM₂, (C) PM₃, (D) PM₄, (E) PM₅ and (F) PM₆ from EtOAc:MeOH extract of *P. malabarica* with integration values

The greater radical scavenging properties of PM₃, PM₄ and PM₆ might be attributed to greater electron donating methoxy/hydroxyl groups (δ 3.5-4.5) whereas PM₁, PM₂ and PM₅ were recorded comparatively lesser number of olefinic/oxygenated groups, and therefore, exhibited significantly lesser bioactivities. The sub-fraction, PM₆ displayed intense signals and greater number of proton integrals at δ 2.5-3.5 and 4.5-6.5 that ascribed to alkenic and electronegative auxochromes, such as alkoxy/alkyl halide/functionalized hydride H of the substituted alkanols followed by PM₃ and PM₄. In general, the fractions PM₃, PM₄ and PM₆ derived from EtOAc:MeOH extract of *P. malabarica* showed greater proton integrals than other column fractions when these potentially electronegative regions were taken into consideration. A significant co-linearity was found among bioactive potentials and deshielded electronegative functionalities present in the intermediate fractions of EtOAc:MeOH extract of *P. malabarica*.

The proton NMR based bioactivity analyses of intermediate fractions (PM₁-PM₆) suggested that the sub-fractions, PM₃, PM₄ and PM₆ could be considered as promising candidate fractions for further chromatographic purifications to isolate bioactive principles.

Table 6.2.: Types and integral values of protons obtained from the ¹H NMR spectra of sub-fractions of EtOAc:MeOH extract of *P. malabarica*

Proton signal (δ)	Proton integral (ΣH)					
	PM ₁	PM ₂	PM ₃	PM ₄	PM ₅	PM ₆
0.1-2.0	45.14	18.00	106.93	76.71	21.00	42.24
2.0-2.5	2.33	3.23	14.04	5.60	1.40	4.07
2.5-3.5	0.69	1.70	1.78	1.66	0.25	15.56
3.5-4.5	1.13	0.86	1.76	3.05	0.26	3.28
4.5-6.5	1.61	2.58	3.13	2.70	0.11	18.14
6.5-8.5	0.05	0.01	0.51	0.09	0.00	0.11

6.3.1.3. Isolation of bioactive secondary metabolites from EtOAc:MeOH extract of *P. malabarica*

The sub-fractions, such as PM₃, PM₄ and PM₆ were selected as candidate fractions for the isolation of bioactive compounds. The yield (in mg and in %), retention

factor (R_f), bioactivities (antioxidant/anti-inflammatory) of each column/flash/PTLC sub-fractions obtained from the candidate fractions were recorded in Table 6.3.-6.5.

The fraction, PM₃ (6.42 g; 12.84%) was subjected to vacuum liquid chromatography using the step-wise elution of *n*-hexane/EtOAc/MeOH to furnish 8 sub-groups, PM₃₋₁ to PM₃₋₈. Among these, column fractions, such as PM₃₋₃ (1.52 g; 3.04%) and PM₃₋₁ (1.50 g; 3.00%) were exhibited significantly higher antioxidant activities with respect to scavenge DPPH (IC_{50} 0.99 and 0.65 mg/mL, respectively) and ABTS⁺ (IC_{50} 0.94 and 0.69 mg/mL, respectively) radicals. The anti-inflammatory effects were also greater for PM₃₋₃ (IC_{50} anti-COX-2 0.98 and IC_{50} anti-5-LOX 1.03 mg/mL) and PM₃₋₁ (IC_{50} anti-COX-2 0.71 and IC_{50} anti-5-LOX 0.73 mg/mL) when compared to other fractions ($IC_{50} > 1.00$ mg/mL).

The sub-fraction, PM₃₋₃ was flash chromatographed using *n*-hexane/ EtOAc/ MeOH to yield four sub-fractions (PM₃₋₃₋₁ through PM₃₋₃₋₄) (Table 6.3.). The fraction, PM₃₋₃₋₁ (189 mg; 0.38%) and PM₃₋₃₋₂ (246 mg; 0.49%) were exhibited significantly greater antioxidant activities (IC_{50} DPPH inhibition 1.06 and 0.95 mg/mL, respectively; IC_{50} ABTS⁺ inhibition (1.08 and 0.97 mg/mL, respectively) radicals. The anti-inflammatory effects were greater for PM₃₋₃₋₁ (IC_{50} anti-COX-2 1.21 mg/mL and IC_{50} anti-5-LOX 1.10 mg/mL) and PM₃₋₃₋₂ (IC_{50} anti-COX-2 1.01 mg/mL and IC_{50} anti-5-LOX 1.10 mg/mL) when compared to other fractions ($IC_{50} > 1.00$ mg/mL for anti-COX-2 and anti-5-LOX). The fractions, PM₃₋₃₋₁ and PM₃₋₃₋₂ were fractionated over preparatory TLC to afford pure compounds, **10** (PM₃₋₃₋₁₋₁; 82 mg; yield 0.16%) and **9** (PM₃₋₃₋₂₋₁; 148 mg; yield 0.30%).

The sub-fraction, PM₃₋₁ was flash chromatographed using *n*-hexane/ EtOAc/MeOH to furnish two fractions (PM₃₋₁₋₁-PM₃₋₁₋₂) (Table 6.3.). The fractions, PM₃₋₁₋₁ (654 mg; 1.31%) and PM₃₋₁₋₂ (668 mg; 1.34%) were displayed higher antioxidant (IC_{50} ~0.72 and ~0.83 mg/mL, respectively) and anti-inflammatory (IC_{50} ~0.76 and ~0.93 mg/mL, respectively) potentials. The sub-fraction, PM₃₋₁₋₁ was purified through PTLC using *n*-hexane:EtOAc (24:1, v/v) to yield compound **3** (PM₃₋₁₋₁₋₁; 75 mg; yield 0.15%) along with a mixture, PM₃₋₁₋₁₋₂ (409 mg; 0.82%). Likewise, the sub-fraction PM₃₋₁₋₂ purified through PTLC using *n*-hexane:EtOAc (24:1, v/v) to yield compound **5** (PM₃₋₁₋₂₋₂; 90 mg; 0.18%) along with a mixture, PM₃₋₁₋₂₋₁ (406 mg; 0.81%).

Table 6.3.: Yield (in mg and in %), retention factor (R_f), bioactivities (antioxidant/anti-inflammatory) of column/flash/PTLC fractions obtained from the sub-fraction, PM₃ of EtOAc:MeOH extract of *P. malabarica*

	#Yield		R _f	*Bioactive potentials (IC ₅₀ value; mg/mL)			
	mg	%		Antioxidant		Anti-inflammatory	
				DPPH	ABTS ⁺	COX-2	5-LOX
PM ₃ CC (<i>n</i> -hexane/EtOAc/MeOH)	6420	12.84		0.73 ± 0.03	0.94 ± 0.07	0.89 ± 0.03	0.87 ± 0.01
PM ₃₋₁ (2% <i>n</i> -hexane)	1500	3.00		0.65 ± 0.01	0.69 ± 0.02	0.71 ± 0.02	0.73 ± 0.02
PM ₃₋₂ (6% EtOAc: <i>n</i> -hexane)	513	1.03		2.35 ± 0.05	2.42 ± 0.04	2.16 ± 0.04	2.12 ± 0.00
PM ₃₋₃ (10% EtOAc: <i>n</i> -hexane)	1520	3.04		0.99 ± 0.02	0.94 ± 0.01	0.98 ± 0.00	1.03 ± 0.02
PM ₃₋₄ (15% EtOAc: <i>n</i> -hexane)	640	1.28		1.17 ± 0.08	2.35 ± 0.05	1.85 ± 0.04	1.07 ± 0.01
PM ₃₋₅ (25% EtOAc: <i>n</i> -hexane)	227	0.45		2.42 ± 0.04	2.12 ± 0.00	1.42 ± 0.03	1.26 ± 0.07
PM ₃₋₆ (50% EtOAc: <i>n</i> -hexane)	540	1.08		1.92 ± 0.04	2.16 ± 0.04	1.25 ± 0.00	1.21 ± 0.02
PM ₃₋₇ (90% EtOAc: <i>n</i> -hexane)	329	0.66		1.55 ± 0.03	1.23 ± 0.05	1.17 ± 0.08	1.69 ± 0.01
PM ₃₋₈ (50% EtOAc:MeOH)	260	0.52		1.84 ± 0.03	1.36 ± 0.04	1.76 ± 0.02	1.68 ± 0.09
PM ₃₋₁ FC (<i>n</i> -hexane/EtOAc/MeOH)	1500	3.00		0.75	0.59 ± 0.06	0.69 ± 0.06	0.68 ± 0.06
PM ₃₋₁₋₁	654	1.31					
PM ₃₋₁₋₂	668	1.34					
PM ₃₋₁₋₁ PTLC (4% EtOAc: <i>n</i> -hexane)	654	1.31					
PM ₃₋₁₋₁₋₁ (Compound 3)	75	0.15					
PM ₃₋₁₋₁₋₂	409	0.82	0.32	1.76 ± 0.02	1.45 ± 0.01	1.36 ± 0.04	1.68 ± 0.09

PM₃₋₁₋₂ PTLC (4% EtOAc:<i>n</i>-hexane)	668	1.34					
PM ₃₋₁₋₂₋₁	406	0.81	0.64	0.99 ± 0.00	1.05 ± 0.05	1.03 ± 0.04	1.04 ± 0.05
PM₃₋₁₋₂₋₂ (Compound 5)	90	0.18	0.48	0.73 ± 0.07	0.79 ± 0.07	0.85 ± 0.07	0.82 ± 0.07
PM₃₋₃ FC (<i>n</i>-hexane/EtOAc/MeOH)	1520	3.04					
PM₃₋₃₋₁	189	0.38		1.06 ± 0.03	1.08 ± 0.02	1.21 ± 0.01	1.10 ± 0.02
PM₃₋₃₋₂	246	0.49		0.95 ± 0.01	0.97 ± 0.02	1.01 ± 0.04	1.10 ± 0.07
PM ₃₋₃₋₃	423	0.85		2.32 ± 0.01	2.26 ± 0.04	2.45 ± 0.05	2.49 ± 0.04
PM ₃₋₃₋₄	467	0.93		1.37 ± 0.08	1.36 ± 0.07	1.75 ± 0.04	1.99 ± 0.04
PM₃₋₃₋₁ PTLC (2% EtOAc:<i>n</i>-hexane)	189	0.38					
PM₃₋₃₋₁₋₁ (Compound 10)	82	0.16	0.39	1.01 ± 0.09	1.12 ± 0.09	1.15 ± 0.09	1.02 ± 0.09
PM₃₋₃₋₂ PTLC (2% EtOAc:<i>n</i>-hexane)	246	0.49					
PM₃₋₃₋₂₋₁ (Compound 9)	148	0.30	0.48	0.81 ± 0.09	0.98 ± 0.09	0.92 ± 0.09	0.96 ± 0.09

[#]The percentage of yield was calculated on the basis of crude EtOAc:MeOH extract (50.0 g EtOAc:MeOH crude extract weight). CC-column chromatography; FC-flash chromatography; PTLC-preparative thin layer chromatography; EtOAc-ethyl acetate; MeOH-methanol. The samples were analyzed in triplicate (n=3) and expressed as mean ± standard deviation. *The IC₅₀ values were reported as mg/mL

The fraction PM₄ (3.53 g; 7.06%) was flash chromatographed with gradient elution of *n*-hexane/EtOAc/MeOH to acquire seven (PM₄₋₁ to PM₄₋₇) fractions based on TLC (Table 6.4). The percentage yields for sub-fractions, PM₄₋₁ (716 mg), PM₄₋₂ (896 mg), PM₄₋₃ (794 mg), PM₄₋₄ (531 mg) and PM₄₋₅ (362 mg) were 1.43%, 1.79%, 1.59%, 1.06% and 0.72%, respectively, and these were found to be greater when compared to PM₄₋₆ (65 mg; 0.13%) and PM₄₋₇ (0.79 g; 0.16%). The sub-fractions, PM₄₋₁ to PM₄₋₅ were recorded higher antioxidant potentials against DPPH and ABTS⁺ radicals with lower IC₅₀ values (0.75-0.95 and 0.78-1.01 mg/mL, respectively) when compared to those recorded with PM₄₋₆-PM₄₋₇ (> 1.20 mg/mL). Similarly, the COX-2 and 5-LOX inhibitory potentials were found to be greater for PM₄₋₁ to PM₄₋₅ (IC₅₀ 0.79-0.97 and 0.79-1.10 mg/mL, respectively) compared to those recorded with PM₄₋₆-PM₄₋₇ (IC₅₀ > 1.45 and > 1.55 mg/mL, respectively).

The sub-fraction, PM₄₋₁ was further fractionated over PTLC on silica gel using *n*-hexane:EtOAc (49:1, v/v) to yield the compound **8** (PM₄₋₁₋₁; 90 mg; 0.18%) as major component. The fractionation of PM₄₋₃ over PTLC utilizing *n*-hexane:EtOAc (22:3, v/v) afforded compound **7** (PM₄₋₃₋₁; 118 mg; 0.24%). The fraction, PM₄₋₄ was further purified by PTLC over silica gel (GF₂₅₄) using *n*-hexane/EtOAc (43:7, v/v) to afford compound **6** (PM₄₋₄₋₁; 95 mg; 0.19%). The purification of sub-fraction, PM₄₋₂ over preparatory TLC (GF₂₅₄) using *n*-hexane:EtOAc (47:3 v/v) was yielded compound **4** (PM₄₋₂₋₁; 110 mg; 0.22%) as major component with bioactive potentials (Table 6.4.). The fraction, PM₄₋₅ was flash chromatographed using gradient elution of *n*-hexane/EtOAc to acquire three sub-groups (PM₄₋₅₋₁-PM₄₋₅₋₃). The yields of the sub-fractions, PM₄₋₅₋₁ (64 mg; 0.13%) and PM₄₋₅₋₂ (0.82 mg; 0.16%) were found to be lesser and recorded lower bioactive potentials when compared to PM₄₋₅₋₃. The bioactive sub-fraction, PM₄₋₅₋₃ (139 mg; 0.28%) was isolated by PTLC using EtOAc:*n*-hexane (10:90, v/v) solvent system to acquire compound **1** (PM₄₋₅₋₃₋₁; 65 mg; 0.13%) (Table 6.4.).

Table 6.4.: Yield (in mg and in %), retention factor (R_f), bioactivities (antioxidant/anti-inflammatory) of column/flash/PTLC fractions obtained from the sub-fraction, PM₄ of EtOAc:MeOH extract of *P. malabarica*

	#Yield		R _f	*Bioactive potentials (IC ₅₀ value; mg/mL)			
	mg	%		Antioxidant		Anti-inflammatory	
				DPPH	ABTS ⁺	COX-2	5-LOX
PM ₄ FC (<i>n</i> -hexane/EtOAc/MeOH)	3530	7.06		0.68 ± 0.03	0.95 ± 0.05	0.88 ± 0.03	0.84 ± 0.01
PM ₄₋₁	716	1.43		0.90 ± 0.03	0.98 ± 0.01	0.95 ± 0.04	1.03 ± 0.04
PM ₄₋₂	896	1.79		0.75 ± 0.01	0.78 ± 0.02	0.79 ± 0.02	0.79 ± 0.01
PM ₄₋₃	794	1.59		0.95 ± 0.02	1.01 ± 0.01	0.97 ± 0.06	1.10 ± 0.02
PM ₄₋₄	531	1.06		0.80 ± 0.01	0.82 ± 0.01	0.91 ± 0.03	0.90 ± 0.02
PM ₄₋₅	362	0.72		0.83 ± 0.04	0.86 ± 0.02	0.86 ± 0.01	0.85 ± 0.01
PM ₄₋₆	65	0.13		1.23 ± 0.05	1.36 ± 0.04	1.45 ± 0.01	1.55 ± 0.03
PM ₄₋₇	79	0.16		1.69 ± 0.01	1.68 ± 0.09	1.76 ± 0.02	1.84 ± 0.03
PM ₄₋₁ PTLC (2% EtOAc: <i>n</i> -hexane)	716	1.43	0.75	0.78 ± 0.06	0.92 ± 0.06	0.95 ± 0.06	1.02 ± 0.06
PM ₄₋₁₋₁ (Compound 8)	90	0.18					
PM ₄₋₂ PTLC (6% EtOAc: <i>n</i> -hexane)	896	1.79	0.38	0.56 ± 0.06	0.67 ± 0.06	0.72 ± 0.06	0.76 ± 0.07
PM ₄₋₂₋₁ (Compound 4)	110	0.22					
PM ₄₋₃ PTLC (12% EtOAc: <i>n</i> -hexane)	794	1.59	0.43	0.76 ± 0.06	0.96 ± 0.06	0.92 ± 0.06	1.06 ± 0.07
PM ₄₋₃₋₁ (Compound 7)	118	0.24					
PM ₄₋₄ PTLC (14% EtOAc: <i>n</i> -hexane)	531	1.06					

PM₄₋₄₋₁ (Compound 6)	95	0.19	0.65	0.65 ± 0.06	0.78 ± 0.06	0.82 ± 0.06	0.75 ± 0.07
PM₄₋₅ FC (<i>n</i>-hexane/EtOAc/MeOH)	362	0.72					
PM ₄₋₅₋₁	64	0.13		1.05 ± 0.01	1.04 ± 0.00	1.02 ± 0.02	1.03 ± 0.01
PM ₄₋₅₋₂	82	0.16		1.04 ± 0.01	1.03 ± 0.04	1.03 ± 0.01	1.09 ± 0.04
PM₄₋₅₋₃	139	0.28		0.75 ± 0.01	0.86 ± 0.02	0.86 ± 0.01	0.90 ± 0.04
PM₄₋₅₋₃ PTLC (10% EtOAc:<i>n</i>-hexane)	139	0.28					
PM₄₋₅₋₃₋₁ (Compound 1)	65	0.13	0.61	0.65 ± 0.06	0.74 ± 0.06	0.74 ± 0.06	0.81 ± 0.07

[#]The percentage of yield was calculated on the basis of crude EtOAc:MeOH extract (50.0 g EtOAc:MeOH crude extract weight). CC-column chromatography; FC-flash chromatography; PTLC-preparative thin layer chromatography; EtOAc-ethyl acetate; MeOH-methanol. The samples were analyzed in triplicate (n=3) and expressed as mean ± standard deviation. *The IC₅₀ values were reported as mg/mL

Table 6.5.: Yield (in mg and in %), retention factor (R_f), bioactivities (antioxidant/anti-inflammatory) of column/flash/PTLC fractions obtained from the sub-fraction, PM₆ of EtOAc:MeOH extract of *P. malabarica*

	#Yield		R _f	*Bioactive potentials (IC ₅₀ value; mg/mL)				
	mg	%		Antioxidant		Anti-inflammatory		
				DPPH	ABTS ⁺	COX-2	5-LOX	
PM ₆ CC (<i>n</i> -hexane/EtOAc/MeOH)	18000	36.00		0.83 ± 0.03	0.84 ± 0.07	0.92 ± 0.03	0.89 ± 0.01	
PM ₆₋₁ (2% <i>n</i> -hexane)	1123	2.25		1.05 ± 0.06	1.09 ± 0.05	1.23 ± 0.01	1.25 ± 0.02	
PM ₆₋₂ (6% EtOAc: <i>n</i> -hexane)	841	1.68		1.12 ± 0.00	1.16 ± 0.04	1.35 ± 0.08	1.42 ± 0.04	
PM ₆₋₃ (10% EtOAc: <i>n</i> -hexane)	2136	4.27		0.85 ± 0.00	0.86 ± 0.01	0.92 ± 0.03	0.96 ± 0.04	
PM ₆₋₄ (15% EtOAc: <i>n</i> -hexane)	1258	2.52		1.07 ± 0.01	1.21 ± 0.02	1.25 ± 0.00	1.42 ± 0.03	
PM ₆₋₅ (25% EtOAc: <i>n</i> -hexane)	1943	3.89		2.12 ± 0.00	2.16 ± 0.04	2.35 ± 0.05	2.42 ± 0.04	
PM ₆₋₆ (50% EtOAc: <i>n</i> -hexane)	1569	3.14		1.17 ± 0.08	1.26 ± 0.07	1.85 ± 0.04	1.92 ± 0.04	
PM ₆₋₃ FC (<i>n</i> -hexane/EtOAc/MeOH)	2136	4.27			0.82 ± 0.01	0.80 ± 0.03	0.90 ± 0.02	0.94 ± 0.02
PM ₆₋₃₋₁	746	1.49						
PM ₆₋₃₋₂	568	1.14						
PM ₆₋₃₋₃	345	0.69						
PM ₆₋₃₋₁ PTLC (40% EtOAc: <i>n</i> -hexane)	746	1.49	0.57	0.79 ± 0.02	0.76 ± 0.01	0.89 ± 0.03	0.92 ± 0.01	
PM ₆₋₃₋₁₋₁ (Compound 2)	92	0.18						

[#]The percentage of yield was calculated on the basis of crude EtOAc:MeOH extract (50.0 g EtOAc:MeOH crude extract weight).

CC-column chromatography; FC-flash chromatography; PTLC-preparative thin layer chromatography; TLC-thin layer chromatography; EtOAc-ethyl acetate; MeOH-methanol. The samples were analyzed in triplicate (n=3) and expressed as mean ± standard deviation. *The IC₅₀ values were recorded as mg/mL

The fraction, PM₆ (18.0 g; 36.0%) was subjected to chromatographic fractionation using *n*-hexane/EtOAc/MeOH step-wise elution to yield pooled fractions, named as PM₆₋₁-PM₆₋₆ (Table 6.5.). The sub-fraction, PM₆₋₃ (2136 mg; 4.27%) was registered greater bioactive potentials (IC₅₀ 0.85, 0.86, 0.92 and 0.96 mg/mL for DPPH, ABTS⁺, COX-2 and 5-LOX inhibitory potentials, respectively) when compared to other fractions (IC₅₀ values > 1.05 mg/mL). The sub-fraction, PM₆₋₃ was appeared to be a mixture, and chosen for flash chromatography using *n*-hexane/EtOAc to yield three pooled fractions (PM₆₋₃₋₁-PM₆₋₃₋₃). Repeated PTLC fractionation of PM₆₋₃₋₁ (746 mg; 1.49%) using EtOAc:*n*-hexane (40:60, v/v) yielded **2** (PM₆₋₃₋₁₋₁; 92 mg; 0.18%) as pure compound.

6.3.2. Spectroscopic analysis of bioactive secondary metabolites from EtOAc:MeOH extract of *P. malabarica*

Repetitive chromatographic fractionations of EtOAc:MeOH extract of the edible parts of *P. malabarica* yielded candidate bioactive secondary metabolites. The structures of identified metabolites were ascribed through extensive one (¹H, ¹³C and ¹³⁵DEPT NMR) and two (¹H-¹H COSY, HSQC, HMBC and NOESY) dimensional spectroscopic analyses combined with mass and FTIR experiments. The bioactive secondary metabolites isolated and characterized from the EtOAc:MeOH extract of *P. malabarica* were classified under various classes, such as aryl polyketide derivatives (**1-3**), tetrahydro chromenyl derivatives (**4-5**), isopimarane norditerpenoid (**6**), meroterpeno pyranoids (**7-8**) and cholestenol analogues (**9-10**).

6.3.2.1. Structural characterization of aryl polyketide derivatives (**1-3**)

Polyketide compounds with their pleotropic molecular frameworks and functional properties were reported in previous literatures and an attractive choice of natural product chemists. Polyketides characterize a wide range of natural products that usually contain multiple carbonyl groups (C=O) possessing variety of bio-potential functionalities, such as antioxidant, anti-bacterial, anti-inflammatory, anti-cholesterol, etc. They were biosynthesized by decarboxylative condensation of carboxylic acids through polyketide synthase (PKS) enzymes, which were classified into type-1, 2 and 3. Type-1

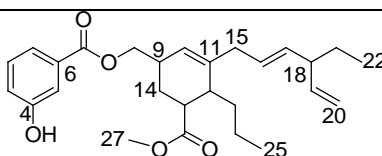
PKS was found to be an assembly of polypeptides similar to type-1 fatty acid synthase (FAS) and which consists of various enzyme domains (acyltransferase, ketoreductase etc.) to form diverse polyketide structures (Yu *et al.*, 2012). Type-2 PKS class belonged to type-2 FAS which was responsible for the biosynthesis of aromatic polyketides (Zhan 2009) whereas type-3 PKS catalyzed the formation of pyrones, chalcones, resorcinolic lipids and polypropionates (Yu *et al.*, 2012). Among all these, aryl polyketides were widely studied due to the promising bio-potentials. Also, these were an interesting class of compounds due to the presence of aromatic functionalities that can enhance its electronic properties (Zhan 2009). Notably, the polyketide compounds exhibited keto-enol resonance stabilization with adjacent $>C=O$ group leading to $-CH=C(-OH)-$ moiety. The greater resonance stabilization, presence of aromatic groups and ease of H-atom release onto DPPH radical to form stable DPPH were the prominent reasons for antioxidative properties of these aryl polyketides.

Several polyketides were reported from marine resources (Chakraborty *et al.*, 2017b), especially from marine shelled mollusks, such as gastropods/bivalves with potential antioxidant activities (Terlau and Olivera 2004). Pyrones, aryls, polypropionates and other related polyketides were previously reported from soft bodied mollusks (Di Marzo *et al.*, 1991). These polyketides were significant of marine mollusks and which were produced by the mollusk itself as part of their defense or communication (Davies-Coleman and Garson 1998; Vardaro *et al.*, 1992). There were few reports available for the occurrence of aryl enclosed polyketides in mollusks (Cutignano *et al.*, 2008) whereas, these were frequent in marine algae or mollusk associated bacteria (Blunt *et al.*, 2011; Chakraborty *et al.*, 2016d). Most of the reported polyketides were pyrone and polypropionate types for example polyketides reported from mollusks, *Cyerce cristallina* and *Onchidium sp.* (Davies-Coleman and Garson 1998; Di Marzo *et al.*, 1991). This is the first report of characterization of three new variants of aryl polyketides, featuring the aryl substituent from marine bivalve clam with potential bioactivities. Fewer studies were concentrated on small molecular bioactive secondary metabolites, such as phenolics, aryl derivatives, benzoates, and pyranoids from bivalves (Sala *et al.*, 2007). However, there have been sustained efforts to isolate newer chemistries of polyketides with bioactive properties compared to previously described molecules. Herein, we focused the structural

characterization of three aryl polyketide derivatives (**1-3**) from *P. malabarica*. Putative biosynthetic pathways catalyzed by polyketide synthase leading to the formation of polyketide compounds were used to corroborate the structural attributions.

6.3.2.1.A. Structural characterization of compound **1** (PM₄₋₅₋₃₋₁)

(13-(Methoxycarbonyl)-11-((*E*)-18-ethylhexa-16,19-dienyl)-12-propylcyclohex-10-enyl)-methyl-4-hydroxy benzoate (**1**)



Yield	65 mg; 0.13%
Physical description	Brown oily
Molecular formula	C ₂₇ H ₃₆ O ₅
Molecular mass	440.2563

The compound **1** was characterized as a hydroxy benzoate metabolite and purified as brown oily compound with molecular formula as C₂₇H₃₆O₅. It exhibited UV absorbance (in MeOH) at λ_{max} (log ϵ 3.90) 286.0 nm was assigned to a chromophore with ester carbonyl and olefinic groups (Figure 6.4.). The purity of the compound was supported by RP C18 HPLC experiments using MeOH:MeCN (3:2, v/v) (R_t 6.79) solvent system (Figure 6.5.).

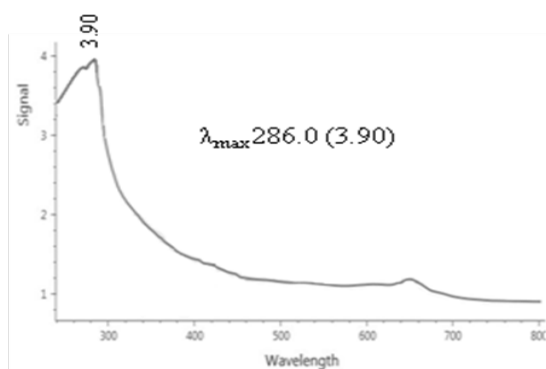


Figure 6.4.: UV spectrum of (13-(methoxycarbonyl)-11-((*E*)-18-ethylhexa-16,19-dienyl)-12-propylcyclohex-10-enyl)-methyl-4-hydroxy benzoate (**1**)

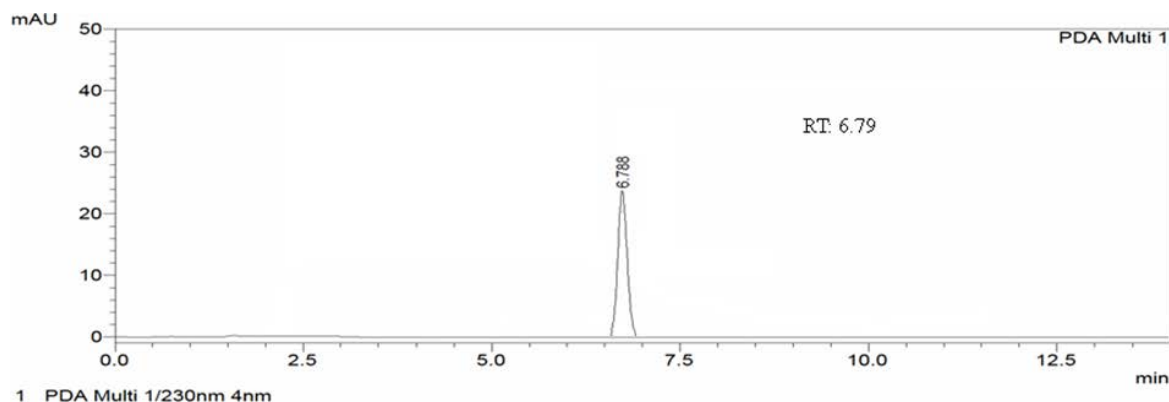


Figure 6.5.: HPLC chromatogram of (13-(methoxycarbonyl)-11-((*E*)-18-ethylhexa-16,19-dienyl)-12-propylcyclohex-10-enyl)-methyl-4-hydroxy benzoate (**1**)

The ^{13}C NMR spectrum of compound **1** displayed 27 peaks, whereas the multiplicities, such as five quaternary, twelve $-\text{CH}$, seven $-\text{CH}_2$ and three $-\text{CH}_3$ were confirmed by $^{135}\text{DEPT}$ experiment (Figure 6.9.-6.10.). The double bond equivalence was recorded as ten including eight double bonds and two ring moieties. Greater chemical shift values and coupling constants of four aromatic resonances at δ 8.10 (H-5, s), 7.12 (d, $J=9.36$ Hz, H-3), 7.36 (t, $J=7.89$ Hz, H-2) and 7.52 (d, $J=10.48$ Hz, H-1) designated the *meta* disubstituted aryl ring, and these attributions were corroborated by previous studies (Chakraborty *et al.*, 2016d; Khan *et al.*, 2015). The ^1H NMR spectrum displayed resonances at $\sim\delta$ 5.3 (proton integral of 3) representing non-conjugated *trans* diene with greater J values (Table 6.6.; Figure 6.8.). The deshielded signal at δ 4.08 (d) was attributed to carboxy methylene and that at δ 3.70 (s) was related to the carboxy methyl groups (Chakraborty *et al.*, 2016d). The cyclohex-10-enyl ring enclosed ^1H NMR signals at δ 2.02 (H-9), 5.35 ($J=8.95$ Hz, H-10), 2.31 (H-12), 1.33 (H-14) and 2.62 (H-13) along with an alkenic quaternary carbon at C-11 (δ 146.92). The ^1H spectrum suggested the presence of *trans* monosubstituted olefinic moiety due to the signals at δ 5.82 (p) and 4.97 (dd) with greater coupling constants ($J=11.26$ and 16.45 Hz, respectively). Further, HMBC correlations from δ 2.03 (H-18) to δ 114.06 (C-20); δ 1.31 (H-21) to δ 129.74 (C-17), 139.28 (C-19); δ 0.88 (H-22) to δ 31.93 (C-18); δ 1.28 (H-24) to δ 146.92 (C-11) and δ 3.70 (H-27) to δ 174.89 (C-26) confirmed the presence of 13-(methoxycarbonyl),11-(18-

ethylhexa-16,19-dienyl) and 12-propyl side chain attachments in **1** (Figure 6.6.B; Figure 6.13.). These attributions further corroborated by the four spin systems in ^1H - ^1H COSY which were H-1 to H-3 (δ 7.52/7.36/7.12) in aryl ring, H-8 (δ 4.08)/2.02 (H-9)/5.35 (H-10) and δ 2.02 (H-9)/1.33 (H-14)/2.62 (H-13)/2.31 (H-12)/1.32 (H-23)/1.28 (H-24)/0.98 (H-25) in 12-propylcyclohex-10-enyl-9-methyl group, H-15 to H-16 (δ 2.85/5.34), H-17 to H-20 (δ 5.34/2.03/5.82/4.97) together with δ 2.03 (H-18)/1.31 (H-21)/0.88 (H-22) in 18-ethylhexa-16,19-dienyl moiety (Figure 6.6.A; Figure 6.11.). The relative stereochemistries at C-9, C-18, C-12 and C-13 were deduced from NOESY interactions (Figure 6.7.; Figure 6.14.). The proton resonances at δ 2.02 (H-9) and 2.03 (H-18) displayed NOE cross peaks with δ 5.35 (H-10) and these were disposed in the similar plane, and therefore, considered as β -oriented. Intense NOE correlations among δ 2.31 (H-12) and 2.62 (H-13) inferred the orientation of protons in an identical plane of reference. However, these protons did not show NOE connections with the β -protons at H-9/H-18, therefore, attributed to α -oriented. The acetoxyl (-COOCH₃) group at C-13 was considered as β -oriented being opposite to α -disposed proton at C-13.

Table 6.6.: NMR spectroscopic data of (13-(methoxycarbonyl)-11-((*E*)-18-ethylhexa-16,19-dienyl)-12-propylcyclohex-10-enyl)-methyl-4-hydroxy benzoate (**1**) in CDCl₃

C. No.	^{13}C	^1H NMR (int.,mult., <i>J</i> in Hz) ^a	COSY	HMBC
1	136.47	7.52 (1H,d,10.48)	H-2	C-7
2	128.25	7.36 (1H,t,7.89)	H-3	-
3	124.45	7.12 (1H,d,9.36)	-	-
4	155.50	-	-	-
5	137.23	8.10 (1H,s)	-	C-7
6	133.63	-	-	-
7	167.98	-	-	-
8	67.55	4.08 (2H,d)	H-9	C-7
9	27.23	2.02 (1H β ,m)	H-10,14	C-10
10	129.73	5.35 (1H β ,d,8.95)	-	-
11	146.92	-	-	-
12	33.82	2.31 (1H α ,m)	H-13,23	C-26,24,9,15
13	30.20	2.62 (1H α ,m)	H-14	-
14	29.36	1.33 (2H,t)	-	C-13,12

15	25.63	2.85 (2H,dd)	H-16	-
16	129.73	5.34 (1H,q,10.48)	-	C-15
17	129.74	5.36 (1H,t,10.46)	H-18	-
18	31.93	2.03 (1H β ,m)	H-19,21	C-19,20
19	139.28	5.82 (1H,p,11.26)	H-20	-
20	114.06	4.97 (2H,dd,16.45,12.31)	-	-
21	22.69	1.31 (2H,m)	H-22	C-17,19
22	14.12	0.88 (3H,t)		C-18, 21
23	31.44	1.32 (2H,m)	H-24	-
24	29.66	1.28 (2H,m)	H-25	C-11
25	19.23	0.98 (3H,t)	-	-
26	174.89	-	-	-
27	50.55	3.70 (3H,s)		C-26

¹H NMR spectra recorded using Bruker AVANCE III 500MHz (AV 500) spectrometer (Bruker, Karlsruhe, Germany) in CDCl₃ as aprotic solvent at ambient temperature with TMS as the internal standard (δ 0 ppm). The ¹H NMR spectra were recorded at 500MHz, while the ¹³C NMR spectra were recorded at 125MHz. ^aValues in ppm, multiplicity and coupling constants (J =Hz) were indicated in parentheses. The assignments were made with the aid of the ¹H-¹H COSY, HSQC, HMBC and NOESY experiments

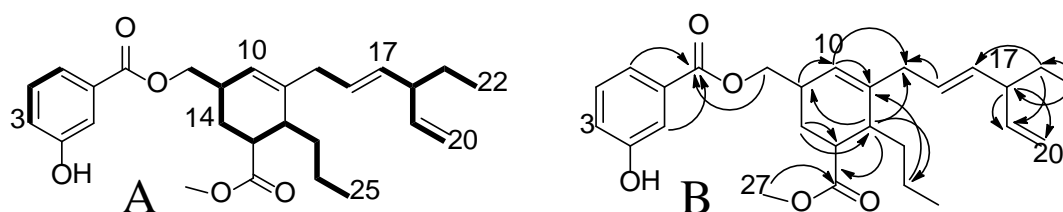


Figure 6.6.: ¹H-¹H COSY (A) and HMBC (B) correlations of (13-(methoxycarbonyl)-11-((*E*)-18-ethylhexa-16,19-dienyl)-12-propylcyclohex-10-enyl)-methyl-4-hydroxy benzoate (1). The key ¹H-¹H COSY couplings have been represented by the bold face bonds. The HMBC couplings were indicated by double barbed arrow

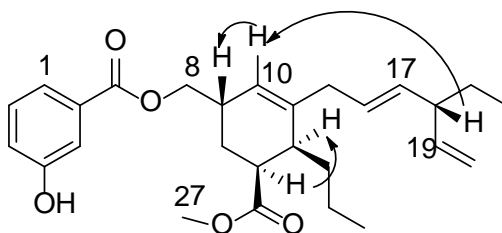


Figure 6.7.: NOESY correlations of (13-(methoxycarbonyl)-11-((*E*)-18-ethylhexa-16,19-dienyl)-12-propylcyclohex-10-enyl)-methyl-4-hydroxy benzoate (**1**). The NOESY relations were represented by double barbed arrow

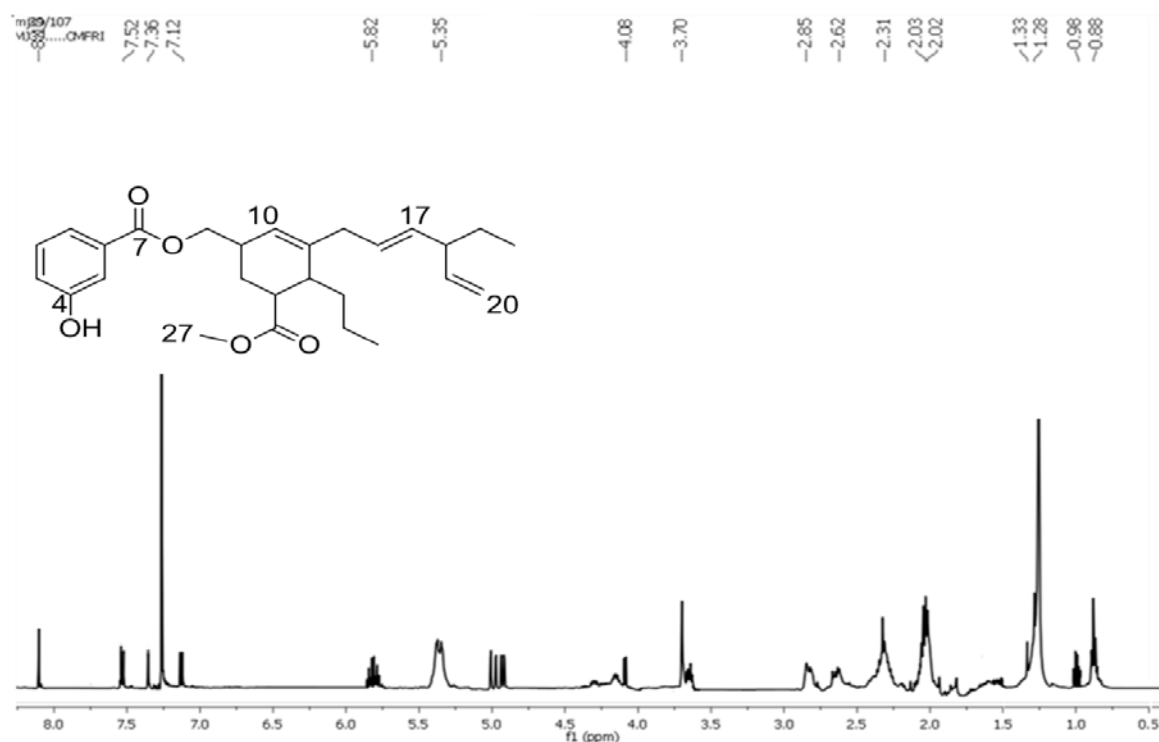


Figure 6.8.: ¹H NMR spectrum of (13-(methoxycarbonyl)-11-((*E*)-18-ethylhexa-16,19-dienyl)-12-propylcyclohex-10-enyl)-methyl-4-hydroxy benzoate (**1**)

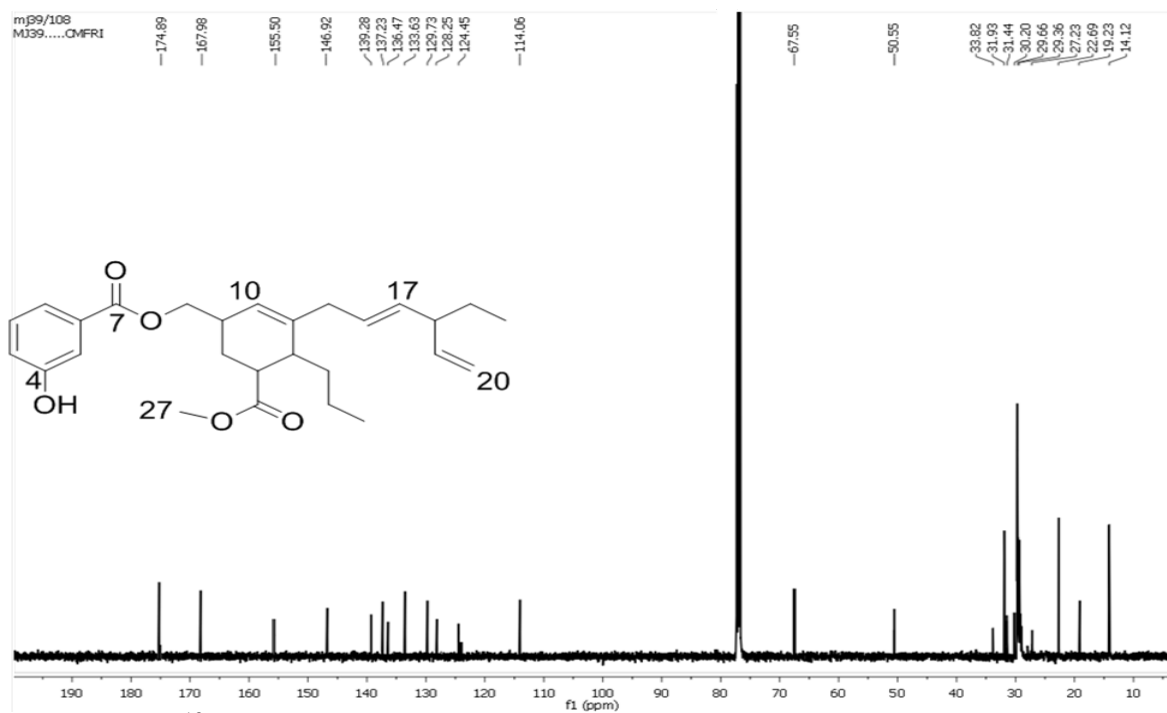


Figure 6.9.: ^{13}C NMR spectrum of (13-(methoxycarbonyl)-11-((*E*)-18-ethylhexa-16,19-dienyl)-12-propylcyclohex-10-enyl)-methyl-4-hydroxy benzoate (**1**)

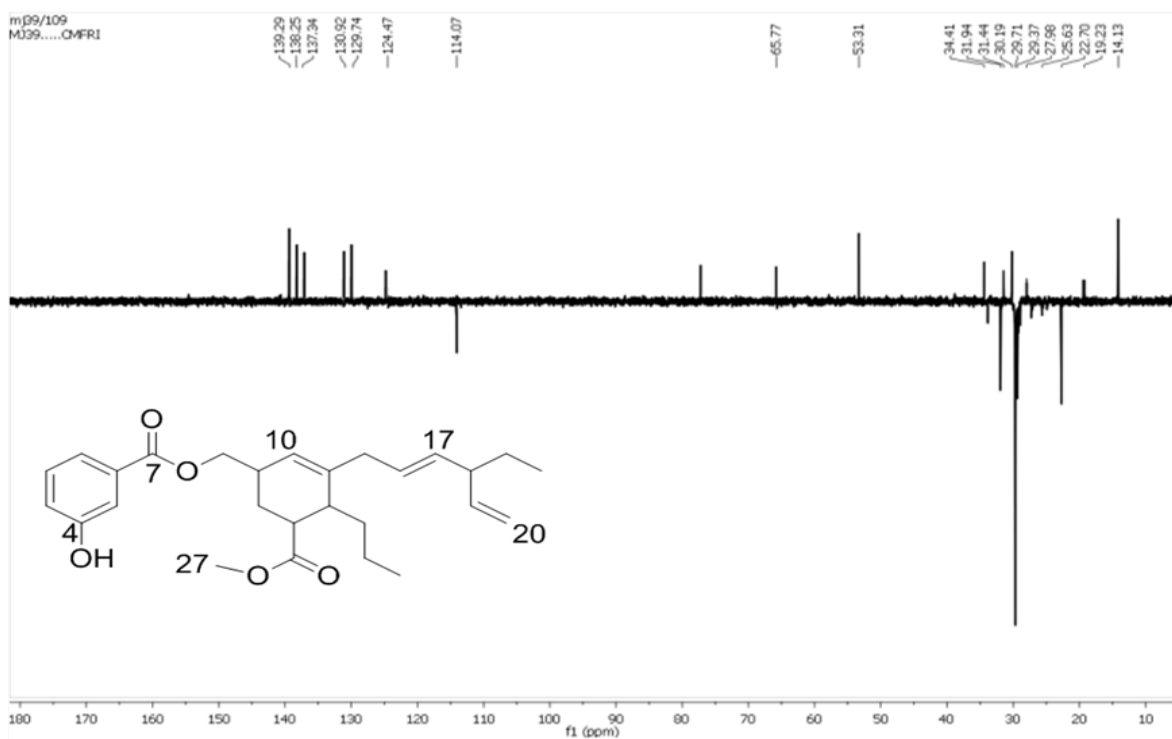


Figure 6.10.: $^{135}\text{DEPT}$ NMR spectrum of (13-(methoxycarbonyl)-11-((*E*)-18-ethylhexa-16,19-dienyl)-12-propylcyclohex-10-enyl)-methyl-4-hydroxy benzoate (**1**)

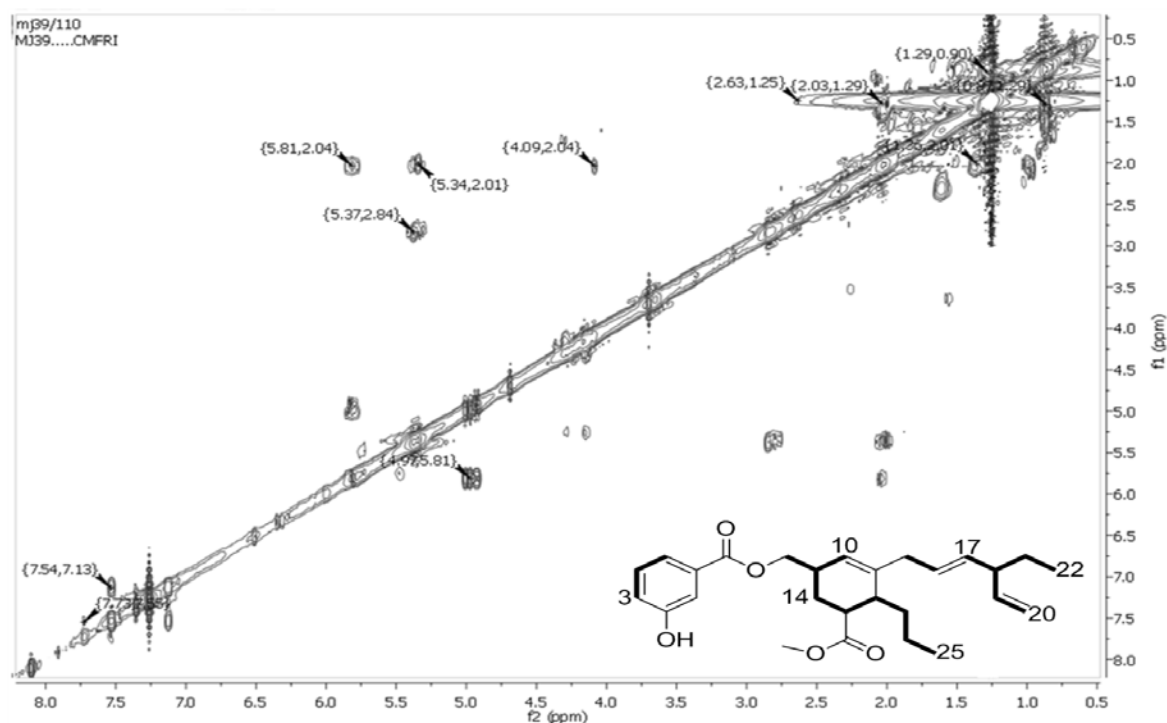


Figure 6.11.: ^1H - ^1H COSY NMR spectrum of (13-(methoxycarbonyl)-11-((*E*)-18-ethylhexa-16,19-dienyl)-12-propylcyclohex-10-enyl)-methyl-4-hydroxy benzoate (**1**)

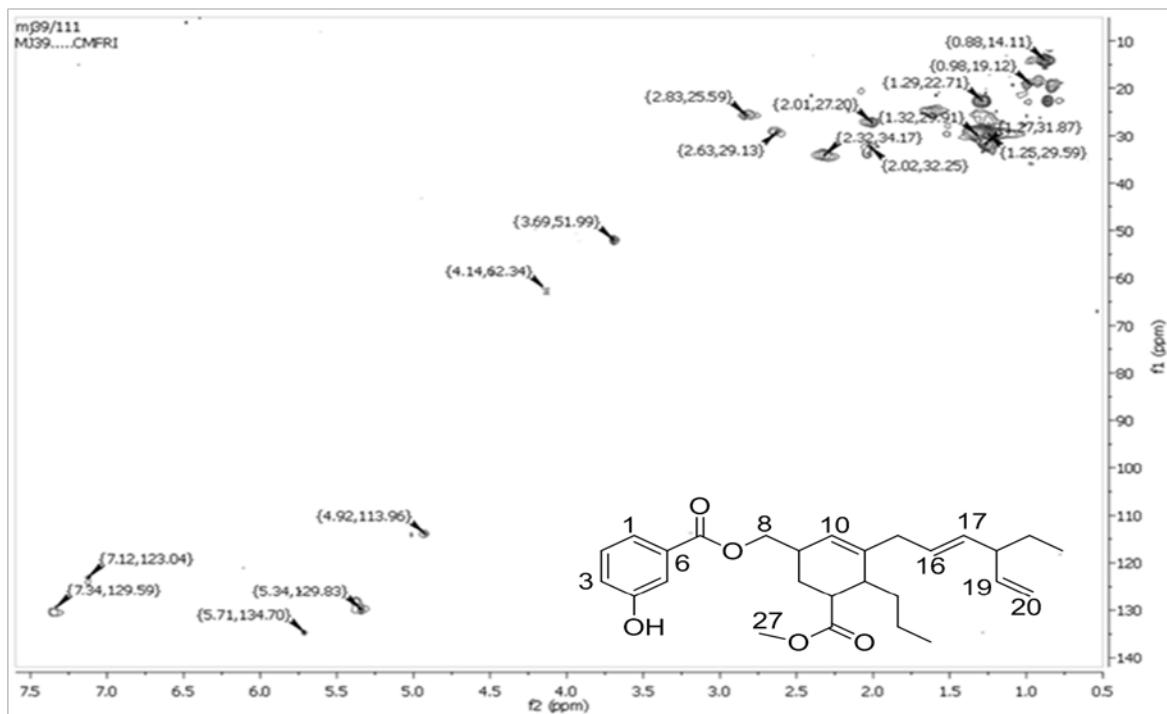


Figure 6.12.: HSQC NMR spectrum of (13-(methoxycarbonyl)-11-((*E*)-18-ethylhexa-16,19-dienyl)-12-propylcyclohex-10-enyl)-methyl-4-hydroxy benzoate (**1**)

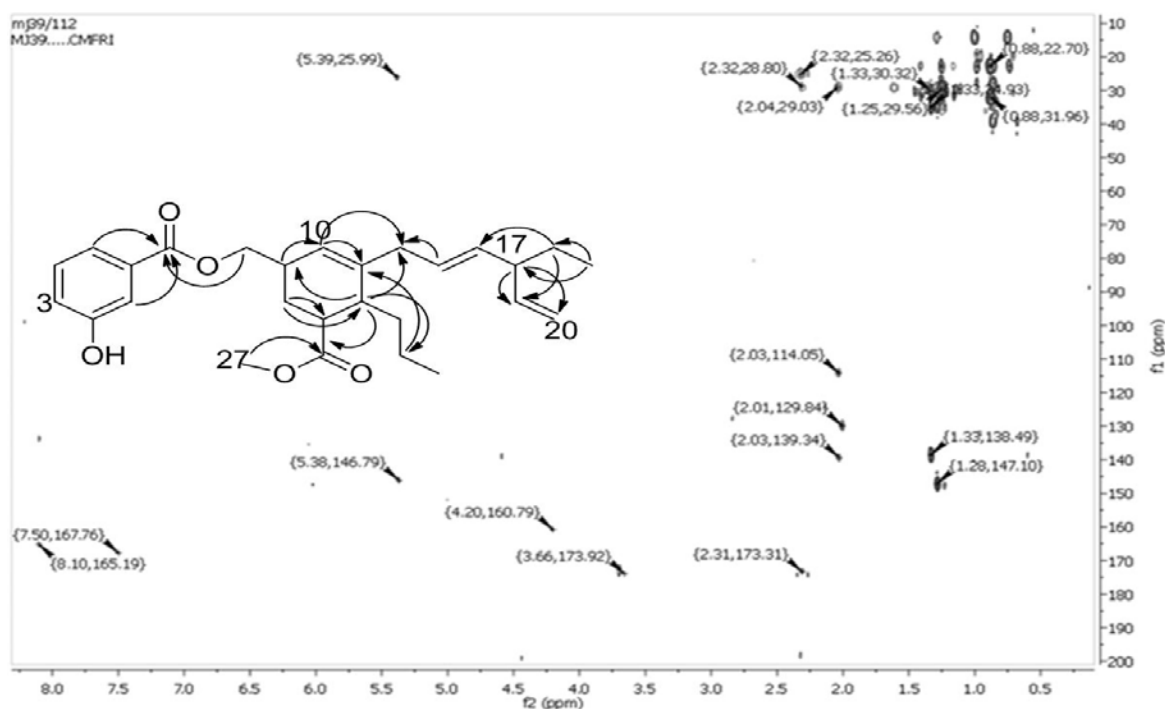


Figure 6.13.: HMBC NMR spectrum of (13-(methoxycarbonyl)-11-((*E*)-18-ethylhexa-16,19-dienyl)-12-propylcyclohex-10-enyl)-methyl-4-hydroxy benzoate (**1**)

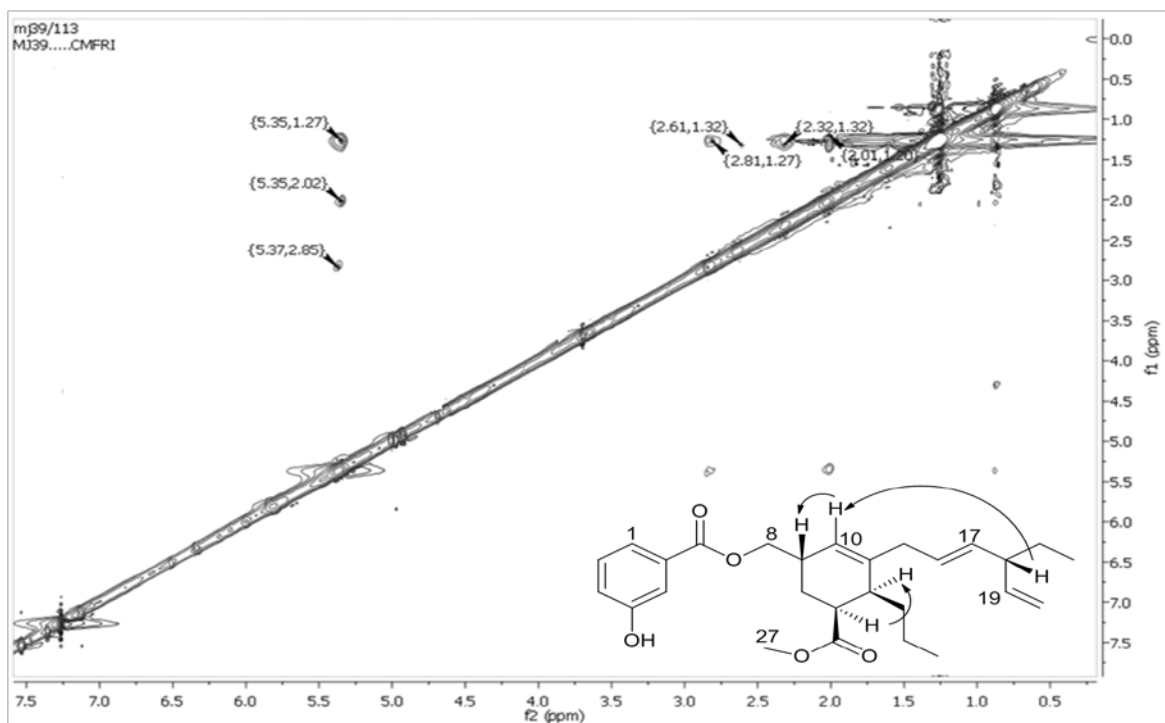


Figure 6.14.: NOESY NMR spectrum of (13-(methoxycarbonyl)-11-((*E*)-18-ethylhexa-16,19-dienyl)-12-propylcyclohex-10-enyl)-methyl-4-hydroxy benzoate (**1**)

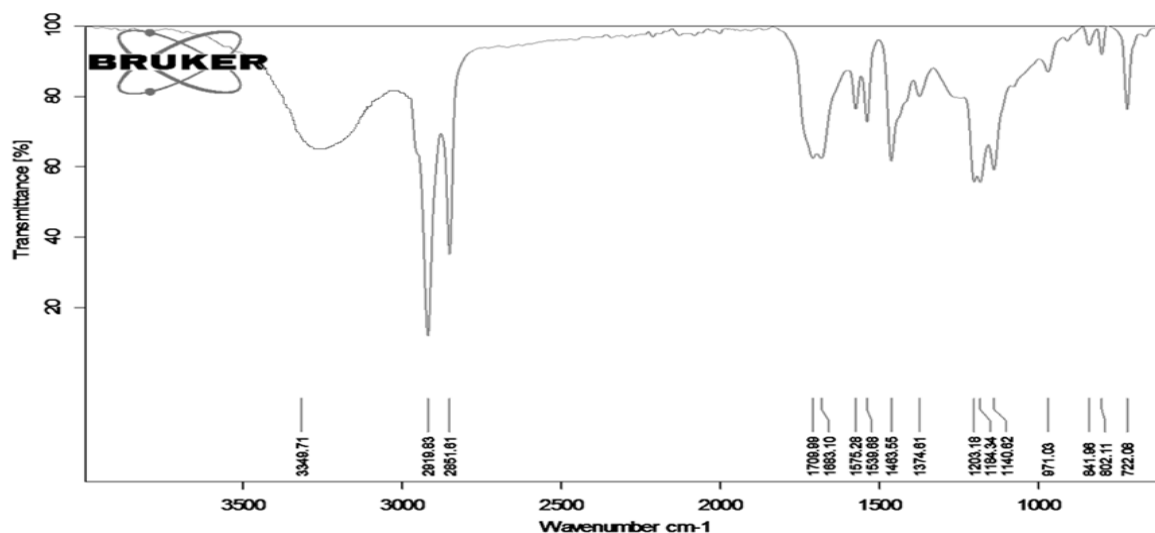


Figure 6.15.: FTIR spectrum of (13-(methoxycarbonyl)-11-((*E*)-18-ethylhexa-16,19-dienyl)-12-propylcyclohex-10-enyl)-methyl-4-hydroxy benzoate (**1**)

The compound **1** exhibited ester carbonyl stretching vibration (1709 cm^{-1}) along with quaternary carbon signals due to δ 167.98 and 174.89 ($-\text{COOCH}_3$). The IR frequency at ~ 1580 and 3349 cm^{-1} represented the aromatic alkene and broad hydroxyl stretching vibrations, respectively. The stretching vibrations at 2919 and 2851 cm^{-1} denoted the C-H alkyl absorptions. The C-C stretching vibrations at $1184\text{--}1140\text{ cm}^{-1}$ and C-H bending vibrations at 1483 cm^{-1} were apparent (Figure 6.15.).

The compound **1** recorded its molecular ion peak at m/z 440 (found m/z 440.2565 $[\text{M}]^+$, cal. for $\text{C}_{27}\text{H}_{36}\text{O}_5$ 440.2563) in the mass spectrum (Figure 6.16.) that underwent elimination of methoxy radical followed by methyl, $\text{CHO}\cdot$, butyl and methyl radicals were yielded the fragmented ions at m/z 409 (**b**), 395 (**c**), 366 (**d**), 311 (**e**) and 297 (**f**), respectively. The latter ion on sequential fragmentations exhibited peaks at m/z 270 (**g**, significant peak), 244 (**h**), 204 (**j**), 191 (**k**, but-9-enyl-4-hydroxy benzoate), 177 (**l**, butyl benzoate) and 160 (**m**). The fragment, **m** further fragmented to **n** with m/z 146 which signified to vinyl benzoate radical on removal of methyl radical. The benzene cation was reported at m/z 77 (**q**) from the fragment, **p** on $\text{CHO}_2\cdot$ radical elimination and which was considered as the base peak of compound **1** (Figure 6.17.).

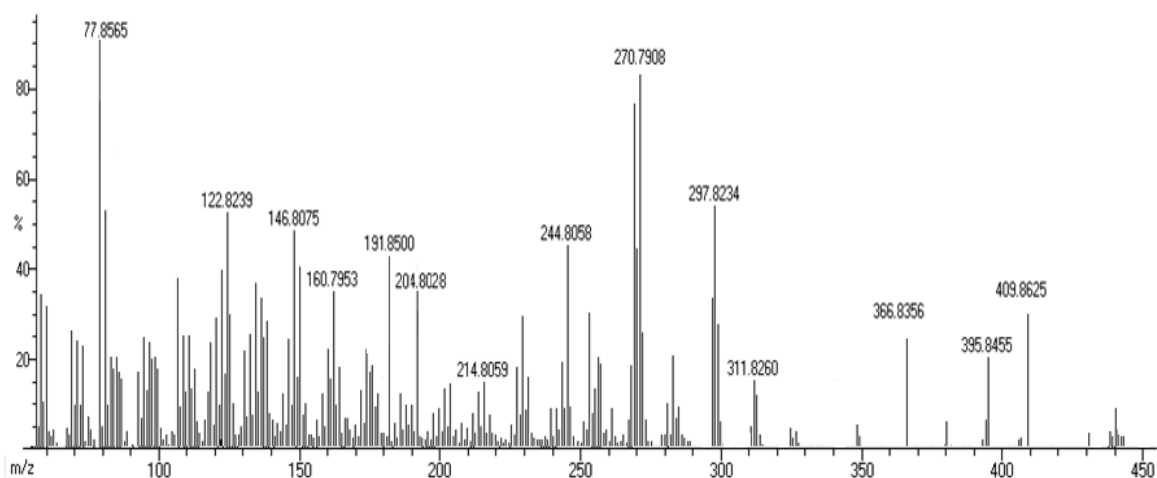


Figure 6.16.: EIMS spectrum of (13-(methoxycarbonyl)-11-((*E*)-18-ethylhexa-16,19-dienyl)-12-propylcyclohex-10-enyl)-methyl-4-hydroxy benzoate (**1**)

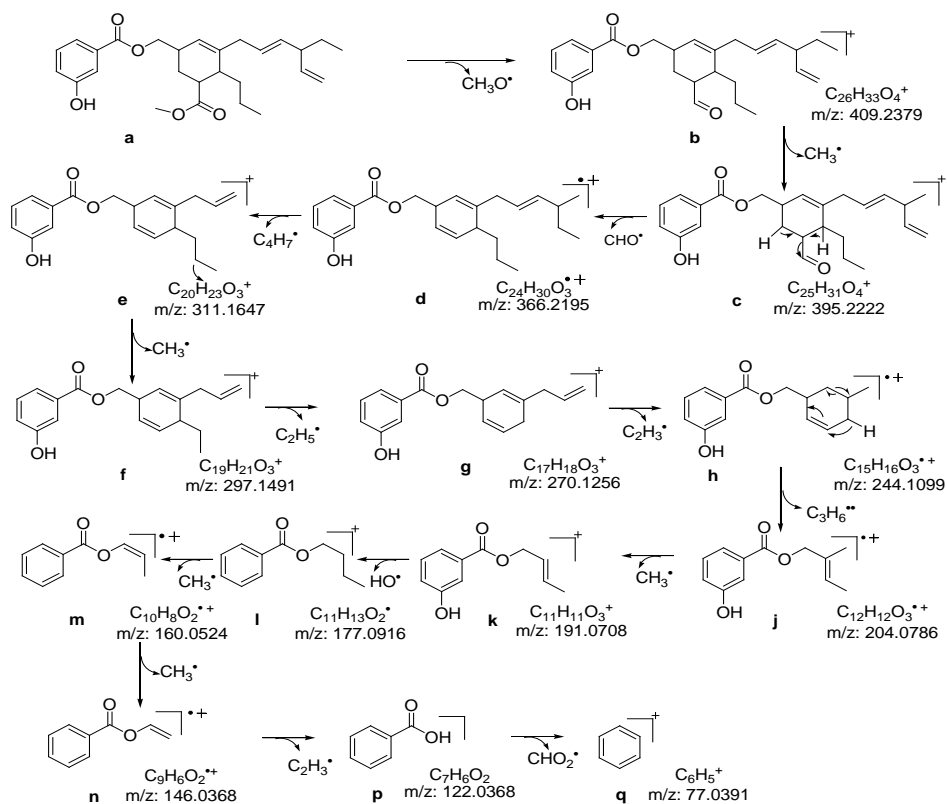


Figure 6.17.: Mass fragmentation pattern of (13-(methoxycarbonyl)-11-((*E*)-18-ethylhexa-16,19-dienyl)-12-propylcyclohex-10-enyl)-methyl-4-hydroxy benzoate (**1**)

6.3.2.1.1. Biogenic origin of the polyketide synthase (PKS) catalyzed aryl polyketide derivative (1)

The PKS-bound malonate and 3-ethylpent-4-enethioate clusters were the building blocks to initiate the formation of the intermediate 5-ethyl-3-oxohept-6-enethioate bound to the biosynthetic enzyme cascade. Subsequent rearrangements and intramolecular cyclizations of the latter afforded PKS-bound methyl-3-((*E*)-4-ethylhexa-2,5-dienyl)-5-(hydroxymethyl)-2-propylcyclohex-3-enecarboxylate. The latter appeared to undergo nucleophilic attack at hydroxyl end (situated terminally) on PKS activated carbonyl carbon of 3-hydroxy benzothioate. Subsequent elimination of acyl carrier protein (ACP)/KS-enzyme cascade by thiolase appeared to result in the formation of **1** (Figure 6.18.).

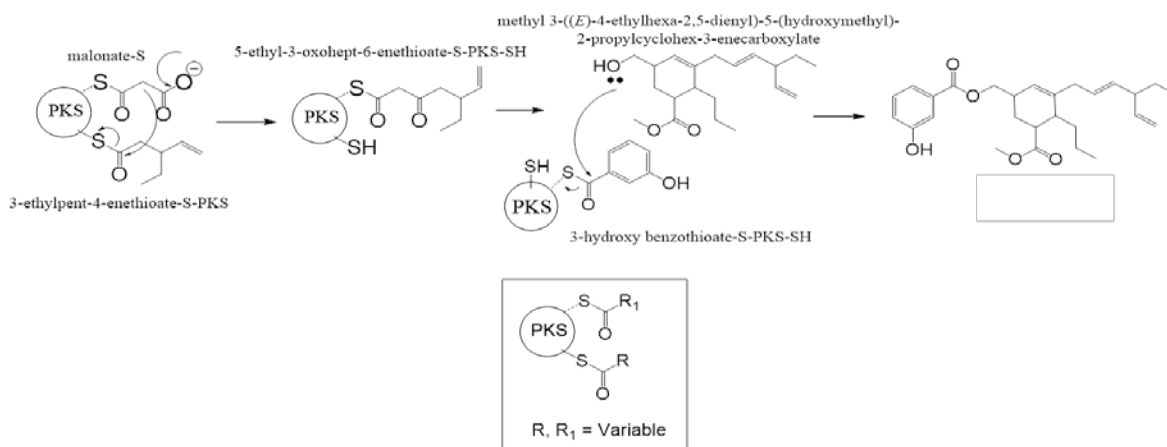
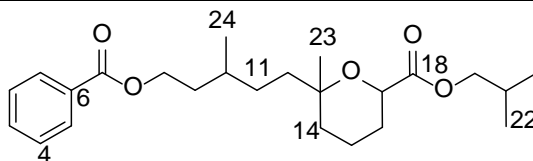


Figure 6.18.: Schematic representation of biosynthetic pathway of (13-(methoxycarbonyl)-11-((*E*)-18-ethylhexa-16,19-dienyl)-12-propylcyclohex-10-enyl)-methyl-4-hydroxy benzoate (**1**)

6.3.2.1.B. Structural characterization of compound 2 (PM₆₋₃₋₁₋₁)

Isobutyl-13-(6-(benzoyloxy)-10-methylpentyl)-tetrahydro-13-methyl-2H-pyran-17-carboxylate (2)



Sample yield	92 mg; 0.18%
Physical description	Yellow oily
Molecular formula	$C_{24}H_{36}O_5$
Molecular mass	404.2563

The titled benzoate derivative (**2**) was purified as yellowish oil, and elucidated as $C_{24}H_{36}O_5$ with detailed NMR/mass spectroscopy and compared with earlier works (Chakraborty *et al.*, 2016d; Chakraborty *et al.*, 2017c). It exhibited UV absorbance (in MeOH) at λ_{\max} (log ϵ 3.50) 261.0 nm, and was assigned to a chromophore with ester carbonyl and olefinic groups (Figure 6.19.). The purity of the compound was supported by RP C18 HPLC experiments using 3:2 (v/v) MeOH:MeCN (R_t 5.32) solvent system (Figure 6.20.).

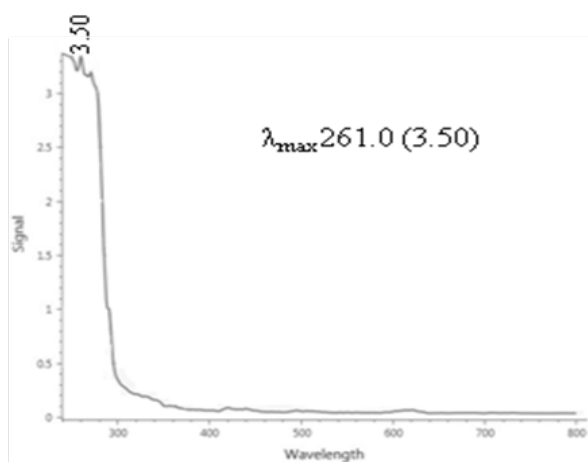


Figure 6.19.: UV spectrum of isobutyl-13-(6-(benzoyloxy)-10-methylpentyl)-tetrahydro-13-methyl-2*H*-pyran-17-carboxylate (**2**)

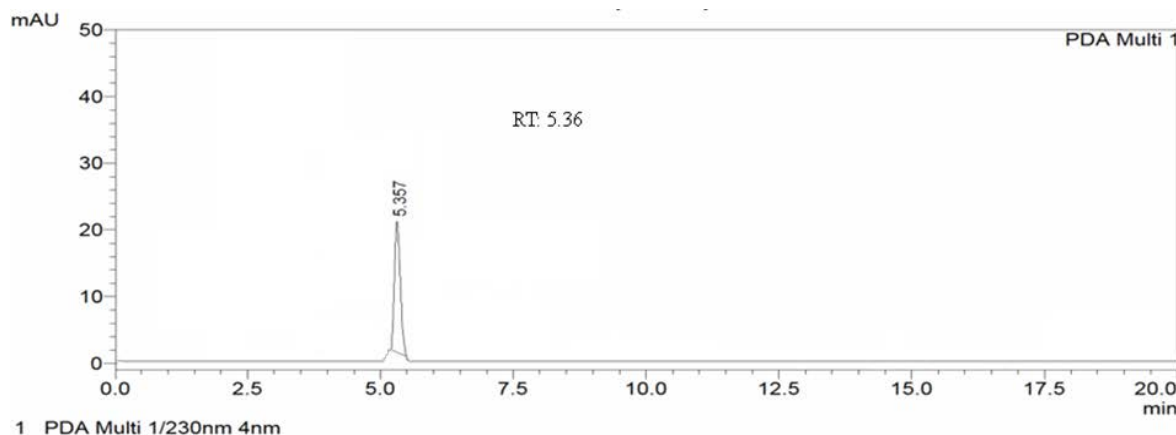


Figure 6.20.: HPLC chromatogram of isobutyl-13-(6-(benzoyloxy)-10-methylpentyl)-tetrahydro-13-methyl-2*H*-pyran-17-carboxylate (**2**)

The NMR signals in aromatic region confirmed the presence of benzyl group and greater chemical shift of aromatic quaternary carbon at C-6 (δ 132.32) was attributed to adjacent $-\underline{\text{C}}(=\text{O})-\text{O}-$ moiety at C-7 (δ 167.69) (Table 6.7.; Figure 6.23.-6.24.). The protons at δ 4.23 and 4.02 displayed HSQC correlations with δ 65.51 (C-8) and 71.77 (C-19), respectively, and were adjacent to carbonyls at C-7 and C-18, respectively (HMBCs). The IR stretching vibration due to aromatic alkene (1599 cm^{-1}) and $^{13}\text{C}/^1\text{H}$ (δ 130-128/7.45-7.65) peaks (HSQC) including the aromatic quaternary carbon at δ 132.32 unambiguously established the presence of aromatic moiety in **2** (Huong *et al.*, 2004) (Figure 6.27.). Seven degrees of unsaturations were recorded, and among which four were related to aryl, one was due to the pyran ring and the remaining two were accounted for the double bonds (C=O). The multiplicities of carbons were established from $^{135}\text{DEPT}$ spectrum, which recognized the possibilities of seven methylenes ($-\text{CH}_2$), four methyls ($-\text{CH}_3$), three methines ($-\text{CH}$) (one oxygenated) along with three quaternary positions. The HMBC correlations due to the aromatic protons δ 7.65 (H-1) and δ 7.45 (H-4) to C-7 (δ 167.69) confirmed the occurrence of monosubstituted benzoyloxy group. The ^1H NMR signal at δ 5.10 ($-\underline{\text{CH}}-$) exhibiting HSQC with δC 72.38 (C-17) was placed between the oxygen atom and carbonyl ($-\underline{\text{C}}=\text{O}$) group of isobutyl-carboxylate chain. The one bond $^1\text{H}-^1\text{H}$ COSY recorded four spin systems, which were attributed to δ 7.65 (H-1)/7.45 (H-2) in the benzyl ring, δ 4.23 (H-8)/1.64 (H-9)/1.37 (H-10)/1.26 (H-11), 0.88 (H-24); δ 1.26 (H-11)/1.52 (H-

12) in methylpentyl chain, δ 1.47 (H-14)/1.34 (H-15)/1.61, 1.27 (H-16)/5.10 (H-17) in pyran ring and δ 4.02 (H-19)/1.97 (H-20)/0.92 (H-21), 0.91 (H-22) in isobutyl end (Figure 6.21.A, 6.26.). The HMBC couplings from δ 4.23 (H-8) to δ 167.69 (C-7), 19.75 (C-10); δ 1.64 (H-9) to δ 13.77 (C-24); δ 1.37 (H-10) to δ 65.51 (C-8); δ 1.52 (H-12) to δ 67.23 (C-13); δ 1.26 (H-11) to δ 38.05 (C-14), 67.23 (C-13); δ 1.18 (H-23) to δ 67.23 (C-13), 19.75 (C-10) and δ 0.88 (H-24) to δ 19.75 (C-10), 30.57 (C-9) unambiguously established the 13-(6-(benzoyloxy)-10-methylpentyl)-tetrahydro-13-methyl-2*H*-pyran moiety in **2** (Figure 6.21.B, 6.28.). This pyran moiety attached to the isobutyl-carboxylate at C-17 was predicted from intense HMBC cross peaks due to δ 5.10 (H-17) to δ 71.77 (C-19), 167.01 (C-18) together with δ 4.02 (H-19) to δ 167.01 (C-18), 19.16 (C-21), 19.13 (C-22) and δ 1.97 (H-20) to δ 19.13 (C-22) thus establishing the structure of **2** (Chakraborty *et al.*, 2017b). Relative spatial configuration of the stereochemical centres at C-17 and C-10 were appropriately described by NOESY correlations (Figure 6.22., 6.29.). The NOE couplings between δ 1.37 (H-10) and 1.61 (H-16) attributed that these were located in similar plane and considered as α -disposed. NOE connections among the protons at δ 5.10 (H-17)/1.27 (H-16)/0.88 (H-24)/1.18 (H-23) assigned them in identical plane of symmetry, whereas these protons did not display NOE cross peaks with the α -oriented H-10 and H-16 protons, and therefore, considered as β -disposed.

Table 6.7.: NMR spectroscopic data of isobutyl-13-(6-(benzoyloxy)-10-methylpentyl)-tetrahydro-13-methyl-2*H*-pyran-17-carboxylate (**2**) in CDCl₃

C. No	¹³ C	¹ H (int.,mult., <i>J</i> in Hz) ^a	COSY	HMBC
1	128.81	7.65 (1H,d,7.15)	H-2	C-2,7
2	130.83	7.45 (1H,t,9.53)	-	C-1
3	130.74	7.46 (1H,t,8.58)	-	-
4	130.90	7.45 (1H,d,10.21)	H-5	C-7
5	128.71	7.64 (1H,d,9.17)	-	-
6	132.32	-	-	-
7	167.69	-	-	-
8	65.51	4.23 (2H,t)	H-9	C-7,9,10
9	30.57	1.64 (2H,m)	H-10	C-8,10,24
10	19.75	1.37 (1H α ,m)	H-11,24	C-8,9,24,13,12

11	31.92	1.26 (2H,m)	H-12	C-10,13,14
12	26.20	1.52 (2H,t)	-	-
13	67.23	-	-	-
14	38.05	1.47 (2H,m)	H-15	C-15
15	18.81	1.34 (2H,m)	H-16	-
16	22.69	1.61 (1H α ,m) 1.27 (1H β ,m)	H-17	C-17
17	72.38	5.10 (1H β ,dd)	-	C-18,19
18	167.01	-	-	-
19	71.77	4.02 (2H,d)	H-20	C-18,20,21,22
20	27.73	1.97 (1H,m)	H-21,22	C-22
21	19.16	0.92 (3H,d)	-	C-19,20
22	19.13	0.91 (3H,d)	-	C-20
23	29.69	1.18 (3H β ,s)	-	C-10, 13
24	13.77	0.88 (3H β ,d)	-	C-9,10

¹H NMR spectra recorded using Bruker AVANCE III 500MHz (AV 500) spectrometer (Bruker, Karlsruhe, Germany) in CDCl₃ as aprotic solvent at ambient temperature with TMS as the internal standard (δ 0 ppm). The ¹H NMR spectra were recorded at 500MHz, while the ¹³C NMR spectra were recorded at 125MHz. ^aValues in ppm, multiplicity and coupling constants (J =Hz) were indicated in parentheses. The assignments were made with the aid of the ¹H-¹H COSY, HSQC, HMBC and NOESY experiments

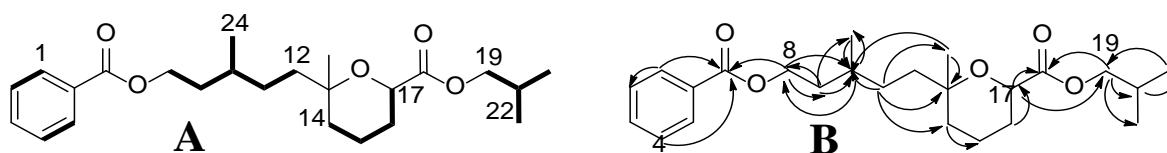


Figure 6.21.: ¹H-¹H COSY (A) and HMBC (B) correlations of isobutyl-13-(6-(benzoyloxy)-10-methylpentyl)-tetrahydro-13-methyl-2H-pyran-17-carboxylate (**2**). The key ¹H-¹H COSY couplings have been represented by the bold face bonds. The HMBC couplings were indicated by double barbed arrow

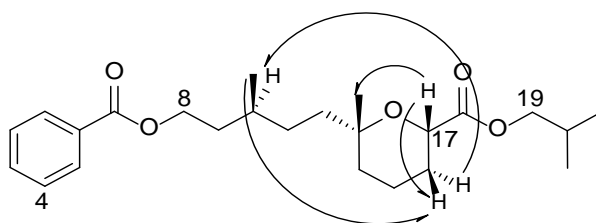


Figure 6.22.: NOESY correlations of isobutyl-13-(6-(benzoyloxy)-10-methylpentyl)-tetrahydro-13-methyl-2*H*-pyran-17-carboxylate (**2**). The NOESY relations were represented by double barbed arrow



Figure 6.23.: ^1H NMR spectrum of isobutyl-13-(6-(benzoyloxy)-10-methylpentyl)-tetrahydro-13-methyl-2*H*-pyran-17-carboxylate (**2**)

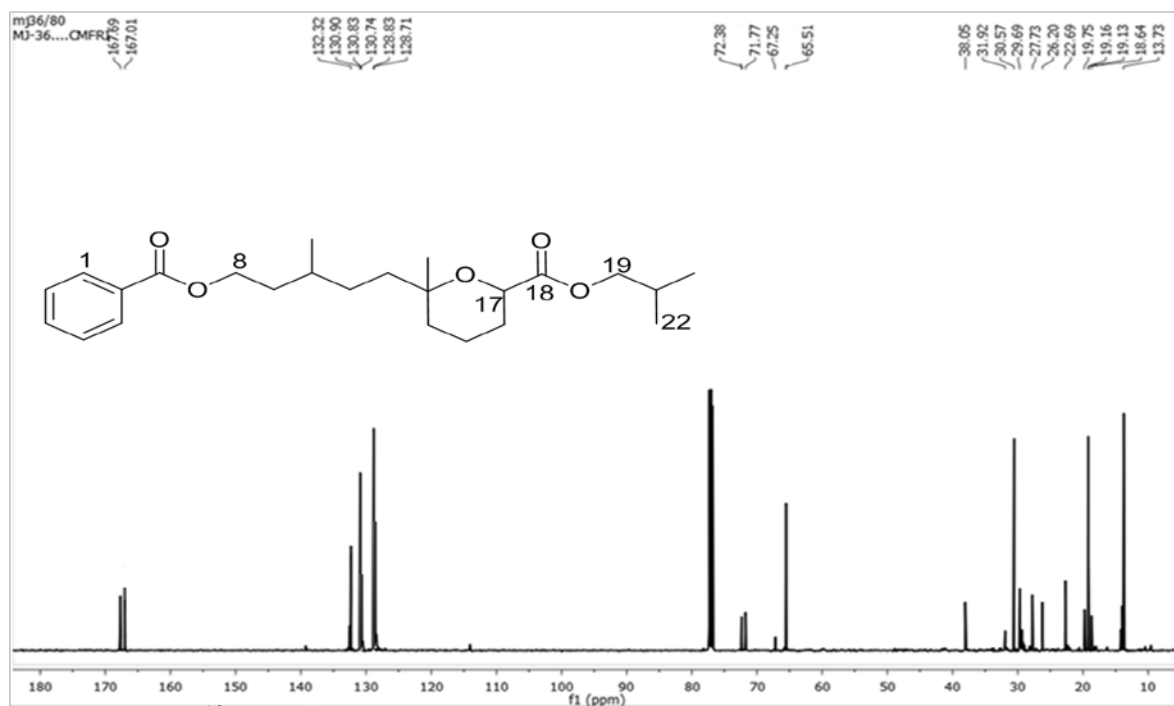


Figure 6.24.: ^{13}C NMR spectrum of isobutyl-13-(6-(benzoyloxy)-10-methylpentyl)-tetrahydro-13-methyl-2*H*-pyran-17-carboxylate (**2**)

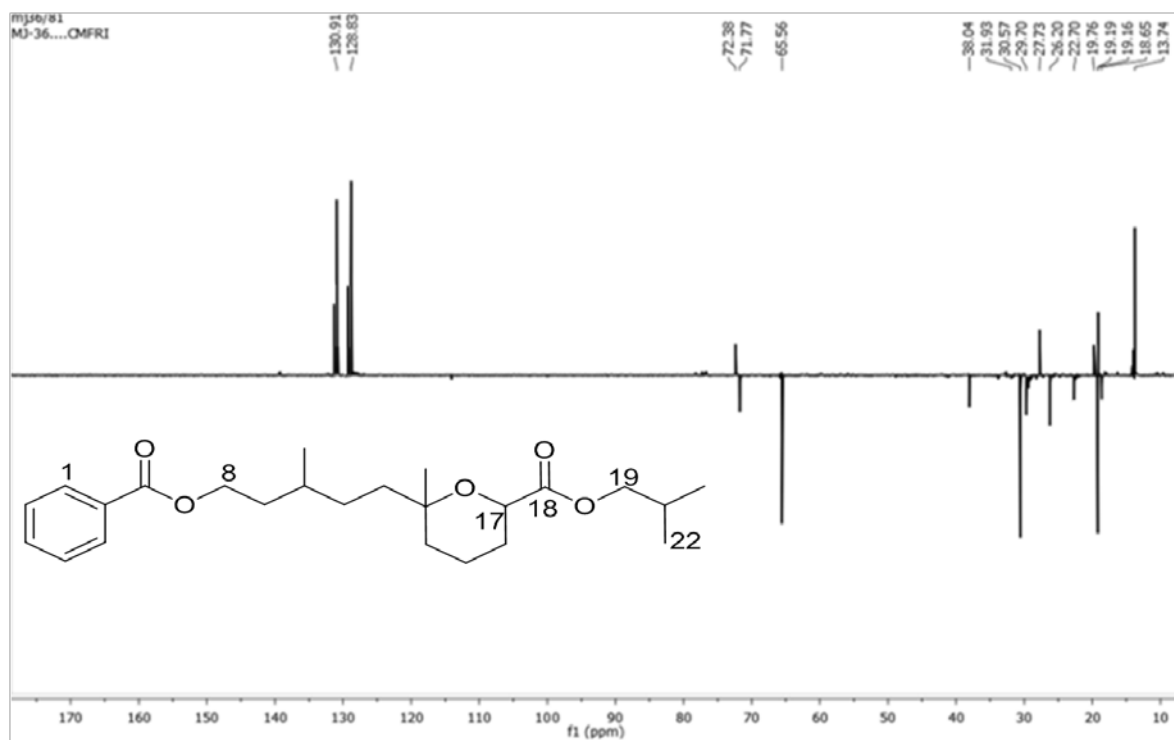


Figure 6.25.: $^{135}\text{DEPT}$ NMR spectrum of isobutyl-13-(6-(benzoyloxy)-10-methylpentyl)-tetrahydro-13-methyl-2*H*-pyran-17-carboxylate (**2**)

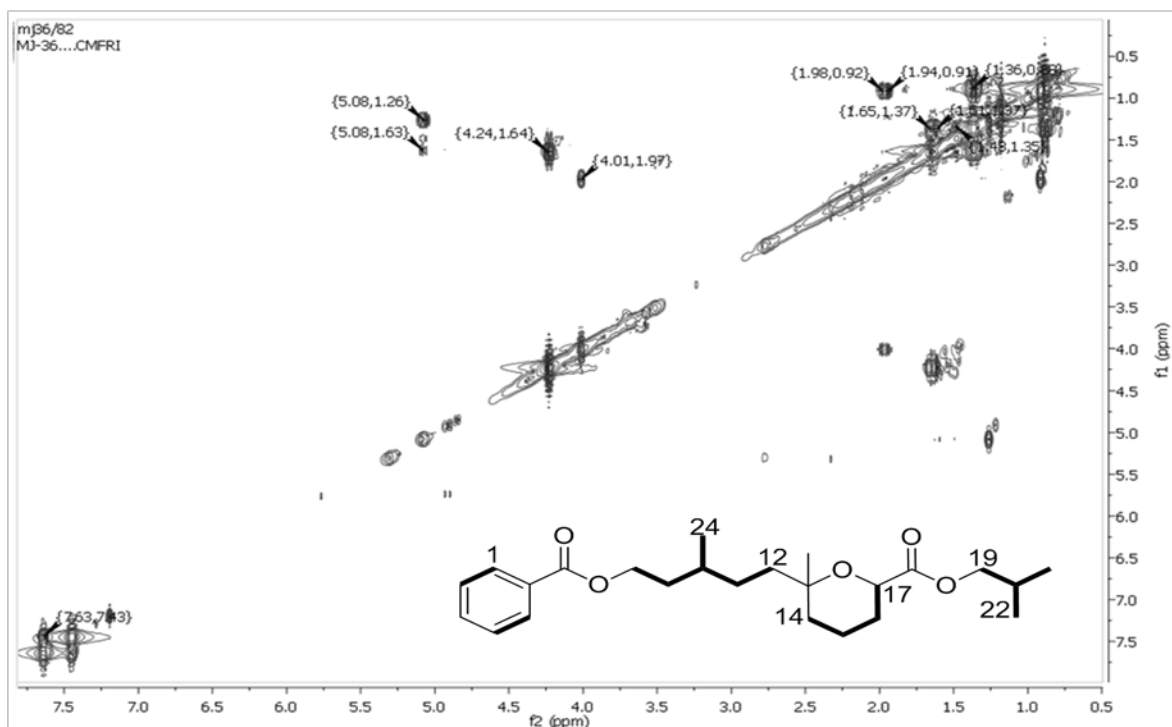


Figure 6.26.: ^1H - ^1H COSY NMR spectrum of isobutyl-13-(6-(benzoyloxy)-10-methylpentyl)-tetrahydro-13-methyl-2*H*-pyran-17-carboxylate (**2**)

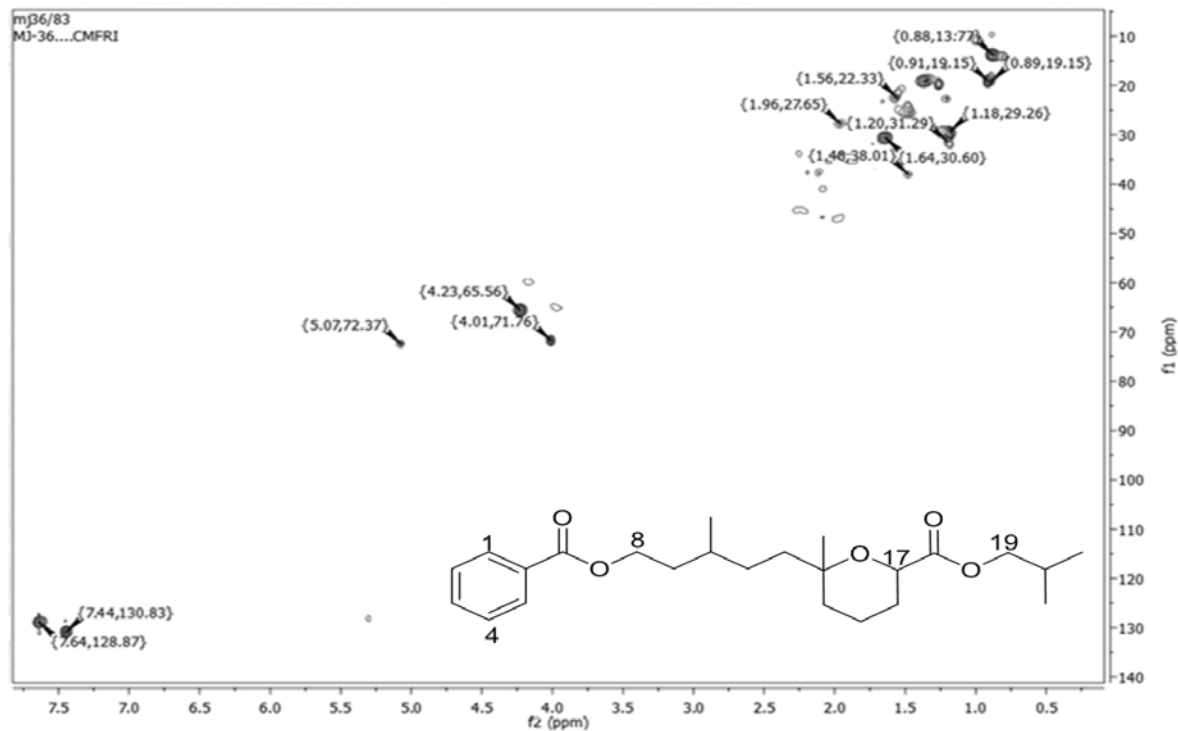


Figure 6.27.: HSQC NMR spectrum of isobutyl-13-(6-(benzoyloxy)-10-methylpentyl)-tetrahydro-13-methyl-2*H*-pyran-17-carboxylate (**2**)

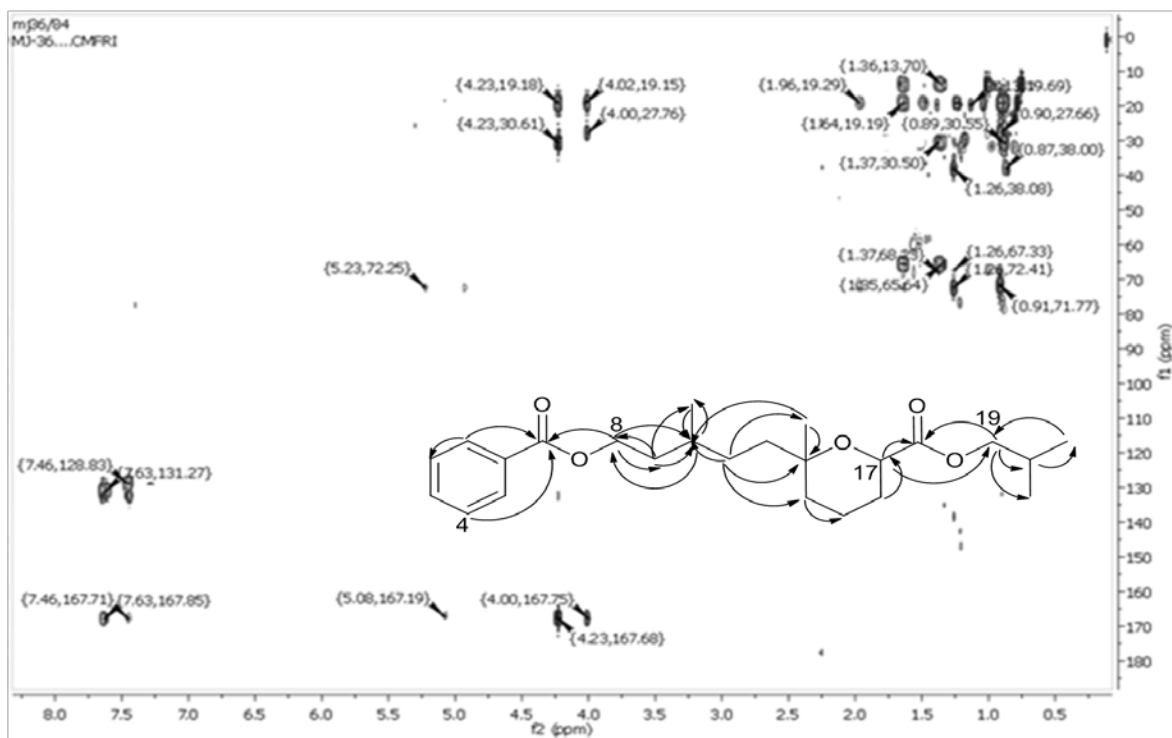


Figure 6.28.: HMBC NMR spectrum of isobutyl-13-(6-(benzoyloxy)-10-methylpentyl)-tetrahydro-13-methyl-2*H*-pyran-17-carboxylate (**2**)

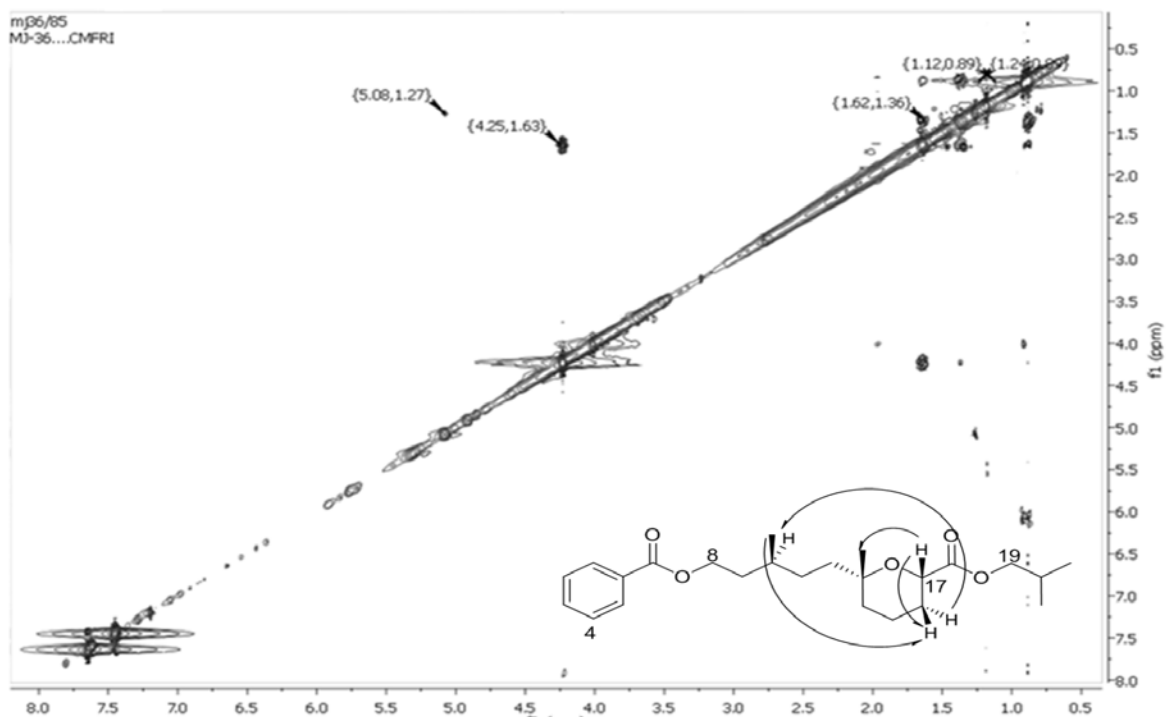


Figure 6.29.: NOESY NMR spectrum of isobutyl-13-(6-(benzoyloxy)-10-methylpentyl)-tetrahydro-13-methyl-2*H*-pyran-17-carboxylate (**2**)

The compound **2** exhibited ester carbonyl stretching vibrations at 1722 cm^{-1} along with aromatic alkenic stretching vibrations at $\sim 1585\text{ cm}^{-1}$. The stretching vibration bands at 2959 , 2930 cm^{-1} denoted the C-H alkyl absorptions. The C-H bending and rocking absorption bands were appeared at 1448 and $703\text{--}651\text{ cm}^{-1}$, respectively (Figure 6.30.).

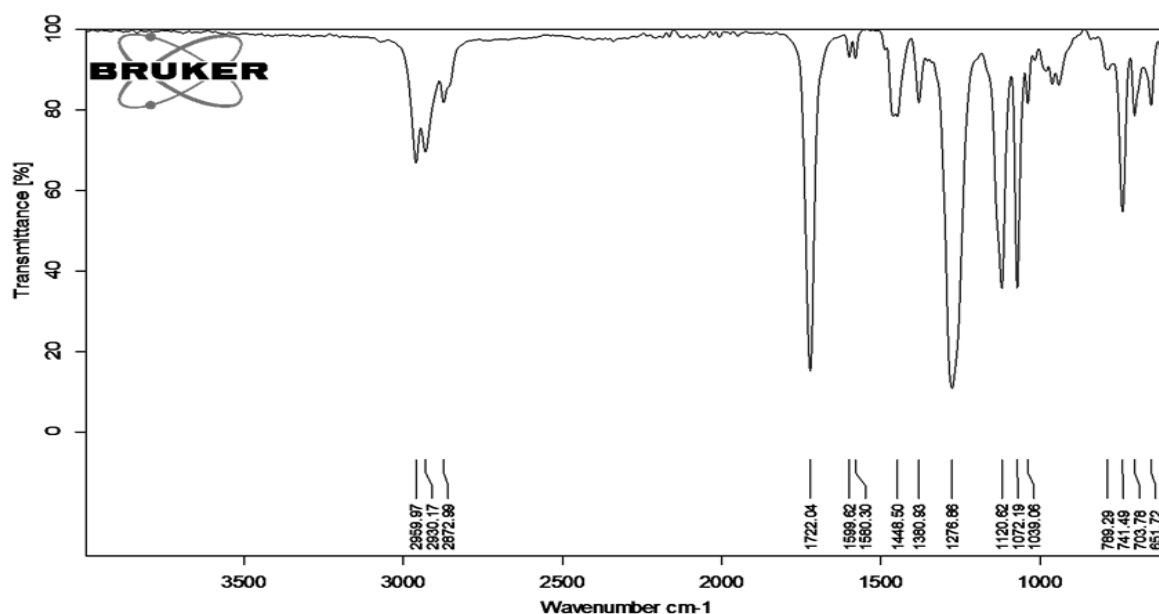


Figure 6.30.: FTIR spectrum of isobutyl-13-(6-(benzoxyloxy)-10-methylpentyl)-tetrahydro-13-methyl-2*H*-pyran-17-carboxylate (**2**)

The compound **2** was registered the molecular ion peak at m/z 404 (found m/z 404.2567 $[\text{M}]^+$, cal. for $\text{C}_{24}\text{H}_{36}\text{O}_5$ 404.2563), which on fragmentation of propyl radical and two sequential methoxy radicals yielded ions at m/z 361 (**b**), 333 (**c**) and 303 (**d**), respectively. The later was found to fragmented at m/z 284 (**e**), 256 (**f**), 232 (**g**) and 191 (**h**) on removal of methyl, two repeated units of $\text{C}_2\text{H}_4\bullet\bullet$ and $\text{C}_2\text{H}_4\text{O}\bullet\bullet$ radicals, respectively. The ethyl benzoate radical was recorded at m/z 149 (**j**) from isopentyl benzoate (m/z 191, **h**) on elimination of propyl moiety, which was further fragmented at m/z 121 (**k**, benzoate cation) on $\text{C}_2\text{H}_5\bullet$ elimination. The fragment, **k** eliminated carboxylate radical to acquire base peak at m/z 77 (**l**) which was corresponded to benzene cation (Figure 6.31., 6.32.).

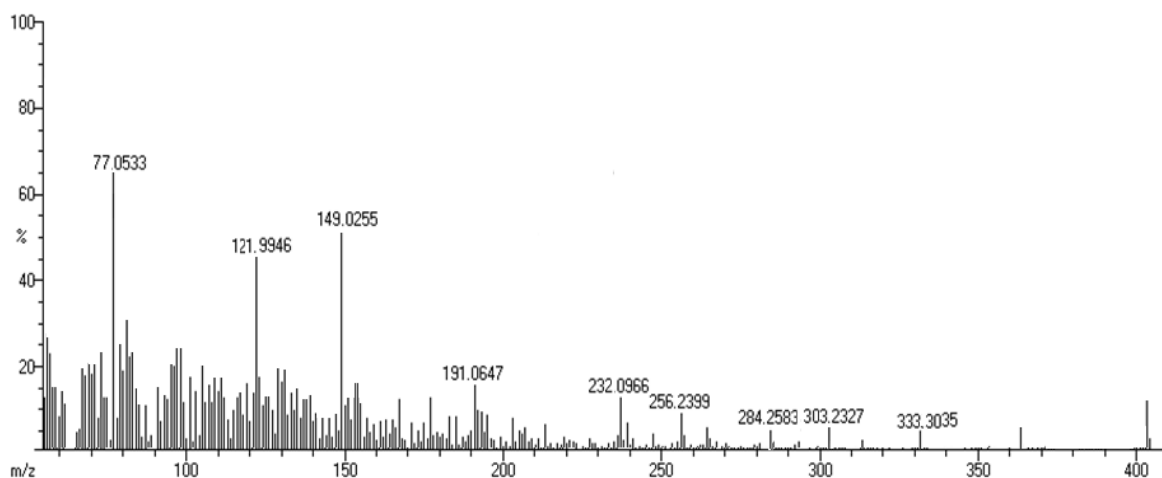


Figure 6.31.: EIMS spectrum of isobutyl-13-(6-(benzoyloxy)-10-methylpentyl)-tetrahydro-13-methyl-2*H*-pyran-17-carboxylate (**2**)

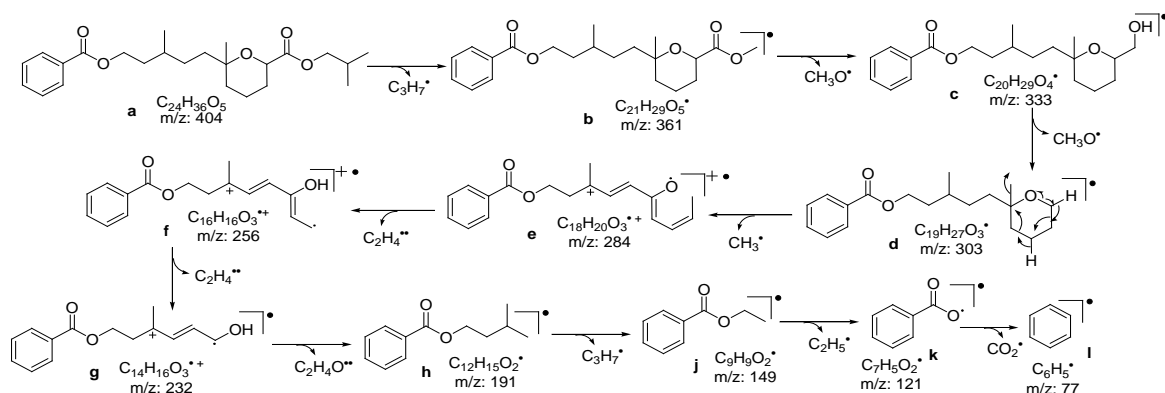


Figure 6.32.: Mass fragmentation pattern of isobutyl-13-(6-(benzoyloxy)-10-methylpentyl)-tetrahydro-13-methyl-2*H*-pyran-17-carboxylate (**2**)

6.3.2.1.2. Biogenic origin of the polyketide synthase (PKS) catalyzed aryl polyketide derivative (**2**)

The PKS-bound malonate and isobutoxycarbonyl moieties were the building blocks to initiate the formation of 2-(isobutoxycarbonyl)-ethanethiote, which has been the backbone for the biosynthesis of **2** (Figure 6.33.). 2-(Isobutoxycarbonyl)-ethanethiote bound to PKS enzyme cascade underwent several rearrangements to yield isobutyl-2,11-dihydroxy-9-methyl-6-oxoundecanoate, which on elimination of hydroxyl group followed by intramolecular cyclization afforded isobutyl-tetrahydro-6-hydroxy-6-(5-hydroxy-3-methylpentyl)-2*H*-pyran-2-carboxylate. The later on methyl transferase and enolreductase

catalyzed condensation with benzothioate bound to PKS acquired compound **2** (Chakraborty *et al.*, 2017b).

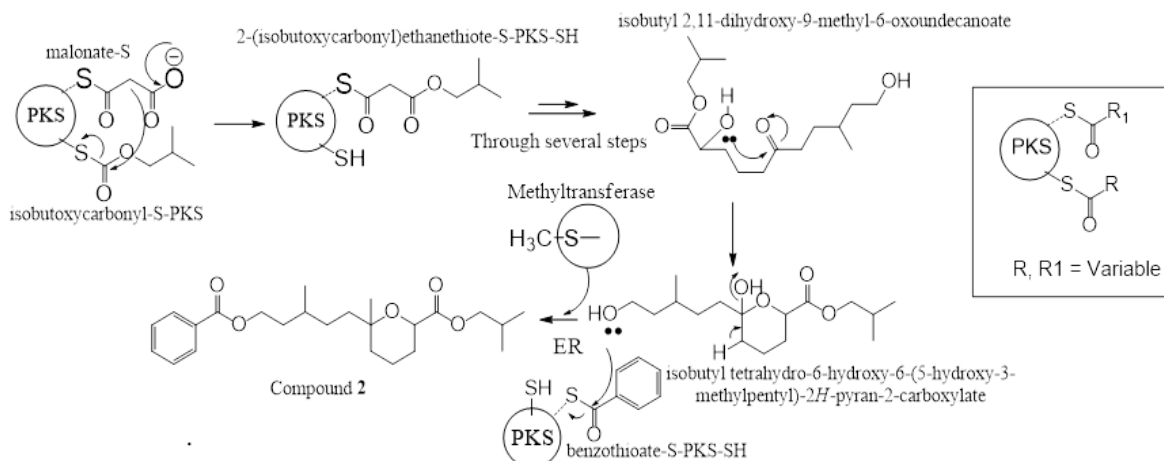
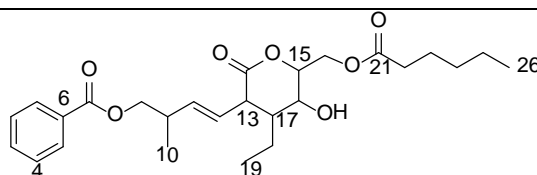


Figure 6.33.: Schematic representation of biosynthetic pathway of isobutyl-13-(6-(benzoyloxy)-10-methylpentyl)-tetrahydro-13-methyl-2*H*-pyran-17-carboxylate (**2**)

6.3.2.1.C. Structural characterization of compound 3 (PM₃₋₁₋₁₋₁)

(*E*)-12-(17-Ethyl-tetrahydro-16-hydroxy-15-(methyl pentanoate)-14-oxo-2*H*-pyran-13-yl)-9-methylbut-11-enyl benzoate (3**)**



Sample yield	75 mg; 0.15%
Physical description	Pale yellow oily
Molecular formula	C ₂₆ H ₃₆ O ₇
Molecular mass	460.2461

Compound **3** was purified as pale yellow oily compound and its molecular formula determined as C₂₆H₃₆O₇. It exhibited UV absorbance (in MeOH) at λ_{max} (log ε 3.80) 274.0 nm was assigned to a chromophore with ester carbonyl and olefinic groups

(Figure 6.34.). The RP C18 HPLC experiments using MeOH:MeCN (3:2, v/v) (R_t 6.28) was supported its purity (Figure 6.35.).

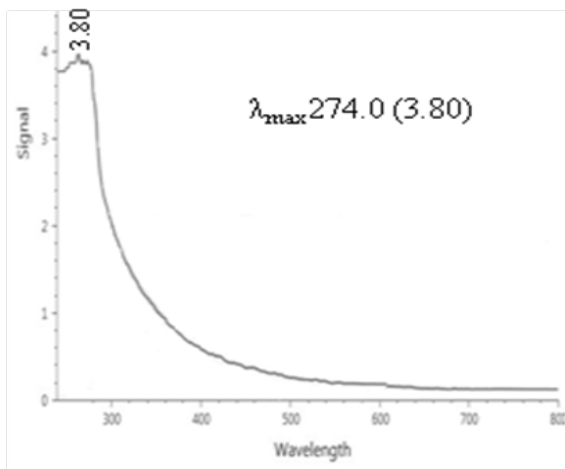


Figure 6.34.: UV spectrum of (*E*)-12-(17-ethyl-tetrahydro-16-hydroxy-15-(methyl pentanoate)-14-oxo-2*H*-pyran-13-yl)-9-methylbut-11-enyl benzoate (**3**)

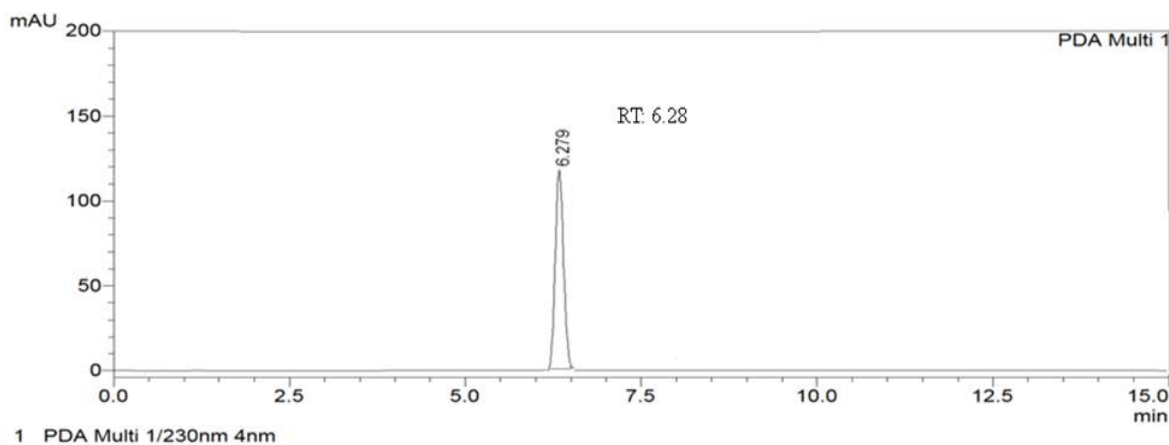


Figure 6.35.: HPLC chromatogram of (*E*)-12-(17-ethyl-tetrahydro-16-hydroxy-15-(methyl pentanoate)-14-oxo-2*H*-pyran-13-yl)-9-methylbut-11-enyl benzoate (**3**)

The characteristic ^{13}C NMR signals registered at δ 167.68, 172.83 and 173.25 were due to ester $\{-\text{C}(=\text{O})-\text{O}-\}$ moieties in which the former belonged to an aromatic ester, whereas the other two were attributed to cyclic or straight chain ester groups. These attributions were appropriately supported by the presence of strong carbonyl IR stretching band (1724 cm^{-1}) along with $^1\text{H}/^{13}\text{C}$ NMR signals at δ 4.09/71.78 and δ 4.32/65.54 (due to

strong electron withdrawing effect of oxygen) (Table 6.8.). The presence of benzyl moieties were ascribed by characteristic peaks at δ 7.50-7.72 in ^1H NMR and their HSQC relations with carbon atoms at δ 128-132 (Figure 6.38., 6.39., 6.42.). The ^1H NMR of **3** exhibited two olefinic signals at δ 5.35 ($J=9.54$ Hz) and 5.37 ($J=9.86$ Hz), which revealed the presence of *trans* oriented (*E*) *vicinal* olefinic protons. The title compound exhibited nine degrees of unsaturation in which four were recognized to aromatic ring, whereas remaining five related to double bonds.

The aromatic signals in ^1H NMR spectrum appeared to be doublets/double doublets with five proton integral, which attributed to the monosubstituted benzyl framework (Chakraborty *et al.*, 2017a). The ^{13}C NMR at δ 132.33 was suggested to the quaternary carbon in aromatic ring and its downfield shift was attributed to the presence of strong electron withdrawing ester group $\{-\text{C}(=\text{O})-\text{O}-\}$ at δ 167.68 (Huong *et al.*, 2004). The deshielded methine proton at δ 4.32 (corresponded to δC 65.54, HSQC) was *geminal* to the hydroxyl group, and was enclosed in oxo-2*H*-pyran ring. The occurrence of hydroxyl group was further confirmed by broad stretching vibration band at 3308 cm^{-1} and deuterium exchange $\{\text{D}_2\text{O}$ (deuterium oxide)- ^1H NMR} experiment. The attachment of carbonyl group to aryl skeleton was supported by intense HMBC cross peaks from δ 7.71 (H-1) to δ 167.68 (C-7) that established that the benzoate moiety was connected to the oxo-2*H*-pyran group through the 9-methylbut-11-ene moiety (Figure 6.36.B, 6.43.). The long range HMBC correlations from δ 4.09 (H-8) to δ 167.68 (C-7), 27.73 (C-9), 19.16 (C-10); δ 2.03 (H-9) to δ 129.92 (C-12); δ 0.98 (H-10, $-\text{CH}_3$) to δ 71.78 (C-8); δ 5.35 (H-11) to δ 27.23 (C-9) attributed the presence of 9-methylbut-11-ene moiety in **3** (Figure 6.36.B). Its attachment to oxo-2*H*-pyran was confirmed by long range HMBCs among δ 2.85 (H-13) and δ 129.80 (C-11). This structure enclosed five spin systems, δ 7.71 (H-1)/7.51 (H-2); 7.53 (H-4)/7.72 (H-5) in benzene ring and δ 4.09 (H-8)/2.03 (H-9)/0.98 (H-10), 5.35 (H-11) in 9-methylbut-11-enyl chain network. The spin systems, δ 5.37 (H-12)/2.85 (H-13) and δ 4.15, 4.29 (H-20)/5.27 (H-15)/4.32 (H-16)/1.73 (H-17)/1.45 (H-18)/0.96 (H-19) were attributed to 17-ethyl-tetrahydro-16-hydroxy-15-methyl-14-oxo-2*H*-pyran (Figure 6.36.A, 6.41.), and these assignments were comparable with lactone ring system of previously described benzoates (Huong *et al.*, 2004). Intense correlations at δ 2.31 (H-22)/1.61 (H-23)/1.30 (H-24)/1.26 (H-

25)/0.89 (H-26) were substantiated the presence of pentanoate side chain. The relative stereochemistries at C-17, C-16, C-13, C-9 and C-15 were predicted from nuclear overhauser effect spectroscopy (NOESY) cross peaks (Figure 6.37., 6.44.). Likewise, NOE correlations were obvious between δ 4.32 (H-16)/5.27 (H-15)/4.15 (H α -20), which depicted that these protons were located at similar plane of geometry and α -orientated. The NOE peaks between δ 2.03 (H-9)/1.73 (H-17)/4.29 (H β -20)/2.85 (H-13) were indicated that these were equiplaner, and disposed at the β -plane of reference. Furthermore, the hydroxyl group (at C-16) was placed at the β -plane of reference, and was disposed at the opposite plane of the α -oriented proton at δ 4.32 (H α -16) and methyl group at C-9, being *trans* to H β -9.

Table 6.8.: NMR spectroscopic data of (*E*)-12-(17-ethyl-tetrahydro-16-hydroxy-15-(methyl pentanoate)-14-oxo-2*H*-pyran-13-yl)-9-methylbut-11-enyl benzoate (**3**) in CDCl₃

C. No	¹³ C	¹ H (int.,mult.,J in Hz) ^a	COSY	HMBC
1	128.83	7.71 (1H,d,8.57)	H-2	C-7,2
2	130.88	7.51 (1H,dd,7.59)	-	C-1
3	130.88	7.54 (1H,dd,9.46)	-	-
4	130.88	7.53 (1H,dd,8.24)	H-5	-
5	128.7	7.72 (1H,d,7.48)	-	-
6	132.33	-	-	-
7	167.68	-	-	-
8	71.78	4.09 (2H,d)	H-9	C-7,9,10
9	27.73	2.03 (1H β ,m)	H-10,11	C-12
10	19.16	0.98 (3H α ,d)	-	C-8
11	129.8	5.35 (1H,t,9.54)	-	C-9
12	129.92	5.37 (1H,t,9.86)	H-13	-
13	25.63	2.85 (1H β ,t)	-	C-11
14	172.83	-	-	-
15	68.88	5.27 (1H α ,dt)	H-16,20	
16	65.54	4.32 (1H α ,t)	H-17	C-14,17,18,20
17	30.58	1.73 (1H β ,p)	H-18	C-16,18,19
18	19.19	1.45 (2H,m)	H-19	
19	13.72	0.96 (3H,t)	-	-
20	62.09	4.15 (1H α ,dd) 4.29 (1H β ,dd)	-	C-14,21,16
21	173.25	-	-	-

22	34.05	2.31 (2H,t)	H-23	C-21,23,24
23	24.82	1.61 (2H,p)	H-24	
24	29.7	1.30 (2H,m)	H-25	C-23
25	22.69	1.26 (2H,m)	H-26	C-24,
26	14.11	0.89 (3H,t)	-	C-24,25

^1H NMR spectra recorded using Bruker AVANCE III 500MHz (AV 500) spectrometer (Bruker, Karlsruhe, Germany) in CDCl_3 as aprotic solvent at ambient temperature with TMS as the internal standard (δ 0 ppm). The ^1H NMR spectra were recorded at 500MHz, while the ^{13}C NMR spectra were recorded at 125MHz. ^aValues in ppm, multiplicity and coupling constants (J =Hz) were indicated in parentheses. The assignments were made with the aid of the ^1H - ^1H COSY, HSQC, HMBC and NOESY experiments

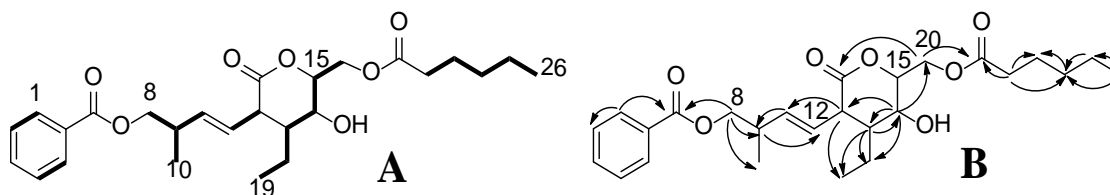


Figure 6.36.: ^1H - ^1H COSY(A) and HMBC (B) correlations of (*E*)-12-(17-ethyl-tetrahydro-16-hydroxy-15-(methylpentanoate)-14-oxo-2*H*-pyran-13-yl)-9-methylbut-11-enyl benzoate (**3**). The key ^1H - ^1H COSY couplings have been represented by the bold face bonds. The HMBC couplings were indicated by double barbed arrow

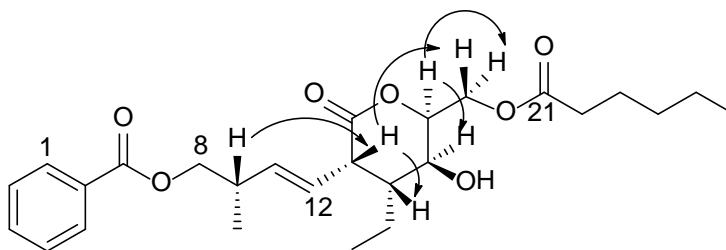


Figure 6.37.: NOESY correlations of (*E*)-12-(17-ethyl-tetrahydro-16-hydroxy-15-(methyl pentanoate)-14-oxo-2*H*-pyran-13-yl)-9-methylbut-11-enyl benzoate (**3**). The NOESY relations were represented by double barbed arrow

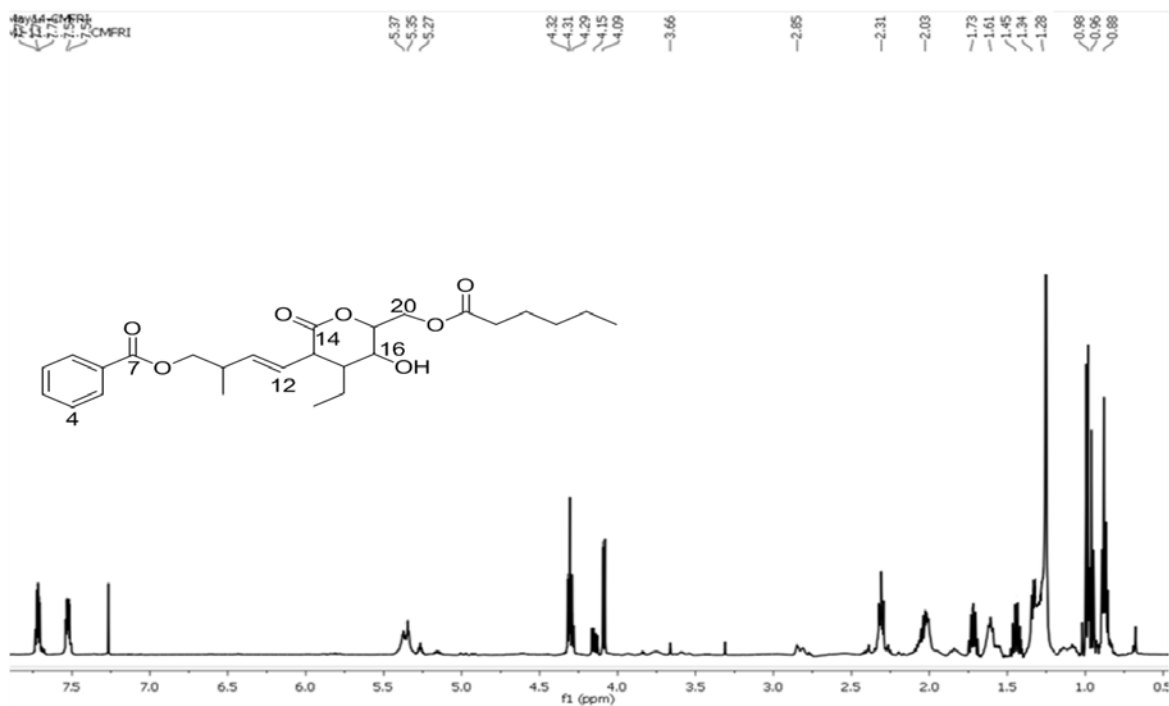


Figure 6.38.: ^1H NMR spectrum of (*E*)-12-(17-ethyl-tetrahydro-16-hydroxy-15-(methyl pentanoate)-14-oxo-2*H*-pyran-13-yl)-9-methylbut-11-enyl benzoate (**3**)

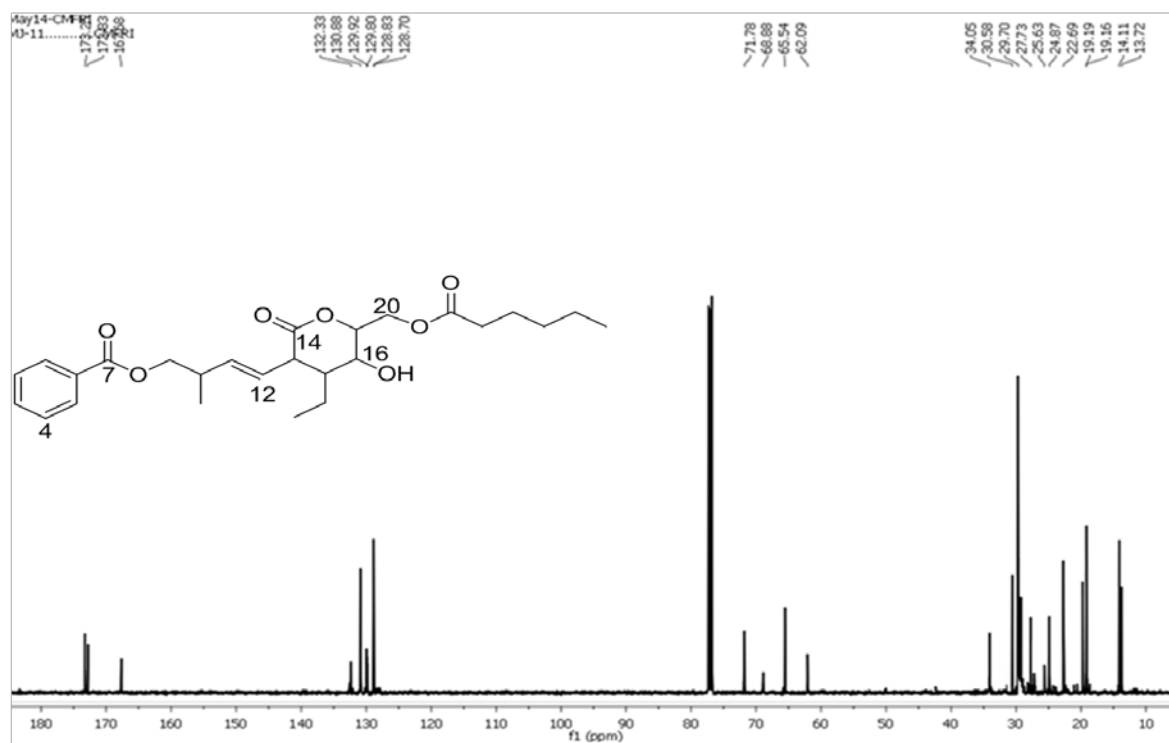


Figure 6.39.: ^{13}C NMR spectrum of (*E*)-12-(17-ethyl-tetrahydro-16-hydroxy-15-(methyl pentanoate)-14-oxo-2*H*-pyran-13-yl)-9-methylbut-11-enyl benzoate (**3**)

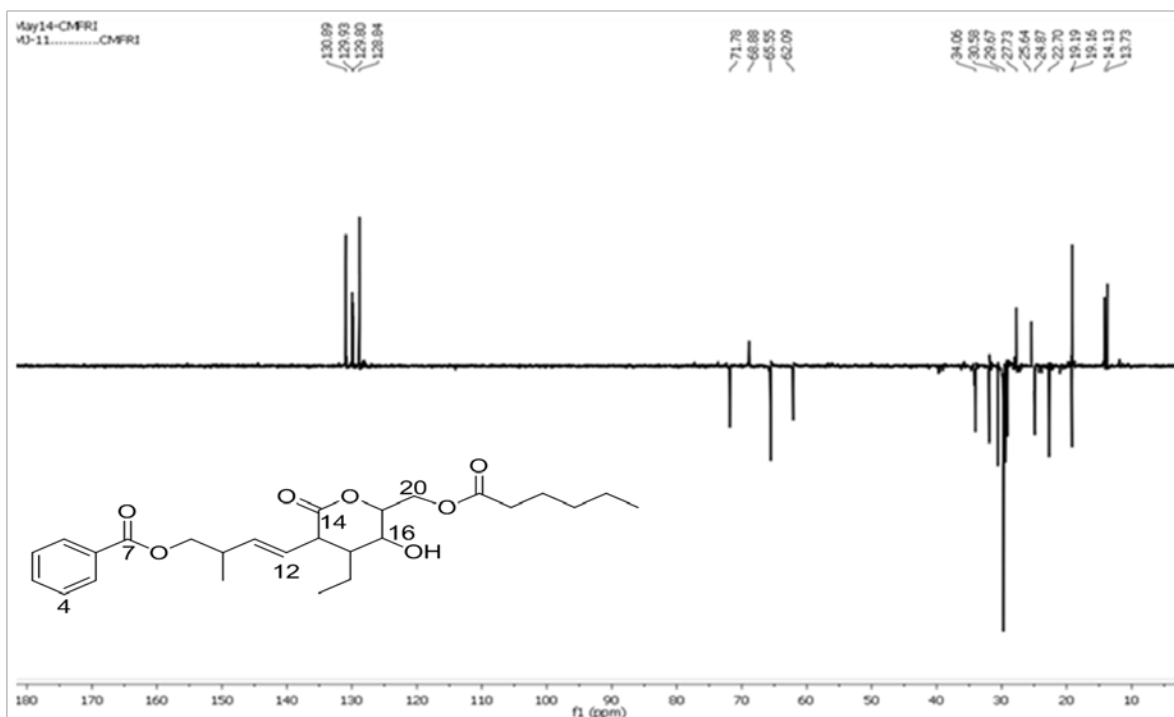


Figure 6.40.: $^{135}\text{DEPT}$ NMR spectrum of (*E*)-12-(17-ethyl-tetrahydro-16-hydroxy-15-(methylpentanoate)-14-oxo-2*H*-pyran-13-yl)-9-methylbut-11-enyl benzoate (**3**)

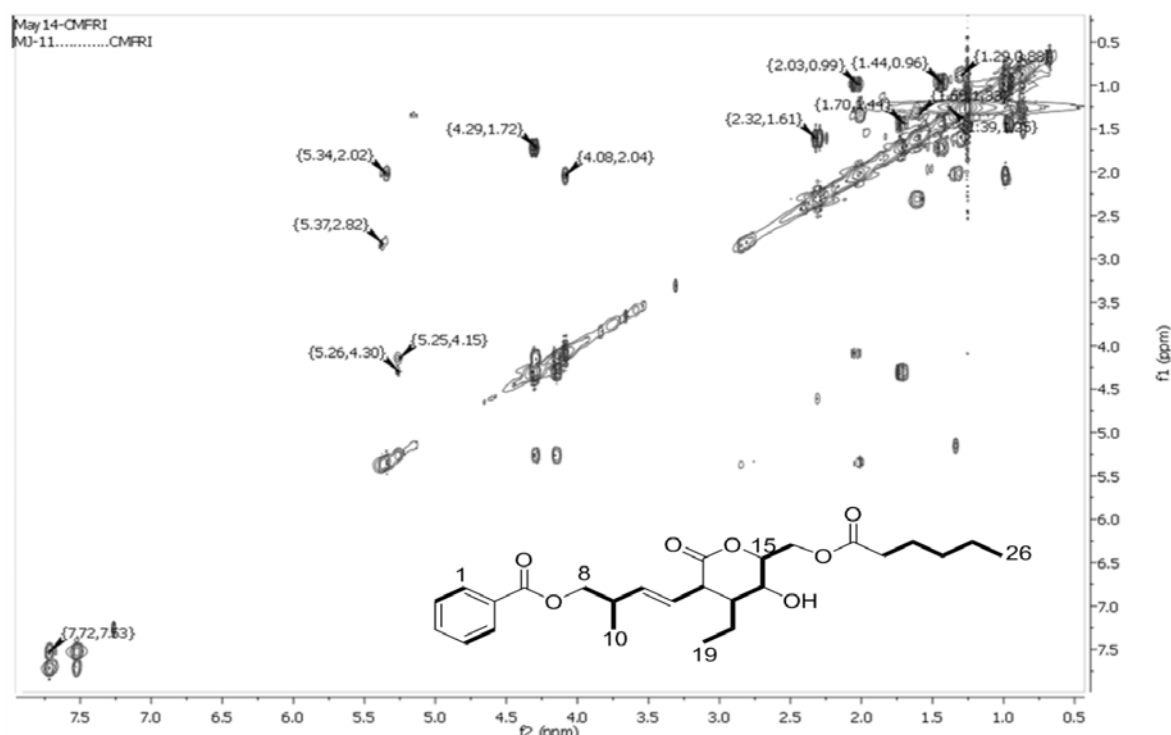


Figure 6.41.: ^1H - ^1H COSY NMR spectrum of (*E*)-12-(17-ethyl-tetrahydro-16-hydroxy-15-(methylpentanoate)-14-oxo-2*H*-pyran-13-yl)-9-methylbut-11-enyl benzoate (**3**)

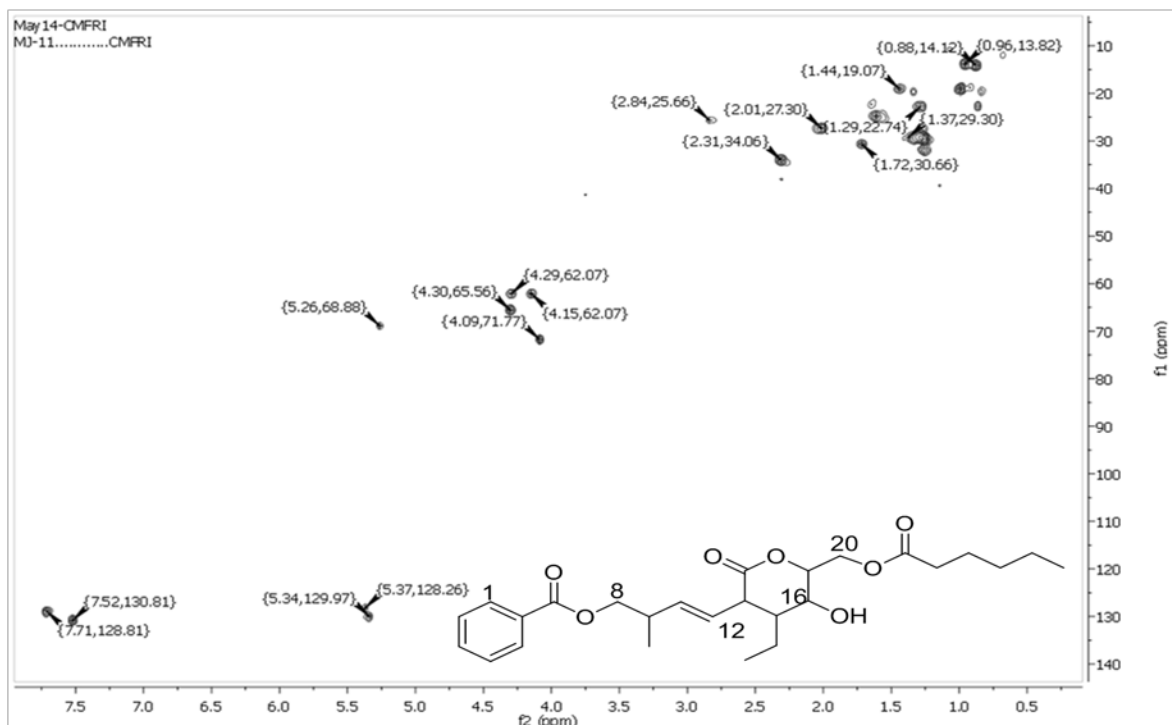


Figure 6.42.: HSQC NMR spectrum of (*E*)-12-(17-ethyl-tetrahydro-16-hydroxy-15-(methylpentanoate)-14-oxo-2*H*-pyran-13-yl)-9-methylbut-11-enyl benzoate (**3**)

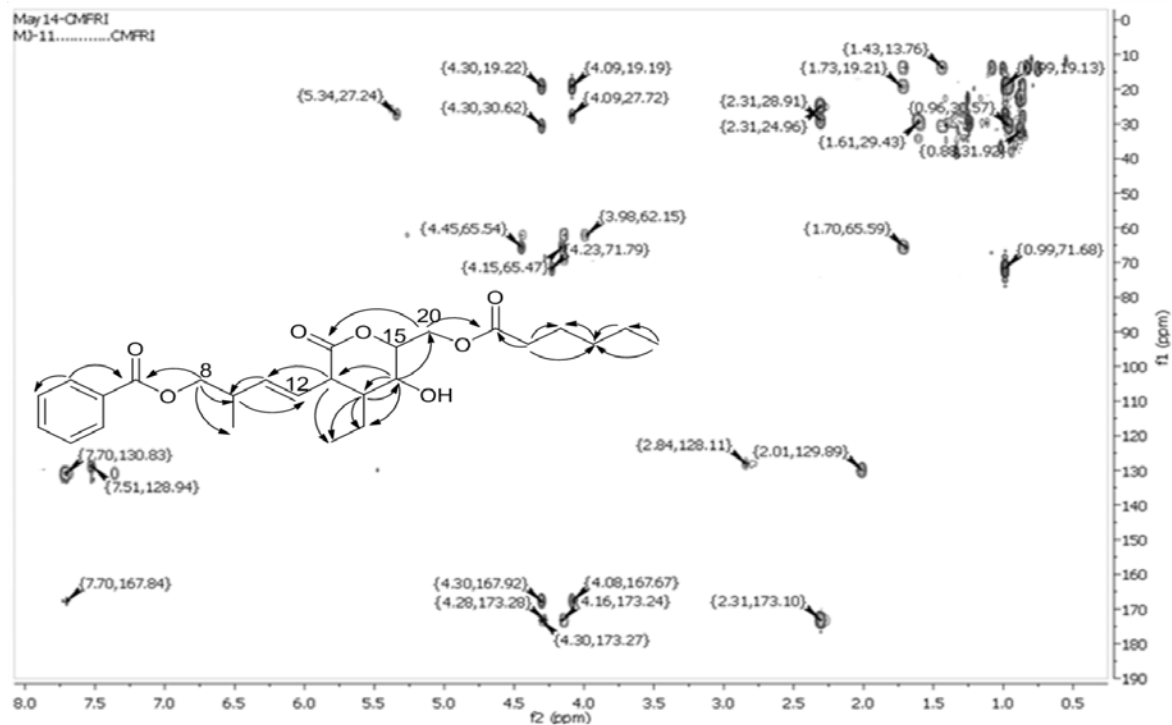


Figure 6.43.: HMBC NMR spectrum of (*E*)-12-(17-ethyl-tetrahydro-16-hydroxy-15-(methylpentanoate)-14-oxo-2*H*-pyran-13-yl)-9-methylbut-11-enyl benzoate (**3**)

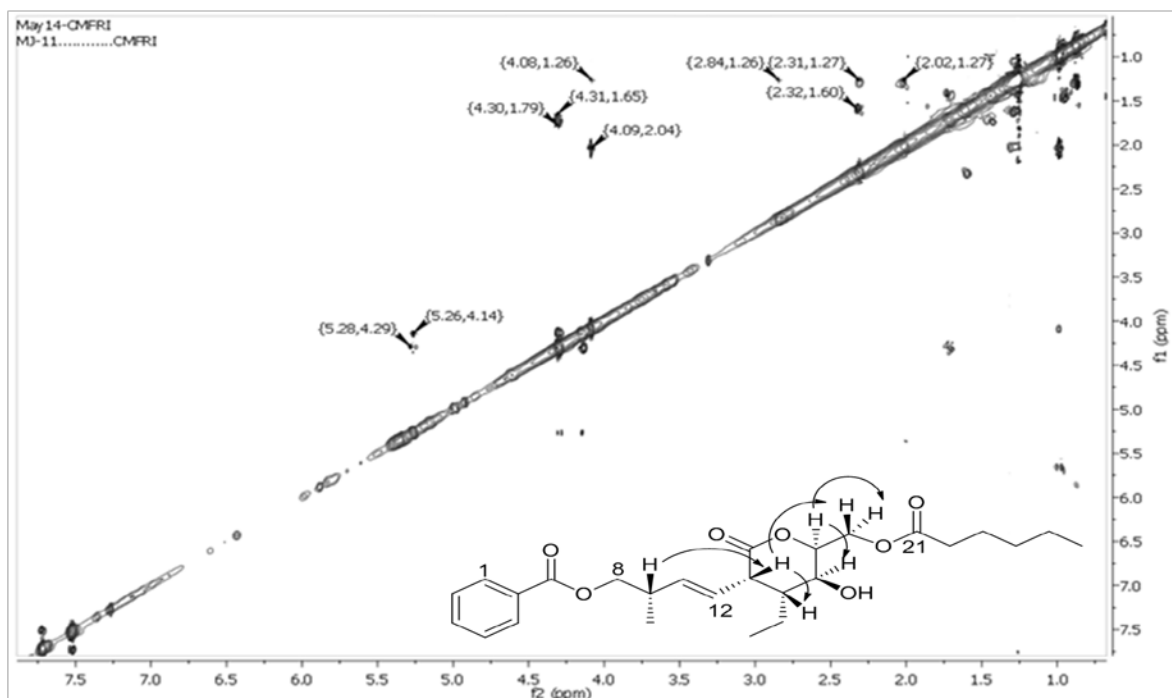


Figure 6.44.: NOESY NMR spectrum of (*E*)-12-(17-ethyl-tetrahydro-16-hydroxy-15-(methylpentanoate)-14-oxo-2*H*-pyran-13-yl)-9-methylbut-11-enyl benzoate (**3**)

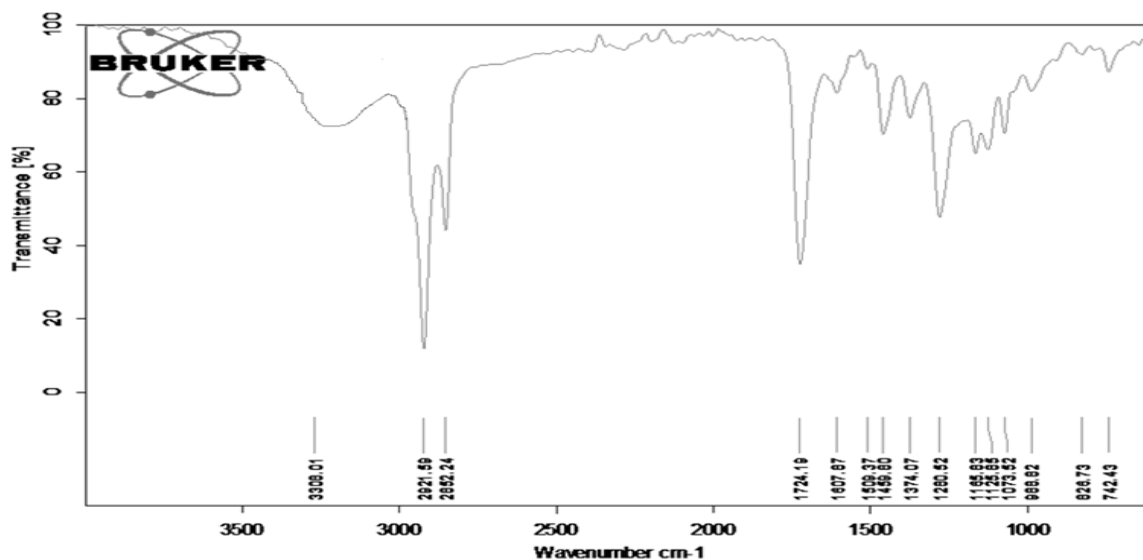


Figure 6.45.: FTIR spectrum of (*E*)-12-(17-ethyl-tetrahydro-16-hydroxy-15-(methylpentanoate)-14-oxo-2*H*-pyran-13-yl)-9-methylbut-11-enyl benzoate (**3**)

The compound **3** exhibited ester carbonyl stretching vibrations at 1724 cm^{-1} and hydroxyl stretching vibrations at 3308 cm^{-1} . The stretching vibrations at $2921\text{--}2852\text{ cm}^{-1}$

denoted the C-H alkyl absorptions. The C-H bending and rocking absorption bands were appeared at 1457 and 742 cm^{-1} (Figure 6.45.).

The compound **3** recorded its molecular ion peak at m/z 460 (EIMS: found m/z 460.2466 $[\text{M}]^+$, cal. for $\text{C}_{26}\text{H}_{36}\text{O}_7$ 460.2461) (Figure 6.46.) that belived to undergo three sequential fragmentation of ethyl radical to get ion fragments at m/z 431 (**b**), 403 (**c**) and 375 (**d**), respectively. The ion fragment at **d** showed fragmentation by the removal of hydroxyl and $\text{C}_2\text{H}_3\text{O}_2^\bullet$ radicals to obtain peaks at m/z 355 (**e**) and 295 (**f**), respectively which was on fragmentation yielded a fragment at m/z 281 (**g**) along with the removal of CH_2^\bullet radical. The molecular ion, **g** resulted in the fragmented ions at m/z 213 (**h**) and 203 (**j**) on elimination of $\text{C}_3\text{H}_3\text{O}_2^\bullet$ and methyl radicals, respectively. The significant peak of vinyl benzoate cation at m/z 147 (**1k**) and a stable benzoate ion at m/z 121 (**l**) were appeared on subsequent elimination of $\text{C}_4\text{H}_7^\bullet$ and $\text{C}_2\text{H}_3^\bullet$ radicals from the fragment **j**. The base peak was apparent at m/z 77 (**m**) for benzene cation on elimination of carboxyl radical from the fragment, **l** (m/z 121) (Figure 6.47.).

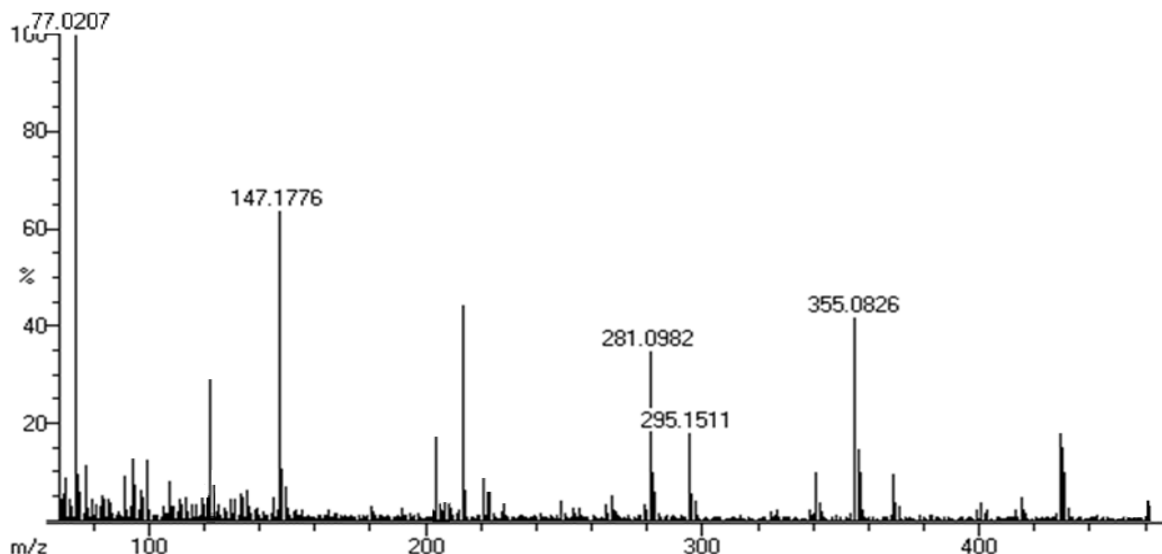


Figure 6.46.: EIMS spectrum of (*E*)-12-(17-ethyl-tetrahydro-16-hydroxy-15-(methyl pentanoate)-14-oxo-2*H*-pyran-13-yl)-9-methylbut-11-enyl benzoate (**3**)

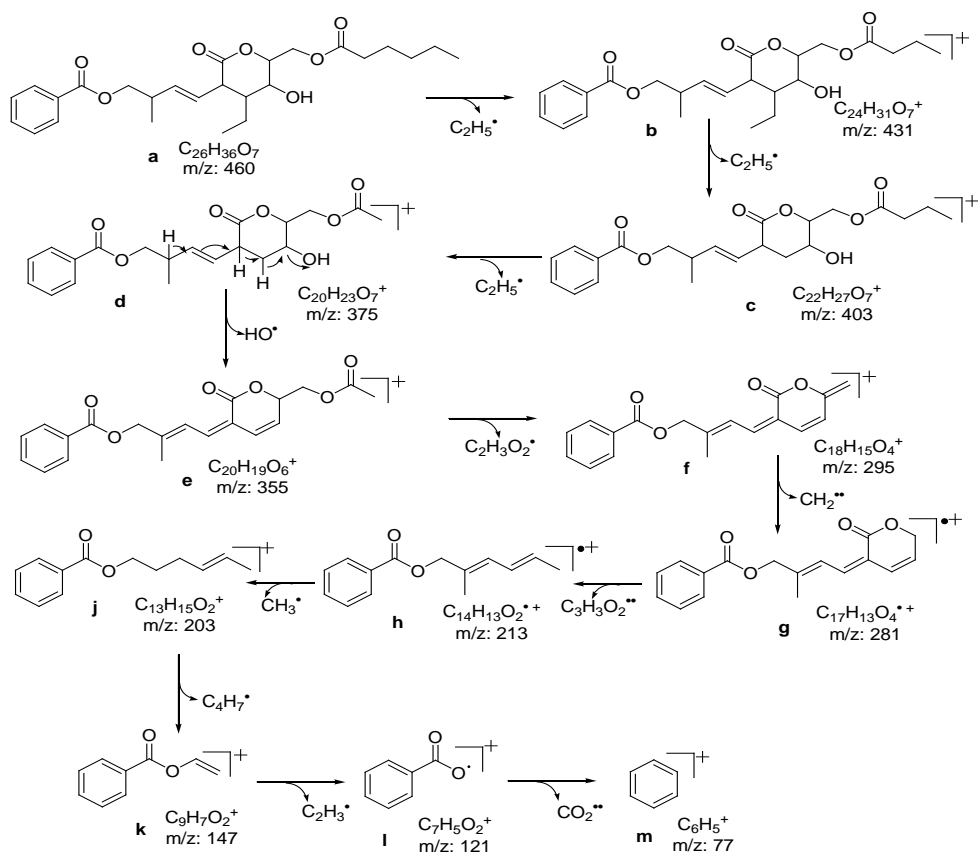


Figure 6.47.: Mass fragmentation pattern of *(E)*-12-(17-ethyl-tetrahydro-16-hydroxy-15-(methylpentanoate)-14-oxo-2*H*-pyran-13-yl)-9-methylbut-11-enyl benzoate (**3**)

6.3.2.1.3. Biogenic origin of the polyketide synthase (PKS) catalyzed aryl polyketide derivative (**3**)

The putative biosynthetic pathway of aryl polyketide **3** was postulated. The intermediate polyketide, 3-ethyl-6-(hexanoyloxy)-4,5-dihydroxy-2-((*E*)-but-1-enyl-3-methyl-hydroxy)-hexane thioate connected to polyketide synthase (PKS) enzyme cascade appeared to undergo intramolecular cyclization to 4-ethyl-tetrahydro-3-((*E*)-4-hydroxy-3-methyl-but-1-enyl)-6-(hydroxymethyl)-2*H*-pyran-2,5-diol. The latter compound undergoes intramolecular rearrangement yielding 4-ethyl-tetrahydro-5-hydroxy-3-((*E*)-4-hydroxy-3-methylbut-1-enyl)-6-(hydroxy-methyl)-pyran-2-one. The ketosynthetase (KS)-catalyzed condensation of 4-ethyl-tetrahydro-5-hydroxy-3-((*E*)-4-hydroxy-3-methylbut-1-enyl)-6-(hydroxymethyl)-pyran-2-one and PKS-bound benzothioate through nucleophilic attack of

terminal hydroxyl of the latter resulted in the formation of titled compound on subsequent elimination of PKS-thiolase (Figure 6.48.) (Chakraborty *et al.*, 2017b; Chakraborty *et al.*, 2017c).

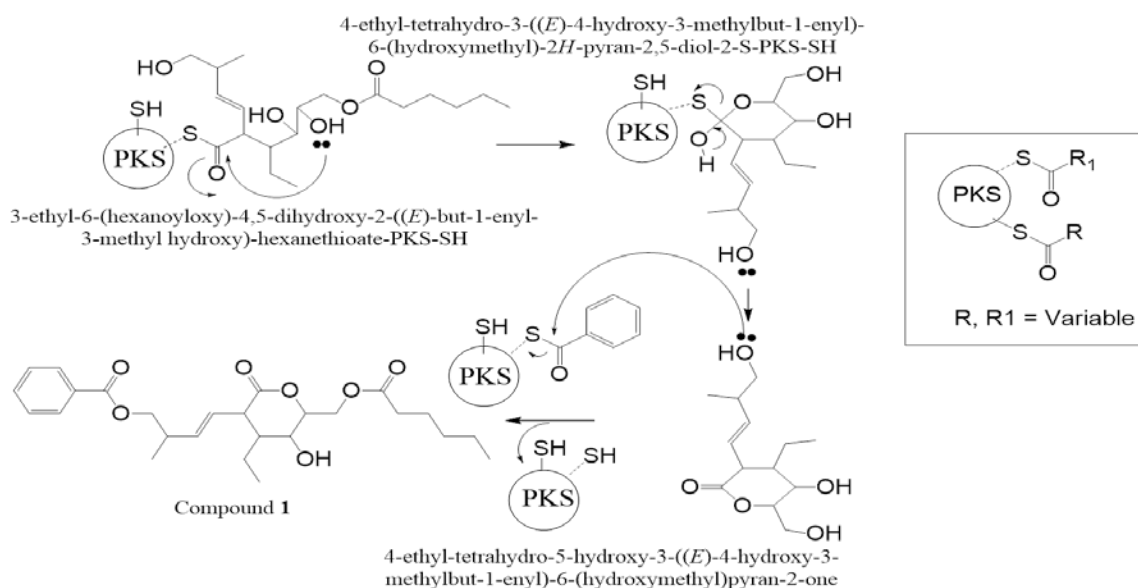


Figure 6.48.: Schematic representation of biosynthetic pathway of (*E*)-12-(17-ethyl-tetrahydro-16-hydroxy-15-(methylpentanoate)-14-oxo-2*H*-pyran-13-yl)-9-methylbut-11-enyl benzoate (**3**)

Polyketide group of compounds constitute a versatile class of secondary metabolites in marine organisms with diverse bioactivities (Chakraborty *et al.*, 2016d; Chakraborty *et al.*, 2017b). Despite the fact that microbial polyketide compounds are of immense health significance, the occurrence of this group of compounds in marine mollusks, one of the affluent origin of functional leads, remained predominantly uninvestigated. In particular, hypothetical biosynthetic routes leading to the formation of polyketide compounds were described in the previous literatures (Chakraborty *et al.*, 2017b). Successive decarboxylative Claisen condensations between various extenders and polyketide skeletons followed by chain enlargements by discrete enzymes appeared to biosynthesize structurally diverse molecules, such as aryl polyketide derivatives isolated from *P. malabarica*. The putative PKS enzyme cascade assisted biosynthetic pathways of

title compounds, and accordingly confirmed the structural features of previously undisclosed aryl polyketide derivatives (**1-3**). This is the first report of characterization of three new variants of aryl substituted polyketide derivatives from mollusks with potential antioxidative and anti-inflammatory properties for use as functional food ingredients.

6.3.2.2. Structural characterization of tetrahydro chromenyl derivatives (4-5)

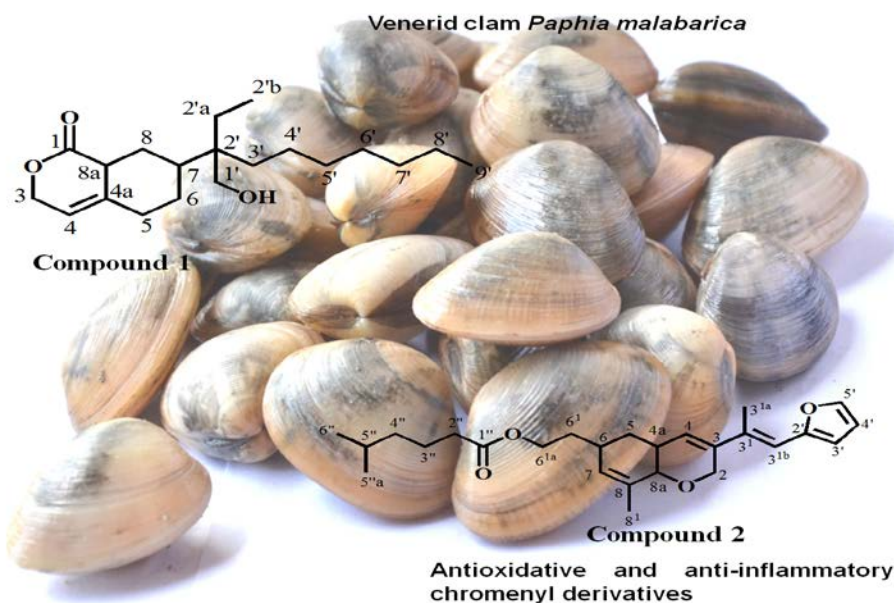


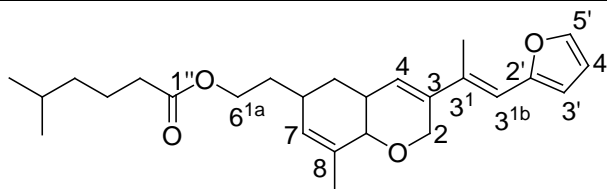
Figure 6.49.: Tetrahydro chromenyl derivatives from *P. malabarica* with bioactive potentials

Naturally and synthetically identified chromene derivatives are valuable pharmacophores, which exhibit important structural and functional peculiarities in natural product research and also reported for biological activities, such as antioxidant (Milan *et al.*, 2011), anti-inflammatory (Nitin *et al.*, 2012), anti-bacterial and anti-tumour properties (Smith *et al.*, 1998). The benzopyrans or pyranones, hydrogenated benzopyrans or pyrones, cyclohexane δ -lactones are the different forms of chromene or chromenone based skeletons (Boeckman *et al.*, 1988). The α -tocopherol is a prominent example of naturally occurring chromene (benzopyran) with significant antioxidant properties and is commercially exploited to prevent lipid peroxidation in food (Kindleysides *et al.*, 2012). A medicinally

important isochromenone secondary metabolite was identified from a fungus, *Camptotheca acuminata* (Lin *et al.*, 2011) and the hydrogenated chromenone from marine green alga were reported (El-Beih *et al.*, 2007). The extensive investigation of naturally derived chromenyl compounds with varying substitutions is imperative to the invention of potential pharmacophore templates for upcoming functional foods, nutraceutical supplements and to prevent peroxide formations in foods. Herein, we have characterized two new substituted tetrahydro chromenyl derivatives with hitherto unreported furanyl-2*H*-chromenyl skeletons (**4**) and isochromen-(5*H*)-one (**5**) from EtOAc:MeOH extract of *P. malabarica*.

6.3.2.2.A. Structural characterization of compound **4** (PM₄₋₂₋₁)

6¹-(3-((*E*)-3^{1b}-(Furan-2'-yl)-prop-3^{1b}-en-3¹-yl)-4a,5,6,8a-tetrahydro-8-methyl-2*H*-chromen-6-yl)-ethyl-5''-methyl-hexanoate (4**)**



Sample yield	110 mg; 0.22%
Physical description	Brown oily
Molecular formula	C ₂₆ H ₃₆ O ₄
Molecular mass	412.2613

The compound, 6¹-(3-((*E*)-3^{1b}-(furan-2'-yl)-prop-3^{1b}-en-3¹-yl)-4a,5,6,8a-tetrahydro-8-methyl-2*H*-chromen-6-yl)-ethyl-5''-methyl-hexanoate (**4**) was isolated as brown oily upon repetitive fractionation. It exhibited UV absorbance (in MeOH) at λ_{max} (log ε 3.98 and 3.90) 284.0 and 286.0 nm assigned to a chromophore with ester carbonyl, furanyl and olefinic groups (Figure 6.50.). The purity of compound **4** was supported by RP C18 HPLC experiments using 3:2 (v/v) MeOH:MeCN (R_t 12.92) solvent system (Figure 6.51.).

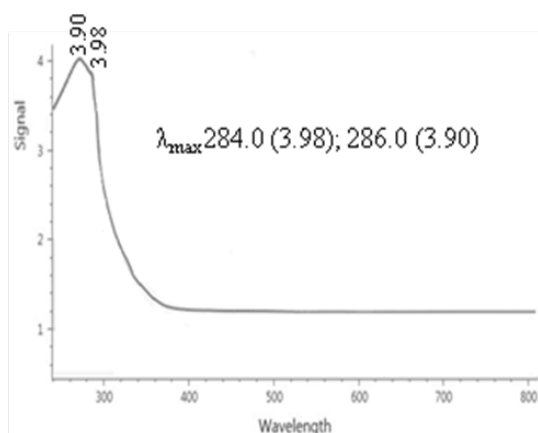


Figure 6.50.: UV spectrum of 6¹-(3-((*E*)-3^{1b}-(furan-2'-yl)-prop-3^{1b}-en-3¹-yl)-4a,5,6,8a-tetrahydro-8-methyl-2*H*-chromen-6-yl)-ethyl-5''-methyl-hexanoate (**4**)

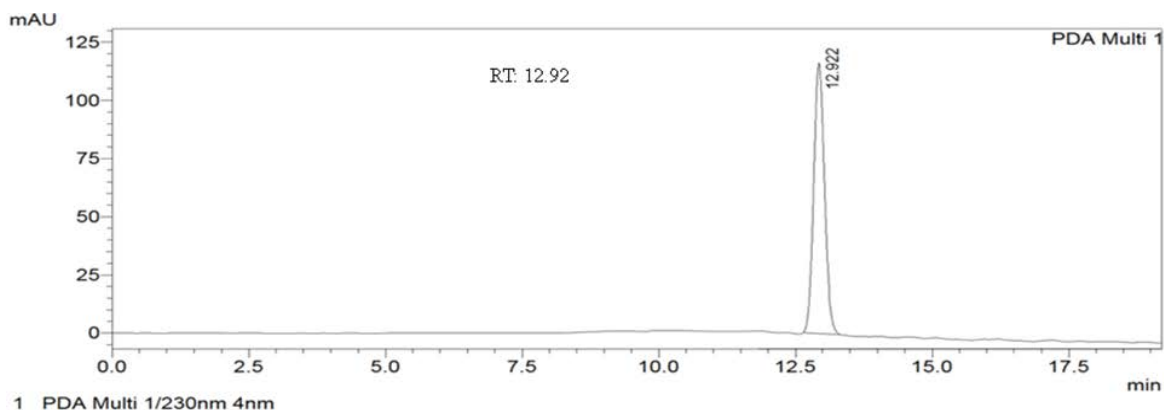


Figure 6.51.: HPLC chromatogram 6¹-(3-((*E*)-3^{1b}-(furan-2'-yl)-prop-3^{1b}-en-3¹-yl)-4a,5,6,8a-tetrahydro-8-methyl-2*H*-chromen-6-yl)-ethyl-5''-methyl-hexanoate (**4**)

The molecular ion peak was registered at m/z 413 (HRESIMS: found m/z 413.2694 $[M+1]^+$, cal. for $C_{26}H_{37}O_4$ 413.2692), which supported the chemical composition of **4** as $C_{26}H_{36}O_4$ (molecular mass: 412.2614) with nine double bond equivalences corresponding to five alkenic and one carbonyl, and three rings. The presence of aromatic ring was confirmed by three noteworthy peaks (δ 7.07, 7.29, 7.46; each with 1H) exhibiting HSQC correlations with the carbons at δ 124.45, 123.97 and 119.10, respectively (Table 6.9.; Figure 6.52., 6.53., 6.58.). The quaternary carbon at δ 152.12 (C-2') was exhibited significant downfield shift, and attributed to the carbon adjacent to an electronegative oxygen atom, which supported the possible substitution at C-2' of the furan ring system.

The long range HMBCs from δ 7.07 (H-4') to δ 123.97 (C-5'), 152.12 (C-2') further confirmed the presence of furan ring system (Figure 6.59.). The ^1H NMR spectrum was exhibited a highly deshielded singlet at δ 6.92 (assigned to H-3^{1b}) showing intense HSQC interaction with the carbon at δ 124.76 (-CH-), which confirmed the presence of an alkenic proton attached to the highly electronegative centre of furan ring system. These attributions were supported by the previously described chemical shift values of Hypofuran B (Ding *et al.*, 2015). The side chain attachment to furan at C-2' was established from the HMBC correlations between δ 6.92 (H-3^{1b}) to δ 152.12 (C-2'), 123.97 (C-5') and that between δ 6.92 (H-3^{1b}) to δ 30.20 (C-3^{1a}), 135.88 (C-3¹) established the presence of 3^{1b}-(furan-2'-yl)-prop-3^{1b}-en-3¹-yl framework with methyl (-CH₃) at its C-3^{1a} position (δH 1.26/ δC 30.20, s). These correlations were further confirmed the attachment of second carbon of prop-3^{1b}-ene to the C-3 of tetrahydro chromene. The ^1H NMR was enclosed two doublets at δ 4.08 and 4.22, which exhibited HSQC correlation with carbon at δ 62.10. The greater chemical shifts of these protons (δ 4.08 and 4.22) were attached to same carbon atom was probably due to the presence of strong electronegative moieties, such as oxygen/olefines. The olefinic signals at δ 5.30/128.80 (assigned to C-4 of tetrahydro chromene) was identified by the comparison of olefinic protons of benzopyran moiety in 6-acetyl-7-hydroxy-2,2-dimethylchromene isolated from *Calea pinnatifida*, in which H-4 proton appeared at highly downfielded region (δ 6.28) due to the adjacent benzene ring (Lima *et al.*, 2015). Likewise, the pyran moiety of 24-*O*-ethylmanoalide from marine sponge *Luffariella variabilis* exhibited comparable ^1H and ^{13}C NMR shifts at C-2 to C-4 positions of title compound (Bialecki *et al.*, 2008). HMBC correlations from δ 4.08 (H-2) to δ 147.06 (C-3); δ 4.22 (H-2) to δ 128.80 (C-4), 135.88 (C-3¹) were further affirmed the presence of tetrahydro benzopyran framework. ^1H - ^1H COSY correlations confirmed that the protons at C-6 and C-8 positions were attached to the ethyl (-CH₂-CH₂-) and methyl { δ 1.36 (s)/ δ 30.21} groups, respectively. The greater chemical shift of proton at δ 4.00 corresponding to δ 64.63 (C-6^{1a}) was due to the vicinity of oxygenated end of carboxylate group present at δ 173.34 (-C(O)-O) (attributed to C-1''). The HSQC spectrum was showed correlation between proton at δ 2.24 with the carbon at δ 34.30 that was found to be at the carbonyl (C=O) end. This compound enclosed three spin systems, such as H-3' to H- 5' { δ 7.46 (H-3')/7.07 (H-

4')/7.29 (H- 5') } in the furan ring; δ 5.30 (H-4)/2.54 (H-4a)/1.38 (H-5)/1.95 (H-6)/5.27 (H-7); δ 2.54 (H-4a)/2.78 (H-8a); δ 1.95 (H-6)/1.54 (H-6¹)/4.00 (H-6^{1a}) for 6¹-tetrahydro-8-methyl-2*H*-chromen-6-yl)-ethyl moiety, and H-2'' to H-6'' (δ 2.24 (H-2'')/1.51 (H-3'')/1.21 (H-4'')/1.98 (H-5'')/0.81 (H-5''a, H-6'') for 5''-methyl-hexanoate side chain (Figure 6.52.A, 6.57.). The long range HMBC correlations between δ 2.54 (H-4a) to δ 31.44 (C-8a); δ 1.38 (H-5) to δ 36.52 (C-4a); δ 2.78 (H-8a) to δ 36.52 (C-4a), 131.16 (C-8), 130.87 (C-7); δ 1.36 (H-8¹) to δ 131.16 (C-8), 31.44 (C-8a), 36.52 (C-4a); δ 1.54 (H-6a) to δ 31.94 (C-5); δ 4.00 (H-6¹) to δ 25.93 (C-6¹), 27.23 (C-6) were supported the presence of 6¹-(4a,5,6,8a-tetrahydro-8-methyl-2*H*-chromen-6-yl)-ethyl fragment (Figure 6.52.B, 6.59.). The HMBC correlations between δ 4.00 (H-6^{1a}) to δ 173.34 (C-1''); δ 2.24 (H-2'') to δ 173.34 (C-1''); δ 0.81(H-6'') to δ 22.70 (C-4''), 29.37 (C-3'') accounted for the presence of 6¹-ethyl-5''-methyl-hexanoate moiety. Likewise, the main carbon connectivity of **4**, featuring tetrahydro-8-methyl-2*H*-chromen-6-yl)-ethyl-5''-methyl-hexanoate framework was established. The relative configurations of the chiral carbons of **4** were established by detailed NOESY (Figure 6.60.). NOESY correlations between δ 1.36 (H-8¹) to δ 2.54 (H-4a); δ 2.78 (H-8a) to δ 1.95 (H-6) and δ 6.92 (H-3^{1b}) to δ 1.36 (H-8¹), indicated that these protons were co-facial, and β -orientated (Figure 6.53.). Consequently, the NOESYs between δ 7.29 (H-5') to δ 1.26 (H-3^{1a}) and from δ 1.26 (H-3^{1a}) to δ 1.98 (H-5'') were showed that these protons disposed at opposite plane of reference to that of H-4a/H-8a, therefore, assigned to be α -oriented. Detailed NOE assignments predicted that the protons at ring junctions (C-8a)/(C-4a) and chiral proton at C-6 were disposed at identical plane of symmetry of title compound, and considered as β -oriented. Based on these, the bulky 6¹-ethyl-5''-methyl-hexanoate group at C-6 position was found to dispose at different plane of reference to that of H-4a/H-8a, and α -oriented.

Table 6.9.: NMR spectroscopic data of 6¹-(3-((*E*)-3^{1b}-(furan-2'-yl)-prop-3^{1b}-en-3¹-yl)-4a,5,6,8a-tetrahydro-8-methyl-2*H*-chromen-6-yl)-ethyl-5''-methyl-hexanoate (**4**) in CDCl₃

C. No.	¹³ C	¹ H (int.,mult., <i>J</i> in Hz) ^a	COSY	HMBC
1	-	-	-	-
2	62.10	4.08 (1H,dd) 4.22 (1H,dd)	- -	C-3 C-4,3 ¹
3	147.06	-	-	-
3 ¹	135.88	-	-	-
3 ^{1a}	30.20	1.26 (3H α ,s)	-	C-3 ¹ ,3
3 ^{1b}	124.76	6.92 (1H β ,s)	-	C-2',5',3 ^{1a} , 3 ¹
4	128.80	5.30 (1H,d,11.20)	H-4a	C-3 ¹
4a	36.52	2.54 (1H β ,dt)	H-5,8a	C-8a
5	31.94	1.38 (2H,t)	H-6	C-4a
6	27.23	1.95 (1H β ,m)	H-6 ¹ ,7	
6 ¹	25.93	1.54 (2H,m)	H-6 ^{1a}	C-5
6 ^{1a}	64.63	4.00 (2H,t)	-	C-6a,6,1''
7	130.87	5.27 (1H,d,11.00)	-	-
8	131.16	-	-	-
8a	31.44	2.78 (1H β ,t)	-	C-4a,8,7
8 ¹	30.21	1.36 (3H β ,s)	-	C-8,8a,4a
1'	-	-	-	-
2'	152.12	-	-	-
3'	119.10	7.46 (1H,d,9.91)	H-4'	
4'	124.45	7.07 (1H,t,10.48)	H-5'	C-5',2'
5'	123.97	7.29 (1H,d,5.51)	-	-
1''	173.34	-	-	-
2''	34.30	2.24 (2H,m)	H-3''	C-1''
3''	29.37	1.51 (2H,m)	H-4''	-
4''	22.70	1.21 (2H,m)	H-5''	-
5''	30.20	1.98 (1H α ,m)	H-5''a,6''	-
5''a	14.10	0.81 (3H,d)	-	C-4'',3''
6''	14.10	0.81 (3H,d)	-	C-3''

¹H NMR spectra recorded using Bruker AVANCE III 500MHz (AV 500) spectrometer (Bruker, Karlsruhe, Germany) in CDCl₃ as aprotic solvent at ambient temperature with TMS as the internal standard (δ 0 ppm). The ¹H NMR spectra were recorded at 500MHz, while the ¹³C NMR spectra were recorded at 125MHz. ^aValues in ppm, multiplicity and

coupling constants (J =Hz) were indicated in parentheses. The assignments were made with the aid of the ^1H - ^1H COSY, HSQC, HMBC and NOESY experiments

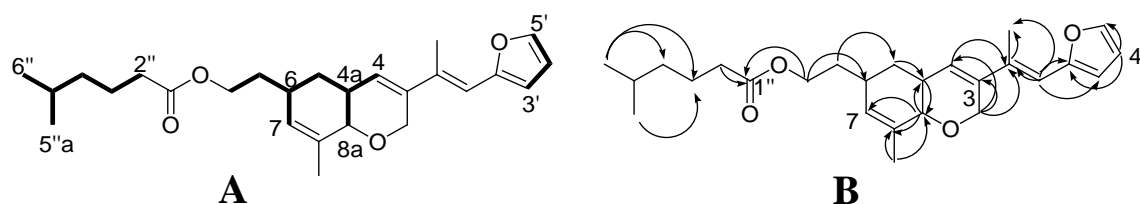


Figure 6.52.: ^1H - ^1H COSY (A) and HMBC (B) correlations of 6¹-(3-((*E*)-3^{1b}-(furan-2'-yl)-prop-3^{1b}-en-3¹-yl)-4a,5,6,8a-tetrahydro-8-methyl-2*H*-chromen-6-yl)-ethyl-5''-methyl-hexanoate (**4**). The key ^1H - ^1H COSY couplings have been represented by the bold face bonds. The HMBC couplings were indicated by double barbed arrow

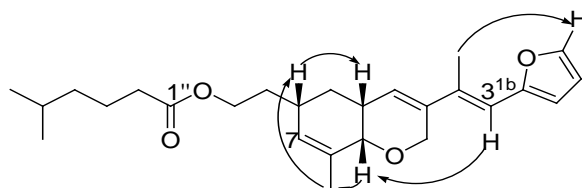


Figure 6.53.: NOESY correlations of 6¹-(3-((*E*)-3^{1b}-(furan-2'-yl)-prop-3^{1b}-en-3¹-yl)-4a,5,6,8a-tetrahydro-8-methyl-2*H*-chromen-6-yl)-ethyl-5''-methyl-hexanoate (**4**). The NOESY relations were represented by double barbed arrow

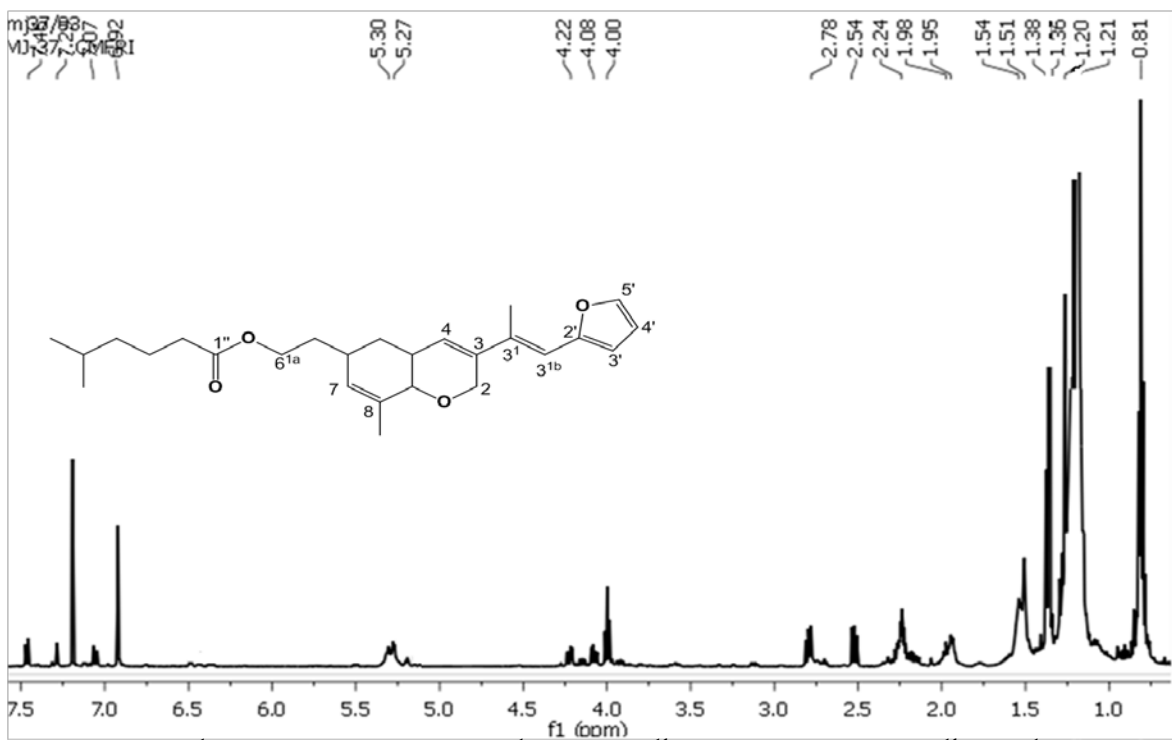


Figure 6.54.: ¹H NMR spectrum of 6¹-(3-((*E*)-3^{1b}-(furan-2'-yl)-prop-3^{1b}-en-3¹-yl)-4a,5,6,8a-tetrahydro-8-methyl-2*H*-chromen-6-yl)-ethyl-5''-methyl-hexanoate (4)

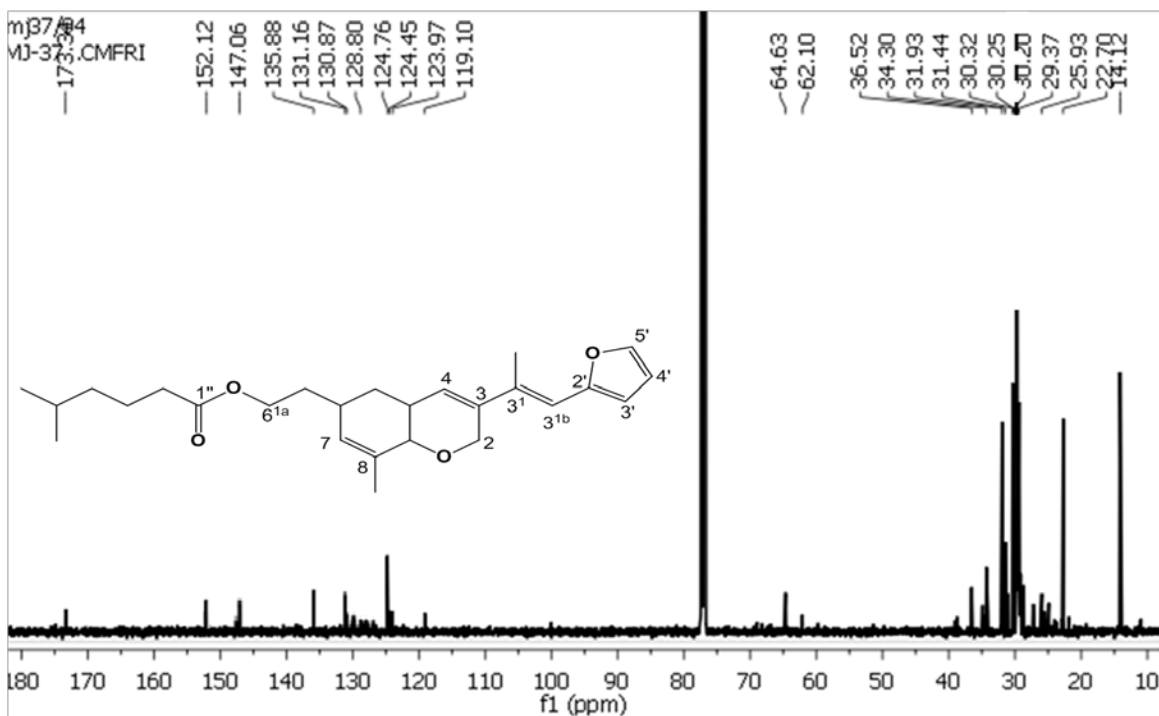


Figure 6.55.: ¹³C NMR spectrum of 6¹-(3-((*E*)-3^{1b}-(furan-2'-yl)-prop-3^{1b}-en-3¹-yl)-4a,5,6,8a-tetrahydro-8-methyl-2*H*-chromen-6-yl)-ethyl-5''-methyl-hexanoate (4)

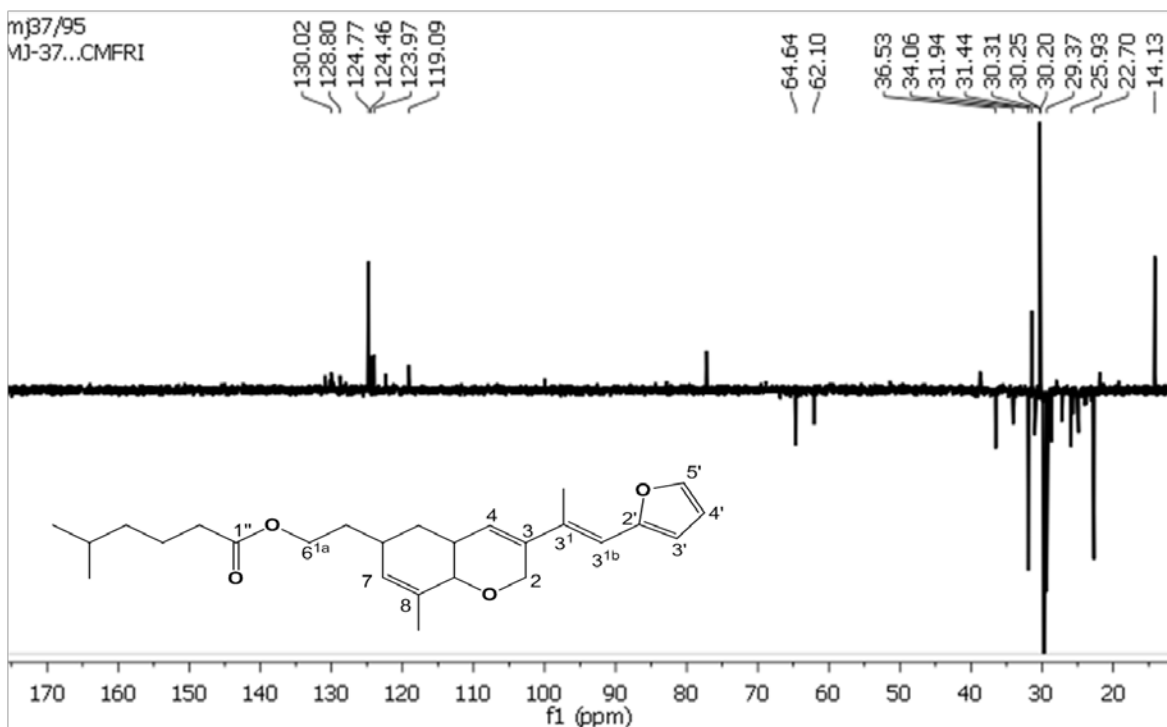


Figure 6.56.: $^{135}\text{DEPT}$ NMR spectrum of $6^1\text{-(3-((E)-3}^{1b}\text{-(furan-2'-yl)-prop-3}^{1b}\text{-en-3}^{1}\text{-yl)-4a,5,6,8a-tetrahydro-8-methyl-2H-chromen-6-yl)-ethyl-5''-methyl-hexanoate}$ (**4**)

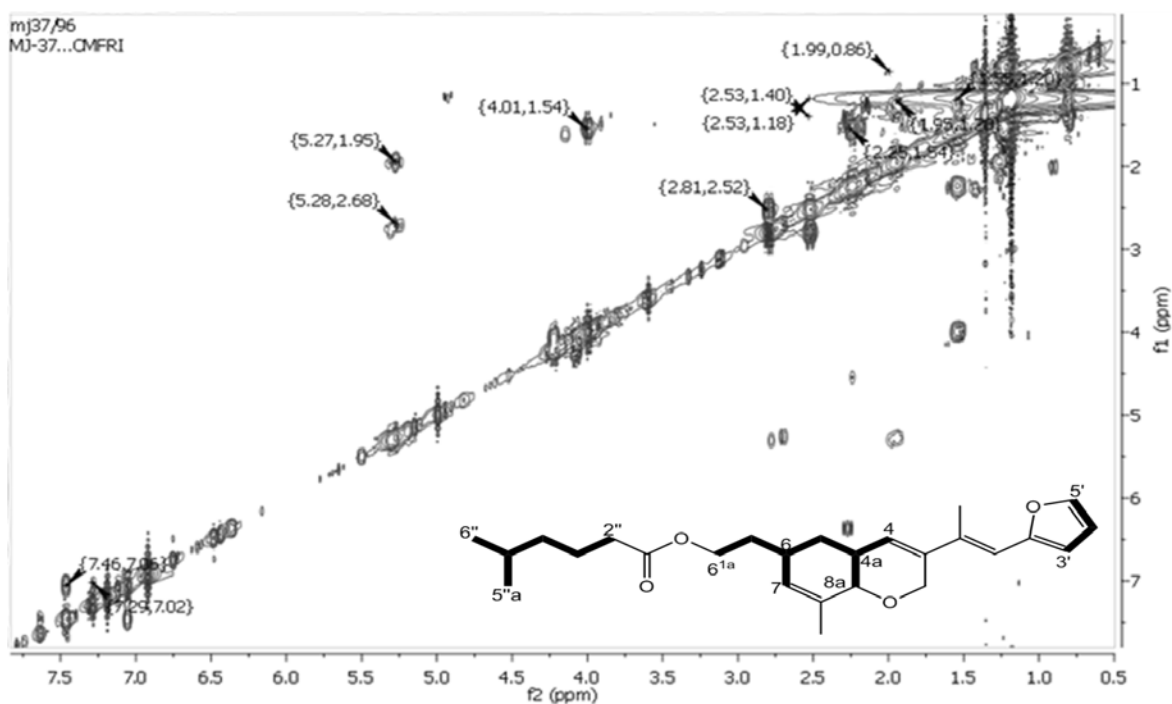


Figure 6.57.: $^1\text{H-}^1\text{H}$ COSY NMR spectrum of $6^1\text{-(3-((E)-3}^{1b}\text{-(furan-2'-yl)-prop-3}^{1b}\text{-en-3}^{1}\text{-yl)-4a,5,6,8a-tetrahydro-8-methyl-2H-chromen-6-yl)-ethyl-5''-methyl-hexanoate}$ (**4**)

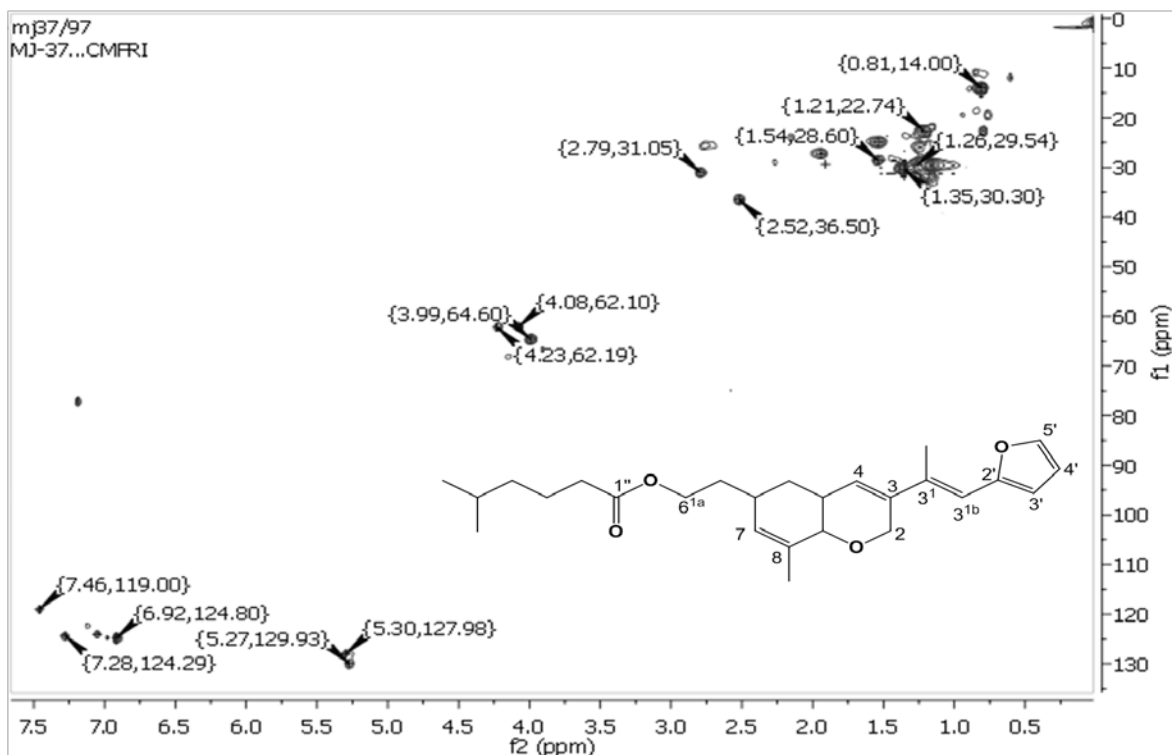


Figure 6.58.: HSQC NMR spectrum of 6¹-(3-((*E*)-3^{1b}-(furan-2'-yl)-prop-3^{1b}-en-3¹-yl)-4a,5,6,8a-tetrahydro-8-methyl-2*H*-chromen-6-yl)-ethyl-5''-methyl-hexanoate (**4**)

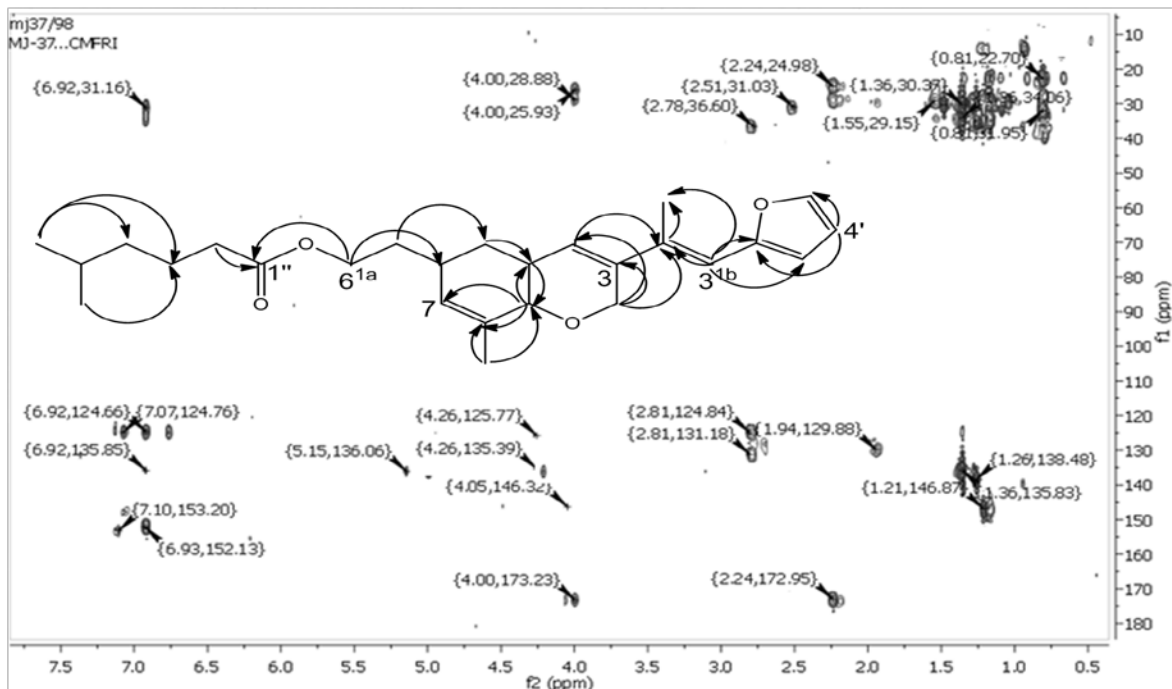


Figure 6.59.: HMBC NMR spectrum of 6¹-(3-((*E*)-3^{1b}-(furan-2'-yl)-prop-3^{1b}-en-3¹-yl)-4a,5,6,8a-tetrahydro-8-methyl-2*H*-chromen-6-yl)-ethyl-5''-methyl-hexanoate (**4**)

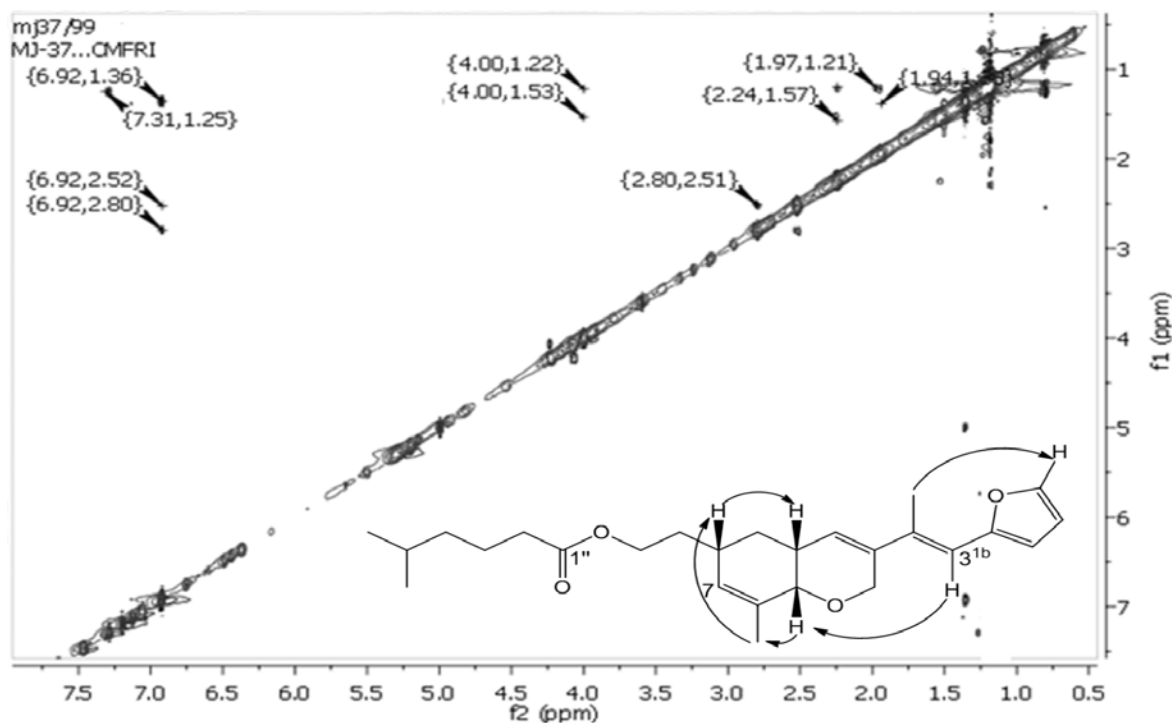


Figure 6.60.: NOESY NMR spectrum of 6¹-(3-((*E*)-3^{1b}-(furan-2'-yl)-prop-3^{1b}-en-3¹-yl)-4a,5,6,8a-tetrahydro-8-methyl-2*H*-chromen-6-yl)-ethyl-5''-methyl-hexanoate (**4**)

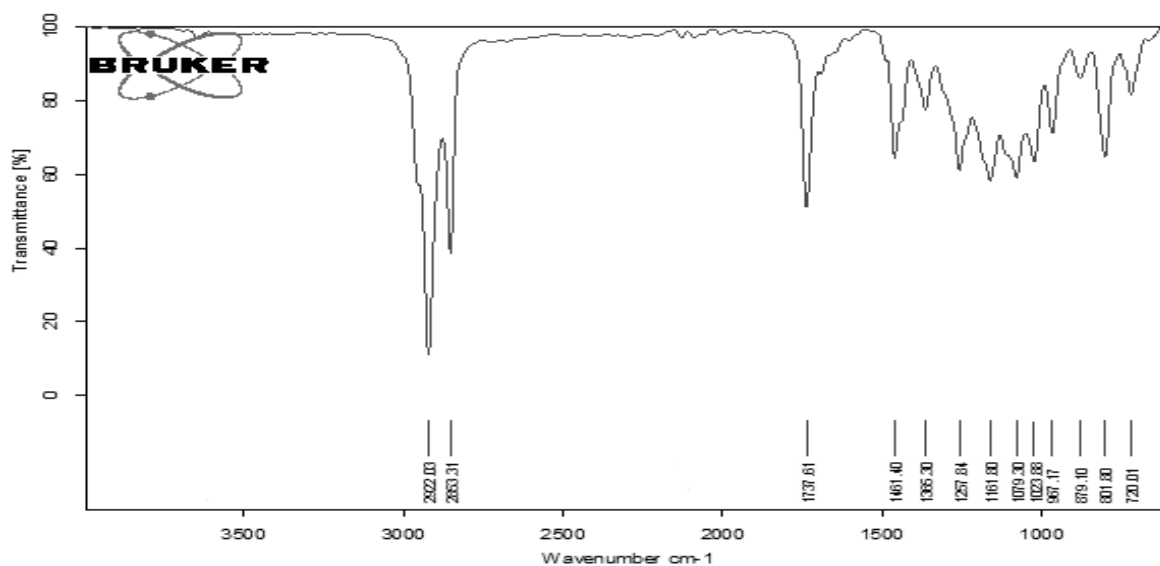


Figure 6.61.: FTIR spectrum of 6¹-(3-((*E*)-3^{1b}-(furan-2'-yl)-prop-3^{1b}-en-3¹-yl)-4a,5,6,8a-tetrahydro-8-methyl-2*H*-chromen-6-yl)-ethyl-5''-methyl-hexanoate (**4**)

IR spectrum indicated the presence of carbonyl and ester stretchings, which were represented by the bending vibrations at 1737 and 1161 cm⁻¹, respectively. Notably, the

intense IR peak at 1079 cm^{-1} represented the C-H bending vibrations of the furan ring. The stretching vibration bands at $2922, 2853\text{ cm}^{-1}$ denoted the occurrences of C-H alkyl absorptions. The C-H bending and rocking absorption bands were appeared at 1481 and 720 cm^{-1} (Figure 6.61.).

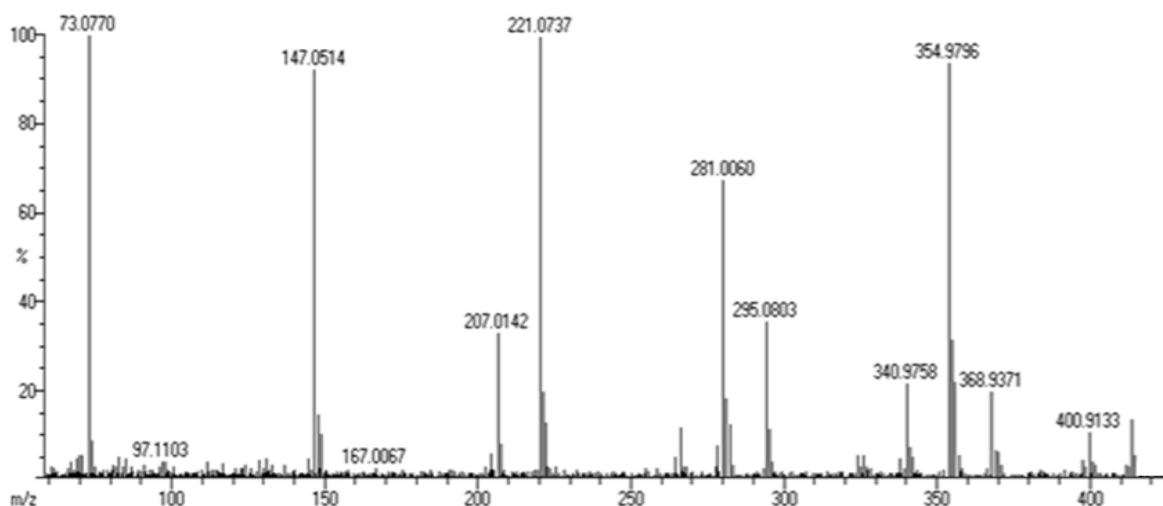


Figure 6.62.: EIMS spectrum of 6^1 -(3-((*E*)- 3^{1b} -(furan-2'-yl)-prop- 3^{1b} -en- 3^1 -yl)-4a,5,6,8a-tetrahydro-8-methyl-2*H*-chromen-6-yl)-ethyl-5''-methyl-hexanoate (**4**)

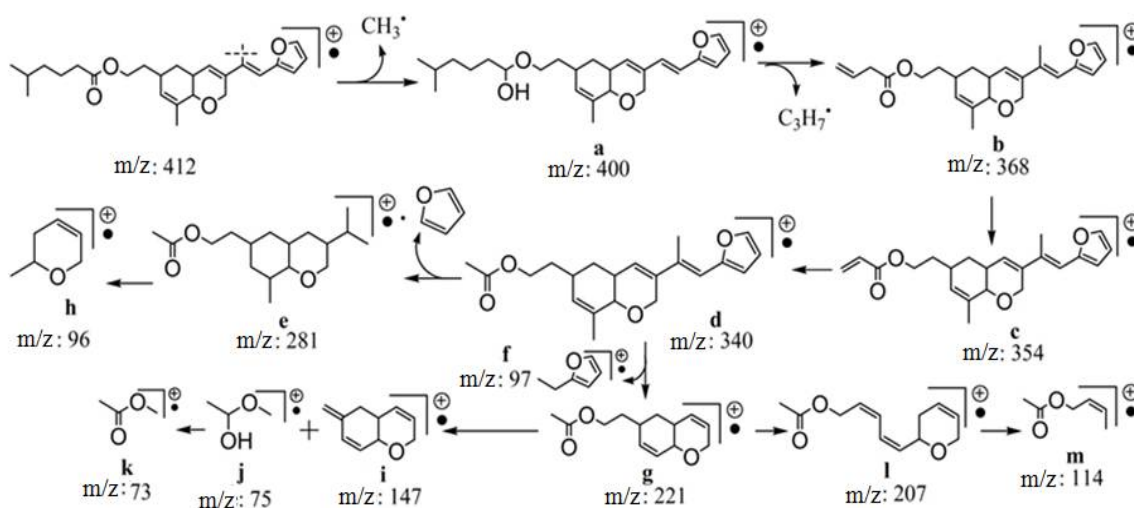
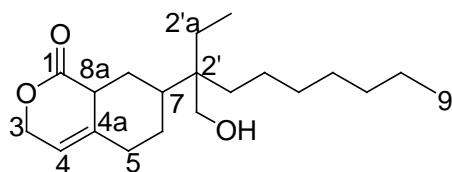


Figure 6.63.: Mass fragmentation pattern of 6^1 -(3-((*E*)- 3^{1b} -(furan-2'-yl)-prop- 3^{1b} -en- 3^1 -yl)-4a,5,6,8a-tetrahydro-8-methyl-2*H*-chromen-6-yl)-ethyl-5''-methyl-hexanoate (**4**)

The molecular ion peak at m/z 413 was appeared to yield fragment ions at m/z 400 (**a**), 368 (**b**), 354 (**c**) and 340 (**d**) (Figure 6.63.-6.64.). The elimination of vinylfuran and furan radical from the fragment ion at m/z 340 yielded the fragments with m/z 281 (**e**) and 221 (**g**). Subsequent fragmentation of the fragment ion at m/z 221 (**g**) resulted into radicals at m/z 207 (**l**), 147 (**i**), 114 (**m**), 96 (**h**) and 73 (**k**) (but-2-en-1-ol). Notably, the fragment ion at m/z 73 ($C_3H_5O_2^{++}$) appeared as base peak (de Carvalho *et al.*, 2001).

6.3.2.2.B. Structural characterization of compound 5 (PM₃₋₁₋₂₋₂)

7-(2'-Ethyl-1'-hydroxynonan-2'-yl)-6,7,8,8a-tetrahydro-3H-isochromen-1-(5H)-one (**5**)



Sample yield	90 mg; 0.18%
Physical description	Yellow oily
Molecular formula	$C_{20}H_{34}O_3$
Molecular mass	322.2508

The compound, 7-(2'-Ethyl-1'-hydroxynonan-2'-yl)-6,7,8,8a-tetrahydro-3H-isochromen-1-(5H)-one, is an isochromenone derivative (**5**) was isolated as a yellowish oil compound. It exhibited UV absorbance (in MeOH) at λ_{max} (log ϵ 3.99) 277.0 nm was assigned to a chromophore with ester carbonyl groups (Figure 6.65.). The purity of the compound was supported by RP C18 HPLC experiments using 3:2 (v/v) MeOH:MeCN (R_t 3.80) solvent system (Figure 6.66.).

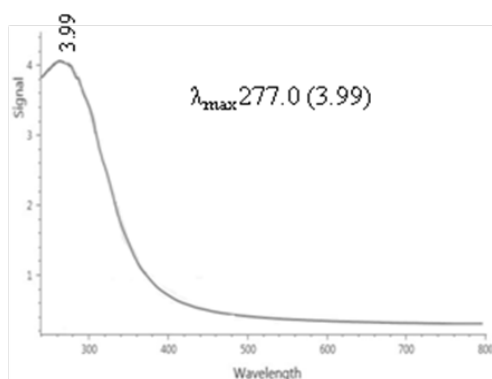


Figure 6.64.: UV spectrum of 7-(2'-ethyl-1'-hydroxynonan-2'-yl)-6,7,8,8a-tetrahydro-3H-isochromen-1-(5H)-one (**5**)

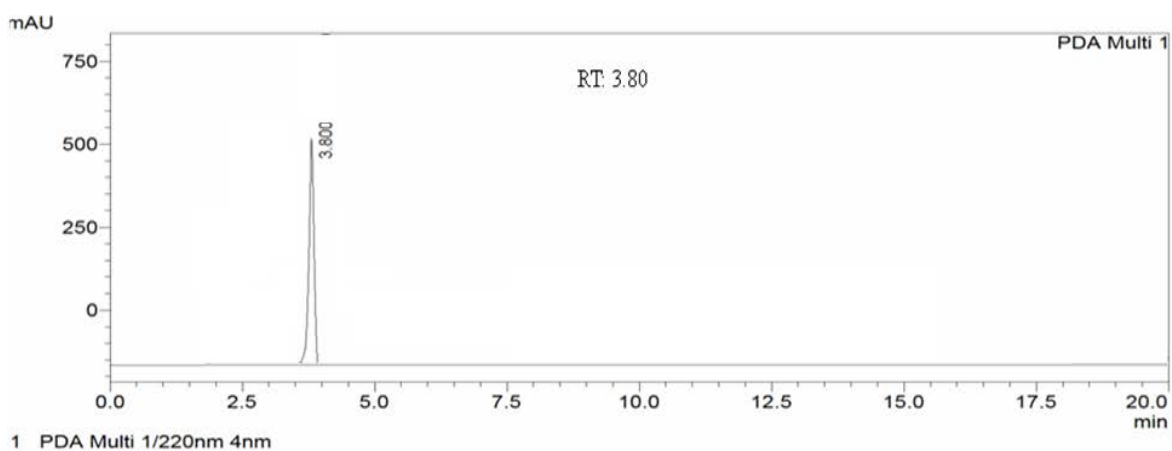


Figure 6.65.: HPLC chromatogram of 7-(2'-ethyl-1'-hydroxynonan-2'-yl)-6,7,8,8a-tetrahydro-3H-isochromen-1-(5H)-one (**5**)

Aromatic region (δ 6.5-8.5) of the compound **5** did not exhibit any notable signals, which confirmed the absence of aromatic moiety (Figure 6.68.). The molecular ion peak at m/z 322 (EIMS: found m/z 322.2512 $[M]^+$, cal. 322.2508) supported the elemental composition of **5** as $C_{20}H_{34}O_3$ with 4 degrees of double bond equivalence (one each of alkene and C=O alongside two rings) based on the characteristic chemical shifts of protons and carbons (1H and ^{13}C NMR) and previously reported NMR values (Table 6.10.) (Li *et al.*, 2015). The ^{13}C NMR exhibited a peak at δ 173.34 (Figure 6.69.), which has been confirmed as quaternary carbon based on DEPT analysis (Figure 6.70.). It was evident from the fact that the chemical shift in the range δ 170-185 apparently forms a part of carbonyl group,

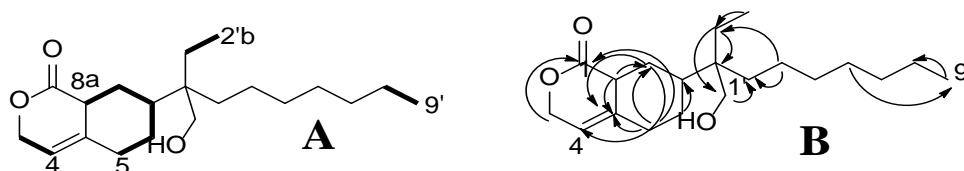
preferably an ester moiety, and thus the carbon at δ 173.34 was attributed to C-1. These chemical shift assignments were in accordance with those reported for previously described 6-hydroxy-5-methylramulosin (El-Beih *et al.*, 2007). The proton attached next to the oxygen of ester group was highly deshielded and registered higher chemical shift of about δ 4.0-4.5, due to the intense electron withdrawing ability of -C(O)O- group. Thus, the highly deshielded ^1H signal at δ 4.28/4.14 exhibited HSQC with δ 61.93 (attributed to C-3) that correspond to the methylene group residing next to an ester linkage (Figure 6.72.). An intense ^1H - ^1H COSY correlation with the protons at δ 5.34 (H-4) to those at δ 4.28/4.14 (assigned as H-3) further affirmed this attributions (Figure 6.71., 6.66.A). The protons at C-3 also exhibited long range HMBC correlation with the carbon at δ 173.34 (C-1) (Figure 6.66.B, 6.73.). The ^{13}C peak appeared at δ 130.89 (C-4) and 144.43 represented a double bond. The highly deshielded proton at δ 5.34 ($J=9.85$ Hz, 1H) attached to the carbon at δ 130.89 (HSQC) was noted. The relatively greater downfield shift of δ 144.43 (attributed to C-4a) referred to a quaternary carbon next to the double bond in the pyranone ring. Notably, the ^{13}C NMR signal appeared at downfield region (δ 144.43) was less intense than the adjacent peak at δ 130.89, because of slow relaxation, and therefore, confirmed as a quaternary carbon. These attributions were corroborated with previous study, which explained that the olefinic proton exhibited resonances at δ 5.0-5.6 (br, $J > 5$ Hz) due to $>\text{C}=\underline{\text{CH}}\text{-CH}_2$ moiety (Goad and Akihisa 1997). The moderately deshielded proton at δ 2.0-2.4 was due to the presence of electron withdrawing groups, and thus, it was inferred that the attachment of carbon atom of carbonyl ($>\text{C}=\text{O}$) to methine ($-\underline{\text{CH}}-$) proton exerted a downfield shift of δ 1.0 than the typical chemical shift of $-\underline{\text{CH}}-$ proton. HMBC correlations determined the proton signal at δ 2.30 (assigned to H-8a) was attached to the carbon of $-\underline{\text{C}}=\text{O}$ (C-1). Further the HMBC correlation between δ 2.30 (H-8a) and δ 144.43, attributed to C-4a, confirmed the presence of hexacyclic ring system with carboxylate moiety (pyranone). The proton at δ 2.31, which was found to be present next to quaternary alkenic carbon (C-4a) exhibited intense ^1H - ^1H COSY correlations between δ 2.31 (H-5)/1.60 (H-6)/1.33 (H-7)/2.01 (H-8)/2.30 (H-8a), which supported the presence of adjacent protons from H-5 to H-8a (Figure 6.71.). Furthermore, HMBC correlations from δ 2.31 (H-5) to δ 173.34 (C-1), 27.22 (C-8), 144.43 (C-4a); δ 1.60 (H-6) to δ 173.34 (C-1), 34.04 (C-7); δ

2.01 (H-8) to δ 144.43 (C-4a), 130.89 (C-4) and δ 2.30 (H-8a) to δ 27.22 (C-8) were unambiguously determined the occurrence of another hexacyclic ring (Figure 6.73.). Thus, the bicyclic system with carboxylate moiety in compound **5** was evident, which was characterized as 6,7,8,8a-tetrahydro-3*H*-isochromen-1-(5*H*)-one, and can be related to the literature of pyrones isolated from marine source (Kim *et al.*, 2014). The previous study on isolation of δ -lactone isochromanone was supported the numbering and framework of elucidated compound (Li *et al.*, 2015). The HMBC correlations from δ 1.33 (H-7) to δ 29.69 (C-4'); δ 1.60 (H-6) to δ 31.77 (C-3') and δ 2.01 (H-8) to δ 31.77 (C-3') were supported the side chain extended from C-7 of tetrahydro isochromenone moiety. The side chain enclosed a highly downfield singlet at δ 3.48 (H-1') was due to a secondary carbon (δ 50.69) attached to the hydroxyl group. The low-field aliphatic resonances from H-3' through H-9' (δ 1.25, 1.28, 1.29, 1.28, 1.27, 1.28 and 0.88, respectively) were accounted for the nonane side chain of **5**. An ethyl group attached at δ 42.41 (C-2') was showed COSY from δ 1.25 (H-2^{1a}) to δ 0.86 (H-2^{1b}) and HMBC from δ 0.86 (H-2^{1b}) to δ 31.92 (C-2^{1a}). The HMBC correlations between δ 1.25 (H-2^{1a}) to δ 50.69 (C-1'), 0.86 (H-2^{1b}), 50.69 (C-1') and from δ 1.28 (H-4') to δ 50.69 (C-1') were supported the positions of hydroxyl and ethyl groups. The total number of carbon atoms were found to be 20 from detailed ¹³C and DEPT analysis, in which two -CH₃, twelve -CH₂ and three -CH groups were apparent. The relative configurations of the chiral carbons, C-8a and C-7 were deduced by detailed NOESY experiments (Figure 6.74.). NOESY correlations were apparent between δ 4.28 (H-3)/5.34 (H-4) and δ 4.14 (H-3)/2.30 (H-8a)/1.33 (H-7), although no correlations were evident between δ 4.28 (H-3) and 2.30 (H-8a) (Figure 6.67.). The protons at ring junction (C-8a) and the side chain attached to the chiral carbon (C-7) were disposed at the identical plane of reference of **5**, and considered to be oriented at the β position, whereas the protons at H-3 (δ 4.28) implied at the α -position. These correlations further confirmed that the bulky side chain bearing 2'-ethyl-1'-hydroxynonan-1-yl moiety was α -oriented.

Table 6.10.: NMR spectroscopic data of 7-(2'-ethyl-1'-hydroxynonan-2'-yl)-6,7,8,8a-tetrahydro-3*H*-isochromen-1-(5*H*)-one (**5**) in CDCl₃

C. No.	¹³ C	¹ H (int.,mult., <i>J</i> in Hz) ^a	COSY	HMBC
1	173.34	-	-	-
2	-	-	-	-
3	61.93	4.28 (1H α ,d) 4.14 (1H β ,d)	H-4 H-4	C-1 C-1
4	130.89	5.34 (1H α , t,9.85)	-	-
4a	144.43	-	-	-
5	34.00	2.31 (2H,t)	H-6	C-1,8,4a
6	24.80	1.60 (2H,m)	H-7	C-1,7,3'
7	34.04	1.33 (1H β ,m)	H-8	C-4'
8	27.22	2.01 (2H,t)	H-8a	C-4a,4,3'
8a	38.20	2.30 (1H β ,t)	-	C-8,4a
1'	50.69	3.48 (2H,s)	-	C-3',2'
2'	42.41	-	-	-
2'a	31.92	1.25 (2H)	H-2'b	C-1',2'
2'b	22.60	0.86 (3H,t)	-	C-1',2'a
3'	31.77	1.25 (2H)	-	-
4'	29.69	1.28 (2H)	-	C-8',3',1'
5'	29.30	1.29 (2H)	-	C-9''
6'	29.20	1.28 (2H)	-	-
7'	29.10	1.27 (2H)	-	-
8'	22.50	1.28 (2H)	H-9'	-
9'	14.10	0.88 (3H,t)	-	C-8'

¹H NMR spectra recorded using Bruker AVANCE III 500MHz (AV 500) spectrometer (Bruker, Karlsruhe, Germany) in CDCl₃ as aprotic solvent at ambient temperature with TMS as the internal standard (δ 0 ppm). The ¹H NMR spectra were recorded at 500MHz, while the ¹³C NMR spectra were recorded at 125MHz. ^aValues in ppm, multiplicity and coupling constants (*J*=Hz) were indicated in parentheses. The assignments were made with the aid of the ¹H-¹H COSY, HSQC, HMBC and NOESY experiments

**Figure 6.66.:** ¹H-¹H COSY (A) and HMBC (B) correlations of 7-(2'-ethyl-1'-hydroxynonan-2'-yl)-6,7,8,8a-tetrahydro-3*H*-isochromen-1-(5*H*)-one (**5**). The key ¹H-¹H COSY

couplings have been represented by the bold face bonds. The HMBC couplings were indicated by double barbed arrow

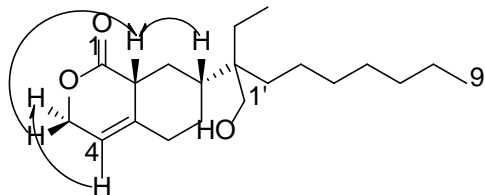


Figure 6.67.: NOESY correlations of 7-(2'-ethyl-1'-hydroxynonan-2'-yl)-6,7,8,8a-tetrahydro-3*H*-isochromen-1-(5*H*)-one (**5**). The NOESY relations were represented by double barbed arrow

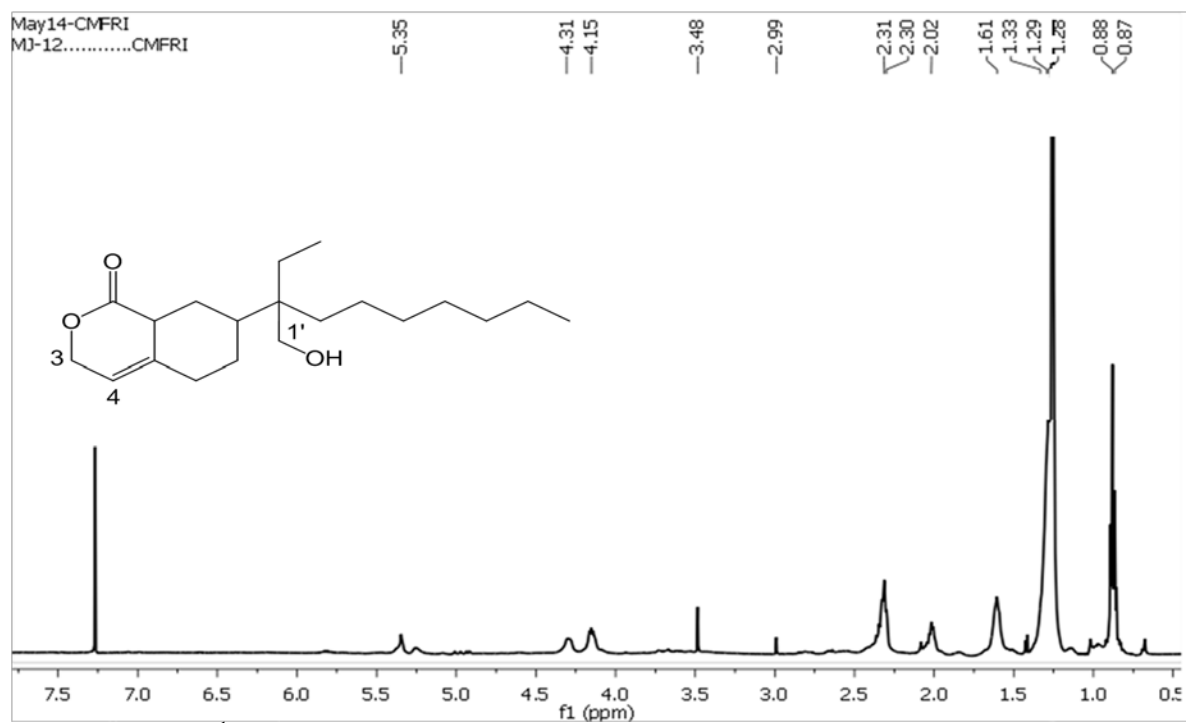


Figure 6.68.: ¹H NMR spectrum of 7-(2'-ethyl-1'-hydroxynonan-2'-yl)-6,7,8,8a-tetrahydro-3*H*-isochromen-1-(5*H*)-one (**5**)

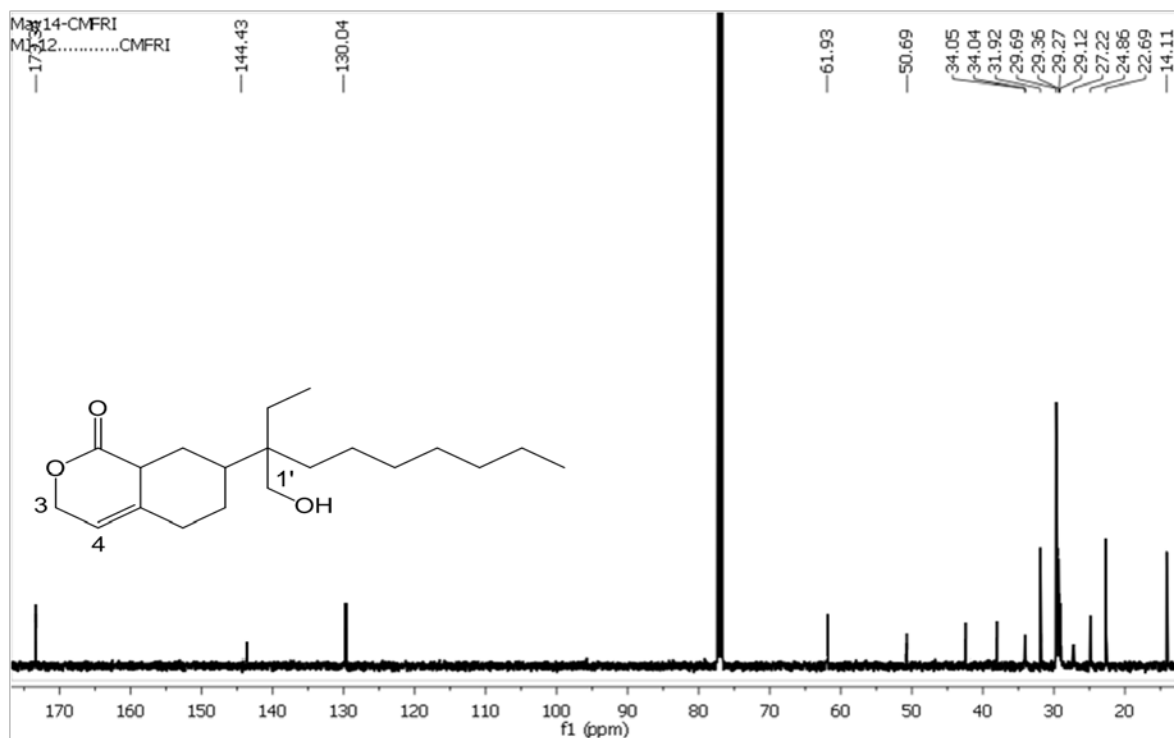


Figure 6.69.: ^{13}C NMR spectrum of 7-(2'-ethyl-1'-hydroxynonan-2'-yl)-6,7,8,8a-tetrahydro-3H-isochromen-1-(5H)-one (5)

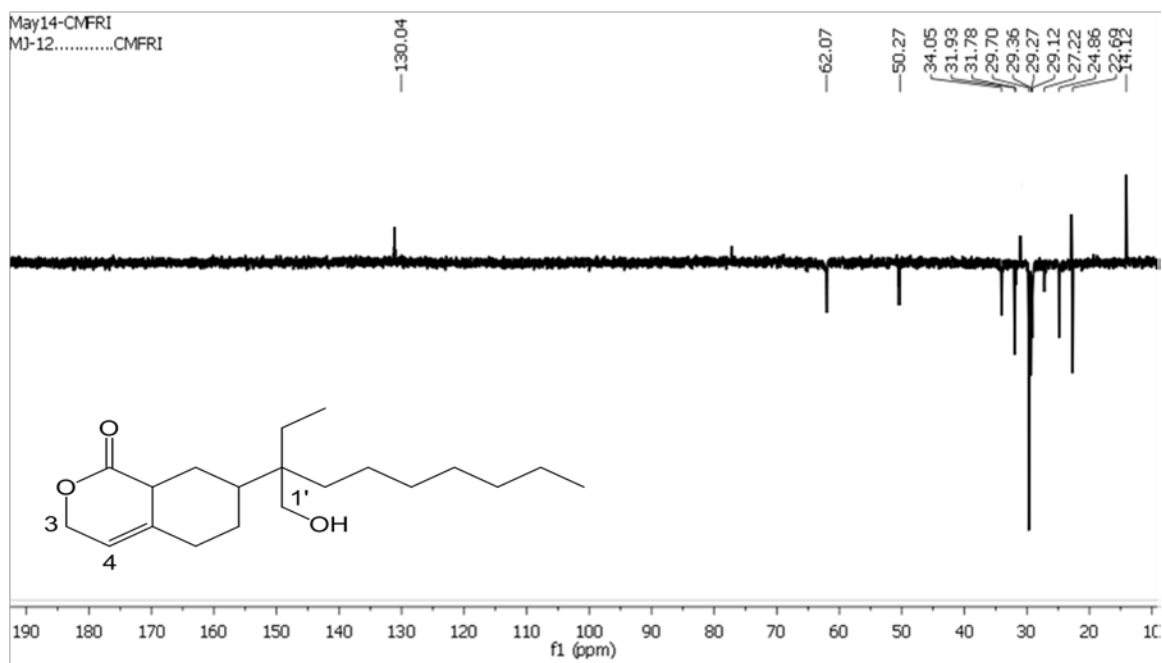


Figure 6.70.: $^{135}\text{DEPT}$ NMR spectrum of 7-(2'-ethyl-1'-hydroxynonan-2'-yl)-6,7,8,8a-tetrahydro-3H-isochromen-1-(5H)-one (5)

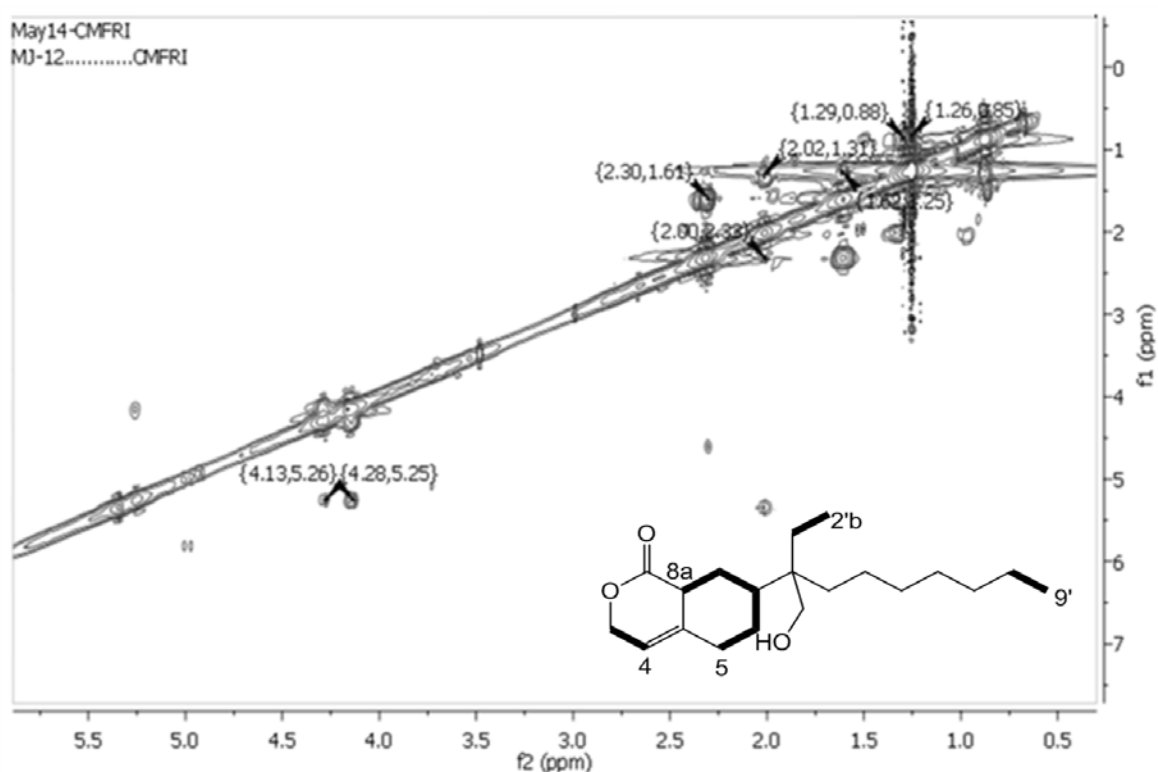


Figure 6.71.: ^1H - ^1H COSY NMR spectrum of 7-(2'-ethyl-1'-hydroxynonan-2'-yl)-6,7,8,8a-tetrahydro-3H-isochromen-1-(5H)-one (**5**)

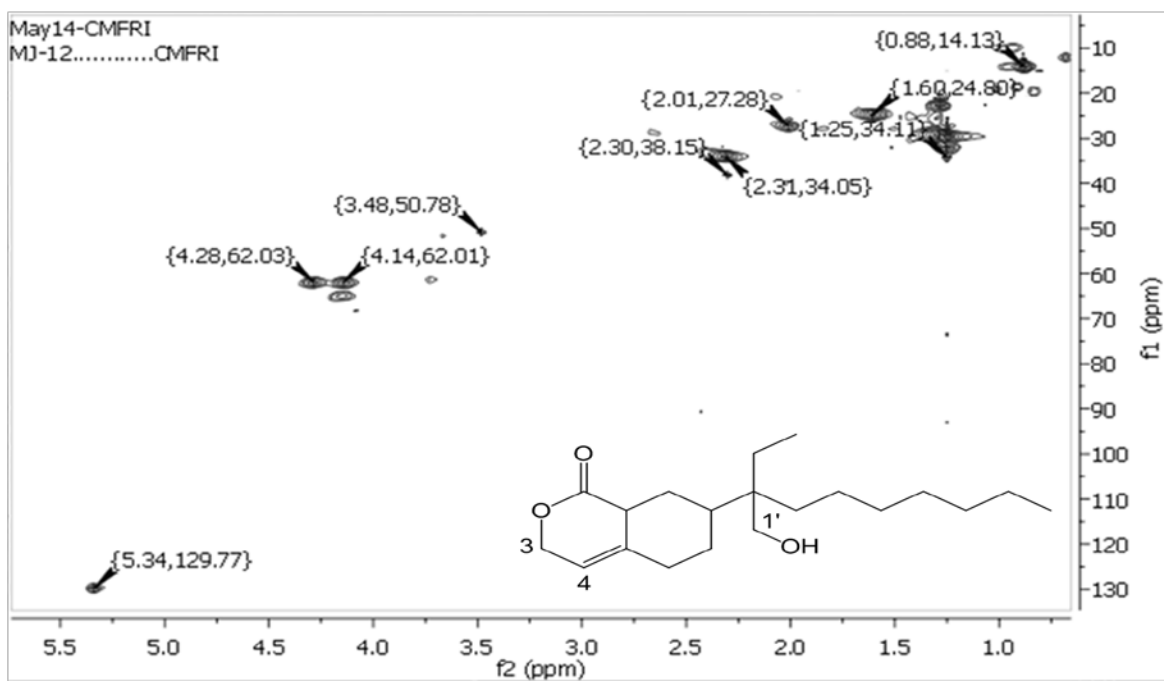


Figure 6.72.: HSQC NMR spectrum of 7-(2'-ethyl-1'-hydroxynonan-2'-yl)-6,7,8,8a-tetrahydro-3H-isochromen-1-(5H)-one (**5**)

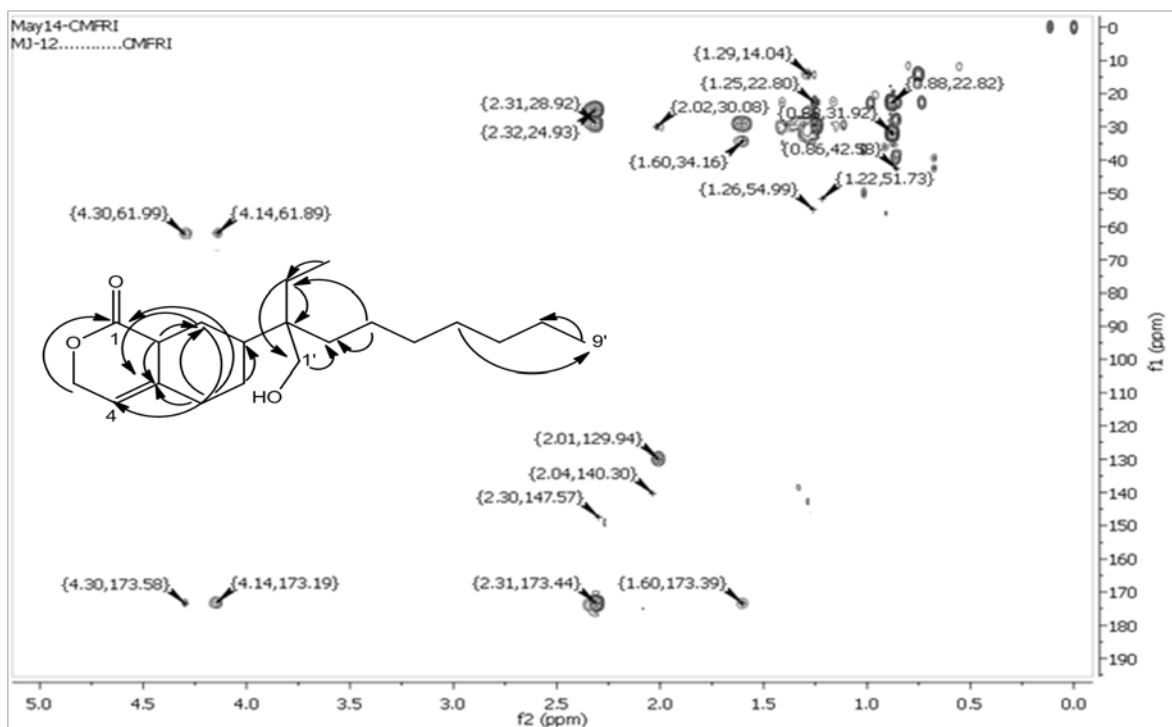


Figure 6.73.: HMBC NMR spectrum of 7-(2'-ethyl-1'-hydroxynonan-2'-yl)-6,7,8,8a-tetrahydro-3H-isochromen-1-(5H)-one (**5**)

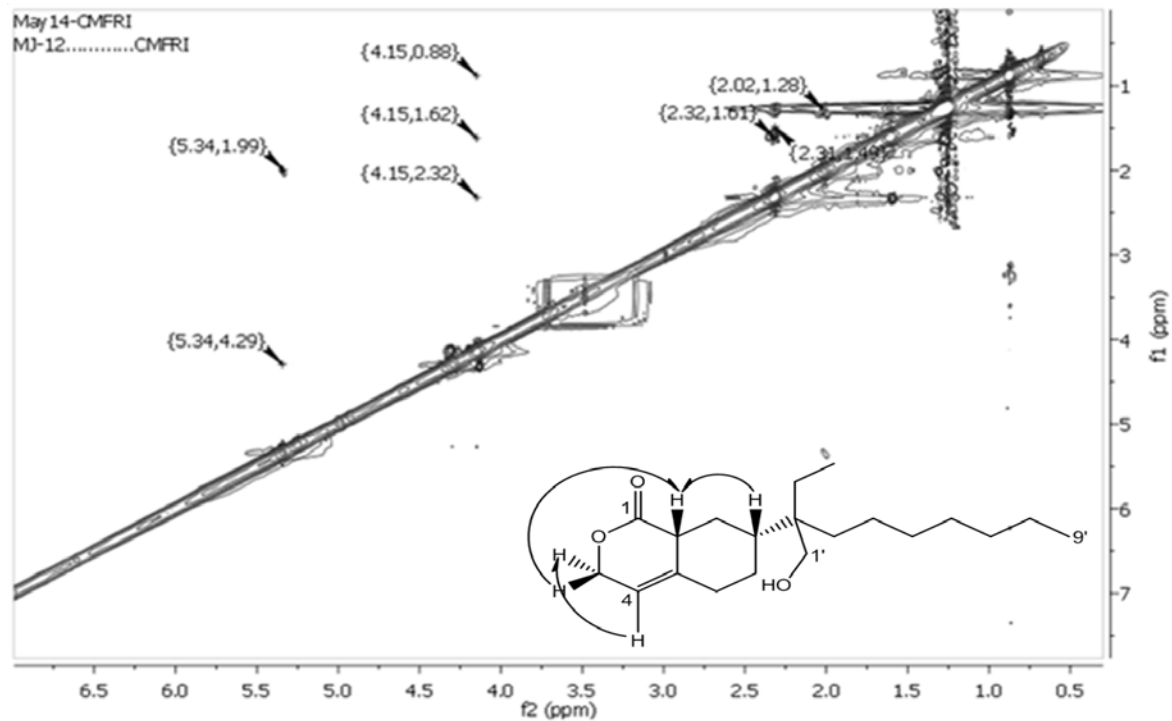


Figure 6.74.: NOESY NMR spectrum of 7-(2'-ethyl-1'-hydroxynonan-2'-yl)-6,7,8,8a-tetrahydro-3H-isochromen-1-(5H)-one (**5**)

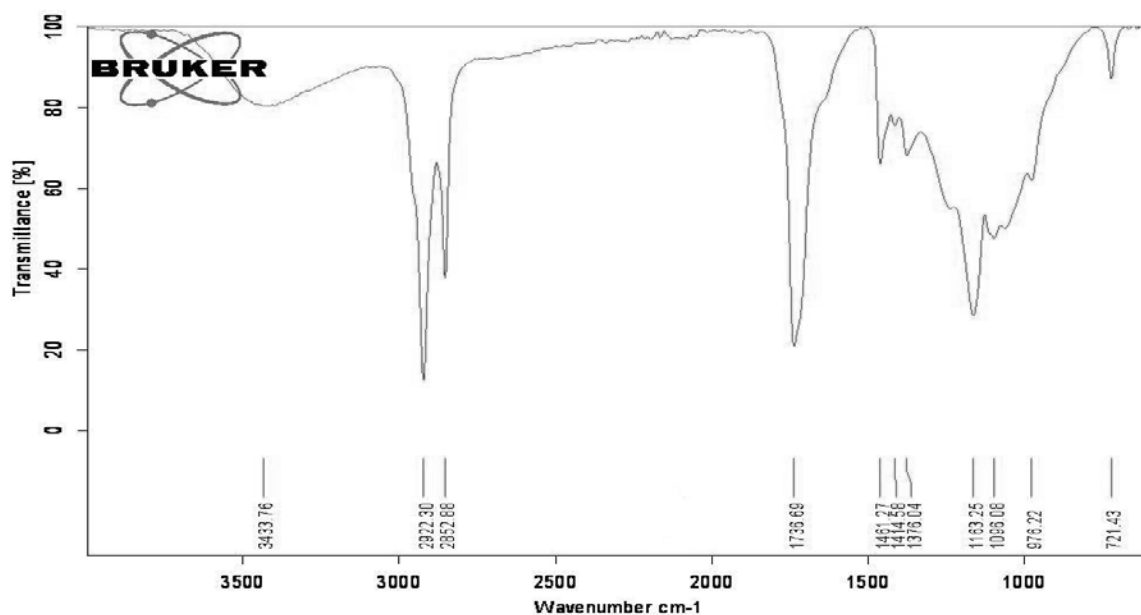


Figure 6.75.: FTIR spectrum of 7-(2'-ethyl-1'-hydroxynonan-2'-yl)-6,7,8,8a-tetrahydro-3*H*-isochromen-1-(5*H*)-one (**5**)

The distinctive IR absorption peak at 3433 cm⁻¹ indicated O-H stretching vibration. The C-H bending and rocking absorption bands were appeared at 1481-1414 and 721 cm⁻¹ (Figure 6.75.). The carbonyl and alkyl stretching vibrations at 1736 and 2922/2852 cm⁻¹, respectively concurred with the structure of **5**.

The mass and fragmentation pattern for compound **5** was given in Figure 6.76., 6.77. The titled compound initially fragmented ethyl radical to yielded a fragment ion at *m/z* 294 (**a**). The later underwent successive side chain elimination of methyl, propyl and hydroxyl radicals resulting in fragments with *m/z* 280 (**b**), 239 (**c**), and 221 (**d**), respectively. The fragment ion, 7-butyl-tetrahydro-3*H*-isochromen-1-(5*H*)-one at *m/z* 208 (**e**) were formed from *m/z* 221 (**d**) by removal of a CH₃• radical. The base peak was recorded at *m/z* 73 (**i**, vinyl formate) that was obtained by the successive fragmentation of fragment ion at *m/z* 208. This base peak was typical to the presence of isochromenone moiety (de Carvalho *et al.*, 2001).

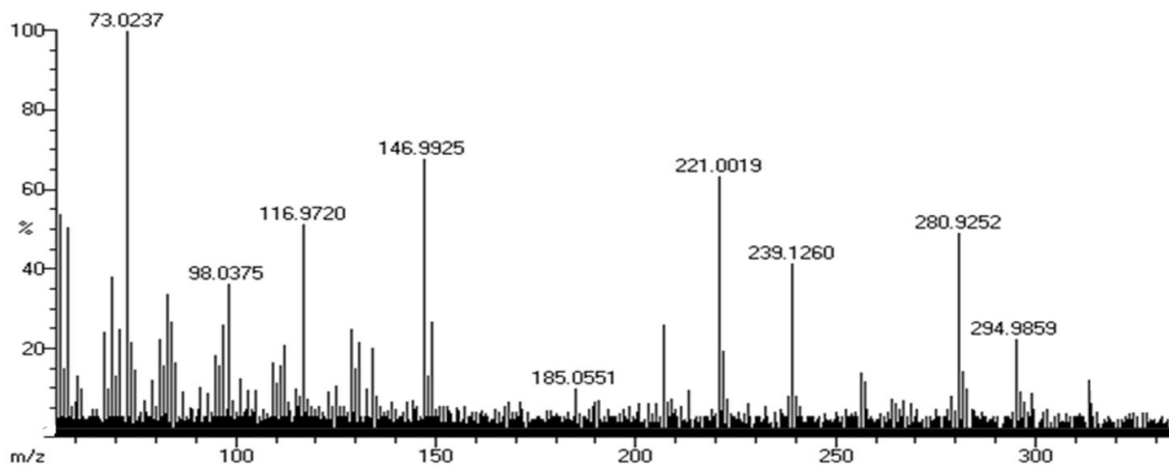


Figure 6.76.: EIMS spectrum of 7-(2'-ethyl-1'-hydroxynonan-2'-yl)-6,7,8,8a-tetrahydro-3H-isochromen-1-(5H)-one (**5**)

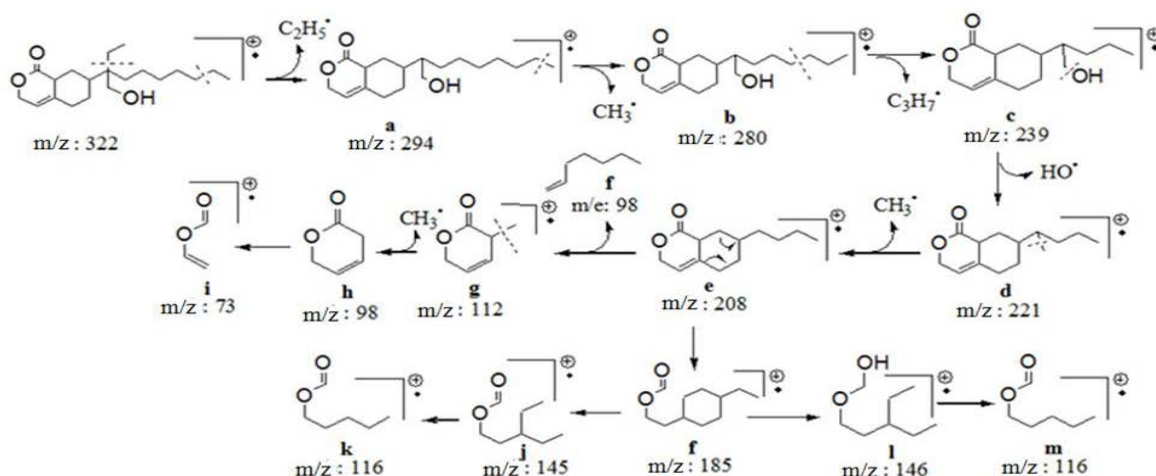


Figure 6.77.: Mass fragmentation pattern of 7-(2'-ethyl-1'-hydroxynonan-2'-yl)-6,7,8,8a-tetrahydro-3H-isochromen-1-(5H)-one (**5**)

Notably, the basic structural framework of **5** was showed significant similarity with α -tocopherol, whereas the benzopyran moiety (of α -tocopherol) was substituted by the hydrogenated benzopyran ring of **5**. However, compound **4** enclosed a hydrogenated benzopyranone moiety with an electronegative heterocyclic centre, a furan ring, and therefore, exhibited greater antioxidative activities. The isochromenone moiety in **5** showed structural similarities with bioactive ramulosin derivative, isolated from *Codium fragile* (El-Beih *et al.*, 2007). Antioxidative roridin was identified from marine sponges and characterized to enclose a chromene moiety (Xu *et al.*, 2006). The isolation and

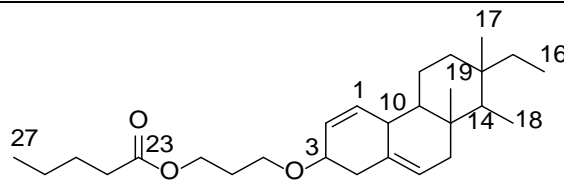
characterization of bioactive natural chromanones and chromenes consisting of benzene ring have been identified and reported (Ballio *et al.*, 1966). Likewise, furan containing metabolites from *Hypocrea koningii*, furanoid terpenes from sea slug *Doriopsilla pelseneeri* and furan fatty acids from *P. canaliculus* were found to be potent DPPH radical scavengers and anti-inflammatory agents (Ding *et al.*, 2015; Gaspar *et al.*, 2005; Wakimoto *et al.*, 2011). These results showed the importance and greater utilities of chromene and isochromenone containing compounds as rancidity deterring agents in food systems.

6.3.2.3. Structural characterization of isopimarane norditerpenoid derivative (6)

Isopimarane and pimarane metabolites were classified as significantly important class of diterpenoids with interesting pharmacological properties, like anti-diabetic, antioxidant and anti-microbial activities, and reported in marine organisms (Porto *et al.*, 2009; Sun *et al.*, 2012). Although, rare in occurrence, three cytotoxic isopimarane diterpenoids from *Excoecaria acerifolia* (Huang *et al.*, 2013) and brominated pimaranes from *Laurencia obtusa* (Takeda *et al.*, 1990) were previously reported. An ent-pimarane diterpenoid tedanol was isolated from the marine sponge *Tedania ignis* and was reported to possess potential anti-inflammatory activity against COX-2 enzyme (Costantino *et al.*, 2009). The bioactive diterpenoids with pimarane skeletons were also described from the marine mollusks, *A. dactylomela* (Schmitz *et al.*, 1982) and *A. pulmonica* (Bian *et al.*, 2014). Herein, we have described the characterization of new rearranged isopimarane norditerpenoid with bioactive potentials.

6.3.2.3.A. Structural characterization of compound 6 (PM_{4.4.1})

18 (4→14),19 (4→8) Bis-abeo-nor-isopimarane-1,5-dien-3-yl-3β-methoxy propyl pentanoate (6)



Sample yield

95 mg; 0.19%

Physical description	White solid
Molecular formula	$C_{27}H_{44}O_3$
Molecular mass	416.3290

The repeated chromatographic separation of EtOAc/MeOH extract of *P. malabarica* yielded a C_{19} isopimarane norditerpenoid derivative (**6**), as white solid. It exhibited UV absorbance (in MeOH) at λ_{\max} (log ϵ 3.12) 270.0 nm was assigned to a chromophore with ester carbonyl and olefinic groups (Figure 6.78.). The purity of the compound was supported by RP C18 HPLC experiments using 3:2 (v/v) MeOH:MeCN (R_t 3.85) (Figure 6.79.).

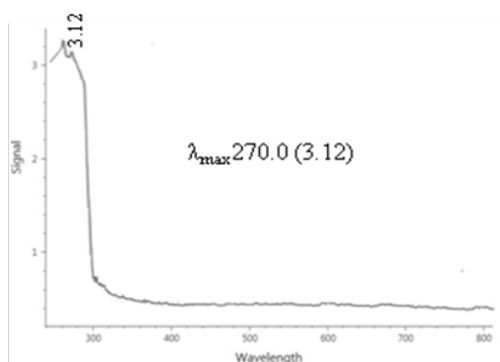


Figure 6.78.: UV spectrum of 18 (4→14),19 (4→8) bis-abeo-nor-isopimarane-1,5-dien-3-yl-3 β -methoxy propyl pentanoate (**6**)

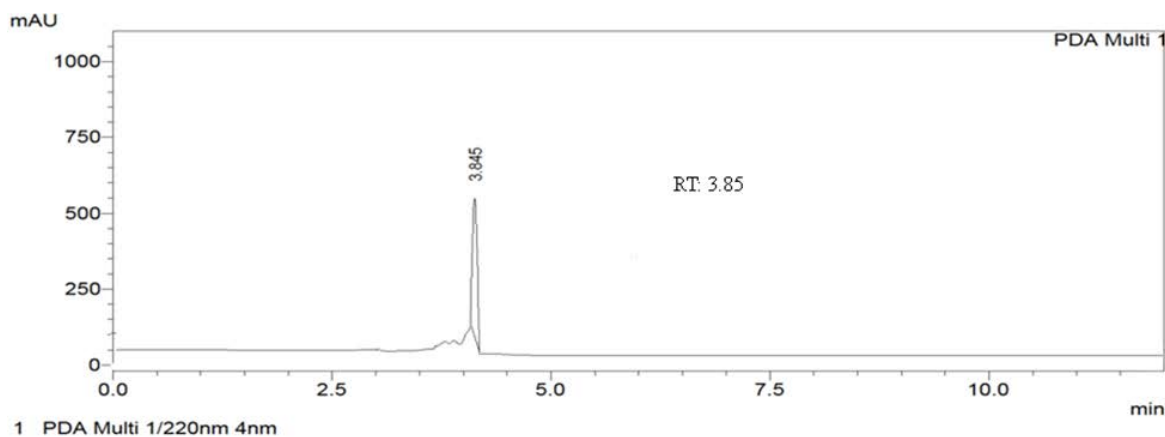


Figure 6.79.: HPLC chromatogram of 18 (4→14),19 (4→8) bis-abeo-nor-isopimarane-1,5-dien-3-yl-3 β -methoxy propyl pentanoate (**6**)

The title compound recorded its molecular ion peak at m/z 416 (EIMS: found m/z 416.3295 $[M]^+$, cal. for $C_{27}H_{44}O_3$, 416.3290). The 1H and ^{13}C NMR analyses confirmed the elemental composition as $C_{27}H_{44}O_3$ having six degree of unsaturation related to two double bonds, three ring systems and a carboxylate group (Table 6.11.; Figure 6.82.-6.83). The ^{13}C NMR and DEPT data along with HSQC established the presence of 19 carbons including four methyls, five methylenes, seven methines (in which one is oxygenated at δ 71.83) and three quaternary carbons, suggesting that the title compound was a norditerpene (Figure 6.83., 6.84., 6.86). Notably, *ent*-pimarane diterpenoid skeleton isolated from *Siegesbeckia orientalis* with 20 carbons including methyl ($-CH_3$) group at C-10 was not apparent in the title compound, thus confirming the presence of norditerpenoid functionality (Wang *et al.*, 2009). A downfield shift of δH 3.53 attached to δC 71.83 was due to the presence of oxygenated functionality at C-3. The characteristic quaternary carbon with greater chemical shift at δ 140.72 (C-5) was apparent as a result of adjacent vinylic group at δH 5.34/ δC 121.72 (C-6) (Sun *et al.*, 2012). The COSY spectrum was exhibited six spin systems, which include δ 5.37 (H-1)/2.81 (H-10); δ 5.38 (H-2)/3.53 (H-3)/2.29 (H-4); δ 5.34 (H-6)/2.01 (H-7); δ 0.91 (H-9)/1.49, 1.85 (H-11)/1.83, 1.08 (H-12); δ 1.12 (H-14)/0.86 (H-18); δ 1.15 (H-15)/0.89 (H-16) (Figure 6.80.A, 6.85.). The HMBC correlations from δ 5.37 (H-1) to δ 31.93 (C-11); δ 5.38 (H-2) to δ 42.24 (C-4); δ 2.29 (H-4) to δ 140.72 (C-5), 121.72 (C-6), 71.83 (C-3); δ 2.01 (H-7) to δ 121.72 (C-6) and δ 0.91 (H-9) to δ 36.50 (C-13), 56.77 (C-14) were revealed the presence of tricyclic norditerpene framework (Figure 6.80.B, 6.87.). The NOESY correlations between δ 1.01 (H-19)/0.68 (H-17) were confirmed the relative configuration of the chiral centre as β and other correlation between δ 5.35 (H-6)/2.01 (H-7)/3.53 (H-3)/2.29 (H-4) established that H-6 and H-3 were α -configured (Figure 6.81., 6.88.). This stereochemical arrangement specifically at H-17 and H-15 (β and α , respectively) was comparable with the isolated isopimarane diterpenoids (Xia *et al.*, 2015). The bulky *-O*-propyl pentanoate group appeared to be equatorially disposed, and therefore, the proton at the junction point (C-3) might be axial and α -oriented. The presence of NOEs among the methyl at C-14 and methine proton at H-3 belonging to the substituted rearranged isopimarane skeleton situated at the junction point connected with *-O*-propyl pentanoate was apparent. The stereochemistry of oxygenated derivative at C-3 was further confirmed

as β based upon literature study of oxygenated pimarane (Sun *et al.*, 2012) and isopimarane diterpenes (Huang *et al.*, 2013). The usual *gem*-dimethyl group (C-18 and C-19) found at C-4 position in isopimarane and 20-nor-isopimarane diterpenoids (Wang *et al.*, 2011) were absent at C-4 in the title compound. However, the $-\text{CH}_3$ groups, such as C-18 and C-19 were appeared at C-14 and C-8 positions, respectively, and therefore, it can be classified as 18 (4 \rightarrow 14),19 (4 \rightarrow 8) bis-abeo-nor-isopimarane. The 3 β -methoxy propyl pentanoate was recognized at C-3 by long range coupling from δ 5.38 (H-2) to δ 29.70 (C-21) and δ 3.64 (H-20) to δ 71.83 (C-3). This linear chain enclosed two spin systems such as δ 3.64 (H-20)/1.61 (H-21)/4.15 (δ H-22) in propyl moiety and δ 2.33 (H-24)/1.63 (H-25)/1.44 (H-26)/0.87 (H-27) in pentanoate chain. The ester carbon, δ 178.23 at C-23 of pentanoate chain was verified by HMBCs, such as δ 2.33 (H-24) to δ 24.75 (C-25), 178.23 (C-23); δ 1.63 (H-25) to δ 33.87 (C-24), 178.23 (C-23) and δ 1.44 (H-26) to δ 33.87 (C-24), 24.75 (C-25).

Table 6.11.: NMR spectroscopic data of 18 (4 \rightarrow 14),19 (4 \rightarrow 8) bis-abeo-nor-isopimarane-1,5-dien-3-yl-3 β -methoxy propyl pentanoate (**6**) in CDCl_3

C. No.	^{13}C	^1H (int.,mult.,J in Hz) ^a	COSY	HMBC
1	129.71	5.37 (1H,t,7.24)	H-10	C-11
2	130.01	5.38 (1H,t,8.51)	H-3	C-4,21
3	71.83	3.53 (1H α ,td)	H-4	-
4	42.24	2.29 (2H,d)	-	C-5,6,3
5	140.72	-	-	-
6	121.72	5.34 (1H,t,6.61)	H-7	-
7	39.52	2.01 (2H,d)	-	C-6
8	42.32	-	-	-
9	50.14	0.91 (1H,m)	H-11	C-13,14
10	28.23	2.81 (1H,dd)	-	C-14
11	31.93	1.49 (1H β ,m) 1.85 (1H α ,m)	H-12 -	- -
12	37.25	1.83 (1H,t) 1.08 (1H,t)	- -	- -
13	36.50	-	-	-
14	56.77	1.12 (1H β ,m)	H-18	-
15	22.69	1.15 (2H,d)	H-16	C-18,19
16	14.11	0.89 (3H,t)	-	C-18,19
17	11.86	0.68 (3H α ,s)	-	C-12,14,8
18	22.82	0.86 (3H,d)	-	C-19,11,8

19	19.39	1.01 (3H α ,s)	-	C-16,13,9,5
20	68.35	3.64 (2H,t)	H-21	C-3
21	29.7	1.61 (2H,m)	H-22	-
22	65.03	4.15 (2H,t)	-	-
23	178.23	-	-	-
24	33.87	2.33 (2H,t)	H-25	C-25,23
25	24.75	1.63 (2H,m)	H-26	C-24,23
26	21.09	1.44 (2H,m)	H-27	C-24,25
27	18.72	0.87 (3H,t)	-	-

^1H NMR spectra recorded using Bruker AVANCE III 500MHz (AV 500) spectrometer (Bruker, Karlsruhe, Germany) in CDCl_3 as aprotic solvent at ambient temperature with TMS as the internal standard (δ 0 ppm). The ^1H NMR spectra were recorded at 500MHz, while the ^{13}C NMR spectra were recorded at 125MHz. ^aValues in ppm, multiplicity and coupling constants (J =Hz) were indicated in parentheses. The assignments were made with the aid of the ^1H - ^1H COSY, HSQC, HMBC and NOESY experiments

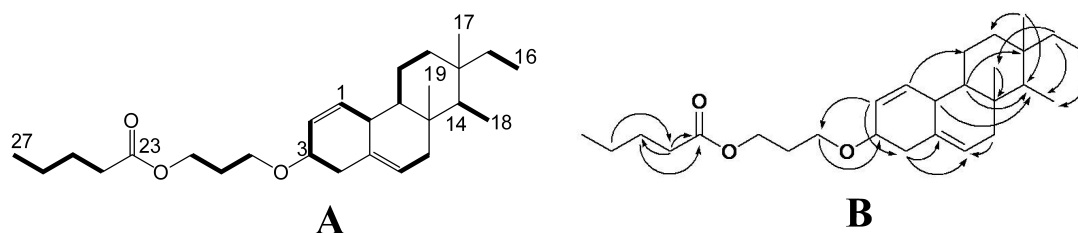


Figure 6.80.: ^1H - ^1H COSY (A) and HMBC (B) correlations of 18 (4 \rightarrow 14),19 (4 \rightarrow 8) bis-abeo-nor-isopimarane-1,5-dien-3-yl-3 β -methoxy propyl pentanoate (**6**). The key ^1H - ^1H COSY couplings have been represented by the bold face bonds

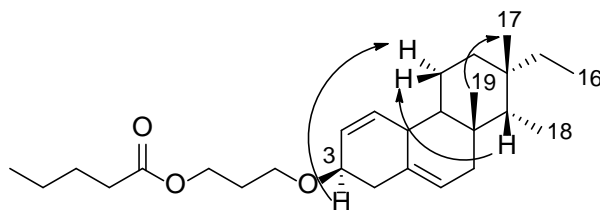


Figure 6.81.: NOESY correlations of 18 (4 \rightarrow 14),19 (4 \rightarrow 8) bis-abeo-nor-isopimarane-1,5-dien-3-yl-3 β -methoxy propyl pentanoate (**6**). The NOESY relations were represented by double barbed arrow

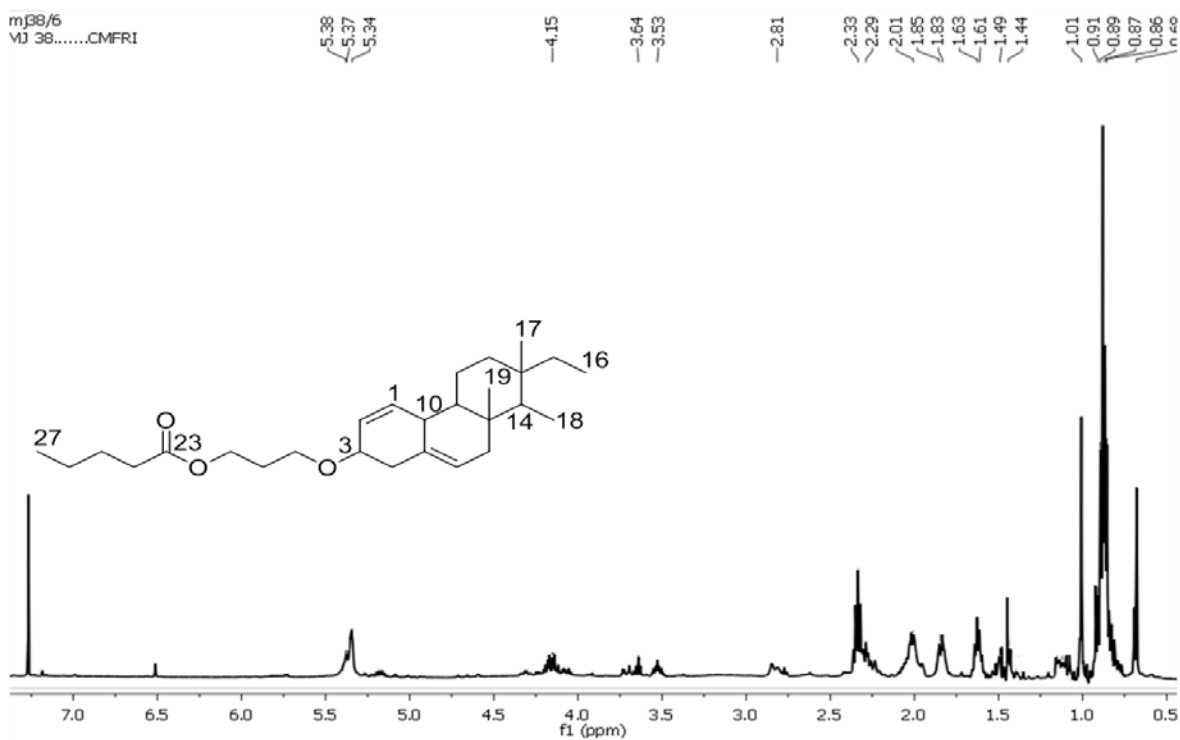


Figure 6.82.: ^1H NMR spectrum of 18 (4 \rightarrow 14),19 (4 \rightarrow 8) bis-abeo-nor-isopimarane-1,5-dien-3-yl-3 β -methoxy propyl pentanoate (**6**)

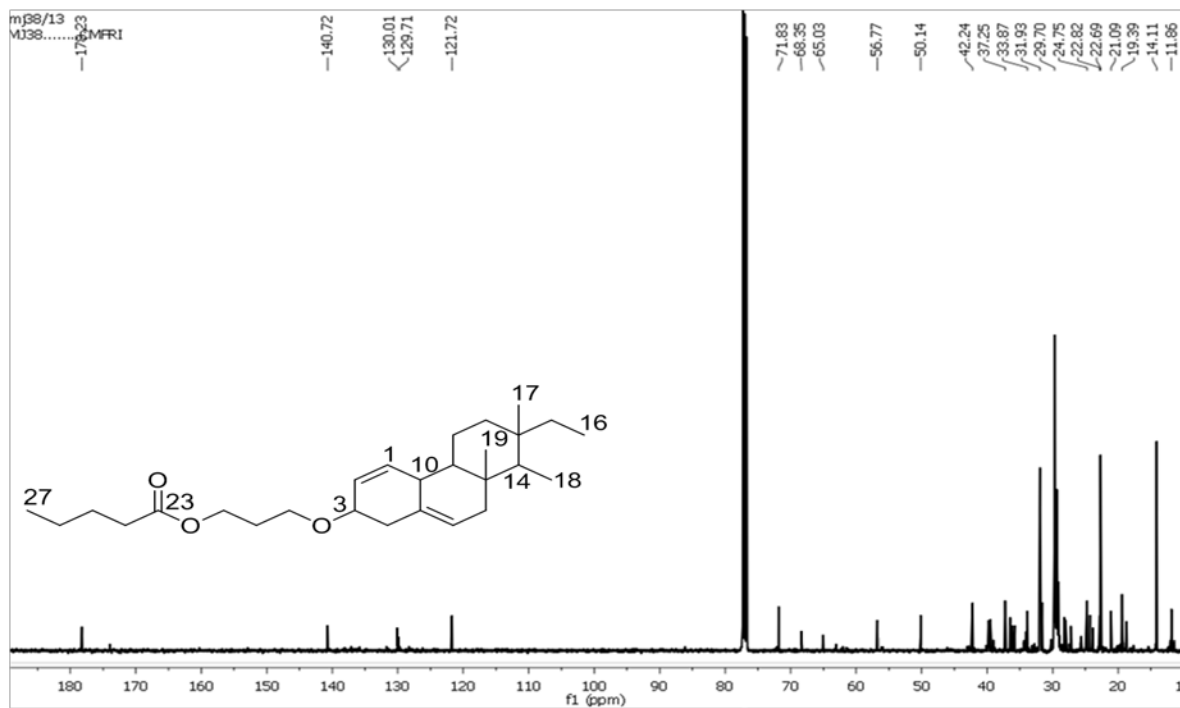


Figure 6.83.: ^{13}C NMR spectrum of 18 (4 \rightarrow 14),19 (4 \rightarrow 8) bis-abeo-nor-isopimarane-1,5-dien-3-yl-3 β -methoxy propyl pentanoate (**6**)

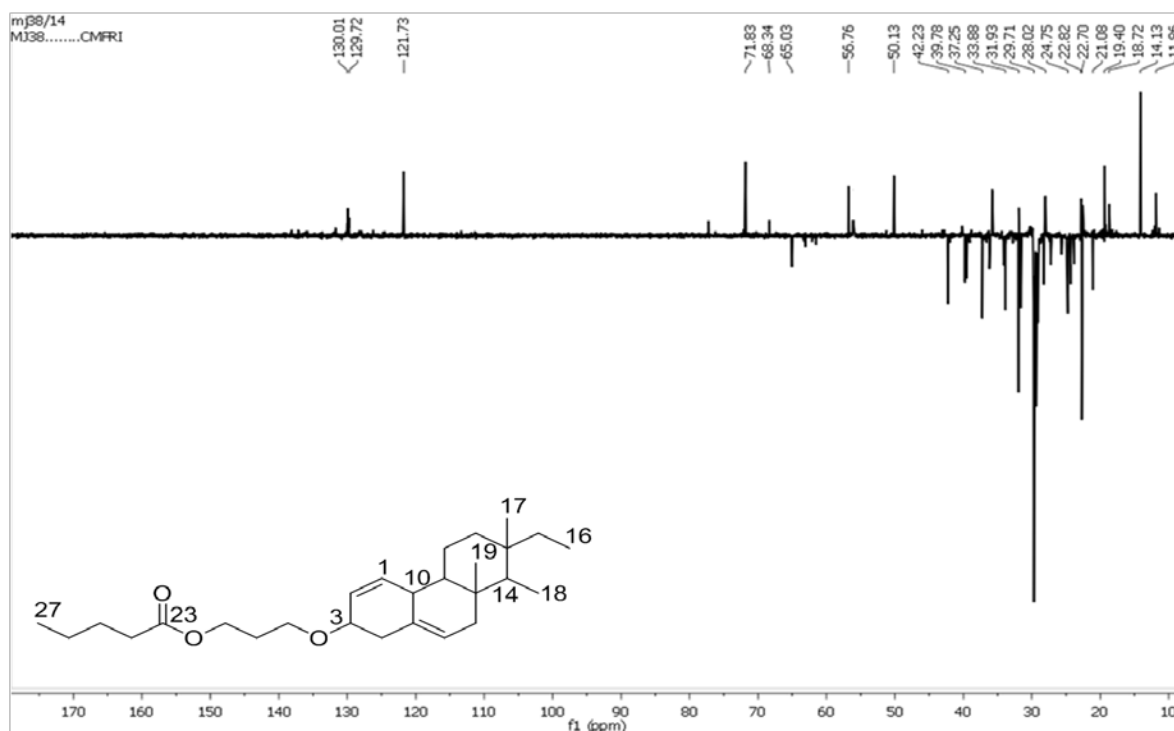


Figure 6.84.: $^{135}\text{DEPT}$ NMR spectrum of 18 (4 \rightarrow 14),19 (4 \rightarrow 8) bis-abeo-nor-isopimarane-1,5-dien-3-yl-3 β -methoxy propyl pentanoate (**6**)

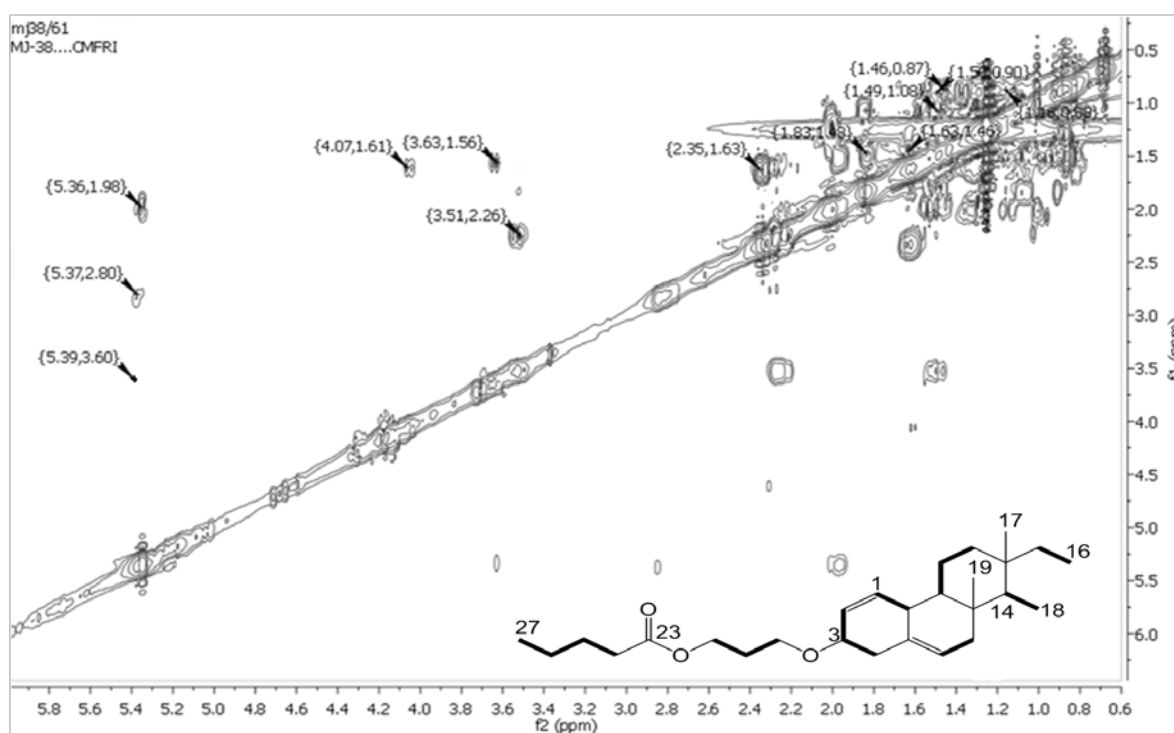


Figure 6.85.: ^1H - ^1H COSY NMR spectrum of 18 (4 \rightarrow 14),19 (4 \rightarrow 8) bis-abeo-nor-isopimarane-1,5-dien-3-yl-3 β -methoxy propyl pentanoate (**6**)

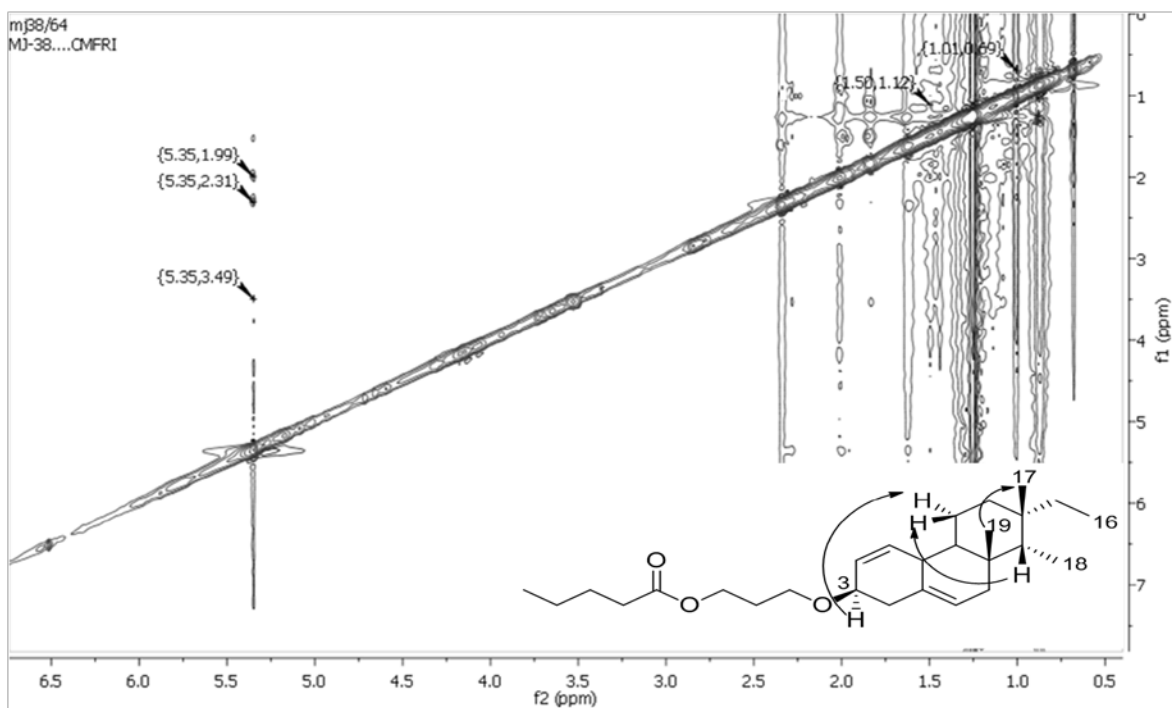


Figure 6.88.: NOESY NMR spectrum of 18 (4→14),19 (4→8) bis-abeo-nor-isopimarane-1,5-dien-3-yl-3 β -methoxy propyl pentanoate (**6**)

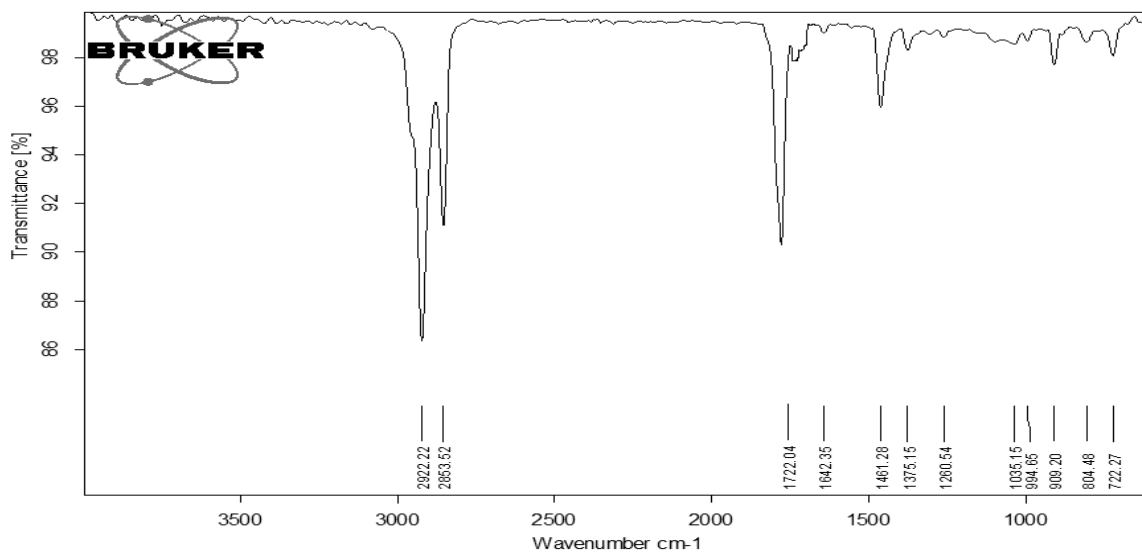


Figure 6.89.: FTIR spectrum of 18 (4→14),19 (4→8) bis-abeo-nor-isopimarane-1,5-dien-3-yl-3 β -methoxy propyl pentanoate (**6**)

The distinctive IR stretching absorption bands at 2922 and 1722 cm^{-1} recognized C-H and C=O vibrations, respectively, whereas those at 1375, 1260 cm^{-1} revealed the

presence of C-O bending vibrations, thereby substantiated the structure of the title compound. The absence of IR stretching absorption bands near 3500 cm^{-1} (assigned to hydroxyl) proposed the absence of characteristic hydroxyl moiety at C-3. Thus, the substitution or derivatisation of hydroxyl moiety at C-3 position with -O-propyl pentanoate chain was further confirmed (Figure 6.89.).

Fragmentation of molecular ion with m/z 416 (Figure 6.90.) was perceived to be accompanied by the loss of a C-4 fragment (butyl radical) resulting in an ion at m/z 359 (a), and has been ascribed to 18 (4→14),19 (4→8) bis-abeo-nor-isopimarane-1,5-diene-3-yl-3 β -methoxy formate. The fragment ion at m/z 286 (c) undergo fragmentation to obtain fragment peak at m/z 256 (d, 18 (4→14),19 (4→8) bis-abeo-nor-isopimarane-1,5-diene), which on subsequent rearrangement yielded the fragments with m/z 229 (e), 206 (f) and 185 (g) (Figure 6.91.) that was comparable with earlier reports (Bromann *et al.*, 2014). The base peak was apparent at m/z 57 (e, butane cation).

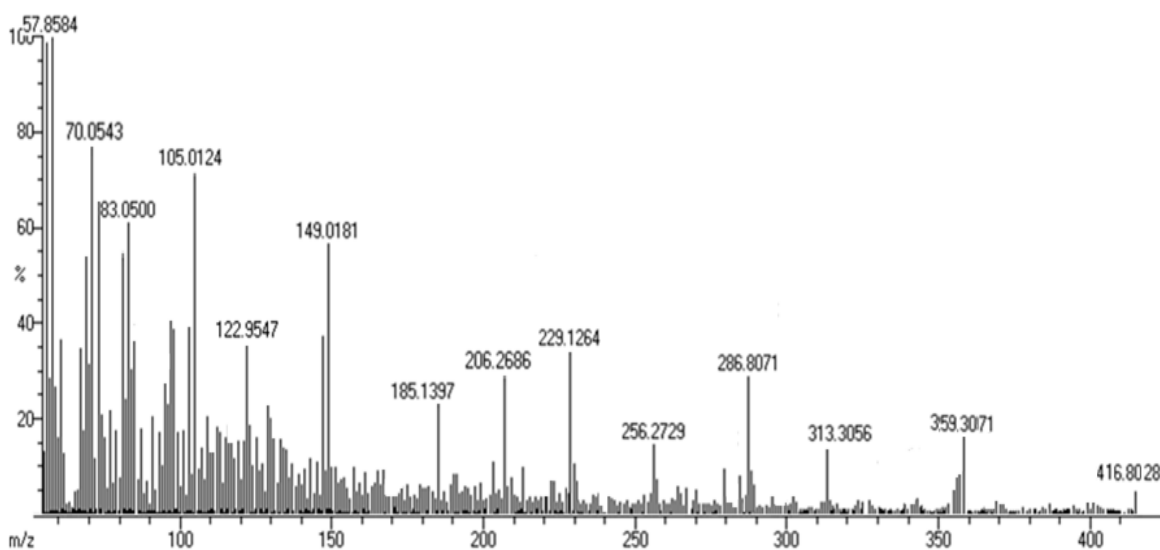


Figure 6.90.: EIMS spectrum of 18 (4→14),19 (4→8) bis-abeo-nor-isopimarane-1,5-diene-3-yl-3 β -methoxy propyl pentanoate (6)

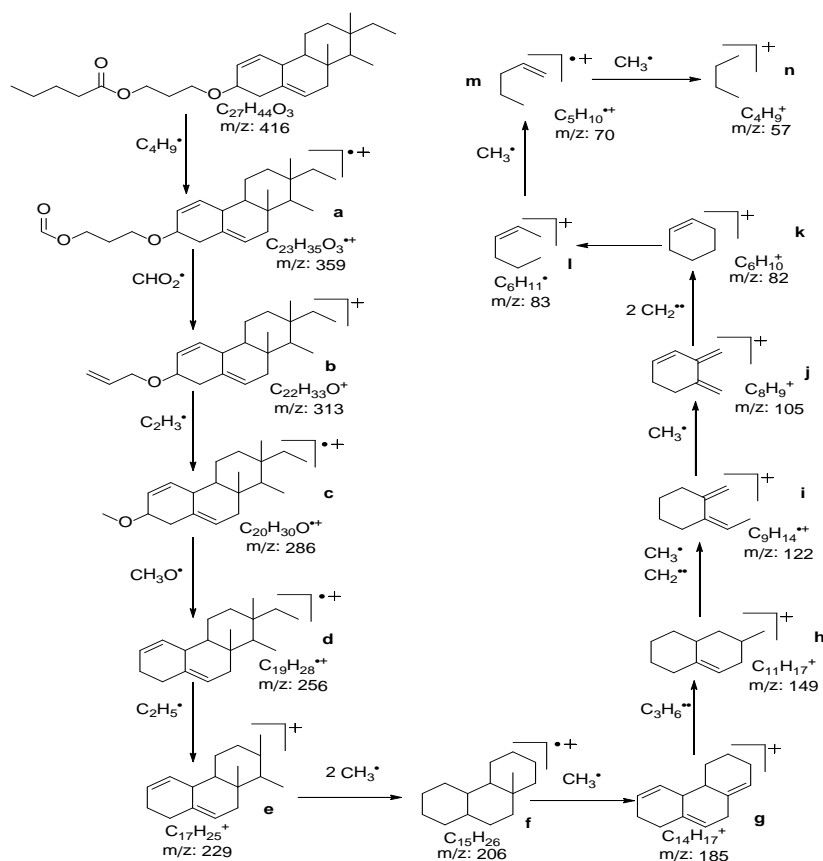


Figure 6.91.: Mass fragmentation pattern of 18 (4→14),19 (4→8) bis-abeo-nor-isopimarane-1,5-diene-3-yl-3β-methoxy propyl pentanoate (**6**)

Previous reports of isopimarane and their derivatives from the natural resources has been envisaged their bioactive potential and pharmacological effects. The potential antioxidative property of entpimara-8(14),15-diene was demonstrated DPPH scavenging activity (Bromann *et al.*, 2014). The anti-bacterial potentials of rare pimarane derivatives with cyclopropane rings at C-3 and C-4 from the isolates of *A. pulmonica* were reported (Bian *et al.*, 2014). The titled C19 isopimarane norditerpenoid enclosed with a straight chain of 3-methoxy propyl pentanoate at the C-3 position of isopimarane skeleton thus, accounted for its potential activity. The ent-pimarane derivative isolated from *T. ignis* (sponge) exhibited *in vivo* inhibitory properties towards COX-2 and iNOS expressions (Costantino *et al.*, 2009). The pimarane diterpenoid, libertellenones (anti-cancer agent) (Oh *et al.*, 2005) and C-19 diterpenoid pimarane were identified from *Ephemerantha fimbriata*

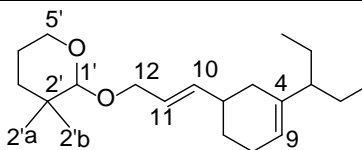
(Ma *et al.*, 1998). The isolated isopimarane norditerpenoid can be a potential lead pharmacophore for therapeutic investigations. The compound **6** represented as the first description of isopimarane norditerpenoid possessing the bis-abeo C19 norditerpenoid framework from a natural bivalve source.

6.3.2.4. Structural characterization of meroterpeno pyranoids (7-8)

Pyran derivatives, an important category of organic compounds, which proved to constitute an important class of heterocycle and were found to occur in marine organisms that attracted a great deal of interest due to their pharmacological potentials (Ciavatta *et al.*, 2011; Cueto *et al.*, 1998a). The occurrence of pyranoids in biological system and their role as precursors in the production of pharmacologically active metabolites as anti-fungal, anti-inflammatory, anti-microbial and anti-cancer compounds from natural and synthetic origin (Arora and Mathur 1963; Goel and Ram 2009). The pyranoid cladiellane diterpenes were isolated from mollusk, *Tritoniopsis elegans* (Ciavatta *et al.*, 2011) and naturally occurring 1-(6-butyl-3,4-dihydro-2*H*-pyran-2yl)-pentanone was reported from marine invertebrate, *Neosadocus maximus* (Rocha *et al.*, 2011). Polyoxygenated monoterpenes, pantopyranoids A-C and pantoisofuranoids A-C and monoterpenes with tetrahydrofuran ring were isolated from marine algae *Pantoneura plocamioides* (Cueto and Darias 1996; Cueto *et al.*, 1998b). In view of this, two unprecedented meroterpeno pyranoids, 1'-((10*E*)-10-(10-(pentan-4-yl)-cyclohex-4-enyl)-allyloxy)-tetrahydro-2',2'-dimethyl-2*H*-pyran (**7**) and 2-((*E*)-deca-1,8-dien-10-yl)-11,12-dihydro-13-propyl-2*H*-pyran (**8**) were isolated from *P. malabarica*.

6.3.2.4.A. Structural characterization of compound 7 (PM₄₋₃₋₁)

1'-((10*E*)-10-(10-(Pentan-4-yl)-cyclohex-4-enyl)-allyloxy)-tetrahydro-2',2'-dimethyl-2*H*-pyran (**7**)



Sample yield

118 mg; 0.24%

Physical description	Light green solid
Molecular formula	$C_{21}H_{36}O_2$
Molecular mass	320.2715

The naturally occurring C_{21} prenylated bisabolene type meroterpenoid, 1'-((10*E*)-10-(10-(pentan-4-yl)-cyclohex-4-enyl)-allyloxy)-tetrahydro-2',2'-dimethyl-2*H*-pyran (**7**), was isolated as light green solid. It exhibited UV absorbance (in MeOH) at λ_{\max} (log ϵ 3.46) 260.0 nm assigned to olefinic groups (Figure 6.92.). The purity of compound was supported by RP C18 HPLC using 3:2 (v/v) MeOH:MeCN (R_t 22.18) experiments (Figure 6.93.).

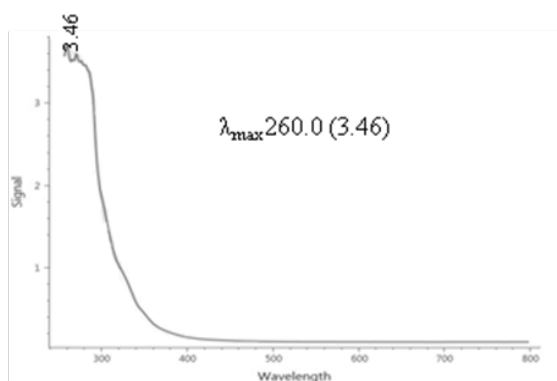


Figure 6.92.: UV spectrum of 1'-((10*E*)-10-(10-(pentan-4-yl)-cyclohex-4-enyl)-allyloxy)-tetrahydro-2',2'-dimethyl-2*H*-pyran (**7**)

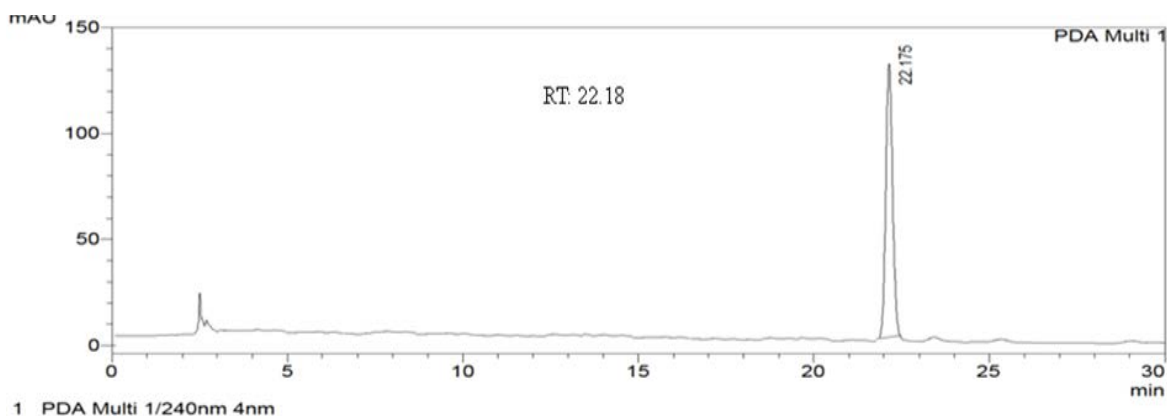


Figure 6.93.: HPLC chromatogram of 1'-((10*E*)-10-(10-(pentan-4-yl)-cyclohex-4-enyl)-allyloxy)-tetrahydro-2',2'-dimethyl-2*H*-pyran (**7**)

The molecular ion peak was recorded at m/z 320 (EIMS: found m/z 320.2718 $[M]^+$, cal. for $C_{21}H_{36}O_2$ 320.2715) and 1H - ^{13}C spectroscopic details established the elemental composition as $C_{21}H_{36}O_2$ with four double bond equivalence enclosing two double bonds and two cyclic systems. The singlet at δ 4.59 (assigned to C-1') attributed to the methine (-CH) group, in which the upfield shift of the corresponding carbon (δ 68.39) was due to the electronegative -O-C moiety (Table 6.12., Figure 6.96.-6.97.). This carbon (C-1') was also attached to an oxygenated side chain as apparent from the HMBC correlations. The long range couplings from δ 4.59 (H-1') to δ 25.74 (C-4'), 39.07 (C-2'), 30.25 (C-2'a), 30.09 (C-2'b) proved that it was a part of pyran moiety. The 1H - 1H COSY revealed that the presence of four spin systems, H-3' to H-6' $\{(\delta$ 1.63, 1.66 (H-3')/1.55, 1.56 (H-4')/3.64 (H-5')) in the pyran ring, H-11 to H-12 $\{(\delta$ 4.12, 4.14 (H-12)/5.35 (H-11)) in the allyloxy chain, H-5 to H-9 $\{(\delta$ 2.02 (H-5)/2.35 (H-6)/1.57, 1.59 (H-7)/1.99, 2.00 (H-8)/5.34 (H-9)) including H-6 to H-10 $\{(\delta$ 2.35 (H-6)/5.38 (H-10)) in the cyclohexenyl ring and from H-1 to H-3 consisting of H-3/H-13/ H-14 $\{(\delta$ 2.31 (H-3)/1.43 (H-13)/0.89 (H-14); δ 0.87 (H-1)/1.42 (H-2)/2.31 (H-3)) in the isopentanyl side chain (Figure 6.94.A, 6.99.). Two intense singlet protons due to methyl (-CH₃) at δ 1.48 and 1.46 showed HSQC correlation with δ 30.25 (C-2'a) and 30.09 (C-2'b), respectively, which were attached to a quaternary carbon at δ 39.07 (Figure 6.100.). This was apparent from the HMBC correlations, δ 1.46/1.48 (C-2'a/2'b) to δ 63.11 (C-5'), 39.07 (C-2'), which proved the attachment of dimethyl groups to the pyran ring (Figure 6.94.B, 6.101.). The HMBC relations between δ 1.55 (H-4') to δ 29.62 (C-3'), 30.25 (C-2'a), 30.09 (C-2'b) and δ 3.64 (H-5') to δ 25.74 (C-4') established the pyran moiety. The attachment of carbon atom in the allyloxy side chain to pyran network was evident. The methine (-CH) groups, δ H 5.38/ δ C 139.27 and δ H 5.35/ δ C 127.67 at H-10 and H-11, respectively with large coupling constants ($J=8.5$ and 9.2 , respectively) was revealed its *trans* (*E*) geometry (assigned to C10=C11). The cyclohexenyl ring system enclosed -C=CH moiety in which the olefinic quaternary carbon (-C=) registered higher chemical shift of δ 143.18 (C-4) compared to the methine (=CH; δ 124.47) and a pentanyl group attached to the quaternary carbon attributed to C-12. This cyclic system was exhibited HMBCs from δ 5.38 (H-10) to δ 31.93 (C-5) and δ 2.35 (H-6) to δ 29.37 (C-7). The spectroscopic data for quaternary olefinic carbon at δ 143.18

(C-4) and the methine at δ 68.39 (C-1') were comparable with 1-(6-butyl-3,4-dihydro-2H-pyran-2-yl)-pentanone (Rocha *et al.*, 2011). The HMBC couplings from δ 0.89 (H-14) to δ 22.69 (C-13); δ 1.43 (H-13) to δ 34.37 (C-3), 143.18 (C-4), 31.93 (C-5); δ 1.42 (H-2) to δ 34.37 (C-3), 143.18 (C-4); δ 0.87 (H-1) to δ 34.37 (C-3), 22.69 (C-2) were confirmed the attachment of isopentanyl moiety to the cyclohexenyl ring. The ^{13}C and DEPT NMR identified 21 carbons, in which four CH_3 , nine CH_2 , six CH were accounted. The relative stereochemistries of **7**, mainly at C-1' and C-6 protons, δ 4.59 and 2.35 were confirmed from NOESY (Figure 6.95., 6.102.). The NOEs between δ 1.55 (H-4')/4.59 (H-1')/2.35 (H-6)/2.00 (H-8) and δ 2.35 (H-6)/4.12 (H-12) demonstrated that these protons were in the same plane of geometry and α -disposed. Further, NOEs among the protons δ 1.99 (H-8), 1.66 (H-3'), 4.14 (H-12) and 1.46 (H-2'b, CH_3) showed that they were disposed in the identical plane of geometry, and disposed at β -orientation. The methyl protons at δ 1.46 (H-2'b) was found to be β disposed with the reference plane due to NOEs with δ 4.14 (H β -12), and not with the protons at δ 4.59 (H α -1') and 2.39 (H α -6). This was further explained the *trans* orientation of the methine and methyl groups at C-6 and C-2'b positions of **7**.

Table 6.12.: NMR spectroscopic data of 1'-((10*E*)-10-(10-(pentan-4-yl)-cyclohex-4-enyl)-allyloxy)-tetrahydro-2',2'-dimethyl-2*H*-pyran (**7**) in CDCl_3

C. No.	^{13}C	^1H (int.,mult., <i>J</i> in Hz) ^a	COSY	HMBC
1	14.15	0.87 (3H,t)	H-2	C-2,3
2	22.69	1.42 (2H,m)	H-3	C-3,4
3	34.37	2.31 (2H,m)	H-13	-
4	143.18	-	-	-
5	31.93	2.02 (2H,d)	H-6	-
6	32.84	2.35 (1H α ,t)	H-7,10	C-7
7	29.37	1.57 (1H,m)	H-8	-
		1.59 (1H,m)	-	-
8	27.23	1.99 (1H β ,t)	H-9	-
		2.00 (1H α ,t)	-	-
9	124.47	5.34 (1H,t,9.22)	-	-
10	139.27	5.38 (1H,t,8.50)	-	C-5
11	127.67	5.35 (1H,q,9.21)	H-12	-
12	65.05	4.12 (1H α ,d)	-	C-11, 2'
		4.14 (1H β ,d)	-	C-1'

13	22.69	1.43 (2H,m)	H-14	C-3,4,5
14	14.15	0.89 (3H,t)	-	C-13,3
1'	68.39	4.59 (1H α ,s)	-	C-4',12,2',2'a,2'b
2'	39.07	-	-	-
2'a	30.25	1.48 (3H α ,s)	-	C-5',2'
2'b	30.09	1.46 (3H β ,s)	-	C-5',3'
3'	29.62	1.63 (1H α ,m)	H-4'	-
		1.66 (1H β ,m)	-	-
4'	25.74	1.55 (1H α ,m)	H-5'	C-3',2'a,2'b
		1.56 (1H β ,m)	-	-
5'	63.11	3.64 (2H,t)	-	C-4'

^1H NMR spectra recorded using Bruker AVANCE III 500MHz (AV 500) spectrometer (Bruker, Karlsruhe, Germany) in CDCl_3 as aprotic solvent at ambient temperature with TMS as the internal standard (δ 0 ppm). The ^1H NMR spectra were recorded at 500MHz, while the ^{13}C NMR spectra were recorded at 125MHz. ^aValues in ppm, multiplicity and coupling constants (J =Hz) were indicated in parentheses. The assignments were made with the aid of the ^1H - ^1H COSY, HSQC, HMBC and NOESY experiments

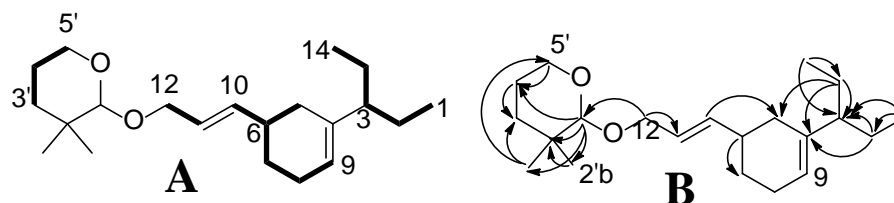


Figure 6.94.: ^1H - ^1H COSY (A) and HMBC (B) correlations of 1'-((10*E*)-10-(10-(pentan-4-yl)-cyclohex-4-enyl)-allyloxy)-tetrahydro-2',2'-dimethyl-2*H*-pyran (**7**). The key ^1H - ^1H COSY couplings have been represented by the bold face bonds. The HMBC couplings were indicated by double barbed arrow

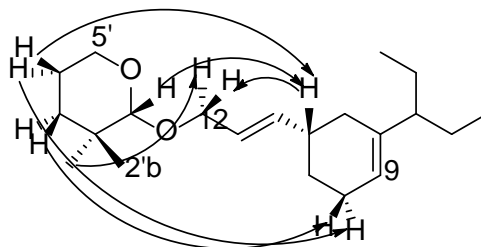


Figure 6.95.: NOESY correlations of 1'-((10*E*)-10-(10-(pentan-4-yl)-cyclohex-4-enyl)-allyloxy)-tetrahydro-2',2'-dimethyl-2*H*-pyran (**7**). The NOESY relations were represented by double barbed arrow

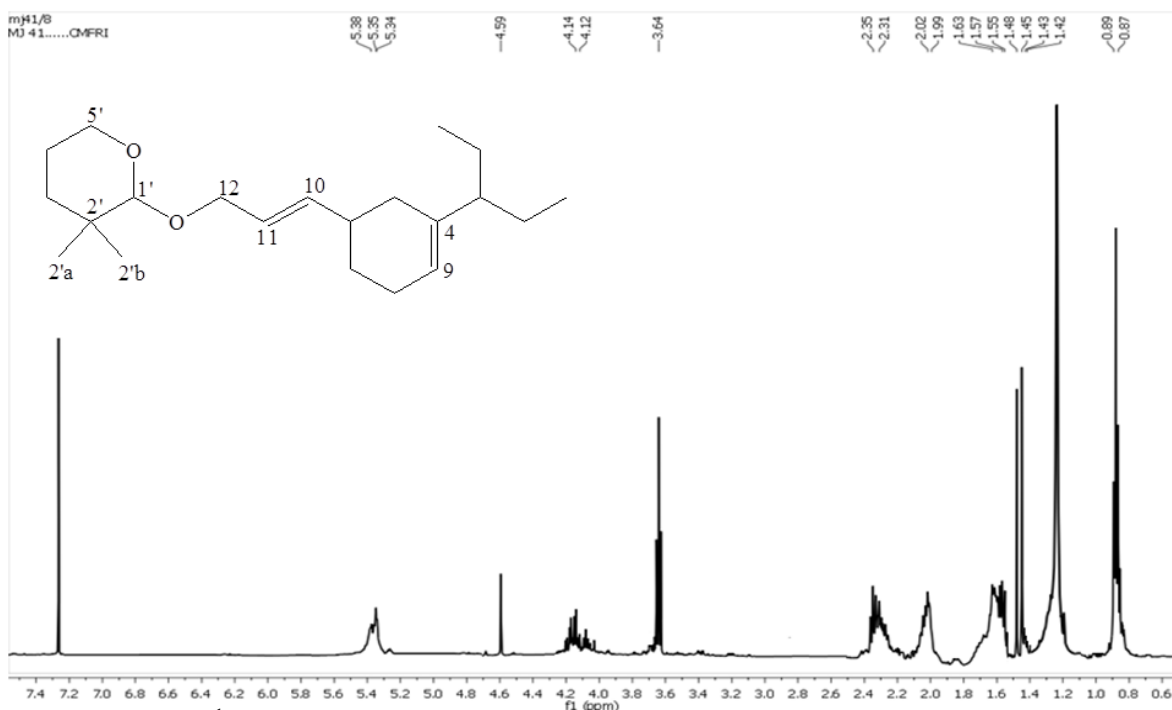


Figure 6.96.: ^1H NMR spectrum of 1'-((10*E*)-10-(10-(pentan-4-yl)-cyclohex-4-enyl)-allyloxy)-tetrahydro-2',2'-dimethyl-2*H*-pyran (7)

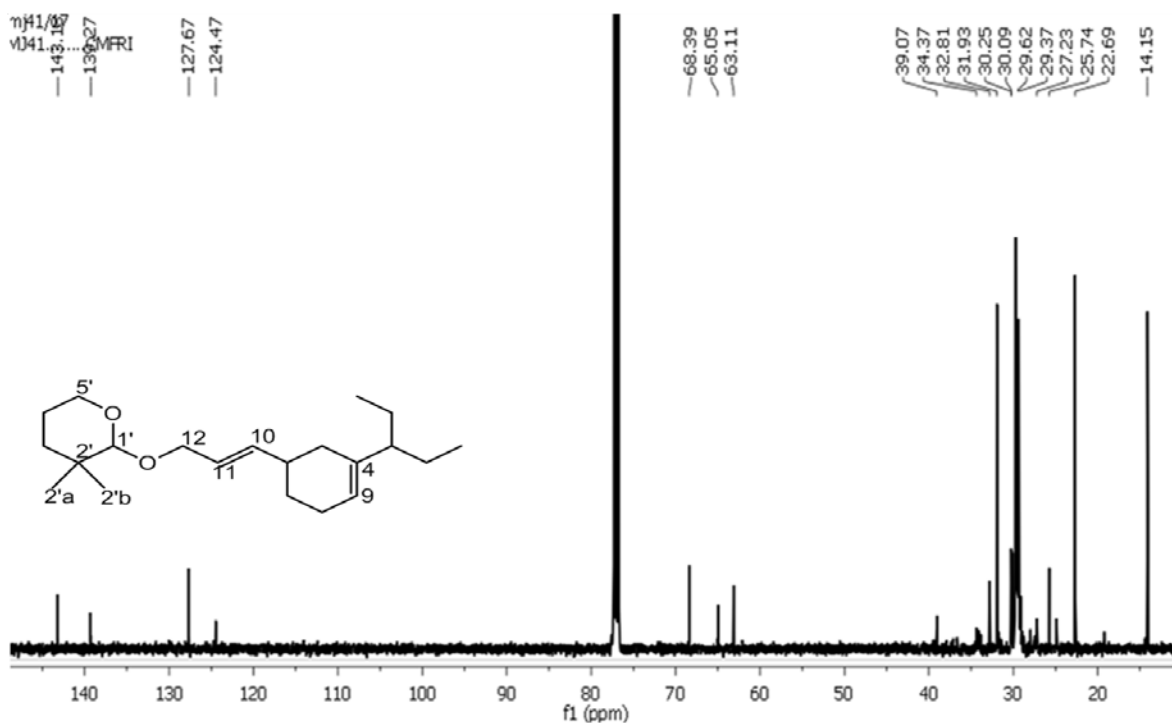


Figure 6.97.: ^{13}C NMR spectrum of 1'-((10*E*)-10-(10-(pentan-4-yl)-cyclohex-4-enyl)-allyloxy)-tetrahydro-2',2'-dimethyl-2*H*-pyran (7)

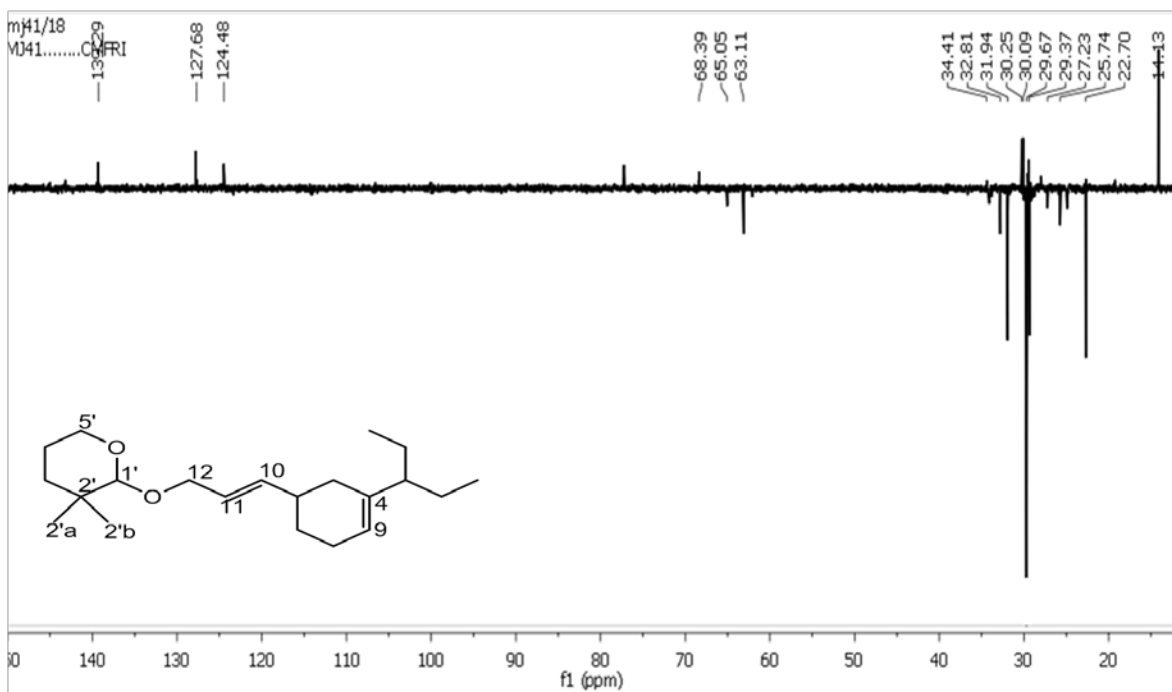


Figure 6.98.: $^{135}\text{DEPT}$ NMR spectrum of 1'-((10*E*)-10-(10-(pentan-4-yl)-cyclohex-4-enyl)-allyloxy)-tetrahydro-2',2'-dimethyl-2*H*-pyran (**7**)

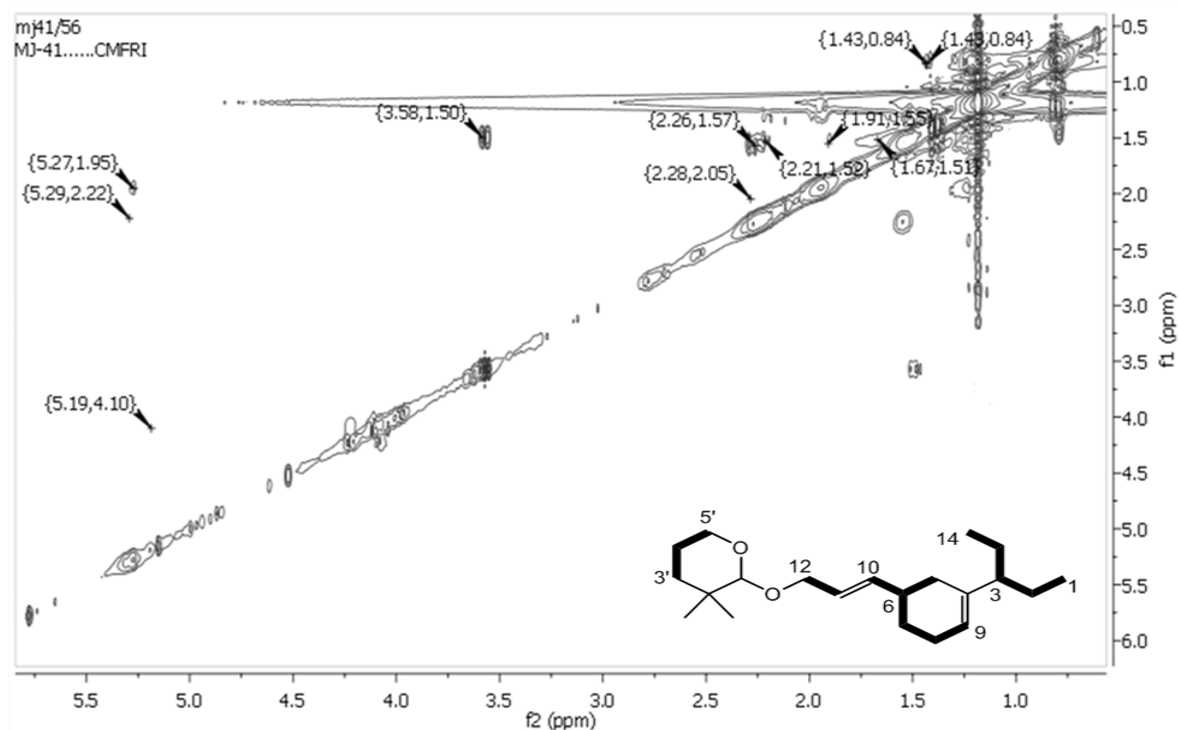


Figure 6.99.: ^1H - ^1H COSY NMR spectrum of 1'-((10*E*)-10-(10-(pentan-4-yl)-cyclohex-4-enyl)-allyloxy)-tetrahydro-2',2'-dimethyl-2*H*-pyran (**7**)

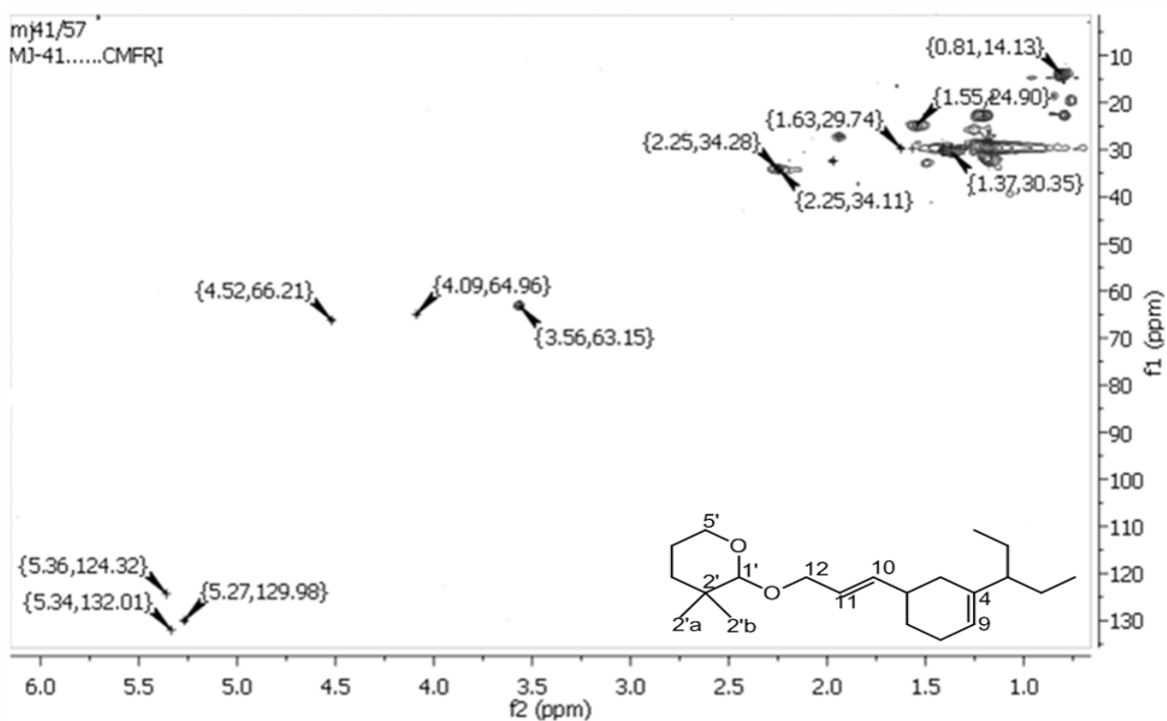


Figure 6.100.: HSQC NMR spectrum of 1'-((10E)-10-(10-(pentan-4-yl)-cyclohex-4-enyl)-allyloxy)-tetrahydro-2',2'-dimethyl-2H-pyran (**7**)

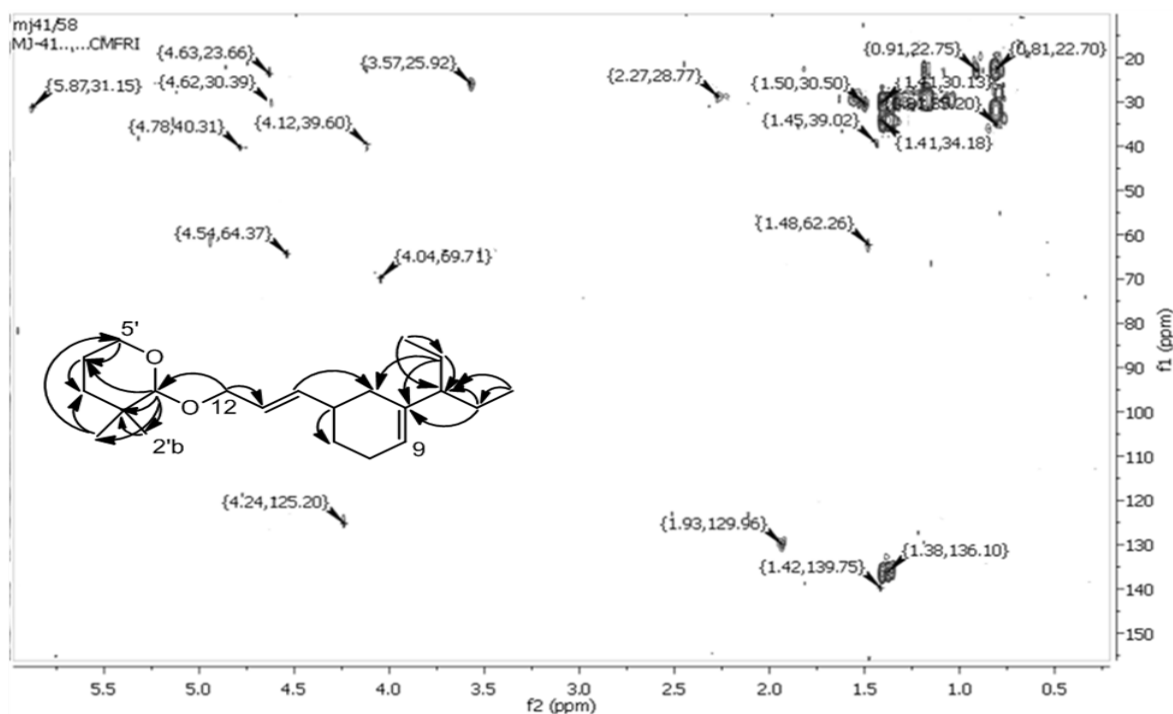


Figure 6.101.: HMBC NMR spectrum of 1'-((10E)-10-(10-(pentan-4-yl)-cyclohex-4-enyl)-allyloxy)-tetrahydro-2',2'-dimethyl-2H-pyran (**7**)

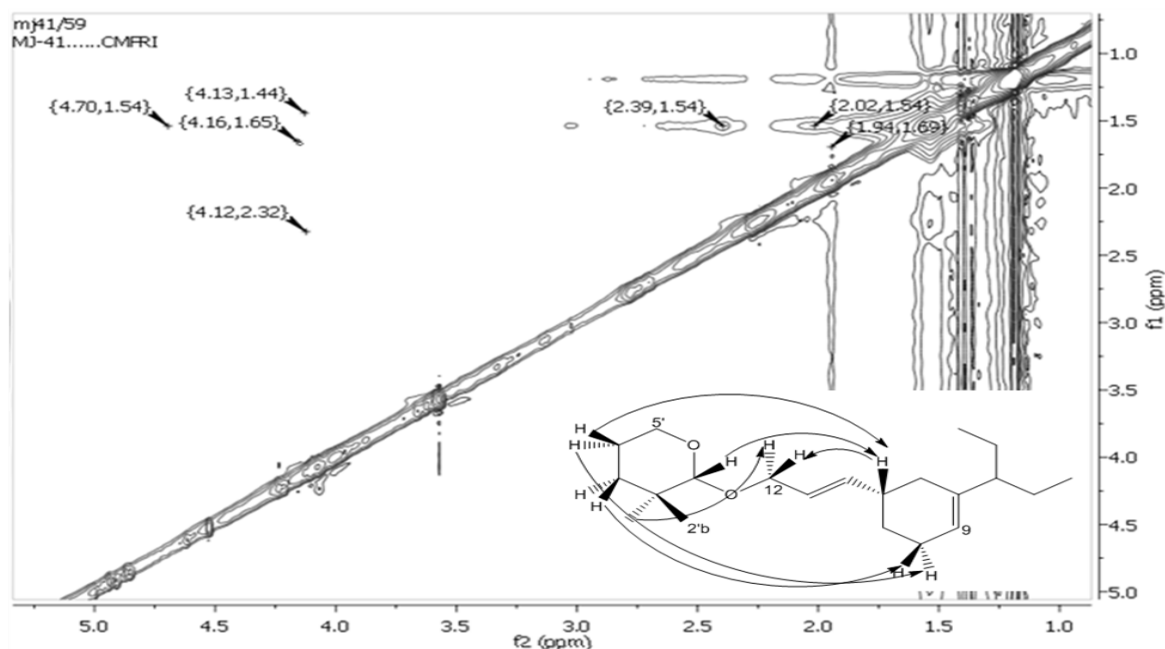


Figure 6.102.: NOESY NMR spectrum of 1'-((10*E*)-10-(10-(pentan-4-yl)-cyclohex-4-enyl)-allyloxy)-tetrahydro-2',2'-dimethyl-2*H*-pyran (**7**)

The characteristic IR absorptions at 2932-2860 cm^{-1} were due to C-H alkane stretching, whereas olefinic (C=C) stretching and =C-H bending were represented by 1661 and 965 cm^{-1} absorption bands, respectively. The characteristic absorption at 1456 cm^{-1} was indicated for C-H groups (Figure 6.103.).

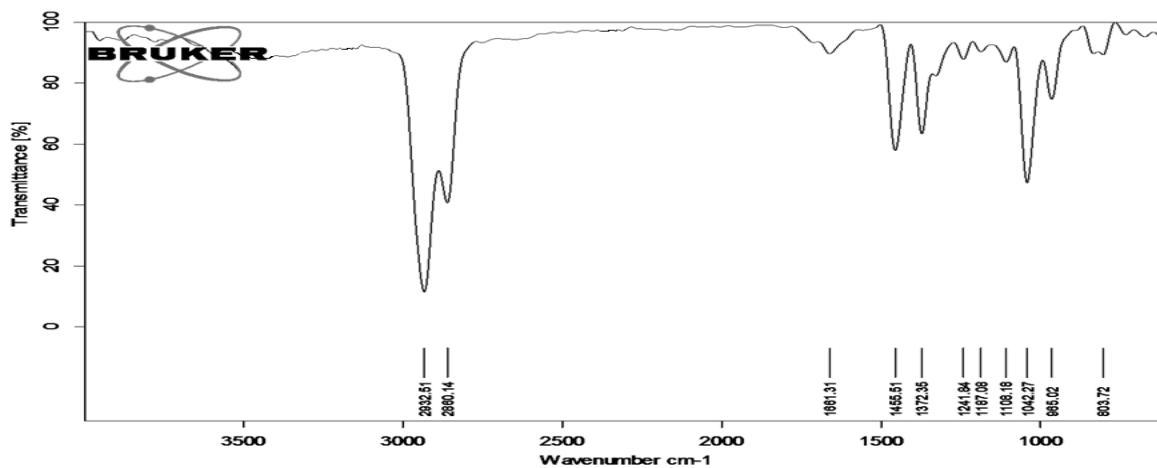


Figure 6.103.: FTIR spectrum of 1'-((10*E*)-10-(10-(pentan-4-yl)-cyclohex-4-enyl)-allyloxy)-tetrahydro-2',2'-dimethyl-2*H*-pyran (**7**)

The molecular ion peak at m/z 320 was appeared to undergo elimination of one $-C_2H_5$ group to yield 1'-(10-(3-propylcyclohexyl)propoxy)-tetrahydro-2',2'-dimethyl-2*H*-pyran (**a**, m/z 296). The elimination of $-C_3H_7$ group from the fragment ion at m/z 296 yielded the fragment with m/z 253 (**b**, attributed to 1'-(3-cyclohexylpropoxy)-tetrahydro-2',2'-dimethyl-2*H*-pyran) and m/z 254 (**c**, 1'-(4-methyloctyloxy)-tetrahydro-2',2'-dimethyl-2*H*-pyran). The elimination of one $-CH_3$ group from the fragment ion at m/z 254 yielded the fragments with m/z 238 (**d**, 1'-(4-methylenehept-1-enyloxy)-tetrahydro-2',2'-dimethyl-2*H*-pyran). The elimination of $-C_3H_5$ group from the fragment ion at m/z 238 yielded the fragments with m/z 198 (**e**, 1'-(pent-2-enyloxy)-tetrahydro-2',2'-dimethyl-2*H*-pyran) and m/z 184 (**f**, 1'-(butoxy)-tetrahydro-2',2'-dimethyl-2*H*-pyran), which on subsequent rearrangement yielded the fragments at m/z 142 (**h**, 1'-(allyloxy)-tetrahydro-2*H*-pyran), 102 (**j**, tetrahydro-2*H*-pyran-2-ol), 86 (pentan-1-ol) and 73 (**l**, but-3-en-1-ol). The fragment peak at m/z 85 (**k**, tetrahydro-2*H*-pyran) appeared as base peak of **7** (Figure 6.104., 6.105.).

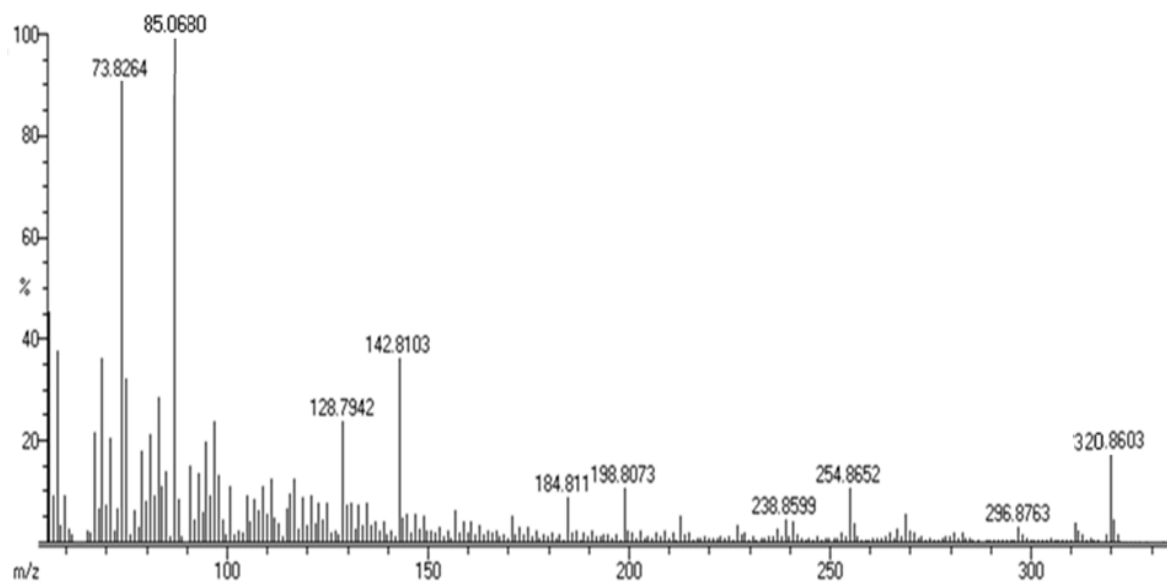


Figure 6.104.: EIMS spectrum of 1'-((10*E*)-10-(10-(pentan-4-yl)-cyclohex-4-enyl)-allyloxy)-tetrahydro-2',2'-dimethyl-2*H*-pyran (**7**)

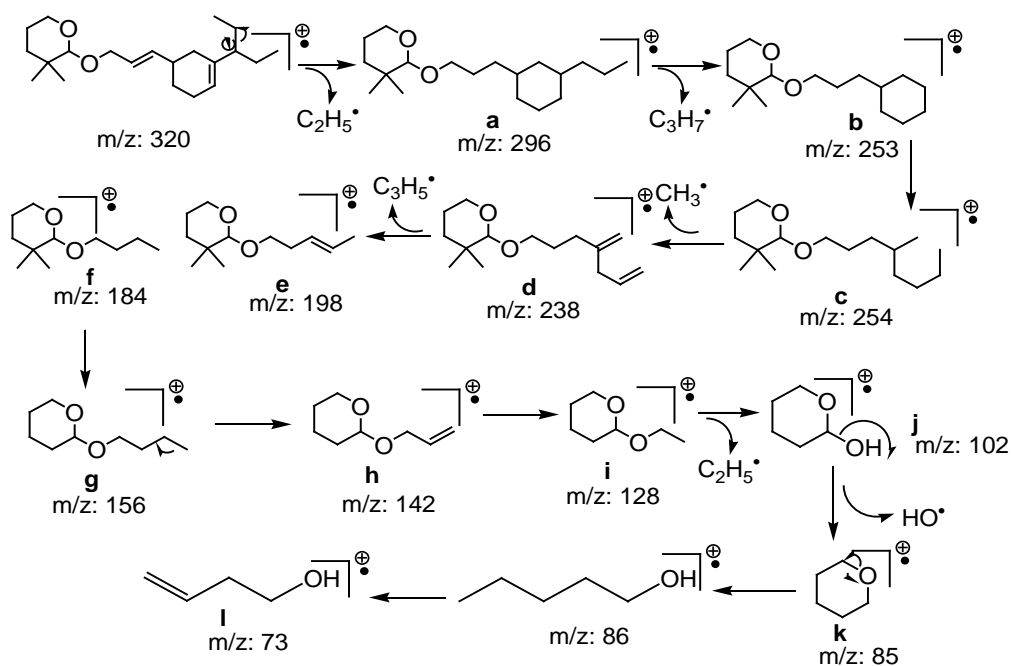
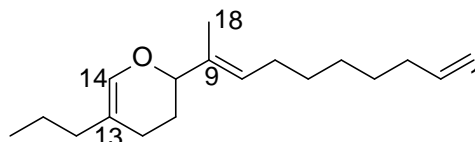


Figure 6.105.: Mass fragmentation pattern of 1'-((10*E*)-10-(10-(pentan-4-yl)-cyclohex-4-enyl)-allyloxy)-tetrahydro-2',2'-dimethyl-2*H*-pyran (**7**)

6.3.2.4.B. Structural characterization of compound **8** (PM₄₋₁₋₁)

2-((*E*)-Deca-1,8-dien-10-yl)-11,12-dihydro-13-propyl-2*H*-pyran (**8**)



Sample yield	90 mg; 0.18%
Physical description	Yellow solid
Molecular formula	C ₁₈ H ₃₀ O
Molecular mass	262.2297

The compound **8**, 2-((*E*)-deca-1,8-dien-10-yl)-11,12-dihydro-13-propyl-2*H*-pyran, a new C₁₈ sesquiterpenoid with prenylated irregular framework, was isolated as yellow solid. It exhibited UV absorbance (in MeOH) at λ_{max} (log ε 3.37) 265.0 nm assigned

to a chromophore with olefinic groups (Figure 6.106.). The purity of the compound was supported by RP C18 HPLC experiments using 3:2 (v/v) MeOH:MeCN (R_t 20.52) (Figure 6.107.).

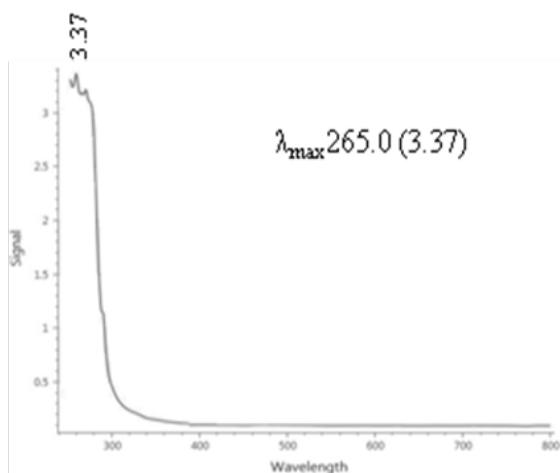


Figure 6.106.: UV spectrum of 2-((*E*)-deca-1,8-dien-10-yl)-11,12-dihydro-13-propyl-2*H*-pyran (**8**)

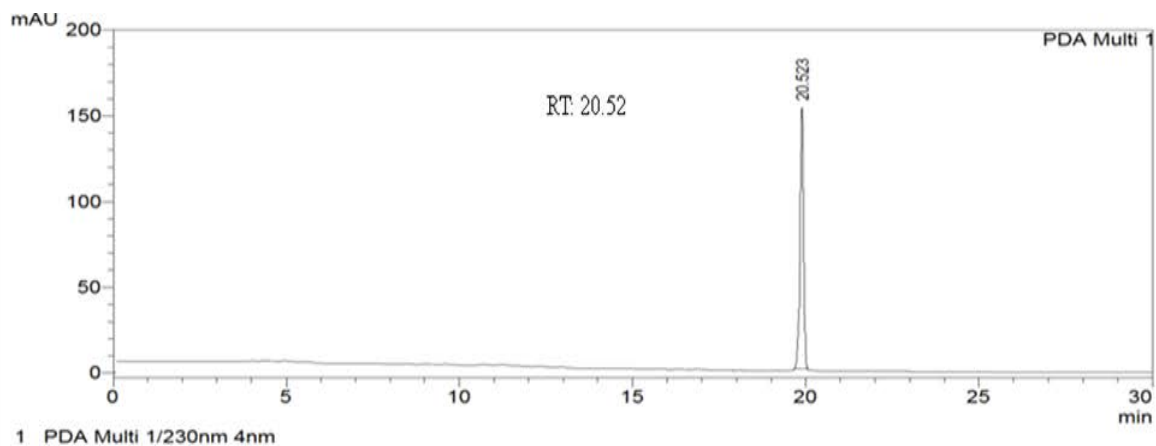


Figure 6.107.: HPLC chromatogram of 2-((*E*)-deca-1,8-dien-10-yl)-11,12-dihydro-13-propyl-2*H*-pyran (**8**)

The title compound was exhibited a molecular ion peak at m/z 262 (EIMS: found m/z 262.2300 $[M]^+$, cal. for $C_{18}H_{30}O$ 262.2297), along with 1H and ^{13}C NMR spectra, signifying the elemental composition as $C_{18}H_{30}O$ with four degrees of unsaturation associated with three double bonds and one ring system (Table 6.13.; Figure 6.110.-6.111.).

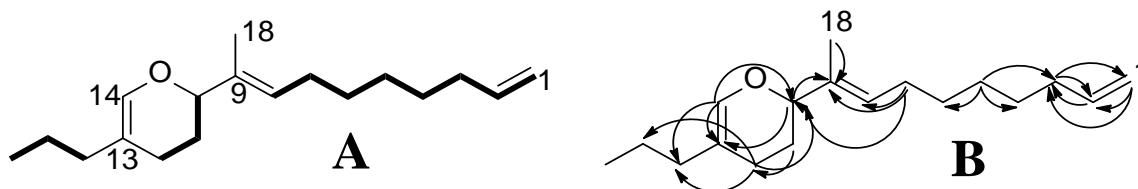
The ^1H - ^1H COSY couplings from δ 4.68 (assigned to H-10)/ δ 1.58, 1.60 (H-11)/ δ 2.02, 2.00 (H-12) were apparent (Figure 6.108.A, 6.113.). The downfield methine (-CH) at δ 4.68 was found to be a triplet, HSQC with δ 108.30 was attributed to the part of a pyran ring system (Figure 6.114.). The quaternary carbon at C-13 (δ 112.37) was recognized as the junction point of pyran ring system and the propyl moiety. However, the lower chemical shift value of quaternary carbon predicted that it might be adjacent to highly electron withdrawing group with high downfield shift at δ C 123.34/ δ H 6.96. The higher chemical shift of this alkenic proton was due to the neighboring oxygen atom and found to be a singlet proton, but not related to an aromatic ring. The HMBC relation from δ 6.96 (assigned as H-14) to δ 108.30 (C-10), 112.37 (C-13); δ 4.68 (H-10) to δ 112.37 (C-13); δ 1.58 (H-11) to δ 29.71 (C-12) and δ 2.02 (H-12) to δ 108.30 (C-10) were established the 2H-pyran ring system (Figure 6.108.B, 6.115.). The signal at δ 112.37 (assigned to C-13) attached to a propyl side chain was evident from the HMBC relations from the protons of propyl moiety to the pyran ring. The two methylenes at δ 37.11 (C-15), 22.70 (C-16) and methyl at δ 14.12 (C-17) were in good concurrence with previously reported 2H-pyranoid, 1-(6-butyl-3,4-dihydro-2H-pyran-2-yl)-pentanone (Rocha *et al.*, 2011). The long couplings from δ 2.02 (H-12) to δ 37.11 (C-15), 22.70 (C-16); δ 1.37 (H-16) to δ 29.71 (C-12) and δ 6.96 (H-14) to δ 37.11 (C-15) were confirmed the attachment to pyran moiety and ^1H - ^1H COSY correlations between δ 2.03 (H-15)/1.37 (H-16)/0.88 (H-17) were established the propyl side chain. The proton at δ 4.68 (H-10) was exhibited HMBC relations with δ 129.91 (C-9) which implied the attachment to the alkenic quaternary carbon of deca-1,8-dien-10-yl side chain. The signal at δ 129.91 was found to be due to the quaternary carbon, and was attached to an alkenic proton, δ 5.35 (corresponding to ^{13}C NMR signal at δ 130.38 at C-8 position) (Wang *et al.*, 2010a). The singlet proton at δ 1.44 (H-18) was attached to δ 30.41 exhibiting HMBC relations to δ 129.91 (C-9), 130.38 (C-8), 31.94 (C-7), 108.30 (C-10). It was found that the groups of carbons from C-1 to C-9 were linearly aligned as assigned by ^1H - ^1H COSY correlation analyses. The ^1H - ^1H COSY correlations from δ 4.94, 5.10 (H-1)/5.81 (H-2)/2.06 (H-3)/1.36 (H-4)/1.26 (H-5)/1.30 (H-6)/1.97 (H-7)/5.35 (H-8) and long range HBMC correlations from δ 1.97 (H-7) to δ 130.38 (C-8), 129.91 (C-9), 108.30 (C-10); δ 1.26 (H-5) to δ 33.83 (C-3), 29.37 (C-4), 28.97 (C-6); δ 2.06 (H-3) to δ

139.27 (C-2), 114.06 (C-1); δ 5.81 (H-2) to δ 114.06 (C-3) and δ 5.01, 4.94 (H-1) to δ 139.27 (C-2), 33.83 (C-3) unambiguously confirmed the presence of side straight chain of **8**. The $>\text{CH}_2$ group at δ 5.01 and δ 4.94 were found to be significantly downfielded due to its terminal position and the presence of highly downfielded alkene ($-\text{CH}=\$, δ 5.81). The geometrical arrangement of these alkenic protons was confirmed from their J values, which were 5.81 ($J=10.24$ Hz), 5.01 ($J=14.51$, 6.90 Hz) and 4.94 ($J=10.22$, 6.41 Hz), thus established the *trans* (*E*) configuration comparable with a related compound, lobatriene, identified from soft coral, (Govindam *et al.*, 2012). The ^{13}C NMR spectrum of this compound in combination with DEPT were indicated the presence of a total of 18 carbons, which enclosed two CH_3 , ten CH_2 , and four CH groups. The relative stereochemistries of the chiral centre of **8**, particularly that of C-10 carrying the methine proton, δ 4.68 (1H, t) was deduced from the NOESY spectrum (Figure 6.109., 6.116.). NOE correlations among the protons, δ 1.60 (H-11)/4.94 (H-1)/5.81 (H-2)/2.00 (H-12)/4.68 (H-10)/5.35 (H-8) suggested the closeness of these groups and their α -position. Further NOE couplings were observed between the protons at δ 1.58 (H-11)/2.02 (H-12)/5.01 (H-1)/1.44 (H-18)/6.96 (H-14) which suggested that these were on the similar of plane of the molecule, and disposed in β -orientation. Additionally, the large coupling constant of 10.2 Hz (each) between the pertinent olefinic protons at 5.81 (related to H-2 α) and δ 5.35 (assigned to H-8 α , bearing C8-C9 double bond) revealed that they were disposed on the same plane of geometry, all these effects were in accord with the observed J values and, thus indicated the stereochemistry. The protons at δ 1.44 (CH_3 , s, C-18) was found to be situated at β -position because of NOE relationship with δ 6.96 (H β -14, s), and has no NOE associations with the protons at δ 4.94 (H α -1) and 4.68 (H α -10) which suggested the *cis*-orientation for the methyl groups at C-18 and olefinic proton at C-14, and that these groups must be disposed on the β -side. The H-10 should be *trans* orientation with the methyl protons at C-18 and olefinic proton at C-14 since there was no cross peak could be detected between the H-14 and H-10 in NOESY experiment.

Table 6.13.: NMR spectroscopic data of 2-((*E*)-deca-1,8-dien-10-yl)-11,12-dihydro-13-propyl-2*H*-pyran (**8**) in CDCl₃

C. No.	¹³ C	¹ H (int.,mult., <i>J</i> in Hz) ^a	COSY	HMBC
1	114.06	5.01 (1H β ,m,14.51,6.90) 4.94 (1H α ,m,10.22,6.41)	H-2 -	C-2 C-3,2
2	139.27	5.81 (1H α ,m,10.24)	H-3	C-3
3	33.83	2.06 (2H,t)	H-4	C-2,1
4	29.37	1.36 (2H,m)	H-5	-
5	29.52	1.26 (2H,m)	H-6	C-3,4,6
6	28.97	1.30 (2H,m)	H-7	-
7	31.94	1.97 (2H,t)	H-8	C-9,8,2
8	130.38	5.35 (1H α ,t,10.6,5.5)	-	-
9	129.91	-	-	-
10	108.30	4.68 (1H α ,t)	H-11	C-13,9
11	26.72	1.58 (1H β ,m) 1.60 (1H α ,m)	H-12 -	C-12 -
12	29.71	2.02 (1H β ,t) 2.00 (1H α ,t)	- -	C-15,16,10 -
13	112.37	-	-	-
14	123.34	6.96 (1H β ,s)	-	C-15,13,10
15	37.11	2.03 (2H,t)	H-16	-
16	22.70	1.37 (2H,m)	H-17	C-12
17	14.12	0.88 (3H,t)	-	C-16
18	30.41	1.44 (3H β ,s)	-	C-9,10,8,7

¹H NMR spectra recorded using Bruker AVANCE III 500MHz (AV 500) spectrometer (Bruker, Karlsruhe, Germany) in CDCl₃ as aprotic solvent at ambient temperature with TMS as the internal standard (δ 0 ppm). The ¹H NMR spectra were recorded at 500MHz, while the ¹³C NMR spectra were recorded at 125MHz. ^aValues in ppm, multiplicity and coupling constants (*J*=Hz) were indicated in parentheses. The assignments were made with the aid of the ¹H-¹H COSY, HSQC, HMBC and NOESY experiments

**Figure 6.108.:** ¹H-¹H COSY (A) and HMBC (B) correlations of 2-((*E*)-deca-1,8-dien-10-yl)-11,12-dihydro-13-propyl-2*H*-pyran (**8**). The key ¹H-¹H COSY couplings have been

represented by the bold face bonds. The HMBC couplings were indicated by double barbed arrow

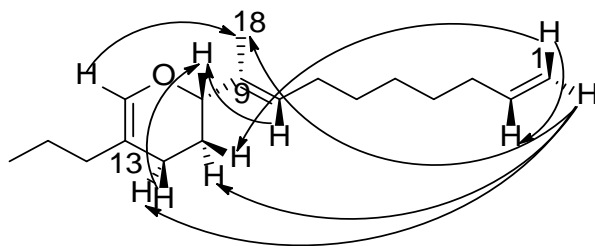


Figure 6.109.: NOESY correlations of 2-((*E*)-deca-1,8-dien-10-yl)-11,12-dihydro-13-propyl-2*H*-pyran (**8**). The NOESY relations were represented by double barbed arrow

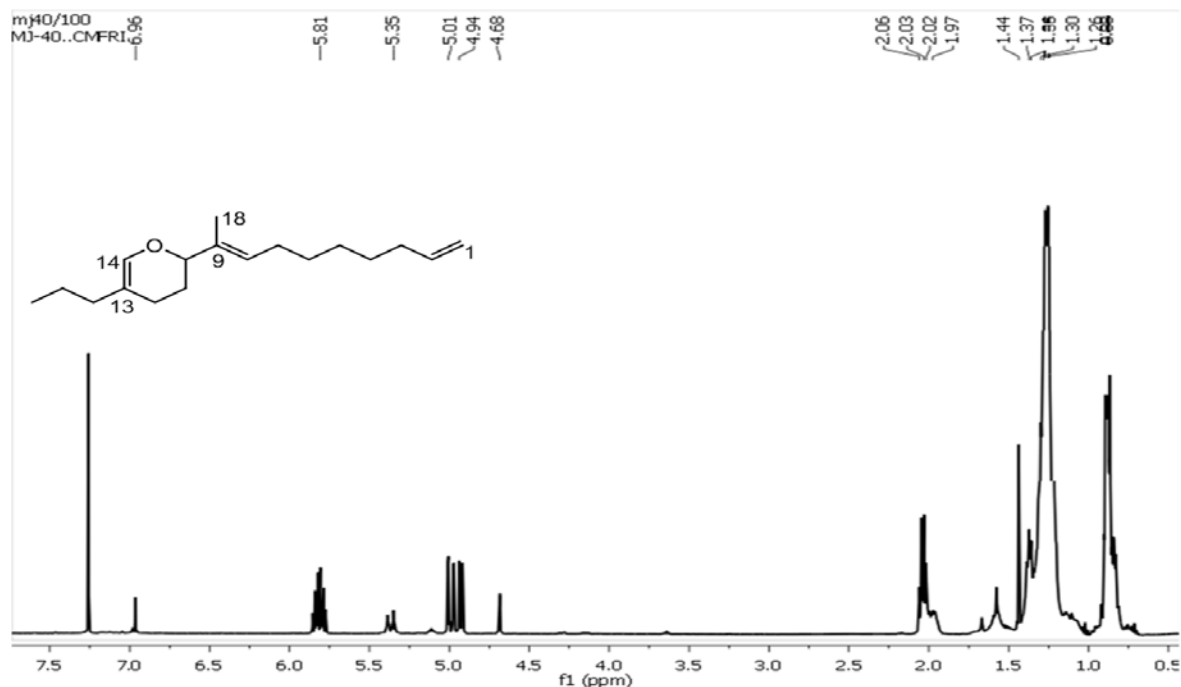


Figure 6.110.: ^1H NMR spectrum of 2-((*E*)-deca-1,8-dien-10-yl)-11,12-dihydro-13-propyl-2*H*-pyran (**8**)

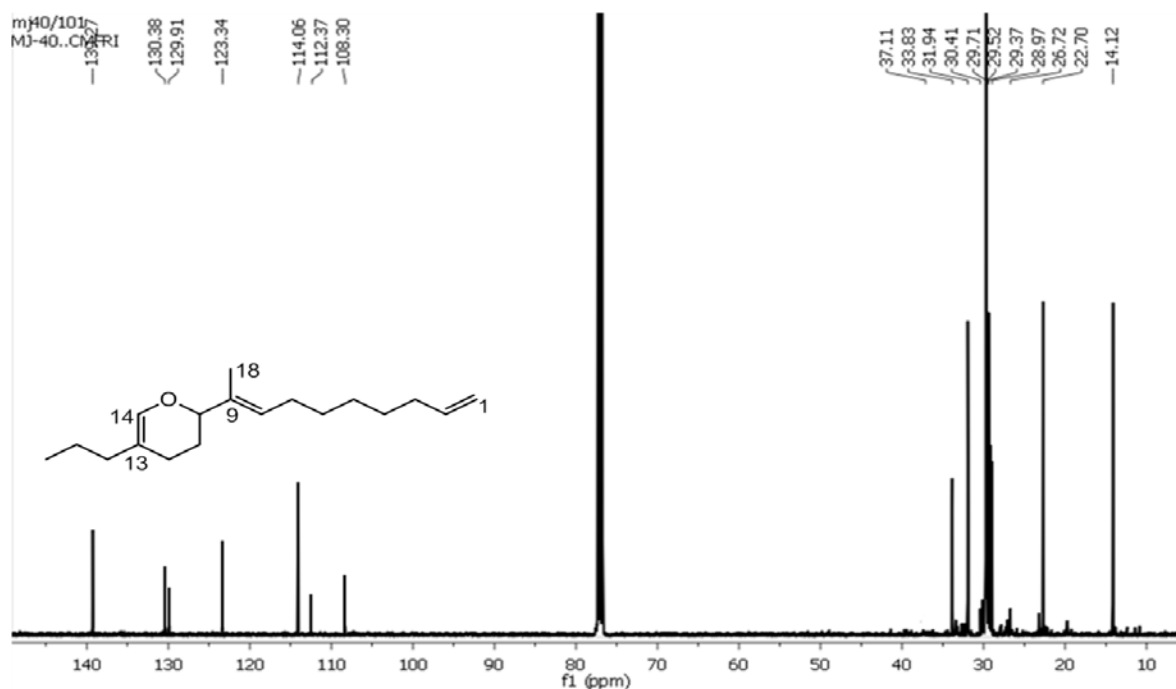


Figure 6.111.: ^{13}C NMR spectrum of 2-((*E*)-deca-1,8-dien-10-yl)-11,12-dihydro-13-propyl-2*H*-pyran (**8**)

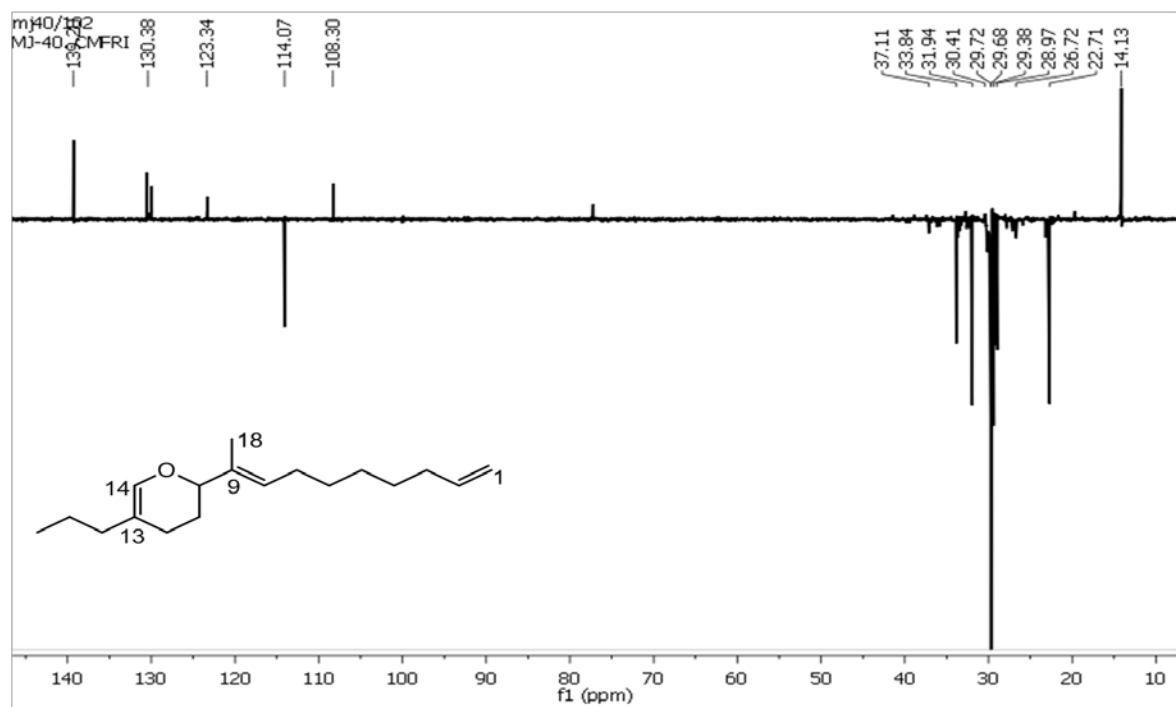


Figure 6.112.: $^{135}\text{DEPT}$ NMR spectrum of 2-((*E*)-deca-1,8-dien-10-yl)-11,12-dihydro-13-propyl-2*H*-pyran (**8**)

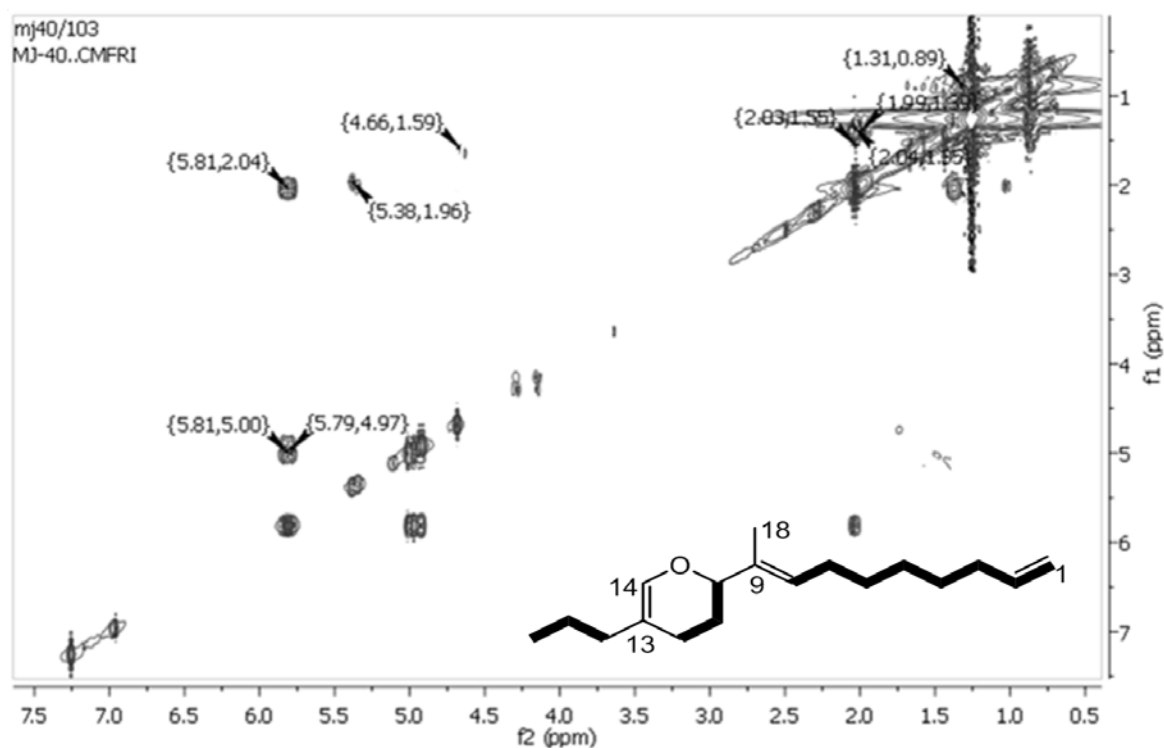


Figure 6.113.: ^1H - ^1H COSY NMR spectrum of 2-((*E*)-deca-1,8-dien-10-yl)-11,12-dihydro-13-propyl-2H-pyran (8)

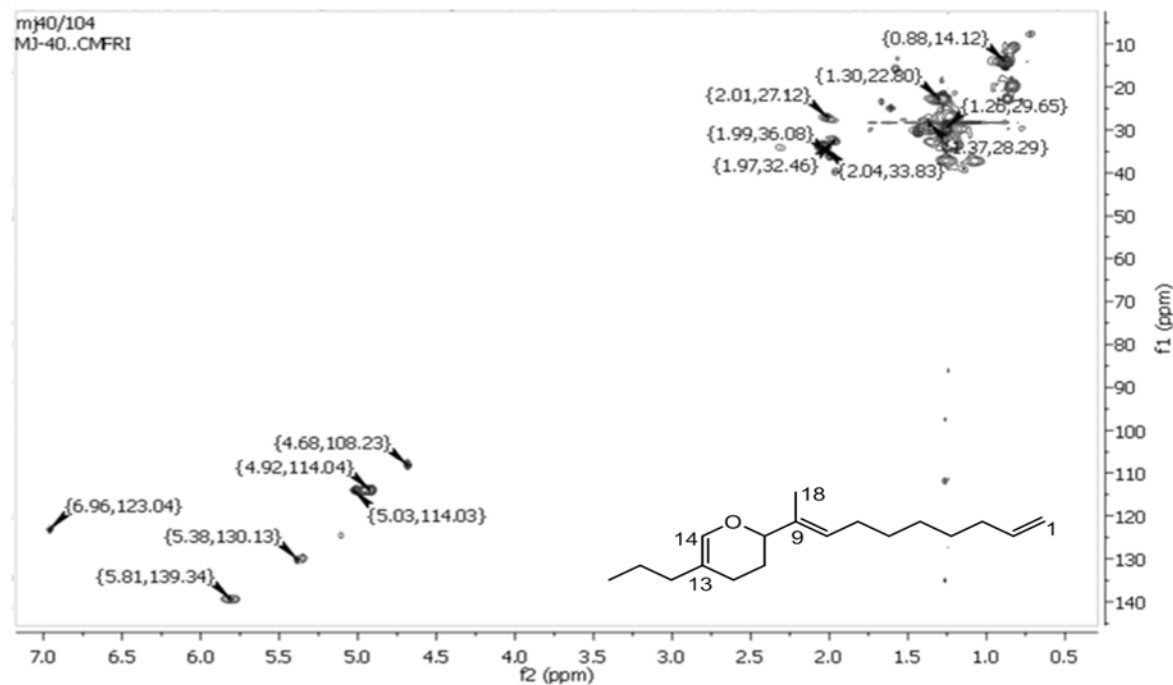


Figure 6.114.: HSQC NMR spectrum of 2-((*E*)-deca-1,8-dien-10-yl)-11,12-dihydro-13-propyl-2H-pyran (8)

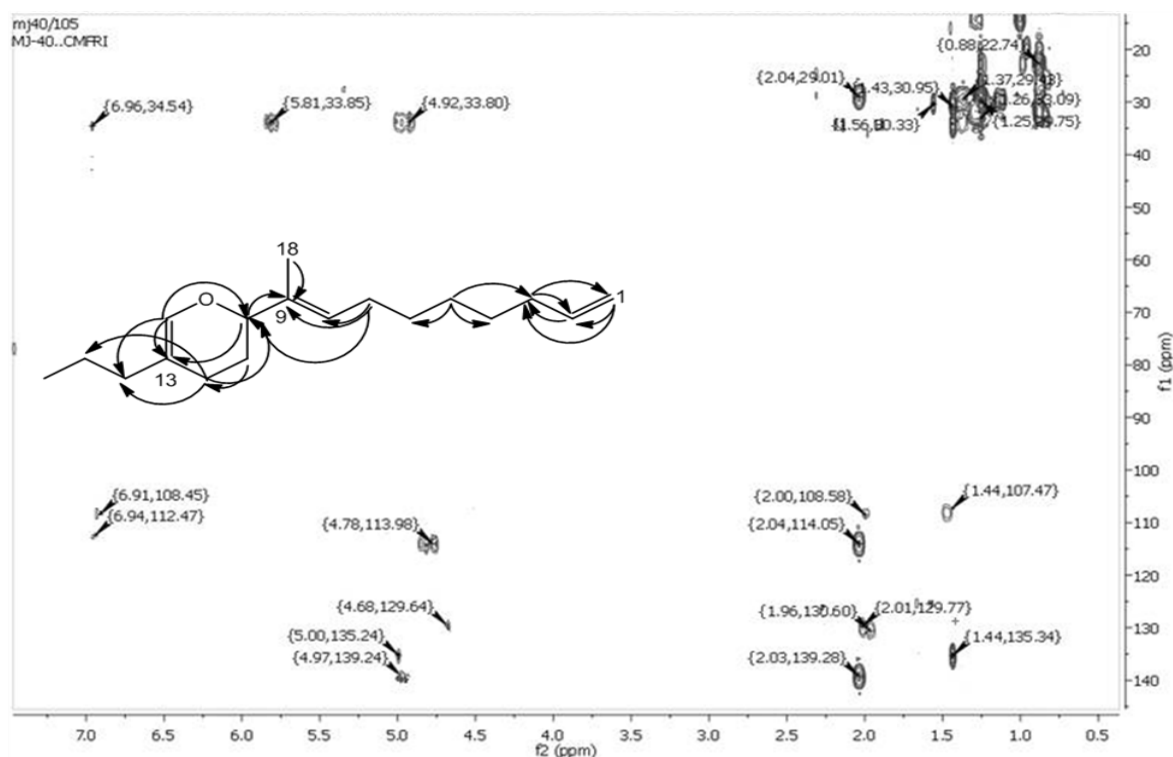


Figure 6.115.: HMBC NMR spectrum of 2-((*E*)-deca-1,8-dien-10-yl)-11,12-dihydro-13-propyl-2*H*-pyran (**8**)

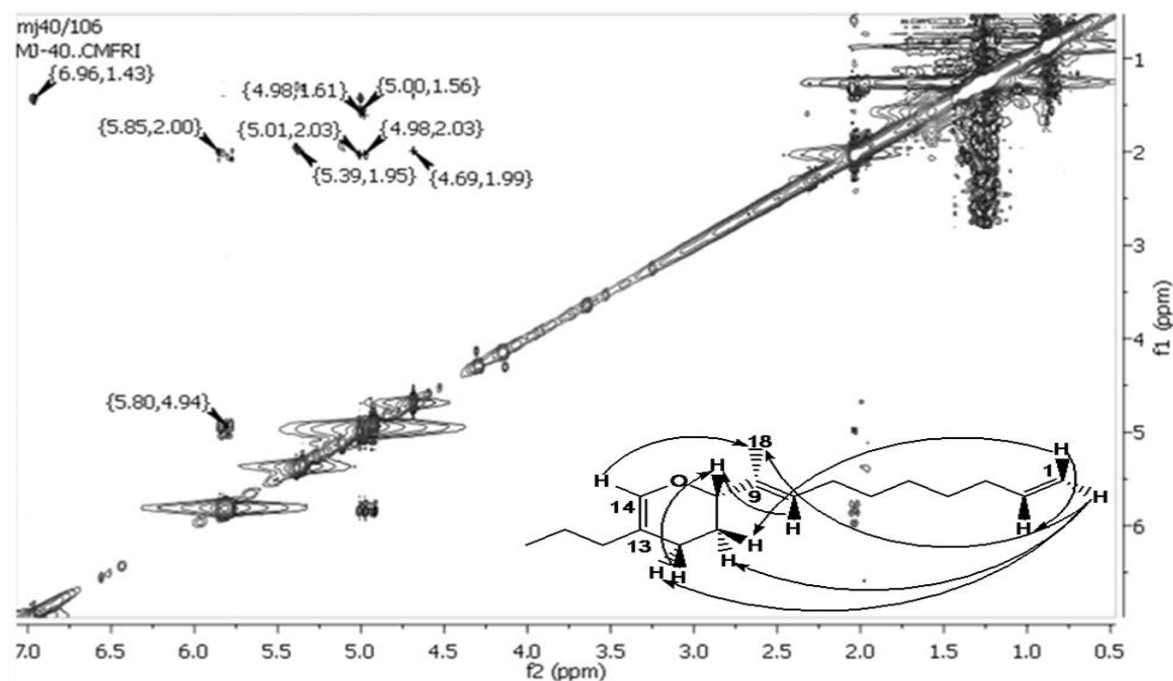


Figure 6.116.: NOESY NMR spectrum of 2-((*E*)-deca-1,8-dien-10-yl)-11,12-dihydro-13-propyl-2*H*-pyran (**8**)

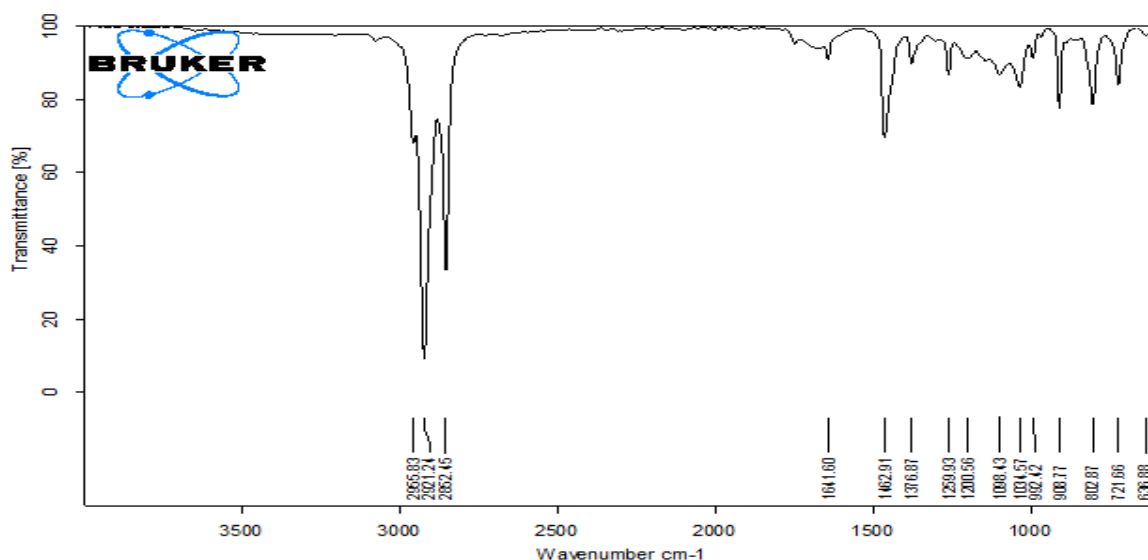


Figure 6.117.: FTIR spectrum of 2-((*E*)-deca-1,8-dien-10-yl)-11,12-dihydro-13-propyl-2*H*-pyran (**8**)

The IR spectrum revealed the presence of olefinic (C=C) and alkyl (C-H) vibrations were represented by the 1641 and 1462 cm^{-1} absorption bands, respectively. The absorption bands at 2955/2852 cm^{-1} indicated C-H stretching vibration (Figure 6.117.), thereby corroborated the prenylated pyranoid framework.

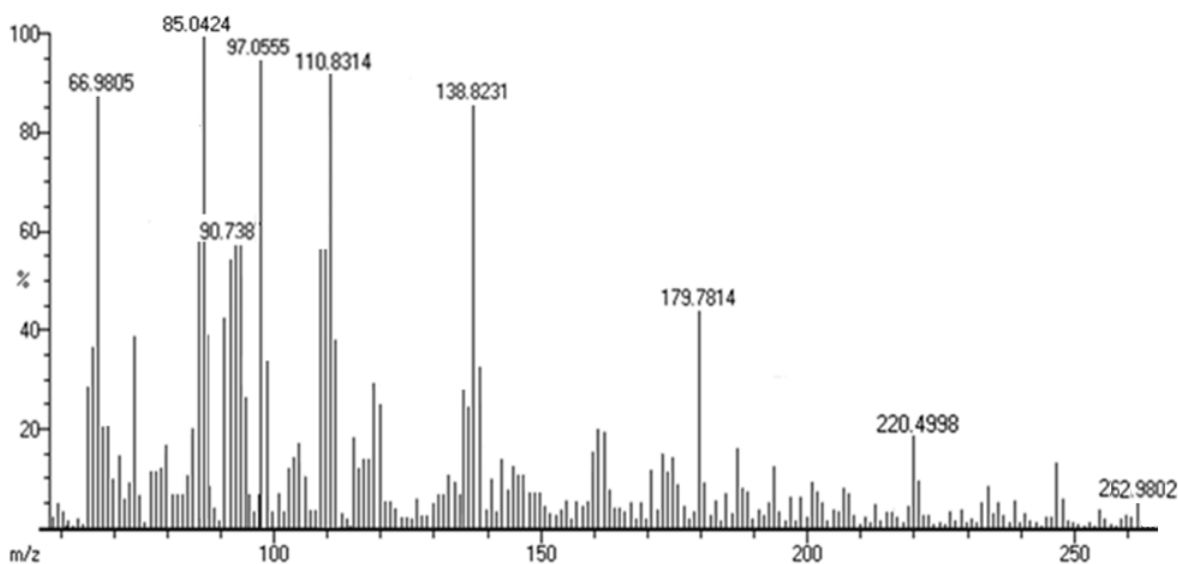


Figure 6.118.: EIMS spectrum of 2-((*E*)-deca-1,8-dien-10-yl)-11,12-dihydro-13-propyl-2*H*-pyran (**8**)

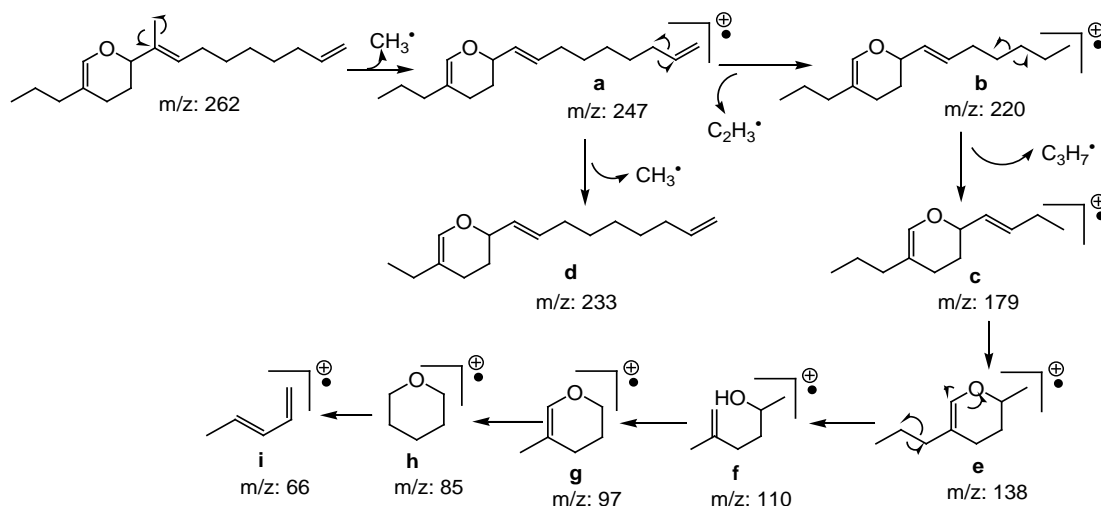


Figure 6.119.: Mass fragmentation pattern of 2-((*E*)-deca-1,8-dien-10-yl)-11,12-dihydro-13-propyl-2*H*-pyran (**8**)

The mass spectrum exhibited molecular ion peak at m/z 262, which appeared to undergo elimination of methyl radical to yield a radical ion fragment at m/z 247 (**a**, dihydro-2-(nona-1,8-dienyl)-13-propyl-2*H*-pyran). The latter underwent fragmentation by eliminating $\cdot\text{CH}_3$ and $\cdot\text{C}_2\text{H}_3$ radicals to obtain fragment peaks at m/z 233 (**d**, 13-ethyl-dihydro-2-(nona-1,8-dienyl)-2*H*-pyran) and m/z 220 (**b**, 2-(hept-1-enyl)-9,10-dihydro-11-propyl-2*H*-pyran), respectively. Fragmentation of the ion at m/z 220 (**b**) was perceived to be accompanied by the loss of a C-3 fragment resulting in an ion at m/z 179 (**c**), which on subsequent rearrangement yielded the fragments at m/z 110 (**f**, 5-methylhex-5-en-2-ol) and 97 (**g**, dihydro-5-methyl-2*H*-pyran). The latter eliminated CH_2O radical to yield m/z 66 (**i**, penta-1,3-diene). The fragment peak at 85 (tetrahydro-2*H*-pyran ion) was found to be the base peak (Figure 6.118.-6.119.).

The pyran derivatives, 2-((*E*)-deca-1,8-dien-10-yl)-11,12-dihydro-13-propyl-2*H*-pyran (**8**) and 1'-((10*E*)-10-(10-(pentan-4-yl)-cyclohex-4-enyl)-allyloxy)-tetrahydro-2',2'-dimethyl-2*H*-pyran (**7**) represent the first description of meroterpeno pyranoids possessing the C18 sesquiterpenoid with prenylated irregular farnesene framework and C21 prenylated bisabolene-type meroterpenoid with the allyloxy linkage coordinating between the C14 meroterpene and substituted tetrahydropyran system from a natural source. These

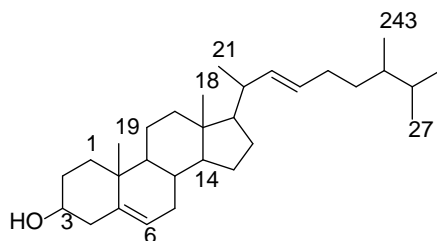
unprecedented meroterpeno pyranoids from *P. malabarica* has bioactive potential as natural antioxidant and anti-inflammatory pharmacophore.

6.3.2.5. Structural characterization of cholestenol derivatives (9-10)

Sterols were known as the bioactive lipid metabolites, and found as major constituents in marine invertebrates, such as sponges, bryozoans and mollusks (Goad and Scheuer 1978). More than 200 sterols of 3β -hydroxy- Δ^5 (or saturated) cholestane nucleus and a C8-C10 side chain occurring in marine organisms were reported (Sarma *et al.*, 2005). In particular, sponges and mollusks were extensively investigated for different types of steroids than invertebrates of other phyla (Joosse 1978; Sica 1980). Among different groups of steroids, poly-oxygenated tetracyclic nucleus with varying degrees of unsaturation and atypical side chain substitution (D'Auria *et al.*, 1993), 3β -cholestane esters, steroids with spiro ring system (Su *et al.*, 2007) and bicyclo[4.4.1] or bicyclo[4.3.1] A/B steroids were predominant among the compounds isolated from marine organisms (Amagata *et al.*, 2003; Wang *et al.*, 2015). We herein described isolation and structure elucidation of two new sterol derivatives, (22*E*)-24¹,24²-methyldihomocholesta-5,22-dien-3 β -ol (**9**) and 23-*gem*-dimethylcholesta-5-en-3 β -ol (**10**) from *P. malabarica*.

6.3.2.5.A. Structural characterization of compound 9 (PM₃₋₃₋₂₋₁)

(22*E*)-24¹,24²-Methyldihomocholesta-5,22-dien-3 β -ol (**9**)



Sample yield	148 mg; 0.30%
Physical description	White solid
Molecular formula	C ₃₀ H ₅₀ O
Molecular mass	426.3862

The (22*E*)-24¹,24²-methyldihomocholesta-5,22-dien-3 β -ol (**9**), a new substituted dihomocholestadienol, was purified as white solid. The ultraviolet absorbance at λ_{max} (log ϵ 1.74) 228.9 nm has been assigned to be chromophores with olefinic system (Figure 6.120.). The purity of the compound was supported by RP C18 HPLC experiments using 6:4 (v/v) MeOH:MeCN (R_t 5.33) (Figure 6.121.).

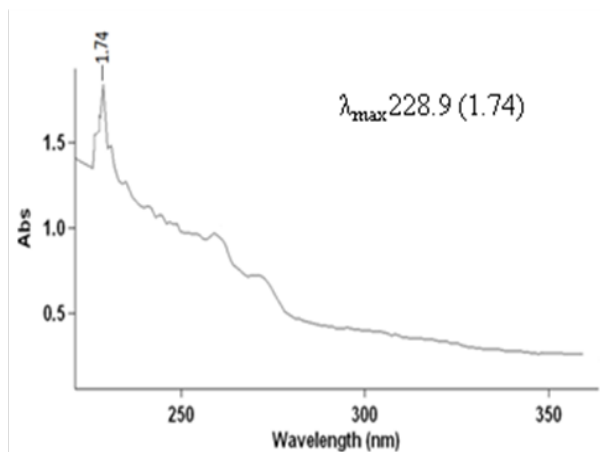


Figure 6.120.: UV spectrum of (22*E*)-24¹,24²-methyldihomocholesta-5,22-dien-3 β -ol (**9**)

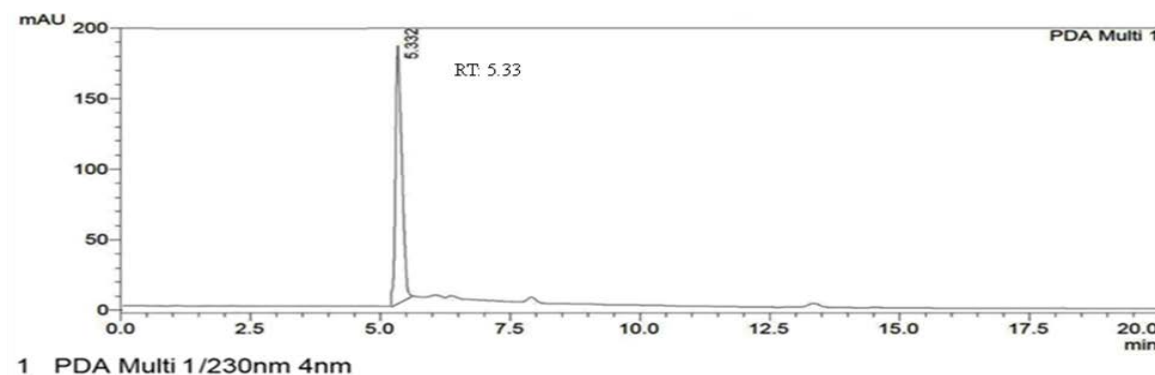


Figure 6.121.: HPLC chromatogram of (22*E*)-24¹,24²-methyldihomocholesta-5,22-dien-3 β -ol (**9**)

Its mass spectrum exhibited a molecular ion peak at m/z 426 (EIMS: found m/z 426.3868 $[M]^+$, cal. 426.3862), which in combination with its ¹H and ¹³C NMR data (Table 6.14.) indicated the elemental composition of (22*E*)-24¹,24²-methyldihomocholest-5,22-dien-3 β -ol (**9**) as C₃₀H₅₀O with six degrees of unsaturation containing two double bonds and four ring systems (Figure 6.124., 6.125.). The ¹³C spectrum of **9** in combination with DEPT

experiments were indicated the occurrence of 30 carbon atoms including one carbinol carbons at δ 71.81 and olefinic carbons at δ 140.76, 121.71, 135.83 and 131.72. A total number of six methyl carbons, ten methylene and eleven methine groups were recorded (Figure 6.125., 6.126.). Since no aromatic signals were recorded in the ^1H data, these peaks appeared downfield above δ 130 were assigned to the olefinic carbons in the ^{13}C spectrum. The olefinic signal at δ 140.76 was appeared at the far downfield region and less intense than other peak at δ 121.71, because of slow relaxation, it must be a quaternary carbon. The intense olefinic signals at δ 131.72 and 135.83 might be due to the fact that these are less substituted carbons and sterically less crowded. The similarity in chemical shift apparently indicated these as sp^2 hybridized ($-\text{CH}=\text{CH}-$) and shifted more upfield relative to the sp hybridized carbon atom. The broad IR absorptions at 3427 cm^{-1} was due to O-H vibrations, which has been supported by the ^1H signal at δ 3.50. The presence of olefinic protons was suggested by ^1H signals at δ 5.35 (1H, dd) with a coupling constant of 5.28 and 3.58 Hz. This supported the presence of *E*-geometrical isomer of the olefinic proton (C-6). The ^1H , ^{13}C and HSQC experiments (Figure 6.128.) attributed the parent steroid nucleus with C-3 hydroxyl at δ 3.50 (δ 71.81) and C5-C6 double bond at δ 5.35 were similar to those reported in the earlier studies (Wilson *et al.*, 1996). The COSY correlations were confirmed between δ 1.83, 1.08 (assigned to H-1)/1.50, 1.82 (H-2)/3.50 (H-3)/2.24, 2.28 (H-4); δ 5.35 (H-6)/1.96, 1.56 (H-7)/0.93 (H-8) and δ 0.96 (H-9)/1.49 (H-11)/2.01, 1.15 (H-12) (Figure 6.127.) along with their H-C connectivities were proposed from the HSQCs and HMBs (Figure 6.128., 6.129.). The ^{13}C NMR signals at C-22 and C-23 (δ 135.83 and 131.72, respectively) in combination with the HSQC experiments (δ 5.18 and 5.17) assigned the olefinic ($-\text{HC}=\text{CH}-$) group at the side chain. The large coupling constants, (*J*) 12.4 and 16.1 Hz of the olefinic protons at H-22 and H-23, respectively attributed to its *trans* (*E*-form) configuration, as supported by the previous studies (Goad and Akihisa 1997). The occurrence of olefinic proton at Δ^{22} (δ 5.18 (H-22) and 5.17 (H-23)) was further confirmed by the long range HMB correlations from δ 0.91 (H-21) to δ 131.72 (C-23) and from δ 1.10 (H-17) to δ 135.83 (C-22) (Figure 6.122.B) along with one bond $^1\text{H}-^1\text{H}$ COSY relations such as δ 1.86 (H-20)/5.18 (H-22); δ 5.17 (H-23)/2.03 (H-24)/1.25 (H-24¹)/1.35 (H-24²)/0.92 (H-24³), 1.52 (H-25) and δ 1.52 (H-25)/0.86 (H-26), 0.87 (H-26) (Figure

6.122.A, 6.127.) (Tian *et al.*, 2011). The HMBC relations from δ 1.35 (H-24²) to δ 22.69 (C-27) and from δ 2.03 (H-24) to δ 28.02 (C-25) supported the occurrence of side chain framework attached to the parent steroid skeleton. Further the long range HMBC correlations such as δ 2.24 (H-4) to δ 31.80 (C-2), 121.71 (C-6), 36.50 (C-10); δ 5.35 (H-6) to δ 36.50 (C-10); δ 1.96 (H-7) to δ 140.76 (C-5), 121.71 (C-6); δ 1.83 (H-1) to δ 71.81 (C-3), 36.50 (C-10); δ 1.49 (H-11) to δ 56.70 (C-14) assigned to the tricyclic framework. ¹H-¹H COSYs were observed among the protons at δ 1.00 (H-14)/1.57, 1.06 (H-15)/1.85 (H-16)/1.10 (H-17). Further the HMBC correlations such as δ 1.00 (H-14) to δ 46.05 (C-8), 50.14 (C-9) and C-H connectivities between δ 1.10 (H-17) and δ 135.83 (C-22), 56.70 (C-14) confirmed the side chain framework. Six methyl groups, including the two angular -CH₃ groups (δ 0.91 and 0.68) were located at the ring junction of A/B and C/D gave rise to sharp peaks at shielded region. The HMBCs between δ 1.01 (H-19) to δ 37.20 (C-1), 31.80 (C-2) and 140.76 (C-5) also attributed the occurrence of C-19 methyl at C-10. The stereochemistries of chiral centers, particularly at C-3, C-17, C-20, C-8 and C-14 were deduced from NOESY (Figure 6.130., 6.123.). NOE couplings were apparent among H α -3/H α -6 suggested the α -side of the molecule. The C-3 hydroxyl group is equatorial and β -oriented (Sun *et al.*, 2013). NOE correlations between H α -6/H α -14 indicated that these groups on their α -disposition. The methine proton at C-21 did not exhibit NOE interactions with Me-18 and Me-19, which were at the β -face of the molecule, thereby indicating that H-21 was at α -position. Based on the interpretations, the compound was deduced as (22*E*)-24¹,24²-methyldihomocholesta-5,22-dien-3 β -ol.

Table 6.14.: NMR spectroscopic data of (22*E*)-24¹,24²-methyldihomocholesta-5,22-dien-3 β -ol (**9**) in CDCl₃

C. No.	¹³ C	¹ H (int.,mult.,J in Hz) ^a	COSY	HMBC
1	37.22	1.83 (1H β ,t) 1.08 (1H α ,t)	H-2 -	C-10,3 C-3
2	31.83	1.50 (1H β ,m) 1.82 (1H,m)	H-3 -	C-3 C-5
3	71.81	3.50 (1H α ,p)	H-4	-
4	42.33	2.24 (1H β ,d) 2.28 (1H α ,d)	- -	C-3,5,6 C-10,2

5	140.76	-	-	-
6	121.71	5.35 (1H α ,dd,5.28,3.58)	H-7	C-10,7
7	31.91	1.56 (1H β ,m)	-	C-5,6
		1.96 (1H α ,t)	-	-
8	46.05	0.93 (1H β ,m)	-	C-7
9	50.14	0.96 (1H α ,m)	H-11	-
10	36.50	-	-	-
11	21.14	1.49 (2H,m)	H-12	C-12,14
12	39.72	2.01 (1H β ,t)	-	C-13
		1.15 (1H α ,t)	-	C-20,9
13	42.32	-	-	-
14	56.70	1.00 (1H,m)	H-15	C-8,9,20
15	24.26	1.57 (1H β ,m)	H-16	C-16,13
		1.06 (1H α ,m)	-	-
16	28.22	1.85 (2H,m)	H-17	-
17	56.16	1.10 (1H β ,m)	-	C-22,14,20,18,16
18	11.68	0.68 (3H β ,s)	-	C-12,20
19	19.40	1.01 (3H β ,s)	-	C-5,2,1
20	42.54	1.86 (1H α ,t)	H-22	-
21	18.39	0.91 (3H α ,d)	-	C-23
22	135.83	5.18 (1H,dd,12.41,6.09)	-	-
23	131.72	5.17 (1H,dt,16.10,7.31)	H-24	-
24	41.90	2.03 (2H,m)	H-24 ¹	C-25
24 ¹	28.42	1.25 (2H,m)	H-24 ²	-
24 ²	35.72	1.35 (1H β ,m)	H-24 ³ ,25	C24 ³ ,27,25
24 ³	20.53	0.92 (3H α ,d)	-	-
25	28.02	1.52 (1H α ,m)	H-26,27	C-26,27
26	19.89	0.86 (3H,d)	-	-
27	22.69	0.87 (3H,d)	-	-

¹H NMR spectra recorded using Bruker AVANCE III 500MHz (AV 500) spectrometer (Bruker, Karlsruhe, Germany) in CDCl₃ as aprotic solvent at ambient temperature with TMS as the internal standard (δ 0 ppm). The ¹H NMR spectra were recorded at 500MHz, while the ¹³C NMR spectra were recorded at 125MHz. ^aValues in ppm, multiplicity and coupling constants (J =Hz) were indicated in parentheses. The assignments were made with the aid of the ¹H-¹H COSY, HSQC, HMBC and NOESY experiments

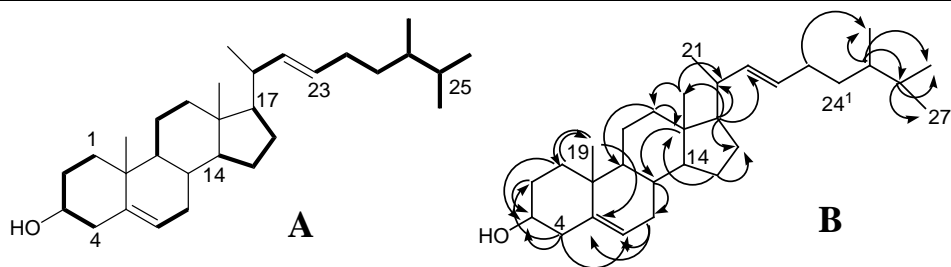


Figure 6.122.: ^1H - ^1H COSY (A) and HMBC (B) correlations of (22E)-24¹,24²-methyl dihomocholesta-5,22-dien-3β-ol (9). The key ^1H - ^1H COSY couplings have been represented by the bold face bonds. The HMBC couplings were indicated by double barbed arrow

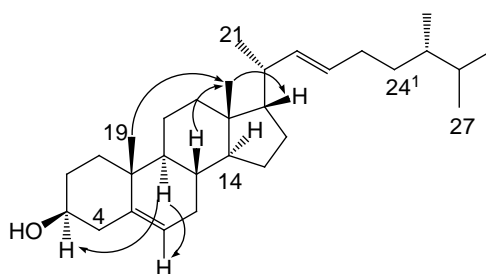


Figure 6.123.: NOESY correlations of (22E)-24¹,24²-methyldihomocholesta-5,22-dien-3β-ol (9). The NOESY relations were represented by double barbed arrow

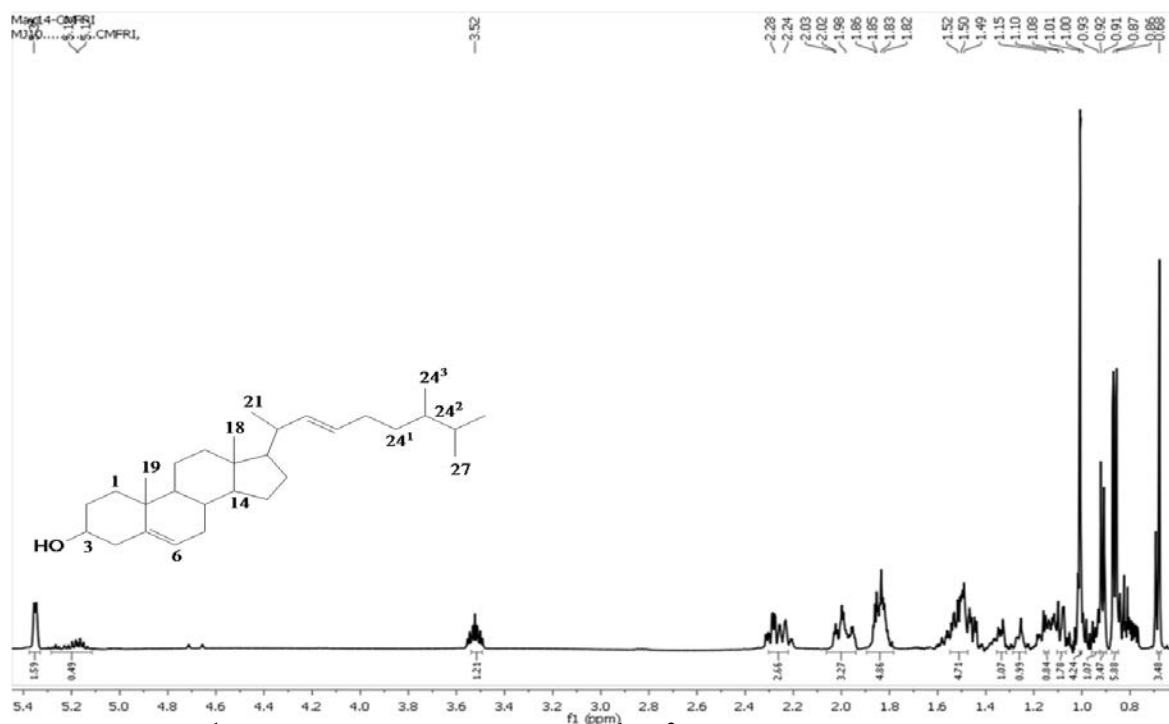


Figure 6.124.: ^1H NMR spectrum of (22E)-24¹,24²-methyldihomocholesta-5,22-dien-3β-ol (9)

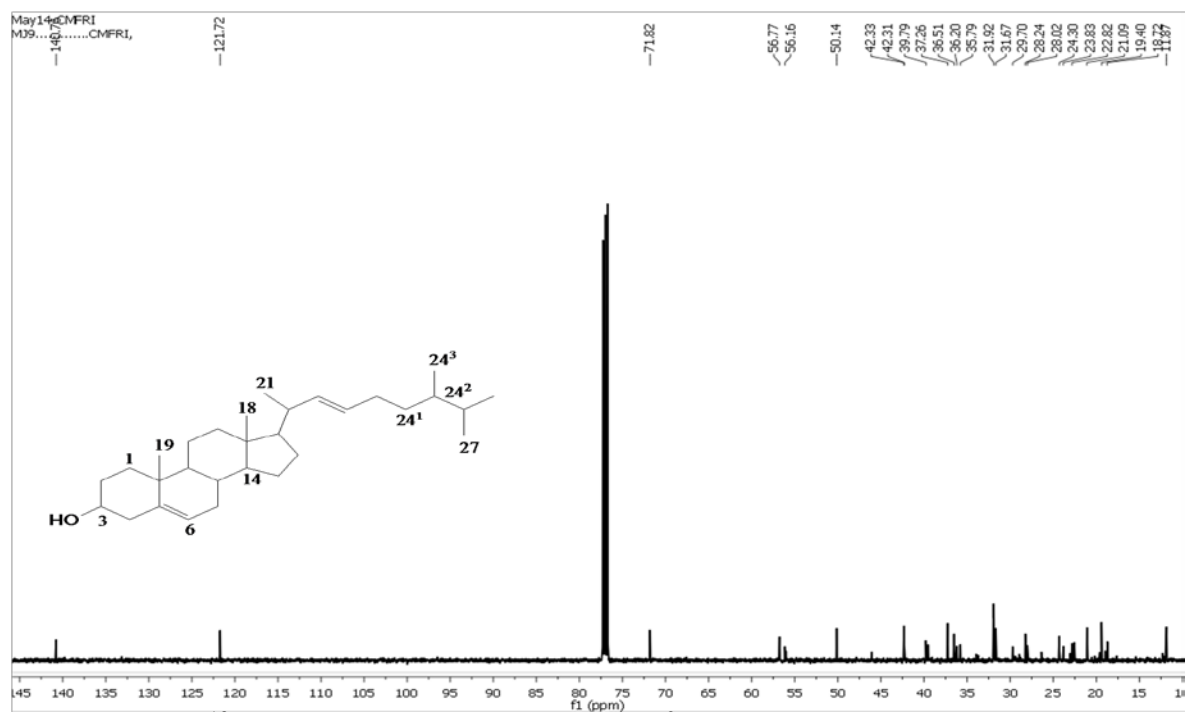


Figure 6.125.: ^{13}C NMR spectrum of (22*E*)-24¹,24²-methyldihomocholesta-5,22-dien-3 β -ol (9)

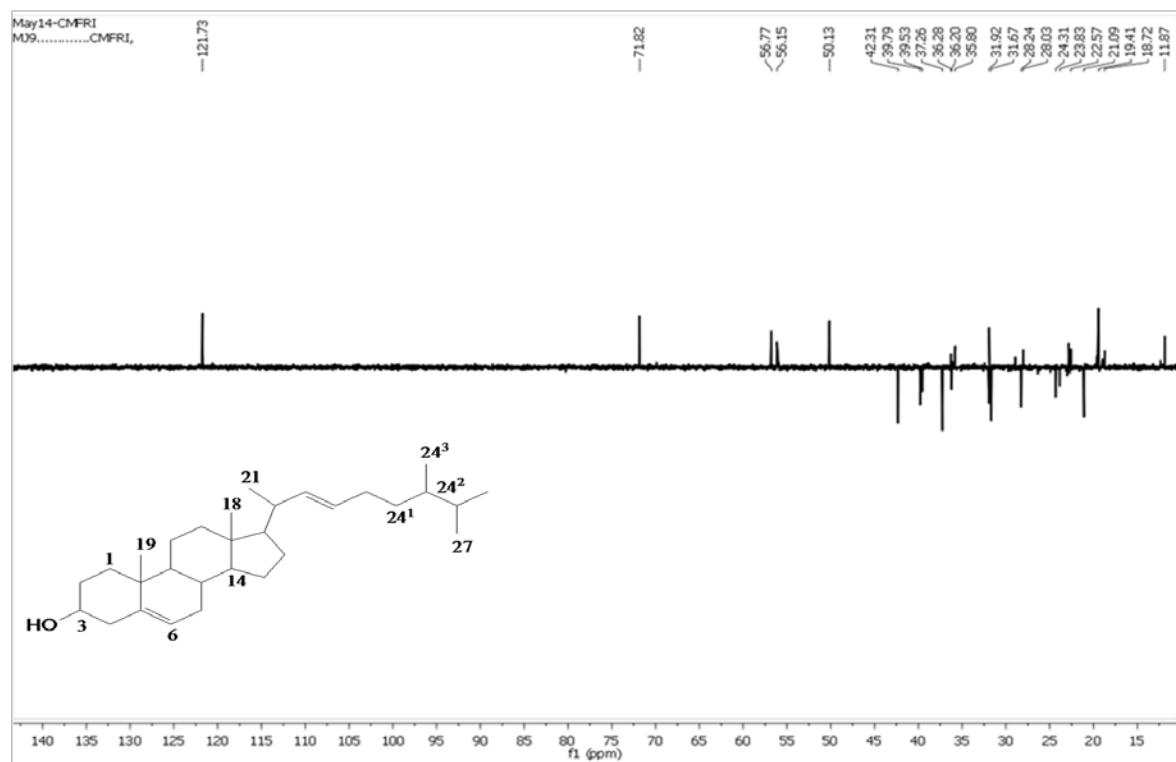


Figure 6.126.: $^{135}\text{DEPT}$ NMR spectrum of (22*E*)-24¹,24²-methyldihomocholesta-5,22-dien-3 β -ol (9)

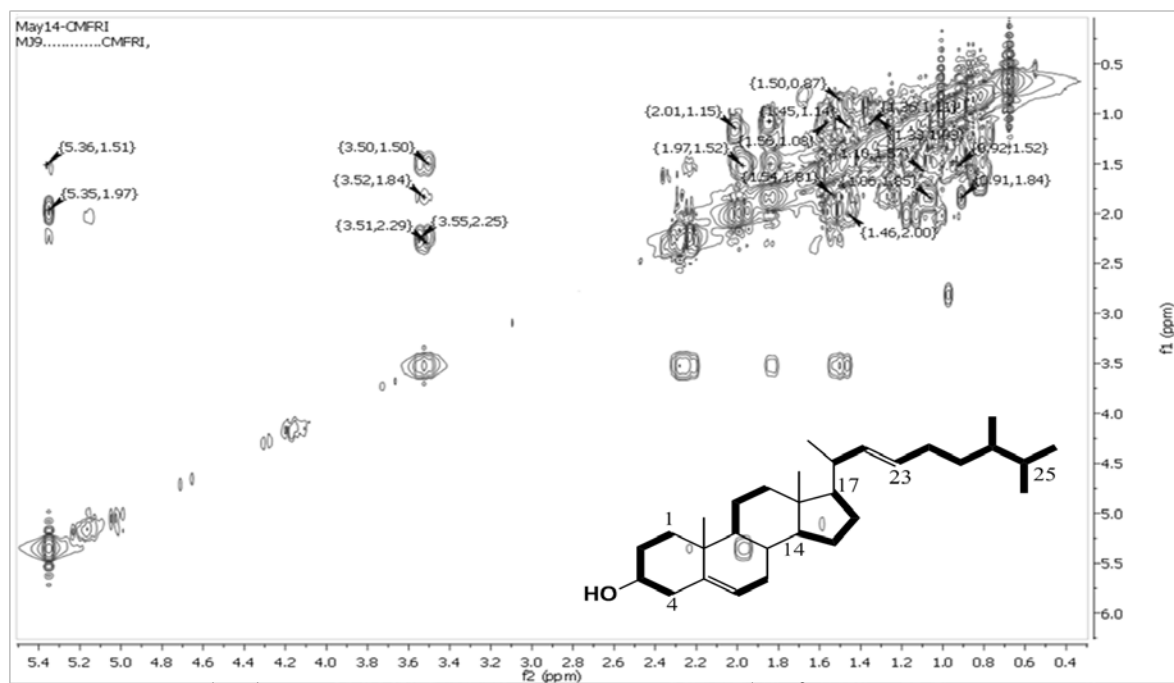


Figure 6.127.: ^1H - ^1H COSY NMR spectrum of (22*E*)-24¹,24²-methyldihomocholesta-5,22-dien-3 β -ol (**9**)

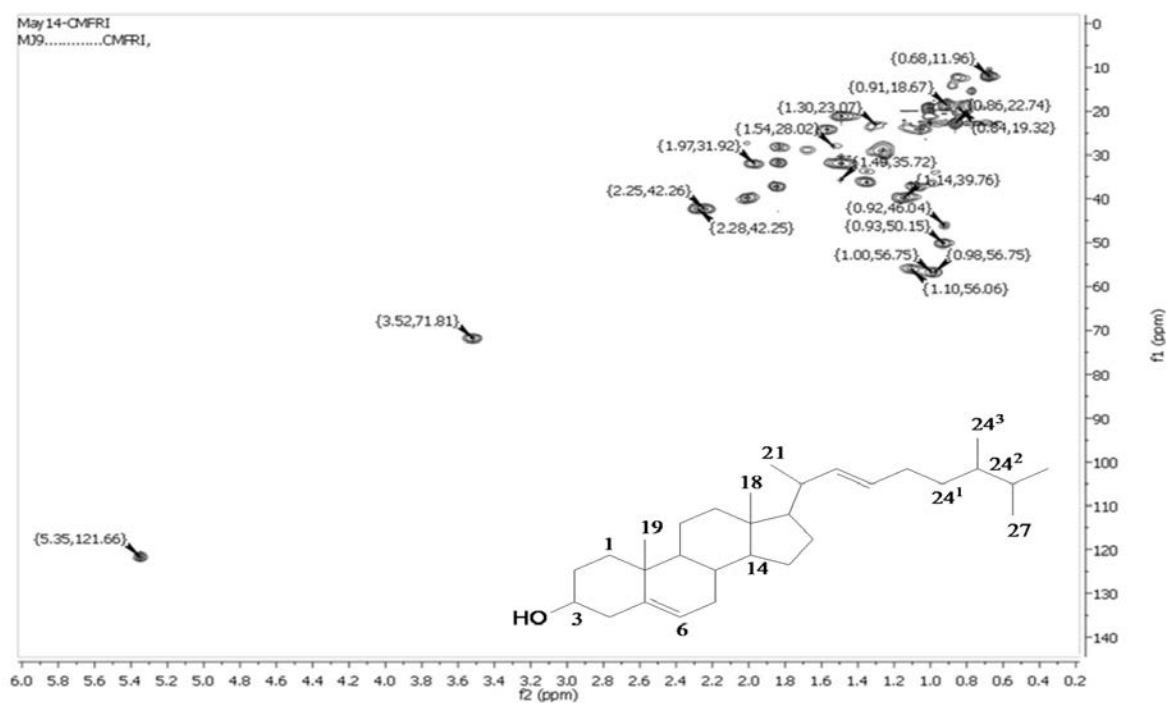


Figure 6.128.: HSQC NMR spectrum of (22*E*)-24¹,24²-methyldihomocholesta-5,22-dien-3 β -ol (**9**)

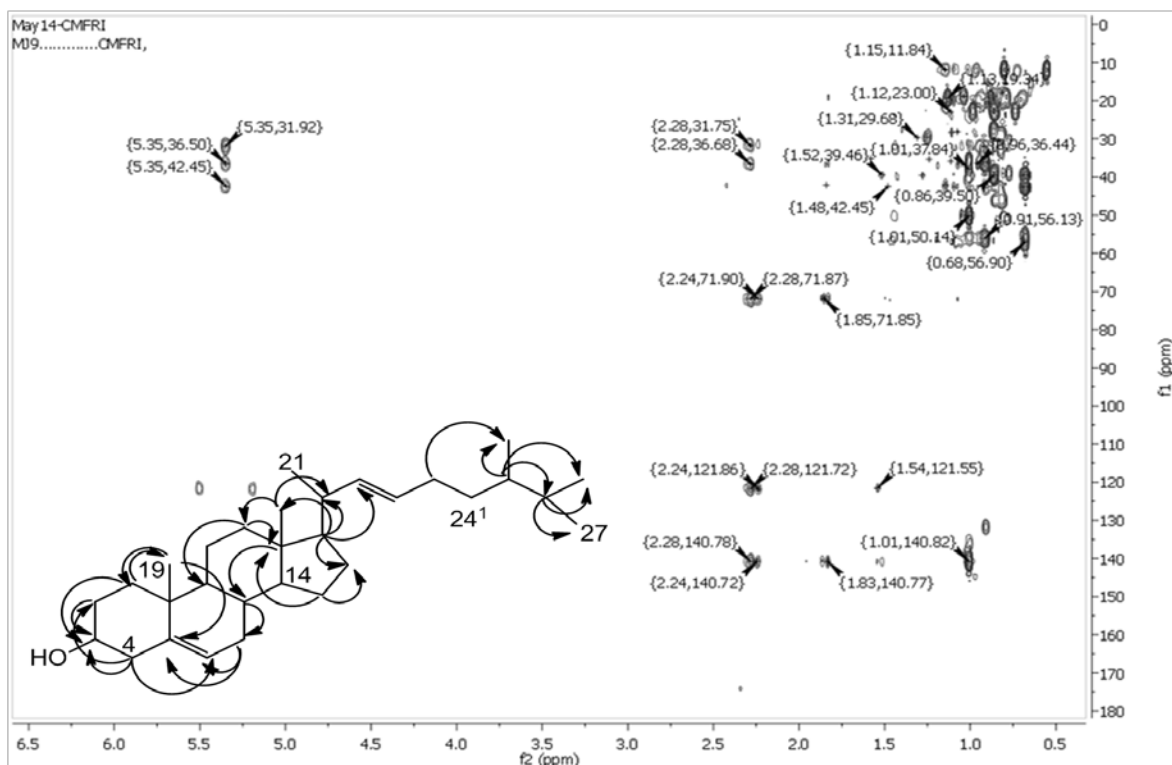


Figure 6.129.: HMBC NMR spectrum of (22*E*)-24¹,24²-methyldihomocholesta-5,22-dien-3 β -ol (**9**)

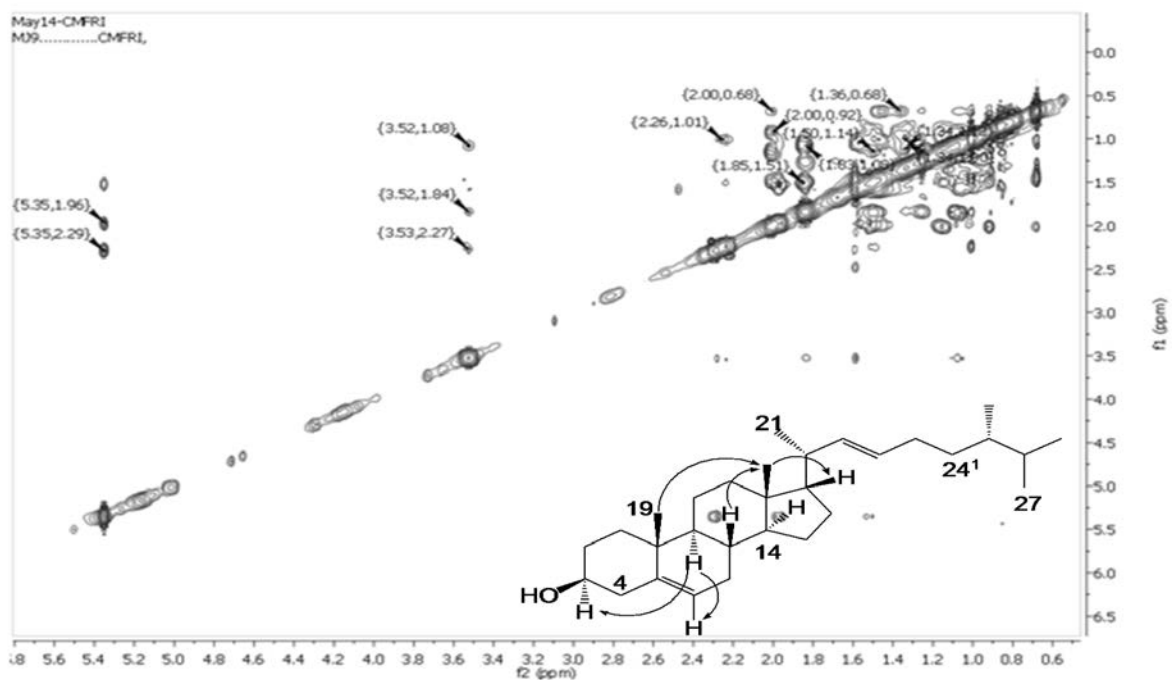


Figure 6.130.: NOESY NMR spectrum of (22*E*)-24¹,24²-methyldihomocholesta-5,22-dien-3 β -ol (**9**)

The IR absorption peak at 3427 cm^{-1} for hydroxyl and at 1664 cm^{-1} to olefinic (C=C) functionalities were recognized. The FTIR absorption bands at 1459, 1332 (C-H rocking), 1243, 1122 (C-C stretch) and 881 ($=\text{C-H}$ bend) cm^{-1} substantiated the structure (Figure 6.131.).

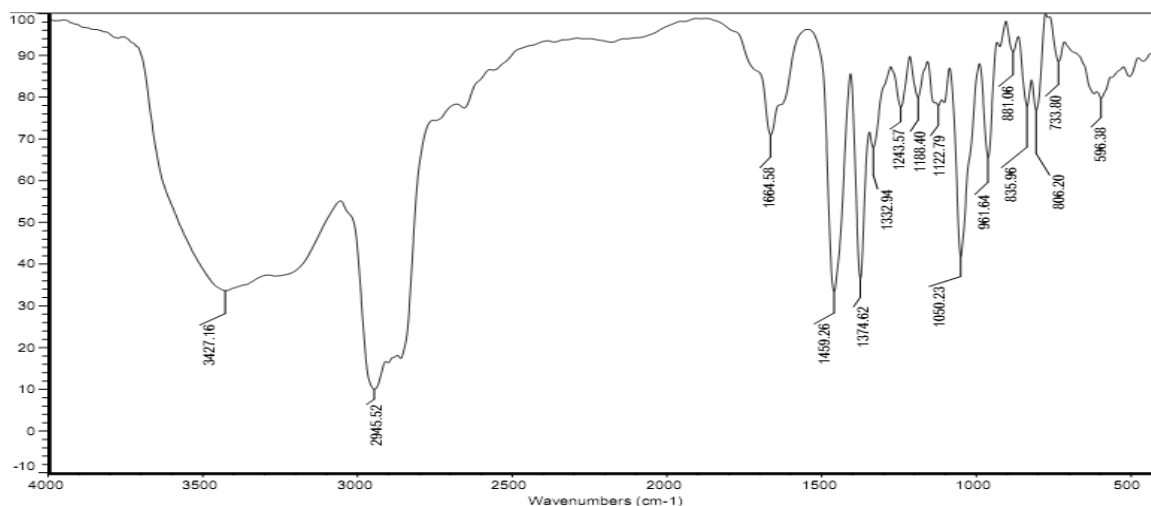


Figure 6.131.: FTIR spectrum of (22E)-24¹,24²-methyldihomocholesta-5,22-dien-3 β -ol (**9**)

The molecular ion peak at m/z 426 ($\text{C}_{30}\text{H}_{50}\text{O}^+$, $[\text{M}]^+$) was appeared to eliminate one molecule of water and an isopropyl group to yield 24¹,24²-methyldihomocholesta-5,22-trien-3 β -ol (**h**) (m/z 409), which underwent side chain elimination followed by rearrangement at ring D to afford a fragment with m/z 229 (**i**). The fragment ion at m/z 357 were formed from m/z 411 (24¹,24²-methyldihomocholesta-5,22-dien-3 β -ol), through a Retro-Diels-Alder mechanism. Fragmentation of the ion at m/z 366 (**b**) was perceived to be accompanied by the loss of a C-6 fragment (assigned to hex-1-ene ion) resulted in an ion at m/z 285 (**c**), which on successive rearrangement afforded fragments at m/z 177 (**d**), 135 (**e**), and 69 (**f**). It is of note that the fragment ion at m/z 69 (C_5H_8^+) appeared as base peak of **9** (Figure 6.132., 6.133.).

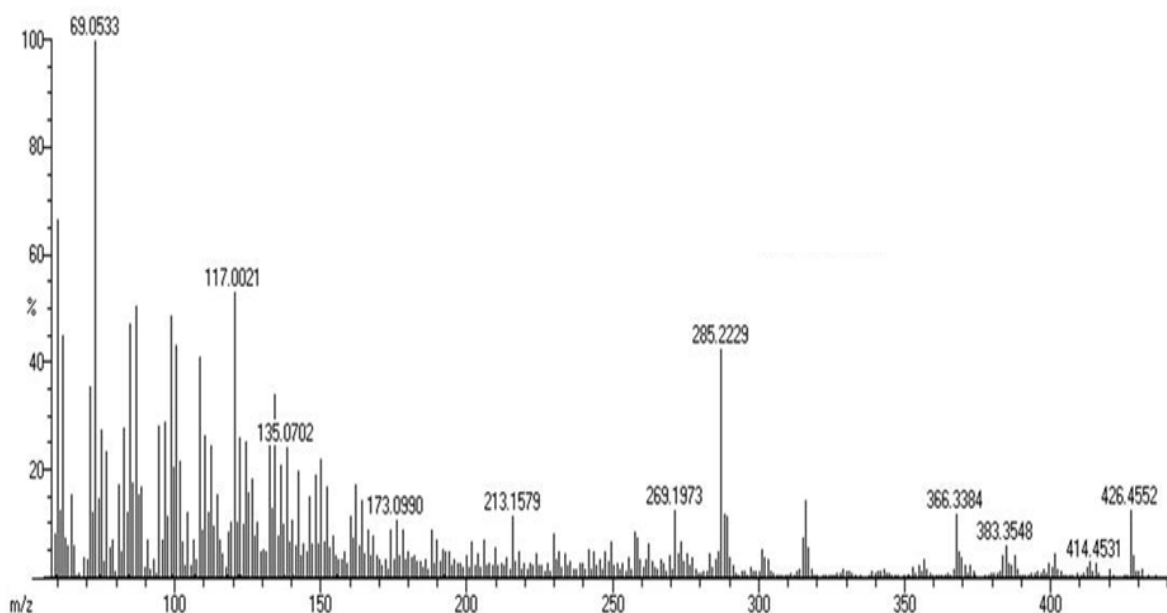


Figure 6.132.: EIMS spectrum of (22E)-24¹,24²-methyldihomocholesta-5,22-dien-3 β -ol (**9**)

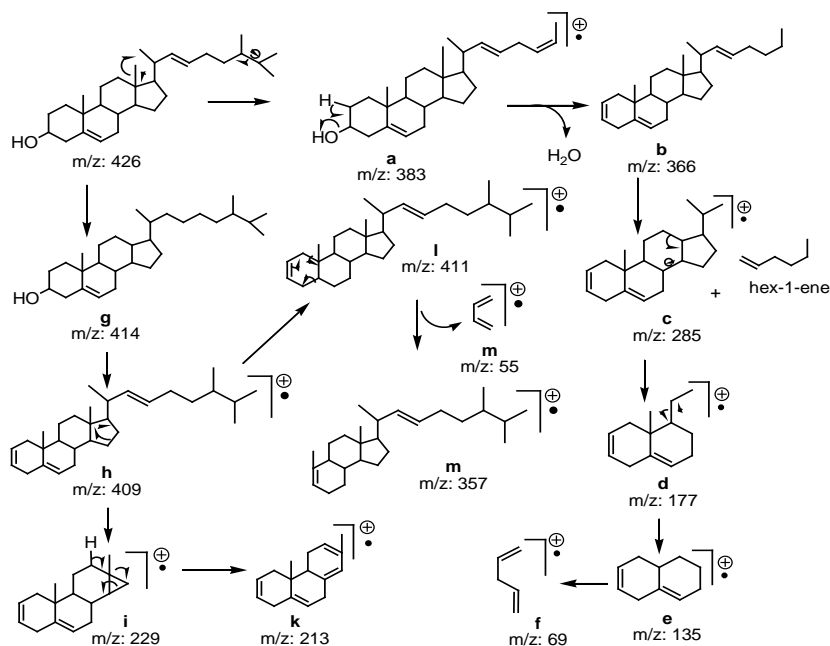
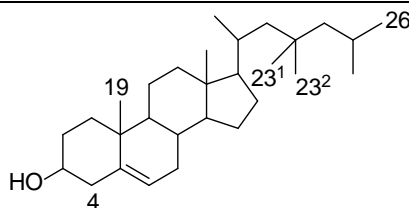


Figure 6.133.: Mass fragmentation pattern of (22E)-24¹,24²-methyldihomocholesta-5,22-dien-3 β -ol (**9**)

6.3.2.5.B. Structural characterization of compound 10 (PM₃₋₃₋₁₋₁)**23-Gem-dimethylcholesta-5-en-3 β -ol (10)**

Sample yield	82 mg; 0.16%
Physical description	White solid
Molecular formula	C ₂₉ H ₅₀ O
Molecular mass	414.3862

The 23-*gem*-dimethylcholesta-5-en-3 β -ol (**10**) is a new cholestenol derivative, in which the side chain at C-17 contains a *gem* dimethyl group at C-23 position. It was isolated as white solid upon repeated chromatography. It exhibited UV absorbance (in MeOH) at λ_{max} (log ϵ 1.36) 226.4 nm assigned to olefinic groups (Figure 6.134.). The purity of the compound was supported by RP C18 HPLC experiments using 6:4 (v/v) MeOH:MeCN (R_t 5.99) (Figure 6.135.).

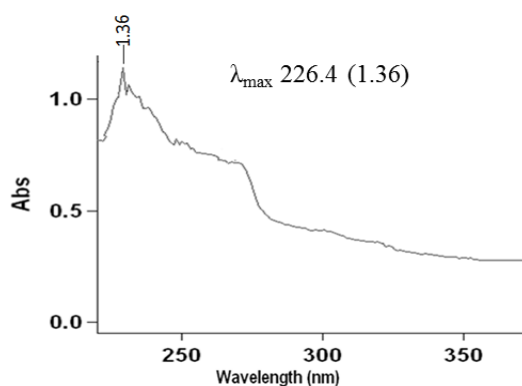


Figure 6.134.: UV spectrum of 23-*gem*-dimethylcholesta-5-en-3 β -ol (**10**)

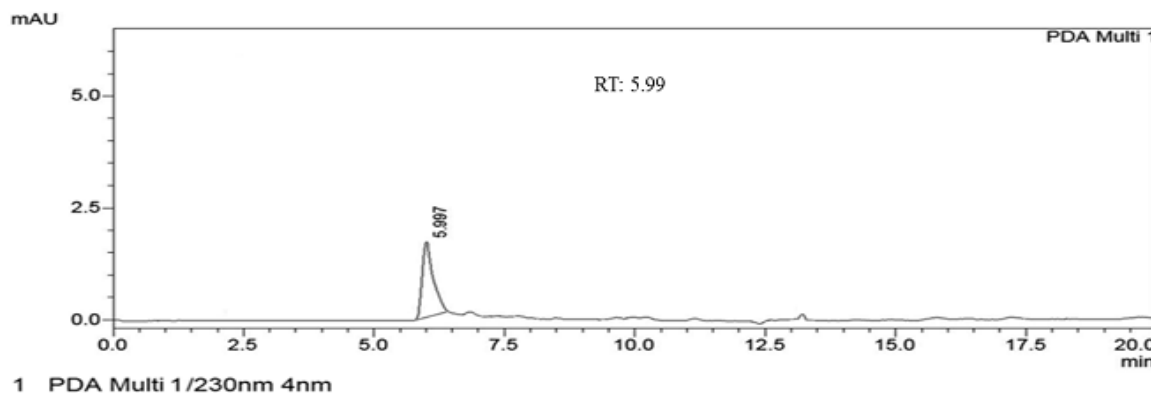


Figure 6.135.: HPLC chromatogram of 23-*gem*-dimethylcholesta-5-en-3 β -ol (**10**)

The molecular ion peak at m/z 414 (EIMS: found m/z 414.3868 $[M]^+$, cal. for $C_{29}H_{50}O$, 414.3862) along with 1H and ^{13}C data (Table 6.15.) was proposed the elemental composition of $C_{29}H_{50}O$ as 23-*gem*-dimethylcholesta-5-en-3 β -ol (**10**) with five degrees of unsaturation containing one double bond and four ring systems. The NMR signal and peak characteristics of **10** were closely related to **9**. The main difference found in the 1H spectrum was the occurrence of an additional double bond which was between C-22 and C-23 in **9**. Previous works on 1H and ^{13}C NMR spectroscopy established the characteristic chemical shifts of various types of protons and carbons of steroids; and based on these data steroid shift assignments were made for the present study. The absence of the characteristic aromatic proton signals in the 1H NMR spectrum confirmed that the four cyclic rings were not of aromatic origin (Figure 6.138.). The 1H NMR spectrum contains several overlapping second order multiplets with the type ABCDEF. The olefinic signals appeared at δ 140.76 and 121.72 in the ^{13}C NMR spectrum were indicated a double bond (Figure 6.139.). The relatively downfield shift at δ 140.76 was referred to quaternary carbon adjacent to a double bond in the cyclic ring. The highly deshielded 1H signal at Δ^5 (H-6, δ 5.35, dd), which was found to be a double doublet due to the adjacent δ 1.98 and 1.52 protons attached to carbon (C-7, δ 31.91) with coupling constant of 5.24 and 3.36 Hz. The presence of an olefinic group in the carbocyclic ring was identified by comparison with cholestene analogues as detailed in a previous literature (Reich *et al.*, 1969). An earlier study of steroid derivatives were explained the olefinic proton resonances in the region δ 5.0-5.6 (br, $J=5$ Hz) due to the $>C=\underline{CH}-CH_2$ skeleton (Goad and Akihisa 1997). The proton at H-3 (δ 3.50) attached to

tertiary carbon (δ 71.82) attributed to hydroxyl group (-OH) was apparent due to pentet splitting pattern in the downfield. The downfield shift of carbinol carbon at C-3 was the result of a greater electron-withdrawing power of the hydroxyl group. It is of note that for the axial cyclohexanols, there is a δ 1 downfield shift of C-3, probably because of smaller 1, 3 interaction of the -OH group with the H-3 relative to the hydroxyl group. Further specific deuteration of the hydroxyl proton was used for identifying the C-3 carbon. The signal for deuterated -OH proton essentially disappeared. The spectroscopic analysis of ^1H , ^{13}C along with ^1H - ^1H COSY, HSQC and HMBC relations allowed the elucidation of a cholestene network with δ 5.35 (H-6) as double bond (δ 121.72) and 3.50 (H-3) hydroxyl (δ 71.8), which was consistent with the literature study (Tian *et al.*, 2011) (Figure 6.138.-6.143.). The COSYs δ 1.85, 1.08 (H-1)/1.50, 1.85 (H-2)/3.50 (H-3)/2.25, 2.29 (H-4) and δ 5.35 (H-6)/1.98, 1.52 (H-7)/0.91 (H-8) were supported the presence of adjacent protons from H-1 to H-4 and H-6 to H-8, respectively (Figure 6.136.A). The HMBC correlations from δ 2.25/2.29 (H-4) to δ 31.66 (attributed to C-2), 71.82 (C-3), 140.76 (C-5), 121.72 (C-6), 36.52 (C-10) and those from δ 5.35 (H-6) to δ 42.31 (C-4), 31.91 (C-7), 36.52 (C-10) were supported the bicyclic framework (Figure 6.136.B). The three high-field methine (-CH-) protons, δ 0.95, 1.10 and 1.02 were allocated to carbons at C-9, C-14 and C-17 positions, respectively. The two quaternary carbons (C-10 and C-13) were attributed to characteristic chemical shift and signal pattern of steroids (Reich *et al.*, 1969). The COSY relations, such as δ 0.95 (H-9)/1.46 (H-11)/2.01, 1.15 (H-12) and δ 1.10 (H-14)/1.56, 1.06 (H-15)/1.83 (H-16)/1.02 (H-17) established the presence of ring C (hexacyclic) and D (cyclopentane), respectively. The HMBCs from δ 1.46 (H-11) to δ 42.52 (C-13); δ 2.01/1.15 (H-12) to δ 42.50 (C-13); δ 0.91 (H-8) to δ 56.11 (C-14) appropriately supported the attachment of hexacyclic ring, C; whereas the correlations from δ 1.83 (H-16) to δ 42.52 (C-13); δ 1.10 (H-14) to δ 28.33 (C-16); δ 1.56 (H-15) to δ 28.33 (C-16) unambiguously described the attachment of cyclopentane (D) moiety in compound **10** as also established by preceding literatures (Diaz-Marrero *et al.*, 2003b). The C-4 proton has been flanked on both side by downfield shifting of functional groups (OH at C-3 and C=C at C-5, 6) and the two H-4 protons are pulled downfield to δ 2.25-2.29 away from the pack of overlapped resonances in ^1H spectrum. The ^{13}C signal at far downfield region (δ 140.76)

was less intense (shorter) than other peak at δ 121.72, due to slow relaxation, it must be quaternary carbon. It is of note that the closeness of protons is the basic modes of relaxation of ^{13}C nuclei, and therefore, carbons not bonded to protons were relax more slowly, therefore recorded a less intense peaks (RD = 1.7 s relaxation delay is short). The more substituted carbon (at C-5) was more desheilded relative to C-6 due to steric crowding effects. The resonances of the cholestene side chain (C-20 to C-27) can readily be identified by comparison with 2,6-dimethyloctane as a model compound as detailed in a previous literature (Reich *et al.*, 1969) and confirmed by ^1H - ^1H COSY. The ^1H - ^1H COSY connections among δ 1.02 (H-17) and 1.35 (H-20) along with their HSQC values confirmed the attachment of side chain, C-20 at C-17 (Diaz-Marrero *et al.*, 2003b). The HMBCs from δ 1.02 (H-17) to δ 18.72 (C-21) and from δ 0.92 (H-21) to δ 42.52 (C-13), 36.27 (C-20) further supported the presence of side chain attachment to the sterol moiety. The two quaternary carbons, C-10 and C-13 were assigned using a long range ^1H - ^{13}C correlation spectrum. A two bond correlation to the methyl protons in each case yields the assignment of C-10 at δ 36.52 and C-13 at δ 42.52. The structure contained four singlets which made the compound different from other reported steroids from mollusks (Santalova *et al.*, 2007). The ^1H spectrum displayed seven upfield methyl signals at δ 1.01 (s), 0.68 (s), 1.59 (s), 1.25 (s), 0.92 (d), 0.86 (d) and 0.87 (d), which were found to exhibit connectivities with carbons at δ 19.41, 11.87, 28.01, 29.72, 18.72, 19.31 and 22.82, respectively based on HSQC. The numbers of carbon atoms were confirmed as 29 through ^{13}C and DEPT analysis in which seven $-\text{CH}_3$, ten $-\text{CH}_2$ and eight $-\text{CH}$ groups with total proton integral of 51.93. The methyl groups, including two *gem*-dimethyl groups give rise to sharp peak at shielded region. The configurations at individual carbons were determined by using the detailed NOESY (Figure 6.144., 6.137.). In NOESY, the proton δ 3.50 (H-3) exhibited correlation with δ 5.35 (H-6)/ δ 2.29 (H α -4), and therefore, have been considered as α -protons, which in turn indicated the β -disposition of -OH at C-3 (Sun *et al.*, 2013; Tian *et al.*, 2011). The methyl groups (H-18 and H-19) of cholestene derivative were correlated with δ 2.25 (H β -4)/2.01 (H β -12)/0.91 (H-8)/1.35 (H-20), which apparently suggested their β -orientation, and the attributions were supported by literature reports (Calderon *et al.*, 2004; Tian *et al.*, 2011).

Table 6.15.: NMR spectroscopic data of 23-*gem*-dimethylcholesta-5-en-3 β -ol (**10**) in CDCl₃

C. No.	¹³ C	¹ H (int.,mult., <i>J</i> in Hz) ^a	COSY	HMBC
1	37.22	1.84 (1H β ,t) 1.08 (1H α ,t)	H-2 -	C-3 -
2	31.66	1.50 (1H β ,m) 1.85 (1H α ,m)	H-3 -	- C-5
3	71.82	3.50 (1H α ,p)	H-4	-
4	42.31	2.25 (1H β ,d) 2.29 (1H α ,d)	- -	C-5,6,3 C-2, 10
5	140.76	-	-	-
6	121.72	5.35 (1H,dd,5.13,3.36)	H-7	C-4,10,7
7	31.91	1.52 (1H β ,t) 1.98 (1H α ,t)	H-8 -	- -
8	46.06	0.91 (1H β ,m)	-	C-4,7
9	50.14	0.95 (1H α ,t)	H-11	-
10	36.52	-	-	-
11	21.09	1.46 (2H, q)	H-12	C-13
12	39.79	2.01 (1H β ,t) 1.15 (1H α ,t)	- -	C-13 -
13	42.52	-	-	-
14	56.11	1.10 (1H α ,m)	H-15	C-16
15	24.21	1.06 (1H β ,m) 1.56 (1H α ,t)	H-16 -	C-16 -
16	28.33	1.83 (2H,t)	H-17	C-13
17	56.72	1.02 (1H β ,m)	H-20	C-21
18	11.87	0.68 (3H β ,s)	-	C-13,12,17
19	19.41	1.01 (3H β ,s)	-	C-5,1,9
20	36.27	1.35 (1H β ,m)	H-22	-
21	18.72	0.92 (3H α ,d)	-	C-13,20
22	36.22	1.14 (2H,d)	-	C-24,25
23	39.61	-	-	-
23 ¹	28.01	1.59 (3H,s)	-	C-25
23 ²	29.72	1.25 (3H,s)	-	C-23
24	23.83	1.30 (2H,d)	H-25	C-23 ²
25	35.71	1.49 (1H,m)	H-26,27	-
26	19.31	0.86 (3H,d)	-	C-26
27	22.82	0.87 (3H,d)	-	C-20

¹H NMR spectra recorded using Bruker AVANCE III 500MHz (AV 500) spectrometer (Bruker, Karlsruhe, Germany) in CDCl₃ as aprotic solvent at ambient temperature with TMS as the internal standard (δ 0 ppm). The ¹H NMR spectra were recorded at 500MHz,

while the ^{13}C NMR spectra were recorded at 125MHz. ^aValues in ppm, multiplicity and coupling constants ($J=\text{Hz}$) were indicated in parentheses. The assignments were made with the aid of the ^1H - ^1H COSY, HSQC, HMBC and NOESY experiments

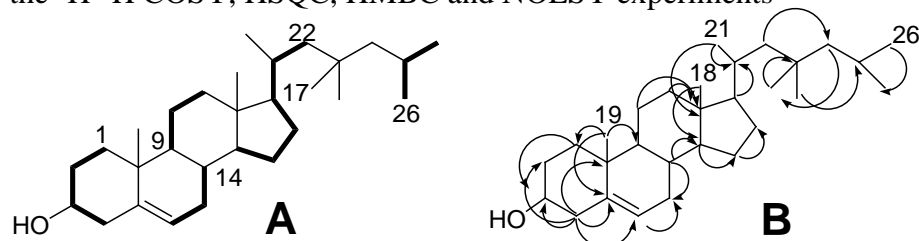


Figure 6.136.: ^1H - ^1H COSY (A) and HMBC (B) correlations of 23-gem-dimethylcholesta-5-en-3β-ol (10). The key ^1H - ^1H COSY couplings have been represented by the bold face bonds. The HMBC couplings were indicated by double barbed arrow

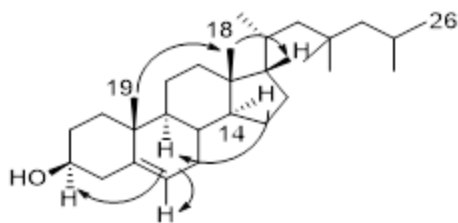


Figure 6.137.: NOESY correlations of 23-gem-dimethylcholesta-5-en-3β-ol (10). The NOESY relations were represented by double barbed arrow

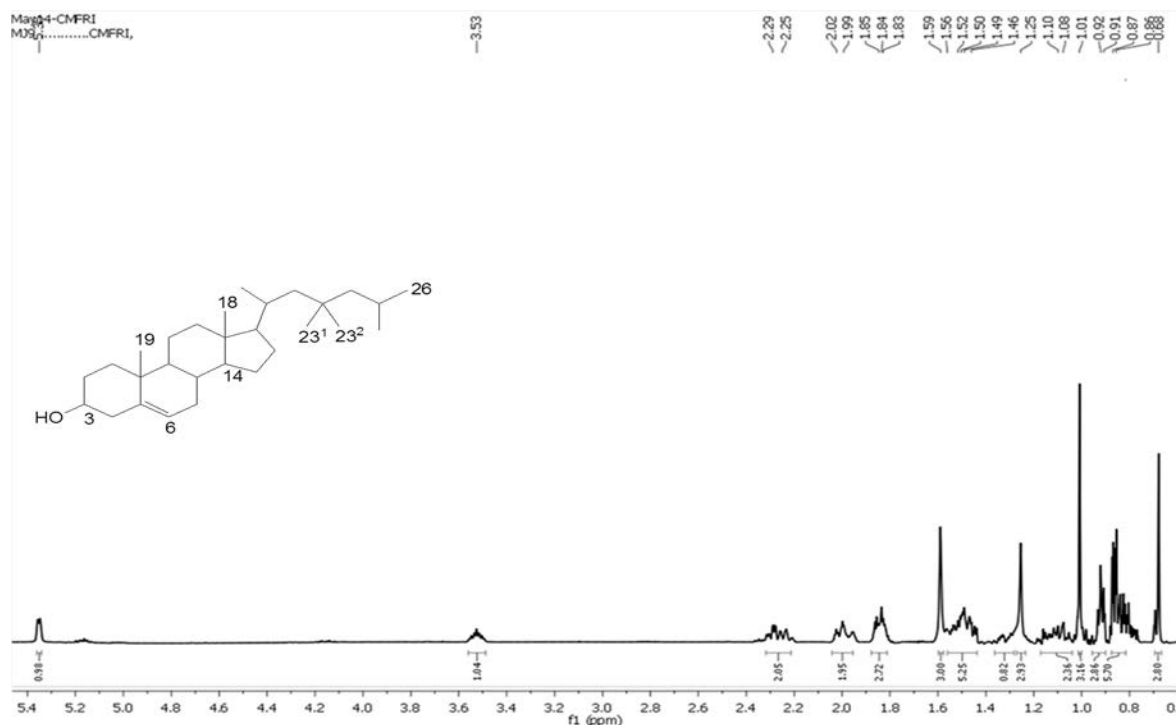
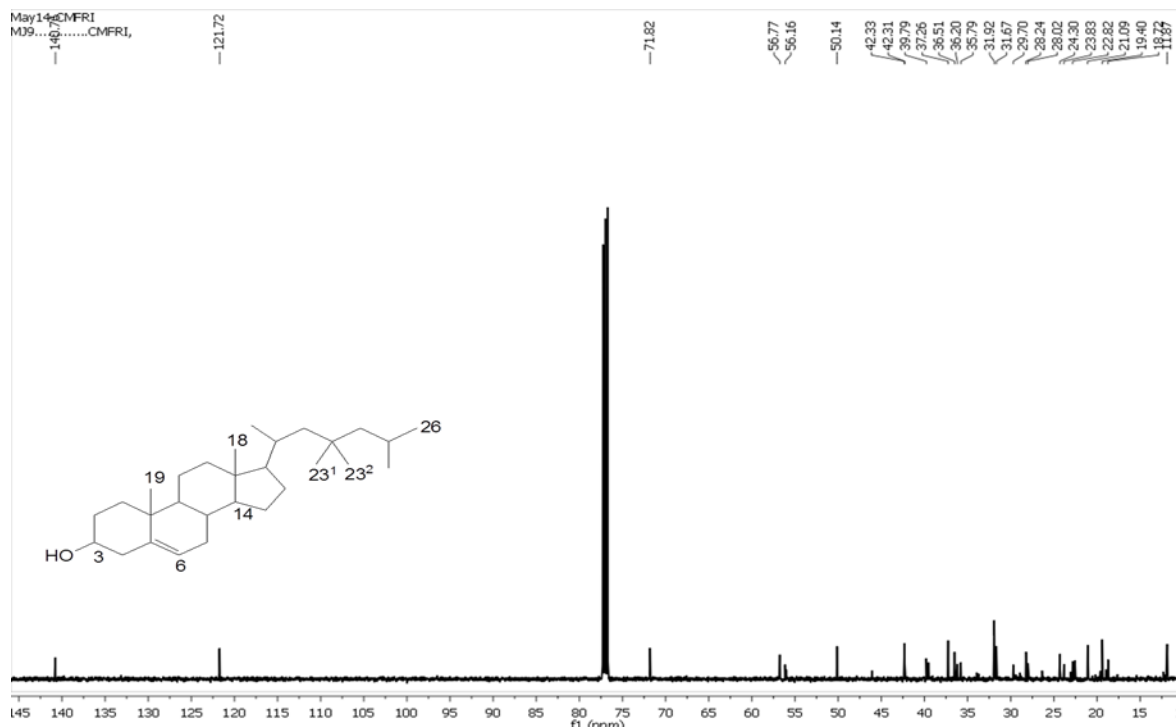
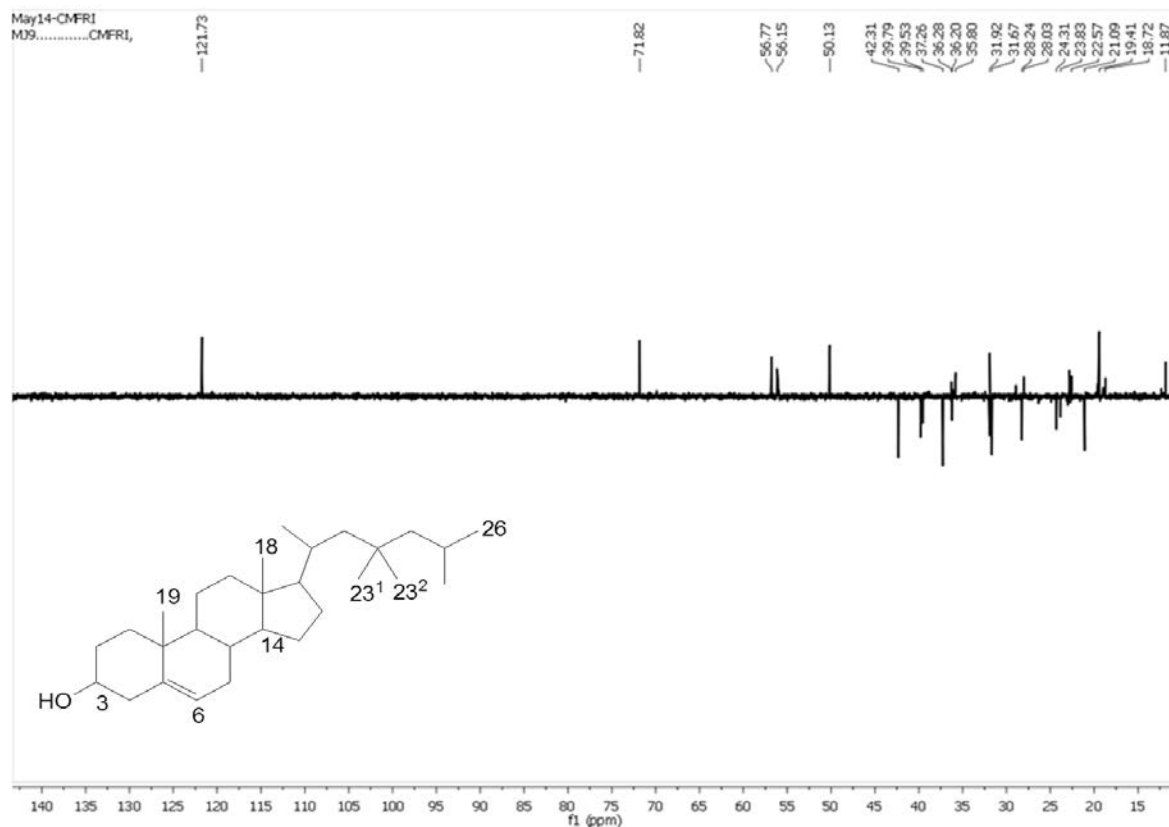
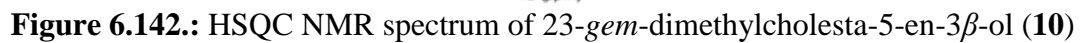
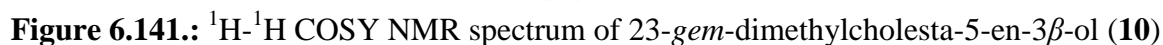


Figure 6.138.: ^1H NMR spectrum of 23-gem-dimethylcholesta-5-en-3β-ol (10)

**Figure 6.139.:** ^{13}C NMR spectrum of 23-gem-dimethylcholesta-5-en-3 β -ol (10)**Figure 6.140.:** $^{135}\text{DEPT}$ NMR spectrum of 23-gem-dimethylcholesta-5-en-3 β -ol (10)



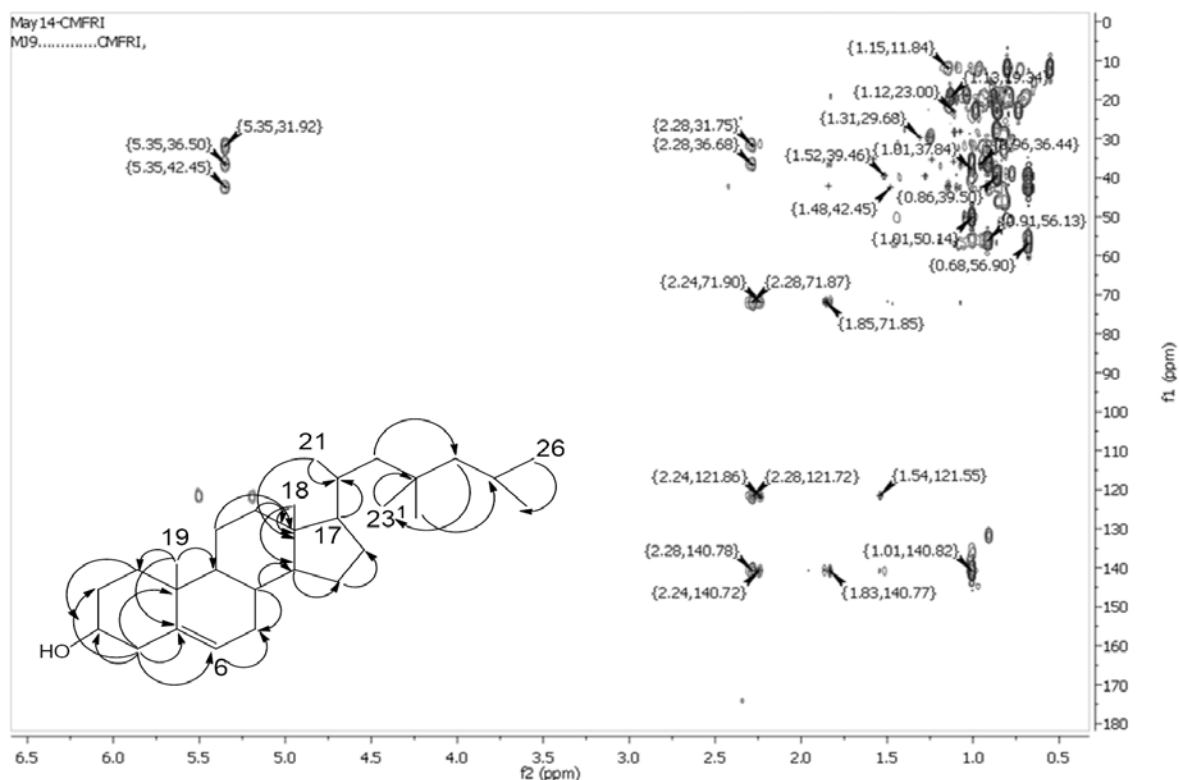


Figure 6.143.: HMBC NMR spectrum of 23-gem-dimethylcholesta-5-en-3 β -ol (10)

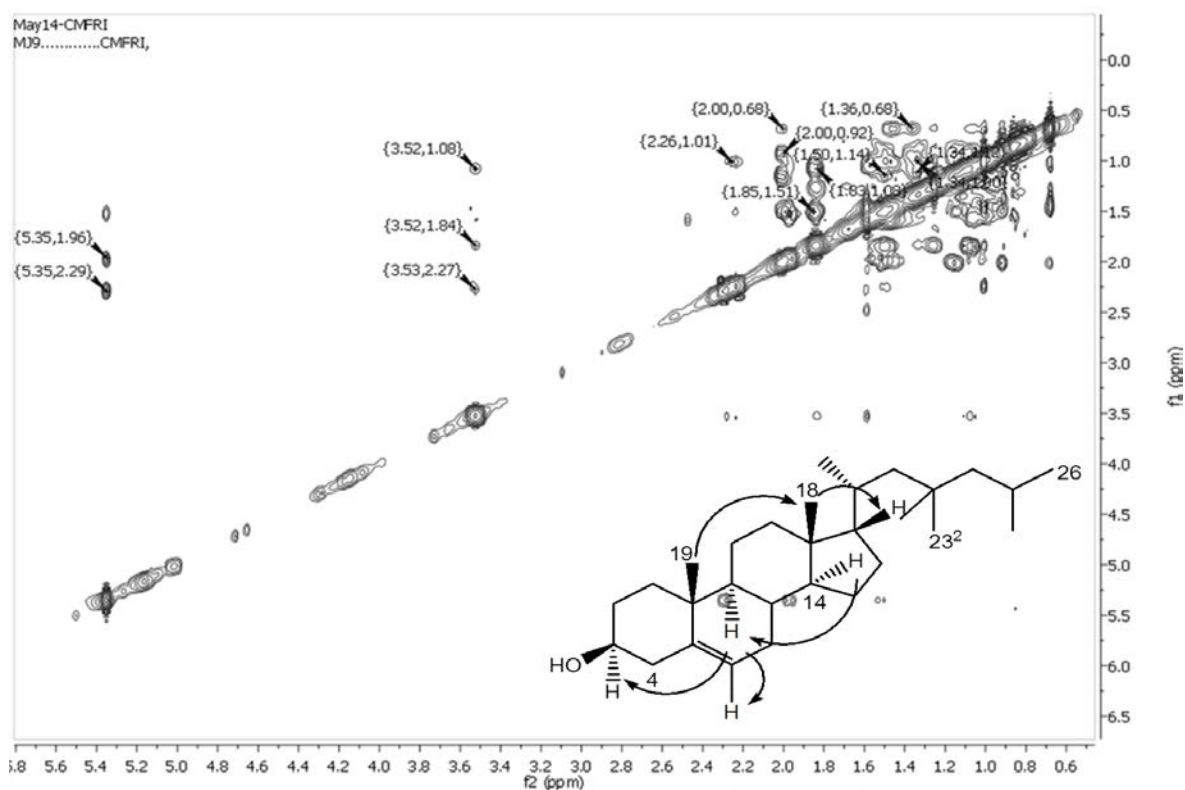


Figure 6.144.: NOESY NMR spectrum of 23-gem-dimethylcholesta-5-en-3 β -ol (10)

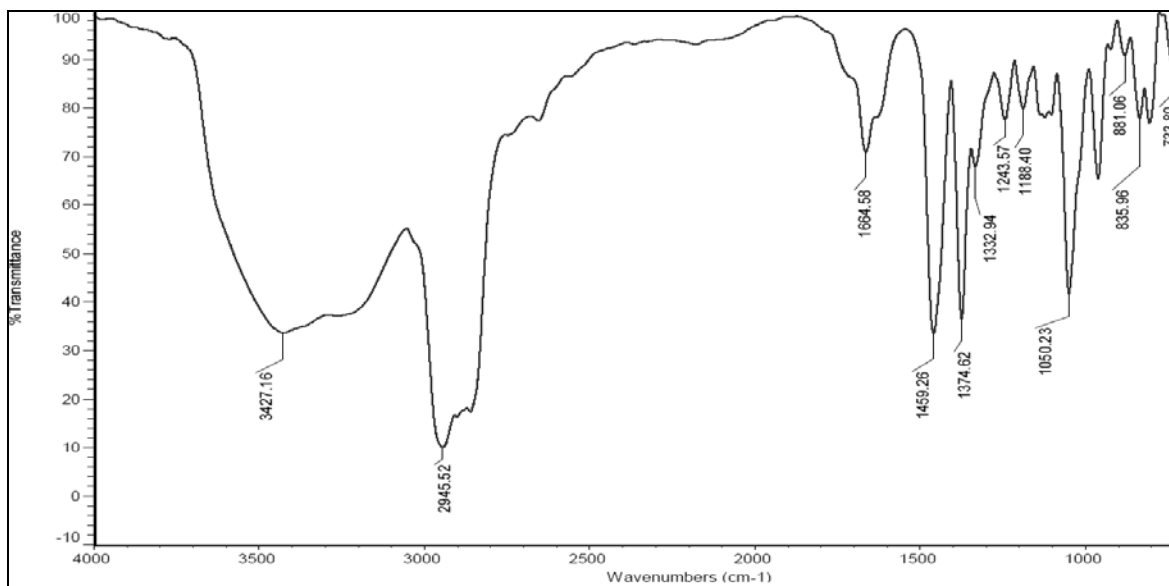


Figure 6.145.: FTIR spectrum of 23-*gem*-dimethylcholesta-5-en-3 β -ol (**10**)

The olefinic (C=C) and alkyl (C-H) groups IR stretching vibrations were represented by the 1664 and 2945 cm⁻¹ absorption bands, respectively. The absorption at 3427 cm⁻¹ indicated O-H stretching vibration. The FTIR peaks at 1243-1188 (C-C stretch) cm⁻¹ were substantiated the substituted cholestene structure (Figure 6.145.).

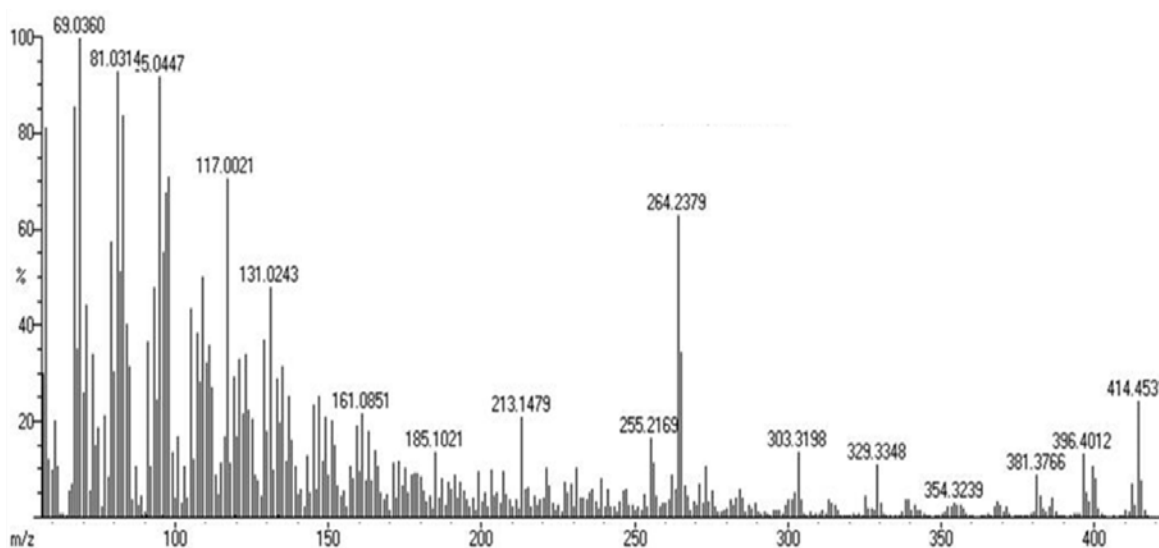


Figure 6.146.: EIMS spectrum of 23-*gem*-dimethylcholesta-5-en-3 β -ol (**10**)

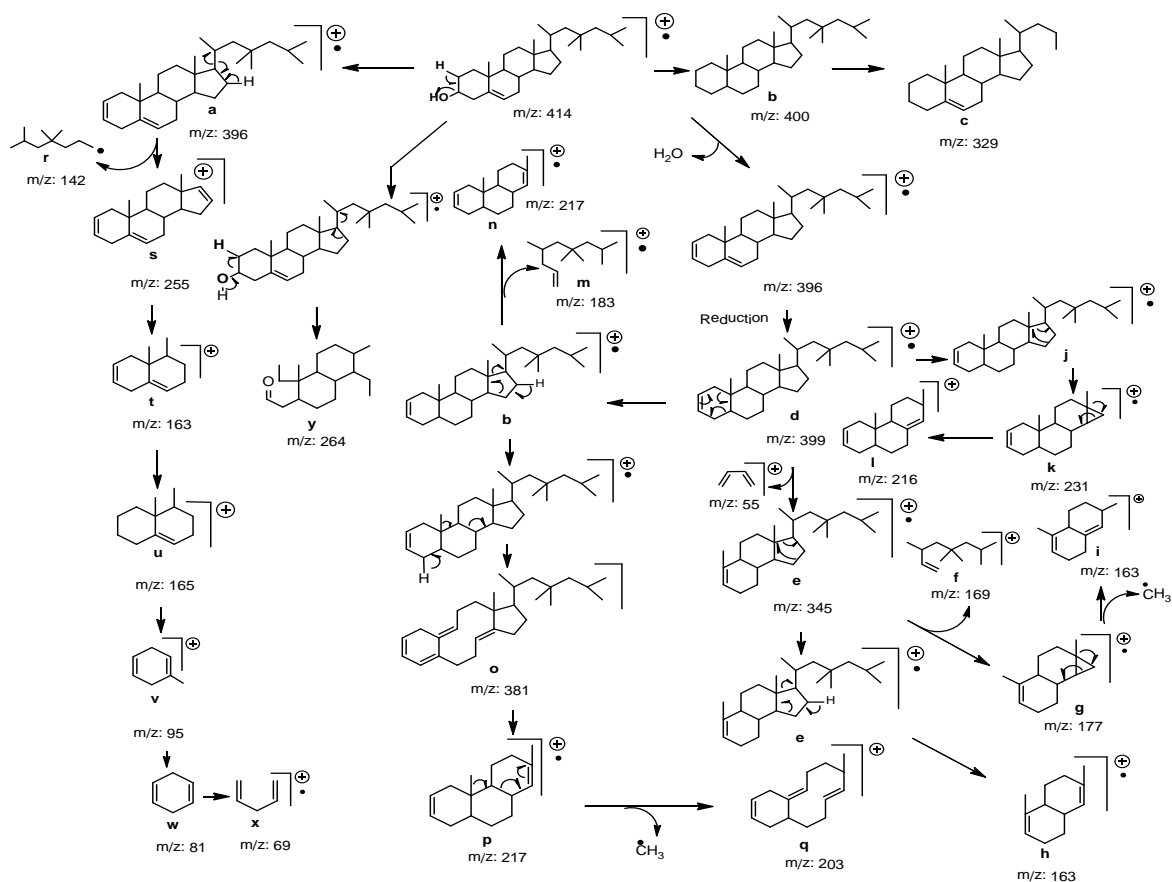


Figure 6.147.: Mass fragmentation pattern of 23-gem-dimethylcholesta-5-en-3 β -ol (**10**)

The molecular ion peak at m/z 414 appeared to undergo elimination of one molecule of water to yield 23-gem-dimethylcholesta-2,5-diene (**10**) (m/z 396). One of the most general types of fragmentation in substituted C-17 steroids was the removal of side chain which led to an copious ion at m/z 255 in the corresponding spectra. The side chain elimination (2,4,4-trimethylheptane) from the fragment ion at m/z 396 yielded the fragment with m/z 255 (**s**), which on successive rearrangements yielded the fragments at m/z 163 (**t**), 95 (**v**), 81 (**w**) and 69 (**x**). The molecular ion peak at 69 (**x**) was found to be the base peak and corresponding to penta-1,4-diene. The ion at m/z 345 formed from m/z 399 (23-gem-dimethylcholesta-2-ene), through a Retro-Diels-Alder mechanism. Further decomposition of the ion at m/z 399 was perceived by the loss of C-18 methyl and resulted in ion at m/z 203. The molecular ion peak at m/z 264 (**y**) resulted from the fragmentation of ions through elimination of water molecule and side chain (Figure 6.146., 6.147.).

More significantly, the marine-derived steroids with their diverse structures were found to exhibit interesting therapeutic properties (Goad and Akihisa 1997; Whitson *et al.*, 2009). Anti-inflammatory properties of steroidal compounds isolated from marine invertebrates against pro-inflammatory COX-2 and cytokines were reported in earlier literatures (Chao *et al.*, 2008; Su *et al.*, 2008; Thao *et al.*, 2013) for example, inhibitory effect of di-unsaturated C-27 polyhydroxy sterols isolated from marine gastropod, *Trimusculus peruvianus* (Diaz-Marrero *et al.*, 2003b). Consequently, the detection and identification of COX-2/5-LOX-specific inhibitors could have a potentially profound impact on the treatment of a number of inflammatory disorders.

6.3.3. Bioactive (antioxidant and anti-inflammatory) potentials of secondary metabolites isolated from EtOAc:MeOH extract of *P. malabarica*

6.3.3.1. Antioxidative potentials of secondary metabolites (1-10) isolated from EtOAc:MeOH extract of *P. malabarica*

The free radical inhibiting activities of title compounds (1-10) isolated from EtOAc:MeOH extract of *P. malabarica* were described in Table 6.16. The antioxidant activities of isolated compounds were determined by *in vitro* DPPH and ABTS⁺ scavenging experiments.

The hydroxy oxo-pyran enclosed benzoate derivative, compound **3** (IC₅₀ 0.59 mg/mL) and furanyl-2*H*-tetrahydro chromenyl derivative, **4** (IC₅₀ 0.56 mg/mL) did not display any significant difference among each other in DPPH radical scavenging activity ($p > 0.05$). The compounds **3-4** were appeared to exhibit significantly greater DPPH scavenging activity when compared to other compounds and commercially available α -tocopherol (IC₅₀ 0.65 mg/mL) (Table 6.16.). No significant difference in scavenging DPPH radical for isopimarane norditerpenoid derivative, **6** (IC₅₀ 0.65 mg/mL) and hydroxy benzoate metabolite, **1** (IC₅₀ 0.65 mg/mL) compared to those displayed by the commercially available antioxidant, α -tocopherol (IC₅₀ 0.65mg/mL) ($p > 0.05$) was apparent. Other compounds, such as benzoate derivative **2** (IC₅₀ 0.79 mg/mL), 3*H*-isochromenone derivative, **5** (IC₅₀ 0.73 mg/mL), meroterpeno pyranoid derivatives, **7-8** (IC₅₀ ~0.77 mg/mL) along with substituted dihomocholestadienol, **9** (IC₅₀ 0.81 mg/mL) did

not display significant differences among each other in DPPH radical scavenging activity ($p > 0.05$), and which were found to be significantly ($p < 0.05$) greater when compared to 23-*gem*-dimethyl cholesterol derivative, **10** (IC_{50} 1.01 mg/mL).

Table 6.16.: *In vitro* antioxidant {2,2-diphenyl-1-picrylhydrazyl (DPPH) and 2,2'-azino-bis(3-ethylbenzothiazoline-6-sulphonic acid) ($ABTS^+$) radical scavenging assays} bioactivities of secondary metabolites (**1-10**) isolated from EtOAc:MeOH extract of *P. malabarica* against commercially available standard, α -tocopherol

Compounds	Antioxidant activities IC_{50} values (mg/mL)	
	*DPPH scavenging activity	* $ABTS^+$ scavenging activity
1	0.65 ± 0.06^a	0.74 ± 0.06^a
2	0.79 ± 0.02^{bd}	0.76 ± 0.01^a
3	0.59 ± 0.06^c	0.69 ± 0.06^b
4	0.56 ± 0.06^c	0.67 ± 0.06^b
5	0.73 ± 0.07^b	0.79 ± 0.07^a
6	0.65 ± 0.06^a	0.78 ± 0.06^a
7	0.76 ± 0.06^{bd}	0.96 ± 0.06^c
8	0.78 ± 0.06^{bd}	0.92 ± 0.06^c
9	0.81 ± 0.09^d	0.98 ± 0.09^c
10	1.01 ± 0.09^e	1.12 ± 0.09^d
α-tocopherol	0.65 ± 0.04^a	0.76 ± 0.05^a

The samples were analyzed in triplicate ($n = 3$) and expressed as mean \pm standard deviation. Means followed by different superscripts (a-e) within the same column indicated significant differences ($p < 0.05$). *The bioactivities were expressed as IC_{50} values (mg/mL)

Likewise, hydroxy oxo-pyran enclosed benzoate derivative, compound **3**, (IC_{50} 0.69 mg/mL) and furanyl-2*H*-tetrahydro chromenyl derivative, **4** (IC_{50} 0.67 mg/mL) did not display any significant difference each other in $ABTS^+$ radical scavenging activity ($p > 0.05$). The compounds **3** and **4** were exhibited significantly greater $ABTS^+$ radical scavenging effects ($p < 0.05$) when compared to other compounds and commercially

available α -tocopherol (IC_{50} 0.76 mg/mL). No significant difference in scavenging $ABTS^+$ radical for isopimarane norditerpenoid derivative, **6** (IC_{50} 0.78 mg/mL), benzoate derivative **2** (IC_{50} 0.76 mg/mL), 3*H*-isochromenone derivative, **5** (IC_{50} 0.79 mg/mL) and hydroxy benzoate metabolite, **1** (IC_{50} 0.74 mg/mL) equated to those displayed by the commercially available antioxidant, α -tocopherol (IC_{50} 0.76 mg/mL) were apparent ($p > 0.05$) (Table 6.16.). These compounds (**1-6**) were exhibited significantly greater $ABTS^+$ radical scavenging potentials ($p < 0.05$) when compared to meroterpeno pyranoid derivatives, **7-8** (IC_{50} 0.92-0.96 mg/mL) and substituted dihomocholestadienol, **9** (IC_{50} 0.98 mg/mL). No significant dissimilarity ($p > 0.05$) was apparent for compounds **7-9** (IC_{50} ~0.95 mg/mL) and, which seemed to be higher when compared to 23-*gem*-dimethyl cholestenol derivative, **10** (IC_{50} 1.12 mg/mL) ($p < 0.05$).

6.3.3.2. Anti-inflammatory potentials of secondary metabolites (1-10) isolated from EtOAc:MeOH extract of *P. malabarica*

The anti-inflammatory potentials of title compounds (**1-10**) isolated from EtOAc:MeOH extract of *P. malabarica* were described in Table 6.17. The anti-inflammatory potentials of isolated compounds were determined by the *in vitro* cyclooxygenase-1/2 and 5-lipoxygenase enzyme inhibitory assays. In addition, the selectivity indices were calculated from the ratio of IC_{50} values of anti-COX-1 to IC_{50} values of anti-COX-2 potentials and the values were compared among the isolated bioactive compounds and standard, ibuprofen (Figure 6.145).

The hydroxy oxo-pyran enclosed benzoate derivative, **3** (IC_{50} 0.83 mg/mL) and hydroxy benzoatemetabolite, **1** (IC_{50} 0.89 mg/mL) were represented significantly greater ($p < 0.05$) inhibitory activity against COX-1 compared to benzoate derivative **2** (IC_{50} 0.95 mg/mL), furanyl-2*H*-tetrahydro-chromenyl derivative, **4** (IC_{50} 0.94 mg/mL), 3*H*-isochromenone derivative, **5** (IC_{50} 1.01 mg/mL), and isopimarane norditerpenoid derivative, **6** (IC_{50} 0.96 mg/mL). The anti-COX-1 potentials were significantly higher ($p < 0.05$) for compounds **1-6** when compared to meroterpeno pyranoids, **7-8** (IC_{50} ~1.06 mg/mL) and cholestenol derivatives, **9-10** (IC_{50} 1.11-1.27 mg/mL). The hydroxy benzoate derivative, **3** (IC_{50} 0.68 mg/mL) was registered greater anti-COX-2 potentials followed by

hydroxy benzoate, **1** (IC₅₀ 0.74 mg/mL) and furanyl-2*H*-tetrahydro-chromenyl, **4** (IC₅₀ 0.72 mg/mL). The anti-COX-2 potentials were significantly greater for compounds, **1**, **3** and **4** ($p < 0.05$) when compared to 3*H*-isochromenone derivative, **5** (IC₅₀ 0.85 mg/mL) benzoate derivative **2** (IC₅₀ 0.89 mg/mL) and isopimarane norditerpenoid, **6** (IC₅₀ 0.82 mg/mL) followed by the compounds, **7-9** (IC₅₀ ~0.93 mg/mL) and 23-*gem*-dimethyl cholesterol derivative, **10** (IC₅₀ 1.15 mg/mL), in descending order. In addition, these compounds, **1-10** were exhibited greater activity against COX-2 than COX-1, and consequently recorded greater selectivity indices (SI, IC₅₀anti-COX-1/IC₅₀anti-COX-2 > 1.05) than ibuprofen (0.63; selective towards constitutive pro-inflammatory enzyme COX-1), a commercial anti-inflammatory drug (Figure 6.148.). The selectivity index was greater for compound, **4** (SI 1.31) followed by **1** (SI 1.20), **3** (SI 1.22), **9** (SI 1.21) and compounds **5-8**, **10** (SI ~1.15) and **2** (SI 1.07), in descending order.

Likewise, hydroxy oxo-pyran enclosed benzoate derivative, compound **3**, isopimarane norditerpenoid derivative, **6** and furanyl-2*H*-tetrahydro chromenyl derivative, **4** did not display any significant difference among each other for anti-5-LOX potentials (IC₅₀ 0.75-0.76 mg/mL; $p > 0.05$). The anti-5-LOX activities of these compounds were significantly greater when compared to other compounds and ibuprofen (IC₅₀ > 0.77 mg/mL; $p < 0.05$). Also, the compounds, hydroxy benzoate metabolite, **1** (IC₅₀ 0.81 mg/mL), 3*H*-isochromenone derivative, **5** (IC₅₀ 0.82 mg/mL) were displayed greater anti-5-LOX activity than that exhibited by the reference inhibitor, ibuprofen whereas, the compounds **2** and **9** were showed activity comparable to ibuprofen (IC₅₀ 0.96 mg/mL) (Table 6.17.).

It is of note that the NSAIDs are used for moderating the pathogenesis due to inflammatory pain and arthritis (Quan *et al.*, 2008), although these drugs were reported to cause deleterious side effects, such as gastric ulcers, CVD and toxicosis on the various organs (Schnitzer *et al.*, 1999). Notably, the adverse implications of NSAIDs were reported to be due to greater anti-COX-1 properties. COX-1 is produces prostaglandins (PGs) which protect the stomach and kidney from damage (Chakraborty *et al.*, 2014a). COX-2 is induced by inflammatory stimuli and produces PGs which contributed to the swelling and

pain of inflammation. The systemic inhibition of the COX-1 leads to a subsequent reduction in cytoprotective PGs required for an effective mucosal defense.

Table 6.17.: *In vitro* anti-inflammatory {cyclooxygenase-1/2 (COX-1/2) and 5-lipoxygenase (5-LOX)) scavenging assays} bioactivities of secondary metabolites (**1-10**) isolated from EtOAc:MeOH extract of *P. malabarica* against commercially available standard, ibuprofen

Compounds	Anti-inflammatory activities		
	IC ₅₀ values (mg/mL)		
	*COX-1 scavenging activity	*COX-2 scavenging activity	*5-LOX scavenging activity
1	0.89 ± 0.05 ^a	0.74 ± 0.06 ^a	0.81 ± 0.07 ^a
2	0.95 ± 0.01 ^b	0.89 ± 0.03 ^b	0.92 ± 0.01 ^b
3	0.83 ± 0.06 ^a	0.68 ± 0.06 ^c	0.76 ± 0.06 ^c
4	0.94 ± 0.03 ^a	0.72 ± 0.06 ^a	0.76 ± 0.07 ^c
5	1.01 ± 0.07 ^b	0.85 ± 0.07 ^b	0.82 ± 0.07 ^a
6	0.96 ± 0.06 ^b	0.82 ± 0.06 ^b	0.75 ± 0.07 ^c
7	1.05 ± 0.01 ^c	0.92 ± 0.06 ^d	1.06 ± 0.07 ^d
8	1.07 ± 0.02 ^c	0.95 ± 0.06 ^d	1.02 ± 0.06 ^d
9	1.11 ± 0.06 ^d	0.92 ± 0.09 ^d	0.96 ± 0.09 ^b
10	1.27 ± 0.07 ^d	1.15 ± 0.09 ^e	1.02 ± 0.09 ^d
Ibuprofen	0.05 ± 0.02 ^e	0.08 ± 0.05 ^f	0.96 ± 0.03 ^b

The samples were analyzed in triplicate (n = 3) and expressed as mean ± standard deviation. Means followed by different superscripts (a-f) within the same column indicated significant differences ($p < 0.05$). *The bioactivities were expressed as IC₅₀ values (mg/mL)

The main undesirable effects of synthetic drugs were due to the inhibition of COX-1, whereas the beneficial effects were due to the inhibition of COX-2. Therefore, the selective COX-2 inhibitors with higher COX-2/COX-1 ratio than NSAIDs seem to be safer. Selective inhibition of COX-2 also provided selective anti-inflammatory effects with reduced organ toxicity risks associated with the COX-1 inhibition. It is of note that the simultaneous inhibition of 5-LOX/COX-2 is important to allow synthesis of lipoxins to

resolve inflammation and attenuate any remaining leukotriene effect. As a result, medical researchers are looking for safer, more efficacious alternatives to both the traditional NSAIDs. It is therefore, necessary to find suitable medications that can inhibit 5-LOX and COX-2 simultaneously while maintaining COX_{1/2} ratio below the threshold limit (preferably lesser than 1.0) for targeted and selective activities against inflammatory response. Apparently, a greater selectivity index (anti-COX-1IC₅₀/anti-COX-2IC₅₀) of the pharmacophores also signified their greater selectivity profile. The greater selectivity index of the secondary metabolites (**1-10**) isolated from EtOAc:MeOH extract of *P. malabarica* (SI > 1.07) (Figure 6.148) explained its greater selectivity profiles than the nonsteroidal anti-inflammatory drug based therapies (e.g., selectivity index of ibuprofen 0.63) (Botting 2006).

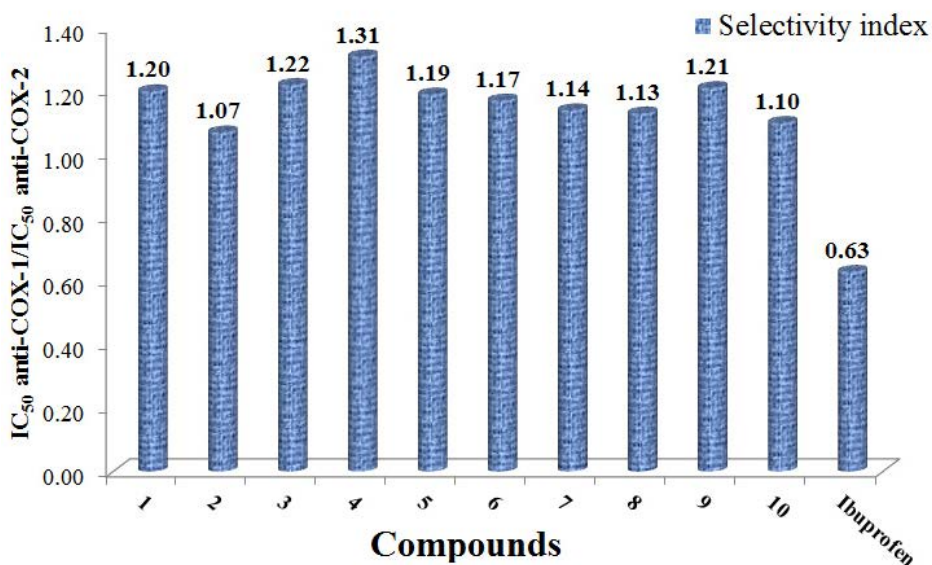


Figure 6.148.: A comparison of selectivity indices (IC₅₀ of anti-COX-1/IC₅₀ of anti-COX-2) of were calculated for the secondary metabolites (**1-10**) isolated from EtOAc:MeOH extract of *P. malabarica* along with commercially available standard, ibuprofen

6.3.4. Structure-activity relationship analysis of secondary metabolites from EtOAc:MeOH extract of *P. malabarica*

6.3.4.1. Structure-activity relationship analysis of secondary metabolites from EtOAc:MeOH extract of *P. malabarica* using various molecular parameters

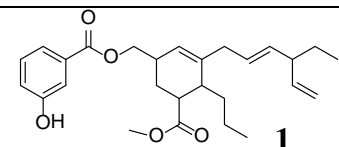
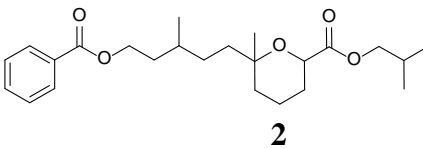
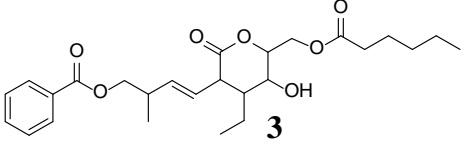
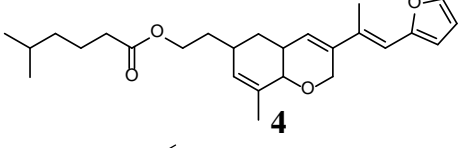
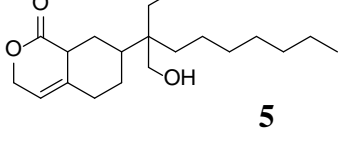
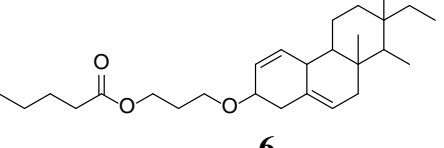
The radical scavenging and anti-inflammatory properties of title compounds (**1-10**) were correlated between their structures and corresponding hydrophobic ($\log P_{ow}$), steric (MR/MV/Pr) and electronic (tPSA/PI) factors to explain their bioactivities (Chakraborty *et al.*, 2017b; Lipinski 2000). The molecular descriptor values for secondary metabolites isolated from *P. malabarica* (**1-10**) and reference compounds, α -tocopherol and ibuprofen were tabulated in the Table 6.18.

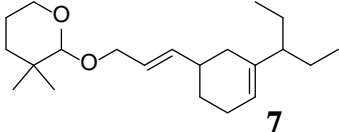
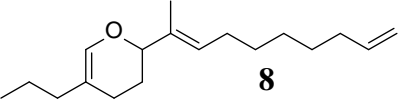
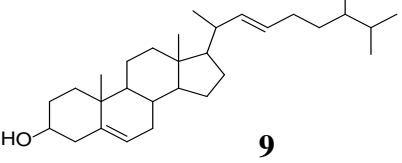
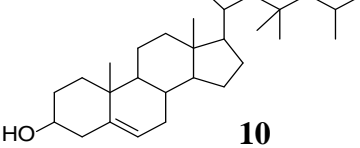
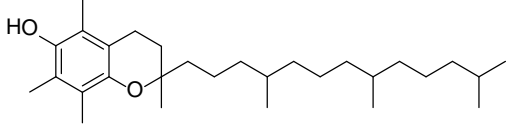
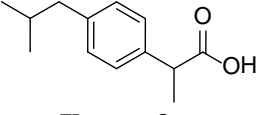
The hydrophobicity of the title compounds, **1-10** were found to be lesser ($\log P_{ow} < 8.3$) when compared to commercially used antioxidant α -tocopherol ($\log P_{ow}$ 9.98). The hydroxy oxo-pyran enclosed benzoate derivative (**3**), furanyl-2*H*-tetrahydro chromenyl (**4**) and 3*H*-isochromenone (**5**) exhibited lesser $\log P_{ow}$ values, which were 4.81, 4.44 and 4.82, respectively and found to be within the acceptable limits (recommended $\log P_{ow}$ 2-5) for optimum hydrophobic-lipophilic properties when compared to α -tocopherol ($\log P_{ow}$ 9.98) (Lipinski 2000). The $\log P_{ow}$ for titled isopimarane norditerpenoid (**6**), benzoate derivatives (**1-2**) and meroterpeno pyranoids, **7-8** were calculated as 6.30, 5.26-6.13 and 5.41-6.05, respectively which was the ratio of 1-octanol to water partition coefficient (Table 6.18.). Antioxidant activities of compounds, **1-6** were greater and their optimum hydrophilic-lipophilic balance demonstrated its utility as a selective pharmacophore. The hydrophobicities of title compounds **1-10** were found to inversely proportional to their intermembrane permeability and bioavailability, which in turn, might negatively affect their bioactivities (Ishige *et al.*, 2001). The significantly greater hydrophobicity of α -tocopherol thus might explain its lesser antioxidant effects than those displayed by title compounds. The bio-potencies of isolated compounds were correlated with their steric bulk values {molar refractivity (MR); molar volume (MV); parachor (Pr)}. The greater steric bulk of α -tocopherol (MR 135.06 cm³/mol; MV 462.7 cm³; Pr 1123 cm³) than those recorded with regard to studied metabolites, **1-8** (MR 85-129 cm³/mol; MV 297-416 cm³; Pr 696-1046

cm³) might possibly explain the relatively lesser bulk hindrance and the greater antioxidative activities of title compounds (Table 6.18.).

It is of note that greater the electronic property, higher is the free radical scavenging and anti-inflammatory activities (Chakraborty *et al.*, 2017c). Notably, the lesser electronic property of α -tocopherol based on total polar surface area, tPSA (29.46) compared to aryl polyketide derivatives, **1-3** (tPSA > 60) and tetrahydro chromenyl derivatives **4-5** (tPSA 44-46) signified the greater electronic interaction of compounds **1-5** resulting in potentially higher free radical scavenging activities. The compound, hydroxy oxo-pyran bearing benzoate derivative, **3** recorded greater tPSA value of 99.13 followed by **1** (tPSA 72.83) and **2** (tPSA 61.83), which was correlated with the greater antioxidative potential of **3** (IC₅₀ < 0.70 mg/mL). Likewise, the studied compounds, **1-5** were displayed greater tPSA values compared to ibuprofen (tPSA 37.30), which accordingly explained its significantly higher inhibiting activities towards pro-inflammatory 5-LOX (IC₅₀ anti-5-LOX 0.76-0.92 mg/mL) against ibuprofen (IC₅₀ 0.96 mg/mL). The electronic property determined by polarisability factor, PI was found to be greater for the title compounds, **1-10** (PI > 30) when compared to ibuprofen (PI 23.96). Similar to the tPSA values, aryl polyketides, **1** (PI 50.33), **3** (PI 50.06) recorded greater PI values followed by tetrahydro chromenyl derivative, **4** (PI 47.85) and aryl polyketide, **2** (PI 44.89) (Table 6.18.). The hydroxy oxo-pyran moiety in **3**, hydroxy benzoate skeleton of **1**, benzoate moiety in **2** and furanyl-chromenyl skeleton in **4** appeared to increase the electron delocalizations and provide free hydrogens to effectively neutralize the free radicals by hydrogen atom transfer (HAT) reaction, which in turn, might possibly minimize the inflammatory responses. The presence of greater numbers of electron-withdrawing groups and centre of unsaturations, such as oxo-pyran, hydroxyl, carboxylates, furanyls, pyrans and aryl moieties in compounds, **1-5** were appeared to increase its electronic property (tPSA **1-5** > 40) than other compounds in the series (tPSA **6** 35.53). Greater number of electronegative centers could be added towards higher bioactive properties due to effective electron-transfer (Cai *et al.*, 2006). Therefore, greater electronic property of **3** appropriately manifested its greater bioactivities compared to those displayed by other compounds.

Table 6.18.: The molecular descriptors of secondary metabolites from EtOAc:MeOH extract of *P. malabarica* (**1-10**) and commercially available products

	Electronic		Steric			Hydrophobic
	tPSA	PI (X10 ⁻²⁴ cm ³)	MR (cm ³ /mol)	MV (cm ³)	Pr (cm ³)	Log P _{ow}
 1	72.83	50.33	129.38	416.9	1034.3	6.13
 2	61.83	44.89	113.39	389.6	956.9	5.26
 3	99.13	50.06	125.15	403.7	1046.5	4.81
 4	44.76	47.85	122.74	394.5	970.7	4.44
 5	46.53	37.10	94.22	315.2	790.8	4.82
 6	35.53	38.93	125.96	337.2	814.6	6.30

 7	18.46	38.93	100.50	337.2	814.6	6.05
 8	9.23	33.33	85.53	297.5	696.7	5.41
 9	20.23	53.02	136.17	433.7	1078.7	8.23
 10	20.23	51.23	130.01	424.1	1049.3	8.19
 α-tocopherol	29.46	53.54	135.06	462.7	1123	9.98
 Ibuprofen	37.30	23.96	60.44	200.1	499.3	3.75

tPSA: Topological Polar Surface Area; Pl: polarizability; MR: molar refractivity; MV: molar volume; Pr: parachor; Log P_{ow} : logarithm of octanol-water coefficient. The molecular descriptors were calculated by using ChemDraw[®] Ultra (CambridgeSoft Corporation, Cambridge, MA, USA; version 8.0) and ACD ChemSketch (Advanced Chemistry Development, Inc., Canada; version 12.0) softwares

The antioxidant activity of title compounds, especially **1-6** were greater than or comparable to α -tocopherol, even though the acceptable lipophilic levels of the former demonstrated it's utility as a selective pharmacophore. Notably, more than 25% of the drugs approved by USFDA were reported to deviate from the boundaries prescribed by Lipinski rule, and this might lead to the undesirable characteristics, such as lesser selectivity and undesirable side effects (Petit *et al.*, 2012). This attributions have been clearly defined by the significantly lesser selectivity indices of the synthetic NSAIDs (ibuprofen, selectivity index lesser than 0.7). The hydrophobic parameter, log P_{ow} appeared to play a predominant role in determining the anti-inflammatory properties, particularly due to the increase in log P_{ow} resulting in lesser COX-2/5-LOX activities as in **3** and **4** (log P_{ow} 4.44-4.82). Hydrophobic molecular descriptor (log P_{ow}) and H-bonding capacity or electronic properties (tPSA/PI) appeared to be closely associated to the pharmacological properties and intermembrane permeability. An earlier literature indicated the close relationship between log P_{ow} and tPSA (Egan and Lauri 2002). It is apparent that the compounds with significantly lesser hydrophobicity could be effectively separated in lipophilic segment of the biological membrane network, and unsuccessful to travel across the hydrophilic part of membrane complex resulting in lesser penetration through the membrane barrier (Wils *et al.*, 1994). A balanced lipophilic-lipophobic index is essentially vital for imparting the target activity and bioavailability of the pharmacophores.

6.3.4.2. Suggested antioxidative mechanism of secondary metabolites from EtOAc:MeOH extract of *P. malabarica* in the DPPH radical model system

The titled three aryl polyketide derivatives, particularly compound **3** was contained a conjugated system that could easily transfer H atom (by hydrogen atom transfer, HAT) to DPPH radical and could form resonance stabilized compounds, thus demonstrating their greater DPPH radical scavenging activity (IC_{50} 0.59 mg/mL). The resonance stabilized forms of three polyketides that would be rearranged intramolecularly and their interaction with the DPPH radical were given in the Figure 6.149. Notably, in the case of compound **3**, there were three reaction sites of antioxidative centres, in which two were at keto (C=O) group. The compound **2** enclosed one active site at keto position,

whereas compound **1** was consisted of two reaction sites in which one was at the keto centre. Apparently, these compounds were exhibited keto-enol resonance stabilization with the adjacent $>C=O$ group leading to $CH=C(-OH)-$ moiety. The greater resonance stabilization, presence of aromatic groups and the ease of H-atom release onto the DPPH radical to form stable DPPH were the prominent reasons for the antioxidative properties of these three aryl polyketide derivatives (**1-3**).

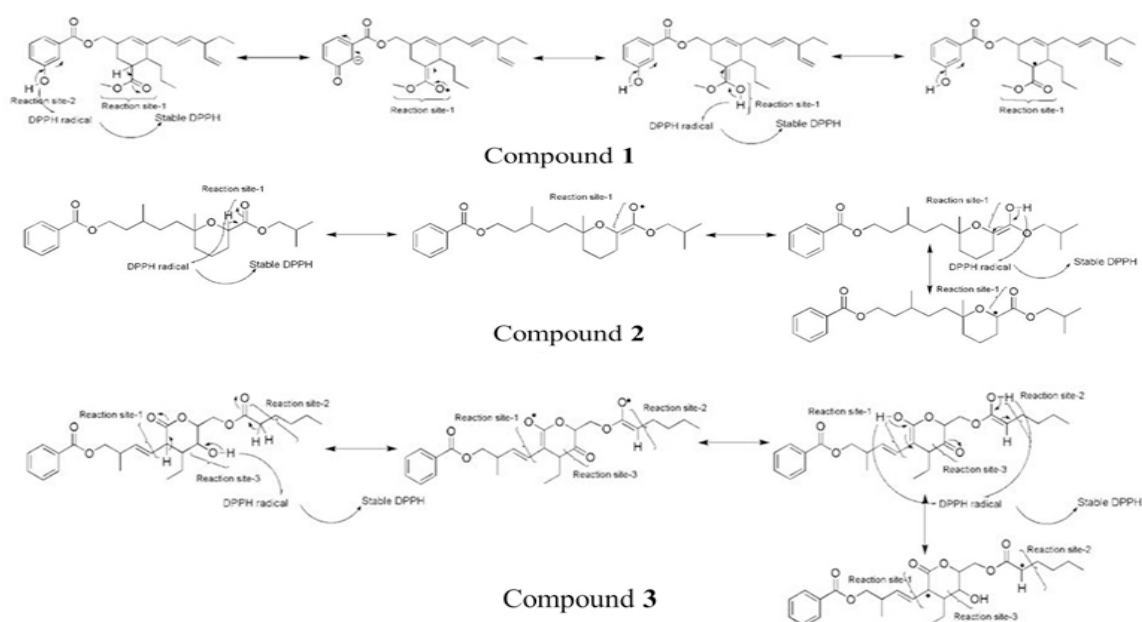


Figure 6.149.: Suggested antioxidative mechanism of aryl polyketides (**1-3**) in DPPH radical model system

Compound **4** was found to contain a conjugated system as 3-(3^{1b}-(furan-2'-yl)-prop-3^{1b}-en-3¹-yl)-dihydro-2*H*-pyran that could easily transfer a H atom (by hydrogen atom transfer, HAT) at C-4a of the tetrahydro-2*H*-chromene framework onto the DPPH radical to form resonance stabilized 3-(3^{1b}-(furan-2'-(5*H*)-ylidene)-propan-3^{1b}-ylidene)-3,6-dihydro-2*H*-pyran skeleton. This might explain the potential DPPH (IC₅₀0.56 mg/mL) radical scavenging activity of **4**. The acidic proton at C-2 of tetrahydro-8-methyl-2*H*-chromene, has been abstracted by DPPH radical by HAT to yield resonance stabilized 6¹-(3-((*E*)-3^{1b}-(furan-2'-yl)-prop-3^{1b}-en-3¹-yl)-6,8a-dihydro-8-methyl-5*H*-chromen-6-yl)-ethyl-5''-methyl

-hexanoate that would be rearranged intramolecularly, and could interact with the DPPH radical (Figure 6.150.). Notably, in the case of compound **4**, there have been two sites of antioxidative reaction centres, one at 3-(3^{1b}-(furan-2'-yl)-prop-3^{1b}-en-3¹-yl)-dihydro-2*H*-pyran, whereas the other was at -CH-C(=O)O- moiety of the ethyl-5-methylhexanoate fragment. Apparently, the proton at C-2'' (in the side chain linked to the tetrahydro chromenyl group) might possibly assist in keto-enol resonance with the adjacent >C=O group (at C-1'') leading to the formation of CH=C(-OH)- moiety by relocating the proton at C-2'' to DPPH radical. However, the second site of antioxidative reaction centre did not effectively participate in the resonance stabilization, and therefore, appeared to exhibit secondary role to stabilize the DPPH radical.

Compound **5** did not possess the extended conjugation, and therefore, could not efficiently transfer an H atom onto the DPPH radical, leading to its lesser antioxidant activity (IC₅₀ 0.73 mg/mL) than those displayed by compound **3-4** (IC₅₀ < 0.60 mg/mL). Compound **5** was found to possess tetrahydro-3*H*-isochromen-1(5*H*)-one moiety, where the olefinic (C=C), and -C(=O)O- groups were located in isolation, and not in extended conjugation. Although the proton at C-8a could potentially form the enolic -C=C(OH)-O- in 6*H*-pyran-1-ol skeleton by DPPH aided abstraction of the acidic proton (C-8a), the abstraction capacity (acidity) of the proton has been weaker, apparently due to lesser electron delocalization. The presence of the free -CH₂OH group, and the free electron pair of the -OH might not effectively participate in the resonance with the tetrahydro chromenyl ring (Figure 6.150.). The proton of -CH₂OH group at the side chain methylnonanol moiety was weakly acidic in nature, and therefore, appeared to form feebly stabilized diphenyl picryl-hydrazine (DPPH-H).

Compound **6** was found to possess two active sites of antioxidant reaction centres, one at the carboxylate linkage in the *O*-propyl pentanoate chain and the second one was located at the -CH-CH=CH-CH(-O-) moiety in cyclic ring. Apparently, the proton in the side chain linked to the ester group might possibly assist in keto-enol resonance with adjacent >C=O group leading to the formation of CH=C(-OH)- moiety by relocating the proton to DPPH radical. The second site of antioxidative reaction centre at the olefinic (C=C) and -C(-O-) groups have been located in conjugation and could easily transfer the

acidic proton to DPPH radical through electron delocalization. Likewise, the antioxidant property of **6** was supported by the suggested mechanism in DPPH model (Figure 6.151.).

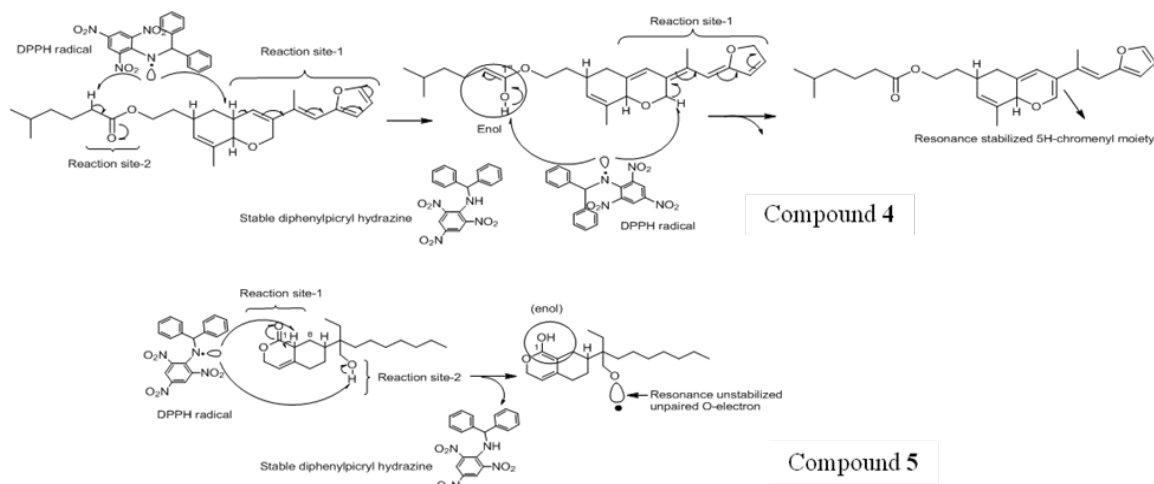


Figure 6.150.: Suggested antioxidative mechanism of tetrahydro chromenyl derivatives (**4-5**) in DPPH radical model system

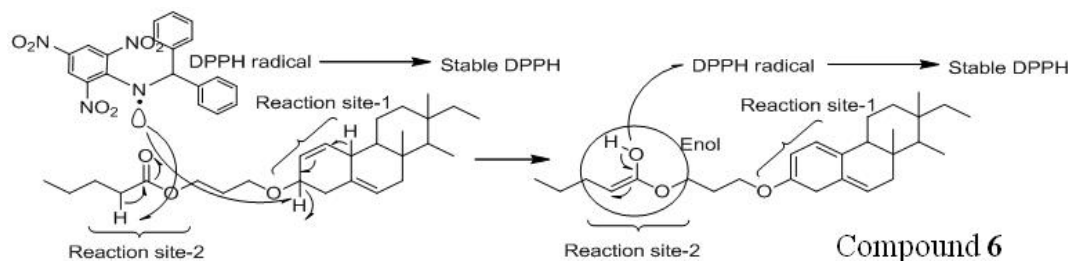


Figure 6.151.: Suggested antioxidative mechanism of isopimarane derivative (**6**) in DPPH radical model system

The compound, **7** was comprised a reaction center in the non-conjugated alkenic system and the compound, **8** enclosed the active center in the pyranil moiety by the delocalization of protons in their vicinity. The protons were not in extended conjugation in both the compounds (**7-8**) and cannot effectively participate in resonance stabilization. Therefore, forms a feebly stabilized DPPH-H and recorded a lower DPPH radical scavenging potential (IC_{50} 0.76-0.78 mg/mL) (Figure 6.152).

The cholestenol derivatives, **9-10** were found to possess one reaction centres at the hydroxyl attached position (C-3) in conjugation with olefinic proton at C-6. The free

electron pair of the -OH might not effectively participate in the resonance with the tetracyclic ring (Figure 6.153.). The protons of -CHOH group located at C-3 position of compounds, **9** and **10** have been weakly acidic in nature, and therefore, might form a weakly stabilized diphenyl picryl-hydrazine (DPPH-H).

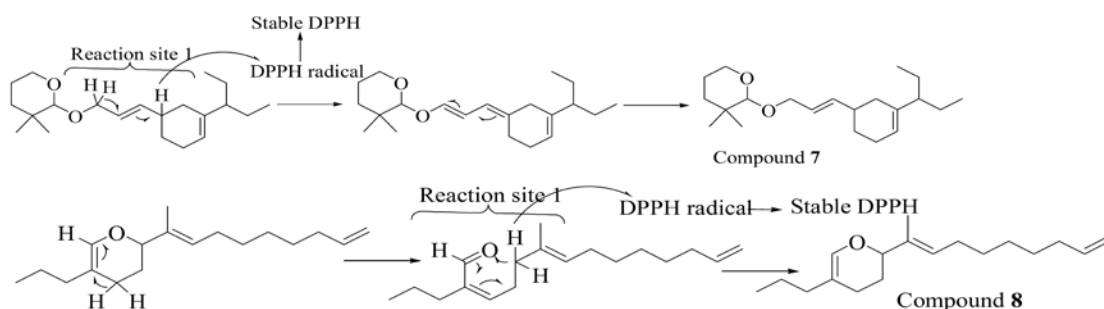


Figure 6.152.: Suggested antioxidative mechanism of meroterpeno pyranoids (**7-8**) in DPPH radical model system

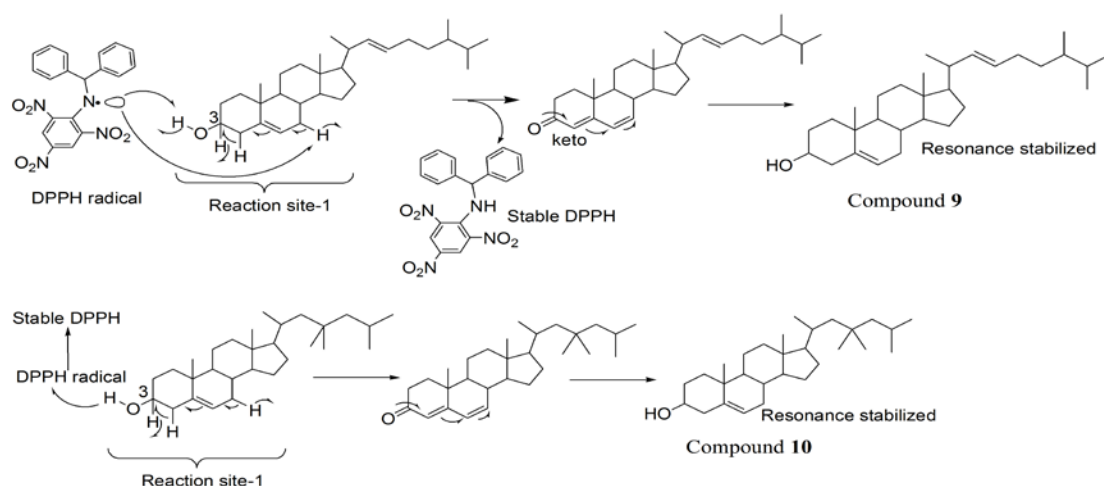


Figure 6.153.: Suggested antioxidative mechanism of cholestenol derivatives (**9-10**) in DPPH radical model system

The proposed antioxidative mechanisms of the titled secondary metabolites (**1-10**) from *P. malabarica* in DPPH radical model system were corroborated with the *in vitro* DPPH radical scavenging model system. The aryl polyketide derivative, **3** was found to contain greater number of active antioxidant reaction centres and possess more number of electronegative groups in conjugation. As a result, it could easily transfer H atom to

neutralize the DPPH radical to form resonance stabilized structures, consequently demonstrating its greater antioxidant activity. Likewise, both the aryl polyketide, **1** and tetrahydro chromenyl derivative, **4** were found to comprise two reaction centres and could easily interact with the DPPH radical, thus the antioxidant potentials were correlated with the suggested mechanism.

6.3.5. *In silico* molecular docking studies of selected compounds (**1-4**, **6**) from *P. malabarica*

The molecular docking studies were revealed the interactions between the selected compounds from *P. malabarica* with the active sites of target enzymes. The molecular docking studies were performed for the compounds isolated from *P. malabarica*, against pro-inflammatory COX-2 and 5-LOX enzymes, respectively, and their RMSD results were analyzed. The docked conformations with lowest binding energies (compounds **1-4**, **6**) were selected for docking visualization to calculate the number of hydrogen bonds and the molecular binding interactions with the active sites of COX-/5-LOX. The number of hydrogen bonds, hydrogen bonded amino acid residues, binding energy, docking score, inhibition constant, intermolecular energy and torsional free energy between the compounds **1-4**, **6** and the active sites of COX-2/5-LOX were recorded in Table 6.19. and 6.20., respectively.

In silico molecular docking studies of selected compounds with COX-2 receptor were revealed that all the docked ligands were bound with the targets. It exhibited lowest binding energies ranging from -7.80 to -9.01 kcal/mol and lowest docking scores of -10.73 to -12.22 kcal/mol (Table 6.18.). Particularly, hydroxy oxo-pyran benzoate derivative, **3** was registered lowest binding energy and docking score of -9.01 and -12.22 kcal/mol, respectively followed by hydroxy benzoate metabolite, **1** (-8.91 and -11.17, respectively) and furanyl-2*H*-tetrahydro chromenyl derivative, **4** (-8.81 and -11.14 kcal/mol, respectively). The enzyme inhibition constants, K_i was found to be lesser for compound **4** (1.71 μ M) than those recorded by **3** (3.59 μ M), **1** (3.30 μ M), **2** (6.52 μ M) and **6** (7.30 μ M), in descending order. Also, the intermolecular energy and torsional free energies were found to be lesser for **1**, **3** and **4** (-10.26 to -12.27 and 2.28 to 2.39 kcal/mol, respectively). The

results were demonstrated the lowest binding energy and docking score of compounds **3** and **4**, which in turn, indicated their greater enzyme inhibition activities against pro-inflammatory inducing enzyme COX-2.

The compound **1** on molecular docking studies against COX-2 were exhibited six hydrogen bonded residues, such as SER 129.A, TRP 125.A, ARG 319.B, GLN 227.B, TYR 220.B, GLY 221.8 (Figure 6.154.A) in active pocket site whereas, compound **2** (TRP 125.A, ASN 130.A, ASP 215.B; Figure 6.154.B) and **3** (ASN 130.A, LEU 131.A, LEU 210.B, LEU 224.B; Figure 6.154.C) exerted four H-bonds each in active site of COX-2. The compounds **4** (LEU 224.B, ARG 319.B; Figure 6.154.D) exhibited two H-bonds whereas, **5** showed five H-bond residues (ARG 319.B, SER 129.A, GLU 222.B, THR 223.B; Figure 6.154.E). The greater number of hydrogen bonds in active site of COX-2 and lesser values of docking parameters (binding energy, docking energy and inhibition constant) were recorded for **3** and **4** and found to be consistent with their greater bio-potentials obtained from *in vitro* anti-COX-2 assay (IC₅₀ 0.68-0.72 mg/mL).

The molecular docking studies of compounds (**1-4, 6**) with pro-inflammatory 5-LOX were revealed their lowest binding energies ranging from 9.55 to 11.02 kcal/mol along with lowest docking scores of 13.24 to 14.41 kcal/mol (Table 6.19.). Notably, hydroxy oxo-pyran enclosed benzoate derivative, **3** was registered lesser binding energy and docking score of 9.55 and 13.24 kcal/mol, respectively followed by that of hydroxy benzoate metabolite, **1** (9.89 and 13.42 kcal/mol, respectively). The enzyme inhibition constants, K_i was found to be lesser for compound **3** (7.12 μM) than those recorded by **4** (7.20 μM), **1** (7.56 μM), **4** (7.34 μM) and **6** (8.21 μM), in descending order. The intermolecular energy and torsional free energies were found to be lesser for compounds **1** and **3** (13.27 to 13.50 and 2.28 to 2.39 kcal/mol, respectively) (Table 6.19.). These results were substantiated the greater enzyme inhibition activities of **3** against pro-inflammatory 5-LOX.

The compound **1** on molecular docking simulation against 5-LOX was displayed three hydrogen bonded residues, such as SER 281.A, GLN 574.A, GLY 569.A (Figure 6.155.A), whereas compound **2** displayed four hydrogen bonds at GLY 570.A, SER 281.A, SER 768.A, SER 768.A, respectively (Figure 6.155.B) in the active pocket of enzyme.

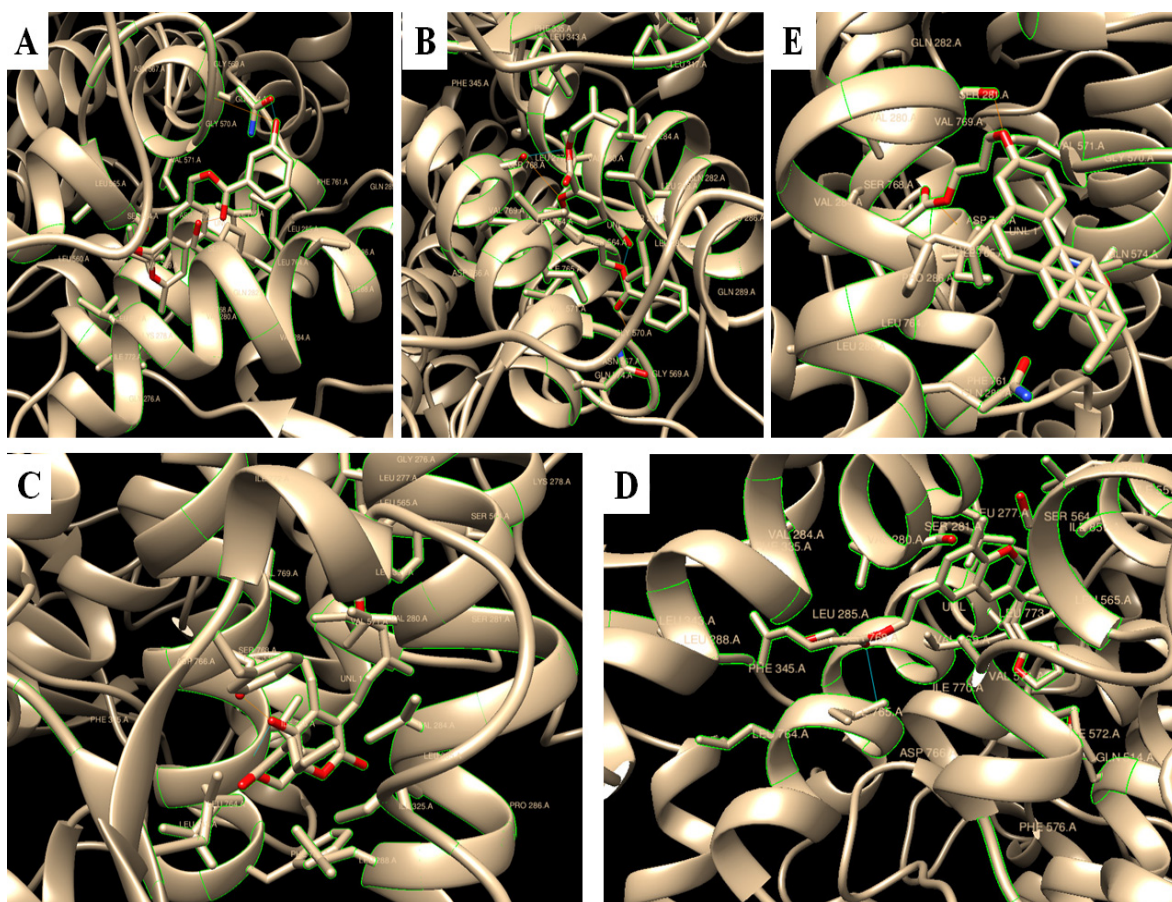


Figure 6.155. The molecular binding interactions of compounds (A) **1**, (B) **2**, (C) **3**, (D) **4** and (E) **6** in the active site of lipoyxygenase (5-LOX) were comprehended from the docking studies. The orange and blue coloured bonds were indicated the H-bonding correlations with 5-LOX

Table 6.19.: Number of hydrogen bonds, hydrogen bonded (H-bonded) amino acid residue, binding energy, docking score, inhibition constant, intermolecular energy and torsional free energy between the ligands (compounds **1-4, 6**) and the active sites of COX-2

Ligands	†No. of H-bonds	#H-bonded amino acid residues	*Binding energy (kcal/mol)	*Docking score (kcal/mol)	*Inhibition constant, Ki (μM)	*Intermolecular energy (kcal/mol)	*Torsional free energy (kcal/mol)
1	6	SER 129.A TRP 125.A ARG 319.B GLN 227.B TYR 220.B GLY 221.8	-8.91	-11.17	3.30	-11.29	2.39
2	4	TRP 125.A TRP 125.A ASN 130.A ASP 215.B	-7.80	-10.73	7.30	-9.79	2.98
3	4	ASN 130.A LEU 131.A LEU 210.B LEU 224.B	-9.01	-12.22	3.59	-12.27	2.28
4	2	LEU 224.B ARG 319.B	-8.81	-11.14	1.71	-10.26	2.39
6	5	ARG 319.B ARG 319.B SER 129.A GLU 222.B THR 223.B	-8.46	-11.01	6.52	-11.15	2.68

†Molecular docking studies were carried out using the software Autodock 4. #Hydrogen bonding interactions between protein and ligand.*Values were obtained from the energy minimization based calculations

Table 6.20.: Number of hydrogen bonds, hydrogen bonded (H-bonded) amino acid residue, binding energy, docking score, inhibition constant, intermolecular energy and torsional free energy between the ligands (compounds **1-4, 6**) and the active sites of 5-LOX

Ligands	†No. of H-bonds	#H-bonded amino acid residues	*Binding energy (kcal/mol)	*Docking score (kcal/mol)	*Inhibition constant, Ki (μM)	*Intermolecular energy (kcal/mol)	*Torsional free energy (kcal/mol)
1	3	SER 281.A GLN 574.A GLY 569.A	9.89	13.42	7.56	13.50	2.39
2	4	GLY 570.A SER 281.A SER 768.A SER 768.A	10.11	14.07	10.32	14.09	2.98
3	2	ILE 765.A SER 768.A	9.55	13.24	7.12	13.27	2.28
4	1	ILE 765.A	10.79	14.41	7.20	14.61	2.39
6	2	ILE 765.A SER 281.A	11.02	13.28	10.09	13.34	2.68

†Molecular docking studies were carried out using the software Autodock 4. #Hydrogen bonding interactions between protein and ligand.*Values were obtained from the energy minimization based calculations

The docking studies of selected compounds (**1-4**, **6**) isolated from *P. malabarica* on the binding sites of 5-LOX/COX-2 showed that these ligands were potential inflammatory inhibitors and it could act as dual 5-LOX/COX-2 inhibitors. The 5-LOX and COX-2 enzymes were reported to be the inductive pro-inflammatory enzymes, and their expression was found to be upregulated in response to inflammatory stimuli. Apparently, simultaneous inhibition of COX-2 and 5-LOX is vital to arrest the inflammatory response in affected individuals. Notably, the binding interactions were explained the significant biological activity of studied compounds. Also, the molecular docking interactions were appropriately visualized the specificity of titled compounds with COX-2 and 5-LOX enzymes, which in turn, ascertained their greater selectivity, in particular, with reference to the compounds, **3** and **4**.

6.4. Conclusions

The rich diversity of venerid bivalve clam, *P. malabarica* in the coastal and marine waters of Kerala represented an unexploited reservoir of bio-potent compounds with valuable pharmaceutical and biomedical use, even though, the scientific investigations to acknowledge the health benefits of these species are confined. The present study is the first of its kind to extensively study this low-value bivalve clam to isolate specialized metabolites of potential pharmacological significance, and characterize in detail by extensive spectroscopic experiments. The ethyl acetate:methanol extract of *P. malabarica* was chromatographically fractionated to acquire bioactive secondary metabolites which were classified under various classes belonging to aryl polyketide derivatives (**1-3**), tetrahydro chromenyl derivatives (**4-5**), isopimarane norditerpenoid (**6**), meroterpeno pyranoids (**7-8**) and cholestenol analogues (**9-10**). The chemical structures of the previous undescribed specialized metabolites were resolved by detailed spectroscopic analysis. Putative biosynthetic pathways catalyzed by polyketide synthase leading to the formation of the title polyketide compounds unambiguously validated the structural attributions of compounds **1-3**.

The isolated compounds were evaluated for its antioxidant (DPPH and ABTS⁺ scavenging) and anti-inflammatory (COX-1/COX-2/5-LOX inhibition) potentials. The

compounds, (E)-12-(17-ethyl-tetrahydro-16-hydroxy-15-(methyl pentanoate)-14-oxo-2H-pyran-13-yl)-9-methyl-but-11-enyl benzoate (**3**) and 6¹-(3-((E)-3^{1b}-(furan-2'-yl)-prop-3^{1b}-en-3¹-yl)-tetrahydro-8-methyl-2H-chromen-6-yl)-ethyl-5''-methyl-hexanoate (**4**) exhibited greater pro-inflammatory 5-lipoxygenase (5-LOX) inhibition potential (IC₅₀ 0.76 mg/mL) than that displayed by ibuprofen (IC₅₀ 0.96 mg/mL) in consonant with significantly greater anti-inflammatory selectivity indices (SI > 1.20) than latter (ibuprofen SI < 1), which inferred the greater selectivity of **3** and **4**. The aryl polyketides (13-(methoxycarbonyl)-11-((E)-18-ethylhexa-16,19-dienyl)-12-propylcyclohex-10-enyl)-methyl-4-hydroxy benzoate (**1**), isobutyl-13-(6-(benzoyloxy)-10-methylpentyl)-tetrahydro-13-methyl-2H-pyran-17-carboxylate (**2**), tetrahydro chromenyl derivative, 7-(2'-ethyl-1'-hydroxynonan-2'-yl)-tetrahydro-3H-isochromen-1-(5H)-one (**5**) and isopimarane norditerpenoid, 18 (4→14),19 (4→8) bis-abeo-nor-isopimarane-1,5-diene-3-yl-3β-methoxy propyl pentanoate (**6**) reported comparable pro-inflammatory 5-lipoxygenase (5-LOX) inhibition potential (IC₅₀ 0.75-0.92 mg/mL) to ibuprofen (IC₅₀ 0.96 mg/mL) and significantly greater anti-inflammatory selectivity indices (SI > 1.05) than the latter (SI < 1). Further, the docking study of selected compounds (**1-4**, **6**) on COX-2 and 5-LOX binding sites displayed that the titled ligands were good inflammatory inhibitors of COX-2/5-LOX enzymes. The specificity of titled compounds with COX-2 and 5-LOX enzymes explained their greater anti-inflammatory selectivity profiles, particularly of aryl polyketide, **3**.

The antioxidant activities of the compound **3** and **4**, as determined by 2,2-diphenyl-1-picrylhydrazyl and 2,2'-azino-bis (3-ethylbenzothiazoline-6-sulphonic acid) radical scavenging activities (IC₅₀ 0.56-59 and 0.67-0.69 mg/mL, respectively) were greater than those recorded with commercially with α-tocopherol (IC₅₀ 0.65 and 0.76 mg/mL, respectively). The compounds, **1**, **2**, **5** and **6** displayed comparable antioxidant potentials (IC₅₀ 0.66-0.79 and 0.74-0.79 mg/mL, respectively) to α-tocopherol. Structure activity correlation studies displayed that the antioxidative and anti-inflammatory properties of the title compounds were directly proportional to their electronic properties and inversely with the hydrophobic and steric bulk characteristics. The proposed antioxidative mechanisms of the reported metabolites in DPPH radical model system were positively correlated with the *in vitro* DPPH radical scavenging assay. This mechanism further supported the greater

antioxidant potentials of the aryl polyketide derivatives (compounds **3** and **1**) followed by tetrahydro chromenyl derivative, **4** which were found to effectively quench the DPPH free radical.

Polyketide compounds along with the tetrahydro chromenyl derivatives bearing pleotropic molecular frameworks and functional properties were reported in previous literatures, and therefore, are the attractive choices of natural product chemists to develop cardinal bioactive pharmacophores in present-day drug discovery. However, there are sustained efforts to isolate newer chemistries of these groups of compounds with higher bioactive properties compared to previously described molecules. Accordingly, investigations with regard to modern functional food research are concentrated to identify and evolve chromene and polyketide derivatives with greater bioactive properties. The previously undescribed aryl polyketides and tetrahydro chromenyl analogues isolated from *P. malabarica* could effectively be utilized as naturally derived antioxidants to improve the shelf-life of food ingredients and to prevent the oxidative stress induced inflammatory diseases.

Mollusks are traditional seafoods with wide variety of bioactive secondary metabolites, in which bivalve clams found in the marine and estuarine habitats were considered to be valuable marine resources of nutritional and commercial importance (Wakimoto *et al.*, 2011). The bivalve clams contributed a significant role in the total fish catch of coastline areas of India and were recognized as predominant seafood resources with traditional health food applications among the coastal populace of the southwest coast of India. Bivalve clams considered as low-value by-catch species, even though these coastal fishery resources held a cardinal part of the aggregate edible mollusks, and preferred food items among the coastal population due to their nutritional importance and easy availability. Among different bivalve clam species, *Villorita cyprinoides* (black clam) and *Paphia malabarica* (yellow-foot clam) are the common resources, abundantly available in the coastal regions of southwest coast of India, and their cultivation methodologies have been developed and standardized. Considering the promising perspective for the utilization of these groups of bivalve clams, and limited research reports on their utilization as potential health foods, their nutritional and pharmaceutical potential began to receive considerable attention. A number of research publications related to nutritional significance, bio-potent functionalities together with isolation, identification and characterization of previously unidentified chemistries from bivalve clams demonstrated their broader possibilities in the pharmaceutical chemistry research and related applications (Blunt *et al.*, 2015; Mohite *et al.*, 2009; Tsai *et al.*, 2008; Wei *et al.*, 2007). Earlier reports suggested the relevance of bivalves as natural bio-potential products, health food supplements, nutraceuticals, food additives and pharmacophores for human well-being (Watanabe *et al.*, 2012).

The free radical generation and oxidative stress is one of the major concerns in the present day life leading to various health problems. The reactive oxygen species were found to be the mediators of various disorders, such as inflammations, atherosclerosis, cancer, diabetes, ulcers, hypertension etc. (Stefanis *et al.*, 1997). Reactive oxygen species were found to generate signals to activate the pro-

inflammatory mediators like COX, LOX isoforms, cytokines, interleukins and chemokines, which develop acute or chronic inflammations. The action of free radicals can be effectively suppressed by various antioxidant supplements. The commercially available antioxidants were reported to be carcinogenic and can lead to organ damages (Schnitzer *et al.*, 1999). Likewise, the non-steroidal anti-inflammatory (NSAIDs) medicines used to treat inflammatory ailments were associated with mild to severe damages of gastrointestinal tract (Weil *et al.*, 1995). In these circumstances, target specified antioxidative and anti-inflammatory compounds from natural resources have been acknowledged to overcome the adverse effects of synthetics. It is to note that the marine organisms were endowed with complex defense pathways to challenge their oxidative stress conditions and to help them synthesizing various specialized and potent bioactive secondary metabolites (Chainy *et al.*, 2016). The soft tissue bivalve clams have been adapted to extreme unfavourable conditions, even though they were not reported for cellular damages. Therefore, it was believed that the cells of these sessile organisms were significant producers of diverse classes of specialized bioactive metabolites with pharmaceutical significance. It is important to note that small molecular weight compounds constitute a major share of bioactives in the marine organisms (Blunt *et al.*, 2015). It is, therefore, imperative to explore these molecules due to their greater bioactivities against various pharmacological models, and also relative ease to synthesize these molecules in laboratory conditions. The potential bioactive templates can also be used as intermediates to synthesize drug candidates/drug-like molecules. Even though, the ratios of marine natural products that can be established into drugs are relatively lesser, it is apparent that the cumulative numbers of bioactive components will be permitted for the curing of human diseases. The promising perspective of bivalve clams, *V. cyprinoides* (family, Corbiculidae) and *P. malabarica* (family, Veneridae) as potential health foods, the investigations of their pharmaceutical applications began to receive substantial consideration. Therefore, the isolation and characterization of low molecular weight bioactive metabolites from the commonly available bivalve clams, *V. cyprinoides* and *P. malabarica* have vital role in the development of functional foods and pharmaceutical lead templates.

The investigation of the nutritional compositions of *V. cyprinoides* and *P. malabarica* in the current study appropriately established their dietary qualities as

functional food candidates. The greater contents of polyunsaturated fatty acids (34.33%), especially, eicosapentaenoic acid (EPA, 7.68%), docosahexaenoic acid (DHA, 14.35%), balanced *n*-3/*n*-6 fatty acid proportion (2.31%) and DHA/EPA (1.88%) were characterized for *P. malabarica* compared to *V. cyprinoides* (Σ PUFA 18.46%; EPA 3.57%; DHA 3.22%; Σ *n*-3/ Σ *n*-6 0.77 and DHA/EPA 0.91%). The balanced essential/non-essential amino acid ratio (> 1.0 mg/100 g wet weight) and vitamin D₃ (> 160 IU) contents in the edible portion of these bivalve clams were recognized these species as high value health food components. The favourable sodium to potassium ratio ($\text{Na/K} > 1.0$) and calcium-phosphorus contents ($\text{Ca+P} > 550$ mg/100 g wet weight) along with greater selenium concentrations ($\text{Se} > 25$ $\mu\text{g}/100$ g wet weight) showed that these bivalves were good sources of well-balanced diet. The present study demonstrated the nutritional qualities of *V. cyprinoides* and *P. malabarica* and suggested their utilities as functional food components.

Anti-inflammatory, anti-hypertensive, antioxidant and anti-diabetic potentials of EtOAc:MeOH (ethyl acetate:methanol) solvent extract of *V. cyprinoides* and *P. malabarica* were assessed by different *in vitro* models. The EtOAc:MeOH extract of *P. malabarica* was demonstrated greater 1,1-diphenyl-2-picryl-hydrazil and 2,2'-azinobis-3-ethylbenzothiozoline-6-sulfonic acid radical scavenging abilities (IC_{50} 0.76 and 1.27 mg/mL, respectively). A higher angiotensin converting enzyme-1 (ACE-1) inhibitory activity coupled with anti-cyclooxygenase-2 and anti-5-lipoxygenase (IC_{50} 1.11, 0.92 and 1.51 mg/mL, respectively) properties along with DPP-4 and α -glucosidase (IC_{50} 1.00 and 1.47 mg/mL, respectively) inhibitory activities registered for EtOAc:MeOH extract of *P. malabarica* than *V. cyprinoides*. This study revealed that the EtOAc:MeOH extract of *P. malabarica* registered greater antioxidative properties, and the activities were showed significant positive correlation with antihypertensive, anti-inflammatory, and anti-diabetic activities. The utilities of spectroscopic tools for analyzing the signature peaks and relative abundance of the vital functional groups present in the solvent extracts, and to furnish with essential rules regarding the presence of electronegative functional groups responsible for the bioactivities were illustrated. A significant co-linearity was found to exist between the electronegative groups present in the downfield position of the NMR spectra and the bioactivities of the EtOAc:MeOH extracts derived from the bivalve clam species.

The bioassay guided chemical prospecting of EtOAc:MeOH extract of bivalve clam *V. cyprinoides* led to isolation of bio-potent metabolites, which were grouped into spirocyclic ether derivatives (**1-2**), irregular meroterpenoids (**3-5**), hexahydro isochromenyl analogues (**6-7**) and cholestenol derivatives (**8-10**). The structures of isolated compounds were unambiguously assigned by 1D (^1H , ^{13}C , $^{135}\text{DEPT}$), 2D (^1H - ^1H COSY, HSQC, HMBC, NOESY) nuclear magnetic resonances (NMR) spectroscopy, fourier transform infrared (FTIR) and mass experiments.

The bioactivity-guided purification of EtOAc:MeOH extract of *V. cyprinoides* resulted in the identification of two spirocyclic ether derivatives namely 16-hydroxyhexyl-(2-ethyl-2,6-dimethyl-1-oxaspiro[4.5]dec-3,8-dien)-10-propanoate (**1**) and (*E*)-18-ethyl-17,19-dihydroxyhept-14-enyl-(2-ethyl-2,6-dimethyl-1-oxaspiro[4.5]dec-3,8-dien)-10-acetate (**2**). These two compounds enclosed a rearranged monocyclofarnesyl framework with a dihydrofuran ring spiro fused to substituted cyclohexene framework, and found to possess an oxaspiro[4.5]deca-dienyl skeleton. The extensive one and two dimensional NMR experimentations (^1H - ^1H COSY, HSQC and HMBC) ascertained that the basic *O*-spirocyclic structural attributions of **1** and **2** were found to be similar, but differed in their side chain attachments. The compound **1** enclosed 16-hydroxyhexyl-10-propanoate at C-10 whereas, **2** enclosed distinctive 18-ethyl-17,19-dihydroxyhept-14-enyl-10-acetate unit at C-10 position. The compounds with *O*-heterocyclic-spiro functionalities were found to be significant bioactive agents among various classes of organic compounds. The spiro compounds were found to enclose two rings shared with one atom (the quaternary spiroatom) and the conformation of the ligands (compounds) has been rigidified by the introduction of ring framework. In this manner, the cyclic derivatives were appeared to experience a reduced conformational stress during the binding to a target site (enzymes or proteins).

The present study demonstrated the identification of three irregular meroterpenoid derivatives bearing oxygen heterocycles (**3-5**) from *V. cyprinoides*. The chromatographic purification of EtOAc:MeOH extract of black clam resulted in the identification of *O*-heterocyclic fused irregular meroterpenoid derivative named as 8-(1,3,3a,4,5,7a-hexahydro-1-(hydroxymethyl)-3-oxoisobenzofuran-4-yl)-ethyl-pentanoate (**3**) along with one each of *O*-heterocyclic pyranone characterized as tetrahydro-3-methoxy-5-((*E*)-8,12-dimethyloct-8-enyl)-pyran-2-one (**4**) and *O*-heterocyclic dihydro

furanone-dihydropyran ring enclosed dihydro-5-(8-(9,12-dihydro-8-methyl-11-propyl-2*H*-pyran-8-yl)-ethyl)-furan-2(3*H*)-one (**5**). The compound **3** was composed with a basic C11 skeleton including the hexahydro oxoisobenzofuran and pentanoate side chain, which were linked through an ethyl linkage. The compound **4** was found to be α -pyrone enclosed sesquiterpene-based C16 prenylated bisabolene type of meroterpenoid, whereas the compound **5** was enclosed an irregular C15 furano meroterpenoid as its basic structural framework. Extensive two dimensional NMR experiments with compound **5** has explained that it was composed of two parts, which were dihydro-furan-2(3*H*)-one part and {8-(9,12-dihydro-8-methyl-11-propyl)-2*H*-pyran-8-yl} part linked through an ethyl moiety. The *O*-heterocyclic skeletons with varying substitutions of electronegative functionalities might play significant functional roles towards the potential biological activities of the irregular meroterpenoid derivatives bearing oxygen heterocycles (**3-5**) from *V. cyprinoides*.

The identification and characterization of two hexahydro isochromenyl meroterpenoids, (10*E*)-butyl-9-(6-ethyl-hexahydro-1*H*-isochromen-3-yl)-pent-10-enoate (**6**) and (12*E*)-(hexahydro-1*H*-isochromen-3-yl)-methyl-hept-12-enoate (**7**) from *V. cyprinoides* were described in the present study. The compound, **6** was an irregularly arranged C20 hexahydro isochromenyl meroterpenoid, whereas the compound **7** was found to be an irregularly arranged C17 isochromenyl meroterpenoid. The extensive NMR experiments proposed that the basic hexahydro isochromenyl frameworks of **6** and **7** were similar, but found to be varied in their side chain attachments. The compound **6** enclosed ethyl moiety at C-6 and butyl-pent-10-enoate side chain at C-3 whereas, in **7**, the ethyl moiety at C-6 was absent and C-3 position was linked to methyl hept-12-enoate. The presence of *O*-heterocyclic tetrahydro chromenyl derivatives with lipophilic side chains might play a noteworthy role towards their potential bioactivities.

The present study also described the characterization of a new abeo-pregnane-type sterol derivative as 19 (10 \rightarrow 5) abeo-20-methyl-pregn-1-en-3-yl-3 β -methoxy-hex-25-enoate (**8**) along with two cholestenol derivatives, which were characterized as (22*E*)-24¹-homocholesta-5,22-dien-(3 β ,24¹ β)-diol (**9**) and (22*E*),(24¹*E*)-24¹,24²-dihomocholesta-5,22,24¹-trien-3 β -ol (**10**). The methyl group (-CH₃-19) at C-10 position of the pregnane steroid derivative, **8** was shifted to C-5, and therefore, it was named as 19 (10 \rightarrow 5) abeo pregnane. Also, the characteristic hydroxyl group at C-3 of sterols was

substituted by the highly electronegative groups like carboxylates, which was apparent from the deshielded proton signal at $\delta \sim 4.5$ (corresponded to ester linkages) in the ^1H NMR spectrum. The two cholesterol derivatives were found to be similar, except the side chain moieties. The cholesta-dienol derivative, **9** was deduced to enclose the olefinic and hydroxyl groups in the side chain framework attached at C-17, whereas the dihomocholesta-trien-ol derivative, **10** was found to possess two isolated alkenes at C-22 and C-24¹ positions in the side chain (attached at C-17).

The spirocyclic ether derivatives, (*E*)-18-ethyl-17,19-dihydroxyhept-14-enyl-(2-ethyl-2,6-dimethyl-1-oxaspiro[4.5]dec-3,8-dien)-10-acetate (**2**) and 16-hydroxy hexyl-(2-ethyl-2,6-dimethyl-1-oxaspiro [4.5]dec-3,8-dien)-10-propanoate (**1**) isolated from *V. cyprinoides* were displayed significantly greater ($p < 0.05$) antioxidant activities against DPPH radical (IC_{50} 0.54 and 0.59 mg/mL, correspondingly) when equated to α -tocopherol and other compounds in series ($\text{IC}_{50} > 0.60$ mg/mL). The antioxidant activity against DPPH radical for the irregular meroterpenoid derivatives bearing oxygen heterocycles (**3-5**) were found to be lesser compared to spirocyclics, even though no significant difference ($p > 0.05$) was apparent for the DPPH radical scavenging potentials of **3-5** (IC_{50} 0.63-0.71 mg/mL) along with α -tocopherol (IC_{50} 0.65 mg/mL). The prenylated spirocyclic ether derivatives, **1** and **2** (IC_{50} 0.62-0.67 mg/mL) along with furano meroterpenoid derivative, **5** (IC_{50} 0.64 mg/mL) not displayed ($p > 0.05$) any significant difference in ABTS⁺ radical scavenging properties, and their antioxidative activities against ABTS⁺ radical were found to be significantly greater ($p < 0.05$) than those exhibited by other compounds in this series and α -tocopherol (IC_{50} 0.76 mg/mL). No significant difference was apparent in ABTS⁺ radical inhibition for the α -pyrone derivative, **4** (IC_{50} 0.76 mg/mL) and hexahydrobenzo furanone, **3** (IC_{50} 0.72 mg/mL) with the reference, α -tocopherol (IC_{50} 0.76 mg/mL).

The spirocyclic ether derivative, **2** exhibited significantly greater ($p < 0.05$) inhibitory activity against constitutive pro-inflammatory COX-1 and inducible isoform COX-2 (IC_{50} 0.86 and 0.65 mg/mL, respectively) when related to other compounds ($\text{IC}_{50} > 0.90$ and > 0.70 mg/mL, respectively) isolated from *V. cyprinoides*. The compound **2** exhibited greater COX-2 inhibitory potential followed by spirocyclic ether derivative **1** (IC_{50} 0.70 mg/mL), hexahydrobenzo furanone, **3** (IC_{50} 0.74 mg/mL) and furano meroterpenoid derivative, **5** (IC_{50} 0.76 mg/mL), in descending order. The

spirocyclic ether derivative, **1** and irregular meroterpenoids **3** and **5** did not record any significant difference among each other with regard to their COX-2 inhibitory potentials ($p > 0.05$). Notably, the greater selectivity index {SI > 1.02 , IC₅₀ (anti-COX-1/anti-COX-2)} of the compounds isolated from *V. cyprinoides* (**1-10**) were appropriately suggested their selective inhibition of the inducible pro-inflammatory COX-2 than the constitutive COX-1. Similarly, the spirocyclic ether derivatives, **1-2** (IC₅₀ 0.75-0.77 mg/mL), hexahydrobenzo furanone, **3** (IC₅₀ 0.76 mg/mL) along with furano meroterpenoid, **5** (IC₅₀ 0.80 mg/mL) were exhibited significantly greater inhibitory potentials ($p < 0.05$) against pro-inflammatory 5-LOX as compared to other compounds and ibuprofen (IC₅₀ > 0.90 mg/mL). No noteworthy variance ($p > 0.05$) in the inhibitory potencies towards 5-LOX was apparent for the irregular meroterpenoid, **4** (IC₅₀ 0.92 mg/mL) and hexahydro isochromenyl meroterpenoids, **6-7** (IC₅₀ ~ 0.97 mg/mL), whereas the bioactivities were appeared to be akin to ibuprofen (IC₅₀ > 0.90 mg/mL).

Structure-activity relationship analysis of the isolated compounds were carried out using hydrophobic parameter (logarithmic scale of the octanol-water partition coefficient, log P_{ow}), electronic descriptor variables (polarizability, PI) together with steric factors {molar refractivity (MR), molar volume (MV), parachor (Pr)}. The spirocyclic ether derivatives, **1** (log P_{ow} 3.79) and **2** (log P_{ow} 3.32) along with hexahydrobenzo furanone, **3** (log P_{ow} 1.81) were exhibited acceptable hydrophilic-lipophilic balance (log P_{ow} 2-5) and found to be lesser than that of reference, α -tocopherol showing significantly greater hydrophobicity (log P_{ow} 9.98). Moreover, the α -pyrone derivative, **4** (log P_{ow} 3.59), furano meroterpenoid, **5** (log P_{ow} 2.25) and hexahydro isochromenyl analogues, **6-7** (log P_{ow} 3.1-4.0) were registered optimum hydrophobic-lipophilic balance (log P_{ow} 2-5). The lesser bulk (steric) parameters of compounds **1-3** (MR 75-120 cm³/mol; MV < 375 cm³; Pr < 960 cm³) might contribute towards their greater radical scavenging potentials compared to α -tocopherol (MV 462.7 cm³; Pr 1123 cm³; MR 135.06 cm³). Also, the compounds **4-7** recorded lesser bulk (steric) parameters (MR < 100 cm³/mol; MV < 350 cm³; Pr < 800 cm³), which might contribute towards their greater antioxidative potential over α -tocopherol. The electronic property as determined by tPSA factor was greater for compounds, **1-3** (tPSA₁ 55.76; tPSA₂ 75.99; tPSA₃ 72.83) as compared to the standards, ibuprofen (tPSA 37.30) and α -tocopherol (tPSA 29.46), which might be correlated with the greater

bioactive potentials of the two irregular spirocyclic ether derivatives (**1-2**) and the irregular meroterpenoid **3**. The bioactivities of the compounds **4-7** were not influenced by their electronic parameters and therefore, found to be insignificant in predicting their bioactive potentials. The lower hydrophobicity ($\log P_{ow}$ 2.25) and lesser steric bulkiness along with greater electronic properties of the compounds, particularly spirocyclic ether derivatives, **1-2**, hexahydrobenzo furanone, **3** and furano meroterpenoid derivative (**5**) imparted towards their greater bioactive potentials and bioavailability as compared to other compounds isolated from the bivalve clam *V. cyprinoides*.

The number of active reaction centers or the number of acidic protons available to neutralize the DPPH radical were predicted by the proposed mechanism of DPPH radical inhibition for the tilted compounds isolated from *V. cyprinoides*. The spirocyclic ether derivatives, **1-2**, hexahydrobenzo furanone, **3** and furano meroterpenoid derivative, **5** were found to enclose greater number of electron-rich active sites that can effectively participate in the resonance stabilization and appeared to exhibit primary role to stabilize the DPPH radical.

Molecular docking studies were determined the relations between the compounds (ligands) and the active sites of target inducible pro-inflammatory enzymes (COX-2 and 5-LOX). The greater numbers of hydrogen bonds in both the active regions of 5-LOX and COX-2 along with the lower values of docking parameters (binding energy, docking energy and inhibition constant) were recorded for compounds **1-5**. In particular, the spirocyclic ether derivative, **2** (COX-2 number of hydrogen bonds-4; 5-LOX number of hydrogen bonds-3) and hexahydrobenzo furanone, **3** (COX-2 number of hydrogen bonds-4; 5-LOX number of hydrogen bonds-3) were found to enclose greater number of enzyme inhibition sites for COX-2 and 5-LOX as determined by the hydrogen bonds. The anti-inflammatory bioactive potentials were evaluated by the *in vitro* 5-LOX and COX-2 inhibition assays for the compounds from *V. cyprinoides* deduced to be coherent with the *in silico* molecular docking calculations.

The chemical investigations of EtOAc:MeOH extract of *P. malabarica* led to the isolation of different metabolites belonging to aryl polyketide derivatives (**1-3**), tetrahydro chromenyl analogues (**4-5**), isopimarane norditerpenoid (**6**), meroterpeno 2H-pyranoids (**7-8**) and cholestenol derivatives (**9-10**). The chemical structures of these

previously undescribed metabolites were resolved by detailed spectroscopic analysis along with mass spectrometric experiments.

The chemical investigation of EtOAc:MeOH extract of *P. malabarica* directed to the isolation of three unprecedented aryl polyketide analogues, such as (13-(methoxycarbonyl)-11-((*E*)-18-ethylhexa-16,19-dienyl)-12-propyl-cyclohex-10-enyl)-methyl-3-hydroxy benzoate (**1**), isobutyl-13-(6-(benzoyloxy)-10-methylpentyl)-tetrahydro-13-methyl-2*H*-pyran-17-carboxylate (**2**) and (*E*)-12-(17-ethyl-tetrahydro-16-hydroxy-15-(methylpentanoate)-14-oxo-2*H*-pyran-13-yl)-9-methyl-but-11-enyl benzoate (**3**). The ^1H aromatic signals (δ 6.5-8.5) of the compounds **2** and **3** exhibited proton integral of five each, which established their monosubstituted benzyl framework, whereas, the compound **1** exhibited four aromatic resonances in which one was found to be singlet proton that designated the presence of meta disubstituted aryl ring of **1**. The putative PKS enzyme cascade-assisted biosynthetic pathways of these previously unreported aryl polyketide compounds (**1-3**) appropriately substantiated their structural attributions.

Previously undescribed tetrahydro chromenyl derivatives, characterized as 6¹-(3-((*E*)-3^{1b}-(furan-2'-yl)-prop-3^{1b}-en-3¹-yl)-4a,5,6,8a-tetrahydro-8-methyl-2*H*-chromen-6-yl)-ethyl-5''-methyl-hexanoate (**4**) and 7-(2'-ethyl-1'-hydroxynonan-2'-yl)-6,7,8,8a-tetrahydro-3*H*-isochromen-1-(5*H*)-one (**5**) were isolated from *P. malabarica*. These were composed of furanyl-2*H*-tetrahydro chromenyl (**4**) and tetrahydro isochromen-(5*H*)-one (**5**) moieties, which were reported for the first time in marine organism. The ^1H NMR spectrum of compound **4** was exhibited a highly deshielded singlet at δ 6.92 showing intense HSQC interaction with the carbon at δ 124.76 (-CH-), which confirmed the presence of an alkenic proton attached to the highly electronegative centre of furan ring system. The presence of furanyl ring in compound **4** was confirmed by three aromatic ^1H NMR resonances. The chromenyl derivatives were valuable pharmacophores which exhibiting important structural and functional peculiarities in natural product research, and receiving more prominent considerations as cardinal bioactive pharmacophores in present-day drug discovery. Although these groups of compounds constitute an important share of natural products, variation in substitution patterns might lead to pharmacophore templates with greater bioactivity and selectivity.

The present study demonstrated the isolation of 18 (4→14),19 (4→8) bis-abeo-nor-isopimarane-1,5-diene-3-yl-3 β -methoxy-propyl pentanoate (**6**), which represented the first description of C19 isopimarane norditerpenoid possessing the bis-abeo C19 norditerpenoid framework from a natural bivalve source. Generally, the ent-pimarane diterpenoid skeletons have 20 carbons including a methyl (-CH₃) group at C-10 whereas, the methyl at C-10 was not apparent in the titled compound, thus confirming the presence of norditerpenoid functionality. The usual *gem*-dimethyl groups (C-18 and C-19) found at C-4 position in isopimarane and 20-nor-isopimarane diterpenoids were absent at C-4 in **6**. However, the -CH₃ (C-18 and C-19) groups at C-4 was shifted to C-14 and C-8 positions, respectively, and therefore, it named as 18 (4→14),19 (4→8) bis-abeo nor-isopimarane. This unprecedented isopimarane derivative isolated from *P. malabrica* would be a potential natural alternative to the commercially available synthetic antioxidants and anti-inflammatory agents.

The present study also reported the identification of two undescribed meroterpeno 2*H*-pyranoids from *P. malabarica*. This is the first report of biogenic allyloxy-(isopentanyl)-cyclohexene (**7**) and 2*H*-pyrans bearing decadienyl (**8**) frameworks from marine organisms. The C18 sesquiterpenoid with irregularly prenylated farnesene skeleton characterized as 2-((*E*)-deca-1,8-dien-10-yl)-11,12-dihydro-13-propyl-2*H*-pyran (**8**). Another compound, 1'-((10*E*)-10-(10-(pentan-4-yl)-cyclohex-4-enyl)-allyloxy)-tetrahydro-2',2'-dimethyl-2*H*-pyran (**7**) was signified the first occurrence of C21 prenylated bisabolene-type meroterpenoid from a natural resource, while tetrahydro-2',2'-dimethyl-2*H*-pyran bonded to cyclohex-4-enyl moiety through the allyloxy bond. The titled compounds were previously undescribed marine natural components possessing the pyranyl regiochemistries and found to be the first depiction of bioactive meroterpeno 2*H*-pyranoids from *P. malabrica*.

The present study was envisaged the isolation of two new sterol derivatives as (22*E*)-24¹,24²-methyldihomocholesta-5,22-dien-3 β -ol (**9**) and 23-*gem*-dimethyl cholesta-5-en-3 β -ol (**10**) from *P. malabarica*. The C-30 dihomosterol and 23-*gem*-dimethyl-3 β -hydroxy- Δ^5 -cholestane skeleton (**9-10**) represent the first examples of steroids possessing the C-30 dihomosterol system (**9**) and 23-*gem*-dimethyl-3 β -hydroxy- Δ^5 -cholestane (**10**) framework from a natural source with bioactive pluralities.

The (*E*)-12-(17-ethyl-tetrahydro-16-hydroxy-15-(methylpentanoate)-14-oxo-2*H*-pyran-13-yl)-9-methyl-but-11-enyl benzoate (**3**) and 6¹-(3-((*E*)-3^{1b}-(furan-2'-yl)-prop-3^{1b}-en-3¹-yl)-4a,5,6,8a-tetrahydro-8-methyl-2*H*-chromen-6-yl)-ethyl-5''-methyl-hexanoate (**4**) were exhibited significantly greater DPPH (IC₅₀ ~0.57 mg/mL) and ABTS⁺ (IC₅₀ ~0.68 mg/mL) scavenging activities ($p < 0.05$) as compared to other compounds in the series and α -tocopherol (IC₅₀ \geq 0.65 mg/mL). The titled C19 isopimarane norditerpenoid from *P. malabarica* not exhibited any significant difference ($p > 0.05$) in scavenging DPPH and ABTS⁺ free radicals (IC₅₀ 0.65 and 0.78 mg/mL, correspondingly) equated to α -tocopherol (IC₅₀ 0.65 and 0.76 mg/mL, respectively). No significant difference was apparent ($p > 0.05$) in ABTS⁺ scavenging potentials among compound **5** (IC₅₀ 0.79 mg/mL) and α -tocopherol (IC₅₀ 0.76 mg/mL, respectively).

The hydroxy benzoate derivative, **3** (IC₅₀ 0.68 mg/mL) was registered greater inhibitory potential against pro-inflammatory COX-2 isoform followed by those of hydroxy benzoate, **1** (IC₅₀ 0.74 mg/mL) and furanyl-2*H*-tetrahydro-chromenyl, **4** (IC₅₀ 0.72 mg/mL), in descending order. The compounds **1**, **3** and **4** were registered greater COX-2 inhibitory potentials as compared to other compounds in this series. The potent 5-LOX inhibitory effects were recorded for the compounds **3**, **6** and **4** (IC₅₀ ~0.76 mg/mL) when related to other compounds and ibuprofen (IC₅₀ $>$ 0.80 mg/mL). The compounds **1** and **3** were demonstrated significantly greater inhibition towards pro-inflammatory 5-LOX (IC₅₀ 0.81 and 0.76 mg/mL, correspondingly) than that revealed by ibuprofen (IC₅₀ 0.96 mg/mL) along with significantly greater selectivity (anti-COX-1IC₅₀/anti-COX-2IC₅₀ $>$ 1.05) indices compared to ibuprofen (SI $<$ 1). Significantly greater 5-LOX inhibitory activities of tetrahydro chromenyl analogues (**4-5**) (IC₅₀ 0.76-0.82 mg/mL) along with isopimarane norditerpenoid (**6**) (IC₅₀ 0.75 mg/mL) compared to ibuprofen (IC₅₀ 0.96 mg/mL) specified their potent anti-inflammatory effects. The greater selectivity (SI $>$ 1.05) of the titled compounds, **1-10** isolated from *P. malabarica* than ibuprofen (SI 0.63) was appropriately demonstrated their selective inhibitory properties towards inflammatory COX-2 over COX-1.

Structure-activity relationship analysis of the compounds isolated from *P. malabarica* revealed the optimum hydrophilic-lipophilic balance of the aryl polyketide, **3** (log P_{ow} 4.81) and tetrahydro chromenyl derivatives (compounds **4-5**) (log P_{ow} 4.44-4.82). The hydrophobic-lipophilic properties of other compounds in the series were found to be

lesser ($\log P_{ow} < 9$) as compared to commercially used antioxidant α -tocopherol ($\log P_{ow}$ 9.98). The hydrophobicity of the compounds was found to be inversely proportional to their intermembrane permeability and bioavailability, and a greater $\log P_{ow}$ value (> 6) negatively affect their bioactive properties. Notably, the lesser electronic property of α -tocopherol (tPSA 29.46) compared to aryl polyketides, **1-3** (tPSA > 60) and tetrahydro chromenyl analogues **4-5** (tPSA 44-46) appropriately signified the greater electronic interaction of the latter resulting in potentially greater free radical scavenging activities. Likewise, greater steric bulk of α -tocopherol (MR 135.06 cm³, Pr 1123 cm³) than those recorded with regard to aryl polyketides (MR 113-126 cm³; Pr ~1000 cm³) and tetrahydro chromenyl analogues, **4-5** (MR 94-122 cm³; Pr 790-970 cm³) explained their greater bioactivities.

The numbers of bioactive reaction centers in the isolated compounds from *P. malabarica* were correlated with their antioxidant potentials in the DPPH radical scavenging model. The aryl polyketide derivatives, particularly **3** was found to possess greater number of conjugated systems that could easily transfer H atom to DPPH radical by hydrogen atom transfer (HAT) mechanism to attain resonance stabilization, thus corroborating its potential DPPH radical scavenging activity (IC₅₀ 0.59 mg/mL). The furanyl-2*H*-tetrahydro chromenyl, **4** and other aryl polyketide derivatives, **1-2** were found to enclose antioxidative centers in their vicinities, and their antioxidant activities were correlated with the proposed DPPH mechanism.

Moreover, the *in silico* molecular docking studies of compounds from *P. malabarica* were carried out to determine their interactions with the active sites of pro-inflammatory inducible COX-2 and 5-LOX enzymes. The greater number of hydrogen bonds (in active regions of 5-LOX and COX-2) and lesser docking parameter values were recorded for compounds **1-4** and **6**. In specific, the aryl polyketide derivatives, **1-3** and C19 isopimarane norditerpenoid, **6** were found to register greater number of enzyme inhibition sites for COX-2 and 5-LOX based on the numbers of H-bonds in their active sites. The *in vitro* 5-LOX and COX-2 anti-inflammatory analysis of the compounds from *P. malabarica* were found to exhibit linearity with the *in silico* molecular docking simulations.

Comprehensive analyses demonstrated that during the last decade, the typical percentages of bioactive compounds amongst the newer compounds are diminishing,

though there are a countless numbers of marine natural compounds yet to be investigated. This may indicated that the research level of bio-potencies is not keeping up with the identification of newer compounds. With innumerable bivalve clams from coastal ecosystem representing a large community of marine fauna, the coastal waters of India are acknowledged for their particular richness. The present study explored these two prominent bivalve clam species as a source for potentially useful bioactive properties, and a library of previously undescribed molecules with prospective bioactive properties against inflammatory mediators and reactive oxygen species. This study is the first of its kind to demonstrate that the low value bivalve clams *V. cyprinoides* and *P. malabarica* are endowed with potential bioactive properties. Furthermore, the newer bioactive compounds from *V. cyprinoides* and *P. malabarica* described in the present study will form copious resources for upcoming bioactivity guided investigations and development of biomedically important new pharmacological leads.

REFERENCES

- Aasen J, MacKinnon SL, LeBlanc P, Walter JA, Hovgaard P, Aune T, Quilliam MA (2005). Detection and identification of spirolides in Norwegian shellfish and plankton. *Chemical Research in Toxicology*, 18(3), 509-515.
- Abele D, Heise K, Pfrtner HO, Puntarulo S (2002). Temperature dependence of mitochondrial function and production of reactive oxygen species in the intertidal mud clam *Mya arenaria*. *Journal of Experimental Biology*, 205, 1831-1841.
- Ahmad TB, Rudd D, Smith J, Kotiw M, Mouatt P, Seymour LM, Liu L, Benkendorff K (2017). Anti-inflammatory activity and structure-activity relationships of brominated indoles from a marine mollusc. *Marine Drugs*, 15(5), 133.
- Ajithkumar P, Jeganathan NS, Balamurugan K, Manvalan R, Radha K (2012). Evaluation of anti-ulcer activity of *Villorita cyprinoides* extract (black water clams) against immobilization stress induced ulcer in albino rats. *Journal of Pharmaceutical Research and Opinion*, 2(6), 55-57.
- Alkanani T, Parrish CC, Thompson RJ, McKenzie CH (2007). Role of fatty acids in cultured mussels, *Mytilus edulis*, grown in Notre Dame Bay, Newfoundland. *Journal of Experimental Marine Biology and Ecology*, 348, 33-45.
- Amagata T, Amagata A, Tenney K, Valeriote FA, Lobkovsky E, Clardy J, Crews P (2003). Unusual C25 steroids produced by a sponge-derived *Penicillium citrinum*. *Journal of Organic Letters*, 5, 4393-4396.
- Amornrut C, Toida T, Imanari T, Woo ER, Park H, Linhardt R, Wu SJ, Kim YS (1999). A new sulfated beta-galactan from clams with anti-HIV activity. *Carbohydrate Research*, 321(1-2), 121-127.
- Anbuselvi S, Chellaram C, Jonesh S, Jayanthi A, Edward JKP (2009). Bioactive potential of coral associated gastropod, *Trochus tentorium* of Gulf of Mannar, Southeastern India. *Journal of Medical Sciences*, 9, 240-244.
- Andersen RJ, Desjardine K, Woods K (2006). Skin chemistry of nudibranchs from the west coast of North America. *Progress in Molecular and Subcellular Biology*, 43, 277-301.
- Andersen RJ, Faulkner DJ, He CH, Van Duyne GD, Clardy J (1985). Metabolites of the marine prosobranch mollusk *Lamellaria* sp. *Journal of the American Chemical Society*, 107, 5492-5495.
- Andrade J, Marin R, Apel M, Raseira M, Henriques A (2012). Comparison of the fatty acid profiles of edible native fruit seeds from Southern Brazil. *International Journal of Food Properties*, 15(4), 815-822.
- Andrianasolo EH, Haramaty L, McPhail KL, White E, Vetriani C, Falkowski P, Lutz R (2011). Bathymodiolamides A and B, ceramide derivatives from a deep-Sea hydrothermal vent invertebrate mussel, *Bathymodiolus thermophilus*. *Journal of Natural Products*, 74, 842-846.

- Annamalai N, Anburaj R, Jayalakshmi S, Thavasi R (2007). Antibacterial activities of green mussel (*Perna viridis*) and edible oyster (*Crassostrea madrasensis*). Research Journal of Microbiology, 2(12), 978-982.
- Antolovic M, Prenzler PD, Patsalides E, McDonald S, Robards K (2002). Methods for testing antioxidant activity. Analyst, 127, 183-198.
- AOAC (1990). Official Methods of Analysis of the Association of Official Analytical Chemists. 15th ed. Washington, D.C.
- AOAC (2005). Official methods of analysis of the association of official analytical chemists International. 18th ed. Gaithersburg, M.D. Association of Analytical Communities, 473.
- Appleton AR, Babcock RC, Copp BR (2001). Novel tryptophan-derived dipeptides and bioactive metabolites from the Sea hare *Aplysia dactylomela*. Tetrahedron, 57, 10181-10189.
- Appleton DR, Sewell MA, Berridge MV, Copp BRJ (2002). A new biologically active malyngamide from a New Zealand collection of the Sea hare *Bursatella leachii*. Journal of Natural Products, 65(4), 630-631.
- Arora RB, Mathur CN (1963). Relationship between structure and anticoagulant activity of coumarin derivatives. British Journal of Pharmacology and Chemotherapy, 20, 29-35.
- Aruoma OI (1994). Nutrition and health aspects of free radicals and antioxidants. Food and Chemical Toxicology, 32, 671-83.
- Aruoma OI (2003). Methodological consideration for characterization for potential antioxidant actions of bioactive components in plants foods. Mutation Research, 532, 9-20.
- Ashour M, Edrada R, Ebel R, Wray V, Watjen W, Padmakumar K, Muller WEG, Lin W H, Proksch P (2006). Kahalalide derivatives from the Indian sacoglossan mollusk *Elysia grandifolia*. Journal of Natural Products, 69(11), 1547-1553.
- Astorga-Espana MS, Rodriguez EM, Romero CD (2007). Comparison of mineral and trace element concentrations in two mollusks from the Strait of Magellan (Chile). Journal of Food Composition and Analysis, 20, 273-279.
- Babu A, Venkatesan V, Rajagopal S. (2011). Fatty acid and amino acid compositions of the gastropods, *Tonna dolium* (Linnaeus, 1758) and *Phalium glaucum* (Linnaeus, 1758) from the Gulf of Mannar, Southeast coast of India. Annals Food Science and Technology, 12(2), 159-163.
- Baby RL, Hasan I, Kabir KA, Naser MN (2010). Nutrient analysis of some commercially important mollusks of Bangladesh. Journal of Scientific Research, 2 (2), 390-396.
- Ballio A, Barcellona S, Santurban B (1966). 5-Methylmellein, a new natural dihydroisocoumarin. Tetrahedron Letters, 7, 3723-3726.
- Balti R, Bougatef A, Sila A, Guillochon D, Dhulster P, Nedjar-Arroume N (2015). Nine novel angiotensin-I converting enzyme (ACE) inhibitory peptides from cuttlefish (*Sepia officinalis*) muscle protein hydrolysates and antihypertensive

- effect of the potent active peptide in spontaneously hypertensive rats. *Food Chemistry*, 170(1), 519-525.
- Baptista M, Repolho T, Maulvault A, Vanessa ML, Luis N, Antonio M, Narcisa B, Rui R (2014). Temporal dynamics of amino and fatty acid composition in the razor clam *Ensis siliqua* (Mollusca: Bivalvia). *Helgoland Marine Research*, 10152, 402-407.
- Bartosz G (2003). Generation of reactive oxygen species in biological systems. *Comments on Toxicology*, 9(1), 5-21.
- Baunbaek D, Trinkler N, Ferandin Y, Lozach O, Ploypradith P, Rucirawat S, Ishibashi F, Iwao M, Meijer L (2008). Anticancer alkaloid Lamellarins inhibit protein kinases. *Marine Drugs*, 6, 514-527.
- Baylac S, Racine P (2003). Inhibition of 5-lipoxygenase by essential oils and other natural fragment extracts. *International Journal of Aromatherapy*, 13(2-3), 138-142.
- Belisle BW, Stickle WB (1978). Seasonal patterns in the biochemical constituents and body component indexes of the muricid gastropod, *Thais haemastoma*. *The Biological Bulletin*, 155, 259-272.
- Benkendorff K, McIver CM, Abbott CA (2011). Bioactivity of the Murex Homeopathic remedy and of extracts from an Australian muricid mollusc against human cancer cells. *Evidence-Based Complementary and Alternative Medicine*, 2011, Article ID 879585, 12 pages.
- Benkendorff K (2010). Molluscan biological and chemical diversity: Secondary metabolites and medicinal resources produced by marine mollusks. *Biological Reviews*, 85, 757-775.
- Bernay B, Baudy-Floch M, Gagnon J, Henry J (2006). Ovarian jelly-peptides (OJPs), a new family of regulatory peptides identified in the cephalopod *Sepia officinalis*. *Peptides*, 27, 1259-1268.
- Besednova NN, Zaporozhets TS, Kovalev NN, Makarenkova ID, Yakovlev YM (2017). Cephalopods: The potential for their use in medicine. *Russian Journal of Marine Biology*, 43(2), 101-110.
- Bialecki AG, Aknin M, Smadja J (2008). 24-*O*-ethylmanoalide, a manoalide-related sesterterpene from the Marine sponge *Luffariella cf. variabilis*. *Molecules*, 13, 3184-3191.
- Bian W-T, You Z-J, Wang C-Y, Shao CL (2014). Brominated pimarane diterpenoids from the Sea hare *Aplysia pulmonica* from the South China Sea. *Chemistry of Natural Compounds*, 50, 557-559.
- Bichurina MA, Nikitina LE, Sovetora MG, Rechina NI, Basedina TV, Boikov YA, Noskov FS (1994). Mussels treat humans and animals. *Voprosy Virusologii*, 3, 134-136.
- Blunt JW, Copp BR, Keyzers RA, Munro MHG, Prinsep MR (2003). Marine natural products. *Natural Product Reports*, 20, 1-48.

- Blunt JW, Copp BR, Keyzers RA, Munro MHG, Prinsep MR (2006). Marine natural products. *Natural Product Reports*, 23, 26-78.
- Blunt JW, Copp BR, Keyzers RA, Munro MHG, Prinsep MR (2012). Marine natural products. *Natural Product Reports*, 29, 144-222.
- Blunt JW, Copp BR, Keyzers RA, Munro MHG, Prinsep MR (2013). Marine natural products. *Natural Product Reports*, 30, 237-323.
- Blunt JW, Copp BR, Keyzers RA, Munro MHG, Prinsep MR (2014). Marine natural products. *Natural Product Reports*, 31, 160-258.
- Blunt JW, Copp BR, Keyzers RA, Munro MHG, Prinsep MR (2015). Marine natural products. *Natural Products Reports*, 32, 116-211.
- Blunt JW, Copp BR, Keyzers RA, Munro MHG, Prinsep MR (2016). Marine natural products. *Natural Product Reports*, 33, 382-431.
- Blunt JW, Copp BR, Munro MH, Northcote PT, Prinsep MR (2011). Marine natural products. *Natural Products Reports*, 28, 196-268.
- Boeckman Jr RK, Blum DM, Ganem B (1988). 3-Trimethylsilyl-3-buten-2-one as Michael acceptor for conjugate-addition-annulation: Cis-4,4a,5,6,7,8-hexahydro-4a,5-dimethyl-2(3H)-naphthalenone. *Organic Synthesis*, 6, 666.
- Booth JD (1983). Studies on twelve common bivalve larvae and bivalve spawning seasons. *New Zealand Journal of Marine and Freshwater Research*, 17, 231-265.
- Borbulevych OY, Jankun J, Selman SH, Skrzypczak-Jankun E (2004). Lipxygenase interactions with natural flavonoid, quercetin, reveal a complex with protocatechuic acid in its X-ray structure at 2.1 Å resolution. *Proteins: structure, function, and bioinformatics*, 54, 13-19.
- Borquaye LS, Darko G, Oklu N, Anson-Yevu C, Ababio A (2016). Antimicrobial and antioxidant activities of ethyl acetate and methanol extracts of *Littorina littorea* and *Galatea paradoxa*. *Cogent Chemistry*, 2, 1161865.
- Botting RM (2006). Inhibitors of cyclooxygenases mechanisms, selectivity and uses. *Canadian Journal of Physiology and Pharmacology*, 57, 113-124.
- Boucaud-Camou E (1990). La Seiche, un animal d'avenir. *La Pêche Maritime*, 69(1342), 321-329.
- Bourdron J, Commeiras L, Audran G, Vanthuyne N, Hubaud JC, Parrain J-L (2007). First total synthesis and assignment of the stereochemistry of crispatenine. *The Journal of Organic Chemistry*, 72, 3770-3775.
- Bowden BF, Coll JC, Mitchell SJ (1980). Studies of Australian soft corals. XXI. A new sesquiterpene from *Nephthea chabrolii* and an investigation of the common clam *Tridacna maxima*. *Australian Journal of Chemistry*, 33(8), 1833-1839.
- Boyle PR, Rodhouse P (2005). *Cephalopods: Ecology and fisheries*. Oxford, Blackwell Science. pp. 452.
- Brayer GD, Sidhu G, Maurus R, Rydberg EH, Braun C, Wang Y (2000). Subsite mapping of the human pancreatic alpha-amylase active site through structural kinetic and mutagenesis techniques. *Biochemical Journal*, 39, 4778-4791.

- Brazao S, Morais S, Boaventura D, Re P, Narciso L, Hawkins SJ (2003). Spatial and temporal variation of the fatty acid composition of *Patella* spp. (Gastropoda: Prosobranchia) soft bodies and gonads. *Comparative Biochemistry and Physiology-B*, 136, 425-441.
- Brito I, Dias T, Diaz-Marrero AR, Darias J, Cueto M (2006). Aplysiadiol from *Aplysia dactylomela* suggested a key intermediate for a unified biogenesis of regular and irregular marine algal bisabolene-type metabolites. *Tetrahedron*, 62(41), 9655-9660.
- Bromann K, Viljanen K, Moreira VM, Yli-Kauhaluoma (2014). Isolation and purification of ent-pimara-8(14),15-diene from engineered *Aspergillus nidulans* by accelerated solvent extraction combined with HPLC. *Journal of Analytical Methods*, 6, 1227-1234.
- Bromley CL, Popplewell WL, Pinchuck SC, Hodgson AN, Davies-Coleman MT (2012). Polypropionates from the South African Marine Mollusk *Siphonaria oculus*. *Journal of Natural Products*, 75, 497-501.
- Brusca RC, Brusca GJ. (1990). *Invertebrates*. Massachusetts USA, Sinauer Associates, Inc., Sunderland.
- Cai YZ, Mei S, Jie X, Luo Q, Corke H (2006). Structure radical scavenging activity relationships of phenolic compounds from traditional Chinese medicinal plants. *Journal of life science*, 78, 2872-2888.
- Calder PC (2004). Long-chain fatty acids and cardiovascular disease: Further evidence and insights. *Nutrition Research*, 24, 761-772.
- Calder PC (2012). The role of marine *n*-3 fatty acids in inflammatory processes, atherosclerosis and plaque stability. *Molecular Nutrition and Food Research*, 56, 1073-1080.
- Calderon GJ, Castellanos L, Duque C, Echigo S, Hara N, Fujimoto Y (2004). Ophirasterol, a new C31 sterol from the marine sponge *Topsentia ophiraphidites*. *Steroids*, 69, 93-100.
- Calter MA, Liao W (2002). First total synthesis of a natural product containing a chiral, β -diketone: Synthesis and stereochemical reassignment of siphonarienedione and siphonarienolone. *Journal of the American Chemical Society*, 124, 13127-13129.
- Camacho-Ruiz A, Mendez ME (2010). Diabetes radicales libres. *In* Diabetes. Eds. Gonzalez JAM, Santillan EOM, Chapa GN, Montiel ID, Falcon AJ, Soto JE. 2nd ed. Pachuca, Hidalgo, Mexico. Universidad Autónoma del Estado de Hidalgo.
- Carbone M, Ciavatta ML, Wang J-R, Cirillo I, Mathieu V, Kiss R, Mollo E, Guo Y-W, Gavagnin M (2013). Extending the record of bis- γ -pyrone polypropionates from marine pulmonate mollusks. *Journal of Natural Products*, 76, 2065-2073.
- Carbone M, Irace C, Costagliola F, Castelluccio F, Villani G, Calado G, Padula V, Cimino G, Cervera JL, Santamaria R, Gavagnin M (2010). A new cytotoxic tambjamine alkaloid from the Azorean nudibranch *Tambja ceutae*. *Medicinal Chemistry Letters*, 20, 2668-2670.

- Carrell RW, Winterbourn CC, Rachmilewitz EA (1975). Activated oxygen and haemolysis. *British Journal of Haematology*, 30, 259-264.
- Cazalet S (2007). *Materia Medica: Repertorium Homeopathicum* (Reversed Kent's Repertory). <http://www.homeoint.org/hidb/kent/index.htm>. Homeopathe International.
- Celik MY, Culha ST, Culha M, Yildiz H, Acarli S, Celik I, Celik P (2014). Comparative study on biochemical composition of some edible marine molluscs at Canakkale coasts: Turkey. *Indian Journal of Geo-Marine Sciences*, 43, 601-606.
- Cesaretti M, Luppi E, Maccari F, Volpi N (2004). Isolation and characterization of a heparin with high anticoagulant activity from the clam *Tapes philippinarum*: Evidence for the presence of a high content of antithrombin III binding site. *Glycobiology*, 14, 1275-1284.
- Chainy GBN, Paital B, Dandapat J (2016). An overview of seasonal changes in oxidative stress and antioxidant defence parameters in some invertebrate and vertebrate species. *Scientifica*, 2016, 8 pages, Article ID 6126570.
- Chakraborty K, Chakkalakal SJ, Joseph D, Asokan PK, Vijayan KK (2016a). Nutritional and antioxidative attributes of green mussel (*Perna viridis* L.) from the southwestern coast of India. *Journal of Aquatic Food Product Technology*, 25(7), 968-985.
- Chakraborty K, Chakkalakal SJ, Joseph D, Joy M (2016b). Nutritional composition of edible Oysters (*Crassostrea madrasensis* L.) from the southwest coast of India. *Journal of Aquatic Food Product Technology*, 25(8), 1172-1189.
- Chakraborty K, Chakkalakal SJ, Joseph D (2014a). Response of pro-inflammatory prostaglandin contents in anti-inflammatory supplements from green mussel *Perna viridis* L. in a time dependent accelerated shelf-life study. *Journal of Functional Foods*, 7, 527-540.
- Chakraborty K, Joseph D, Chakkalakal SJ (2014b). Toxicity profile of a nutraceutical formulation derived from green mussel *Perna viridis*. *BioMed Research International*, 2014, 14 pages Article ID 471565.
- Chakraborty K, Joseph D, Chakkalakal SJ (2014c). Seasonal and inter-annual lipid dynamics of spiny cheek grouper (*Epinephelus diacanthus*) in the southern coast of India. *Journal of the Marine Biological Association of the United Kingdom*, 94(8), 1677-1686.
- Chakraborty K, Joseph D, Joy M, Raola VK (2016d). Characterization of substituted aryl meroterpenoids from red seaweed *Hypnea musciformis* as potential antioxidants. *Food Chemistry*, 212, 778-788.
- Chakraborty K, Joseph D (2015). Inter-annual and seasonal dynamics of amino acid, mineral and vitamin composition of silver belly *Leiognathus splendens*. *Journal of the Marine Biological Association of the United Kingdom*, 95, 817-828.
- Chakraborty K, Joy M, Raola VK, Makkar F (2017a). Angiotensin-I converting enzyme inhibitory activities of common edible cephalopods and their antioxidative

- effects using different *in vitro* models. Journal of Food Biochemistry, 41(1), doi: 10.1111/jfbc.12268.
- Chakraborty K, Joy M, Vijayagopal, P (2016c). Nutritional qualities of common edible cephalopods at the Arabian Sea. International Food Research Journal, 23(5), 1926-1938.
- Chakraborty K, Joy M (2017). Anti-diabetic and anti-inflammatory activities of commonly available cephalopods. International Journal of Food Properties, 20(7), 1655-1665.
- Chakraborty K, Thilakan B, Chakraborty RD, Raola VK, Joy M (2017b). *O*-heterocyclic derivatives with antibacterial properties from marine bacterium *Bacillus subtilis* associated with seaweed, *Sargassum myriocystum*. Applied Microbiology and Biotechnology, 101, 569-583.
- Chakraborty K, Thilakan B, Raola VK, Joy M (2017c). Antibacterial polyketides from *Bacillus amyloliquefaciens* associated with edible red seaweed *Laurenciae papillosa*. Food Chemistry, 218, 427-434.
- Chakraborty K, Vijayan KK, Rao GS, Joseph D, Chakkalakal SJ (2012). A process to isolate anti-inflammatory principles from green mussel *Perna viridis* L. and to prepare a stabilized nutraceutical supplement against inflammatory disorders and a product thereof. Indian Patent Application number 5198/CHE/2012.
- Chandran B, Rameshkumar G, Ravichandran S (2009). Antimicrobial activity from the gill extraction of *Perna viridis* (Linnaeus, 1758). Global Journal of Biotechnology and Biochemistry, 4(2), 88-92.
- Chao CH, Wen ZH, Su JH, Chen IM, Huang HC, Dai CF, Sheu JH (2008). Further study on anti-inflammatory oxygenated steroids from the octocoral *Dendronephthya grifni*. Steroids, 73, 1353-1358.
- Chapman AD (2009). Numbers of living species in Australia and the world. 2nd ed. Australian Biological Resources Study. Canberra, Australia, pp. 31-34.
- Charlet M, Chernysh S, Philippe H, Hetru C, Hoffmann JA, Bulet P (1996). Isolation of several cysteine-rich antimicrobial peptides from the blood of a mollusc, *Mytilus edulis*. Journal of Biological Chemistry, 271(36), 21808-21813.
- Chatterji A, Ansari ZA, Ingole BS, Bichurina MA, Sovetova M, Boikov YA (2002). Indian marine bivalves: Potential source of antiviral drugs. Current Science, 82(10), 1279-1282.
- Chattopadhyay SK, Pattenden G (2000). A total synthesis of the unique tris-oxazole macrolide ulapualide A produced by the marine nudibranch *Hexabranhus sanguineus*. Journal of the Chemical Society Perkin Transactions 1, 2429-2454.
- Cheeseman KH, Slater TF (1993). An introduction to free radicals chemistry. British Medical Bulletin, 49, 481-93.
- Chellaram C, Edward JKP (2009). Anti-inflammatory potential of coral reef associated gastropod, *Drupa margaritcola*. Indian Journal of Science and Technology, 2, 75-77.

- Chen S, Wang J, Xue C, Li H, Sun B, Xue Y, Chai W (2010). Sulfation of a squid ink polysaccharide and its inhibitory effect on tumor cell metastasis. *Carbohydrate Polymers*, 81, 560-566.
- Chen Z, Liu J, Fu Z, Ye C, Zhang R, Song Y, Zhang Y, Li H, Ying H, Liu H (2014). 24(S)-Saringosterol from edible marine seaweed *Sargassum fusiforme* is a novel selective LXR β agonist. *Journal of Agricultural and Food Chemistry*, 62, 6130-6137.
- Chew YL, Lim YY, Omar M, Khoo KS (2008). Antioxidant activity of three edible seaweeds from two areas in southeast Asia. *LWT-Food Science and Technology*, 41, 6, 1067-1072.
- Chioccare F, Misuraca G, Novellino E, Prota G (1979). Occurrence of two new mycosporine-like aminoacids, mytilins A and B in the edible mussel, *Mytilus galloprovincialis*. *Tetrahedron Letters*, 20, 3181-3182.
- Choi JH, Kim KT, Kim SM (2015). Biofunctional properties of enzymatic squid meat hydrolysate. *Preventive Nutrition and Food Science*, 20(1), 67-72.
- Chou T, Kuramoto M, Otani Y, Shikano M, Yazawa K, Uemura D (1996). Pinnaic acid and tauropinnaic acid: Two novel fatty acids composing a 6-azaspiro[4.5]decane unit from the Okinawan bivalve *Pinna muricata*. *Tetrahedron Letters*, 37, 3871-3874.
- Ciavatta ML, Gresa MPL, Gavagnin M, Manzo E, Mollo E, D'Souza L, Cimino G (2006). New caulerpenyne-derived metabolites of an *Elysia sacoglossan* from the south Indian coast. *Molecules*, 11(10), 808-816.
- Ciavatta ML, Manzo E, Mollo E, Mattia CA, Tedesco C, Irace C, Guo Y-W, Li X-B, Cimino G, Gavagnin M (2011). Tritoniopsins A-D, cladiellane-based diterpenes from the South China Sea nudibranch *Tritoniopsis elegans* and its prey *Cladiella krempfi*. *Journal of Natural Products*, 74, 1902-1907.
- Ciavatta ML, Manzo E, Nuzzo G, Villani G, Cimino G, Cervera JL, Malaquias MAE, Gavagnin M (2009). Aplysiopsenes: An additional example of marine polyketides with a mixed acetate/propionate pathway. *Tetrahedron Letters*, 50, 527-529.
- Ciavatta ML, Trivellone E, Villani G, Cimino G (1993). Membrenones: New polypropionates from the skin of the mediterranean mollusc *Pleurobranchus membranaceus*. *Tetrahedron Letters*, 34, 6791-6794.
- Ciavatta ML, Villani G, Trivellone E, Cimino G (1995). Two new labdane aldehydes from the skin of the notaspidean *Pleurobranchaea meckelii*. *Tetrahedron Letters*, 36, 8673-8676.
- Ciminiello P, Dell'Aversano C, Fattorusso E, Forino M, Grauso L, Magno SG, Poletti R, Tartaglione L (2007a). Desulfoyessotoxins from Adriatic mussels: A new problem for seafood safety control. *Chemical Research in Toxicology*, 20(1), 95-98.
- Ciminiello P, Dell'Aversano C, Fattorusso E, Forino M, Grauso L, Santelia FU, Tartaglione L, Moutsos VI, Pitsinos EN, Couladouros EA (2007b).

- Stereostructural determination by a synthetic and NMR-based approach of three oxazinins isolated from Adriatic mussels. *European Journal of Organic Chemistry*, 2007, 5434-5439.
- Ciminiello P, Dell'Aversano C, Fattorusso E, Forino M, Magno S, Di Rosa M, Ianaro A, Poletti R (2002). Structure and stereochemistry of a new cytotoxic polychlorinated sulfolipid from Adriatic shellfish. *Journal of the American Chemical Society*, 124(44), 13114-13120.
- Ciminiello P, Dell'Aversano C, Fattorusso E, Forino M, Magno S, Di Meglio P, Ianaro A, Poletti R (2004). A new cytotoxic polychlorinated sulfolipid from contaminated Adriatic mussels. *Tetrahedron*, 60, 7093-7098.
- Ciminiello P, Dell'Aversano C, Fattorusso E, Forino M, Magno S, Ianaro A, Di Rosa M (2001). Oxazinins-1, -2 and -3 - A Novel toxic compound and its analogues from the digestive glands of *Mytilus galloprovincialis*. *European Journal of Organic Chemistry*, 2001(1), 49-53.
- Ciminiello P, Dell'Aversano C, Fattorusso E, Forino M, Magno S, Santelia FU, Moutsos VI, Pitsinos EN, Couladouros EA (2006). Oxazinins from toxic mussels: Isolation of a novel oxazinins and reassignment of the C-2 configuration of oxazinins-1 and -2 on the basis of synthetic models. *Tetrahedron*, 62 (33), 7738-7743.
- Ciminiello P, Fattorusso E, Forino M, Magno S, Poletti R, Viviani R (1998). Isolation of adriatoxin, a new analogue of yessotoxin from mussels of the Adriatic Sea. *Tetrahedron Letters*, 39, 8897-8900.
- Cimino G, Gavagnin M (2006). *Molluscs: Progress in molecular and subcellular biology subseries marine molecular biochemistry*, Springer-Verlag, Berlin, Heidelberg. pp. 387.
- Cimino G, Ghiselin MT (2001). *Marine natural products chemistry as an evolutionary narrative*. Eds. McKlinton JB, Baker BJ. *Marine Chemical Ecology*, CRC Press, Boca Raton. pp. 115-154.
- Clardy J, Walsh C (2004). Lessons from natural molecules. *Nature*, 432, 829-837.
- Clark KE, Capper A, Della Togna G, Paul VJ, Romero LI, Johns T, Cubilla-Rios L, Capson TL (2013). Ecology- and bioassay-guided drug discovery for treatments of tropical parasitic disease: 5 α ,8 α -epidioxycholest-6-en-3 β -ol isolated from the mollusk *Dolabrifera dolabrifera* shows significant activity against *Leishmania donovani*. *Natural Product Communications*, 8(11), 1537-1540.
- Cleland J, Bernstein S, Ezech A, Faundes A, Glasier A, Innis J (2006). Family planning: The unfinished agenda. *Lancet*, 18, 1810-1827.
- CMFRI Annual Report (2015-2016). Technical Report. CMFRI, Kochi.
- Cobb CS, Ernst E (2006). Systematic review of a marine nutraceutical supplement in clinical trials for arthritis: The effectiveness of the New Zealand green-lipped mussel *Perna canaliculus*. *Clinical Rheumatology*, 25(3), 275-284.

- Conforti F, Loizzo MR, Statti GA, Menichini F (2005). Comparative radical scavenging and anti-diabetic activities of methanolic extract and fractions from *Achillea ligustica*. *Biological and Pharmaceutical Bulletin*, 28, 1791-1794.
- Cooke IR, Whitelaw B, Norman M, Caruana N, Strugnell JM (2015). Toxicity in cephalopods. *In* *Evolution of venomous animals and their toxins*. Dordrecht: Springer-Verlag. pp. 1-15.
- Costa-Lotufo LV, Wilke DV, Jimenez PC, Epifanio RDA (2009). Marine organisms as a source of new pharmaceuticals, history and perspectives. *Quimica Nova*, 32(3), 703-716.
- Costantino V, Fattorusso E, Mangoni A, Perinu C, Cirino G, De Gruttola L, Roviezzo F (2009). Tedanol: a potent anti-inflammatory ent-pimarane diterpene from the Caribbean Sponge *Tedania ignis*. *Journal of Bioinorganic and Medicinal Chemistry*, 17, 542-7547.
- Coval SJ, Schulte GR, Matsumoto GK, Roll DM, Scheuer PJ (1985). Two polypropionate metabolites from the cephalaspidean mollusc *Philinopsis speciosa*. *Tetrahedron Letters*, 26, 5359-5362.
- Cueto M, D'Croz L, Mate JL, San-Martin A, Darias J (2005). Elysiapyrones from *Elysia diomedea*. Do such metabolites evidence an enzymatically assisted electrocyclization cascade for the biosynthesis of their bicyclo[4.2.0]octane Core? *Organic Letters*, 7, 415-418.
- Cueto M, Darias J, Roviroso J, San Martin A (1998a). Tetrahydropyran monoterpenes from *Plocamium cartilagineum* and *Pantoneura plocamioides*. *Journal of Natural Products*, 61, 1466-1468.
- Cueto M, Darias J, Roviroso J, San Martin A (1998b). Unusual polyoxygenated monoterpenes from the Antarctic alga *Pantoneura plocamioides*. *Journal of Natural Products*, 61, 17-21.
- Cueto M, Darias J (1996). Uncommon tetrahydrofuran monoterpenes from Antarctic *Pantoneura plocamioides*. *Tetrahedron*, 52, 5899-5906.
- Cutignano A, Avila C, Domenech-Coll A, d'Ippolito G, Cimino G, Fontana A (2008). First biosynthetic evidence on the phenyl-containing polyketides of the marine mollusc *Scaphander lignarius*. *Journal of Organic Letters*, 10, 2963-2966.
- Cutignano A, Blihoghe D, Fontana A, Villani G, d'Ippolito G, Cimino G (2007). Fusariapyrones, novel polypropionates from the Mediterranean mollusc *Haminoea fusari*. *Tetrahedron*, 63, 12935-12939.
- Cutignano A, Calado G, Gaspa H, Cimino G, Fontana A (2011). Polypropionates from *Bulla occidentalis*: Chemical markers and trophic relationships in cephalaspidean molluscs. *Tetrahedron Letters*, 52, 4595-4597.
- Cutignano A, Fontana A, Renzulli L, Cimino G (2003). Placidenes C-F, novel alpha-pyrone propionates from the Mediterranean sacoglossan *Placida dendritica*. *Journal of Natural Products*, 66, 1399-401.

- Cutignano A, Moles J, Avila C, Fontana A (2015). Granuloside, a unique linear homosesterterpene from the Antarctic nudibranch *Charcotia granulosa*. *Journal of Natural Products*, 78, 1761-1764.
- D'Auria MV, Minale L, Riccio R (1993). Polyoxygenated steroids of marine origin. *Journal of Chemical Reviews*, 93, 1839-1895.
- Daoust J, Fontana A, Merchant CE, de Voogd NJ, Patrick BO, Kieffer T J, Andersen R, Ansellone A (2010). A Sesterterpenoid Isolated from the Nudibranch *Cadlina luteromarginata* and the sponge *Phorbasp* sp., Activates the Camp Signaling Pathway. *Organic Letters*, 12, 3208-3211.
- Darias J, Roviroso J, San Martin A, Diaz AR, Dorta E, Cueto M (2001). Furoplacamoids A-C, novel polyhalogenated furanoid monoterpenes from *Plocamium cartilagineum*. *Journal of Natural Products*, 64, 1383-1387.
- Datta D, Talapatra SN, Swarnakar S (2015). Bioactive compounds from marine invertebrates for potential medicines - An overview. *International Letters of Natural Sciences*, 34, 42-61.
- Davies-Coleman MT, Garson MJ (1998). Marine polypropionates. *Journal of Natural Products Reports*, 15, 477-493.
- de Carvalho MG, Vellosoa CRX, Braz-Filho R, da Costa WF (2001). Acyl-lupeol esters from *Parahancornia amapa* (Apocynaceae). *Journal of Brazilian Chemical Society*, 12(4), 556-559.
- Derochette S, Mouithys-Mickalad A, Franck T, Collienne S, Ceusters J, Deby-Dupont G, Neven P, Serteyna D (2014). NDS27 combines the effect of curcumin lysinate and hydroxypropyl- β -cyclodextrin to inhibit equine PKC δ and NADPH oxidase involved in the oxidative burst of neutrophils. *FEBS Open Bio*, 4, 1021-1029.
- Di Marzo V, Vardaro RR, De Petrocellis L, Villani G, Minei R, Cimino G (1991). Cyercenes, novel pyrones from the ascoglossan mollusk *Cyerce cristallina*, Tissue distribution, biosynthesis and possible involvement in defense and regenerative processes. *Cellular and Molecular Life Sciences*, 47, 1221-1227.
- Dias T, Brito I, Moujir L, Paiz N, Darias J, Cueto M (2005). Cytotoxic Sesquiterpenes from *Aplysia dactylomela*. *Journal of Natural Products*, 68, 1677-1679.
- Diaz-Marrero AR, Dorta E, Cueto M, Roviroso J, San-Martin A, Loyola A (2003a). Labdane diterpenes with a new oxidation pattern from the marine pulmonate *Trimusculus peruvianus*. *Tetrahedron*, 59 (26), 4805-4809.
- Diaz-Marrero AR, Dorta E, Cueto M, Roviroso J, San-Martin A, Loyola A, Darias J (2003b). New polyhydroxylated steroids from the marine pulmonate *Trimusculus peruvianus*. *Archive for Organic Chemistry*, 10, 107-117.
- Diaz-Marrero AR, Porras G, Aragon Z, de la Rosa JM, Dorta E, Cueto M, D'Croz L, Juan M, Darias J (2011). Carijodienone from the Octocoral *Carijoa multiflora*. A spiropregnane-based steroid. *Journal of Natural Products*, 74(2), 292-295.

- Ding G, Qi Y, Liu S, Guo L, Chen X (2012). Photipyrones A and B, new pyrone derivatives from the plant endophytic fungus *Pestalotiopsis photiniae*. *Journal of Antibiotics*, 65, 271-273.
- Ding LJ, Gu B, Jiao W, Yuan W, Li Y, Tang W, Yu H, Liao X, Han B, Li Z, Xu S, Lin H (2015). New furan and cyclopentenone derivatives from the sponge-associated fungus *Hypocrea Koningii*. *Marine Drugs*, 13, 5579-5592.
- Diyabalanage T, Iken KB, McClintock JB, Amsler CD, Baker BJ (2010). Palmadorins A-C, Diterpene glycerides from the Antarctic nudibranch *Austrodoris kerguelenensis*. *Journal of Natural Products*, 73, 416-421.
- Edmonds JS, Francesconi KA, Healy PC, White AH (1982). Isolation and crystal structure of an arsenic-containing sugar sulphate from the kidney of the giant clam, *Tridacna maxima*. X-Ray crystal structure of (2S)-3-[5-deoxy-5-(dimethylarsinoyl)- β -D-ribofuranosyloxy]-2-hydroxypropyl hydrogen sulphate. *Journal of the Chemical Society Perkin Transactions*, 1, 2989-2993.
- Egan WJ, Lauri G (2002). Prediction of intestinal permeability. *Advanced Drug Delivery Reviews*, 54, 273-289.
- El-Beih AA, Kato H, Ohta T, Tsukamoto S (2007). (3R,4aR,5S,6R)-6-hydroxy-5-methyl ramulosin: A new ramulosin derivative from a marine-derived sterile Mycelium. *Chemical and Pharmaceutical Bulletin*, 55, 953-954.
- Ensminger AH, Ensminger ME, Konlande JE, Robson JRK (1995). *In Potassium*. The Concise Encyclopedia of Foods and Nutrition. CRC Press, London. 865-866.
- Escrig JA, Rincon M, Pulido R, Calixto SF (2001). Guava fruit (*Psidium guajava* L) as a new source of antioxidant dietary fibre. *Journal of Agricultural and Food Chemistry*, 49, 5489-5493.
- Estevez MS, Abele D, Puntarulo S (2002). Lipid radical generation in polar (*Laternula elliptica*) and temperate (*Mya arenaria*) bivalves. *Comparative Biochemistry and Physiology-B*, 132, 729-737.
- Fahmy SR, Soliman AM (2013). *In vitro* antioxidant, analgesic and cytotoxic activities of *Sepia officinalis* ink and *Coelatura aegyptiaca* extracts. *African Journal of Pharmacy and Pharmacology*, 7(22), 1512-1522.
- Fang H-Y, Hsu C-H, Chao C-H, Wen Z-H, Wu Y-C, Dai C-F, Sheu J-H (2013). Cytotoxic and anti-inflammatory metabolites from the soft coral *Scleronephthya gracillimum*. *Marine Drugs*, 11, 1853-1865.
- FAO, WHO, UNU 2007. Protein and amino acid requirements in human nutrition. Report of a Joint WHO/FAO/UNU Expert Consultation. Geneva, WHO. WHO Technical Report Series 935.
- FAO, WHO (1990). Report of the joint FAO/WHO expert consultation on protein quality evaluation. Bethesda, MD. FAO/WHO.
- FAO (2012). The state of world fisheries and aquaculture 2012. Food and agriculture organization of the United Nations.
- FAO (2014). The state of World fisheries and aquaculture opportunities and challenges. Rome. pp. 243.

- FAO (2015). Fishery statistical collections: Global capture production. Food and Agriculture Organization of the United Nations.
- Faulkner DJ (1999). Marine natural products. Natural Product Reports, 16, 155-198.
- Faulkner DJ (2000a). Marine natural products. Natural Product Reports, 17, 7-55.
- Faulkner DJ (2000b). Highlights of marine natural products chemistry (1972-1999). Natural Product Reports, 17, 1-6.
- Federov SN, Shubina LK, Kalinovsky AI, Lyakhova EG, Stonik VA (2000). Structure and absolute configuration of a new rearranged chamigrane-type sesquiterpenoid from the Sea hare *Aplysia sp.* Tetrahedron Letters, 41, 1979-1982.
- Fernandes E, Costa D, Toste SA, Lima JLFC, Reis S (2004). *In vitro* scavenging activity for reactive oxygen and nitrogen species by nonsteroidal anti-inflammatory indole, pyrrole, and oxazole derivative drugs. Free Radical Biology and Medicine Journal, 37, 1895-1905.
- Findlay JA, Li G (2002). Novel terpenoids from the Sea Hare *Aplysia punctata*. Canadian Journal of Chemistry, 80(12), 1697-1707.
- Fischedick JT, Pesic M, Podolski-Renic A, Bankovic J, de Vos RCH, Peric M, Todorovic S, Tanic N (2013). Cytotoxic activity of sesquiterpene lactones from *Inula britannica* on human cancer cell lines. Phytochemistry Letters, 6, 246-252.
- Folch J, Lees M, Stanley GHS (1957). A simple method for the isolation and purification of total lipids from animal tissues. Journal of Biological Chemistry, 226, 497-509.
- Fontana A, Avila C, Martinez E, Ortea J, Trivellone E, Cimino G (1993). Defensive allomones in three species of Hypselodoris (gastropoda: Nudibranchia) from the Cantabrian Sea. Journal of Chemical Ecology, 19(2), 339-356.
- Food and Nutrition Board (2007). Seafood choices balancing benefits and risks. Food and Nutrition Board, Institute of Medicine, National Academies Press, Washington, D.C.
- Francesconi KA, Stick RV, Edmonds JS (1991). An arsenic-containing nucleoside from the kidney of the giant clam, *Tridacna maxima*. Journal of the Chemical Society, Chemical Communications, 14, 928-929.
- Fu X, Hong EP, Schmitz FJ (2000). New polypropionate pyrones from the Philippine sacoglossan mollusc *Placobranchus ocellatus*. Tetrahedron, 56, 8989-8993.
- Fu X, Palomar AJ, Hong EP, Schmitz FJ, Valeriote FA (2004). Cytotoxic lissoclimide-type diterpenes from the molluscs *Pleurobranchus albiguttatus* and *Pleurobranchus forskalii*. Journal of Natural Products, 67, 1415-1418.
- Fujiwara Y, Maoka T, Ookubo M, Matsuno T (1992). Crassostreaxanthins A and B: Novel marine carotenoids from the oyster *Crassostrea gigas*. Tetrahedron Letters, 33, 4941-4944.
- Fung A, Hamid N, Lu J (2013). Fucoxanthin content and antioxidant properties of *Undaria Pinnatifida*. Food Chemistry, 136(2), 1055-1062.

- Gaspar H, Gavagnin M, Calado G, Castelluccio F, Mollo E, Cimino G (2005). Pelseneeriol-1 and -2: New furanosesquiterpene alcohols from porostome nudibranch *Doriopsilla pelseneeri*. *Tetrahedron*, 61, 11032-11037.
- Gaspar H, Santos S, Carbone M, Rodrigues AS, Rodrigues AI, Uriz MJ, Feio SMS, Melck D, Humanes M, Gavagnin M (2008). Isomeric furanosesquiterpenes from the Portuguese marine sponge *Fasciospongia* sp. *Journal of Natural Products*, 71, 2049-2052.
- Gavagnin M, Carbone M, Mollo E, Cimino G (2003a). Further chemical studies on the Antarctic nudibranch *Austrodoris kerguelensis*: New terpenoid acylglycerols and revision of the previous stereochemistry, *Tetrahedron*, 59, 5579-5583.
- Gavagnin M, Carbone M, Mollo E, Cimino G (2003b). Austrodoral and austrodoric acid: Nor-sesquiterpenes with a new carbon skeleton from the Antarctic nudibranch *Austrodoris kerguelensis*. *Tetrahedron letters*, 44 (7), 1495-1498.
- Gavagnin M, Carbone M, Nappo M, Mollo E, Roussis V, Cimino G (2005). First chemical study of anaspidean *Syphonota geographica*: Structure of degraded sterols aplykurodinone -1 and -2. *Tetrahedron*, 61 (3), 617-621.
- Gavagnin M, Mollo E, Castelluccio F, Montanaro D, Ortea J, Cimino G (1997). A novel dietary sesquiterpene from the marine sacoglossan *Tridachia crispata*. *Journal of Natural Products*, 10(2), 151-156.
- Gavagnin M, Mollo E, Cimino G, Ortea J (1996). A new γ -dihydropyrone-propionate from the Caribbean sacoglossan *Tridachia crispata*. *Tetrahedron letters*, 37 (24), 4259-4262.
- Gavagnin M, Mollo E, Docimo T, Guo Y-W, Cimino G (2004). Scalarane metabolites of the nudibranch *Glossodoris rufomarginata* and its dietary sponge from the south China Sea. *Journal of Natural Products*, 67, 2104-2107.
- Gavagnin M, Mollo E, Montanaro D (2000). Chemical studies of Caribbean sacoglossans: Dietary relationships with green algae and ecological implications. *Journal of Chemical Ecology*, 26, 1563-1578.
- Gavagnin M, Ungur N, Mollo E, Templado J, Cimino G (2002). Structure and synthesis of a progesterone homologue from the skin of the Dorid Nudibranch *Aldisa smaragdina*. *European Journal of Organic Chemistry*, 9, 1500-1504.
- Giugliano D, Ceriello A, Paolisso G (1995). Diabetes mellitus, hypertension, and cardiovascular disease, which role for oxidative stress? *Metabolism*, 44 (3), 363-368.
- Goad LJ, Akihisa T (1997). Analysis of sterols. Blackie Academic and Professional, London. Chapman & Hall, 2-6 Boundary Row.
- Goad LJ, Scheuer PJ (1978). Marine natural products. Academic Press, New York. 2, pp. 76-172.
- Goel A, Ram VJ (2009). Natural and synthetic 2H-pyran-2-ones and their versatility in organic synthesis. *Tetrahedron*, 65, 7865-7913.
- Goldberg ED (1975). The mussel watch: A first step in global marine monitoring. *Marine Pollution Bulletin*, 6, 111-132.

- Gonzalez PM, Malanga G, Puntarulo S (2015). Cellular oxidant antioxidant network: Update on the environmental effects over marine organisms. *The Open Marine Biology Journal*, 9, 1-13.
- Gopalakrishnan S, Vijayavel K (2009). Nutritional composition of three estuarine bivalve mussels, *Perna viridis*, *Donax cuneatus* and *Meretrix meretrix*. *International Journal of Food Science and Technology*, 60 (6), 458-63.
- Gosling E (2002). Bivalve mollusks, biology, ecology and culture. Fishing News Books. Blackwell Publishing, UK. pp. 443.
- Gosling E (2015). Phylogeny and evolution of bivalve molluscs. *In* Marine bivalve molluscs. 2nd ed. John Wiley & Sons, Ltd., Chichester, UK. Chapter 1.
- Govindam SVS, Yoshioka Y, Kanamoto A, Fujiwara T, Okamoto T, Ojika M (2012). Cyclolobatriene, a novel prenylated germacrene diterpene, from the soft coral *Lobophytum pauciflorum*. *Bioorganic and Medicinal Chemistry Journal*, 20, 687-692.
- Govindarajulu J, Anand M, Chelladurai G, Kumaraguru A (2016). Bioactive potential of some economically important marine gastropods along the Gulf of Mannar region, southeast coast of India. *Journal of Coastal Life Medicine*, 4(8), 608-611.
- Gulcin I (2007). Comparison of *in vitro* antioxidant and anti-radical activities of L-tyrosine and L-dopa. *Amino Acids*, 32, 431-438.
- Hadacek F, Bachmann G (2015). Low-molecular-weight metabolite systems chemistry. *Frontiers in environmental science*, 3 (12), 1-21.
- Halliwell B, Gutteridge JMC (2006). Free radicals in biology and medicine. 4th ed. Clarendon Press, Oxford, New York.
- Halliwell B (2007). Biochemistry of oxidative stress. *Biochemical Society Transactions*, 35, 1147-1150.
- Hamann MT, Scheuer PJ, Kahalide F (1993). A Bioactive Depsipeptide from the Sacoglossan Mollusk *Elisia refescens* and the Green Alga *Byopsis* sp. *Journal of the American Chemical Society*, 115, 5825-5826.
- Hamdan II, Afifi FU (2004). Studies on the *in vitro* and *in vivo* hypoglycemic activities of some medicinal plants used in treatment of diabetes in Jordanian traditional medicine. *Journal of Ethnopharmacology*, 93, 117-121.
- Hamed I, Ozogul F, Ozogul Y, Regenstein JM (2015). Marine bioactive compounds and their health benefits: A review. *Comprehensive Reviews in Food Science and Food Safety*, 14.
- Han TS, Teichert RW, Olivera BM, Bulaj G (2008). Conus venoms-a rich source of peptide-based therapeutics. *Current Pharmaceutical Design*, 14, 2462-2479.
- Herbert DG, Hamer ML, Mander M, Mkhize N, Prins F (2003). Invertebrate animals as a component of the traditional medicine trade in KwaZulu-Natal, South Africa. *African Invertebrates*, 44, 327-344.
- Heslinga GA (1989). Biology and culture of the giant clam. *In* clam mariculture in North America. Eds. Manzi JJ, Castagna M. Elsevier Science Publishing Company Inc., New York. pp. 293-322.

- HMSO (2001). Nutritional aspects of cardiovascular disease: Report on health and social subjects. Department of health, London. 37-46.
- Hochlowski JE, Coll JC, Faulkner DJ, Biskupiak JE, Ireland CM, Zheng Q-T, He C-H, Clardy J (1984). Novel metabolites of four Siphonaria species. Journal of the American Chemical Society, 106, 6748-6750.
- Hochlowski JE, Faulkner DJ, Matsumoto GK, Clardy J (1983). Norrisolide, a novel diterpene from the dorid nudibranch *Chromodoris norrisi*. The Journal of Organic Chemistry, 48, 1141-1142.
- Hodzic Z, Pasalic H, Memisevic A, Scrabovic M, Saletovic M, Poljakovic M (2009). The influence of total phenols content on antioxidant capacity in the whole grain extracts. European Journal of Scientific Research, 28, 471-477.
- Holmquist B, Bunning P, Riordan JF (1979). A continuous spectrophotometric assay for angiotensin converting enzyme. Journal of Analytical Biochemistry, 95, 540-548.
- Hooper C, Day R, Slocombe R, Handler J, Benkendorff K (2007). Stress and immune responses in abalone: Limitations in current knowledge and investigative methods based on other models. Fish and Shellfish Immunology, 22, 363-379.
- Hu T, Curtis JM, Oshima Y, Quilliam MA, Walter JA, Watson-Wright WM, Wright JLC (1995). Spirolides B and D, two novel macrocycles isolated from the digestive glands of shellfish. Journal of the Chemical Society, Chemical Communications, 21, 2159-2161.
- Hu T, Curtis JM, Walter JA, Wright JLC (1996). Characterization of biologically inactive spirolides E and F: Identification of the spirolide pharmacophore. Tetrahedron Letters, 37, 7671-7674.
- Huang S-C, Kuo P-C, Hung H-Y, Pan T-L, Chen F-A, Wu T-S (2016). Ionone derivatives from the mycelium of *Phellinus linteus* and the inhibitory effect on activated rat hepatic stellate cells. International Journal of Molecular Sciences, 17, 681.
- Huang SZ, Ma QY, Fang WW, Xu FQ, Peng H, Dai HF, Zhou J, Zhao YX (2013). Three new isopimarane diterpenoids from *Excoecaria acerifolia*. Journal of Asian Natural Products Research, 15, 750-755.
- Huang X, Deng Z, Zhu X, van Ofwegen L, Proksch P, Lin W (2006). Krempenes A-D: A series of unprecedented pregnane-type steroids from the marine soft coral *Cladiella krempfi*. Helvetica Chimica Acta, 89(9), 2020-2026.
- Huang X-C, Li J, Li Z-Y, Shi L, Guo Y-W (2008). Sesquiterpenes from the Hainan Sponge *Dysidea septosa*. Journal of Natural Products, 71, 1399-1403.
- Huang ZH, Chen YX, Zhao Y, Zuo ZH, Chen M (2005). Antioxidant responses in *Meretrix meretrix* exposed to environmentally relevant doses of tributyltin. Environmental Toxicology and Pharmacology, 20(1), 107-111.

- Huber M (2010). Compendium of bivalves. A full-color guide to 3300 of the World's marine bivalves. A status on bivalvia after 250 years of research. Conch Books, Hackenheim.
- Huong DT, Kamperdick C, Sung TV (2004). Homogentisic acid derivatives from *Miliusa balansae*. Journal of Natural Products, 67, 445-447.
- Imai T, Sakai S (1961). Study on the breeding of the Japanese oyster, *Crassostrea gigas*. Tohoku Journal of Agricultural Research, 12, 125-171.
- Ioannou E, Nappo M, Avila C, Vagias C, Roussis V (2009). Metabolites from the Sea hare *Aplysia fasciata*. Journal of Natural Products, 72, 1716-1719.
- Iqbal K, Khan A, Khattak MMAK (2004). Biological significance of ascorbic acid (vitamin C) in human health - A review. Pakistan Journal of Nutrition, 3(1), 5-13.
- Ishida H, Nozawa A, Hamano H, Naoki H, Fujita T, Kaspar HF, Tsuji K (2004). Brevetoxin B5, a new brevetoxin analog isolated from cockle *Austrovenus stutchburyi* in New Zealand, the marker for monitoring shellfish neurotoxicity. Tetrahedron Letters, 45, 29-33.
- Ishige K, Schubert D, Sagara Y (2001). Flavonoids protect neuronal cells from oxidative stress by three distinct mechanisms. Free Radical Biology and Medicine, 30(4), 433-446.
- Ito S, Nardi G, Prota G (1976). Structure of aldenochromines A and B, the iron (III) binding amino-acids of a unique group of peptides, adenochromes from *Octopus vulgaris*. Journal of the Chemical Society, Chemical Communications, 24, 1042-1043.
- Iwakoshi E, Hisada M, Minakata H (2000). Cardioactive peptides isolated from the brain of a Japanese octopus, *Octopus minor*. Peptides, 21(5), 623-630.
- James KJ, Sierra MD, Lehane M, Magdalena AB, Furey A. (2003). Detection of five new hydroxyl analogues of azaspiracids in shellfish using multiple tandem mass spectrometry. Toxicon, 41, 277.
- Jeevitha M, Athiperumalsami T, Kumar V (2013). Dietary fibre, mineral, vitamin, amino acid and fatty acid content of seagrasses from Tuticorin Bay, southeast coast of India. Phytochemistry, 90, 135-146.
- Jena KB, Jagtap TG, Verlecar XN (2010). Antioxidative potential of *Perna viridis* and its protective role against ROS induced lipid peroxidation and protein carbonyl. Current Trends in Biotechnology and Pharmacy, 4, 862-870.
- Jin Q, Lee JW, Jang H, Choi JE, Lee D, Hong JT, Kim Y, Lee MK, Hwang BY (2016). Sesquiterpenes from *Inula japonica* with inhibitory effects on nitric oxide production in murine macrophage RAW 264.7 Cells. Journal of Natural Products, 79(6), 1548-1553.
- Joosse J (1978) Endocrinology of molluscs. Actualites sur les Hormones d'Invertebres. Colloques Internationaux CNRS, 251, 107-123.

- Kaiser AR, Pitombo LF, Pinto AC (2001). Complete ^1H and ^{13}C NMR assignments of chamigrenes from *Aplysia dactilomela*. *Magnetic resonance in chemistry*, 39, 147-149.
- Kamio M, Kicklighter CE, Nguyen L, Germann MW, Derby CD (2011). Isolation and structural elucidation of novel mycosporine-like amino acids as alarm cues in the defensive ink secretion of the Sea hare *Aplysia californica*. *Helvetica Chimica Acta*, 94, 1012-1018.
- Kanda A, Minakata H (2006). Isolation and characterization of a novel small cardioactive peptide-related peptide from the brain of *Octopus vulgaris*. *Peptides*, 27(7), 1755-1761.
- Kanofsky JR (1986). Catalysis of singlet oxygen production in the reaction of hydrogen peroxide and hypochlorous acid by 1,4-diazabicyclo[2.2.2]octane (DABCO). *Biochemical and Biophysical Research Communications*, 134, 777-782.
- Kanofsky JR (1989). Singlet oxygen production by biological systems. *Chemico-Biological Interactions*, 70, 1-28.
- Karawita R, Siriwardhana N, Lee KW, Heo MS, Yeo IK, Lee YD, Jeon YJ (2004). Reactive oxygen species scavenging, metal chelating, reducing power and lipid peroxidation inhibition properties of different solvent fractions from *Hizikia fusiformis*. *European Food Research and Technology Journal*, 220, 363-371.
- Karthigayan S, Sri Balasubashini M, Sengottuvelan M, Balasubramanian T, Somasundaram ST (2006). Anticancer principles from salivary gland extract of *Octopus agcina*. *International Journal of Cancer Research*, 2, 242-252.
- Kaviarasan T, Sankar RS, Yogamoorthi A (2011). Studies in ultra structure of egg capsule wall of snails using scanning electron microscope. *Journal of Coastal Environment*, 2(2), 143-50.
- Kawashima H, Ohnishi M, Ogawa S (2013). Distribution of unusual cholesterol precursors, 4-methyl and 4,4-dimethylsterols with δ^8 unsaturation in gonads of marine archaeogastropods. *Journal of Oleo Science*, 62, 465-470.
- Khan AL, Ali L, Hussain J, Rizvi TS, Al-Harrasi A, Lee IJ (2015). Enzyme inhibitory radicicol derivative from endophytic fungus *Bipolaris sorokiniana* LK12, associated with *Rhazya stricta*. *Molecules*, 20, 12198-12208.
- Khlebnikov AI, Schepetkin IA, Domina NG, Kirpotina LN, Quinn MT (2007). Improved quantitative structure-activity relationship models to predict antioxidant activity of flavonoids in chemical, enzymatic, and cellular systems. *Bioorganic & Medicinal Chemistry*, 15, 1749-1770.
- Kiem PV, Nhiem NX, Quang NV, Minh CV, Nam NH, Cuc NT, Anh HLT, Tai BH, Yen PH, Cuong NX, Thao NP, Hoai NT, Kim NY, Park SJ, Hyun KS (2013). New butenolide and pentenolide from *Dysidea cinerea*. *Natural Product Communication*, 8(12), 1751-1752.
- Kigoshi H, Itoh T, Ogawa T, Ochi K, Okada M, Suenaga K, Yamada K (2001). Stereoselective synthesis of pinnamine, an alkaloidal marine toxin from *Pinna muricata*. *Tetrahedron Letters*, 42, 7461-7471.

- Kilcoyne J, Twiner MJ, McCarron P, Crain S, Giddings SD, Foley B, Rise F, Hess P, Wilkinsand AL, Miles CO (2015). Structure elucidation, relative LC-MS response and *in vitro* toxicity of azaspiracids 7-10 isolated from mussels (*Mytilus edulis*). Journal of Agricultural and Food Chemistry, 63(20), 5083-5091.
- Kim E-K, Hwang J-W, Kim Y-S, Ahn C-B, Jeon Y-J, Kweon HJ, Bahk YY, Moon S-H, Jeon B-T, Park P-J (2013). A novel bioactive peptide derived from enzymatic hydrolysis of *Ruditapes philippinarum*: Purification and investigation of its free-radical quenching potential. Process Biochemistry, 48, 325-330.
- Kim H, Elvitigala DAS, Lee Y, Lee S, WhangI, Lee J (2012). Ferritin H-like subunit from Manila clam (*Ruditapes philippinarum*): Molecular insights as a potent player in host antibacterial defense. Fish and Shellfish Immunology, 3, 926-936.
- Kim HL, Kang SG, Kim IC, Kim SJ, Kim DW, Ma SJ, Gao T, Li H, Kim MU, Lee TH (2006). *In vitro* anti-hypertensive, antioxidant and anticoagulant activities of extracts from *Haliotis discus hannai*. Journal of the Korean Society of Food Science and Nutrition, 35, 835-840.
- Kim JD, Lall SP (2000). Amino acid composition of wholebody tissue of Atlantic halibut (*Hippoglossus hippoglossus*), yellowtail flounder (*Pleuronectes ferruginea*) and Japanese flounder (*Paralichthys olivaceus*). Aquaculture, 187(3-4), 367-373.
- Kim Y, Ogura H, Akasaka K, Oikawa T, Matsuura N, Imada C, Yasuda H, Igarashi Y (2014). Nocapyrones: α - and γ -pyrones from a marine-derived *Nocardiopsis* sp. Marine Drugs, 12, 4110-4125.
- Kindleysides S, Quek SY, Miller MR (2012). Inhibition of fish oil oxidation and the radical scavenging activity of New Zealand seaweed extracts. Food Chemistry, 133, 1624-1631.
- Kohen R, Nyska A (2002). Oxidation of biological systems Oxidative stress phenomena, antioxidants, redox reactions, and methods for their quantification. Toxicologic Pathology, 30(6), 620-650.
- Kojima K, Ham T, Kato T (1980). Rapid chromatographic purification of dipeptidyl peptidase-IV in human submaxillary gland. Journal of Chromatography, 189, 233-240.
- Kornprobst J-M (2010). Encyclopedia of marine natural products. Wiley-Blackwell, 1.
- Kraffe E, Soudant P, Marty Y, Kervarec N (2005). Docohexaenoic acid and eicosapentaenoic acid enriched cardiolipin in the manila clam *Ruditapes philippinarum*. Lipids, 40, 619-624.
- Kreuzer R (1984). Cephalopods: Handling, processing and products. Fisheries Technical Paper No. 254, FAO, Italy, Rome. pp. 108.
- Kulisic T, Radonic A, Katalinic V, Milos M (2004). Use of different methods for testing antioxidative activity of oregano essential oil. Food Chemistry, 85, 633-640.

- Kuo C-Y, Juan Y-S, Lu M-C, Chiang MY-N, Dai C-F, Wu Y-C, Sung P-J (2014). Pregnane-type steroids from the formosan soft coral *Scleronephthya flexilis*. *International Journal of Molecular Sciences*, 15, 10136-10149.
- Lacy F, Kailasam MT, O'Connor DT, Schmid-Schonbein GW, Parmer RJ (2000). Plasma hydrogen peroxide production in human essential hypertension: Role of heredity, gender, and ethnicity. *Journal of Hypertension*, 36(5), 878-884.
- Lah R, Smith J, Savins D, Dowell A, Bucher D, Benkendorff K (2017). Investigation of nutritional properties of three species of marine turban snails for human consumption. *Food Science and Nutrition*, 5(1), 14-30.
- Laneuville O, Breuer DK, DeWitt DL, Hla T, Funck CD, Smith WL (1994). Differential inhibition of human prostaglandin endoperoxide H synthases-1 and -2 by nonsteroidal anti-inflammatory drugs. *Journal of Pharmacology and Experimental Therapeutics*, 271, 927-934.
- Larsen LN, Dahl E, Bremer J (1996). Peroxidative oxidation of leuco dichlorofluorescein by prostaglandin H synthase in prostaglandin biosynthesis from polyunsaturated fatty acids. *BBA Molecular and Cell Biology of Lipids*, 1299(1), 47-53.
- Lee CG, Kwon HK, Ryu JH, Kang SJ, Im CR, Kim JI, Im SH (2010). Abalone visceral extract inhibit tumor growth and metastasis by modulating COX-2 levels and CD8 β T cell activity. *BMC Complementary and Alternative Medicine*, 10, 60.
- Lee PG (1995). Nutrition of cephalopods: Fuelling the system. *Marine and Fresh Water Behaviour and Physiology*, 25, 35-51.
- Leiva GE, Castilla JC (2002). A review of the world marine gastropod fishery: Evolution of catches, management and the Chilean experience. *Reviews in Fish Biology and Fisheries*, 11, 283-300.
- Levander OA, Burk RF (1994). In *Selenium*. Eds. Ziegler EE, Filer JJ. Present knowledge in nutrition. 7th ed. ILSI Press, Washington, D.C. pp. 320-328.
- Li C, Yang B, Fenstemacher R, Turkson J, Cao S (2015). Lycopodiellactone, an unusual d-lactone-isochromanone from Hawaiian plant-associated fungus *Paraphaeosphaeria neglecta* FT462. *Tetrahedron Letters*, 56, 1724-1727.
- Li D, Sinclair AJ (2002). Macronutrient innovations: The role of fats and sterols in human health. *Asia Pacific Journal of Clinical Nutrition*, 11(S6), S155-S162.
- Li W, Li X-B, Li L, Li R-J, Lou H-X (2015a). α -Pyrone derivatives from the endolichenic fungus *Nectria* sp. *Phytochemistry Letters*, 12, 22-26.
- Lima TC, Santos ADC, Costa DTM, Souza RJ, Barison A, Steindel M, Biavattia MW (2015). Chromenes from leaves of *Calea pinnatifida* and evaluation of their leishmanicidal activity. *Revista Brasileira de Farmacognosia*, 25(1), 7-10.
- Lin L, Lv S, Li B (2012). Angiotensin-I-converting enzyme (ACE)-inhibitory and antihypertensive properties of squid skin gelatin hydrolysates. *Food Chemistry*, 131(1), 225-230.

- Lin T, Wang GH, Lin X, Hu ZY, Chen QC, Xu Y, Zhang ZK, Chen HF (2011). Three new oblongolides from *Phomopsis* sp. XZ-01 and endophytic fungus from *Camptotheca acuminata*. *Molecules*, 16, 3351-3359.
- Lindsay RC (1996). Food additives. In *Food Chemistry*. Eds. Fennema OR. Marcel Dekker, Inc., New York. 12, pp. 778-780.
- Lin-rui C, Qing L, Zhen-Xing S, Yu-Chao Y, Lin S (2012). Antioxidant and antibacterial activities of polysaccharides from Chinese surf clam (*Mactra chinensis*). *Food Science*, 33(7), 101-104.
- Lipinski B (2001). Pathophysiology of oxidative stress in diabetes mellitus. *Journal of Diabetes and its Complications*, 15 (4), 203-210.
- Lipinski C, Hopkins A (2004). Navigating chemical space for biology and medicine. *Nature*, 432, 855-861.
- Lipinski CA (2000). Drug-like properties and the causes of poor solubility and poor permeability. *Journal of Pharmacological and Toxicological Methods*, 44, 235-249.
- Liu H, Yin L, Board PG, Han X (2012). Expression of selenocysteine-containing glutathione S-transferase in eukaryote. *Protein Expression and Purification*, 84(1), 59-63.
- Liu H, Zhang H, Zheng H, Wang S, Guo Z, Zhang G (2014). PUFA biosynthesis pathway in marine scallop *Chlamys nobilis* Reeve. *Journal of Agricultural and Food Chemistry*, 62, 12384-12391.
- Lopez-Macia A, Jimenez JC, Royo M, Giralt E, Albericio F (2001). Synthesis and structure determination of Kahalalide F^{1,2}. *Journal of the American Chemical Society*, 123, 11398-11401.
- Lordan S, Ross RP, Stanton C (2011). Marine bioactives as functional food ingredients: Potential to reduce the incidence of chronic diseases. *Marine Drugs*, 9(6), 1056-1100.
- Lowry OH, Rosebrough NJ, Farr AL, Randall RJ (1951). Protein measurement with the Folin phenol reagent. *Journal of Biological Chemistry*, 193, 265-275.
- Luan H, Wang L, Wu H, Jin Y, Ji J (2011). Antioxidant activities and antioxidative components in the surf clam, *Mactra veneriformis*. *Natural Product Research*, 25(19), 1838-1848.
- Luppi E, Cesaretti M, Volpi N (2005). Purification and characterization of heparin from the Italian clam *Callista chione*. *Biomacromolecules*, 6, 1672-1678.
- Lushchak VI (2011). Environmentally induced oxidative stress in aquatic animals. *Aquatic Toxicology*, 101(1), 13-30.
- Ma GX, Yin L, Wang TS, Pan Y, Guo LW (1998). A 19-carbon pimarane-type diterpenoid from *Ephemerantha fimbriata*. *Pharmaceutical Biology*, 36, 66-68.
- Macielag MJ (2011). Chemical properties of antimicrobials and their uniqueness. In *Antibiotic discovery and development*. Eds. Dougherty TJ, Pucci MJ. Springer, New York. pp. 793-820.

- Manker DC, Faulkner DJ (1987). Diterpenes from the marine pulmonate *Trimusculus reticulatus*. *Tetrahedron*, 43, 3677-3680.
- Manning Jr RD, Tian N, Meng S (2005). Oxidative stress and antioxidant treatment in hypertension and the associated renal damage. *American Journal of Nephrology*, 25(4), 311-317.
- Manzo E, Ciavatta ML, Gavagnin M, Mollo E, Wahidulla S, Cimino G (2005a). New γ -pyrone propionates from the Indian Ocean sacoglossan *Placobranchus ocellatus*. *Tetrahedron Letters*, 46, 465-468.
- Manzo E, Ciavatta ML, Gavagnin M, Puliti R, Mollo E, Guo Y-W, Mattia CA, Mazzarella L, Cimino G (2005b). Structure and absolute stereochemistry of novel C-15 halogenated acetogenins from the anaspidean mollusc *Aplysia dactylomela*. *Tetrahedron*, 61(31), 7456-7460.
- Manzo E, Ciavatta ML, Gavagnin M, Mollo E, Guo Y-W, Cimino G (2004). Isocyanide terpene metabolites of *Phyllidiella pustulosa*, a nudibranch from the South China Sea. *Journal of Natural Products*, 67(10), 1701-4.
- Manzo E, Gavagnin M, Bifulco G, Cimino P, Di Micco S, Ciavatta ML, Guo YW, Cimino G (2007a). Aplysiols A and B, squalene-derived polyethers from the mantle of the Sea hare *Aplysia dactylomela*. *Tetrahedron*, 63, 9970-9978.
- Manzo E, Gavagnin M, Somerville MJ, Mao S-C, Ciavatta ML, Mollo E, Schupp PJ, Garson MJ, Guo Y-W, Cimino G (2007b). Chemistry of Glossodoris nudibranchs: Specific occurrence of 12-keto scalaranes. *Journal of Chemical Ecology*, 33(12), 2325-2336.
- Mao S-C, Gavagnin M, Mollo E, Guo Y-W (2011). A new rare asteriscane sesquiterpene and other related derivatives from the Hainan aeolid nudibranch *Phyllodesmium magnum*. *Biochemical Systematics and Ecology*, 39, 408-411.
- Maoka T, Akimoto N, Murakoshi M, Sugiyama K, Nishino H (2010). Carotenoids in clams, *Ruditapes philippinarum* and *Meretrix petechialis*. *Journal of Agricultural and Food Chemistry*, 58, 5784-5788.
- Maoka T, Akimoto N, Yim M-J, Hosokawa M, Miyashita K (2008). A new C37-skeletal carotenoid from the clam, *Paphia amabilis*. *Journal of Agricultural and Food Chemistry*, 56, 12069-12072.
- Maoka T, Etoh T, Borodina AV, Soldatov AA (2011). A series of 19'-hexanoyl oxyfucoxanthin derivatives from the Sea mussel, *Mytilus galloprovincialis*, grown in the black Sea, Ukraine. *Journal of Agricultural and Food Chemistry*, 59, 13059-13064.
- Maoka T, Fujiwara Y, Hashimoto K, Akimoto N (2005a). Carotenoids in three species of corbicula clams, *Corbicula japonica*, *Corbicula sandai*, and *Corbicula* sp. (Chinese freshwater corbicula clam). *Journal of Agricultural and Food Chemistry*, 53(21), 8357-8364.
- Maoka T, Fujiwara Y, Hashimoto K, Akimoto N (2005b). Structures of new carotenoids with a 3,4-dihydroxy- β -end group from the oyster *Crassostrea gigas*. *Chemical and Pharmaceutical Bulletin*, 53, 1207-1209.

- Maoka T, Fujiwara Y, Hashimoto K, Akimoto N (2007). Characterization of fucoxanthin and fucoxanthinol esters in the Chinese surf clam, *Macra chinensis*. *Journal of Agricultural and Food Chemistry*, 55(4), 1563-1567.
- Maoka T, Hashimoto K, Akimoto N, Fujiwara Y (2001). Structures of five new carotenoids from the oyster *Crassostrea gigas*. *Journal of Natural Products*, 64, 578-581.
- Maoka T, Yokoi S, Matsuno T (1989). Comparative biochemical studies of carotenoids in nine species of Cephalopoda. *Comparative Biochemistry and Physiology-B*, 92(2), 247-250.
- Maoka T (1997). A new apocarotenoid from marine shellfish *Mytilus coruscus*. *Journal of Natural Products*, 60(6), 616-617.
- Martel-Pelletier J, Lajeunesse D, Reboul P, Pelletier J (2003). Therapeutic role of dual inhibitors of 5-LOX and COX, selective and nonselective non-steroidal anti-inflammatory drugs. *Annals of the Rheumatic Diseases*, 62(6), 501-509.
- Mates JM, Perez-Gomez C, De Castro IN (1999). Antioxidant enzymes and human diseases. *Clinical Biochemistry*, 32, 595-603.
- Mathy-Hartert M, Deby-Dupont GP, Reginster JY, Ayache N, Pujol JP, Henrotin YE (2002). Regulation by reactive oxygen species of interleukin-1 beta, nitric oxide and prostaglandin E(2) production by human chondrocytes. *Osteoarthritis and Cartilage*, 10, 547-55.
- Matsunaga S, Fusetani N, Hashimoto K, Koseki K, Noma M, Noguchi H, Sankawa U (1989). Bioactive marine metabolites. 25. Further kabiramides and halichondramides, cytotoxic macrolides embracing trisoxazole, from the Hexabanchus egg masses. *The Journal of Organic Chemistry*, 54, 1360-1363.
- Matsuno T (2001). Aquatic animal carotenoids. *Fisheries Science*, 67, 771-783.
- McCall MR, Frei B (1999). Can antioxidant vitamins materially reduce oxidative damage in humans? *Free Radical Biology and Medicine*, 26, 1034-53.
- McCarron P, Rourke WA, William H, Pooley B, Quilliam MA (2012). Identification of pinnatoxins and discovery of their fatty acid ester metabolites in mussels (*Mytilus edulis*) from eastern Canada. *Journal of Agricultural and Food Chemistry*, 60 (6), 1437-1446.
- McClintock JB, Baker BJ (2001). *Marine chemical ecology*, CRC Press, New York.
- McPhail KL, Davies-Coleman MT, Starmer J (2001). Sequestered chemistry of the Arminacean nudibranch *Leminda millecra* in Algoa Bay, South Africa. *Journal of Natural Products*, 64, 1183-1190.
- McPhail KL, Davies-Coleman MT (2005). (3Z)-Bromofucin from a South African Sea hare. *Natural Product Research*, 19(5), 449-452.
- McPhee S, Hodges LD, Wright PF, Wynne PM, Kalafatis N, Harney DW, Macrides TA (2007). Anti-cyclooxygenase effects of lipid extracts from the New Zealand green-lipped mussel, *Perna canaliculus*. *Comparative Biochemistry and Physiology-B: Biochemistry and Molecular Biology*, 146(3), 346-356.

- Metcalf LD, Schimtz AA, Pleka JR (1966). Rapid preparation of fatty acid esters from lipids for gas chromatographic analyses. *Analytical Chemistry*, 38, 514-515.
- Milan M, Mirjana M, Desanka B, Sanja M, Neda N, Vladimir M, Vukovic N, Sukdolak S, Solujic S (2011). *In vitro* antioxidant of selected 4-hydroxy-chromene-2-one derivatives-SAR, QSAR and DFT studies. *International Journal of Molecular Sciences*, 12(5), 2822-2841.
- Miliou H, Fintikaki M, Tzitzinakis M, Kountouris T, Verriopoulos G (2006). Fatty acid composition of the common octopus, *Octopus vulgaris*, in relation to rearing temperature and body weight. *Aquaculture*, 256, 311-322.
- Mirshahi M, Mirshahi P, Negro S, Soria J, Sreekumar PK, Kotnala S, Therwath A, Chatterji A (2009). Extract of Indian green mussel, *Perna viridis* (L.) shows inhibition of blood capillary formation *in vitro*. *Pertanika Journal of Tropical Agricultural Science*, 32(1), 35-42.
- Mitra D, Chatterji A (2004). Indian green mussel (*Perna viridis*) as a source of anti-HIV activity. US Patent #6,770,302 3.
- Miyamoto T, Sakamoto K, Arao K, Komori T, Higuchi R, Sasaki T (1996). Cytotoxic spongian diterpenoids, from the nudibranch *Chromodoris obsoleta*. *Tetrahedron*, 52, 8187-8198.
- Mohamed KS, Venkatesan V, Kripa V, Prema D, Joseph M, Alloycious PS, Sharma J, Valsala KK, Saji Kumar KK, Ragesh N, Bose J, Mohan A (2013). Fishery management plan for Ashtamudi lake clam resources. CMFRI Special Publication No: 114, pp. 48.
- Mohite SA, Mohite AS, Singh H (2009). On condition index and percentage edibility of the shortneck clam *Paphia malabarica* (Chemnitz) from estuarine regions of Ratnagiri, west coast of India. *Aquatic Research*, 73, 40-69.
- Morais S, Boaventura D, Narcisoa L, Re P, Stephen JHD (2003). Gonad development and fatty acid composition of *Patella depressa* Pennant (Gastropoda: Prosobranchia) populations with different patterns of spatial distribution, in exposed and sheltered sites. *Journal of Experimental Marine Biology and Ecology*, 294, 61-80.
- Moreno-Felix C, Wilson-Sanchez G, Cruz-Ramirez S-G, Velazquez-Contreras C, Plascencia-Jatomea M, Acosta A, Machi-Lara L, Aldana-Madrid M-L, Ezquerro-Brauer J-M, Rocha-Alonzo F, Burgos-Hernandez A (2013). Bioactive lipidic extracts from Octopus (*Paraoctopus limaculatus*): Antimutagenicity and antiproliferative studies. 2013, 12 pages, Article ID 273582.
- Morteau O (2000). Prostaglandins and inflammation: the cyclooxygenase controversy. *Archivum Immunologiae et Therapia Experimentalis*, 48, 437-480.
- Murata K, Satake M, Naoki H, Kaspar HF, Yasumoto T (1998). Isolation and structure of a new brevetoxin analog, brevetoxin B2, from greenshell mussels from New Zealand. *Tetrahedron*, 54(5-6), 735-742.

- Murphy KJ, Mooney BD, Mann NJ, Nichols PD, Sinclair AJ (2002). Lipid, FA, and sterol composition of New Zealand green lipped mussel (*Perna canaliculus*) and Tasmanian blue mussel (*Mytilus edulis*). *Lipids*, 37(6), 587-595.
- Murphy MP (2009). How mitochondria produce reactive oxygen species. *Biochemical Journal*, 417(1), 1-13.
- Murray J, Burt JR (2001). The composition of fish. Torry Advisory Note No. 38, Ministry of Technology, Torry Research Station, Aberdeen, UK. pp. 14.
- Nagash YS, Nazeer RA, Kumar NSS (2010). *In vitro* antioxidant activity of solvent extracts of mollusks (*Loligo duvauceli* and *Donax strateus*) from India. *World Journal of Fish and Marine Sciences*, 2, 240-245.
- Nawar WF (1996). Lipids. *In Food Chemistry*. Eds. Fennema O. 3rd ed. Marcel Dekker, New York. pp. 225-320.
- Ninh TD, Nagashima Y, Shiomi K (2007). Water-soluble and lipid-soluble arsenic compounds in Japanese flying squid *Todarodes pacificus*. *Journal of Agricultural and Food Chemistry*, 55, 3196-3202.
- Nischwitz V, Kanaki K, Pergantis SA (2006). Mass spectrometric identification of novel arsiniothiyl-sugars in marine bivalves and algae. *Journal of Analytical Atomic Spectrometry*, 21, 33-40.
- Nitin K, Sushil K, Himanshu G, Sharma PK (2012). 3-Hydroxy-2-(substituted phenyl)-4H-chromen-4-one derivatives-synthesis, spectral characterization and pharmacological screening. *World Research Journal of Biochemistry*, 1(1), 1-5.
- Njinkoue JM, Barnathan G, Miralles J, Gaydou EM, Samb A (2002). Lipids and fatty acids in muscle, liver and skin of three edible fish from the Senegalese coast: *Sardinella maderensis*, *Sardinella aurita* and *Cephalopholis taeniops*. *Comparative Biochemistry and Physiology-B: Biochemistry and Molecular Biology*, 31, 395-402.
- Norte M, Cataldo F, Gonzalez AG, Rodriguez ML, Ruiz-Perez C (1990). New metabolites from the marine mollusc *siphonaria grisea*. *Tetrahedron*, 46, 1669-1678.
- O'Boyle NM, Banck M, James CA, Morley C, Vandermeersch T, Hutchison GR (2011). Open Babel: An open chemical toolbox. *Journal of Cheminformatics*, 3, 33.
- Odeleye T, Li Y, White WL, Nie S, Chen S, Wang J, Lu J (2016). The antioxidant potential of the New Zealand surf clams. *Food Chemistry*, 204, 141-149.
- Oh DC, Jensen PR, Kauffman CA, Fenical W (2005). Libertellenones A-D: Induction of cytotoxic diterpenoid biosynthesis by marine microbial competition. *Bioorganic and Medicinal Chemistry*, 13, 5267-5273.
- Okuzumi M, Fujii T (2000). Nutritional and functional properties of squid and cuttlefish. Eds. Okuzumi M, Fujii T. National Cooperative Association of Squid Processors. 35th Anniversary Commemorative Publication, Tokyo. pp. 223.

- Orban E, Di Lena G, Nevigato T, Casini I, Marzetti A, Caproni R, Santorini R, Giulini G (2006). Nutritional and commercial quality of the striped venus clam, *Chamelea gallina*, from the Adriatic Sea. Food Chemistry, 101, 1063-1070.
- Orban E, Di Lena G, Nevigato T, Casini I, Marzetti A, Caproni R (2002). Seasonal changes in meat content, condition index and chemical composition of mussels (*Mytilus galloprovincialis*) cultured in two different Italian sites. Food Chemistry, 77, 57-65.
- Ouyang M-A (2006). A new adenosyl-alkaloid from *Ostrea rivularis*. Natural Product Research, 20, 79-83.
- Ozyurt G, Duysak O, Akama E, Tureli C (2006). Seasonal change of fatty acids of cuttlefish *Sepia officinalis* L. (mollusca: cephalopoda) in the north eastern Mediterranean Sea. Food Chemistry, 95, 382-385.
- Paiva SAR, Russell RM (1999). β -Carotene and other carotenoids as antioxidants. Journal of the American College of Nutrition, 18(5), 426-433.
- Pan M-H, Huang Y-T, Chang C-I, Ho C-T, Pan BS (2007). Apoptotic-inducing epidioxysterols identified in hard clam (*Meretrix lusoria*). Food Chemistry, 102, 788-795.
- Parente L, Perretti M (2003). Advances in the pathophysiology of constitutive and inducible cyclooxygenases, two enzymes in the spotlight. Biochemical Pharmacology, 65, 1530-159.
- Parker SR, Cutler HG, Jacyno JM, Hill RA (1997). Biological activity of 6-pentyl-2H-pyran-2-one and its analogs. Journal of Agricultural and Food Chemistry, 45(7), 2774-2776.
- Pawar RT, Nagvenkar SS, Jagtap TG (2013). Protective role of edible clam *Paphia malabarica* (Chemnitz) against lipid peroxidation and free radicals. Turkish Journal of Biochemistry, 38 (2), 138-144.
- Periyasamy N, Murugan S, Bharadhirajan P (2014). Biochemical composition of marine bivalve *Donax incarnatus* (Gmelin, 1791) from Cuddalore southeast coast of India. International Journal of advances in Pharmacy, Biology and Chemistry, 3(3), 575-582.
- Perron F, Albizati KF (1989). Chemistry of spiroketals. Chemical Reviews, 89(7), 1617-1661.
- Petit J, Meurice N, Kaiser C, Maggiora G (2012). Softening the rule of five-where to draw the line? Bioorganic and Medicinal Chemistry, 20, 5343-5351.
- Pettit GR, Kamano Y, Kizu H, Dufresne C, Herald CL, Bontems RJ, Schmidt JM, Boettner F E, Nieman RA (1989). Isolation and structure of the cell growth inhibitory depsipeptides Dolastatins 11 and 12. Heterocycles, 1989, 28, 553-558.
- Pettit GR, Tang Y, Knight JC (2005). Antineoplastic agents. 545. Isolation and structure of turbotatins 1-4 from the Asian marine mollusk *Turbo stenogyris*. Journal of Natural Products, 68 (7), 974-978.
- Pierce G, Valavanis V, Guerra A, Jereb P, Orsi-Relini L, Bellido J, Katara I, Piatkowski U, Pereira J, Balguerias E, Sobrino I, Lefkadiou E, Wang J,

- Santurtun M, Boyle P, Hastie L, MacLeod C, Smith J, Viana M, Gonzalez A (2008). A review of cephalopod environment interactions in European Seas. *Hydrobiologia*, 612, 49-70.
- Pla D, Marchal A, Olsen CA, Francesch A, Cuevas C, Albericio F, Alvarez M (2006). Synthesis and structure-activity relationship study of potent cytotoxic analogues of the marine alkaloid Lamellarin D. *Journal of Medicinal Chemistry*, 49(11), 3257-3268.
- Porto TS, Rangel R, Furtado NAJC, De Carvalho TC, Martins CG, Veneziani RCS, Da Costa FB, Vinholis AHC, Cunha WR, Heleno VCG (2009). Pimarane-type diterpenes: Antimicrobial activity against oral pathogens. *Molecules*, 14, 191-199.
- Poyton RO, Ball KA, Castello PR (2009). Mitochondrial generation of free radicals and hypoxic signaling. *Trends in Endocrinology and Metabolism*, 20, 332-340.
- Prota G, Ito S, Nardi G. (1977). The Chemistry of adenochrome(S). *In Marine Natural Products Chemistry*. Eds. Faulkner DJ, Fenical WH. Nato Conference Series, Springer, Boston, M.A. 1.
- Putz A, Kehraus S, Diaz-Agras G, Wagele H, König GM, Dotofide (2011). Guanidine-interrupted terpenoid from the marine slug *Doto pinnatifida* (Gastropoda, Nudibranchia). *European Journal of Organic Chemistry*, 3733-3737.
- Quan LD, Thiele GM, Tian J, Wang D (2008). The development of novel therapies for rheumatoid arthritis. *Expert Opinion on Therapeutic Patents*, 18, 723-738.
- Rajaganapathi J, Kathiresan K, Singh TP (2002). Purification of anti-HIV protein from purple fluid of the Sea hare *Bursatella leachii* de Blainville. *Marine Biotechnology*, 4, 447-453.
- Ramasamy M, Balasubramanian U (2012). Identification of bioactive compounds and antimicrobial activity of marine clam *Anadara granosa* (linn.). *International Journal of Science and nature*, 3(2), 263-266.
- Ramasamy M, Balasubramanian U (2014). Study on antimicrobial activity of marine of bivalves *Meretrix casta* (Chemnitz) and *Anadara granosa* (Linn) from Muthupet and Tutcorin Southeast coast of India. *International Journal of Science and Nature*, 5(1), 109-112.
- Ramesh X, Ayyakkannu K (1992). Nutritive value of *Chicoreus ramosus*: A status report. Proceedings of second workshop of the tropical marine mollusc programme (TMMP) at Annamalai University, India, 4th to 14th May, 1992. Eds. Hylleberg J, Ayyakkannu K, Khokiattiwong S. Phuket Marine Biology Center, 10, 14.
- Ravi C, Karthiga A, Venkatesan V (2012). Isolation and biomedical screening of the tissue extracts of two marine gastropods *Hemifusus pugilinus* (Born, 1778) and *Natica didyma* (Roding, 1798). *Asian Fisheries Science Journal*, 25, 158-169.
- Reich HJ, Jautelat M, Messe MT, Weigert FJ, Roberts JD (1969). Nuclear magnetic resonance spectroscopy, Carbon-13 spectra of steroids. *Journal of the American Chemical Society*, 91, 7445-7454.

- Rice-Evans CA, Miller NJ, Paganga G (1996). Structure-antioxidant activity relationships of flavonoids and phenolic acids. *Free Radical Biology and Medicine*, 20, 933-956.
- Rocha DFO, Hamilton K, Goncalves CCS, Machado G, Marsaioli AJ (2011). 6-Alkyl-3,4-dihydro-2H-pyrans: Chemical secretion compounds in neotropical harvestmen. *Journal of Natural Products*, 74, 58-663.
- Rovirosa J, San-Martin A (2006). A novel metabolite from the Chilean mollusk *Siphonaria lessoni*. *Quimica Nova*, 29(1), 52-53.
- Russo C, Olivieri O, Girelli D, Faccini G, Zenari ML, Lombardi S, Corrocher R (1998). Antioxidant status and lipid peroxidation in patients with essential hypertension. *Journal of Hypertension*, 16(9), 1267-1271.
- Russo G, Tringali G (1983). Hemagglutinating and antibacterial activity in hemolymph of *Octopus vulgaris*. *Revue Internationale d'Océanographie Medicale*, 70/71, 49-54.
- Russo GL, Nisco ED, Fiore G, Donato PD, d'Ischia M, Palumbo A (2003). Toxicity of melanin-free ink of *Sepia officinalis* to transformed cell lines: Identification of the active factor as tyrosinase. *Biochemical and Biophysical Research Communications*, 308, 293-299.
- Ryan KA, Smith MF Jr, Sanders MK, Ernst PB (2004). Reactive oxygen and nitrogen species differentially regulate Toll-like receptor 4-mediated activation of NF-kappa B and interleukin-8 expression. *Infection and Immunity*, 72, 2123-2130.
- Saba S (2011). Bivalve culture optimisation of three autochthonous species (*Ruditapes decussatus*, *Mytilus galloprovincialis* and *Ostrea edulis*) in a central-western Mediterranean lagoon (Porto Pozzo, northern Sardinia). PhD Thesis, Università degli Studi di Sassari, Dottore di Ricerca, Scienze Zootecniche.
- Saito H, Aono H (2014). Characteristics of lipid and fatty acid of marine gastropod *Turbo cornutus*: High levels of arachidonic and *n*-3 docosapentaenoic acid. *Food Chemistry*, 145, 135-144.
- Saito H (2007). Identification of novel *n*-4 series polyunsaturated fatty acids in a deep-Sea clam, *Calymene phaseoliformis*. *Journal of Chromatography A*, 1163(1-2), 247-259.
- Sakata K, Yamamoto Y, Ishikawa H, Yagi A, Etoh H, Ina K (1990). Chlorophyllone-a, a new pheophorbide- α related compound isolated from *Ruditapes philippinarum* as an antioxidative compound. *Tetrahedron Letters*, 31(8), 1165-1168.
- Sala GD, Cutignano A, Fontana A, Spinella A, Calabrese G, Coll AD, d'Ippolito G, Monica CD, Cimino G (2007). Towards the biosynthesis of the aromatic products of the Mediterranean mollusc *Scaphander lignarius*: Isolation and synthesis of analogues of lignarenones. *Tetrahedron*, 63(30), 7256-7263.
- Salo-Vaananen P, Mattila P, Lehtikainen K, Salmela-Molsa E, Piironen V (2000). Simultaneous HPLC analysis of fat-soluble vitamins in selected animal products after small-scale extraction. *Journal of Agricultural and Food Chemistry*, 71, 535-543.

- Sanmugam A, Subhapradha N, Suman S, Ramasamy P, Saravanan R, Shanmugam V, Srinivasan A (2012). Characterization of biopolymer "Chitosan" from the shell of Donacid clam (Linnaeus, 1758) and its antioxidant activity. *International Journal of Pharmacy and Pharmaceutical Sciences*, 4460-4465.
- Santalova EA, Denisenko VA, Chernyshev AV, Gavagnin M, Sanamyan KE (2007). Ketosteroids from the far-east marine prosobranch mollusk *Onchidiopsis variegata*. *Chemistry of Natural Compounds*, 43, 86-89.
- Santos-Silva J, Bessa RJB, Santos-Silva F (2002). Effect of genotype, feeding system and slaughter weight on the quality of light lambs: II. Fatty acid composition of meat. *Livestock Production Science*, 77, 187-194.
- Sarma NS, Krishna MSR, Rao SR (2005). Sterol ring system oxidation pattern in marine sponges. *Marine Drugs* 3, 84-111.
- Sasaki K, Wright JLC, Yasumoto T (1998). Identification and characterization of pectenotoxin (PTX) 4 and PTX7 as spiroketal stereoisomers of two previously reported pectenotoxins. *The Journal of Organic Chemistry*, 63, 2475-2480.
- Satake M, Terasawa K, Kadowaki Y, Yasumoto T (1996). Relative configuration of yessotoxin and isolation of two new analogs from toxic scallops. *Tetrahedron Letters*, 37, 5955-5958.
- Schmeer MR, Huala CV (1965). Mercene: *In vivo* effects of mollusc extracts on sarcoma 180. *Annals of the New York Academy of Sciences*, 118, 605-610.
- Schmitz FJ, Gopichand Y, Michaud DP, Prasad RS, Retnaley S. (1981). Recent developments in research on metabolites from Caribbean marine invertebrates. *Pure Applied Chemistry*, 51, 853-865.
- Schmitz FJ, McDonald FJ, Vanderahl DJ (1978). Marine natural products: Sesquiterpene alcohols and ethers from the Sea hare *Aplysia dactylomela*. *The Journal of Organic Chemistry*, 43(21), 4220-4225.
- Schmitz FJ, McDonald FJ (1974). Marine natural products: Dactyloxene-B, a sesquiterpene ether from the Sea hare, *Aplysia dactylomela*. *Tetrahedron letters*, 29, 2541-2544.
- Schmitz FJ, Michaud DP, Schmidt PC (1982). Marine natural products: Parguerol, deoxyparguerol and isoparguerol. New brominated diterpenes with modified pimarane skeletons from the Sea hare *Aplysia dactylomela*. *Journal of the American Chemical Society*, 104, 6415-6423.
- Schnitzer J, Kamin M, Olson WH (1999). Tramadol allows reduction of naproxen dose among patients with naproxen-responsive osteoarthritis pain. *Arthritis and Rheumatology*, 42, 1370-1377.
- Schofield C, Ashworth A (2002). Why have mortality rates for severe malnutrition remained so high? World Health Organisation. World health report Geneva. *Bulletin of the World Health Organization*. 74, 223-229.
- Schwartsmann G, Da Rocha AB, Berlinck RGS, Jimeno J (2001). Marine organisms as a source of new anticancer agents. *The Lancet Oncology*, 2, 221-225.

- Selwood AI, Miles CO, Wilkins AL, Van Ginkel R, Munday R, Rise F, McNabb P (2010). Isolation, structural determination and acute toxicity of pinnatoxins E, F and G. *Journal of Agricultural and Food Chemistry*, 58, 6532-6542.
- Senan VP, Sherief PM, Nair JR (2013). Anticancer property of purified fraction C2 of cuttlefish (*Sepia pharaonis*) ink on cervical cancer cells. *Indo American Journal of Pharmaceutical Research*, 3(9), 7444-7454.
- Seo JK, Crawford JM, Stone KL, Noga EJ (2005). Purification of a novel arthropod defensin from the American oyster, *Crassostrea virginica*. *Biochemical and Biophysical Research Communications*, 338, 1998-2004.
- Sevanian A, Ursini F (2000). Lipid peroxidation in membranes and low-density lipoproteins: Similarities and differences. *Free Radical Biology and Medicine*, 29, 306-311.
- Shan B, Cai Y-Z, Brooks JD, Corke H (2007). The *in vitro* antibacterial activity of dietary spice and medicinal herb extracts. *International Journal of Food Microbiology*, 117, 112-119.
- Shubina LK, Fedorov SN, Kalinovskiy AI, Dmitrenok AS, Jin JO, Song MG, Kwak JY, Stonik VA (2007). Four new chamigrane sesquiterpenoids from the opisthobranch mollusk *Aplysia dactylomela*. *Russian Chemical Bulletin*, 56(10), 2109-2114.
- Sica D. (1980). Sterols from some molluscs. *Comparative Biochemistry and Physiology*, 65B, 407-410.
- Simopoulos AP (2009). Omega-6/omega-3 essential fatty acids: Biological effects. *World Review of Nutrition and Dietetics*, 99, 1-16.
- Siriwardhana N, Kalupahana NS, Moustaid MN (2012). Health benefits of *n*-3 polyunsaturated fatty acids: Eicosapentaenoic acid and docosahexaenoic acid. *Advances in Food and Nutrition Research*, 65, 211-222.
- Smith WP, Sollis LS, Howes DP, Cherry CP, Starkey DI, Cobley NK (1998). Dihydropyran-carboxamides related to Zanamivir: A new series of inhibitors of Influenza virus Sialidases. Discovery, synthesis, biological activity, and structure-activity relationships of 4-guanidino and 4-amino-4H-pyran-6-carboxamides. *Journal of Medicinal Chemistry*, 41, 787-797.
- Smoothey AF (2013). Habitat-associations of turban snails on intertidal and subtidal rocky reefs. *PLOS ONE*, 8(5), e61257.
- Soliman AM, Fahmy SR, El-Abied SA (2015). Anti-neoplastic activities of *Sepia officinalis* ink and *Coelatura aegyptiaca* extracts against Ehrlich ascites carcinoma in Swiss albino mice. *International Journal of Clinical and Experimental Pathology*, 8(4), 3543-3555.
- Somerville MJ, Katavic PL, Lambert LK, Pierens GK, Blanchfield JT, Cimino G, Mollo E, Gavagnin M, Banwell MG, Garson MJ (2012). Isolation of Thuridillins D-F, diterpene metabolites from the Australian sacoglossan mollusk *Thuridilla splendens*: Relative configuration of the epoxylactone ring. *Journal of Natural Products*, 75(9), 1618-1624.

- Sostres C, Gargallo CJ, Arroyo MT, Lanas A (2010). Adverse effects of non-steroidal anti-inflammatory drugs (NSAIDs, aspirin and coxibs) on upper gastrointestinal tract. *Best Practice and Research: Clinical Gastroenterology*, 24(2), 121-132.
- Sreejamole KL, Radhakrishnan CK, Padikkala J (2011). Anti-inflammatory activities of aqueous/ethanol and methanol extracts of *Perna viridis* Linn. in mice. *Inflammopharmacology*, 19, 335-341.
- Sreejamole KL, Radhakrishnan CK (2013). Antioxidant and cytotoxic activities of ethyl acetate extract of the Indian green mussel *Perna viridis*. *Asian Journal of Pharmaceutical and Clinical Research*, 6(3), 197-201.
- Sreekumar PK (2007). Identification of radioprotective activity in the extract of Indian green mussel *Perna viridis* (L). Ph.D Thesis. Goa University.
- Srilatha G, Chamundeeswari K, Ramamoorthy K, Sankar G, Varadharajan D (2013). Proximate, amino acid, fatty acid and mineral analysis of clam, *Meretrix casta* (Chemnitz) from Cuddalore and Parangipettai coast, south east coast of India. *Journal of Marine Biology and Oceanography*, 2, 2-7.
- Stefanis L, Burke RE, Greene LA. (1997). Apoptosis in neurodegenerative disorders. *Current Opinion in Neurology*, 10, 299-305.
- Su JH, Lin FY, Huang HC, Dai CF, Wu YC, Hu WP, Hsu CH, Sheu JH (2007). Novel steroids from the soft coral *Nephthea chabroliei*. *Tetrahedron*, 63, 703-707.
- Su JH, Lo CL, Lu Y, Wen ZH, Huang CY, Dai CF, Sheu JH (2008). Anti-inflammatory polyoxygenated steroids from the soft coral *Sinularia* sp. *Bulletin of the Chemical Society of Japan*, 81, 1616-1620.
- Suciati, Lambert LK, Garson MJ (2011). Structures and anatomical distribution of oxygenated diterpenes in the Australian nudibranch *Chromodoris reticulate*. *Australian Journal of Chemistry*, 64, 757-765.
- Sudhakar GRL, Vincent SGP (2014). Purification and characterization of a novel C-type haemolytic lectin for clot lysis from the fresh water clam *Villorita cyprinoides*: A possible natural thrombolytic agent against myocardial infarction. *Fish and Shellfish Immunology*, 36, 367-373.
- Suja N, Mohamed KS (2010). The black clam, *Villorita cyprinoides* fishery in the State of Kerala, India. *Marine Fisheries Review*, 72(3), 48-61.
- Sun L, Li D, Tao M, Chen Y, Dan F, Zhang W (2012). Scoparanes C-G: New oxygenated pimarane diterpenes from the marine sediment-derived fungus *Eutypella scoparia* FS26. *Marine Drugs*, 10, 539-550.
- Sun L-L, Fu X-M, Li X-B, Xing Q, Wang C-Y (2013). New 18-oxygenated polyhydroxy steroid from a South China Sea soft coral *Sarcophyton* sp. *Natural Product Research*, 27, 2006-2011.
- Suntornchashweij S, Chaichit N, Isobe M, Suwanborirux K (2005). Hectochlorin and morpholine derivatives from the Thai Sea hare, *Bursatella leachii*. *Journal of Natural Products*, 68, 951-955.

- Suntornchashwej S, Suwanborirux K, Koga K, Isobe M (2007). Malynamide X: The first (7R)-lyngbic acid that connects to a new tripeptide backbone from the Thai Sea hare *Bursatella leachii*. *Asian Journal of Organic Chemistry*, 2, 114-122.
- Supatra K, Soottawat B, Hideki K, Tsai YH (2013). Chemical compositions and nutritional value of Asian hard clam (*Meretrix lusoria*) from the coast of Andaman Sea. *Food Chemistry*, 141, 4138-4145.
- Tabassum A, Bristow RG, Venkateswaran V (2010). Ingestion of selenium and other antioxidants during prostate cancer radiotherapy, a good thing? *Cancer Treatment Reviews*, 36, 230-234.
- Takada N, Iwatsuki M, Suenaga K, Uemura D (2000). Pinnamine, an alkaloidal marine toxin, isolated from *Pinna muricata*. *Tetrahedron Letters*, 41(33), 6425-6428.
- Takada N, Suenaga K, Yamada K, Zheng SZ, Chen HS, Uemura, D (1999). Isolation and structures of attenols A and B. Novel bicyclic triols from the Chinese bivalve *Pinna attenuata*. *Chemistry Letters*, (10), 1025-1026.
- Takahashi H, Kusumi T, Kan Y, Satake M, Yasumoto T (1996). Determination of the absolute configuration of yessotoxin, a polyether compound implicated in diarrhetic shellfish poisoning, by NMR spectroscopic method using a chiral anisotropic reagent, methoxy-(2-naphthyl)acetic acid. *Tetrahedron Letters*, 37, 7087-7090.
- Takeda S, Kurosawa E, Komiyama K, Suzuki T (1990). The structures of cytotoxic diterpenes containing bromine from the marine red alga *Laurencia obtusa* (Hudson) Lamouroux. *Bulletin of the Chemical Society of Japan*, 63, 3066-3072.
- Tarui A, Shibata K, Takahashi S, Kera Y, Munegumi T, Yamada RH (2003). N-methyl-D-glutamate and N-methyl-L-glutamate in *Scapharca broughtonii* (Mollusca) and other invertebrates. *Comparative Biochemistry and Physiology-B: Biochemistry and Molecular Biology*, 134(1), 79-87.
- Taylor AG, Savage C (2006). Fatty acid composition of New Zealand green-lipped mussels, *Perna canaliculus*: Implications for harvesting for *n*-3 extracts. *Aquaculture*, 261, 430-439.
- Terlau H, Olivera BM (2004). Conus venoms: A rich source of novel ion channel-targeted peptides. *Physiological Reviews*, 84, 41-68.
- Thao PN, Cuong XN, Luyen TTB, Quang HT, Hong Hanh TT, Kim S, Koh SY, Nam HN, Kiem VP, Minh VC, Kim HY (2013). Anti-inflammatory components of the starfish *Astropecten polyacanthus*. *Marine Drugs*, 11, 2917-2926.
- Tian RX, Tang H-F, Li Y-S, Lin H-W, Chen X-L, Ma N, Yao M-N, Zhang P-H (2011). New cytotoxic oxygenated sterols from the marine bryozoan *Cryptosula pallasiana*. *Marine Drugs*, 9, 162-183.
- Tiffany LB, Bui LM (2002). Improvement of arthritic signs in dogs fed green lipped mussel (*Perna canaliculus*). *Journal of Nutrition*, 132, 634S-1636S.

- Tilvi S, Naik CG (2007). Tandem mass spectrometry of kahalalides: Identification of two new cyclic depsipeptides, kahalalide R and S from *Elysia grandifolia*. *International Journal of Mass Spectrometry*, 42(1), 70-80.
- Treschow AP, Hodges LD, Wright PF, Wynne PM, Kalafatis N, Macrides TA (2007). Novel anti-inflammatory omega-3 PUFAs from the New Zealand green-lipped mussel, *Perna canaliculus*. *Comparative Biochemistry and Physiology-B: Biochemistry and Molecular Biology*, 147(4), 645-656.
- Trivedi DP, Doll R, Khaw KT (2003). Effect of four monthly oral vitamin D₃ (cholecalciferol) supplementation on fractures and mortality in men and women living in the community: randomised double blind controlled trial. *British Medical Journal*, 326, 469-475.
- Tsai JS, Chen JL, Pan BS (2008). ACE inhibitory peptides identified from the muscle protein hydrolysate of hard clam (*Meretrix lusoria*). *Process Biochemistry*, 43, 743-747.
- Tsukamoto S, Yamashita Y, Ohta T (2005). New cytotoxic and antibacterial compounds isolated from the Sea hare, *Aplysia kurodai*. *Marine Drugs*, 3(2), 22-28.
- Twede VD, Miljanich G, Olivera BM, Bulaj G (2009). Neuroprotective and cardioprotective conopeptides: An emerging class of drug leads. *Current Opinion in Drug Discovery and Development*, 12, 231-239.
- Tymiak AA, Rinehart KL Jr (1983). Structures of kellestinins-I and II, antibacterial metabolites of the marine mollusk *Kelletia kelletii*. *Journal of the American Chemical Society*, 105, 7396-7401.
- Uddin MH, Otsuka M, Muroi T, Ono A, Hanif N, Matsuda S, Higa T, Tanaka (2009). Deoxymanoalides from the nudibranch *Chromodoris willani*. *Chemical and Pharmaceutical Bulletin*, 57, 885-887.
- Ulbricht TLV, Southgate DAT (1991). Coronary heart disease: Seven dietary factors. *The Lancet*, 338, 985-992.
- Unusan N (2007). Change in proximate, amino acid and fatty acid contents in muscle tissue of rainbow trout (*Oncorhynchus mykiss*) after cooking. *Journal of Food Science and Technology*, 42, 1087-1093.
- Vagias C, Tsitsimpikou C, Rapti T, Roussis V (2000). 1,1'-Dimethyl-[2,2']-Bipyridyldiium salt from the bivalve *Callista chione*. *Natural Product Letters*, 14(6), 425-428.
- van Wyk WW, Froneman PW, Bernard KS, Davies-Coleman MT. (2007). New Isocopalane diterpene diester from a sub-Antarctic marine nudibranch. *Archives for Organic Chemistry*, 121-128.
- Vapaatalo, H (1986). Free radicals and anti-inflammatory drugs. *Medical Biology*, 64(1), 1-7.
- Vardaro RR, Di Marzo V, Cimino G (1992). Placidenes: Cyercene-like polypropionate c-pyrones from the mediterranean ascoglossan mollusk *Placida dendritica*. *Tetrahedron Letters*, 33, 2875-2878.

- Vardaro RR, Di Marzo V, Crispino A, Cimino G (1991). Cyercenes, novel polypropionate pyrones from the autotomizing mediterranean mollusc *cyerce cristallina*. *Tetrahedron*, 47, 5569-5576.
- Venkateswarlu Y, Biabani MAF, Reddy MVR, Chavakula R, Rao JV (1994). A new sesquiterpene from the Andaman sponge *Dysidea herbacea*. *Journal of Natural Products*, 57(6), 827-828.
- Vijayabaskar P, Shiyamala V (2012). Antioxidant properties of seaweed poly-phenol from *Turbinaria ornata* (Turner) J. Agardh, (1848). *Asian Pacific Journal of Tropical Biomedicine*, 2, S90-S98.
- Virdis A, Duranti E, Taddei S (2011). Oxidative stress and vascular damage in hypertension: Role of Angiotensin II. *International Journal of Hypertension*, 2011, 7 pages, Article ID 916310.
- Wakimoto T, Kondo H, Nii H, Kimura K, Egami Y, Oka Y, Yoshid M, Kida E, Ye Y, Akahoshi S, Asakawa T, Matsumura K, Ishida H, Nukaya H, Tsuji K, Kan T, Abe I (2011). Furan fatty acid as an anti-inflammatory component from the green-lipped mussel *Perna canaliculus*. *Proceedings of the National Academy of Sciences*, 108(42), 17533-17537.
- Walne PR (1976). Experiments on the culture in the Sea of the Butterfish *Venerupis decussata* L. *Aquaculture*, 8, 371-381.
- Wanasundara UN, Shahidi F (1999). Concentration of omega 3-polyunsaturated fatty acids of seal blubber oil by urea complexation: Optimization of reaction conditions. *Food Chemistry*, 65, 41-49.
- Wang F, Cheng XL, Li YJ, Shi S, Liu JK (2009). ent-Pimarane diterpenoids from *Siegesbeckia orientalis* and structure revision of a related compound. *Journal of Natural Products*, 72, 2005-2008.
- Wang F, Zhu T, Zhang M, Lin A, Zhua W, Gu Q (2010a). Structural determination of aspericins A-C, new furan and pyran derivatives from the marine-derived fungus *Rhizopus* sp. 2-PDA-61, by 1D and 2D NMR spectroscopy. *Magnetic Resonance in Chemistry*, 48, 155-158.
- Wang JL, Limburg D, Graneto MJ, Springer J, Hamper JR, Liao S, Pawlitz JL, Kurumbail RG, Maziasz T, Talley JJ, Kiefer JR, Carter J (2010b). The novel benzopyran class of selective cyclooxygenase-2 inhibitors. Part 2: The second clinical candidate having a shorter and favorable human half-life. *Bioorganic and Medicinal Chemistry Letters*, 20, 7159-716.
- Wang W, Lee TG, Patil RS, Mun B, Yang I, Kim H, Hahn D, Won DH, Lee J, Lee Y (2015). Monanchosterols A and B, bioactive bicyclo[4.3.1]steroids from a Korean sponge *Monanchora* sp. *Journal of Natural Products*, 78, 368-373.
- Wang XN, Bashyal BP, Wijeratne EMK, U'Ren JM, Liu MX, Gunatilaka MK, Arnold AE, Gunatilaka AAL (2011). Smardaesidins A-G, isopimarane and 20-nor-isopimarane diterpenoids from *Smardaea* sp., a fungal endophyte of the moss *Ceratodon purpureus*. *Journal of Natural Products*, 74, 2052-2061.

- Wang Y, He H, Wang G, Wu H, Zhou B, Chen X, Zhang Y (2010c). Oyster (*Crassostrea gigas*) hydrolysates produced on a plant scale have antitumor activity and immunostimulating effects in BALB/c Mice. *Marine Drugs*, 8, 255-268.
- Watanabe M, Fuda H, Jin S, Sakurai T, Ohkawa F, Hui S-P, Takeda S, Watanabe T, Koike T, Chiba H (2012). Isolation and characterization of a phenolic antioxidant from the pacific oyster (*Crassostrea gigas*). *Journal of Agricultural and Food Chemistry*, 60, 830-835.
- Wei N, Lin XK, Niu RL, Li HY (2007). Overview on anticancer agents from *Meretrix meretrix*. *Food Drug* (in Chinese), 9, 63-65.
- Weil J, Colin-Jones D, Langman M (1995). Prophylactic aspirin and risk of peptic ulcer bleeding. *British Medical Journal*, 310, 827-30.
- Wermuth CG (1996). Strategies in the search for new lead compounds or original working hypotheses. *In The practice of medicinal chemistry*. Eds. Wermuth CG. Academic, London. pp. 81.
- Wessels A, Konig GM, Wright AD (2000). New natural product isolation and comparison of the secondary metabolite content of three distinct samples of the Sea hare *Aplysia dactylomela* from Tenerife. *Journal of Natural Products*, 63(7), 920-928.
- Whitehouse MW, Macrides TA, Kalafatis N, Betts WH, Haynes DR, Broadbent J (1997). Anti-inflammatory activity of a lipid fraction (Lyprinol) from the New Zealand green-lipped mussel. *Inflammopharmacology*, 5, 237-246.
- Whitson EL, Bugni TS, Chockalingam PS, Concepcion GP, Feng X, Jin G, Harper MK, Mangalindan GC, McDonald LA, Ireland CM (2009). Fibrosterol sulfates from the Philippine sponge *Lissodendoryx* (Acanthodoryx) *fbrosa*: Sterol dimers that inhibit PKC ζ . *The Journal of Organic Chemistry*, 74, 5902-5908.
- Wilcox CS (2002). Reactive oxygen species: Roles in blood pressure and kidney function. *Current Hypertension Reports*, 4, 160-166.
- Williams DE, Andersen RJ (1987). Terpenoid metabolites from skin extracts of the dendronotid nudibranch *Tochuina tetraquetra*. *Canadian Journal of Chemistry*, 65, 2244.
- Wils P, Warnery A, Phung-Ba V, Legrain S, Scherman D (1994). High lipophilicity decreases drug transport across intestinal epithelial cells. *Journal of Pharmacology and Experimental Therapeutics*, 269, 654-658.
- Wilson WK, Sumpter RM, Warren JJ, Rogers PS, Ruan B, Schroepfer GJ (1996). Analysis of unsaturated C27 sterols by nuclear magnetic resonance spectroscopy. *Journal of Lipid Research*, 37, 1529-1555.
- Wu CJ, Cheng J, Shi XL (2013). Preparation of ACE inhibitory peptides from *Mytilus coruscus* hydrolysate using uniform design. *International Journal of Biomedical Research*, 2013, Article ID 290120, 6 pages.

- Xia X, Qi J, Liu Y, Jia A, Zhang Y, Liu C, Gao C, She Z (2015). Bioactive isopimarane diterpenes from the fungus, *Epicoccum* sp. HS-1, associated with *Apostichopus japonicus*. *Marine Drugs*, 13, 1124-1132.
- Xie W, Chen C, Lui X, Wang B, Sun Y, Yan M (2012). *Meretrix meretrix*: Activity components and their bioactivities. *Life Science Journal*, 9(3), 756-762.
- Xu J, Takasaki A, Kobayashi H, Oda T, Yamada J, Mangindaan REP, Ukai K, Nagai H, Namikoshi M (2006). Four new macrocyclic trichothecenes from two strains of marine-derived fungi of the genus *Myrothecium*. *Journal of Antibiotics*, 59, 451-455.
- Xu XL, Li TM, Zhang CR (1999). Study on antihyperglycemia and antihyperlipemia action of hydrolysate of *Meretrix meretrix* Linnaeus. *Chinese Journal of Biochemical Pharmaceutics* (in Chinese), 20(6), 298-299.
- Yamada K, Ojika M, Ishigaki T, Yoshida Y (1993). Aplyronine A, a potent antitumor substance and the congeners aplyronines B and C isolated from the Sea hare *Aplysia kurodai*. *Journal of the American Chemical Society*, 115(23), 11020-11021.
- Yamada K, Okija M, Kigoshi H, Suenaga K (2000). Cytotoxic substances from opisthobranch molluscs. In *Drugs from the Sea*. Eds. Fusetani N. Karger Publishers AG, Basel. pp. 59-73.
- Yamamoto K, Sakata K, Watanabe N, Yagi A, Brinen LS, Clardy J (1992). Chlorophyllonic acid and methyl ester, a new chlorophyll a related compound isolated as an antioxidant from short-necked clam, *Ruditapes philippinarum*. *Tetrahedron Letters*, 33(18), 2587-2588.
- Yamazaki M (1993). Antitumor and antimicrobial glycoproteins from Sea hare. *Comparative Biochemistry and Physiology-C*, 105(2), 141-146.
- Young IS, Woodside JV (2001). Antioxidants in health and disease. *Journal of Clinical Pathology*, 54, 176-86.
- Yu D, Xu F, Zeng J, Zhan J (2012). Type III Polyketide synthases in natural product biosynthesis. *Life*, 64(4), 285-295.
- Zarai Z, Frikha F, Balti R, Miled N, Gargouri Y, Mejdoub H (2011). Nutrient composition of the marine snail (*Hexaplex trunculus*) from the Tunisian Mediterranean coasts. *Journal of the Science of Food and Agriculture*, 91, 1265-1270.
- Zhan J (2009). Biosynthesis of bacterial aromatic polyketides. *Current Topics in Medicinal Chemistry*, 9, 1598-1610.
- Zhang W, Gavagnin M, Guo Y-W, Mollo E, Ghiselin MT, Cimino G (2007). Terpenoid metabolites of the nudibranch *Hexabranchus sanguineus* from the South China Sea. *Tetrahedron*, 63(22), 4725-4729.
- Zhao GD, Su B (1992). The preliminary studies on the Lectin from Sea clam (*Meretrix meretrix*). *Journal of Zhong Shan University (Natural Science)* (in Chinese), 31(3), 66-74.

- Zhao H-Y, Shao C-L, Li Z-Y, Han L, Cao F, Wang C-Y (2013). Bioactive pregnane steroids from South China Sea Gorgonian *Carijoa* sp. *Molecules*, 18, 3458-3466.
- Zheng Y, Tice CM, Singh SB (2014). The use of spirocyclic scaffolds in drug discovery. *Bioorganic and Medicinal Chemistry Letters*, 24, 3673-3682.
- Zhivotovsky B, Orrenius S (2011). Calcium and cell death mechanisms: A perspective from the cell death community. *Cell Calcium*, 50, 211-221.
- Zhong J-P, Wang G, Shang J-H, Pan JQ, Li K, Huang Y, Liu HZ (2009). Protective effects of squid ink extract towards Hemopoietic injuries induced by cyclophosphamine. *Marine Drugs*, 7(1), 9-18.
- Zlatanov S, Laskaridis K, Feist C, Sagredos A (2006). Proximate composition, fatty acid analysis and protein digestibility-corrected amino acid score of three Mediterranean cephalopods. *Molecular Nutrition and Food Research*, 50, 967-970.

PUBLICATIONS

Sl No	Authors	Title, Volume, Pages, DOI	Journal, ISSN, Impact factor	Year
Published Research Articles				
1	<u>Minju Joy</u> & Kajal Chakraborty	Antioxidative and anti-inflammatory pyranoids and isochromenyl analogues from Corbiculid bivalve clam, <i>Villorita cyprinoides</i> , 251, 125-134, 10.1016/j.foodchem.2018.01.059	Food Chemistry 0308-8146 4.946	2018
2	<u>Minju Joy</u> & Kajal Chakraborty	Biogenic antioxidative and anti-inflammatory aryl polyketides from the venerid bivalve clam <i>Paphia malabarica</i> , 237, 169-180, 10.1016/j.foodchem.2017.05.087	Food Chemistry 0308-8146 4.946	2017
3	<u>Minju Joy</u> & Kajal Chakraborty	Specialized oxygenated heterocyclics from <i>Villorita cyprinoides</i> with cyclooxygenase-2 and 5-lipoxygenase inhibitory properties, 106, 164-172, 10.1016/j.foodres.2017.12.066	Food Research International 0963-9969 3.520	2018
4	<u>Minju Joy</u> & Kajal Chakraborty	Previously undisclosed bioactive sterols from corbiculid bivalve clam <i>Villorita cyprinoides</i> with anti-inflammatory and antioxidant potentials, 135, 1-8, 10.1016/j.steroids.2018.04.007	Steroids 0039-128X 2.523	2018
5	<u>Minju Joy</u> & Kajal Chakraborty	First report of two new antioxidative meroterpeno 2 <i>H</i> -pyranoids from short-necked yellow-foot clam <i>Paphia malabarica</i> (family: Veneridae) with bioactivity against pro-inflammatory cyclooxygenases and lipoxygenase, 31(6), 615-625, 10.1080/14786419.2016.1209670	Natural Product Research 1478-6419 1.928	2017

-
- | | | | | |
|----|---|---|---|------|
| 6 | <u>Minju Joy</u>
& Kajal
Chakraborty | An unprecedented antioxidative isopimarane norditerpenoid from bivalve clam, <i>Paphia malabarica</i> with anti-cyclooxygenase and lipoxygenase potential, 55(1), 819-824, 10.1080/13880209.2017.1280061 | Pharmaceutical Biology
1388-0209
1.918 | 2017 |
| 7 | <u>Minju Joy</u>
& Kajal
Chakraborty | Previously undescribed antioxidative and anti-inflammatory chromenyls bearing 3 <i>H</i> -isochromenone and furanyl-2 <i>H</i> -chromenyl skeletons from the venerid clam, <i>Paphia malabarica</i> , 26(8), 1708-1722, 10.1007/s00044-017-1886-x | Medicinal Chemistry Research
1554-8120
1.607 | 2017 |
| 8 | <u>Minju Joy,</u>
Kajal
Chakraborty
& Vamshi
Krishna
Raola | New sterols with anti-inflammatory potentials against cyclooxygenase-2 and 5-lipoxygenase from <i>Paphia malabarica</i> , 31(11), 1286-1298, 10.1080/14786419.2016.1242001 | Natural Product Research
1478-6419
1.928 | 2017 |
| 9 | <u>Minju Joy,</u>
Kajal
Chakraborty
&
Vijayagopal
Pananghat | Comparative bioactive properties of bivalve clams against different disease molecular targets, 40(4), 593-602, 10.1111/jfbc. 12256 | Journal of Food Biochemistry
1745-4514
1.552 | 2017 |
| 10 | <u>Minju Joy</u>
& Kajal
Chakraborty | Nutritional qualities of the low-value bivalve mollusks <i>Paphia malabarica</i> and <i>Villorita cyprinoides</i> at the estuarine waters of the southwestern coast of India, 26(1), 54-70, 10.1080/10498850.2015.1092486 | Journal of Aquatic Food Product Technology
1049-8850
0.682 | 2017 |

PAPERS IN CONFERENCES

Sl. No.	Title	International/ National/State	Status
1	<u>Minju Joy</u> , Kajal Chakraborty, P. Vijayagopal. (2014). Nutritional composition of black clam <i>Villorita cyprinoides</i> (family, corbiculidae). <i>Book of abstracts in the Marine Biological Association of India, Marine Ecosystems Challenges and Opportunities-2 (MECOS-2)</i> , pp. 243-244.	International	Presented
2	<u>Minju Joy</u> , Kajal Chakraborty. (2019). Dual cyclooxygenase-2 and 5-lipoxygenase inhibitory properties of previously undescribed oxygenated heterocyclic metabolites from Corbiculid black clam <i>Villorita cyprinoides</i> from the Vembanad Lake of Kerala. <i>Albertian Knowledge Summit 2019</i> . CHEM OP1918.	International	Presented
2	<u>Minju Joy</u> , Kajal Chakraborty. (2017). Antioxidative and anti-inflammatory polyketides from bivalve clam <i>Paphia malabarica</i> . <i>Book of abstracts in 11th Indian Fisheries and AquaCulture Forum (IFAF)</i> , pp. 426-427.	International	Presented
3	<u>Minju Joy</u> , Kajal Chakraborty. (2017). Isolation and characterization of secondary metabolites from <i>Paphia malabarica</i> . <i>Book of abstracts in Current Trends in Chemistry (CTriC2017)</i> . pp. 55.	National	Presented
4	<u>Minju Joy</u> , Kajal Chakraborty. (2017). Antioxidant chromenyl derivatives from the bivalve clam, <i>Paphia malabarica</i> . <i>Book of</i>	National	Presented

- abstracts in Green Chemistry for Environmental Sustainability*, pp. 26-27.
- 5 **Minju Joy**, Kajal Chakraborty. (2017). Bioactive State Presented
 properties of bivalve clams against different
 disease molecular targets. *Proceedings of extended
 abstracts in 29th Kerala Science Congress*, pp.
 236-240.